WILEY VCH

Edited by Xin-Yuan Liu and Guosheng Liu

# Catalytic Asymmetric Radical Reactions

Foreword by Professor Mukund P. Sibi

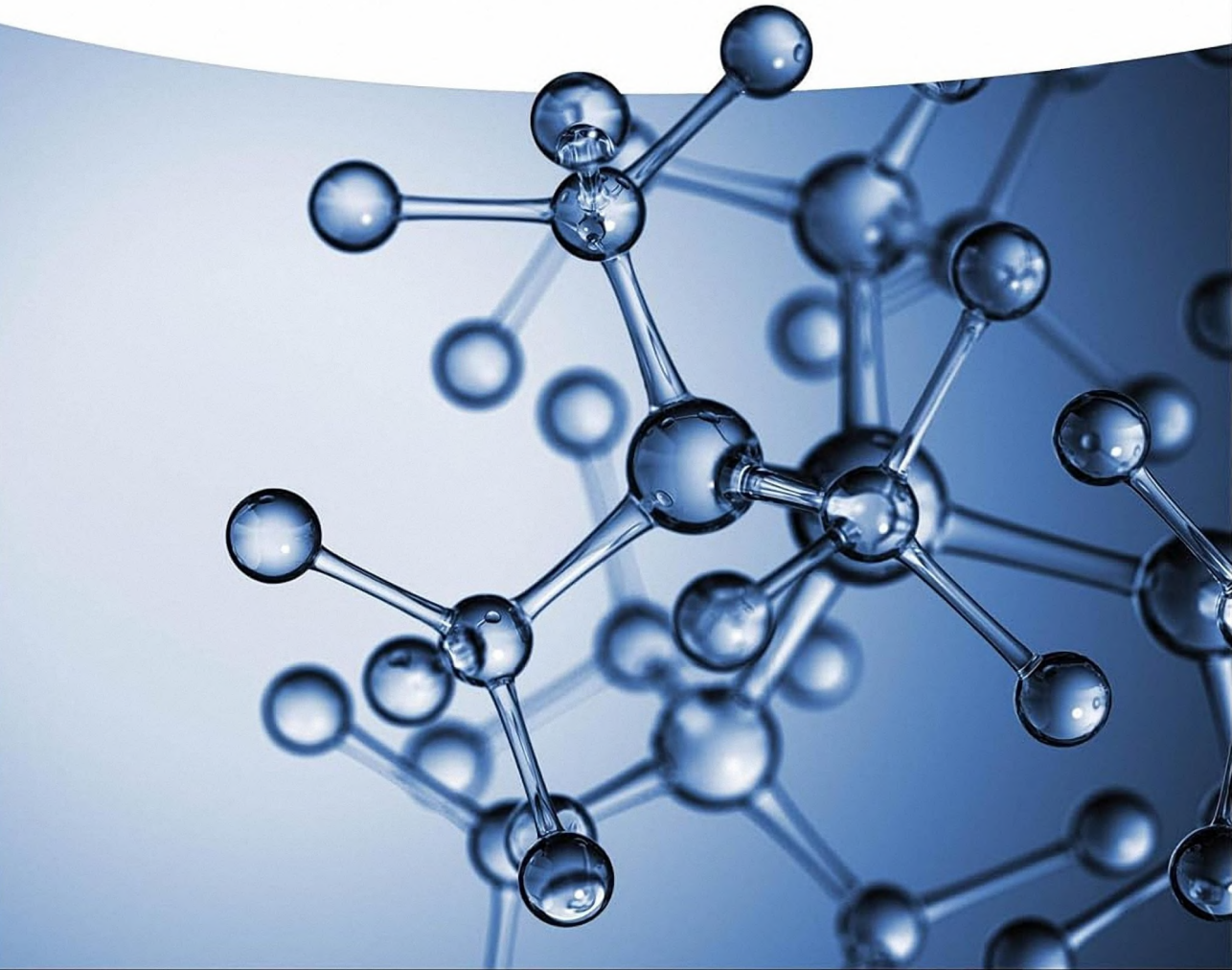

**Catalytic Asymmetric Radical Reactions**

# Catalytic Asymmetric Radical Reactions

*Edited by Xin-Yuan Liu and Guosheng Liu*

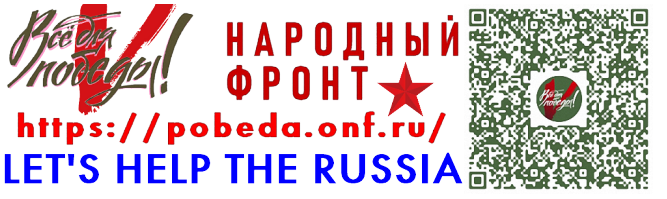


WILEY VCH

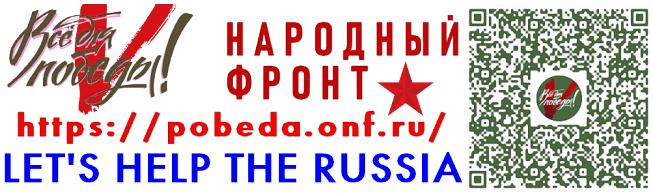


**Editors**

***Prof. Xin-Yuan Liu***
Southern University of Science & Technology (SUSTech)
No. 1088 Xueyuan Road
Nanshan District
Shenzhen 518055
China

***Prof. Guosheng Liu***
Shanghai Institute of Organic Chemistry (SIOC)
Chinese Academy of Sciences (CAS)
345 Lingling Road
Shanghai 200032
China

**Cover Image:** © BlackJack3D/Getty Images

All books published by **WILEY-VCH** are carefully produced. Nevertheless, authors, editors, and publisher do not warrant the information contained in these books, including this book, to be free of errors. Readers are advised to keep in mind that statements, data, illustrations, procedural details or other items may inadvertently be inaccurate.

**Library of Congress Card No.:** applied for

**British Library Cataloguing-in-Publication Data**
A catalogue record for this book is available from the British Library.

**Bibliographic information published by the Deutsche Nationalbibliothek**
The Deutsche Nationalbibliothek lists this publication in the Deutsche Nationalbibliografie; detailed bibliographic data are available on the Internet at <http://dnb.d-nb.de>.

© 2025 WILEY-VCH GmbH, Boschstraße 12, 69469 Weinheim, Germany

The manufacturer's authorized representative according to the EU General Product Safety Regulation is WILEY-VCH GmbH, Boschstraße 12, 69469 Weinheim, Germany, e-mail: Product_Safety@wiley.com.

All rights reserved (including those of translation into other languages, text and data mining and training of artificial technologies or similar technologies). No part of this book may be reproduced in any form – by photoprinting, microfilm, or any other means – nor transmitted or translated into a machine language without written permission from the publishers. Registered names, trademarks, etc. used in this book, even when not specifically marked as such, are not to be considered unprotected by law.

**Print ISBN:** 978-3-527-35028-5
**ePDF ISBN:** 978-3-527-83663-5
**ePub ISBN:** 978-3-527-83665-9
**oBook ISBN:** 978-3-527-83664-2

**Typesetting** Straive, Chennai, India

# Contents

**Foreword** *xi*
**Preface** *xiii*

**1 Iron-Catalyzed Radical Asymmetric Reactions** *1*
*Yajun Li, Changqing Ye, and Hongli Bao*
1.1 Introduction *1*
1.2 Asymmetric Oxidative Coupling of C—H Bonds *4*
1.2.1 Coupling for Binaphthyl Synthesis *4*
1.2.2 Coupling of Other C—H Bonds *7*
1.3 Asymmetric C—C Coupling of Alkyl Halides *11*
1.4 Asymmetric C—N Bond Formation *13*
1.5 Conclusion *18*
References *19*

**2 Cobalt-Catalyzed Asymmetric Radical Reactions** *23*
*Duo-Sheng Wang and X. Peter Zhang*
2.1 Introduction *23*
2.2 [Co(II)(Por)]-Catalyzed Asymmetric Radical Transformations via Metalloradical Catalysis *25*
2.2.1 [Co(II)(Por)]-Catalyzed Asymmetric Radical Cyclopropanation *26*
2.2.2 [Co(II)(Por)]-Catalyzed Asymmetric Radical C—H Alkylation *36*
2.2.3 Radical Cyclopropenation and Cascade Reactions *39*
2.2.4 [Co(II)(Por)]-Catalyzed Asymmetric Radical Aziridination *40*
2.2.5 [Co(II)(Por)]-Catalyzed Asymmetric Radical C—H Amination *47*
2.3 Cobalt-Catalyzed Asymmetric Hydrofunctionalization of Alkenes *54*
2.3.1 With O-nucleophile *55*
2.3.2 With *N*-nucleophile *58*
2.3.3 With C-nucleophile *60*
2.3.4 Miscellaneous *61*
2.4 Co-Catalyzed Asymmetric Radical Cross-Coupling Reactions *63*
2.4.1 Asymmetric Kumada Cross-Coupling *64*
2.4.2 Asymmetric Negishi Cross-Coupling *66*
2.4.3 Miscellaneous *68*

2.5 Summary and Outlook *70*
Acknowledgments *71*
References *71*

**3 Nickel-Catalyzed Electrophile–Nucleophile and Related Asymmetric Radical Cross-Coupling** *77*
*Yate Chen and Wangqing Kong*
3.1 Introduction *77*
3.2 Asymmetric Cross-Coupling of Organohalides with Organometallic Reagents *78*
3.2.1 Cross-Coupling of Organohalides with Aryl and Primary Alkylzinc Reagents *78*
3.2.2 Cross-Coupling of Organohalides with Secondary Alkylzinc Reagents *87*
3.2.3 Cross-Coupling of Organohalides with Organozirconium, Organoindium, Organotitanium, and Grignard Reagents *92*
3.2.4 Cross-Coupling of Organohalides with Organosilicon and Organoboron Reagents *95*
3.3 Asymmetric Cross-Coupling with Redox Auxiliaries *101*
3.4 Asymmetric Cross-Coupling with Aliphatic $C(sp^3)$—H Bonds *107*
3.5 Asymmetric Redox-Neutral Alkene Functionalization *115*
3.6 Summary and Outlook *120*
References *121*

**4 Nickel-Catalyzed Asymmetric Cross-Electrophile Couplings and Related Asymmetric Radical Cross-Couplings** *127*
*Lingling Chu, Shengqing Zhu, Jian Qin, and Yaheng Zhao*
4.1 Introduction *127*
4.2 Asymmetric $C(sp^2)$—$C(sp^3)$ Cross-Electrophile Couplings *129*
4.2.1 Asymmetric Couplings of $C(sp^3)$ Halides with $C(sp^2)$ Halides *129*
4.2.1.1 Couplings with Acyl Chlorides *129*
4.2.1.2 Couplings with Alkenyl Halides *131*
4.2.1.3 Couplings with Aryl Halides *133*
4.2.2 Asymmetric Couplings of $C(sp^2)$-Halides with $C(sp^3)$ Pseudo-Electrophiles *136*
4.2.2.1 Couplings with Epoxides *136*
4.2.2.2 Couplings with Aziridines *137*
4.2.3 Asymmetric $C(sp^3)$—$C(sp^2)$ XECs Enabled by Metallaphotoredox or Electrocatalysis *137*
4.3 Asymmetric Reductive Difunctionalization of Alkenes with Electrophiles *144*
4.3.1 Two-Component Asymmetric Couplings with Tethered Alkenes *144*
4.3.1.1 Tethered Activated Alkenes *144*
4.3.1.2 Tethered Nonactivated Alkenes *146*

4.3.2 Three-Component Asymmetric Coupling with Alkenes *151*
4.4 Conclusion *154*
List of Abbreviations *154*
References *155*

**5 Copper-Catalyzed Oxidative Asymmetric Radical Cross-Coupling of C($sp^3$)—H Bonds** *159*
*Pinhong Chen and Guosheng Liu*
5.1 Introduction *159*
5.2 Asymmetric Cyanation of C($sp^3$)—H Bonds *160*
5.3 Asymmetric Arylation of C($sp^3$)—H Bonds *167*
5.4 Asymmetric Alkynylation of C($sp^3$)—H Bonds *169*
5.5 Asymmetric Fluoroalkylation of C($sp^3$)—H Bonds *173*
5.6 Asymmetric Amination of C($sp^3$)—H Bonds *175*
5.7 Conclusion *179*
References *179*

**6 Copper-Catalyzed Enantioconvergent Radical Cross-Coupling Under Thermal Conditions** *181*
*Xiao-Yang Dong, Zhong-Liang Li, and Xin-Yuan Liu*
6.1 Introduction *181*
6.2 Chiral Anionic Ligands-Tuned Enantioconvergent Radical Cross-Coupling Under Mild Thermal Conditions *183*
6.2.1 Chiral Anionic Tridentate N,N,P-Ligands *184*
6.2.2 Chiral Anionic Tridentate N,N,N-Ligands *193*
6.2.3 Hemilabile Chiral Anionic N,N,N-Ligands *195*
6.2.4 Chiral Anionic N,N,N-Ligands with Long Spreading Side Arm *198*
6.2.5 Other Ligands in Copper-Catalyzed Enantioconvergent Radical Cross-Coupling Reactions *200*
6.3 Conclusion *203*
References *203*

**7 Manganese-Catalyzed Asymmetric Radical Reactions** *207*
*Min Cao, Huai-Ri Sun, and Lei Liu*
7.1 Introduction *207*
7.2 Manganese-Catalyzed Asymmetric Transformation *208*
7.2.1 Manganese-Catalyzed Enantioselective C—H Bond Hydroxylation *208*
7.2.2 Manganese-Catalyzed Enantioselective C—H Azidation *213*
7.3 Manganese-Catalyzed Enantioselective Desymmetrization Through C—H Bond Oxidation *214*
7.3.1 C—H Bond Oxidation to Alcohols *214*
7.3.2 C—H Bond Oxidation to Ketones *218*
7.3.3 C—H Bond Oxidation to Lactones *220*
7.4 Manganese-Catalyzed Kinetic Resolution Through C—H Bond Oxidation *221*
7.5 Conclusion *225*
References *225*

**8 Photoredox/Earth-Abundant Metal-Catalyzed Asymmetric Radical Reactions** *229*
*Peng-Zi Wang, Wen-Jing Xiao, and Jia-Rong Chen*
8.1 Introduction *229*
8.2 Photoredox/Copper-Catalyzed Asymmetric Radical Reactions *232*
8.2.1 Dual Catalysis by Merge of a Chiral Copper Catalyst and an Additional Photocatalyst *232*
8.2.2 Bifunctional Catalysis by a Single Chiral Copper Catalyst *241*
8.3 Photoredox/Nickel-Catalyzed Asymmetric Radical Reactions *248*
8.3.1 Redox-Neutral Enantioselective Radical Transformations Enabled by Dual Photoredox/Nickel Catalysis *248*
8.3.2 Enantioselective Reductive Cross-Couplings *257*
8.4 Dual Photoredox/Chromium or Cobalt-Catalyzed Asymmetric Radical Reactions *262*
8.5 Conclusion *267*
References *267*

**9 Precious Transition Metal-Catalyzed Asymmetric Radical Reactions** *273*
*Changhua Song, Liang Liu, and Shouyun Yu*
9.1 Introduction *273*
9.2 Pd-Catalyzed Asymmetric Radical Reactions *273*
9.3 Rhodium-Catalyzed Asymmetric Radical Reactions *283*
9.4 Iridium-Catalyzed Asymmetric Radical Reactions *284*
9.5 Summary and Perspectives *285*
References *285*

**10 Chiral Lewis Acid-Catalyzed Asymmetric Radical Transformations** *287*
*Yu-Mei Lin, Haichao Huang, Jiabin Liao, Yuhang He, and Lei Gong*
10.1 Introduction *287*
10.2 Asymmetric Radical Reactions Initiated by Classical Chemical Methods *288*
10.2.1 Enantioselective Conjugate Radical Addition Reactions *288*
10.2.2 Enantioselective Hydrogen Atom Transfer Reactions *291*
10.2.3 Radical Cyclization *296*
10.2.4 Other Reactions *299*
10.3 Merging CLA Catalysis with Photocatalysis *304*
10.3.1 CLA-Catalyzed Asymmetric Photochemical Reactions in the Absence of External Photosensitizers *305*
10.3.2 CLA-Catalyzed Asymmetric Photochemical Reactions in the Presence of External Photosensitizers *314*
10.4 Merging CLA Catalysis with Electrochemical Reactions *324*
10.5 Conclusion *326*
References *327*

**11 Chiral-at-Metal Complex-Catalyzed Asymmetric Radical Reactions** *333*
*Jiajia Ma*
11.1 Introduction *333*
11.2 Asymmetric Radical Reactions Enabled by Chiral-at-Iridium Lewis Acid *335*
11.2.1 Radicals Dissociated out of Chiral-at-Iridium Complexes *336*
11.2.2 Radicals Delocalized on the Ligand Sphere of Chiral-at-Iridium Complexes *339*
11.3 Asymmetric Radical Reactions Enabled by Chiral-at-Rhodium Lewis Acid *340*
11.3.1 Radicals Dissociated out of Chiral-at-Rhodium Complexes *341*
11.3.1.1 Electrophilic Radicals Interfacing with Rhodium-Enolate *341*
11.3.1.2 Nucleophilic Radicals Interfacing with Rhodium-Enone *344*
11.3.2 Radicals Delocalized on the Ligand Sphere of Chiral-at-Rhodium Complexes *347*
11.3.2.1 Ligand Sphere Radical by Single Electron Transfer of Rhodium Complexes *349*
11.3.2.2 Ligand Sphere Biradical by Direct Photoexcitation of Rhodium Complexes *359*
11.4 Asymmetric Radical Reactions Enabled by Substitutionally Inert Chiral-at-Iridium Complexes *363*
11.5 Summary *367*
Acknowledgments *367*
References *367*

**12 Chiral Photochemical Reactions in Supramolecular Assemblies** *371*
*Yanling Shen, Yulin Mao, Tong Shan, Wanhua Wu, and Cheng Yang*
12.1 Introduction *371*
12.2 Chiral Photoreactions with Cyclodextrins *372*
12.3 Supramolecular Photochirogenesis with Chiral Zeolites *384*
12.4 Chiral Photoreactions with Chiral Templates *387*
12.5 Supramolecular Photochirogenesis with Biomolecular Hosts *390*
12.6 Supramolecular Photochirogenesis with Circularly Polarized Light in Supramolecular Systems *393*
12.7 Supramolecular Photochirogenesis in Other Supramolecular Systems *396*
References *399*

**13 Organocatalysis via Covalent Bonds for Asymmetric Radical Transformations** *403*
*Danqing Zheng*
13.1 Introduction *403*
13.2 Aminocatalysis for Asymmetric Radical Transformations *404*

13.2.1 Enamine Catalysis for Asymmetric Radical Transformations *404*
13.2.1.1 Enamine Catalysis via α-Iminyl Radical Cation Intermediates *404*
13.2.1.2 Enamine Catalysis via Radical Addition to Enamine Intermediates *418*
13.2.2 Iminium Catalysis for Asymmetric Radical Transformations *424*
13.2.2.1 Radical Coupling *425*
13.2.2.2 Radical Addition *428*
13.3 Nitrogen-Heterocyclic Carbene Catalysis for Asymmetric Radical Transformations *433*
13.4 Conclusion *438*
References *438*

**14 Organocatalysis via Hydrogen Bonding for Asymmetric Radical Transformations** *443*
*Xu Ban, Xiangbin Bai, and Zhiyong Jiang*
14.1 Introduction *443*
14.2 Asymmetric Cycloaddition via H-Bonding Organocatalysis *444*
14.3 Asymmetric Cyclization via H-Bonding Organocatalysis *457*
14.4 Asymmetric Radical Addition via H-Bonding Organocatalysis *461*
14.5 Asymmetric Minisci Reaction via H-Bonding Organocatalysis *467*
14.6 Asymmetric Radical Cross-Coupling via H-Bonding Organocatalysis *471*
14.7 Asymmetric Protonation via H-Bonding Organocatalysis *477*
14.8 Asymmetric Radical/Polar Crossover Reaction via H-Bonding Organocatalysis *484*
14.9 Deracemization via H-Bonding Organocatalysis *489*
14.10 Summary and Perspective *493*
References *494*

**15 Covalent Interaction (S-/Sn-/B-Centered Radical)-Induced Asymmetric Radical Reactions** *499*
*Yee Lin Phang, Feng-Lian Zhang, and Yi-Feng Wang*
15.1 Introduction *499*
15.2 Thiyl Radicals *500*
15.3 Stannyl Radicals *512*
15.4 Boryl Radicals *513*
15.5 Conclusions *518*
References *518*

**Index** *521*

# Foreword

Radical reactions have emerged as a powerful tool with unique advantages in organic synthesis. Their high reactivity, tolerance of many reactive functionalities, and reduced sensitivity to steric crowding make them invaluable in organic synthesis, drug discovery, and materials science. However, harnessing the potential of radical reactions to access chiral molecules through catalytic asymmetric transformations has been a formidable challenge in the twentieth century, mainly due to the difficulty in stereocontrol over the highly reactive radical species. Over the past two decades, the chemistry community has witnessed a surge of innovative research in the development of asymmetric catalytic methods for enantioselective radical reactions. Organic chemists have dedicated their efforts to developing novel strategies, catalysts, and reaction conditions to achieve stereocontrol in reactions with radical intermediates. Despite this flurry of activity, there has been a conspicuous absence of a comprehensive resource that consolidates and presents these advancements in a systematic manner. This edited volume, *Catalytic Asymmetric Radical Reactions*, aims to fill that void.

Catalytic enantioselective radical reactions have evolved significantly since the seminal reports in 1996 using chiral Lewis acid catalysis. Early methods were often plagued by high catalyst loadings, excess of radical initiators and radical precursors, limitations of competent radical traps, and the use of highly toxic radical chain reagents such as tin hydrides. These drawbacks have led to the development of other catalytic methodologies over the past two decades. Synergistic photoredox and other forms of catalysis (using chiral Lewis acids, chiral Brønsted acids, hydrogen-bonding compounds, polarity reversal catalysts, etc.) expanded the scope of radical traps used and introduced alternate ways of quenching – with radicals, nucleophiles, or electrophiles (generated by radical polar crossover reactions of intermediates). The photoredox catalysts used in most of the synergistic catalytic methods are Ir- and Ru-based systems that are expensive and less readily available. These limitations can be overcome by developing green and sustainable organophotoredox systems. Recent advancements in chiral base metal (Fe, Cu, Co, Ni, Mn) catalyzed enantioselective radical reactions should enable the development of methodologies that expand the radical reactions to larger numbers of substrates in green and sustainable ways. An emerging trend in the field of catalytic enantioselective radical transformations is the use of enzymatic catalysis

to control absolute stereochemistry, although it has not been discussed in this book. Remarkable transformations have been demonstrated using this promising greener mode of catalysis. Enzymatic catalysis poses disadvantages including enzyme engineering and reaction scale-up but is optimal in terms of toxicity profile. This methodology has a bright future when used individually or synergistically with other catalytic systems.

This edited volume brings together the collective expertise of researchers in the field, each contributing a chapter on a specific area of catalytic asymmetric radical reactions. The collection begins with an in-depth exploration of transition metal-catalyzed reactions, covering a wide range of metals from iron to precious transition metals. The chapters in this section not only detail the reaction mechanisms but also showcase the reaction scope and the impact of these reactions on the synthesis of chiral molecules. The next section outlines the exploration of chiral Lewis acids and chiral-at-metal-catalyzed asymmetric radical reactions. The contributions in this part shed light on the unique activation modes and stereochemical outcomes enabled by these catalysts. The organocatalysis section rounds off the book, highlighting the power of covalent and noncovalent interactions in asymmetric radical transformations. Chiral amines and phosphoric acids, among other organocatalysts, have proven to be effective in achieving high levels of enantioselectivity, and the chapters here provide a comprehensive overview of these fascinating reactions.

I believe that this edited volume will serve as an essential reference for researchers, students, and industrial chemists alike. It offers a view of the current state of the art in catalytic asymmetric radical reactions, from the fundamental concepts to the most recent breakthroughs. By presenting the strategies and achievements in this field, it will inspire the next generation of chemists to further explore and expand the boundaries of asymmetric radical catalysis. The editor and all the contributors for the volume should be commended for their invaluable expertise and hard work in preparing their chapters. Their dedication has made this edited volume possible. The continued participation of the scientific community should be recognized for their contributions to this exciting area of research. This edited volume will serve as a catalyst for further discovery in the field of catalytic asymmetric radical reactions.

*Mukund P. Sibi*
North Dakota State University
Fargo, North Dakota 58108-6050
United States 2025

# Preface

Asymmetric synthesis is of great importance in the field of organic chemistry as it allows for the direct synthesis of valuable enantiomerically enriched molecules. Radical species, characterized by unpaired electrons, serve as highly reactive intermediates that are integral to a wide range of chemical transformations, such as organic synthesis, polymerization, and biological processes. In contrast to ionic reactions, radical reactions usually have high reactivity, good functional group tolerance, and less sensitivity to steric crowding. Therefore, the development of catalytic asymmetric radical reactions should be highly appealing but has been less recognized in the history of organic synthesis. The lag might stem from a long-standing misconception that radicals are highly reactive and uncontrollable species, which renders the enantiocontrol challenging. Over the past two decades, however, there has been an extraordinary surge in the development of numerous catalytic asymmetric radical reactions, driven by innovations in chiral Lewis acid catalysis, organocatalysis, transition metal catalysis, and enzymatic catalysis, with the rapid advancement of photo- and electrocatalysis further accelerating progress in the field. Meanwhile, our interest in this field dates back to before 2016, when both the editors of this book published their first publication of the topic independently, drawing on their expertise in transition metal catalysis. Since then, we have devoted sustainable effort to developing chiral copper catalysis for the asymmetric radical transformations of simple chemical feedstocks, including C—H functionalization, difunctionalization of alkenes, and cross-coupling of alkyl halides. Concurrently, a growing array of innovative strategies has emerged in this field, promoting a recognition of the need for a comprehensive summary that encompasses the diverse methodologies developed to date. At this moment, we were honored to receive an invitation from Wiley Publishing to contribute a book dedicated to catalytic asymmetric radical reactions. This opportunity provided the impetus for the creation of the present book.

The content of this book is organized into 3 main parts, encompassing 15 chapters in total. Chapters 1 through 9 provide a comprehensive overview of transition metal-catalyzed asymmetric radical reactions, encompassing both earth-abundant 3d transition metal catalysts – such as iron, cobalt, nickel, copper, and manganese, and precious metal catalysts, including palladium, rhodium, and iridium. Chapter 1 summarizes iron-catalyzed radical asymmetric reactions, utilizing various chiral

ligands to facilitate the construction of chiral C—C and C—X bonds in reactions such as C—H functionalization, alkene difunctionalization, and the cross-coupling of racemic alkyl halides. Chapter 2 presents cobalt-catalyzed radical transformations through strategic ligand design, focusing on three key systems: [Co(Por)]-based metalloradical catalysis enabling stereocontrolled cyclopropanation, aziridination, C—H functionalization, and radical cascade reactions, [Co(salen)]-catalyzed hydrofunctionalization of alkenes involving metal-hydride hydrogen atom transfer (MHAT), and cross-coupling of alkyl halides with organometallic reagents. Chapter 3 highlights the advances in nickel-catalyzed asymmetric radical cross-coupling reactions of racemic alkyl halides and organometallic reagents. In addition, other radical precursors beyond alkyl halides are also discussed to illustrate the broad applicability of asymmetric radical cross-coupling reactions. Chapter 4 summarizes the development of nickel-catalyzed asymmetric radical cross-electrophile coupling reactions under reductive conditions, which circumvent the need for air- or moisture-sensitive organometallic reagents. This chapter mainly introduces the scope of the coupled electrophiles and further highlights their application in alkene difunctionalization. In Chapter 5, copper-catalyzed asymmetric radical cross-coupling of C($sp^3$)—H bonds via a radical relay process is presented. The discussion in this chapter emphasizes diverse bond-formation reactions of the resulting radicals, encompassing cyanation, arylation, alkynylation, trifluoromethylation, and amination with various chiral ligands. In Chapter 6, copper-catalyzed enantioconvergent radical cross-coupling reactions of racemic alkyl halides with diverse nucleophiles under thermal conditions are presented. The discussion herein predominantly focuses on the design of chiral ligands for tuning the reducing capability of copper to initiate the radical reaction and creating a chiral environment to achieve the enantiocontrol of radicals. Chapter 7 summarizes manganese-catalyzed asymmetric radical reactions, primarily covering C—H oxidation and related enantioselective desymmetrization. Chapter 8 discusses recent progress in photoredox and earth-abundant metal-catalyzed asymmetric radical reactions, highlighting their ability to generate diverse radical species and enable chiral C—C and C—X bond formations under mild conditions. Chapter 9 highlights the advances in precious transition metal-catalyzed asymmetric radical reactions, involving palladium, rhodium, and iridium catalysis. Since they are reluctant to the single-electron transfer process, a photocatalyst is often incorporated into the reaction system to facilitate the generation of radical species.

Chapters 10 and 11 focus on Lewis acid-catalyzed asymmetric radical reactions. Chapter 10 provides an overview of asymmetric radical reactions catalyzed by classic chiral Lewis acids, such as chiral boranes and metals bearing bidentate, tridentate, or multidentate chiral ligands. Chapter 11 highlights the chiral-at-metal complex-catalyzed asymmetric radical reactions, enabling numerous transformations such as alkylation, alkenylation, amination, addition, deracemization, and rearrangement. Chapter 12 presents asymmetric photochemical reactions within supramolecular assemblies, emphasizing the impact of the chiral host framework and the synergistic effects of non-covalent interactions on photoreaction

stereoselectivity. It also discusses the influence of external environmental factors such as temperature, solvent, and pressure.

Chapters 13 through 15 focus on organocatalyzed asymmetric radical reactions. Chapter 13 summarizes the advances in organocatalysis via covalent bonds for asymmetric radical transformations. The discussion in this chapter is organized based on different modes of organocatalysis, including chiral amine-catalyzed transformations of carbonyl compounds and nitrogen-heterocyclic carbene (NHC) catalysis. Chapter 14 focuses on the role of hydrogen-bonding interactions in asymmetric radical transformations. It is categorized into eight radical transformations including radical cycloaddition, radical cyclization, radical addition, radical coupling, Minisci reactions, asymmetric protonation, radical/polar crossover reactions, and deracemizations. In Chapter 15, advances in the use of covalent interactions involving sulfur-, stannyl-, and boron-centered radicals to achieve high enantioselectivity in radical transformations are presented. The discussion focuses on how such covalent interactions between the substrate and radical species modulate both the reactivity and stereochemical outcome. In addition, the enzymatic catalysis has progressed rapidly to realize asymmetric radical reactions, but this topic is not covered in this book.

We would like to acknowledge the dedicated efforts of many friends and their collaborators who wrote the corresponding chapters and made this book a reality, including Hongli Bao from Fujian Institute of Research on the Structure of Matter, X. Peter Zhang from Boston College, Wangqing Kong from Wuhan University, Lingling Chu from Donghua University, Lei Liu from Shandong University, Wenjing Xiao and Jia-Rong Chen from Central China Normal University, Shouyun Yu from Nanjing University, Lei Gong from Xiamen University, Jiajia Ma from Shanghai Jiaotong University, Cheng Yang from Sichuan University, Danqing Zheng from Nanjing Tech University, Zhiyong Jiang from Henan Normal University, and Yi-Feng Wang from University of Science and Technology of China. We also want to extend our gratitude to our group members Pinhong Chen from Shanghai Institute of Organic Chemistry and Xiao-Yang Dong from Great Bay University, who helped us accomplish Chapters 5 and 6. In particular, Zhong-Liang Li from Great Bay University is acknowledged for his invaluable assistance in organizing and proofreading all the chapters. Professor Mukund Sibi is greatly appreciated for his support of this book and his willingness to contribute a Foreword, which serves as a remarkable introduction to the content of this book. We also appreciate people from Wiley Publishing, Dr. Lifen Yang, Priyadarshini Natarajan, Naveen Kumaran Shanmugam, and Jona Nussbeck, for their kind assistance.

*Xin-Yuan Liu*
Southern University of Science and Technology
Shenzhen, China

*Guosheng Liu*
Shanghai Institute of Organic Chemistry (CAS)
Shanghai, China

# 1

# Iron-Catalyzed Radical Asymmetric Reactions

*Yajun Li, Changqing Ye, and Hongli Bao*

*State Key Laboratory of Structural Chemistry, Key Laboratory of Coal to Ethylene Glycol and Its Related Technology, Center for Excellence in Molecular Synthesis, Fujian Institute of Research on the Structure of Matter, Chinese Academy of Sciences, Fuzhou, P. R. China*

## 1.1 Introduction

The remarkable earth's abundance and low toxicity of iron make it an environmentally benign and economically viable alternative to conventional transition-metal catalysts. Over the past several decades, the development of iron-catalyzed reactions has exemplified the ingenuity and innovation within the organic chemistry community, and iron catalysis has become a cornerstone in modern organic synthesis, revolutionizing the way chemists construct complex molecules [1–9]. Harnessing the unique reactivity of iron, researchers have developed a diverse array of transformations that have not only expanded the synthetic toolbox but also addressed sustainability challenges in the field. From unconventional bond formations to intricate cascade reactions, iron catalysis has demonstrated exceptional versatility and efficiency, offering a promising platform for the continued advancement of sustainable synthetic methodologies.

Iron-catalyzed asymmetric reactions have garnered significant attention in the field of organic chemistry, with several excellent reviews documenting the remarkable progress achieved [10–18]. The development of chiral ligands and the elucidation of their role in controlling the enantioselectivity of iron-catalyzed reactions has been a key focus. Chiral porphyrins, chiral bipyridines, chiral salens, chiral bisoxazolines (BOX) and pyridine bisoxazolines (PyBOX), chiral diamines, chiral diphosphines, chiral binaphthyls, and planar-chiral ferrocenyls were among the most studied ligands for iron catalysis. The continuous exploration and refinement of iron-catalyzed asymmetric reactions showcase their potential as powerful tools in asymmetric synthesis. For example, iron-catalyzed enantioselective oxidation, hydride transfer, activation of Lewis basic substrates, carbene transfer, nitrene transfer, and more provide transformative strategies for accessing enantioenriched compounds sustainably.

In this chapter, we will introduce the advancements in iron-catalyzed radical asymmetric reactions. In this field, iron-porphyrins play an important role in biomimetic radical asymmetric catalysis. By using metalloporphyrins as the catalysts, researchers have been able to successfully mimic several types of reactions, including epoxidation [19–21], cyclopropanation [22–24], sulfoxidation [25–27], C—H amination/hydroxylation [28, 29], and so on. Several reviews on metalloporphyrin catalysis have been well documented to cover the remarkable achievements [30–39]. On the other hand, the Arnold group elegantly pioneered the use of P411-mutants derived from well-known cytochromes P450 in organic reactions. Their work has led to great successes in radical asymmetric C—H functionalization [40–50], cyclopropanation [51–58], and so on [59–69]. Important reviews on the reactions of P411-mutants and cytochromes P450 have been published [70–76]. Therefore, these are out of the scope of this chapter and will only be briefly depicted (Schemes 1.1 and 1.2).

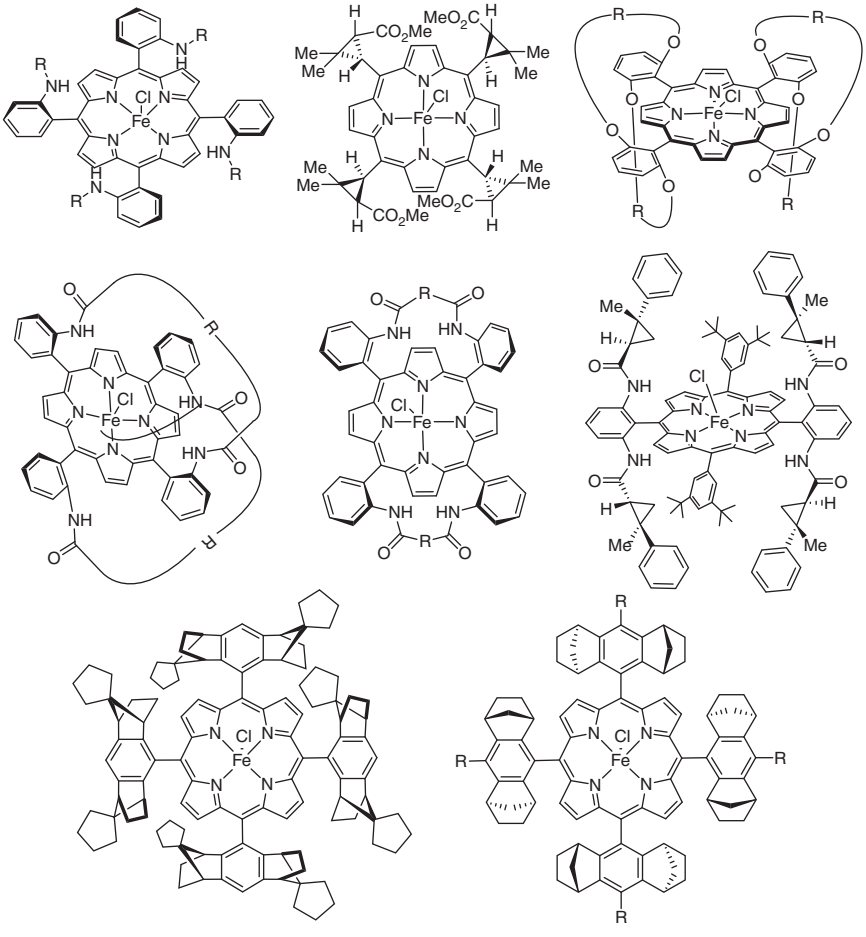

**Scheme 1.1** Selected iron-porphyrins for radical asymmetric catalysis.

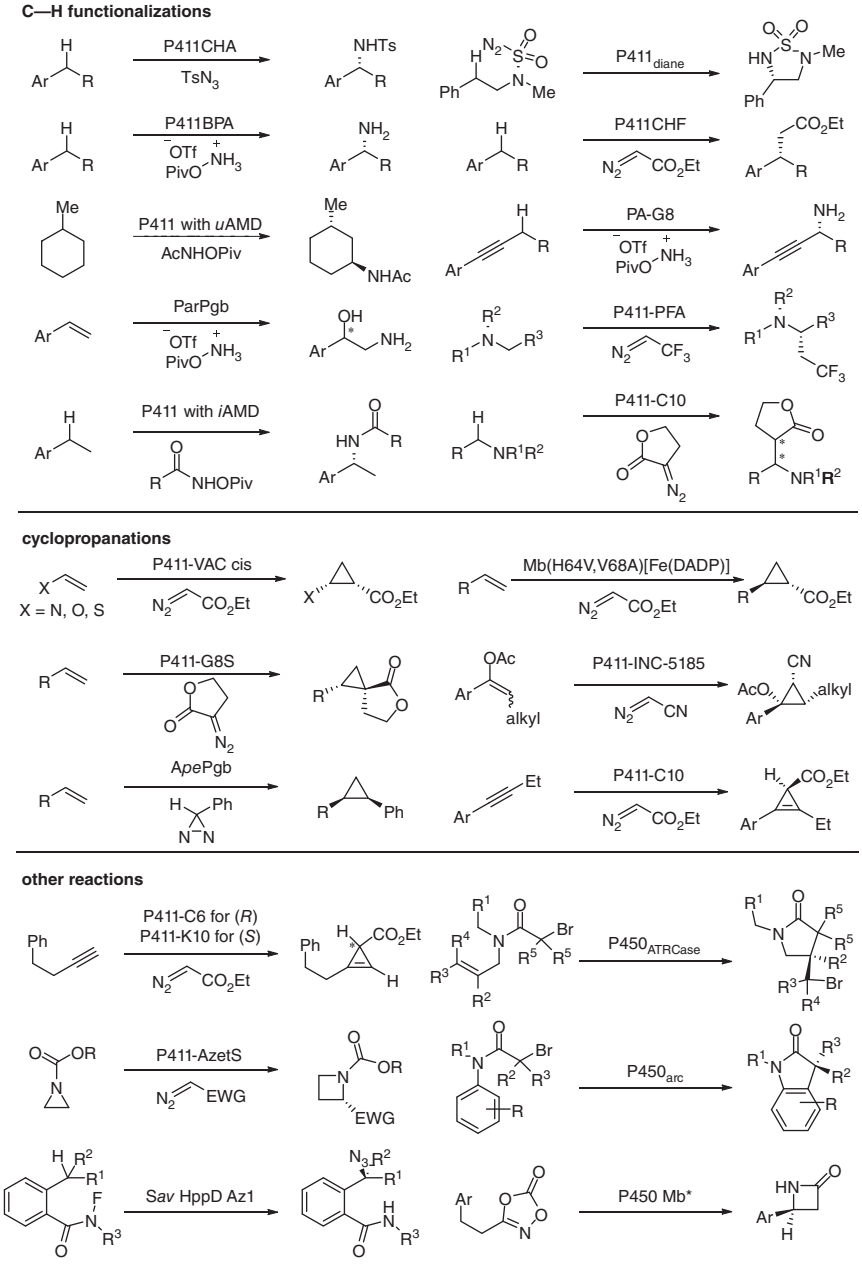


**Scheme 1.2** Engineered cytochrome P450s for radical asymmetric catalysis.

Sibi and coworkers have made substantial contributions to the advancement of radical asymmetric chemistry and a comprehensive survey of the progress achieved in enantioselective radical reactions has recently been updated [77–79]. However, the utilization of iron/chiral ligand complexes in asymmetric radical

reactions is unexpectedly underdeveloped [80–87]. This may stem from two pivotal reasons: (i) the challenge in controlling the enantioselectivity of highly reactive radicals; (ii) iron's capacity to adopt various oxidation states and partake in a diverse range of radical-mediated elementary processes. This chapter aims to elucidate how asymmetry is controlled in iron-catalyzed radical asymmetric catalysis.

## 1.2 Asymmetric Oxidative Coupling of C—H Bonds

### 1.2.1 Coupling for Binaphthyl Synthesis

Transition-metal-mediated oxidative C—H/C—H coupling reactions represent one of the most straightforward and powerful tools in modern organic synthetic chemistry [88–90]. In 2010, Katsuki and coworkers pioneered the studies on iron-catalyzed radical asymmetric oxidative C—H/C—H coupling for the synthesis of $C_1$-symmetric 1,1′-bi-2,2′-naphthols (BINOLs) (Scheme 1.3) [91]. Using the

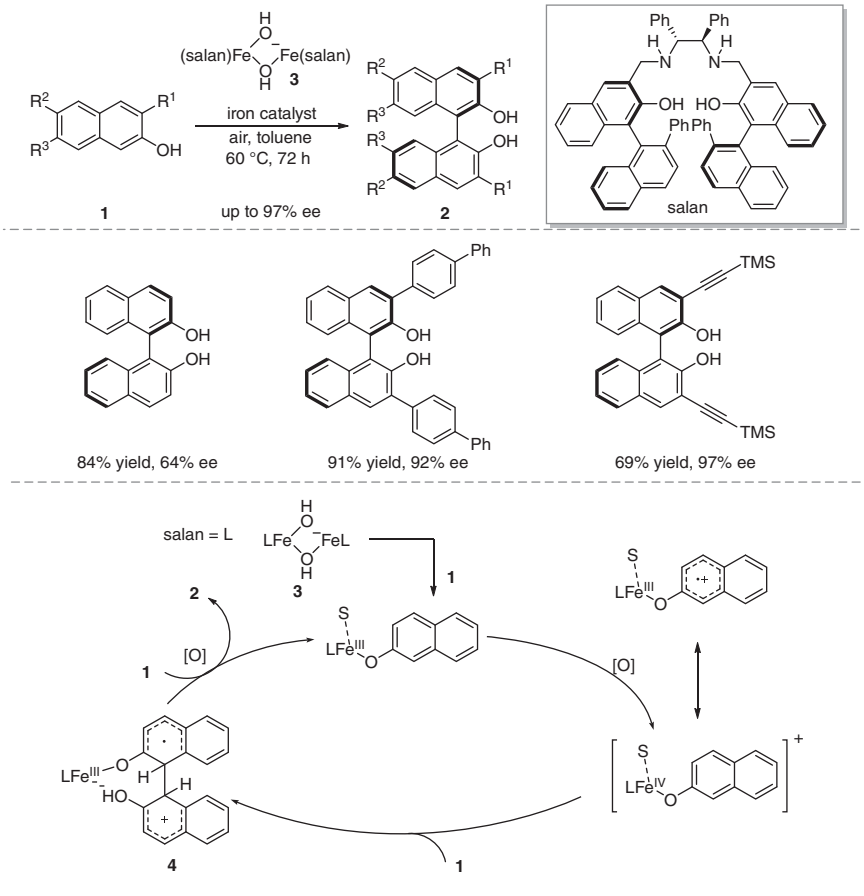


**Scheme 1.3** Iron-catalyzed C—H/C—H cross-coupling of 2-naphthols.

iron(salan) complex as the catalyst, a range of 2-naphthols **1** underwent the aerobic oxidative cross-coupling reactions and many highly enantiopure BINOLs **2** can be obtained with up to 95% enantiomeric excess (ee). The mechanistic studies suggested that the (di-$\mu$-hydroxo)iron$^{III}$(salan) catalyst **3** first underwent ligand exchange with a 2-naphthol **1** to form the 2-naphtholated iron$^{III}$(salan) species. The latter was oxidized to form the 2-naphtholated iron$^{IV}$(salan) species, which then asymmetrically reacted with another molecule of 2-naphthol **1** to give the radical cation species **4** that was associated with the iron$^{III}$(salan) core. After further oxidation and dissociation, the final chiral BINOL **2** was produced and the iron catalyst was recycled. The oxidation of 2-naphtholated iron$^{III}$(salan) to 2-naphtholated iron$^{IV}$(salan) species might be the rate-determining step of this iron-catalyzed oxidative coupling.

In 2016, the Pappo group disclosed that enantioselective oxidative homocoupling and cross-coupling of 2-naphthols can be catalyzed by chiral iron phosphate complexes **5** (Scheme 1.4) [92]. Enantioenriched $C_1$- and $C_2$-symmetric BINOLs can be smoothly produced in up to 92% ee. After reaction condition screening, the chiral phosphonic acid (CPA) with 4-$^t$Bu-Ph substituents was found to be the best chiral ligand. Di-*tert*-butyl peroxide (DTBP) was used as the oxidant and 1,2-dichloroethane (DCE)/1,1,1,3,3,3-hexafluoroisopropanol (HFIP) was used as the mixed solvent. Based on kinetic studies, an iron-catalyzed oxidative radical-anion coupling mechanism was proposed. They point out that the use of CPAs as ligands may provide a general platform for the application of chiral iron catalysts in asymmetric synthesis.

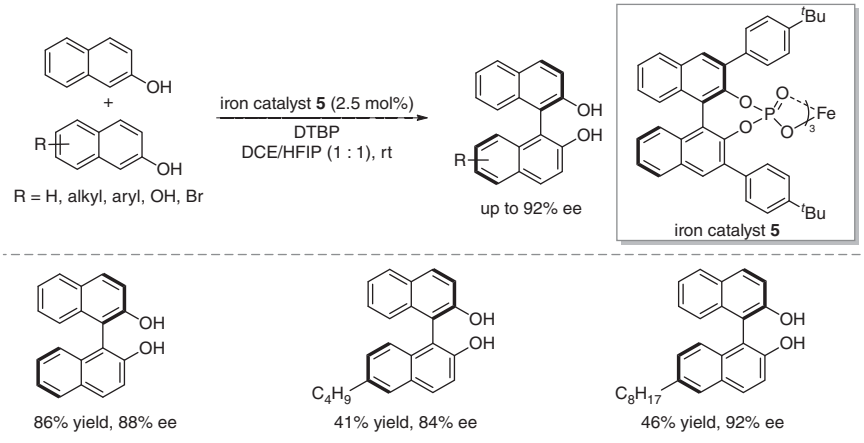


**Scheme 1.4** Iron-catalyzed C–H/C–H cross-coupling of 2-naphthols.

Bryliakov and coworkers tested a series of bipyrrolidine-derived iron aminopyridine complexes as the catalysts in the oxidative homocoupling of 2-naphthols [93]. However, when the reaction was carried out in chlorobenzene at 50 °C, only up to 56% ee was obtained. While the Ishihara group reported a chiral diphosphine oxide–iron(II) complexes ((*S*)-xylyl-$^i$PrO-BIPHEP-oxide: $Fe(OTf)_2$) for oxidative

homocoupling of 2-naphthols with *tert*-butyl hydroperoxide (TBHP) as the oxidant. The $C_1$-symmetric BINOLs were generated in up to 98% yield and 92% ee [94].

2-Amino-2′-hydroxy-1,1′-binaphthyls (NOBINs), as a kind of biaryl compounds bearing axial chirality, frequently serve as building blocks, ligands, or catalysts in asymmetric transformations [95]. In 2022, Pappo and coworkers developed an interesting asymmetric oxidative C—H/C—H cross-coupling between 2-naphthols and 2-aminonaphthalene derivatives **6** (Scheme 1.5) [96]. This cross-coupling reaction was catalyzed by a novel type of chiral redox disulfonate iron complex $[Fe((R_a)\text{-BINSate})]^+$ (BINSate = 1,1′-binaphthalene-2,2′-disulfonate), which was in situ generated from iron salt and (*Ra*)-BINSA **8**. Under the optimal reaction conditions with lauroyl peroxide (LPO) as the oxidant and boron-trifluoride-etherate $BF_3 \cdot OEt_2$ as the additive, the selective cross-coupling reactions proceeded smoothly, providing the NOBINs **7** in good yields and high enantioselectivities.

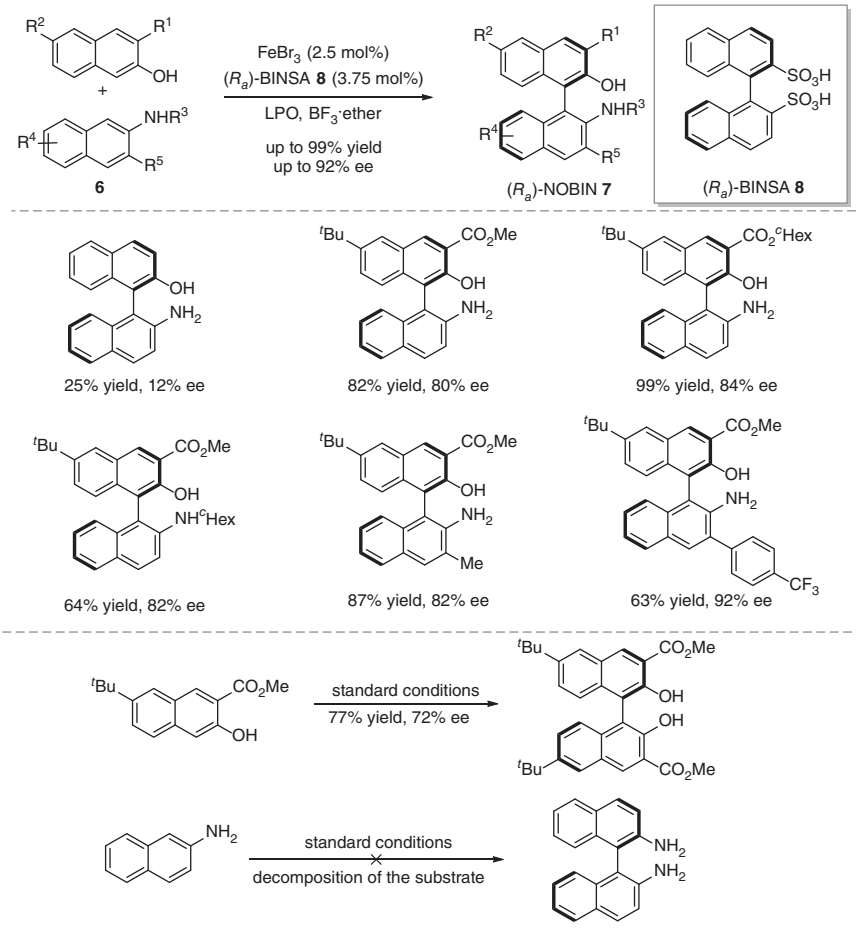


**Scheme 1.5** Iron-catalyzed C—H/C—H cross-coupling of 2-naphthols and 2-aminonaphthalene derivatives.

Without $BF_3 \cdot OEt_2$, the [Fe($(R_a)$-BINSate)]$^+$ complex would catalyze the oxidative homocoupling of a 2-naphthol derivative to afford the corresponding BINOL as the product, while the homocoupling of 2-aminonaphthalene led to the complete decomposition of the substrate. These results suggested that a radical–nucleophile coupling mechanism was involved. Moreover, the high-resolution mass spectrometry (HRMS) study and the nonlinear effect experiment suggested the involvement of mono-ligand/mono-iron species during the selectivity-determining step.

The Knölker group found that the iron/CPA complex enabled the asymmetric C—H/C—H coupling of 2-aminonaphthalene derivatives (Scheme 1.6) [97]. After examination of more than 10 different chiral phosphonic acids, it was found that the use of triphenylsilylated CPA **10** afforded the best result. The coupled 2,2′-bis(arylamino)-1,1′-biaryls **9** can be obtained in up to 97% yield and 90% ee. However, the enantioselectivity was poor for most substrates. Notably, higher yields can be obtained for phenyl naphthyl amines, and heavily electron-rich substituents are required for diphenyl amines to afford better yields and chemoselectivity. A similar mechanism proceeding via a radical cation-chiral phosphate ion pair was proposed.

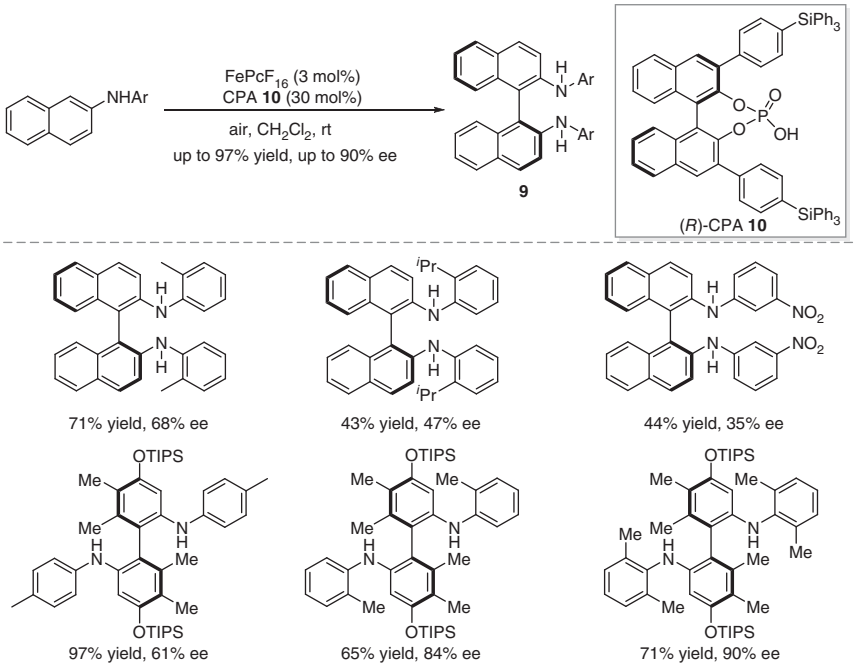


**Scheme 1.6** Iron-catalyzed homocoupling of 2-aminonaphthalene derivatives.

### 1.2.2 Coupling of Other C—H Bonds

In 2012, the Katsuki group found that if the 1-position of 2-naphthol was blocked by a substituent, these 2-naphthols would react with nitroalkanes **11** to

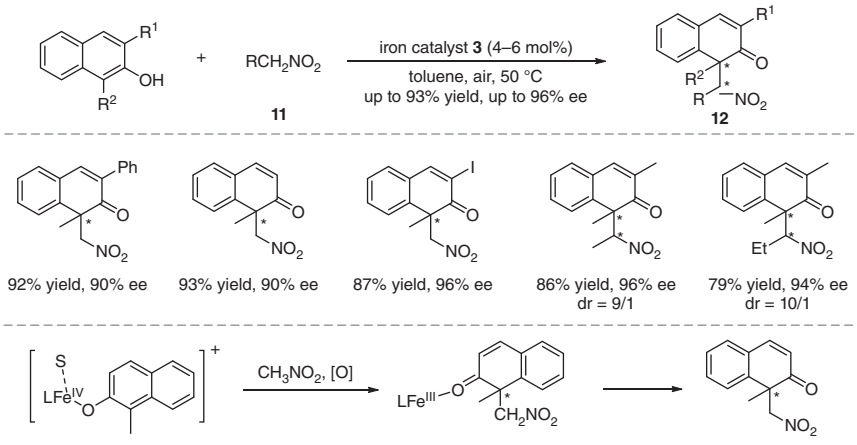


**Scheme 1.7** Iron-catalyzed coupling of 2-naphthols and nitroalkanes.

generate the enantioenriched products with an all-carbon quaternary stereocenter (Scheme 1.7) [98]. In the presence of the previously discussed iron(salan) complex **3** as the catalyst, the reactions simultaneously underwent oxidative dearomatization/asymmetric construction of the all-carbon quaternary stereocenter in an intermolecular manner to produce the products **12** in up to 93% yield and 96% ee. This iron(salan) complex-catalyzed asymmetric aerobic oxidative coupling of 2-naphthols and nitroalkanes was supposed to involve the nucleophilic attack of the nitroalkane to the radical cation species.

Pappo and coworkers explored the asymmetric cross-dehydrogenative coupling of 2-naphthols with β-ketoester derivatives (Scheme 1.8) [99]. At room temperature, the chiral iron phosphate catalyst derived from iron salt and ligand **15** and DTBP in a mixed solvent of $PhCF_3$/HFIP would only result in the homocoupling of 2-naphthols. Interestingly, the coupling of 2-naphthols with β-ketoester derivatives

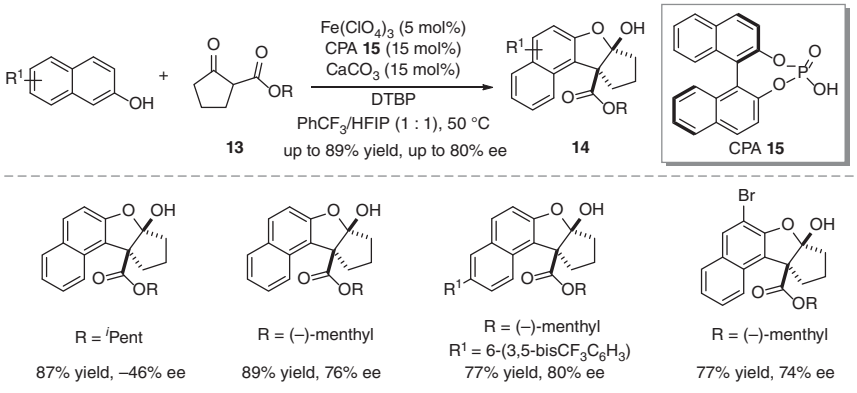


**Scheme 1.8** Iron-catalyzed cross-coupling of 2-naphthols and β-ketoester derivatives.

**13** proceeds smoothly at elevated temperatures, yielding the corresponding polycyclic hemiacetals **14** in good yields. Extensive screening of CPA ligands revealed a correlation between the size of the 3,3′-substituents of the phosphoric acid and the diastereoselectivity of the product. Notably, the use of chiral auxiliary (−)-menthyl was found to be crucial for enantiocontrol. The mechanism studies supported that the coupling took place between two associated ligands via a radical–anion coupling mechanism.

The significance and interest in heterobiaryl compounds with axial chirality have been growing across various fields. However, the enantioselective synthesis of these compounds through direct oxidative methods remains a significant challenge. In 2022, Smith and coworkers developed an iron-catalyzed oxidative cross-coupling of 2-naphthols and NH-free indoles for the synthesis of atropisomeric heterobiaryl compounds (Scheme 1.9) [100]. The chiral PyBOX ligand **18** was found to be the best one, and the cross-coupling product **17** can be obtained with high levels of chemoselectivity and enantioselectivity. The measurement of the oxidation potentials of 2-tert-butylindole and 2-isopropylphenyl 3-hydroxy-2-naphthoate clearly showed that the indole exhibited a lower oxidation potential compared to the

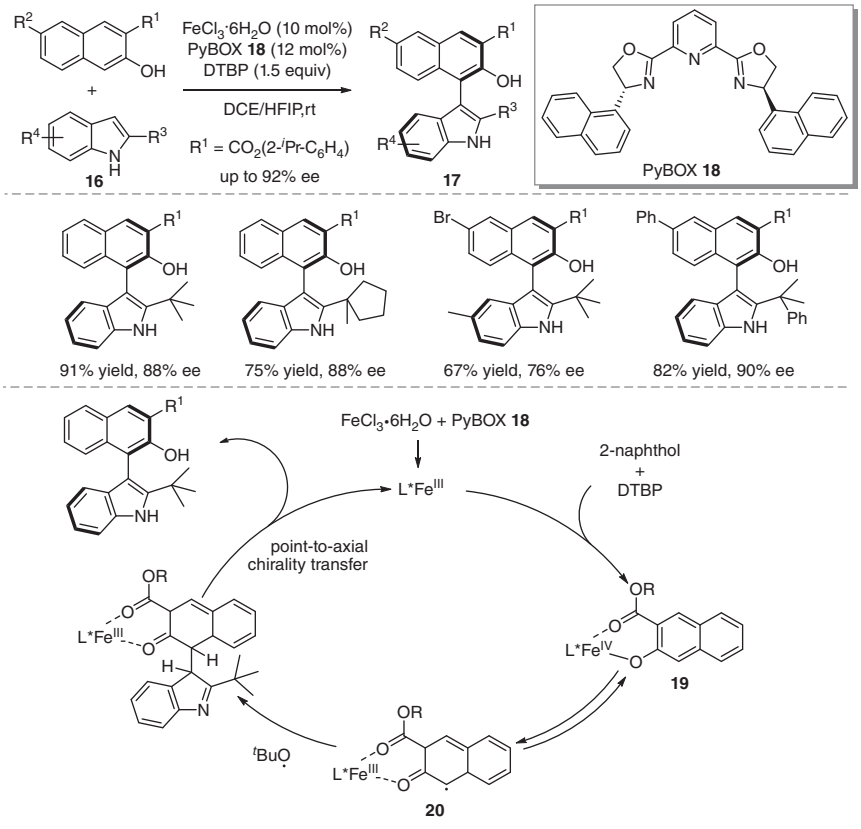


**Scheme 1.9** Iron-catalyzed cross-coupling of 2-naphthols and indoles.

naphthol component under standard conditions. Interestingly, the cross-coupling of 2-naphthols and NH-free indoles **16** was found to exclusively produce the cross-coupled products **17** without any competing homocoupling products. These findings suggest that the oxidation of the heterocyclic component does not significantly contribute to the catalytic cycle. Further mechanistic investigations, including radical clock experiment, HRMS, electron paramagnetic resonance (EPR) spectroscopy, and the Hammett plot analysis, supported the radical-involved mechanism.

First, the PyBOX ligand associated with the Fe(III) salt to form an octahedral Fe/PyBOX complex, which underwent ligand exchange with the 2-naphthol to produce a complex with the 2-naphthol binding in a bidentate fashion. Second, the single-electron transfer of the Fe(III) complex by DTBP afforded an Fe(IV) complex **19** and an accompanying *tert*-butoxy radical, and the subsequent reversible single-electron transfer generates the Fe(III)-ligated naphthoxy radical **20**. Then, directly controlled by the chiral ligand, the π-nucleophilic indole could facially attack the Fe(III)-ligated naphthoxy radical via an outer-sphere mechanism in the presence of the *tert*-butoxy radical to afford the coupling product, followed by ligand exchange to enable release of the enantioenriched heterobiaryl and an Fe(III) complex for the next catalytic cycle.

The previous work covers dehydrogenative coupling in which at least one $sp^2$-hybridized carbon was involved. The cross-dehydrogenative coupling of two inert C($sp^3$)—H bonds would generate two adjacent $sp^3$-hybridized carbons [101, 102]. In 2024, Feng, Liu, and coworkers reported an iron-catalyzed radical asymmetric dehydrogenative coupling of 2-acylimidazoles **21** with benzylic and allylic hydrocarbons as well as nonactivated alkanes **22** (Scheme 1.10) [103]. In this

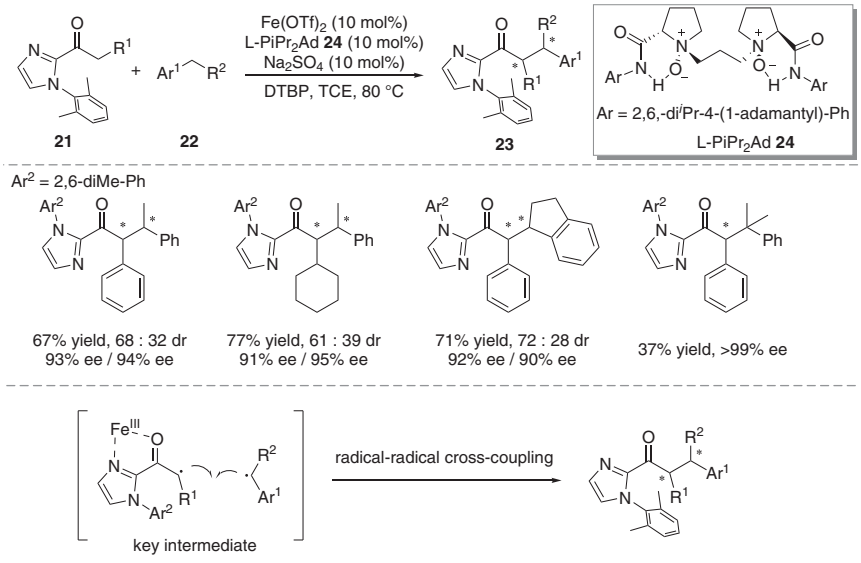


**Scheme 1.10** Iron-catalyzed coupling of two inert C($sp^3$)—H bonds.

method, the two inert C($sp^3$)—H bonds were enantioselectively coupled. The readily available and tunable *N*,*N*′-dioxide ligand L-PiPr$_2$Ad **24** and DTBP exhibited excellent asymmetric induction. Based on the Density functional theory (DFT) calculation and control experiments, a radical-radical cross-coupling mechanism was proposed.

## 1.3 Asymmetric C—C Coupling of Alkyl Halides

The Kumada reaction is a widely employed method in organic synthesis, which involves the cross-coupling of an organohalide with an organometallic compound. In 2015, the Nakamura group developed the first iron-catalyzed asymmetric Kumada reaction (Scheme 1.11) [104]. The enantioselective cross-coupling of α-haloesters **25** with aryl Grignard reagents **26** was conducted in the presence of Fe(acac)$_3$/chiral biphosphine ligand **28**. Good yields and high ee values of the coupled products **27** were obtained. Deprotection of the coupled products led to carboxylic acids, and further co-crystallization with octylamine constituted a nice approach for the synthesis of enantiopure dexibuprofen **29**. As supported by the control experiments, the reaction involved the abstraction of a halogen

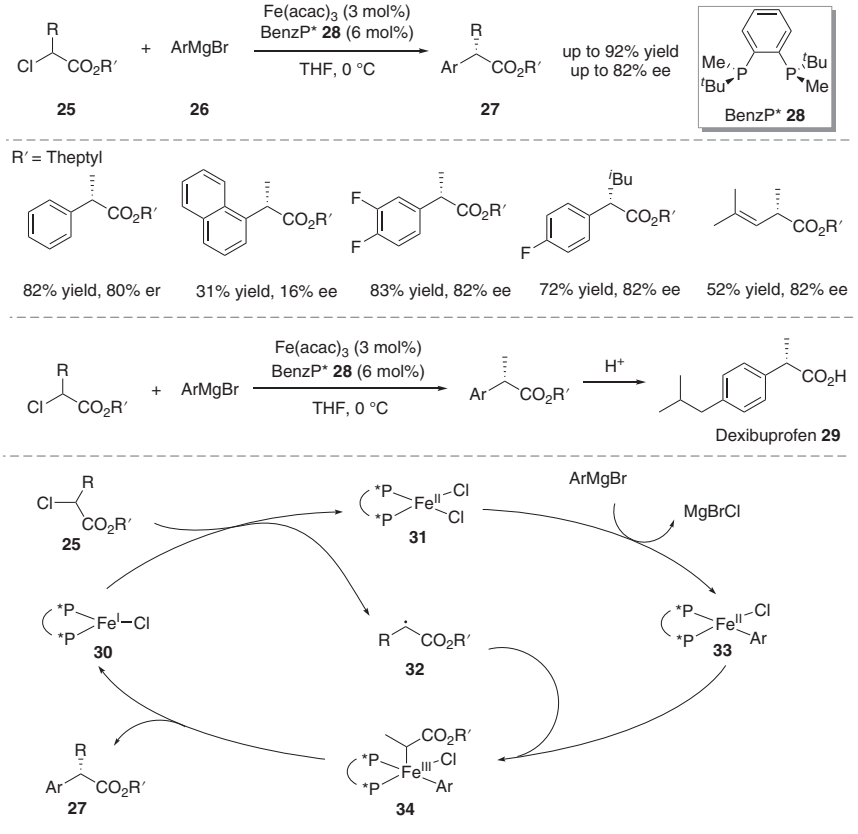


**Scheme 1.11** Iron-catalyzed asymmetric Kumada reaction.

from α-haloesters to generate an alkyl radical intermediate and underwent a Fe(III)—Fe(II)—Fe(I) catalytic cycle.

Shortly after that, the authors conducted theoretical calculations to further investigate the mechanism [105]. It was found that $Fe^{I}$(BenzP*)Cl complex **30** was the active intermediate for the C—Cl bond activation to provide L*$Fe^{II}Cl_2$ **31** and an alkyl radical **32**. The formation of the C—C bond through an inner-sphere mechanism was the selectivity-determining step. Transmetalation of the L*$Fe^{II}Cl_2$ **31** with aryl Grignard reagent generated a L*Ar$Fe^{II}$Cl species **33**, which bonded with the alkyl radical **32** to afford a L*$Fe^{III}$ species **34**. The reductive elimination afforded the coupling product **27** and regenerated the L*$Fe^{I}$Cl complex **30** that enabled the halogen atom abstraction process. The theoretical study provided important mechanistic insights into the iron-catalyzed cross-coupling reactions and is very important for the development of iron-based catalysts for highly stereoselective synthetic organic transformations. At the same time, Gutierrez and coworkers have also performed DFT studies on this iron-catalyzed Kumada coupling and further supported the proposed mechanism [106].

In 2023, Gutierrez and coworkers reported an iron-catalyzed enantioselective three-component coupling reaction (Scheme 1.12) [107]. In the presence of $Fe(acac)_3$/BenzP* as the catalytic system, the cross-couplings of vinyl boronates **35**, (fluoro)alkyl halides **36**, and Grignard reagents reacted well to produce the enantioenriched boro-products, which were transferred into the corresponding chiral alcohols **37** with high efficiency. The α-boryl radicals **38** generated from the addition of alkyl radicals to vinyl boronates was supposed to be involved.

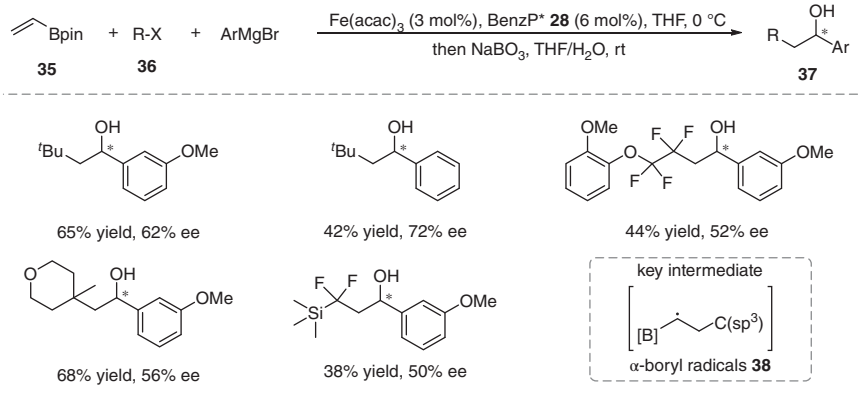


**Scheme 1.12** Iron-catalyzed radical asymmetric three-component coupling.

In 2019, the Nakamura group reported an iron-catalyzed Suzuki–Miyaura coupling reaction (Scheme 1.13) [108]. In the presence of catalytic amounts of $FeCl_2$ and (*R*,*R*)-QuinoxP* **41**, the cross-coupling of *tert*-butyl α-bromopropionate **39** and lithium arylborates **40** took place to afford various optically active α-arylpropionic acids after cascade hydrolysis.

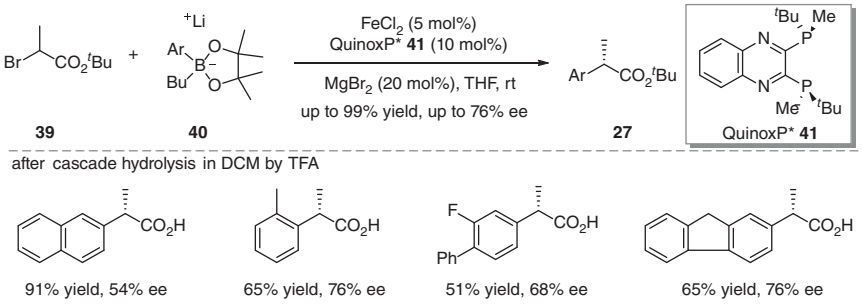


**Scheme 1.13** Iron-catalyzed asymmetric Suzuki–Miyaura coupling.

## 1.4 Asymmetric C—N Bond Formation

The C—N bond is one of the most common chemical bonds found in both natural and synthetic molecules. Numerous naturally occurring organic compounds, pharmaceuticals, agrochemicals, and functional materials include at least one nitrogen atom, highlighting the widespread importance of this bond in various fields. The Xu group made preliminary attempts at iron-catalyzed radical asymmetric C—N bond formation [109, 110]. The use of $Fe(NTf_2)_2$/chiral BOX ligand induced the enantioselectivity. Both of the (*E*)- and (*Z*)-olefins with a functionalized hydroxylamine were transferred into *syn*-hydroxyl oxazolidinone with the same ee and dr (82% ee, dr > 20 : 1), which suggested a radical mechanism.

In 2020, Bao and coworkers reported the pioneering achievement of the first radical asymmetric carboazidation, a significant milestone even in light of notable advancements in achiral carboazidation reactions (Scheme 1.14) [111]. The catalytic complex was composed of $Fe(OTf)_2$ and Haixi-BOX ligand **45**. Many inexpensive industrial chemical feedstocks, including styrenes **42**, alkyl halides, fluoroalkyl halides, and $TMSN_3$ **43**, are viable substrates for the iron-catalyzed radical asymmetric carboazidation of olefins, with LPO serving as a radical initiator. Mechanistic studies revealed that this process involved the generation of a carbon radical, and the reaction may undergo a group transfer mechanism. It was supposed that the stereocontrol at the radical center was achieved through the synergistic effects of van der Waals and $\pi$ interactions in the rigid chiral space created by the tridentate chiral NON-pincer ligand and iron. The generated chiral organoazides **44** can be transferred into valuable chiral primary amines, chiral phosphoramides, chiral benzylic 1,2,4-triazin-5(4*H*)-ones, chiral triazoles, and so on. The incorporation of natural product moieties, such as an estradiol derivative or a botulin derivative, emphasized the utility of this method. Furthermore, the obtained (*S*)-3-amino-3-phenylpropanoic acid through simple transformations served as a key intermediate for the synthesis of the anti-HIV drug Maraviroc.

Based on the mechanistic studies and DFT calculations, a catalytic cycle was proposed (Scheme 1.15). Upon ligand exchange with $TMSN_3$ **43**, the ligated $Fe^{II}$ complex **46** would be transferred into the azido $Fe^{II}$ species **47**. Then, a single-electron transfer (SET) process occurred between **47** and LPO to afford the crucial iron(III) azide

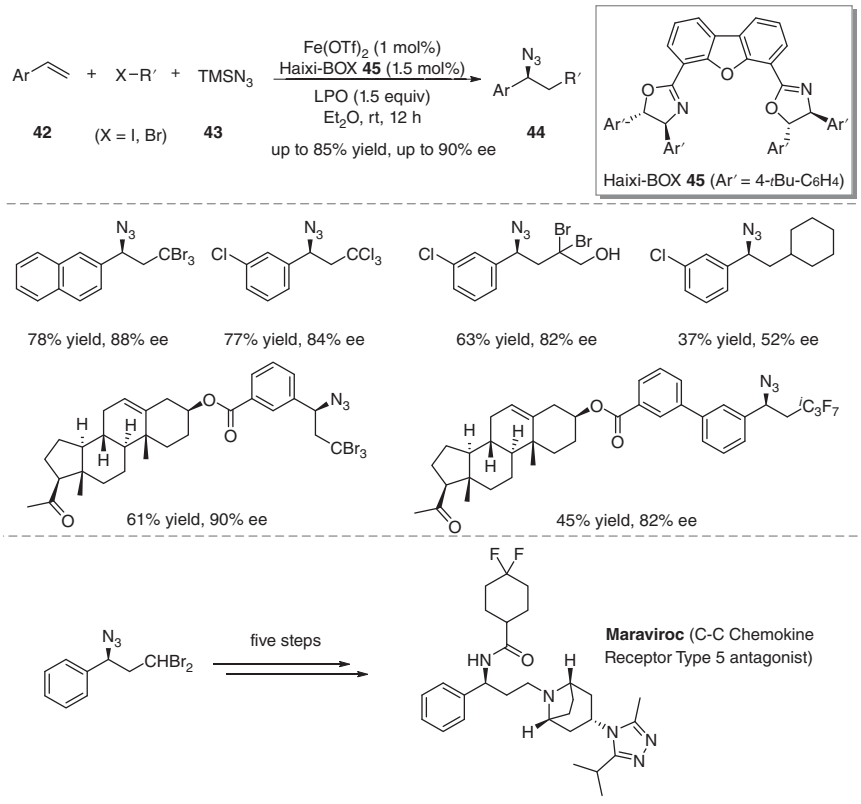


**Scheme 1.14** Iron-catalyzed radical asymmetric carboazidation of styrenes.

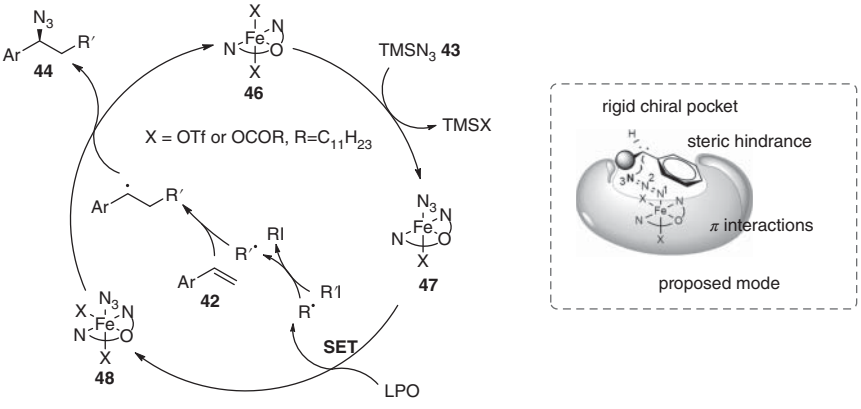


**Scheme 1.15** The mechanism for iron-catalyzed radical asymmetric carboazidation.

species **48** and an alkyl radical R. Meanwhile, the alkyl radical abstracted the iodine atom from the (fluoro)alkyl iodide to form the fluoroalkyl radical R′, which was then added to a styrene to generate a benzylic radical **49**. The interaction between the iron(III) azide species **48** and the benzylic radical **49** led to the final product **44**.

Notably, the outer-sphere group transfer of the azido functionality was anticipated to occur on the N3-position, as depicted in Scheme 1.15.

Shortly thereafter, the Bao group expanded on their work by achieving an iron-catalyzed intermolecular asymmetric diazidation of di- or tri-substituted styrenes (Scheme 1.16) [112]. This advancement enabled the synthesis of a range of chiral diazidation products **50** that were previously inaccessible, which are essential for the generation of various nitrogen-containing compounds. Mechanistic studies suggest that the reaction proceeds via a radical pathway, wherein the stereocontrol of an acyclic radical is potentially achieved through a group transfer mechanism.

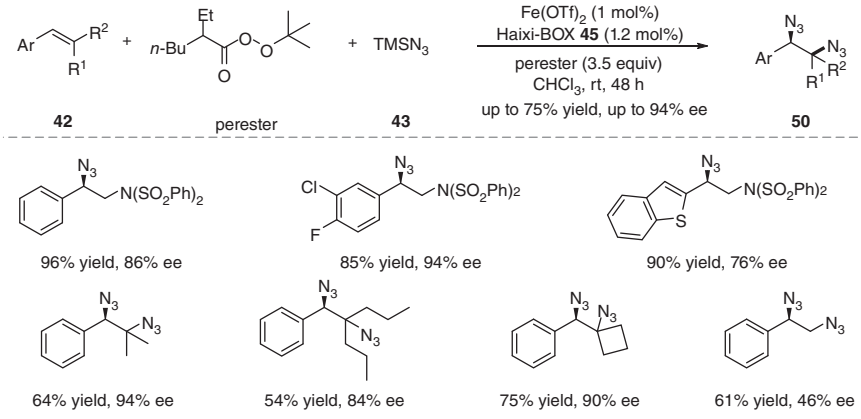


**Scheme 1.16** Iron-catalyzed asymmetric aminoazidation and diazidation of styrenes.

In 2021, the Bao group developed an iron-catalyzed asymmetric azidation of benzylic peresters using $TMSN_3$ **43** (Scheme 1.17) [113]. The chiral Haixi-BOX

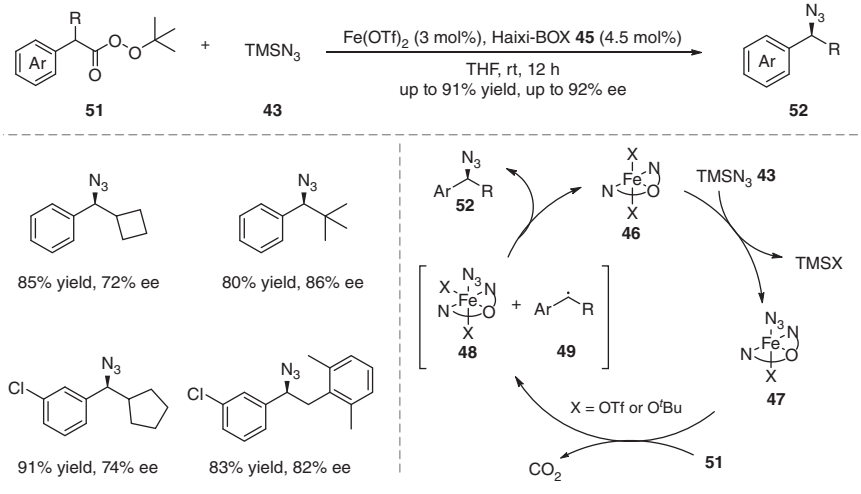


**Scheme 1.17** Iron-catalyzed asymmetric azidation of benzyl peresters.

ligand **45** showed superior performance in this process. Various benzylic peresters **51** exhibited excellent reactivity, yielding enantioenriched azides **52** with high yields and good enantioselectivities under mild reaction conditions. Notably, the generated hydrocarbon radicals lack strong interactions. The resulting chiral benzyl azides **52** can be utilized in click reactions, phosphoramidation, and reductive amination reactions. The exchange of ligand between the L*Fe(II) species **46** and $TMSN_3$ **43** produced the L*Fe(II)-azide species **47**, which then underwent SET with the perester **51** to generate the L*Fe(III)-azide species **48** and the resulting benzylic radical **49**. An outer-sphere group transfer led to the formation of the final product **52** and the active catalyst **46**.

In 2021, Feng and coworkers disclosed an $Fe(OTf)_2$/chiral *N*,*N*′-dioxide complex-catalyzed radical enantioselective carboazidation and diazidation of α,β-unsaturated ketones and amides (Scheme 1.18) [114]. Alkyl peroxides **54**, Togni's reagent **55**, fluoroalkyl halides, and $TMSN_3$ **43** were well tolerated under the mild reaction conditions, and many substituted alkenes **53** were sequentially converted into α-azido carbonyl derivatives **56** with high enantioselectivity. Mechanistic studies and DFT calculations suggest that a radical pathway was involved and the azido transferred to the radical intermediate via an intramolecular five-membered transition state with the internal nitrogen of the Fe—$N_3$ species. A wide array

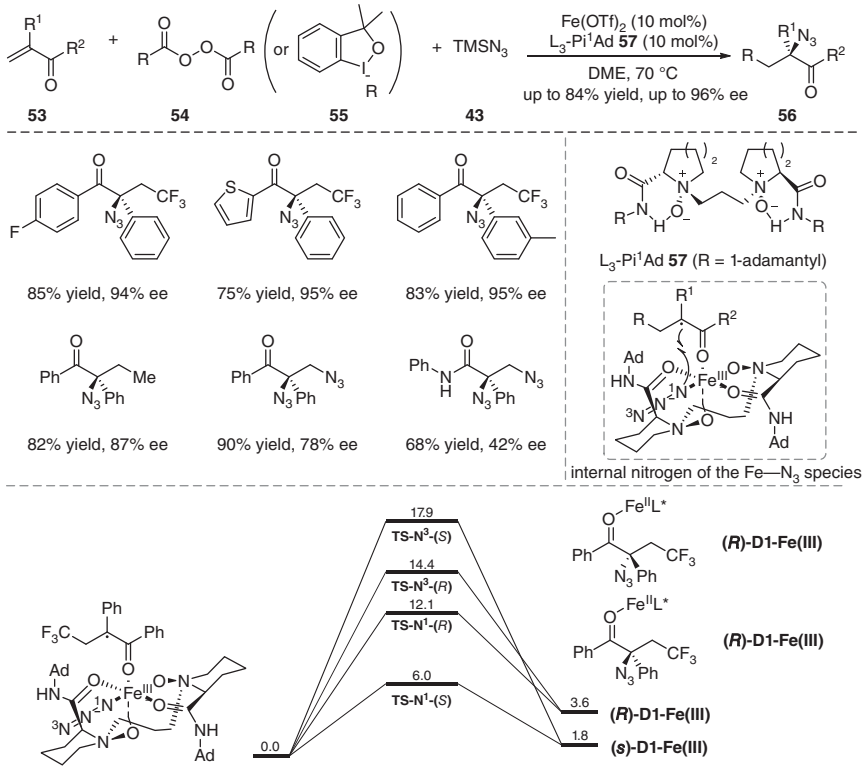


**Scheme 1.18** Iron-catalyzed asymmetric azidation of alkenes.

of chiral α-azido carbonyl derivatives, which could be further transformed into highly valuable chiral amino ketones, amino alcohols, and vicinal diamines, were synthesized by this efficient protocol.

In 2023, Wang and coworkers developed an enantioselective radical decarbonylative azidation (Scheme 1.19, top) [115]. Catalyzed by the complex of $Fe^{II}$/BOX, various aldehydes **58** underwent radical decarbonylation to generate the benzyl radicals, which abstracted the azido group from the azido-Fe species to produce the enantioenriched azides **59**. Notably, *tert*-butylperoxybenzoate (TBPB) served as the radical initiator. The Lian group established an iron-catalyzed approach for the enantioselective synthesis of chiral β-azido sulfones (Scheme 1.19, bottom) [116]. SOgen: tetrabromothiophene S,S-dioxide **63** was selected as the sulfur dioxide source. A series of BOX ligands have been evaluated. The iron-catalyzed four-component reactions afforded the corresponding heavily functionalized azides **64** in good yields and high enantioselectivity.

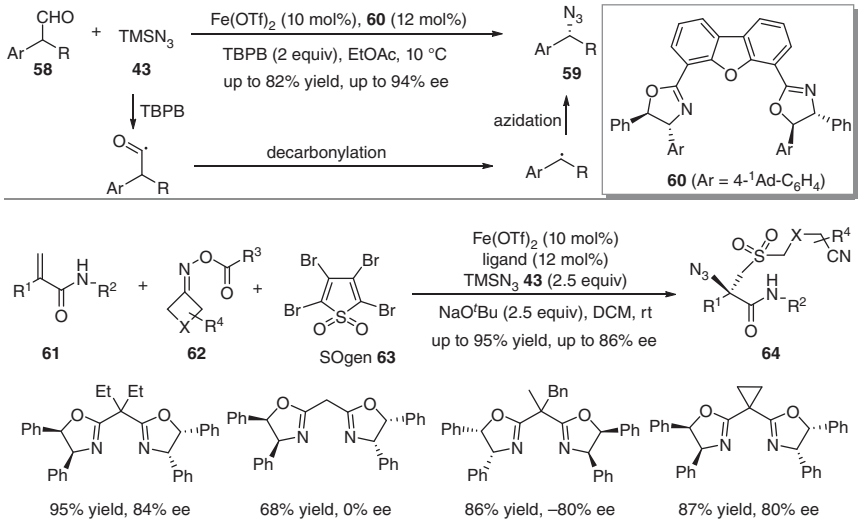


**Scheme 1.19** Iron-catalyzed decarbonylative azidation and four-component reactions.

In 2008, the Bolm group made preliminary attempts on iron-catalyzed radical asymmetric aziridination of alkenes. The PyBOX ligand offered the synthetically valuable aziridine with moderate ee [117]. The Meggers group developed a Fe/tetradentate N4-ligand-catalyzed asymmetric ring contraction of isoxazoles **65** to 2*H*-azirines **66** (Scheme 1.20, top) [118]. They can be easily transferred into chiral aziridine, α-methyl phenylalanine ester, β-hydroxy and β-methoxy phenylalanine derivatives. Mechanistic studies revealed that heterolytic cleavage of the N—O bond induced by SET from the iron center and stereocontrolled C—N bond formation via intramolecular radical addition were found to be crucial. Very closely, Meggers and coworkers reported a ring construction of *N*-aroyloxyureas to form chiral 2-imidazolidinones **68** in up to 99% yield and with up to 95% ee (Scheme 1.20,

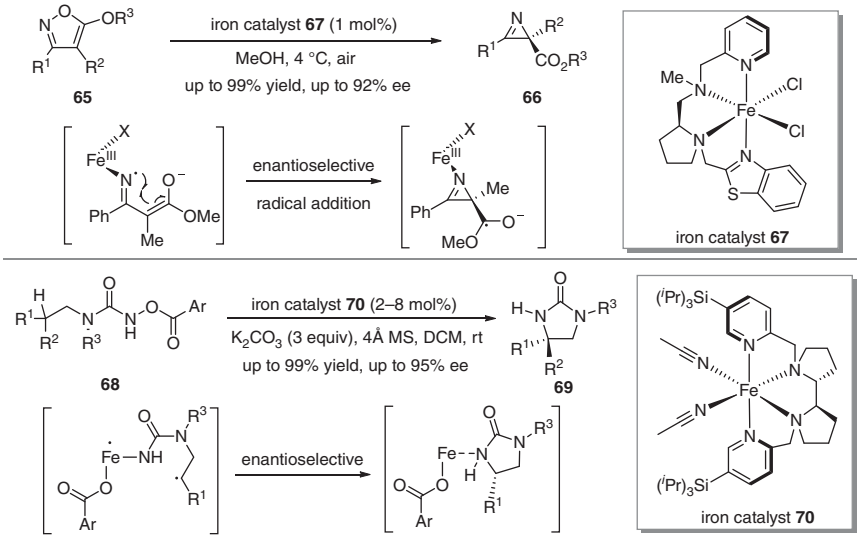


**Scheme 1.20** Iron-catalyzed asymmetric radical ring contraction and C—H amination.

bottom) [119]. This iron-catalyzed enantioselective C($sp^3$)—H amination facilitated the rapid construction of chiral nitrogen-containing heterocycles **69**, which can be hydrolyzed to yield valuable chiral vicinal diamines in a single step. Mechanistic studies suggested that the C—N bond formation step was enantioselectively controlled by the chiral iron complex.

## 1.5 Conclusion

This chapter compiles the advancements in iron-catalyzed radical asymmetric reactions. Stemming from Groves' pioneering work on catalytic radical asymmetric epoxidations facilitated by chiral iron-porphyrins, considerable progress has been made, predominantly in porphyrin-based biomimetic asymmetric catalysis. In consideration of the ongoing demand for new, economical, and sustainable reactions, recent years have witnessed advancements in chiral iron catalysis employing non-porphyrin-based ligands. A diverse array of chiral ligands, including chiral oxazolines, bidentate chiral phosphines, chiral phosphoric acids, chiral salens, chiral $C_2$ symmetric *N*,*N*′-dioxide ligands, and chiral bipyridines, have proven to be exceptional chiral auxiliaries, ensuring high levels of asymmetric induction in the field. By using these ligands, a wide range of noteworthy reactions extending beyond traditional epoxidations and cyclopropanations have been successfully achieved, facilitating enantioconvergent and sustainable construction of chiral C—C, C—N, C—O, and C—X bonds. Detailed insights into the catalytic models and mechanisms underpinning these radical asymmetric reactions are provided. Notably, great successes in enzymatic radical asymmetric synthesis should also be highly commended.

Despite the current ground-breaking developments that demonstrate the significance of iron-catalyzed radical asymmetric synthesis, this field remains underdeveloped, and many challenges need to be well addressed. First, the scope of reaction types is still narrow. Efforts should focus on exploring more efficient catalytic asymmetric transformations, particularly those that emulate natural processes. Second, there is a critical requirement for the design of new categories of chiral ligands that can expand the portfolio of this field. Third, more comprehensive understandings of the catalytic mechanism employed in iron catalysis would be vital for revealing the essence of enantiocontrol. It is evident that iron catalysis will continue to be a prominent topic in the forthcoming years. The pursuit of cost-effective, sustainable, and enantioselective methods is pivotal for the evolution of future organic synthetic chemistry.

## References


1 Bolm, C., Legros, J., Le Paih, J., and Zani, L. (2004). *Chem. Rev.* 104: 6217–6254.
2 Díaz, D.D., Miranda, P.O., Padrón, J.I., and Martín, V.S. (2006). *Curr. Org. Chem.* 10: 457–476.
3 Bauer, E.B. (2015). *Top. Organomet. Chem.* 50: 1–18.
4 Bauer, I. and Knolker, H.J. (2015). *Chem. Rev.* 115: 3170–3387.
5 Furstner, A. (2016). *ACS Cent. Sci.* 2: 778–789.
6 Bauer, E.B. (2017). *Isr. J. Chem.* 57: 1131–1150.
7 Fang, G.-C., Cheng, Y.-F., Yu, Z.-L. et al. (2019). *Top. Curr. Chem.* 377: 23.
8 Rana, S., Biswas, J.P., Paul, S. et al. (2021). *Chem. Soc. Rev.* 50: 243–472.
9 Liu, Y., Shing, K.-P., Lo, V.K.-Y., and Che, C.-M. (2023). *ACS Catal.* 13: 1103–1124.
10 Gopalaiah, K. (2013). *Chem. Rev.* 113: 3248–3296.
11 Srour, H., Le Maux, P., Chevance, S., and Simonneaux, G. (2013). *Coord. Chem. Rev.* 257: 3030–3050.
12 Ollevier, T. and Keipour, H. (2015). *Top. Organomet. Chem.* 50: 259–309.
13 Ollevier, T. (2016). Catal. *Sci. Technol.* 6: 41–48.
14 Loup, J., Dhawa, U., Pesciaioli, F. et al. (2019). *Angew. Chem. Int. Ed.* 58: 12803–12818.
15 Pellissier, H. (2019). *Coord. Chem. Rev.* 386: 1–31.
16 Achar, T.K., Maiti, S., Jana, S., and Maiti, D. (2020). *ACS Catal.* 10: 13748–13793.
17 Casnati, A., Lanzi, M., and Cera, G. (2020). *Molecules* 25: 3889.
18 Liu, Y., You, T., Wang, H.-X. et al. (2020). *Chem. Soc. Rev.* 49: 5310–5358.
19 Groves, J.T. and Myers, R.S. (1983). *J. Am. Chem. Soc.* 105: 5791–5796.
20 Collman, J.P., Zhang, X., Lee, V.J. et al. (1993). *Science* 261: 1404–1411.
21 Collman, J.P., Wang, Z., Straumanis, A. et al. (1998). *J. Am. Chem. Soc.* 121: 460–461.
22 Mansuy, D., Battioni, P., Renaud, J.P., and Guerin, P. (1985). *J. Chem. Soc. Chem. Commun.* 155–156.

**23** Gross, Z., Galili, N., and Simkhovich, L. (1999). *Tetrahedron Lett.* 40: 1571–1574.
**24** Lee, W.-C.C., Wang, D.-S., Zhu, Y., and Zhang, X.P. (2023). *Nat. Chem.* 15: 1569–1580.
**25** Naruta, Y., Tani, F., and Maruyama, K. (1990). *J. Chem. Soc. Chem. Commun.* 1378–1380.
**26** Naruta, Y., Tani, F., and Maruyama, K. (1991). *Tetrahedron: Asymmetry* 2: 533–542.
**27** Mahammed, A. and Gross, Z. (2005). *J. Am. Chem. Soc.* 127: 2883–2887.
**28** Groves, J.T. and Viski, P. (1989). *J. Am. Chem. Soc.* 111: 8537–8538.
**29** Wang, H.-H., Shao, H., Huang, G. et al. (2023). *Angew. Chem. Int. Ed.* 62: e202218577.
**30** Sessler, J.L. and Seidel, D. (2003). *Angew. Chem. Int. Ed.* 42: 5134–5175.
**31** Rose, E., Andrioletti, B., Zrig, S., and Quelquejeu-Etheve, M. (2005). *Chem. Soc. Rev.* 34: 573–583.
**32** Chen, Z. and Yin, G. (2015). *Chem. Soc. Rev.* 44: 1083–1100.
**33** Barona-Castano, J.C., Carmona-Vargas, C.C., Brocksom, T.J., and de Oliveira, K.T. (2016). *Molecules* 21: 310.
**34** Huang, X. and Groves, J.T. (2017). *J. Biol. Inorg. Chem.* 22: 185–207.
**35** Pereira, M.M., Dias, L.D., and Calvete, M.J.F. (2018). *ACS Catal.* 8: 10784–10808.
**36** Singh, R. and Mukherjee, A. (2019). *ACS Catal.* 9: 3604–3617.
**37** Weissenborn, M.J. and Koenigs, R.M. (2020). *ChemCatChem* 12: 2171–2179.
**38** Ahmad, I. and Shagufta, S.R. (2022). *Tetrahedron* 104: 132604.
**39** Xiao, X., Xu, K., Gao, Z.-H. et al. (2023). *Sci. China Chem.* 66: 1553–1633.
**40** Prier, C.K., Zhang, R.K., Buller, A.R. et al. (2017). *Nat. Chem.* 9: 629–634.
**41** Yang, Y., Cho, I., Qi, X. et al. (2019). *Nat. Chem.* 11: 987–993.
**42** Jia, Z.J., Gao, S., and Arnold, F.H. (2020). *J. Am. Chem. Soc.* 142: 10279–10283.
**43** Athavale, S.V., Gao, S., Liu, Z. et al. (2021). *Angew. Chem. Int. Ed.* 60: 24864–24869.
**44** Athavale, S.V., Gao, S., Das, A. et al. (2022). *J. Am. Chem. Soc.* 144: 19097–19105.
**45** Liu, Z., Qin, Z.-Y., Zhu, L. et al. (2022). *J. Am. Chem. Soc.* 144: 80–85.
**46** Mai, B.K., Neris, N.M., Yang, Y., and Liu, P. (2022). *J. Am. Chem. Soc.* 144: 11215–11225.
**47** Gao, S., Das, A., Alfonzo, E. et al. (2023). *J. Am. Chem. Soc.* 145: 20196–20201.
**48** Zhang, J., Huang, X., Zhang, R.K., and Arnold, F.H. (2019). *J. Am. Chem. Soc.* 141: 9798–9802.
**49** Zhang, R.K., Chen, K., Huang, X. et al. (2019). *Nature* 565: 67–72.
**50** Zhou, A.Z., Chen, K., and Arnold, F.H. (2020). *ACS Catal.* 10: 5393–5398.
**51** Brandenberg, O.F., Prier, C.K., Chen, K. et al. (2018). *ACS Catal.* 8: 2629–2634.
**52** Chen, K., Zhang, S.-Q., Brandenberg, O.F. et al. (2018). *J. Am. Chem. Soc.* 140: 16402–16407.
**53** Knight, A.M., Kan, S.B.J., Lewis, R.D. et al. (2018). *ACS Cent. Sci.* 4: 372–377.
**54** Carminati, D.M. and Fasan, R. (2019). *ACS Catal.* 9: 9683–9697.
**55** Chen, K. and Arnold, F.H. (2020). *J. Am. Chem. Soc.* 142: 6891–6895.

**56** Suzuki, K., Shisaka, Y., Stanfield, J.K. et al. (2020). *Chem. Commun.* 56: 11026–11029.

**57** Porter, N.J., Danelius, E., Gonen, T., and Arnold, F.H. (2022). *J. Am. Chem. Soc.* 144: 8892–8896.

**58** Mao, R., Wackelin, D.J., Jamieson, C.S. et al. (2023). *J. Am. Chem. Soc.* 145: 16176–16185.

**59** Chen, K., Huang, X., Kan, S.B.J. et al. (2018). *Science* 360: 71–75.

**60** Cho, I., Prier, C.K., Jia, Z.J. et al. (2019). *Angew. Chem. Int. Ed.* 58: 3138–3142.

**61** Cui, H.-B., Xie, L.-Z., Wan, N.-W. et al. (2019). *Green Chem.* 21: 4324–4328.

**62** Xie, L., Chen, K., Cui, H. et al. (2020). *ChemBiochem* 21: 1820–1825.

**63** Steck, V., Carminati, D.M., Johnson, N.R., and Fasan, R. (2020). *ACS Catal.* 10: 10967–10977.

**64** Goldberg, N.W., Knight, A.M., Zhang, R.K., and Arnold, F.H. (2019). *J. Am. Chem. Soc.* 141: 19585–19588.

**65** Huang, X., Garcia-Borras, M., Miao, K. et al. (2019). *ACS Cent. Sci.* 5: 270–276.

**66** Miller, D.C., Lal, R.G., Marchetti, L.A., and Arnold, F.H. (2022). *J. Am. Chem. Soc.* 144: 4739–4745.

**67** Zhou, Q., Chin, M., Fu, Y. et al. (2021). *Science* 374: 1612–1616.

**68** Rui, J., Zhao, Q., Huls, A.J. et al. (2022). *Science* 376: 869–874.

**69** Roy, S., Vargas, D.A., Ma, P. et al. (2023). *Nat. Catal.* 7: 65–76.

**70** Meunier, B., de Visser, S.P., and Shaik, S. (2004). *Chem. Rev.* 104: 3947–3980.

**71** Poulos, T.L. (2014). *Chem. Rev.* 114: 3919–3962.

**72** Cook, D.J., Finnigan, J.D., Cook, K. et al. (2016). *Advances in Protein Chemistry and Structural Biology*, vol. 105, 105–126. Elsevier Ltd.

**73** Hammer, S.C., Knight, A.M., and Arnold, F.H. (2017). *Curr. Opin. Green Sustain. Chem.* 7: 23–30.

**74** Fasan, R., Jennifer Kan, S.B., and Zhao, H. (2019). *ACS Catal.* 9: 9775–9788.

**75** Guo, M., Corona, T., Ray, K., and Nam, W. (2019). *ACS Cent. Sci.* 5: 13–28.

**76** Hanefeld, U., Hollmann, F., and Paul, C.E. (2022). *Chem. Soc. Rev.* 51: 594–627.

**77** Sibi, M.P. and Porter, N.A. (1998). *Acc. Chem. Res.* 32: 163–171.

**78** Sibi, M.P., Manyem, S., and Zimmerman, J. (2003). *Chem. Rev.* 103: 3263–3296.

**79** Mondal, S., Dumur, F., Gigmes, D. et al. (2022). *Chem. Rev.* 122: 5842–5976.

**80** Wang, F., Chen, P., and Liu, G. (2018). *Acc. Chem. Res.* 51: 2036–2046.

**81** Wang, K. and Kong, W. (2018). *Chin. J. Chem.* 36: 247–256.

**82** Gu, Q.-S., Li, Z.-L., and Liu, X.-Y. (2019). *Acc. Chem. Res.* 53: 170–181.

**83** Li, Z.-L., Fang, G.-C., Gu, Q.-S., and Liu, X.-Y. (2020). *Chem. Soc. Rev.* 49: 32–48.

**84** Genzink, M.J., Kidd, J.B., Swords, W.B., and Yoon, T.P. (2022). *Chem. Rev.* 122: 1654–1716.

**85** Nagib, D.A. (2022). *Chem. Rev.* 122: 15989–15992.

**86** Yao, W., Bergamino, E.A.B., and Ngai, M.Y. (2022). *ChemCatChem* 14: e202101292.

**87** Yang, C.-J., Liu, L., Gu, Q.-S., and Liu, X.-Y. (2024). *CCS Chem.* 6: 1612–1627.

**88** Liu, C., Liu, D., and Lei, A. (2014). *Acc. Chem. Res.* 47: 3459–3470.

**89** Liu, C., Yuan, J., Gao, M. et al. (2015). *Chem. Rev.* 115: 12138–12204.

**90** Yang, Y., Lan, J., and You, J. (2017). *Chem. Rev.* 117: 8787–8863.
**91** Egami, H., Matsumoto, K., Oguma, T. et al. (2010). *J. Am. Chem. Soc.* 132: 13633–13635.
**92** Narute, S., Parnes, R., Toste, F.D., and Pappo, D. (2016). *J. Am. Chem. Soc.* 138: 16553–16560.
**93** Tkachenko, N.V., Lyakin, O.Y., Samsonenko, D.G. et al. (2018). *Catal. Commun.* 104: 112–117.
**94** Horibe, T., Nakagawa, K., Hazeyama, T. et al. (2019). *Chem. Commun.* 55: 13677–13680.
**95** Ding, K., Li, X., Ji, B. et al. (2005). *Curr. Org. Synth.* 2: 499–545.
**96** Dyadyuk, A., Vershinin, V., Shalit, H. et al. (2022). *J. Am. Chem. Soc.* 144: 3676–3684.
**97** Fritsche, R.F., Schuh, T., Kataeva, O., and Knölker, H.J. (2023). *Chem. Eur. J.* 29: e202203269.
**98** Oguma, T. and Katsuki, T. (2012). *J. Am. Chem. Soc.* 134: 20017–20020.
**99** Narute, S. and Pappo, D. (2017). *Org. Lett.* 19: 2917–2920.
**100** Surgenor, R.R., Liu, X., Keenlyside, M.J.H. et al. (2022). *Nat. Chem.* 15: 357–365.
**101** Li, Z., Cao, L., and Li, C.-J. (2007). *Angew. Chem. Int. Ed.* 46: 6505–6507.
**102** Tanaka, T., Hashiguchi, K., Tanaka, T. et al. (2018). *ACS Catal.* 8: 8430–8440.
**103** Xu, N., Pu, M., Yu, H. et al. (2024). *Angew. Chem. Int. Ed.* 63: e202314256.
**104** Jin, M., Adak, L., and Nakamura, M. (2015). *J. Am. Chem. Soc.* 137: 7128–7134.
**105** Sharma, A.K., Sameera, W.M.C., Jin, M. et al. (2017). *J. Am. Chem. Soc.* 139: 16117–16125.
**106** Lee, W., Zhou, J., and Gutierrez, O. (2017). *J. Am. Chem. Soc.* 139: 16126–16133.
**107** Youshaw, C.R., Yang, M.-H., Gogoi, A.R. et al. (2023). *Org. Lett.* 25: 8320–8325.
**108** Iwamoto, T., Okuzono, C., Adak, L. et al. (2019). *Chem. Commun.* 55: 1128–1131.
**109** Liu, G.-S., Zhang, Y.-Q., Yuan, Y.-A., and Xu, H. (2013). *J. Am. Chem. Soc.* 135: 3343–3346.
**110** Li, H., Shen, S.-J., Zhu, C.-L., and Xu, H. (2018). *J. Am. Chem. Soc.* 140: 10619–10626.
**111** Ge, L., Zhou, H., Chiou, M.-F. et al. (2020). *Nat. Catal.* 4: 28–35.
**112** Lv, D., Sun, Q., Zhou, H. et al. (2021). *Angew. Chem. Int. Ed.* 60: 12455–12460.
**113** Wang, K., Li, Y., Li, X. et al. (2021). *Org. Lett.* 23: 8847–8851.
**114** Liu, W., Pu, M., He, J. et al. (2021). *J. Am. Chem. Soc.* 143: 11856–11863.
**115** Wang, R., Wang, C.-Y., Liu, P. et al. (2023). *Sci. Adv.* 9: eadh5195.
**116** Luo, L., Zhang, X., Huang, C., and Lian, Z. (2024). *Org. Chem. Front.* 11: 1678–1684.
**117** Nakanishi, M., Salit, A.F., and Bolm, C. (2008). *Adv. Synth. Catal.* 350: 1835–1840.
**118** Steinlandt, P.S., Hemming, M., Xie, X. et al. (2023). *Chem. Eur. J.* 29: e202300267.
**119** Cui, T., Ye, C.X., Thelemann, J. et al. (2023). *Chin. J. Chem.* 41: 2065–2070.

# 2

# Cobalt-Catalyzed Asymmetric Radical Reactions

*Duo-Sheng Wang and X. Peter Zhang*

*Department of Chemistry, Merkert Chemistry Center, Boston College, Chestnut Hill, MA, USA*

## 2.1 Introduction

Cobalt, as one of the earth's abundant metals, has garnered significant attention in organic synthesis due to its versatile reactivity. Notably, Co-catalyzed radical transformations, especially their asymmetric variants, have emerged as powerful tools for accessing chiral molecules (Scheme 2.1) [1–7]. These transformations are attractive due to their high reactivity, mild reaction conditions, and excellent control over enantioselectivity, driving increasing research efforts in this area. Among these, the Zhang group utilized Co(II)-porphyrin complexes, [$Co^{II}$(**P**)], as metalloradical catalysts to activate diazo and azide compounds, leading to the formation of α-Co(III)-alkyl and α-Co(III)-aminyl radicals. These metal-entangled radicals have been employed in a variety of transformations, including cyclopropanation [8], C—H alkylation [9], aziridination [10, 11], and C—H amination reactions [12], among others (Scheme 2.1a). The success of this chemistry is largely due to the use of dianionic porphyrin ligands with tetradentate coordination to cobalt, which forms a stable square planar complex (Scheme 2.1d). In some cases, the addition of an axial ligand is used to fine tune the reactivity and selectivity of the reactions. Another significant class of reactions involves the Co(II)-catalyzed hydrofunctionalization of alkenes via Co(III)–hydride-mediated hydrogen atom transfer (MHAT) [1, 13]. In this process, a Co(II) complex is oxidized by an extra oxidant, leading to the formation of a Co(III) complex that subsequently reacts with silane to generate the Co(III)—H species (Scheme 2.1b). This species transfers a hydrogen atom to the alkene, following the Markovnikov rule, to form a more stable alkyl radical coupled with the [Co(II)] species. The alkyl radical can then recombine with the [Co(II)] to produce [Co(III)]-alkyl complex, a reversible step that generally favors the formation of the complex. This [Co(III)]-alkyl intermediate can be further oxidized to a cationic [Co(IV)]-alkyl species, which undergoes nucleophilic substitution to yield the hydrofunctionalization product while regenerating the [Co(II)] complex. For these transformations, salen-type ligands, which are similar

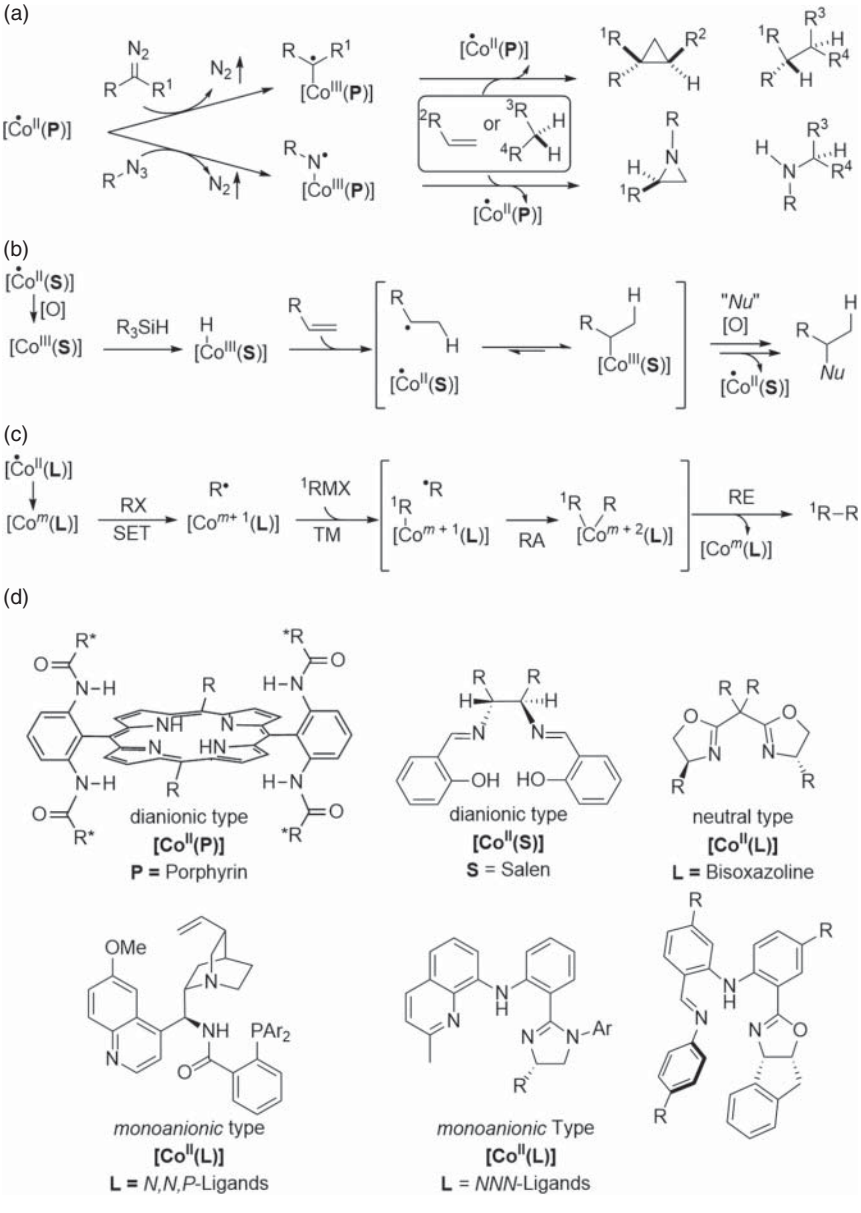


**Scheme 2.1** General overview of Co-catalyzed asymmetric radical reactions. (a) [$Co^{II}$(P)-catalyzed asymmetric reactions, (b) [$Co^{II}$(S)-catalyzed asymmetric hydrofunctionalization of alkenes via MHAT, (c) [$Co^{m}$(L)-catalyzed cross-coupling of alkyl halides with organometallic compounds, (d) typical ligands employed for Co-catalyzed radical transformations.

to porphyrin ligands but allow for *cis*-coordination, have proven beneficial due to their ability to facilitate reductive elimination (RE) ($Co^{II}$(**S**), Scheme 2.1d). The third type of reaction involves the reduction of the Co(II) complex to a lower-valent species Co($m$), such as Co(I) or Co(0), in the presence of organometallic reagents like Grignard or organozinc compounds (Scheme 2.1c) [5]. This reduced cobalt species then participates in a single-electron transfer (SET) with alkyl halides (RX), generating Co($m+1$) and an organic radical (R·). The Co($m+1$) species subsequently undergoes transmetalation (TM) with the organometallic reagent $^1$RMX, followed by radical addition (RA) to form a Co($m+2$)-alkyl species with *cis*-coordination of the R and $^1$R groups. The final step involves RE, which produces the cross-coupling product $^1$R—R and regenerates the active Co($m$) catalyst. In these reactions, neutral bisoxazoline ligands and monoanionic *N,N,P*- or *N,N,N*-tridentate ligands have been widely explored (Co(**L**), Scheme 2.1d).

In all these transformations, ligand design plays crucial role in achieving high yield and selectivity, driving ongoing efforts to develop new ligands and explore their reactivity. This chapter will focus on Co-catalyzed asymmetric radical transformations, primarily categorizing them into these three types of transformations.

## 2.2 [Co(II)(Por)]-Catalyzed Asymmetric Radical Transformations via Metalloradical Catalysis

Among recent advancements in addressing reactivity and stereoselectivity issues in radical chemistry [14–23], metalloradical catalysis (MRC) has emerged as a powerful approach [3, 8, 24–31]. MRC leverages metal-centered radicals as one-electron catalysts to homolytically activate substrates, generating metal-entangled organic radicals that govern the reaction pathway and stereochemical outcome of catalytic radical process [12, 31–36]. Metalloradicals, in this context, refer to open-shell transition-metal complexes with unpaired electrons that exhibit radical-like homolytic reactivity. One notable example is the use of Co(II) complexes of porphyrins [Co(II)(Por)], which act as stable 15-electron metalloradicals [3, 24]. These complexes have proven to be effective catalysts for the homolytic activation of metalloradicophiles including various diazo and azide compounds, leading to the formation of α-Co(III)-alkyl radicals [37–39] and α-Co(III)-aminyl radicals [40–42], respectively (Scheme 2.2). The detailed mechanism of how [Co(Por)] activates these metalloradicophiles is shown in Scheme 2.2.

The unique electronic configuration of the [Co(II)(Por)] complex, with its single electron located in the $dz^2$ orbital perpendicular to the porphyrin plane, enables it to engage in radical recombination with diazo and azide compounds (Scheme 2.2) [38–44]. This process forms γ-Co(III)-diazo ($\mathbf{I}_{\mathbf{Diazo}}$) and γ-Co(III)-azide radicals ($\mathbf{I}_{\mathbf{Azide}}$), which subsequently undergo radical β-scission with releasing dinitrogen gas as driving force, yielding the α-Co(III)-alkyl ($\mathbf{II}_{\mathbf{Diazo}}$) and α-Co(III)-aminyl radical intermediates ($\mathbf{II}_{\mathbf{Azide}}$), respectively (Scheme 2.2). These α-Co(III)-alkyl and α-Co(III)-aminyl radical intermediates have been successfully characterized using electron paramagnetic resonance (EPR) spectroscopy together with radical

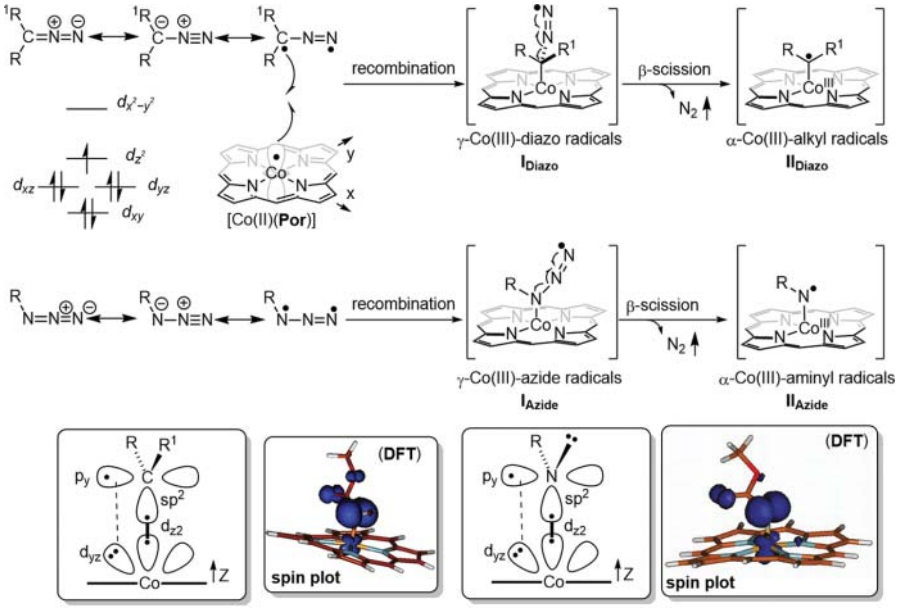


**Scheme 2.2** Metalloradical activation of diazo and azide compounds by [Co(II)(Por)].

trapping experiments [40, 45–58]. It was further supported by density functional theory (DFT) calculation studies which clearly show the spin is located at the C- and N-centers, respectively [48, 51–55, 57–61]. These fully occupied $d_\pi$ orbital of the Co(II) is forbidden to form a π-bond but through the half π-bonding interaction could help stabilize the radicals in the p-orbital of the C- and N-atoms (as depicted in Scheme 2.2).

These intermediates, stabilized and confined by the cobalt porphyrin complex, retain their radical character and undergo typical radical reactions [38–44]. The distinct radical nature of these intermediates has led to a wealth of novel reactivity, providing the field of organic synthesis with a powerful strategy for innovative bond disconnections and connections. These include RA and hydrogen atom abstraction (HAA, intramolecular or intermolecularly), followed by radical substitution (RS) or β-scission, ultimately yielding products such as cyclopropanes, aziridines, and C—H alkylation or amination products, along with the regeneration of the [Co(II)(Por)] metalloradical catalysts (Scheme 2.3). The success of these transformations is largely attributed to the design and synthesis of supporting porphyrin ligands. By fine tuning the electronic, steric, and chiral properties of these ligands, the reactivity and stereoselectivity of the aforementioned radical processes can be effectively controlled, enabling the development of a range of stereoselective radical transformations.

### 2.2.1 [Co(II)(Por)]-Catalyzed Asymmetric Radical Cyclopropanation

As illustrated in Scheme 2.4, the general mechanism for [Co(Por)]-catalyzed radical cyclopropanation started with metalloradical activation (MRA) of diazo compound

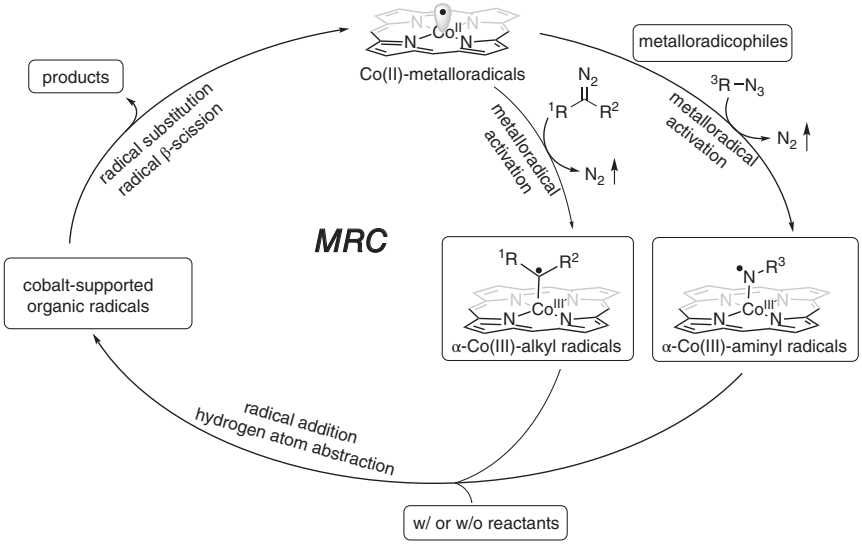


**Scheme 2.3** [Co(II)(Por)]-catalyzed asymmetric radical transformation with diazo and azide compounds via MRC.

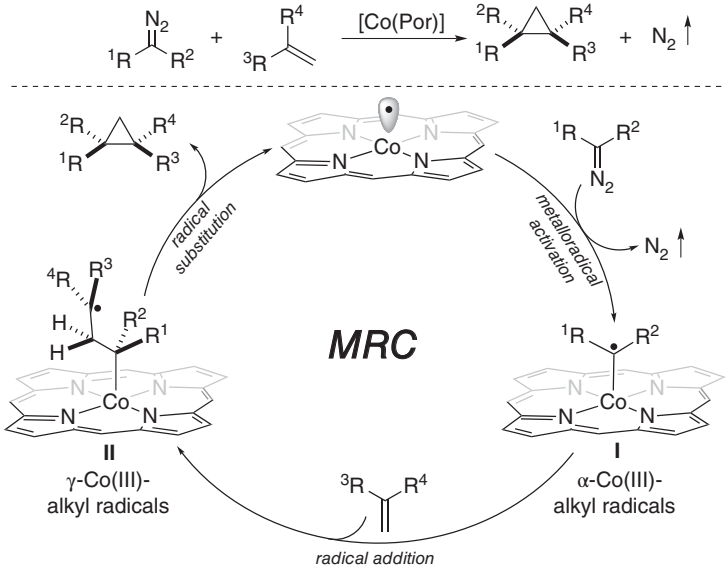


**Scheme 2.4** General catalytic cycle of intermolecular olefin cyclopropanation via Co(II)-MRC.

by [Co(Por)], generating α-Co(III)-alkyl radical intermediate **I**. This intermediate then undergoes RA to the olefin, resulting in the formation of the γ-Co(III)-alkyl radical intermediate **II**. Finally, intermediate **II** undergoes RS (3-exo-tet radical cyclization) with homolytic cleavage of the weak Co—C bond, yielding the cyclopropane product and regenerating the catalyst to complete the catalytic cycle. The section will describe examples of [Co(Por)]-catalyzed asymmetric olefin cyclopropanation based on different classes of diazo compounds as metalloradicophiles, with a particular emphasis on the developing of porphyrin ligands to address enantioselectivity issues. The stepwise radical mechanism of this process is strongly supported by several experimental observations [51, 55, 57, 58], including EPR spectrum, radical trapping experiments using TEMPO, and deuterium labeling studies on styrene, which revealed σ-bond rotation indicative of the presence of a radical intermediate. This behavior contrasts with the concerted metallocarbene mechanism, where such bond rotation would not occur. Furthermore, theoretical studies using DFT calculations also support the stepwise radical pathway [51, 55, 57, 58, 61]. Overall, the Zhang group developed a conceptual novel approach for generating various cyclopropane compounds with high yields and stereoselectivity. The success of this methodology can be attributed to the strategic design and synthesis of tailored catalysts.

The first examples of [Co(Por)]-catalyzed intermolecular olefin cyclopropanation were independently reported by the groups of Cenini and Zhang in 2003 [62, 63]. Cenini and coworkers disclosed that simple [Co(TPP)] (TPP = tetraphenylporphyrin) complexes can serve as efficient catalysts for the selective cyclopropanation of styrene and its derivatives with ethyl diazoacetate (EDA), achieving moderate-to-excellent yields with a preference for *trans* diastereoselectivity [62]. In parallel, Zhang and coworkers showed that [Co(Por)] complexes offer superior reactivity and selectivity for stereoselective cyclopropanation compared to other common metalloporphyrin catalysts [63]. A key advantage of the [Co(Por)]-based catalytic system is its ability to operate with alkenes as the limiting reagents, eliminating the need for slow addition of diazo compounds. It was also demonstrated that both the diastereoselectivities and enantioselectivities of [Co(Por)]-catalyzed cyclopropanation reactions could be finely tuned by using different chiral porphyrin ligands (Scheme 2.5). For example, employing a chiral camphanic-acid-based $D_4$-symmetric porphyrin (**P1**) as the ligand, asymmetric cyclopropanation of styrene with EDA led to cyclopropane product in 73% yield with cis/trans = 64/36 (77% ee and 62% ee, respectively). In contrast, using an L-threitol-based porphyrin (**P2**), *trans*-product was slightly favored (cis/trans = 48/52), with 31% ee and 10% ee, respectively. This modest yet noteworthy stereoselectivity provided the first evidence that asymmetric induction in catalytic cyclopropanation mediated by Co(II)-porphyrin complexes is achievable.

In 2004, Zhang and coworkers pioneered the development of structurally well-defined Co(II)-complexes of $D_2$-symmetric chiral amidoporphyrins [Co($D_2$-Por*)] (Scheme 2.6) [64]. The synthesis of the catalyst started with building dipyrrolemethane from commercially available 2,6-dibromobenzaldehyde (Dipyrromethane). Subsequent construction of 5,10-bis(2′,6′-dibromophenyl) porphyrin (Bromoporphyrin) synthons was with various readily available aldehydes.

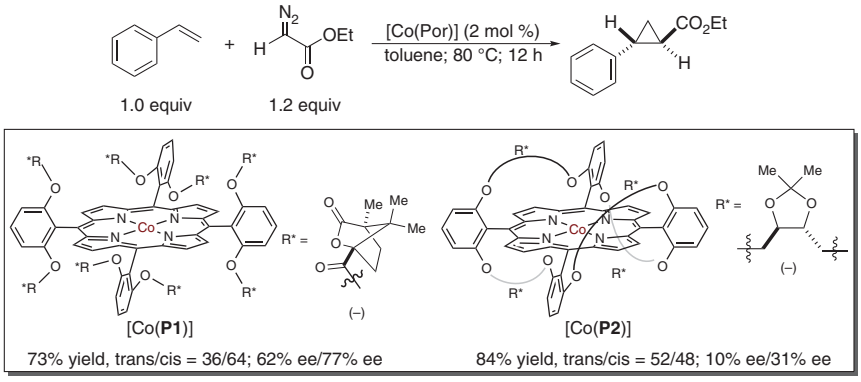


**Scheme 2.5** [Co($D_4$-Por)]-catalyzed asymmetric cyclopropanation of styrene with EDA.

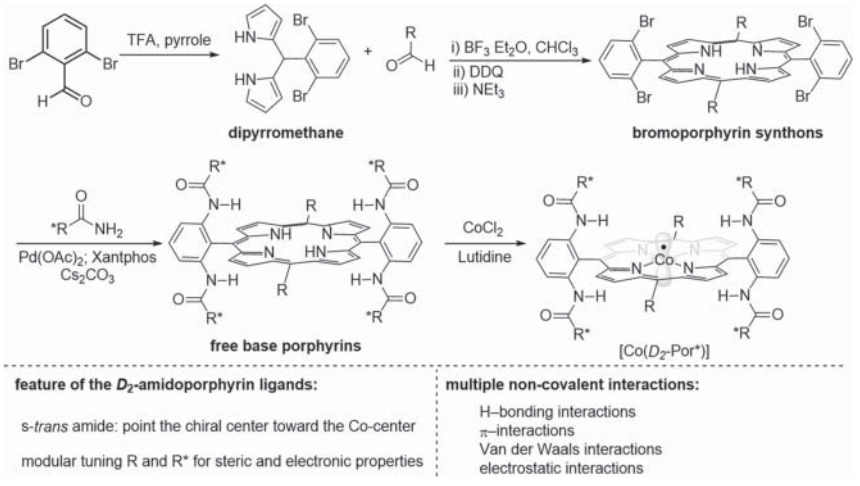


**Scheme 2.6** Modular construction of Co(II)-complexes of $D_2$-symmetric chiral amidoporphyrins [Co($D_2$-Por*)].

The key step for introducing chiral units to the porphyrin was achieved through robust palladium-catalyzed amidation reactions. This approach enabled the creation of a family of $D_2$-symmetric chiral amidoporphyrins with diverse electronic, steric, and chiral properties by varying both the chiral R* and *meso*-R groups of the porphyrin ligands (free base porphyrin). The chiral amide scaffold was later found to be crucial for achieving the desired reactivity and selectivity in various transformations. Due to the restricted *s*-trans configuration of the amide, the chiral elements on the R* group are oriented toward the reaction center, effectively inducing stereoselectivity. Additionally, the N—H unit serves as a potential H-bond donor, enhancing the interaction between the catalyst and reactants and further rigidifying the geometry to regulate the reaction process. The *meso*-R groups can introduce extra steric and electronic factors that significantly influence the reaction's performance. As a result of these well-established procedures, a variety

of [Co($D_2$-Por*)] complexes have been synthesized to enhance their efficacy for specific transformations which will be discussed in the following sections.

The first generation of [Co($D_2$-Por*)] catalyst [Co(**P3**)] (**P3** = 3,5-Di$^t$Bu-Chen Phyrin), featuring with dimethyl-substituted cyclopropane-containing amide unit, was found to be a privileged catalyst for effective cyclopropanation reactions. It showed excellent performance for the asymmetric cyclopropanation of styrene with EDA and *tert*-butyl diazoacetate (*t*BDA) (Scheme 2.7) [64]. The addition of a substoichiometric amount of 4-(dimethylamino)pyridine (DMAP) was found to be crucial for achieving high reactivity and stereoselectivity, due to its positive *trans*-effect on the metal center [65]. Higher enantioselectivity was achieved, yielding a predominantly trans product (trans/cis > 99/1) in 84% yield with 95% ee. The amido scaffold of the [Co($D_2$-Por*)] complex has proven essential for achieving high stereoselectivities, especially in terms of enantioselectivity [66, 67]. [Co(**P3**)] was later found to be effective for asymmetric cyclopropanation of a broad scope of styrene derivatives with varied steric and electronic properties with diazoacetates (Scheme 2.7) [68]. Remarkably, it can be extended to electron-deficient olefins, which sets it apart from typical electrophilic metallocarbene-mediated cyclopropanation (Scheme 2.7) [69]. In addition to alkyl diazoacetates, succinimidyl diazoacetates were also found to be effective metalloradicophiles for Co(II)-catalyzed asymmetric radical cyclopropanation of alkenes (Scheme 2.7) [70], resulting in enantioenriched succinimidyl cyclopropyl carboxylates that serve as valuable synthons for reactions with various amines, yielding a wide range of chiral cyclopropyl carboxamides while retaining the original enantiomeric purity. In 2008, Gallo, Rose, and coworkers reported the synthesis of Co(II) complexes of $C_2$-symmetric chiral bis-binaphthyl porphyrins

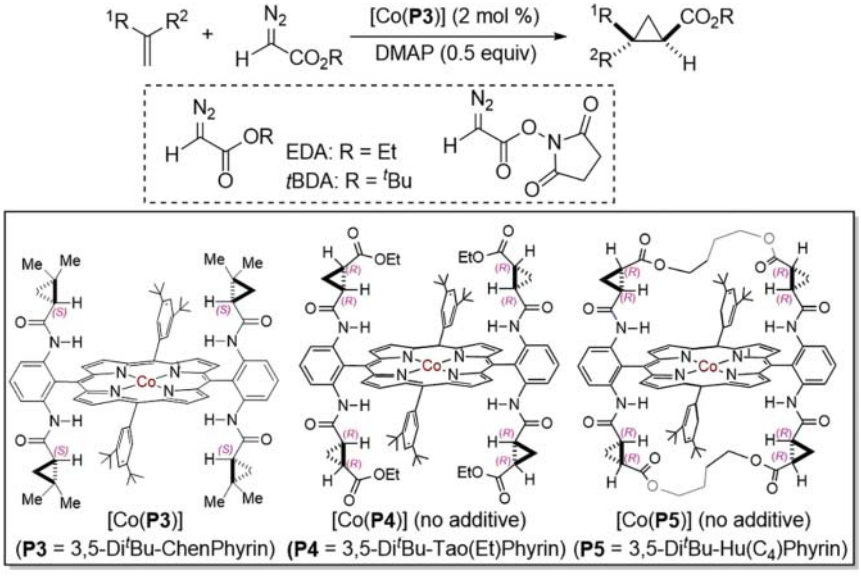


**Scheme 2.7** [Co(Por)]-catalyzed asymmetric cyclopropanation of alkene with diazoacetates.

and applied them to asymmetric olefin cyclopropanation with EDA, and only moderate diastereoselectivity and enantioselectivity were observed [71]. These results clearly showed $D_2$-symmetric amidoporphyrin was the key to achieve the excellent performance which can be attributed to the formation of a chiral pocket created by the chiral amide arms and meso-aromatic groups, which efficiently transfer chiral information from the ligand to the reaction partners. Notably, the N—H and α-carbonyl C—H units can engage in dual hydrogen-bonding interactions with the ester C=O group of the diazo compound. These interactions are thought to stabilize the key transition states and guide the reaction process within the chiral environment of the catalyst, enhancing both selectivity and reactivity. The addition of DMAP was proposed to form 5-coordination complex which makes the opposite side have a more rigidified chiral environment for further increased selectivity.

In 2019, Zhang and coworkers synthesized a new generation of Co(II) complexes of $D_2$-symmetric chiral porphyrins, known as [Co(HuPhyrin)]. These complexes feature alkyl bridges that span two chiral amide units on either side of the porphyrin plane, creating a chiral, cavity-like environment conductive to enhanced stereocontrol [72]. The bridging effect on catalytic performance was exemplified in the asymmetric cyclopropanation of styrene with EDA, where the bridged catalysts [Co(**P5**)] (**P5** = 3,5-Di$^t$Bu-Hu($C_4$)Phyrin) exhibited superior reactivity and stereoselectivity compared to the open analogue [Co(**P4**)] (**P4** = 3,5-Di$^t$Bu-Tao(Et)Phyrin) and the original [Co(**P3**)] (**P3** = 3,5-Di$^t$Bu-ChenPhyrin). [Co(**P5**)] delivered the corresponding cyclopropane product in 93% yield with a 95 : 5 dr and 96% ee, without the need for DMAP as an additive (Scheme 2.7). Notably, the catalytic performance can be fine-tuned by the length of the alkyl bridges, highlighting an important consideration for future catalyst design and development.

As shown in Scheme 2.8, using Co(**P3**)] as the catalyst, the highly stereoselective cyclopropanation of various styrene derivatives, electron-deficient alkenes, and aliphatic alkenes was achieved with acceptor/acceptor-substituted diazo compounds such as α-nitrodiazoacetates [73], α-cyanodiazoacetates [74], α-ketodiazoacetates [75], and α-formyldiazoacetates [76]. These diazo compounds, possessing H-bonding donors on both substituents, facilitated enhanced multiple H-bonding interactions with the chiral amide N—H units on the porphyrin ligand. This interaction rigidified the chiral environment and enabled excellent stereocontrol of the cyclopropanation without requiring DMAP as an additive.

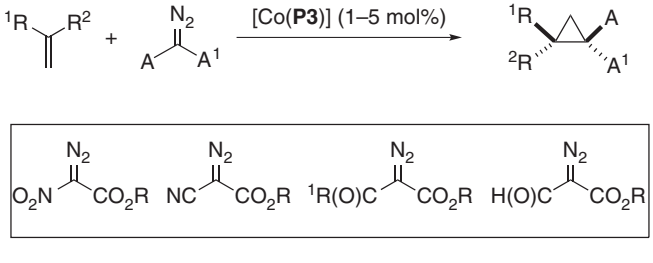


**Scheme 2.8** [Co(**P3**)]-Catalyzed asymmetric cyclopropanation of alkene with acceptor/acceptor-substituted diazo compounds.

In addition to intermolecular cyclopropanation, [Co(**P3**)] was found to be effective for asymmetric intramolecular cyclopropanation of allyl α-diazoacetates with various functional groups and substitution patterns for producing the corresponding [3.1.0] bicyclic products in good-to-high yields, with complete diastereocontrol and good enantiocontrol (Scheme 2.9, top) [77]. In 2023, [Co(**P3**)] was employed for intramolecular cyclopropanation of 2-vinylaryl diazomalonates enabling asymmetric radical bicyclization to construct cyclopropane-fused tricyclic chromanones (Scheme 2.9, bottom). This reaction achieved excellent yields along with remarkable control over both diastereoselectivities and enantioselectivities for the newly created contiguous stereogenic centers [58].

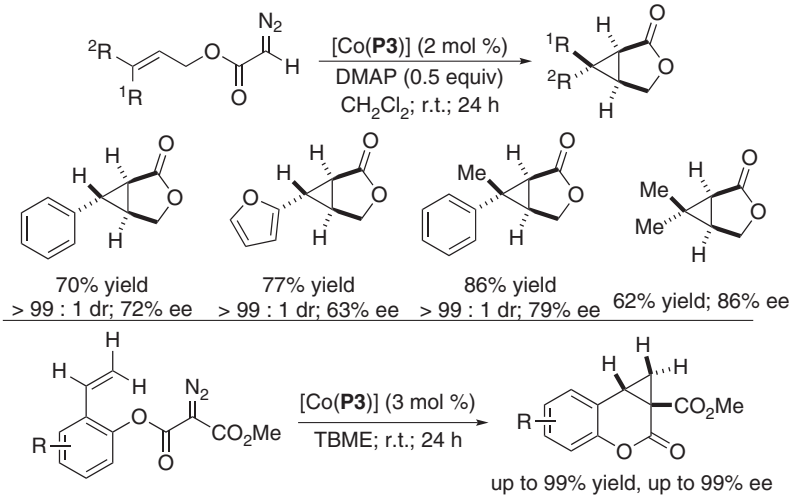


**Scheme 2.9** [Co(**P3**)]-catalyzed intramolecular cyclopropanation.

Zhang and coworkers revealed that the cyclopropane-contained chiral amide was not a prerequisite for achieving effective control over reactivity and enantioselectivity. In 2008, they synthesized [Co(**P6**)] (**P6** = 2,6-DiMeO-RuppelPhyrin) and [Co(**P7**)] (**P7** = 2,6-DiMeO-ZhuPhyrin), incorporating methoxy group and cyclic tetrahydrofuran units. These structural modifications enabled intramolecular O—H—N H-bonding and introduced 2,6-DiMeO substituents on the *meso*-phenyl rings, creating a more rigidified chiral environment and enhancing asymmetric induction [78, 79]. Both catalysts were effectively employed for the cyclopropanation of alkenes with diazosulfones, obviating the need for DMAP as an additive. Notably, [Co(**P7**)] exhibited broad applicability, achieving high yields with excellent diastereoselectivity and enantioselectivity for a wide array of styrene derivatives and electron-deficient olefins. This process produced well-defined cyclopropyl sulfones with remarkable efficiency (Scheme 2.10).

In 2022, the Zhang group demonstrated that the metalloradical catalyst [Co(**P8**)] (**P8** = 3,5-Di$^t$Bu-Xu(2′-Naph)Phyrin), with extended aromatic ring on the chiral amide unit which potentially brings π interactions, could activate unsymmetrical

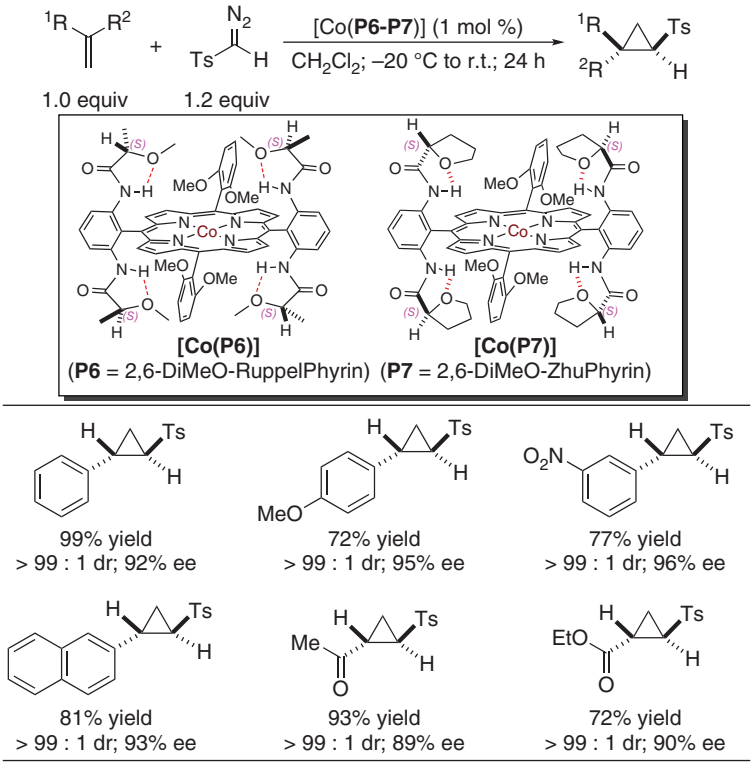


**Scheme 2.10** [Co(Por)]-Catalyzed asymmetric cyclopropanation of alkene with diazosulfones.

methyl phenyl diazomalonate (MPDM) with effective differentiation of its two similar ester groups for asymmetric cyclopropanation of a wide range of olefins, and tolerates various functional groups, resulting in a streamlined synthesis of chiral 1,1-cyclopropanediesters with high yields, diastereoselectivity, and enantioselectivity (Scheme 2.11) [57].

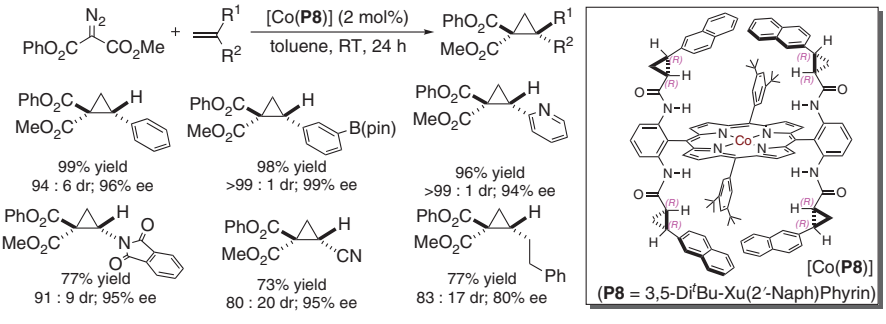


**Scheme 2.11** [Co(**P8**)]-Catalyzed asymmetric cyclopropanation of alkene with methyl phenyl diazomalonate.

By substituting one of the methyl groups in **P3** with a phenyl group to introduce two chiral centers into the cyclopropane ring, a new chiral porphyrin ligand, **P9** (3,5-Di$^t$Bu-QingPhyrin), was synthesized. The corresponding catalyst [Co(**P9**)] demonstrated high efficiency in catalyzing the asymmetric intramolecular cyclopropanation of various α-acceptor-substituted allyl diazoacetates. This reaction led to the formation of 3-oxabicyclo [3.1.0] hexan-2-one derivatives with three contiguous stereogenic centers, achieving high yields and excellent stereoselectivities (Scheme 2.12) [80].

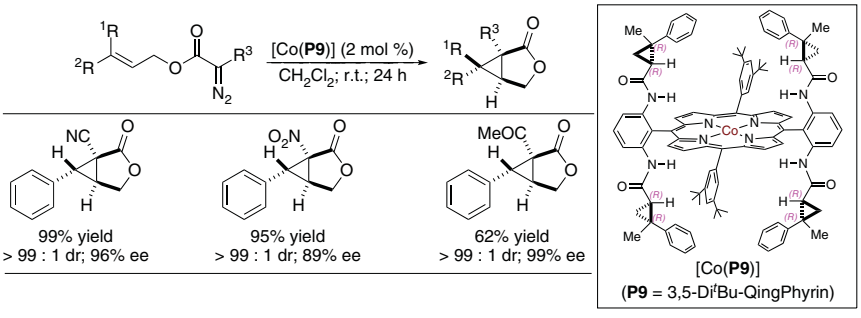


**Scheme 2.12** [Co(**P9**)]-Catalyzed asymmetric intramolecular cyclopropanation.

Efforts to develop asymmetric olefin cyclopropanation with donor-substituted diazo compounds have been limited due to their low stability. To overcome this, *N*-sulfonylhydrazones have been used as stable precursors for in situ diazo generation, expanding substrate scope for carbene transfer reactions [81]. However, applying this strategy in Co(II)-MRC requires addressing key challenges (Scheme 2.13): synchronizing diazo generation with MRA to avoid thermal side reactions and managing base effects that can hinder catalyst performance. Improved [Co(Por)] catalysts are needed for rapid diazo activation under basic conditions.

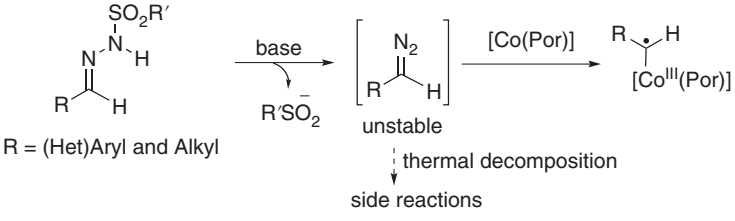


**Scheme 2.13** In situ generation of unstable diazo from *N*-sulfonylhydrazones.

Zhang and coworkers enhanced asymmetric induction for donor-substituted diazo compounds by incorporating an *ortho*-methoxy group in the α-phenyldiazomethanes to enable H-bonding with the chiral ligands. Using [Co(**P8**)] (**P8** = 3,5-Di$^t$Bu-Xu(2′-Naph)Phyrin), they achieved high stereoselectivity and yields in radical cyclopropanation of a wide range of olefins, including styrenes, nonaromatic and

electron-deficient substrates (Scheme 2.14) [82]. This system also facilitated cyclopropanation of dehydroaminoesters, producing (*Z*)-α-aminocyclopropanecarboxylates with high enantioselectivities under mild conditions [51].

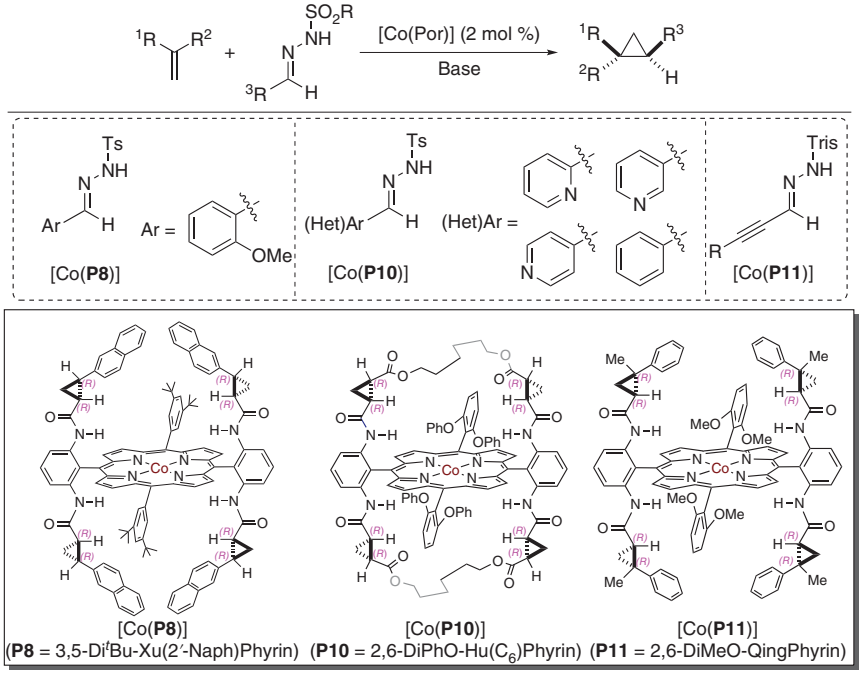


**Scheme 2.14** [Co(Por)]-catalyzed asymmetric cyclopropanation of alkene with in situ-generated donor/H-substituted diazo compounds.

While aryldiazomethanes are effective metalloradicophiles, heteroaryl diazomethanes can also be employed to synthesize biologically relevant heteroaryl cyclopropanes. In 2018, Chattopadhyay and coworkers used in situ-generated pyridyl diazomethanes from *N*-tosylhydrazones, activated by [Co(TPP)], to form α-Co(III)-pyridyl radicals for cyclopropanation of alkenes [83]. Building on this, Zhang and coworkers in 2021 developed an asymmetric variant using [Co(**P10**)] (**P10** = 2,6-DiPhO-Hu($C_6$)Phyrin), a bridged catalyst with phenoxy groups on *meso*-aryl substituents. These features created a rigidified cavity with noncovalent interactions, including π–π interactions, enabling high enantioselectivity without directing groups (Scheme 2.14) [61]. This method efficiently converted various pyridinyl and phenyl diazomethanes into chiral heteroaryl/aryl cyclopropanes with excellent diastereo- and enantioselectivity.

In 2022, Zhang and coworkers introduced the first asymmetric catalytic system capable of using in situ-generated α-alkynyldiazomethanes for Co(II)-MRC cyclopropanation [55]. The [Co(**P11**)] (**P11** = 2,6-DiMeO-QingPhyrin) catalyst, with 2,6-DiMeO groups at the meso-aryl substituent, provided a tailored steric, electronic, and chiral environment to promote efficient noncovalent interactions, enabling high yields and selectivity.

Building on the success of intermolecular cyclopropanation with in situ-generated aryldiazomethanes, Zhang and coworkers in 2023 developed a new catalyst, [Co(**P12**)] (**P12** = 2,6-DiMe-QingPhyrin), by replacing the 2,6-DiMeO groups with 2,6-DiMe groups. This catalyst effectively promoted the asymmetric radical bicyclization of α-aryldiazomethanes containing dangling alkene units, enabling the synthesis of valuable tricyclic chromanes, key structures in many biologically active compounds and pharmaceuticals (Scheme 2.15) [58]. The reaction proceeded with excellent yields and precise diastereo- and enantioselectivity for newly formed contiguous stereogenic centers. Notably, this methodology was instrumental in the first asymmetric total synthesis of the natural product (+)-**Radulanin J**, showcasing its synthetic utility.

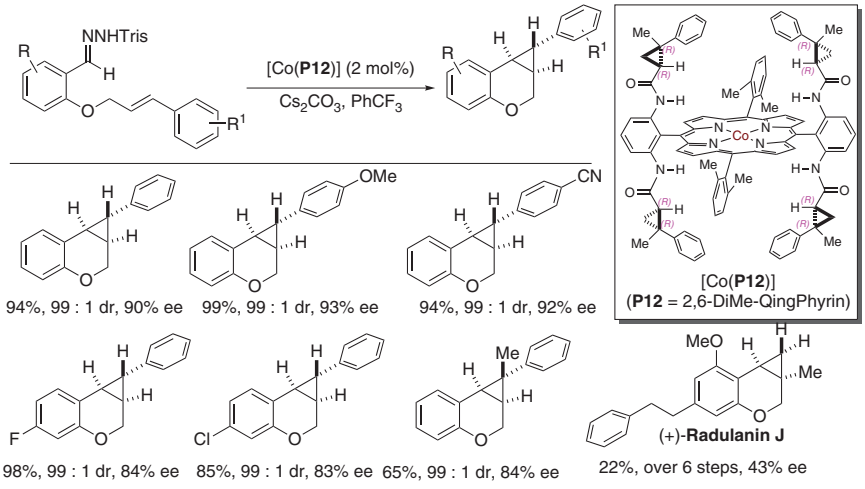


**Scheme 2.15** [Co(**P12**)]-Catalyzed intramolecular asymmetric cyclopropanation with in situ-generated aryldiazomethanes.

### 2.2.2 [Co(II)(Por)]-Catalyzed Asymmetric Radical C—H Alkylation

C—H alkylation is a powerful tool for constructing C—C bonds, but activating inert C—H bonds with precise chemo-, regio-, and stereoselectivity remains challenging [84–88]. Catalysts based on $Rh_2$ [89], Cu [90], Ru [91], and Fe [92] have been highly effective for C—H alkylation using acceptor- and donor/acceptor-substituted diazo compounds. However, reactions with acceptor/acceptor-substituted diazo compounds are less developed due to their low reactivity and challenges in controlling regio- and enantioselectivity during C—H insertion. Similarly, donor- and donor/donor-substituted diazo compounds remain underexplored due to their tendency to undergo side reactions, and methodologies for their use are still underdeveloped. One major challenge is the intrinsic low reactivity of these diazo compounds, which hinders the formation of metallocarbene intermediates.

To overcome these challenges, Zhang and coworkers developed a Co(II)-based MRC system for asymmetric intramolecular C—H alkylation of various diazo

for achieving significant success in cyclization reactions with varying ring sizes (Scheme 2.16) [45, 46, 53, 93, 94]. The process involves the activation of diazo compounds to form α-Co(III)-alkyl radicals **I**, followed by *1,n*-HAA of the distal C—H bond to form ω-Co(III)-alkyl radicals **II**. A final RS step yields the desired product, regenerating the [Co(Por)] catalyst (Scheme 2.16).

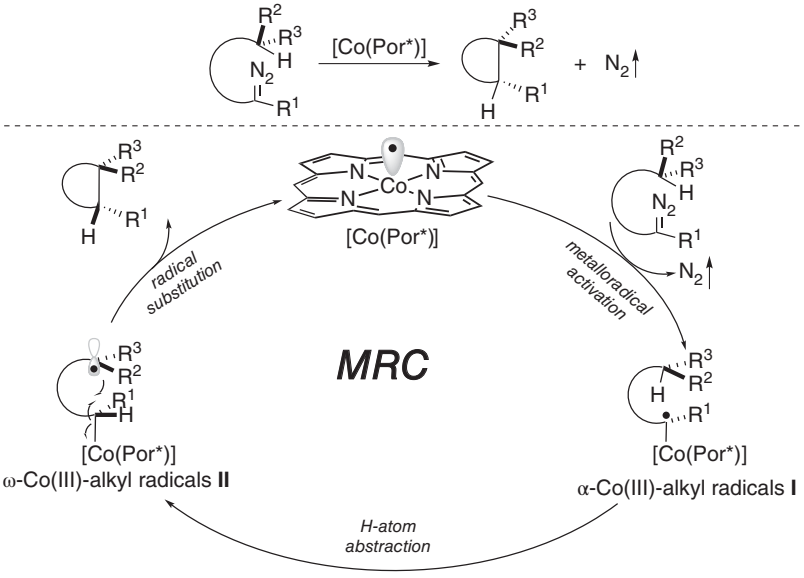


**Scheme 2.16** General mechanism for intramolecular radical C—H alkylation via [Co(Por)]-MRC.

In 2015, Zhang and coworkers applied this system to asymmetric intramolecular 1,5-C—H alkylation of α-methoxycarbonyl-α-diazosulfones, enabling the efficient synthesis of 5-membered sulfolanes with excellent stereoselectivity (Scheme 2.17) [93]. The breakthrough was facilitated by a new $D_2$-symmetric chiral amidoporphyrin ligand (**P13** = 3,5-Di$^i$Pr-Xu(4-$^t$Bu)Phyrin), which showed remarkable tolerance to both electron-rich and electron-deficient C—H bonds. The method also displayed features unique to radical pathways, such as high functional group tolerance and excellent chemoselectivity for allylic and allenic C—H bonds.

In 2018, Zhang and coworkers extended Co(II)-based MRC to intramolecular 1,5-C—H alkylation with donor-substituted diazo compounds by employing the $D_2$-symmetric chiral amidoporphyrin **P14** (2,6-DiPhO-QingPhyrin) (Scheme 2.17) [46]. This [Co(**P14**)]-based system enabled efficient activation of *ortho*-aminoaryldiazomethanes, facilitating the enantioselective intramolecular alkylation of various C—H bonds, including benzylic, propargylic, and non-activated aliphatic substrates. The system produced a broad array of chiral 2-substituted indolines in high yields and excellent enantioselectivities at room temperature. The approach also demonstrated notable functional group tolerance, compatibility with heteroaromatic units, and high chemo- and regioselectivity, making it a versatile tool for the synthesis of chiral molecules.

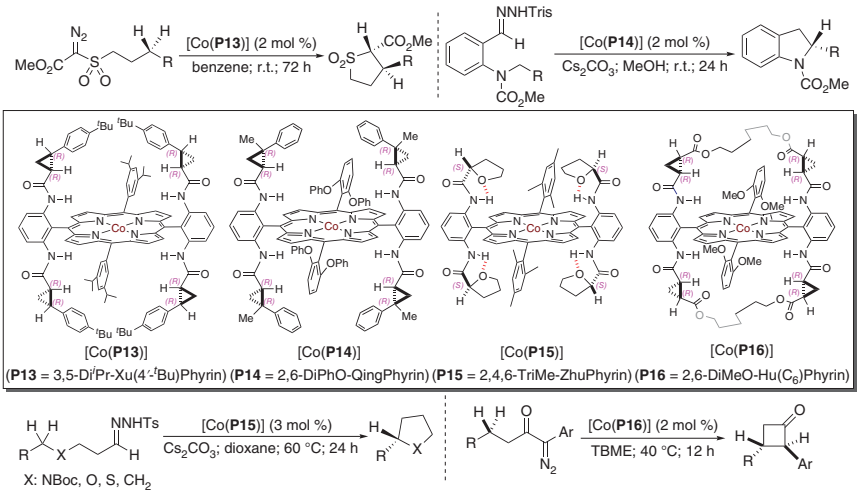


**Scheme 2.17** [Co(Por)]-catalyzed intramolecular radical C—H alkylation.

Zhang further demonstrated that aliphatic aldehyde-derived *N*-sulfonylhydrazones could generate linear aliphatic diazomethanes for enantioselective C—H alkylation [45]. Utilizing the chiral ligand **P15** (2,4,6-TriMe-ZhuPhyrin), [Co(**P15**)] activated these diazo compounds to form α-Co(III)-alkyl radicals. This system enabled the transformation of simple aliphatic aldehydes into chiral α-substituted pyrrolidines and other important 5-membered ring structures in high yields and enantioselectivities (Scheme 2.17). Notably, the catalyst exhibited regioselectivity, favoring homobenzylic over benzylic C—H bonds for the selective synthesis of pyrrolidines. This regioselectivity emphasizes the preference for 1,5-HAA over 1,6-HAA.

Traditional alkyl radicals typically favor 1,5- and 1,6-HAA over the entropically and enthalpically disfavored 1,4-HAA. However, by leveraging MRC principles, Zhang developed a novel catalytic radical system incorporating 1,4-HAA followed by 4-exo-tet RS to achieve asymmetric 1,4-C—H alkylation. This strategy enables the stereoselective construction of cyclobutanone frameworks from α-aryldiazoketones (Scheme 2.17) [53]. The success of this transformation hinged on the introduction of **P16** (2,6-DiMeO-Hu($C_6$)Phyrin), a finely tuned chiral porphyrin ligand. This design created an optimal steric, electronic, and chiral environment, stabilized radical intermediates through noncovalent interactions, and enabled mild reaction conditions. The system yielded enantioenriched α,β-disubstituted cyclobutanones with excellent diastereo- and enantioselectivity.

In 2020, de Bruin and coworkers advanced the field of MRC by developing a *1,6*-HAA process tailored for constructing 8-membered ring products [95]. This innovative methodology capitalized on the sequential 1,6-HAA followed by 8-exo-tet RS, which successfully enabled the synthesis of monobenzocyclooctadienes. They explored the asymmetric version of this reaction using the first-generation catalyst [Co(**P3**)], originally developed by Zhang's group. Although the enantioselectivity

achieved with [Co(**P3**)] was relatively low, the study was significant in demonstrating the feasibility of constructing chiral 8-membered ring systems via this sequential 1,6-HAA/8-exo-tet RS process.

### 2.2.3 Radical Cyclopropenation and Cascade Reactions

Zhang and coworkers expanded the scope of Co(II)-MRC by developing a highly enantioselective cyclopropenation system, employing a novel chiral metalloradical catalyst [Co(**P17**)] (**P17** = 3,5-DiMes-ChenPhyrin), which features extended aromatic substituent at the 3,5-positions of the meso-phenyl ring (Scheme 2.18) [96]. This innovative system enables the asymmetric cyclopropenation of a broad range of aryl- and vinyl-substituted terminal alkynes using various acceptor/acceptor-substituted diazo compounds. Significantly, this methodology represents the first application of α-cyanodiazoacetates and α-cyanodiazoacetamides in asymmetric cyclopropenation. The process showcased exceptional functional group tolerance, as demonstrated by its compatibility with phenylacetylene derivatives bearing sensitive groups like aldehyde, hydroxyl, and amine. The resulting enantioenriched cyclopropenes, featuring all-carbon quaternary stereogenic centers, are highly valuable as chiral intermediates in synthetic chemistry. This advancement not only highlights the versatility of Co(II)-MRC in addressing challenging transformations but also underscores its potential for generating structurally complex and stereochemically rich molecules for diverse synthetic applications.

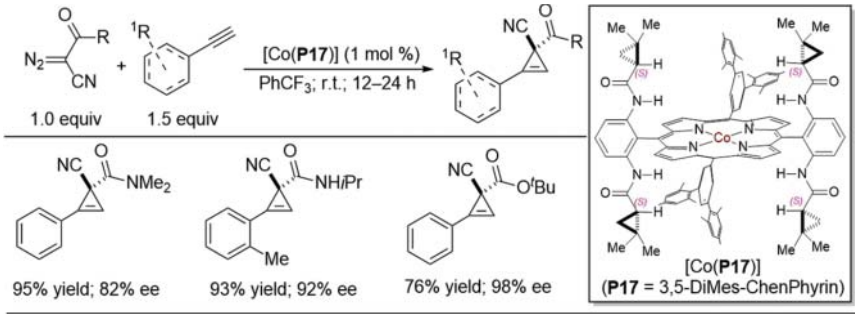


**Scheme 2.18** [Co(**P17**)]-catalyzed asymmetric cyclopropenation of alkynes with acceptor/acceptor-substituted diazo compounds.

As depicted in Scheme 2.19, the γ-Co(III)-vinyl radical intermediate **II**, generated via RA of the α-Co(III)-alkyl radical **I**, can undergo diverse transformations beyond RS. Notably, when the substrate contains an alkene unit, it can preferentially undergo a 5-exo-trig RA to form the ε-Co(III)-alkyl radical (III), outcompeting the 3-exo-tet RS. Intermediate **III** can then proceed through a 3-exo-trig RA, generating a β-Co(III)-alkyl radical **IV**, which undergoes rapid radical β-scission via a formal $S_H2'$ RS process. This cascade sequence culminates in the formation of cyclopropane-fused tetrahydrofurans while regenerating the [Co(Por)] catalyst,

completing the catalytic cycle. Using the same catalyst, [Co(**P17**)], this methodology efficiently yields multisubstituted cyclopropane-fused tetrahydrofurans with three contiguous stereogenic centers, including two all-carbon quaternary centers, in high yields with excellent stereoselectivities. This transformation showcases the potential of Co(II)-MRC for enabling intricate radical cascade reactions with exceptional control over stereochemistry.

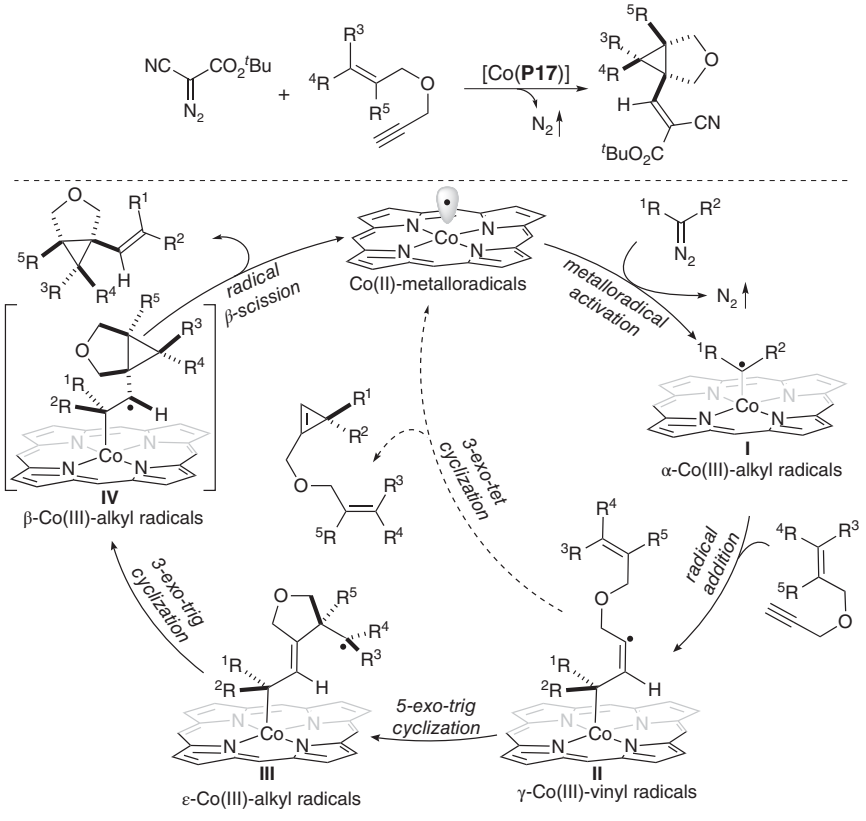


**Scheme 2.19** Enantioselective radical cascade for the construction of bicyclic structures with 1,6-enyne.

### 2.2.4 [Co(II)(Por)]-Catalyzed Asymmetric Radical Aziridination

In addition to activating various diazo compounds for asymmetric transformations, [Co($D_2$-Por*)] have demonstrated exceptional efficiency in activating organic azides for the catalytic radical aziridination of alkenes [97–106]. This methodology enables the formation of the smallest three-membered *N*-heterocycles with excellent control over reactivity and enantioselectivity, achieved through a stepwise radical mechanism (Scheme 2.20). The catalytic cycle begins with MRA of azide compounds, releasing dinitrogen gas as the driving force to form the α-Co(III)-aminyl radical intermediates **I**. These intermediates undergo RA to alkenes, generating the

corresponding γ-Co(III)-alkyl radical intermediates **II**. Subsequently, the reaction proceeds through RS step, yielding the enantioenriched aziridine products while regenerating the [Co(II)(Por)] catalyst to complete the cycle.

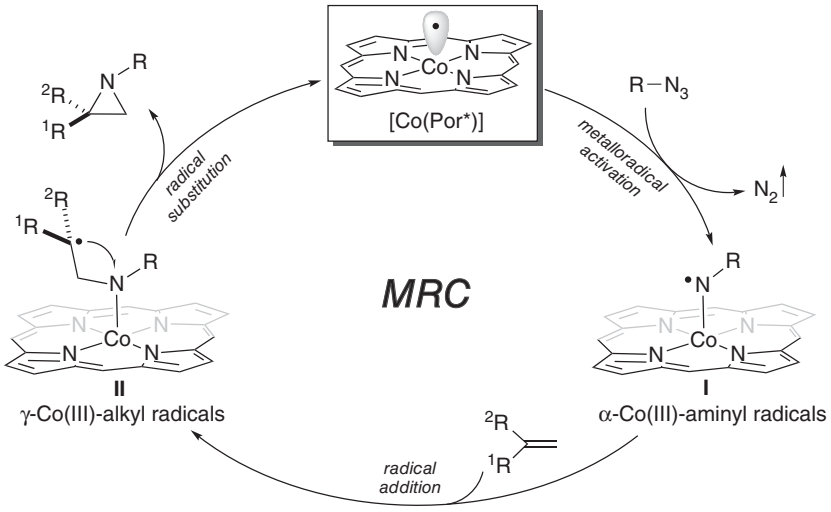


**Scheme 2.20** Proposed catalytic cycle for aziridination of alkenes with organic azides via Co(II)-MRC.

In 2006, the Zhang group successfully developed the catalytic aziridination of styrene derivatives using the commercially available diphenylphosphoryl azide (DPPA) as nitrogen source. The reaction, catalyzed by [Co(TPP)], produced *N*-phosphorus-substituted aziridines. However, achieving satisfactory yields required relatively high catalyst loadings, highlighting a need for more efficient systems [97]. In 2008, the group introduced their first-generation chiral catalyst [Co(**P3**)] for the asymmetric aziridination of styrene derivatives. This system achieved up to 71% ee, although high catalyst loading (10 mol%) remained necessary to achieve good yields (Scheme 2.21) [98]. These limitations prompted efforts to enhance both the reactivity and stereoselectivity of the catalytic system through improved catalyst design.

In 2014, Zhang and coworkers introduced [Co(**P18**)] (**P18** = 3,5-DiMes-QingPhyrin), featuring mesityl groups at the 3,5-positions of the meso-phenyl ring. These mesityl substituents improved reactivity and stereoselectivity, likely via favorable aromatic interactions. Using bis(2,2,2-trichloroethyl)phosphoryl azide ($TcepN_3$) as the nitrogen source, the refined system achieved significant improvements: up to 99% yield and 85% ee with only 2 mol% catalyst loading (Scheme 2.21) [102]. While $TcepN_3$ is not commercially available, it can be synthesized on a multigram scale from readily accessible starting materials [107]. Despite these advancements, the substrate scope of this system remains primarily limited to mono-substituted styrene derivatives.

In 2009, the group extended their work to develop a broadly applicable asymmetric aziridination system using various arylsulfonyl azides [99]. The optimal catalyst

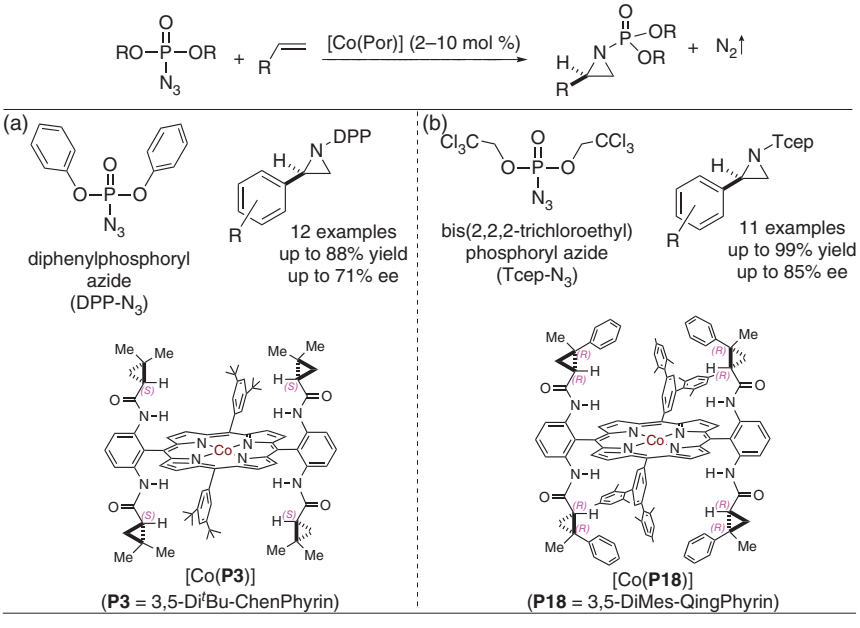


**Scheme 2.21** Aziridination of styrene derivatives with phosphoryl azides. (a) With DPP-$N_3$, (b) with Tcep-$N_3$.

[Co(**P7**)] (**P7** = 2,6-DiMeO-ZhuPhyrin) demonstrated remarkable efficacy when paired with $TcesN_3$ (trichloroethoxysulfonyl azide), enabling aziridination of both aromatic and aliphatic olefins under mild conditions (Scheme 2.22) [100]. This method provided *N*-Tces-aziridines in high yields with excellent enantioselectivities, representing the first highly effective and enantioselective approach for a wide range of simple olefins without requiring additional substrate functionalities. The system's operational simplicity and recyclability further enhance its utility. Through a straightforward precipitation/filtration protocol, the catalytic system can be

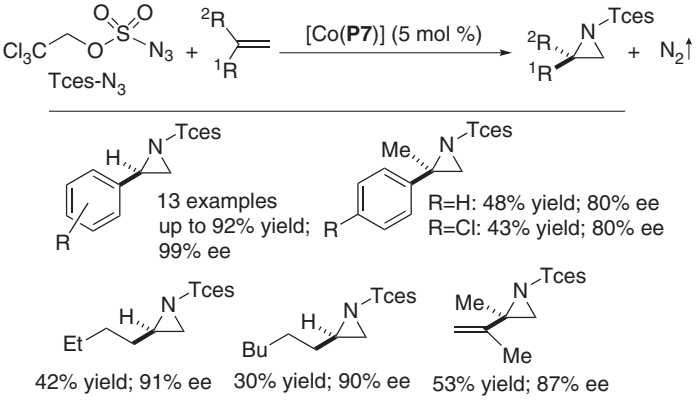


**Scheme 2.22** Aziridination of alkenes with $TcesN_3$ azides via Co(II)-MRC.

reused multiple times without significant loss in activity or selectivity. Additionally, the inclusion of $Pd(OAc)_2$ enhances yields, likely by activating the alkene substrates. This approach showcases the versatility and potential of Co(II)-MRC in asymmetric aziridination, providing a robust platform for constructing enantioenriched aziridines across diverse substrates.

In 2016, Zhang and coworkers advanced [Co(Por)]-catalyzed aziridination with a non-chiral system, targeting allylic sulfamoyl azides to produce bicyclic aziridines with exceptional yields (up to 99%) [104]. The synthetic utility of these sulfonylated [3.1.0] bicyclic diaza aziridines was demonstrated through ring-opening reactions with various nucleophiles, such as trimethylsilyl azide, thiophenol, and benzylamine. These nucleophiles attacked the exo-position under mild conditions, forming five-membered thiadiazolidine dioxide derivatives in good-to-excellent yields, showcasing the versatility of this catalytic system.

In 2024, Zhang's group introduced the first enantioselective radical *N*-heterobicyclization of *N*-allylsulfamoyl azides using a bridged [Co(Por)] catalyst, marking a major milestone in Co(II)-MRC. This system enabled the construction of chiral [3.1.0]-bicyclic sulfamoyl aziridines with outstanding yields, high diastereoselectivity, and impressive enantioselectivity (Scheme 2.23) [59]. The ligand design emerged as a critical determinant of both the catalytic reactivity and the enantioselectivity of the products. [Co(**P19**)] (**P19** = 3,5-Di$^t$Bu-Tao($^t$Bu)Phyrin), featuring bulky $^t$Bu esters groups on its chiral amide unit, catalyzed the reaction with excellent yield (99%) but modest enantioselectivity (37% ee). [Co(**P20**)] (**P20** = 3,5-Di$^t$Bu-Hu($C_8$)Phyrin), incorporating a $C_8$-alkyl bridge between the ester groups, created a cavity-like environment, which improved the enantioselectivity to 49% ee while retaining the 99% yield. With [Co(**P21**)] (**P21** = 3,5-Di$^t$Bu-Hu($C_6$)Phyrin), reducing the alkyl bridge length to $C_6$ significantly enhanced enantioselectivity to an impressive 90% ee without compromising the 99% yield. This represents a key example of how ligand tuning can optimize catalytic performance. [Co(**P5**)] (**P5** = 3,5-Di$^t$Bu-Hu($C_4$)Phyrin): A further shortening of the alkyl bridge to $C_4$ created an overly tight cavity environment, leading to reduced reactivity and enantioselectivity. This catalyst delivered only 13% yield with 84% ee, highlighting the delicate balance required in ligand design. Experimental and computational studies revealed a novel mode of asymmetric induction mediated by a radical intermediate containing a kinetically stable chiral radical center. The ability to control enantioface selectivity in this system hinges on fine-tuning the ligand environment to influence the dynamics of the reaction. These findings underscore the pivotal role of innovative ligand design in advancing MRC for asymmetric transformations.

Cenini and coworkers demonstrated the activation of aryl azides by Co(II)(Por) for benzylic C—H amination, but the reactions resulted showed low yields and uncontrolled reactivity [108, 109]. Similarly, attempts to use aryl azides for styrene aziridination with Co(II)(Por) and Ru(II)(Por) catalysts resulted in low yields and uncontrolled reactivity [106, 110], attributed to the lack of coordination groups like sulfonyl or phosphoryl moieties that enhance catalyst interactions. Fluorinated azides, however, offer improved reactivity and enantioselectivity due

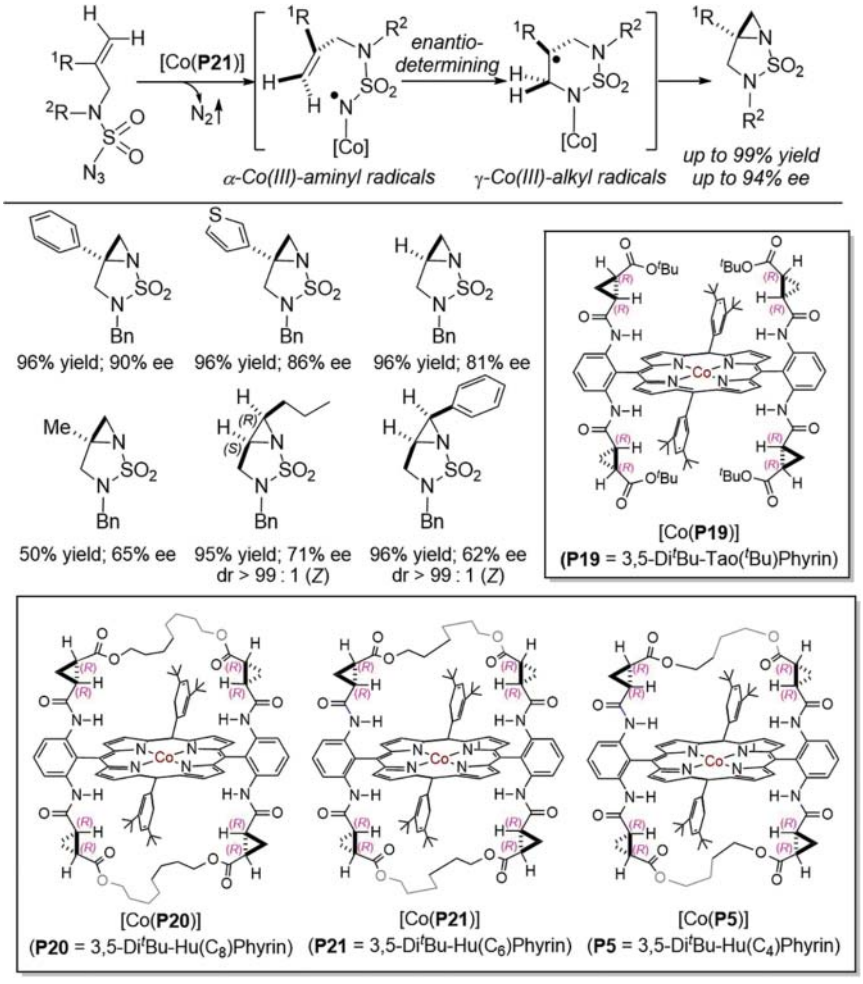


**Scheme 2.23** Intramolecular aziridination of allylic sulfamoyl azides via Co(II)-MRC.

to their electron-deficient nature and fluorine's ability to act as H-bond acceptors. Easily synthesized from commercially available fluoroanilines, these azides enable efficient access to enantioenriched *N*-fluoroaryl aziridines.

In 2013, the Zhang group reported a highly enantioselective aziridination of alkenes using fluoroaryl azides as the nitrogen source [101]. Catalyzed by [Co(**P8**)] (**P8** = 3,5-Di'Bu-Xu(2′-Naph)Phyrin), the reaction was applicable to a wide range of styrene derivatives and heteroaromatic alkenes (Scheme 2.24). The introduction of ortho-fluorine atoms in the azide was key to achieving high reactivity and enantioselectivity, as these substituents formed hydrogen bonds with the amide NH units of the catalyst. These interactions rigidified the geometry, lowered the activation barrier, and enabled enantio-control. Supporting this mechanism, no reaction occurred with 3,4,5-trifluorophenyl azide, which lacks ortho-fluorine substituents. This method represents the first catalytic system for asymmetric olefin

aziridination using aryl azides, proceeding at room temperature without additives and producing nitrogen gas as the sole by-product.

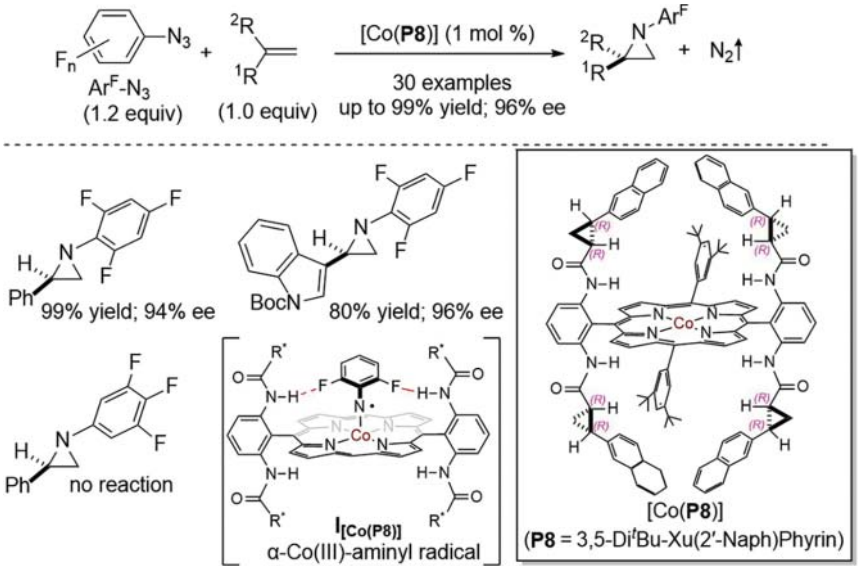


**Scheme 2.24** Aziridination with fluoroaryl azides as nitrogen source.

While carbonyl azides are rarely used for olefin aziridination due to their instability and tendency for Curtius rearrangement [111], intramolecular aziridination offers a valuable route to fused bicyclic aziridines [112–114]. These strained chiral [3.1.0]-bicyclic aziridines serve as intermediates for synthesizing biologically important compounds like oxazolidinones and vicinal amino alcohols [105]. In 2017, the Zhang group developed a [Co(Por)]-catalyzed asymmetric approach for constructing fused bicyclic aziridines using allyl azidoformates as nitrogen sources via a stepwise radical mechanism (Scheme 2.25) [105]. Using the optimized chiral amidoporphyrin ligand 3,5-Di$^t$Bu-QingPhyrin (**P9**), the reaction achieved high yields and excellent stereoselectivities. To address the instability of 3-oxa-1-azabicyclo [3.1.0] hexan-2-one products, in situ ring opening with nucleophiles was employed, directly converting them into 2-oxazolidinones. This process underscores the utility of these optically active bicyclic aziridines as versatile chiral building blocks for stereoselective synthesis.

In 2021, the Zhang group reported the enantioselective intermolecular radical aziridination of alkenes using carbonyl azides, specifically $TrocN_3$ (2,2,2-trichloroethoxycarbonyl azide), as nitrogen source (Scheme 2.26) [52]. $TrocN_3$ offers distinct advantages over other nitrogen precursors, including its straightforward synthesis from commercially available 2,2,2-trichloroethoxy chloroformate and the ease of deprotection of the resulting aziridine products to generate N—H aziridines.

Using the chiral amidoporphyrin ligand 3,5-Di$^t$Bu-QingPhyrin (**P9**), the cobalt(II) complex proved to be an efficient catalyst that could activate $TrocN_3$ at

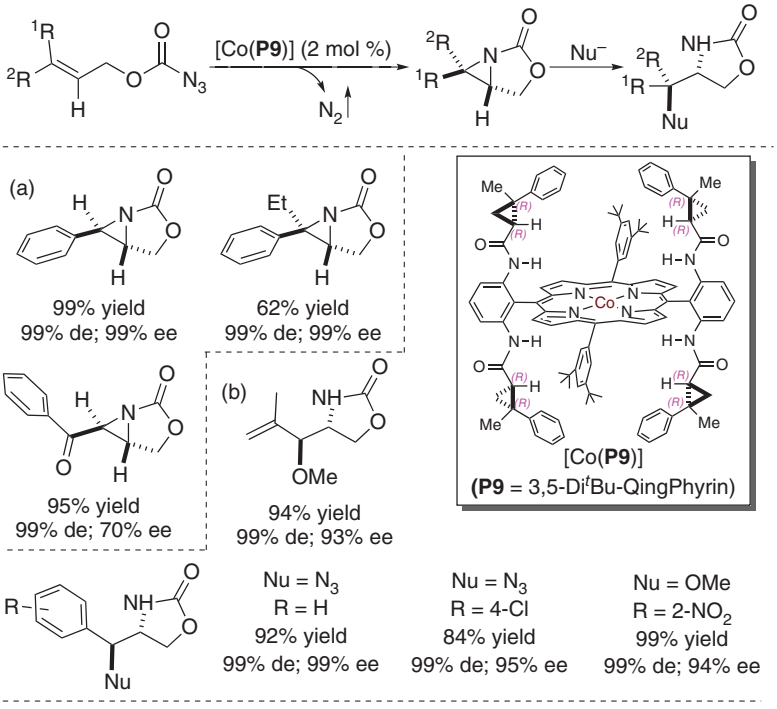


**Scheme 2.25** Asymmetric radical bicyclization of allyl azidoformate. (a) Stable bicyclic aziridines, (b) in situ-ring opening of bicyclic aziridines by nucleophiles.

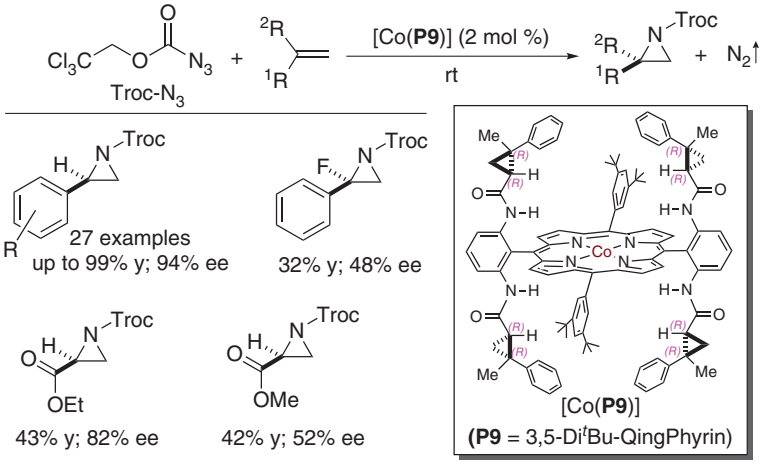


**Scheme 2.26** Aziridination of styrene derivatives with $TrocN_3$.

room temperature. This enabled the effective aziridination of a broad range of styrene derivatives with varied steric and electronic properties, delivering the aziridines in excellent yields and enantioselectivities (Scheme 2.26). Notably, the catalytic system was also applicable to 1,1-disubstituted styrenes, as demonstrated by the productive formation of aziridine bearing a tertiary fluoride stereocenter from the reaction of α-fluorostyrene (Scheme 2.26). Furthermore, the addition of a catalytic amount of $Pd(OAc)_2$ enabled the Co(II)-based metalloradical system to aziridinate electron-deficient alkenes, such as ethyl and methyl acrylates, which are known to be challenging substrates for aziridination by catalytic systems involving electrophilic metallonitrenes as key intermediates (Scheme 2.26).

### 2.2.5 [Co(II)(Por)]-Catalyzed Asymmetric Radical C—H Amination

The Co-catalyzed radical C—H amination provides a straightforward approach for constructing C—N bonds with a broad range of substrates. Both intramolecular and intermolecular versions of this transformation have been extensively developed by the Zhang group using Co(II)-MRC (Scheme 2.27) [40, 42]. The reaction mechanism begins with the MRA of azide compounds, generating α-Co(III)-aminyl radicals $\mathbf{I_A}$ and $\mathbf{I_B}$. These intermediates then undergo a crucial HAA step: $\mathbf{I_A}$ engages in intramolecular *1,n*-HAA of a distal C—H bond, while $\mathbf{I_B}$ performs an intermolecular HAA on external C—H substrates, leading to the formation of ω-Co(III)-alkyl radicals $\mathbf{II_A}$ and ∞-Co(III)-alkyl radicals $\mathbf{II_B}$, respectively. Finally, an RS step yields the desired C—H amination products, with the release of the [Co(Por)] catalyst to complete the catalytic cycle.

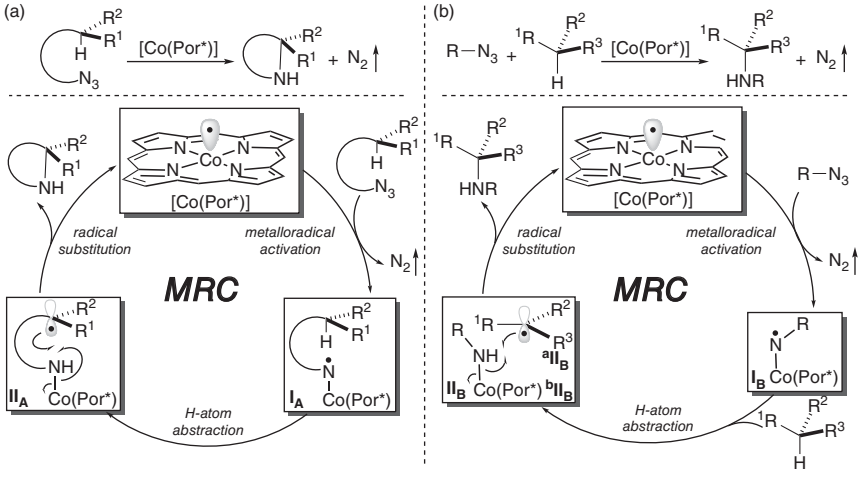


**Scheme 2.27** Proposed catalytic cycle for intramolecular and intermolecular C—H amination with organic azides via Co(II)-MRC. (a) Intramolecular radical C—H amination, (b) intermolecular radical C—H amination.

In 2019, Zhang and coworkers developed Co(II)-based metalloradical systems for the asymmetric 1,5-C—H amination of both arylsulfonyl and alkylsulfonyl azides

under neutral and nonoxidative conditions, using [Co(**P7**)] (**P7** = 2,6-DiMeO-ZhuPhyrin) and [Co(**P22**)] (**P22** = 2,6-DiMeO-Qing(4′-Me)Phyrin), respectively (Scheme 2.28) [47]. These catalytic systems were shown to be highly effective for enantioselective radical amination, not only with benzylic C—H bonds of varied steric and electronic properties but also with allylic C—H bonds, demonstrating excellent chemoselectivity and compatibility with heteroaryl groups. The result was the stereoselective construction of functionalized 5-membered cyclic sulfonamides in high yields with outstanding enantioselectivities. This work represents one of the most general and selective catalytic systems for asymmetric intramolecular C—H amination of sulfonyl azides. The remarkable reactivity and selectivity observed in the Co(II)-based asymmetric 1,5-C—H amination are attributed to its underlying stepwise radical mechanism, which is strongly supported by various lines of experimental evidence.

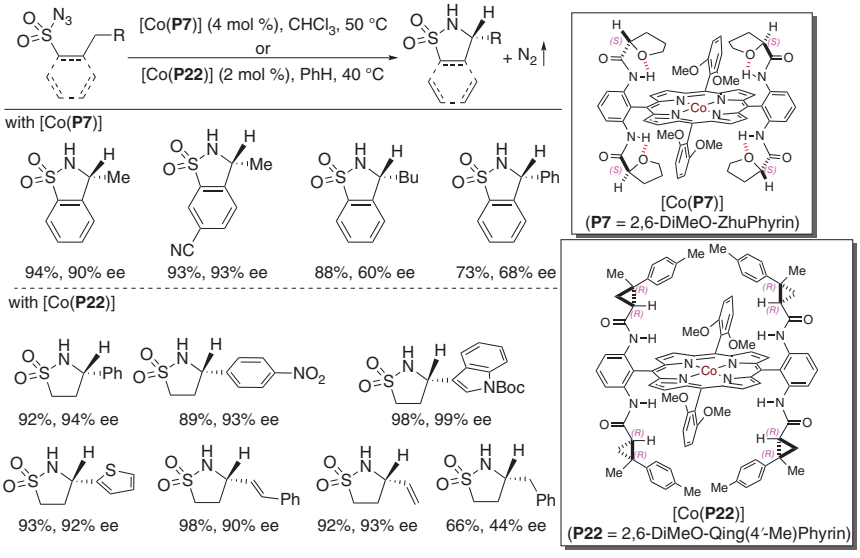


**Scheme 2.28** 1,5-C—H amination of sulfonyl azides via Co(II)-MRC.

In 2018, Zhang and coworkers utilized [Co(**P11**)] (**P11** = 2,6-DiMeO-QingPhyrin) as a catalyst to develop the first highly asymmetric catalytic system for the intramolecular 1,6-C($sp^3$)—H amination of sulfamoyl azides (Scheme 2.29) [115]. The Co(II)-based metalloradical system effectively activated a variety of sulfamoyl azides to aminate wide range of C($sp^3$)—H bonds to deliver six-membered cyclic sulfamides in high yields with excellent enantioselectivities. The Co(II)-catalyzed amination process exhibited a remarkable degree of functional-group tolerance and exceptional level of chemoselectivity, which can be attributed to its unique stepwise radical mechanism. Furthermore, the resulting optically active sulfamides could be readily converted into synthetically useful 1,3-diamines without any loss in enantiopurity.

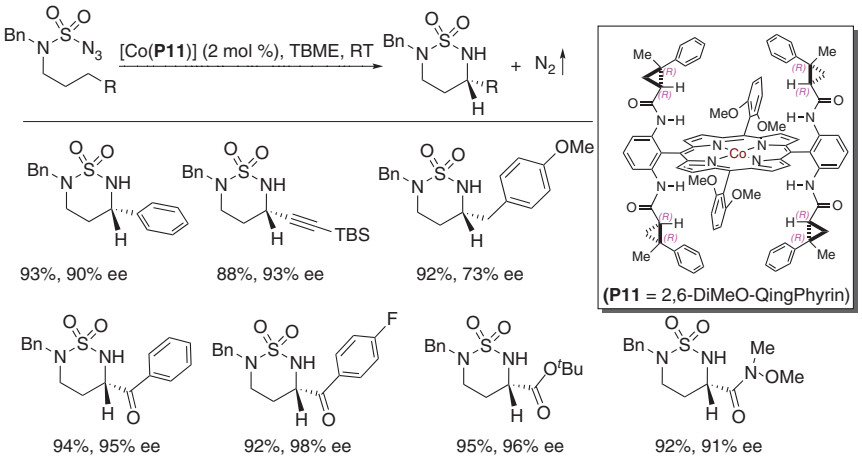


**Scheme 2.29** 1,6-C—H amination of sulfamoyl azides via Co(II)-MRC.

Zhang and coworkers extended the scope of Co(II)-MRC in 2020 by developing a deracemizative functionalization of racemic tertiary C($sp^3$)—H bonds, enabling the stereoselective synthesis of chiral molecules with quaternary stereocenters (Scheme 2.30) [50]. Using the [Co(**P11**)], they achieved an enantioconvergent radical amination process. This method leverages a sequence of H-atom abstraction, radical racemization, and RS under controlled conditions, leading to efficient asymmetric induction. Mechanistic studies indicate that the $D_2$-symmetric ligand environment of [Co(**P11**)] is essential, providing a balanced setting that promotes 1,6-H-atom abstraction, enables racemization of prochiral radical intermediates, and facilitates stereoselective RS for construction of C—N bonds. Operating under mild conditions, the Co(II)-based system catalyzes 1,6-amination of racemic tertiary

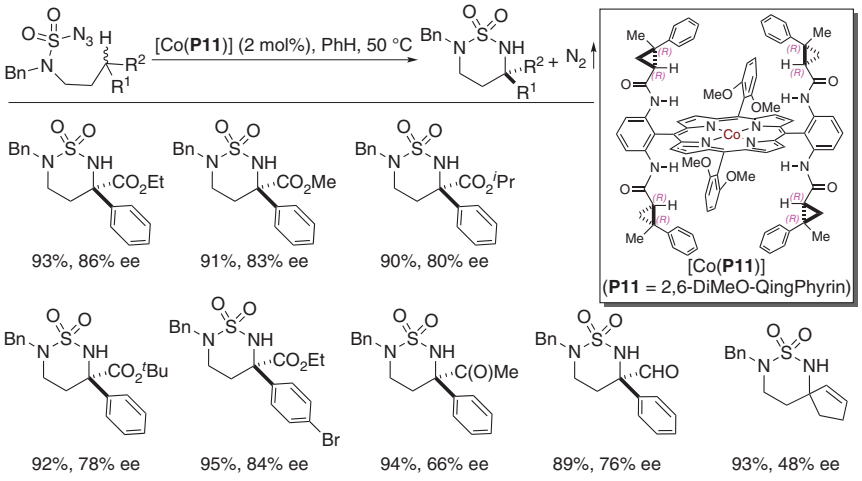


**Scheme 2.30** Enantioconvergent 1,6-C—H amination of sulfamoyl azides via Co(II)-MRC.

C—H bonds in sulfamoyl azides, generating six-membered cyclic sulfamides with chiral α-tertiary amines at the newly formed quaternary stereocenter in excellent yield and enantioselectivity. This approach, which allows direct conversion of C—H bonds into quaternary stereocenters with functional diversity, offers promising applications in organic synthesis, exemplified by the stereoselective construction of bicyclic *N*-heterocycles.

In 2019, Zhang and coworkers pioneered a unique mode of asymmetric induction in radical process by combining enantiodifferentiative H-atom abstraction (HAA) with stereoretentive RS under Co(II)-based MRC (Scheme 2.31) [48]. This approach enabled the first asymmetric system for the stereoselective synthesis of strained five-membered cyclic sulfamides via radical 1,5-C—H amination of sulfamoyl

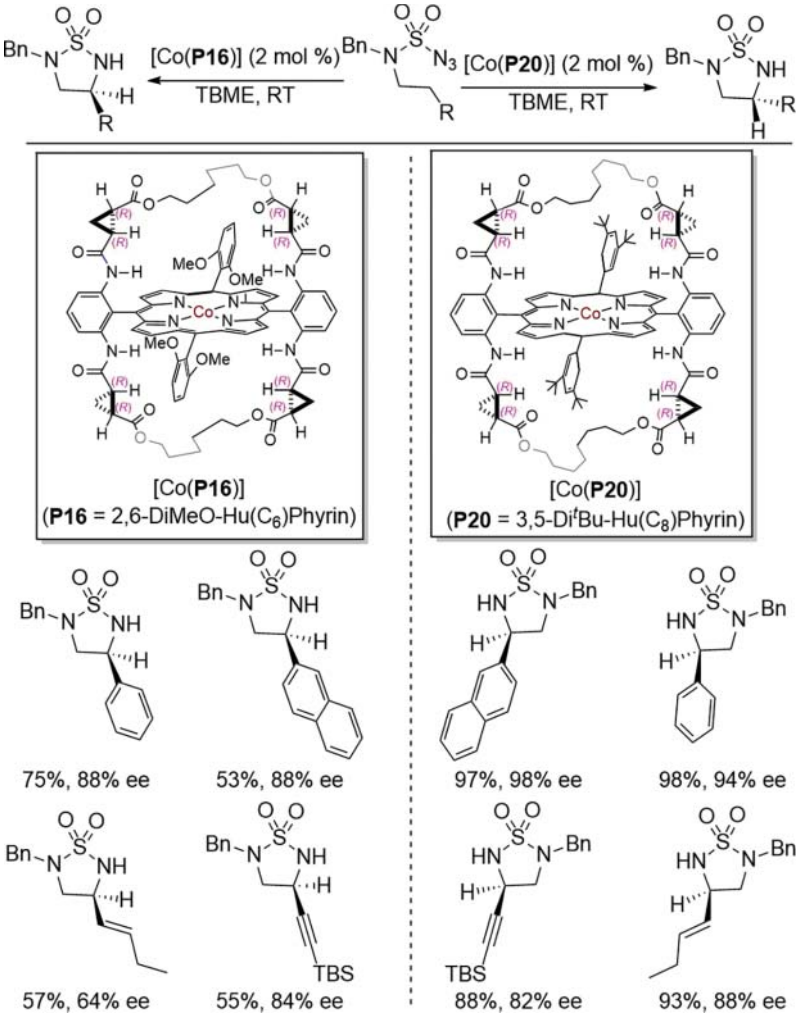


**Scheme 2.31** Enantiodivergent 1,5-C—H amination of sulfamoyl azides via Co(II)-MRC.

azides. The success of this system hinged on the use of tunable bridged HuPhyrin ligands, which create a chiral cavity modifiable through distal alkyl bridges and remote nonchiral substituents. This flexibility allowed precise control over both the degree and direction of asymmetric induction during catalysis. Two metalloradical catalysts, [Co(**P16**)] (**P16** = 2,6-DiMeO-Hu($C_6$)Phyrin) and [Co(**P20**)] (**P20** = 3,5-Di$^t$Bu-Hu($C_8$)Phyrin), which differ only in bridge length and substituent position, were found effective for enantiodivergent radical C—H amination, achieving high enantioselectivity under mild conditions. This system accommodates a broad range of C($sp^3$)—H substrates and produces both enantiomers of cyclic sulfamides with high enantioenrichment. Experimental and computational studies provided stereochemical models explaining asymmetric induction, offering valuable insights for designing catalysts for enantioselective radical reactions. This study highlights the potential of radical processes for stereoselective synthesis, including enantiodivergent strategies for producing chiral molecules.

In 2022, Zhang and coworkers introduced a versatile method for synthesizing chiral amines with β-functionalities, starting from readily available alcohols by combining radical and ionic chemistries (Scheme 2.32) [56]. This approach achieves formal 1,2-difunctionalization of alcohols via an enantioselective 1,5-C—H radical amination of alkoxysulfonyl azides, followed by a stereospecific ring opening of the resulting five-membered cyclic sulfamidates with nucleophiles. The method showcases site-selective, stereospecific ring opening with a range of nucleophiles and employs an optimized Co(II)-based MRC system for enantioselective 1,5-C($sp^3$)—H amination. Key to the process was the ligand 2,6-DiMeO-Hu($C_6$)Phyrin (**P16**), which enabled the activation of various alkoxysulfonyl azides at room temperature, yielding chiral sulfamidates with high diastereo- and enantioselectivity. Mechanistic studies revealed insights into the radical mechanism and asymmetric induction within the Co(II)-based system. This combined radical-ionic strategy efficiently

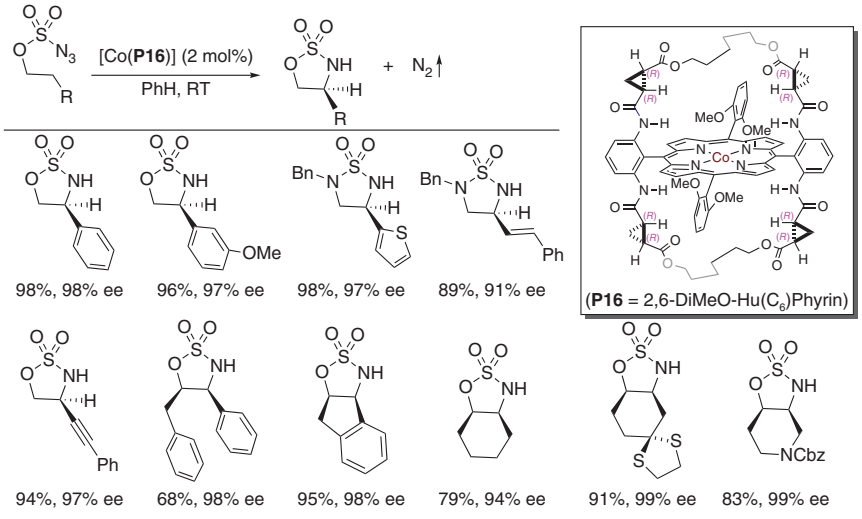


**Scheme 2.32** 1,5-C—H amination of alkoxysulfonyl azides via Co(II)-MRC.

constructs linear and cyclic molecules with multiple contiguous stereocenters, a challenge for other methods. Given the prevalence of chiral amines in bioactive molecules, this approach holds significant potential for applications in organic synthesis and drug discovery.

In 2020, Zhang and coworkers introduced the first highly enantioselective system for intermolecular radical C—H amination, utilizing [Co(**P23**)] (**P23** = 2,6-DiPhS-QingPhyrin) as the catalyst (Scheme 2.33) [49]. Operating under mild conditions with C—H substrates as the limiting reagent, this Co(II)-catalyzed process features a broad substrate scope and high chemoselectivity, facilitating the synthesis of chiral amino acid derivatives with excellent enantioselectivities. The success of this approach stems from the fine-tuning of the $D_2$-symmetric chiral amidoporphyrin ligand, enhancing noncovalent attractive interactions that are essential for controlling both reactivity and enantioselectivity. Unlike traditional metallonitrene insertion, this enantioselective C—H amination follows a stepwise radical pathway comprising three steps: (i) MRA of organic azides, (ii) intermolecular HAA from C—H substrates, and (iii) RS for C—N bond formation. This novel radical pathway marks a major advancement in the field and holds promise as a versatile strategy for synthesizing chiral amine derivatives.

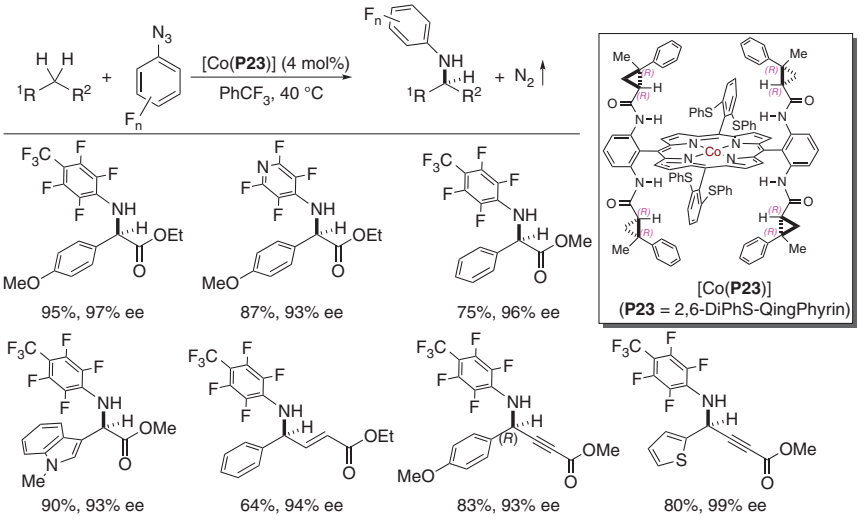


**Scheme 2.33** Intermolecular benzylic C—H amination with fluoroaryl azides via Co(II)-MRC.

In 2023, Zhang and coworkers developed an MRC strategy for achieving concurrent control over multiple convergences and selectivities in radical reactions (Scheme 2.34) [60]. Using the $D_2$-symmetric chiral amidoporphyrin ligand ChenPhyrin (**P24**) with an unsubstituted meso-phenyl ring, the Co(II)-catalyst [Co(**P24**)] effectively activated a range of fluoroaryl azides for radical allylic C—H

amination of trisubstituted alkenes, yielding α-tertiary amino acid derivatives with high stereoselectivity under mild conditions. This system demonstrated exceptional chemoselectivity, regioselectivity, diastereoselectivity, and enantioselectivity, achieving multiple stereochemical convergences. For substrates lacking a phenyl ring at the tertiary position, [Co(**P23**)] (**P23** = 2,6-DiPhS-QingPhyrin) provided good enantioselectivity. Notably, this approach accommodates isomeric mixtures of alkenes, offering practical advantages. The success of this radical C—H amination methodology relied on optimizing the ligand's cavity-like structure to enhance noncovalent interactions with substrates, addressing the challenges of reactivity and selectivity in radical chemistry through precise catalyst design. This work showcases the potential of MRC to enable new synthetic methods in radical chemistry, inspiring further advancements in catalyst-driven control of complex transformations.

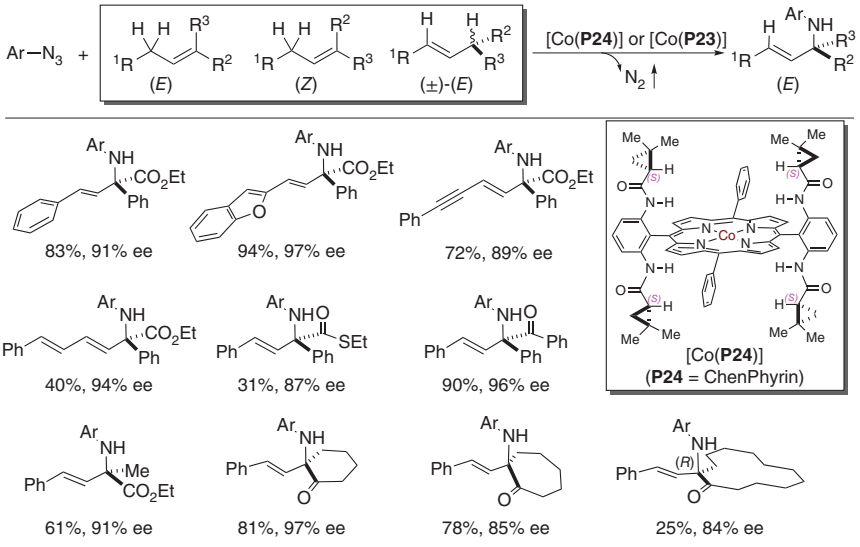


**Scheme 2.34** Intermolecular convergent C—H amination with fluoroaryl azides via Co(II)-MRC.

In 2017, de Bruin and colleagues introduced a [Co(Por)]-catalyzed approach for intramolecular C—H amination of aliphatic azide compounds, enabling the formation of five-membered *N*-heterocyclic structures (Scheme 2.35) [116]. Their study revealed that adding di-*tert*-butyldicarbonate ($Boc_2O$) prevented competitive binding of the amine product, which greatly enhanced the reaction rate. To achieve enantioselectivity in the ring-closing amination, they developed a new chiral cobalt-porphyrin catalyst, [Co(**P25**)], incorporating four (1*S*)-(-)-camphanic-ester groups in the second coordination sphere. Although the reaction required elevated temperatures (80 °C), it provided modest enantioselectivities, reaching up to 46% ee in the ring closure of (4-azidobutyl) benzene. This work highlighted the potential of finely tuned cobalt catalysts in achieving selective C—H amination.

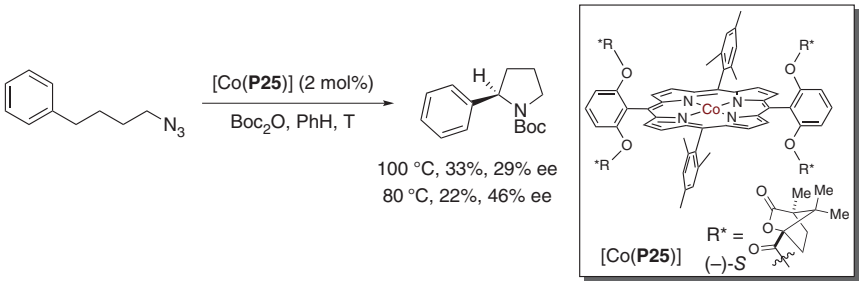


**Scheme 2.35** Intramolecular C—H amination with aliphatic azides via Co(II)-MRC.

## 2.3 Cobalt-Catalyzed Asymmetric Hydrofunctionalization of Alkenes

Co-catalyzed asymmetric hydrofunctionalization of alkenes with nucleophiles in the presence of extra oxidants involving metal-hydride-mediated hydrogen atom transfer (MHAT) has been widely explored and achieved great progress [1, 4]. The general reaction mechanism for these transformations is illustrated in Scheme 2.36; it is initiated with the oxidation of a $[L_nCo^{II}]$ complex to a $[L_nCo^{III}X]$ species.

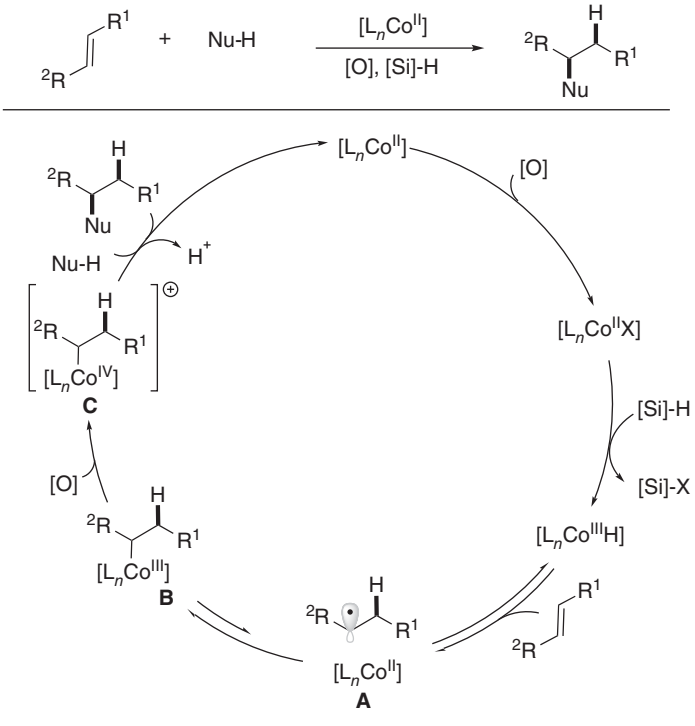


**Scheme 2.36** General catalytic cycle for Co-catalyzed hydrofunctionalization of alkenes involving MHAT.

This species readily transforms into the hydride complex [$L_nCo^{III}H$] upon interaction with a silane ([Si]—H). This [$L_nCo^{III}H$] complex then transfers a hydrogen atom to the alkene following Markovnikov selectivity, yielding a more stable alkyl radical coupled with [$L_nCo^{II}$] species (intermediate **A**). This step is usually reversible and could lead to double-bond migration products. The resulting alkyl radical can either recombine with the [$L_nCo^{II}$] to form a [$L_nCo^{III}$]-alkyl complex (intermediate **B**) or undergo further transformations. The recombination is reversible, with equilibrium favoring the [$L_nCo^{III}$]-alkyl complex state. Subsequently, intermediate **B** can be oxidized to the cationic [$L_nCo^{IV}$]-alkyl complex (intermediate **C**). This species undergoes nucleophilic substitution by a nucleophile to furnish the hydrofunctionalization product, regenerating the [$L_nCo^{II}$] catalyst and completing the catalytic cycle. The choice of oxidant and silane significantly influences the reaction's outcome. The mechanism of electron transfer with [$L_nCo^{II}$] during the initial oxidation step remains ambiguous. It is unclear whether two [$L_nCo^{III}$] complexes are generated simultaneously in a concerted oxidation. Additionally, depending on the oxidant employed, intermediate **B** may not require further oxidation to [$L_nCo^{IV}$]. Instead, direct RS of **B** could yield the desired product, with regeneration of the [$L_nCo^{II}$] species, thus completing the catalytic cycle through an alternate pathway.

As summarized in Scheme 2.37, [Co(Salen)] complexes are effective catalysts for asymmetric hydrofunctionalization of alkenes. While [Co(Salen)] shares similarities with [Co(Por)] in MRC, it is structurally more flexible, exhibiting different coordination chemistry and reaction patterns. Chiral elements in [Co(Salen)] are typically introduced through diamine backbones, such as 1,2-diaminocyclohexane and 1,2-diamino-1,2-diphenylethane, while the salicylaldehyde moiety introduces steric bulk to influence reactivity and enhance chirality.

### 2.3.1 With O-nucleophile

The Co-catalyzed hydroalkoxylation of alkene with oxygen-based nucleophiles (alcohol solvents) via the MHAT mechanism was first pioneered by Shigehisa and coworkers in 2013 [117]. This strategy was later extended to intramolecular reactions using O- or heteroatom-based nucleophiles with a [(Salen)$Co^{II}$]/NFTP (*N*-fluoro-2,4,6-trimethylpyridinium salt) catalytic system. In 2016, the Shigehisa group explored enantioselective hydroalkoxylation for cyclized product formation, achieving 28% ee with chiral β-oxoaldiminatocobalt(II) complexes [Co(**S1**)] (Scheme 2.38) [118]. Despite the modest enantiocontrol, this study demonstrated the feasibility of enantioselective reactions, sparking further research with a focus on ligand design.

In 2019, Pronin and coworkers achieved a breakthrough in Co-catalyzed asymmetric intramolecular hydroalkoxylation of tertiary allylic alcohols, producing chiral epoxides with excellent enantioselectivity for the first time using the MHAT process (Scheme 2.39) [119]. The key to this high enantioselectivity was the incorporation of a dibenzofuran scaffold at the ortho-position of the phenyl ring in the [Co(**S2**)] catalyst. The authors proposed that the cationic [$Co^{IV}$(**S2**)] species is stabilized by a

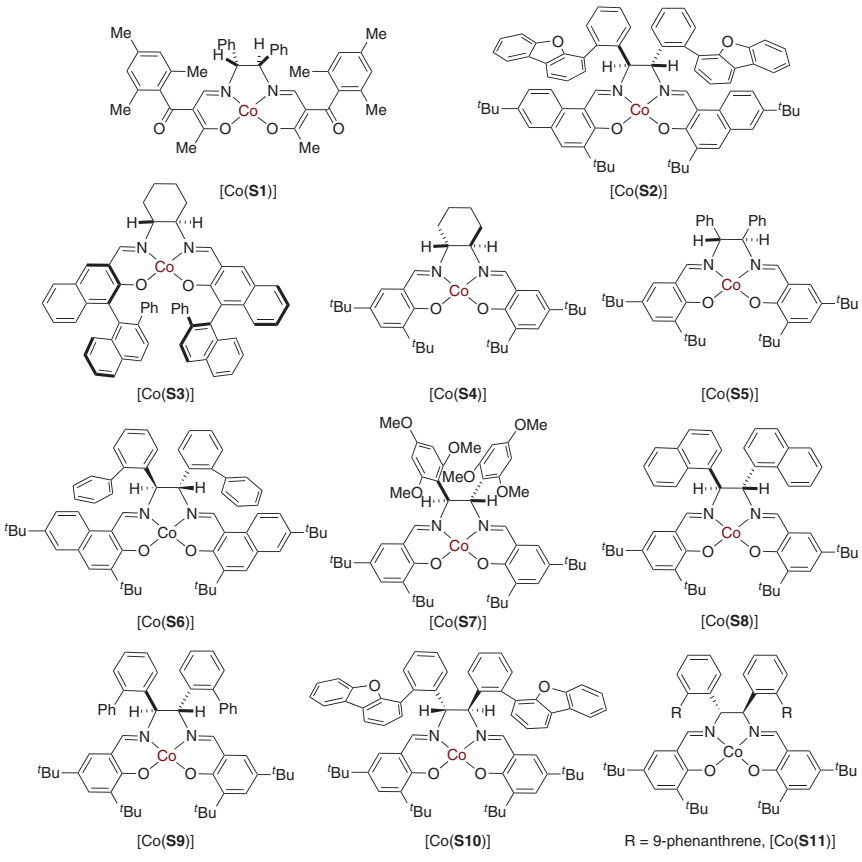


**Scheme 2.37** [Co(Salen)] complexes employed in hydrofunctionalization of alkenes.

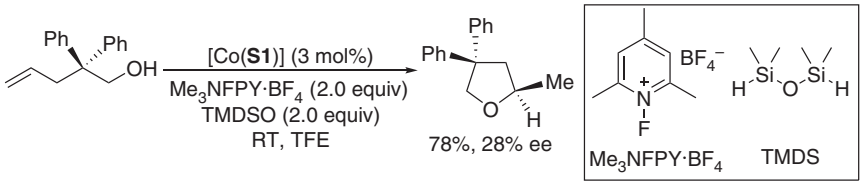


**Scheme 2.38** Initial attempt of asymmetric intramolecular hydroalkoxylation of alkenes via Co(H)-involved MHAT.

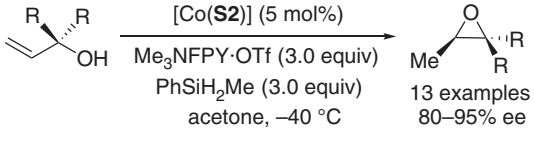


**Scheme 2.39** The first highly enantioselective hydroalkoxylation of tertiary allylic alcohols.

cation-π interaction between the salen motif and biaryl substituents, which provides enthalpic stabilization to the radical cation species, aiding asymmetric induction.

Around the same time, Shigehisa and co-workers developed the [Co(**S3**)] catalyst, which features a chiral cyclohexyl diamine backbone and additional axial chirality from the binaphthyl moiety. This catalyst was effective in catalyzing the enantioselective hydroalkoxylation of alkenyl alcohols, leading to the synthesis of enantioenriched tetrahydrofurans with *N*-fluoro-2,4,6-collidinium tetrafluoroborate as the oxidant (Scheme 2.40) [120]. Notably, the absolute configuration and enantioselectivity of the chiral tetrahydrofuran product were found to be highly sensitive to the steric hindrance of the silane reagents used.

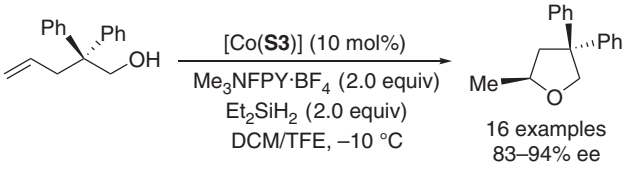


**Scheme 2.40** Silane-controlled enantioselective intramolecular hydroalkoxylation of alkenes.

In 2019, Zhu and coworkers reported the first example of a Co-catalyzed intermolecular hydrofunctionalization reaction of alkenes with oxygen-based nucleophiles, using a hypervalent iodine(III) reagent as the oxidant (Scheme 2.41) [121]. The catalyst [Co(**S4**)], featuring a chiral cyclohexyl diamine backbone and bulky tert-butyl groups on the phenyl ring, achieved a low but measurable level of stereocontrol (5% ee), with the enantiomer showing −7% ee. This provided valuable evidence of catalyst-controlled stereoselectivity at the Co(IV) oxidation state. Mechanistic studies indicated that the reaction proceeds via a unique bimetallic-mediated pathway, involving two distinct Co-species: an alkylcobalt(III) complex and a Co-bound nucleophile. This dual-cobalt system facilitates C—O bond formation, offering new insights into cobalt-catalyzed transformations and highlighting a distinct mechanism for C–nucleophile bond formation.

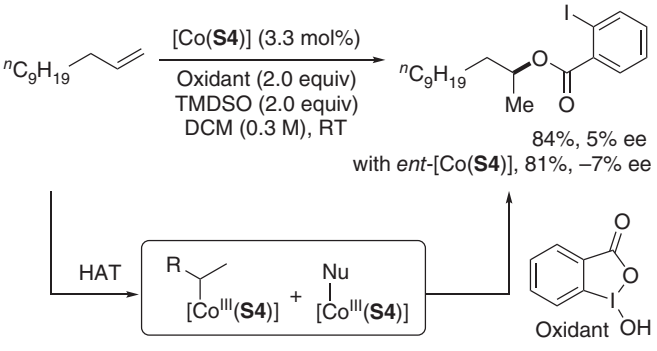


**Scheme 2.41** Bimetallic-mediated hydroacyloxylation of alkenes.

Zhu later introduced a novel electricity-driven method for Co-catalyzed oxidative hydrofunctionalization of alkenes, eliminating the need for stochiometric chemical oxidants (Scheme 2.42) [122]. Key mechanistic evidence for the involvement of a [$Co^{IV}$] intermediate came from an attempted asymmetric synthesis using a chiral Co-Salen complex, [Co(**S5**)], featuring a chiral 1,2-diamino-1,2-diphenylethane backbone and bulky tert-butyl groups on the phenyl ring, which yielded the hydroalkoxylation product with 31% ee. Building on this, Kim developed an analogous electrochemical oxidation process for hydroetherification, enabling the modular synthesis of alkyl aryl ethers. This method utilized a broad range of alkenes and phenols under controlled electrical conditions in a 1,1,1,3,3,3-hexafluoro-2-propanol (HFIP) cosolvent system (Scheme 2.42) [123]. With [Co(**S6**)], featuring a biphenyl diamine backbone and bulky tert-butyl groups on the naphthyl ring of aldehydes, up to 40% ee was achieved in the reaction between 4-*t*-butyl styrene and 4-methoxyphenol. While the enantioselectivity was modest, these results provide strong evidence for catalyst-controlled stereoselectivity, further supporting the involvement of a Co(IV) intermediate in these transformations.

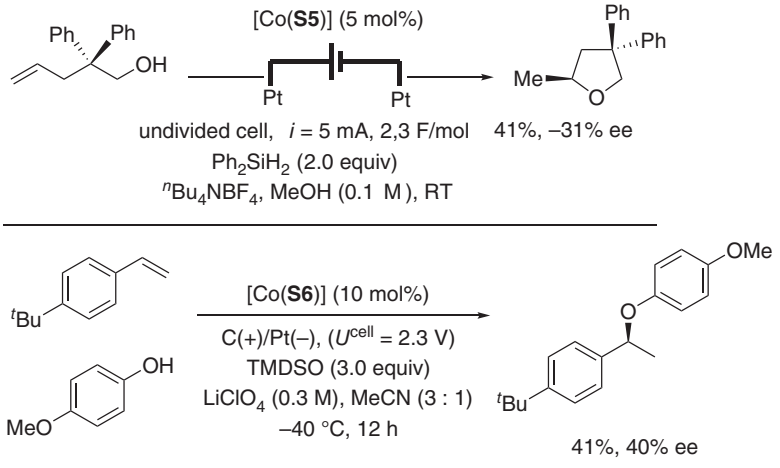


**Scheme 2.42** Electrocatalytic oxidative hydroetherification of alkenes.

### 2.3.2 With *N*-nucleophile

The use of nitrogen nucleophiles in Co-hydride-mediated oxidative HAT reactions offers an elegant strategy for stereoselective C—N bond formation, a key transformation in the synthesis of biologically active natural products, pharmaceuticals, agrochemicals, and materials. In 2020, Akai and co-workers explored the asymmetric hydroamination of non-activated alkenes with benzotriazoles, employing an optically active Co(salen) complex [Co(**S5**)], along with *N*-fluoropyridinium salt and phenylsilane reagent. However, this approach achieved only up to 16% ee (Scheme 2.43, top) [124]. When 5-phenyl tetrazole

was used as the *N*-nucleophile, asymmetric induction of 4-phenyl-1-butene did not exceed 20% ee, even with various chiral Co catalysts. For instance, [Co(**S7**)], featuring a chiral 1,2-diamino-1,2-diphenylethane backbone with 2,4,6-tri-MeO on the phenyl ring and bulky tert-butyl groups on the phenyl ring of the salicylaldehyde moiety, afforded 17% ee (Scheme 2.43, middle) [125]. Similarly, hydroamination of activated indene with tetrazole catalyzed by [Co(**S8**)], which has a 1,2-diamino-1,2-diphenylethane backbone with 1-naphthyl substituents replacing the phenyl ring and bulky tert-butyl groups, provided 81% yield but only 18% ee. Interestingly, performing the reaction at 0 °C with [Co(**S6**)] as the catalyst significantly improved enantioselectivity to 66% ee, although the yield dropped to 24% (Scheme 2.43, bottom). This highlights the sensitivity of the reaction to temperature and catalyst design, emphasizing the need for further optimization.

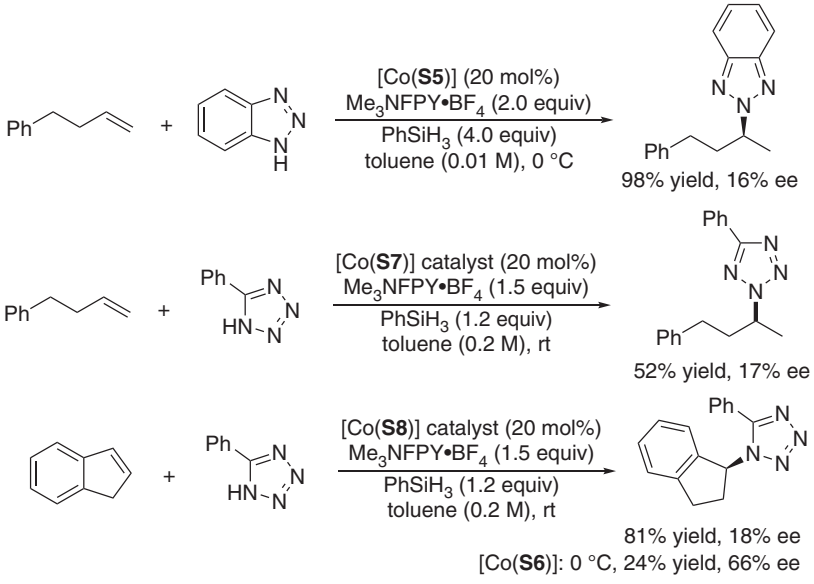


**Scheme 2.43** Asymmetric hydroamination of alkenes with *N*-heterocycles.

In 2021, the Zhang group achieved a significant milestone by reporting the first efficient Co-catalyzed intermolecular, highly enantioselective hydroamination of alkenes, using *N*-fluorobenzenesulfonimide (NFSI) as both oxidant and *N*-source (Scheme 2.44) [126]. Extensive optimization of reaction parameters led to the

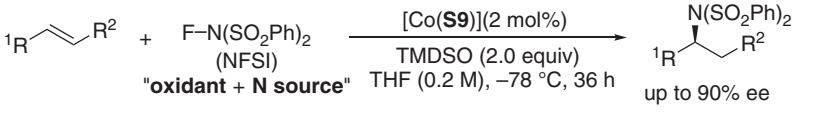


**Scheme 2.44** Co-Catalyzed highly enantioselective hydroamination of alkenes with NFSI.

identification of the optimal conditions: a chiral Co(salen) catalyst [Co(**S9**)] (2 mol%), which incorporates an *o*-biaryl-substituted biphenyl group on the diamine backbone and bulky tert-butyl groups on the phenyl ring, in the presence of tetramethyldisiloxane (TMDSO) as the hydrogen donor in dry THF at −78 °C. Under these conditions, the method efficiently converted a broad range of alkenes, including styrenes, vinylnaphthalenes, heteroaryl-substituted alkenes, and internal alkenes, into the corresponding chiral amines with good-to-excellent yields and enantioselectivities, achieving up to 90% ee.

In 2023, the Zhang group introduced a groundbreaking asymmetric variant of the Co-hydride-mediated oxidative HAT reaction, enabling the coupling of arylalkenes with a wide range of Lewis basic secondary amines (Scheme 2.45) [127]. This innovative approach employed a dibenzofuran-containing chiral Co(Salen) complex, [Co(**S10**)], as the catalyst, with *tert*-butyl peroxide benzoic acid (TBPB) as the oxidant, phenylmethylsilane ($PhMeSiH_2$) as the hydrogen donor, and acetonitrile as the solvent at −20 °C. The reaction proved to be an efficient and straightforward method for synthesizing chiral α-tertiary amines, achieving moderate-to-excellent yields and enantioselectivities (Scheme 2.45).

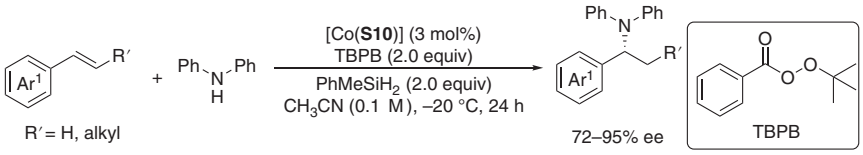


**Scheme 2.45** Co-Catalyzed highly enantioselective hydroamination of alkenes with secondary amines.

### 2.3.3 With C-nucleophile

C-based nucleophiles, such as electron-rich arenes, have also been utilized in asymmetric oxidative MHAT reactions for the formation of chiral C—C bonds. In 2022, the Zhang group successfully developed the first example of CoH-catalyzed symmetric hydrofunctionalization using C-nucleophiles, achieving highly enantioselective hydroarylation between styrene and *N*-methyl indole derivatives (Scheme 2.46) [128]. This breakthrough represents a significant milestone in CoH-catalyzed asymmetric hydrofunctionalization by enabling C—C bond formation through oxidative HAT. The optimized reaction conditions involved the use of a chiral Co(Salen) complex, [Co(**S11**)], as the catalyst (3 mol%), featuring a 9-phenanthryl

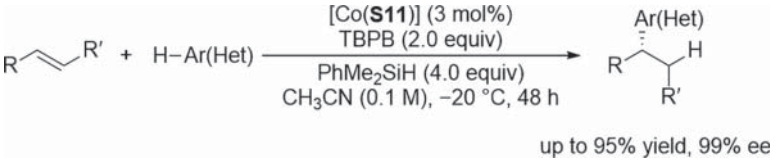


**Scheme 2.46** Co-Catalyzed first highly enantioselective hydroarylation of alkenes.

group at the ortho-position of the phenyl substituent on the diamine backbone. Dimethylphenylsilane ($PhMe_2SiH$) served as the hydrogen donor, while tert-butyl peroxybenzoate (TBPB) was employed as the oxidant.

### 2.3.4 Miscellaneous

The merger of Co-mediated HAT and Cu-promoted radical transformations has opened new avenues in asymmetric MHAT chemistry. In 2020, the Lin group developed a highly enantioselective hydrocyanation of conjugated alkenes by integrating these two metal-mediated radical processes within an anodically coupled electrocatalytic system (Scheme 2.47) [129]. The optimal conditions involved using a Co(salen) complex [Co(**S12**)] (0.5 mol%), $Cu(OTf)_2$ (5 mol%), and a chiral bidentate *N,N*-ligand **L1** (10 mol%) in the presence of phenylsilane ($PhSiH_3$), which resulted in the formation of the hydrocyanation product in 79% yield and 91% ee. Mechanistic studies revealed that the C-centered radical, generated from the Co-catalyzed HAT process, enters the cyanation cycle, undergoing a single-electron oxidative addition to [$Cu^{II}$]—CN species to form a formally [$Cu^{III}$] intermediate. This intermediate then undergoes RE to complete the hydrocyanation reaction. This electrochemical strategy allows for the precise control of the applied potential, avoiding the use of stoichiometric oxidants and providing a broadly applicable method for hydrocyanation with high functional group tolerance and a wide substrate scope.

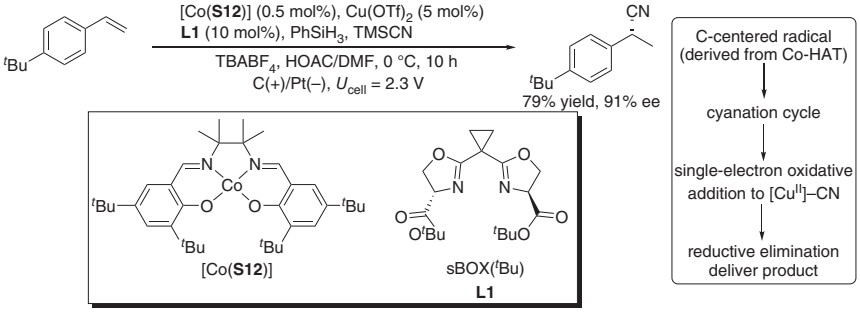


**Scheme 2.47** Dual electrocatalysis enables enantioselective hydrocyanation of alkenes.

It is worth noting that the Lu group successfully demonstrated a Co-catalyzed asymmetric intermolecular Markovnikov hydroamination of non-activated alkenes, using tert-butyl 2-diazo-phenylacetate as the *N*-source, proceeding via an MHAT mechanism (Scheme 2.48) [130]. This reaction utilized a newly developed chiral *N,N,N*-tridentate ligand, *N*-imidazolinylphenyl 8-aminoquinoline (IPAQ, **L2**), which provided chiral hydroamination products with good enantioselectivity (77–84% ee). The reaction mechanism, as depicted in Scheme 2.48, begins with the formation of cobalt hydride species [CoH] (**A**) from the reaction of $Co(OAc)_2$ with the ligand and silane. This species undergoes a metal hydride HAT process, generating a carbon radical intermediate and cobalt species (**B**). Due to the possible

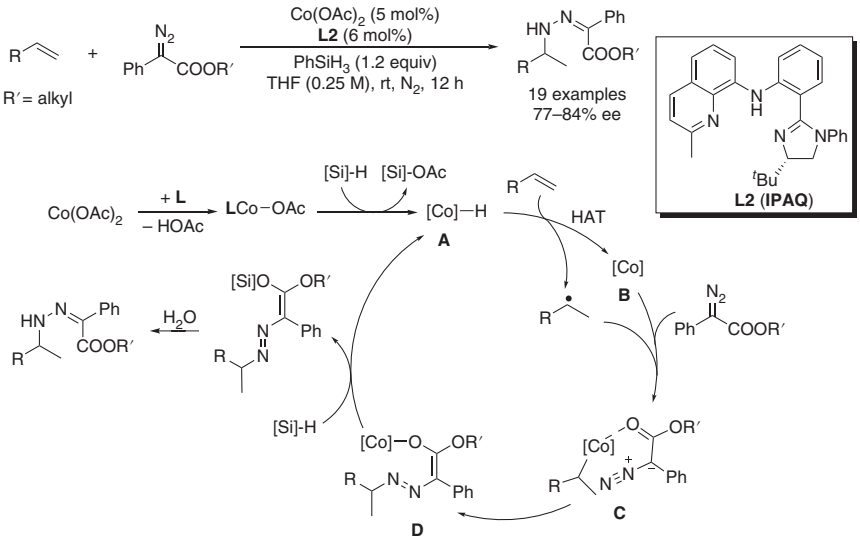


**Scheme 2.48** Co-Catalyzed hydroamination of alkenes with diazo compounds as nitrogen source.

redox non-innocent nature of the ligand, the oxidation state of cobalt may fluctuate throughout the reaction. Cobalt species **B** is proposed to coordinate with the diazo compound, and a one-electron oxidation of the carbon radical intermediate produces a cobalt–carbon species (**C**). This species undergoes alkyl group migration from cobalt to the nitrogen atom, generating cobalt oxide species (**D**). An alternative pathway, where the carbon radical directly attacks the cobalt-coordinated diazo compound, cannot be excluded. Cobalt species **D** is believed to react with hydrosilane, regenerating the cobalt hydride species (**A**) and forming a vinyl silyl ether intermediate, which then undergoes hydrolysis and isomerization to yield the final product.

In 2022, Lu and coworkers expanded the aforementioned catalytic system to a sequential hydrosilylation/hydrohydrazidation of readily available terminal alkynes with hydrosilanes and diazo compounds, resulting in the formation of 1,2-N,Si compounds with good functional group tolerance (Scheme 2.49) [131]. This process involved two mechanistically distinct transformations: cobalt-catalyzed alkyne insertion for hydrosilylation and the HAT process for the hydrohydrazidation of alkenyl silane, both efficiently carried out in a one-pot reaction using 1 mol% of cobalt as the solo metal catalyst. The asymmetric variant of this reaction was also explored with *N*-oxazolinylphenyl 8-aminoquinoline (OPAQ, **L3**) as ligand, yielding chiral products with up to 86% ee. Notably, a phenomenon termed "ligand relay" was observed, in which the cobalt transitions from diphosphine ligand to an *NNN*-tridentate ligand during the reaction. This transition, confirmed by absorption measurements, highlights ligand relay as a potentially powerful strategy for metal-catalyzed sequential reactions involving a single metal catalyst.

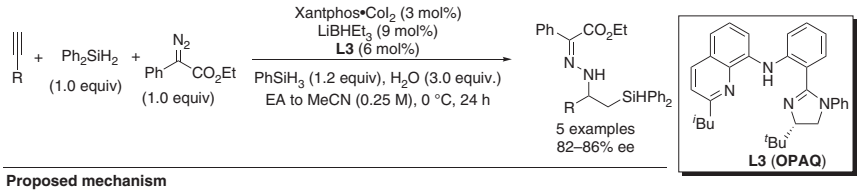


**Proposed mechanism**

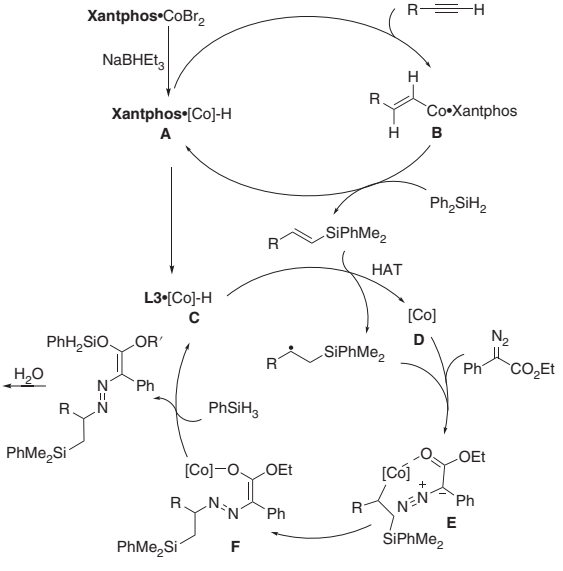


**Scheme 2.49** Ligand relay for Co-catalyzed sequential hydrosilylation and hydrohydrazidation of terminal alkynes.

## 2.4 Co-Catalyzed Asymmetric Radical Cross-Coupling Reactions

The Co-catalyzed radical cross-coupling reactions generally proceed via a proposed mechanism illustrated in Scheme 2.50. The Co(II) precatalyst is initially reduced by aryl or alkyl metal reagents, such as zinc reagents or Grignard reagents, to form the active catalytic species $L_nCo^m$, which initiates the reaction. This low-valent $L_nCo^m$ species then undergoes an SET with alkyl halides, generating a prochiral alkyl radical and forming the $L_nCo^{m+1}$ species. Subsequently, a TM occurs between the $L_nCo^{m+1}$ species and the organic metal reagent, leading to the formation of $L_n(R)Co^{m+1}$. This intermediate then recombines with the prochiral alkyl radical to produce the $L_nR_1RCo^{m+2}$ complex. Finally, an RE step furnishes the desired coupling product (R-$R^1$) while regenerating the active $L_nCo^m$ species, thus completing the catalytic cycle.

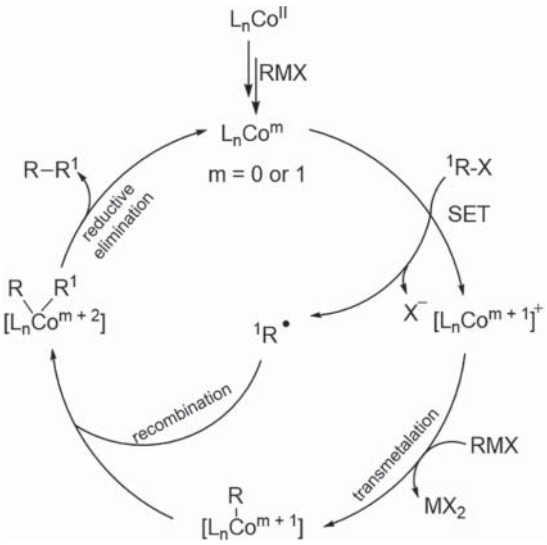


**Scheme 2.50** General catalytic cycle for Co-catalyzed radical cross-coupling reactions.

### 2.4.1 Asymmetric Kumada Cross-Coupling

Pioneered by Oshima and coworkers, Co-catalyzed radical-type Kumada cross-coupling has been successfully developed for the reactions between alkyl halides and various Grignard reagents. In 2002, the Oshima group explored the asymmetric Kumada cross-coupling [132, 133] between tertiary alkyl bromide compound and allylmagnesium chloride, utilizing a Co complex with a chiral bisphosphine ligand [$CoCl_2$((-)-chiraphos)]. Initial results demonstrated that while the reaction achieved significant enantioselectivity (ranging from 14% ee to 22% ee) at low temperatures, it was not yet satisfactory for broader application. Nonetheless, this study showcased the potential of cobalt-catalyzed asymmetric allylation, highlighting its novel utility in transition-metal-catalyzed radical reactions. In 2006, the same group [134] extended their work by using cobalt(II) chloride in combination with chiral diamine ligands for the cross-coupling of alkyl halides with arylmagnesium reagents. They observed notable enantioselectivity in the phenylation of cyclic halides, achieving up to 22% ee. These results emphasized the crucial role of ligand design in enhancing both reactivity and enantioselectivity, sparking increased research interest in the development of cobalt-catalyzed asymmetric radical transformations.

In 2014, Zhong, Bian, and coworkers developed the first Co-catalyzed highly enantioselective Kumada cross-coupling reaction using bisoxazoline ligand **L4**, achieving high yields and excellent enantioselectivities (Scheme 2.51) [135]. This method enabled the coupling of a wide range of readily available aryl Grignard reagents with 28 different α-bromo esters, producing α-arylated esters with high enantioselectivity in most cases. The reactions were readily scalable to gram quantities, and the cross-coupling products could be transformed into enantioenriched α-arylcarboxylic

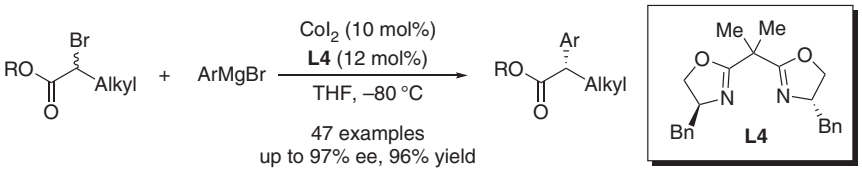


**Scheme 2.51** Co-catalyzed asymmetric Kumada cross-coupling of racemic α-bromo esters and aryl Grignard reagents.

acids and primary alcohols without compromising the ee. Additionally, this approach facilitates the synthesis of new enantioenriched α-arylpropionic esters and has potential applications in the development of nonsteroidal anti-inflammatory drugs (NSAIDs). This utility of this method was further demonstrated through its application in the asymmetric synthesis of (*S*)-fenoprofen (in 3 steps) and the total synthesis of (*S*)-*ar*-turmerone. The advantages of this system include the lower toxicity of cobalt compared to nickel and its lower cost relative to palladium. Moreover, the ability to use Grignard reagents with various α-bromo esters without the need for bulky OR groups enhances the method's practicality and broad applicability.

In 2016, the same group developed four new cyclopropane-based bisoxazoine ligands, featuring ethyl, isobutyl, sec-butyl, and phenylethyl substituents on the oxazoline ring. Among these, ligand **L5** exhibited exceptional performance in Co-catalyzed cross-coupling reactions between α-bromo esters and aryl Grignard reagents (Scheme 2.52) [136]. Specifically, the cross-coupling reaction between *p*-isobutylphenyl Grignard reagent and α-bromopropanoates successfully produced ibuprofen esters with high yields and good enantioselectivities. Following hydrolysis and recrystallization, they achieved the enantioselective synthesis of (*S*)-ibuprofen with an impressive 98% ee.

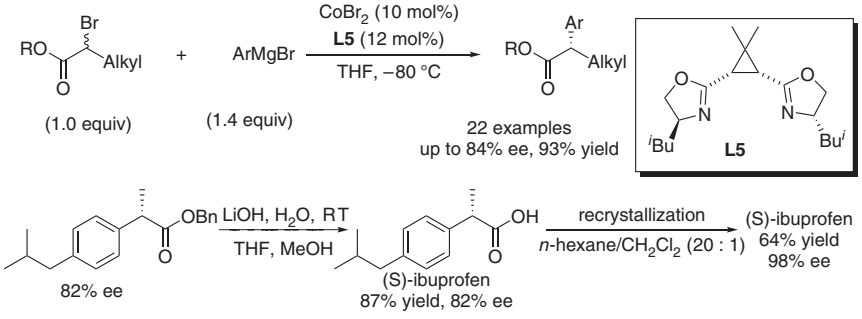


**Scheme 2.52** Co-catalyzed asymmetric Kumada cross-coupling of racemic α-bromo esters and aryl Grignard reagents with cyclopropane-based bisoxazoline ligands.

In 2020, the same group extended the scope of asymmetric Kumada cross-coupling reactions to include alkenyl Grignard reagents [137]. Using a cobalt complex with the chiral bisoxazoline ligand **L6**, they achieved good yields and high enantioselectivities in the reaction between isobutenyl magnesium bromide and various racemic α-bromo esters (Scheme 2.53). When other alkenyl Grignard reagents

were employed, even better enantioselectivity was observed using the biphenyl bisoxazoline ligand **L7**. The enantioselectivity was further enhanced by the addition of LiI, which is believed to stabilize the cobalt ate complex, thereby improving the reaction's stereoselectivity. This enantioselective Kumada alkenylation was successfully applied to the formal synthesis of the California red scale pheromone, and preliminary mechanistic investigations suggested the involvement of radical intermediates.

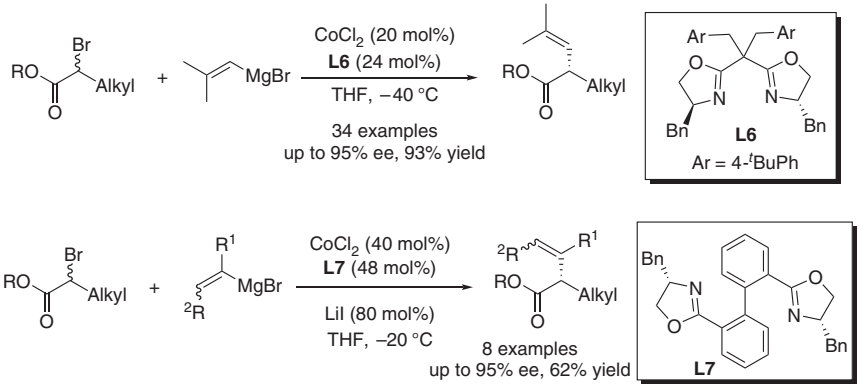


**Scheme 2.53** Co-catalyzed asymmetric Kumada cross-coupling of racemic α-bromo esters and alkenyl Grignard reagents.

### 2.4.2 Asymmetric Negishi Cross-Coupling

In 2018, Bian and coworkers developed the first cobalt-catalyzed enantioselective Negishi cross-coupling reaction and the first arylation of α-halo esters with arylzinc halides (Scheme 2.54) [138]. They employed cobalt complexes of bisoxazoline ligands as catalysts, with the 4-fluorobenzyl bisoxazoline ligand **L8** demonstrating excellent performance, achieving a 94% yield and 92% ee. Subsequently, the same group utilized this methodology for the synthesis of drug molecules, including (*R*)-cinacalcet [139] and (*S*)-preclamol [140].

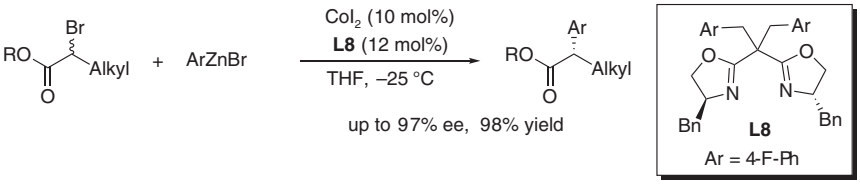


**Scheme 2.54** Co-catalyzed asymmetric Negishi cross-coupling of racemic α-bromo esters with arylzinc reagents.

In 2020, Shen and coworkers developed a cobalt-catalyzed asymmetric cross-coupling reaction of α-bromo-α-fluorotoluene derivatives with various aryl zincates, which were generated in situ from lithium aryl *n*-butyl pinacol boronates

and $ZnBr_2$ under mild conditions. This method provides a versatile, efficient, and convenient approach for the rapid access of optically pure α-fluorinated diarylmethane derivatives (Scheme 2.55) [141]. The key to the success of this reaction was the use of the bisoxazoline ligand **L9**, featuring a steric hindered diphenylmethyl substituent. This approach, which offers advantages over nickel catalysis in certain aspects, significantly expands the toolkit for cobalt-catalyzed asymmetric cross-coupling reactions of secondary alkyl halides.

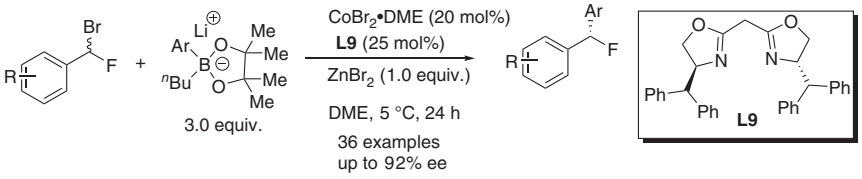


**Scheme 2.55** Co-catalyzed asymmetric Negishi cross-coupling of fluorinated secondary benzyl bromide and lithium aryl boronates/$ZnBr_2$.

In 2021, Liu and coworkers developed a cobalt-catalyzed enantioconvergent radical Negishi $C(sp^3)$—$C(sp^2)$ cross-coupling of racemic benzyl chlorides, enabling access to enantioenriched 1,1-diarylmethanes with good yields and moderate enantioselectivities (Scheme 2.56) [142]. A key factor in this success was the innovative use of a chiral multidentate anionic *N,N,P*-ligand **L10**, which was employed to fine-tune the chiral environment of the cobalt catalyst, allowing for enantiocontrol over the highly reactive prochiral alkyl radical species. This development represents a significant complement to the existing Co/chiral bisoxazoline catalysis and opens new avenues for cobalt-catalyzed enantioconvergent cross-coupling reactions.

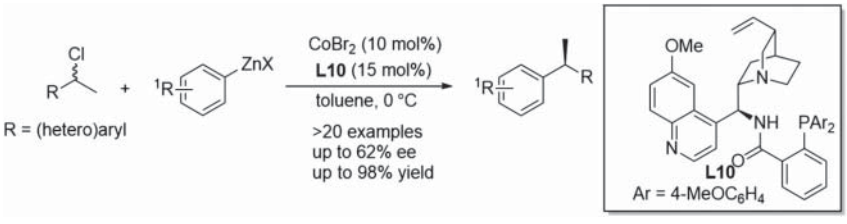


**Scheme 2.56** Co-catalyzed enantioconvergent radical Negishi cross-coupling with chiral multidentate *N,N,P*-ligand.

In 2023, Lu and coworkers developed a general method for cobalt-catalyzed enantioconvergent cross-coupling of α-bromoketones with aryl zinc reagents (Scheme 2.57), enabling the synthesis of chiral ketones containing α-tertiary stereogenic centers with high enantioselectivities [143]. A critical factor in the success was the introduction of chiral unsymmetric *N,N,N*-tridentate ligands **L11**, which enhanced both reactivity and selectivity. Detailed mechanistic studies indicate that the process is radical in nature, involving a Co(I) complex as the active catalytic species.

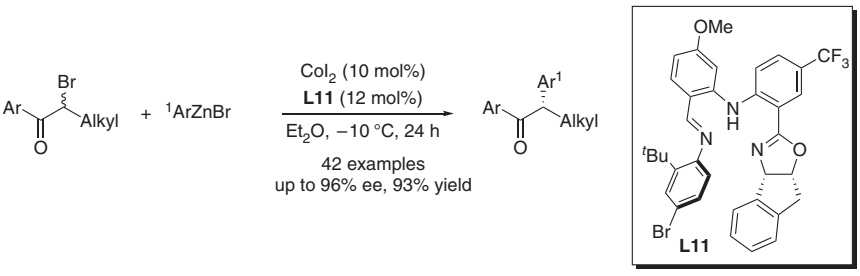


**Scheme 2.57** Co-catalyzed enantioconvergent radical Negishi cross-coupling with α-bromoketones.

### 2.4.3 Miscellaneous

In 2021, Fu and coworkers reported a [Co(**L12**)]-catalyzed enantioselective C($sp^3$)—C($sp^3$) coupling reaction between readily available fluoroalkenes and alkyl halides (Scheme 2.58) [144]. This reaction facilitates the streamlined synthesis of chiral fluoroalkanes by introducing an aliphatic C—F stereogenic center at a desired position within an alkyl chain. The reaction demonstrates catalyst-controlled enantioselectivity, eliminating the need for traditional directing or auxiliary groups. Preliminary mechanistic studies suggest that hydrometalation is both the turnover-limiting and stereodetermining step. This cobalt catalytic system inspired the exploration of additional asymmetric coupling reactions.

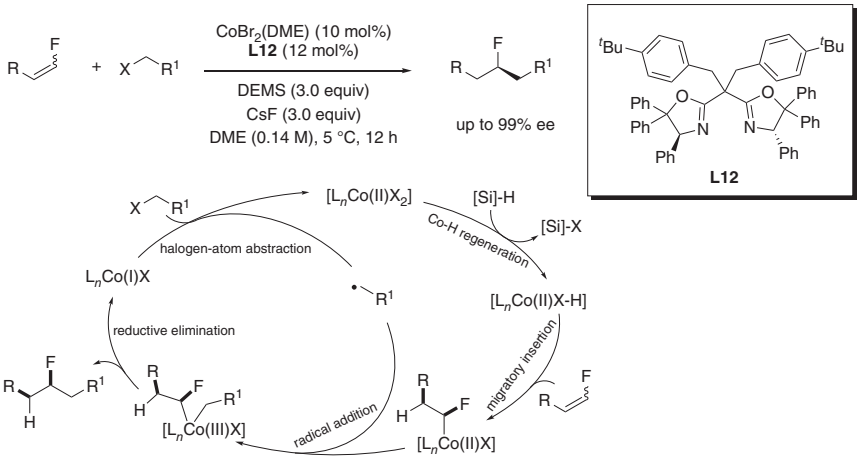


**Scheme 2.58** Co-catalyzed enantioselective C($sp^3$)—C($sp^3$) coupling.

In 2023, the Fu group extended their research to include facial-selective cyclopropene hydroalkylation using a low-valent CoH-catalytic system with **L13** as supporting ligand (Scheme 2.59) [145]. Based on relevant literature and mechanistic experiments, they proposed a reaction mechanism as outlined in Scheme 2.59. The [Co$^I$H] species (**B**) is generated from the reaction between [Co$^I$X] (**A**) with

DEMS in the presence of CsF. The [$Co^{I}H$] (**B**) then inserts into the cyclopropane, forming a cyclopropyl cobalt species (**C**). The [$Co^{I}$]-alkyl species (**C**) subsequently reacts with an alkyl halide, producing an alkyl radical and a [$Co^{II}$]-alkyl species (**D**). The [$Co^{II}$]-alkyl species (**D**) captures the alkyl radical to form the [$Co^{III}$]-alkyl species (**E**). Finally, RE from **E** yields the desired product and regenerates the initial catalyst **A**. The syn-hydrometalation of [$Co^{I}$-H] across the cyclopropene substrate is proposed to be the stereodetermining step; however, an alternative pathway involving [$Co^{II}H$] insertion should not be completely overlooked.

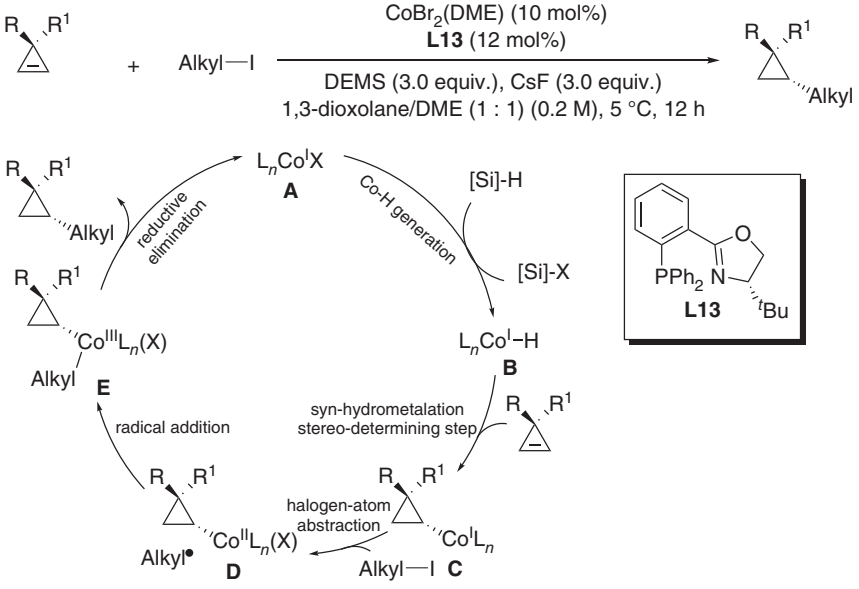


**Scheme 2.59** Co-catalyzed facial-selective hydroalkylation of cyclopropenes.

In 2024, the same group described a ligand-controlled cobalt-hydride-catalyzed regio-, enantio-, and diastereoselective oxyheterocyclic alkene hydroalkylation (with **L14** and **L15** as ligands) (Scheme 2.60) [146]. This methodology differs from previous approaches that required chelation-directing groups to form five- or six-membered metallacycles or involved activated alkenes with conjugated functional groups. The developed method enables the synthesis of $C_2$- or $C_3$-alkylated tetrahydrofurans and tetrahydropyrans with good regio- and enantioselectivities, utilizing both conjugated and unconjugated oxyheterocyclic alkenes. Specifically, the hydroalkylation of C2-substituted 2,5-dihydrofuran facilitates the simultaneous construction of 1,3-distereocenters, providing an innovative synthetic route to tetrahydrofuran skeleton compounds featuring multiple chiral centers. Notably, this reaction exhibits a broad substrate scope and good functional group tolerance, making it suitable for the postmodification of diverse drug molecules and natural products, thereby expanding the library of lead compounds for pharmaceutical chemistry. Mechanistic studies and preliminary DFT calculations indicate the critical roles of

both the ligands and substrate oxygen atoms in controlling stereoselectivity. The RE step is identified as the rate-determining step, while alkene hydrometalation serves as the stereodetermining step. This cobalt-hydride-catalyzed cross-coupling reaction may inspire further exploration of noncanonical auxiliary groups, offering insights into the reactivity and selectivity of cobalt catalysts. Preliminary results, including enantioselectivity control in the hydroalkylation of norbornene and 2,5-norbornadiene, reinforce confidence in this cobalt-hydride catalytic system's ability to achieve enantioselectivity without relying on auxiliary groups.

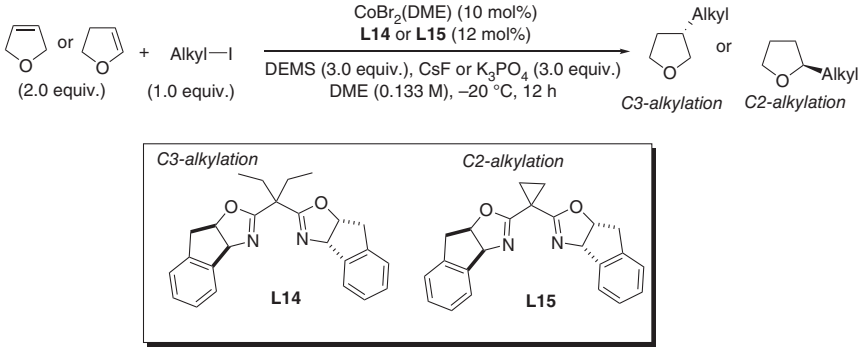


**Scheme 2.60** Ligand-controlled Co-catalyzed regio-, enantio-, and diastereoselective oxyheterocyclic alkene hydroalkylation.

In 2023, Zhao and coworkers developed a cobalt-catalyzed remote borylation of alkyl (pseudo)halides (alkyl-X, where X = I, Br, Cl, OTs) using pinacolborane (HBPin) (Scheme 2.61). This method presents a robust approach for generating valuable chiral secondary organoboronates from racemic alkyl halides by employing Co(salen) as the precatalyst along with chiral *N,N,N*-tridentate ligand **L16** [147]. Preliminary mechanistic studies suggested that a radical reaction pathway is involved, and further research will focus on achieving a detailed understanding of the reaction mechanism.

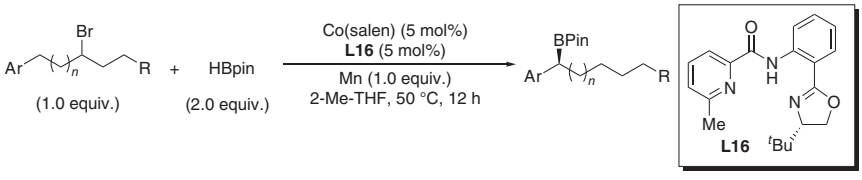


**Scheme 2.61** Co-catalyzed asymmetric remote borylation of alkyl halides.

## 2.5 Summary and Outlook

The advancement of [Co(Por)]-based MRC has facilitated the synthesis of chiral molecules, with potential applications in pharmaceutical synthesis. Significant

achievements have been made in the cyclopropanation of olefins using a wide array of diazo compounds, particularly for constructing chiral cyclopropane scaffolds. However, further development is needed in employing donor/donor- and donor/acceptor-substituted diazo compounds, which remain underexplored in [Co(Por)]-based systems. For intramolecular C—H alkylation, [Co(Por)]-based MRC has shown promise in constructing chiral five- and four-membered rings. Yet, the synthesis of larger ring structures via C—H alkylation still requires further development, as does the establishment of intermolecular C—H alkylation methods for C—C bond formation. In asymmetric aziridination and radical heterobicyclization, advancements have been made in synthesizing *N*-heterocyclic compounds, though with limited applications to complex targets. Expanding this methodology to a broader range of structurally intricate molecules could open new pathways in synthetic chemistry. Intramolecular 1,5- and 1,6-C—H aminations have been effectively established, and significant progress has been made in intermolecular C—H amination, particularly with benzylic and allylic substrates. However, intermolecular C—H amination involving nonactivated substrates remains an unchartered area, presenting a promising opportunity for future research. Additionally, Co(III)(H)-mediated MHAT has been applied to the hydrofunctionalization of alkenes with various nucleophiles, including N-, O-, and C-based species, using silanes and oxidants. The recent hydrothiolation of alkenes developed by the Zhong and Wu groups exemplifies the potential of this approach, though enantioselectivity has yet to be achieved [148]. Expanding these methodologies to incorporate additional nucleophiles could significantly advance the field. Moreover, Co-catalyzed radical cross-coupling reactions of metal reagents and electrophiles have been demonstrated in a limited scope, highlighting the need to broaden the substrate range and enhance functional group tolerance. Developing new supporting ligands tailored to expand the scope of Co-catalyzed radical transformations presents a promising direction for advancing this field. In this regard, ligand design will be central to unlocking broader reactivity, enhancing stereocontrol, and enabling the efficient synthesis of diverse chiral molecules.

## Acknowledgments

We are grateful for financial support by the National Institutes of Health (R01-GM132471 and R01-GM102554) and in part by the National Science Foundation (CHE-2154885).

## References

**1** Zhang, G. and Zhang, Q. (2023). *Chem Catal.* 3: 100526.

**2** Yoshikai, N. (2022). Cobalt-catalyzed asymmetric C-H functionalization. In *Handbook of CH-Functionalization* (ed. D. Maiti), 1–19. Wiley.

3 X. Wang, X. Peter Zhang, Catalytic radical approach for selective carbene transfers via cobalt(II)-based metalloradical catalysis. In *Transition Metal-Catalyzed Carbene Transformations*, J. Wang, C.-M. Che, M. P. Doyle, Eds. Wiley: 2022; pp 25–66.

4 Yin, Y.-N., Ouyang, D.-C., Wang, J.-J., and Zhu, R. (2020). *Sci. Sin. Chim.* 50: 1217–1232.

5 Guérinot, A. and Cossy, J. (2020). *Acc. Chem. Res.* 53: 1351–1363.

6 Wang, K. and Kong, W. (2018). *Chin. J. Chem.* 36: 247–256.

7 Pellissier, H. and Clavier, H. (2014). *Chem. Rev.* 114: 2775–2823.

8 Lee, W.-C.C. and Zhang, X.P. (2022). *Trends Chem.* 4: 850–851.

9 Zhang, X.P. and Cui, X. (2014). *Asymmetric C-H Functionalization by Transition Metal-Catalyzed Carbene Transfer Reactions*, 86. Elsevier B.V.

10 Wang, D.-S. and Zhang, X.P. (2024). *Comprehensive Chirality*, 2e (ed. J. Cossy), 158–179. Oxford: Academic Press.

11 Jiang, H. and Zhang, X.P. (2012). *Comprehensive Chirality* (ed. E.M. Carreira and H. Yamamoto), 168–182. Elsevier B.V.

12 Lu, H. and Zhang, X.P. (2011). *Chem. Soc. Rev.* 40: 1899–1909.

13 Shevick, S.L., Wilson, C.V., Kotesova, S. et al. (2020). *Chem. Sci.* 11: 12401–12422.

14 Huo, H., Shen, X., Wang, C. et al. (2014). *Nature* 515: 100.

15 Hashimoto, T., Kawamata, Y., and Maruoka, K. (2014). *Nat. Chem.* 6: 702–705.

16 Kainz, Q.M., Matier, C.D., Bartoszewicz, A. et al. (2016). *Science* 351: 681.

17 Lin, J.-S., Dong, X.-Y., Li, T.-T. et al. (2016). *J. Am. Chem. Soc.* 138: 9357–9360.

18 Zhang, W., Wang, F., McCann, S.D. et al. (2016). *Science* 353: 1014–1018.

19 Kern, N., Plesniak, M.P., McDouall, J.J.W., and Procter, D.J. (2017). *Nat. Chem.* 9: 1198–1204.

20 Proctor, R.S.J., Davis, H.J., and Phipps, R.J. (2018). *Science* 360: 419–422.

21 Li, J., Zhang, Z., Wu, L. et al. (2019). *Nature* 574: 516–521.

22 Nakafuku, K.M., Zhang, Z., Wappes, E.A. et al. (2020). *Nat. Chem.* 12: 697.

23 Chen, J.-J., Fang, J.-H., Du, X.-Y. et al. (2023). *Nature* 618: 294–300.

24 Lee, W.-C.C. and Zhang, X.P. (2024). *Angew. Chem. Int. Ed.* 63: e202320243.

25 Lee, W.-C.C., Wang, D.-S., Zhu, Y., and Zhang, X.P. (2023). *Nat. Chem.* 15: 1569–1580.

26 Agasti, S., Beltran, F., Pye, E. et al. (2023). *Nat. Chem.* 15: 535–541.

27 Das, S., Ehlers, A.W., Patra, S. et al. (2023). *J. Am. Chem. Soc.* 145: 14599–14607.

28 Smith, D.M., Pulling, M.E., and Norton, J.R. (2007). *J. Am. Chem. Soc.* 129: 770–771.

29 Kapat, A., Sperger, T., Guven, S., and Schoenebeck, F. (2019). *Science* 363: 391–396.

30 Mendel, M., Karl, T.M., Hamm, J. et al. (2024). *Nature* 631: 80–86.

31 Kuo, J.L., Hartung, J., Han, A., and Norton, J.R. (2015). *J. Am. Chem. Soc.* 137: 1036–1039.

32 Demarteau, J., Debuigne, A., and Detrembleur, C. (2019). *Chem. Rev.* 119: 6906.

**33** Huang, H.-M., Garduño-Castro, M.H., Morrill, C., and Procter, D.J. (2019). *Chem. Soc. Rev.* 48: 4626–4638.

**34** Zhang, X.-X. and Wayland, B.B. (1994). *J. Am. Chem. Soc.* 116: 7897.

**35** Gansäuer, A., Hildebrandt, S., Michelmann, A. et al. (2015). *Angew. Chem. Int. Ed.* 54: 7003.

**36** Roy, S., Khatua, H., Das, S.K., and Chattopadhyay, B. (2019). *Angew. Chem. Int. Ed.* 58: 11439.

**37** Intrieri, D., Carminati, D.M., and Gallo, E. (2016). *Dalton Trans.* 45: 15746.

**38** Belof, J.L., Cioce, C.R., Xu, X. et al. (2011). *Organometallics* 30: 2739–2746.

**39** Lu, H., Dzik, W.I., Xu, X. et al. (2011). *J. Am. Chem. Soc.* 133: 8518–8521.

**40** Lyaskovskyy, V., Suarez, A.I.O., Lu, H. et al. (2011). *J. Am. Chem. Soc.* 133: 12264–12273.

**41** Olivos Suarez, A.I., Jiang, H., Zhang, X.P., and de Bruin, B. (2011). *Dalton Trans.* 40: 5697–5705.

**42** Goswami, M., Lyaskovskyy, V., Domingos, S.R. et al. (2015). *J. Am. Chem. Soc.* 137: 5468–5479.

**43** Dzik, W.I., Xu, X., Zhang, X.P. et al. (2010). *J. Am. Chem. Soc.* 132: 10891–10902.

**44** Dzik, W.I., Zhang, X.P., and de Bruin, B. (2011). *Inorg. Chem.* 50: 9896–9903.

**45** Wang, Y., Wen, X., Cui, X., and Zhang, X.P. (2018). *J. Am. Chem. Soc.* 140: 4792–4796.

**46** Wen, X., Wang, Y., and Zhang, X.P. (2018). *Chem. Sci.* 9: 5082–5086.

**47** Hu, Y., Lang, K., Li, C. et al. (2019). *J. Am. Chem. Soc.* 141: 18160–18169.

**48** Lang, K., Torker, S., Wojtas, L., and Zhang, X.P. (2019). *J. Am. Chem. Soc.* 141: 12388–12396.

**49** Jin, L.-M., Xu, P., Xie, J., and Zhang, X.P. (2020). *J. Am. Chem. Soc.* 142: 20828–20836.

**50** Lang, K., Li, C., Kim, I., and Zhang, X.P. (2020). *J. Am. Chem. Soc.* 142: 20902–20911.

**51** Lee, W.-C.C., Wang, D.-S., Zhang, C. et al. (2021). *Chem* 7: 1588–1601.

**52** Riart-Ferrer, X., Sang, P., Tao, J. et al. (2021). *Chem* 7: 1120–1134.

**53** Xie, J., Xu, P., Zhu, Y. et al. (2021). *J. Am. Chem. Soc.* 143: 11670–11678.

**54** Zhang, C., Wang, D.-S., Lee, W.-C.C. et al. (2021). *J. Am. Chem. Soc.* 143: 11130–11140.

**55** Ke, J., Lee, W.-C.C., Wang, X. et al. (2022). *J. Am. Chem. Soc.* 144: 2368–2378.

**56** Lang, K., Hu, Y., Lee, W.-C.C., and Zhang, X.P. (2022). *Nat. Synth.* 1: 548–557.

**57** Wang, J., Xie, J., Cindy Lee, W.-C. et al. (2022). *Chem Catal.* 2: 330–344.

**58** Lee, W.-C.C., Wang, J., Zhu, Y., and Zhang, X.P. (2023). *J. Am. Chem. Soc.* 145: 11622–11632.

**59** Xu, H., Wang, D.-S., Zhu, Z. et al. (2024). *Chem* 10: 283–298.

**60** Xu, P., Xie, J., Wang, D.-S., and Zhang, X.P. (2023). *Nat. Chem.* 15: 498–507.

**61** Wang, X., Ke, J., Zhu, Y. et al. (2021). *J. Am. Chem. Soc.* 143: 11121–11129.

**62** Penoni, A., Wanke, R., Tollari, S. et al. (2003). *Eur. J. Inorg. Chem.* 2003: 1452–1460.

**63** Huang, L., Chen, Y., Gao, G.-Y., and Zhang, X.P. (2003). *J. Organomet. Chem.* 68: 8179–8184.

**64** Chen, Y., Fields, K.B., and Zhang, X.P. (2004). *J. Am. Chem. Soc.* 126: 14718–14719.

**65** Chen, Y. and Zhang, X.P. (2006). *Synthesis* 2006: 1697–1700.

**66** Chen, Y., Gao, G.-Y., and Peter Zhang, X. (2005). *Tetrahedron Lett.* 46: 4965–4969.

**67** Chen, Y. and Zhang, X.P. (2004). *J. Organomet. Chem.* 69: 2431–2435.

**68** Chen, Y. and Zhang, X.P. (2007). *J. Organomet. Chem.* 72: 5931–5934.

**69** Chen, Y., Ruppel, J.V., and Zhang, X.P. (2007). *J. Am. Chem. Soc.* 129: 12074–12075.

**70** Ruppel, J.V., Gauthier, T.J., Snyder, N.L. et al. (2009). *Org. Lett.* 11: 2273–2276.

**71** Fantauzzi, S., Gallo, E., Rose, E. et al. (2008). *Organometallics* 27: 6143.

**72** Hu, Y., Lang, K., Tao, J. et al. (2019). *Angew. Chem. Int. Ed.* 58: 2670–2674.

**73** Zhu, S., Perman, J.A., and Zhang, X.P. (2008). *Angew. Chem. Int. Ed.* 47: 8460–8463.

**74** Zhu, S., Xu, X., Perman, J.A., and Zhang, X.P. (2010). *J. Am. Chem. Soc.* 132: 12796.

**75** Xu, X., Zhu, S., Cui, X. et al. (2013). *Angew. Chem. Int. Ed.* 52: 11857.

**76** Xu, X., Wang, Y., Cui, X. et al. (2017). *Chem. Sci.* 8: 4347–4351.

**77** Ruppel, J.V., Cui, X., Xu, X., and Zhang, X.P. (2014). *Org. Chem. Front.* 1: 515–520.

**78** Zhu, S., Ruppel, J.V., Lu, H. et al. (2008). *J. Am. Chem. Soc.* 130: 5042.

**79** Zhu, S., Cui, X., and Zhang, X.P. (2012). *Eur. J. Inorg. Chem.* 2012: 430–434.

**80** Xu, X., Lu, H.J., Ruppel, J.V. et al. (2011). *J. Am. Chem. Soc.* 133: 15292.

**81** Xia, Y. and Wang, J. (2017). *Chem. Soc. Rev.* 46: 2306.

**82** Wang, Y., Wen, X., Cui, X. et al. (2017). *J. Am. Chem. Soc.* 139: 1049.

**83** Roy, S., Das, S.K., and Chattopadhyay, B. (2018). *Angew. Chem. Int. Ed.* 57: 2238.

**84** Wencel-Delord, J., Dröge, T., Liu, F., and Glorius, F. (2011). *Chem. Soc. Rev.* 40: 4740.

**85** Newton, C.G., Wang, S.-G., Oliveira, C.C., and Cramer, N. (2017). *Chem. Rev.* 117: 8908.

**86** Wang, C.-S., Dixneuf, P.H., and Soulé, J.-F. (2018). *Chem. Rev.* 118: 7532.

**87** Giri, R., Shi, B.-F., Engle, K.M. et al. (2009). *Chem. Soc. Rev.* 38: 3242.

**88** Xue, X.-S., Ji, P., Zhou, B., and Cheng, J.-P. (2017). *Chem. Rev.* 117: 8622.

**89** Chan, W.-W., Lo, S.-F., Zhou, Z., and Yu, W.-Y. (2012). *J. Am. Chem. Soc.* 134: 13565.

**90** Díaz-Requejo, M.M., Belderraín, T.R., Nicasio, M.C. et al. (2002). *J. Am. Chem. Soc.* 124: 896.

**91** Choi, M.K.-W., Yu, W.-Y., and Che, C.-M. (2005). *Org. Lett.* 7: 1081.

**92** Li, Y., Huang, J.-S., Zhou, Z.-Y. et al. (2002). *J. Am. Chem. Soc.* 124: 13185–13193.

**93** Cui, X., Xu, X., Jin, L.-M. et al. (2015). *Chem. Sci.* 6: 1219–1224.

**94** Zhou, M., Lankelma, M., van der Vlugt, J.I., and de Bruin, B. (2020). *Angew. Chem. Int. Ed.* 59: 11073–11079.

**95** Epping, R.F.J., Vesseur, D., Zhou, M., and de Bruin, B. (2023). *ACS Catal.* 13: 5428–5448.

**96** Cui, X., Xu, X., Lu, H. et al. (2011). *J. Am. Chem. Soc.* 133: 3304–3307.

**97** Gao, G.-Y., Jones, J.E., Vyas, R. et al. (2006). *J. Organomet. Chem.* 71: 6655–6658.

**98** Jones, J.E., Ruppel, J.V., Gao, G.-Y. et al. (2008). *J. Organomet. Chem.* 73: 7260–7265.

**99** Ruppel, J.V., Jones, J.E., Huff, C.A. et al. (2008). *Org. Lett.* 10: 1995–1998.

**100** Subbarayan, V., Ruppel, J.V., Zhu, S. et al. (2009). *Chem. Commun.* 28: 4266–4268.

**101** Jin, L.-M., Xu, X., Lu, H. et al. (2013). *Angew. Chem. Int. Ed.* 52: 5309–5313.

**102** Tao, J., Jin, L.-M., and Zhang, X.P. (2014). *Beilstein J. Org. Chem.* 10: 1282.

**103** Subbarayan, V., Jin, L.-M., Cui, X., and Zhang, X.P. (2015). *Tetrahedron Lett.* 56: 3431–3434.

**104** Jiang, H., Lang, K., Lu, H. et al. (2016). *Angew. Chem. Int. Ed.* 55: 11604–11608.

**105** Jiang, H., Lang, K., Lu, H. et al. (2017). *J. Am. Chem. Soc.* 139: 9164–9167.

**106** Caselli, A., Gallo, E., Ragaini, F. et al. (2006). *Inorg. Chim. Acta* 359: 2924–2932.

**107** Lu, H., Tao, J., Jones, J.E. et al. (2010). *Org. Lett.* 12: 1248–1251.

**108** Cenini, S., Gallo, E., Penoni, A. et al. (2000). *Chem. Commun.* 22: 2265–2266.

**109** Ragaini, F., Penoni, A., Gallo, E. et al. (2003). *Chem. Eur. J.* 9: 249–259.

**110** Fantauzzi, S., Gallo, E., Caselli, A. et al. (2005). *Organometallics* 24: 4710–4713.

**111** Smith, P.A.S. (1946). *Org. React.* 3: 337–449.

**112** Müller, P. and Fruit, C. (2003). *Chem. Rev.* 103: 2905–2920.

**113** Pellissier, H. (2010). *Tetrahedron* 66: 1509–1555.

**114** Degennaro, L., Trinchera, P., and Luisi, R. (2014). *Chem. Rev.* 114: 7881–7929.

**115** Li, C., Lang, K., Lu, H. et al. (2018). *Angew. Chem. Int. Ed.* 57: 16837–16841.

**116** Kuijpers, P.F., Tiekink, M.J., Breukelaar, W.B. et al. (2017). *Chem. Eur. J.* 23: 7945–7952.

**117** Shigehisa, H., Aoki, T., Yamaguchi, S. et al. (2013). *J. Am. Chem. Soc.* 135: 10306–10309.

**118** Shigehisa, H., Hayashi, M., Ohkawa, H. et al. (2016). *J. Am. Chem. Soc.* 138: 10597–10604.

**119** Discolo, C.A., Touney, E.E., and Pronin, S.V. (2019). *J. Am. Chem. Soc.* 141: 17527–17532.

**120** Ebisawa, K., Izumi, K., Ooka, Y. et al. (2020). *J. Am. Chem. Soc.* 142: 13481–13490.

**121** Zhou, X.-L., Yang, F., Sun, H.-L. et al. (2019). *J. Am. Chem. Soc.* 141: 7250–7255.

**122** Yang, F., Nie, Y.-C., Liu, H.-Y. et al. (2022). *ACS Catal.* 12: 2132–2137.

**123** Park, S.H., Jang, J., Shin, K., and Kim, H. (2022). *ACS Catal.* 12: 10572–10580.

**124** Yahata, K., Kaneko, Y., and Akai, S. (2020). *Org. Lett.* 22: 598–603.

**125** Yahata, K., Kaneko, Y., and Akai, S. (2020). *Chem. Pharm. Bull.* 68: 332–335.

**126** Qin, T., Lv, G., Meng, Q. et al. (2021). *Angew. Chem. Int. Ed.* 60: 25949–25957.

**127** Miao, H., Guan, M., Xiong, T. et al. (2023). *Angew. Chem. Int. Ed.* 62: e202213913.
**128** Qin, T., Lv, G., Miao, H. et al. (2022). *Angew. Chem. Int. Ed.* 61: e202201967.
**129** Song, L., Fu, N., Ernst, B.G. et al. (2020). *Nat. Chem.* 12: 747–754.
**130** Shen, X., Chen, X., Chen, J. et al. (2020). *Nat. Commun.* 11: 783.
**131** Sun, Y., Guo, J., Shen, X., and Lu, Z. (2022). *Nat. Commun.* 13: 650.
**132** Tsuji, T., Yorimitsu, H., and Oshima, K. (2002). *Angew. Chem. Int. Ed.* 41: 4137–4139.
**133** Ohmiya, H., Tsuji, T., Yorimitsu, H., and Oshima, K. (2004). *Chem. Eur. J.* 10: 5640–5648.
**134** Ohmiya, H., Yorimitsu, H., and Oshima, K. (2006). *J. Am. Chem. Soc.* 128: 1886–1889.
**135** Mao, J., Liu, F., Wang, M. et al. (2014). *J. Am. Chem. Soc.* 136: 17662–17668.
**136** Liu, F., Bian, Q., Mao, J. et al. (2016). *Tetrahedron Asymmetry* 27: 663–669.
**137** Zhou, Y., Wang, L., Yuan, G. et al. (2020). *Org. Lett.* 22: 4532–4536.
**138** Liu, F., Zhong, J., Zhou, Y. et al. (2018). *Chem. Eur. J.* 24: 2059–2064.
**139** Sun, X., Wang, X., Liu, F. et al. (2019). *Chirality* 31: 682–687.
**140** Zhou, Y., Liu, C., Wang, L. et al. (2019). *Synlett* 30: 860–862.
**141** Huang, W., Wan, X., and Shen, Q. (2020). *Org. Lett.* 22: 4327–4332.
**142** Li, Z., Cheng, X.-Y., Yang, N.-Y. et al. (2021). *Organometallics* 40: 2215–2219.
**143** Wang, J., Shen, X., Chen, X. et al. (2023). *J. Am. Chem. Soc.* 145: 24958–24964.
**144** Li, Y., Nie, W., Chang, Z. et al. (2021). *Nat. Catal.* 4: 901–911.
**145** Zhang, Z.-L., Li, Z., Xu, Y.-T. et al. (2023). *Angew. Chem. Int. Ed.* 62: e202306381.
**146** Li, Z., Liu, B., Yao, C.-Y. et al. (2024). *J. Am. Chem. Soc.* 146: 3405–3415.
**147** Zhang, M., Ye, Z., and Zhao, W. (2023). *Angew. Chem. Int. Ed.* 62: e202306248.
**148** Zhang, R.-J., Li, X.-R., Liang, R.-B. et al. (2024). *Org. Lett.* 26: 591–596.

# 3

# Nickel-Catalyzed Electrophile–Nucleophile and Related Asymmetric Radical Cross-Coupling

*Yate Chen and Wangqing Kong*

*The Institute for Advanced Studies, Wuhan University, Wuhan, China*

## 3.1 Introduction

Transition-metal-catalyzed cross-couplings, which canonically refer to the coupling of organic electrophiles to organometallic reagents, open new paradigms and redefine synthetic strategies for preparing enantiomerically enriched molecules. It is generally accepted that the main obstacle to metal-catalyzed cross-coupling of alkyl electrophiles is the facile β-hydride elimination of the alkyl-metal intermediate generated by oxidative addition. Palladium is the most commonly used catalyst in cross-coupling reactions, and the β-hydride elimination of alkyl-Pd(II) is usually very rapid [1, 2]. Although Pd-catalyzed cross-couplings of organometallic nucleophiles with unactivated alkyl electrophiles containing β-hydrogens have been successfully achieved, they have been limited to primary alkyl electrophiles [3–5]. Mechanistic studies reveal that oxidative addition to the C—X bond in the Pd-catalyzed cross-coupling proceeds via an $S_N2$ rather than a radical pathway.

In contrast, nickel is a sustainable, low-cost, and abundant element that undergoes facile oxidative addition due to its smaller size, allowing the use of much less reactive electrophiles in cross-coupling reactions [1, 2]. Furthermore, the β-H elimination of nickel tends to be slower than that of palladium because the activation barrier for β-H elimination in the nickel system is significantly higher than that of the corresponding palladium species [6]. In addition, nickel readily accesses multiple oxidation states. The Ni(0)/Ni(II) catalytic cycle is widespread, and the accessibility of Ni(I) and Ni(III) oxidation states allows for distinct reaction modes and radical mechanisms [7–10].

This chapter discusses advances in nickel-catalyzed electrophile–nucleophile and related asymmetric radical cross-couplings, highlighting the chirality control modes of various coupling partners as well as newly developed radical precursors.

## 3.2 Asymmetric Cross-Coupling of Organohalides with Organometallic Reagents

### 3.2.1 Cross-Coupling of Organohalides with Aryl and Primary Alkylzinc Reagents

Organozinc reagents are readily prepared by the oxidative addition of zinc to alkyl, allyl, or benzyl halides, or by transmetalation reactions. They are less reactive than many other analogous organometallic reagents, such as organolithium and Grignard reagents. Transition-metal-catalyzed cross-coupling of organohalides with organozinc reagents (Negishi coupling) has been widely used in organic synthesis as a powerful tool for C—C bond formation. Nickel-catalyzed Negishi coupling can be operated under diverse mechanisms depending on the coupling partners, allowing the coupling of $sp^3$, $sp^2$, and sp carbon atoms, opening a new reaction mode and redefining synthetic strategies for the preparation of enantioenriched molecules.

The first efficient catalytic enantioselective cross-coupling of secondary alkyl electrophiles with organozinc reagents was developed by Fu and coworkers in 2005 [11]. In the presence of (*i*-Pr)-PyBox **L1**, the cross-coupling of racemic α-bromoamide **1** with primary organozinc reagents tolerates a range of functional groups, providing the desired products **2** in good yields and high enantioselectivities (Scheme 3.1).

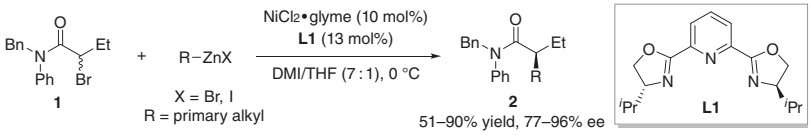


**Scheme 3.1** Enantioselective cross-coupling of α-bromoamides with primary organozinc reagents.

Although the catalytic asymmetric α-functionalization of amides has been described, α-aryl ketones tend to enolize under basic conditions, and the α-functionalization of amides cannot be applied to the asymmetric synthesis of α-aryl ketones. Fu's group further established a nickel/PyBox-catalyzed enantioselective cross-coupling of racemic α-bromoketones **3** with arylzinc reagents to access α-aryl ketones **4** with good yields and enantiomeric excess (ee) values (Scheme 3.2) [12]. This stereoconvergent C—C bond formation occurs at –30 °C

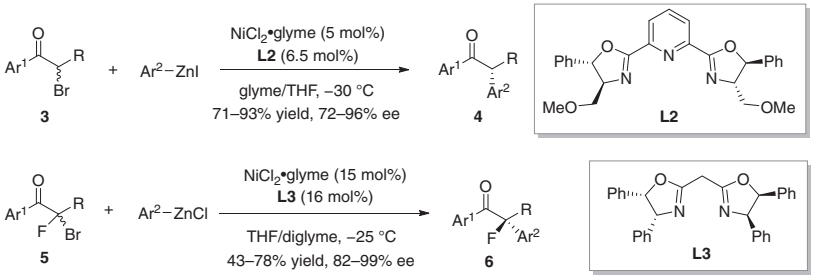


**Scheme 3.2** Enantioselective cross-coupling of α-bromoketones with arylzinc reagents.

in the absence of an activating agent, allowing the generation of potentially labile tertiary stereocenters.

The same reaction conditions (PyBox **L2**) for the asymmetric α-arylation of α-halo-α-fluoro ketones **5** did not work well in the construction of tertiary α-fluorinated ketones. The Box ligand **L3** was demonstrated to be effective in the selective reaction of a C—Br (or C—Cl) bond in the presence of a C—F bond, providing high-value-added chiral tertiary alkyl fluorides **6** with excellent enantioselectivity. This method for the selective cross-coupling of geminal dihalide electrophiles is not limited to α-bromo-α-fluoroketones; racemic α-chloro-α-fluoroketones are also compatible (Scheme 3.2) [13].

The incorporation of a trifluoromethyl ($CF_3$) group into organic molecules results in dramatic changes in properties, including biological activity, compared to non-fluorinated compounds. Fu and coworkers achieved enantioconvergent cross-coupling of arylzinc reagents with $CF_3$-substituted racemic secondary alkyl halides **7** using the Ni/(Ph)-Box (**L4**) catalytic system. This approach provides an efficient way to generate tertiary stereocenters that bear a $CF_3$ substituent without the need for an additional activating/directing group. In addition, a variety of other enantioenriched fluorinated compounds **8**, including perfluoroalkyl, $CF_2Cl$, $CF_2COPh$, and $CF_2CO_2Et$, could also be obtained under the same conditions (Scheme 3.3) [14].

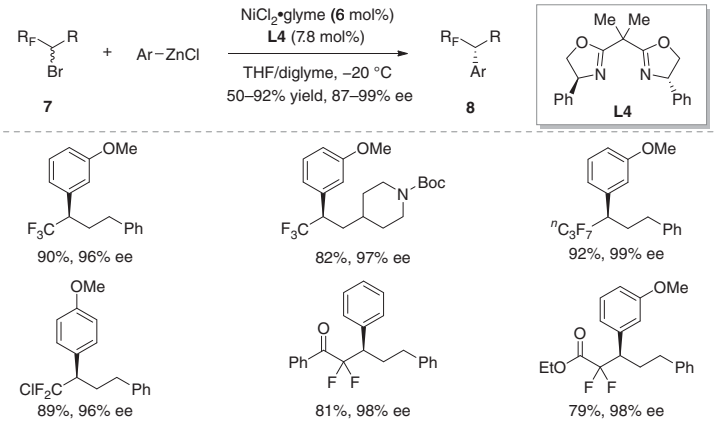


**Scheme 3.3** Enantioselective cross-coupling of $CF_3$-substituted alkyl halides with organozinc reagents.

Many bioactive compounds bear a cyano group attached to a stereogenic carbon, and nitriles serve as versatile precursors to a variety of functional groups, including aldehydes, ketones, amides, carboxylic acids, and amines. Fu and coworkers described the nickel-catalyzed enantioselective arylation and alkenylation of racemic α-halonitriles **9** with arylzinc and alkenylzinc reagents, respectively. A series of enantioenriched α-arylnitriles and allylic nitriles **10** were obtained using (*i*-Pr)-Box **L5** as a ligand (Scheme 3.4) [15]. The cross-coupling of α-halonitriles

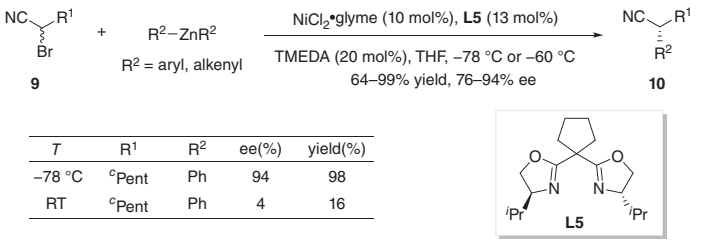


| T | $R^1$ | $R^2$ | ee(%) | yield(%) |
|---|---|---|---|---|
| –78 °C | $^c$Pent | Ph | 94 | 98 |
| RT | $^c$Pent | Ph | 4 | 16 |

**Scheme 3.4** Enantioselective cross-coupling of α-bromonitriles with organozinc reagents.

with arylzinc reagents must occur at a very low temperature (–78 °C), which is critical for enantioselective control.

Both sulfonamides and sulfones are useful intermediates in organic synthesis, and the enantioenriched benzylsulfonamides and sulfones display a range of biological activities. α-Halosulfonyl compounds are generally poor substrates for $S_N2$ reactions, and the sulfonyl group does not effectively stabilize an adjacent radical. Fu's group developed a nickel-catalyzed stereoconvergent Negishi arylation of racemic alkyl electrophiles **11** with organozinc reagents to afford benzylic sulfonamides and sulfones **12** with good ee (Scheme 3.5) [16].

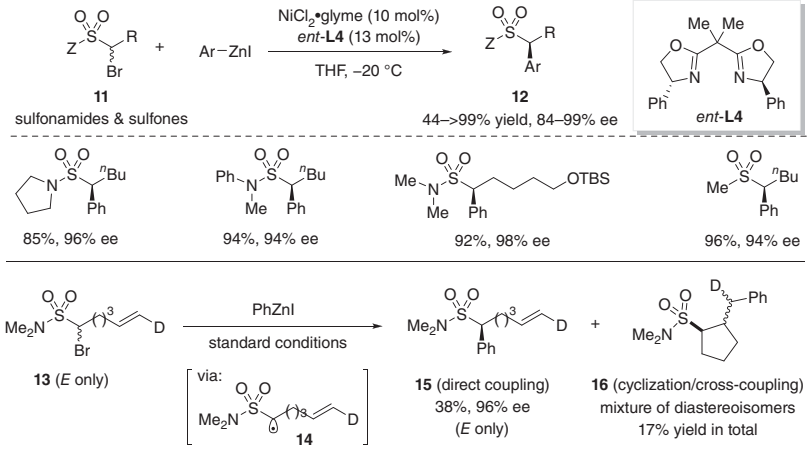


**Scheme 3.5** Enantioselective cross-coupling of α-bromo sulfonamides/sulfones with arylzinc reagents.

The Negishi coupling of α-bromo sulfonamide bearing a pendant olefin **13** with PhZnI afforded a 38% yield of the direct (uncyclized) cross-coupling product **15** and a 17% combined yield of the cyclized cross-coupling product **16**. The cyclopentane derivatives *cis*-**16** and *trans*-**16** are both a 1 : 1 mixture of diastereomers, consistent with the expected radical cyclization of intermediate **14**, rather than the migratory insertion of PhZnI into the alkene followed by reductive elimination.

Chiral aliphatic amines are widespread substructures in pharmaceutical molecules, natural products, and organic materials, and serve as common chiral

building blocks in the asymmetric synthesis of natural products, drugs, pesticides, and functional materials. Fu and coworkers established a nickel/PyBox-catalyzed cross-coupling of alkylzinc reagents with racemic α-amino alkyl chlorides **17** to afford protected dialkylamines **18** in good yields and excellent enantioselectivities (Scheme 3.6) [17]. The same group further achieved the enantioselective cross-coupling of an array of organozinc reagents with racemic α-haloglycine derivatives **19**, enabling ready access to various protected α-amino acids **20** (Scheme 3.6) [18].

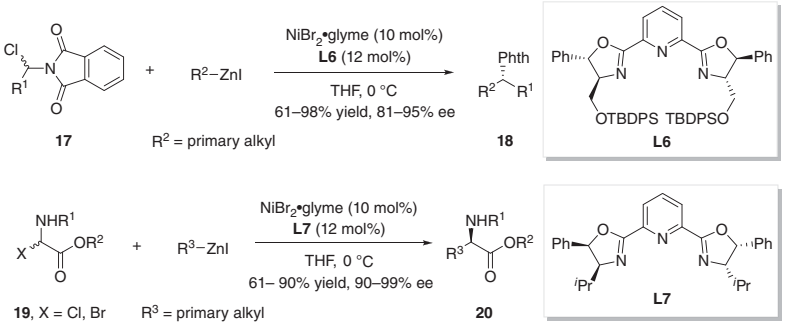


**Scheme 3.6** Asymmetric cross-coupling of organozinc reagents with α-amino alkyl halides.

Organoboron compounds play an important role in the fields of materials science, biochemistry, and organic synthesis. Matteson developed a robust and general strategy for the synthesis of alkylboronate esters **22** by coupling α-halogenated borates with organolithium or organomagnesium reagents [19, 20]. This strategy serves as a foundational approach for the synthesis of enantioenriched alkylboronate esters using stoichiometric chiral auxiliaries **23**. Aggarwal further developed an elegant related method, using enantioenriched α-lithiated benzoates to produce alkylboronate esters, including in an iterative fashion [21].

In 2016, Fu and colleagues achieved a Matteson-like coupling in a mechanistically distinct way. Specifically, the nickel-catalyzed stereoconvergent alkyl–alkyl cross-coupling of racemic α-halogenborates **21** with organozinc reagents leads to the generation of alkylboronate esters **22** with high enantioselectivity [22]. This method provides straightforward access to a diverse range of enantioenriched alkylboronate esters, in which boron is bound to a stereogenic carbon. A derivative of cholesterol was also a suitable electrophile (selective reaction of the α-chloride to boron, rather than the chloride at the 3-position), leading to each of the desired coupling products with high stereoselectivity. In both cases, the stereochemistry of the ligand **L8** rather than that of the substrate, is the predominant determinant of the stereochemistry of the products (Scheme 3.7).

Chiral organosilanes have attracted great interest in medicinal chemistry because replacing carbon with silicon can improve pharmacological properties (e.g. enhanced lipophilicity and potency) without element-specific toxicity due to the presence of silicon. Fu's group reported the enantioconvergent cross-coupling of

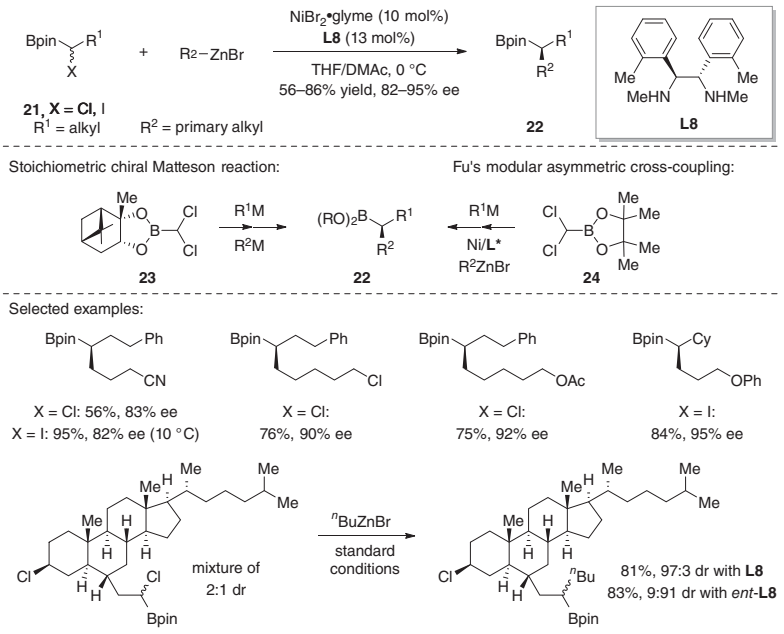


**Scheme 3.7** Stereoconvergent coupling of α-halogenborates with organozinc reagents.

racemic α-halosilanes **25** with alkylzinc reagents, achieving good enantioselectivity under mild conditions, thereby providing access to enantioenriched organosilanes **26** (Scheme 3.8) [23]. Mechanistic studies reveal that the chiral catalyst reacts with both enantiomers of the electrophile, without kinetic resolution, providing an enantioenriched product via irreversible C—Br bond cleavage.

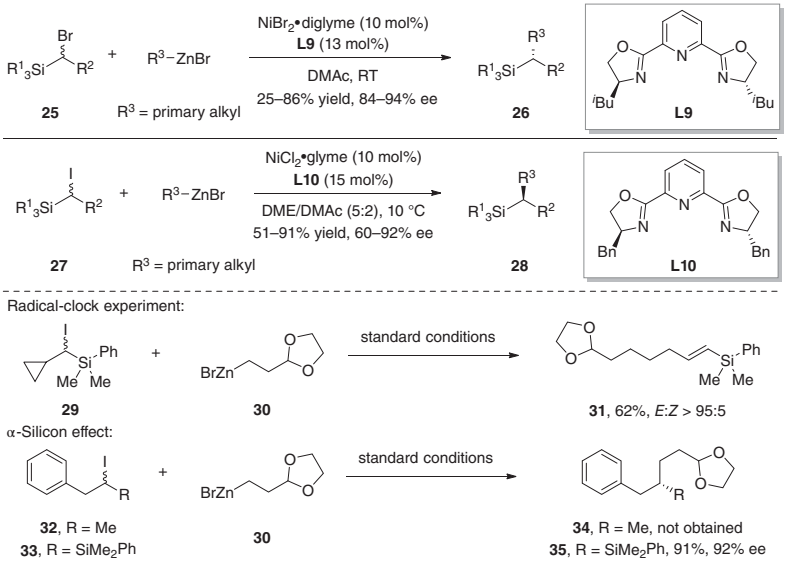


**Scheme 3.8** Enantioselective cross-coupling of α-halosilanes with organozinc reagents.

Oestreich independently reported almost simultaneously the enantioselective C($sp^3$)—C($sp^3$) cross-coupling of racemic α-silylated alkyl iodides **27** with alkylzinc reagents [24], enabling the flexible synthesis of chiral silanes **28**. Cyclopropyl α-iodo alkylsilane **29** was synthesized and reacted with alkylzinc **30** to give the ring-opened product **31**, confirming that the reaction undergoes a radical process. Moreover, when the silyl group (**33**) was replaced by a methyl substituent **32**, the cross-coupling product **34** was not obtained, indicating that the α-silicon group plays a role in stabilizing the alkyl radical (Scheme 3.8).

Significant progress has been made in the development of methods for the synthesis of carbon–carbon bonds through the enantioconvergent substitution reaction of racemic alkyl electrophiles with carbon nucleophiles. To date, high enantioselectivities have only been observed in cross-coupling reactions where the electrophile bears a directing group or a p/π orbital close to the leaving group. Fu's group further developed the asymmetric Negishi coupling reaction of primary alkylzinc reagents with secondary benzylic halides **36** without directing groups [25]. For cyclic benzyl bromides, this method consistently provided chiral indanes **37** with greater than 90% ee. However, the asymmetric Negishi reaction of acyclic secondary benzylic bromides with organozinc reagents achieved only moderate enantioselectivity (Scheme 3.9).

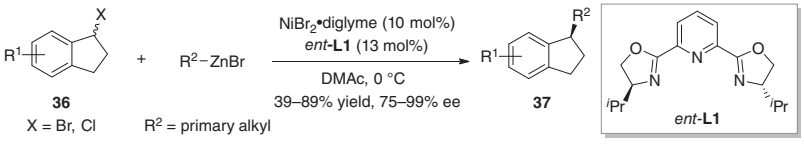


**36**
X = Br, Cl

R2 = primary alkyl

**37**

**Scheme 3.9** Enantioselective cross-coupling of benzylic halides with alkylzinc reagents.

Although the asymmetric Negishi coupling of benzyl halides with alkylzinc reagents has been achieved, the process proved ineffective when arylzincs were used as nucleophiles. A continuing challenge in the field of stereoconvergent cross-coupling is the use of oxygen-based, rather than halogen, leaving groups. The importance of this goal stems partly from the fact that the conversion of alcohols to more reactive oxygen-based leaving groups is usually achieved under Brønsted basic conditions, whereas their conversion to alkyl halides is usually accomplished under Brønsted acidic conditions.

In 2013, Fu and coworkers extended the scope of the nickel-catalyzed asymmetric Negishi reaction of benzylic electrophiles to benzylic mesylates, which were generated in situ by the treatment of benzyl alcohols **38** with methanesulfonyl chloride. A series of enantioenriched 1,1-diarylalkanes **39** were obtained in good yields with high enantioselectivity (Scheme 3.10) [26]. The utility of this reaction was illustrated in the gram-scale synthesis of (*S*)-sertraline tetralone **41**, a precursor to the leading antidepressant drug Zoloft.

Metal-catalyzed enantioselective cross-coupling of allylic electrophiles with carbon nucleophiles has been intensively studied, with most research focusing on Pd-catalyzed reactions of allylic esters/carbonates with enolates. Fu and coworkers accomplished the asymmetric Negishi cross-coupling of racemic secondary allylic

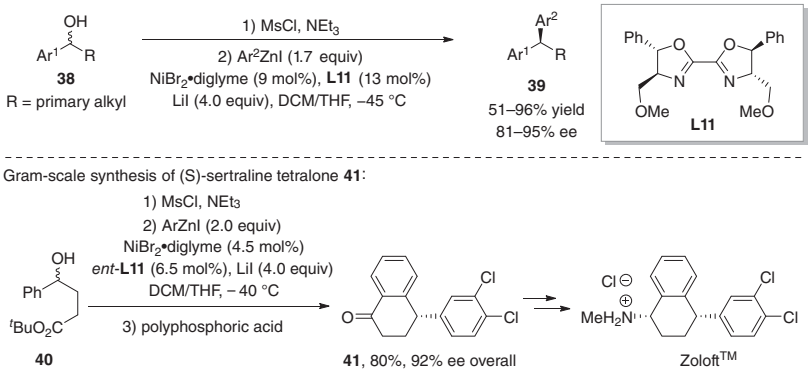


**Scheme 3.10** Stereoconvergent cross-coupling of benzylic alcohols with arylzinc reagents.

chlorides **42** with alkylzinc bromides (Scheme 3.11) [27]. The regioselectivity was consistently high for 2° and 3° alkyl (**44**), as well as for the electron-withdrawing group (**45**), with one substituent positioned at the α-position and another at the γ-position of the allyl unit. However, it was moderate when both substituents were primary alkyl groups (**46**).

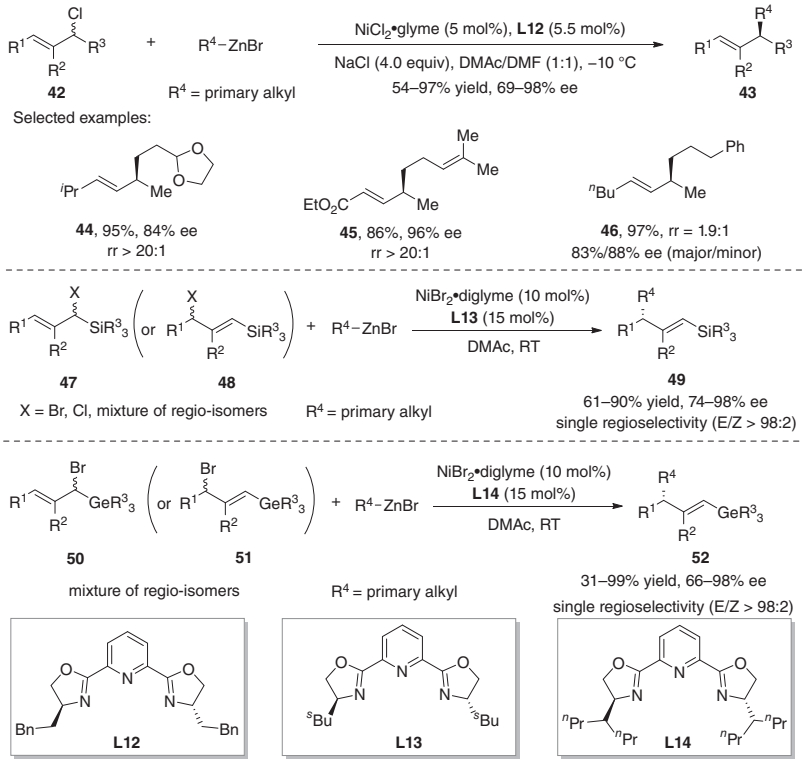


**Scheme 3.11** Enantioselective cross-coupling of allylic chlorides with alkylzinc reagents.

Taking advantage of the directing role of silyl groups in transition-metal-catalyzed allyl displacement, Oestreich and coworkers reported the enantio- and diastereoselective synthesis of exclusively alkyl-substituted acyclic allylic systems with a stereocenter in the allylic position. This was accomplished through nickel-catalyzed $C(sp^3)$—$C(sp^3)$ cross-coupling of regioisomeric mixtures of racemic α-/γ-silylated allylic halides **47** and **48** with primary alkylzinc reagents. The silyl group steers the displacement of the allylic group to form the vinylsilane regioisomer, and the resulting $C(sp^2)$—Si bond plays a crucial role in facilitating the installation of various $C(sp^3)$ substituents in subsequent steps (Scheme 3.11) [28, 29].

Oestreich further demonstrated the nickel-catalyzed enantio- and regioconvergent alkylation of regioisomeric mixtures of racemic germylated allylic bromides **50** and **51** with alkylzinc reagents [30]. The cornerstone of this success lies in the development of a new hept-4-yl-substituted PyBox ligand **L14**, which enables the synthesis of various chiral vinyl germanes **52** in excellent yields and enantioselectivities (Scheme 3.11). The resulting chiral germanes can be converted by a halodegermylative protocol [31] to γ-stereogenic vinyl halides, which are valuable synthetic building blocks, without loss of optical purity.

Chiral alkynes are fundamental building blocks in organic synthesis, serving as privileged synthons for designing new reactions. Fu's group further developed the nickel-catalyzed asymmetric Negishi cross-coupling of racemic propargylic carbonates with organozinc reagents (Scheme 3.12) [32, 33]. The TMS substituent on the alkyne plays a crucial role in improving the stereoselectivity of the reaction (**54** and **56**). In 2021, Oestreich reported the nickel-catalyzed regioselective cross-coupling of α-silylated propargylic bromides **57** with primary alkylzinc reagents for the synthesis of allenylsilanes **58** with moderate enantioselectivity. The high regioselectivity is

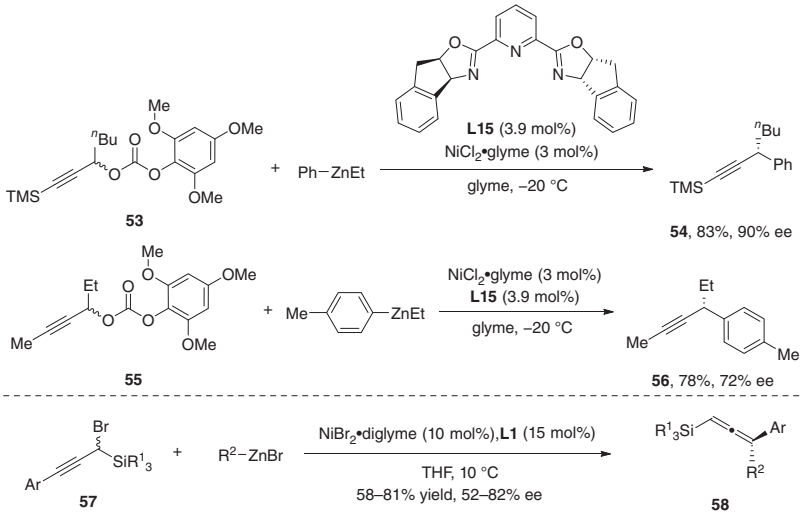


**Scheme 3.12** Enantioselective coupling of propargylic (pseudo)-halides with organozinc reagents.

governed by the bulky silyl group, and the C($sp^2$)—C($sp^3$) bond formation occurs exclusively at the γ-position of the propargyl electrophile (Scheme 3.12) [34].

To gain insights into the mechanism, Fu and colleagues designed a series of experiments to investigate the asymmetric arylation of propargyl bromides (Scheme 3.13) [35]. Asymmetric coupling of propargylic bromide **59** with diphenylzinc using $^{i}$Pr-PyBox (ent-**L1**) afforded product **54** in 77% yield and 82% ee (Scheme 3.13a). The reaction of phenylnickel(I) complex **60** with propargylic bromide **59** indeed afforded the target product **54**, but the yield and stereoselectivity were significantly reduced (Scheme 3.13b). The phenylnickel(II) complex **61** reacts with the propargylic bromide **59** to furnish the coupling product **54** in substantially higher yield and ee than in the case of the phenylnickel(I) complex **60** (Scheme 3.13c). These results suggest that the phenylnickel(II) complex **61** is the possible intermediate in the catalyzed process.

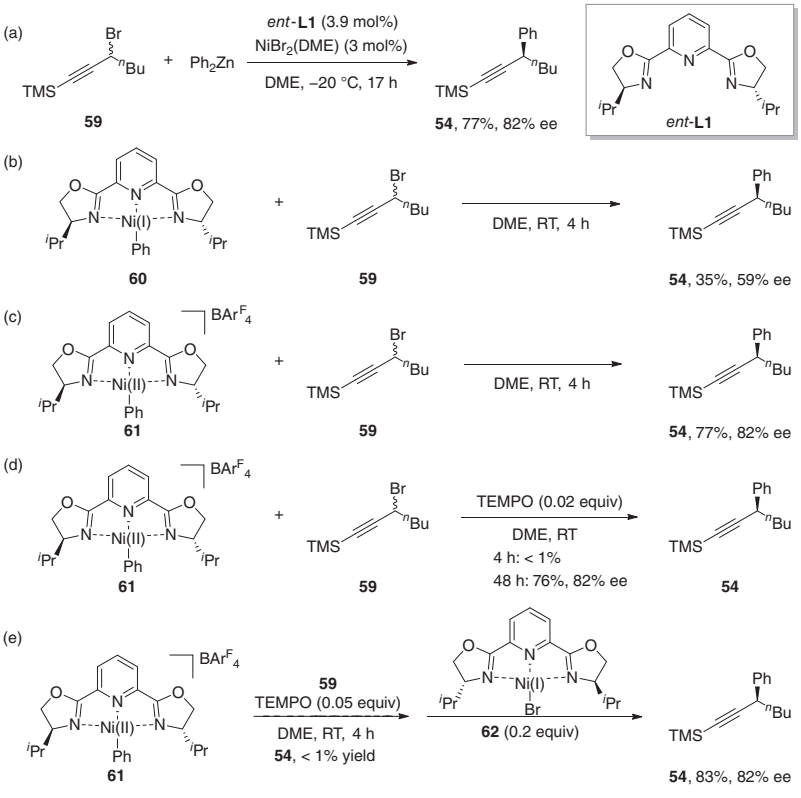


**Scheme 3.13** Mechanistic study of Negishi arylations of propargylic bromides.

The reaction of the phenylnickel(II) complex **61** with propargylic bromide **59** proceeds in the dark at the same rate as under ambient light and is inhibited by a substoichiometric amount of TEMPO. However, the cross-coupling proceeds to completion after 48 h, demonstrating a TEMPO-induced induction period (Scheme 3.13d). When employing the nickel(I) bromide complex **62** as

the initiator with the opposite enantiomer of the PyBox ligand compared with the phenylnickel(II) complex **61**, the ee of the coupled product **54** was unchanged (Scheme 3.13e). This result suggests that the enantioselectivity of the carbon–carbon bond formation process depends on the configuration of the PyBox ligand bound to the phenylnickel(II) complex **61**.

Previous studies have shown that the cross-coupling of propargylic bromides with arylzinc reagents proceeds via a transmetalation-first pathway. Based on the above mechanistic studies, Fu and coworkers proposed a radical chain mechanism in which the C—Br bond is cleaved during the bimetallic oxidative addition transiently generating a propargyl radical **66**, as well as a series of nickel(I)/(II)/(III) intermediates (Scheme 3.14).

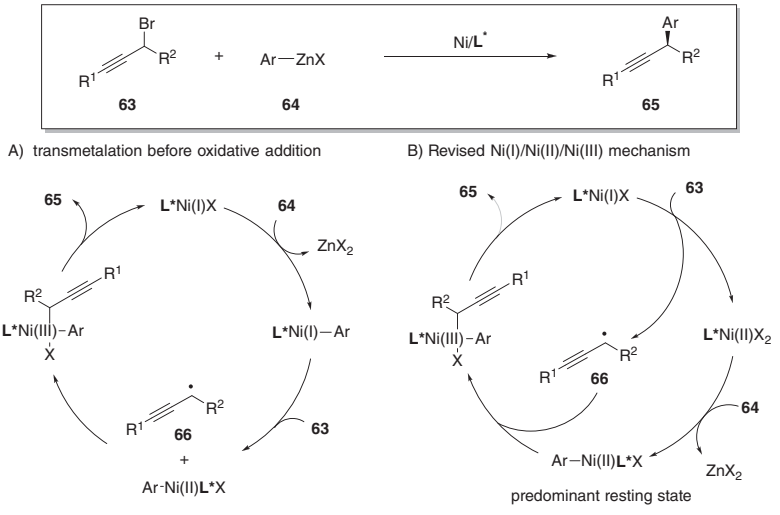


**Scheme 3.14** Plausible mechanism of Negishi arylations of propargylic bromides.

### 3.2.2 Cross-Coupling of Organohalides with Secondary Alkylzinc Reagents

The organozinc reagents discussed in the literature mentioned above are limited to aryl and primary alkyl ones. However, when it comes to secondary alkylzincs, the reactivity is quite different. Extending the scope of asymmetric processes to include secondary–secondary cross-coupling remains one of the key challenges in the field.

Fu's group reported the first nickel-catalyzed asymmetric cross-coupling of secondary electrophiles with secondary nucleophiles, specifically stereoconvergent Negishi reactions of racemic benzylic bromides **67** with cycloalkylzinc reagents **68** (Scheme 3.15) [36]. In contrast to most previous studies of enantioselective Negishi cross-couplings, tridentate PyBox ligands were ineffective in this process. However, the bidentate isoquinoline-oxazoline ligand **L16** provided good yields and excellent enantioselectivity. The use of acyclic alkylzinc reagents ($^{i}$PrZnI and $^{n}$PrZnI) as coupling partners led to the discovery of a highly unusual isomerization, generating a mixture of branched and linear cross-coupling products **71** and **72**.

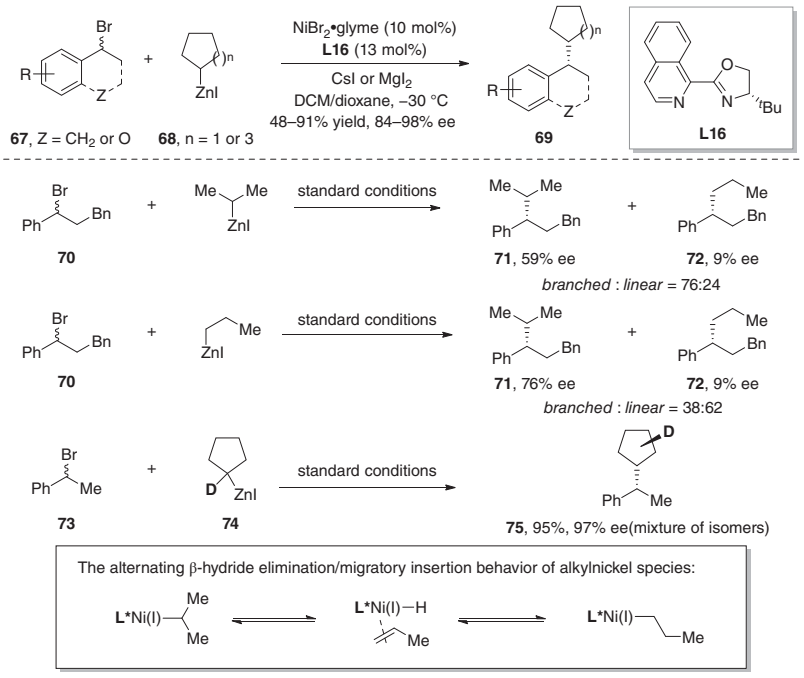


**Scheme 3.15** Enantioselective coupling of secondary benzylic bromides with cycloalkylzinc reagents.

In addition, the Negishi reaction of (1-bromoethyl)benzene **73** with deuterium-labeled cyclopentyl zinc reagent **74** produced five deuterium-containing coupling products **75** in approximately equal quantities. These results suggest that the isomerization process proceeds through β-hydride elimination/β-migratory insertion of the alkyl-nickel species.

Pyrrolidines with an alkyl substituent at the 2-position are important in both chemistry and biology. In 2013, Fu's group reported the enantioconvergent alkyl–alkyl cross-coupling of racemic α-zincated *N*-Boc pyrrolidine (in situ preparation by treating *N*-Boc pyrrolidine **76** with $^{s}$BuLi followed by transmetalation with $ZnI_2$) with unactivated alkyl halides to generate 2-alkylpyrrolidines **77** with good ee (Scheme 3.16) [37]. A range of cyclic and acyclic unactivated secondary alkyl bromides proceeded with excellent enantioselectivities but generally in moderate yields. In contrast, moderate ee was observed for primary alkyl halides.

An enantioenriched organozinc reagent (*S*)-**79** was prepared from the corresponding stannane reagent through Sn–Li exchange, followed by transmetalation with $ZnI_2$. When reagent (*S*)-**79** was coupled with cyclohexyl iodide using either (*R,R*)-**L17** or (*S,S*)-**L17**, the stereochemistry of the cross-coupling product **80** was primarily dependent on the stereochemistry of the ligand rather than the organozinc nucleophile **79**. The pathway for stereoconvergence in the present method does not involve a dynamic kinetic resolution of the organometallic coupling partner, in contrast to a previous report of an enantioconvergent alkyl–alkenyl cross-coupling. A deuterium labeling study ruled out stereomutation via the

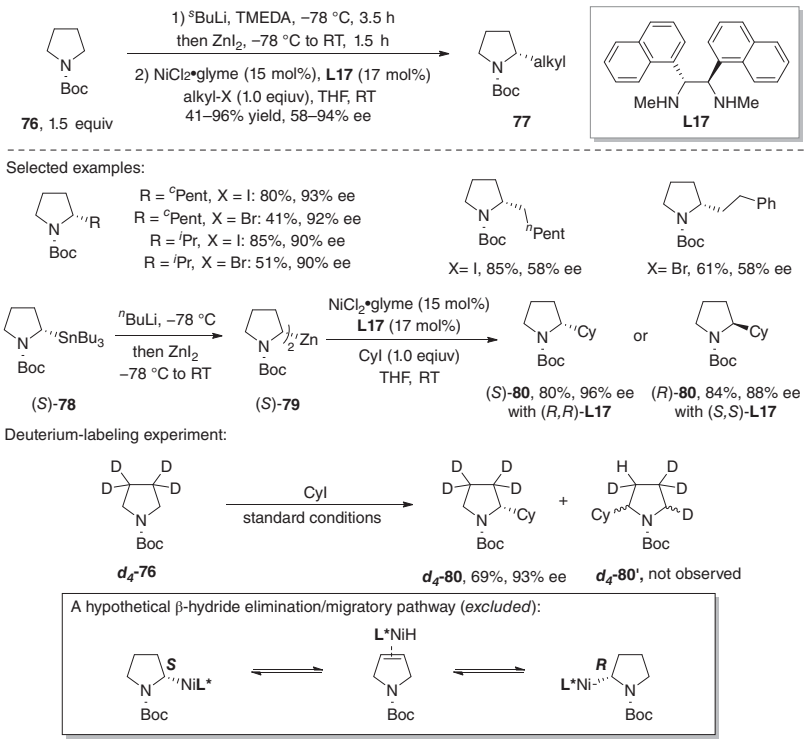


**Scheme 3.16** Enantioconvergent Negishi coupling of α-zincated *N*-Boc-pyrrolidine with alkyl halides.

β-hydride elimination/β-migratory insertion pathway observed in the Ni-catalyzed alkyl–alkyl coupling described above. This difference may be due to the presence of coordination of the ortho-*N*-Boc, which stabilizes the α-nickelate *N*-Boc pyrrolidine (Scheme 3.16).

In 2022, Fu's group reported a nickel-catalyzed enantioconvergent cross-coupling of racemic Reformatsky reagents **82** with primary alkyl iodides. The resulting α-alkylated amides **83** can be converted into a diverse array of chiral molecules (Scheme 3.17) [38]. The chiral alkyl-Ni(II) complex **84** was isolated and characterized by X-ray single-crystal diffraction, showing it as the main resting state of nickel during catalysis. The structure of the alkyl-nickel complex **84** showed that nickel is bound to the stereogenic α-carbon of the carbonyl group, and the stereochemistry of which corresponds to the major enantiomer observed in the coupled product.

Vicinal stereocenters are found in many natural and unnatural compounds. Although metal-catalyzed cross-coupling reactions of unactivated alkyl electrophiles are emerging as powerful tools in organic synthesis, the generation of vicinal stereocenters has been rarely reported. A chiral nickel/diamine catalyst can mediate doubly stereoconvergent alkyl–alkyl cross-coupling. Specifically, this catalyst enables the coupling of racemic pyrrolidine-derived nucleophiles **79** with cyclic alkyl halides **85** (as mixtures of stereoisomers) to produce vicinal stereocenters with good stereoselectivity (Scheme 3.18) [39]. When the asymmetric cross-coupling

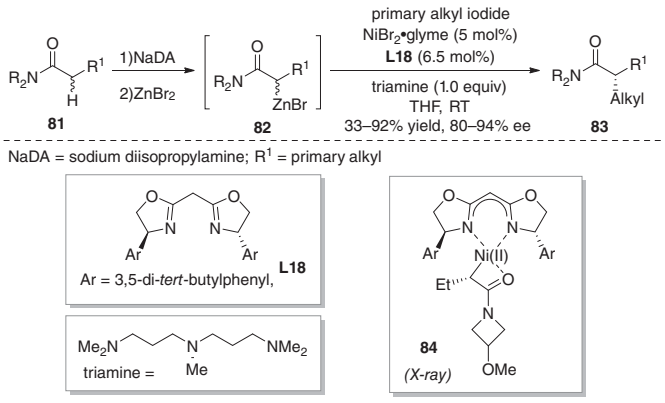


**Scheme 3.17** Enantioconvergent cross-coupling of α-zincated amides with alkyl iodides.

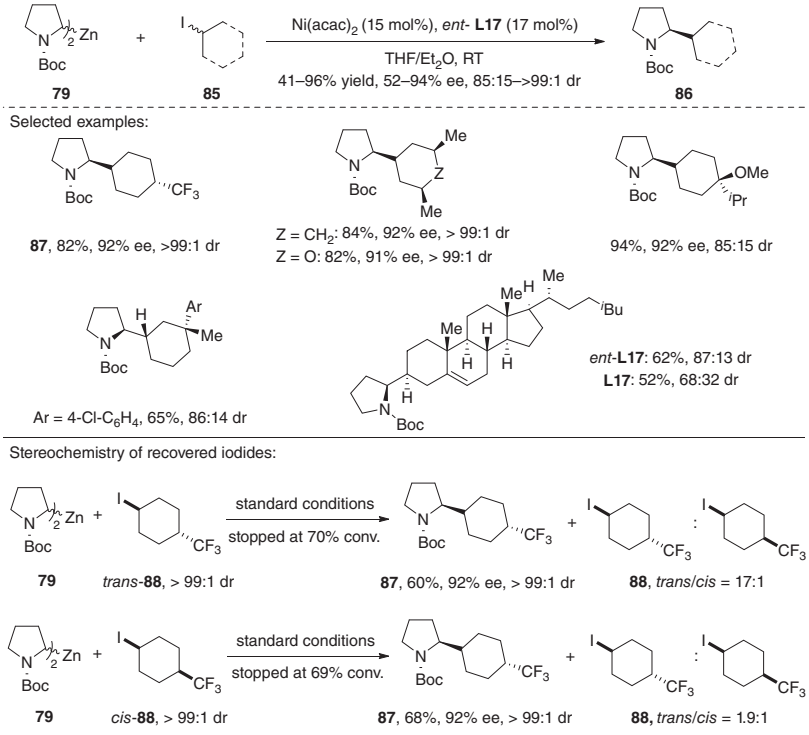


**Scheme 3.18** Enantioconvergent cross-coupling of α-zincated *N*-Boc-pyrrolidines with alkyl iodides.

of α-zincated *N*-Boc pyrrolidine **79** with single diastereoisomers of alkyl iodide **88** was performed, the alkyl iodide **88** was found to undergo isomerization during the reaction. The two isomers of the electrophile do not interconvert in the presence of an iodide source, suggesting that reversible iodine transfer between the alkyl radical and nickel is a more likely pathway. Possible mechanisms for this isomerization

include halogen exchange via $S_N2$ reactions and reversible transfer of the iodine radical from alkyl iodides to nickel catalysts.

Classical substitution reactions via $S_N1$ and $S_N2$ pathways are limited in their ability to generate C—C bonds (due to side reactions such as rearrangements and eliminations) and to control stereochemistry when starting with readily available racemic materials. Fu et al. further disclosed the doubly enantioconvergent substitution reactions of racemic secondary propargylic bromides **90** with racemic β-zincated amides **89** using a Ni/pyridine-oxazoline-based catalyst (Scheme 3.19) [40]. Both enantiomers of the two racemic starting materials were converted to a particular stereoisomer of the desired products **91** with good stereoselectivity.

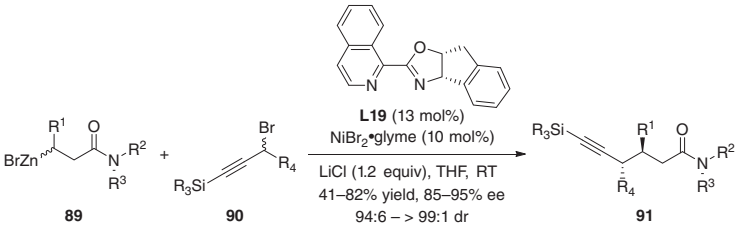


**Scheme 3.19** Doubly enantioconvergent substitution reactions of racemic β-zincated amides by racemic propargylic bromides.

In 2020, Zhang's group developed an enantiodivergent strategy to efficiently synthesize an array of synthetically useful chiral cyclopropanes **94** from racemic cyclopropylzinc reagents **92** (Scheme 3.20) [41]. This strategy relies on a two-step enantiodivergent relay coupling process of the racemic cyclopropylzinc reagents

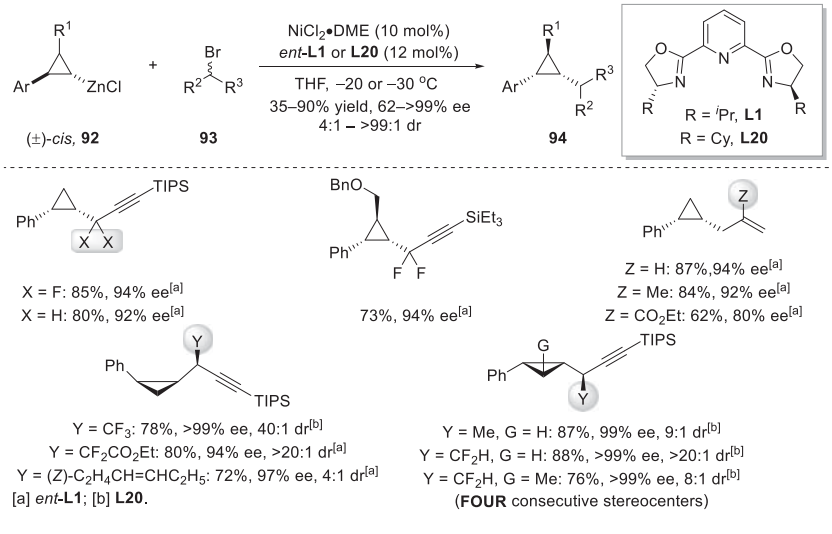


**Scheme 3.20** Asymmetric Negishi reaction of cyclopropyliczinc reagents and alkyl electrophiles.

**92** with two electrophiles. Initially, it entails the kinetic resolution of racemic cis-cyclopropylzinc reagents through a nickel-catalyzed enantioselective coupling with alkyl electrophiles. Subsequently, the process proceeds with a stereospecific relay coupling of the remaining enantiomeric cyclopropylzinc reagent.

### 3.2.3 Cross-Coupling of Organohalides with Organozirconium, Organoindium, Organotitanium, and Grignard Reagents

In addition to organozinc reagents, other metal reagents, including organozirconium reagents, organoindium reagents, Grignard reagents, etc., have also been used in nickel-catalyzed stereoselective cross-coupling reactions with alkyl halides. Alkenyl zirconium compounds are attractive alkenyl metals for cross-coupling, mainly because they are readily prepared by the reaction of a commercially available Schwartz reagent ($Cp_2ZrHCl$) with alkynes. Fu and coworkers developed the first nickel-catalyzed cross-coupling of secondary α-haloketones **95** with alkenylzirconium reagents to generate potentially labile β,γ-unsaturated ketones **96** with good enantioselectivity (Scheme 3.21) [42]. The same group expanded the scope of stereoconvergent cross-couplings of α-bromosulfonamides **11** with alkenyl metal reagents. Very low yields were obtained using alkenylzinc reagents, while alkenylzirconium reagents served as suitable nucleophiles, providing allylic sulfonamides **97** with good enantioselectivity (Scheme 3.21) [16].

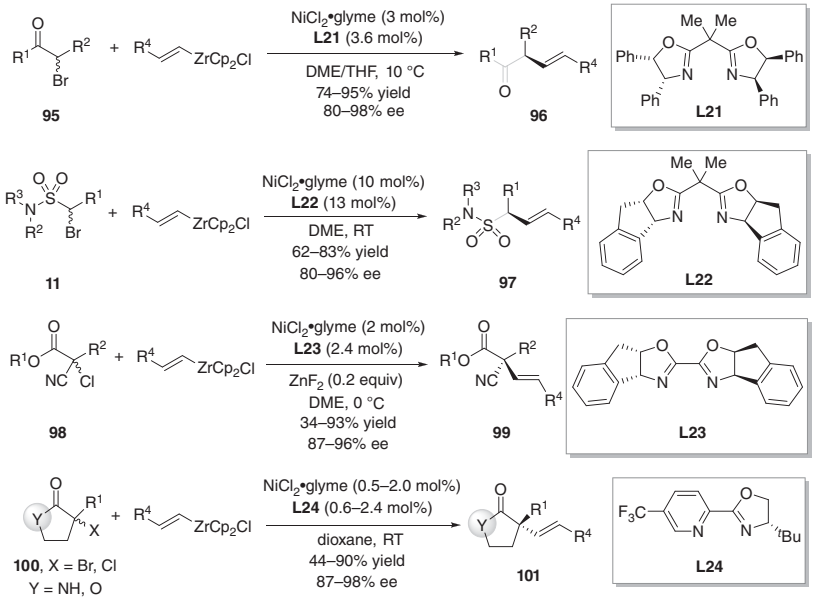


**Scheme 3.21** Asymmetric α-alkenylation of organohalides with alkenyl zirconium reagents.

Numerous reports have established that transition metals can catalyze the enantioconvergent nucleophilic substitution of racemic secondary alkyl electrophiles via a

radical pathway. Nevertheless, the exploration of the corresponding cross-coupling of tertiary electrophiles with organometallic nucleophiles to construct quaternary stereocenters with good enantioselectivity remains underexplored. In 2021, Fu and colleagues developed a nickel-catalyzed enantioconvergent substitution of both acyclic and cyclic racemic tertiary alkyl electrophiles (**98** and **100**) with organometallic nucleophiles (alkenylzirconium reagents) [43]. This cross-coupling, which probably proceeds via a radical pathway, occurs under mild and convenient conditions with remarkable functional group compatibility, providing carbonyl compounds **99** and **101** bearing α-quaternary centers in good yields and enantioselectivities (Scheme 3.21).

Organoindium compounds are useful reagents in metal-catalyzed cross-coupling reactions. Trialkynyl lithium reagents are prepared by treating the corresponding alkynyl lithium reagents with $InCl_3$. The key features of indium reagents are their high versatility, non-toxicity, and ability to transfer all three metal-linking groups to electrophiles. Sarandeses et al. reported the first nickel-catalyzed enantioselective cross-coupling reaction of alkynyl organoindium reagents with racemic benzyl bromides **102** [44]. The reaction is performed at room temperature using $NiBr_2$·diglyme and (*S*)-($^i$Pr)-PyBox as the catalytic system (Scheme 3.22).

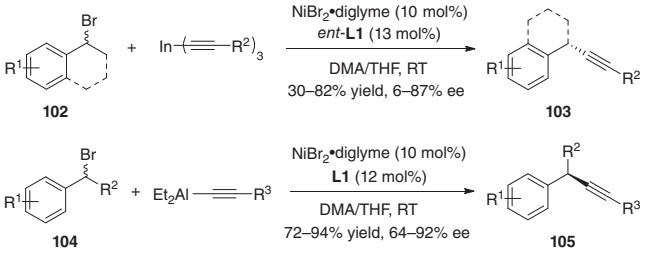


**Scheme 3.22** Asymmetric alkynylation with alkynyl indium and aluminum reagents.

Organoaluminum reagents have been widely applied in cross-coupling reactions due to the high reactivity and Lewis acidity of the aluminum center. Zhou and coworkers reported the first example of an enantioselective cross-coupling reaction of secondary benzylic bromides **104** with alkynyl aluminum reagents [45]. Chiral propargyl compounds **105** bearing (hetero)-aromatic groups were obtained in high yield and good enantioselectivity using $NiBr_2$·diglyme and (*R*)-$^i$Pr-PyBox as the catalytic system (Scheme 3.22).

Organotitanium reagents exhibit broader functional group tolerance than the corresponding Grignard reagents due to their lower nucleophilicity and basicity, and they display faster transmetalation rates compared to the corresponding organozinc reagents [46]. Gandelman and coworkers disclosed the synthesis of chiral $CF_3$-substituted thioethers **107** by a Ni-catalyzed stereoconvergent cross-coupling of aryl-titanium reagents [47]. Organotitanium species have been proven to be beneficial compared to the commonly used organomagnesium and organozinc counterparts (Scheme 3.23). The same group further extended the method to the synthesis of α-$CF_3$-substituted benzhydryls. The use

of an aryl-titanate-based nucleophile enabled the synthesis of a variety of chiral 1,1-diaryl-2,2,2-trifluoroethanes **111** starting from α-$CF_3$-benzyl bromides **110** in high yields and excellent enantioselectivities (Scheme 3.23) [48].

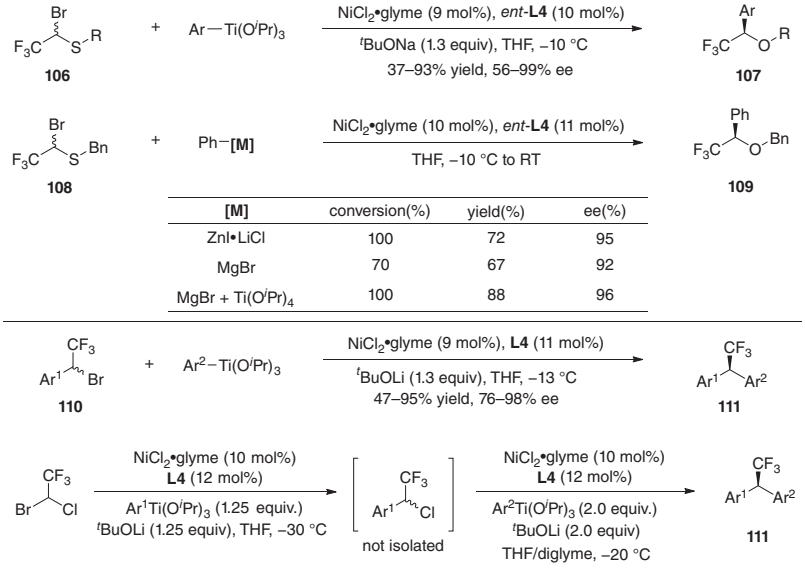


**Scheme 3.23** Asymmetric arylation of secondary alkyl halides using organotitanium reagents.

Grignard reagents can be conveniently synthesized from organic halides and exhibit high reactivity. The transition-metal-catalyzed coupling of organic electrophiles with Grignard reagents (Kumada reaction) was one of the first cross-coupling reactions developed. In 1976, Kumada described the first Ni-catalyzed enantioconvergent coupling of a racemic benzylic Grignard reagent (PhCHMeMgCl) with an alkenyl halide (bromo ethylene) to generate an enantioenriched allylbenzene [49, 50]. Due to the high activity of Grignard reagents, only moderate stereoselectivity was obtained. It was not until 2010 that Fu's group realized the enantioconvergent Kumada coupling of alkyl electrophiles and aryl Grignard reagents (Scheme 3.24) [51]. The reaction must be performed at very low temperatures (–60 °C) to maintain high ee, as the racemization of α-aryl ketones occurs easily by enol isomerization under the Brønsted basic reaction conditions.

In 2019, the group investigated the detailed mechanism of the aforementioned Ni/Box-catalyzed enantioconvergent α-arylation of racemic α-bromo ketones **95** [52]. Compared with previous studies on nickel-catalyzed cross-coupling of Grignard reagents with alkyl electrophiles employing tridentate ligands, a different catalytic cycle was proposed. Mechanistic experiments support a pathway for carbon–carbon bond formation via a radical chain process, in which nickel(I) complexes act as the chain-carrying radical, and the organonickel(II) complex **113** is the predominant resting state of the catalyst.

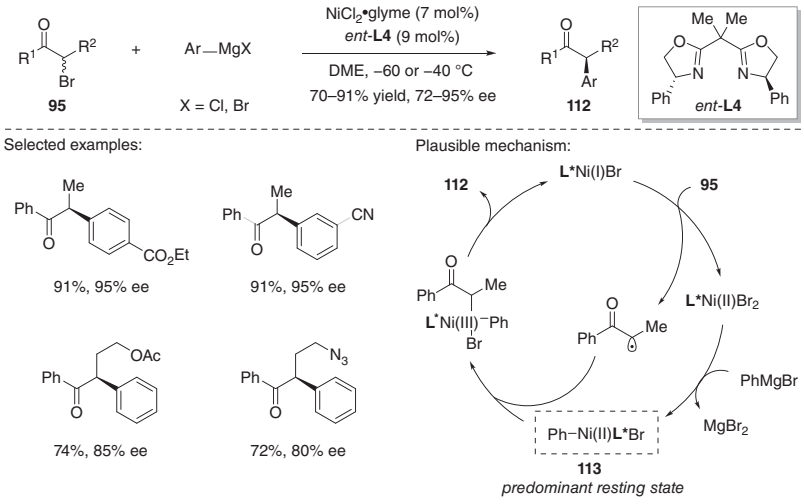


**Scheme 3.24** Asymmetric cross-coupling of α-bromoketones with Grignard reagents.

### 3.2.4 Cross-Coupling of Organohalides with Organosilicon and Organoboron Reagents

Organoboron and organosilicon compounds are highly stable and widely used in organic synthetic chemistry. In 2008, Fu and coworkers reported the first nickel/diamine-catalyzed asymmetric Hiyama coupling reaction of α-bromo esters **114** with organosilanes, providing α-aryl and α-alkenyl esters **115** with good enantioselectivity [53]. The fluoride activator (TBAT) plays an important role in determining the efficiency of the cross-coupling process. The steric hindrance of the ester group has a significant effect on controlling the stereoselectivity of the reaction, and the 2,6-di-tert-butyl-4-methylphenyl-substituted one proves to be the most effective (Scheme 3.25).

Gandelman and coworkers developed a catalytic stereoconvergent approach to the synthesis of enantioenriched α-trifluoromethyl- and perfluoroalkyl-containing benzylic and allylic ethers **117** by nickel-catalyzed stereoconvergent Hiyama cross-coupling (Scheme 3.25) [54]. This reaction utilizes a bifunctional electrophile **116** bearing both a trifluoromethyl and a functional group as direct substituents of the reactive center. This method represents a conceptually different approach to synthesize chiral $CF_3$-substituted alcohols and ethers in high yields and enantioselectivities. Irradiation with blue or white light was found to accelerate the nickel-catalyzed Hiyama arylation.

The asymmetric Suzuki arylation of racemic α-haloamides **119** with arylboron reagents was first accomplished by Fu's group via nickel/chiral diamine ligand catalysis (Scheme 3.26) [55]. The resulting α-aryl amides **120** can be transformed into enantioenriched α-arylcarboxylic acids and primary alcohols. A mechanistic study suggests that the selectivity may reflect the discrimination of the two enantiomers of α-chloroamides by the chiral catalyst via an irreversible oxidative addition process.

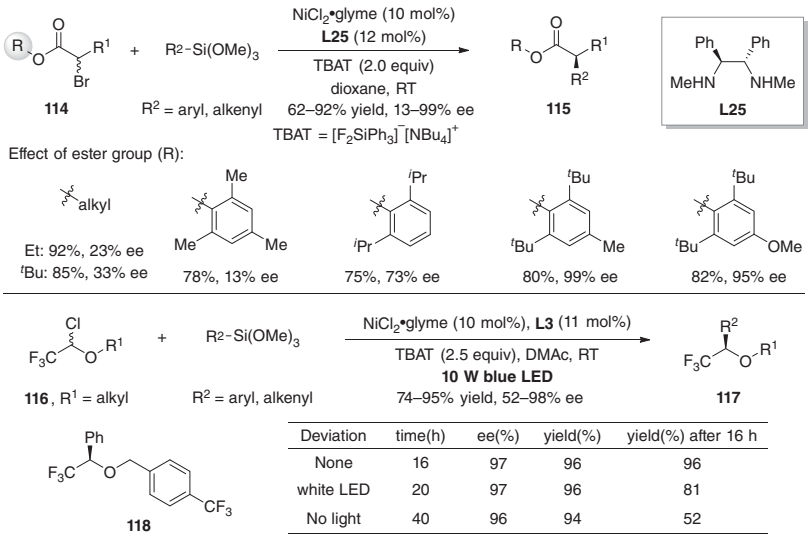


| Deviation | time(h) | ee(%) | yield(%) | yield(%) after 16 h |
|---|---|---|---|---|
| None | 16 | 97 | 96 | 96 |
| white LED | 20 | 97 | 96 | 81 |
| No light | 40 | 96 | 94 | 52 |

**Scheme 3.25** Asymmetric Hiyama α-arylation of α-bromo esters.

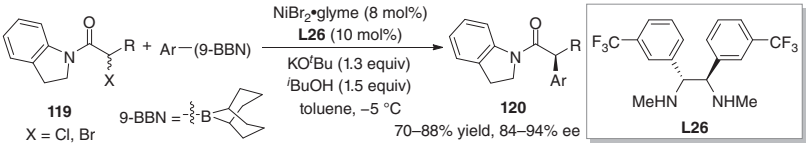


**Scheme 3.26** Asymmetric Suzuki α-arylation of α-chloro amides.

The trifluoromethoxy functional group is a unique fluorinated group that has received a great deal of attention in medicinal chemistry and agrochemistry. In 2017, Shen and coworkers reported the asymmetric Suzuki-Miyaura coupling of α-bromobenzyl trifluoromethyl ethers **121** with a variety of lithium aryl boronates **122** (Scheme 3.27) [56]. This reaction proceeded smoothly to obtain $CF_3O$-substituted stereogenic centers **123** with high enantioselectivity. A variety of common functional groups, such as fluoride, chloride, bromide, ester, enolizable ketone, nitro, cyano, amino, and vinyl moieties, were well tolerated. 3-Substituted phthalides are important motifs widely present in biologically active

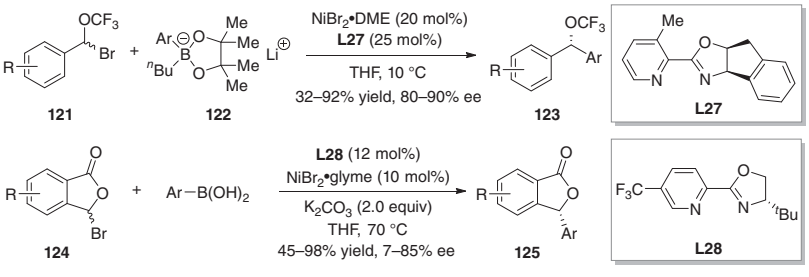


**Scheme 3.27** Asymmetric cross-coupling of 3-bromo-phthalides with arylboronic acids.

natural products. Feng's group demonstrated the feasibility of nickel-catalyzed Suzuki-Miyaura cross-coupling of racemic 3-bromo-phthalides **124** with arylboronic acids to access chiral 3-aryl-phthalides **125** in moderate to excellent yields and enantioselectivities (Scheme 3.27) [57].

Shen and coworkers developed a versatile protocol to access 1,1-diaryl fluoroalkanes **127** via nickel/Pyrox-catalyzed asymmetric Suzuki-Miyaura coupling of α-bromobenzyl trifluoro-/difluoro-/mono-fluoromethanes **126** with a variety of lithium aryl zincates that were in situ generated from the reaction of lithium organoboronates **122** with 1.0 equivalent of $ZnBr_2$ (Scheme 3.28) [58].

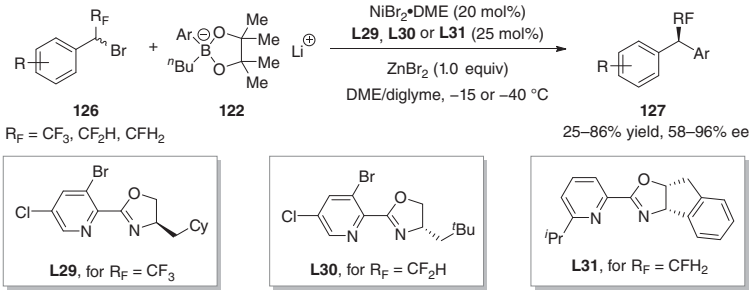


**Scheme 3.28** Asymmetric coupling of α-bromobenzyl fluoroalkanes with lithium aryl boronates.

Organoboron compounds usually undergo transmetalation with catalysts to give key organometallic intermediates via a two-electron process in cross-coupling reactions. Compared with arylboron reagents, alkylboron reagents, especially secondary and tertiary boron reagents, are less nucleophilic due to the non-polar nature of $C(sp^3)$—B bonds. In most cases, excess base and harsh conditions are necessary for facilitating transmetalation, thus limiting functional group tolerance and increasing unwanted side reactions. The challenge of alkylboron transmetalation is recognized to stem from mechanistic limitations inherent in the two-electron nature of the conventional process, where reactivity is inversely proportional to the heterolytic C—B bond strength, thus predisposing $Csp^3$ nucleophiles to failure in cross-coupling reactions.

A highly progressive work in enantioselective alkyl–alkyl cross-coupling, the stereoconvergent Suzuki coupling of alkyl-(9-BBN) with homobenzylic bromides, was first established by Fu in 2008 (Scheme 3.29) [59]. A variety of racemic β-arylated secondary alkyl bromides underwent asymmetric alkylation with good enantioselectivity. The chiral Ni/**L26** complex discriminates the two alkyl groups of the alkyl halide through secondary interactions between the $CH_2Ar$ substituent and the catalyst. Consistent with the suggestion that proper positioning of the aromatic group is important for obtaining good ee (**130**–**132**), products **133** and **134** were obtained with low enantioselectivities under standard conditions.

In addition to β-aryl groups, β-oxygen (**135**) [60], β-nitrogen (**140**) [61], γ-sulfonamide, γ-sulfone (**146**) [62], and γ-amide (**151**) [63], etc. [64, 65], were also demonstrated to be effective directing groups that facilitate asymmetric alkylation with alkylboranes (Scheme 3.30). The presence of the directing group is very

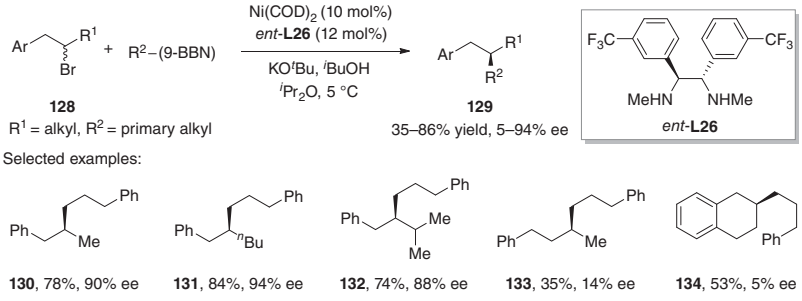


**Scheme 3.29** Asymmetric Suzuki coupling of homobenzylic bromides with alkylboranes.

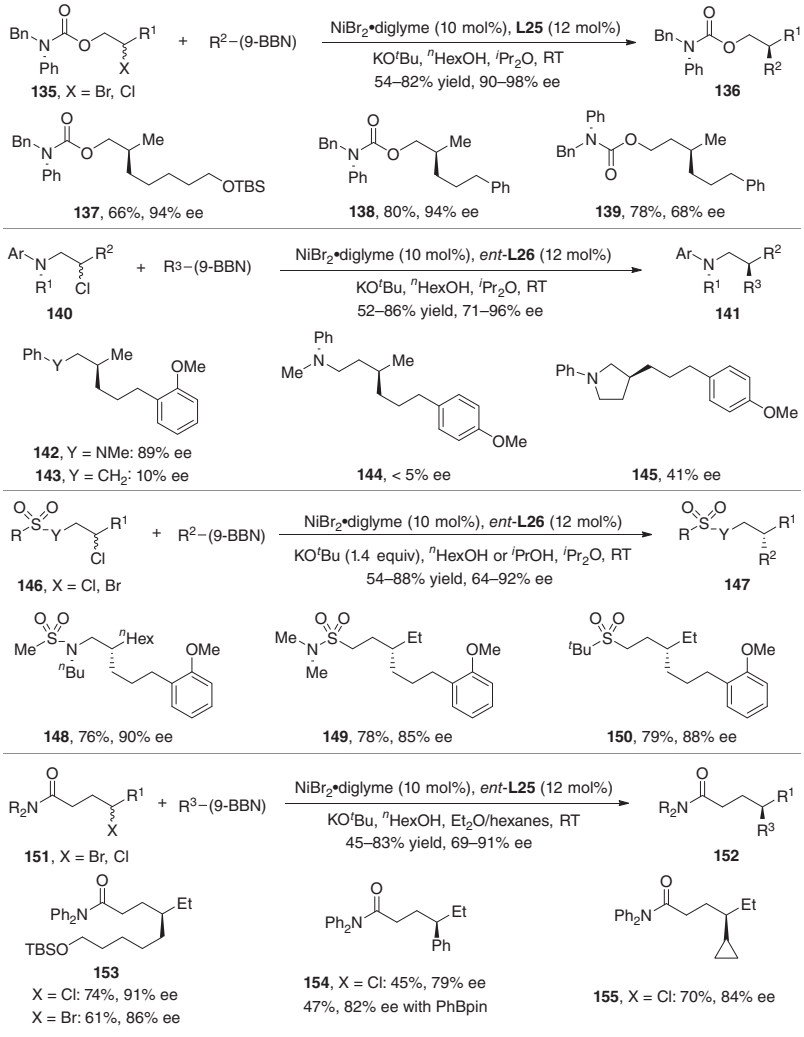


**Scheme 3.30** Asymmetric Suzuki cross-coupling of alkyl halides with alkylboranes.

important. If the position of the directing group is changed, the stereoselectivity is significantly reduced, as indicated by the formation of products **139**, **143**, **144**, and **145**.

Potassium organotrifluoroborates were identified as promising partners in cross-coupling, as previous reports have documented their ability to act as carbon radical sources upon single-electron oxidation [66, 67]. In 2014, Molander's group reported the photoredox/nickel dual-catalyzed cross-coupling of potassium organotrifluoroborates with aryl bromides. The transformation was extended to the stereoconvergent cross-coupling of a racemic trifluoroborate **156** with an aryl bromide to afford the 1,1-diarylethane product **157** with 50% ee (Scheme 3.31) [68]. The same group further developed an asymmetric cross-coupling of potassium alkoxymethyl trifluoroborate **158** with acyl chloride to give ketone **159** in 91% yield with 62% ee (Scheme 3.31) [69].

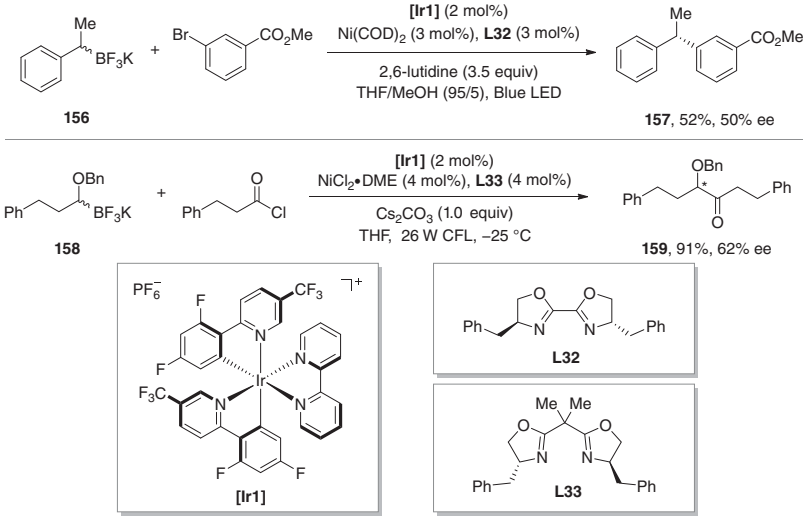


**Scheme 3.31** Asymmetric cross-coupling of organotrifluoroborates with aryl bromides or acyl chlorides by photoredox/nickel dual catalysis.

In 2017, Doyle's group described the enantioselective desymmetrization of cyclic meso-anhydrides **160** with benzyl trifluoroborates by dual photoredox and nickel/Box catalysis (Scheme 3.32) [70]. This reaction allows access to *trans*

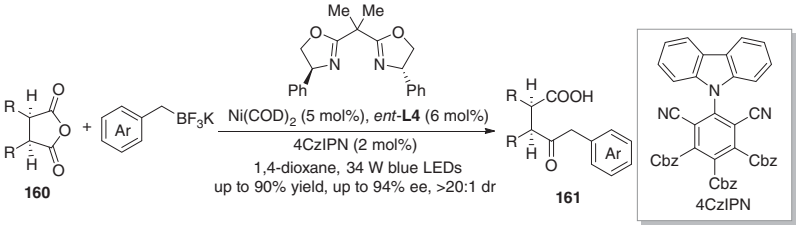


**Scheme 3.32** Desymmetrization of cyclic meso-anhydrides with benzyl trifluoroborates.

keto-acid products with high enantioselectivity from *cis* meso-anhydrides. A mechanism involving decarbonylation and Ni—C bond homolysis of Ni(II) adducts is proposed.

Reisman and coworkers reported an asymmetric cross-coupling of secondary α-*N*-heterocyclic trifluoroborates **162** with aryl bromides using Ni/photoredox dual catalysis (Scheme 3.33) [71]. In particular, the solubility of the *N*-heterobenzylic $BF_3K$ salts could be leveraged as a handle for controlling radical generation. A series of chiral five-membered heterocycles, including pyrroles (**164**, **165**, and **166**), azaindole (**167**), pyrazole (**168**), phthalimide (**169**), and pyrrolidine (**170**), were successfully intercalated into target molecules with moderate to excellent enantioselectivity.

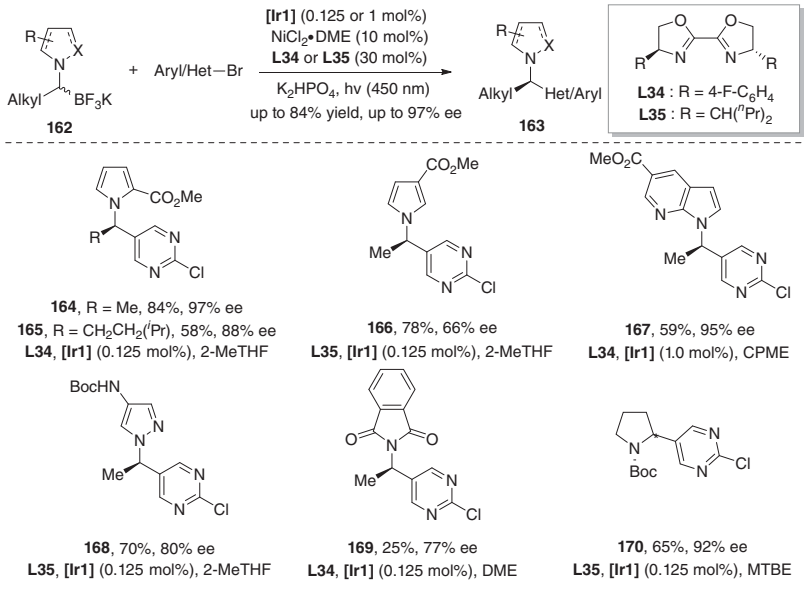


**Scheme 3.33** Asymmetric cross-coupling of α-*N*-heterobenzylic trifluoroborates with aryl bromides.

It was originally believed that Ni(0) catalysts first undergo oxidative addition with aryl bromides to provide aryl-nickel(II) complexes. Oxidative fragmentation of the alkyl trifluoroborate by the photoredox catalyst yields a C-centered radical, which is rapidly captured by this Ni(II) complex. Reductive elimination from the resulting Ni(III) species yields the cross-coupled product and Ni(I) complex (Scheme 3.34, path a). Molander and Kozlowski performed density functional theory (DFT) calculations to disclose the reaction mechanism [72]. The calculations reveal a new reaction pathway involving alkyl-nickel(I) complexes generated by the addition of alkyl radicals to Ni(0), which may operate in parallel with previously proposed mechanisms (Scheme 3.34, path b). Analysis of the enantioselective variant of the transformation reveals an unexpected manifold for stereoinduction, involving

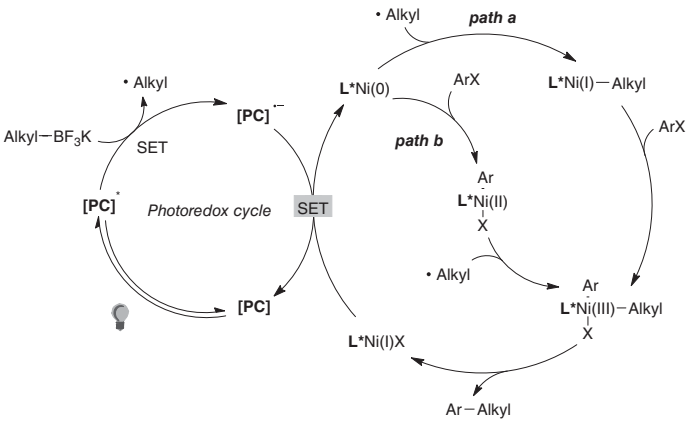


**Scheme 3.34** Possible mechanism for the dual photoredox/nickel-catalyzed cross-coupling of organotrifluoroborates with aryl bromides

dynamic kinetic resolution of a Ni(III) intermediate, where the stereodetermining step is reductive elimination.

Ni-catalyzed cross-coupling of alkyl halides is mainly used for the stereoselective construction of C—C bonds. In 2018, Fu and coworkers expanded the scope of nickel/PyBox-catalyzed stereoconvergent cross-coupling of alkyl chlorides to construct carbon–heteroatom bonds. Specifically, the conversion of benzylic chlorides **171** into synthetically useful enantioenriched benzylic boronic esters **172** was accomplished [73]. Notably, functional groups such as ether (**175**), ester (**176**), and primary alkyl chloride (**177**) are compatible with the borylation conditions (Scheme 3.35).

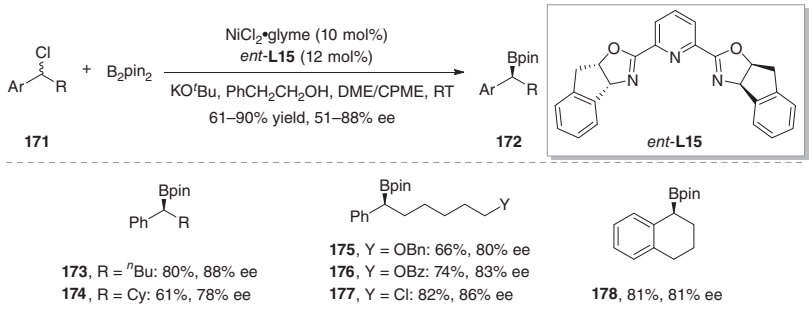


**Scheme 3.35** Enantioconvergent Miyaura borylation of benzylic chlorides.

## 3.3 Asymmetric Cross-Coupling with Redox Auxiliaries

A "redox auxiliary" is defined as an easily removable moiety that can be temporarily installed on a substrate to enable its activation by single-electron transfer processes [74]. Typical auxiliaries include xanthates, phosphites, and oxalates,

activated through electron transfer or light irradiation. Carbon–carbon bond formation based on redox auxiliaries offers an excellent complementary approach to conventional cross-coupling of organometallic nucleophiles with organohalides.

In 2014, MacMillan's group developed a photoredox/nickel dual-catalysis platform that enables carboxylate oxidation-$CO_2$ extrusion, a general mechanism for nucleophile activation. As a result, carboxylic acids can be utilized instead of organometallic nucleophiles, such as organozinc or organoboron reagents, in nickel-catalyzed cross-coupling reactions. [75]. In 2016, Fu and MacMillan developed the asymmetric decarboxylation arylation of α-amino acids **179** with aryl bromides through the synergistic merger of photoredox and nickel catalysis [76]. This protocol converts a variety of naturally abundant α-amino acids and readily available aryl halides to valuable enantioenriched benzylamines with high ee. The utility of this reaction was demonstrated in the synthesis of the cores of pharmacologically active molecules (**181** and **182**) (Scheme 3.36).

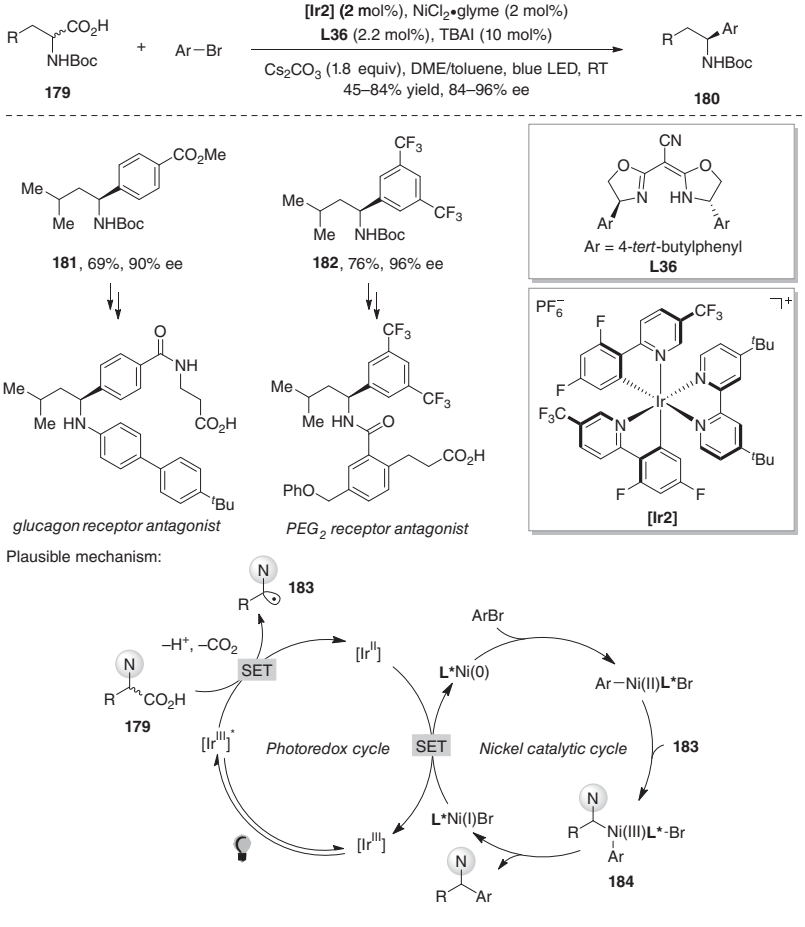


**Scheme 3.36** Enantioselective cross-coupling of α-amino acids with aryl bromides.

Mechanistically, the process involves deprotonation of the α-amino acid by a base, followed by oxidation through single-electron transfer with the excited-state Ir(III)* complex. This oxidation generates a carboxyl radical, which undergoes rapid $CO_2$ extrusion to form an α-amino radical **183**. Oxidative addition of Ni(0) species to the aryl halide produces a Ni(II) intermediate, which is rapidly intercepted by the α-amino radical to form the organometallic Ni(III) adduct **184**. Subsequent reductive elimination provides the desired α-amino arylation product **180** and regenerates the Ni(I) species. Finally, single-electron reduction of the Ni(I) species with Ir(II) yields the catalytically active Ni(0) catalyst.

*N*-benzyl heterocycles are an important class of heterocycles in the pharmaceutical industry, with many examples of commercial drugs and bioactive molecules. Davidson and coworkers reported a dual nickel/photoredox-catalyzed modular approach for the preparation of enantiomerically enriched *N*-benzyl heterocycles **186** via decarboxylative arylation of α-heterocyclic carboxylic acids **185** (Scheme 3.37) [77]. However, only moderate enantioselectivities were achieved. As mentioned above, Fu and MacMillan achieved excellent stereoselective control when using carbamate-protected amino acids as substrates. In this system, the protecting group on nitrogen may play a role as a coordinating moiety. Indeed, increased stereoselectivity was observed when a carbonyl functional group was introduced into the heterocycle (**189**). This finding suggests that the protecting group on nitrogen may be a directing group.

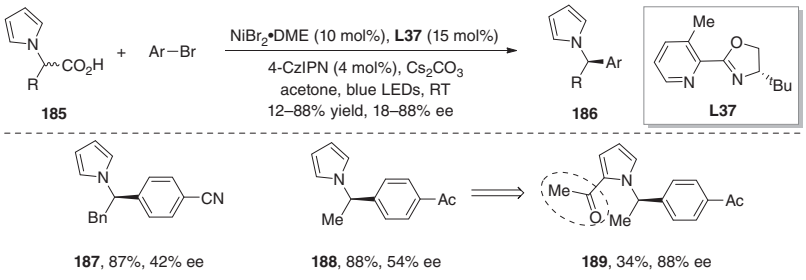


**Scheme 3.37** Synthesis of *N*-benzyl heterocycles via decarboxylative arylation of α-heterocyclic carboxylic acids.

4-Alkyl-1,4-dihydropyridines (alkyl-DHPs) can be prepared from aldehydes in one step. Melchiorre and colleagues demonstrated that alkyl-DHPs possess a dual reactivity profile. Excitation with violet light turns alkyl-DHPs into strong reducing agents that can activate reagents via single-electron transfer (SET) while undergoing homolytic cleavage to directly generate alkyl radicals [78]. The same group further developed photochemical asymmetric nickel-catalyzed α-acylation of anhydrides with alkyl-DHPs to afford enantioenriched α-substituted ketones **192** and **193** (Scheme 3.38) [79].

Mechanistically, upon excitation, racemic alkyl-DHPs can act as precursors of alkyl radicals and as strong reducing agents to generate catalytically active Ni(0) from Ni(I). The oxidative addition of Ni(0) to anhydrides, followed by the capture

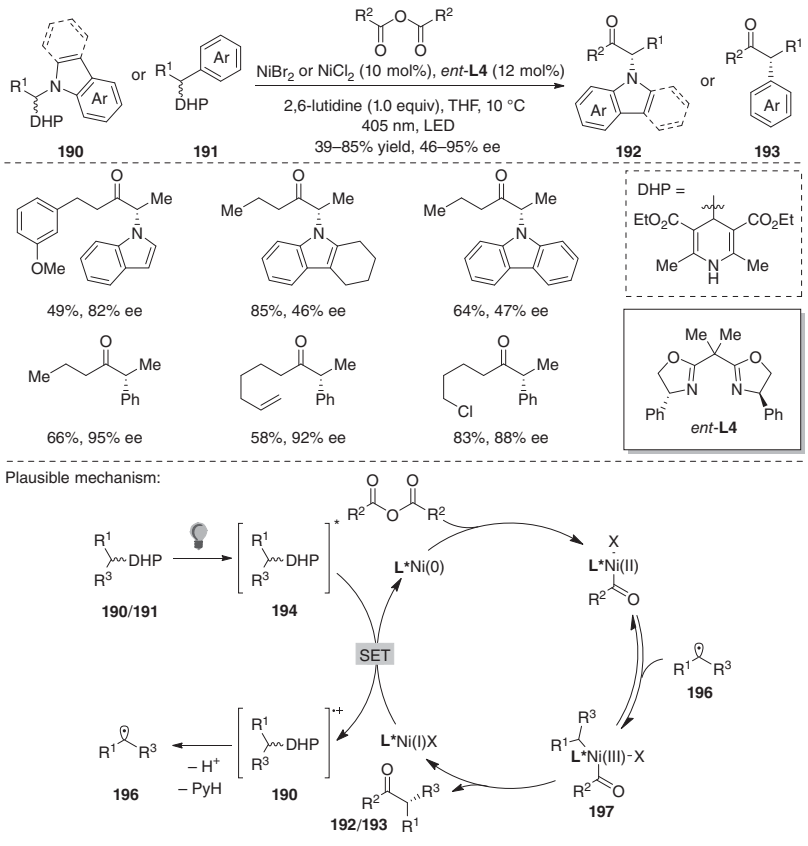


**Scheme 3.38** Asymmetric cross-coupling of alkyl-DHPs with anhydrides via dual photoredox/nickel catalysis.

of the resulting alkyl radicals, affords the acyl-Ni(III)-alkyl species **197**, which undergoes reductive elimination to deliver the target products.

*N*-Hydroxyphthalimide (NHP) esters are readily available, stable alternatives to Barton esters, derived from the corresponding carboxylic acids. As a type of redox-active compound, NHP esters can accept one electron via single-electron transfer, followed by cleavage of the N—O bond to generate the corresponding carbon-centered radicals. In 2021, Fu and coworkers reported a nickel-catalyzed asymmetric cross-coupling of alkylzinc reagents with NHP esters of α-amino acids using chiral diamine ligand **L38**, allowing the generation of enantioenriched dialkylamines **199** from commercially available amino acid derivatives **198** (Scheme 3.39) [17].

Similar to α-amino NHP esters **198**, α-oxy TCNHP esters **200** can generate the corresponding α-oxy radicals. Baran's group developed an enantioselective decarboxylative Negishi-type alkylation of readily available racemic α-oxy carboxylates, providing an efficient route to valuable chiral dialkyl carbinols **201** (Scheme 3.39) [80]. The nature of the ligand is critical to control the reactivity and

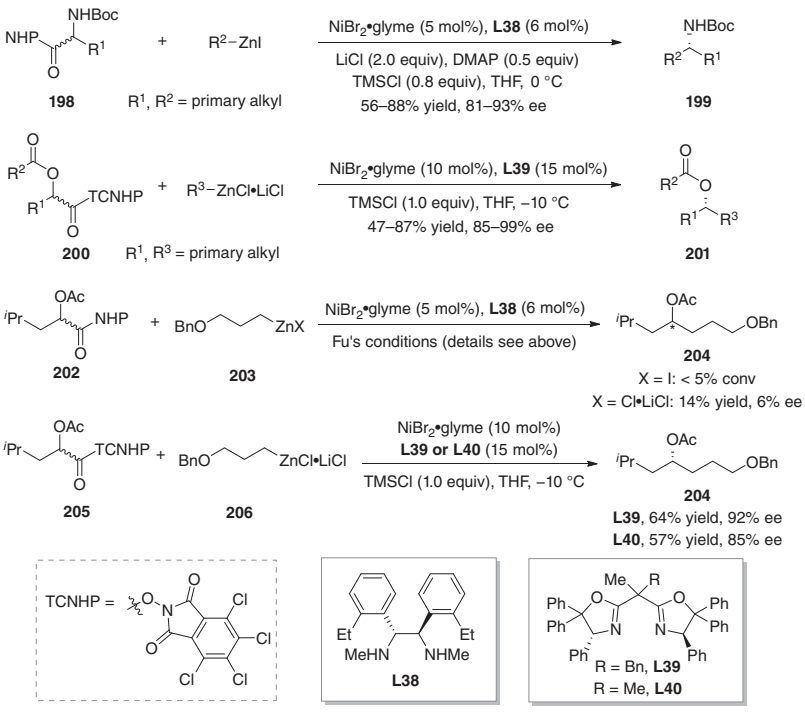


**Scheme 3.39** Asymmetric Negishi α-alkylation using NHP esters as radical precursors.

stereoselectivity of the reaction. The reaction of α-acetoxy redox-active ester **202** and organozinc reagent **203** using Fu's conditions resulted in low yield and ee. In the presence of chiral bis-oxazoline ligand **L39**, TCNHPI ester **205** and alkyl zinc reagent **206** were smoothly coupled, affording dialkyl acetate **204** in 64% yield and 92% ee.

Cyclopropanes are versatile building blocks that participate in various transformations in organic synthesis by exploiting their inherent high ring strain. Cyclopropanols have been widely applied in the synthesis of β-functionalized ketones, involving intermediates of homoenolates or β-keto radicals generated via ring-opening pathways. In 2020, Huang and Rueping disclosed a general strategy for the activation of a diverse set of readily available cyclic alcohols for the remote and site-specific arylation of ketones via photoredox and nickel catalysis [81]. Subsequently, Li and coworkers reported a photoredox and nickel dual-catalyzed asymmetric β-arylation of cyclopropanols **207** with aryl bromides (Scheme 3.40) [82]. This dual-catalytic transformation features a broad substrate scope and good functional group tolerance, providing facile access to a wide array of enantioenriched β-aryl ketones **208** in good yields with satisfactory enantioselectivities.

Mechanistically, the excited photocatalyst Ir(III)* oxidizes cyclopropanols **207** via a proton-coupled electron transfer (PCET) process to generate the key alkoxy radical

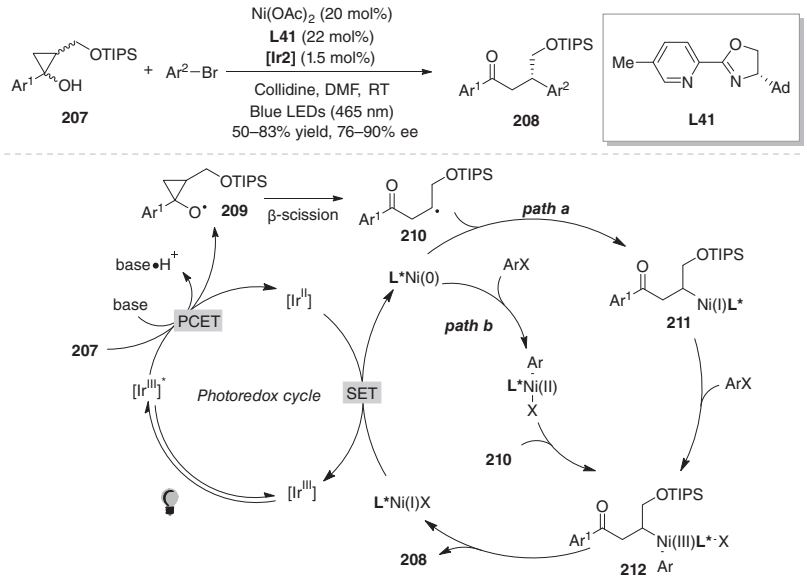


**Scheme 3.40** Asymmetric β-arylation of cyclopropanols.

intermediate **209**. Subsequent ring-opening through β-scission leads to a secondary alkyl radical **210**, which can engage in nickel-catalyzed cross-coupling.

Zhang's group developed a nickel/bisphosphine-catalyzed stereoconvergent cross-coupling of epoxides with alkenyl boronic acids [83]. Spiroepoxyoxindoles **213** were converted to homoallylic alcohols **214** bearing quaternary carbon stereogenic centers with good to excellent enantioselectivities (Scheme 3.41). The radical trapping reaction with TEMPO (2,2,6,6-tetramethylpiperidine-1-oxyl) supported

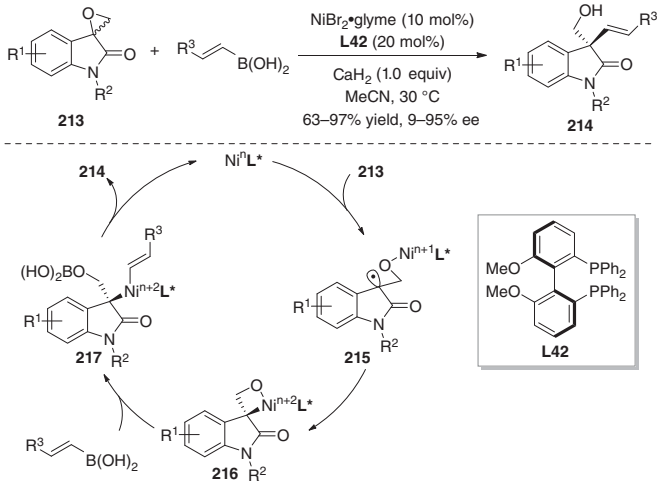


**Scheme 3.41** Stereoconvergent cross-coupling of epoxides with alkenyl boronic acids.

a single-electron transfer mechanism via a stabilized tertiary radical intermediate **215**. A possible reaction mechanism was proposed. Two consecutive SET-type oxidative additions of nickel to epoxides **213** afford a four-membered oxanickelacycle intermediate **216**, which undergoes transmetalation with alkenyl boronic acids, followed by reductive elimination to give the target chiral homoallylic alcohol **214**.

## 3.4 Asymmetric Cross-Coupling with Aliphatic C($sp^3$)—H Bonds

The inert C($sp^3$)—H bonds are ubiquitous motifs in organic molecules. The direct enantioselective C($sp^3$)—H functionalization is undoubtedly a transformative approach to accessing high-value chiral molecules. However, the intrinsic chemical inertness and too much similarity in polarity of C($sp^3$)—H bonds have made the regio- and stereoselective transformation of these hydrocarbons an almost insurmountable task. Among the few available strategies, transition-metal-catalyzed, directing group-assisted C–H activation has been successfully established for the regio- and enantioselective functionalization of C($sp^3$)—H bonds [84, 85]. In addition, the concerted metal carbenoid/nitrenoid C—H insertion reaction enables the direct enantioselective conversion of hydrocarbons to chiral molecules [86, 87]. In recent years, the combination of hydrogen atom transfer (HAT) with nickel catalysis has emerged as a powerful strategy for the direct functionalization of feedstock hydrocarbons. The proposed mechanism for this class of reactions involves hydrogen atom abstraction from hydrocarbons to generate carbon-centered radicals, which then engage in nickel-catalyzed cross-coupling [64, 75, 88–98]. The mild reaction protocol avoids the need for exogenous directing groups and organometallic reagents, representing an attractive complementary strategy to conventional C($sp^3$)—H activation reactions.

In 2019, Lu and coworkers reported the first enantioselective benzylic C($sp^3$)—H arylation via photoredox/nickel dual catalysis using their self-designed chiral bis-imidazoline (BiIM) ligand [99]. Using an iridium photocatalyst with DMBP as a co-photocatalyst and the sterically hindered **L49** as a ligand, the reaction of ethylbenzene with methyl 4-bromobenzoate afforded 1,1-diaryl alkane **218** in 44% yield and 90% ee under the irradiation of blue LEDs (Scheme 3.42). Subsequently, Huo and colleagues reported a similar enantioselective benzylic β-C($sp^3$)—H arylation of amides [100]. The β-amide group was found to play a crucial role in asymmetric induction. Arylation of the γ-amide (**222**) resulted in a marked decrease in enantioselectivity. Replacing the β-amide with a weak directing group, such as a β-ketone (**223**) or a β-ester (**224**), led to a significant reduction in efficiency and enantioselectivity (Scheme 3.42).

Compared with the arylation of benzylic C($sp^3$)—H bonds, the alkenylation of benzylic C($sp^3$)—H bonds is more challenging because the photocatalytic *E*/*Z* isomerization of alkenes is easily carried out via an energy transfer pathway under visible light irradiation. Lu and coworkers further achieved stereo- and enantioselective alkenylation of benzylic C($sp^3$)—H bonds via photoredox/nickel catalysis

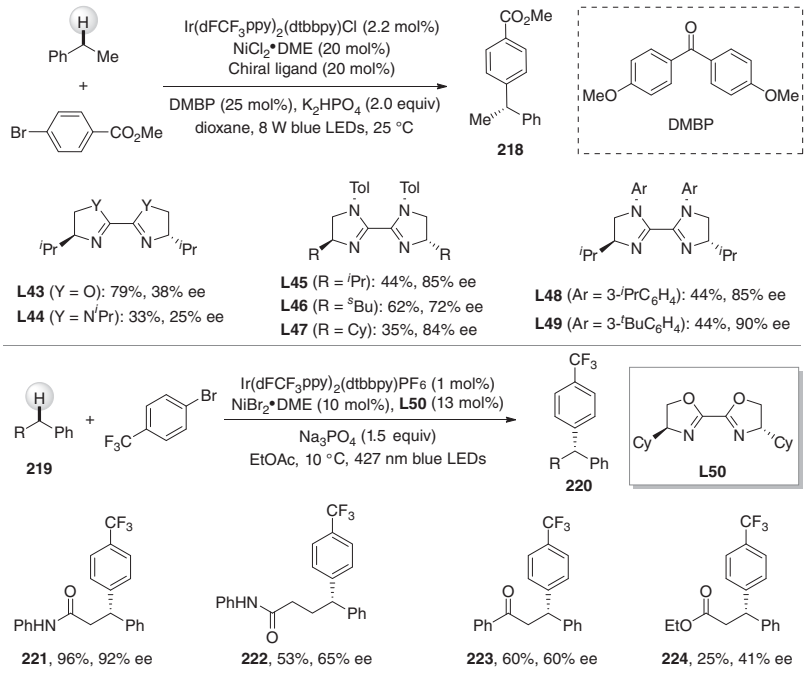


**Scheme 3.42** Enantioselective benzylic C($sp^3$)–H arylation.

(Scheme 3.43) [101]. Readily available alkylbenzenes and alkenyl bromides undergo the cross-coupling reaction smoothly to afford chiral allylic compounds **225** in up to 93% ee and >20/1 *E*/*Z* ratio with good functional group tolerance. Stilbene **226** or **227**, as a triplet-energy inhibitor, was used in the stereoconvergent synthesis of alkenes through declining photocatalytic *E*/*Z* isomerization of the product.

Almost simultaneously, the Huo group independently developed an enantioselective benzylic C($sp^3$)—H bond alkenylation for the stereodivergent synthesis of both *E*- and *Z*-alkenes **228** (Scheme 3.43) [102]. Tunable *Z*/*E* selectivity is achieved by energy transfer catalysis using iridium photocatalysts with different counteranions, $PF_6^-$ for *Z*-selectivity (thermodynamically disfavored) and $Cl^-$ for *E*-selectivity. This is consistent with the previous hypotheses by Yoon [103] and Meyer [104] that more coordinating counteranions lead to shorter lifetimes or lower triplet-excited-state energies.

Subsequently, Huo and coworkers reported an asymmetric benzylic C—H acylation of alkylarenes employing carboxylic acids as acyl surrogates for the synthesis of α-aryl ketones (Scheme 3.44) [105]. The mild and straightforward protocol converts various feedstock carboxylic acids and simple alkylbenzenes to highly valuable α-aryl ketones **229** with high enantioselectivities. Murakami's group further reported the benzylic C($sp^3$)—H carbamoylation of ethylbenzene with isocyanate under visible light irradiation in the presence of an iridium photoredox catalyst and a bromide anion. However, the α-aryl amide **230** was obtained in low yield and moderate stereoselectivity (Scheme 3.43) [106].

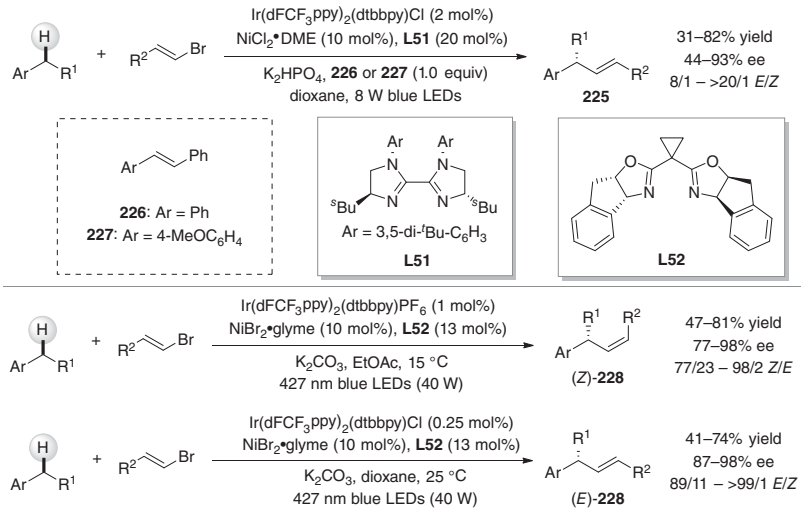


**Scheme 3.43** Stereo- and enantioselective benzylic C(sp³)—H alkenylation.

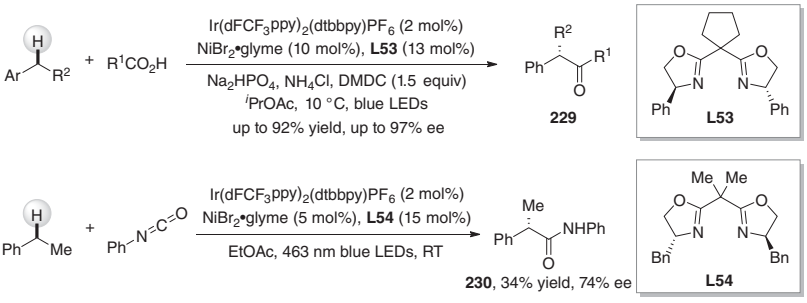


**Scheme 3.44** Enantioselective benzylic C(sp³)—H acylation and carbamoylation.

The ubiquity of saturated amines in a myriad of biologically active molecules has prompted chemists to develop noninvasive site-selective C(sp³)—H functionalization as a platform for structural diversity. In 2016, Doyle's group reported the first example of α-amino C(sp³)—H arylation with aryl halides using a nickel-photoredox dual catalyst system. Gratifyingly, the use of a chiral Biox ligand **L55** generated 2-arylpyrrolidine **231** with moderate enantioinduction, demonstrating the ability of the nickel catalyst to dictate facial selectivity in the arylation protocol (Scheme 3.45) [107].

To address this gap, Montgomery and Martin developed the enantioselective α-amino C(sp³)—H arylation of aliphatic secondary amides **232** with aryl halides. The corresponding α-arylated products **233** could be obtained in high levels of enantioselectivity with comparable yields (Scheme 3.45) [108].

Chiral α-aryl *N*-heterocycles are common structural motifs in many natural products and pharmaceuticals, but their access via asymmetric catalysis remains challenging. Huo and coworkers developed a general and modular approach for the

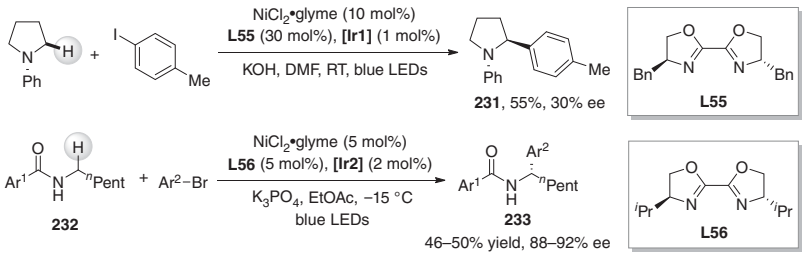


**Scheme 3.45** α-Amino C($sp^3$)—H arylation via dual nickel/photoredox-catalysis.

direct enantioselective α-arylation of saturated azacycles **234** via nickel/photoredox dual catalysis (Scheme 3.46) [109]. This process utilizes the HAT ability of photoeliminated chlorine radicals to convert *N*-heterocycles to the corresponding α-amino alkyl radicals, which are then coupled with ubiquitous and inexpensive (hetero)aryl chlorides. This protocol features a broad substrate scope, including lactams (**236**, **237**), cyclic amides (**238**–**241**), and cyclic carbamates (**242**–**244**), which are all compatible. Furthermore, the ring size (**236**, **237**, and **238**–**241**) has a limited effect on the level of stereocontrol. It is worth mentioning that the benzoyl protecting group on the nitrogen plays a crucial role in achieving high stereoselectivity, which may act as a directing group or as a handle for stereoselective induction.

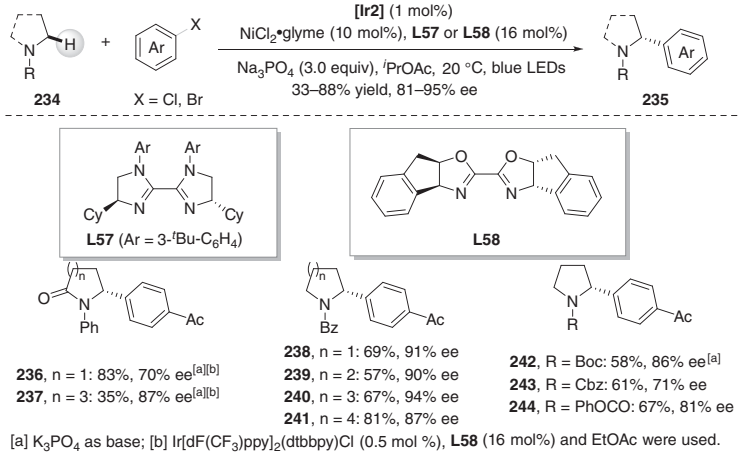


**Scheme 3.46** Enantioselective α-amino C($sp^3$)—H arylation of amides.

The same group further developed the enantioselective α-amino C($sp^3$)—H acylation of acyclic amides **245** with carboxylic acids. This protocol enables the cross-coupling of various carboxylic acids with readily available *N*-alkylbenzamides to produce high-value α-aminoketones **246** with high enantioselectivity under mild conditions (Scheme 3.47) [110].

Enantioselective α-amino C($sp^3$)—H acylation of acyclic amides was further extended to cyclic amides **247** by the same group (Scheme 3.48) [111]. The challenging issue of regioselectivity was settled by choosing chlorine radicals, which are more polarity-matched (local electrophilicity of Cl**.** and Br**.**: 3.8 eV vs 3.6 eV) [112,

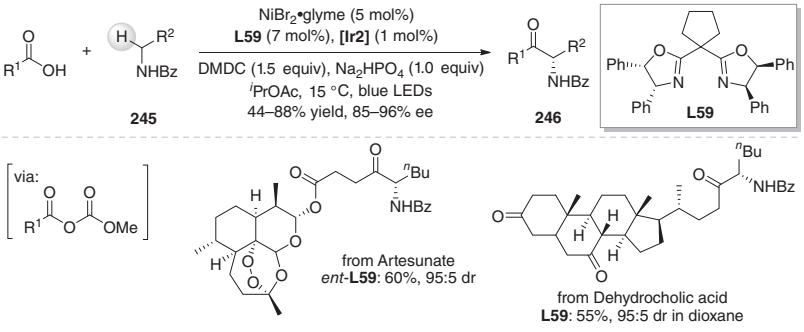


**Scheme 3.47** Enantioselective α-amino C(sp³)—H acylation of acyclic amides.

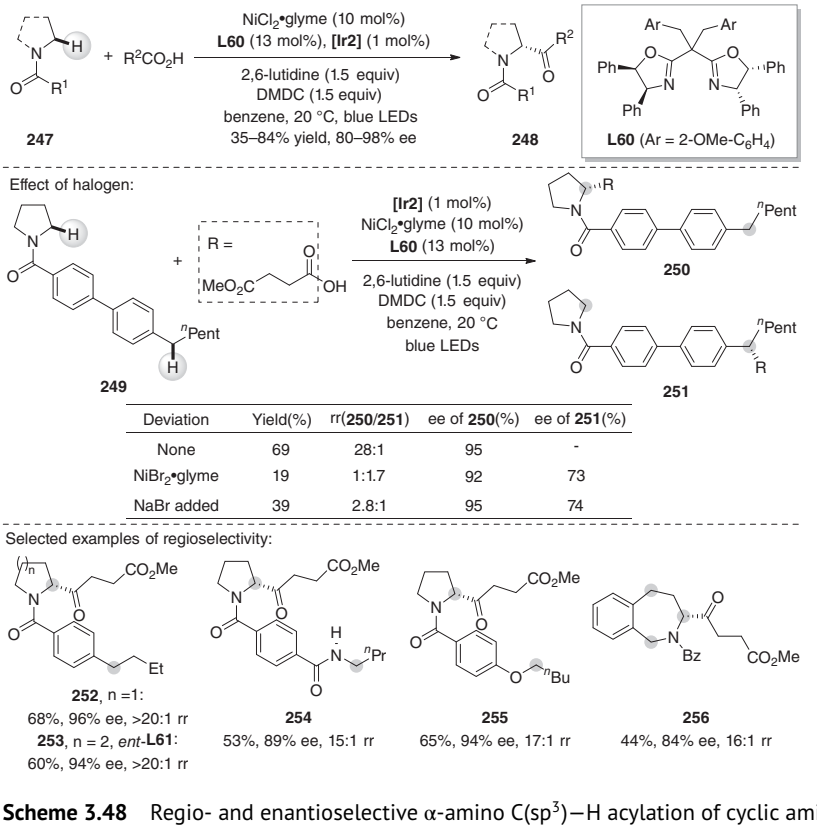


| Deviation | Yield(%) | rr(**250**/**251**) | ee of **250**(%) | ee of **251**(%) |
|---|---|---|---|---|
| None | 69 | 28:1 | 95 | - |
| $NiBr_2$•glyme | 19 | 1:1.7 | 92 | 73 |
| NaBr added | 39 | 2.8:1 | 95 | 74 |




**Scheme 3.48** Regio- and enantioselective α-amino C(sp³)—H acylation of cyclic amides.

113] and thermodynamically stable than bromine radicals (BDEs of H—Cl and H—Br: 103 kcal/mol vs 88 kcal/mol), as HAT abstractors. Control experiments confirmed this hypothesis: once bromine was introduced, the reactivity and selectivity of the α-amino C(sp³)—H acylation of amide **249** with 4-methoxy-4-oxobutanoic acid decreased significantly. Excellent regioselectivities were maintained in the presence of benzylic C(sp³)—H bonds (**250**, **252**, **253**, and **256**) or α-oxy C(sp³—H bonds (**255**). Cyclic tertiary amides are preferentially acylated over acyclic secondary

amides (**254**) because the former have a more fixed conformation due to restricted rotation, resulting in a stronger interaction between the lone pair of electrons on the nitrogen and the adjacent C—H bond [114].

Based on the above results, a possible mechanism was proposed and is shown in Scheme 3.49. Initially, Ni(II) dichloride is oxidized by the excited photocatalyst to afford Ni(III) trichloride species, which is photolyzed to provide Cl· and regenerate Ni(II) dichloride. The photoeliminated Cl· undergoes selective HAT with the most hydridic α-amino C—H bond to produce a prochiral α-amino radical, which is trapped by Ni(I) chloride to form alkyl-Ni(II) chloride. A single-electron transfer (SET) between the Ni(II) complex and the reduced photocatalyst will regenerate the ground-state photocatalyst and simultaneously provides an alkyl-Ni(I) complex. Oxidative addition of alkyl-Ni(I) complexes with in situ activated carboxylic acids yields Ni(III) species. Finally, reductive elimination provides an enantiomerically enriched coupling product and regenerates the active Ni(I) chloride catalyst.

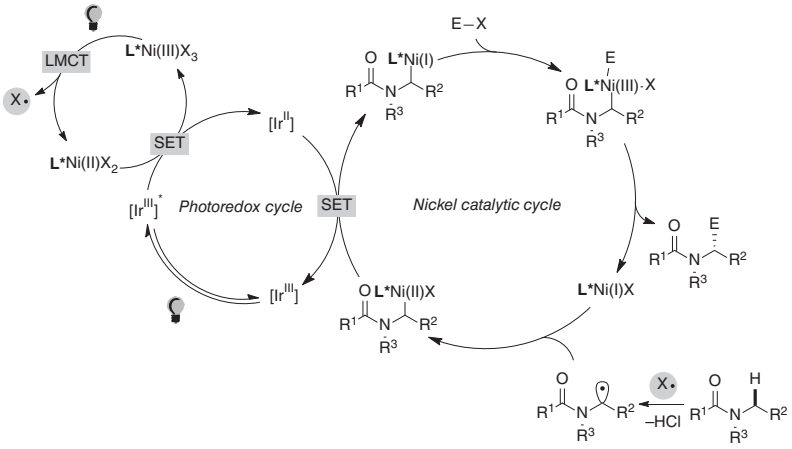


**Scheme 3.49** Plausible mechanism for α-amino C($sp^3$)—H functionalization.

Asymmetric α-oxygen C($sp^3$)—H functionalization is an ideal approach to afford synthetically attractive enantiomerically enriched alcohols and their derivatives. In 2018, Martin et al. designed a catalytic platform employing a synergistic combination of nickel and triplet-excited diaryl ketone catalysts for the utilization of saturated feedstocks as functional handles in C($sp^3$)—H arylation. Asymmetric α-oxy C($sp^3$)—H arylation of THF was also achieved, but only with low enantioselectivity (54% ee) (Scheme 3.50) [115].

The introduction of protecting groups into the nitrogen heterocycle not only modulates the BDEs of the α-amino C($sp^3$)—H bonds but also acts as a functional handle for stereoselective control. Unlike azacycles, planar oxacycles have similar steric hindrance and lack functional handles, making the catalytic enantiomeric differentiation of small oxacycles extremely challenging.

Recently, Kong and coworkers addressed the enantioselective C($sp^3$)—H functionalization of oxacycles without exogenous directing groups by utilizing a synergistic catalyst consisting of a tunable chiral PHOX-nickel catalyst and a commercially available diaryl ketone photocatalyst (Scheme 3.51) [116]. This elegant platform

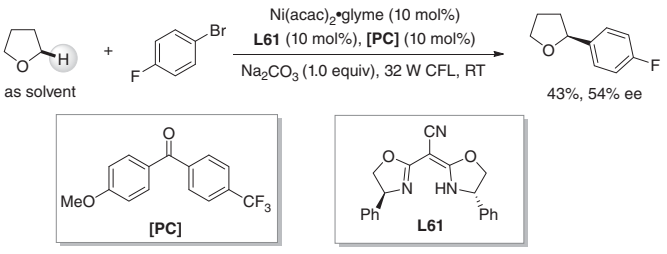


**Scheme 3.50** α-Oxy C(sp³)—H arylation via dual nickel/photoredox-catalysis.

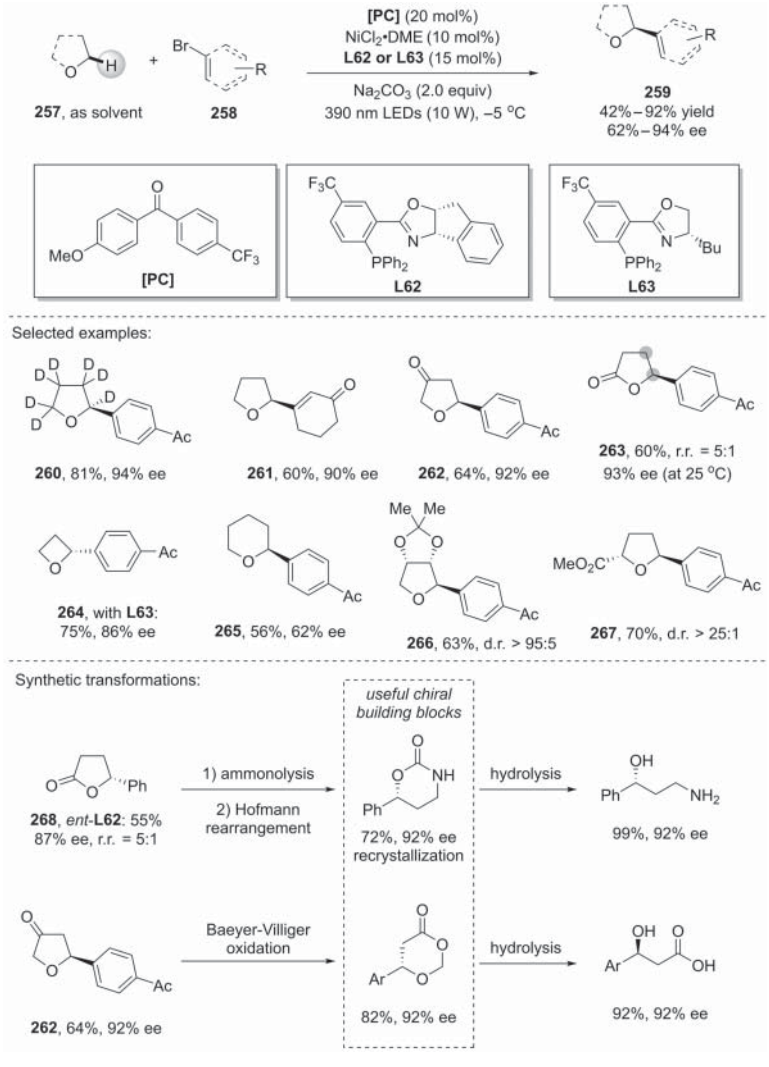


**Scheme 3.51** Enantioselective α-oxy C(sp³)—H functionalization.

tolerates diverse aryl bromides, heteroaryl bromides, and alkenyl bromides (**261**), which have also been demonstrated as suitable electrophilic partners. Various oxacycles, including deuterium-labeled tetrahydrofuran (**260**), tetrahydrofuran-3-one (**262**), and γ-butyrolactone (**263**), retain potent reactivity and enantioselectivity. The size of the ring has a great influence on the control of stereoselectivity. Both five-membered oxacycles and oxetane (**264**) achieved high stereoselectivity, while the stereoselectivity of oxane (**265**) was reduced. The utility of this protocol was further demonstrated in the late-stage functionalization of natural products and the synthesis of many pharmaceutically relevant molecules.

DFT calculations were also performed to gain a deeper insight into the reaction mechanism (Scheme 3.52). Initially, upon light irradiation, the ketone sensitizer **PC** is excited to generate a triplet-excited state, **PC***, which can capture a hydrogen atom from THF to produce a carbon-centered radical. The radical addition of the resulting carbon-centered radical to the chiral Ni(I) species is the stereoselectivity-determining step. A single-electron transfer (SET) between the alkyl-Ni(II) complex and the reduced photocatalyst $\mathbf{PC}^-$ will regenerate the ground-state photocatalyst while simultaneously providing the alkyl-Ni(I) complex. Oxidative addition of the alkyl-Ni(I) complex to aryl bromides, followed by reductive elimination, provides chiral α-functionalized oxacycles and regenerates the active Ni(I) chloride catalyst.

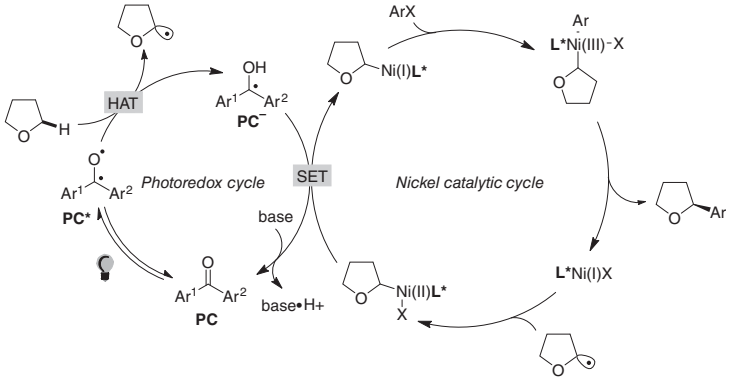


**Scheme 3.52** Plausible mechanism of enantioselective α-oxy C($sp^3$)—H functionalization

Nitroalkanes are broadly useful building blocks in organic synthesis. Watson's group reported the nickel-catalyzed asymmetric alkylation of nitroalkanes using α-bromoamides **269**, the first example of asymmetric nitroalkane alkylation using haloalkane electrophiles (Scheme 3.53) [117]. This method enables the formation of highly enantioenriched β-nitroamides **270** from readily available α-bromoamides **269** using mild reaction conditions that are compatible with a wide range of functional groups.

Mechanistically, reduction of the Ni(II) precatalyst by $Et_2Zn$ leads to the formation of the Ni(0) complex, which then undergoes a disproportionation reaction with excess Ni(II) complex to generate an active Ni(I) catalyst. Deprotonation of the acidic

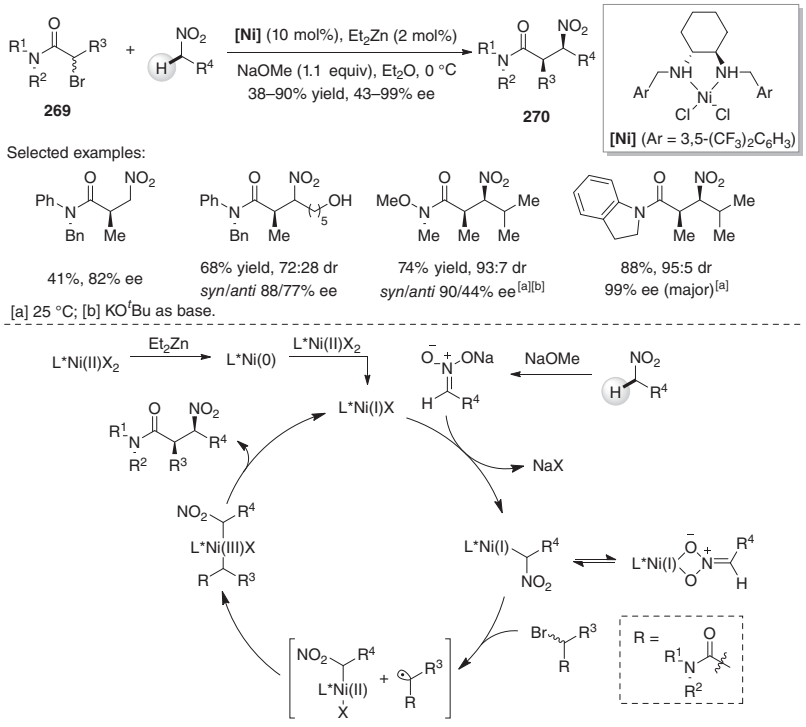


**Scheme 3.53** Enantioselective α-alkylation of nitroalkanes.

nitroalkane by the alkoxide base produces a nitronate anion, which undergoes anion exchange with the Ni(I) complex to yield the Ni(I) nitrogen nitronate. This Ni(I) complex then reacts with the alkyl bromide via oxidative addition followed by reductive elimination to provide the observed product and regenerate the catalyst.

## 3.5 Asymmetric Redox-Neutral Alkene Functionalization

Due to the versatile reactivity of the C=C bond and the easy availability of many unfunctionalized alkenes, alkenes are excellent starting materials in organic synthesis. Difunctionalization of alkenes by simultaneously adding two different functional groups on the double bond in one operation, allows rapid access to complex molecules with great potential for industrial applications, thus attracting much attention from researchers over the past few decades. Such transformations involving intramolecular carbon-nickelation of alkenes, followed by intermolecular nucleophilic or electrophilic trapping of the resulting σ-alkyl-nickel intermediate, have been extensively explored. Although transition-metal-catalyzed asymmetric oxidative [118–127], reductive [128–140], and redox-neutral [141–145] difunctionalization of alkenes has been developed, this section mainly focuses on the nickel-catalyzed redox-neutral strategy.

The Fu group determined that a nickel/1,2-diamine-based catalyst accomplished two distinct enantioselective transformations: create a stereocenter by the cyclization of arylboron reagent **271**, which bears a pendant olefin, as well as the control of the absolute stereochemistry of a second stereocenter through an enantioconvergent coupling with secondary alkyl halide **272** (Scheme 3.54) [146]. Mechanistically, transmetalation of organoboron reagent **271** with nickel, followed by migratory insertion into the alkenes, generates the alkyl-nickel(I) intermediate **274**. Single-electron transfer of alkyl halides with **272** generates the corresponding alkyl radical and alkyl-nickel(II) intermediate **275**. A nucleophilic attack of alkyl radicals on alkyl-nickel(II), followed by reductive elimination, yields the target product **273**. However, applying this approach to the catalytic asymmetric generation of quaternary stereocenters was unsuccessful, yielding only modest stereoselectivity (**278**).

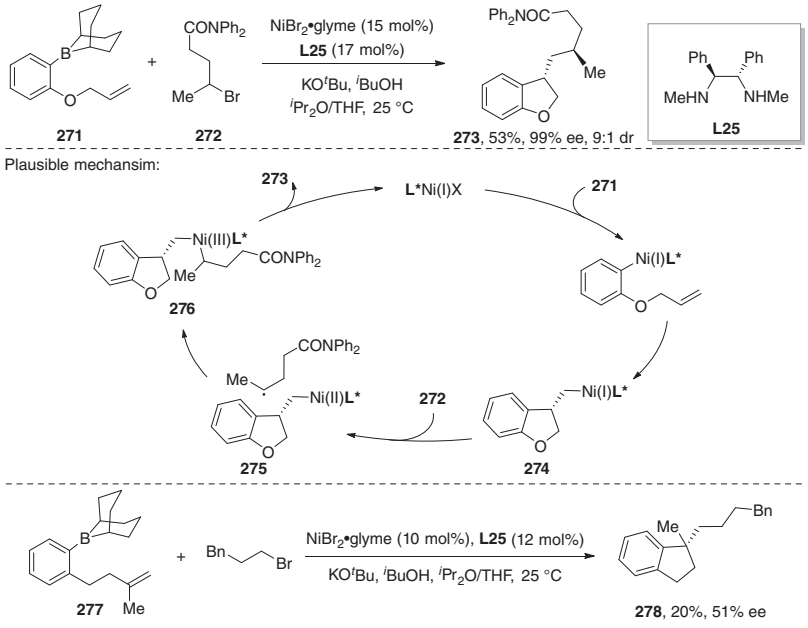


**Scheme 3.54** Enantioselective cyclization/cross-coupling of arylboron with alkyl electrophiles.

Wang and coworkers developed the enantioselective acyl-carbamoylation of alkenes via the combination of HAT photo- and asymmetric nickel catalysis. This protocol provided a variety of 3,3-disubstituted oxindoles **281** bearing a quaternary stereogenic center with excellent enantiomeric excess from aryl carbamoyl chloride-tethered alkenes **279** and aldehydes **280** under the cooperative catalysis of TBADT and Ni-PHOX complex (Scheme 3.55) [147]. Preliminary mechanistic investigations suggest that a Ni(III)-mediated migratory insertion might be engaged as the enantiodetermining step in the catalytic cycle wherein the acyl radical is generated by TBADT from the aldehyde through acyl C—H activation.

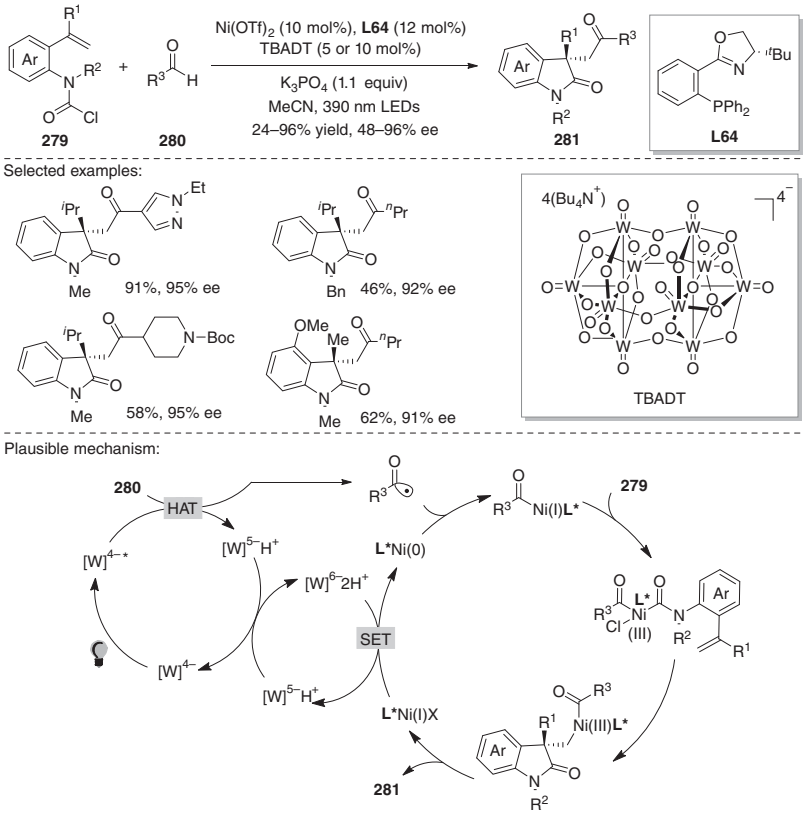


**Scheme 3.55** Enantioselective acyl-carbamoylation of alkenes.

In 2020, Chu and coworkers reported the intermolecular asymmetric three-component carboarylation of alkenes with tertiary and secondary alkyltrifluoroborates and aryl bromides through synergistic photoredox/nickel catalysis [148]. This redox-neutral protocol allows for facile and divergent access to a wide array of enantioenriched β-alkyl-α-arylated carbonyls **282**, phosphonates, and sulfones in high yields and excellent enantioselectivities (Scheme 3.56). Computational and experimental studies were carried out that were consistent with a Ni(0)/Ni(II)/Ni(III) catalytic cycle, with the radical addition to the tetrahedron Ni(II) species as the stereodetermining step.

The same group further reported a similar asymmetric carbo-alkenylation of vinyl phosphonates, providing a diverse array of α-alkenyl phosphonates from vinyl phosphonates, alkenyl halides, and alkyl trifluoroborates (Scheme 3.57) [149]. Furthermore, by simple modification of the triplet energy of the photocatalyst employed, both enantioenriched *trans* and *cis* α-alkenyl phosphonates **283** can be divergently accessed. Computational and experimental studies support a radical cascade sequence, with α-phosphonate controlling the trajectory of radical capture by a chiral tetrahedral alkenyl nickel(II) species in the enantioselectivity-determining step.

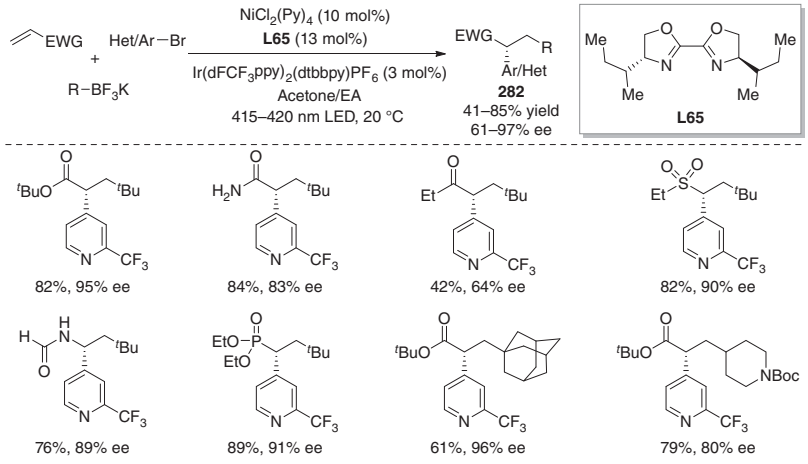


**Scheme 3.56** Asymmetric three-component carboarylation of alkenes.

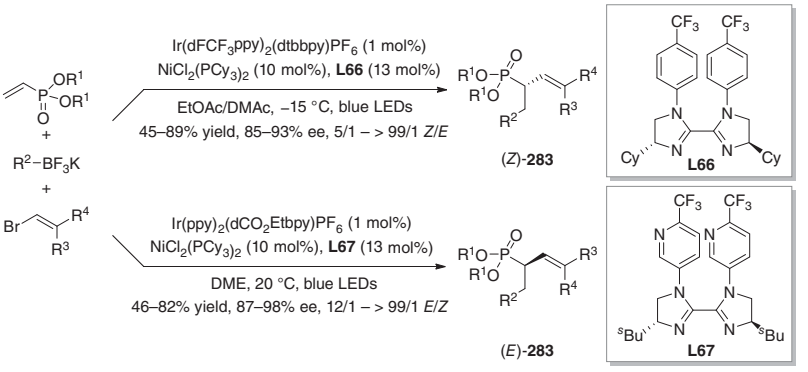


**Scheme 3.57** Enantioselective alkyl-alkenylation of vinyl phosphonates.

Shu and Nevado reported the enantioselective alkenyl-sulfonylation of styrenes [150] and aryl-sulfonylation of enamides [151], respectively (Scheme 3.58). The reaction, involving the simultaneous formation of a C—C and a C—S bond across the π-system, uses a dual nickel/photoredox catalytic system to produce both β-aryl and β-alkenyl sulfones in high yields with excellent stereocontrol. Control experiments support the involvement of a secondary alkyl radical intermediate generated through the radical addition of a sulfonyl radical to the double bond. Moreover, stoichiometric and cross-over experiments suggest an underlying Ni(0)/Ni(I)/Ni(III) pathway operative in these transformations.

Yin and coworkers reported the nickel-catalyzed diastereo- and enantioselective alkyl-borylation of heterocyclic alkenes, providing a rapid and modular protocol for constructing a diversity of 2,4-disubstituted heterocycles (Scheme 3.59) [152]. The reaction is initiated by the transmetalation of the nickel catalyst with $B_2Pin_2$ to form a Ni(II)–Bpin species. The migratory insertion of the Ni(II)–Bpin species into the alkene, followed by chain-walking via β-hydride elimination and further migratory

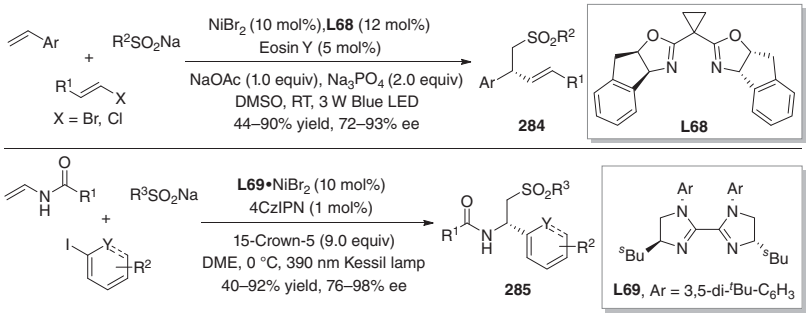


**Scheme 3.58** Enantioselective alkenyl- and aryl-sulfonylation of alkenes.

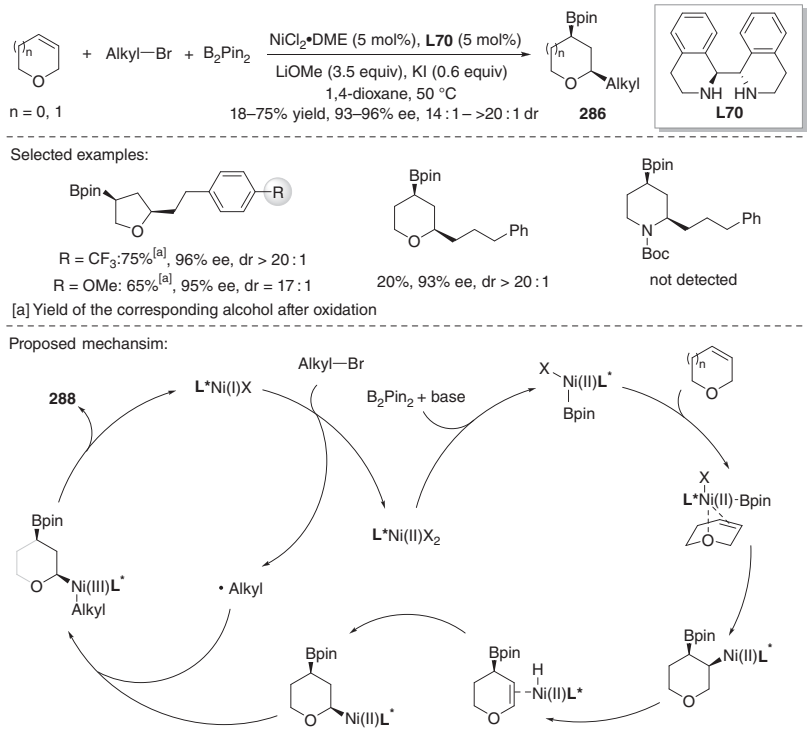


**Scheme 3.59** Diastereo- and enantioselective alkyl-borylation of heterocyclic alkenes.

insertion, leads to the formation of an α-oxygen alkyl-nickel(II) species. This nickel intermediate reacts with an alkyl radical, generated from the alkyl bromide and a Ni(I) species, resulting in the formation of a Ni(III) species. The reductive elimination of the Ni(III) species produces the migratory carboboration product. The stereochemical outcome suggests that the olefin intermediate does not dissociate from nickel during chain-walking.

The same group further reported an asymmetric nickel-catalyzed borylative coupling of terminal alkenes with nonactivated alkyl halides, providing a

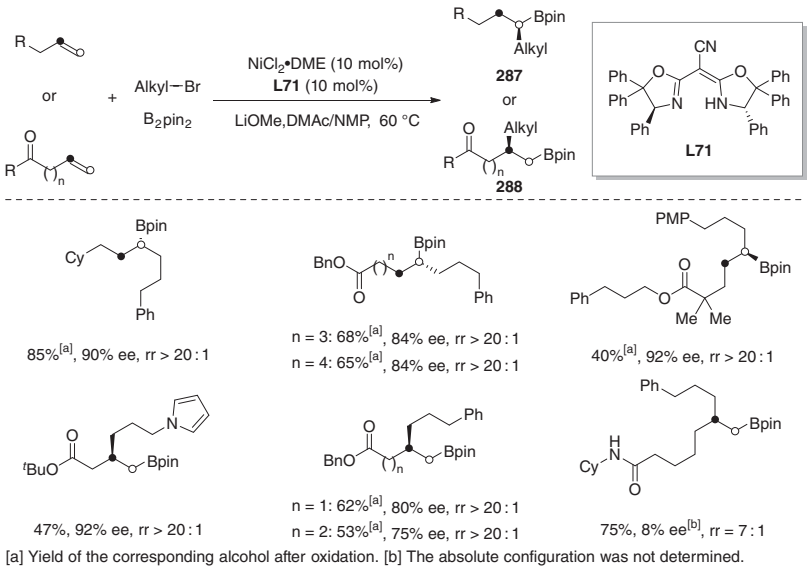


[a] Yield of the corresponding alcohol after oxidation. [b] The absolute configuration was not determined.

**Scheme 3.60** Enantioselective alkyl-borylation of terminal alkenes.

three-component strategy to access α- and β-stereogenic boronic esters from easily accessible starting materials (Scheme 3.60) [153]. The regioselectivity of this approach is strongly influenced by the alkene partners. Nonactivated terminal alkenes without strong coordinating groups provide 1,1-alkyl-borylation products **287** via chain-walking involving a stable α-boron-nickel intermediate. Borylation of terminal alkenyl esters/amides yields 1,2-alkylborated products **288** involving five- or six-membered cyclic nickel intermediates. The carbonyl of the ester strongly coordinates with nickel, inhibiting the elimination of β-hydride and thus the chain-walking process.

Of particular note is that while the regioselectivity is neither affected by the alkyl electrophile partner nor by the ester and amide protecting groups, the enantioselectivity is strongly substrate-dependent, with many substrates leading to very low stereoselectivity.

## 3.6 Summary and Outlook

Nickel-catalyzed electrophile–nucleophile and related asymmetric radical cross-couplings have flourished since the early 2000s, demonstrating the unparalleled potential of nickel in asymmetric C—C bond formation. The majority of protocols employ commercially available nickel catalysts and chiral nitrogen-containing ligands under mild reaction conditions. While significant progress has been made in the field, some issues and challenges remain.

Asymmetric cross-coupling is still mainly limited to the construction of $C(sp^3)$—$C(sp^2)$ bonds, and the asymmetric construction of $C(sp^3)$—$C(sp^3)$ bonds is

still very rare. To obtain a wider range of $Csp^3$ coupling partners that can be used as alkyl radical precursors, radical generation mechanisms other than organohalides should be explored. The direct functionalization of C—H compounds using synergistic photoredox/nickel catalysis is an exciting new direction. This strategy not only expands the source of alkyl radicals but also addresses the inherent disadvantages of using heterogeneous metal-reducing agents.

Overall, Ni-catalyzed cross-coupling can afford the desired products in good yields with high stereoselectivities and has been applied to the synthesis of natural products. We believe that the field will continue to develop and revolutionize the way carbon–carbon bonds are constructed in an enantioselective manner.

## References


1 Rudolph, A. and Lautens, M. (2009). *Angew. Chem. Int. Ed.* 48: 2656–2670.
2 Jana, R., Pathak, T.P., and Sigman, M.S. (2011). *Chem. Rev.* 111: 1417–1492.
3 Iwasaki, T. and Kambe, N. (2014). Coupling Reactions between $sp^3$-carbon centers. In: *Comprehensive Organic Synthesisc*, vol. 3 (ed. P. Knochel and G.A. Molander), 337–391. Amsterdam: Elsevier.
4 Manolikakes, G. (2014). Coupling Reactions between $sp^3$ and $sp^2$ carbon centers. In: *Comprehensive Organic Synthesis*, vol. 3 (ed. P. Knochel and G.A. Molander), 392–464. Amsterdam: Elsevier.
5 Choi, J. and Fu, G.C. (2017). *Science* 356: eaaf7230.
6 Lin, B.-L., Liu, L., Fu, Y. et al. (2004). *Organometallics* 23: 2114–2123.
7 Fu, G.C. (2017). *ACS Cent. Sci.* 3: 692–700.
8 Tasker, S.Z., Standley, E.A., and Jamison, T.F. (2014). *Nature* 509: 299–309.
9 Jahn, U. (2011). *Top. Curr. Chem.* 320: 323–452.
10 Devasagayaraj, A., Stüdemann, T., and Knochel, P. (1996). *Angew. Chem. Int. Ed.* 34: 2723–2725.
11 Fischer, C. and Fu, G.C. (2005). *J. Am. Chem. Soc.* 127: 4594–4595.
12 Lundin, P.M., Esquivias, J., and Fu, G.C. (2009). *Angew. Chem. Int. Ed.* 48: 154–156.
13 Liang, Y. and Fu, G.C. (2014). *J. Am. Chem. Soc.* 136: 5520–5524.
14 Liang, Y. and Fu, G.C. (2015). *J. Am. Chem. Soc.* 137: 9523–9526.
15 Choi, J. and Fu, G.C. (2012). *J. Am. Chem. Soc.* 134: 9102–9105.
16 Choi, J., Martín-Gago, P., and Fu, G.C. (2014). *J. Am. Chem. Soc.* 136: 12161–12165.
17 Yang, Z., Freas, D.J., and Fu, G.C. (2021). *J. Am. Chem. Soc.* 143: 2930–2937.
18 Yang, Z., Freas, D.J., and Fu, G.C. (2021). *J. Am. Chem. Soc.* 143: 8614–8618.
19 Matteson, D.S. (1989). *Chem. Rev.* 89: 1535–1551.
20 Matteson, D.S. (1995). *Stereodirected Synthesis with Organoboranes. Reactivity and Structure Concepts in Organic Chemistry*, vol. 32. Berlin: Springer.
21 Burns, M., Essafi, S., Bame, J.R. et al. (2014). *Nature* 513: 183–188.
22 Schmidt, J., Choi, J., Liu, A. et al. (2016). *Science* 354: 1265–1269.

**23** Schwarzwalder, G.M., Matier, C.D., and Fu, G.C. (2019). *Angew. Chem. Int. Ed.* 58: 3571–3574.

**24** Yi, H., Mao, W., and Oestreich, M. (2019). *Angew. Chem. Int. Ed.* 58: 3575–3578.

**25** Arp, F.O. and Fu, G.C. (2005). *J. Am. Chem. Soc.* 127: 10482–10483.

**26** Do, H., Chandrashekar, E.R.R., and Fu, G.C. (2013). *J. Am. Chem. Soc.* 135: 16288–16291.

**27** Son, S. and Fu, G.C. (2008). *J. Am. Chem. Soc.* 130: 2756–2757.

**28** Kranidiotis-Hisatomi, N. and Oestreich, M. (2022). *Org. Lett.* 24: 4987–4991.

**29** Kranidiotis-Hisatomi, N., Yi, H., and Oestreich, M. (2021). *Angew. Chem. Int. Ed.* 60: 13652–13655.

**30** Brösamlen, D. and Oestreich, M. (2023). *Org. Lett.* 25: 1901–1906.

**31** Fricke, C., Deckers, K., and Schoenebeck, F. (2020). *Angew. Chem. Int. Ed.* 59: 18717–18722.

**32** Oelke, A.J., Sun, J., and Fu, G.C. (2012). *J. Am. Chem. Soc.* 134: 2966–2969.

**33** Smith, S.W. and Fu, G.C. (2008). *J. Am. Chem. Soc.* 130: 12645–12647.

**34** Xu, Y., Yi, H., and Oestreich, M. (2021). *Organometallics* 40: 2194–2197.

**35** Schley, N.D. and Fu, G.C. (2014). *J. Am. Chem. Soc.* 136: 16588–16593.

**36** Binder, J.T., Cordier, C.J., and Fu, G.C. (2012). *J. Am. Chem. Soc.* 134: 17003–17006.

**37** Cordier, C.J., Lundgren, R.J., and Fu, G.C. (2013). *J. Am. Chem. Soc.* 135: 10946–10949.

**38** Tong, X., Schneck, F., and Fu, G.C. (2022). *J. Am. Chem. Soc.* 144: 14856–14863.

**39** Mu, X., Shibata, Y., Makida, Y., and Fu, G.C. (2017). *Angew. Chem. Int. Ed.* 56: 5821–5824.

**40** Huo, H., Gorsline, B.J., and Fu, G.C. (2020). *Science* 367: 559–564.

**41** An, L., Tong, F., Zhang, S., and Zhang, X. (2020). *J. Am. Chem. Soc.* 142: 11884–11892.

**42** Lou, S. and Fu, G.C. (2010). *J. Am. Chem. Soc.* 132: 5010–5011.

**43** Wang, Z., Yang, Z., and Fu, G.C. (2021). *Nat. Chem.* 13: 236–242.

**44** Caeiro, J., Sestelo, J.P., and Sarandeses, L.A. (2008). *Chem. Eur. J.* 14: 741–746.

**45** Fang, H., Yang, Z., Zhang, L. et al. (2016). *Org. Lett.* 18: 6022–6025.

**46** Manolikakes, G., Dastbaravardeh, N., and Knochel, P. (2007). *Synlett* 13: 2077–2080.

**47** Varenikov, A. and Gandelman, M. (2019). *J. Am. Chem. Soc.* 141: 10994–10999.

**48** Varenikov, A., Shapiro, E., and Gandelman, M. (2020). *Org. Lett.* 22: 9386–9391.

**49** Hayashi, T., Tajika, M., Tamao, K., and Kumada, M. (1976). *J. Am. Chem. Soc.* 98: 3718–3719.

**50** Hayashi, T., Konishi, M., Fukushima, M. et al. (1982). *J. Am. Chem. Soc.* 104: 180–186.

**51** Lou, S. and Fu, G.C. (2010). *J. Am. Chem. Soc.* 132: 1264–1266.

**52** Yin, H. and Fu, G.C. (2019). *J. Am. Chem. Soc.* 141: 15433–15440.

**53** Dai, X., Strotman, N.A., and Fu, G.C. (2008). *J. Am. Chem. Soc.* 130: 3302–3303.

**54** Varenikov, A. and Gandelman, M. (2018). *Nat. Commun.* 9: 3566.

**55** Lundin, P.M. and Fu, G.C. (2010). *J. Am. Chem. Soc.* 132: 11027–11029.

**56** Huang, W., Wan, X., and Shen, Q. (2017). *Angew. Chem. Int. Ed.* 56: 11986–11989.

**57** Xu, S., Zhang, R., Zhang, S., and Feng, C. (2021). *Org. Biomol. Chem.* 19: 4492–4496.

**58** Huang, W., Hu, M., Wan, X., and Shen, Q. (2019). *Nat. Commun.* 10: 2963.

**59** Saito, B. and Fu, G.C. (2008). *J. Am. Chem. Soc.* 130: 6694–6695.

**60** Owston, N.A. and Fu, G.C. (2010). *J. Am. Chem. Soc.* 132: 11908–11909.

**61** Lu, Z., Wilsily, A., and Fu, G.C. (2011). *J. Am. Chem. Soc.* 133: 8154–8157.

**62** Wilsily, A., Tramutola, F., Owston, N.A., and Fu, G.C. (2012). *J. Am. Chem. Soc.* 134: 5794–5797.

**63** Zultanski, S.L. and Fu, G.C. (2011). *J. Am. Chem. Soc.* 133: 15362–15364.

**64** Jiang, X., Sakthivel, S., Kulbitski, K. et al. (2014). *J. Am. Chem. Soc.* 136: 9548–9551.

**65** Jiang, X. and Gandelman, M. (2015). *J. Am. Chem. Soc.* 137: 2542–2547.

**66** Molander, G.A., Colombel, V., and Braz, V.A. (2011). *Org. Lett.* 13: 1852–1855.

**67** Lockner, J.W., Dixon, D.D., Risgaard, R., and Baran, P.S. (2011). *Org. Lett.* 13: 5628–5631.

**68** Tellis, J.C., Primer, D.N., and Molander, G.A. (2014). *Science* 345: 433–436.

**69** Amani, J., Sodagar, E., and Molander, G.A. (2016). *Org. Lett.* 18: 732–735.

**70** Stache, E.E., Rovis, T., and Doyle, A.G. (2017). *Angew. Chem. Int. Ed.* 56: 3679–3683.

**71** Lacker, C.R., DeLano, T.J., Chen, E.P. et al. (2022). *J. Am. Chem. Soc.* 144: 20190–20195.

**72** Gutierrez, O., Tellis, J.C., Primer, D.N. et al. (2015). *J. Am. Chem. Soc.* 137: 4896–4899.

**73** Wang, Z., Bachman, S., Dudnik, A.S., and Fu, G.C. (2018). *Angew. Chem. Int. Ed.* 57: 14529–14532.

**74** Tyson, E.L., Farney, E.P., and Yoon, T.P. (2012). *Org. Lett.* 14: 1110–1113.

**75** Zuo, Z., Ahneman, D.T., Chu, L. et al. (2014). *Science* 345: 437–440.

**76** Zuo, Z., Cong, H., Li, W. et al. (2016). *J. Am. Chem. Soc.* 138: 1832–1835.

**77** Pezzetta, C., Bonifazi, D., and Davidson, R.W.M. (2019). *Org. Lett.* 21: 8957–8961.

**78** Buzzetti, L., Prieto, A., Roy, S.R., and Melchiorre, P. (2017). *Angew. Chem. Int. Ed.* 56: 15039–15043.

**79** Gandolfo, E., Tang, X., Roy, S.R., and Melchiorre, P. (2019). *Angew. Chem. Int. Ed.* 58: 16854–16858.

**80** Gao, Y., Zhang, B., Levy, L. et al. (2022). *J. Am. Chem. Soc.* 144: 10992–11002.

**81** Huang, L., Ji, T., and Rueping, M. (2020). *J. Am. Chem. Soc.* 142: 3532–3539.

**82** Wang, J. and Li, X. (2022). *Chem. Sci.* 13: 3020–3026.

**83** Wu, L., Yang, G., and Zhang, W. (2019). *CCS Chem.* 1: 623–631.

**84** Rouquet, G. and Chatani, N. (2013). *Angew. Chem. Int. Ed.* 52: 11726–11743.

**85** Saint-Denis, T.G., Zhu, R., Chen, G. et al. (2018). *Science* 359: eaao4798.

**86** Davies, H.M.L. and Liao, K. (2019). *Nat. Rev. Chem.* 3: 347–360.

**87** Hayashi, H. and Uchida, T. (2020). *Eur. J. Org. Chem.* 2020: 909–916.

**88** Twilton, J., Le, C., Zhang, P. et al. (2017). *Nat. Rev. Chem.* 1: 0052.

**89** Wang, C., Dixneuf, P.H., and Soulé, J.F. (2018). *Chem. Rev.* 118: 7532–7585.
**90** Milligan, J.A., Phelan, J.P., Badir, S.O., and Molander, G.A. (2019). *Angew. Chem. Int. Ed.* 58: 615–6163.
**91** Cheng, W.-M. and Shang, R. (2020). *ACS Catal.* 10: 9170–9196.
**92** Zhu, C., Yue, H., Jia, J., and Rueping, M. (2021). *Angew. Chem. Int. Ed.* 60: 17810–17831.
**93** Cheung, K.P.S., Sarkar, S., and Gevorgyan, V. (2022). *Chem. Rev.* 122: 1543–1625.
**94** Lipp, A., Badir, S.O., and Molander, G.A. (2021). *Angew. Chem. Int. Ed.* 60: 1714–1726.
**95** Mondal, S., Dumur, F., Gigmes, D. et al. (2022). *Chem. Rev.* 122: 5842–5976.
**96** Kariofillis, S.K. and Doyle, A.G. (2021). *Acc. Chem. Res.* 54: 988–1000.
**97** Chan, A.Y., Perry, I.B., Bissonnette, N.B. et al. (2022). *Chem. Rev.* 122: 1485–1542.
**98** Holmberg-Douglas, N. and Nicewicz, D.A. (2022). *Chem. Rev.* 122: 1925–2016.
**99** Cheng, X., Lu, H., and Lu, Z. (2019). *Nat. Commun.* 10: 3549.
**100** Zhang, W., Shu, X., Huan, L. et al. (2021). *Org. Biomol. Chem.* 19: 9407–9409.
**101** Cheng, X., Li, T., Liu, Y., and Lu, Z. (2021). *ACS Catal.* 11: 11059–11065.
**102** Xu, J., Li, Z., Xu, Y. et al. (2021). *ACS Catal.* 11: 13567–13574.
**103** Farney, E.P., Chapman, S.J., Swords, W.B. et al. (2019). *J. Am. Chem. Soc.* 141: 6385–6391.
**104** Li, G., Swords, W.B., and Meyer, G.J. (2017). *J. Am. Chem. Soc.* 139: 14983–14991.
**105** Huan, L., Shu, X., Zu, W. et al. (2021). *Nat. Commun.* 12: 3536.
**106** Kawasaki, T., Yamazaki, K., Tomono, R. et al. (2021). *Chem. Lett.* 50: 1684–1687.
**107** Ahneman, D.T. and Doyle, A.G. (2016). *Chem. Sci.* 7: 7002–7006.
**108** Rand, A.W., Yin, H., Xu, L. et al. (2020). *ACS Catal.* 10: 4671–4676.
**109** Shu, X., Zhong, D., Lin, Y. et al. (2022). *J. Am. Chem. Soc.* 144: 8797–8806.
**110** Shu, X., Huan, L., Huang, Q., and Huo, H. (2020). *J. Am. Chem. Soc.* 142: 19058–19064.
**111** Shu, X., Zhong, D., Huang, Q. et al. (2023). *Nat. Commun.* 14: 125.
**112** Ruffoni, A., Mykura, R.C., Bietti, M., and Leonori, D. (2022). *Nat. Synth.* 1: 682–695.
**113** de Vleeschouwer, F., van Speybroeck, V., Waroquier, M. et al. (2007). *Org. Lett.* 9: 2721–2724.
**114** Milan, M., Carboni, G., Salamone, M. et al. (2017). *ACS Catal.* 7: 5903–5911.
**115** Shen, Y., Gu, Y., and Martin, R. (2018). *J. Am. Chem. Soc.* 140: 12200–12209.
**116** Xu, S., Ping, Y., Li, W. et al. (2023). *J. Am. Chem. Soc.* 145: 5231–5241.
**117** Devannah, V., Sharma, R., and Watson, D.A. (2019). *J. Am. Chem. Soc.* 141: 8436–8440.
**118** Jensen, K.H. and Sigman, M.S. (2008). *Org. Biomol. Chem.* 6: 4083–4088.
**119** McDonald, R.I., Liu, G., and Stahl, S.S. (2011). *Chem. Rev.* 111: 2981–3019.
**120** Egami, H. and Sodeoka, M. (2014). *Angew. Chem., Int. Ed.* 53: 8294–8308.
**121** Merino, E. and Nevado, C. (2014). *Chem. Soc. Rev.* 43: 6598–6608.

**122** Yin, G., Mu, X., and Liu, G. (2016). *Acc. Chem. Res.* 49: 2413–2423.
**123** Crossley, S.W.M., Obradors, C., Martinez, R.M., and Shenvi, R.A. (2016). *Chem. Rev.* 116: 8912–9000.
**124** Wang, F., Chen, P., and Liu, G. (2018). *Acc. Chem. Res.* 51: 2036–2046.
**125** Lin, J., Song, R.-J., Hu, M., and Li, J.-H. (2019). *Chem. Rec.* 19: 440–451.
**126** Jiang, H. and Studer, A. (2020). *Chem. Soc. Rev.* 49: 1790–1811.
**127** Li, Z., Fang, G., Gu, Q., and Liu, X.-Y. (2020). *Chem. Soc. Rev.* 49: 32–48.
**128** Qi, X. and Diao, T. (2020). *ACS Catal.* 10: 8542–8556.
**129** Poremba, K.E., Dibrell, S.E., and Reisman, S.E. (2020). *ACS Catal.* 10: 8237–8246.
**130** Luo, Y., Xu, C., and Zhang, X. (2020). *Chin. J. Chem.* 38: 1371–1394.
**131** Ping, Y. and Kong, W. (2020). *Synthesis* 52: 979–992.
**132** Pan, Q., Ping, Y., and Kong, W. (2023). *Acc. Chem. Res.* 56: 515–535.
**133** Ping, Y., Song, H., and Kong, W. (2022). *Chin. J. Org. Chem.* 42: 3302–3321.
**134** Wang, K., Ding, Z., Zhou, Z., and Kong, W. (2018). *J. Am. Chem. Soc.* 140: 12364–12368.
**135** Qin, X., Lee, M.W.Y., and Zhou, J.S. (2017). *Angew. Chem. Int. Ed.* 56: 12723–12726.
**136** Ping, Y., Wang, K., Pan, Q. et al. (2019). *ACS Catal.* 9: 7335–7342.
**137** Li, Y., Ding, Z., Lei, A., and Kong, W. (2019). *Org. Chem. Front.* 6: 3305–3309.
**138** Jin, X. and Wang, C. (2019). *Angew. Chem. Int. Ed.* 58: 6722–6726.
**139** Ma, T., Chen, Y., Li, Y. et al. (2019). *ACS Catal.* 9: 9127–9133.
**140** Chen, X., Yue, J., Wang, K. et al. (2021). *Angew. Chem. Int. Ed.* 60: 14068–14075.
**141** Coombs, J.R. and Morken, J.P. (2016). *Angew. Chem., Int. Ed.* 55: 2636–2649.
**142** Kc, S. and Giri, R. (2018). *J. Org. Chem.* 83: 3013–3022.
**143** Dhungana, R.K., Kc, S., Basnet, P., and Giri, R. (2018). *Chem. Rec.* 18: 1314–1340.
**144** Ping, Y., Li, Y., Zhu, J., and Kong, W. (2019). *Angew. Chem., Int. Ed.* 58: 1562–1573.
**145** Derosa, J., Apolinar, O., Kang, T. et al. (2020). *Chem. Sci.* 11: 4287–4296.
**146** Cong, H. and Fu, G.C. (2014). *J. Am. Chem. Soc.* 136: 3788–3791.
**147** Fan, P., Lan, Y., Zhang, C., and Wang, C. (2020). *J. Am. Chem. Soc.* 142: 2180–2186.
**148** Guo, L., Yuan, M., Zhang, Y. et al. (2020). *J. Am. Chem. Soc.* 142: 20390–20399.
**149** Li, X., Yuan, M., Chen, F. et al. (2023). *Chem* 9: 154–169.
**150** Liu, M. and Shu, W. (2023). *JACS Au* 3: 1321–1327.
**151** Du, X., Cheng-Sánchez, I., and Nevado, C. (2023). *J. Am. Chem. Soc.* 145: 12532–12540.
**152** Ding, C., Ren, Y., Sun, C. et al. (2021). *J. Am. Chem. Soc.* 143: 20027–20034.
**153** Li, Z., Shi, H., Chen, X. et al. (2023). *J. Am. Chem. Soc.* 145: 13603–13614.

# 4

# Nickel-Catalyzed Asymmetric Cross-Electrophile Couplings and Related Asymmetric Radical Cross-Couplings

*Lingling Chu, Shengqing Zhu, Jian Qin, and Yaheng Zhao*

*State Key Laboratory for Modification of Chemical Fibers and Polymer Materials, Center for Advanced Low-Dimension Materials, College of Chemistry and Chemical Engineering, Donghua University, Shanghai, China*

## 4.1 Introduction

Transition metal-catalyzed cross-coupling reactions have numerous important applications in chemical synthesis, medicinal chemistry, and materials science [1–3]. Conventionally, one carbon electrophile and one carbon nucleophile, each with different reactivity, are used to ensure excellent chemoselectivity in cross-couplings. Recently, the development of cross-electrophile coupling (XEC), which employs two different carbon electrophiles as coupling partners under reductive conditions, has drawn increasing attention [4–17]. This strategy bypasses the need for pre-prepared carbon nucleophiles, particularly air- or water-sensitive organometallic agents, providing an attractive complement to conventional electrophile–nucleophile couplings with improved substrate scope and functional group compatibility. Nevertheless, a central challenge in XEC systems is selectivity control: (i) chemoselectivity, i.e. cross-coupled products vs homo-coupled dimers, due to the similar chemical propensity of the two electrophiles for the transition metal catalyst (oxidative addition); and (ii) stereoselectivity, typically when $sp^3$-hybridized stereocenters are forged via XECs. Although there has been notable progress toward cross-electrophile couplings with excellent chemoselectivity by employing different types of electrophiles, such as C($sp^2$) and C($sp^3$) electrophiles, the development of catalytic asymmetric XECs has remained underexploited until recently.

Nickel-catalyzed cross-couplings represent an empowering method for constructing chemical bonds in chemical synthesis [18–28]. The characteristic properties of nickel, such as high pairing energy, low electronegativity, and facile accessibility to various valence states ($Ni^0$, $Ni^I$, $Ni^{II}$, $Ni^{III}$, $Ni^{IV}$), allow for its important application in facilitating cross-couplings with $sp^3$-hybridized substrates, particularly XECs with C($sp^3$) electrophiles. With the diverse and easily accessible chiral ligand skeletons for

nickel catalysis, impressive progress has been made in asymmetric XECs via nickel catalysis [11, 15, 24, 26].

This chapter highlights recent advances and applications of asymmetric radical-based cross-electrophile coupling (XEC) via nickel catalysis. It includes discussions on synthetic applications and the mechanisms behind these important studies. The article is first categorized by reaction types (XECs between two electrophiles and XECs with alkenes and electrophiles) and then by the electrophile types. Discoveries enabled by other transition metal catalysts, those without enantioselective control, or those not involving radical intermediates, have been reviewed elsewhere and are beyond the scope of this treatise [5–17].

Before going through specific examples, we briefly discuss a generally proposed catalytic cycle for Ni-catalyzed asymmetric XEC cross-coupling with C($sp^3$) electrophiles, though the actual mechanism could be more complex. As shown in Scheme 4.1c, the reaction starts with an active Ni(0) species. Reduction of a Ni(II) precursor by a reductant (Mn, Zn, etc.) forms the Ni(0) species **I**, which undergoes oxidative addition with a C($sp^2$) electrophile to generate an organonickel(II) species **II**. On the other hand, the Ni(I)-halide species is responsible for the activation of C($sp^3$) electrophile, generating an alkyl radical and Ni(II) species

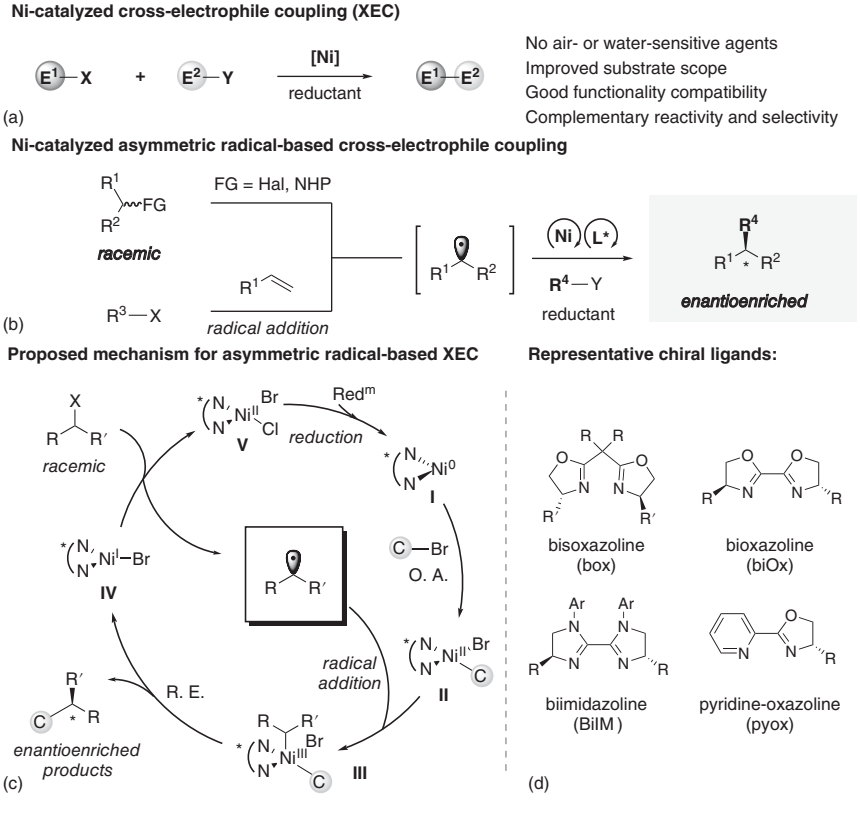


**Scheme 4.1** Ni-catalyzed asymmetric cross-electrophile coupling (XEC).

via a single-electron transfer (SET) process. The formed alkyl radical that adds to the organonickel(II) species **II** to deliver a Ni(III) intermediate **III**, followed by facile reductive elimination to form the final coupled product and the Ni(I)-halide species **IV**. Chiral bidentate and tridentate *N*-ligands, such as bisoxazoline (box), bioxazoline (biOx), bi-imidazoline (BiIM), and pyridine-oxazoline (pyox), are commonly employed chiral ligands for asymmetric Ni-catalyzed radical XEC reactions, probably due to the redox reactivity of these ligands further to stabilize the nickel intermediates (Scheme 4.1d).

## 4.2 Asymmetric C(sp²)—C(sp³) Cross-Electrophile Couplings

### 4.2.1 Asymmetric Couplings of C(sp³) Halides with C(sp²) Halides

#### 4.2.1.1 Couplings with Acyl Chlorides

Reisman and coworkers reported the first example of a nickel-catalyzed asymmetric XEC reaction. In 2013, they demonstrated the asymmetric cross-coupling of acyl chlorides with α-substituted benzyl chlorides in the presence of $NiCl_2$•DME and the chiral box ligand **L1**, using Mn as the stoichiometric reductant, 2,6-dimethyl benzoic acid (DMBA), and 3 Å molecular sieves (3 Å MS) as additives, to access enantioenriched α, α-disubstituted ketones in good yields and high enantiomeric excess (ee) (Scheme 4.2) [29]. This mild, base-free protocol is compatible with a wide range of acyl and benzyl chlorides, showing good functional group tolerance. Control experiments revealed that adding DMBA is indispensable to increasing cross-coupling efficiency, probably by inhibiting the homocoupling of benzyl chlorides. Furthermore, the isopropylidene bridge of ligand **L1** proved crucial. The authors proposed a sequential reduction catalytic cycle involving a stereo-convergent oxidative addition of the benzylic chloride.

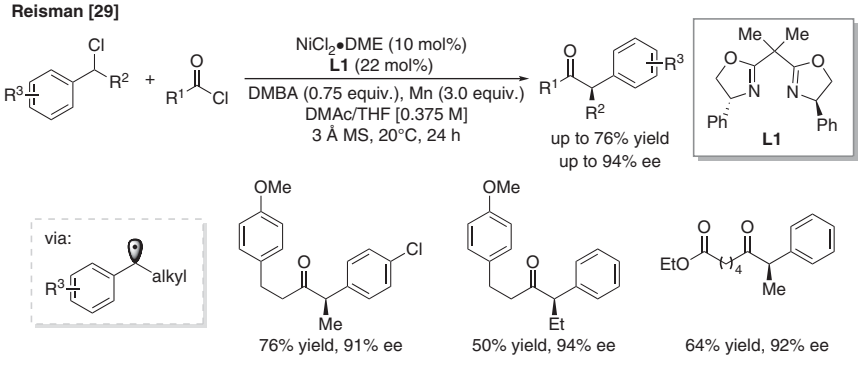


**Scheme 4.2** Acylation of benzyl chlorides. Source: Reisman [29]/American Chemical Society.

The introduction of polyfluoroalkyl groups into molecules can significantly improve their physical and biological properties, making the efficient construction

of polyfluoroalkyl-substituted stereocenters highly desirable by chemists [30, 31]. In 2022, Wang et al. reported a Ni-catalyzed asymmetric reductive acylation of α-$CF_3$ alkyl bromides, achieving high yields and excellent ee (Scheme 4.3, top) [32]. This protocol employs $NiCl_2$•DME and a sterically hindered phenanthrene methyl box ligand **L2** as the catalyst combination, with Mn as the reductant, forging a wide range of enantioenriched α-$CF_3$ substituted ketones with broad functional group compatibility. Further reduction of chiral α-$CF_3$-substituted ketones by $NaBH_4$ generates the corresponding chiral β-$CF_3$-substituted alcohols in moderate to good yields. This method is applicable for the late-stage synthetic modification of complex molecules, offering great potential for developing biologically active $CF_3$-containing drugs.

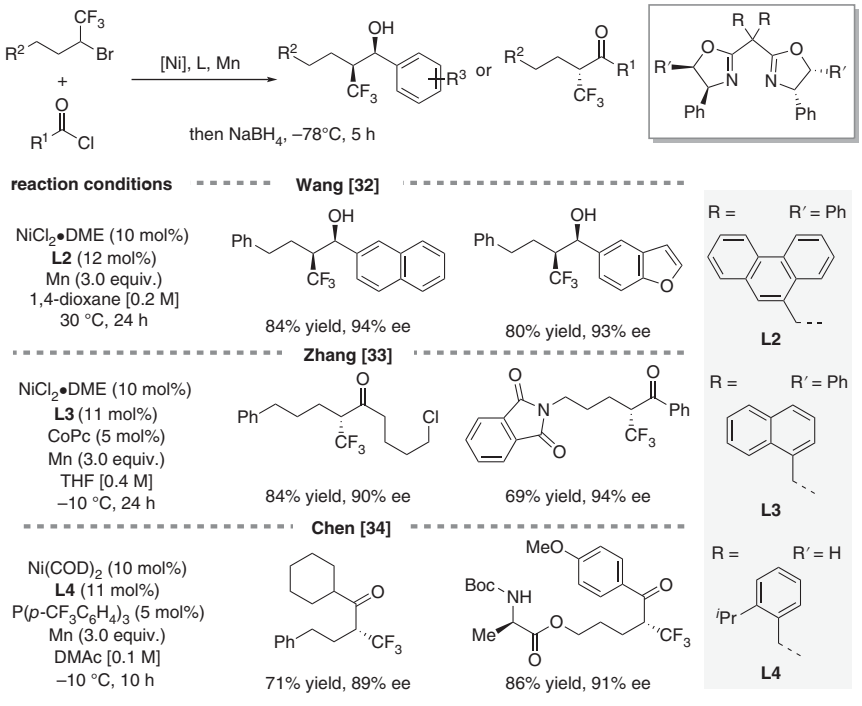


**Scheme 4.3** Acylation of α-$CF_3$ alkyl bromides.

Simultaneously, two other research groups reported similar XEC reactions between acyl chlorides and α-$CF_3$ alkyl bromides in the presence of Mn via nickel catalysis (Scheme 4.3). Zhang's protocol used 5 mol% of cobalt phthalocyanine (CoPc) as an additive to significantly improve coupling efficiency, probably by facilitating the generation of α-$CF_3$ alkyl radicals from the corresponding alkyl bromides (Scheme 4.3, middle) [33]. Chen's protocol employed phosphine as a co-ligand to facilitate the oxidative addition of the acyl chloride to the nickel species, ensuring a sufficient concentration of acyl nickel species to capture the unstable α-$CF_3$ alkyl radicals (Scheme 4.3, bottom) [34]. They also found that the phosphine

co-ligand was beneficial to the stereoselective control of this transformation. Both reactions were compatible with aryl and aliphatic acyl chlorides. A radical chain mechanism involving α-$CF_3$ alkyl radicals is proposed for these XEC reactions.

#### 4.2.1.2 Couplings with Alkenyl Halides

In 2014, Reisman and coworkers reported a Ni-catalyzed asymmetric XEC of vinyl bromides and benzyl chlorides to forge chiral alkenes bearing stereogenic, aryl-substituted tertiary allylic centers with high yields and excellent ee (Scheme 4.4, top) [35]. This reaction utilizes $NiCl_2$•DME and the IndaBOX **L5** ligand as the catalyst combination, $Mn^0$ as the reductant, and NaI as the additive, tolerating a wide range of vinyl bromides and benzylic chlorides, including cyclic benzylic chlorides. The bite angle of the chiral ligands significantly affects the reaction efficiency, with the cyclopropyl-linked box ligand **L5** being optimal. Furthermore, the addition of NaI has been shown to improve the coupling efficiency, probably via the in situ generation of organic iodides or the facilitation of the SET event between Mn and nickel. In 2018, Reisman and coworkers expanded the alkyl electrophile scope of the asymmetric XEC reaction to (chlorobenzyl)silanes (Scheme 4.4, bottom) [36]. Using the IndaBOX ligand **L5**, this reaction employs Mn as the stoichiometric reductant and CoPc as the additive. This combination enables the straightforward access to a wide range of enantioenriched allylic silanes, which serve as versatile building blocks for many stereoselective transformations under mild conditions.

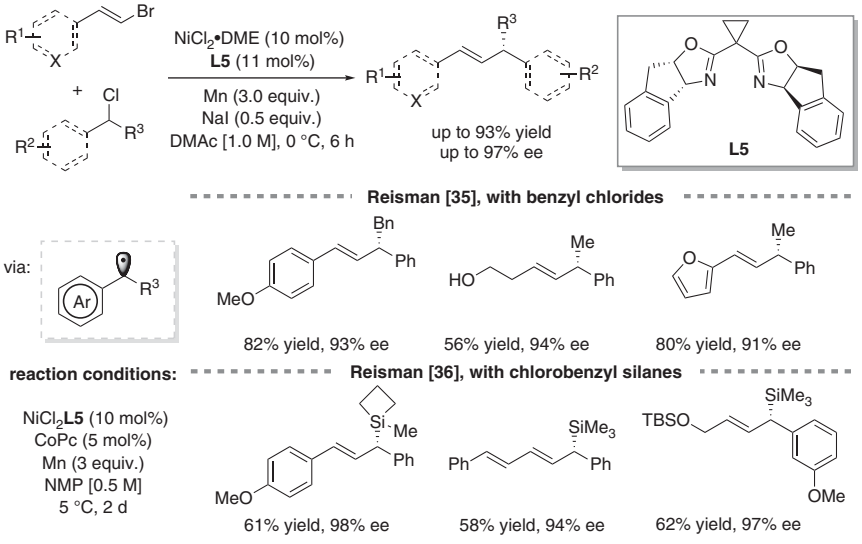


**Scheme 4.4** Alkenylation of alkyl chlorides.

Besides organohalides, carboxylic acid-derived redox-active *N*-hydroxyphthalimide (NHP) esters can undergo SET reduction to release the corresponding alkyl radicals. Therefore, they can participate in catalytic XEC reactions [37–41]. In 2017, the Reisman group successfully developed an asymmetric reductive

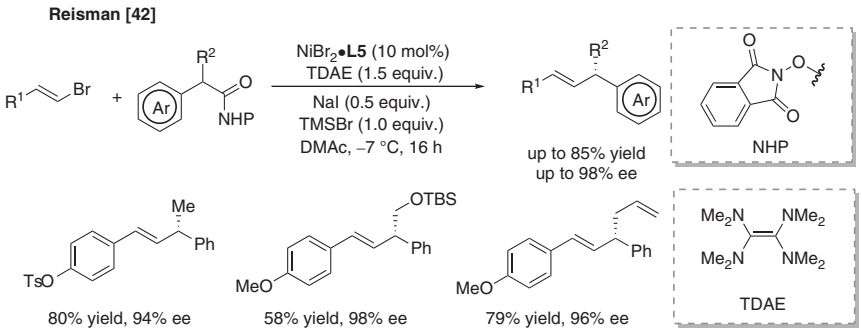


**Scheme 4.5** Benzylation of alkenyl bromides with N-hydroxyphthalimide esters. Source: Reisman [42]/American Chemical Society.

alkenylation of NHP esters via nickel catalysis (Scheme 4.5) [42]. Compared to the previous asymmetric alkenylation of benzylic chlorides [35], this reaction uses tetrakis(dimethylamino)ethylene (TDAE) as the stoichiometric reductant and TMSBr as the additive. Both aryl- and alkyl-substituted alkenyl bromides are applicable, yielding moderate to good yields and excellent enantioselectivity. Recent mechanistic studies of these asymmetric alkenylation reactions [43] suggest that activation of NHP esters is facilitated by a combination of TDAE and TMSBr, rather than by low-valent nickel species, as is the case in the Ni/Mn/benzylic chloride system. The activation mode of alkyl electrophiles leads to divergent mechanistic scenarios for these two asymmetric alkenylation reactions.

In 2022, Wu and Sun et al. developed a Ni-catalyzed asymmetric reductive alkenylation with secondary α-chlorosulfones as alkyl electrophiles by utilizing chiral box ligand **L6** in the presence of Mn as the reductant and $MgBr_2$ as the additive. This strategy enables the enantioselective synthesis of α-allylic sulfones with good tolerance of various functional group under mild conditions (Scheme 4.6) [44]. Due to the low reactivity, a high loading of nickel catalyst and chiral ligands and relatively long reaction times are required.

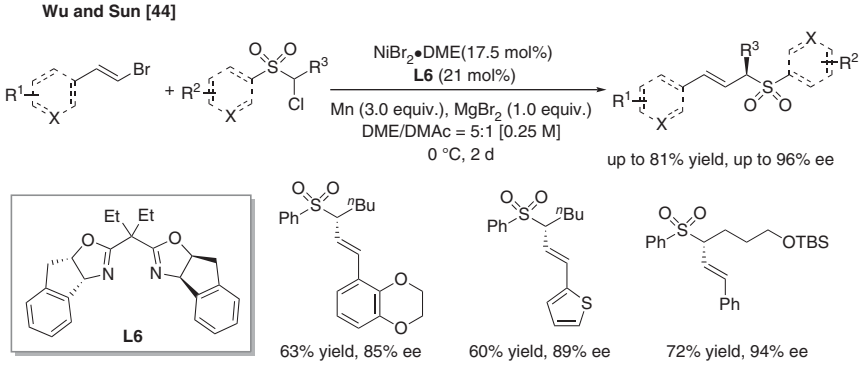


**Scheme 4.6** Alkenylation of α-sulfonyl alkyl chlorides with alkenyl bromides. Source: Wu and Sun [44]/American Chemical Society.

### 4.2.1.3 Couplings with Aryl Halides

The asymmetric cross-electrophile coupling with aryl halides, one of the most widely employed coupling partners in XEC reactions, provides an important platform for forging α-aryl stereogenic centers presented in many bioactive molecules.

In 2015, Reisman et al. reported a nickel-catalyzed asymmetric XEC between heteroaryl iodides and secondary α-chloronitriles to access α-aryl alkylnitriles with good yields and high enantioselectivity (Scheme 4.7) [45]. This reaction combines $NiBr_2$•DME and chiral phosphino-oxazoline (PHOX) ligand **L7** with Mn as the reductant and TMSCl as the additive. The use of the PHOX ligand, which is more electron-rich than the commonly employed box ligands, is critical to improve the reaction efficiency. The authors assume that the PHOX ligand could increase the oxidative addition rate of heteroaryl iodides to Ni(0) species and slow down the hydrodechlorination rate of α-chloronitriles. DMMB-PHOX **L7** was evaluated as the optimal ligand for obtaining the best yields and enantioselectivity. The mild conditions are compatible with a wide range of iodo-heteroaromatics, including pharmaceutically relevant pyridines, pyrimidines, and piperidines.

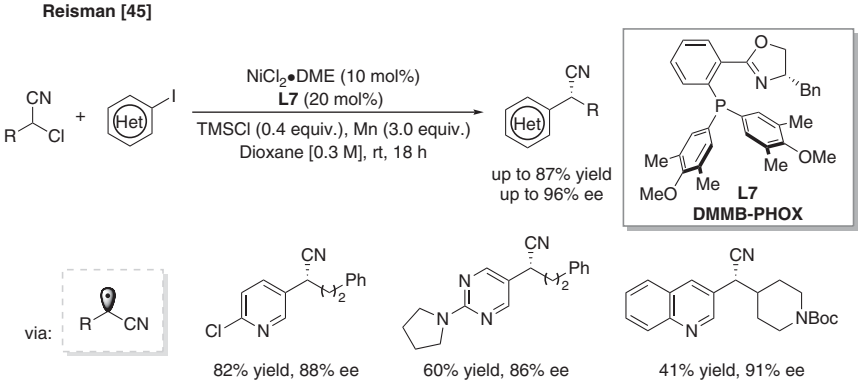


**Scheme 4.7** Arylation of α-chloroalkyl nitriles with aryl iodides. Source: Reisman [45]/ American Chemical Society.

Later, Reisman et al. utilized a chiral bioxazoline (biOx) ligand to achieve two additional examples of asymmetric XEC reactions between (hetero)aryl iodides and racemic secondary alkyl chlorides (α-chloroarenes and α-chloroesters) via nickel catalysis (Scheme 4.8) [46, 47]. The length of the alkyl chains on the chiral biOx ligands has a pronounced effect on both coupling efficiency and enantioselective control. Specifically, biOx ligands with bis 4-heptyl substitution were identified as optimal. Based on the multivariate linear regression analysis of the case of α-chloroesters, the effect of steric matching between the chiral ligand and α-chloroesters is the major effect for excellent stereoselectivity. A radical chain mechanism was proposed for this XEC coupling.

In 2021, Wang and coworkers utilized the same chiral 4-heptyl biOx ligand to develop a nickel-catalyzed asymmetric cross-electrophile coupling of α-$CF_3$-containing alkyl bromides with (hetero)aryl halides, forging a series of

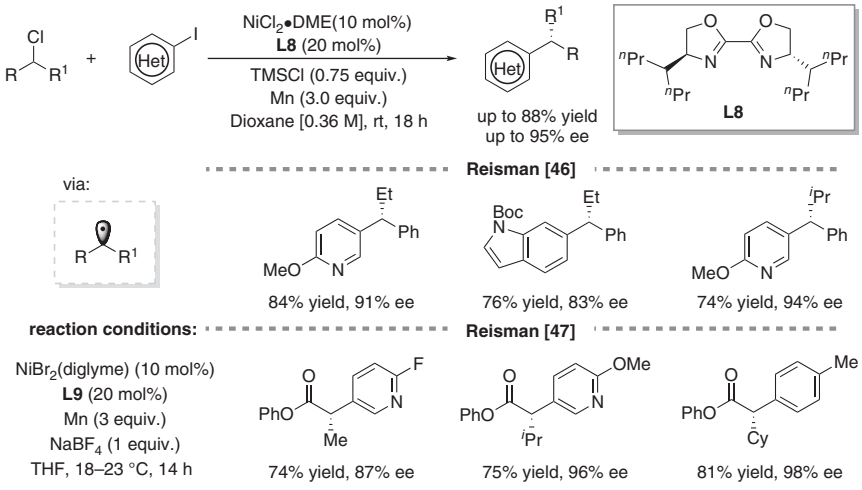


**Scheme 4.8** Arylation of alkyl chlorides with aryl iodides.

enantioenriched α-$CF_3$ alkanes under mild conditions (Scheme 4.9) [48]. With TBAI as the additive, this reaction proceeds with good efficiency, high enantioselectivity, and broad substrate scope for both aryl halides and α-trifluoromethyl bromides. It provides an efficient platform for synthesizing chiral $CF_3$-containing biologically active compounds.

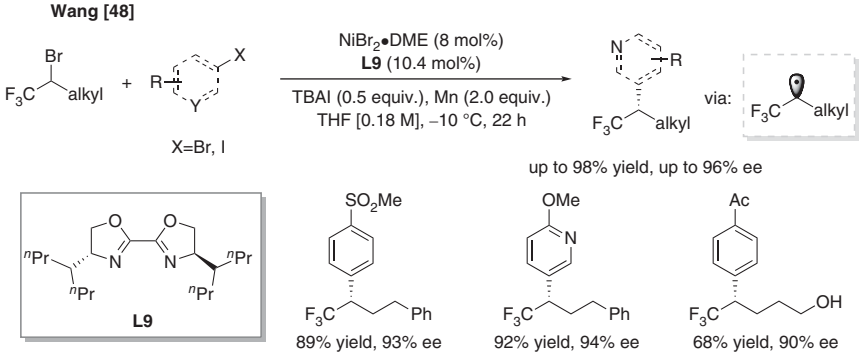


**Scheme 4.9** Arylation of α-$CF_3$ alkyl bromides. Source: Wang [48]/John Wiley & Sons.

In 2021, Gong and coworkers disclosed an enantioselective reductive arylation of α-chlorosulfones to access enantioenriched α-arylated sulfones (Scheme 4.10) [49]. Similar to Reisman's findings, the use of a chiral box ligand, with a cyclopropyl linker, Zn, and $MgCl_2$ was shown to achieve high enantioselective control. Mechanistic investigations also pointed to a radical chain pathway involving α-sulfonyl radicals.

Also in 2021, Xu and coworkers developed an XEC coupling of α-iodofluoroalkylboronates and (hetero)aryl iodides via nickel catalysis (Scheme 4.11) [50].

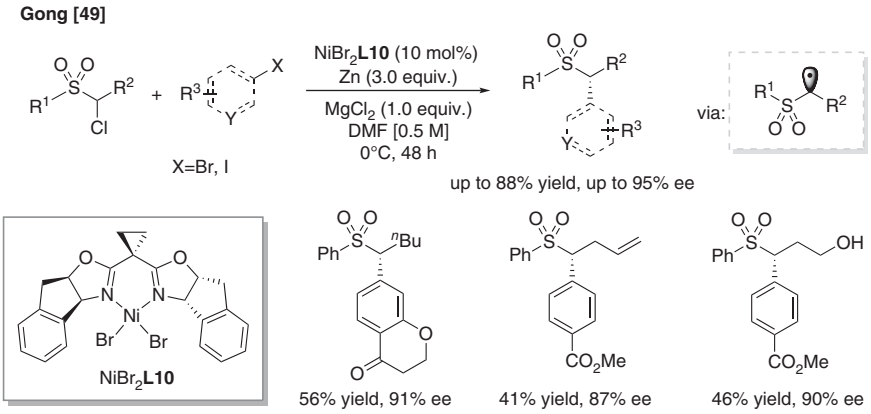


**Scheme 4.10** Arylation of α-chlorosulfones with aryl halides. Source: Adapted from Gong [49].

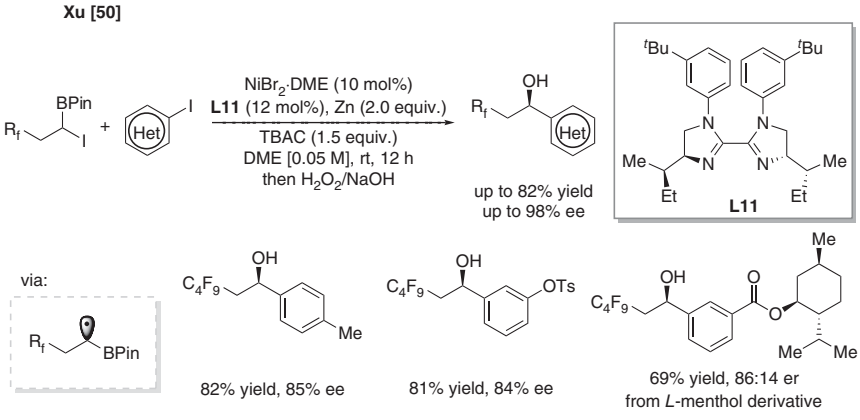


**Scheme 4.11** Arylation of α-borylalkyl iodides with aryl iodides. Source: Xu [50]/American Chemical Society.

With a combination of catalytic $NiBr_2$•DME and chiral bi-imidazoline (BiIM) ligand **L11** in the presence of stoichiometric tetrabutylammonium chloride (TBAC) and Zn, this reaction enables the straightforward access to a wide range of enantioenriched α-aryl-fluoroalkyl boronates with high yields and excellent ee under mild conditions. The employed alkyl electrophiles, α-iodo-perfluoroalkyl boronates, can be readily accessible via atom transfer radical addition (ATRA) reactions of perfluoroalkyl iodides and vinylboronates. Based on their mechanistic studies, the authors reasoned that the exogenous chloride ion could accelerate the Zn-mediated reduction of $Ni^{II}X_2$ species to generate Ni(0), which then captures the α-boroalkyl radicals.

## 4.2.2 Asymmetric Couplings of C($sp^2$)-Halides with C($sp^3$) Pseudo-Electrophiles

### 4.2.2.1 Couplings with Epoxides

Epoxides are important building blocks for the synthesis of substituted alcohols [51, 52]. Recently, considerable attention has been devoted to engaging epoxides as alkyl electrophiles in catalytic XEC reactions [5, 6, 53]. In 2015, Weix and coworkers disclosed the first example of asymmetric XEC of aryl halides with *meso*-epoxides as C($sp^3$)-electrophiles via dual nickel and titanium catalysis, delivering a series of enantioenriched trans-β-arylcycloalkanols under mild conditions (Scheme 4.12, top) [54]. This reaction is driven by a catalytic combination of $NiCl_2$•DME/2,2′-bipyridine and the chiral titanocene catalyst **12** in the presence of stoichiometric Mn and $Et_3N$·HCl. A key step is the chiral titanocene-mediated enantioselective generation of a β-titanoxy carbon radical, the involvement of which is supported by the ring-opening/rearrangement reaction of cyclooctadiene monoxide from the meso-epoxide. Subsequent interception of the chiral carbon

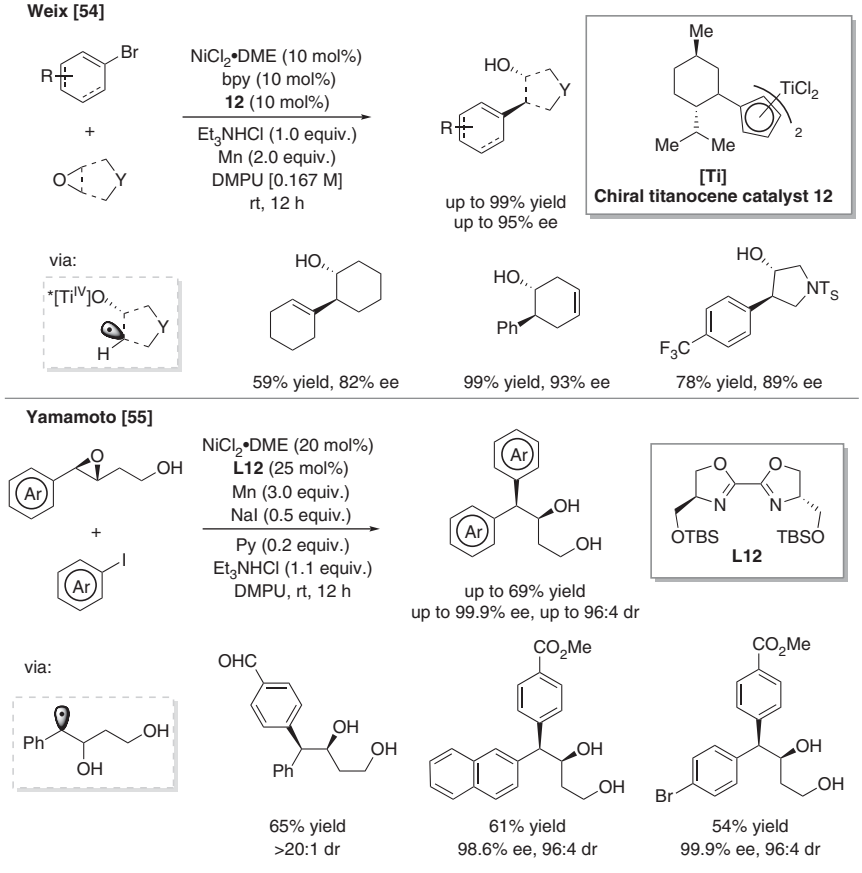


**Scheme 4.12** Alkylation of aryl iodides with epoxides.

radical by the arylnickel species would finally forge the second C(sp³)—C(sp²) bond to deliver the β-aryl alcohols.

In 2017, Yamamoto et al. developed an asymmetric nickel-catalyzed regio- and stereoselective cross-electrophile coupling of 3,4-epoxyalcohols with aryl iodides (Scheme 4.12, bottom) [55]. With the use of $NiCl_2$•DME and the C2-symmetric oxazoline ligand **L12**, a series of enantioenriched 4,4-diaryl-1,3-diols can be formed with high efficiency and excellent ee. The tethered alcohol group is critical to ensure the regioselective opening of epoxides at the C4 position. Additives such as NaI, pyridine, and $Et_3N$·HCl could be beneficial to activate epoxides.

### 4.2.2.2 Couplings with Aziridines

Like epoxides, the ring strain of aziridines makes them highly reactive and versatile building blocks for synthesizing amines and derivatives [56, 57]. In 2017, Doyle, Sigman et al. reported an asymmetric XEC reaction of styrenyl aziridines with aryl iodides in the presence of Mn via nickel catalysis (Scheme 4.13) [58]. With $NiCl_2$•DME and the chiral 4-heptyl-biOx ligand **L8**, a series of enantioenriched 2-aryl phenethylamines could be obtained from racemic aziridines with high efficiency and excellent regioselectivity. By employing the multivariate analysis tools, the authors revealed that a long, branched alkyl chain, which can significantly enhance steric effects and allow for possible noncovalent interactions (NCIs) of the chiral biOx ligands is optimal for the enantioselective control. This phenomenon is echoed by a recent asymmetric photoredox and nickel work developed by Chu and Guiterrez [59].

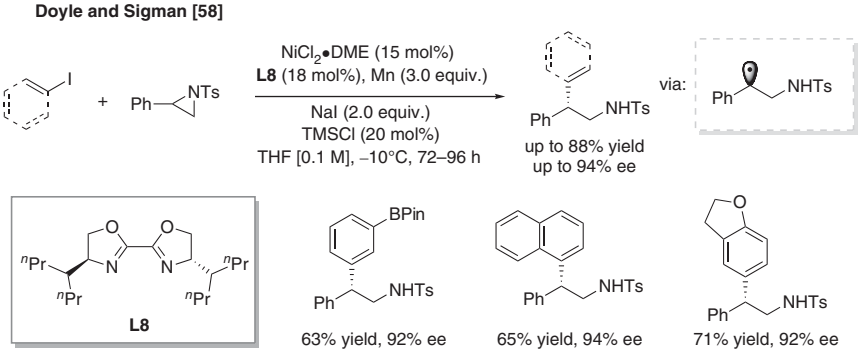


**Scheme 4.13** Alkylation of aryl iodides with aziridines. Source: Doyle and Signman [58]/ American Chemical Society/CC BY 4.0.

## 4.2.3 Asymmetric C(sp³)—C(sp²) XECs Enabled by Metallaphotoredox or Electrocatalysis

Synergistic photoredox/nickel catalysis has emerged as an efficient platform for constructing C—C bonds under exceptionally mild conditions [60–68]. The capability of photoredox catalysis in generating alkyl radicals from diverse electrophiles under reductive conditions incorporates it well with nickel-catalyzed XEC strategies. One

significant advantage of dual photoredox/nickel-catalyzed XEC reactions is to avoid the utilization of stoichiometric metals.

In 2020, Mao and Walsh et al. disclosed an enantioselective reductive arylation of α-chloro esters via dual photoredox and nickel catalysis (Scheme 4.14) [69]. With a combination of catalytic $Ni(COD)_2$, chiral biOx ligand **L9**, and 1,2,3,5-tetrakis(carbazole-9-yl)-4,6-dicyanobenzene (4CzIPN), this asymmetric XEC reaction proceeded smoothly in the presence of Hantzsch esters (HEH) (reductant) and N,N-dicyclohexylmethylamine ($Cy_2NMe$) (base) with the irradiation of blue LEDs. The mild conditions tolerate good substrate compatibility, delivering a diverse range of enantioenriched α-aryl esters with good yields and high ee. The authors proposed a mechanism involving Ni(0/I/II/III) for this dual catalytic XEC reaction: SET reduction of photoexcited 4CzIPN* by HEH gives the reducing $4CzIPN^{\bullet-}$, which is responsible for two SET reduction events of α-chloroesters and Ni(I) to release α-ester alkyl radical and regenerate Ni(0), respectively.

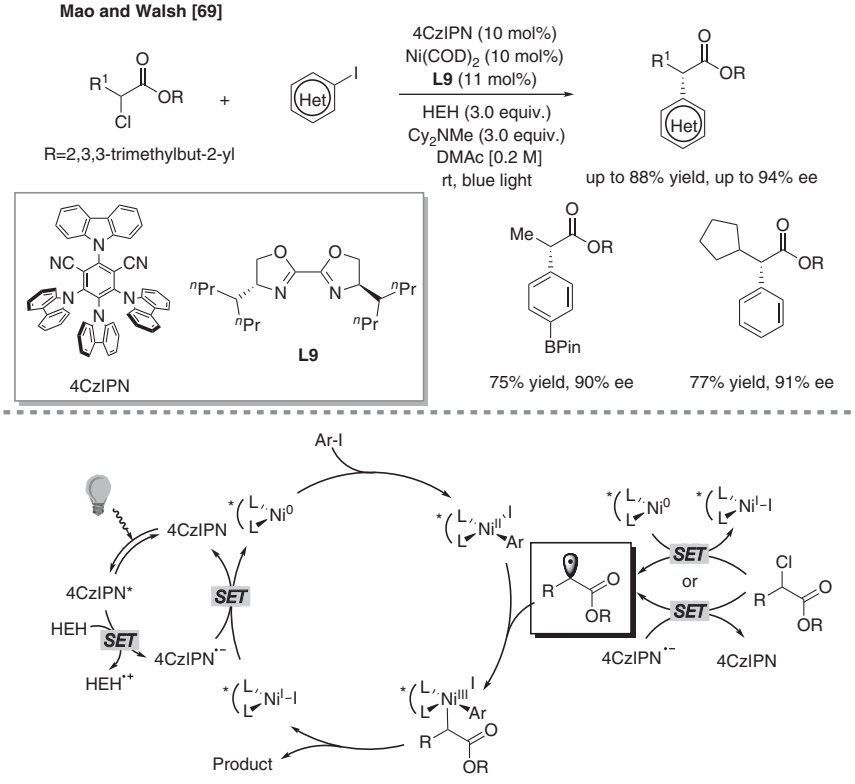


**Scheme 4.14** Arylation of α-chloroesters with aryl iodides. Source: Mao and Walsh [69]/ John Wiley & Sons.

In 2021, Doyle et al. disclosed a dual Ni/photoredox-catalyzed cross-electrophile coupling between aryl epoxides and aryl iodides to forge a variety of enantioenriched 2,2-diaryl alcohols with 4CzIPN as the photocatalyst, chiral bi-imidazoline

(BiIM) **L13** as the ligand, and $Et_3N$ as the reductant (Scheme 4.15) [70]. Mechanistic studies indicated that two distinct activation modes for these two electrophiles, i.e. aryl iodides undergo oxidative addition with $LnNi^0$ species, while epoxides undergo ring-opening by in situ generated HX to form halohydrin and finally produce alkyl radicals via the SET reduction. Furthermore, the use of multivariate linear regression (MVLR) analysis demonstrated that the electronic effect, instead of steric hindrance, of the biOx and BiIM ligands could be responsible for the enantioinduction differences, and higher ee were obtained with the more electron-donating BiIM ligands.

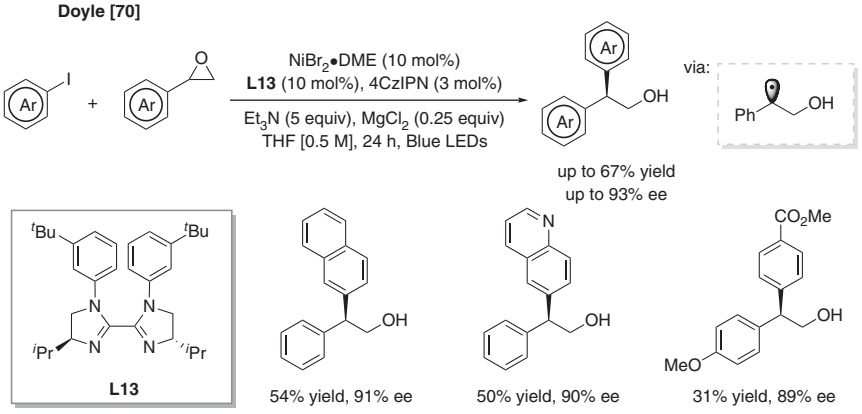


**Scheme 4.15** Arylation of epoxides with aryl iodides. Source: Doyle [70]/American Chemical Society.

In 2021, Xu and coworkers developed a dual Ni/photoredox-catalyzed XEC between α-borylalkyl chlorides and aryl iodides in the presence of catalytic 4CzIPN, $NiBr_2$•DME, and chiral diamine **L14** together with stoichiometric HEH and $Et_3N$, accessing to a wide range of enantioenriched α-aryl alkylboronates with high efficiency, excellent enantioselectivity, and good functional group tolerance (Scheme 4.16) [71]. They also extended this dual-catalyzed asymmetric XEC strategy to α-$CF_3$ alkyl bromides, enabling the enantioselective construction of chiral trifluoromethylated alkanes with aryl halides by using chiral BiIM ligand **L13** [72].

In 2021, Lu and coworkers reported a Ni/photoredox-catalyzed enantioselective XEC of benzylic chlorides with aryl bromides to yield enantioenriched 1,1-diaryl alkanes (Scheme 4.17, top) [73]. This protocol employed $[Ir(dFCF_3ppy)_2(dtbbpy)]Cl$, $NiCl_2$•DME, and chiral BiIM **L11** as the catalyst combination, together with HEH/DIPEA and blue LEDs. More electron-rich BiIM ligands enabled efficient couplings with aryl bromides, which are more economical than corresponding aryl iodides. In addition, alkenyl bromines and chlorides were competent coupling partners in this XEC protocol to form corresponding enantioenriched *trans*-alkene compounds with high stereoselectivity. Stilbene was used as a triplet-energy-transfer inhibitor to modulate photoinduced *E/Z* isomerization to achieve *trans*-selectivity. In 2022, Mao et al. also developed an asymmetric XEC reaction of alkenyl bromides

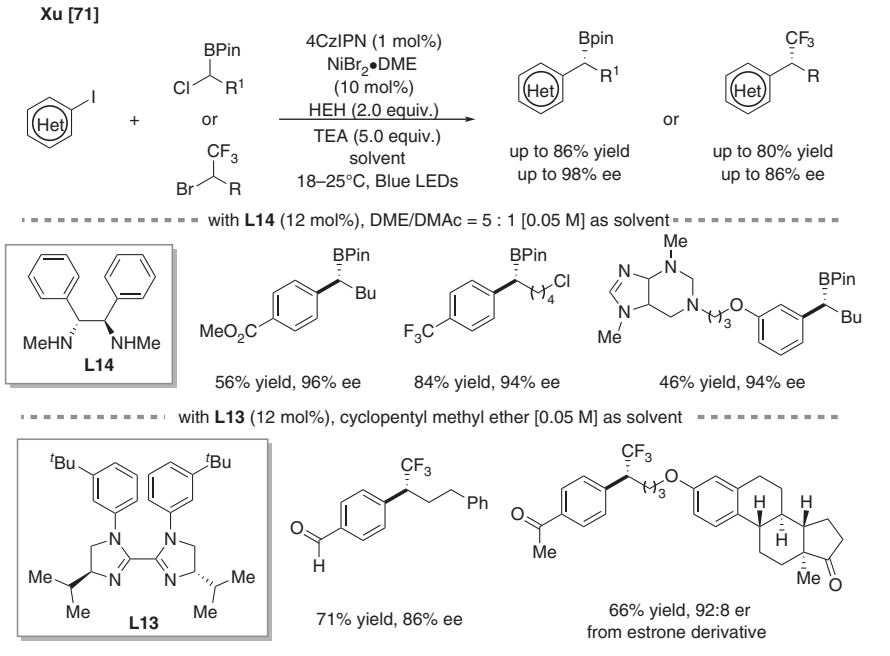


**Scheme 4.16** Arylation of alkyl halides with aryl iodides. Source: Xu [71]/Springer Nature CC BY 4.0.

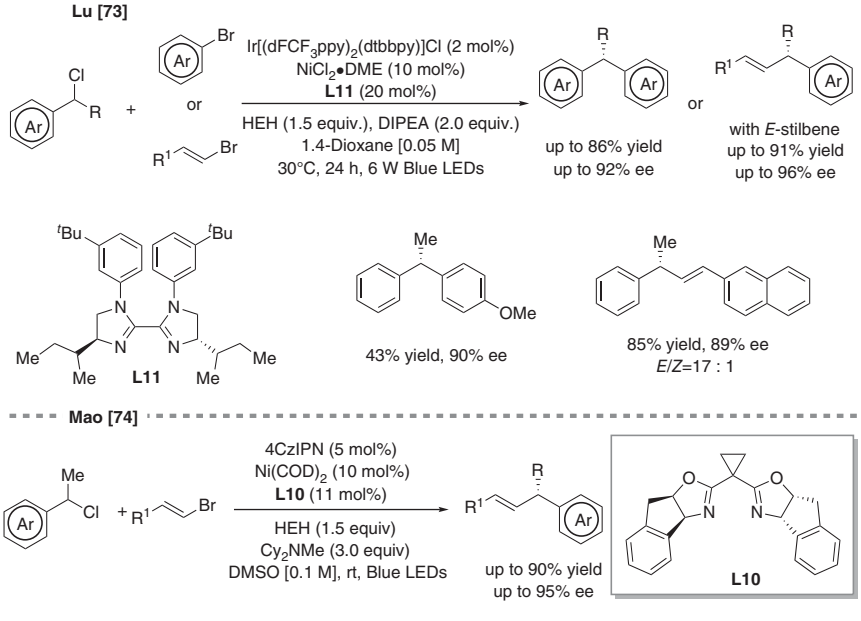


**Scheme 4.17** Arylation and alkenylation of benzyl chlorides.

with benzyl chlorides to access enantioenriched allylic compounds (Scheme 4.17, bottom) [74]. Unlike Lu's report, this work utilized organic photocatalyst 4CzIPN and cyclopropyl-linked bis(oxazoline) **L10.**

Chiral phosphine-containing compounds are important structural units that widely exist in organic synthesis. Based on their previous work, in 2022, Xu et al. disclosed another Ni/photoredox-catalyzed asymmetric XEC reaction of α-bromo phosphonates with (hetero)aryl iodides for the direct synthesis of enantioenriched α-aryl phosphonates (Scheme 4.18) [75]. With catalytic 4CzIPN/$NiBr_2$•DME/chiral BiIM **L11** in the presence of HEH as a reductant and $Cs_2CO_3$ as a base, this mild protocol demonstrated broad substrate compatibility with high enantioselectivity. Simple synthetic manipulations of the resulting α-aryl phosphonates led to several chiral phosphine-containing ligands. Mechanistic studies disclosed that the SET reduction of α-bromo phosphonates by $4CzIPN^{\bullet-}$, instead of low-valent Ni species, could be the main pathway for radical generation. Moreover, the alkyl radical capture by the ligated (aryl)Ni(II) species could be the enantiodetermining step based on the density functional theory (DFT) computations.

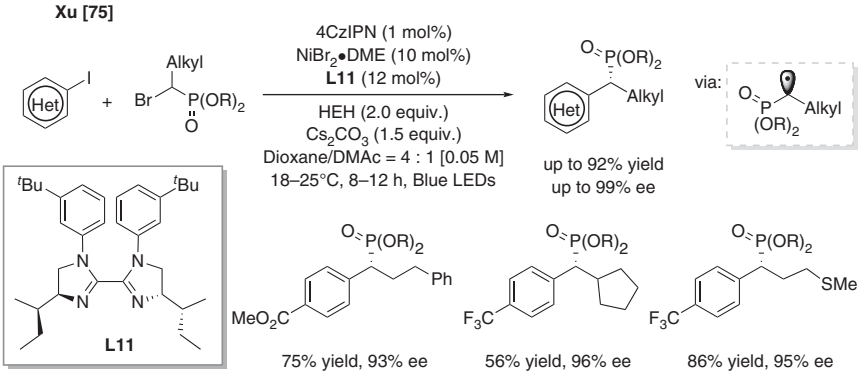


**Scheme 4.18** Arylation of α–phosphoryl alkyl bromides with aryl iodides. Source: Xu [75]/American Chemical Society.

Very recently, Xu et al. expanded the dual photoredox/nickel asymmetric XEC reaction to more challenging alkyl electrophiles and reported the asymmetric $C(sp^3)$-$C(sp^3)$ XEC reaction of α-chloroboronates with alkyl iodides (Scheme 4.19) [76]. With the commonly employed 4CzIPN/$NiBr_2$•DME catalyst and reductant combination, this protocol employed a simple methylene-linked bis(oxazoline) **L15** as the chiral ligand and $Mg(OTf)_2$/water as additives to access a series of enantioenriched α,α-dialkyl boronic esters in moderate to good yields and excellent enantioselectivity. Synthetic applications were demonstrated via the rapid synthesis of important chiral bioactive molecules (*R*)-δ-decalactone. Mechanistic investigations revealed that the two alkyl electrophiles could release corresponding radicals through low-valent Ni species or reductive $4CzIPN^{\bullet-}$-enabled SET events. Primary alkyl iodides formed out-of-cage radicals, and a radical-rebound mechanism was proposed for the activation of α-chloroboronates.

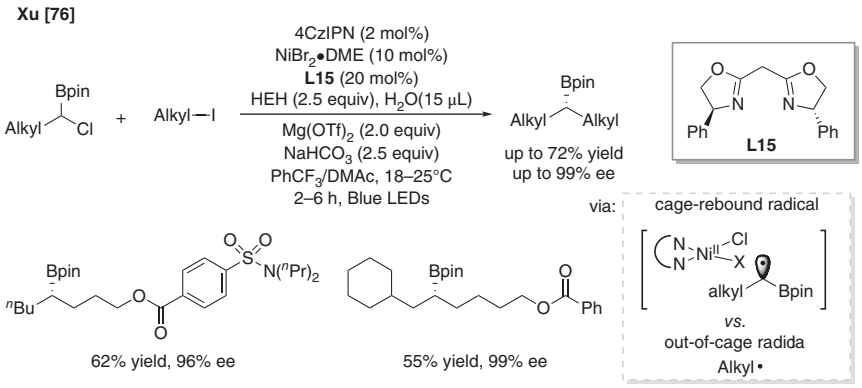


**Scheme 4.19** Alkylation of α-boryl alkyl chlorides with alkyl iodides. Source: Xu [76]/American Chemical Society.

In 2019, Reisman and coworkers developed an electrochemically driven nickel-catalyzed asymmetric XEC between alkenyl bromides and benzylic chlorides (Scheme 4.20) [77]. The substrate scope is generally broad to afford the corresponding enantioenriched α-alkenyl benzylic compounds with high efficiency and ee. Unlike previous protocols that employed super-stoichiometric metal powder reductants, this method uses electric current to turn over the nickel catalyst. Nevertheless, this electrochemical protocol still needs the use of a sacrificial Zn anode with an RVC cathode.

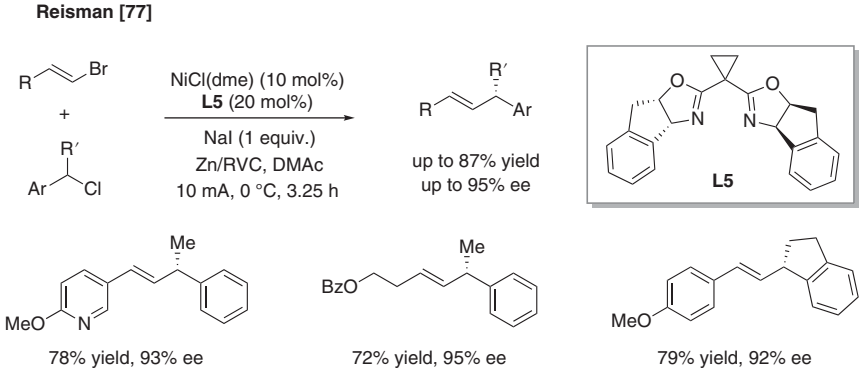


**Scheme 4.20** Electrochemically driven alkenylation of benzylic chlorides. Source: Reisman [77]/American Chemical Society.

In 2022, Mei and coworkers developed paired electrolysis-enabled asymmetric XEC of aryl bromides with α-chloro esters to afford enantioenriched α-aryl esters with good yields and ee (Scheme 4.21) [78]. The reaction has good substrate compatibility and can synthesize various nonsteroidal anti-inflammatory drug derivatives. Mechanistic investigations revealed that alkyl radicals are generated from α-chloro esters through a sequential oxidative electron transfer process at the anode, while the nickel catalyst is reduced to a lower oxidation state at the cathode.

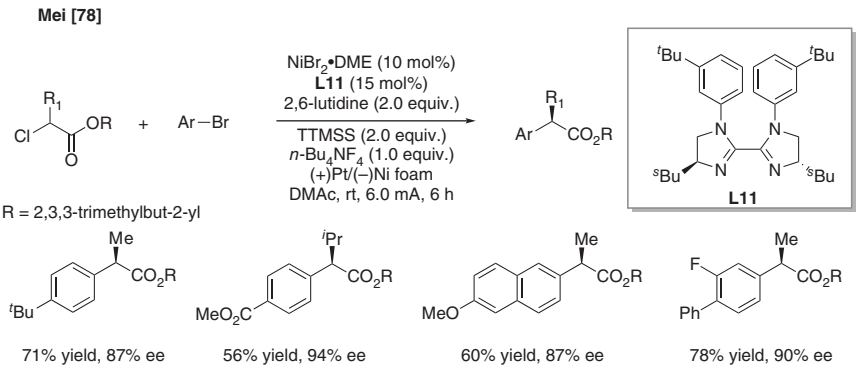


**Scheme 4.21** Electrolysis-enabled arylation of α-chloroesters. Source: Mei [78]/Springer Nature/CC BY 4.0.

In 2023, Nevado and coworkers reported an electrolysis-enabled nickel-catalyzed asymmetric XEC of aryl aziridines and alkenyl bromides, affording a series of enantioenriched β-aryl homoallylic amines (Scheme 4.22) [79]. This method merges a constant current electrolysis process in a single cell with triethylamine as a sustainable electron donor, avoiding the utilization of active metal electrodes as sacrificial anodes. Moreover, the successful preparation of some pharmacologically relevant substrates demonstrates the synthetic potential of this reaction. At the same time, Mei et al. also developed an asymmetric XEC reaction with aryl aziridines and aryl iodides via electrochemical synthesis [80]. In this reaction, an electron-rich BiIM ligand **L16** was used to improve reactivity and selectivity.

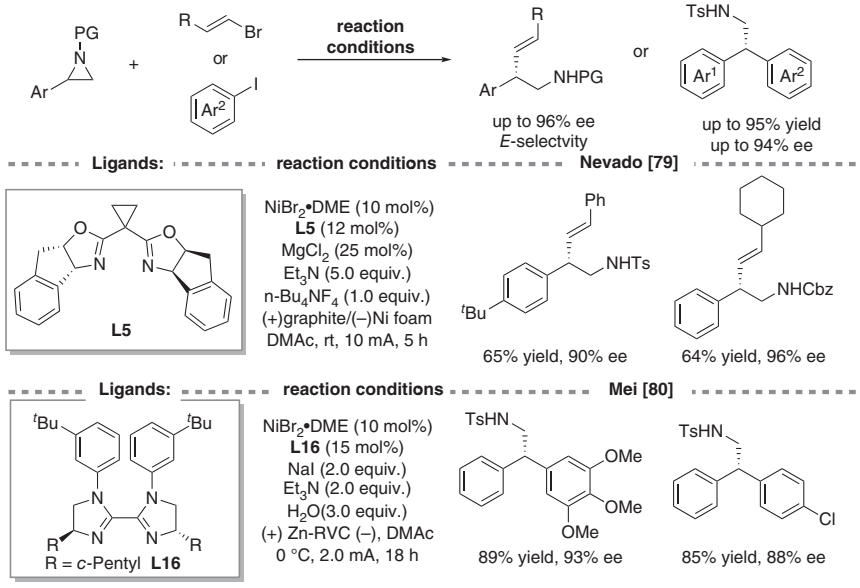


**Scheme 4.22** Electrolysis-enabled alkenylation or arylation of aryl aziridines.

## 4.3 Asymmetric Reductive Difunctionalization of Alkenes with Electrophiles

Alkenes are one of the most abundant feedstocks in chemical synthesis. Transition metal-catalyzed difunctionalization of alkenes represents an attractive approach to increase molecular complexity by incorporating two functional groups over double bonds in one pot [81–89]. Typically, 1,2-difunctionalization of alkenes with an electrophile and a nucleophile is redox-neutral, which can usually provide good chemo- and regioselectivity based on the intrinsic difference in reactivity of the nucleophile and electrophile. A significant challenge in the catalytic difunctionalization of alkenes with two electrophiles, which avoids using air-sensitive organometallic species, is the chemo- and regioselectivity. Typically, the use of two electrophiles with different redox potentials, steric hindrance, and activation mode has been proved efficient in achieving control of chemo- and regioselectivity, with the employment of chiral ligands to achieve the most challenging enantioselectivity.

### 4.3.1 Two-Component Asymmetric Couplings with Tethered Alkenes

#### 4.3.1.1 Tethered Activated Alkenes

In 2018, Kong and coworkers disclosed a Ni-catalyzed asymmetric reductive difunctionalization of acrylamide-tethered aryl bromides and other aryl bromides to forge an array of enantioenriched bis-heterocycles bearing all-carbon quaternary centers under mild conditions (Scheme 4.23, top) [90]. This reaction employed $Ni(COD)_2$ and chiral Phosferrox ligand **L17** as the catalyst combination, together with $Zn/B_2pin_2$ as the terminal reductants, KI as the additive, and $K_3PO_4$ as the base. The mild conditions tolerate a broad range of aryl bromides and diverse functional groups. Based on preliminary mechanistic studies, the authors proposed a reaction pathway involving the oxidative addition of tethered aryl bromides to Ni(0), followed by intramolecular carbonickelation to give a σ-alkyl-Ni(II) species. This migratory insertion could be the enantiodetermining step for this reaction. Subsequent SET reduction of σ-alkyl-Ni(II), followed by a second oxidative addition with aryl bromide or transmetalation between σ-alkyl-Ni(II) and aryl-Ni(II), would finally deliver the diarylation products.

Based on this mechanistic scenario, employing different types of electrophiles to intercept the σ-alkyl-Ni(II) species in the presence of reductants would allow for diverse difunctionalizations of bromoaryl-tethered acrylamides. Indeed, in 2019, Kong and coworkers employed vinyl bromides and *gem*-difluoroalkenes as the second electrophile to develop asymmetric reductive arylalkenylation of bromoaryl-tethered acrylamides via nickel catalysis, respectively (Scheme 4.23, bottom). In the cross-electrophile coupling reaction with vinyl bromides, chiral biOx ligand **L18** was used with Zn as a reductant to provide enantioenriched oxindoles with good ee [91]. The authors also used these chiral oxindoles to accomplish formal syntheses of (+)-physovenine and (+)-physostigmine. In the cross-electrophile coupling with of *gem*-difluoroalkenes, a chiral pyox ligand **L19** together with Mn as the reductant and $MgCl_2$ as the additive were used for

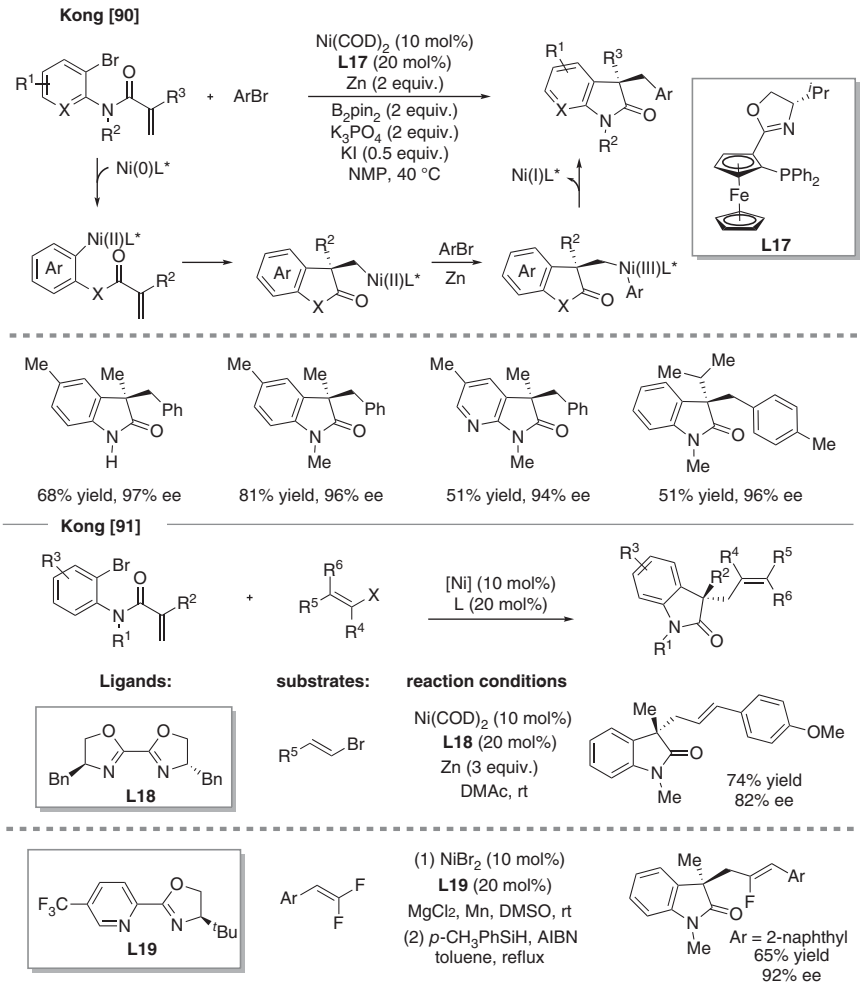


**Scheme 4.23** Intramolecular arylation and alkenylation of acrylamides.

producing the enantioenriched mono-fluoroalkene incorporated indolines with high efficiency and high ee [92]. Adding *p*-thiocresol as an additive was found to be beneficial to maintain high *E*-selectivity of the resulting monofluoroalkenes, probably by inhibiting undesired *E*/*Z* isomerization.

In 2020, Wang and coworkers developed an asymmetric reductive carboalkylation of acyl chloride-tethered styrenes with primary and secondary alkyl iodides via nickel catalysis (Scheme 4.24, top) [93]. This reaction proceeded with 20 mol% of $NiBr_2$•DME and chiral pyox **L20** to afford enantioenriched oxindoles bearing quaternary stereogenic centers with moderate yields and enantioselectivity. In 2021, Chen and coworkers developed a nickel-catalyzed asymmetric reductive alkylarylation of bromoaryl-tethered enamides with alkyl iodides in the presence of Zn as the reductant to deliver enantioenriched dialkyl-substituted isoindoline skeletons

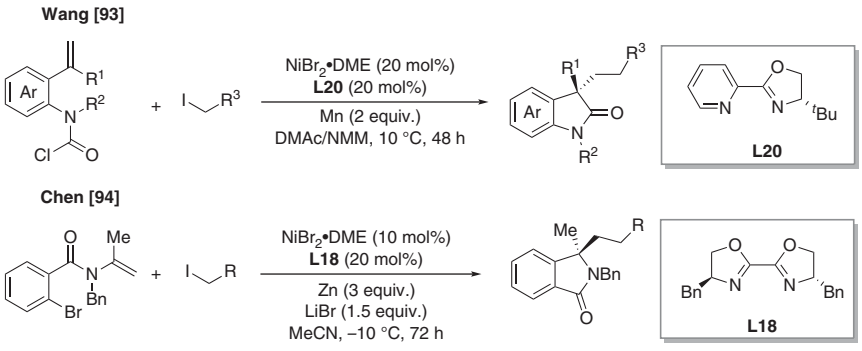


**Scheme 4.24** Enantioenriched oxindole synthesis with alkyl iodides. Source: Wang [93]/ Springer Nature/CC BY 4.0.

(Scheme 4.24, bottom) [94]. Chiral biOx **L18** was the optimal ligand, and the additive LiBr significantly improved the coupling efficiency.

#### 4.3.1.2 Tethered Nonactivated Alkenes

In 2019, Shu and coworkers developed an enantioselective cross-electrophile aryl-alkenylation reaction of iodoaryl-tethered unactivated alkenes with vinyl triflates in the presence of Mn via nickel catalysis (Scheme 4.25) [95]. Using catalytic $NiI_2$ and chiral pyox **L19**, the reaction proceeded with equimolar amounts of alkenes and alkenyl triflates to deliver enantioenriched heterocyclic products, including dihydrobenzofurans, indolines, and indanes, in good yields and excellent ee. The incorporated alkenes were leveraged for further synthetic manipulations, while only tethered 1,1-disubstituted alkenes were applicable. Mechanistically, an enantioselective intramolecular migratory insertion of (aryl)nickel into the tethered alkene was proposed for this asymmetric reaction.

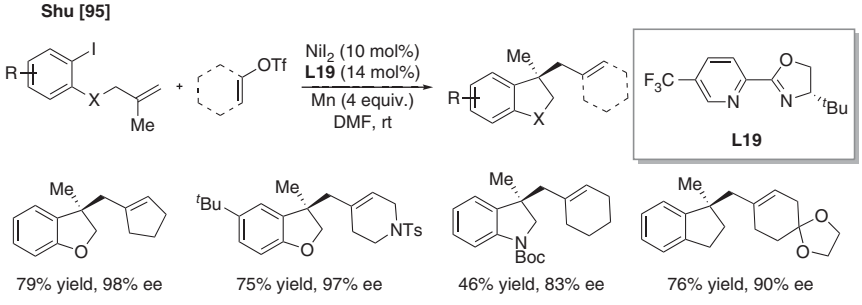


**Scheme 4.25** Intramolecular aryl-alkenylation of alkenes with alkenyl triflates. Source: Shu [95]/American Chemical Society.

With allylic carbonates as the second electrophiles, in 2021, Wang and coworkers disclosed an asymmetric reductive aryl-allylation of alkene-tethered aryl iodides with allylic carbonates in the presence of $NiCl_2$•DME, chiral pyox ligand **L20**, and

Zn (Scheme 4.26) [96]. Both acyclic and cyclic allyl carbonates were suitable partners to afford enantioenriched indanes and dihydrobenzofurans with high ee.

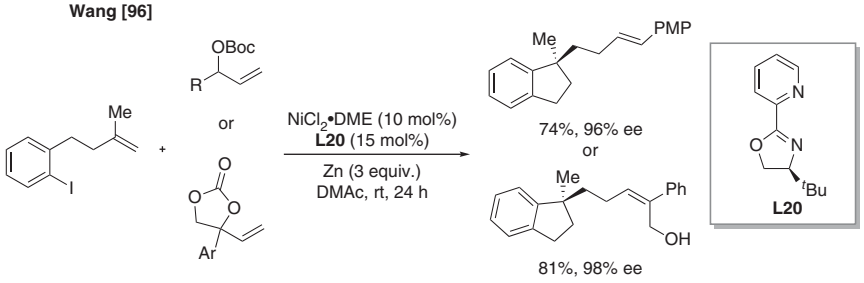


**Scheme 4.26** Intramolecular aryl-allylation of alkenes with allyl carbonates. Source: Wang [96]/Royal Society of Chemistry.

In 2019, Wang and coworkers developed an asymmetric reductive alkylarylation of bromoaryl-tethered alkenes with alkyl bromides in the presence of catalytic $NiBr_2$•DME/chiral biOx ligand **L18** and stoichiometric Zn (Scheme 4.27, top) [97]. Under the established conditions, enantioenriched benzene-fused five-membered cyclic products bearing a quaternary stereocenter were obtained with good efficiency and enantioselectivity. In this case, six-membered products were obtained with significantly decreased ee. Later, the Wang group extended it to an asymmetric XEC reaction of iodoaryl-tethered alkenes and benzylic chlorides with chiral pyox **L20** as the ligand (Scheme 4.27, bottom) [98].

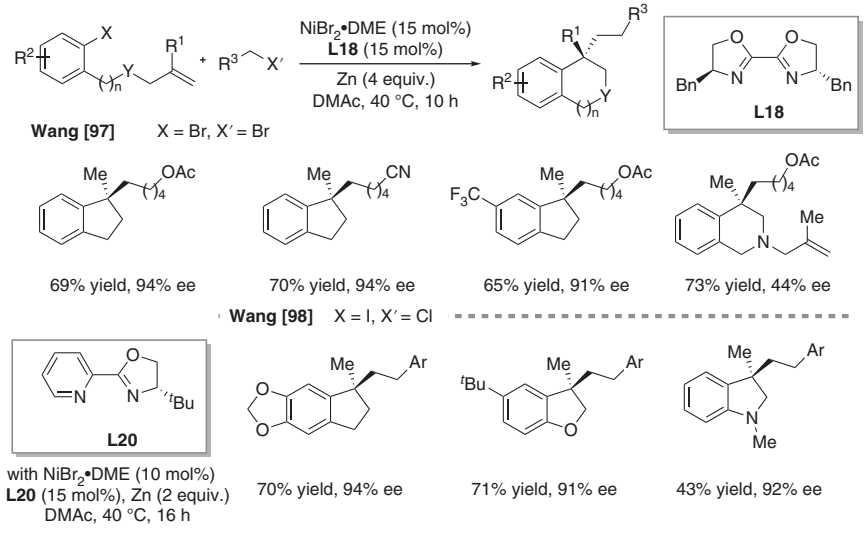


**Scheme 4.27** Aryl-alkylation of alkenes with alkyl halides.

In 2022, Chen and coworkers developed a nickel-catalyzed asymmetric XEC reaction of acyl chloride-tethered alkenes with alkyl iodides to forge a series of

enantioenriched six-membered nitrogen-based heterocycles with high efficiency (Scheme 4.28) [99]. Using catalytic $Ni(ClO_4)_2 \bullet 6H_2O$ and the newly developed 8-Quniox ligand **L21** in the presence of stoichiometric Mn and LiI, this protocol proceeded via a more challenging 6-exo-trig cyclization to access six-membered lactams, including 3,4-dihydroquinolinones and 2-piperidinones in high enantioselectivity. Both 1,1-disubstituted alkenes and terminal alkenes worked well, while only primary alkyl iodides were compatible.

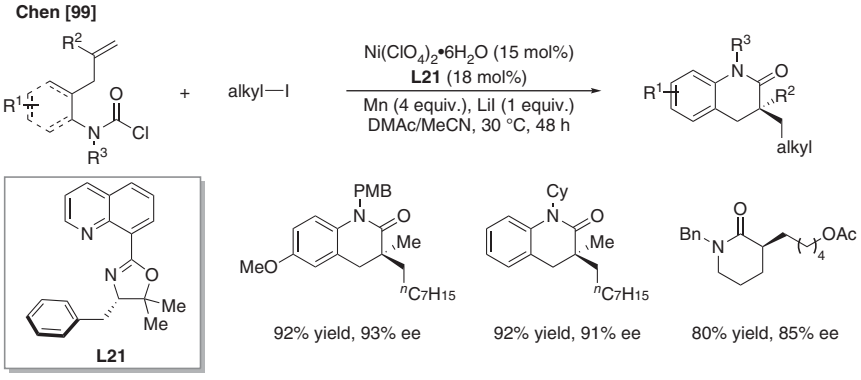


**Scheme 4.28** Intramolecular alkyl-acylation of alkenes with alkyl iodides. Source: Chen [99]/Springer Nature/CC BY 4.0.

In 2020, Zhu and coworkers utilized O-benzoyl-hydroxylamines as electrophilic aminating agents to develop the first example of asymmetric reductive 1,2-carboamination of tethered alkenes via nickel catalysis (Scheme 4.29) [100]. With catalytic $NiI_2$, chiral pyox **L22**, and CoPc in the presence of stoichiometric Zn and TMSCl, a variety of enantioenriched alkylamines bearing aryl-substituted quaternary carbon centers can be straightforwardly constructed with excellent enantioselectivity under mild conditions. The mild conditions are tolerated with many functional groups. Mechanistically, a similar enantiodetermining migratory insertion of (aryl)nickel(II) into tethered alkene to form (alkyl)nickel(II) species, followed by SET reduction and electrophilic amination, was proposed.

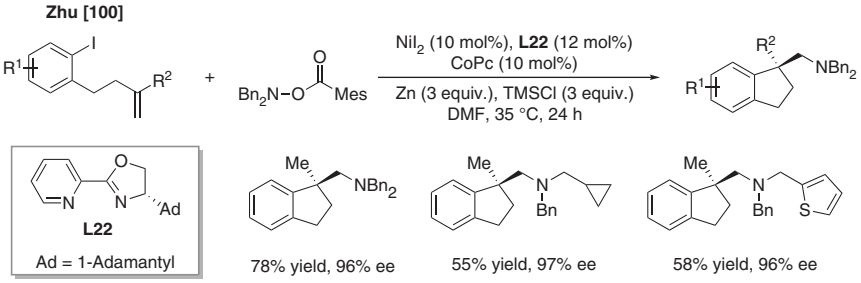


**Scheme 4.29** Aryl-amination of alkenes with O-acyl hydroxylamines. Source: Zhu [100]/John Wiley & Sons.

The nickel-catalyzed asymmetric reductive cyclization of nonaromatic-tethered mono-substituted alkenes remains underexploited, probably due to the inherent challenge in stereoselective migratory insertion. In 2020, Chen and coworkers utilized a newly designed chiral 8-quinoline imidazoline ligand (Quinim) to achieve the asymmetric reductive cyclization of mono-substituted alkene-tethered carbamoyl chlorides with primary alkyl iodides via nickel catalysis (Scheme 4.30, top) [101]. Employing catalytic $Ni(cod)_2$ and *t*-Bu Quinim **L23** and stoichiometric Mn and LiBr, this protocol allowed for the efficient assembly of enantioenriched α-alkylated pyrrolidinones from simple alkene-tethered carbamoyl chlorides with high enantiomeric excess. Preliminary mechanistic studies revealed that the intramolecular migratory insertion of carbamoyl nickel species into the alkene could be the enantiodetermining step.

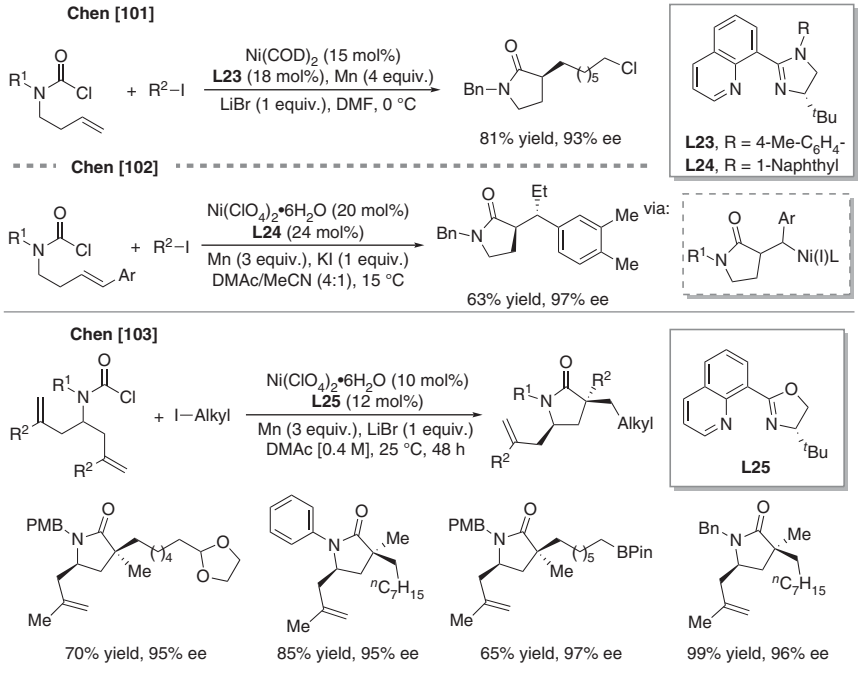


**Scheme 4.30** Intramolecular alkyl-acylation of alkenes with alkyl iodides.

In 2022, the Chen group expanded this system to internal alkene-tethered carbamoyl chlorides to forge a series of chiral pyrrolidinones bearing vicinal stereogenic centers with excellent diastereo- and enantioselectivity (Scheme 4.30, middle) [102]. Using 1-naphthyl-substituted Quinim **L24** was critical for selective control. This asymmetric reductive protocol was also applicable to 1,1-disubstituted alkenes. A slightly different reaction pathway, in which SET reduction of acylnickel(II) proceeded prior to the enantiodetermining migratory insertion into the alkene, was proposed based on DFT calculations.

At the same time, Chen and coworkers also developed a desymmetric carbamoylalkylation of carbamoyl chloride-tethered 1,6-dienes with alkyl iodides via nickel-catalyzed asymmetric cross-electrophile coupling with chiral Quinim **L25** as the ligand (Scheme 4.30, bottom) [103]. A wide range of enantioenriched pyrrolidinones bearing two stereogenic centers were constructed with high diastereo- and enantioselectivity. Both disubstituted and mono-substituted alkenes were applicable, and the resulting products can be further manipulated. The authors reasoned that the intramolecular migratory insertion of carbamoyl-Ni(I) species into one of the pendant alkenes could be the stereo-determining step, and the interaction between the second pendant alkene and nickel species could set the diastereoselectivity.

In 2021, Shu and coworkers developed a nickel-catalyzed asymmetric reductive divinylation of 2-bromo-1,6-dienes with vinyl bromides (Scheme 4.31, top) [104]. Using $NiBr_2$ and chiral *t*-Bu-pyox ligand **L26** as the catalyst combination, this protocol was compatible with N-, O-, and C-tethered bromo-dienes and various alkenyl bromides, enabling efficient access to enantioenriched cyclic architectures with high chemo-, regio-, and enantioselectivity. The addition of $AgBF_4$ could improve the selectivity of the cyclization product when the methyl group was replaced with a more sterically hindered substituent (Scheme 4.31, top). In 2022, the same group reported a nickel-catalyzed asymmetric iminoalkylation reaction of

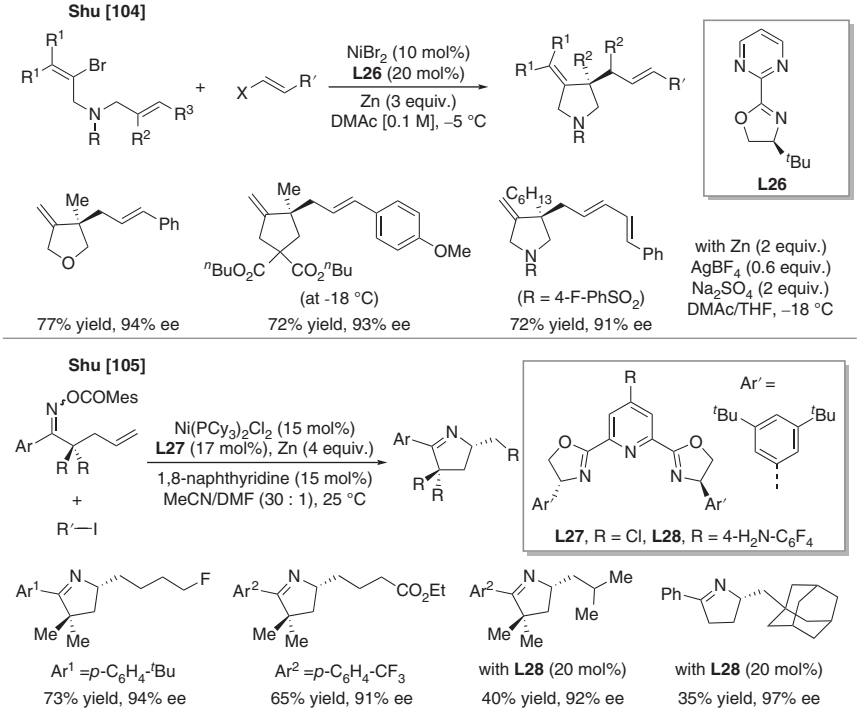


**Scheme 4.31** Alkenyl-cyclization of 2-bromo-1,6-dienes with alkenyl halides.

oxime ester-tethered alkenes with alkyl iodides by employing newly defined chiral PyBox ligands **L27** and **L28** (Scheme 4.31, bottom) [105].

### 4.3.2 Three-Component Asymmetric Coupling with Alkenes

In 2019, Diao and coworkers reported an asymmetric diarylation reaction of styrenes with aryl bromides in the presence of Zn via nickel catalysis (Scheme 4.32) [106]. Using $NiBr_2$•DME as the nickel catalyst, chiral biOx **L29** as the ligand, and *N*-oxyl radical additive (ABNO) as the co-ligand, a series of enantioenriched α,α,β-triarylated ethane scaffolds were forged with high efficiency and ee. Mechanistically, the involvement of benzylic radicals was supported by the formation of benzylic dimers and *trans*-diarylated products in the case of indene.

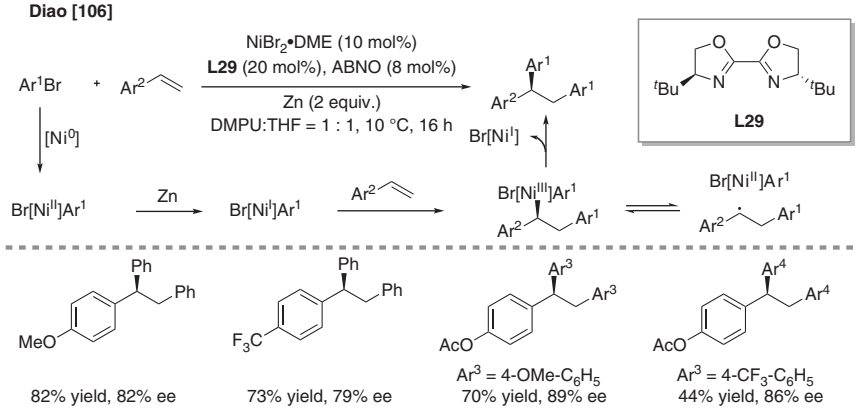


**Scheme 4.32** Diarylation of styrenes with aryl bromides. Source: Diao [106]/John Wiley & Sons.

It is more challenging to conquer the selectivity in three-component reductive difunctionalization of alkenes, particularly nonactivated alkenes, with two different carbon electrophiles. In 2020, Chu and coworkers reported the first example of asymmetric three-component reductive 1,2-alkylarylation of nonactivated alkenes with aryl halides and alkyl halides via nickel catalysis (Scheme 4.33) [107]. Using $NiCl_2$•DME and chiral 4-heptyl-substituted biOx **L9** or the newly designed 5-nonyl-substituted biOx **L30** in the presence of Mn and TMSCl, a wide range of nonactivated alkenes, aryl halides, and alkyl halides underwent efficient and selective couplings to afford enantioenriched benzylic compounds under mild conditions. The authors reasoned that a weak coordination effect between the pendant carbonyl group and nickel intermediates would synergistically facilitate the control of regio- and enantioselectivity. Various functionalized chiral β-fluoroalkyl aryl-alkanes with excellent enantioselectivity were constructed.

Later, Nevado and coworkers developed a Ni-catalyzed asymmetric reductive dicarbofunctionalization of enamines with aryl halides and alkyl halides (Scheme 4.34) [108]. This protocol used biOx **L31** as the chiral ligand and TDAE as

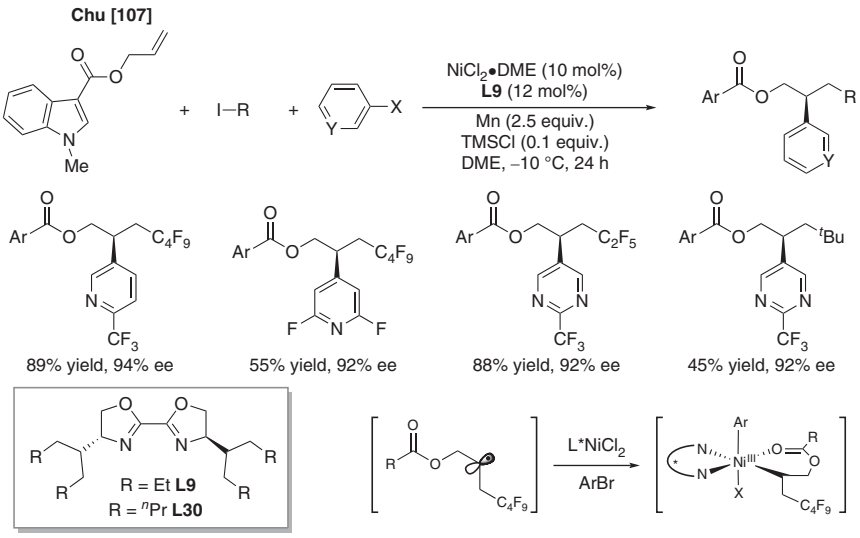


**Scheme 4.33** Three-component carboarylation of unactivated alkenes with fluoroalkyl iodides. Source: Chu [107]/American Chemical Society.

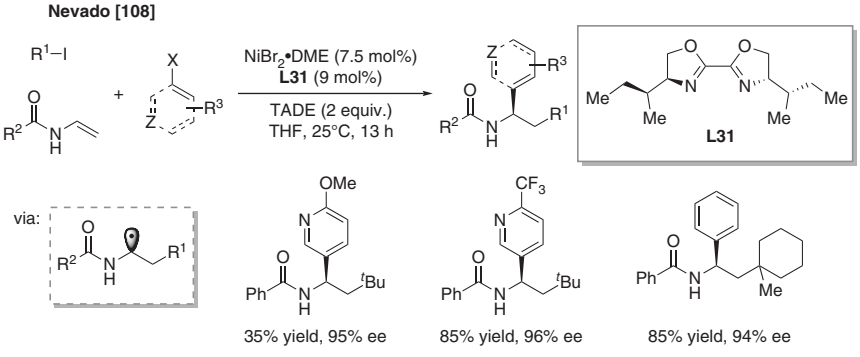


**Scheme 4.34** Carboarylation of activated alkenes with alkyl iodides. Source: Nevado [108]/American Chemical Society.

the organic reductant, affording the corresponding enantioenriched α-aryl amides with high efficiency and excellent ee. DFT calculations revealed that the interaction of the carbonyl group of enamines with the nickel center in the transition state could enable partial de-coordination of the biOx ligand, leading to a stereodefined outcome.

Recently, Chu and coworkers developed a nickel-catalyzed asymmetric reductive three-component carboalkenylation of β,γ-alkenyl ketones with alkyl halides and cis-vinyl halides (Scheme 4.35) [109]. This reaction employed $Ni(COD)_2$ and chiral biOx **L31** as the catalyst combination, together with Mn as the reductant and benzoic acid as the additive, to forge a diverse range of synthetically valuable enantioenriched β-alkenyl ketones with high efficiency and excellent enantioselectivity.

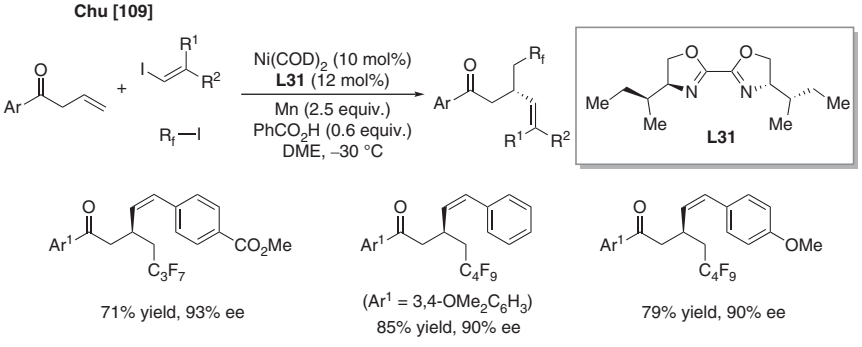


**Scheme 4.35** Carboalkenylation of unactivated alkenes with fluoroalkyl- and alkenyl iodides. Source: Chu [109]/American Chemical Society.

The addition of benzoic acid significantly improved the yields by inhibiting the competitive formation of styrenyl-$C_4F_9$ side products. Similar to their previous studies, this reaction involved a radical addition to the alkene, followed by alkyl radical capture by the chiral nickel complex, where the chelation between the pendant ketone group and the chiral nickel species was critical for achieving high enantioselectivity.

In 2021, Mao, Walsh et al. reported an enantioselective three-component reductive carboarylation of acrylates via Ni/photoredox dual catalysis (Scheme 4.36) [110]. Using a combination of catalytic 4CzIPN, $NiBr_2$, and chiral BiIM ligand **L13**, this reaction proceeded smoothly in the presence of HEH as the reductant, $Et_3N$ as the base, and blue LED irradiation, constructing enantioenriched α-aryl carbonyls in good yields and high ee. In addition to tertiary alkyl bromines, secondary and primary alkyl bromines or iodides were also competent coupling partners, albeit with lower yields and selectivity.

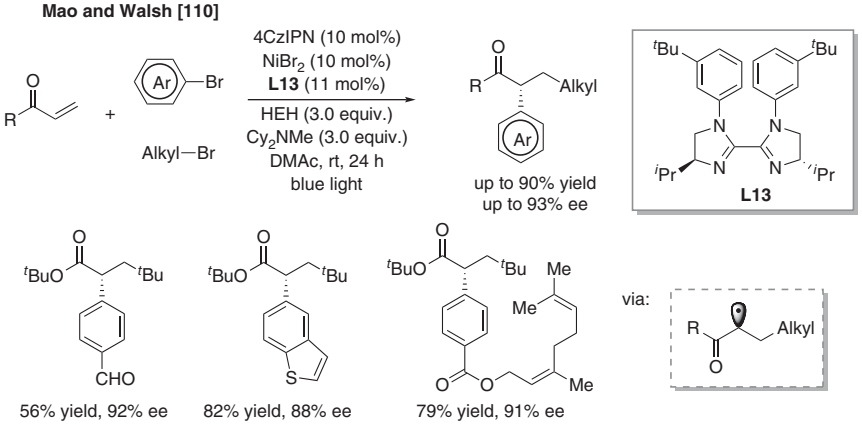


**Scheme 4.36** Carboarylation of acylate esters with alkyl- and aryl bromides. Source: Mao and Walsh [110]/Springer Nature/CC BY 4.0.

## 4.4 Conclusion

In recent years, extraordinary advances have been made in Ni-catalyzed asymmetric cross-electrophile couplings, providing a powerful platform for constructing diverse chiral motifs without the need for organometallic agents under mild conditions. However, several synthetic challenges remain, including the use of more diverse and readily accessible electrophiles, taming the intriguing chemo-, regio-, and stereoselectivity issues between two similar electrophiles, achieving planar chirality with $C(sp^2)$-electrophiles, and improving the practical applications of asymmetric XECs remain to be further exploitations.

## List of Abbreviations

| | |
|---|---|
| 4CzIPN | 2,4,5,6-tetra(9H-Carbazol-9-yl)-isophthalonitrile |
| ABNO | 9-Azabicyclo[3.3.1] nonane *N*-oxyl |
| Ad | 1-Adamantyl |
| ATRA | Atom transfer radical addition |
| box | Bisoxazoline |
| BiIM | Bi-imidazoline |
| biox | Bioxazoline |
| COD | Cyclooctadiene |
| CoPc | Cobalt(II) phthalocyanine |
| DFT | Density functional theory |
| DIPEA | *N,N*-Diisopropylethylamine |
| DMAc | *N,N*-Dimethyl acetamide |
| DMBA | Dimethyl benzoic acid |
| DME | 1,2-Dimethyl ethane |
| DMF | *N,N*-Dimethylformamide |
| DMPU | *N,N*-Dimethylpropyleneurea |
| DMSO | Dimethyl sulfoxide |
| dr | Diastereomeric ratio |
| ee | Enantiomeric excess |
| FG | Functional group |
| HEH | Hantzsch ester |
| LEDs | Light-emitting diodes |
| MS | Molecular sieve |
| MVLR | Multivariate linear regression |
| NCIs | Noncovalent interactions |
| NHP | *N*-Hydroxy phthalimide |
| NMM | *N*-Methylmorpholine |
| NMP | *N*-Methyl pyrrolidone |
| O.A. | Oxidative addition |
| PHOX | Phosphino-oxazoline |
| PyBox | Pyridine-bisoxazoline |

| | |
|---|---|
| pyox | pyridine-oxazoline |
| R.E. | Reductive elimination |
| RVC | Reticulated vitreous carbon |
| SET | Single-electron transfer |
| TBAC | Tetrabutylammonium chloride |
| TDAE | Tetrakis(dimethylamino)ethylene |
| TEA | Triethylamine |
| THF | Tetrahydrofuran |
| TMSCl | Chlorotrimethylsilane |
| TTMSS | Tris(trimethylsilyl)silane |
| XECs | Cross-electrophile couplings |

## References


1 Hegedus, L.S. and Söderberg, B.C.G. (2010). *Transition Metals in the Synthesis of Complex Organic Molecules*, 3rde. South Orange, NJ: University Science Books.
2 de Meijere, A., Bräse, S., and Oestreich, M. (2014). *Metal-Catalyzed Cross-Coupling Reactions and More*. Weinheim, Germany: Wiley.
3 Wu, X.-F. (2023). *C–C Cross Couplings with 3d Base Metal Catalysts*. Cham: Springer International Publishing.
4 Carnahan, E.M., Protasiewicz, J.D., and Lippard, S.J. (1993). *Acc. Chem. Res.* 26: 90–97.
5 Everson, D.A. and Weix, D.J. (2014). *J. Org. Chem.* 79: 4793–4798.
6 Knappke, C.E.I., Grupe, S., Gärtner, D. et al. (2014). *Chem. Eur. J.* 20: 6828–6842.
7 Weix, D.J. (2015). *Acc. Chem. Res.* 48: 1767–1775.
8 Hanna, L.E. and Jarvo, E.R. (2015). *Angew. Chem. Int. Ed.* 54: 15618–15620.
9 Gu, J., Wang, X., Xue, W., and Gong, H. (2015). *Org. Chem. Front.* 2: 1411–1421.
10 Wang, X., Dai, Y., and Gong, H. (2016). Nickel-catalyzed reductive couplings. *Top. Curr. Chem.* 374: 43.
11 Lucas, E.L. and Jarvo, E.R. (2017). *Nat. Rev. Chem.* 1: 0065.
12 Holmes, M., Schwartz, L.A., and Krische, M.J. (2018). *Chem. Rev.* 118: 6026–6052.
13 Li, Y., Fan, Y., and Jia, Q. (2019). *Chin. J. Org. Chem.* 39: 350–362.
14 Pang, X., Peng, X., and Shu, X.-Z. (2020). *Synthesis* 52: 3751–3763.
15 Poremba, K.E., Dibrell, S.E., and Reisman, S.E. (2020). *ACS Catal.* 10: 8237–8246.
16 Pang, X., Su, P.-F., and Shu, X.-Z. (2022). *Acc. Chem. Res.* 55: 2491–2509.
17 Liu, Y., Li, P., Wang, Y., and Qiu, Y. (2023). *Angew. Chem. Int. Ed.* 62: e202306679.
18 Tasker, S.Z., Standley, E.A., and Jamison, T.F. (2014). *Nature* 509: 299–309.
19 Ananikov, V.P. (2015). *ACS Catal.* 5: 1964–1971.
20 Su, B., Cao, Z.-C., and Shi, Z.-J. (2015). *Acc. Chem. Res.* 48: 886–896.
21 Diccianni, J.B. and Diao, T. (2019). *Trends Chem.* 1: 830–844.

**22** Boit, T.B., Bulger, A.S., Dander, J.E., and Garg, N.K. (2020). *ACS Catal.* 10: 12109–12126.

**23** Clevenger, A.L., Stolley, R.M., Aderibigbe, J., and Louie, J. (2020). *Chem. Rev.* 120: 6124–6196.

**24** Diccianni, J., Lin, Q., and Diao, T. (2020). *Acc. Chem. Res.* 53: 906–919.

**25** Ogoshi, S. (2020). *Nickel Catalysis in Organic Synthesis*. Weinheim, Germany: Wiley.

**26** Zhu, S., Zhao, X., Li, H., and Chu, L. (2021). *Chem. Soc. Rev.* 50: 10836–10856.

**27** Sun, X.-Y., Yao, B.-Y., Xuan, B. et al. (2022). *Chem Catal.* 2: 3140–3162.

**28** Kranthikumar, R. (2022). *Organometallics* 41: 667–679.

**29** Cherney, A.H., Kadunce, N.T., and Reisman, S.E. (2013). *J. Am. Chem. Soc.* 135: 7442–7445.

**30** Müller, K., Faeh, C., and Diederich, F. (2007). *Science* 317: 1881–1886.

**31** Hagmann, W.K. (2008). *J. Med. Chem.* 51: 4359–4369.

**32** Wu, B.-B., Xu, J., Bian, K.-J. et al. (2022). *J. Am. Chem. Soc.* 144: 6543–6550.

**33** Wu, J., Wu, H., Liu, X. et al. (2022). *Org. Lett.* 24: 4322–4327.

**34** Lin, D., Chen, Y., Dong, Z. et al. (2023). *CCS Chem.* 5: 1386–1397.

**35** Cherney, A.H. and Reisman, S.E. (2014). *J. Am. Chem. Soc.* 136: 14365–14368.

**36** Hofstra, J.L., Cherney, A.H., Ordner, C.M., and Reisman, S.E. (2018). *J. Am. Chem. Soc.* 140: 139–142.

**37** Cornella, J., Edwards, J.T., Qin, T. et al. (2016). *J. Am. Chem. Soc.* 138: 2174–2177.

**38** Huihui, K.M.M., Caputo, J.A., Melchor, Z. et al. (2016). *J. Am. Chem. Soc.* 138: 5016–5019.

**39** Konev, M.O. and Jarvo, E.R. (2016). *Angew. Chem. Int. Ed.* 55: 11340–11342.

**40** Qin, T., Cornella, J., Li, C. et al. (2016). *Science* 352: 801–805.

**41** Wang, J., Qin, T., Chen, T.-G. et al. (2016). *Angew. Chem. Int. Ed.* 55: 9676–9679.

**42** Suzuki, N., Hofstra, J.L., Poremba, K.E., and Reisman, S.E. (2017). *Org. Lett.* 19: 2150–2153.

**43** Turro, R.F., Wahlman, J.L.H., Tong, Z.J. et al. (2023). *J. Am. Chem. Soc.* 145: 14705–14715.

**44** Geng, J., Sun, D., Song, Y. et al. (2022). *Org. Lett.* 24: 1807–1811.

**45** Kadunce, N.T. and Reisman, S.E. (2015). *J. Am. Chem. Soc.* 137: 10480–10483.

**46** Poremba, K.E., Kadunce, N.T., Suzuki, N. et al. (2017). *J. Am. Chem. Soc.* 139: 5684–5687.

**47** DeLano, T.J., Dibrell, S.E., Lacker, C.R. et al. (2021). *Chem. Sci.* 12: 7758–7762.

**48** Min, Y., Sheng, J., Yu, J.-L. et al. (2021). *Angew. Chem. Int. Ed.* 60: 9947–9952.

**49** Sun, D., Ma, G., Zhao, X. et al. (2021). *Chem. Sci.* 12: 5253–5258.

**50** Wang, D. and Xu, T. (2021). *ACS Catal.* 11: 12469–12475.

**51** Nielsen, L.P.C. and Jacobsen, E.N. (2006). Catalytic asymmetric epoxide ring-opening chemistry. In: *Aziridines and Epoxides in Organic Synthesis*, 229–269. Weinheim, Germany: Wiley.

**52** Huang, C.-Y. and Doyle, A.G. (2014). *Chem. Rev.* 114: 8153–8198.

**53** Moragas, T., Correa, A., and Martin, R. (2014). *Chem. Eur. J.* 20: 8242–8258.

**54** Zhao, Y. and Weix, D.J. (2015). *J. Am. Chem. Soc.* 137: 3237–3240.
**55** Banerjee, A. and Yamamoto, H. (2017). *Org. Lett.* 19: 4363–4366.
**56** Hu, X.E. (2004). *Tetrahedron* 60: 2701–2743.
**57** Stanković, S., D'Hooghe, M., Catak, S. et al. (2012). *Chem. Soc. Rev.* 41: 643–665.
**58** Woods, B.P., Orlandi, M., Huang, C.-Y. et al. (2017). *J. Am. Chem. Soc.* 139: 5688–5691.
**59** Guo, L., Yuan, M., Zhang, Y. et al. (2020). *J. Am. Chem. Soc.* 142: 20390–20399.
**60** Prier, C.K., Rankic, D.A., and MacMillan, D.W.C. (2013). *Chem. Rev.* 113: 5322–5363.
**61** Cavalcanti, L.N. and Molander, G.A. (2016). *Top. Curr. Chem.* 374: 39.
**62** Gui, Y.-Y., Sun, L., Lu, Z.-P., and Yu, D.-G. (2016). *Org. Chem. Front.* 3: 522–526.
**63** Lang, X., Zhao, J., and Chen, X. (2016). *Chem. Soc. Rev.* 45: 3026–3038.
**64** Skubi, K.L., Blum, T.R., and Yoon, T.P. (2016). *Chem. Rev.* 116: 10035–10074.
**65** Twilton, J., Le, C., Zhang, P. et al. (2017). *Nat. Rev. Chem.* 1: 0052.
**66** Zhang, H.-H., Chen, H., Zhu, C., and Yu, S. (2020). *Sci. China Chem.* 63: 637–647.
**67** Zhu, C., Yue, H., Chu, L., and Rueping, M. (2020). *Chem. Sci.* 11: 4051–4064.
**68** Chan, A.Y., Perry, I.B., Bissonnette, N.B. et al. (2022). *Chem. Rev.* 122: 1485–1542.
**69** Guan, H., Zhang, Q., Walsh, P.J., and Mao, J. (2020). *Angew. Chem. Int. Ed.* 59: 5172–5177.
**70** Lau, S.H., Borden, M.A., Steiman, T.J. et al. (2021). *J. Am. Chem. Soc.* 143: 15873–15881.
**71** Zheng, P., Zhou, P., Wang, D. et al. (2021). *Nat. Commun.* 12: 1646.
**72** Zhou, P., Li, X., Wang, D., and Xu, T. (2021). *Org. Lett.* 23: 4683–4687.
**73** Li, T., Cheng, X., Lu, J. et al. (2022). *Chin. J. Chem.* 40: 1033–1038.
**74** Lu, Q., Guan, H., Wang, Y.-E. et al. (2022). *J. Org. Chem.* 87: 8048–8058.
**75** Wang, H., Zheng, P., Wu, X. et al. (2022). *J. Am. Chem. Soc.* 144: 3989–3997.
**76** Zhou, J., Wang, D., Xu, W. et al. (2023). *J. Am. Chem. Soc.* 145: 2081–2087.
**77** DeLano, T.J. and Reisman, S.E. (2019). *ACS Catal.* 9: 6751–6754.
**78** Liu, D., Liu, Z.-R., Wang, Z.-H. et al. (2022). *Nat. Commun.* 13: 7318.
**79** Hu, X., Cheng-Sánchez, I., Cuesta-Galisteo, S., and Nevado, C. (2023). *J. Am. Chem. Soc.* 145: 6270–6279.
**80** Wang, Y.-Z., Wang, Z.-H., Eshel, I.L. et al. (2023). *Nat. Commun.* 14: 2322.
**81** McDonald, R.I., Liu, G., and Stahl, S.S. (2011). *Chem. Rev.* 111: 2981–3019.
**82** Merino, E. and Nevado, C. (2014). *Chem. Soc. Rev.* 43: 6598–6608.
**83** Crossley, S.W.M., Obradors, C., Martinez, R.M., and Shenvi, R.A. (2016). *Chem. Rev.* 116: 8912–9000.
**84** Yin, G., Mu, X., and Liu, G. (2016). *Acc. Chem. Res.* 49: 2413–2423.
**85** Dhungana, R.K., Kc, S., Basnet, P., and Giri, R. (2018). *Chem. Rec.* 18: 1314–1340.
**86** Giri, R. and Kc, S. (2018). *J. Org. Chem.* 83: 3013–3022.
**87** Zhang, J.-S., Liu, L., Chen, T., and Han, L.-B. (2018). *Chem. Asian J.* 13: 2277–2291.

**88** Jiang, H. and Studer, A. (2020). *Chem. Soc. Rev.* 49: 1790–1811.
**89** Li, Y., Wu, D., Cheng, H.-G., and Yin, G. (2020). *Angew. Chem. Int. Ed.* 59: 7990–8003.
**90** Wang, K., Ding, Z., Zhou, Z., and Kong, W. (2018). *J. Am. Chem. Soc.* 140: 12364–12368.
**91** Li, Y., Ding, Z., Lei, A., and Kong, W. (2019). *Org. Chem. Front.* 6: 3305–3309.
**92** Ma, T., Chen, Y., Li, Y. et al. (2019). *ACS Catal.* 9: 9127–9133.
**93** Lan, Y. and Wang, C. (2020). *Commun. Chem.* 3: 45.
**94** Fang, K., Huang, W., Shan, C. et al. (2021). *Org. Lett.* 23: 5523–5527.
**95** Tian, Z.-X., Qiao, J.-B., Xu, G.-L. et al. (2019). *J. Am. Chem. Soc.* 141: 7637–7643.
**96** Lin, Z., Jin, Y., Hu, W., and Wang, C. (2021). *Chem. Sci.* 12: 6712–6718.
**97** Jin, Y. and Wang, C. (2019). *Angew. Chem. Int. Ed.* 58: 6722–6726.
**98** Jin, Y., Yang, H., and Wang, C. (2020). *Org. Lett.* 22: 2724–2729.
**99** Zhang, C., Wu, X., Xia, T. et al. (2022). *Nat. Commun.* 13: 5964.
**100** He, J., Xue, Y., Han, B. et al. (2020). *Angew. Chem. Int. Ed.* 59: 2328–2332.
**101** Wu, X., Qu, J., and Chen, Y. (2020). *J. Am. Chem. Soc.* 142: 15654–15660.
**102** Wu, X., Turlik, A., Luan, B. et al. (2022). *Angew. Chem. Int. Ed.* 61: e202207536.
**103** Wu, X., Luan, B., Zhao, W. et al. (2022). *Angew. Chem. Int. Ed.* 61: e202111598.
**104** Qiao, J.-B., Zhang, Y.-Q., Yao, Q.-W. et al. (2021). *J. Am. Chem. Soc.* 143: 12961–12967.
**105** Jia, X.-G., Yao, Q.-W., and Shu, X.-Z. (2022). *J. Am. Chem. Soc.* 144: 13461–13467.
**106** Anthony, D., Lin, Q., Baudet, J., and Diao, T. (2019). *Angew. Chem. Int. Ed.* 58: 3198–3202.
**107** Tu, H.-Y., Wang, F., Huo, L. et al. (2020). *J. Am. Chem. Soc.* 142: 9604–9611.
**108** Wei, X., Shu, W., García-Domínguez, A. et al. (2020). *J. Am. Chem. Soc.* 142: 13515–13522.
**109** Wang, F., Pan, S., Zhu, S., and Chu, L. (2022). *ACS Catal.* 12: 9779–9789.
**110** Qian, P., Guan, H., Wang, Y.-E. et al. (2021). *Nat. Commun.* 12: 6613.

# 5

# Copper-Catalyzed Oxidative Asymmetric Radical Cross-Coupling of C($sp^3$)—H Bonds

*Pinhong Chen and Guosheng Liu*

*State Key Laboratory of Organometallic Chemistry and Shanghai Hong Kong Joint Laboratory in Chemical Synthesis, Center for Excellence in Molecular Synthesis, Shanghai Institute of Organic Chemistry, University of Chinese Academy of Sciences, Chinese Academy of Sciences, Shanghai, China*

## 5.1 Introduction

C—H bonds are the most abundant functional groups in organic compounds. Direct C—H functionalization arguably represents the most straightforward and atom-economical transformation in organic synthesis. Instead of manipulating functional groups, the new logic relies on the controllable functionalization of specific C—H bonds, even in the presence of supposedly more reactive functional groups. For a general comparison, direct C—H functionalization could substantially streamline the synthesis of target molecules via step- and atom-economy than canonical strategies.

The key challenge is achieving good selectivity under the forcing conditions necessary to activate inert C—H bonds. Numerous strategies have been developed to achieve this target over the past decades. Among these, the radical C—H functionalization via hydrogen atom transfer (HAT) represents one of the most powerful approaches and allows a unique profile of reactivity and selectivity complementary to ionic chemistry in which electrons move in pairs. Although elegant methods of C($sp^3$)—H oxidation have been developed using transition metal complexes as catalysts to mimic the modes of enzyme catalysis, the rapid radical rebound process limits its further application in installing other functional groups and enantioselectivity control.

Alternatively, a diffusible carbon radical species formed through HAT could be trapped by a second species or catalysts to afford the C($sp^3$)—H functionalized products, known as a copper–catalyzed radical relay pathway (Scheme 5.1). Meanwhile, the copper catalyst has shown impressive controllability and reactivity in radical-mediated cross-coupling reactions. Thus, the copper-catalyzed radical relay offers a substantial opportunity to expand the regime of radical-mediated C($sp^3$)—H bond functionalization, and significant progress has been achieved in the last decades. The HAT process can proceed intermolecularly with an external radical generated by reduction with copper, as well as intramolecularly with

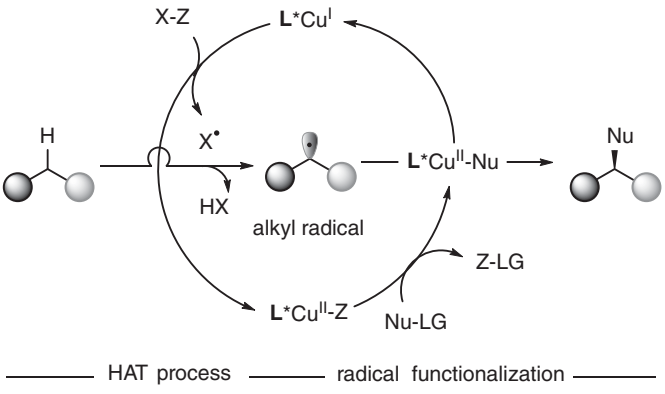


**Scheme 5.1** Copper-catalyzed radical relay strategy for benzylic C—H bonds.

an internal radical. More importantly, the asymmetric version of radical C—H functionalization could be achieved by introducing appropriate chiral ligands or chiral anions.

In this chapter, we summarize the advancements in copper-catalyzed asymmetric functionalization of C(sp³)—H bonds via a radical relay process. This chapter is classified based on the bond-formation types of carbon radicals, including cyanation, arylation, alkynylation, trifluoromethylation, and amination.

## 5.2 Asymmetric Cyanation of C(sp³)—H Bonds

In 2016, Liu, Stahl, and coworkers established an innovative approach to achieve an enantioselective cyanation of benzylic C—H bonds via a copper-catalyzed radical relay (Scheme 5.2) [1]. This transformation converted benzylic C—H bonds into chiral nitriles using C—H substrates as limiting reagents. The reaction featured mild conditions, broad functional group tolerance, and exceptional regioselectivity (**2a—2d**). A variety of 1-alkyl-substituted (hetero)arenes, including the precursor to a CCR1 receptor antagonist, could be converted into chiral nitriles (**2e**) in good yields and enantioselectivity.

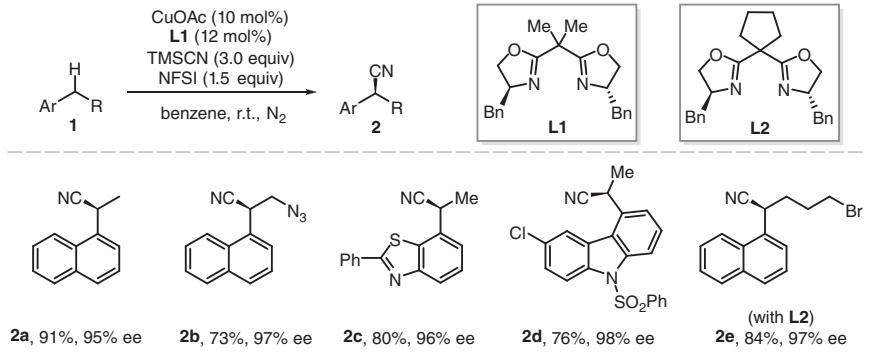


**Scheme 5.2** Copper-catalyzed asymmetric cyanation of benzylic C—H bonds.

The site selectivity of HAT favors the benzylic position adjacent to the naphthalene with the substrates bearing two benzylic positions (Scheme 5.3). When changing the *para* substituents from electron-donating to electron-deficient groups, the site selectivity increases from 12 : 1 to 29 : 1 (**2f—2i**). The reaction of enantiomerically pure homobenzylic acetate (*R*)-**1j** with each of the enantiomers of ligand **L2** led to products with excellent diastereoselectivity, which reflected high levels of catalyst rather than substrate-controlled stereoselectivity.

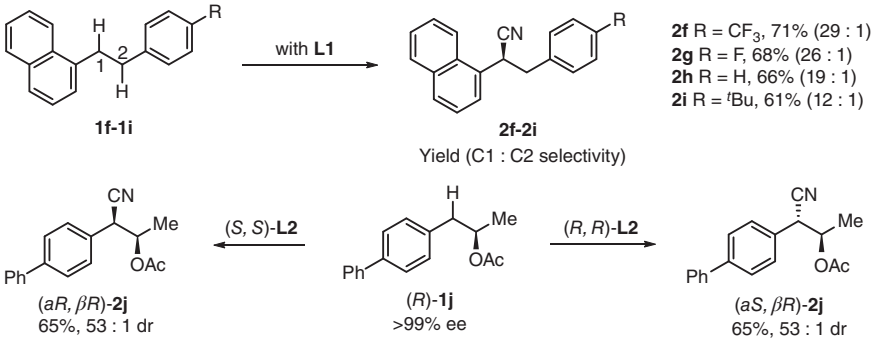


**Scheme 5.3** Selectivity in asymmetric cyanation of benzylic C—H bonds.

A preliminary mechanism study was performed by density functional theory (DFT) calculations (Scheme 5.4). A benzylic radical reacts with (**L1**)$Cu^{II}(CN)_2$ species to afford the benzyl—$Cu^{III}$ species with a low barrier. In contrast, the subsequent $sp^3$ C—CN reductive elimination of $Cu^{III}$ species generates the benzylic nitrile products with a higher barrier. This calculation suggested that the formation of the

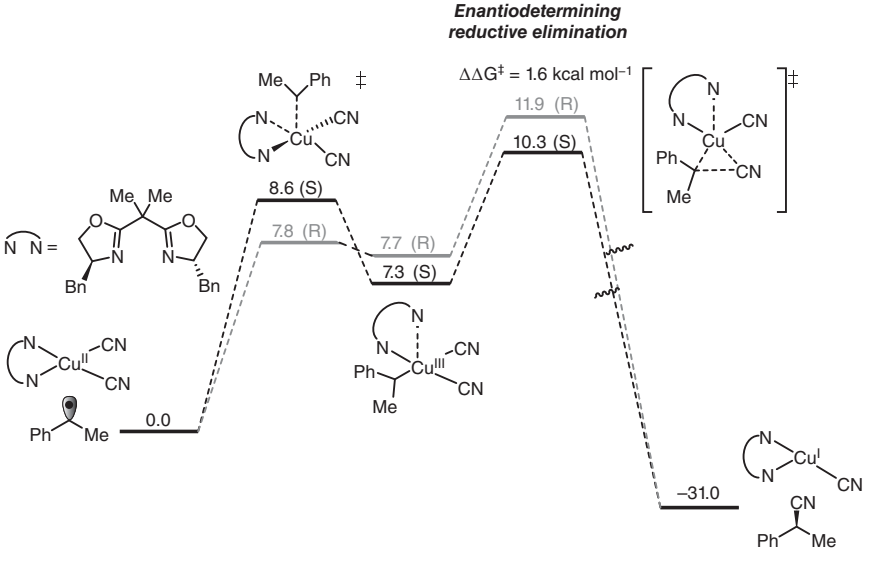


**Scheme 5.4** DFT calculation of asymmetric cyanation of benzylic radical.

alkyl–$Cu^{III}$ species is reversible, with the reductive elimination step being pivotal for controlling enantioselectivity. This seminal work represents one of the most efficient methods for synthesizing chiral nitriles through C—H functionalization.

In the above radical relay catalysis, the HAT process and the radical trap are generated simultaneously in the same redox event. However, the rate constant of HAT of alkylarenes is electronically sensitive and highly substrate-dependent, typically with a reactivity sequence of electron-rich (E-rich) > electron-neutral (E-neutral) > electron-poor (E-poor). Meanwhile, not only acting as a HAT acceptor, L*Cu—[N·] could potentially undergo the oxidative cross–coupling with the nucleophiles or react with low-valent Cu(I), resulting in the oxidative homocoupling of nucleophiles and catalyst deactivation. Thus, limited substrate scope was observed in radical relay catalysis, with E-neutral and E-poor alkylarenes showing poor reactivity. Recent reports indicated that the copper-catalyzed radical relay not only integrates well with photoredox chemistry [2] but has also been successfully adapted to electrochemistry by the Lin group [3]. This provides an opportunity to achieve green asymmetric transformations by circumventing the need for stoichiometric amounts of oxidants/reductants. Thus, Liu and coworkers established a new catalytic system that could independently regulate the HAT step and $Cu^{II}/Cu^{I}$ speciation, in which a decoupled radical relay was proposed for the highly efficient asymmetric C($sp^3$)—H cyanation (Scheme 5.5) [4]. The HAT step for benzylic radical formation was

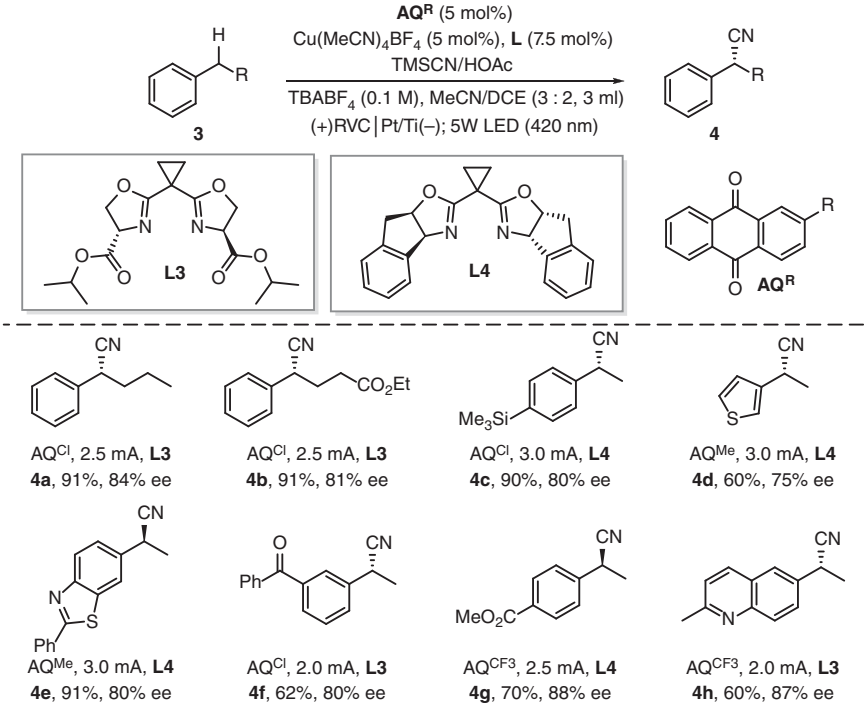


**Scheme 5.5** Electrophoto- and copper-catalyzed asymmetric cyanation of benzylic C–H bonds.

regulated by tuning the electronic property of the anthraquinone–type photocatalyst, and the speciation of $Cu^{II}/Cu^{I}$ to effectively capture the transient radical intermediate was modulated by the applied current, respectively. This method significantly expanded the substrate scope from E-poor to highly E-rich alkylarenes and exhibited remarkable functional group tolerance. For example, E-neutral and E-rich substrates could give **4a**–**4c** in excellent yields with good enantioselectivities, surpassing the less than 40% yield obtained under previous conditions. Substrates with highly E-rich and E-poor arenes and heteroarenes (**4d**–**4h**) could also yield acceptable results. Xu developed the same reaction concurrently [5].

With further investigation on the regioselective C—H cyanation, Liu, Lin, and coworkers found that the site selectivity of HAT could be controlled by a tunable Cu(II)–bound N-centered radical (NCR) [6]. Thus, the regio-, stereo-, and enantioselective allylic C—H cyanation was realized via the copper-catalyzed

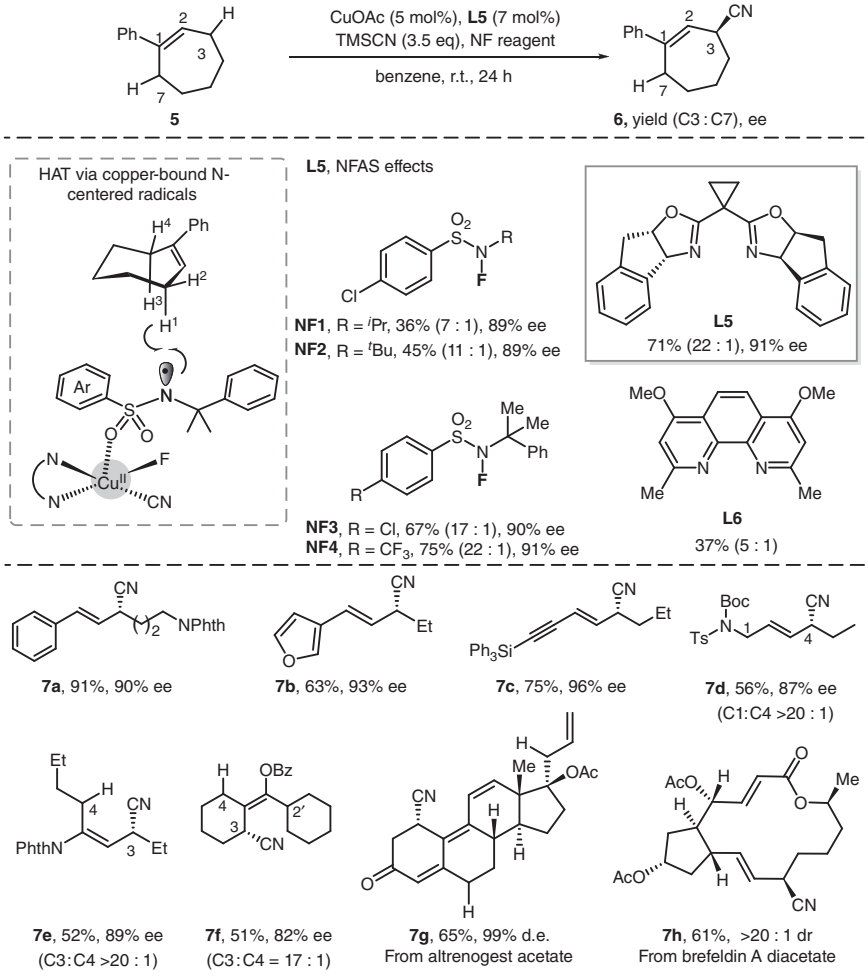


**Scheme 5.6** Copper-catalyzed asymmetric cyanation of allylic C—H bonds.

radical relay (Scheme 5.6). Preliminary screening indicated that the site-selective HAT of the substrate **5**, bearing two sets of allylic C—H bonds, was affected by *N*-fluoroalkylsulfonamide (NFAS) and ligands. Modification of NFAS exhibited a great effect on the site selectivity and efficiency of this reaction. For example, a bulkier alkyl group on the nitrogen atom led to both better selectivity and yield (from **NF1** at 36% yield, C3 : C7 = 7 : 1 to **NF3** at 67% yield, C3 : C7 = 17 : 1). The introduction of an electron-deficient aryl group could further improve the site selectivity (**NF4**, C3 : C7 = 22 : 1). Similar enantiomeric excess values (89–91%) were obtained with different NCR precursors **NF1**–**NF4**, indicating that NCR precursors are not involved in the enantioselective radical trapping process. Notably, changing the ligand from **L5** to **L6** resulted in a remarkable drop in regioselectivity from 22 : 1 to 5 : 1. These results suggested that the HAT process is not solely controlled by a free NCR. A Cu(II)–bound NCR is proposed for the high regioselectivity, which is supported by experiments and computational studies.

This transformation exhibited good functional group compatibility, giving rise to products **7a**–**7c** in excellent yields and enantioselectivity. Moreover, excellent site selectivity was demonstrated in the presence of multiple allylic C—H bonds (**7d**–**7f**), and the late-stage functionalization of complex alkene-containing molecules, including drug derivatives (**7g**–**7h**), was also showcased. This strategy offers an alternative solution to site-specific and enantioselective C—H oxidation reactions, including those with allylic and other types of C—H bonds.

The enantioselective copper-catalyzed cyanation of propargylic C—H bonds via radical relay was later established by Liu and coworkers, providing an efficient and straightforward tool for the construction of structurally diverse chiral allenyl nitriles in good yields with excellent enantioselectivities (Scheme 5.7) [7]. A novel $Box^{OH}$ ligand **L7**, bearing two gem-substituted hydroxymethyl groups, proved the best ligand. The TMS-protected ligand **L8** exhibited a result similar to that of **L7**,

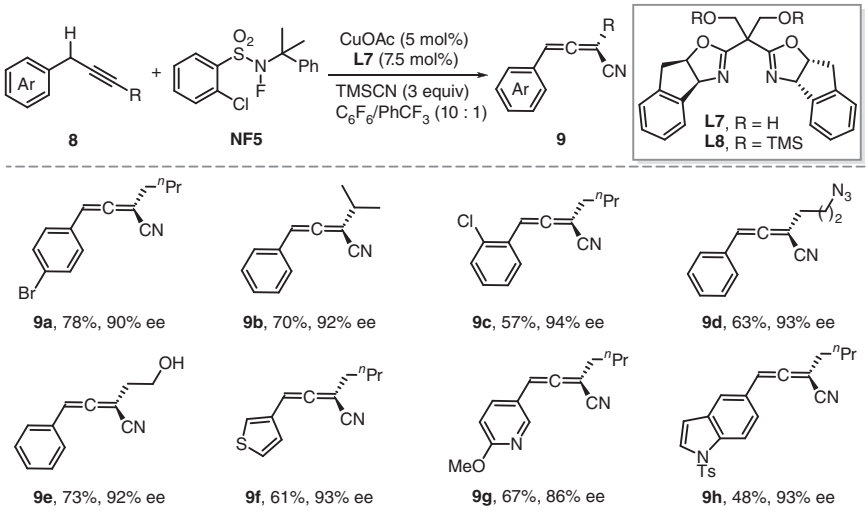


**Scheme 5.7** Copper-catalyzed asymmetric cyanation of propargylic C–H bonds.

indicating the protection of the hydroxyl groups in **L7** with TMSCN occurred in the reaction. This reaction features good functional group tolerance. The substrate with an *ortho*-chlorine yielded products **9c** with a higher ee but a slightly lower yield. Substrates with azide (**9d**), a free hydroxyl group (**9e**), and heteroarenes such as thiophene (**9f**), pyridine (**9g**), and indole (**9h**) were all suitable for this reaction. In addition, the chiral allene products can be readily converted to other chiral compounds via axis-to-center chirality transfer.

A key Cu(II)—bound NCR species reported in our previous allylic C—H bond cyanation was also observed in the site-selective propargylic HAT process (Scheme 5.6). Moreover, DFT calculations were conducted to measure the propargylic C—H bond dissociation energy (BDE) (Scheme 5.8). In the substrate **8i**, the BDE of the C—H bond at the α-C position (78.9 kcal mol$^{-1}$) is lower than that of the C—H bond at the $\delta$-C position (88.4 kcal mol$^{-1}$), thus allowing for the exclusive hydrogen atom abstraction of the α-C—H bond to give **9i** as a single product. In addition, compared to substrate, alkyne **8j** bearing a relatively inert propargylic C—H bond (BDE = 85.7 kcal mol$^{-1}$) exhibited poor reactivity, where only 35% conversion was observed, which also consisted of the rate-determining HAT step. Thus, an

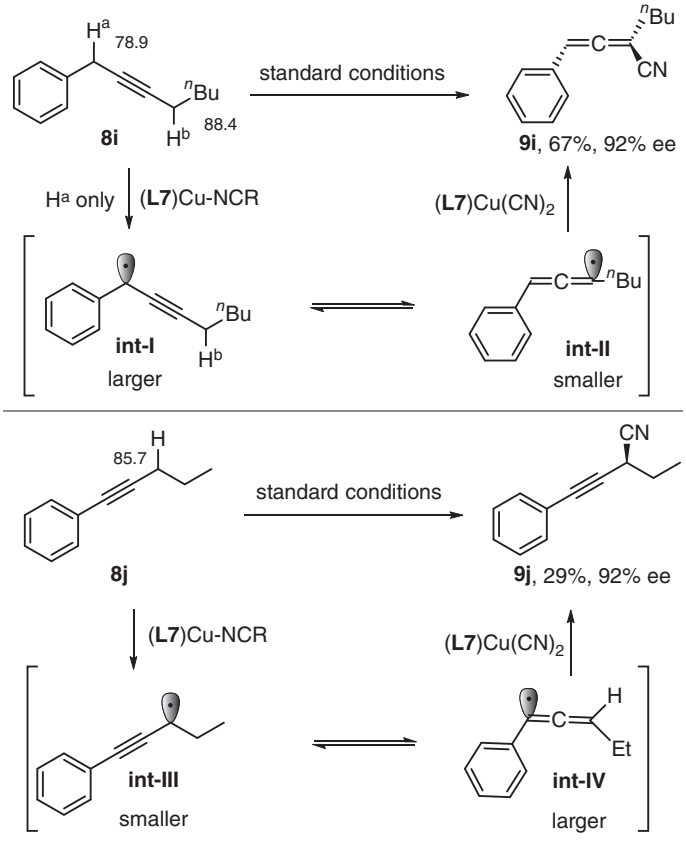


**Scheme 5.8** Regioselectivity in asymmetric cyanation of propargylic C—H bonds.

intramolecular 1,5-HAT process was applied for the efficient generation of a propargylic radical, and finally achieving the enantioselective cyanation of propargylic C—H bonds by combining photoredox catalysis with the copper-catalyzed radical relay [8].

Other than applying a copper-bound NCR, the regioselectivity can be governed by substrates via an intramolecular 1,5-HAT. Inspired by the classic Hofmann-Löffler-Freytag reaction, known for its ability to selectively produce $\delta$-C-centered radicals from N—X substrates [9], Nagib and coworkers intercepted the remote carbon radical by a chiral copper complex to achieve a copper-catalyzed enantioselective C—H cyanation (Scheme 5.9) [10]. The enantioenriched products could be further converted into valuable chiral piperidines. Notably, the ratio of copper and ligand played a crucial role in suppressing the background reaction and enhancing the reaction efficiency. More importantly, the formal synthesis of the anticancer drug (niraparib) further demonstrated the synthetic utility.

Meanwhile, several other groups have also developed similar protocols, which take advantage of 1,5-HAT from N- or O-centered radicals to achieve excellent regioselectivity (Scheme 5.10). Wang and coworkers reported an enantioselective remote C—H cyanation via an NCR generated by single-electron reduction of an N—F substrate

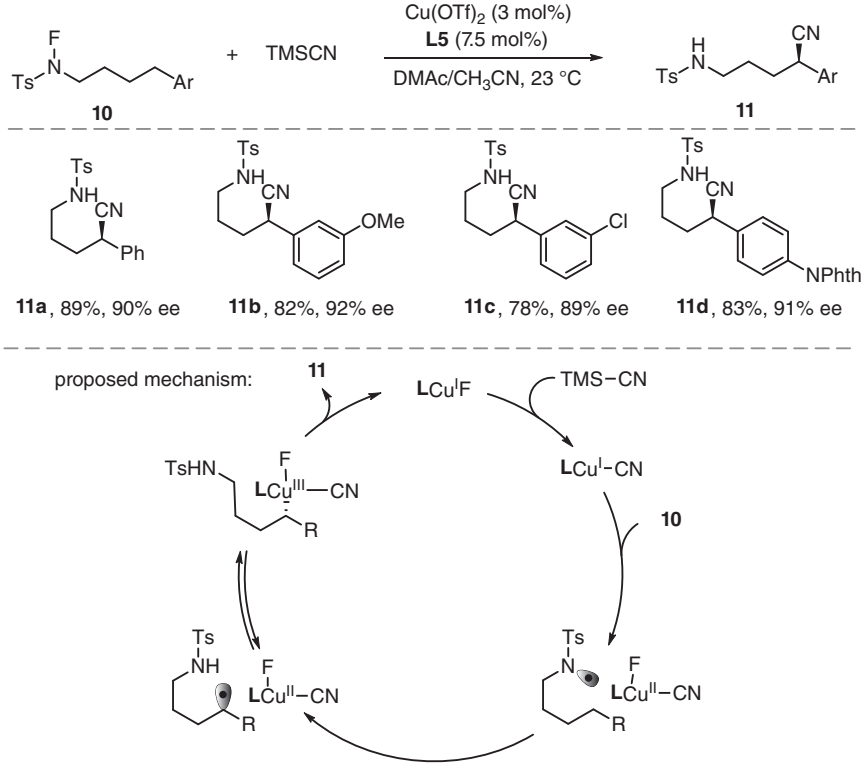


**Scheme 5.9** Copper-catalyzed asymmetric cyanation of C—H bonds via intramolecular 1,5-HAT.

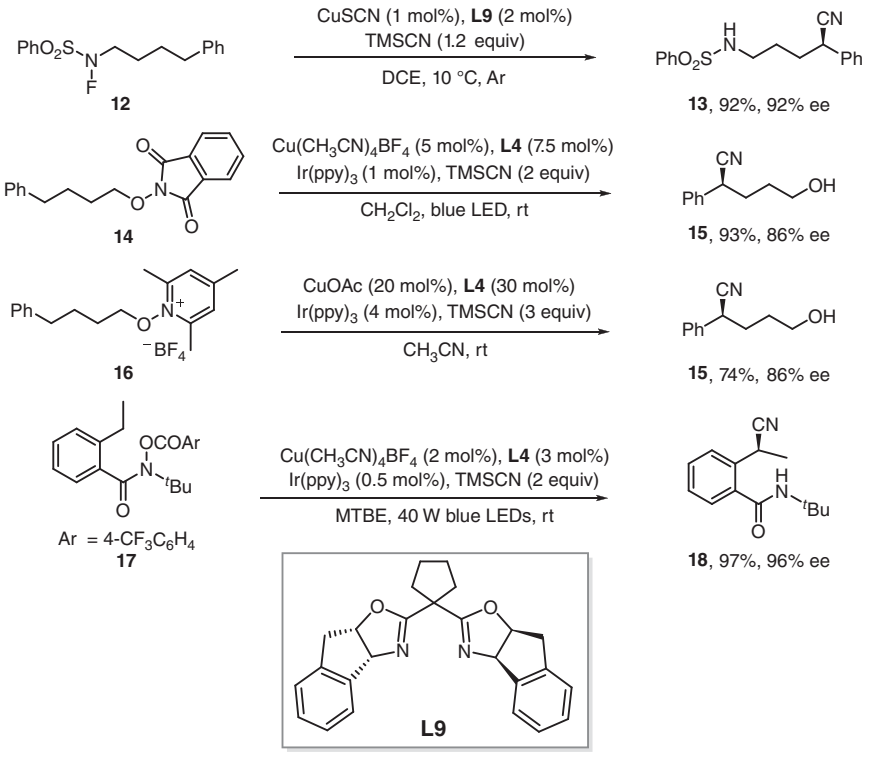


**Scheme 5.10** Asymmetric cyanation of benzylic C—H bonds via 1,5-HAT.

**12** to afford enantioenriched $\delta$-amino nitrile **13** [11]. Instead of cleaving N—F bonds, N—O bonds could be reduced to generate heteroatom radicals by merging photoredox catalysis and copper catalysis. Liu and coworkers developed an enantioselective remote C—H cyanation via an oxygen radical generated by an N—O bond with photoredox catalysis [12]. In this reaction, *N*-hydroxyphthalimide ether **14** was reduced by a photoredox catalyst to generate an oxygen-centered radical, which underwent 1,5-HAT to form a $\delta$-carbon radical. The carbon radical was trapped by a chiral copper catalyst to install the cyanide group enantioselectively, yielding $\delta$-hydroxyl nitrile **15** in excellent yield and enantioselectivity. Zhu and coworkers also achieved a similar C—H cyanation of N—alkoxypyridinium salt **16** with a chiral Box ligand to give the same $\delta$-hydroxyl nitrile **15** [13]. Yu and coworkers also applied a similar strategy and realized enantioselective remote C—H cyanation of amides **17** [14].

## 5.3 Asymmetric Arylation of C(sp³)—H Bonds

Transition metal-catalyzed cross-coupling reactions represent one of the most important methods to construct C($sp^2$)—C($sp^3$) bonds. Using C($sp^3$)—H substrates as the cross-coupling partner has drawn increasing attention due to their good atom- and step-economy. In 2017, the Liu group [15] and the Stahl group [16]

independently reported a copper-catalyzed benzylic C—H arylation. Both reactions underwent a radical relay mechanism, and the trap of the formed carbon radical by $ArCu^{II}$ species afforded the desired product. Besides using arylboronic acids as nucleophiles, the Chang group developed a copper-catalyzed C($sp^3$)—H polyfluoroarylation using polyfluoroarenes as nucleophiles and DTBP as the oxidant for the generation of an oxygen-centered radical [17]. However, the copper-catalyzed enantioselective C—H arylation via a radical relay was hard to achieve, due to the less reactivity of the Box ligand. In 2019, Liu and coworkers developed the enantioselective arylation of benzylic C—H bonds, which provided an attractive protocol for synthesizing enantiomerically enriched 1,1-diarylalkanes (Scheme 5.11) [18]. The steric hindrance of bulky chiral copper complexes is required to control enantioselectivity but undermines the efficiency of transmetalation between the $(L^*)Cu^{II}$ species and $PhB(OH)_2$. As a result, the active benzylic radicals could not be captured efficiently by a low concentration of $(L^*)Cu^{II}Ar$ species. To solve this dilemma, a directing group was introduced onto the chiral ligand (**L10**) to accelerate the transmetalation step, therefore leading to a higher concentration of $(L^*)Cu^{II}Ar$ and inhibiting the side reaction. This reaction demonstrated impressive chemo- and enantioselectivity. However, the C—H substrate scope was limited to alkyl naphthalenes (**21a**–**21h**), and slightly lower yields were obtained with alkyl benzenes (**21d**).

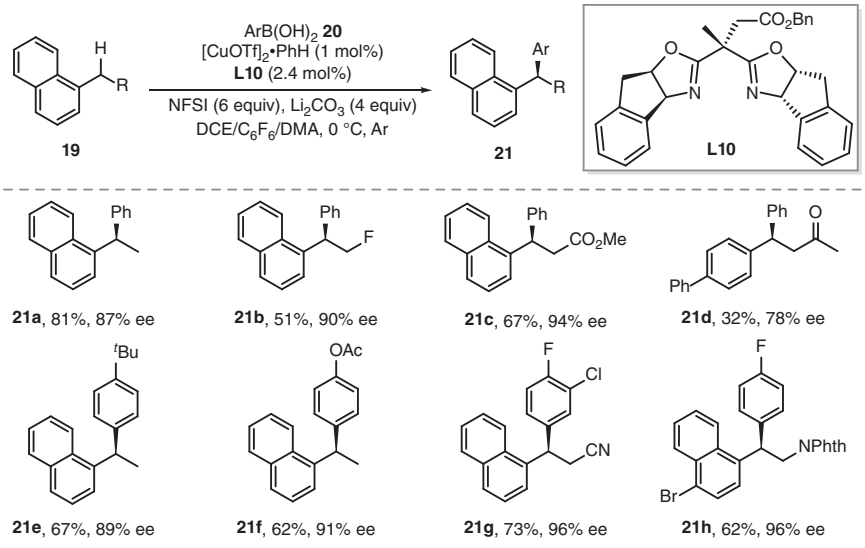


**Scheme 5.11** Copper-catalyzed asymmetric arylation of benzylic C–H bonds.

The copper-catalyzed remote C—H arylation via an intramolecular HAT was later independently developed by Zhu's group [19] and Nagib's group [20]. However, only racemic reactions of amides were tested with 2,2′-bipyridine and 1,10-phenanthroline as the ligands in Zhu's strategies. In contrast, Nagib's strategy employed a Box ligand **L11**, providing the chiral diaryl amide **23** in 59% yield with

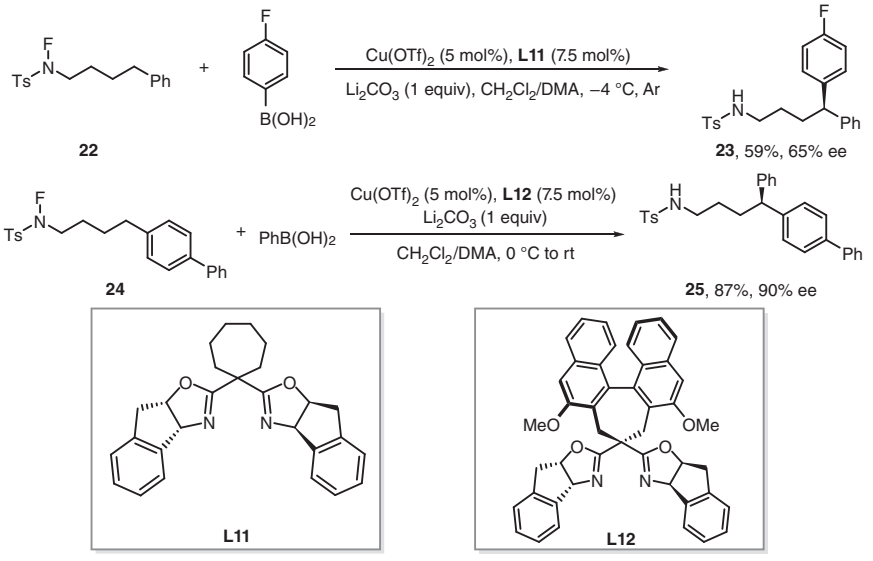


**Scheme 5.12** Copper-catalyzed asymmetric remote arylation of C—H bonds via 1,5-HAT.

65% ee (Scheme 5.12). Later, Maruoka's group developed a chiral BN-Box hybrid ligand **L12**, which could further enhance the enantioselectivity of $\delta$-C—H arylation of *N*-fluorotosylamide to over 90% ee [21]. Nevertheless, general methods to achieve enantioselective C—H arylation with broad substrate scopes via a copper-catalyzed radical relay still need to be developed.

## 5.4 Asymmetric Alkynylation of C(sp³)—H Bonds

Chiral alkynes are widely used in the synthesis of biologically active molecules and functional molecules due to their electronic properties and diversified transformations. The copper-catalyzed asymmetric C—H alkynylation via a radical relay offered an efficient method to install the alkynyl group selectively from inert C—H bonds.

Based on their previous work on asymmetric trifluoromethylalkynylation of alkenes [22], Liu and coworkers established the first enantioselective benzylic C—H alkynylation of simple alkyl arenes via a copper-catalyzed radical relay (Scheme 5.13) [23]. The reaction efficiency could be promoted using $Na_2CO_3$ as the base and 1,2,4,5-tetrafluorobenzene as the solvent. The ligand screening revealed that the steric hindrance of Box ligands had a significant effect on the enantioselectivity. Finally, ligand **L13** bearing a cyclopentyl group was the best choice to give the chiral benzyl alkynes with up to 98% ee. The reaction also featured a broad substrate scope, and many alkyl arenes and heteroarenes were compatible with the reaction conditions (**28a**–**28h**). Impressively, alkylbenzenes, which exhibited poor reactivity and low enantioselectivity in the asymmetric benzylic C—H arylation,

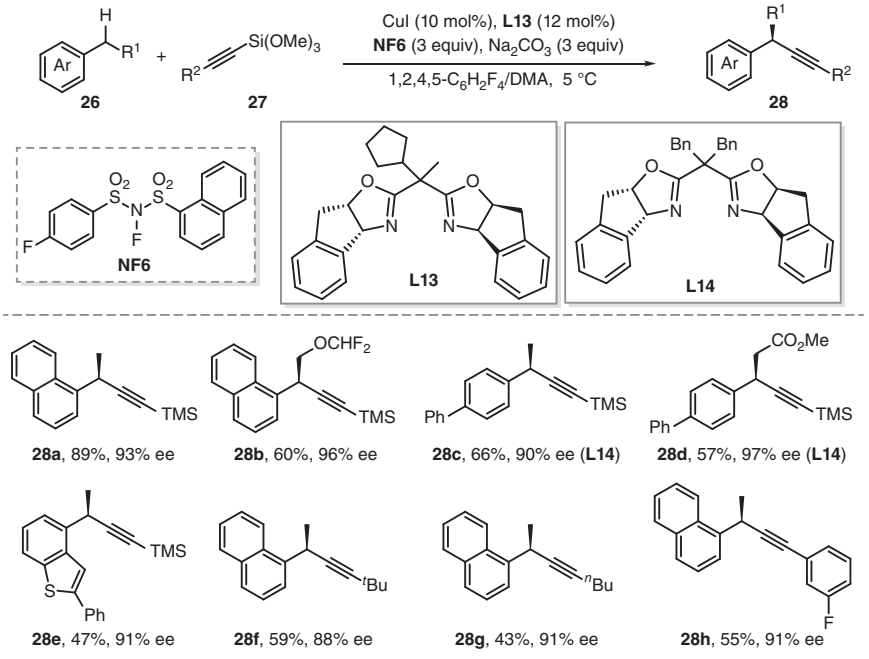


**Scheme 5.13** Copper-catalyzed asymmetric alkynylation of benzylic C–H bonds.

could be employed as substrates for the asymmetric alkynylation to afford the corresponding products with ligand **L14** in moderate to good yields with excellent enantioselectivities (**28c**, **28d**).

It is noteworthy that substrate **26i**, bearing two sets of different benzylic C—H bonds, preferentially yielded the enantioenriched alkynylation product **28i** in 49% yield with 94% ee, which was converted into terminal alkyne **29** in 92% yield without loss of optical purity upon exposure to ammonium fluoride. This reaction provides an efficient approach for the synthesis of a potent GPR40 agonist AMG 837 (Scheme 5.14). Interestingly, the N—F reagents also exhibited a remarkable effect on the yields and enantioselectivities. This phenomenon indicated that the generated bisarenesulfonimide should be involved in the enantioselective capture of benzylic radicals by chiral L*$Cu^{II}$–alkynyl species, presumably due to coordination of the bisarenesulfonimide to a $Cu^{II}$ center. Control experiments and DFT calculations were performed and supported that the C—C bond formation stemmed from a $Cu^{III}$ intermediate rather than an outer-sphere radical addition–elimination pathway. Later, the Kramer group demonstrated that using alkynylboronic esters as nucleophilic coupling partners instead of alkynylsilanes could achieve the racemic benzylic C—H alkynylation with 4,4′-di-*tert*-butyl-2,2′-bipyridine as the ligand [24].

The variants of the Hofmann-Löffler-Freytag reaction in remote C—H alkynylation were investigated by several groups [25]. In 2020, Wang and coworkers realized a copper-catalyzed enantioselective remote C—H alkynylation of sulfonamides (**12**) to give the alkynyl amide **30** in excellent yield and enantioselectivity (Scheme 5.15) [26]. The chiral Box-copper complex was used to reduce the N—F bond to generate

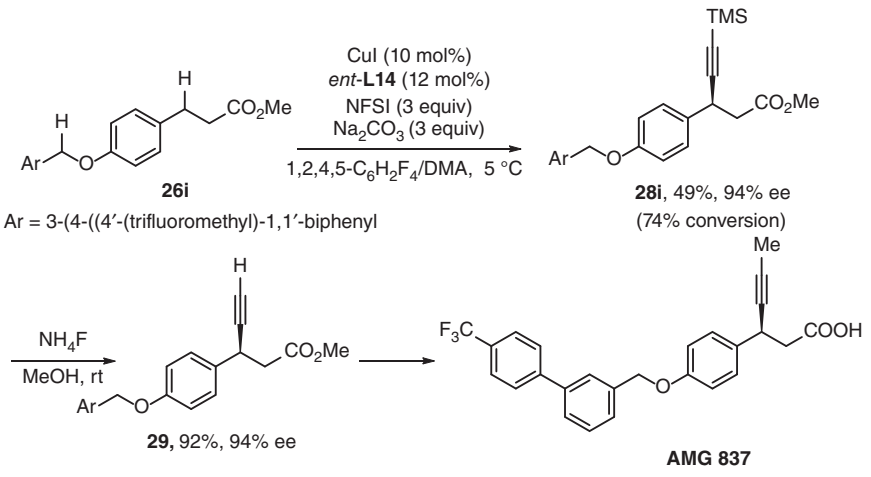


**Scheme 5.14** Selectivity in copper-catalyzed asymmetric alkynylation of benzylic C—H bonds.

an NCR and capture the carbon radical formed via 1,5-HAT. Similar to Liu's reaction, alkynylsilanes were the only successful alkynylating reagents in this reaction.

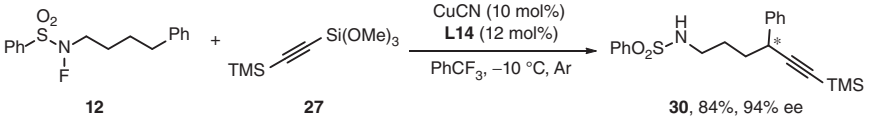


**Scheme 5.15** Copper-catalyzed asymmetric remote alkynylation of C—H bonds via 1,5-HAT.

Recently, Liu and coworkers reported a copper/chiral cinchona alkaloid–based N,N,P-ligand catalyst for the asymmetric oxidative cross-coupling of unactivated C(sp³)—H bonds with terminal alkynes (Scheme 5.16) [27]. The use of *N*-fluoroamides **31** as the mild oxidants is essential to generate the corresponding amidyl radicals while avoiding the Glaser homocoupling. Alkynes, including phenyl rings bearing electron-donating or -withdrawing groups at different positions and alkyl groups, reacted smoothly to afford **33a–33h** in good yields with excellent enantioselectivity. Heterobenzylic and propargylic C—H bonds were all applicable. Mechanistic studies indicated that copper phenylacetylide with chiral cinchona alkaloid-based N,N,P-ligand **L15** might be the initial complex to start the reaction. After intramolecular 1,5(6)-HAT of the amidyl radical, the C(sp³)—C(sp) bond formed via reductive elimination of a $Cu^{III}$ intermediate with **L15**, giving the enantioenriched products **33**.

The intermolecular version was later reported with high to excellent enantioselectivity (Scheme 5.17) [28]. Critical to the success was the rational design of chiral N,N,P(O)-ligands bearing chiral oxazoline and pentavalent phosphine oxide building blocks in place of the easily oxidized tertiary alkyl amine and trivalent aryl phosphine. The ligand could not only tolerate the strong oxidative conditions requisite

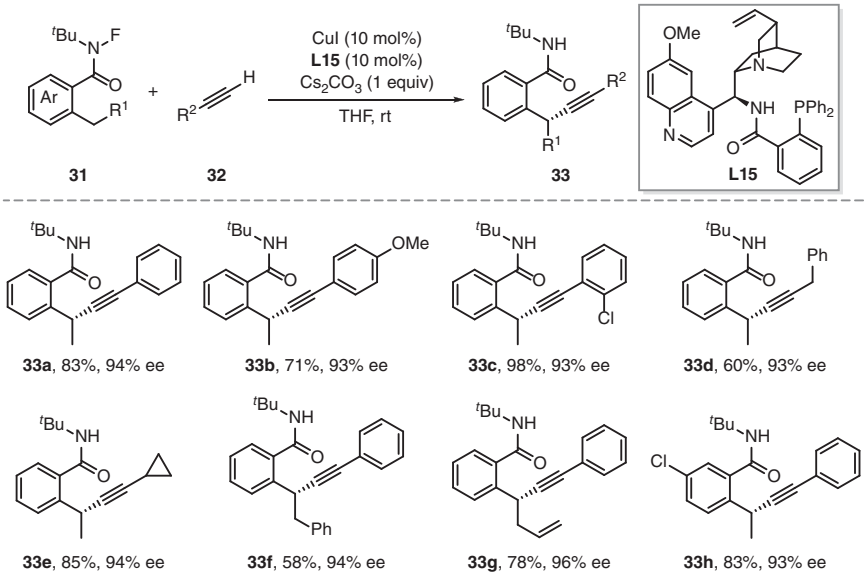


**Scheme 5.16** Copper-catalyzed intramolecular asymmetric oxidative cross-coupling of C—H bonds with alkynes.

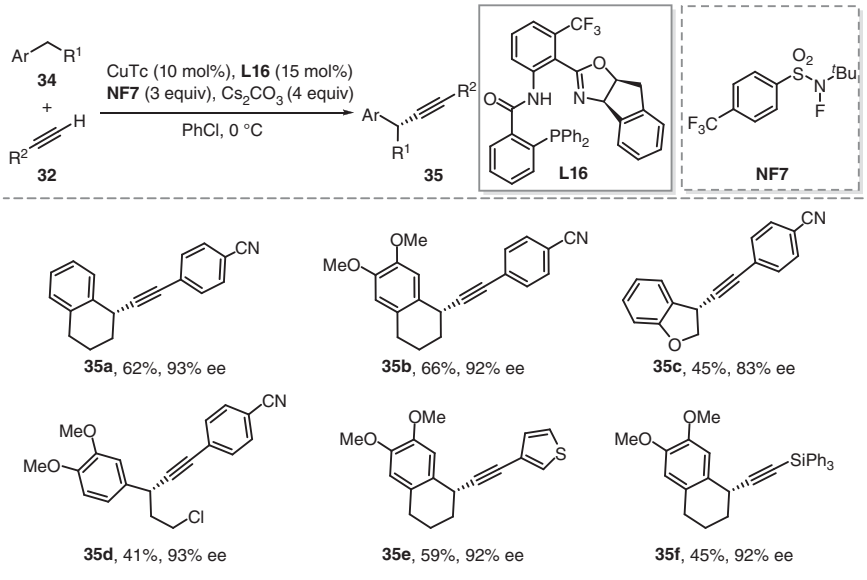


**Scheme 5.17** Copper-catalyzed intermolecular asymmetric oxidative cross-coupling of C—H bonds with alkynes.

for intermolecular hydrogen atom abstraction (HAA) processes but also induce the challenging enantiocontrol. Both cyclic and acyclic benzylic C—H bonds underwent the alkynylation reaction successfully to afford the corresponding products **3a**–**3e** in up to 84% yield and 94% ee. For the alkynes, many (hetero)aryl, alkyl, and silylated alkynes were well tolerated to give **3f** and **3g** with up to 92% ee. Generally, the alkyl alkynes gave rise to the coupling product in less efficiency and lower ee. The enantioselective alkynylation of acyclic allylic C—H bonds was also achieved after further modification of the chiral ligands.

## 5.5 Asymmetric Fluoroalkylation of C($sp^3$)—H Bonds

Fluorinated groups such as $CF_3$ attract increasing attention due to their important roles in pharmaceuticals and agrochemicals. Therefore, tremendous efforts have been devoted to developing novel methodologies to introduce fluorinated groups via C—H functionalization, especially in an enantioselective pathway. Direct C($sp^3$)—H trifluoromethylation via a radical relay was underdeveloped due to the lack of methods for trifluoromethylation of alkyl radicals. Several groups demonstrated the copper-mediated trifluoromethylation of alkyl radicals via $CF_3$ transfer from $Cu^{II}$—$CF_3$ intermediates [29]. For example, Li and coworkers successfully developed a general copper-catalyzed protocol for benzylic C($sp^3$)—H trifluoromethylation [30]. Meanwhile, MacMillan and coworkers developed an elegant procedure for general C($sp^3$)—H trifluoromethylation using Togni reagent II via the merger of decatungstate photocatalysis with copper catalysis [31]. Despite the great progress in C—H trifluoromethylation, the asymmetric version of C—H trifluoromethylation via a radical relay has not been realized yet.

Recently, Liu and coworkers accomplished an enantioselective trifluoromethylation of alkyl radicals derived from the ring-opening process of cyclopropanols [32]. Inspired by this result, they developed the first enantioselective radical trifluoromethylation of benzylic C—H bonds by a cooperative photoredox and copper catalysis system (Scheme 5.18) [33]. A combination of anthraquinone photosensitizers $AQ^{Cl}$ and NQ was effective for the reaction, giving the desired products **37a**–**37h** with up to 81% yield. This reaction features a broad substrate scope and excellent functional group compatibility, thus providing straightforward access to structurally diverse benzylic trifluoromethylation products in good yields with excellent enantioselectivities. For alkyl arenes containing two or more sets of C—H bonds, the reaction occurred exclusively at the less hindered benzylic C—H bond (**37g** and **37h**).

Merging cooperative photoredox catalysis with copper catalysis is essential for the reaction (Scheme 5.19). In the photocatalytic cycle, the photosensitizer AQ is excited by blue light to afford the active diradical AQ*. This species abstracts the hydrogen atom at the benzylic position to generate the benzylic radical and an active AQH radical. Meanwhile, in the copper catalytic cycle, the $L^*Cu^{I}$ catalyst is initially oxidized by the Togni-II reagent to generate the $L^*Cu^{III}$—$CF_3$ species. This species acts as an efficient oxidant to convert AQH radical to AQ, thereby efficiently

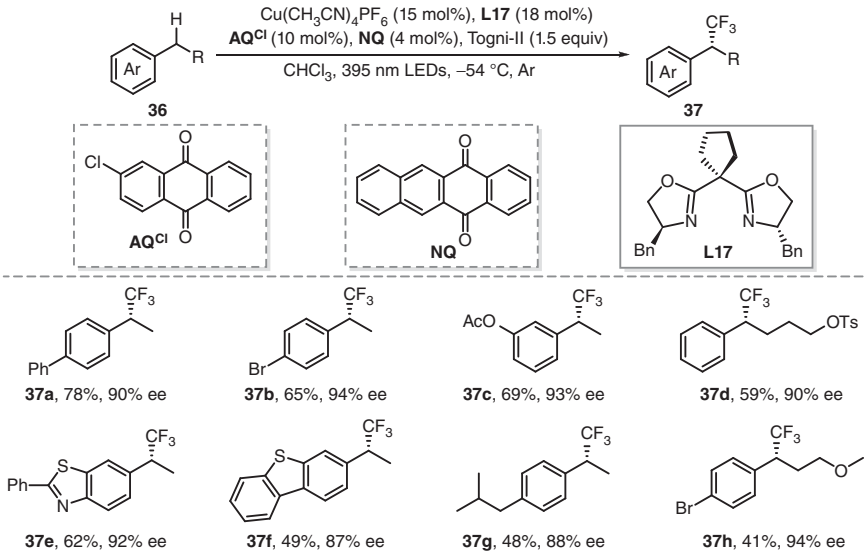


**Scheme 5.18** Copper-catalyzed asymmetric trifluoromethylation of C–H bonds.

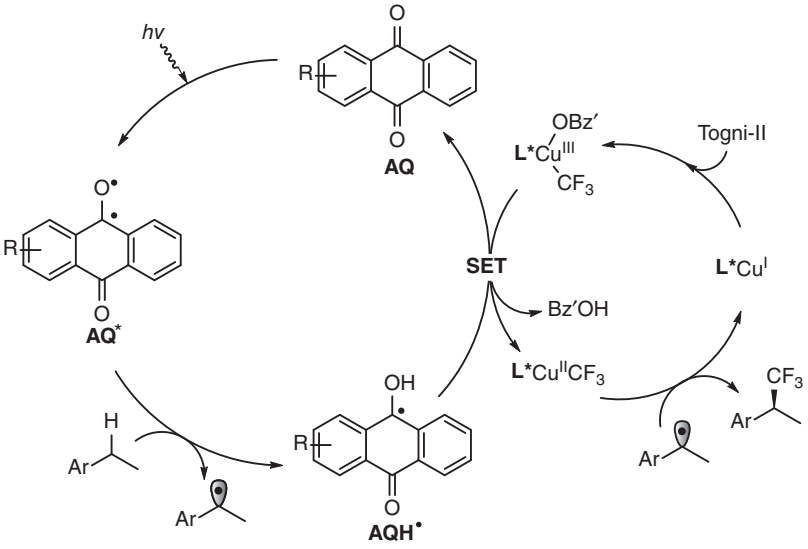


**Scheme 5.19** Mechanism of copper-catalyzed asymmetric trifluoromethylation of C–H bonds.

completing the photocatalytic cycle. Subsequently, the simultaneously released $L^*Cu^{II}—CF_3$ species can trap the benzylic radical in an enantioselective manner to yield the desired product. The bond formation process possibly involves a reductive elimination of the $Cu^{III}$ species. While photoredox catalysis is used to generate benzylic radicals from alkyl arenes through a HAT process, copper catalysis is used for the enantioselective trifluoromethylation of the benzylic radicals.

## 5.6 Asymmetric Amination of C(sp³)—H Bonds

Direct oxidation of ubiquitous C(sp³)—H bonds to install carbon–heteroatom bonds is of great significance to avoid tedious functional group manipulations that are required for the synthesis of target functional molecules. The classic Kharasch-Sosnovsky reaction with copper catalysis has been expanded to incorporate heteroatom units via a radical relay. Inspired by the Kharasch-Sosnovsky reaction, Katsuki and Clark made initial attempts to study asymmetric oxidative C—H amination with peroxycarbamate as both oxidant and nitrogen source in the presence of Cu/chiral bis(oxazoline) catalyst [34]. However, low yield and enantioselectivity were observed for cyclic alkenes. Recently, the efficiency of copper-catalyzed C(sp³)—H amination has been well solved with peroxides and NFSI as the oxidants [35]. However, the development of catalytic asymmetric methods has proven a formidable challenge.

In 2020, Nagib and coworkers disclosed a regio- and enantioselective C—H amination of alcohols by merging radical chaperone, energy transfer, and asymmetric copper catalysis (Scheme 5.20) [36]. In this transformation, oxime imidates **39** generated from alcohols **38** were converted to the imidate radicals that undergo an intramolecular 1,5-HAT process. Notably, the generated carbon radical was imidated enantioselectively with a chiral copper catalyst. The chiral oxazolines **40** can be hydrolyzed to chiral β-amino alcohols **41**. A variety of alcohols containing benzylic, allylic, and propargylic C—H bonds (**40a–40f**) were suitable for this strategy. Notably, aliphatic alcohols bearing large β-methylene units could also give **40g** and **40h** with good enantioselectivities. These results suggest that the role of the aryl group is merely to act as a sterically repulsive, catalyst-recognition element.

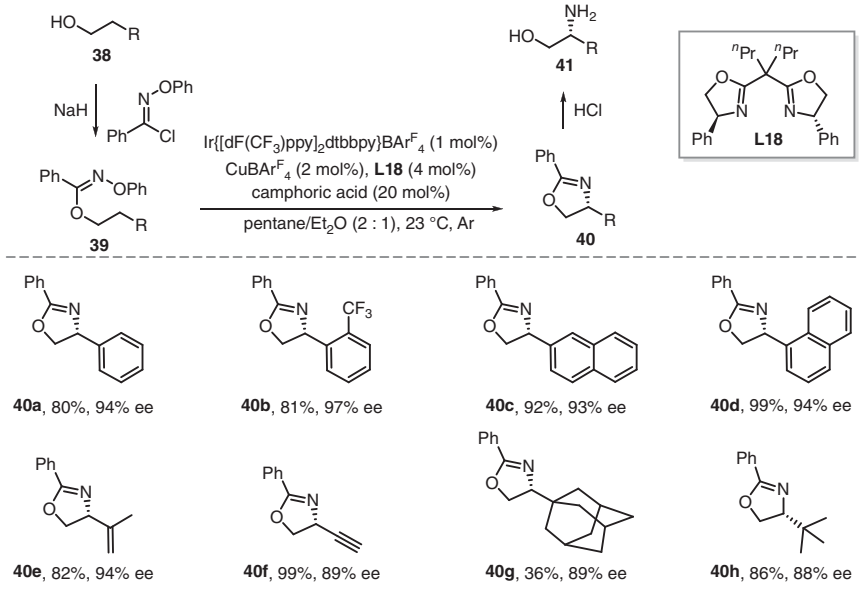


**Scheme 5.20** Copper-catalyzed asymmetric intramolecular amination of C—H bonds.

The asymmetric tertiary C(sp³)—H bond functionalization is extremely rare due to the steric sensitivity in the construction of quaternary stereocenters. In 2020, Liu and coworkers developed a dual Cu/chiral phosphoric acid (CPA) catalysis for the radical enantioconvergent tertiary C(sp³)—H amination (Scheme 5.21) [37]. This transformation converted readily available racemic ketones **42** into enantioenriched quaternary stereocenters. The racemic hydrazones **43** as E/Z mixtures were readily available in one step from racemic ketones **42** and N-arylsulfonohydrazides, in which 4-methoxy-phenylsulfonohydrazide (4-$MeOC_6H_4NHNH_2$) showed the best reaction efficiency. Various functional groups were compatible with the mild reaction conditions, providing the desired products **45a**–**45g** in moderate to good yield with good to excellent enantioselectivity. The aliphatic ketones **42c** also underwent the reaction to deliver **45c** with promising enantioselectivity. Mechanistic studies indicated that $Cu^I$ reacts with CPA-activated peroxide via SET to afford a highly reactive *tert*-butoxy radical accompanied by the formation of the crucial chiral $Cu^{II}$ phosphate complex. After intermolecular hydrogen abstraction of the weak N—H bond in hydrazine, subsequent irreversible intramolecular 1,5-HAT gives rise to prochiral tertiary alkyl radical, followed by asymmetric radical functionalization to afford the desired products.

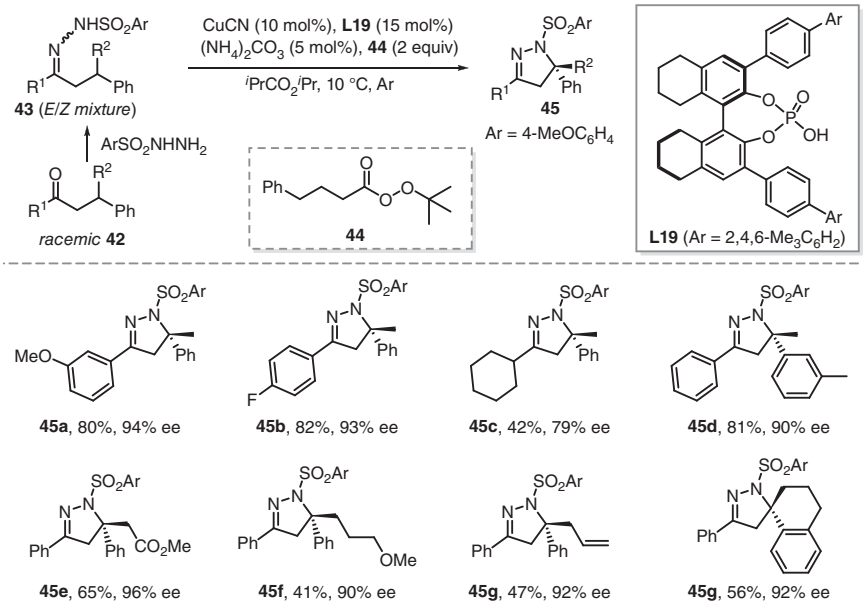


**Scheme 5.21** Copper-catalyzed asymmetric intramolecular amination of tertiary C—H bonds.

They later applied the redox $Cu^I$/CPA catalytic system to the intramolecular enantioselective oxidative C—H amination of acyclic allylic and benzylic substrates (Scheme 5.22) [38]. The alkyl amines in substrates **46** were protected with a urea group, which was supposed to deactivate the C—H bond adjacent to the amine toward HAT. 4-methoxy-NHPI (N-hydroxyphthalimide) was used

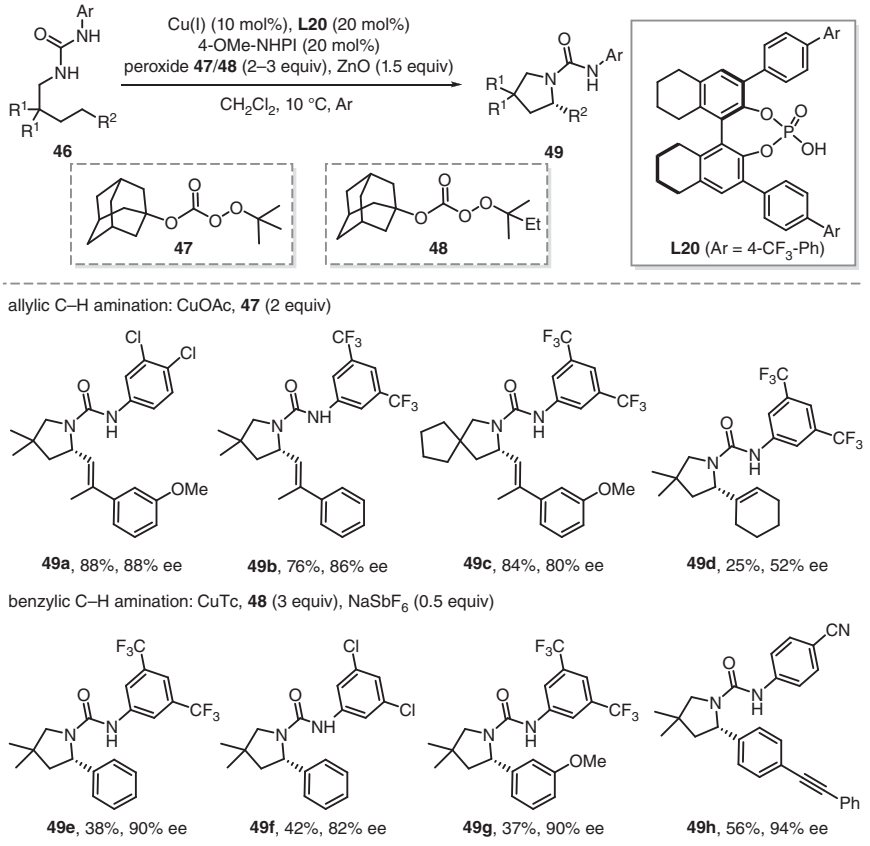


**Scheme 5.22** Copper-catalyzed asymmetric intramolecular amination of C–H bonds.

as a stable and chemoselective HAT mediator precursor. Allylic substrates with electron-withdrawing groups ($CF_3$, $NO_2$, etc.) on the aromatic rings of urea at the different positions and various aryl substituents (OMe, Me) at the alkenyl group are tolerated and afforded the α-alkenyl pyrrolidines **49a–49d**. However, the reaction efficiency of benzylic C—H amination is lower than that observed in allylic C—H amination. In some cases, the C—H oxidation side-product and the cross-coupling product of the benzylic radical and PINO were obtained. Benzylic substrates with different ureas bearing electron-withdrawing groups underwent C—H amination smoothly to yield the products **49e–49h** in 38–56% yields with up to 94% ee.

Despite these advances, the enantioselective intermolecular benzylic C—H amination for the installation of primary amines and amides remains a big challenge. In 2023, Zhou and coworkers disclosed a copper-catalyzed enantioselective intermolecular C—H amination (Scheme 5.23) [39]. The reaction employed di-*tert*-butylperoxide (DTBP) as the oxidant to generate the *tert*-butoxyl radical. A cationic copper with large and weak coordinating counterions is vital for high yield and enantioselectivity, and tetrakis[3,5-bis(trifluoromethyl)phenyl]borate anion ($BAr_F$) is the best choice. Alkylarenes **50** with one or more electron-withdrawing

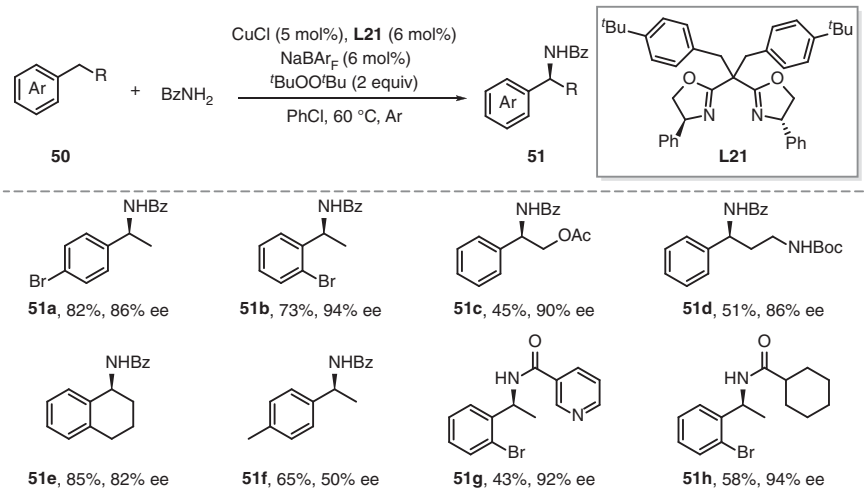


**Scheme 5.23** Copper-catalyzed asymmetric intermolecular amination of C–H bonds.

halogen atoms on the aryl ring were well tolerated (**51a**, **51b**). However, the presence of electron-donating groups (such as Me, OMe) dramatically decreased the enantioselectivity (**51f**). Functional groups on the alkyl chain exhibited good compatibility (**51c**, **51d**). Both aryl and aliphatic amides were suitable amide sources for the reaction.

At the same time, Lian, Kramer, and coworkers developed an enantioselective intermolecular radical amidation and amination of benzylic C—H bonds via dual copper and photocatalysis (Scheme 5.24) [40]. DTBP was irradiated with 425 nm light to generate the *tert*-butoxyl radical, facilitating the reaction to occur at a

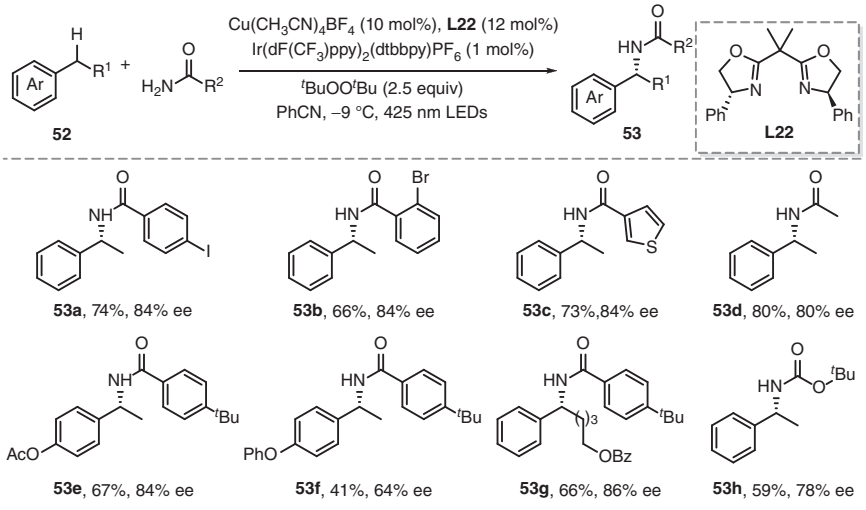


**Scheme 5.24** Copper-catalyzed asymmetric intermolecular amination of C–H bonds.

temperature of −9 °C. However, the enantioselectivity was only slightly influenced by temperature. A strongly coordinating counterion or benzoyl peroxide was detrimental to the amidation reaction. Alkylarenes bearing various substituents led to **53a**–**53h** in good yields and enantioselectivities. The method is compatible with late-stage C—H functionalization. Both aryl and alkyl amides, as well as carbamates, serve as feasible nucleophiles. Even cheap $^{15}N$ labeling ammonium chloride is applicable, offering easy access to $^{15}N$-labeled amides and amines.

## 5.7 Conclusion

Based on the copper-catalyzed radical relay strategy, a series of asymmetric C—H functionalization reactions have been developed and recognized as an important tool in organic synthesis. For the key enantioselective functionalization of carbon radicals, there are mainly three classes of chiral ligands that have been employed, including chiral Box ligands and cinchona alkaloid-based P, N-ligands, as well as chiral phosphoric acids. So far, the installed functional groups mainly focus on carbon nucleophiles, such as cyanide, aryl, alkynyl, trifluoromethyl and amine groups. In contrast, the heteroatom functional groups are only installed in the racemic version, and the enantioselective version is rare. Recently, the copper-catalyzed asymmetric amination of C—H bonds has been developed, suggesting the potential for C–heteroatom bond formation via a copper-catalyzed radical relay. More attention should be paid to the chiral ligand design to realize more C–heteroatom bond formation. As for C—H bonds, benzylic, allylic, and propargylic ones have been well studied. Photocatalysis and electrocatalysis may provide new types of HAT reagents, thereby enabling the asymmetric functionalization of inert C—H bonds. These reactions will deliver new sustainable synthetic tools for the efficient assembly of valuable chiral compounds.

## References


1 Zhang, W., Wang, F., McCann, S.D. et al. (2016). *Science* 353: 1014–1018.
2 Wang, D., Zhu, N., Chen, P. et al. (2017). *J. Am. Chem. Soc.* 139: 15632–15635.
3 Fu, N., Song, L., Liu, J. et al. (2019). *J. Am. Chem. Soc.* 141: 14480–14485.
4 Fan, W., Zhao, X., Deng, Y. et al. (2022). *J. Am. Chem. Soc.* 144: 21647–21682.
5 Cai, C.-Y., Lai, X.-L., Wang, Y. et al. (2022). *Nat. Catal.* 5: 943–951.
6 Li, J., Zhang, Z., Wu, L. et al. (2019). *Nature* 574: 516–521.
7 Lu, R., Yang, T., Chen, X. et al. (2021). *J. Am. Chem. Soc.* 143: 14451–14457.
8 Deng, Y., Lu, R., Chen, P., and Liu, G. (2023). *Chem. Commun.* 59: 4656–4659.
9 Kumar, G., Pradhan, S., and Chatterjee, I. (2020). *Chem. Asian J.* 15: 651–672.
10 Zhang, Z., Zhang, X., and Nagib, D.A. (2019). *Chem* 5: 3127–3134.
11 Wang, C.-Y., Qin, Z.-Y., Huang, Y.-L. et al. (2019). *iScience* 21: 490–498.
12 Cheng, Z., Chen, P., and Liu, G. (2019). *Acta Chim. Sin.* 77: 856–860.
13 Bao, X., Wang, Q., and Zhu, J. (2019). *Angew. Chem. Int. Ed.* 58: 2139–2143.
14 Chen, H., Jin, W., and Yu, S. (2020). *Org. Lett.* 22: 5910–5914.

**15** Zhang, W., Chen, P., and Liu, G. (2017). *J. Am. Chem. Soc.* 139: 7709–7712.

**16** Vasilopoulos, A., Zultanski, S.L., and Stahl, S.S. (2017). *J. Am. Chem. Soc.* 139: 7705–7708.

**17** Xie, W., Heo, J., Kim, D., and Chang, S. (2020). *J. Am. Chem. Soc.* 142: 7487–7496.

**18** Zhang, W., Chen, P., and Liu, G. (2019). *Angew. Chem. Int. Ed.* 58: 6425–6429.

**19** (a) Li, Z., Wang, Q., and Zhu, J. (2018). *Angew. Chem. Int. Ed.* 57: 13288–13292. (b) Bao, X., Wang, Q., and Zhu, J. (2019). *Chem. Eur. J.* 25: 11630–11634.

**20** Zhang, Z., Stateman, L.M., and Nagib, D.A. (2019). *Chem. Sci.* 10: 1207–1211.

**21** Sakurai, S., Matsumoto, A., Kano, T., and Maruoka, K. (2020). *J. Am. Chem. Soc.* 142: 19017–19022.

**22** Fu, L., Zhou, S., Wan, X. et al. (2018). *J. Am. Chem. Soc.* 140: 10965–10969.

**23** Fu, L., Zhang, Z., Chen, P. et al. (2020). *J. Am. Chem. Soc.* 142: 12493–12500.

**24** Buendia, M.B., Balin, J.-G.J., Andersen, M.E. et al. (2022). *Synlett* 33: 150–154.

**25** (a) Cao, Z., Li, J., Sun, Y. et al. (2021). *Chem. Sci.* 12: 4836–4840. (b) Li, Z., Torres-Ochoa, R.O., Wang, Q., and Zhu, J. (2020). *Nat. Commun.* 11: 403.

**26** Wang, C.-Y., Qin, Z.-Y., Huang, Y.-L. et al. (2020). *Org. Lett.* 22: 4006–4009.

**27** Zhang, Z.-H., Dong, X.-Y., Du, X.-Y. et al. (2019). *Nat. Commun.* 10: 5689.

**28** Liu, L., Guo, K.-X., Tian, Y. et al. (2021). *Angew. Chem. Int. Ed.* 60: 26710–26717.

**29** (a) Shen, H., Liu, Z., Zhang, P. et al. (2017). *J. Am. Chem. Soc.* 139: 9843–9846. (b) Tan, X., Liu, Z., Shen, H. et al. (2017). *J. Am. Chem. Soc.* 139: 12430–12433. (c) Kautzky, J.A., Wang, T., Evans, R.W., and MacMillan, D.W.C. (2018). *J. Am. Chem. Soc.* 140: 6522–6526. (d) Paeth, M., Carson, W., Luo, J.-H. et al. (2018). *Chem. Eur. J.* 24: 11559–11563. (e) Guo, S., AbuSalim, D.I., and Cook, S.P. (2018). *J. Am. Chem. Soc.* 140: 12378–12382.

**30** Xiao, H., Liu, Z., Shen, H. et al. (2019). *Chem* 5: 940–949.

**31** Sarver, P.J., Bacauanu, V., Schultz, D.M. et al. (2020). *Nat. Chem.* 12: 459–467.

**32** Jiang, C., Wang, L., Zhang, H. et al. (2020). *Chem* 6: 2407–2419.

**33** Xu, P., Fan, W., Chen, P., and Liu, G. (2022). *J. Am. Chem. Soc.* 144: 13468–13474.

**34** (a) Kohmura, Y., Kawasaki, K., and Katsuki, T. (1997). *Synlett* 12: 1456–1458. (b) Clark, J.S. and Roche, C. (2005). *Chem. Commun.* 2005: 5175–5177.

**35** (a) Pelletier, G. and Powell, D.A. (2006). *Org. Lett.* 8: 6031–6034. (b) Ni, Z., Zhang, Q., Xiong, T. et al. (2012). *Angew. Chem. Int. Ed.* 51: 1244–1247. (c) Tran, B.L., Li, B., Driess, M., and Hartwig, J.F. (2014). *J. Am. Chem. Soc.* 136: 2555–2563. (d) Liu, S., Achou, R., Boulanger, C. et al. (2020). *Chem. Commun.* 56: 13013–13016. (e) Suh, S.-E., Chen, S.-J., Mandal, M. et al. (2020). *J. Am. Chem. Soc.* 142: 11388–11393. (f) Chen, S.-J., Golden, D.L., Krska, S.W., and Stahl, S.S. (2021). *J. Am. Chem. Soc.* 143: 14438–14444.

**36** Nakafuku, K.M., Zhang, Z., Wappes, E.A. et al. (2020). *Nat. Chem.* 12: 697–704.

**37** Yang, C.-J., Zhang, C., Gu, Q.-S. et al. (2020). *Nat. Catal.* 3: 539–546.

**38** Ye, L., Tian, Y., Meng, X. et al. (2020). *Angew. Chem. Int. Ed.* 59: 1129–1133.

**39** Dai, L., Chen, Y.-Y., Xiao, L.-J., and Zhou, Q.-L. (2023). *Angew. Chem. Int. Ed.* 62: e202304427.

**40** Chen, X., Lian, Z., and Kramer, S. (2023). *Angew. Chem. Int. Ed.* 62: e202217638.

# 6

# Copper-Catalyzed Enantioconvergent Radical Cross-Coupling Under Thermal Conditions

*Xiao-Yang Dong[1], Zhong-Liang Li[1], and Xin-Yuan Liu[2]*

*[1]Dongguan Key Laboratory of Interdisciplinary Science for Advanced Materials and Large Scale Scientific Facilities, School of Physical Science, Great Bay University, Dongguan, China*
*[2]Shenzhen Grubbs Institute, Department of Chemistry, and Guangming Advanced Research Institute, Southern University of Science and Technology, Shenzhen, China*

## 6.1 Introduction

Over the past decades, transition-metal-catalyzed cross-coupling reactions have become a highly effective strategy for synthesizing target compounds. These reactions offer a convenient and efficient process that has found applications in many fields, including synthetic chemistry, drug discovery, and materials science [1–4]. Notably, Pd-catalyzed cross-coupling reactions were recognized with the 2010 Nobel Prize in Chemistry for their groundbreaking contribution to C—C bond formation, providing a robust method for research in both laboratory and industry settings [5–7]. While classical research in this field primarily concentrated on C($sp^2$)—C/X cross-coupling for achiral products, progress in meeting the rising demand for chiral products has been limited. Consequently, there is an urgent demand for the development of more convenient, highly efficient, and cost-effective methods for asymmetric reactions. Specifically, the utilization of broad alkyl electrophiles combined with nucleophiles for enantioconvergent C($sp^3$)—C/X reactions would introduce new possibilities for creating three-dimensional molecules [8–13]. However, several challenges need to be addressed to facilitate this process. First, the oxidative addition of alkyl electrophiles is more challenging compared to aryl/alkenyl halides. Second, there is a lack of effective enantioconvergent strategies to achieve asymmetric transformation, as the classical transition metal palladium generally follows a concerted insertion pathway [14, 15].

In recent years, significant advancements have been made in the field of enantioconvergent radical C($sp^3$)—C cross-coupling of racemic alkyl halides with chiral nickel [16], cobalt [17], and iron [18] catalysts by Fu and others [19–21]. The key factors that enable the accomplishment of these reactions are the exceptional single electron transfer (SET) ability possessed by first-row transition metals, which allows for the reduction of racemic alkyl halides to prochiral radicals [21]. Additionally, the chiral metal catalysts can interact with the prochiral radical, leading to the

formation of single enantiomeric coupling products through a uniform pathway (Scheme 6.1a) [22]. This strategy represents a gentle approach to enantioconvergent transformation. These reactions involving nucleophiles have primarily focused on carbon-based organometallic reagents, while the electrophiles have been limited to secondary ones possessing activating or directing groups.

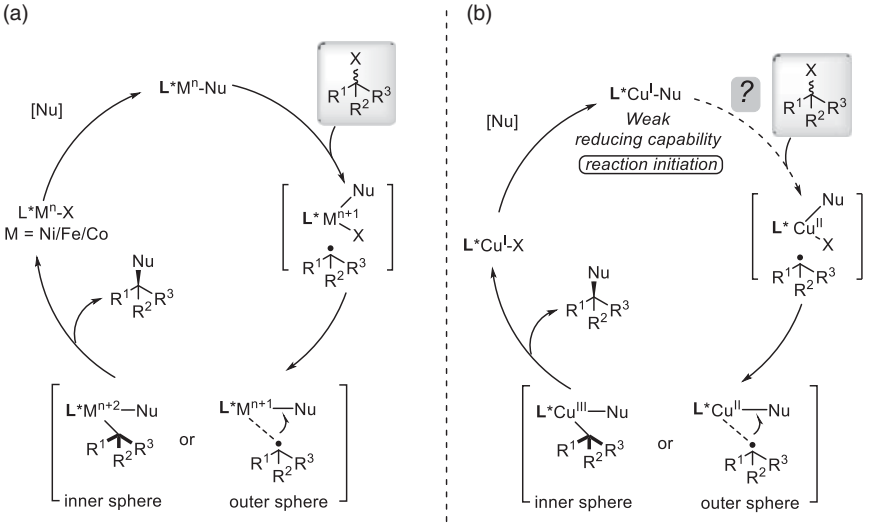


**Scheme 6.1** (a) Transition-metal-catalyzed enantioconvergent radical cross-coupling of alkyl halides. (b) Challenges for copper-catalyzed enantioconvergent radical cross-coupling.

Copper is an abundant first-row transition metal [23–25] with multiple valence states, including Cu(0), Cu(I), Cu(II), Cu(III). In particular, the metalloradical Cu(II) has a tendency to form new chemical bonds through its interaction with alkyl radicals [26]. Numerous copper-catalyzed radical asymmetric reactions have been developed to construct chiral C($sp^3$)—C/X bonds, using chiral ligands like bisoxazolines and phosphoric acids [27–29]. However, progress in the enantioconvergent cross-coupling of racemic alkyl halides with copper catalysts has been limited, mainly due to the lower reducing capability of copper compared to nickel, cobalt, and iron catalysts at the ground state, making it challenging to initiate the reaction under mild thermal conditions (Scheme 6.1b). Various strategies have been conceptualized to enhance the reducing capability of copper catalysts for gentle initiation of the enantioconvergent process.

This chapter aims to demonstrate these copper-catalyzed strategies for reaction initiation and enantioselectivity control in recent years. First, the use of photoinduced conditions in the excited state to initiate the reaction is an effective strategy for enantioconvergent transformation from the groups of Fu, Peters, and others. Here, we will briefly summarize this strategy, as more details will be discussed in Chapter 8. Second, chiral anionic ligands have been found to enhance the reducing capacity of copper under thermal conditions, allowing for the inclusion of various nucleophiles in the cross-coupling. Therefore, the strategic development of

multidentate chiral anionic ligands by Liu and others will be introduced to initiate the enantioconvergent transformations under thermal conditions (Scheme 6.2). Finally, a summary and outlook will be provided for this emerging field.

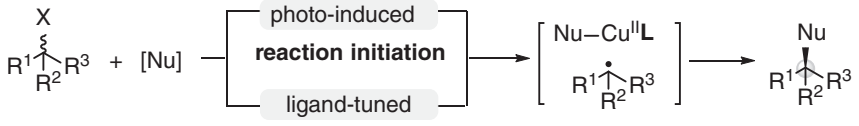


- irradiation to the excited state of copper(I) complex under photoinduced conditions
- design of multidentate chiral anionic ligand under mild thermal conditions

**Scheme 6.2** Design of copper-catalyzed enantioconvergent radical cross-coupling.

## 6.2 Chiral Anionic Ligands-Tuned Enantioconvergent Radical Cross-Coupling Under Mild Thermal Conditions

It is challenging to activate the strong C–halogen bond of racemic alkyl halides to generate the prochiral radicals under thermal conditions due to the limited reducing capability of the copper catalyst [30–32]. However, if the active ground-state Cu(I) catalyst could be irradiated to the excited state, it is possible to activate alkyl halides. This would result in a photoinduced copper-catalyzed strategy that combines the advantages of feasible activation of electrophiles and copper catalysis. Using the photoinduced strategy, Fu, Peters, and others have successfully achieved photoinduced copper-catalyzed arylations and alkylations of various nucleophiles, including *N*-heterocycles, phenols, thiols, amides, anilines, alcohols, alkyl amines, cyanide, and others (Scheme 6.3) [33–42]. In recent years, they have also made

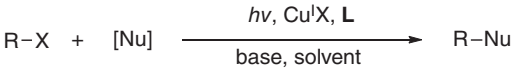


[Nu]: N-heterocycles, phenols, thiols, amides, anilines, alcohols, alkyl amines, cyanide

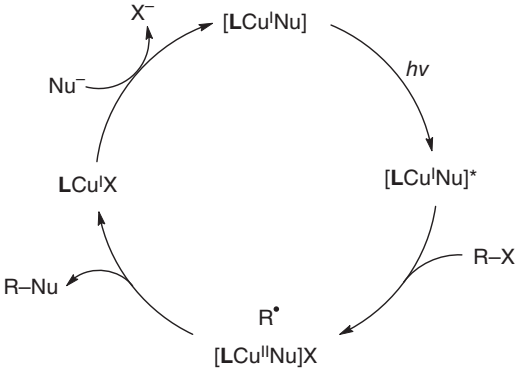


**Scheme 6.3** A typical catalytic cycle for photoinduced Cu-catalyzed radical cross-coupling.

advancements in the field of photoinduced copper-catalyzed enantioconvergent radical C($sp^3$)—C/N cross-coupling. They have established various methods for initiating the reaction through different photoinduced modes [43–46]. This specific topic will be discussed in detail in Chapter 8.

The elegant approach of developing a photoactive copper catalyst in its excited state effectively initiates the reaction, overcoming the limited reducing ability of the copper catalyst, as demonstrated by Fu, Peters, and others. This innovative strategy successfully enables copper-catalyzed radical enantioconvergent C($sp^3$)—C/N cross-couplings of various racemic electrophiles. An alternative approach to achieve the enantioconvergent cross-coupling of racemic alkyl halides is through the design of electron-rich chiral ligands [47]. These ligands would enhance the high reducing capability of copper, allowing the reaction to be initiated under thermal conditions. On account of this concept, the design and synthesis of multidentate anionic chiral ligands offer a gentle solution to both the challenges of reaction initiation and stereoselectivity control (Scheme 6.4). Furthermore, these anionic ligands may effectively suppress the oxidative homocoupling of nucleophiles by saturating the coordinating site of copper [48]. This section will primarily focus on the development of copper-catalyzed enantioconvergent cross-coupling using multidentate anionic chiral ligands.

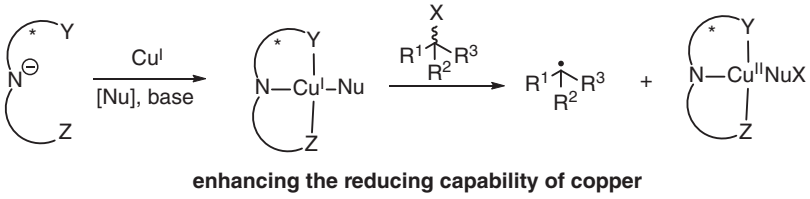


**Scheme 6.4** The initiation modes of chiral anionic ligands-tuned enantioconvergent cross-coupling.

### 6.2.1 Chiral Anionic Tridentate N,N,P-Ligands

Chiral phosphorus acids (CPAs) are a family of chiral ligands that have found wide applications in organic catalysis and transition-metal catalysis [27–29]. In recent years, the Liu group has made significant advancements in the field by developing a series of Cu/CPA-catalyzed radical asymmetric difunctionalization of alkenes [28, 29]. Initially, they discovered that when CPA is used as a monodentate anionic ligand in conjunction with copper, it can activate highly active radical precursors, such as the Togni reagent, resulting in good enantioselectivity for substrates possessing a directing group [49]. Building on this, they expanded their catalytic system by introducing a pyridine-type ligand and achieved radical asymmetric oxytrifluoromethylation of alkenes [50]. It was found that pyridine provided an additional coordination site to stabilize the chiral copper intermediate. Subsequently, they accomplished Cu/anionic N,N-ligand-catalyzed radical asymmetric oxytrifluoromethylation of alkenyl oximes [51]. This approach introduced

a catalytic model that combines a monodentate anionic ligand with an additional achiral ligand into a single catalyst, resulting in enhanced stability of the copper complex and a more rigid chiral environment (Scheme 6.5).

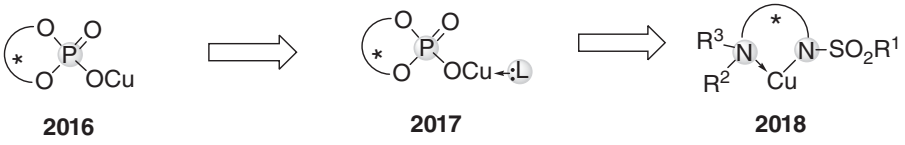


**Scheme 6.5** The development of the catalytic mode for Cu/chiral anionic ligands of Liu's group.

Inspired by their previous work and the above concept of ligand design, the Liu group has synthesized a library of multidentate anionic N,N,P-ligands derived from cinchona-alkaloid-based Dixon's ligand [52–55] since 2019. These ligands exhibit various steric hindrances and electric properties on the phosphine substituents. The Cu/N,N,P-ligand complex shows a significantly stronger reducing capability than simple copper salts.

They initially employed this catalytic system to conduct enantioconvergent radical C($sp^3$)—C(sp) cross-coupling of racemic secondary alkyl halides and terminal alkynes. This particular reaction is of great significance in organic synthesis and the synthesis of natural products. However, there have been very few reports of similar reactions. The achievement of the enantioconvergent radical C($sp^3$)—C(sp) cross-coupling requires enhancing the reducing capacity of copper to initiate the reaction, inhibiting the Glaser homocoupling of terminal alkynes, and creating a controlled chiral environment to achieve enantioselectivity. The investigation of ligands revealed that commercially available mono- and bi-phosphine ligands yielded poor results, with some cases producing trace products and side Glaser homocoupling products. Fortunately, the tridentate N,N,P-ligand was able to promote the reaction smoothly with 50% ee and effectively inhibit the Glaser homocoupling. Further investigation into the steric bulkiness and electronic properties of the *P*-aryl ring in N,N,P-ligands showed that electron-rich groups at the *ortho* or *meta* positions were beneficial for both yield and enantiocontrol. Among the ligands examined, **L13** proved to be the most effective ligand (Scheme 6.6).

More than 120 examples of chiral alkynes were obtained with impressive yield and enantioselectivity (up to 99% ee) [56]. The range of alkyl halides included benzyl bromide or chloride, allyl bromide, propargyl bromide, α-bromo amide, and α-bromo nitrile. The scope of alkynes covers (hetero)aryl, alkyl, and silyl terminal alkynes. Notably, the reaction system tolerated industrial acetylene and propyne well, showcasing its potential for industrial applications. Furthermore, this protocol facilitated the synthesis of numerous drug analogues and natural products. (Scheme 6.7).

Based on the findings of the control experiments, a viable mechanism is postulated as follows. In the presence of a base, the alkynes, $Cu^I$, and **L** combine to form an **L**$Cu^I$Nu complex. This intermediate exhibits a strong reducing capability to convert

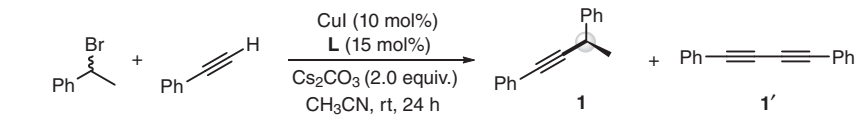


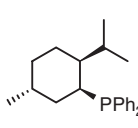


**L1**
**1** trace; **1′** 22%

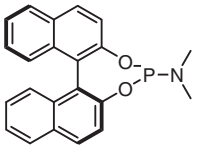


**L2**
**1** trace; **1′** trace

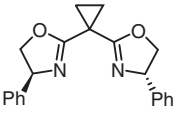


**L3**
**1** trace; **1′** 52%

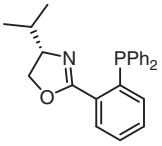


**L4**
**1** trace; **1′** 34%

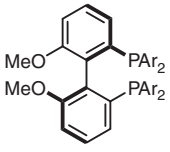


**L5** (Ar = 3,5-$^t$Bu$_2$-4-MeO-C$_6$H$_2$)
**1** trace; **1′** trace

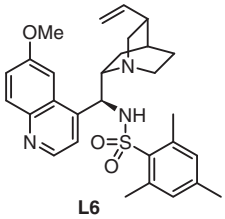


**L6**
**1** trace; **1′** 42%

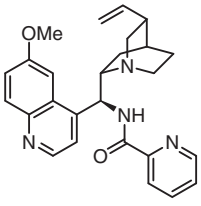


**L7**
**1** trace; **1′** trace

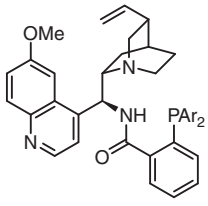


| | Ar | 1 |
|---|---|---|
| **L8** | Ph | 81%, 50% ee |
| **L8** | Ph | 89%, 82% ee[a] |
| **L9** | 4-MeOC$_6$H$_4$ | 83%, 85% ee[a] |
| **L10** | 2,4,6-Me$_3$C$_6$H$_2$ | 50%, 89% ee[a] |
| **L11** | 2-Naphthyl | 82%, 80% ee[a] |
| **L12** | 3,5-(CF$_3$)$_2$C$_6$H$_3$ | 75%, 75% ee[a] |
| **L13** | 3,5-$^t$Bu$_2$C$_6$H$_3$ | 90%, 94% ee[a] |

[a]CuTc (10 mol%) and Et$_2$O were used.

**Scheme 6.6** Ligand effect of enantioconvergent radical C(sp$^3$)—C(sp) cross-coupling.

racemic alkyl halides into prochiral alkyl radicals and generate an **L**Cu$^{II}$NuX complex. Subsequently, the complex **L**Cu$^{II}$NuX reacts with the prochiral alkyl radicals to produce the desired chiral coupling products and release **L**Cu$^{I}$X. (Scheme 6.8).

Subsequently, they also successfully realized several types of asymmetric radical alkynylation reactions from diverse radical precursors by using the Cu/N,N,P-ligand catalytic system. The *N*-hydroxyphthalimide (NHP)-type esters of carboxylic acids were employed as radical precursors and coupled with terminal alkynes catalyzed by Cu/N,N,P-ligand, which acted as a dual photo and coupling catalyst without the need for additional photosensitizers (Scheme 6.8a) [57]. This decarboxylative coupling approach offered an alternative method for coupling with alkyl halides that was previously considered challenging or impractical. Additionally, a three-component asymmetric radical 1,2-carboalkynylation of alkenes and 1,4-carboalkynylation of 1,3-enynes with alkyl halides and terminal alkynes has also been realized (Scheme 6.8b, c) [58, 59]. Notably, both reactions exhibited a wide range of applicability with respect to alkenes, 1,3-enynes, and terminal alkynes,

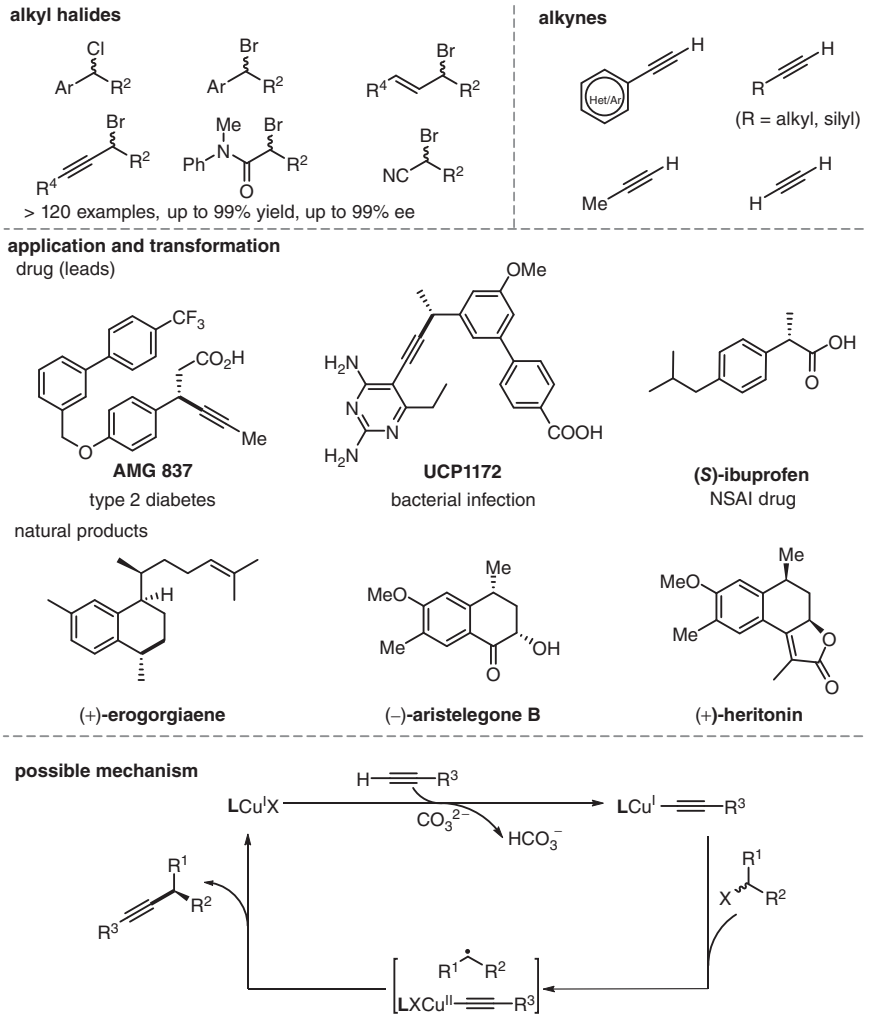


**Scheme 6.7** Scope and application of C($sp^3$)—C(sp) cross-coupling.

particularly when employing primary, secondary, and tertiary carbon-based radical precursors of various chemical structures. Furthermore, the Cu/N,N,P- and Cu/N,N,P(O)-ligand catalytic system has been developed to enable the intramolecular and intermolecular oxidative cross-coupling of C($sp^3$)—C(sp) bonds with terminal alkynes, respectively (Scheme 6.8c, 6.8e) [60, 61]. This can be achieved through either intramolecular or intermolecular hydrogen atom abstraction (HAA) processes.

In 2022, Zhang and colleagues developed an enantioconvergent radical C($sp^3$)—C(sp) cross-coupling of racemic alkyl halides and terminal alkynes (Scheme 6.9) [62]. This work was achieved by employing two distinct types of oxazoline-derived anionic N,N,P-ligands. The first type of ligand **L18** contained a chiral center incorporated in the oxazoline moiety, which preferred α-silyl benzyl

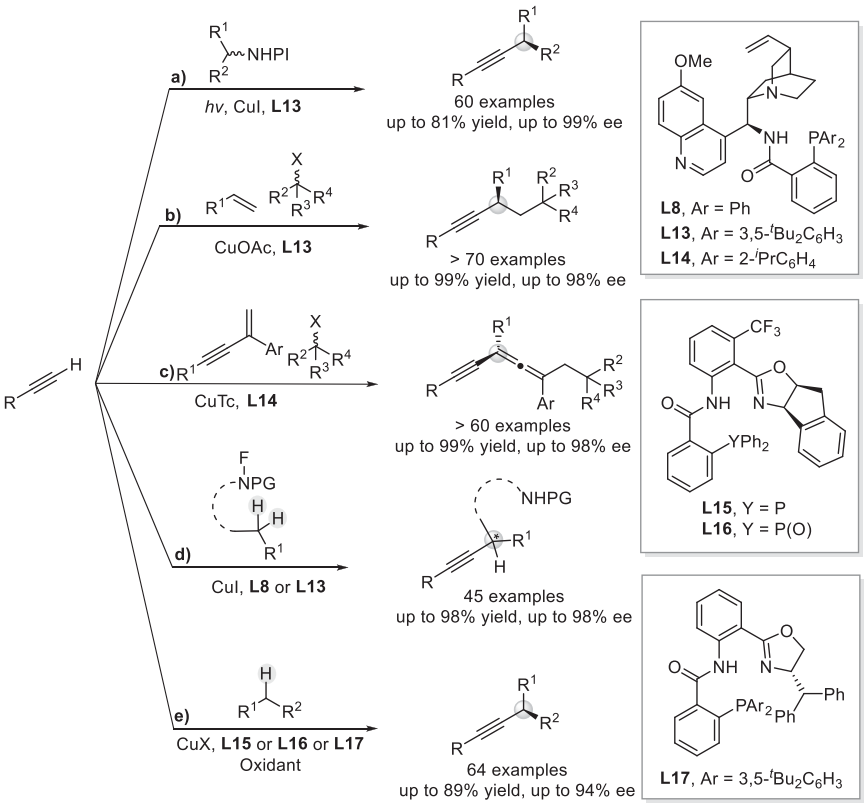


**Scheme 6.8** Cu/anionic ligand-catalyzed diverse asymmetric radical reactions of alkynes.

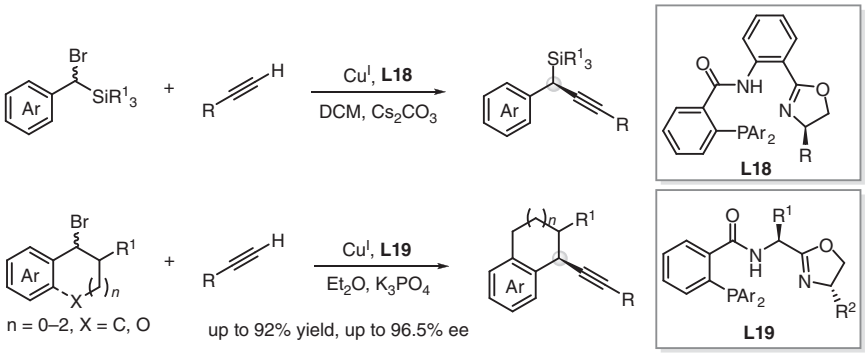


**Scheme 6.9** Zhang's enantioconvergent radical C($sp^3$)–C(sp) cross-coupling.

halides. The second type of ligand **L19** featured a new chiral center positioned between the 2-diphenylphos-phinobenzamide and oxazoline moiety, which was particularly beneficial for the coupling of benzo-fused cyclic α-halides. It is worth mentioning that the N,N,P-ligands utilized in this study were found to enhance the reducing capacity of copper, thereby enabling the conversion of alkyl halides into prochiral radicals.

Organoboron reagents are a class of stable and low-toxic reagents, which have found extensive application in Suzuki-Miyaura cross-coupling. In 2020, Liu and colleagues utilized the Cu/N,N,P-ligand system to accomplish an enantioconvergent radical Suzuki-Miyaura C($sp^3$)—C($sp^2$) cross-coupling of racemic alkyl halides with arylboronate esters [63] (Scheme 6.10). N,N,P-ligand **L13** demonstrated moderate yield and enantioselectivity, while ligands bearing steric hindrance at the *ortho* position had a great influence on enantiocontrol, and **L20** was the most effective ligand. Notably, the addition of $H_2O$ was found to be a critical factor in achieving high yields, attributable to its role in accelerating the transmetalation process. Mechanistic studies revealed that the catalytic cycle proceeds via the radical pathway. A diverse range of cross-coupling products (>50 examples, up to 97% ee) were obtained from (hetero)benzyl and propargyl bromides/chlorides and aryl and heteroarylboronate esters.

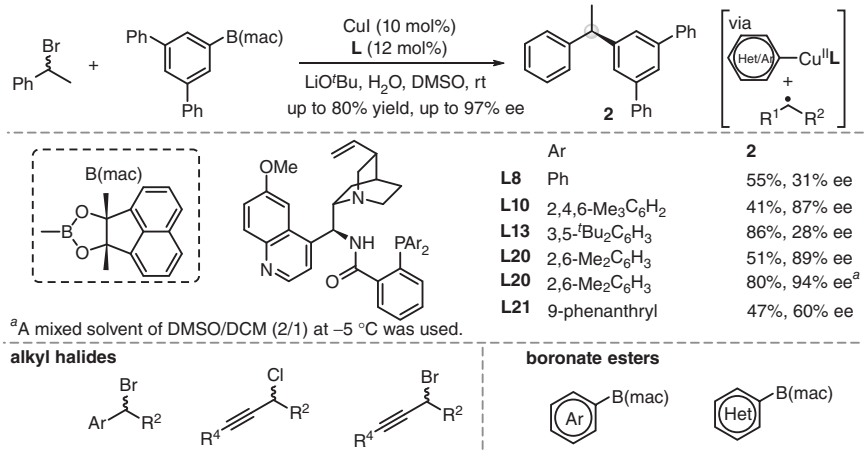


**Scheme 6.10** Enantioconvergent radical Suzuki-Miyaura C($sp^3$)—C($sp^2$) cross-coupling.

Azoles are an essential structural motif found in various bioactive compounds. These molecules exhibit an acidic C($sp^2$)—H bond that readily undergoes transmetalation with copper catalysts in the presence of a base. The coupling of alkyl halides with azoles typically occurs at high temperatures. In 2020, Liu and colleagues accomplished an enantioconvergent radical C($sp^3$)—C($sp^2$) cross-coupling of benzyl bromides with azoles by using a copper/chiral N,N,P-ligand catalyst [64]. The role of the catalyst is to initiate the radical process under mild conditions, effectively suppressing the racemization of the α proton of the resulting chiral alkylated azoles at otherwise high temperatures. Various azoles, including 1,3,4-oxadiazoles, oxazoles, benzo[*d*]oxazoles, and 1,3,4-triazoles, can be coupled to afford a diverse range of chiral azoles with up to 95% ee (Scheme 6.11).

Chiral amines are significant in organic synthesis, pharmaceuticals, and other disciplines. The direct enantioconvergent cross-coupling of alkyl halides with ammonia is challenging due to the strong coordination of ammonia with copper. In 2021, the Liu group utilized the Cu/N,N,P-ligand catalytic system to achieve

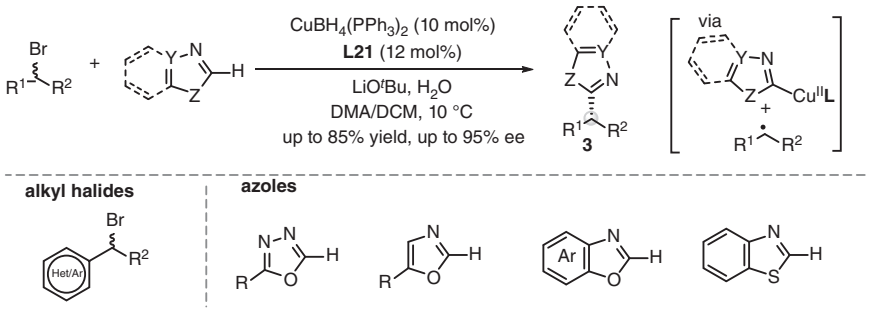


**Scheme 6.11** Enantioconvergent radical C($sp^3$)—C($sp^2$) cross-coupling with azoles.

an enantioconvergent radical C—N cross-coupling of secondary alkyl halides with sulfoximines [65] (Scheme 6.12). In this strategy, sulfoximines serve as a good surrogate for ammonia. Interestingly, the electronic and steric properties of the *meta* substituents on the P-aryl rings of N,N,P-ligands greatly influenced the reaction efficiency and enantioselectivity. The sterically crowded ligands **L24** and **L25** are beneficial for both yield and ee of the coupling products. A wide range of secondary alkyl halides, including (hetero)benzyl halides, propargyl bromides, α-bromo ketones, α-bromo nitriles, and α-bromo amides, were suitable for the coupling reaction, leading to diverse α-chiral sulfoximines. Interestingly, a general trend for these two ligands: the bulkier ligand **L25** was effective for less sterically crowded alkyl halides, while the less bulky ligand **L24** worked well for sterically crowded substrates. Subsequent transformations of the products allowed them to obtain various common chiral *N*-containing building blocks, such as simple amines,

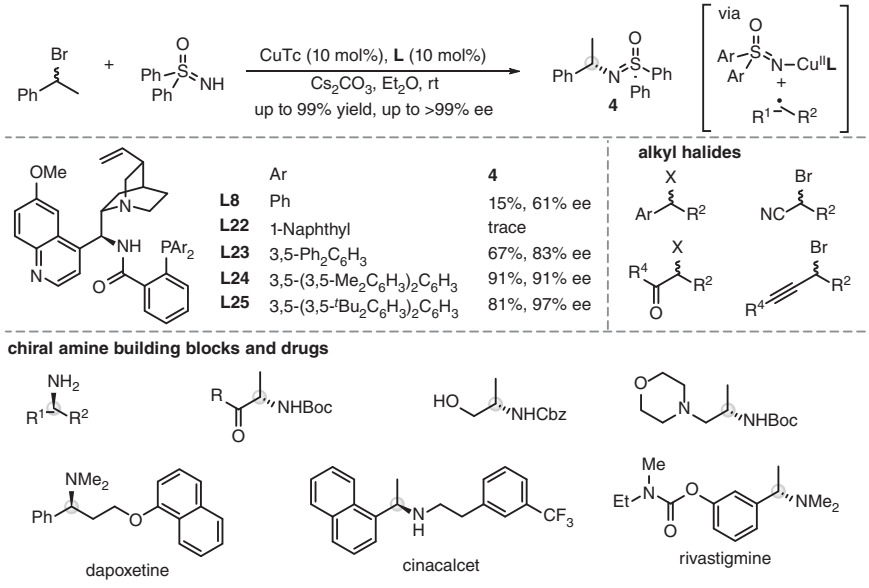


**Scheme 6.12** Enantioconvergent radical C($sp^3$)—N cross-coupling with sulfoximines.

α-amino ketones, 1,2-amino alcohols, and 1,2-diamines. Moreover, this strategy proved to be a useful tool for the synthesis of *N*-containing chiral drugs, including dapoxetine, cinacalcet, and rivastigmine.

Chiral phosphorus compounds play a crucial role as building blocks in synthetic chemistry, catalysts, and medicine. The C($sp^3$)—P cross-coupling of racemic alkyl halides and phosphorus nucleophiles remains challenging due to various factors. These challenges include the strong background $S_N2$ reaction, competition between the P nucleophile and ligand, leading to the poisoning of the reaction, the weak reducing capability of copper catalysts, and the homocoupling side product of P nucleophiles. Therefore, the key to achieving this enantioconvergent transformation lies in the selective rational design of a catalytic system and the choice of P nucleophile source. In 2023, the Liu group successfully employed their Cu/anionic ligand system to achieve the enantioconvergent radical Michaelis–Becker-type C($sp^3$)—P cross-coupling of racemic alkyl halides and H-phosphonates [66]. Ligand screening revealed that the presence of a 3,5-substituted electronic donating group on the P-aryl phenyl moiety of the ligand was beneficial for both yield and enantiocontrol, while also inhibiting the formation of homocoupling side products. Among the ligands tested, the 3,5-$^t$Bu ligand (**L13**) was the most effective. This reaction demonstrated good tolerance toward a range of alkyl halides and H-phosphonates, including benzyl-, heterobenzyl-, propargyl-, and α-aminocarbonyl alkyl halides, affording high yields and enantioselectivities. Mechanistic studies indicated that the reaction proceeds through a radical pathway, offering a complementary approach for the synthesis of diverse chiral phosphorus compounds (Scheme 6.13).

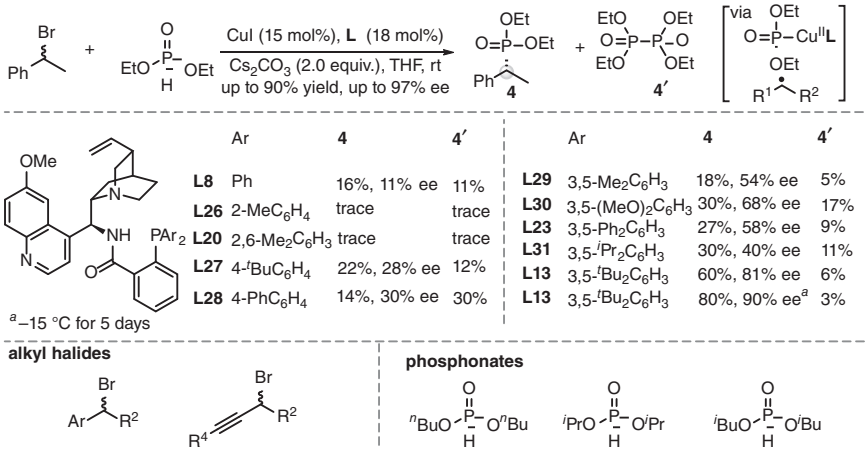


**Scheme 6.13** Enantioconvergent radical C($sp^3$)—P cross-coupling with H-phosphonates.

α-Chiral organosulfur compounds are essential building blocks in various fields, such as organic synthesis and biochemistry. However, accessing these compounds through copper-catalyzed enantioconvergent C($sp^3$)—S cross-coupling is challenging due to the poison effect of the metal catalyst and uncontrollable background reactions. Interestingly, the biosynthesis of C($sp^3$)—S bonds occurs through

the radical homolytic substitution of metalloenzymic iron–sulfur complexes by carbon-centered radicals, offering a potential solution to these challenges. Building on this concept, the Liu group successfully achieved Cu-catalyzed enantioconvergent radical C($sp^3$)—S cross-coupling using their Cu/multidentate chiral anionic ligand catalytic system [67]. The choice of sulfur source is crucial for the success of this reaction, with sodium 3,5-dimethylbenzenesulfonothioate being the most effective. The use of 3,5-substituted N,N,P-ligands improves the yield and enantioselectivity. Using **L31** as a ligand, they achieved the target compound with 81% yield and 92% ee for the model reaction of benzyl alkyl halide. They also explored the use of sodium benzenesulfonothioate as a sulfur nucleophile for propargyl bromide with **L33**, and benzothioic S-acid as a sulfur nucleophile for tertiary alkyl chloride with **L34**. The reaction tolerates a range of racemic secondary/tertiary alkyl halides and various sulfur nucleophiles, providing access to α-chiral alkyl thiols and organosulfur compounds with different oxidation states. These compounds are valuable for the synthesis of building blocks, ligands, and drugs in subsequent transformations (Scheme 6.14).

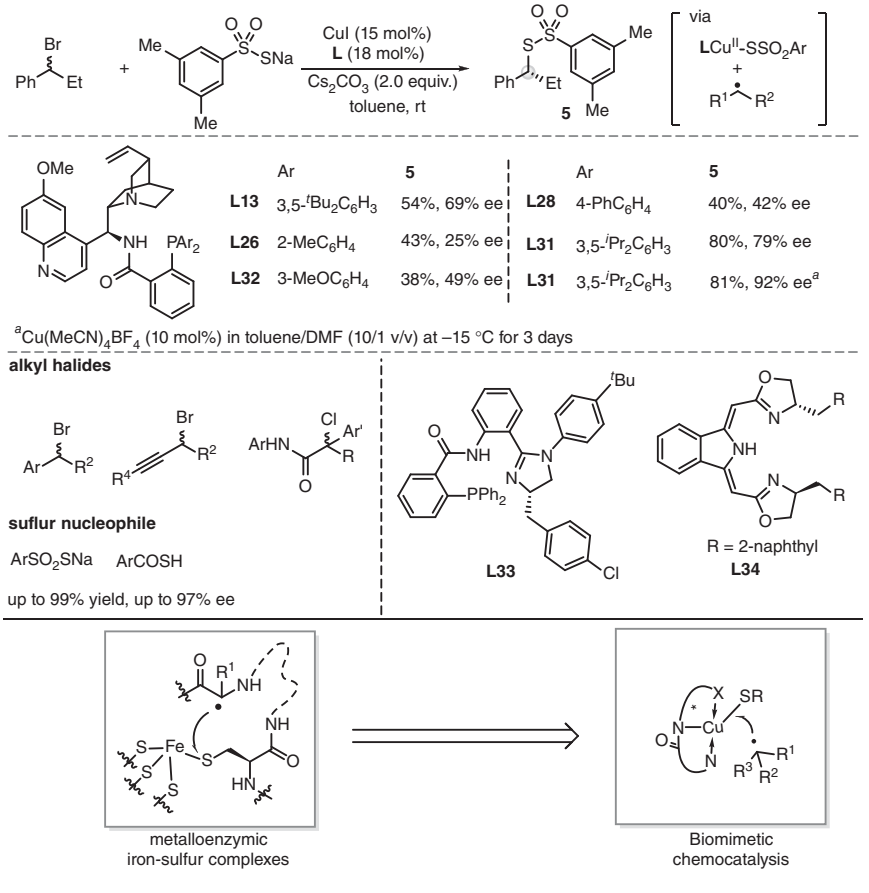


**Scheme 6.14** Enantioconvergent radical C($sp^3$)—S cross-coupling.

### 6.2.2 Chiral Anionic Tridentate N,N,N-Ligands

In comparison to the use of an amine surrogate as a nucleophile for the synthesis of chiral amines, the direct utilization of unprotected amines or ammonia for the one-step enantioconvergent *N*-alkylation holds greater appeal and significance. However, the resolution of those challenges, including the high Lewis basicity of aliphatic amines for the poison of metal catalysis, weakly acidic N—H bonds of amines to deprotonation, and background $S_N2$ reactions, are critical factors for the successful completion of this transformation. By modifying a chiral multidentate anionic ligand to adjust the binding affinities of the amine, a viable solution can be found to overcome these difficulties.

After numerous attempts, a variety of multidentate anionic N,N,N-ligands were synthesized, allowing for a general and practical copper-catalyzed enantioconvergent *N*-alkylation of aliphatic amines and ammonia with diverse racemic α-carbonyl alkyl chlorides. In the initial results, this reaction exhibited a significant background reaction even in the absence of copper and ligand. The cinchona alkaloid-derived bidentate sulfonamide N,N-anionic ligand (**L35**, **L36**) yielded the desired product with moderate yield and ee, but also produced a substantial amount of side products. However, the incorporation of an external 8-quinolinyl group to form a tridentate sulfonamide N,N,N-anionic ligand (**L38**) resulted in the formation of the chiral product with high yield and ee, significantly reducing the formation of side products. Furthermore, the tridentate sulfonamide N,N,N-anionic ligand derived from cyclohexanediamine (**L41**) was suitable for alkyl amide electrophiles. Additionally, the ligand **L42** was compatible with tertiary alkyl chlorides. This strategy enabled the conversion of over 100 aliphatic amines, and even ammonia, into α-chiral aliphatic amines with high yields and ee, demonstrating its potential application in both academic research and the pharmaceutical industry (Scheme 6.15) [68].

The mechanism of this reaction differs from the previous study on sulfoximine coupling. When the dual nucleophile containing both sulfoximine and aliphatic amine was subjected to the standard reaction conditions, the aliphatic amine exhibited a highly selective *N*-alkylation. Through a series of control experiments, they proposed the following reaction mechanism: the α-carbonyl alkyl chloride and Cu(I) react to form the cuprate intermediate **I** in the presence of a base. This intermediate then undergoes an intramolecular oxidative addition, resulting in the equilibrium between **II** and **III**. Subsequently, the amine attacks **III** through an out-sphere pathway, leading to the formation of **IV**. Finally, ligand exchange occurs, resulting in the formation of the final chiral products and the regeneration of intermediate **I** (Scheme 6.16).

The utilization of (hetero)aromatic amines in asymmetric C—N bond formation is a gentle approach to synthesizing chiral aromatic amines. In 2023, the Liu group successfully demonstrated the enantioconvergent cross-coupling of (hetero)aromatic amines with racemic alkyl halides, resulting in the synthesis of diverse chiral *N*-alkyl (hetero)aromatic amines [69]. While the enantioconvergent C—N cross-coupling of aliphatic amines has been extensively studied, it is important to

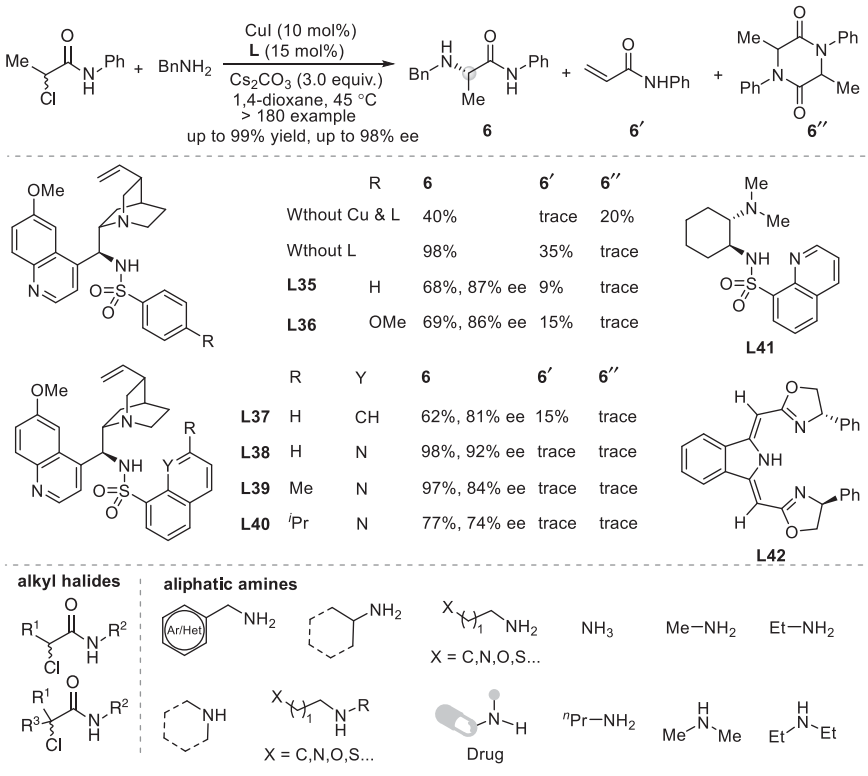


| | R | 6 | 6′ | 6″ |
|---|---|---|---|---|
| Wthout Cu & L | | 40% | trace | 20% |
| Wthout L | | 98% | 35% | trace |
| L35 | H | 68%, 87% ee | 9% | trace |
| L36 | OMe | 69%, 86% ee | 15% | trace |

| | R | Y | 6 | 6′ | 6″ |
|---|---|---|---|---|---|
| L37 | H | CH | 62%, 81% ee | 15% | trace |
| L38 | H | N | 98%, 92% ee | trace | trace |
| L39 | Me | N | 97%, 84% ee | trace | trace |
| L40 | $^{i}$Pr | N | 77%, 74% ee | trace | trace |

**Scheme 6.15** Enantioconvergent radical *N*-alkylation of aliphatic amines.

note that the reaction mechanism for aromatic amines is different. The stronger acidity of aromatic amines allows for the formation of a Cu(I)-amino complex in the presence of a base. This complex then reduces alkyl halides to prochiral alkyl radicals using multidentate anionic ligands. The **L**Cu(II)-amino complex interacts with the prochiral alkyl radicals, leading to the asymmetric C—N cross-coupling through either a Cu(III) intermediate or radical addition to the Cu—N bond. In their study, they employed an oxazline-derived sulfonamide N,N,N-ligand (**L46**) for the enantioconvergent C—N cross-coupling of tertiary alkyl halides with aromatic amines, and an N,N,P-ligand (**L47**) for propargyl halides. This reaction exhibited a broad substrate scope, accommodating various secondary/tertiary alkyl halides and (hetero)aromatic amines (Scheme 6.17).

Additionally, in the same year, they also developed a copper-catalyzed enantioconvergent C($sp^3$)—N cross-coupling of aromatic amines with racemic tertiary α-bromo-β-lactams (Scheme 6.18) [70]. This reaction utilized a similar tridentate anionic N,N,N-ligand (**L48**) and demonstrated tolerance toward a variety of racemic tertiary α-bromo-β-lactams and different types of aromatic amines. The mechanism for this reaction is similar to their previous work, proceeding via a radical process as depicted in Scheme 6.17.

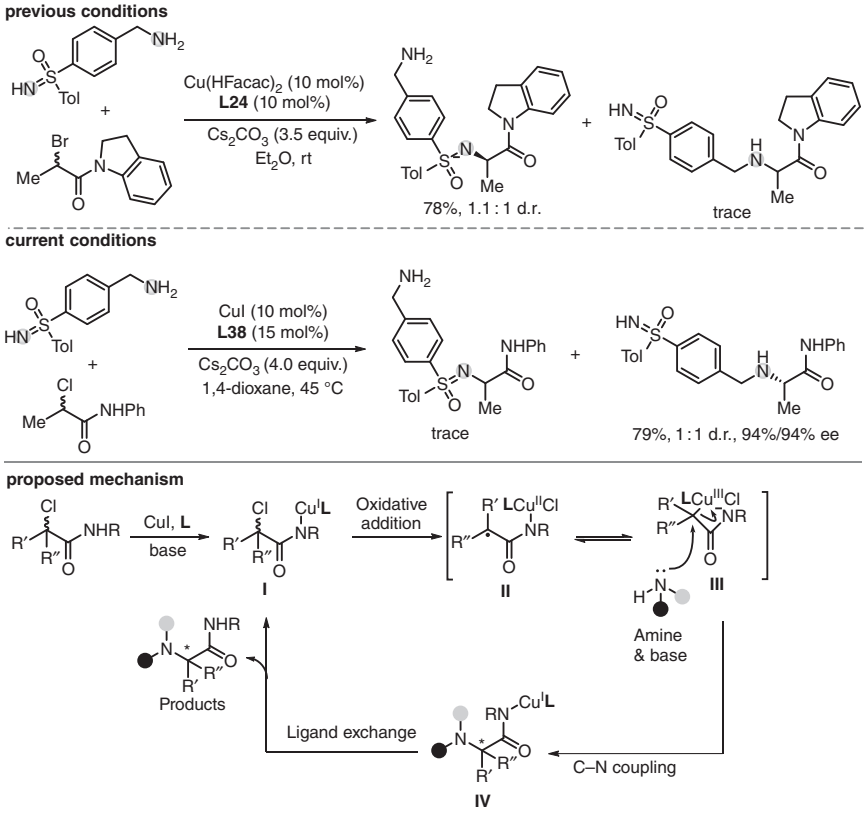


**Scheme 6.16** Proposed mechanism for enantioconvergent radical *N*-alkylation.

### 6.2.3 Hemilabile Chiral Anionic N,N,N-Ligands

Alkenylboronate esters are readily available organoboron reagents. If alkenylboronate esters can be successfully coupled with racemic alkyl halides, it would enable the synthesis of valuable chiral alkenes. The Liu group continued to explore this process. However, only low yields and enantioselectivities have been achieved using the Cu/N,N,P-ligand catalytic system. This suggests that the enantiocontrol model may differ between alkenylcopper and alkynyl- or (hetero)arylcopper complexes, necessitating the design of new chiral ligands to address this issue. Subsequently, other types of ligands were synthesized and tested. It was found that the bidentate N,N-ligand (**L35**) only yielded trace amounts of the coupling product, albeit with good enantioselectivity, while the tridentate N,N,N-ligand (**L38**) gave good yields but poor enantioselectivity. This result indicated that the forthcoming ligand should possess two crucial characteristics. First, the in situ generated copper complex with a tridentate state should have sufficient reducing capacity to convert alkyl halides to prochiral radicals. Second, the enantiocontrol step of

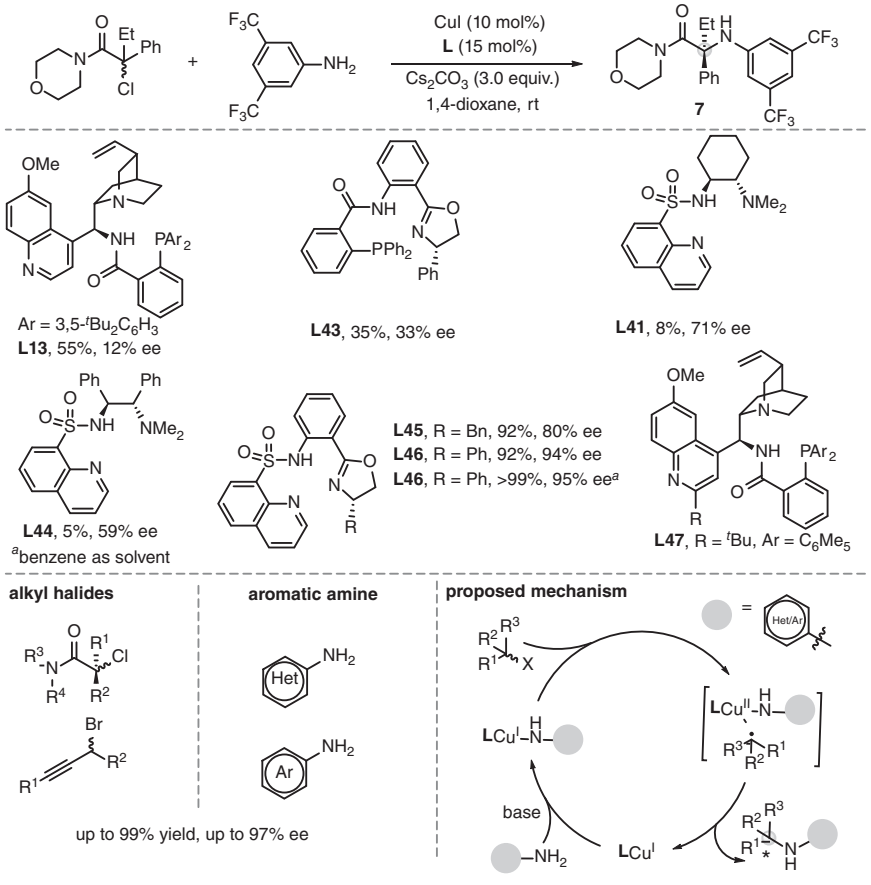


**Scheme 6.17** Enantioconvergent radical C($sp^3$)—N cross-coupling of aromatic amines.

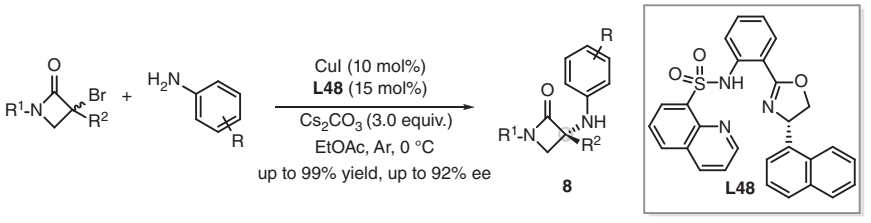


**Scheme 6.18** Enantioconvergent radical C($sp^3$)—N cross-coupling of aromatic amines with tertiary α-bromo-β-lactams.

bond formation between alkenyl copper and the prochiral radical should occur in a bidentate manner. A hemilabile coordination model is proposed for the initiation of the reaction and the enantiocontrol step. Based on this concept, a methyl group was introduced at the *ortho* position of one coordinating quinoline ring (**L39**),

enhancing the steric hindrance to confer the hemilabile feature to the ligand. Finally, the newly developed hemilabile chiral N,N,N-ligand **L39** was employed to successfully accomplish the challenging reactions [71]. Other chiral skeletons of this type of ligand (**L49**, **L50**) also yielded the desired coupling products. The scope of this coupling reaction is broad and delivers highly chiral alkenes with ee reaching up to 99% (Scheme 6.19).

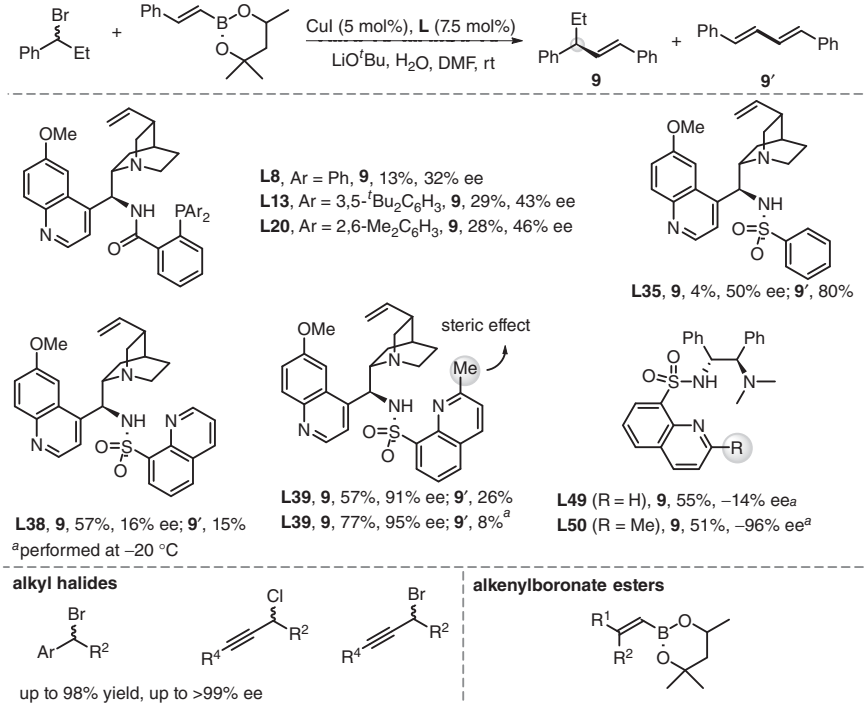


**Scheme 6.19** Hemilabile ligand design in enantioconvergent radical Suzuki-Miyaura C($sp^3$)−C($sp^2$) cross-coupling with alkenylboronates.

Chiral α-quaternary β-lactams hold significant importance as an active category of molecules in drug synthesis. However, achieving asymmetric cross-coupling of racemic tertiary α-bromide-β-lactams requires addressing the challenges of reaction initiation and enantiocontrol, specifically in controlling the crowdness of tertiary prochiral radicals. In 2023, the Liu research group employed the hemilabile N,N,N-ligand to achieve copper-catalyzed enantioconvergent C($sp^3$)—C($sp^2$) cross-coupling of tertiary α-bromide-β-lactams with aryl- and alkenylboronate esters (Scheme 6.20) [72]. This reaction demonstrated a broad functional group tolerance, encompassing various tertiary α-bromo-β-lactams as well as aryl-, heteroaryl-, and alkenylboronate esters. Importantly, the mechanistic study revealed that the **L**Cu(I) complex serves as the active species for reducing alkyl halides to prochiral radicals without transmetalation.

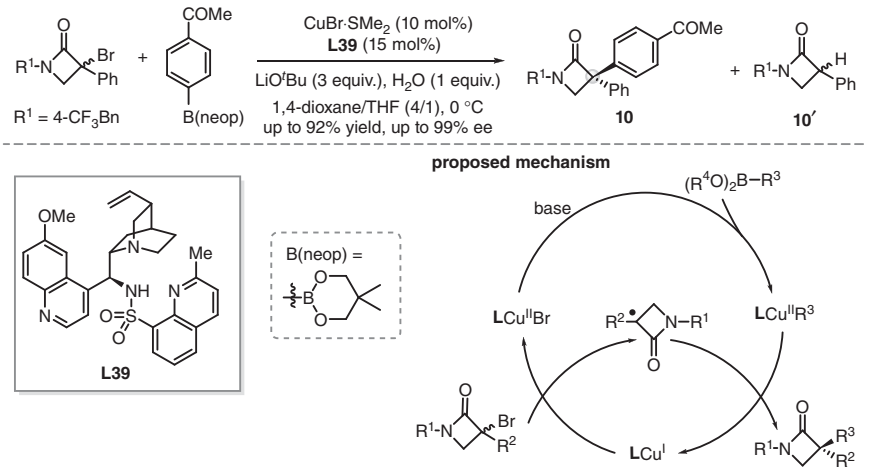


**Scheme 6.20** Suzuki-Miyaura cross-coupling of tertiary α-bromide-β-lactams.

### 6.2.4 Chiral Anionic N,N,N-Ligands with Long Spreading Side Arm

In recent years, there has been significant progress in enantioconvergent radical C($sp^3$)—C cross-coupling of secondary alkyl halides. In comparison, the cross-coupling of tertiary alkyl electrophiles to form fully substituted carbon stereocenters is still rare. This is primarily due to the steric hindrance associated with tertiary alkyl radicals and the challenge of differentiating three different carbon substituents in terms of enantioselectivity. Recently, Fu and his colleagues reported the first enantioconvergent radical C($sp^3$)—C($sp^2$/$sp^3$) cross-coupling of racemic tertiary alkyl halides using nickel/bisoxazoline catalysts [73].

Building upon the advantages of the anionic-ligand catalytic system, the Liu group studied the enantioconvergent radical C($sp^3$)—C(sp) cross-coupling of tertiary alkyl halides with terminal alkynes. In the initial study, they screened multiple N,N,P-ligands and achieved a high yield but low enantioselectivity in the formation of chiral products. To address this issue, they employed DFT calculation with coworkers to investigate the key factors influencing enantioselectivity. The preliminary DFT calculation revealed a preference for an outer-sphere radical substitution-type C—C bond formation process in the coupling step between the prochiral tertiary alkyl radical and alkynyl group. This finding contrasted with previous work on secondary alkyl radicals but aligned with Fu's and Peters' research on photoinduced Cu-catalyzed asymmetric C—N cross-coupling using racemic tertiary alkyl chloride [43]. The outer-sphere process may have less effective enantiodiscriminating interactions due to its greater distance from the first coordination sphere around the copper centers than the inner-sphere pathway. Based on this analysis, they proposed the design of new ligands with specific features: (i). limited steric congestion in the immediate vicinity of the first coordination sphere to accommodate sterically bulky tertiary alkyl radicals easily; (ii). a long spreading side arm for efficient interaction with one or both substrates in the outer side of the second

coordination sphere to enable effective stereodiscrimination. Subsequently, they synthesized a series of novel amide-derived anionic N,N,N-ligands and discovered that the ligand with a long spreading side arm played a critical role in controlling enantioselectivity. Finally, they successfully conducted enantioconvergent radical C($sp^3$)—C(sp) cross-coupling of tertiary alkyl halides and terminal alkynes using the newly designed anionic N,N,N-ligands with mild reaction conditions [74]. The reaction exhibited excellent tolerance toward tertiary α-aminocarbonyl alkyl chlorides and bromides while maintaining good functional group compatibility and superior enantioselectivity. This remarkable transformation demonstrates its promising application in the synthesis of challenging enantioenriched quaternary carbon building blocks. The X-ray structural analysis of the Cu/N,N,N-ligand complex showed an anionic tridentate coordination mode of the ligand. With the support of systematic control experiments and DFT calculation, the results provided clear evidence that this reaction proceeded through the outer-sphere radical group transfer pathway (Scheme 6.21).

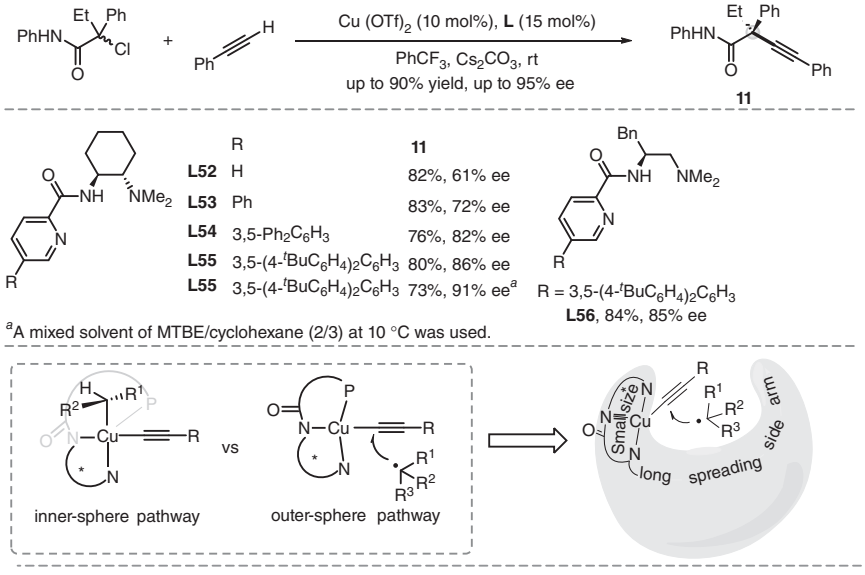


**Scheme 6.21** New chiral anionic N,N,N-ligands for the coupling of tertiary alkyl halides.

The chiral unnatural α,α-disubstituted amino acids are a class of valuable building blocks in the fields of biochemistry and medicinal chemistry. In 2023, the Liu group achieved an enantioconvergent radical C—N cross-coupling of tertiary alkyl halides with sulfoximines using an N,N,N-ligand (**L57**) that possesses a long spreading side arm [75]. It exhibits a broad substrate scope, accommodating various tertiary alkyl halides and sulfoximines, and delivers good yields and enantioselectivity. The resulting chiral C—N cross-coupling products can be easily converted to α,α-disubstituted α-amino amide, amino acid ester, 1,2-amino alcohol, and 1,2-diamine using a straightforward procedure (Scheme 6.22).

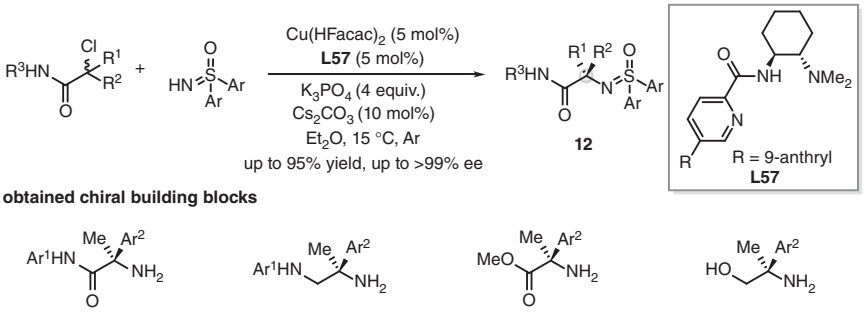


**Scheme 6.22** The enantioconvergent C($sp^3$)—N coupling of tertiary alkyl halides with sulfoximines.

### 6.2.5 Other Ligands in Copper-Catalyzed Enantioconvergent Radical Cross-Coupling Reactions

Alcohols and phenols belong to a significant category of oxygen-based nucleophiles that react with alkyl halides. This reaction of alcohols and alkyl halides can be traced back to the development of the Williamson ether synthesis in 1850. However, achieving asymmetric synthesis of chiral ethers presents a major challenge due to the prevalence of strong $S_N2$ background reactions. In 2023, the Fu research group made a significant breakthrough by developing a copper-catalyzed enantioconvergent C($sp^3$)—O cross-coupling method [76]. This method involved the reaction of α-haloamides with various alcohols and phenols using an anionic bisoxazoline ligand. Remarkably, this reaction proceeded under mild conditions and yielded valuable chiral α-oxylamides with diverse functional groups in high yields and enantioselectivity. Mechanistic studies revealed that the in situ generated copper complex, in the presence of a base, facilitated the reduction of the alkyl halide to a prochiral radical, leading to the formation of the $LCu^{II}Br$ complex. Subsequently, a ligand substitution reaction occurred between the $LCu^{II}Br$ complex and the O-nucleophile, followed by the trapping of alkyl radicals to form a Cu(III) species. Furthermore, the same Cu(III) species could be obtained from the aziridinone intermediate through the reaction with LCu(I) and O-nucleophiles. Finally, the last step involved reductive elimination to access the chiral products and regenerate the LCu(I) complex (Scheme 6.23).

Zhang and colleagues have accomplished the asymmetric radical C($sp^3$)—C(sp) cross-coupling of α-bromoamides with terminal alkynes utilizing the copper/chiral bisoxazoline diphenylalanine (BOPA) catalyst [77]. Their mechanistic analysis suggests that the chiral ligand **L59** and copper formed an anionic copper complex in the presence of a base to enhance the reducing capability of the copper catalyst, thereby initiating the reaction. The formation of the C($sp^3$)—C(sp) bond is proposed to occur through either a Cu(III) complex intermediate or an out-of-cage pathway. The reaction displays a wide range of β,γ-alkynyl amides with high enantioselectivity; however, the alkyl electrophiles are limited to α-bromoamides, possibly due to the weak reducing capacity of the copper complex. This limitation has been previously

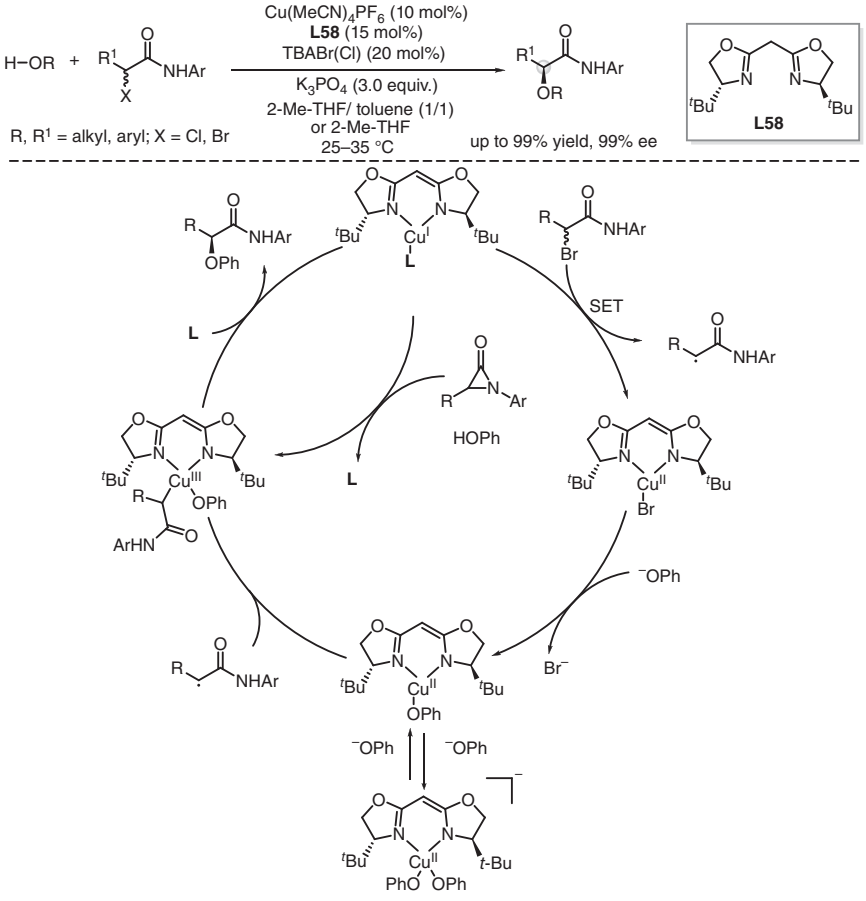


**Scheme 6.23** Enantioconvergent radical C($sp^3$)—O cross-coupling of O-nucleophiles.

observed in their cross-coupling reaction of benzyl bromides and azoles, which required the assistance of photocatalysis for initiation. They have also used a similar Cu/BOPA system to achieve the enantioconvergent C($sp^3$)—C(sp) cross-coupling of tertiary alkyl bromides with alkynes [78]. This reaction could tolerate diverse tertiary alkyl bromides and terminal alkynes (Scheme 6.24).

In the year 2022, the Liu group developed a unique chiral *N*-donor hybrid ligand (**L61**), which incorporates acyclic guanidine, amide, and pyridine motifs. They utilized this ligand in the copper-catalyzed radical enantioconvergent C($sp^3$)—C(sp) cross-coupling reaction [79]. The reaction resulted in the coupling products with high yields and enantioselectivity. The guanidine, amide, and pyridine units play a critical role in coordinating with Cu(I) to form an active complex. This complex facilitates the reduction of alkyl halides to prochiral radical species (Scheme 6.25).

The Ito group has made a significant breakthrough in the enantioconvergent C($sp^3$)—B cross-coupling of racemic benzyl chlorides [80]. Their study involved

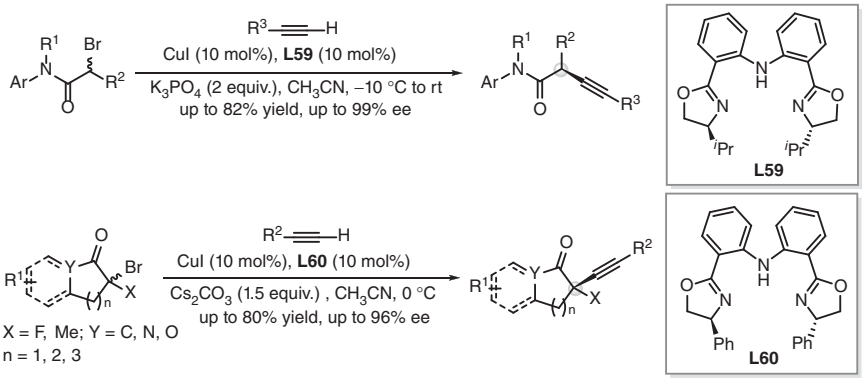


**Scheme 6.24** Zhang's BOPA-ligand for enantioconvergent C($sp^3$)—C(sp) cross-coupling.

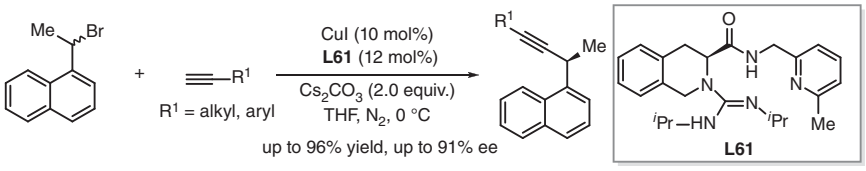


**Scheme 6.25** The chiral guanidine hybrid ligand for enantioconvergent cross-coupling.

the utilization of copper/chiral bisphosphine ligands, resulting in the formation of corresponding chiral benzylboronates. The success of this transformation was attributed to the development of a chiral quinoxaline-based bisphosphine ligand, denoted as **L62**, which was designed with quadrant-by-quadrant structure modulation. This ligand was found to engage in noncovalent interactions with the benzyl radical, thereby achieving a high ee. Based on their comprehensive mechanistic investigation, they proposed that the catalytically active species responsible for the enantioconvergent radical transformation is the alkoxide-coordinated $LCu^{I}Bpin$ complex (Scheme 6.26).

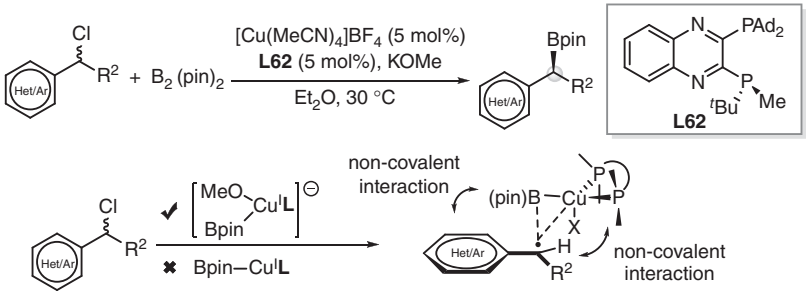


**Scheme 6.26** Ito's enantioconvergent C($sp^3$)—B cross-coupling.

## 6.3 Conclusion

The copper-catalyzed enantioconvergent radical cross-coupling has emerged as a potent strategy in chiral molecule synthesis. However, the strategy encounters the challenging oxidative addition step due to the relatively weak reducing capacity of copper. To address this challenge, it is imperative to develop innovative strategies that overcome the hurdles of reaction initiation. This chapter summarizes the recent advancements in copper-catalyzed enantioconvergent radical cross-coupling, focusing on the concept of ligand design for reaction initiation. Liu and others have made contributions by developing multidentate anionic ligands to enhance the reducing capacity of copper complexes and convert alkyl halides into prochiral radicals. This approach has enabled the coupling of activated secondary/tertiary alkyl halides with diverse nucleophiles.

Despite significant advancements in this field, many challenges remain that must be overcome. While the enantioconvergent cross-coupling has seen successful utilization of various nucleophiles such as B, C, N, O, P, S, and others, the asymmetric cross-coupling of C—F and C—Si remains rare. In terms of electrophiles, most reactions have been focused on activated alkyl halides that give rise to π-stabilized alkyl radicals. The exploration of unactivated alkyl halides is challenging due to the lack of stabilization. Notably, the understanding of the enantio-determining bond formation mechanism significantly lags. The collaboration of control experiments with diverse techniques, such as electron paramagnetic resonance spectroscopy, X-ray analysis, and DFT calculation, is essential for elucidating the mechanism. Thus, the development of more catalytic systems is a longstanding goal. Both the strategies of photoinduced reactions and the design of novel ligand systems represent effective methodologies for initiating reactions and controlling enantioselectivity. Additionally, it would be advantageous to explore other tactics, such as electrochemistry, to further expand the reaction scope.

## References


1 Miyaura, N. and Buchwald, S.L. (2002). *Cross-Coupling Reactions: A Practical Guide*, vol. 219. Germany: Springer.
2 Buskes, M.J. and Blanco, M.J. (2020). *Molecules* 25: 3493.
3 Brown, D.G. and Bostrom, J. (2016). *J. Med. Chem.* 59: 4443–4458.
4 Nobuyoshi, Y. (2002). *J. Organomet. Chem.* 253: 279–287.
5 Johansson Seechurn, C.C., Kitching, M.O., Colacot, T.J., and Snieckus, V. (2012). *Angew. Chem. Int. Ed.* 51: 5062–5085.
6 De Meijere, A., Bräse, S., and Oestreich, M. (2014). *Metal Catalyzed Cross-coupling Reactions and More*. Weinheim, Germany: Wiley-VCH.
7 Ruiz-Castillo, P. and Buchwald, S.L. (2016). *Chem. Rev.* 116: 12564–12649.
8 Bhat, V., Welin, E.R., Guo, X., and Stoltz, B.M. (2017). *Chem. Rev.* 117: 4528–4561.

**9** Rössler, S.L., Petrone, D.A., and Carreira, E.M. (2019). *Acc. Chem. Res.* 52: 2657–2672.
**10** Sidera, M. and Fletcher, S.P. (2015). *Nat. Chem.* 7: 935–939.
**11** Li, B., Li, T., Aliyu, M.A. et al. (2019). *Angew. Chem. Int. Ed.* 58: 11355–11359.
**12** Wendlandt, A.E., Vangal, P., and Jacobsen, E.N. (2018). *Nature* 556: 447–451.
**13** Zhang, X., Ren, J., Tan, S.M. et al. (2019). *Science* 363: 400–404.
**14** Rudolph, A. and Lautens, M. (2009). *Angew. Chem. Int. Ed.* 48: 2656–2670.
**15** Kambe, N., Iwasaki, T., and Terao, J. (2011). *Chem. Soc. Rev.* 40: 4937–4947.
**16** Fischer, C. and Fu, G.C. (2005). *J. Am. Chem. Soc.* 127: 4594–4595.
**17** Mao, J., Liu, F., Wang, M. et al. (2014). *J. Am. Chem. Soc.* 136: 17662–17668.
**18** Jin, M., Adak, L., and Nakamura, M. (2015). *J. Am. Chem. Soc.* 137: 7128–7134.
**19** Cherney, A.H., Kadunce, N.T., and Reisman, S.E. (2015). *Chem. Rev.* 115: 9587–9652.
**20** Choi, J. and Fu, G.C. (2017). *Science* 356: eaaf7230.
**21** Fu, G.C. (2017). *ACS Cent. Sci.* 3: 692–700.
**22** Mondal, S., Dumur, F., Gigmes, D. et al. (2022). *Chem. Rev.* 122: 5842–5976.
**23** Kochi, J.K. (1974). *Acc. Chem. Res.* 7: 351–360.
**24** McCann, S.D. and Stahl, S.S. (2015). *Acc. Chem. Res.* 48: 1756–1766.
**25** Stanley, L.M. and Sibi, M.P. (2008). *Chem. Rev.* 108: 2887–2902.
**26** Ribelli, T.G., Matyjaszewski, K., and Poli, R. (2018). *J. Coord. Chem.* 71: 1641–1668.
**27** Wang, F., Chen, P., and Liu, G. (2018). *Acc. Chem. Res.* 51: 2036–2046.
**28** Gu, Q.-S., Li, Z.-L., and Liu, X.-Y. (2020). *Acc. Chem. Res.* 53: 170–181.
**29** Li, Z.-L., Fang, G.-C., Gu, Q.-S., and Liu, X.-Y. (2020). *Chem. Soc. Rev.* 49: 32–48.
**30** Hossain, A., Bhattacharyya, A., and Reiser, O. (2019). *Science* 364: eaav9713.
**31** Le, C., Chen, T.Q., Liang, T. et al. (2018). *Science* 360: 1010–1014.
**32** Zhang, L., Israel, E.M., Yan, J., and Ritter, T. (2022). *Nat. Synth.* 1: 376–381.
**33** Creutz, S.E., Lotito, K.J., Fu, G.C., and Peters, J.C. (2012). *Science* 338: 647–650.
**34** Uyeda, C., Tan, Y., Fu, G.C., and Peters, J.C. (2013). *J. Am. Chem. Soc.* 135: 9548–9552.
**35** Ziegler, D.T., Choi, J., Munoz-Molina, J.M. et al. (2013). *J. Am. Chem. Soc.* 135: 13107–13112.
**36** Tan, Y., Muñoz-Molina, J.M., Fu, G.C., and Peters, J.C. (2014). *Chem. Sci.* 5: 2831–2835.
**37** Bissember, A.C., Lundgren, R.J., Creutz, S.E. et al. (2013). *Angew. Chem. Int. Ed.* 52: 5129–5133.
**38** Do, H.Q., Bachman, S., Bissember, A.C. et al. (2014). *J. Am. Chem. Soc.* 136: 2162–2167.
**39** Ratani, T.S., Bachman, S., Fu, G.C., and Peters, J.C. (2015). *J. Am. Chem. Soc.* 137: 13902–13907.
**40** Johnson, M.W., Hannoun, K.I., Tan, Y. et al. (2016). *Chem. Sci.* 7: 4091–4100.
**41** Ahn, J.M., Ratani, T.S., Hannoun, K.I. et al. (2017). *J. Am. Chem. Soc.* 139: 12716–12723.
**42** Ahn, J.M., Peters, J.C., and Fu, G.C. (2017). *J. Am. Chem. Soc.* 139: 18101–18106.
**43** Kainz, Q.M., Matier, C.D., Bartoszewicz, A. et al. (2016). *Science* 351: 681–684.

**44** Cho, H., Suematsu, H., Oyala, P.H. et al. (2022). *J. Am. Chem. Soc.* 144: 4550–4558.

**45** Chen, C., Peters, J.C., and Fu, G.C. (2021). *Nature* 596: 250–256.

**46** Li, C., Chen, B., Ma, X. et al. (2021). *Angew. Chem. Int. Ed.* 60: 2130–2134.

**47** Patten, T.E. and Matyjaszewski, K. (1999). *Acc. Chem. Res.* 32: 895–903.

**48** Leophairatana, P., Samanta, S., De Silva, C.C., and Koberstein, J.T. (2017). *J. Am. Chem. Soc.* 139: 3756–3766.

**49** Lin, J.-S., Dong, X.-Y., Li, T.-T. et al. (2016). *J. Am. Chem. Soc.* 138: 9357–9360.

**50** Cheng, Y.-F., Dong, X.-Y., Gu, Q.-S. et al. (2017). *Angew. Chem. Int. Ed.* 56: 8883–8886.

**51** Li, X.-T., Gu, Q.-S., Dong, X.-Y. et al. (2018). *Angew. Chem. Int. Ed.* 57: 7668–7672.

**52** Sladojevich, F., Trabocchi, A., Guarna, A., and Dixon, D.J. (2011). *J. Am. Chem. Soc.* 133: 1710–1713.

**53** Ortín, I. and Dixon, D.J. (2014). *Angew. Chem. Int. Ed.* 53: 3462–3465.

**54** de la Campa, R., Ortín, I., and Dixon, D.J. (2015). *Angew. Chem. Int. Ed.* 54: 4895–4898.

**55** Manzano, R., Datta, S., Paton, R.S., and Dixon, D.J. (2017). *Angew. Chem. Int. Ed.* 56: 5834–5838.

**56** Dong, X.-Y., Zhang, Y.-F., Ma, C.-L. et al. (2019). *Nat. Chem.* 11: 1158–1166.

**57** Xia, H.-D., Li, Z.-L., Gu, Q.-S. et al. (2020). *Angew. Chem. Int. Ed.* 59: 16926–16932.

**58** Dong, X.-Y., Cheng, J.-T., Zhang, Y.-F. et al. (2020). *J. Am. Chem. Soc.* 142: 9501–9509.

**59** Dong, X.-Y., Zhan, T.-Y., Jiang, S.-P. et al. (2021). *Angew. Chem. Int. Ed.* 60: 2160–2164.

**60** Zhang, Z.-H., Dong, X.-Y., Du, X.-Y. et al. (2019). *Nat. Commun.* 10: 5689.

**61** Liu, L., Guo, K.-X., Tian, Y. et al. (2021). *Angew. Chem. Int. Ed.* 60: 26710–26717.

**62** Guo, R., Sang, J., Xiao, H. et al. (2022). *Chin. J. Chem.* 40: 1337–1345.

**63** Jiang, S.-P., Dong, X.-Y., Gu, Q.-S. et al. (2020). *J. Am. Chem. Soc.* 142: 19652–19659.

**64** Su, X.-L., Ye, L., Chen, J.-J. et al. (2021). *Angew. Chem. Int. Ed.* 60: 380–384.

**65** Zhang, Y.-F., Dong, X.-Y., Cheng, J.-T. et al. (2021). *J. Am. Chem. Soc.* 143: 15413–15419.

**66** Wang, L.-L., Zhou, H., Cao, Y.-X. et al. (2023). *Nat. Synth.* 2: 430–438.

**67** Tian, Y., Li, X.-T., Liu, J.-R. et al. (2024). *Nat. Chem.* 16: 466–475.

**68** Chen, J.-J., Fang, J.-H., Du, X.-Y. et al. (2023). *Nature* 618: 294–300.

**69** Chen, J.-J., Zhang, J.-Y., Fang, J.-H. et al. (2023). *J. Am. Chem. Soc.* 145: 14686–14696.

**70** Zheng, J.-J., Liu, W.-L., Gu, Q.-S. et al. (2023). *Precis. Chem.* 1: 576–582.

**71** Wang, P.-F., Yu, J., Guo, K.-X. et al. (2022). *J. Am. Chem. Soc.* 144: 6442–6452.

**72** Wang, F.-L., Liu, L., Yang, C.-J. et al. (2022). *Angew. Chem. Int. Ed.* 62: e202214709.

**73** Wang, Z., Yang, Z.P., and Fu, G.C. (2021). *Nat. Chem.* 13: 236–242.

**74** Wang, F.-L., Yang, C.-J., Liu, J.-R. et al. (2022). *Nat. Chem.* 14: 949–957.

**75** Zhang, Y.-F., Wang, J.-H., Yang, N.-Y. et al. (2023). *Angew. Chem. Int. Ed.* 62: e202302983.
**76** Chen, C. and Fu, G.C. (2023). *Nature* 618: 301–307.
**77** Mo, X., Chen, B., and Zhang, G. (2020). *Angew. Chem. Int. Ed.* 59: 13998–14002.
**78** Mo, X., Huang, H., and Zhang, G. (2022). *ACS Catal.* 12: 9944–9952.
**79** Li, J., Ning, L., Tan, Q. et al. (2022). *Org. Chem. Front.* 9: 6312–6318.
**80** Iwamoto, H., Endo, K., Ozawa, Y. et al. (2019). *Angew. Chem. Int. Ed.* 58: 11112–11117.

# 7

# Manganese-Catalyzed Asymmetric Radical Reactions

*Min Cao[1,2], Huai-Ri Sun[2], and Lei Liu[1]*

[1] *School of Chemistry and Chemical Engineering, Shandong University, Jinan, China*
[2] *School of Pharmaceutical Sciences and Institute of Materia Medica, Shandong First Medical University, Jinan, China*

## 7.1 Introduction

The emerging field of asymmetric catalysis has shifted toward research on first-row transition elements due to the unique property of environmental friendliness and relative abundance in the Earth's crust. According to this view, manganese stands out as an attractive candidate for catalysis. Apart from the fact that it is the third most abundant metal in the Earth's crust, it is also non-toxic and biocompatible, playing important roles in metabolism and antioxidant systems [1–6]. Moreover, the valence electron configuration of elemental manganese is $3d^5 4s^2$, and the variable oxidation states of manganese (−3 to +7) endow it with tremendous potential in modern organic synthesis [7–9].

Chiral manganese catalysts have played an important role in the recent advances in asymmetric catalysis owing to the cost-effective and sustainable benefit [10–18]. Among them, manganese-catalyzed enantioselective radical reactions hold great value, opening new avenues in the field. The reactions occur under mild reaction conditions and show good functional group tolerance. However, the high reactivity of radicals, which are generally planar or nearly planar intermediates, poses challenges in controlling both reactivity and enantioselectivity in radical transformations [19–22]. Despite these challenges, the development of diverse chiral ligands has led to considerable achievements in manganese-catalyzed asymmetric radical reactions [15–18].

In this chapter, we will summarize the development of manganese-catalyzed asymmetric radical reactions, which have typically focused on enantioselective oxidation to date. They are divided into the following three categories based on reaction types, including: (i) asymmetric transformations, which involve the conversion of prochiral substrates to chiral products; (ii) oxidative desymmetrizations, where symmetrical molecules are converted into chiral products; and (iii) kinetic resolutions (KRs), which involve the enantio-differentiating transformation of one enantiomer of the given racemate.

## 7.2 Manganese-Catalyzed Asymmetric Transformation

### 7.2.1 Manganese-Catalyzed Enantioselective C—H Bond Hydroxylation

Chiral transition metal complexes have contributed to the progress in enantioselective C—H bond oxidation. Among them, chiral manganese-catalyzed enantioselective C—H bond hydroxylation has received considerable attention, which typically proceeds through a radical rebound mechanism involving hydrogen atom abstraction (HAA) and the subsequent oxygen rebound (Scheme 7.1) [23–26].

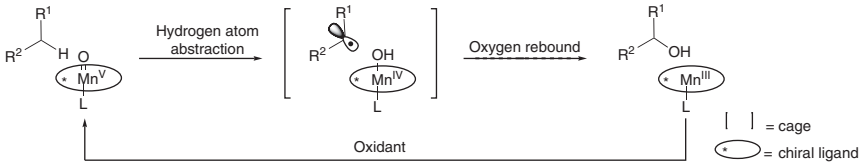


**Scheme 7.1** The radical rebound mechanism for manganese-catalyzed C—H hydroxylation.

In 1990, Groves and co-workers reported the enantioselective hydroxylation reaction of benzylic C—H bonds utilizing sophisticated manganese tetraphenylporphyrin complex **C1** as a catalyst (Scheme 7.2) [27]. The enantiocontrol was hypothesized to originate from the selectivity of the hydrogen abstraction step and the relative rate of radical cage collapse. As depicted in Scheme 7.2, the orientation of the binaphthyl bridge was demonstrated to be pivotal for enantioselectivity,

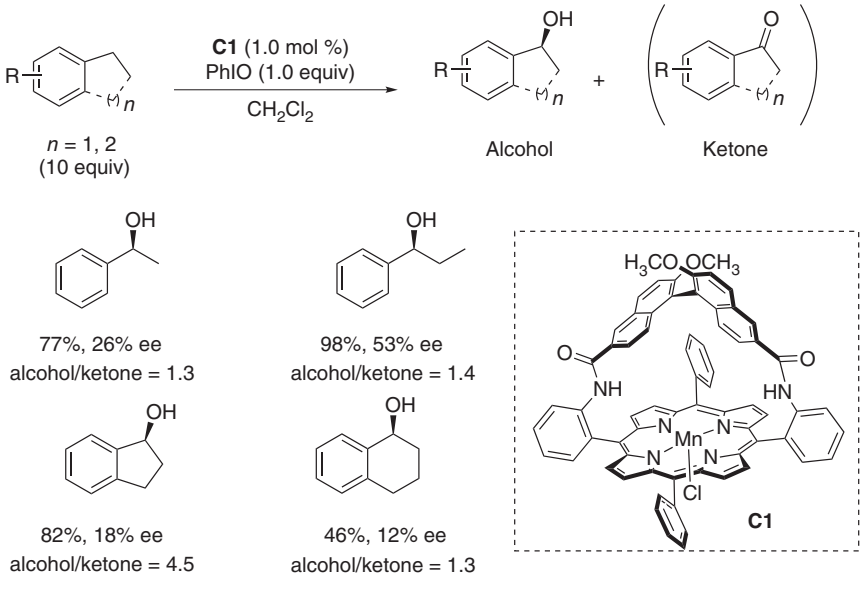


**Scheme 7.2** Chiral Mn(III)–porphyrin complex catalyzed enantioselective benzylic C—H hydroxylation.

as it might provide noncovalent interactions between catalyst and substrate for enantiocontrol. The hydroxylation of a series of benzylic compounds yielded chiral alcohol products with moderate enantiomeric excess (12–53% ee). Additionally, ketones were always obtained as the obvious by-products in every hydroxylation reaction. Although the chemo- and enantioselectivities of this asymmetric C—H hydroxylation were not optimal, these pioneering results are valuable for the design of more efficient chiral catalysts.

In 1998, the Katsuki group found that concave (salen)manganese (III) complexes exhibited promising enantioselection properties in the hydroxylation of substituted ethylbenzenes with iodosobenzene as oxidant (Scheme 7.3) [28]. Under the optimized conditions, the corresponding chiral alcohols were obtained from benzylic C—H oxidation with modest yields and relatively good to high ee. An experimental investigation revealed that high-viscosity solvent provided better enantiocontrol. This might be attributed to the formation of a stout solvent cage, which effectively suppressed undesired radical escape. Further competitive deuterium kinetic isotope effect ($k_H/k_D = 4.6 \pm 1$) indicated that hydrogen atom abstraction might be involved in the rate-determining step.

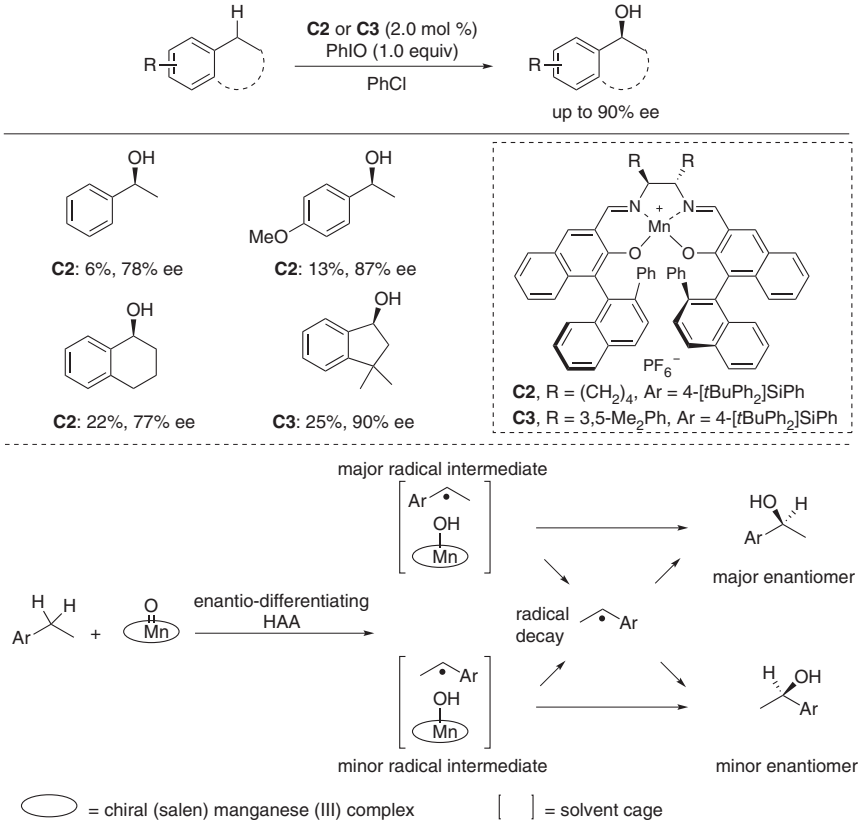


**Scheme 7.3** Mn(III)–salen complexes catalyzed enantioselective C—H oxidation.

In 2004, the Murahashi group synthesized Mn(III)–salen complex **C4** bearing a chiral binaphthyl strapping unit for enantioselective hydroxylation of indane (Scheme 7.4) [29]. The reaction required a much excess of indane substrate, affording corresponding alcohol in 20% yield and 34% ee. The crucial factor enhancing the hydroxylation efficiency and enantioselectivity was the compulsory use of 1,5-dicyclohexylimidazole as a donor additive. This additive effectively blocks the unstrapped side of the catalyst, thereby guiding the oxo manganese species into the chiral cavity.

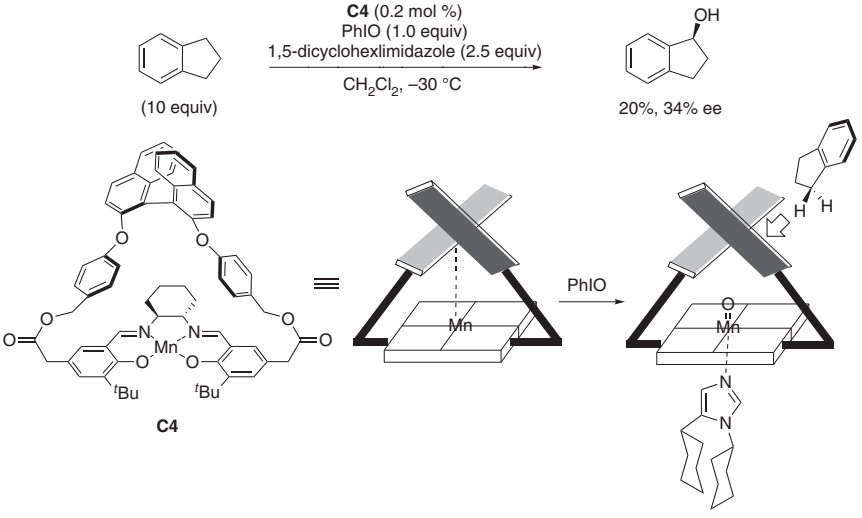


**Scheme 7.4** Enantioselective hydroxylation of indane with a bridged (salen)manganesecomplex.

The pursuit of environmentally sustainable catalyst systems for asymmetric transformation represents one of the ultimate objectives of modern organic chemistry. In 2012, Simonneaux and co-workers made important strides in this area by developing an efficient enantioselective hydroxylation reaction (Scheme 7.5) [30]. This reaction was catalyzed by a water-soluble chiral manganese porphyrin **C5** with $H_2O_2$ as the oxidant. The oxidation proceeded with high conversions (typically 88–100%) and moderate enantioselectivities (32–57% ee). Notably, to achieve relatively high yields

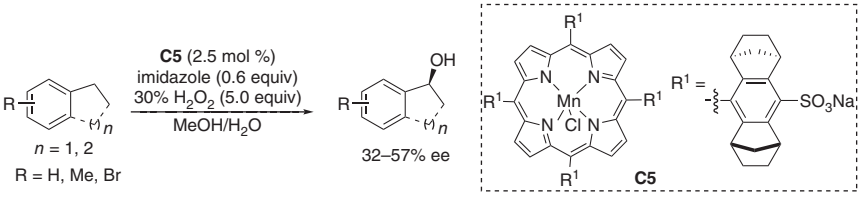


**Scheme 7.5** Mn(III)–porphyrin complex catalyzed C–H hydroxylation with $H_2O_2$.

and enantioselectivities, $H_2O_2$ and imidazole additive need to be added slowly to the reaction mixture over a period of 1 h at 25 °C. This operation process is critical for optimizing the reaction's performance.

Aminopyridine ligands have emerged as appealing frameworks in asymmetric catalysis, and the corresponding metal complexes have demonstrated versatility and efficacy in catalytic asymmetric oxidation reactions [31, 32]. Bryliakov and co-workers reported that chiral bis-amino-bis-pyridine manganese complexes were capable of catalyzing the asymmetric oxidation of arylalkanes with $H_2O_2$ in the presence of carboxylic acid additives (Scheme 7.6) [33]. The use of suitable chiral carboxylic acid additives (*N*-Boc-*L*-proline) proved to be crucial to enhancing the enantioselectivity (up to 89% ee). The improvement might be attributed to the chiral additive's ability to interact with the catalyst and thus influence the stereochemical

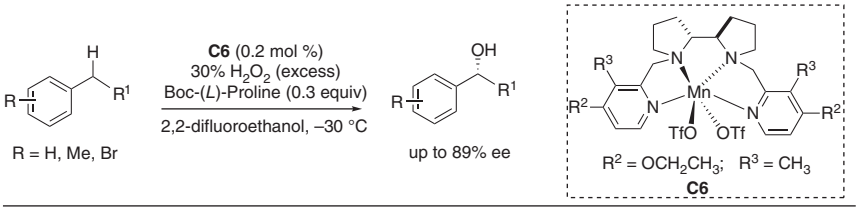


(a)

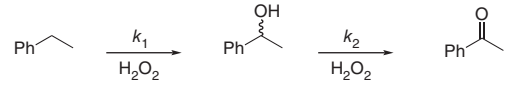


| Solvent | Maximum yield, % (at conversion, %) | % ee at maximum yield | $k_1/k_2$ |
|---|---|---|---|
| $CH_3CN$ | 6.5 (19) | 39 | 0.07 |
| | 17 (51) | 38 | 0.24 |
| | 33 (58) | 61 | 0.84 |
| 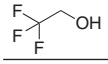 | 45 (75) | 59 | 1.61 |

(b)

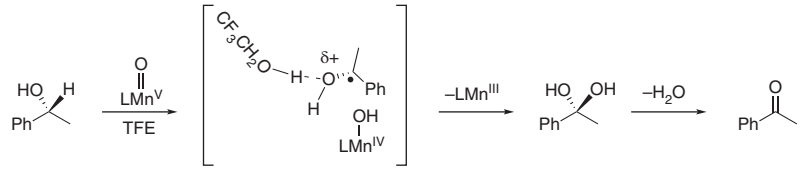


Deactivation of adjacent C–H groups in alcohols

**Scheme 7.6** Manganese-catalyzed enantioselective hydroxylation of arylalkanes using fluorinated alcohol as a solvent. (a) The solvent effect on the reaction, (b) proposed working model of the effect trifluoroethanol.

outcome of the reaction. They further performed detailed mechanistic studies to understand the reaction pathway. The observed primary kinetic isotope effect ($k_H/k_D = 3.5–3.6$) revealed that C—H bond cleavage might be involved in the rate-determining step. Additionally, they found that fluorinated solvents played a crucial role in suppressing the undesired overoxidation (Scheme 7.6a), which might be ascribed to the hydrogen bonding between the alcohol product and the solvent reducing the nucleophilicity of alcohol (Scheme 7.6b). In subsequent studies, the Bryliakov group expanded the reaction scope to asymmetric hydroxylation of a range of 3,4-dihydrocoumarin and 3,4-dihydroquinolinone derivatives [34].

The Bach group has demonstrated that hydrogen-bonding catalysts are effective for enantioselective C—H hydroxylation (Scheme 7.7) [35]. They designed a manganese porphyrin complex featuring a remote binding site that can provide two-point hydrogen-bonding interactions between the substrate and the catalyst. The asymmetric oxidation of 3,4-dihydroquinolones with iodosylbenzene proceeded at the $C^4$ methylene moiety of the heterocyclic skeleton with high enantioselectivity (87–99% ee). The method is compatible with a range of functional groups, including ether, trifluoromethylsulfonyloxyl, and halide (Scheme 7.7a). The enantiocontrol decreased remarkably (5% ee) when the NH group on the substrate was replaced by an NMe one, supporting the hypothesis that the hydrogen bonding should be crucial to the high selectivity (Scheme 7.7b). Further studies showed that the substrate scope could be extended to 3-alkyl and 3-benzylquinolones [36].

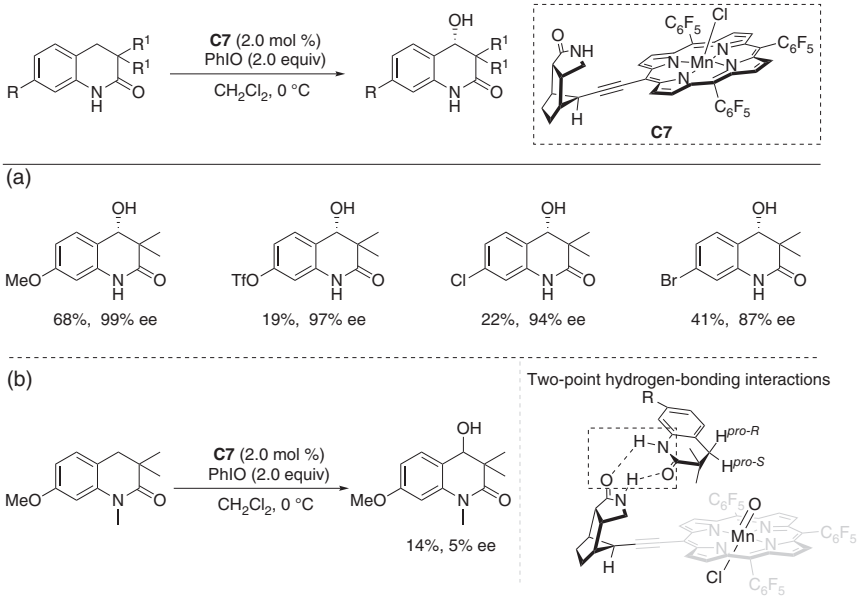


**Scheme 7.7** Manganese-catalyzed enantioselective hydroxylation of 3,4-dihydroquinolones enabled by hydrogen-bonding interaction. (a) Representative examples, (b) control reaction.

### 7.2.2 Manganese-Catalyzed Enantioselective C—H Azidation

Besides hydroxylation, the radical rebound strategy is also applicable to asymmetric C—H azidation reactions. In this aspect, the Groves group reported the first investigation on asymmetric C—H azidation catalyzed by Jacobsen-type Mn(salen) complex in the presence of PhIO as an oxidant and $NaN_3$ as azide source (Scheme 7.8) [37]. While only one isolated example of specific celestolide was illustrated with moderate chemo- and enantioselectivities (60% yield, 70% ee), the pioneering exploration demonstrated the capability of manganese catalysts for enantioselective radical substitution of C—H bonds with C—$N_3$ bonds.

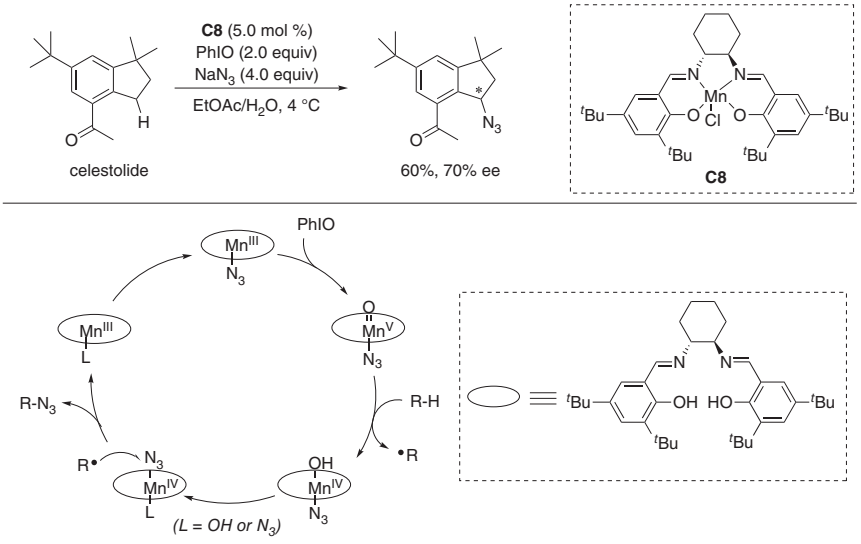


**Scheme 7.8** Chiral manganese-salen-catalyzed enantioselective C—H azidation of celestolide.

Inspired by Groves' seminal work, Jiang and co-workers reported that chiral metallosalen-based ZrMOFs (MOFs = metal–organic frameworks) can catalyze asymmetric C—H azidation reactions (Scheme 7.9) [38]. Several arylalkanes were competent components, providing corresponding benzylic azides with good chemo- and enantioselectivities. The observed selectivities were ascribed to the rigid framework and well-decorated catalytic microenvironment of MOFs.

Later, Liu and co-workers described the manganese-catalyzed enantioselective radical benzylic C—H azidation of indoline compounds, rapidly furnishing a series of structurally diverse $C^3$-azido-substituted indolines (Scheme 7.10) [39]. The key of the work lies in the discovery of a suitable Mn-salen catalyst **C10** with a matched combination of central and axial chiralities. By utilizing this well-elaborated chiral manganese catalyst, both prochiral indolines and racemic $C^3$-alkyl-substituted indolines are suitable substrates, and corresponding secondary and tertiary azides are obtained in good yields and good-to-excellent enantioselectivities (up to 95% ee) (Scheme 7.10a). Tetrahydroquinone-type substrates are also demonstrated with good

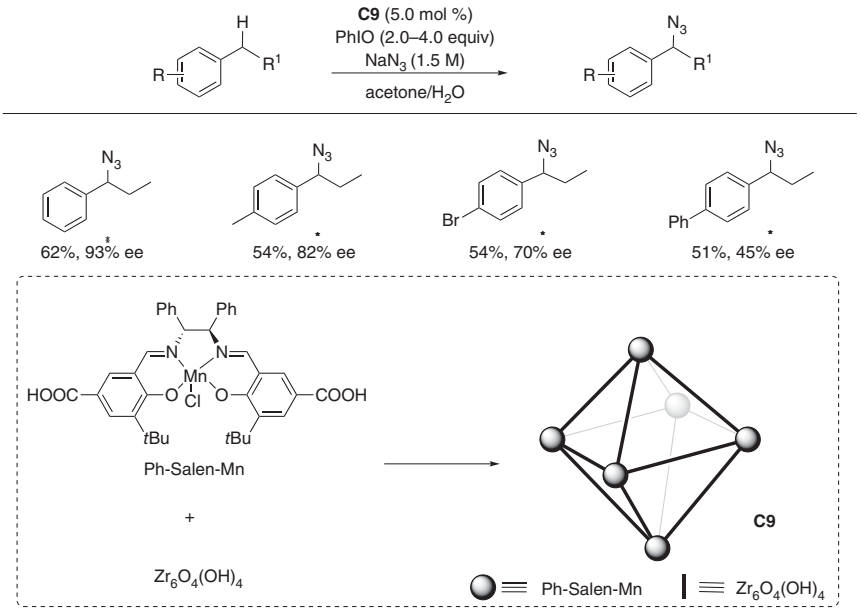


**Scheme 7.9** Chiral zirconium–metallosalen frameworks for enantioselective benzylic C–H azidation.

chemoselectivity together with moderate ee. A radical clock experiment was performed to prove that the carbon-centered radical might be generated (Scheme 7.10b). ESI-MS studies were conducted to help understand the role of the manganese complex in the catalytic cycle. The reaction proceeds via a sequence of hydrogen atom abstraction followed by enantio-determining radical azidation (Scheme 7.10c). DFT calculations reveal the origin of stereoselectivity from a $\pi\cdots\pi$ interaction between chiral manganese catalyst and alkyl radical intermediate (Scheme 7.10d).

## 7.3 Manganese-Catalyzed Enantioselective Desymmetrization Through C—H Bond Oxidation

### 7.3.1 C—H Bond Oxidation to Alcohols

Catalytic desymmetrization of symmetrical compounds, such as prochiral and meso moieties, via enantiotopic selective oxidation of C—H bonds provides a practical platform for the synthesis of optically pure compounds with single to multiple stereogenic centers by simple manipulation. In this context, chiral manganese complexes have been identified as appealing catalysts to achieve this objective.

In 1988, Katsuki and coworkers pioneered the studies on Mn-salen complex catalyzed enantioselective C—H oxidation of meso-pyrrolidine and meso-tetrahydrofuran derivatives (Scheme 7.11) [40, 41]. By adopting the oxidative desymmetrization strategy, they developed an efficient synthetic methodology to access chiral lactams and lactones, which typically serve as building blocks in

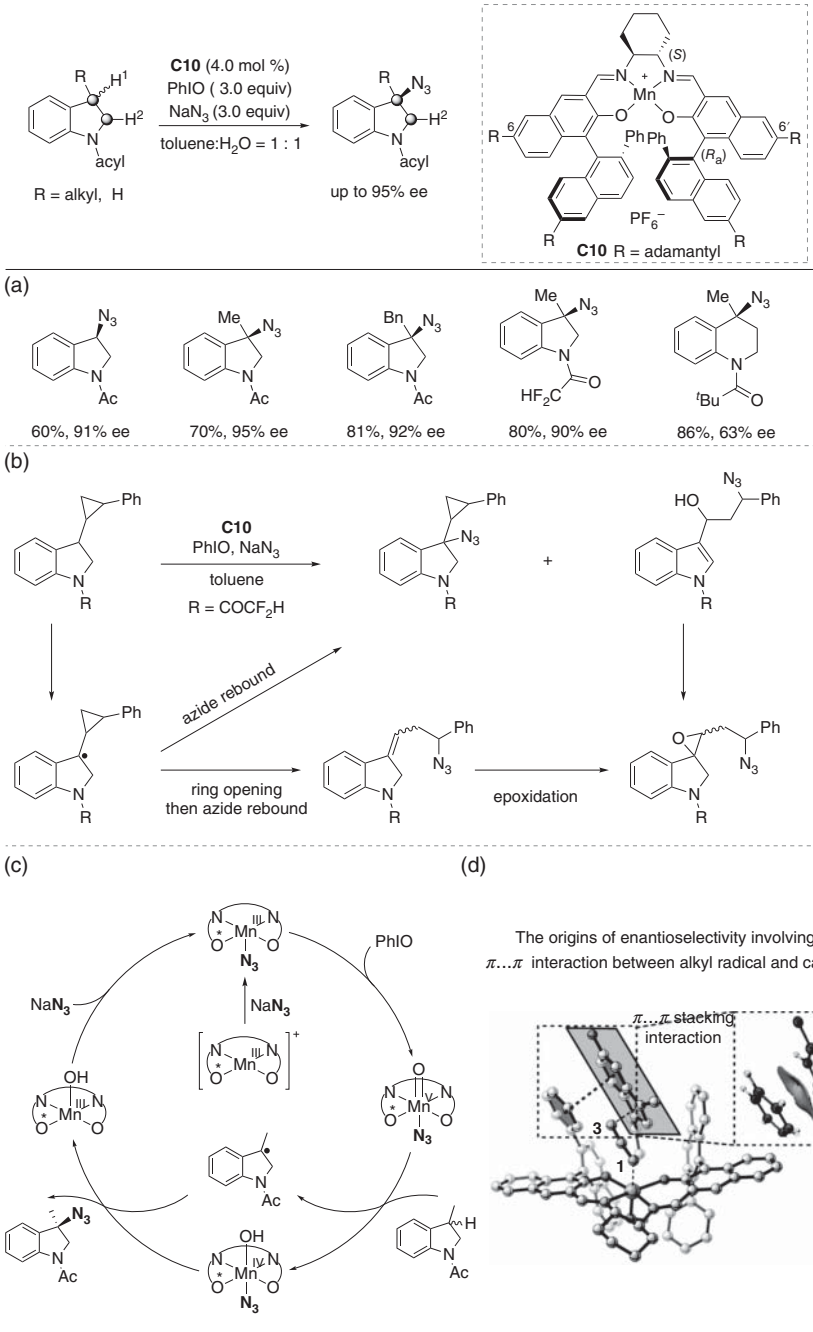


**Scheme 7.10** Manganese-catalyzed site- and enantioselective benzylic C—H azidation of indolines. (a) Selected examples, (b) radical probe, (c) a plausible mechanistic pathway, (d) interaction in stereo-determining state structure.

many biological molecules. Notably, carbon atoms adjacent to heteroatoms were preferentially oxidized to corresponding chiral hemiaminals and lactols, which were further oxidized by the Jones reagent providing chiral lactams or lactones in moderate-to-good enantioselectivity.

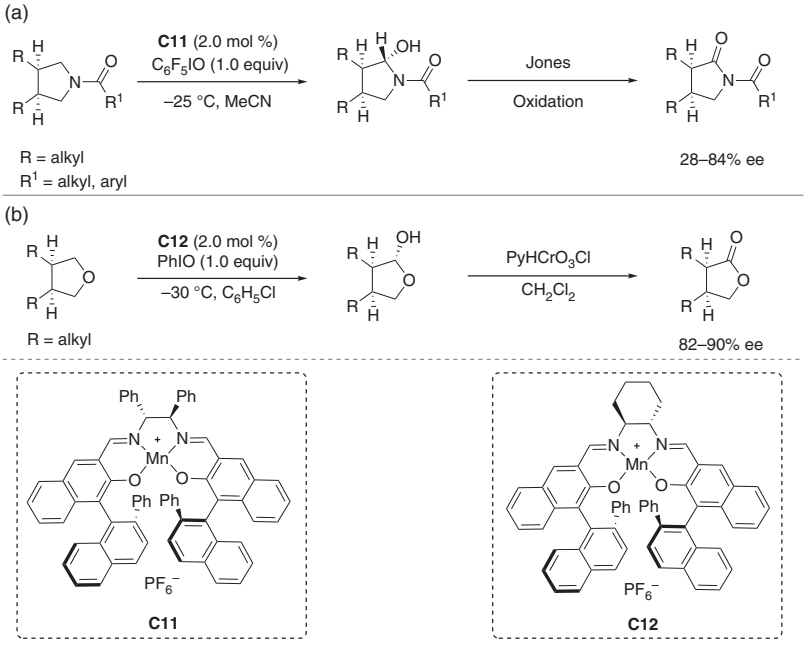


**Scheme 7.11** Enantioselective desymmetrization of meso-pyrrolidine and tetrahydrofuran derivatives catalyzed by Mn-salen complexes. (a) Asymmetric oxidative desymmetrization of meso-pyrrolidine, (b) asymmetric oxidative desymmetrization of meso-tetrahydrofuran.

In 2020, Sun and co-workers designed aminopyridine manganese complex **C13**, which catalyzed asymmetric hydroxylation of indane-derived symmetrical ketones with $H_2O_2$ as an oxidant in the presence of 2,2-dimethylbutanoic acid as an additive (Scheme 7.12) [42]. The enantioselective oxidation proceeded smoothly, providing corresponding benzylic alcohols with good-to-excellent diastereo- and enantioselectivities (up to 95% ee, up to >95 : 5 dr). Furthermore, spirocyclic 2,3-dihydroquinolin-4(1*H*)-ones were suitable substrates with up to 95% ee. Importantly, based on experimental and density functional theory (DFT) evidence, they proposed that the carbonyl directing group appears to be crucial to enhance selectivity due to the possible hydrogen bonding interaction between the Mn(V)-oxo species, 2,2,2-trifluoroethanol, and the carbonyl group (Scheme 7.12b, c).

In 2023, Costas and co-workers disclosed a tetradentate aminopyridine-based manganese complex **C14** that catalyzes asymmetric hydroxylation of unactivated tertiary C—H bonds in symmetric cyclohexane derivatives (Scheme 7.13) [43].

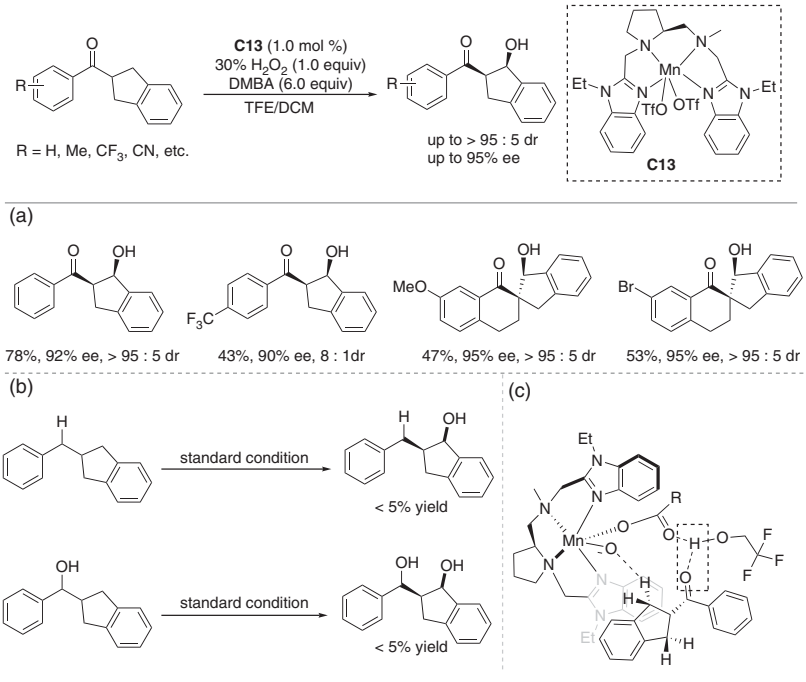


**Scheme 7.12** Enantioselective desymmetrization of carbonyl-group-substituted indane derivatives through manganese-catalyzed C—H oxidation. (a) Selected examples, (b) control experiments, (c) transition state for enantioselective oxidation of C($sp^3$)—H.

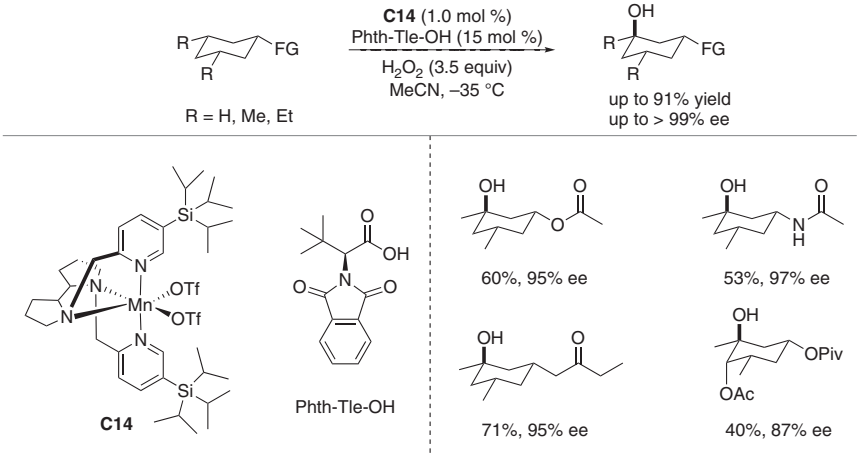


**Scheme 7.13** Enantioselective tertiary C—H bond hydroxylation of *cis*-3,5-dimethyl-substituted cyclohexane derivatives.

This state of the art for non-directed desymmetrization approach proceeded through stereoretentive C—H hydroxylation, allowing the generation of multiple stereogenic centers (up to 4) in a single step. The reaction features good functional group compatibility, and a range of substrates bearing esters, amides, ketones are well tolerated. A careful optimization of manganese catalysts guaranteed good regio- and enantioselectivity together with moderate-to-good yields for multiple-substituted cyclohexanol products. A comprehensive conformational search of the catalyst–substrate complexation pattern was performed. Theoretical calculations established the origin of enantioselectivity due to the weak noncovalent interactions fitting the substrate into the catalytic site precisely.

### 7.3.2 C—H Bond Oxidation to Ketones

In 2017, Costas, Bietti, and co-workers reported a study on site- and enantioselective oxidative desymmetrization of monosubstituted cyclohexanes using sterically demanding tetradentate amino-pyridine manganese complex **C15** as catalyst (Scheme 7.14) [44]. The method employed hydrogen peroxide as an oxidant, and a suitable carboxylic acid additive proved to be crucial to the reaction enantiocontrol. A series of chiral *N*-cyclohexylalkanamides were produced in good yields and good-to-excellent site- and enantioselectivities (up to 85% yield, 96% ee, >99 : 1 for $C^3$ over $C^4$). In 2018, the same group further disclosed an enantioselective oxidative desymmetrization of respective *cis*-1,4-, *trans*-1,3-, and *cis*-1,2-cyclohexanediamide derivatives catalyzed by manganese complex with acetic acid as additive [45].

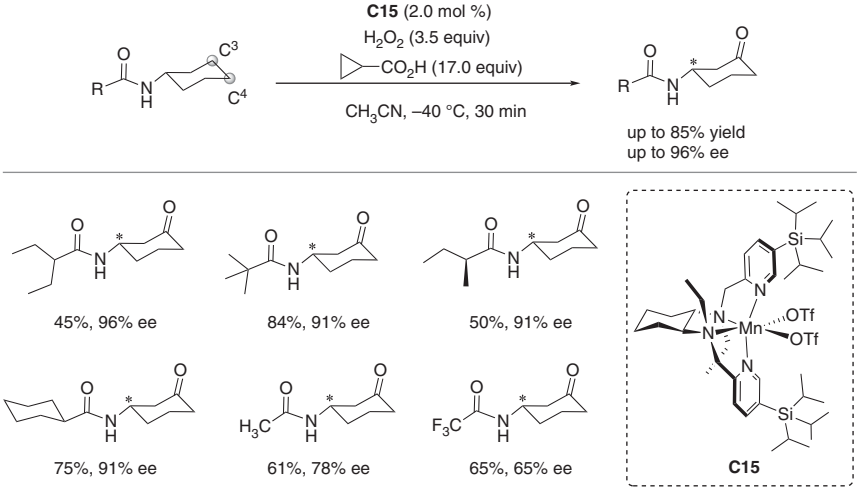


**Scheme 7.14** Enantioselective oxidative desymmetrization of monosubstituted cycloalkanes catalyzed by manganese complex.

In 2018, the Sun group reported an enantioselective oxidative desymmetrization of ketone-based spirocyclic compounds using manganese complex **C13** as catalyst and

hydrogen peroxide as oxidant, providing straightforward access to corresponding chiral spirocyclic $\beta,\beta'$-diketones in good-to-excellent yields and enantioselectivities (up to 98% ee) (Scheme 7.15) [46]. The method was suitable for gram-scale synthesis of chiral spirocyclic diketones. In 2019, the Sun group further expanded the scope of enantioselective oxidative desymmetrization to spirocyclic oxindoles and spirocyclic 2,3-dihydroquinolin-4-ones with excellent enantiocontrol by using the same catalytic system (Scheme 7.16 a, b) [47].

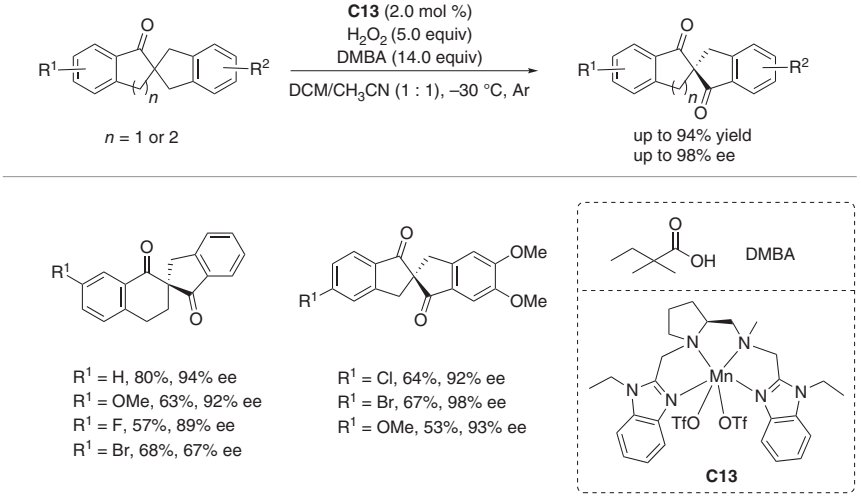


**Scheme 7.15** Enantioselective oxidative desymmetrization of ketone-based spirocyclic hydrocarbons through manganese catalysis.

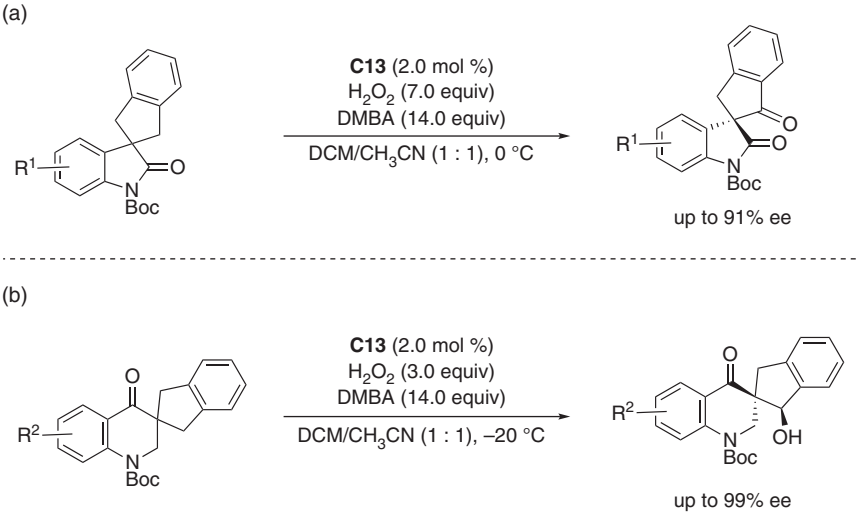


**Scheme 7.16** Enantioselective oxidative desymmetrization of spirocyclic oxindoles and dihydroquinolinones through manganese catalysis. (a) Asymmetric oxidation of spirocyclic oxindoles, (b) asymmetric oxidation of spirocyclic 2,3-dihydroquinolin-4-ones.

### 7.3.3 C—H Bond Oxidation to Lactones

In 2019, Costas, Bietti, and co-workers achieved a manganese-catalyzed enantioselective intramolecular lactonization of unactivated methylene C—H bonds of substituted adamantaneacetic acids with hydrogen peroxide in the presence of trifluoromethanesulfonic acid (Scheme 7.17) [48]. This reaction tolerated a series of functional groups, including aryl motif, hydroxyl group, halogen, ester, and amide, affording corresponding $\gamma$-lactones in good site- and enantioselectivity (up to 99% ee). The isotopic labeling experiments showed that both pathways may operate at comparable rates (1 : 1 ratio) after HAA, which includes (i) OH stereoretentive oxygen rebound and intramolecular esterification, assisted by externally added strong Brønsted acid and (ii) OC(O)R stereoretentive oxygen rebound. Subsequently, the Costas and Bietti group further expanded the enantioselective lactonization strategy to unactivated primary and secondary C($sp^3$)—H bonds in readily available carboxylic acids (Scheme 7.18) [49].

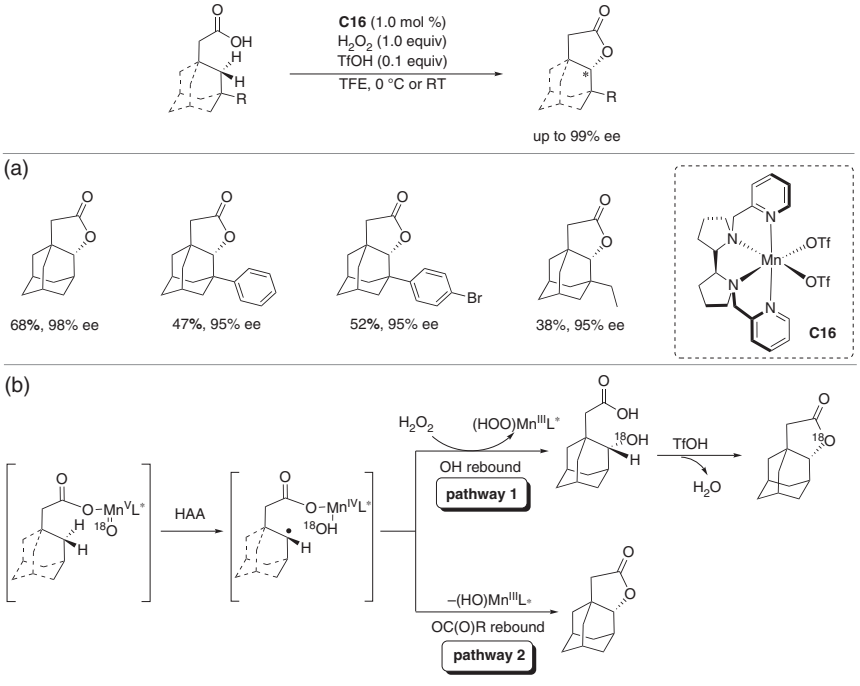


**Scheme 7.17** Enantioselective intramolecular lactonization of methylene C—H bonds of adamantaneacetic acids catalyzed by manganese complex. (a) Selected examples, (b) a plausible mechanistic pathway.

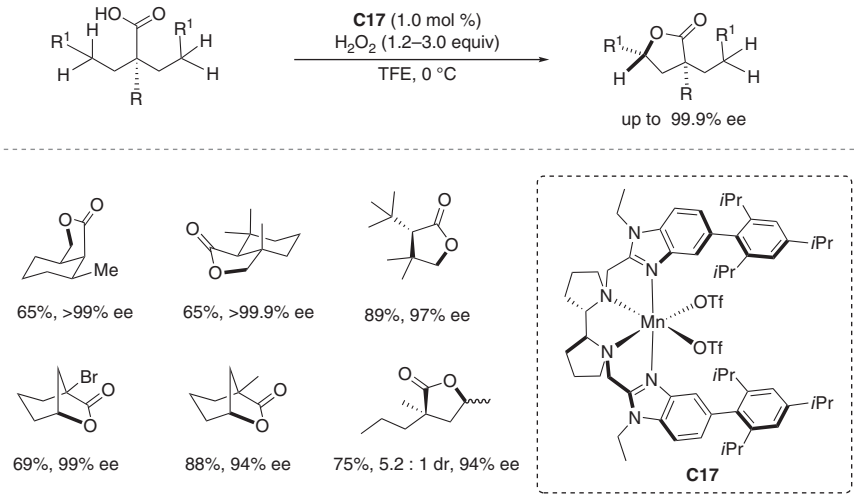


**Scheme 7.18** Enantioselective C—H lactonization of carboxylic acids to form chiral lactones.

## 7.4 Manganese-Catalyzed Kinetic Resolution Through C—H Bond Oxidation

KR is a powerful strategy in the field of asymmetric synthesis. This process is highly valued for its ability to produce enantiopure compounds from racemic starting materials, leveraging the different reactivity rates of the two enantiomers toward a chiral catalyst (Scheme 7.19) [50–52]. Manganese-catalyzed KR of secondary alcohols is one of the most well-explored reactions, and several reviews have highlighted these achievements [53, 54]. In the chapter, we emphasize manganese-catalyzed KR reactions of racemic compounds other than alcohols involving radical intermediate.

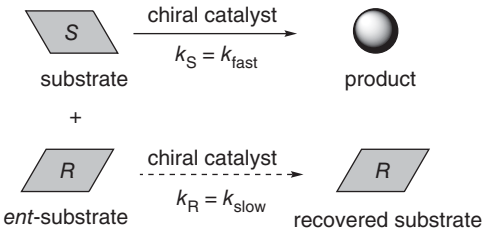


**Scheme 7.19** The principle of kinetic resolution.

In 2020, the Liu group reported a Mn-catalyzed site- and enantio-differentiating oxidation of C—H bonds in saturated cyclic ethers including tetrahydrofurans, tetrahydropyrans, and other medium-sized ones with diverse substituent patterns (Scheme 7.20) [55]. The oxidative KR strategy provides a versatile platform for constructing chiral cyclic ethers (up to 98% ee) together with chiral secondary alcohols (up to 95% ee) with excellent enantioselectivity. Notably, this protocol has also exhibited synthetic values by late-stage oxidative KR of biologically active molecules that are otherwise difficult to access. In this process, the reaction mechanism and origins of stereoselectivity were elucidated by combined experiments and computational studies. The experimental results indicated that the matched enantiomer undergoes a hydrogen atom transfer (HAT) followed by oxygen rebound, providing the chiral secondary alcohols (Scheme 7.20b). DFT calculations reveal that the $\pi\cdots\pi$ interaction between manganese complex **C18** and matched enantiomer is beneficial

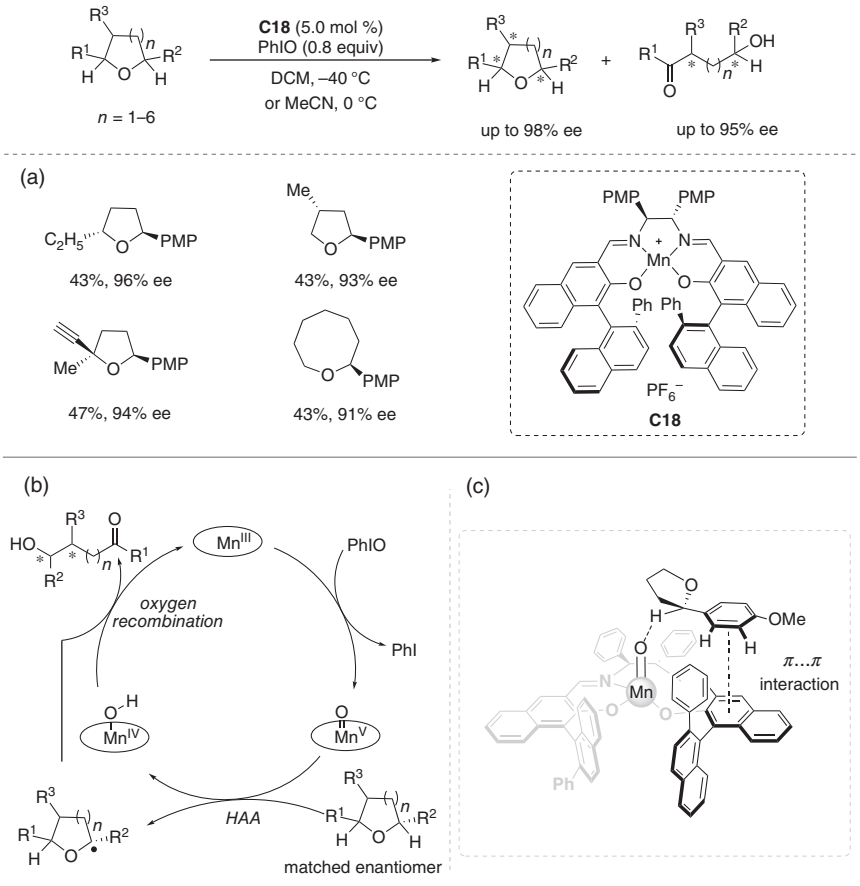


**Scheme 7.20** Mn-catalyzed oxidative kinetic resolution of saturated cyclic ethers. (a) Selected examples, (b) a plausible mechanistic pathway, (c) noncovalent interaction in stereo-determining transition state structures.

for improving the efficiency of KR (Scheme 7.20c). In 2021, Liu and co-workers further expanded the oxidative KR protocol to cyclic benzylic ethers [56].

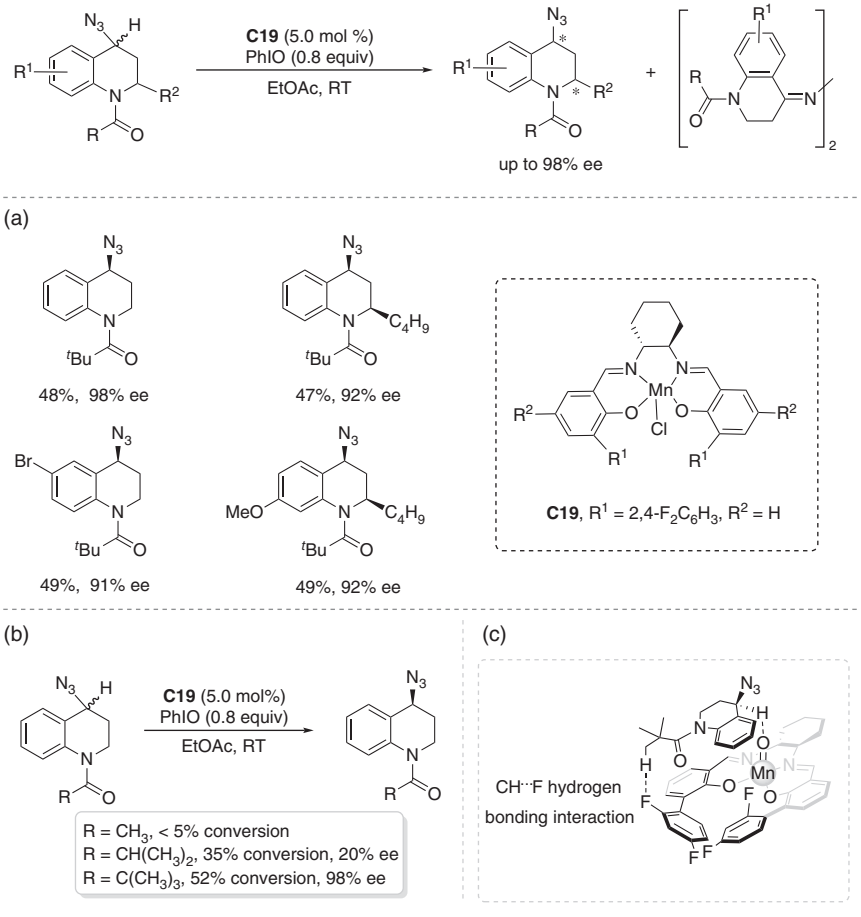


**Scheme 7.21** Mn-catalyzed oxidative kinetic resolution of cyclic benzylic azides. (a) Selected examples, (b) the *N*-acyl substituent effect for organic azides, (c) stereoselectivity-determining transition states.

Besides racemic ethers, organic azides have also been exploited as substrates for Mn-catalyzed oxidative KR reactions. In 2022, Liu and co-workers documented an elegant enantioselective C($sp^3$)—H oxidation of tetrahydroquinoline- based organic azides catalyzed by manganese complex with PhIO as the oxidant (Scheme 7.21) [57]. This oxidative KR protocol affords the corresponding optically cyclic benzylic azides in excellent enantioselectivities (up to 98% ee). Control experiments show that the substituents on the *N*-acyl moieties were crucial to the oxidation reactivity and selectivity (Scheme 7.21b). The reactivity and stereoselectivity were gradually enhanced as the increasing number of methyl groups at the *α*-position of the amide moiety. In addition, detailed computational studies elucidate that the driving

force behind the oxidative KR lies in the CH···F hydrogen bonding interaction between *tert*-butyl group of matching enantiomer and 2,4-difluorophenyl moiety of catalyst **C19**.

Recently, Liu and coworkers described a manganese-catalyzed enantioselective hydroxylation of tertiary propargylic C($sp^3$)—H bonds in acyclic systems in the presence of PhIO as an oxidant (Scheme 7.22) [58]. This oxidative KR protocol is shown to tolerate a diverse array of functional groups, allowing facile access to structurally diverse tertiary propargyl alcohols with good-to-excellent chemo- and

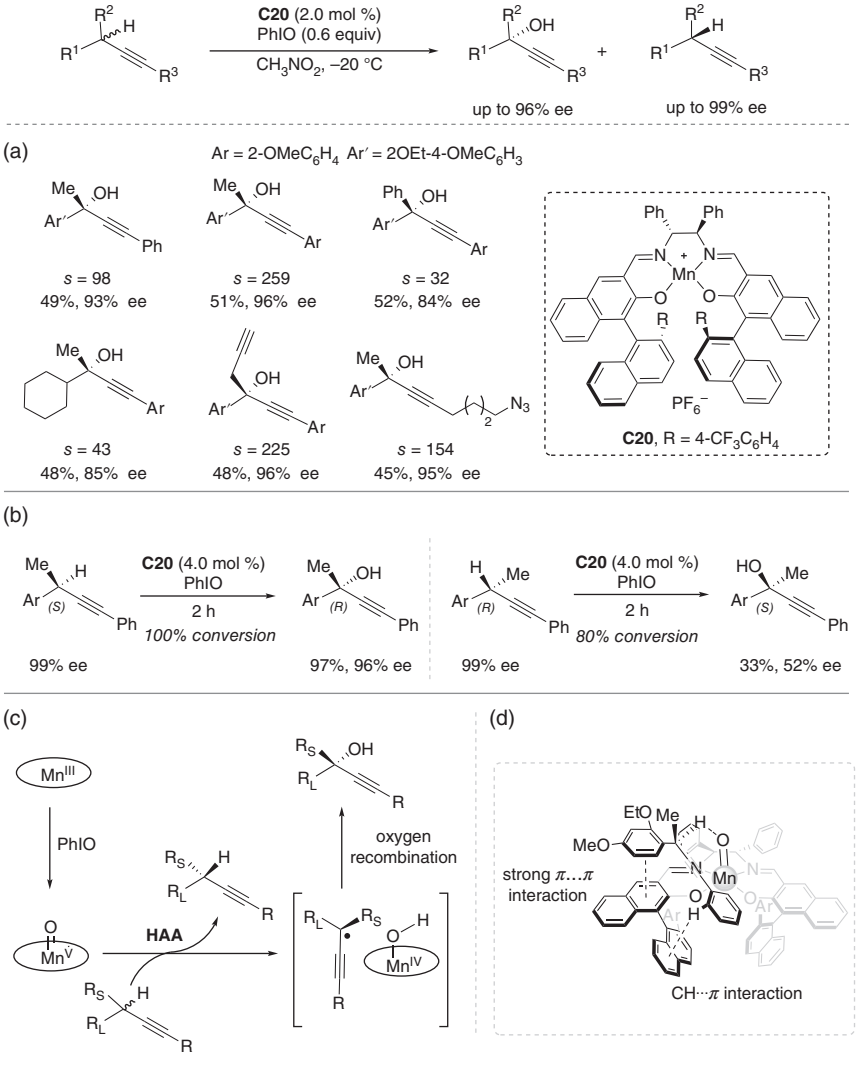


**Scheme 7.22** Mn-catalyzed enantioselective hydroxylation of tertiary propargylic C($sp^3$)—H bonds. (a) Selected examples, (b) controlled experiments: hydroxylation of respective (*S*) and (*R*) isomer, (c) a plausible mechanistic pathway, (d) transition state for enantio-differentiating.

enantio-discrimination (up to 96% ee). Experiments were conducted to gain insight into the reaction mechanism. The observed KIE values revealed that C—H abstraction might be involved in the rate-determining step. Additionally, hydroxylation of respective (*S*)- and (*R*)-isomer of alkynes under standard conditions gave products with opposite configurations enantiopure, suggesting the existence of stereoretentive oxygen recombination (Scheme 7.22b). These studies indicated that the reaction might undergo a rate-determining HAA and subsequent stereoretentive oxygen recombination (Scheme 7.22c). In addition, DFT calculations also proved that the excellent stereoselectivity might be attributed to the $\pi\cdots\pi$ and C—H$\cdots\pi$ interaction between the catalyst and matched enantiomer during the HAA (Scheme 7.22d).

## 7.5 Conclusion

Radical-mediated asymmetric catalysis has emerged as an important research field within the chemistry community. As one of the most popular earth-abundant metals, manganese has played a pivotal role in the development of asymmetric radical reactions, providing a powerful platform for constructing diverse chiral molecules. Despite considerable advances, a series of challenges have remained unsolved. The transformation category is still limited to oxidation reactions. Besides, the reaction mechanisms remain elusive due to the lack of direct characterizations of the involved manganese intermediates. Consequently, there is considerable space for further exploration of manganese-catalyzed asymmetric radical reactions. Future efforts should be made to expand the reaction types and deepen the understanding of the reaction mechanisms. It is anticipated that the field of manganese-catalyzed asymmetric radical reactions will continue to be a focal point of future research.

## References


1 Emsley, J. (2001). *Nature's Building Blocks: An A-Z. Guide to the Elements-Manganese*, 249–253. Oxford: Oxford University Press.
2 Law, N.A., Caudle, M.T., and Pecoraro, V.L. (1998). *Advances in Inorganic Chemistry*, vol. 46 (ed. A.G. Sykes), 305–440. New York: Academic Press.
3 Wieghardt, K. (1989). *Angew. Chem. Int. Ed.* 28: 1153–1172.
4 Tchounwou, P.B., Yedjou, C.G., and Sutton, A.K. (2012). *D. J. EXS* 101: 133–164.
5 For the teratogenicity of metals, the toxicity ($LD_{50}$) of the following metals were determined to be cadmium (3) > arsedic (9) > cobalt (38) > copper (58) > indium (121) > molybdenum (333) > manganese (765) > iron (1185) ($\mu$g/egg), see: Gilani, S.H. and Alibhai, Y. (1990). *J. Toxicol. Environ. Health* 30: 23–31.
6 Christianson, D.W. (1997). *Prog. Biophys. Mol. Biol.* 67: 217–252.
7 Holzwarth, M.S. and Plietker, B. (2013). *ChemCatChem* 5: 1650–1679.
8 Das, K., Waiba, S., Jana, A., and Maji, B. (2022). *Chem. Soc. Rev.* 51: 4386–4464.
9 Maayuri, R. and Gandeepan, P. (2023). *Org. Biomol. Chem.* 21: 441–464.
10 Giri, R., Shi, B.-F., Engle, K.M. et al. (2009). *Chem. Soc. Rev.* 38: 3242–3272.

**11** Bryliakov, K.P. (2017). *Chem. Rev.* 117: 11406–11459.
**12** Milan, M., Bietti, M., and Costas, M. (2018). *Chem. Commun.* 54: 9559–9570.
**13** Gandeepan, P., Müller, T., Zell, D. et al. (2019). *Chem. Rev.* 119: 2192–2452.
**14** Woźniak, Ł. and Cramer, N. (2019). *Trends Chem.* 1: 471–484.
**15** Zhang, C., Li, Z.-L., Gu, Q.-S., and Liu, X.-Y. (2021). *Nat. Commun.* 12: 475–483.
**16** Mondal, S., Dumur, F., Gigmes, D. et al. (2022). *Chem. Rev.* 122: 5842–5976.
**17** Wang, X., He, J., Wang, Y.-N. et al. (2024). *Chem. Rev.* 124: 10192–10280.
**18** Yang, C.-J., Liu, L., Gu, Q.-S., and Liu, X.-Y. (2024). *CCS Chem.* 6: 1612–1627.
**19** Sibi, M.P. and Porter, N.A. (1999). *Acc. Chem. Res.* 32: 163–171.
**20** Bar, G. and Parsons, A.F. (2003). *Chem. Soc. Rev.* 32: 251–263.
**21** Sibi, M.P., Manyem, S., and Zimmerman, J. (2003). *Chem. Rev.* 103: 3263–3295.
**22** Golden, D.L., Suh, S.-E., and Stahl, S.S. (2022). *Nat. Rev. Chem.* 6: 405–427.
**23** Liu, W., Cheng, M.-J., Nielsen, R.J. et al. (2017). *ACS Catal.* 7: 4182–4188.
**24** Huang, X. and Groves, J.T. (2017). *J. Biol. Inorg. Chem.* 22: 185–207.
**25** de Montellano, P.R.O. (2010). *Chem. Rev.* 110: 932–948.
**26** Chakrabarty, S., Wang, Y., Perkins, J.C., and Narayan, A.R.H. (2020). *Chem. Soc. Rev.* 49: 8137–8155.
**27** Groves, J.T. and Viski, P. (1990). *J. Organomet. Chem.* 55: 3628–3634.
**28** Hamada, T., Ihie, R., Mihara, J. et al. (1998). *Tetrahedron* 54: 10017–10028.
**29** Murahashi, S.-I., Noji, S., and Komiya, N. (2004). *Adv. Synth. Catal.* 346: 195–198.
**30** Srour, H., Maux, P.L., and Simonneaux, G. (2012). *Inorg. Chem.* 51: 5850–5856.
**31** Sun, W. and Sun, Q. (2019). *Acc. Chem. Res.* 52: 2370–2381.
**32** Olivo, G., Cussj, O., and Costas, M. (2016). *Chem. Asian J.* 11: 3148–3158.
**33** Ottenbacher, R.V., Talsi, E.P., Rybalova, T.V., and Bryliakov, K.P. (2018). *ChemCatChem* 10: 5323–5330.
**34** Ottenbacher, R.V., Talsi, E.P., and Bryliakov, K.P. (2020). *J. Catal.* 390: 170–177.
**35** Burg, F., Gicquel, M., Breitenlechner, S. et al. (2018). *Angew. Chem. Int. Ed.* 57: 2953–2957.
**36** Burg, F., Breitenlechner, S., Jandl, C., and Bach, T. (2020). *Chem. Sci.* 11: 2121–2129.
**37** Huang, X., Bergsten, T.M., and Groves, J.T. (2015). *J. Am. Chem. Soc.* 137: 5300–5303.
**38** Li, J., Ren, Y., Yue, C. et al. (2018). *ACS Appl. Mater. Interfaces* 10: 36047–36057.
**39** Cao, M., Wang, H., Ma, Y. et al. (2022). *J. Am. Chem. Soc.* 144: 15383–15390.
**40** Punniyamurthy, T., Miyafuji, A., and Katsuki, T. (1998). *Tetrahedron Lett.* 39: 8295–8298.
**41** Miyafuji, A. and Katsuki, T. (1998). *Tetrahedron* 54: 10339–10348.
**42** Sun, Q. and Sun, W. (2020). *Org. Lett.* 22: 9529–9533.
**43** Palone, A., Casadevall, G., Ruiz-Barragan, S. et al. (2023). *J. Am. Chem. Soc.* 145: 15742–15753.
**44** Milan, M., Bietti, M., and Costas, M. (2017). *ACS Cent. Sci.* 3: 196–204.
**45** Milan, M., Bietti, M., and Costas, M. (2018). *Org. Lett.* 20: 2720–2723.
**46** Qiu, B., Xu, D., Sun, Q. et al. (2018). *ACS Catal.* 8: 2479–2487.
**47** Qiu, B., Xu, D., Sun, Q. et al. (2019). *Org. Lett.* 21: 618–622.

**48** Cianfanelli, M., Olivo, G., Milan, M. et al. (2020). *J. Am. Chem. Soc.* 142: 1584–1593.
**49** Call, A., Capocasa, G., Palone, A. et al. (2023). *J. Am. Chem. Soc.* 145: 18094–18103.
**50** Breuer, M., Ditrich, K., Habicher, T. et al. (2004). *Angew. Chem. Int. Ed.* 43: 788–824.
**51** Vedejs, E. and Jure, M. (2005). *Angew. Chem. Int. Ed.* 44: 3974–4001.
**52** Fogassy, E., Nogradi, M., Kozma, D. et al. (2006). *Org. Biomol. Chem.* 4: 3011–3030.
**53** Pellissiera, H. (2011). *Adv. Synth. Catal.* 353: 1613–1666.
**54** Ahmad, I., Shagufta, and AlMallah, A.R. (2017). *Chirality* 29: 798–810.
**55** Sun, S., Yang, Y., Zhao, R. et al. (2020). *J. Am. Chem. Soc.* 142: 19346–19353.
**56** Sun, S., Ma, Y., Liu, Z., and Liu, L. (2021). *Angew. Chem. Int. Ed.* 60: 176–180.
**57** Ye, P., Feng, A., Wang, L. et al. (2022). *Nat. Commun.* 13: 1621–1630.
**58** Cao, M., Wang, H., Hou, F. et al. (2024). *J. Am. Chem. Soc.* 146: 18396–18406.

НАРОДНЫЙ ФРОНТ
https://pobeda.onf.ru/
LET'S HELP THE RUSSIA



# 8

# Photoredox/Earth-Abundant Metal-Catalyzed Asymmetric Radical Reactions

*Peng-Zi Wang, Wen-Jing Xiao, and Jia-Rong Chen*

*College of Chemistry, Central China Normal University, Wuhan, China*

## 8.1 Introduction

Visible light is considered a safe, cost-effective, and renewable source of chemical energy to facilitate the transformation of organic molecules. Compared to extensively studied UV light-induced reactions, the utilization of visible light avoids issues typically associated with UV-mediated photodegradation and eliminates the need for specialized equipment. Over the past few decades, there have been a large number of outstanding studies on photoredox-catalyzed reactions, which have proved that such an activation mode is a robust tool in organic synthesis [1–5]. In sharp contrast to traditional two-electron mechanism-based reactions, this visible light-driven activation mode provides convenient access to diverse highly reactive radical species under mild conditions. As such, numerous transformations that are otherwise inaccessible under thermal conditions can be achieved by using photocatalysts with different redox potentials (Figure 8.1).

Mechanistically, in a typical experimental setup, visible light from sources such as sunlight, LED lights, or standard household lamps is absorbed by a photocatalyst (PC) to generate its excited state (PC*), thereby initiating a single-electron-transfer (SET), energy-transfer (EnT), or hydrogen atom transfer (HAT) process (Scheme 8.1a). In a SET process, the excited photocatalyst (PC*) is a stronger reducing and oxidizing agent compared to the ground state. As a result, despite the fact that organic compounds themselves often cannot absorb visible light, this photoinduced redox chemistry can generate various reactive radical cation or radical anion intermediates from the closed-shell substrates [6–10]. An EnT process defines the catalytic cycle, wherein the excited photocatalyst can subsequently transfer its excited triplet state energy to a substrate, thus allowing activation into its triplet excited state (Sub.*) [11–18]. It should be noted that some photoredox catalysts can also act as HAT catalysts, which abstract a hydrogen atom from substrates through homolytic cleavage of C–H bonds [19–25].

Pioneering studies by MacMillan, Bach, Meggers, Yoon, and Melchiorre [26–30] have demonstrated that dual catalysis can offer solutions to ionic pathway-based

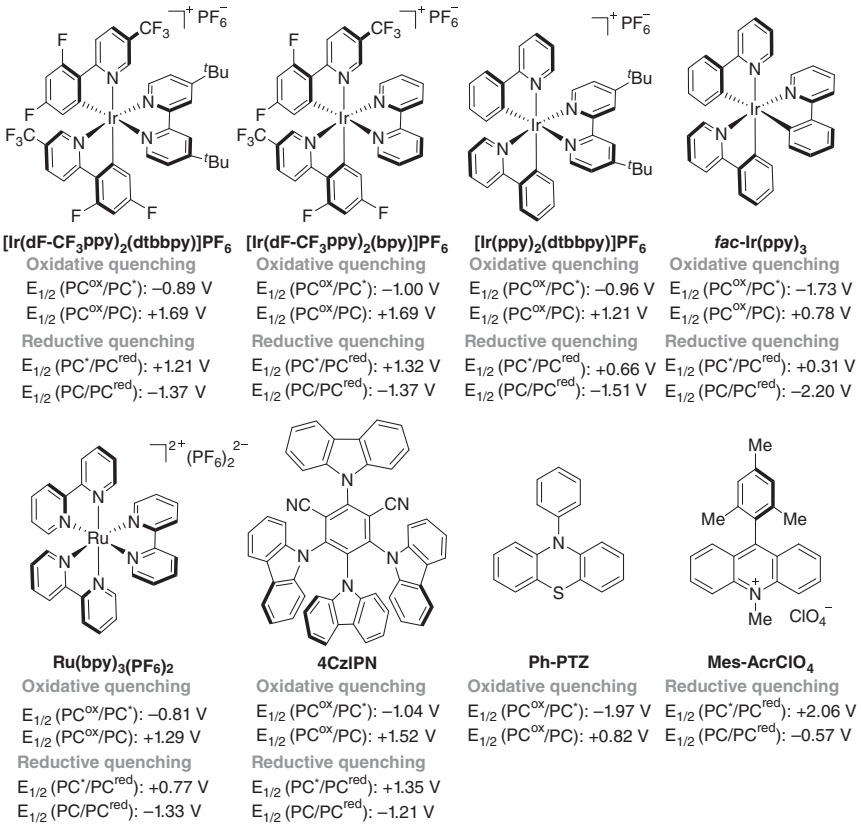


**Figure 8.1** Commonly used photoredox catalysts in metallaphotoredox catalysis.

synthetic problems. Therefore, these works have inspired synthetic chemists to seek more practical stereoselective strategies for the photochemical process [31–40]. These strategies are mainly based on the combination of photocatalysis with various other catalytic methods, including carbene catalysis, Brønsted acid catalysis, transition-metal catalysis, as well as Lewis acid catalysis. Among these dual catalytic strategies, dual photoredox/metal catalysis stands out as the most powerful and versatile method to develop visible light-driven asymmetric transformations. Given the ready availability of a large number of structurally diverse chiral ligands, great opportunities exist for synthesizing chiral molecules under sustainable conditions (Figure 8.2). Compared to traditional transition-metal-catalyzed coupling reactions, the introduction of photoredox catalysis makes the reaction milder and greener, enabling precise control over the reactivity of free radicals and even some contra-thermodynamic transformations. In this chapter, we will survey recent representative advances in enantioselective radical transformations enabled by the combination of photocatalysts with various earth-abundant metals such as copper, nickel, chromium, and cobalt, according to different catalytic modes (Scheme 8.1b).

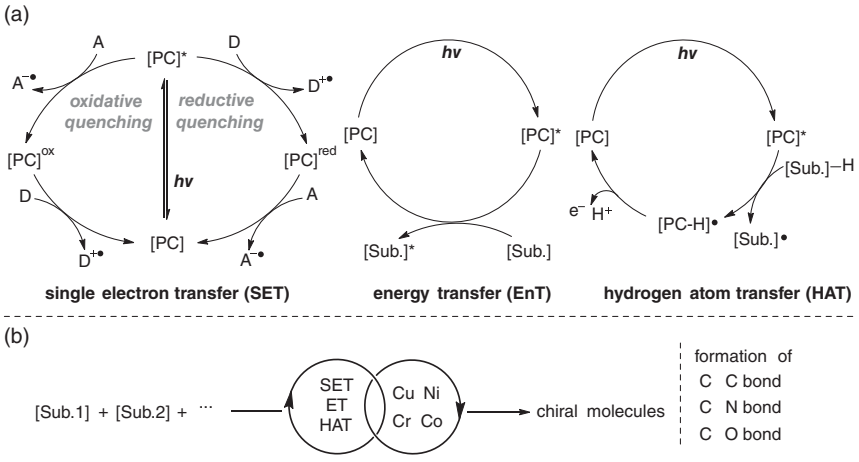


**Scheme 8.1** General visible-light-driven photocatalytic cycles and photoredox/metal catalysis. (a) General photocatalytic quenching cycles. (b) Photoredox/earth-abundant metal-catalyzed asymmetric radical reactions. A, Acceptors; D, Donors; Sub, Substrates.

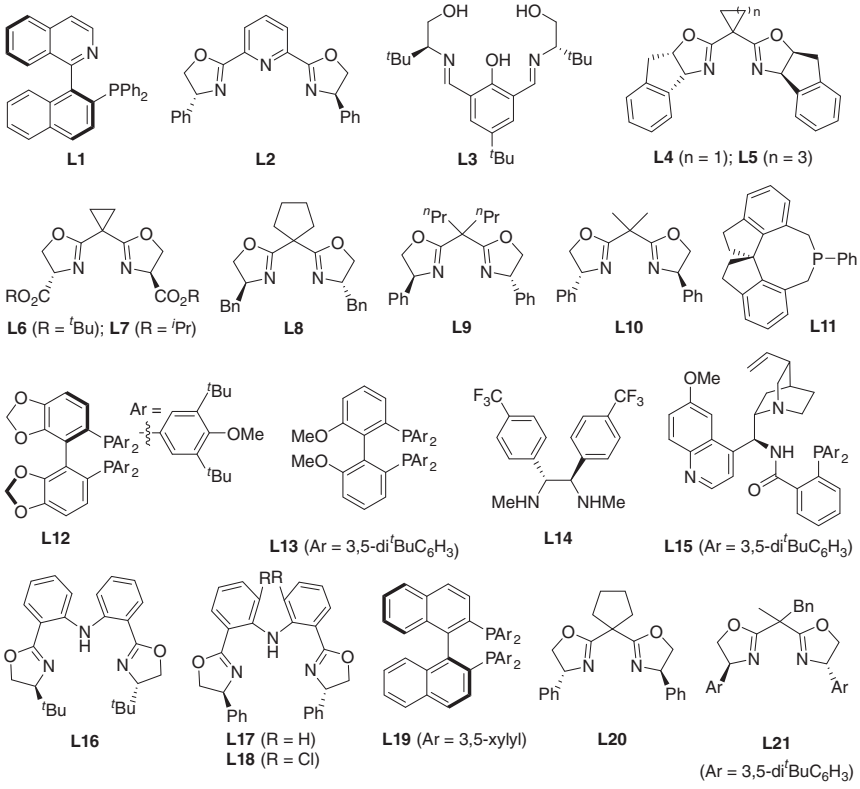


**Figure 8.2** Commonly used chiral ligands in metallaphotoredox catalysis.

## 8.2 Photoredox/Copper-Catalyzed Asymmetric Radical Reactions

Copper is the first earth-abundant transition metal used in the catalytic construction of C—C and C—X bonds (X = heteroatom) [41, 42]. The pioneering work of Ullman in 1901 disclosed the advent of copper-catalyzed C—C cross-coupling reactions. Shortly thereafter, Ullman and Goldberg further expanded this methodology to C—X cross-coupling reactions between 1903 and 1906. Due to its low toxicity and cost-effectiveness, copper has been extensively utilized in transition-metal catalysis since then. In addition to engagement in polar mechanisms, copper can also function as a SET reagent to initiate redox-based radical reactions. The iconic example is the Kharasch–Sosnovsky reaction, which involves copper-catalyzed allylic C—H oxidations [43]. The asymmetric variants were achieved by employing appropriate chiral ligands or counterparts. However, the known methods still have some limitations, such as the weak reducing capability of copper-based catalysts, narrow substrate scope, limited scope of radical precursors, and limited types of chemical bonds that could be formed.

The introduction of visible light photoredox catalysis offers new possibilities for addressing these challenges. Photoredox-catalyzed single-electron transfer provides milder and greener reaction conditions for the controlled generation of various radicals, which thus holds great potential to expand the scope of copper-catalyzed radical cross-couplings. Photoredox/copper-based asymmetric catalytic strategies usually involve two activation modes: dual catalysis by combining a chiral copper catalyst and an additional photocatalyst, and bifunctional catalysis using a single chiral copper catalyst [44–47]. In this context, a variety of photoinduced asymmetric copper-catalyzed reactions have recently been developed using versatile chiral ligands [48, 49].

### 8.2.1 Dual Catalysis by Merge of a Chiral Copper Catalyst and an Additional Photocatalyst

In 2015, Li reported the first example of the enantioselective cross-dehydrogenative-coupling (CDC) reaction of tetrahydroisoquinolines **1** by employing a dual photoredox/copper catalytic strategy, wherein $(BzO)_2$ functions as an oxidant (Scheme 8.2a) [50]. Specifically, by employing a combination of an iridium photocatalyst and a chiral copper(I) salt, *N*-aryl-tetrahydroisoquinolines **1** reacted smoothly with terminal alkynes **2** under the irradiation of visible light to produce the corresponding 1-alkynyl tetrahydroisoquinolines **3** in good yield with high enantioselectivities. As for the proposed mechanism, the transformation begins with a SET process between the photoexcited Ir(III) catalyst and *N*-aryl-tetrahydroisoquinolines **1**, producing an Ir(II) catalyst and an amine cation radical. The latter species can be further converted to iminium ion intermediate **1-A** after the release of a hydrogen atom abstracted by the generated BzO radical. Finally, nucleophilic addition of the chiral Cu(I)-acetylide complex to electrophilic **1-A** results in the corresponding products **3**. Following this

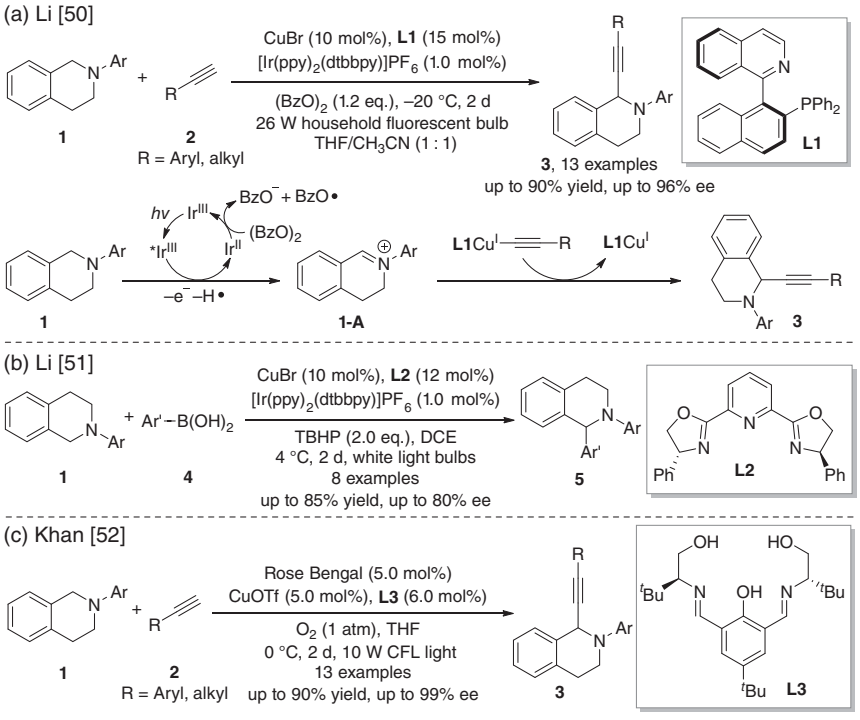


**Scheme 8.2** Dual photoredox/copper-catalyzed asymmetric dehydrogenative cross-couplings of *N*-aryl tetrahydroisoquinolines. Sources: (a) Li [50]/Royal Society of Chemistry. (b) Adapted from Li [51]. (c) Khan [52]/Elsevier.

work, Li and coworkers further realized an efficient photoredox-catalyzed asymmetric arylation reaction of $sp^3$ C–H bonds of *N*-aryl-tetrahydroisoquinolines **1** with arylboronic acids **4** as nucleophiles (Scheme 8.2b) [51]. In the presence of an external oxidant, *tert*-butyl hydroperoxide (TBHP), and a chiral PyBox **L2**, the arylated products **5** are produced in good yields with modest enantioselectivities. Later, using a combination of organic dyes-based photoredox catalysts like Rose Bengal and an in situ generated Cu(I)-chiral complex, Khan and coworkers also developed the aerobic dehydrogenative alkynylation of *N*-aryl tetrahydroisoquinolines (Scheme 8.2c) [52].

The group of Liu has pioneered the field of copper-catalyzed asymmetric radical-involved C—H functionalization through a radical relay strategy [53, 54]. Since the first introduction of this concept in enantioselective benzylic C($sp^3$)—H cyanation [55], Liu and coworkers have accomplished a range of copper-catalyzed enantioselective radical cross-coupling reactions. *N*-Hydroxyphthalimide (NHP) esters that can be obtained from diverse carboxylic acids are a versatile class of redox-active radical precursors [56]. In 2017, the groups of Liu and Lin reported an enantioselective decarboxylative radical cyanation of NHP esters **6** and trimethylsilyl cyanide **(**TMSCN) by merging photoredox catalysis and copper catalysis (Scheme 8.3a) [57]. Mechanistically, under the irradiation of blue LEDs, substrate **6** undergoes SET reduction by the excited state of the photocatalyst and

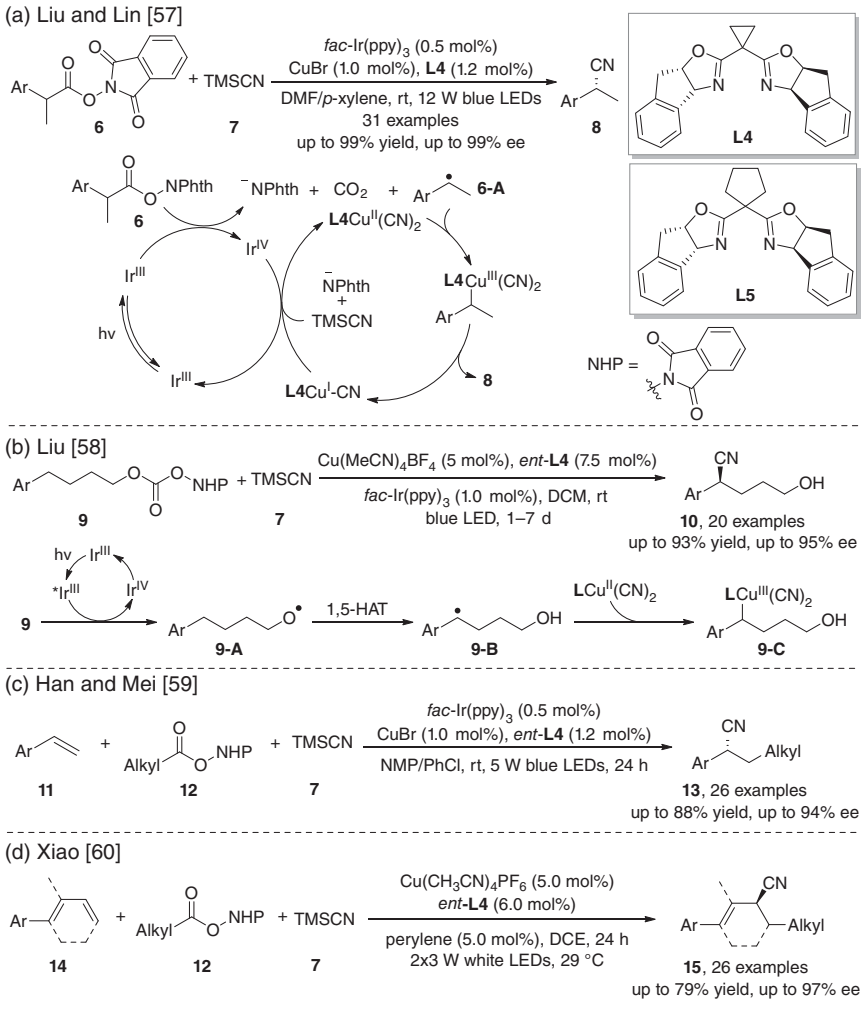


**Scheme 8.3** Dual photoredox/copper-catalyzed enantioselective benzylic and allylic cyanation with *N*-hydroxyphthalimide esters as radical precursors. Sources: (a) Liu and Lin [57]/American Chemical Society. (b) Adapted from Liu [58], (c) Han and Mei [59]/American Chemical Society. (d) Xiao [60]/American Chemical Society.

sequential decarboxylation to produce the benzylic radical **6-A**. The generated oxidizing Ir(IV) catalyst can oxidize copper(I) to copper(II) species and regenerate its ground state. On the other hand, the chiral copper(II) species is able to capture the benzylic radicals to deliver a copper(III) intermediate, followed by reductive elimination to afford the desired chiral benzyl nitriles **8**. Notably, a diverse range of benzyl nitriles, including the key chiral intermediates of some bioactive compounds, can be efficiently produced with excellent yields and enantioselectivity by using a chiral bis(oxazoline) (Box) ligand **L4** under mild conditions. Inspired by this success, the same group developed a similar strategy to realize enantioselective remote C($sp^3$)—H cyanation (Scheme 8.3b) [58]. In this process, the *O*-centered

radical **9-A** generated from *N*-hydroxyphthalimide ethers **9** via SET reduction can trigger a 1,5-HAT process to form the benzylic radical species **9-B**. Then, the new carbon radical **9-B** could be trapped by a copper(II) catalyst to install a cyanide group enantioselectively. Similarly, Zhu and coworkers also achieved an enantioselective example of C($sp^3$)—H cyanation by employing *N*-alkoxypyridinium salts as a radical precursor [61]. Moreover, Han, Mei, and coworkers successfully extended this protocol to a three-component 1,2-difunctionalization of alkenes using NHP esters **12** as alkylation reagents (Scheme 8.3c) [59]. This method features high efficiency and enantioselectivity, as well as a broad substrate scope with respect to NHP esters. A range of primary, secondary, and tertiary alkyl-substituted substrates are well accommodated, while the scope of radical acceptors is limited to aryl alkenes, probably because the aryl group could stabilize the formed carbon radicals. Remarkably, a three-component enantioselective allylic cyanation reaction of NHP esters **12**, TMSCN, and 1,3-dienes **14** has been reported by Xiao and coworkers by using the organic photocatalyst perylene and chiral copper catalyst (Scheme 8.3d) [60]. Under the mild and redox-neutral conditions, a diverse range of 1,2-functionalized chiral allyl cyanides **15** is produced in generally good yield and high enantioselectivity. Besides, 1,3-enynes have proven to be compatible with this reaction, providing practical access to valuable chiral propargylic cyanides. However, internal acyclic dienes and nonactivated dienes fail to participate in this reaction system under the current catalytic conditions.

Besides NHP esters, oxime esters can also serve as alkyl radical precursors where N—O bonds can be reduced to generate imine radicals by merging photoredox and copper catalysis. For example, in 2019, Wang and coworkers described the enantioselective ring-opening cyanation of oxime esters for constructing chiral 1,6-dinitriles **17** (Scheme 8.4a) [62]. When using five-membered cyclooctene oxime esters, it is necessary to combine a chiral copper(I) catalyst and *fac*-Ir$(ppy)_3$ as the photocatalyst, while a single copper catalyst is efficient for cyclobutanone-derived oxime esters due to the inherent higher ring strain. Almost at the same time, Xiao, Chen, and coworkers reported a similar strategy, wherein an organic photocatalyst, Ph-PTZ, was used to replace the precious metal-based photocatalyst (Scheme 8.4b) [63]. Mechanistically, cyanoalkyl radicals **16-B** generate in situ by a photocatalytic iminyl radical **16-A** triggered C—C bond cleavage event from the redox-active oxime esters and can be trapped by chiral copper species to form the final product **17** via a proposed copper(III) intermediate **16-C**. Besides the two types of substrates mentioned above, cycloketone oxime esters with larger ring sizes are incapable of engaging in the ring-opening process through this method. Interestingly, noncyclic oxime esters also exhibit the potential to be alkyl radical precursors under visible light-induced redox conditions [68, 69]. Building on previous works, Xiao, Chen, and coworkers developed an intermolecular, highly enantioselective three-component radical vicinal dicarbofunctionalization (DCF) reaction of alkenes, using oxime esters and TMSCN, by dual photoredox and copper catalysis (Scheme 8.4c) [64]. Under mild conditions, this reaction demonstrates broad substrate scope and high functional group tolerance, providing a general approach for synthesizing optically active β-cyano ketones **19** and alkyldinitriles **20**.

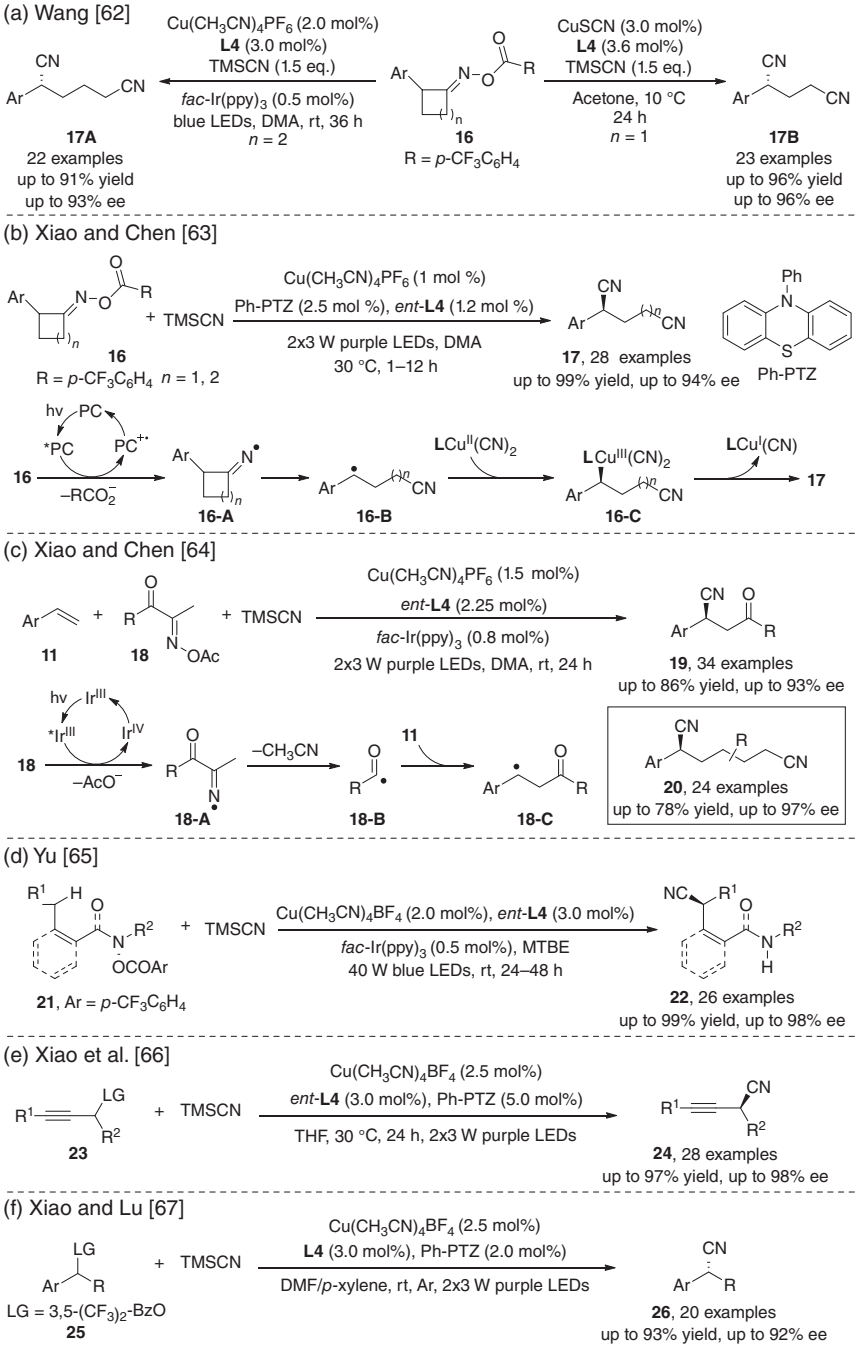


**Scheme 8.4** Dual photoredox/copper-catalyzed enantioselective asymmetric deoxygenative cyanation. Sources: (a) Wang [62]/Springer Nature/CC BY 4.0. (b) Xiao and Chen [63]/American Chemical Society. (c) Xiao and Chen [64]/John Wiley & Sons. (d) Yu [65]/American Chemical Society. (e) Adapted from Xiao et al. [66]. (f) Xiao and Lu [67]/John Wiley & Sons.

In 2020, Yu and coworkers demonstrated a site-selective C($sp^3$)—H cyanation of *O*-acyl hydroxamides **21** (Scheme 8.4d) [65]. Key to the success of this protocol relies on the nitrogen radical-mediated intramolecular HAT, which enables the generation of a more stable radical species to participate in the following enantioselective cross-coupling. However, limited success was achieved about non-benzylic remote C($sp^3$)—H cyanation, and often with low enantioselectivity.

Under photoredox conditions, alkyl radicals can be generated through C—O bond cleavage of propargyl esters and benzyl esters. In 2019, Xiao and coworkers reported the first asymmetric propargylic radical cyanation through the synergistic photoredox and copper catalysis strategy (Scheme 8.4e) [66]. In this reaction, a SET process first occurs between propargyl esters **23** and the excited state of the organic photocatalyst Ph-PTZ to generate propargyl radicals and the oxidizing photocatalyst, which can oxidize copper(I) species to copper(II) species. The resultant chiral copper(II) complex functions as an efficient organometallic catalyst to capture the propargyl radical and allow its coupling with cyanide in an enantiocontrolled manner. Therefore, a range of optically active propargyl cyanides **24** is produced with high reaction efficiency and enantioselectivity. Similarly, an enantioselective dehydrogenative cyanation of benzyl alcohols has been accomplished for synthesizing chiral benzyl nitriles by the same group (Scheme 8.4f) [67].

Molecular photoelectrocatalysis, combining electrochemistry with molecular photocatalysis, has emerged as a powerful tool for addressing long-standing synthetic challenges in recent years [70]. This technology enables oxidative transformations to occur under mild electrode potentials without external chemical oxidants, offering abundant opportunities for the development of selective and efficient synthetic methodologies. Thus, the field of asymmetric electrocatalysis has become a new frontier in organic synthesis and received growing interest [71–76].

Recently, Xu and Song successfully integrated photoelectrocatalysis with asymmetric copper catalysis to accomplish a highly enantioselective decarboxylative cyanation of carboxylic acids. By employing cerium/copper relay catalysis, a wide range of chiral nitriles **26** is obtained with excellent yields and enantioselectivities (Scheme 8.5a) [77]. In this reaction, a cerium salt acts as the photocatalyst for the decarboxylation of the carboxylic acid to generate a benzylic radical, while a chiral copper complex is utilized for the stereoselective C—CN bond formation. According to the proposed mechanism, $Ce(OTf)_3$ reacts with $^nBu_4NCl$ to form $[CeCl_6]^{3-}$, which is subsequently oxidized at the anode to generate $[CeCl_6]^{2-}$. Sequential interaction with carboxylate **27** and photoinduced ligand-to-metal charge transfer (LMCT) results in the formation of benzylic radical **27-A** and regeneration of $[CeCl_6]^{3-}$. Further trap of benzylic radical **27-A** by chiral copper(II) species leads to the formation of chiral copper(III) species, followed by reductive elimination to afford the corresponding chiral nitrile **26** and copper(I) species. The copper(I) species can be further oxidized into copper(II) species at the anode. Later, Xu's group successfully achieved the direct enantioselective cyanation of alkylarenes **28** as benzylic radical precursors, obviating the need for activated precursors to generate alkyl radicals (Scheme 8.5b) [78]. High yields and enantioselectivities are

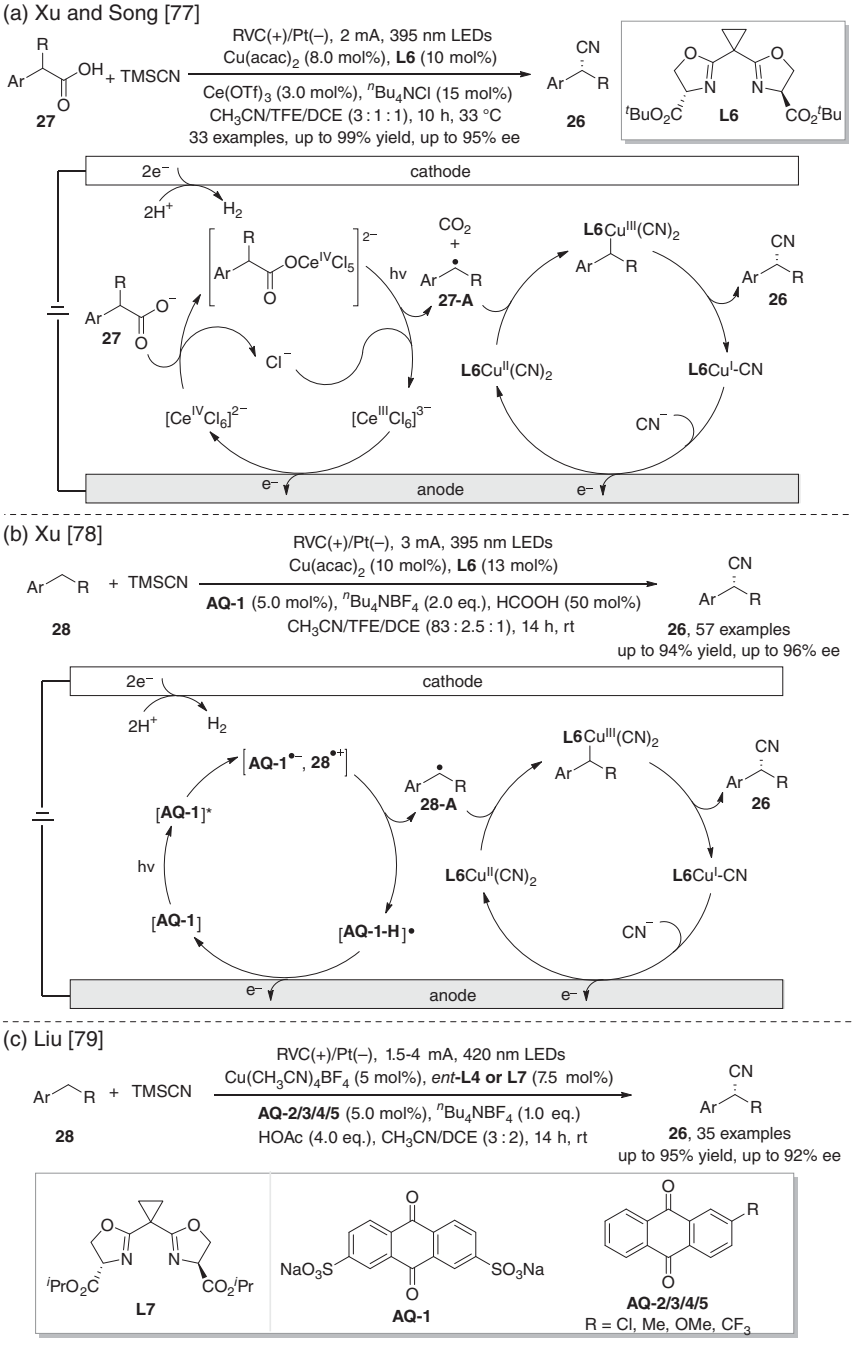


**Scheme 8.5** Enantioselective radical cyanation through photoelectrochemical asymmetric copper catalysis. Sources: (a) Xu and Song [77]/American Chemical Society. (b) Xu [78]/John Wiley & Sons. (c) Liu [79]/American Chemical Society.

achieved for a diverse range of chiral nitriles **26** utilizing **AQ-1** as a HAT photocatalyst in conjunction with chiral Box ligand **L6**. Photoelectrocatalysis is the key to the success of highly site-selective cyanation of multiple benzylic sites, thereby eliminating the necessity for any chemical oxidant and enabling its potential application in the late-stage diversification of complex bioactive molecules and natural products. According to the proposed mechanism, upon photoexcitation, the photocatalyst **AQ-1** can be converted to its excited state, which undergoes SET with alkylarene **28** to form an ion-radical pair. Sequential proton transfer generates a benzylic radical **28-A** and semiquinone radical, which is further oxidized at the anode to regenerate **AQ-1**. The benzylic radical **28-A** would then engage in the analogous enantioselective cyanation process mentioned above.

In analogy with the aforementioned report, Liu and Wang have reported a similar enantioselective cyanation, wherein highly efficient benzylic C—H functionalization was accomplished with exceptional stereocontrol through the utilization of dual photoelectrocatalysis/copper catalysis (Scheme 8.5c) [79]. More recently, Xu and coworkers disclosed a novel photoelectron catalytic method for the enantioselective heteroarylcyanation of alkenes via C—H functionalization [80]. This reaction employs an acridinium salt in conjunction with a chiral copper complex as a coupling catalyst, thereby effectively synthesizing enantioenriched nitriles from readily accessible aryl alkenes and unfunctionalized heteroarenes. Notably, this process represents a rare example of catalytic asymmetric arene radical cation-mediated alkene functionalization.

In addition to the cyanation of alkylarenes, the asymmetric trifluoromethylation of benzylic C—H bonds of alkylarenes is also an attractive but challenging task for chemists. Remarkably, Liu and coworkers have established the first example of an enantioselective radical trifluoromethylation reaction on benzylic C—H bonds through a cooperative photoredox and copper catalysis system (Scheme 8.6) [81]. This protocol allows convenient synthesis of various structurally diverse benzylic

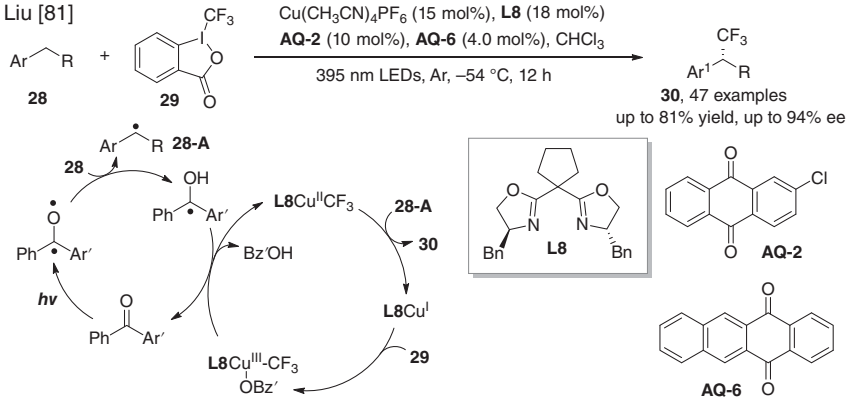


**Scheme 8.6** Dual photoinduced copper-catalyzed asymmetric radical trifluoromethylation of benzylic C—H bonds. Source: Adapted from Liu [81].

trifluoromethylated compounds **30** with good yields and high levels of enantioselectivity. In this process, the photocatalyst facilitates the generation of benzylic radicals from alkylarenes **28** through a HAT process, while the chiral copper complex engages in the ensuing enantioselective trifluoromethylation. Specifically, upon photoexcitation, the photosensitizer is converted into its diradical form, which abstracts a hydrogen atom from alkylarenes **28** to produce benzylic radicals **28-A**. On the other hand, the oxidative addition of copper(I) species with Togni-II reagent **29** results in the formation of copper(III) species, which can be reduced to copper(II) species along with the regeneration of the organic photosensitizer. Then, the capture of benzylic radicals **28-A** by chiral copper(II) species triggers subsequent cross-coupling and affords the desired chiral products **30**, regenerating copper(I) species.

The construction of a C—N bond is involved in five out of the six most commonly employed chemical reactions utilized in drug discovery [84]. As a result, a great deal of modern synthetic efforts have been devoted to designing strategies for direct C—H amination [85, 86]. By employing visible light-driven energy-transfer activation and copper catalysis, Nagib and coworkers reported a robust photoinduced enantioselective radical C($sp^3$)—H amination in 2020, providing access to a diverse array of chiral oxazolines **32** with high yields and enantioselectivities (Scheme 8.7a) [82]. Notably, the $[BArF_4]^-$ counterion of catalysts exhibited superior enantioselectivity compared to other counterions, and a bulky chiral acid played a pivotal role in both yield and enantioselectivity. It is proposed that substrate **31** initially coordinates with copper(I) species, which features a chiral Box ligand and a chiral carboxylate, to generate copper(I) imidate complex **31-A**. Upon excitation, an energy-transfer process occurs between the Ir photocatalyst and **31-A**, resulting in the formation of *N*-centered radical **31-B** via triplet sensitization of the oxime N—O bond to facilitate

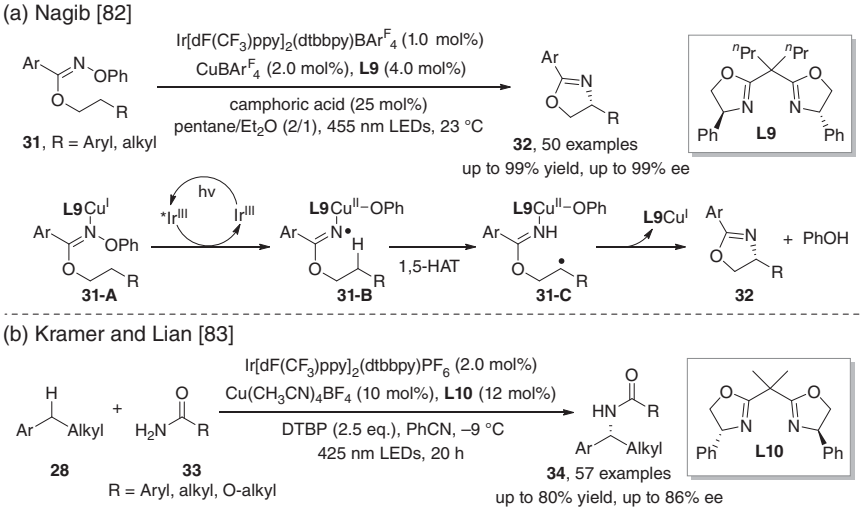


**Scheme 8.7** Dual photoredox/copper-catalyzed enantioselective radical C—H amination reactions. Sources: (a) Nagib [82]/John Wiley & Sons. (b) Kramer and Lian [83]/John Wiley & Sons.

net photoinduced oxidative addition. The resulting intermediate **31-B** can undergo enantio- and regioselective HAT to yield chiral β-radical **31-C**, which can engage in the following coupling transformation to produce enantioenriched oxazoline via copper(III) or copper(II) intermediate, along with release of PhOH and regeneration of copper(I) catalyst. In comparison with intramolecular amination, seeking catalytic strategies toward the enantioselective intermolecular installation of primary amines and amides at the benzylic C—H position remains a preeminent challenge due to the competitive radical-polar crossover pathway. Kramer, Lian, and coworkers described the first HAT-initiated intermolecular benzylic C—H amidation and amination reactions (Scheme 8.7b) [83]. In this process, the enantioselective installation of C—N bonds is enabled by the combination of a chiral copper catalyst and Ir-based photocatalyst, which is considered to effectively prevent the radical-polar crossover that often renders developing enantioselective variants difficult.

### 8.2.2 Bifunctional Catalysis by a Single Chiral Copper Catalyst

In contrast to dual catalysis that involves combining a chiral copper catalyst with an external photocatalyst, chiral ligand/copper or ternary chiral ligand/copper/nucleophile complexes can serve as bifunctional catalysts in photoinduced enantioselective cross-coupling reactions. Specifically, these chiral complexes simultaneously work as both the photocatalyst and the source of asymmetric induction. However, implementing bifunctional catalysis using a single chiral copper catalyst is challenging due to its relatively weak visible-light absorption ability, short excited-state lifetimes, and limited reduction potential window.

In 2016, the groups of Peters and Fu reported a pioneering study that introduced a novel photoinduced enantioselective C($sp^3$)—N cross-coupling strategy by utilizing a complex of copper(I) catalyst and a chiral phosphine ligand as a bifunctional catalyst (Scheme 8.8a) [87]. By utilizing activated alkyl chlorides **35** as alkyl radical precursors and chiral phosphine ligand **L11**, a wide range of chiral C—N coupling products **37** bearing a quaternary carbon stereocenter were synthesized with high yields and enantioselectivities. Based on density functional theory (DFT) calculations and detailed mechanistic studies [90], a reasonable reaction mechanism is also proposed. The initial ligand exchange between the copper(I) catalyst and nucleophile generates a complex **36-B**, which reaches its excited-state upon light irradiation. The subsequent SET process leads to the formation of an alkyl radical **35-A** and a copper(II) complex, which reacts with another nucleophile to generate complex **36-C**. The following interaction with the alkyl radical gives rise to intermediate **36-D**, which undergoes cross-coupling reactions to afford the desired product while regenerating **36-B**. Notably, it was proposed that this process does not involve the formation of an alkylcopper(III) intermediate. Recently, the same group reported a photoinduced copper-catalyzed enantioselective coupling between racemic tertiary alkyl halides **38** or **39** and anilines **40** for synthesizing more advanced amines (Scheme 8.8b) [88]. It is noteworthy that the utilization of uncommon electrophiles, such as alkyl fluoride and alkyl carbonate, has been demonstrated as examples under similar reaction conditions.

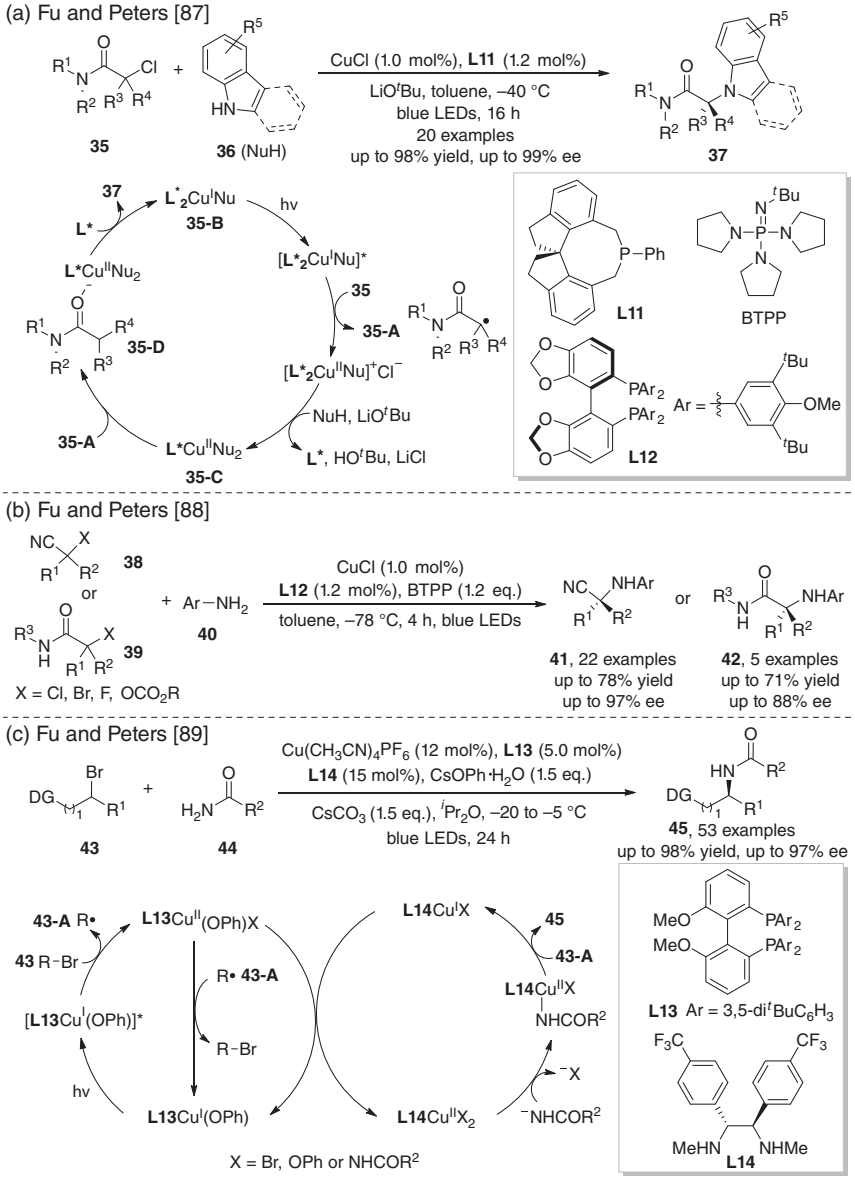


**Scheme 8.8** Photoinduced copper-catalyzed enantioselective radical cross-coupling for formation of C–N bonds. Sources: (a) Adapted from Fu and Peters [87]. (b) Fu and Peters [88]/American Chemical Society. (c) Fu and Peters [89]/John Wiley & Sons.

In addition to amines, Fu and coworkers also expanded the substrate scope of nitrogen nucleophiles to amides by exploiting photoinduced copper catalysis. This protocol provides access to diverse chiral secondary amides **45** with high yields and enantioselectivities (Scheme 8.8c) [89]. Notably, the success of this strategy depends on the use of three classes of ligands to generate two catalytic systems in situ, which

work in a cooperative manner. Specifically, a bidentate phosphine **L13** and a phenoxide coordinate with Cu(I) salt to result in a photocatalyst, which possesses sufficient excited-state lifetime and reduction potential for activating the relatively strong C—Br bond of the unactivated electrophile. Moreover, a bidentate chiral diamine **L14** coordinates with Cu(I) salt to facilitate enantioselective C—N bond formation. Furthermore, a tandem photo- and biocatalytic dynamic kinetic resolution of secondary alcohols and amines for synthesizing chiral amides has been successfully accomplished by utilizing Candida antarctica lipase B (CALB), a commercially available lipase, in conjunction with a heteroleptic copper complex [91].

Aside from phosphine ligands, a range of photoinduced copper-catalyzed asymmetric radical reactions have been developed employing versatile chiral ligands, including Box-type ligands and their variants, and chiral alkaloid-derived multidentate *N*,*N*,*P*-ligands. These catalytic systems provide many methods for the synthesis of a variety of chiral organic molecules. For instance, in 2019, Wang and Xu reported a general visible light-induced copper-catalyzed three-component cyanofluoroalkylation reaction of aryl alkenes (Scheme 8.9) [92]. It was proposed that, under the irradiation of violet LED, the bifunctional chiral copper(I) cyanide coordinated with Box ligands to serve as both a photoredox catalyst for the SET event and an asymmetric cross-coupling catalyst for enantioselective C($sp^3$)—C(sp) bond formation. This transformation shows mild reaction conditions, high reaction efficiency, excellent enantioselectivities, and a broad substrate scope of fluoroalkyl iodides. However, the styrene substrates with strong electron-withdrawing groups, nonconjugated alkenes, and conjugated dienes are incompatible with the reaction conditions.

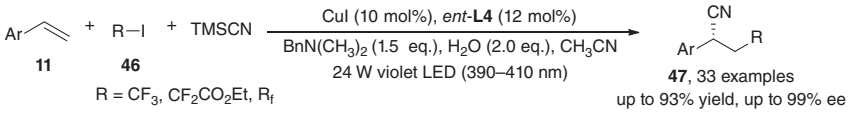


**Scheme 8.9** Photoinduced copper-catalyzed enantioselective radical cyanofluoroalkylation of alkenes. Source: Adapted from Xu and Wang [92].

In addition to chiral copper cyanide, it was found that chiral copper acetylide can also be utilized as a bifunctional catalyst in photoinduced enantioselective radical coupling reactions. In 2020, the Liu group reported a photoinduced copper-catalyzed asymmetric radical decarboxylative alkynylation between terminal alkynes **48** and NNHP-type esters **49** (Scheme 8.10a) [93]. This strategy provides a versatile platform for constructing chiral C($sp^3$)—C(sp) bonds, where the in situ generated chiral copper(I) acetylide, coordinated with cinchona alkaloid-derived N,N,P-ligand **L15**, acts as a dual catalyst for both photoactivation and radical cross-coupling. By fine-tuning the parent NHP-type esters to *N*-hydroxy 2,3-naphthalimide (NNaphth)-derived esters **49**, the undesired homodimerization of terminal alkynes and alkyl radicals can be effectively suppressed. Besides aryl-substituted NHP-type esters, the allylic and aminocarbonyl substrates are also suitable for the reaction to afford the expected products with good enantioselectivities, albeit in low yields. Unfortunately, the homobenzylic substrate yielded a racemic coupling product, while the

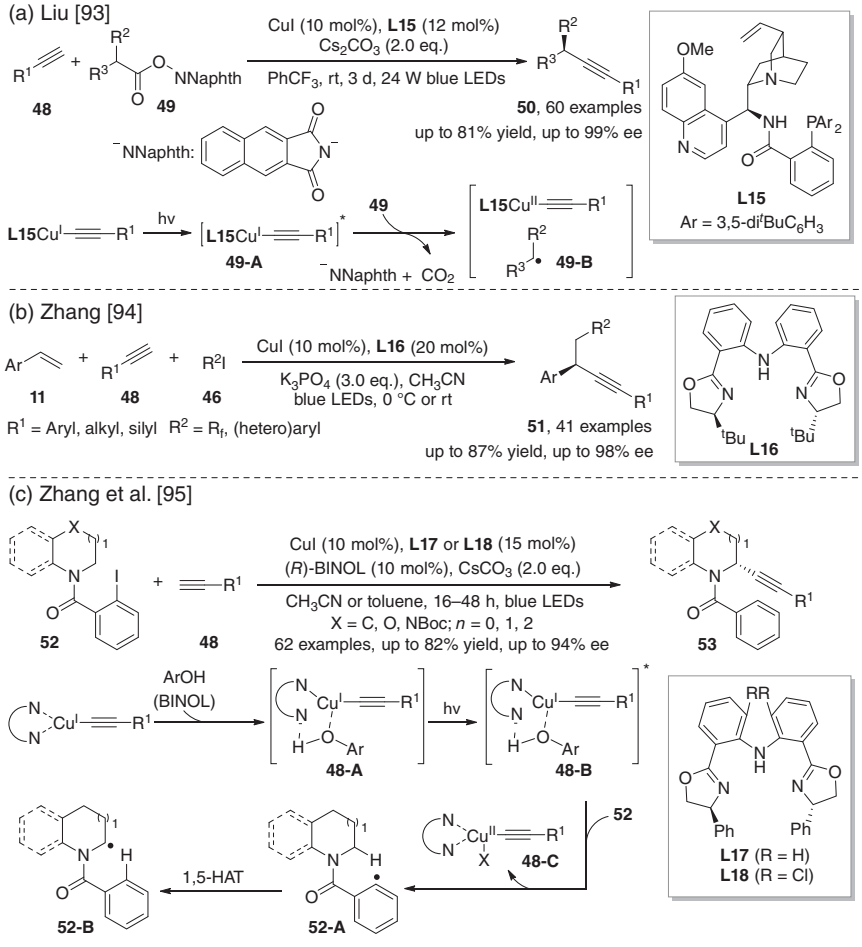


**Scheme 8.10** Photoinduced copper-catalyzed asymmetric C($sp^3$)—H radical alkynylation. Sources: (a) Liu [93]/John Wiley & Sons. (b) Zhang [94]/American Chemical Society. (c) Zhang et al. [95]/John Wiley & Sons.

tertiary substrates failed to provide the desired products. According to the proposed mechanism, a photoactive complex **49-A** is first formed from the chiral copper(I) catalyst and acetylene **48** in the presence of $Cs_2CO_3$. Then, this complex is excited to its photoexcited state **49-A*** upon visible light irradiation. Subsequently, the excited copper acetylide **49-A*** can donate an electron to NNHP-type ester **49**, resulting in the formation of chiral copper(II) complex and radical intermediate **49-B,** followed by the decarboxylation process. Finally, this intermediate **49-B** undergoes C($sp^3$)—C(sp) bond-forming cross-coupling with chiral copper(II) complex, leading to chiral alkyne products **50** with the release of copper(I) species to complete the catalytic cycle. Employing a single chiral complex consisting of a copper acetylide complex and a bisoxazoline diphenylamine ligand **L16**, Zhang and coworkers developed a novel copper-catalyzed enantioselective 1,2-dicarbofunctionalization

of alkenes under visible light irradiation (Scheme 8.10b) [94]. In this process, unactivated alkenes and disubstituted styrenes are not compatible. Later, Zhang, Qi, and Guo reported a photoinduced copper-catalyzed asymmetric C($sp^3$)—H alkynylation of unactivated cyclic 2-iodo-benzamides **52** (Scheme 8.10c) [95]. By employing intramolecular 1,5-HAT and the chiral bisoxazoline diphenylamine (BOPA) ligand, a wide range of chiral propargyl amines were successfully obtained with high yields and enantioselectivities. It was proposed that a stable hydrogen-bonding complex **48-A** derived from copper(I) acetylide complex and BINOL may be a possible key intermediate in this process, and BINOL plays an important role in improving the reduction potential of the copper(I) complex. Thus, the photoexcitation SET from the excited-state copper complex **48-B** to an electrophile can generate a copper(II) acetylide **48-C** and a phenyl radical **52-A**. Then, a facile phenyl radical-based 1,5-HAT event creates an α-amino carbon-centered radical intermediate **52-B**. Finally, the copper(II) complex **48-C** undergoes enantioselective cross-coupling with radical intermediate **52-B** to yield the corresponding product **53** and regenerate a chiral copper(I) complex.

In addition to chiral copper cyanide and copper acetylide, the Box/copper(I)/azole complex has also proven to be remarkably efficient as a bifunctional catalyst in photoinduced enantioselective cross-coupling reactions. In 2021, Zhang and coworkers achieved a highly enantioselective alkylation reaction between azoles **54** and secondary alkyl bromides **55** (Scheme 8.11) [96]. However, unactivated alkyl bromides, α-bromoketones, and pseudo halides such as these with OMs group fail to participate in this reaction. Key to the success of this protocol is the generation of a photoactive complex from copper(I) salt, azole substrate, and chiral bisoxazoline diphenylamine ligand.

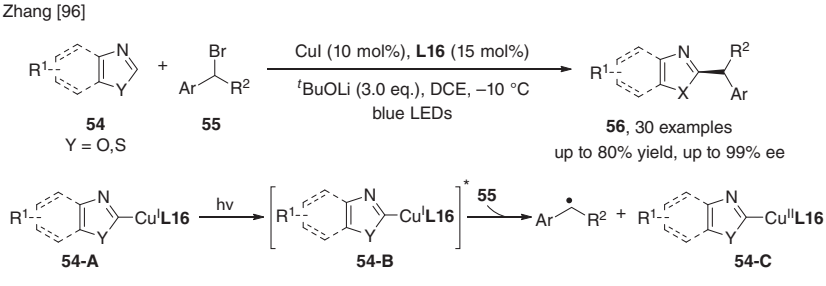


**Scheme 8.11** Photoinduced copper-catalyzed asymmetric radical alkylation of azoles. Source: Zhang [96]/John Wiley & Sons.

In 2021, Wang and Xu reported a visible-light-induced copper-catalyzed enantioselective C($sp^3$)—H alkylation using chiral bisphosphine ligand **L19**, providing access to unnatural α-amino acids **59** bearing primary, secondary, and tertiary alkyl fragments in good yields with high enantioselectivities (Scheme 8.12) [97]. The presence of a quinoline auxiliary played a crucial role in this reaction by coordinating with the chiral copper complex to generate a novel chiral photoactive species, thereby effectively controlling the stereochemistry and suppressing the competing

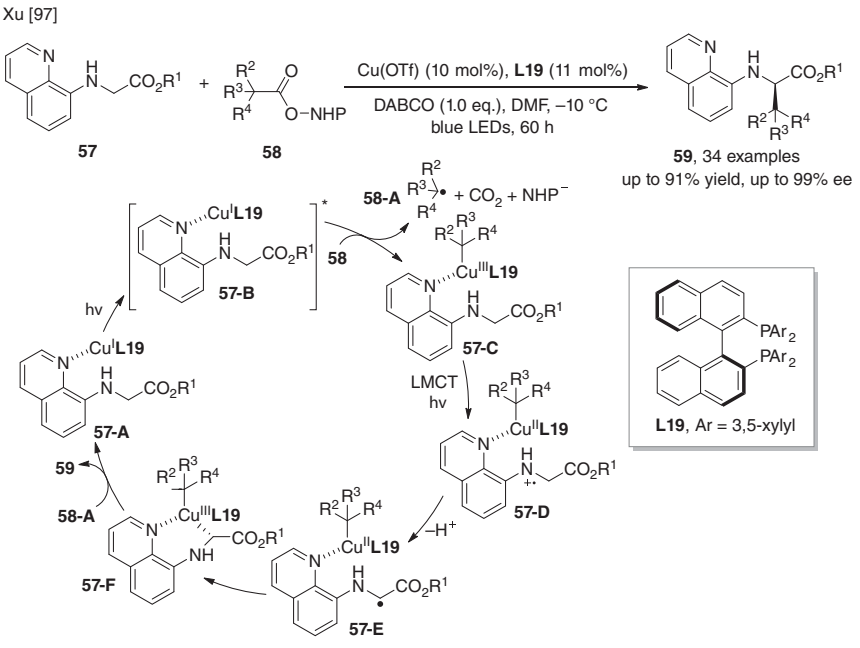


**Scheme 8.12** Photoinduced copper-catalyzed enantioselective C($sp^3$)—H alkylation. Source: Xu [97]/American Chemical Society.

racemic background reaction. As shown in the proposed mechanism, substrate **57** initially coordinates with the chiral copper(I) complex to form intermediate **57-A**, which is excited to **57-B** upon visible light irradiation. Then, SET happens between **57-B** and NHP esters **59** to yield an alkyl radical **58-A**, followed by recombination of substrate-bound copper(II) species to form the intermediate **57-C**. Intramolecular LMCT of intermediate **57-C** leads to a new radical cation **57-D**, which undergoes deprotonation to produce α-amino carbon radical **57-E**. Sequential intramolecular recombination with copper results in copper(III) species **57-F**, followed by reductive elimination to afford the desired product **59**.

Xiao, Chen, and coworkers have demonstrated for the first time that the in situ-formed ternary ligand/copper/carboxylate complex could serve as both the photoactive catalyst and coupling catalyst in enantioselective C—O bond-forming reactions. Using this concept, they recently developed an interesting visible-light-driven copper-catalyzed asymmetric allylic C—O coupling between readily available 1,3-dienes **60** and oxime esters **61** with a chiral copper complex (Scheme 8.13a) [98]. In this process, the chiral copper catalyst functions not only as the photoredox catalyst for generating alkyl radicals but also as the source for asymmetric induction. Building on the catalytic strategy, they further developed a three-component variant using exogenous carboxylic acids **64** as *O*-nucleophiles and Boc-protected oxime esters **63** as radical precursors (Scheme 8.13b) [99]. Note that the minor structural modification of oxime esters is critical to the reaction, which can avoid the competing coupling of the carbonate anion formed in the

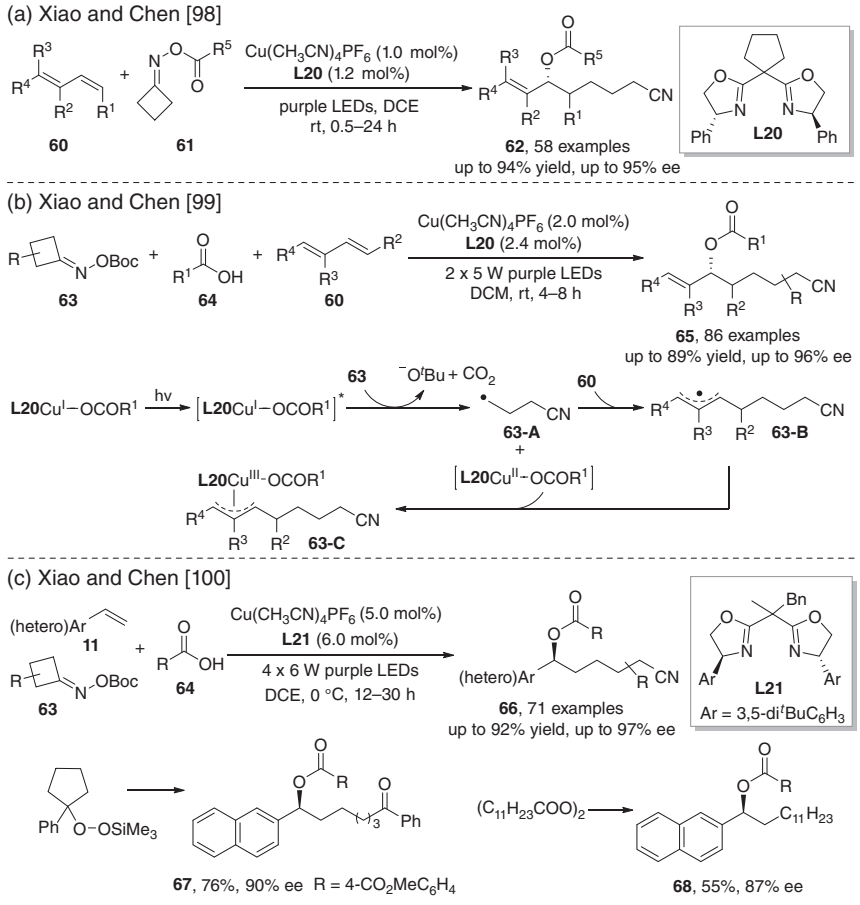


**Scheme 8.13** Photoinduced copper-catalyzed enantioselective radical C—O coupling. Sources: (a) Xiao and Chen [98]/American Chemical Society. (b) Adapted from Xiao and Chen [99]. (c) Xiao and Chen [100]/American Chemical Society.

initial radical-generating step. This modular protocol exhibits broad substrate scope and good functional group tolerance, particularly regarding the carboxylic acids and 1,3-dienes, providing modular access to valuable chiral allylic esters **65** with excellent regio- and enantioselectivities. Mechanistically, the SET reduction of the oxime ester **63** forms a cyanoalkyl radical **63-A**, which can be trapped by 1,3-dienes to form an allylic radical **63-B**. This intermediate can participate in the subsequent asymmetric radical C—O coupling via a high-valent Cu(III) species.

Encouraged by these results, the same group further extended the catalytic system to the asymmetric three-component radical carboesterification of (hetero)aryl alkenes (Scheme 8.13c) [100]. For this transformation, a major challenge can be attributed to the involvement of easily oxidizable benzylic-type radicals and the dearth of efficient coordinating groups to direct the enantioselective coupling pathway. It was envisioned that an aryl $\pi$-allyl-copper(III) complex could be formed

from a benzylic radical with a chiral copper catalyst to facilitate the asymmetric C—O cross-coupling. The majority of the commonly employed Box-type ligands exhibited moderate enantioselectivities in this reaction. Nevertheless, by finely tuning the ligand scaffold, a Box ligand **L21** featuring 3,5-bis(tert-butyl)phenyl groups has been identified as the optimal candidate, demonstrating exceptional high enantioselectivity. DFT calculations also suggest that the observed high enantioselectivity arises from the formation of an aryl enyl $[\sigma + \pi]$-copper complex between the incipient $sp^3$-hybridized carbon radical and carboxylic acid, which thus induces highly enantioselective cross-coupling. This working hypothesis is also in accordance with the substrate scope; as such, naphthyl and extended-conjugated alkenes have proven superior over simple styrene. Remarkably, as for the radical precursors, in addition to cycloketone-derived oxime esters, both alkylsilyl peroxide and lauroyl peroxide (LPO) have proven to be suitable precursors to alkyl radicals, with the corresponding products **67** and **68** being obtained with satisfactory results. Except for carboesterification of the allyl and benzyl positions, Xiao, Chen, and coworkers also reported a radical-mediated three-component coupling of 1,3-enynes, oxime esters, and carboxylic acids with photoinduced copper catalysis. This protocol provides access to a library of valuable cyanoalkylated propargylic esters with good yield and excellent enantioselectivities [101].

## 8.3 Photoredox/Nickel-Catalyzed Asymmetric Radical Reactions

Nickel catalysis has been well established as a versatile methodology for facilitating cross-coupling reactions, including Suzuki-Miyaura, Negishi, Hiyama, Stille, and Kumada coupling reactions [102]. Cooperative photoredox/nickel catalysis, pioneered by Molander, MacMillan, and Doyle, offers new prospects for the cleavage and reconstruction of specific carbon–carbon or carbon–heteroatom bonds. In such catalytic systems, a diverse array of common functionalities, including abundant carboxylic acids, organoboron reagents, aldehydes, and even inert C—H bonds, can be readily transformed into the corresponding carbon-centered radicals, which can subsequently participate in nickel-catalyzed cross-coupling reactions to form new chemical bonds. As such, the use of organometallic reagents can be avoided. However, the high reactivity and instability of various open-shell radical species have often presented significant challenges in the development of enantioselective transformations, even when utilizing chiral nickel complexes. Over the past few years, substantial efforts have been dedicated to controlling the stereochemistry of the transformation of these active intermediates, especially the asymmetric variants [103–106].

### 8.3.1 Redox-Neutral Enantioselective Radical Transformations Enabled by Dual Photoredox/Nickel Catalysis

In 2014, Molander and coworkers reported a powerful photoredox/nickel dual system for the coupling of potassium benzyltrifluoroborates **70** with aryl bromides

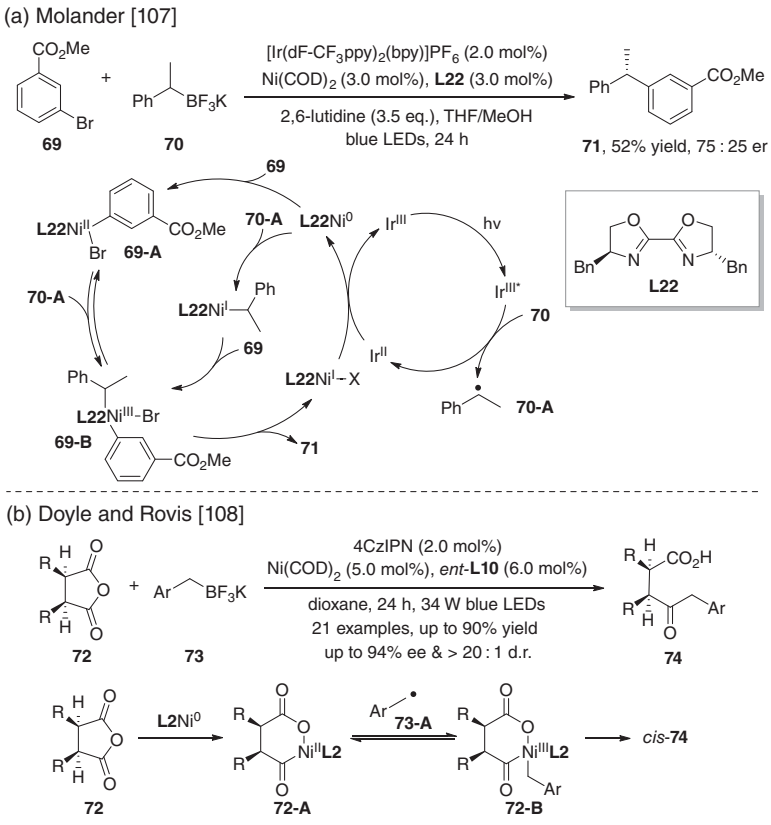


**Scheme 8.14** Dual photoredox/nickel-catalyzed enantioselective cross-coupling of benzylic trifluoroborates. Sources: (a) Adapted from Molander [107]. (b) Doyle and Rovis [108]/John Wiley & Sons.

**69** under mild conditions (Scheme 8.14a) [107]. The groundbreaking achievement utilizes alkyl radicals as nucleophilic coupling partners instead of organometallic nucleophiles, rendering it unattainable through the single use of either nickel catalysis or photoredox catalysis alone. Using a chiral bisoxazoline ligand **L22**, they demonstrated that an arylative product **71** can be generated with moderate enantioselectivity (50% ee). Although only a single example was examined for the asymmetric induction, yet it represents the first example of enantioselective photoredox/nickel-catalyzed cross-coupling reactions. As for the mechanism, the authors proposed a Ni(0)-Ni(II)-Ni(III)-Ni(I) cycle consisting of oxidative addition, radical trapping, and reductive elimination as the key steps. However, DFT calculations revealed that both outlined catalytic cycles are feasible, but the Ni(0)-Ni(I)-Ni(III)-Ni(I) cycle is more favorable due to a lower energy barrier [109]. This mechanism involves the radical addition of an alkyl radical **70-A** to Ni(0) species, delivering a Ni(I) intermediate. The following oxidative addition of aryl bromide **69** to Ni(I) species generates a Ni(III) intermediate. Moreover, the final reductive elimination was computationally determined to serve as the enantiodetermining

step. In a subsequent study, the group of Molander also utilized an alkyltrifluoroborate as the nucleophile coupling partner to react with aryl- and heteroaryl bromides, affording the arylation products with modest enantioselectivities [110].

In 2017, Doyle, Rovis, and coworkers demonstrated a photoredox/nickel-catalyzed enantioselective desymmetrization of cyclic meso-anhydrides **72** with benzyl trifluoroborates **73** (Scheme 8.14b) [108]. In this process, a wide range of sterically and electronically diverse trifluoroborates and cyclic anhydrides can be successfully cross-coupled in this protocol with excellent diastereo- and enantioselectivities. Mechanistically, the authors propose that the reaction was initiated through the enantiodetermining oxidative addition of cyclic anhydrides prior to benzylic radical capture. This proposed catalytic pathway differs from the mechanism mentioned above via a Ni(0)/(I)/(III) pathway [109], which suggests that radical capture occurs before oxidative addition.

Besides potassium trifluoroborates as radical precursors, the groups of MacMillan and Doyle have also developed a seminal photoredox/nickel-catalyzed decarboxylative arylation of amino acids [111]. In 2016, MacMillan and Fu proved that such transformations can be rendered enantioselective by utilizing a chiral cyano-Box ligand **L23** (Scheme 8.15a) [112]. Various naturally occurring amino acids **76** are readily coupled with aryl- and heteroaryl bromides **75**, resulting in enantioenriched benzylic amine products **77**, including pharmaceutically relevant derivatives. However, electron-neutral aryl halides only exhibited modest ee (66%) and comparable yield in this system. It was proposed that a photoinduced SET between amino acids and photoexcited iridium-based catalyst generates an α-amino carbon radical **76-A**, which interacts with the Ni(II) species to afford the corresponding chiral product **77** through a Ni(0)/(II)/(III)/(I) pathway. Recently, Davidson and Bonifazi demonstrated that a chiral pyridineoxazoline ligand **L24** enables rapid synthesis

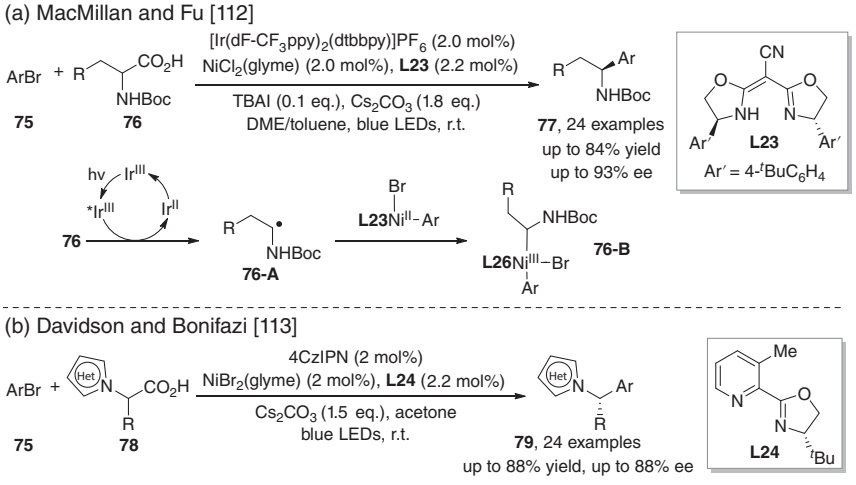


**Scheme 8.15** Dual photoredox/nickel-catalyzed enantioselective decarboxylative arylation. Sources: (a) Adapted from MacMillan and Fu [112]. (b) Adapted from Davidson and Bonifazi [113].

of enantioenriched *N*-benzylic heterocycles with α-heterocyclic carboxylic acids **78** through dual nickel and photoredox catalysis (Scheme 8.15b) [113]. It is found that a directing group on the heterocyclic moiety of carboxylic acid substrates is crucial for efficient asymmetric induction, while electron-neutral and electron-rich aryl bromides are ineffective electrophiles in this process.

Besides the use of trifluoroborates and carboxylic acids as radical precursors, considerable efforts have been devoted to expanding the range of nucleophilic radical coupling partners of photoredox/nickel-catalyzed processes. In this context, Melchiorre and coworkers reported an elegant example of photoinduced nickel-catalyzed enantioselective acylation of 4-alkyl-1,4-dihydropyridines (DHPs) **80** without the need for any additional photosensitizer. This method provides access to a wide variety of enantioenriched α-substituted ketones **82** (Scheme 8.16) [114]. This process is proposed to begin with the direct excitation of DHPs **80** to their excited states, which can function as a strong SET reductant [115]. Consequently, an electron transfer occurs between the photoexcited DHP substrate and Ni(I) species, resulting in a Ni(0) complex and a carbon-centered radical **80-A**. Subsequently, the oxidative addition of an anhydride **81** to Ni(0) species yields the Ni(II) complex, which readily intercepts the initially formed radical **80-A** to form Ni(III) species. The final reductive elimination followed by a SET process produces the acylation product **82** and regenerates the Ni(0) complex.

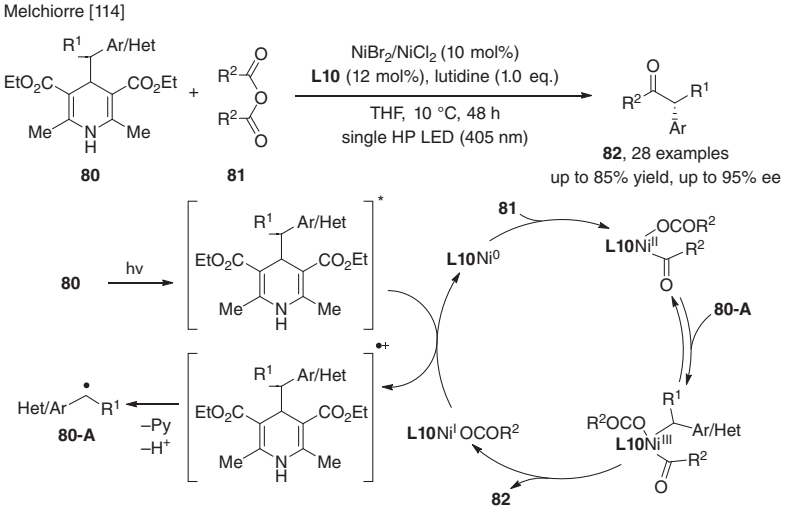


**Scheme 8.16** Photoredox/nickel-catalyzed enantioselective radical acylation reaction between 4-alkyl-1,4-dihydropyridines and anhydrides. Source: Melchiorre [114]/John Wiley & Sons.

In addition to the two-component radical asymmetric reactions, the application of photoredox/nickel dual catalysis to three-component variants can also be achieved using an oxidative radical generation strategy. For instance, the groups of Chu and Gutierrez disclosed an enantioselective three-component carboarylation of alkenes **83** with secondary and tertiary alkyltrifluoroborates **84** and aryl bromides **75** in 2020

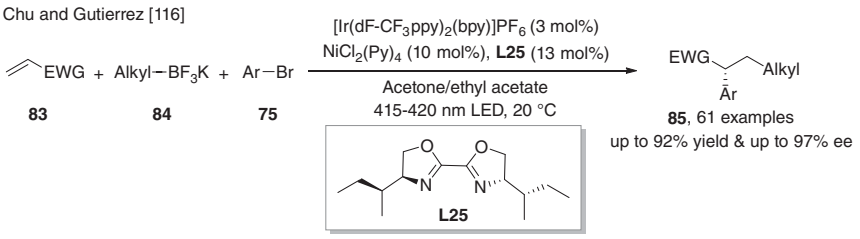


**Scheme 8.17** Dual photoredox/nickel-catalyzed enantioselective three-component radical carboarylation of alkenes. Source: Chu and Gutierrez [116]/American Chemical Society.

(Scheme 8.17) [116]. Under visible light-driven redox-neutral conditions, this synergistic catalytic system enables direct access to structurally diverse chiral α-arylated carbonyls **85** with excellent efficiency and enantioselectivities from readily available starting materials. Besides, the synthetic potential of this catalytic strategy has also been demonstrated through the divergent and enantioselective synthesis of flurbiprofen analogs and piragliatin lead compounds. Computational and experimental studies were conducted, identifying a favored Ni(0)/(II)/(III)/(I) catalytic cycle. It was hypothesized that the radical addition to the tetrahedral Ni(II) center, rather than reductive elimination, serves as the stereodetermining step.

As depicted above, the asymmetric radical transformations of carboxylates and trifluoroborates as alternatives to organometallic reagents have demonstrated promising enantioselectivity in various carbon–carbon bond formations. However, the direct functionalization of inert C($sp^3$)—H bonds is still a synthetically appealing but formidable challenge in organic synthesis [117–121]. In addition to SET-mediated direct C($sp^3$)—H functionalization, the activation of C($sp^3$)—H bonds can also be achieved through a visible light-driven HAT mechanism.

In 2018, Martin and coworkers demonstrated the feasibility of combining a triplet ketone sensitizer and a nickel catalyst to enable direct C($sp^3$)—H radical arylation reactions (Scheme 8.18a) [122]. A notable feature is that the cost-effective and straightforward triplet-excited ketone **AQ-7** can serve as both a HAT catalyst and a SET catalyst, integrating nickel-catalyzed fragment cross-coupling with triplet catalysis. This approach offers a complementary strategy for addressing the long-standing challenge in enantioselective C($sp^3$)—H functionalization reactions. When employing ligand **L26**, an enantiomeric excess of 54% was achieved. In a follow-up study, a dual nickel and photoredox system was developed for C($sp^3$)—H arylation and alkylation of benzamides (Scheme 8.18b) [123]. The chiral Box ligand **L27** exhibited effective asymmetric induction with up to 92% ee; however, only three examples (**90**) were reported for this enantioselective reaction.

In 2019, Lu and coworkers reported an elegant approach for direct enantioselective benzylic C($sp^3$)—H arylation of alkylbenzenes **28** with aryl bromides **75** via a dual photoredox/nickel catalysis strategy (Scheme 8.19a) [124]. A chiral bis(imidazoline) catalyst **L28** has proven to be effective for this transformation. This protocol provides an opportunity for enantioselective synthesis of 1,1-diarylalkanes using abundant

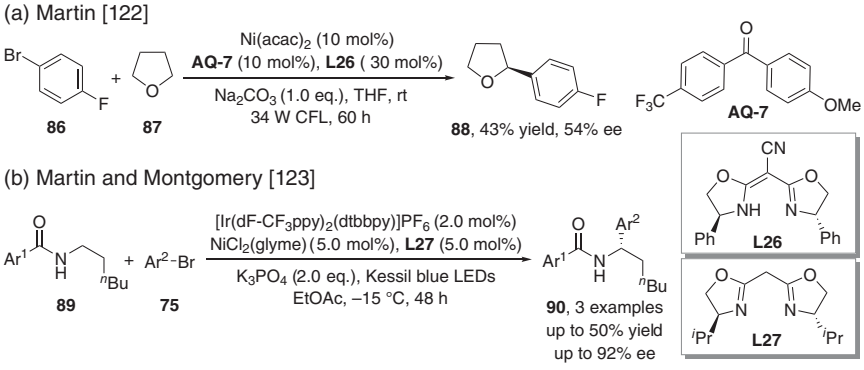


**Scheme 8.18** Dual photoredox/nickel-catalyzed direct asymmetric C($sp^3$)—H radical arylation. Sources: (a) Martin [122]/American Chemical Society. (b) Adapted from Martin and Montgomery [123].

C($sp^3$)—H precursors, featuring high step- and atom-economy. The key to the success of this protocol is that the bromine radical generated in situ serves as a HAT reagent to activate the inert benzylic C—H bond. The proposed mechanism involves the oxidative addition of aryl bromide **75** with a chiral Ni(0) catalyst, resulting in a Ni(II) species. This intermediate then undergoes SET with the excited photocatalyst, leading to a bromine radical and a Ni(II) species. Subsequently, the bromine radical abstracts a hydrogen atom from substrate **28** with bis(4-methoxyphenyl)methanone (DMBP) as a cocatalyst, generating a benzyl radical **28-A**, which can be trapped by aryl Ni(II) species to afford a Ni(III) complex. The reductive elimination of the Ni(III) complex affords the chiral 1,1-diaryl alkanes **91** and produces a Ni(I) complex, which could undergo single-electron reduction by the Ir(II) species to regenerate the Ni(0) species and the photocatalyst Ir(III) complex. Notably, Huo and coworkers demonstrated that such bromine radical-mediated C($sp^3$)—H cleavage strategy is also applicable to enantioselective β-C($sp^3$)—H arylation of *N*-phenylbenzenepropanamides with a range of structurally diverse (hetero)aryl bromides, which provides the arylation products in up to 96% yield with up to 95% ee [127]. The carbonyl group of amides plays a crucial role in the efficient asymmetric induction by complexation of the oxygen atom of the amide moiety with nickel species. The importance of chelation for enantioinduction has also been observed in decarboxylative arylation of α-heterocyclic carboxylic acids by Davidson and Bonifazi [113].

In addition to enantioselective C($sp^3$)—H arylation, Lu and coworkers expanded this protocol to the enantioselective benzylic C—H alkenylation of alkylbenzenes **28** with vinyl bromides **92** in subsequent studies, providing a variety of *E*-alkenes **95** with good enantioselectivities (Scheme 8.19b) [125]. The stilbenes **93** and **94**, possessing significantly lower triplet energies, have been used for the first time in the stereoconvergent synthesis of alkenes by suppressing the photoinduced *E*/*Z* isomerization of the products. Although this protocol is not applicable for synthesizing thermodynamically unfavored *Z* isomers and needs a large excess of

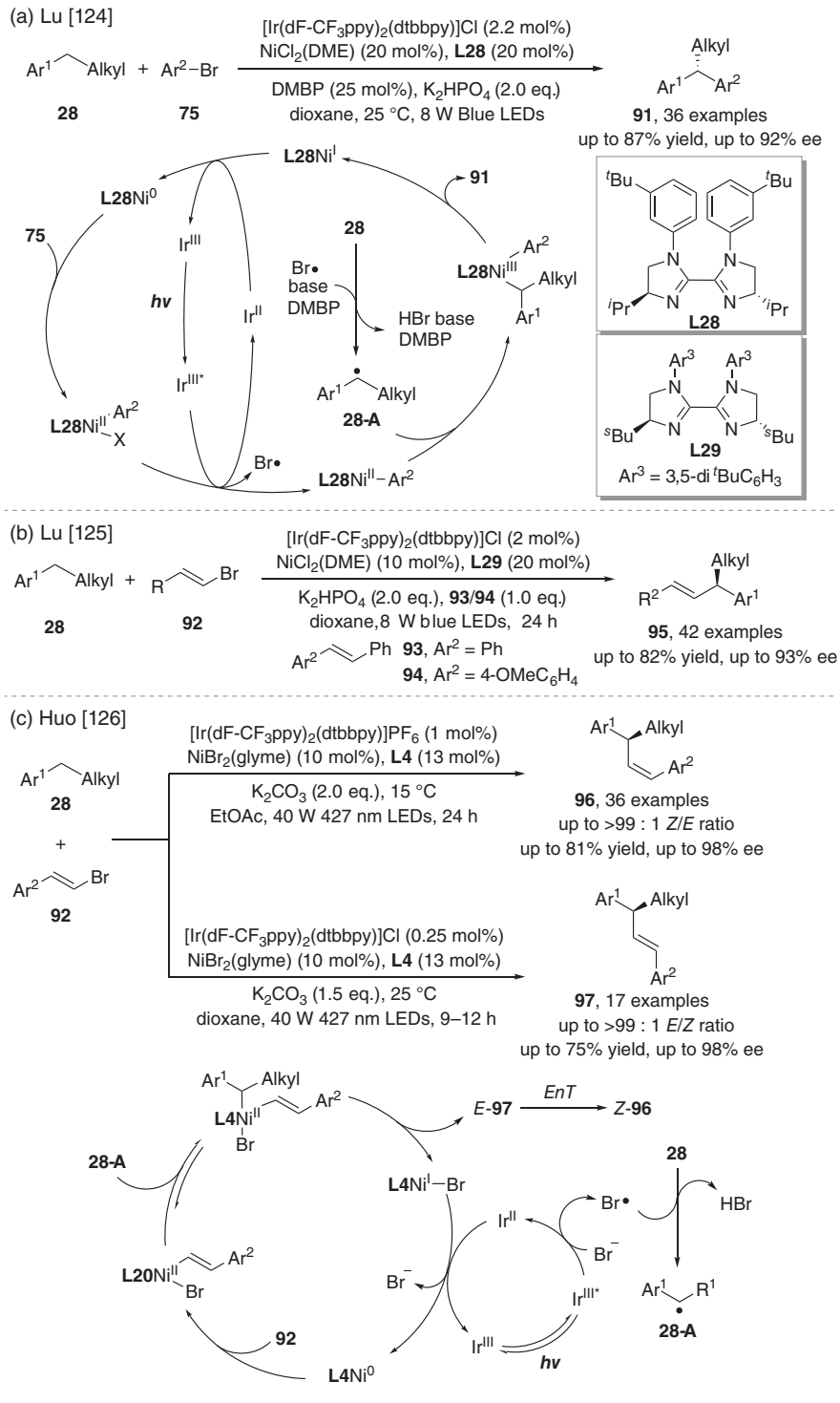


**Scheme 8.19** Dual photoredox/nickel-catalyzed enantioselective benzylic C($sp^3$)—H arylation and alkenylation of alkylbenzenes. Sources: (a) Lu [124]/Springer Nature/CC BY 4.0. (b) Lu [125]/American Chemical Society. (c) Huo [126]/American Chemical Society.

C—H coupling partners, it showcased the practicality of vinyl electrophiles in dual photoredox/nickel-catalyzed asymmetric carbon–carbon bond formation.

At almost the same time, Huo and coworkers independently reported a stereodivergent and enantioselective alkenylation reaction with tunable *Z*/*E*-selectivity (Scheme 8.19c) [126]. This protocol allows the simultaneous synthesis of enantioenriched *Z*- and *E*-olefins under slightly modified conditions, providing an alternative approach to accessing stereodefined and highly functionalized olefins. Importantly, the *Z*/*E* selectivity is simply tuned by the counteranion effect of the Ir-based photocatalyst. The use of $[PF_6]^-$ counteranion readily generates thermodynamically unfavored *Z*-olefins, facilitating more efficient energy transfer for *E*/*Z* alkene isomerization. On the other hand, photocatalyst with chloride anions produces the corresponding *E* isomers. These findings are also in accordance with Yoon and Meyer's elegant studies on counteranion effects of photocatalysts, which demonstrated that a more coordinating counteranion can decrease lifetime or triplet excited-state energy [128, 129]. Based on this concept, Chu, Gutierrez, and coworkers also developed a dual photoredox/nickel-catalyzed asymmetric three-component radical cross-coupling reaction of available vinyl phosphonates, alkenyl halides, and alkyl trifluoroborates [130]. This protocol provides convenient access to a diverse array of α-alkenyl phosphonates in good yields and with excellent chemo-, region-, stereo-, and enantioselectivities. The key to the success of this reaction lies in the fact that different photocatalysts with variable triplet energy levels can produce *trans* and *cis* α-alkenyl phosphonates individually.

Although significant progress has been made in dual photoredox/nickel-catalyzed C($sp^3$)—H functionalization, the sporadic successful protocols are typically limited to the use of aryl halides as electrophiles and often require a large excess of C—H coupling partners for an effective HAT process. In 2020, Huo and coworkers reported a direct enantioselective acylation of α-amino C($sp^3$)—H bonds with carboxylic acids **98** to construct highly valuable and enantioenriched α-amino ketones **100**, which requires only three equivalents of C—H nucleophiles for highly effective C($sp^3$)—H acylation (Scheme 8.20a) [131]. The key to the success of this protocol relies on the bromine radical-mediated HAT of an α-amino C($sp^3$)—H bond, which produces a prochiral α-amino carbon radical, and the formation of acyl electrophiles in situ through the activation of dimethyl dicarbonate (DMDC). This hypothesis is mechanistically distinct from the photoinduced bromine radical-mediated HAT process described by Lu [124]. Specifically, a dissociated bromide anion is oxidized by the excited photocatalyst to produce a bromine radical. Subsequent HAT between an *N*-alkyl benzamide **99** and the bromine radical generates a prochiral α-amino radical **99-A**. Concurrently, the oxidative addition of Ni(0) complex with an in situ-activated carboxylic acid **98-A** results in a Ni(II) species that can readily intercept the α-amino radical **99-A**, leading to a Ni(III) complex. The final enantiodetermining reductive elimination produces the enantioenriched acylation product **100** and a Ni(I) complex.

In a subsequent study, the same group expanded this strategy to benzylic C($sp^3$)—H acylation with alkylbenzenes. A variety of alkylbenzenes and carboxylic acids can be readily cross-coupled through such a dual catalytic system

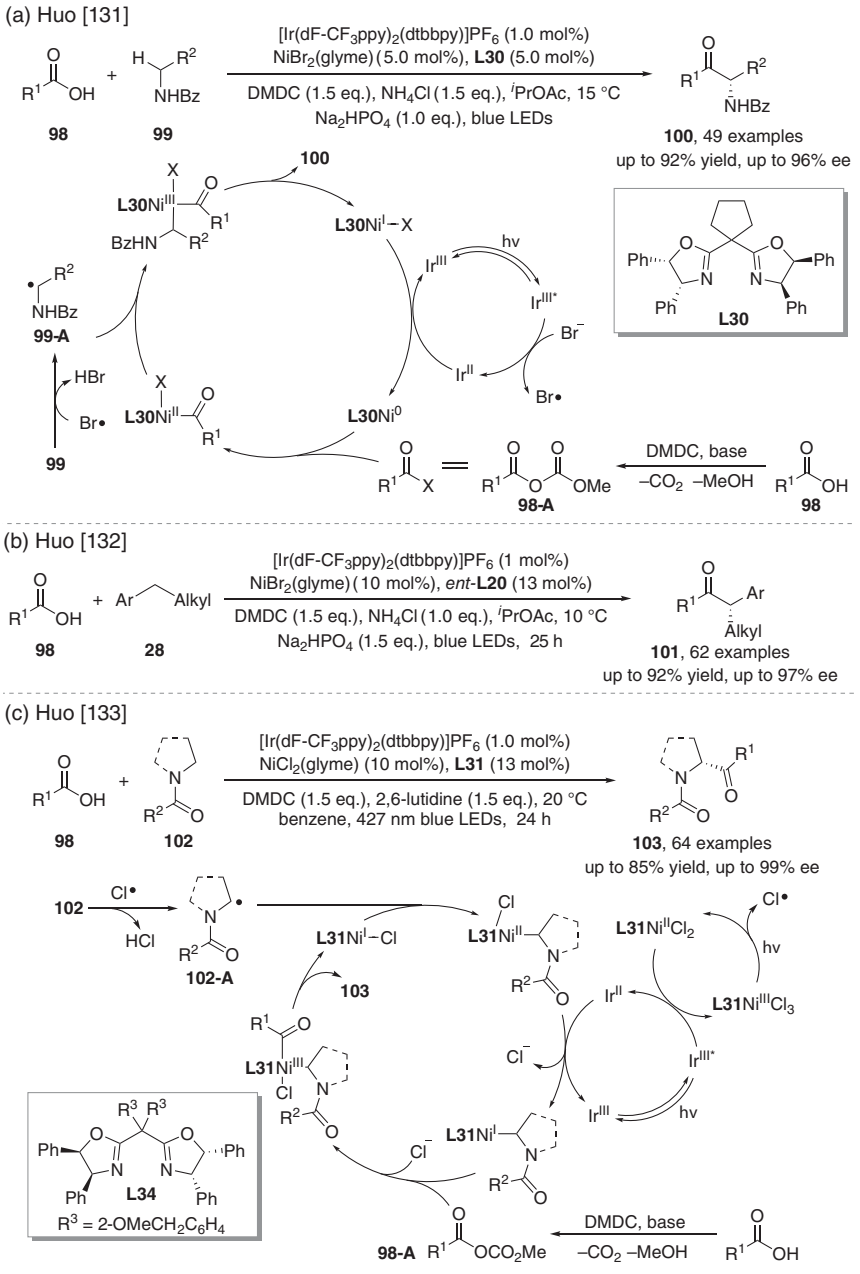


**Scheme 8.20** Photoredox/nickel-dual-catalyzed enantioselective radical C($sp^3$)—H acylation. Sources: (a) Adapted from Huo [131]. (b) Huo [132]/Springer Nature/CC BY 4.0. (c) Huo [133]/Springer Nature/CC BY 4.0.

(Scheme 8.20b) [132]. Moreover, by replacing the in situ-activated carboxylic acids with commercially available chloroformates, this catalytic platform can be applied to the efficient synthesis of chiral α-aryl esters with high enantioselectivities. The carbamoylation of benzylic C—H bonds with isocyanates for the synthesis of α-aryl amides was also achieved by Murakami and coworkers through a similar bromine-radical-mediated C—H activation strategy. They disclosed a single example of the synthesis of enantioenriched α-aryl amide in 34% yield and with 74% ee [134].

Recently, Huo and coworkers reported a site- and enantioselective α-acylation of saturated *N*-heterocycles **102** by utilizing the HAT reactivity of photogenerated chlorine radical to selectively functionalize cyclic α-amino C($sp^3$)—H bonds (Scheme 8.20c) [133]. According to the proposed mechanism, a Ni(II) dichloride is oxidized by the excited photocatalyst to form Ni(III) trichloride species. Subsequently, the photolysis of this Ni(III) trichloride complex generates a chloride radical and regenerates the Ni(II) dichloride. Then, the photogenerated chloride radical selectively abstracts a hydrogen atom of the most hydridic α-amino C($sp^3$)—H bond to produce a prochiral α-amino carbon radical **102-A**. The radical capture by a Ni(I) chloride occurs, followed by SET reduction with a reduced photocatalyst to produce a Ni(I)-alkyl complex. This complex then undergoes oxidative addition with an in situ-activated carboxylic acid to form a Ni(III) complex, which undergoes reductive elimination to yield the enantioenriched coupling products **103**.

In addition to C($sp^3$)—H bonds, C($sp^2$)—H bonds can also serve as nucleophilic coupling partners for the nickel photoredox-catalyzed enantioselective radical transformations. For example, Wang and coworkers reported a highly enantioselective acyl-carbamoylation of alkenes via the cooperative catalysis of a chiral nickel/PHOX **L32** complex and tetrabutylammonium decatungstate (TBADT) (Scheme 8.21a) [135]. This protocol provides access to various oxindoles **106** bearing a quaternary stereogenic center in a highly enantioselective manner. In this process, TBADT functions as a bifunctional photocatalyst to mediate both HAT and SET pathways. It is proposed that the mechanism involves the capture of the acyl radical **105-A**, oxidative addition of carbamoyl chloride followed by intramolecular migratory insertion, and reductive elimination to yield the cross-coupled product **106** and a Ni(I) species. The migratory insertion step is proposed to be the enantiodetermining step. However, an alternative pathway cannot be ruled out, which involves the oxidative addition of carbamoyl chloride to a low-valent Ni(0) complex followed by acyl radical addition for the formation of the Ni(III) species. Shortly thereafter, the same group also achieved an asymmetric imino-acylation of oxime ester-tethered alkenes **107** using readily available aldehydes as the acyl radical sources, allowing the synthesis of highly enantioenriched pyrrolines **108** under mild reaction conditions (Scheme 8.21b) [136].

### 8.3.2 Enantioselective Reductive Cross-Couplings

Recently, nickel-catalyzed reductive cross-coupling (RCC) reactions, which involve the coupling of two electrophiles in the presence of a terminal reductant, have emerged as a robust platform for the construction of diverse

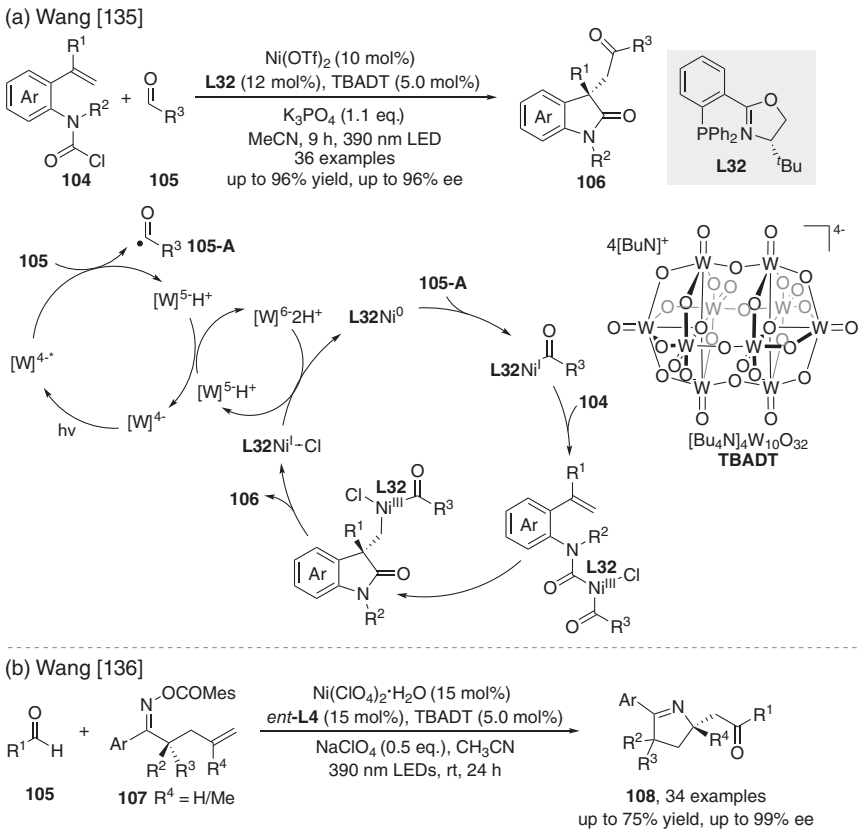


**Scheme 8.21** Photoredox/nickel dual catalyzed enantioselective radical acylation of alkenes. Sources: (a) Adapted from Wang [135]. (b) Wang [136]/John Wiley & Sons.

carbon–carbon bonds with high levels of enantiocontrol [137, 138]. In this context, photoredox/nickel-catalyzed RCC has also received considerable attention. Most methods require a stoichiometric amount of heterogeneous metal dust as a terminal reductant, making them sensitive to stirring rates, metal purity, and mesh size. In this regard, the use of Hantzsch ester (HEH) as an organic reducing agent presents some obvious advantages.

In 2020, Mao, Walsh, and coworkers reported a dual photoredox/nickel-catalyzed asymmetric RCC of α-chloroesters **110** with aryl iodides **109** by using a chiral box ligand **L33** (Scheme 8.22a) [139]. This reaction enables the facile synthesis of valuable α-aryl esters with good yields and enantioselectivities, which are biologically privileged structures commonly found in nonsteroidal anti-inflammatory drugs. The authors proposed that the α-chloroesters **110** can undergo SET with a reduced photocatalyst or Ni(I) species, resulting in α-carbonyl radicals **110-A**. Simultaneously, the aryl iodides **109** undergo oxidative addition with a Ni(0) complex, leading to a Ni(II) species which can subsequently intercept the radical **110-A** to give a high-valent Ni(III) complex. Finally, a facile reductive elimination

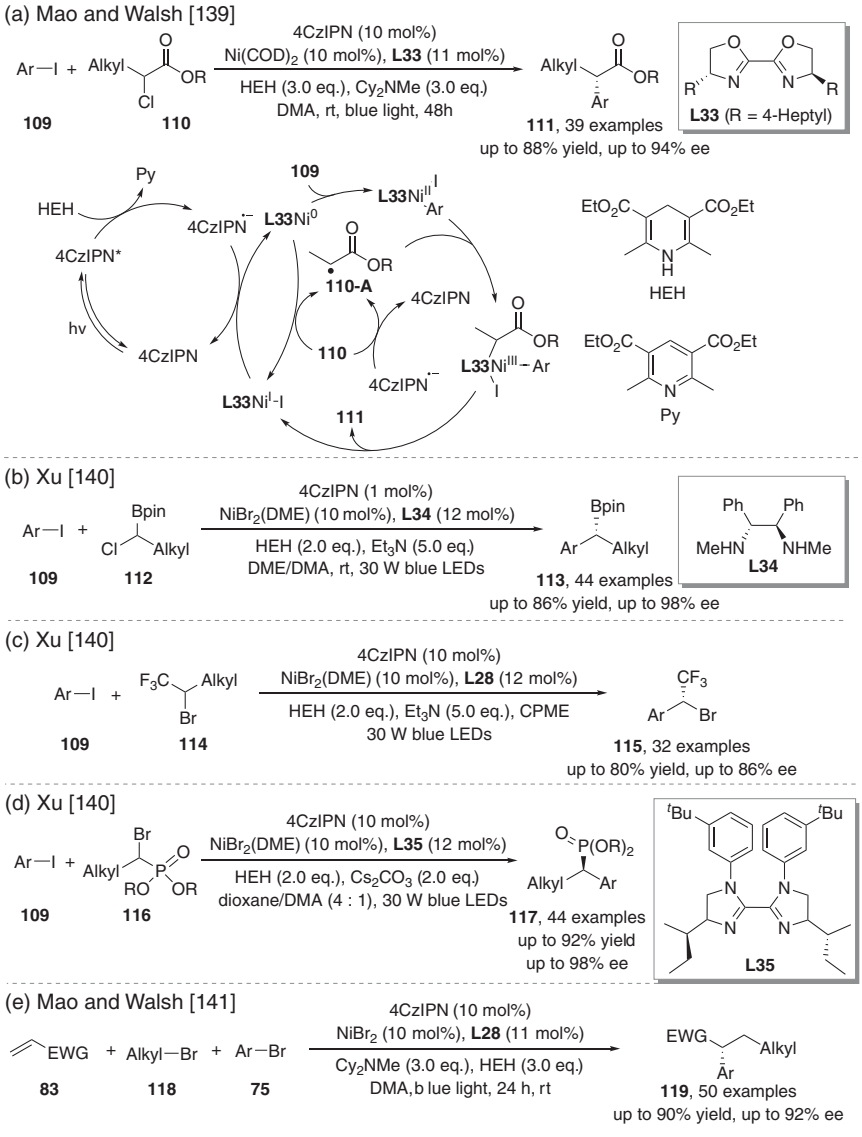


**Scheme 8.22** Dual photoredox/nickel-catalyzed asymmetric reductive arylation. Sources: (a) Wang [142]. (b–d) Adapted from Xu and Wang [142]. (e) Wu [144].

occurs to yield the desired product **111** in an enantioselective manner. The highly reducing Hantzsch esters are utilized to reduce the photoexcited photocatalyst and complete the entire catalytic cycle.

Notably, α-chloroboronates **112** [142], α-$CF_3$-substituted alkyl bromides **114** [143], and α-bromophosphates **116** [144] are also shown to be competent coupling partners for cross-electrophile coupling with aryl iodides in a mechanistically similar manner to α-chloroesters (Scheme 8.22b–d). This dual catalytic regime

exhibits high reaction efficiency and good functional group compatibility. Substrates bearing diverse functional groups can be converted into valuable chiral compounds with good to excellent yields and enantioselectivities. In addition to the aforementioned dual photoredox/nickel catalytic approach, Xu and coworkers have developed a non-photochemical protocol for the enantioselective construction of perfluoroalkyl-containing molecules from α-iodoboronate substrates [140]. This transformation features the use of zinc as a terminal reductant and chloride ions play a pivotal role in accelerating the reduction of Ni(II) species. Mao, Walsh, and coworkers further extended this photoredox/nickel RCC strategy to a three-component variant (Scheme 8.22e) [141]. In this process, tertiary alkyl bromides, secondary alkyl iodides, and (hetero)aryl bromides can proceed smoothly under mild conditions, while primary alkyl iodides showed inferior efficiency. In contrast to the aforementioned Chu's work that involves an overall redox-neutral process, this reductive protocol provides an alternative approach for preparing enantioenriched α-aryl esters from readily available and bench-stable starting materials.

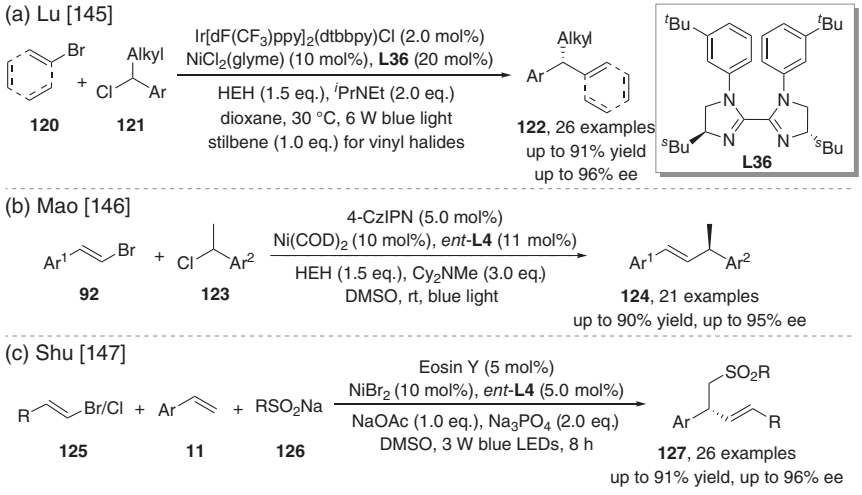


**Scheme 8.23** Dual photoredox/nickel-catalyzed asymmetric reductive alkenylation. Sources: (a) Adapted from Lu [145]. (b) Adapted from Mao [146]. (c) Shu [147]/American Chemical Society.

In 2022, Lu and coworkers applied their catalytic system to the RCC of aryl/alkenyl bromides with benzylic chlorides (Scheme 8.23a) [145]. They demonstrated that aryl and alkenyl bromides, as well as alkenyl chlorides, could be coupled with benzylic chlorides when using a chiral nickel/bis(imidazoline) **L36** catalyst. Considering that the iridium photocatalysts can easily influence the *E*/*Z* isomerizations of the product via an energy-transfer pathway, stoichiometric formal inhibitor stilbene was added to achieve synthetically useful levels of selectivity between *Z* and *E* isomers. Simultaneously, Mao and coworkers reported an enantioselective RCC of vinyl bromides **92** and benzyl chlorides **123** with organic photocatalyst Eosin Y(Scheme 8.23b) [146]. The key features of this method include a wide substrate scope, and no need for

preformed organometallic reagents and stoichiometric metal reductants. Notably, this strategy can be extended to a three-component variant for synthesizing enantioenriched β-chiral sulfones **127** using sodium benzene sulfinates **126** as radical precursors (Scheme 8.23c) [147].

Besides alkyl halides, styrene oxides have also been exploited as competent coupling partners in dual photoredox/nickel-catalyzed RCC reactions. In 2021, Doyle and coworkers documented an elegant enantioselective RCC of racemic styrene oxides **128** with aryl iodides **109** for constructing enantioenriched 2,2-diaryl alcohols **129** (Scheme 8.24a) [148]. Furthermore, N-Ts-protected aziridines can also afford satisfactory results under standard reaction conditions. It is proposed that the nucleophilic ring-opening of epoxide **128** by HX forms the halohydrin intermediate **128-A**, which can undergo SET or halogen atom abstraction (HAA) to generate the corresponding secondary benzylic radical **128-B**, facilitating subsequent enantioselective transformations. Notably, Huo and coworkers demonstrated an unprecedented asymmetric RCC between α-amino acid derivatives **130** with aryl bromides, which provides modular access to enantioenriched benzylic amines **131** with excellent yield and enantioselectivities (Scheme 8.24b) [149]. Distinct from previous studies, this protocol relies on the photocatalytic generation of the α-hydroxyalkyl radical **132-A** from benzyl alcohol **132** to effectively convert alkyl

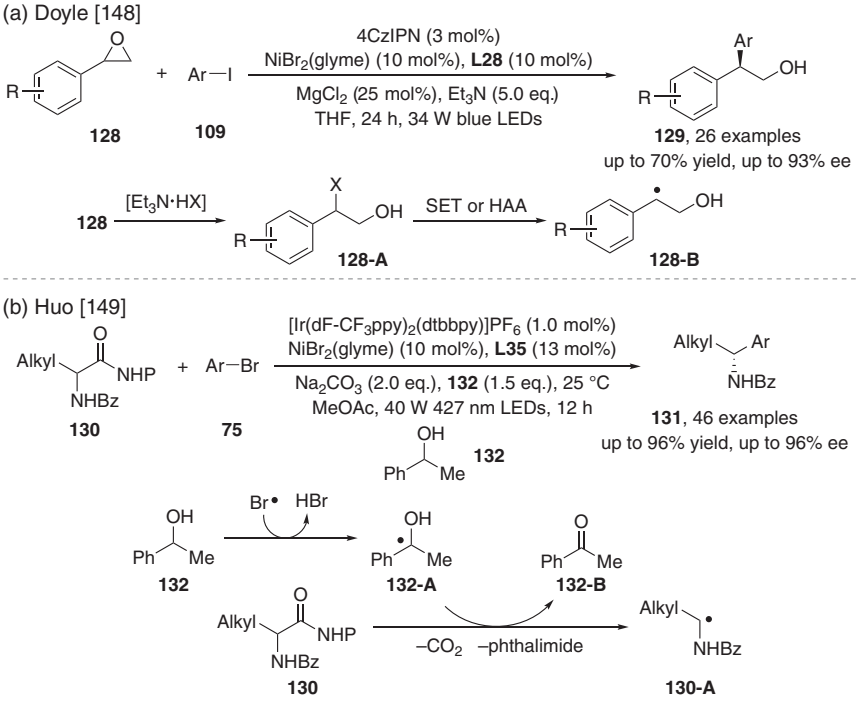


**Scheme 8.24** Dual photoredox/nickel-catalyzed enantioselective cross-electrophile coupling reactions. Sources: (a) Doyle [148]/American Chemical Society. (b) Adapted from Huo [149].

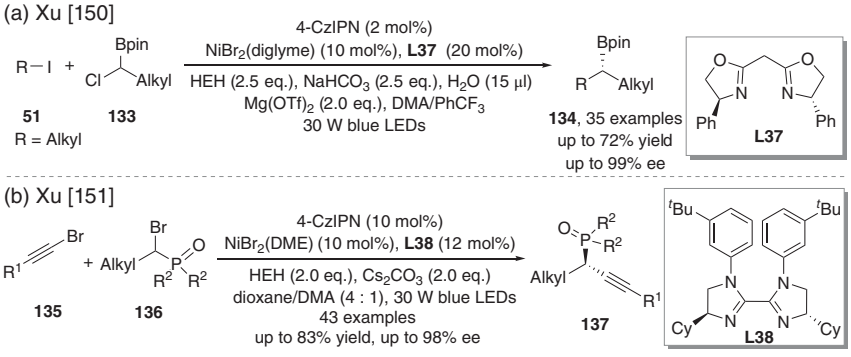


**Scheme 8.25** Dual photoredox/nickel-catalyzed asymmetric reductive C($sp^3$/sp)—C($sp^3$) cross-couplings. Sources: (a) Adapted from Xu [150]. (b) Adapted from Xu [151].

electrophiles into corresponding alkyl radicals **130-A**, which are subsequently enantioselectively coupled with aryl bromides **75**.

Although Ni-catalyzed asymmetric C($sp^3$)—C($sp^2$) cross-couplings have been well established, the enantioselective C($sp^3$)—C($sp^3$) couplings remain a long-standing challenge. The major reasons can be attributed to the sluggish oxidative addition of alkyl halides and the inherent difficulty in the control of stereochemistry. Based on their previous related studies, Xu and coworkers developed a novel enantioconvergent C($sp^3$)—C($sp^3$) RCC between two different alkyl halides via a dual photoredox/nickel catalytic strategy (Scheme 8.25a) [150]. This protocol demonstrates several salient advantages, including the use of readily available unactivated alkyl iodides, mild reaction conditions, broad substrate scopes, and excellent functional group compatibility. The proposed mechanism suggests that it proceeds via the oxidative addition of α-chloroboronates with Ni(I) species rather than Ni(0) species.

Despite many impressive advances in the synthetic applications of the dual photoredox/nickel catalytic system in asymmetric cross-couplings, its further exploration in enantioselective C(sp)—C($sp^3$) bond formation remains limited and challenging. In 2023, Xu and coworkers described an enantioconvergent reductive C(sp)—C($sp^3$) cross-coupling of α-bromophosphonates **136** with alkynyl bromide **135** under a dual photoredox/nickel catalytic condition (Scheme 8.25b) [151]. Importantly, this mild method offers a modular and direct approach for synthesizing chiral α-alkynyl phosphonates **137** with excellent enantioselectivities. A possible mechanism is also proposed for the reaction, which involves the generation of alkyl radicals from **136** via the photocatalytic cycle and the oxidation addition of Ni(0) species with alkynyl bromides.

## 8.4 Dual Photoredox/Chromium or Cobalt-Catalyzed Asymmetric Radical Reactions

In addition to the merger of asymmetric nickel or copper catalysis with photoredox catalysis, asymmetric chromium catalysis can also be employed in

metallaphotoredox-catalyzed cross-coupling reactions, particularly for the Nozaki-Hiyama-Kishi (NHK) reaction [152, 153]. With such a strategy, a range of chemo- and diastereoselective allylations of aldehydes using versatile radical precursors could be achieved. In this context, in 2018, Glorius and coworkers reported a diastereoselective allylation of aldehydes by employing a combination of photoredox and chromium catalysis, resulting in the corresponding highly functionalized allyl alcohols with excellent yields and diastereoselectivities (Scheme 8.26a) [154]. It is noteworthy that when an enantiopure bisoxazoline ligand **L39** was employed in the reaction of 4-fluorobenzaldehyde **138** and *N*-allyl-diphenylamine **139**, a moderate enantiomeric excess (20% ee) for product **140** was obtained. This pioneering work confirms the viability of synthesizing chiral homoallyl alcohols using this strategy.

In 2019, Kanai, Mitsunuma, and coworkers successfully achieved a highly enantioselective asymmetric allylation of aldehydes by utilizing a combination of an organophotoredox acridinium catalyst **144** and a chiral chromium complex (Scheme 8.26b) [155]. In this process, both cyclic and linear alkenes are competent substrates, yielding the corresponding homoallylic alcohols **143** with exceptional diastereo- and enantioselectivity. Mechanistically, the reaction commences photoexcitation of the photocatalyst **144** to its excited state, which can then be quenched by alkene **142a** to generate the reduced photocatalyst and a radical cation **142-A**. This intermediate undergoes deprotonation to generate an allyl radical **142-B**, which was captured by chiral low-valent chromium(II) species to form chiral chromium(III) allyl species **142-C**. It is proposed that the nucleophilic carbonyl addition step occurs via a possible six-membered Zimmerman-Traxler transition state [158, 159], thus producing enantioenriched chromium alkoxide **142-D** in a syn-selective manner. Protonolysis of **142-D** affords the desired homoallylic alcohol **143** and an oxidized chromium(III) complex. Finally, both catalytic cycles are closed through a SET process between the reduced photocatalyst and oxidized chromium(III) complex. It has been confirmed that the addition of $Mg(ClO_4)_2$ markedly enhances both reactivity and enantioselectivity due to the increased concentration of cation radical **142-A**.

In 2022, Glorius and coworkers demonstrated that allylsilanes can be used as suitable allyl sources in NHK reactions (Scheme 8.26c) [156]. By combining photocatalytic activation and chromium catalysis, they achieved an enantioselective cross-coupling of aldehydes **141** with allylsilanes **145**, providing straight access to valuable chiral homoallylic alcohols **146**. As for the working hypothesis, the authors excluded the concerted pathway and proposed a chain reaction mechanism based on DFT calculations.

Exploration of unactivated olefins in NHK reactions is of great significance but remains highly challenging. In 2020, the group of Kanai developed a dual catalytic system by merging photoredox-mediated HAT catalysis with asymmetric chromium catalysis to address this issue (Scheme 8.26d) [157]. Specifically, they developed a ternary hybrid catalyst system comprising a photoredox catalyst **150**, a HAT catalyst **151**, and a chiral chromium complex. The thiophosphoric imide **151** was used as a HAT catalyst to generate sulfur radicals under photoredox catalysis, which can activate the allylic C—H bond of **148** and produce the corresponding allylic radicals **148-A**. This strategy can significantly expand the substrate range

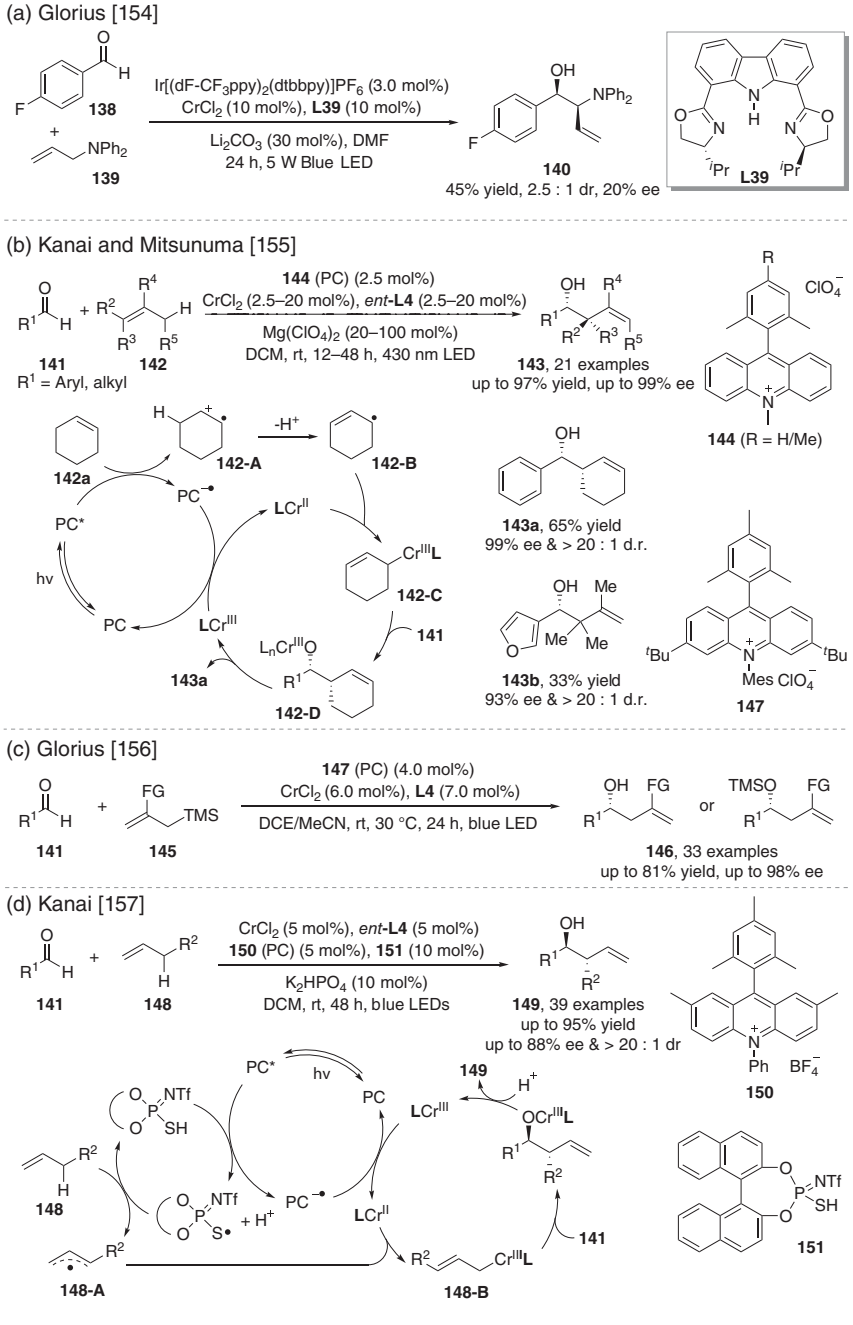


**Scheme 8.26** Dual photoredox/chromium-catalyzed asymmetric radical allylation of aldehydes. Sources: (a) Adapted from Glorius [154]. (b) Kanai and Mitsunuma [155]/John Wiley & Sons. (c) Adapted from Glorius [156]. (d) Kanai [157]/American Chemical Society.

of alkenes, including feedstock lower alkenes. A three-component NHK reaction of alkyl-substituted Hantzsch esters, 1,3-dienes, and aldehydes was subsequently developed by the group of Glorius using dual photoredox and chromium catalysis [160]. In this process, the key step is the addition of Hantzsch ester-derived alkyl radicals to 1,3-butadienes to form allyl radicals. This elegant protocol offers a promising method for accessing valuable chiral homoallylic alcohols from cost-effective and readily available industrial feedstocks.

The regio- and stereoselective 1,4-functionalization of easily available 1,3-enynes could provide practical access to chiral allene derivatives. Extensive efforts have been focused on this field; however, most reactions proceed through ionic pathways, and only limited success has been achieved in radical-involved processes [161–163]. Recently, Wang and coworkers developed a three-component asymmetric 1,4-dialkylation of 1,3-enynes via dual photoredox and chromium catalysis, allowing for constructing chiral allenols **154** with simultaneous control of axial and central elements (Scheme 8.27) [164]. Alkyl-substituted Hantzsch esters **153** and secondary organotrifluoroborates have proven to be privileged alkyl radical precursors in the 1,4-functionalization of enynes **152** with aryl and aliphatic aldehydes **141**, affording the desired coupling products, thus obviating the use of stoichiometric amounts of metal reductants. Besides, NHPI esters **12** could also participate in the reaction smoothly under the slightly modified conditions with HEH as the reductant, resulting in allenols **155** with moderate yields and high stereoselectivities. However, this catalytic system is not effective for 1,3-enynes with substituents on the carbon–carbon double bond. Detailed mechanistic studies suggest that this reaction proceeds via a radical-involved redox-neutral pathway.

Cobalt-catalyzed cross-couplings have been recognized as one of the most potent methodologies for constructing various C—C bonds [165, 166]. Despite its significance as a 3d metal, cobalt has been comparatively less explored than its neighboring elements, nickel and copper, in terms of application in asymmetric radical couplings. One major reason is that the high catalytic activity exhibited

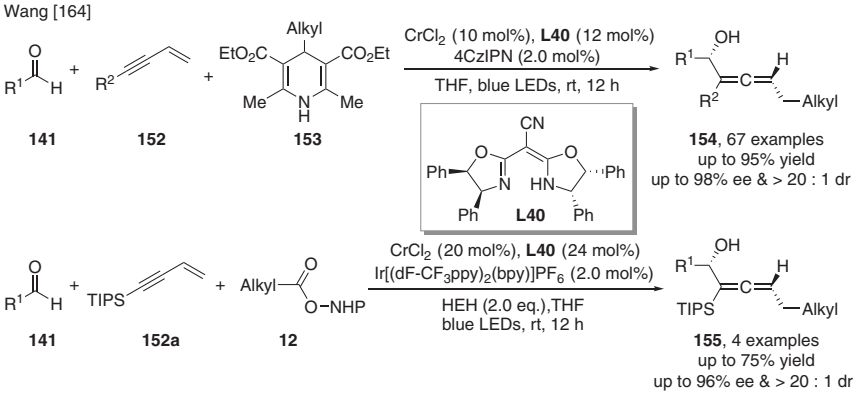


**Scheme 8.27** Dual photoredox/chromium-catalyzed asymmetric radical 1,4-functionalization of 1,3-enynes. Source: Wang [164]/Springer Nature/CC BY 4.0.

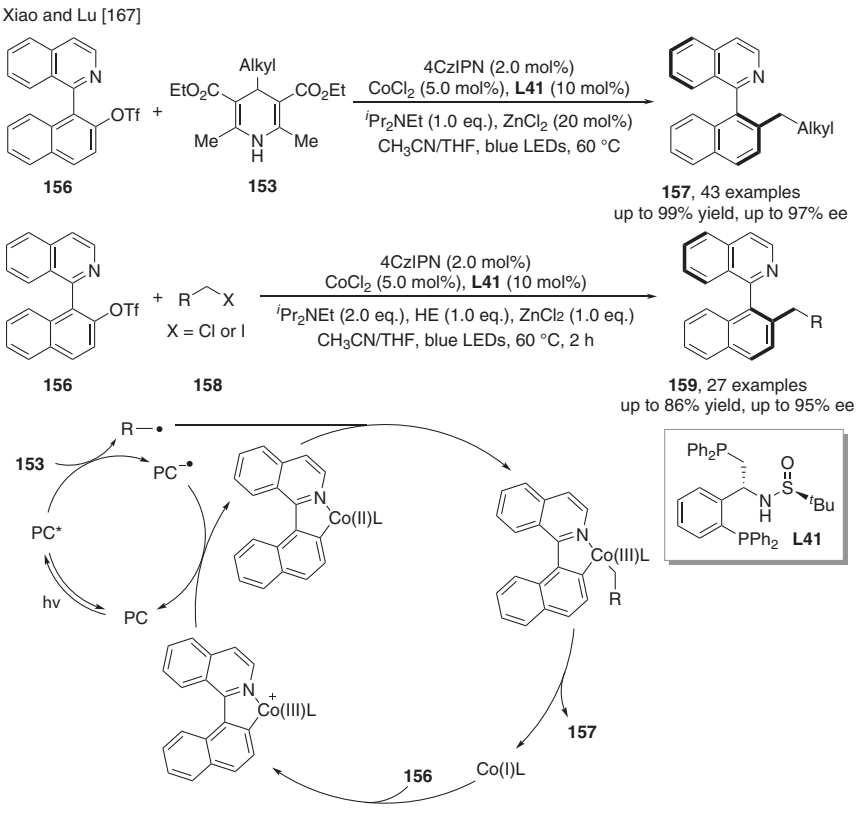


**Scheme 8.28** Dual photoredox/cobalt-catalyzed radical-mediated dynamic kinetic asymmetric cross-coupling for construction of axially chiral heterobiaryls. Source: Adapted from Xiao and Lu [167].

by cobalt salts themselves may compete with chiral ligand-promoted asymmetric couplings, leading to significant racemic background reactions.

Xiao, Lu, and coworkers have developed a metallaphotoredox-catalyzed dynamic kinetic asymmetric transformation of racemic heterobiaryls **156** with 1,4-dihydropyridine (DHP) substrates **153** as radical precursors under visible light irradiation (Scheme 8.28) [167]. The combination of chiral polydentate ligand **L41** and cobalt is identified as the best chiral catalyst for enantioselective radical couplings, leading to a diverse range of chiral heterobiaryl products **157** with generally high efficiency and stereoselectivity. This process has also proven to be applicable for RCC reactions of alkyl halides **158**. Notably, the potential of this methodology was further demonstrated by the facile conversion of these axially chiral heterobiaryl products into promising catalysts and ligands, as well as chiral fluorescent materials. As shown in the proposed mechanism, a photoexcited photocatalyst can be reduced by substrate **153** via a SET process, resulting in a reduced photocatalyst and an alkyl radical **153-A**. On the other hand, the chiral Co(I) complex undergoes oxidative addition with **156** to produce an aryl Co(III) intermediate, which can be further reduced

to a Co(II) intermediate, with regeneration of the ground state photocatalyst. Then, radical **153-A** is captured by the Co(II) species to form a Co(III) intermediate, which undergoes reductive elimination to afford the desired product **157**.

## 8.5 Conclusion

Over the past decade, the integration of visible light photocatalysis with earth-abundant metals (e.g., copper, nickel, cobalt, and chromium) has presented remarkable opportunities for expanding the scope of asymmetric cross-coupling reactions. In this avenue, the merger of the transition-metal-based chiral complex with the photoredox or energy-transfer catalyst and a single metal-based bifunctional catalyst has been developed. Notably, most of them are not easily accessible via thermal processes. Given the obvious advantages of visible light photocatalysis and these earth-abundant metals, these catalyst systems hold great promise for promoting green and sustainable synthetic chemistry, and many developments are likely still to come. However, there are still several challenges that need to be overcome. First, the known scope of radicals that can be efficiently captured by chiral metal catalysts is still limited to a few classes of stabilized prochiral alkyl radicals. Expanding their applicability to non-stabilized prochiral radical species is highly desirable and challenging because of the unselective radical addition step. Second, while the enantioselective C—C bond formation has witnessed great advances, enantioselective C–heteroatom bond formation remains a significant challenge [168]. Third, the pool of chiral ligands is mainly limited to chiral Box ligands and phosphine ligands, which leads to some restrictions on the scope of coupling partners. To further expand this field, there is a need to explore other chiral ligand scaffolds and design bifunctional ligands or metal catalysts. Finally, considerable research efforts should also be devoted to the exploration of base metals such as manganese and iron in photoinduced asymmetric radical transformations.

## References


1 Wang, H., Tian, Y.-M., and König, B. (2022). *Nat. Rev. Chem.* 6: 745–755.
2 Rivas, M., Palchykov, V., Jia, X., and Gevorgyan, V. (2022). *Nat. Rev. Chem.* 6: 544–561.
3 Pitre, S.P. and Overman, L.E. (2022). *Chem. Rev.* 122: 1717–1751.
4 Genzink, M.J., Kidd, J.B., Swords, W.B., and Yoon, T.P. (2022). *Chem. Rev.* 122: 1654–1716.
5 Chan, A.Y., Perry, I.B., Bissonnette, N.B. et al. (2022). *Chem. Rev.* 122: 1485–1542.
6 Mariano, P.S. (1983). *Acc. Chem. Res.* 16: 130–137.
7 Bauld, N.L. (1989). *Tetrahedron* 45: 5307–5363.
8 Yoon, U.C. and Mariano, P.S. (1992). *Acc. Chem. Res.* 25: 233–240.
9 Pandey, G. (1992). *Synlett* 546–552.

**10** Zhang, N., Samanta, S.R., Rosen, B.M., and Percec, V. (2014). *Chem. Rev.* 114: 5848–5958.

**11** Strieth-Kalthoff, F., James, M.J., Teders, M. et al. (2018). *Chem. Soc. Rev.* 47: 7190–7202.

**12** Molloy, J.J., Morack, T., and Gilmour, R. (2019). *Angew. Chem. Int. Ed.* 58: 13654–13664.

**13** Strieth-Kalthoff, F. and Glorius, F. (2020). *Chem* 6: 1888–1903.

**14** Grosskopf, J., Kratz, T., Rigotti, T., and Bach, T. (2022). *Chem. Rev.* 122: 1626–1653.

**15** Bera, M., Lee, D.S., and Cho, E.J. (2021). *Trends Chem.* 3: 877–891.

**16** Lee, D.S., Soni, V.K., and Cho, E.J. (2022). *Acc. Chem. Res.* 55: 2526–2541.

**17** Zhu, M., Zhang, X., Zheng, C., and You, S.L. (2022). *Acc. Chem. Res.* 55: 2510–2525.

**18** Nevesely, T., Wienhold, M., Molloy, J.J., and Gilmour, R. (2022). *Chem. Rev.* 122: 2650–2694.

**19** Ravelli, D., Fagnoni, M., Fukuyama, T. et al. (2017). *ACS Catal.* 8: 701–713.

**20** Stateman, L., Nakafuku, K., and Nagib, D. (2018). *Synthesis* 50: 1569–1586.

**21** Capaldo, L., Quadri, L.L., and Ravelli, D. (2020). *Green Chem.* 22: 3376–3396.

**22** Chen, H. and Yu, S. (2020). *Org. Biomol. Chem.* 18: 4519–4532.

**23** Guo, W., Wang, Q., and Zhu, J. (2021). *Chem. Soc. Rev.* 50: 7359–7377.

**24** Capaldo, L., Ravelli, D., and Fagnoni, M. (2022). *Chem. Rev.* 122: 1875–1924.

**25** Chang, L., An, Q., Duan, L. et al. (2022). *Chem. Rev.* 122: 2429–2486.

**26** Nicewicz, D.A. and MacMillan, D.W.C. (2008). *Science* 322: 77–80.

**27** Alonso, R. and Bach, T. (2014). *Angew. Chem. Int. Ed.* 53: 4368–4371.

**28** Huo, H., Shen, X., Wang, C. et al. (2014). *Nature* 515: 100–103.

**29** Du, J., Skubi, K.L., Schultz, D.M., and Yoon, T.P. (2014). *Science* 344: 392–396.

**30** Arceo, E., Jurberg, I.D., Álvarez-Fernández, A., and Melchiorre, P. (2013). *Nat. Chem.* 5: 750–756.

**31** DiRocco, D.A. and Rovis, T. (2012). *J. Am. Chem. Soc.* 134: 8094–8097.

**32** Proctor, R.S.J., Davis, H.J., and Phipps, R.J. (2018). *Science* 360: 419–422.

**33** Yin, Y., Dai, Y., Jia, H. et al. (2018). *J. Am. Chem. Soc.* 140: 6083–6087.

**34** Blum, T.R., Miller, Z.D., Bates, D.M. et al. (2016). *Science* 354: 1391–1395.

**35** Tröster, A., Alonso, R., Bauer, A., and Bach, T. (2016). *J. Am. Chem. Soc.* 138: 7808–7811.

**36** Silvi, M., Verrier, C., Rey, Y.P. et al. (2017). *Nat. Chem.* 9: 868–873.

**37** Ma, J., Rosales, A.R., Huang, X. et al. (2017). *J. Am. Chem. Soc.* 139: 17245–17248.

**38** Lipp, A., Badir, S.O., and Molander, G.A. (2020). *Angew. Chem. Int. Ed.* 60: 1714–1726.

**39** Shin, N.Y., Ryss, J.M., Zhang, X. et al. (2019). *Science* 366: 364–369.

**40** Fu, M.-C., Shang, R., Zhao, B. et al. (2019). *Science* 363: 1429–1434.

**41** Giri, R., Brusoe, A., Troshin, K. et al. (2018). *J. Am. Chem. Soc.* 140: 793–806.

**42** Altman, R.A. and Buchwald, S.L. (2007). *Nat. Protoc.* 2: 2474–2479.

**43** Kharasch, M.S. and Sosnovsky, G. (1958). *J. Am. Chem. Soc.* 80: 756.

**44** Zhong, M., Pannecoucke, X., Jubault, P., and Poisson, T. (2020). *Beilstein J. Org. Chem.* 16: 451–481.
**45** Engl, S. and Reiser, O. (2022). *Chem. Soc. Rev.* 51: 5287–5299.
**46** Xiong, Y., Li, S., Xiao, H., and Zhang, G. (2021). *Synthesis* 53: 4327–4340.
**47** Beaudelot, J., Oger, S., Perusko, S. et al. (2022). *Chem. Rev.* 122: 16365–16609.
**48** Hossain, A., Bhattacharyya, A., and Reiser, O. (2019). *Science* 364: eaav9713.
**49** Song, L., Cai, L., Gong, L., and Van der Eycken, E.V. (2023). *Chem. Soc. Rev.* 52: 2358–2376.
**50** Perepichka, I., Kundu, S., Hearne, Z., and Li, C.-J. (2015). *Org. Biomol. Chem.* 13: 447–451.
**51** Querard, P., Perepichka, I., Zysman-Colman, E., and Li, C.-J. (2016). *Beilstein J. Org. Chem.* 12: 2636–2643.
**52** Kumar, G., Verma, S., Ansari, A. et al. (2017). *Catal. Commun.* 99: 94–99.
**53** Wang, F., Chen, P., and Liu, G. (2018). *Acc. Chem. Res.* 51: 2036–2046.
**54** Zhang, P. and Chen, G.L. (2022). *Chem. Soc. Rev.* 51: 1640–1658.
**55** Zhang, W., Wang, F., McCann, S.D. et al. (2016). *Science* 353: 1014–1018.
**56** Okada, K., Okamoto, K., and Oda, M. (1988). *J. Am. Chem. Soc.* 110: 8736–8738.
**57** Wang, D., Zhu, N., Chen, P. et al. (2017). *J. Am. Chem. Soc.* 139: 15632–15635.
**58** Cheng, Z., Chen, P., and Liu, G. (2019). *Acta Chim. Sin.* 77: 856–860.
**59** Sha, W., Deng, L., Ni, S. et al. (2018). *ACS Catal.* 8: 7489–7494.
**60** Lu, F.-D., Lu, L.-Q., He, G.-F. et al. (2021). *J. Am. Chem. Soc.* 143: 4168–4173.
**61** Bao, X., Wang, Q., and Zhu, J. (2019). *Angew. Chem. Int. Ed.* 58: 2139–2143.
**62** Wang, T., Wang, Y.-N., Wang, R. et al. (2019). *Nat. Commun.* 10: 5373.
**63** Chen, J., Wang, P.-Z., Lu, B. et al. (2019). *Org. Lett.* 21: 9763–9768.
**64** Wang, P.-Z., Gao, Y., Chen, J. et al. (2021). *Nat. Commun.* 12: 1815.
**65** Chen, H., Jin, W., and Yu, S. (2020). *Org. Lett.* 22: 5910–5914.
**66** Lu, F.-D., Liu, D., Zhu, L. et al. (2019). *J. Am. Chem. Soc.* 141: 6167–6172.
**67** Chen, H.-W., Lu, F.-D., Cheng, Y. et al. (2020). *Chin. J. Chem.* 38: 1671–1675.
**68** Fan, X., Lei, T., Chen, B. et al. (2019). *Org. Lett.* 21: 4153–4158.
**69** Cheng, Y.-Y., Lei, T., Su, L. et al. (2019). *Org. Lett.* 21: 8789–8794.
**70** Yan, M., Kawamata, Y., and Baran, P.S. (2017). *Chem. Rev.* 117: 13230–13319.
**71** Buglioni, L., Raymenants, F., Slattery, A. et al. (2022). *Chem. Rev.* 122: 2752–2906.
**72** Barham, J.P. and Konig, B. (2020). *Angew. Chem. Int. Ed.* 59: 11732–11747.
**73** Wu, S., Kaur, J., Karl, T.A. et al. (2022). *Angew. Chem. Int. Ed.* 61: e202107811.
**74** Huang, H., Steiniger, K.A., and Lambert, T.H. (2022). *J. Am. Chem. Soc.* 144: 12567–12583.
**75** Zhang, W., Carpenter, K.L., and Lin, S. (2020). *Angew. Chem. Int. Ed.* 59: 409–417.
**76** Kim, H., Lambert, T.H., and Lin, S. (2020). *J. Am. Chem. Soc.* 142: 2087–2092.
**77** Lai, X.-L., Chen, M., Wang, Y. et al. (2022). *J. Am. Chem. Soc.* 144: 20201–20206.
**78** Cai, C.-Y., Lai, X.-L., Wang, Y. et al. (2022). *Nat. Catal.* 5: 943–951.
**79** Fan, W., Zhao, X., Deng, Y. et al. (2022). *J. Am. Chem. Soc.* 144: 21674–21682.

**80** Lai, X.L. and Xu, H.C. (2023). *J. Am. Chem. Soc.* 145: 18753–18759.
**81** Xu, P., Fan, W., Chen, P., and Liu, G. (2022). *J. Am. Chem. Soc.* 144: 13468–13474.
**82** Nakafuku, K.M., Zhang, Z., Wappes, E.A. et al. (2020). *Nat. Chem.* 12: 697–704.
**83** Chen, X., Lian, Z., and Kramer, S. (2023). *Angew. Chem. Int. Ed.* 62: e202217638.
**84** Roughley, S.D. and Jordan, A.M. (2011). *J. Med. Chem.* 54: 3451–3479.
**85** Park, Y., Kim, Y., and Chang, S. (2017). *Chem. Rev.* 117: 9247–9301.
**86** Davies, H.M.L. and Manning, J.R. (2008). *Nature* 451: 417–424.
**87** Kainz, Q.M., Matier, C.D., Bartoszewicz, A. et al. (2016). *Science* 351: 681–684.
**88** Lee, H., Ahn, J.M., Oyala, P.H. et al. (2022). *J. Am. Chem. Soc.* 144: 4114–4123.
**89** Chen, C., Peters, J.C., and Fu, G.C. (2021). *Nature* 596: 250–256.
**90** Cho, H., Suematsu, H., Oyala, P.H. et al. (2022). *J. Am. Chem. Soc.* 144: 4550–4558.
**91** Minozzi, C., Dowe, N., Beaucage, N., and Collins, S.K. (2023). *ACS Catal.* 13: 8347–8353.
**92** Guo, Q., Wang, M., Peng, Q. et al. (2019). *ACS Catal.* 9: 4470–4476.
**93** Xia, H.-D., Li, Z.-L., Gu, Q.-S. et al. (2020). *Angew. Chem. Int. Ed.* 59: 16926–16932.
**94** Zhang, Y., Sun, Y., Chen, B. et al. (2020). *Org. Lett.* 22: 1490–1494.
**95** Guo, R., Xiao, H., Li, S. et al. (2022). *Angew. Chem. Int. Ed.* 61: e202208232.
**96** Li, C., Chen, B., Ma, X. et al. (2021). *Angew. Chem. Int. Ed.* 60: 2130–2134.
**97** Qi, R., Wang, C., Huo, Y. et al. (2021). *J. Am. Chem. Soc.* 143: 12777–12783.
**98** Chen, J., Liang, Y.-J., Wang, P.-Z. et al. (2021). *J. Am. Chem. Soc.* 143: 13382–13392.
**99** Wang, P.-Z., Wu, X., Cheng, Y. et al. (2021). *Angew. Chem. Int. Ed.* 60: 22956–22962.
**100** Wang, P.-Z., Liang, Y.-J., Wu, X. et al. (2022). *ACS Catal.* 12: 10925–10937.
**101** Li, G.-Q., Meng, F.-R., Xiao, W.-J., and Chen, J.-R. (2023). *Org. Chem. Front.* 10: 2773–2781.
**102** Tasker, S.Z., Standley, E.A., and Jamison, T.F. (2014). *Nature* 509: 299–309.
**103** Li, Z., Li, C., Ding, Y., and Huo, H. (2022). *Coord. Chem. Rev.* 460: 214479.
**104** Zhu, S., Zhao, X., Li, H., and Chu, L. (2021). *Chem. Soc. Rev.* 50: 10836–10856.
**105** Diccianni, J.B. and Diao, T. (2019). *Trends Chem.* 1: 830–844.
**106** Zhu, S., Li, H., Li, Y. et al. (2023). *Org. Chem. Front.* 10: 548–569.
**107** Tellis, J.C., Primer, D.N., and Molander, G.A. (2014). *Science* 345: 433–436.
**108** Stache, E.E., Rovis, T., and Doyle, A.G. (2017). *Angew. Chem. Int. Ed.* 56: 3679–3683.
**109** Gutierrez, O., Tellis, J.C., Primer, D.N. et al. (2015). *J. Am. Chem. Soc.* 137: 4896–4899.
**110** Ryu, D., Primer, D.N., Tellis, J.C., and Molander, G.A. (2016). *Chem. Eur. J.* 22: 120–123.
**111** Zuo, Z., Ahneman, D.T., Chu, L. et al. (2014). *Science* 435: 437–440.
**112** Zuo, Z., Cong, H., Li, W. et al. (2016). *J. Am. Chem. Soc.* 138: 1832–1835.

**113** Pezzetta, C., Bonifazi, D., and Davidson, R.W.M. (2019). *Org. Lett.* 21: 8957–8961.

**114** Gandolfo, E., Tang, X., Raha Roy, S., and Melchiorre, P. (2019). *Angew. Chem. Int. Ed.* 58: 16854–16858.

**115** Wang, P.-Z., Chen, J.-R., and Xiao, W.-J. (2019). *Org. Biomol. Chem.* 17: 6936–6951.

**116** Guo, L., Yuan, M., Zhang, Y. et al. (2020). *J. Am. Chem. Soc.* 142: 20390–20399.

**117** Saint-Denis, T.G., Zhu, R.-Y., Chen, G. et al. (2018). *Science* 359: eaao4798.

**118** Zhang, C., Li, Z.-L., Gu, Q.-S., and Liu, X.-Y. (2021). *Nat. Commun.* 12: 475.

**119** Holmberg-Douglas, N. and Nicewicz, D.A. (2022). *Chem. Rev.* 122: 1925–2016.

**120** Chu, J.C.K. and Rovis, T. (2018). *Angew. Chem. Int. Ed.* 57: 62–101.

**121** Cao, H., Tang, X., Tang, H. et al. (2021). *Chem Catal.* 1: 523–598.

**122** Shen, Y., Gu, Y., and Martin, R. (2018). *J. Am. Chem. Soc.* 140: 12200–12209.

**123** Rand, A.W., Yin, H., Xu, L. et al. (2020). *ACS Catal.* 10: 4671–4676.

**124** Cheng, X., Lu, H., and Lu, Z. (2019). *Nat. Commun.* 10: 3549.

**125** Cheng, X., Li, T., Liu, Y., and Lu, Z. (2021). *ACS Catal.* 11: 11059–11065.

**126** Xu, J., Li, Z., Xu, Y. et al. (2021). *ACS Catal.* 11: 13567–13574.

**127** Zhang, W., Shu, X., Huan, L. et al. (2021). *Org. Biomol. Chem.* 19: 9407–9409.

**128** Farney, E.P., Chapman, S.J., Swords, W.B. et al. (2019). *J. Am. Chem. Soc.* 141: 6385–6391.

**129** Li, G., Swords, W.B., and Meyer, G.J. (2017). *J. Am. Chem. Soc.* 139: 14983–14991.

**130** Li, X., Yuan, M., Chen, F. et al. (2023). *Chem* 9: 154–169.

**131** Shu, X., Huan, L., Huang, Q., and Huo, H. (2020). *J. Am. Chem. Soc.* 142: 19058–19064.

**132** Huan, L., Shu, X., Zu, W. et al. (2021). *Nat. Commun.* 12: 3536.

**133** Shu, X., Zhong, D., Huang, Q. et al. (2023). *Nat. Commun.* 14: 125.

**134** Kawasaki, T., Yamazaki, K., Tomono, R. et al. (2021). *Chem. Lett.* 50: 1684–1687.

**135** Fan, P., Lan, Y., Zhang, C., and Wang, C. (2020). *J. Am. Chem. Soc.* 142: 2180–2186.

**136** Wang, R. and Wang, C. (2023). *Chem. Sci.* 14: 6449–6456.

**137** Poremba, K.E., Dibrell, S.E., and Reisman, S.E. (2020). *ACS Catal.* 10: 8237–8246.

**138** Jin, Y. and Wang, C. (2020). *Synlett* 31: 1843–1850.

**139** Guan, H., Zhang, Q., Walsh, P.J., and Mao, J. (2020). *Angew. Chem. Int. Ed.* 59: 5172–5177.

**140** Wang, D. and Xu, T. (2021). *ACS Catal.* 11: 12469–12475.

**141** Qian, P., Guan, H., Wang, Y.-E. et al. (2021). *Nat. Commun.* 12: 6613.

**142** Zheng, P., Zhou, P., Wang, D. et al. (2021). *Nat. Commun.* 12: 1646.

**143** Zhou, P., Li, X., Wang, D., and Xu, T. (2021). *Org. Lett.* 23: 4683–4687.

**144** Wang, H., Zheng, P., Wu, X. et al. (2022). *J. Am. Chem. Soc.* 144: 3989–3997.

**145** Li, T., Cheng, X., Lu, J. et al. (2022). *Chin. J. Chem.* 40: 1033–1038.

**146** Lu, Q., Guan, H., Wang, Y.-E. et al. (2022). *J. Organomet. Chem.* 87: 8048–8058.

**147** Liu, M.-S. and Shu, W. (2023). *JACS Au* 3: 1321–1327.

**148** Lau, S.H., Borden, M.A., Steiman, T.J. et al. (2021). *J. Am. Chem. Soc.* 143: 15873–15881.
**149** Li, Z., Huan, L., Li, J. et al. (2023). *Angew. Chem. Int. Ed.* 62: e202305889.
**150** Zhou, J., Wang, D., Xu, W. et al. (2023). *J. Am. Chem. Soc.* 145: 2081–2087.
**151** Wang, H., Wu, X., and Xu, T. (2023). *Angew. Chem. Int. Ed.* 62: e202218299.
**152** Okude, Y., Hirano, S., Hiyama, T., and Nozaki, H. (1977). *J. Am. Chem. Soc.* 99: 3179–3181.
**153** Namba, K., Wang, J., Cui, S., and Kishi, Y. (2005). *Org. Lett.* 7: 5421–5424.
**154** Schwarz, J.L., Schäfers, F., Tlahuext-Aca, A. et al. (2018). *J. Am. Chem. Soc.* 140: 12705–12709.
**155** Mitsunuma, H., Tanabe, S., Fuse, H. et al. (2019). *Chem. Sci.* 10: 3459–3465.
**156** Schäfers, F., Dutta, S., Kleinmans, R. et al. (2022). *ACS Catal.* 12: 12281–12290.
**157** Tanabe, S., Mitsunuma, H., and Kanai, M. (2020). *J. Am. Chem. Soc.* 142: 12374–12381.
**158** Hiyama, T., Kimura, K., and Nozaki, H. (1981). *Tetrahedron Lett.* 22: 1037–1040.
**159** Wessjohann, L.A. and Scheid, G. (1999). *Synthesis* 1: 1–36.
**160** Schwarz, J.L., Huang, H.-M., Paulisch, T.O., and Glorius, F. (2020). *ACS Catal.* 10: 1621–1627.
**161** Zeng, Y., Chiou, M.F., Zhu, X. et al. (2020). *J. Am. Chem. Soc.* 142: 18014–18021.
**162** Dong, X.-Y., Zhan, T.-Y., Jiang, S.-P. et al. (2021). *Angew. Chem. Int. Ed.* 60: 2160–2164.
**163** Wang, F., Wang, D., Zhou, Y. et al. (2018). *Angew. Chem. Int. Ed.* 57: 7140–7145.
**164** Zhang, F.-H., Guo, X., Zeng, X., and Wang, Z. (2022). *Nat. Commun.* 13: 5036.
**165** Hapke, M. and Hilt, G. (ed.) (2020). *Cobalt Catalysis in Organic Synthesis*. Wiley-VCH.
**166** Kojima, M. and Matsunaga, S. (2020). *Trends Chem.* 2: 410–426.
**167** Jiang, X., Xiong, W., Deng, S. et al. (2022). *Nat. Catal.* 5: 788–797.
**168** Wang, P.-Z., Chen, J.-R., and Xiao, W.-J. (2023). *J. Am. Chem. Soc.* 145: 17527–17550.

# 9

# Precious Transition Metal-Catalyzed Asymmetric Radical Reactions

*Changhua Song, Liang Liu, and Shouyun Yu*

*School of Chemistry and Chemical Engineering, Nanjing University, Nanjing, China*

## 9.1 Introduction

Precious metal (Pd, Ir, Ru, Rh, etc.) catalysis plays an important role in homogeneous catalysis and has established predictable chemistry after decades of research [1]. Compared with earth-abundant transition metals (Co, Ni, Cu, etc.), precious metals have a larger atomic radius, higher electronegativities, and potential involvement of two-electron processes with unique features in organometallic chemistry [2]. Therefore, the single electron transfer process catalyzed by precious metal, especially the asymmetric radical transformation, is rarely reported. This chapter highlights recent advances in precious transition metal-catalyzed asymmetric radical reactions. The precious metals described in this chapter act as metal centers, which can effectively capture and stabilize free-radical intermediates. Precious transition metal catalysis, in which metals act as Lewis acids, is not included in this chapter.

## 9.2 Pd-Catalyzed Asymmetric Radical Reactions

Palladium catalysis, as a powerful catalyst in the formation of C—C, C—O, C—N bonds, etc., has established a powerful method for countless synthetic transformations [3–9]. Pd-catalyzed asymmetric transformations have been developed through the design of catalysts and ligands [10–13], and many asymmetric strategies are being reported in this area [14–21]. However, palladium-catalyzed construction of chiral compounds via radical pathways has been rarely reported. Recent advances in photocatalysis and electrochemistry have pushed forward the field of palladium-catalyzed asymmetric radical transformations. This synergetic mechanistic prototype involves the generation of radical species through photocatalysis or electrochemistry and the capture of radical intermediates into the stereogenic center via a Pd-effected radical rebound [22–26]. The chiral palladium complex affords the dual advantages of an electron-transfer mediator and stereochemical discrimination [27].

In 2015, Tunge et al. [28] reported a radical decarboxylative allylation of α-amino and phenylacetic allyl esters via palladium and photoredox cocatalysis (Scheme 9.1). They hypothesized that higher energy radicals should undergo reductive elimination by forming metal-bound radical intermediates rather than free radical coupling. The stability of radicals affects the enantioselectivity of the forming C—C bonds. When the radical intermediates produced by decarboxylation are unstable, C—C bond formation occurs within the coordination sphere of the chiral palladium complex (*path b*) with moderate enantioselectivity (50% ee). In contrast, stabilized radical intermediates lead to nearly racemic products through radical-radical cross-coupling (*path a*).

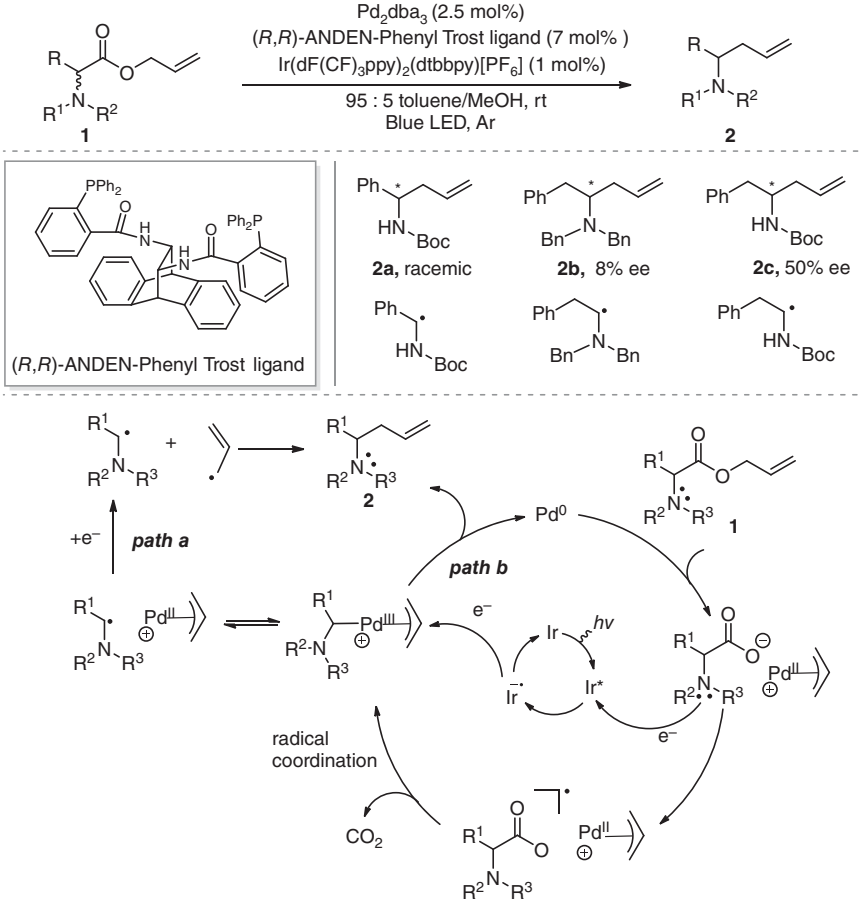


**Scheme 9.1** Dual catalytic decarboxylative allylations of α-amino acids.

In 2018, Yu et al. [29] reported a highly enantioselective photoredox/palladium cocatalytic allylic alkylation reaction (Scheme 9.2). In the field of asymmetric allylic alkylation (AAA), controlling regioselectivity to generate chiral–branched products remains a significant challenge. The single substitution of allylic electrophiles

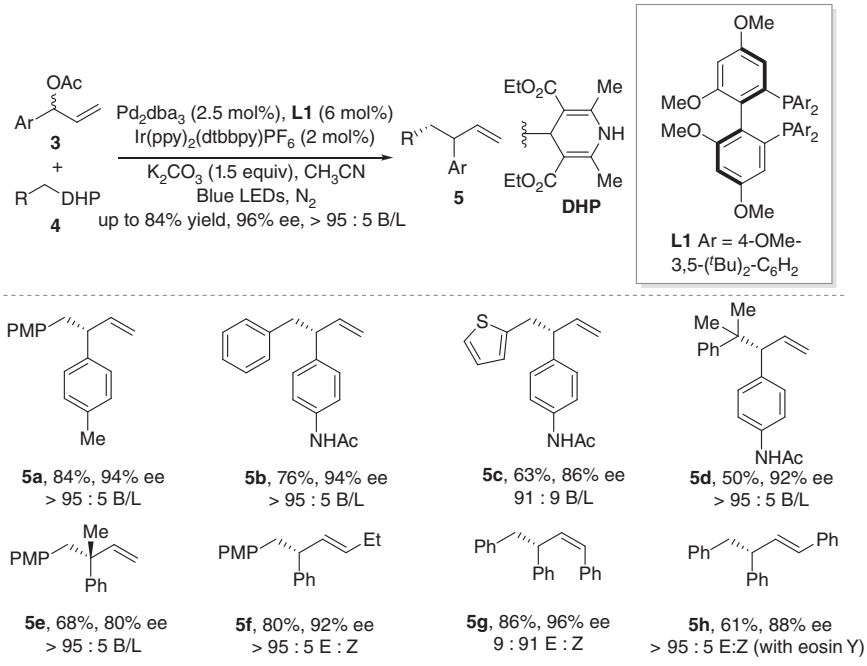


**Scheme 9.2** Enantioselective allylic alkylation enabled by photoredox/palladium cocatalysis.

typically results in achiral linear products unless prochiral nucleophilic reagents are employed. The branch regioselectivity and dynamic kinetic resolution effect of this reaction are normally challenging in the traditional Pd-catalyzed AAA reactions. 4-Alkyl-1,4-dihydropyridines acted as the formal "hard" nucleophiles under photoredox conditions, which were difficult to obtain under classic allylic alkylation conditions. The desired products could be generated with good regio-, enantio-, and *E*/*Z* selectivities from the reactions of primary, secondary, and tertiary alkyl radicals with various racemic aromatic allylic acetates, including 1,3-disubstituted unsymmetric allylic esters. In addition, the configuration of alkene products (**5g**, **5h**) can be controlled by selecting suitable photocatalysts.

A plausible mechanism is proposed (Scheme 9.3) where the reductive quenching of the visible-light excited Ir(III)* by dihydropyridine gives the corresponding alkyl radical and a low-valent Ir(II) complex. In the meantime, the oxidative addition of Pd(0) into allyl ester gives a Pd-π-allyl species, which then traps the alkyl radical to produce a Pd(III) species. Reductive elimination from the Pd(III) species gives the alkylation product and a Pd(I) species. Finally, the low-valent Ir(II) complex reduces the Pd(I) species and regenerates Ir(III) and Pd(0), closing both catalytic cycles.

In 2020, Yu et al. [30] described a photoredox/Pd-cocatalyzed enantioselective and branch regioselective allylic alkylation reaction (Scheme 9.4). *N*-methyl anilines used as the formal "hard" alkyl nucleophiles without preactivation. The only by-product is acetic acid, reflecting a good atom economy of this reaction.

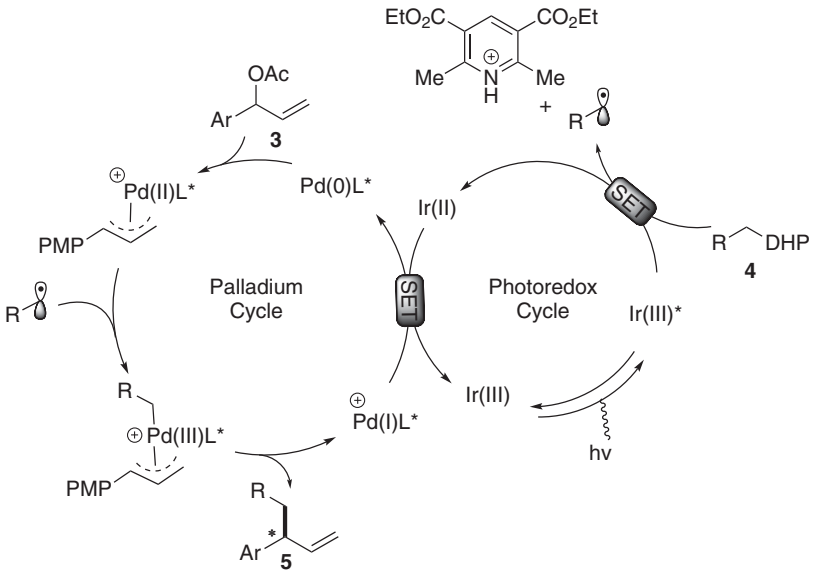


**Scheme 9.3** Proposed mechanism for photoredox/palladium cocatalyzed-AAA reaction.

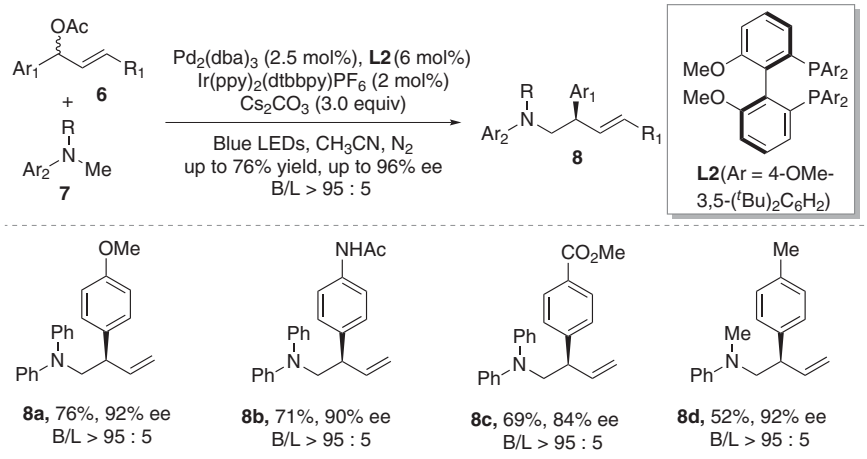


**Scheme 9.4** Enantioselective α-allylation of anilines by photoredox/palladium cocatalysis.

Various chiral homoallyl amines are obtained with moderate to good yields and enantioselectivities, providing an efficient pathway to synthesize chiral homoallylic amines.

In 2020, Yu et al. [31] introduced straightforward access to optically active diarylalkanes from racemic diarylmethyl carbonates through the combination of the photoredox and palladium catalysis under mild reaction conditions (Scheme 9.5). Amenable with carbonates featuring various substituents on an aryl or naphthyl ring with 4-alkyl-1,4-dihydropyridines, this method achieves moderate yields and good enantioselectivity (up to 80% yield and 83% ee). It expands the scope of

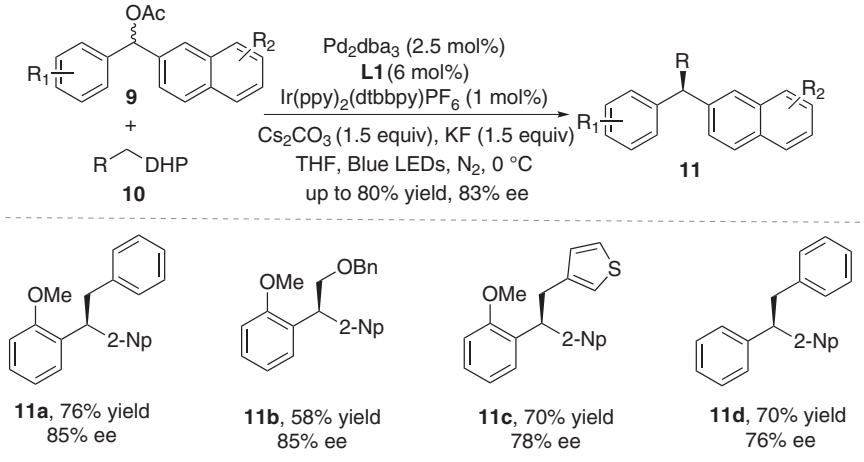


**Scheme 9.5** Photoredox/palladium-cocatalyzed enantioselective alkylation of secondary benzyl carbonates.

asymmetric Pd-catalyzed benzylic substitution reactions and serves as a potential alternative. Control experiments were conducted to confirm that this reaction undergoes a DYKAT process and that the configuration of secondary benzyl carbonates has no influence on the stereochemistry of the products, which is entirely controlled by the chiral ligands.

In 2021, Yu et al. [32] developed a dual photoredox/palladium enantioselective alkylation of 4-alkyl-1,4-dihydropyridines with Morita–Baylis–Hillman (MBH) adducts (Scheme 9.6). By optimizing the reaction conditions, they used Ding's spiroketal-based bis-(phosphine) (SKP) as the chiral ligand, which had been successfully used in $S_N2$-type enantioselective substitutions of MBH adducts with palladium. The $S_N2$-type products were predominant, and the competitive $S_N2'$-type

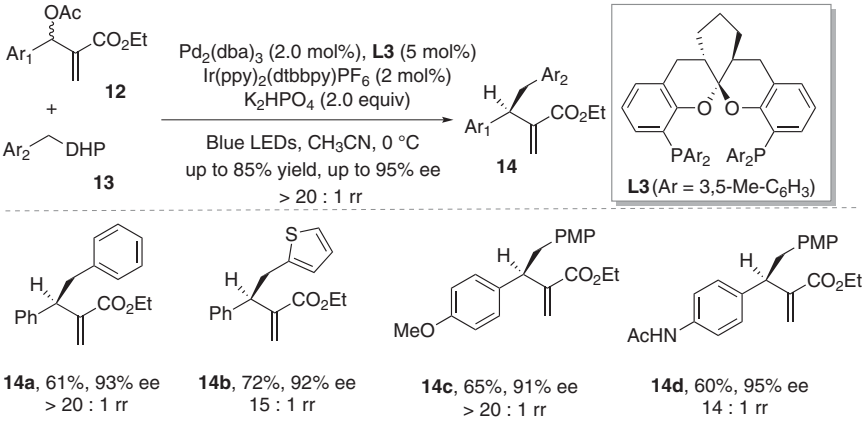


**Scheme 9.6** Enantioselective radical $S_N2$-type alkylation using dual photoredox/palladium catalysis.

pathway was inhibited. By utilizing photoredox in combination with palladium/SKP ligand, the compatibility of this catalytic strategy was demonstrated, successfully achieving satisfactory regio- and enantioselective radical $S_N2$-type alkylation under mild conditions and expanding the substrate scope of these reactions.

In 2021, Yu et al. [33] described a dual photoredox/Pd catalytic protocol for regio-, diastereo-, and enantioselective reductive homocoupling of allylic electrophiles (Scheme 9.7). Diisopropylethylamine or Hantzsch ester served as a homogeneous organic reductant. These chiral 1,5-dienes have the potential to serve as chiral ligands in asymmetric synthesis and can be further modified to create other important chiral ligands. Mechanistically, an allylic radical can be generated from the corresponding allylic electrophile under photoredox conditions. The allylic radical was uncovered by radical trapping experiments. When the radical trapping reagent (TEMPO) was added, the reaction efficiency decreased dramatically and the ally-TEMPO adduct could be isolated. Meanwhile, the oxidative addition of the allylic electrophile to the Pd(0) complex delivers the Pd(II)-π-allyl species. The synthesized π-allylpalladium complex can also provide the reductive homocoupling product, demonstrating that the π-allyl-palladium complex might be the key intermediate. The allylic radical is then trapped by the π-allyl palladium complex to provide the Pd(III) complex. Reductive elimination of the Pd(III) complex gives a C2-symmetrical chiral 1,5-diene.

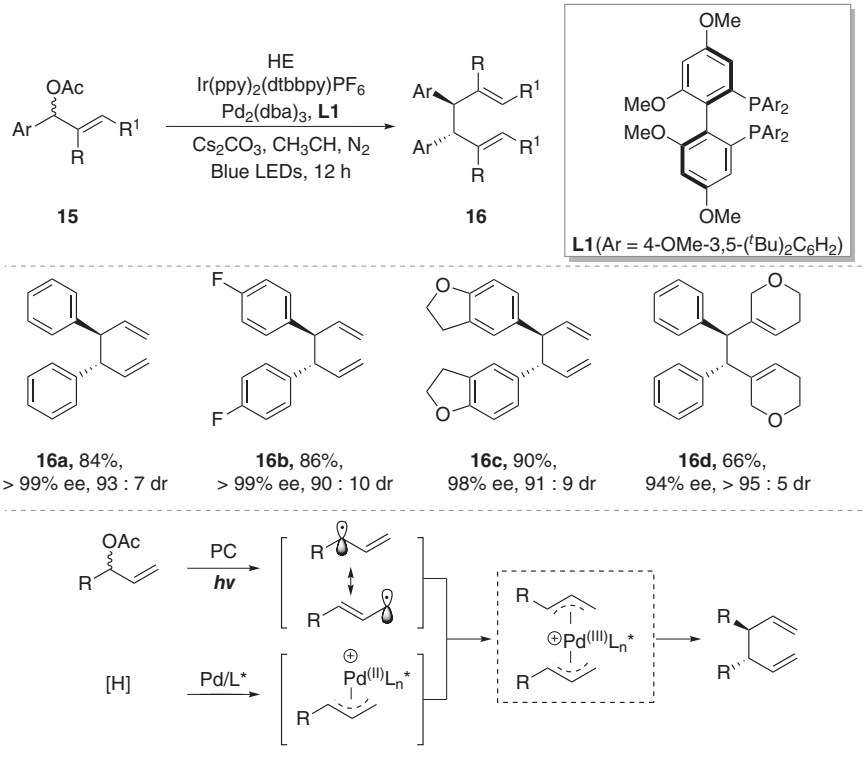


**Scheme 9.7** Photoredox/Pd-cocatalyzed reductive homocoupling of allylic electrophiles.

In 2022, Zhang and Yu et al. [34] reported a palladium-photoredox-catalyzed regio- and enantioselective decarboxylative allylic benzylation (Scheme 9.8). Benzyl carboxylic acids were chosen as atom formal economical and environmentally friendly benzylic nucleophiles. Carbon dioxide was produced as the only by-product. Furthermore, vinyl epoxides could also serve as the Pd-π-allyl precursors to afford various chiral homoallylic alcohols bearing all-carbon quaternary stereocenters with a simple adjustment to the reaction conditions.

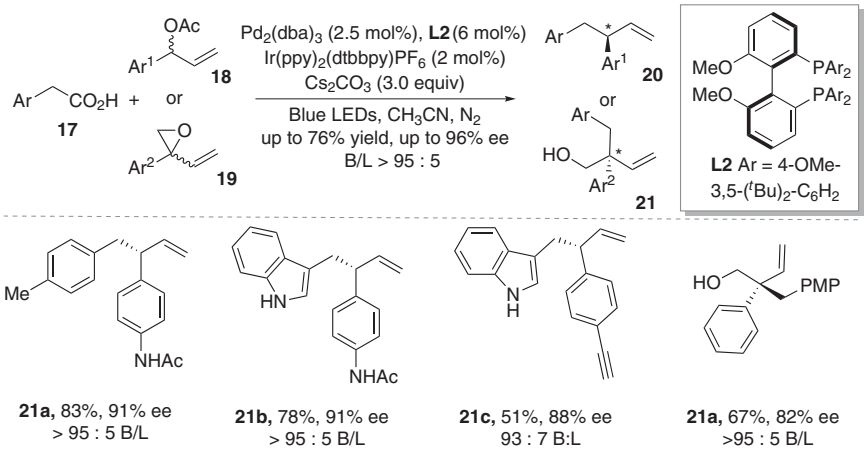


**Scheme 9.8** Palladium/photoredox-catalyzed regio- and enantioselective decarboxylative allylic benzylation.

In 2022, Zhang and Yu et al. [35] described a regio- and enantioselective reductive cross-coupling of allylic acetates under dual photoredox/palladium catalysis (Scheme 9.9). Hantzsch ester served as the reductant. The reductive cross-coupling of allylic acetates with tertiary/secondary alkyl bromides is compatible. The mechanistic study shows that this reaction follows a radical pathway, and the use of a chiral Pd complex allows for the regulation of both regio- and enantioselectivities.

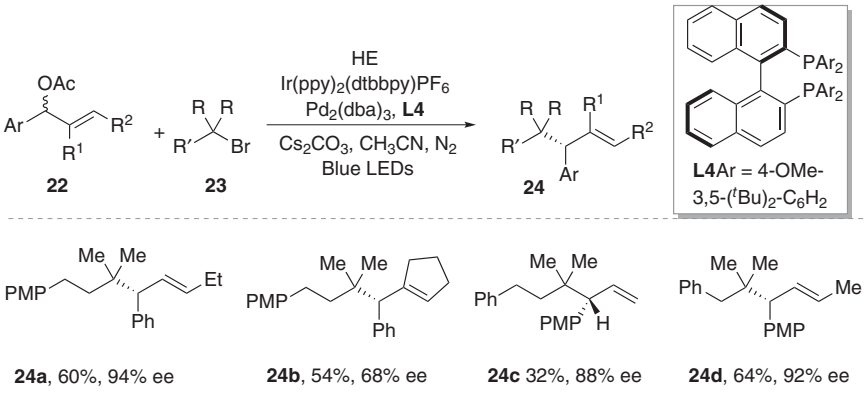


**Scheme 9.9** Dual photoredox/palladium-catalyzed enantioselective reductive cross-coupling.

This strategy provides an efficient pathway to direct and stereoselective construction of C($sp^3$)—C($sp^3$) bonds under mild reaction conditions.

In 2021, Breit et al. [36] developed an enantioselective and regioselective decarboxylative hydroaminoalkylation of alkoxylallenes with the dual photoredox/palladium catalyst (Scheme 9.10). Alkoxyallenes were used as the allylic precursor and α-amino acids as radical precursors, leading to protected vinyl 1,2-amino alcohols in good yields with high levels of regio- and enantioselectivity. A plausible mechanism is proposed wherein the palladium catalyst undergoes oxidative addition with an amino acid, leading to the formation of palladium hydride species **A**. Then, migratory insertion of the intermediate **A** to the allene generates a π-allyl palladium species **B**. The decarboxylation via a reductive quenching process of the visible-light excited Ir(III)* complex resulted in an intermediate **D**. Reductive elimination from Pd(III) species gives the desired product and Pd(I) species. Finally, the low-valent Ir(II) complex reduces Pd(I) species, which will regenerate Ir(III) and Pd(0) to close both catalytic cycles.

In 2022, Breit et al. [37] developed a dual photoredox/palladium-catalyzed regio-, diastereo-, and enantioselective decarboxylative hydroaminoalkylation. They used

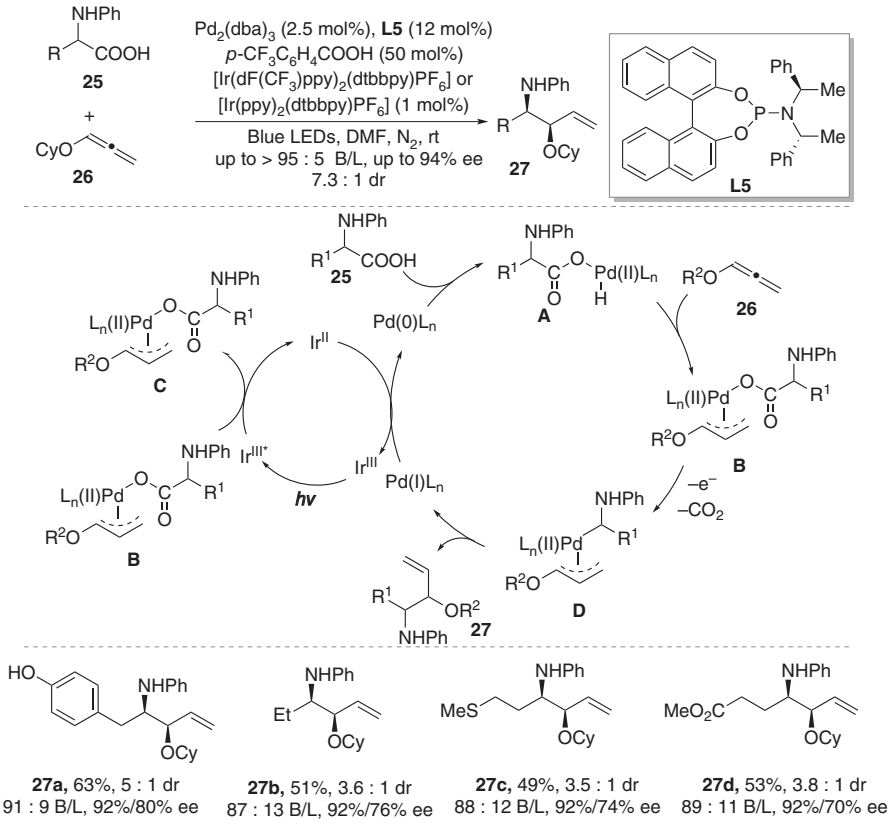


**Scheme 9.10** Dual photoredox/palladium-catalyzed decarboxylative hydroaminoalkylation of allenes.

α-amino acids as radical precursors. According to mechanistic studies, the process of this transformation involves a reversible hydropalladation of 1,3-dienes. This reaction shows good functional group tolerance and excellent diastereo- and enantioselectivity, providing an efficient pathway to synthesize vicinal amino ethers (Scheme 9.11).

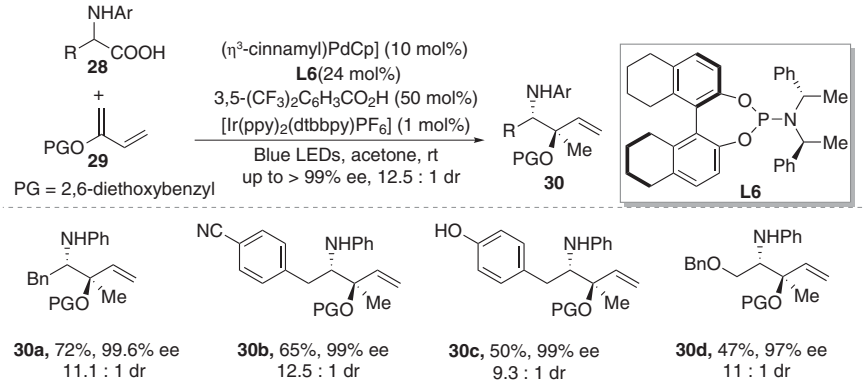


**Scheme 9.11** Enantioselective decarboxylative hydroaminoalkylation enabled by dual palladium/photoredox catalysis.

In 2022, Gevorgyan et al. [38] reported an asymmetric allylic C—H amination to access branched allylic amines (Scheme 9.12). This method relies on an uncommon role of aryl bromide as an oxidant in palladium catalysis. The key to the effective transformation is to find a balance between the selectivity and reactivity of aryl radicals. Under the excitation of visible light, palladium and aryl bromide undergo single-electron transfer to produce aryl radicals and a Pd(I) intermediate, followed by subsequent oxidation of an alkene through hydrogen atom transfer. Then Pd(I) intermediate traps allyl radicals to form a π-allyl Pd(II) complex for a third formal oxidation. Finally, the π-allyl Pd(II) complex could be intercepted by an aliphatic amine to give the C—H amination product.

In 2022, Cheng et al. [39] reported an asymmetric allyl pyridinylation with 4-CN-pyridine driven by electrochemistry (Scheme 9.13). They utilize 4-CN-pyridines as the source of pyridine, which becomes active in the solution below its reduction potential rather than directly at the electrode interface, thus preventing the formation of unpredictable species. These reactions are catalyzed by a Pd/chiral diphosphine complex, which functions as both an electron-transfer mediator and a chiral catalyst. A plausible mechanism is proposed: $PdCl_2L^*$ is first reduced to a Pd(0)L* intermediate. The oxidative addition of Pd(0) into allyl ester gives a Pd-π-allyl species **C**. After undergoing cathodic reduction, the Pd-π-allyl species **C** forms a Pd species **D**, which then transfers an electron to 4-CN-pyridine, resulting in the generation of a Pd species **E** and a radical intermediate. Complex **E** accepts another electron from the cathode to produce a Pd species **F**, which traps the generated radical to produce a Pd(II) species **G**. The reductive elimination from the Pd(II) species gives the desired product and Pd(0) species.

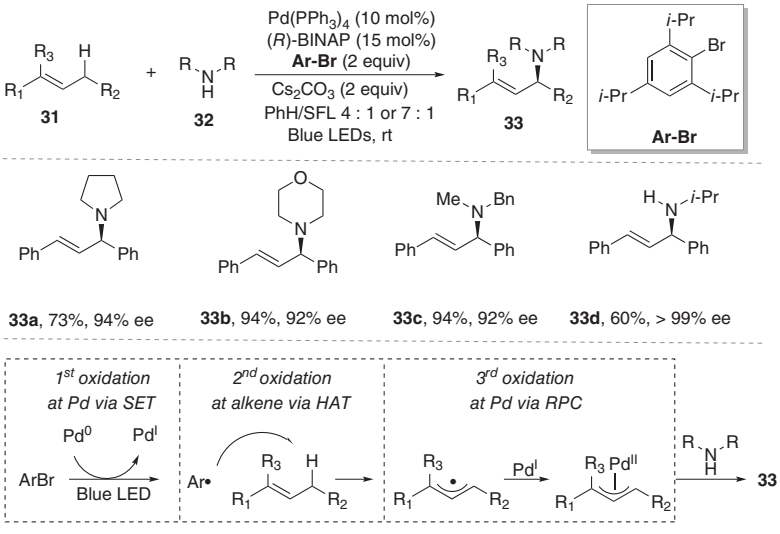


**Scheme 9.12** Light-promoted palladium-catalyzed asymmetric intermolecular allylic C—H amination.

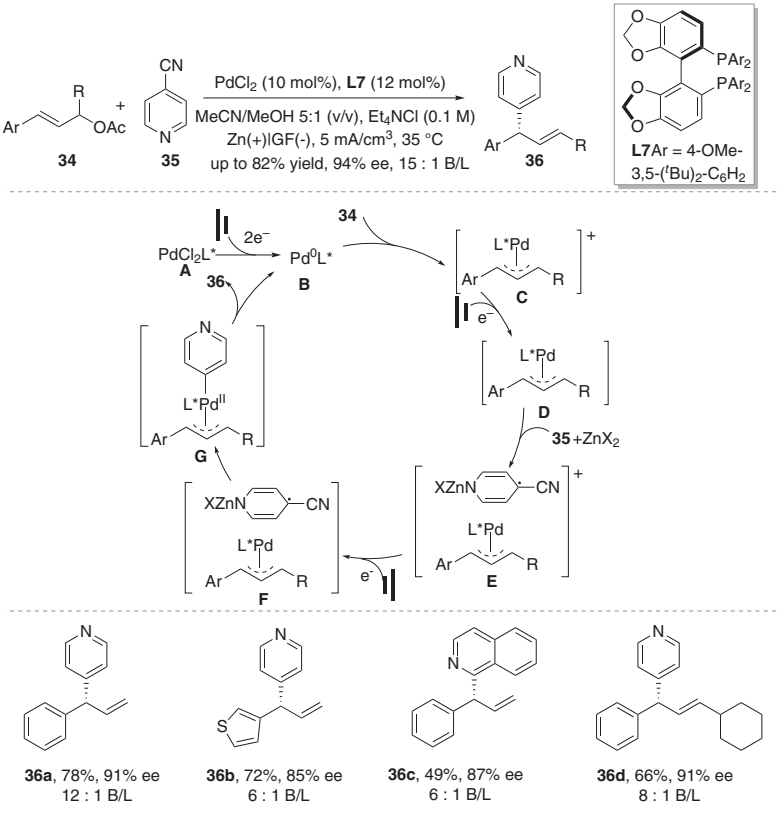


**Scheme 9.13** Enantioselective electroreductive palladium-catalyzed pyridinylation.

## 9.3 Rhodium-Catalyzed Asymmetric Radical Reactions

In addition to palladium, the rhodium catalyst has been utilized in asymmetric radical reactions. Eric Megggers [40] has accomplished a series of works in this field. However, the rhodium-catalyzed asymmetric radical reactions in which the rhodium center can intercept the generated radical are still rare.

In 2017, Ready and co-workers [41] described a rhodium-catalyzed enantioselective radical addition of $BrCX_3$ ($X$ = Cl or Br) to terminal olefins to afford optically active secondary bromides (Scheme 9.14). With $[Rh(cod)Cl]_2$ as the optimal catalyst, *p*-tol-DIOP (**L8**) as the optimal ligand, the addition of $BrCCl_3$ to vinyl arenes could undergo the radical addition reaction in good yields and enantioselectivity (up to 98% yield, 90% ee). Both experimental and computational studies revealed an asymmetric atom-transfer radical addition mechanism (Scheme 9.14, bottom). The bromine radical is abstracted by Rh(I)Cl species to generate the $\bullet CX_3$ radical and a Rh(II)BrCl species. The subsequent addition of the $\bullet CX_3$ radical to styrene **37** affords the benzylic radical. Oxidative addition of benzylic radical to Rh(II) to provide the

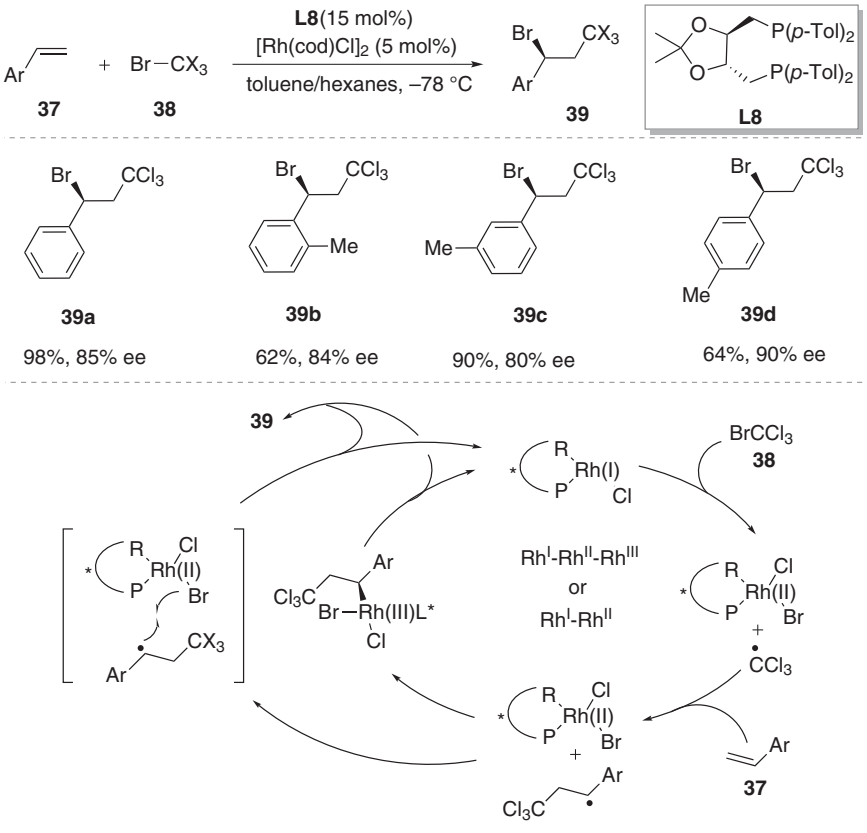


**Scheme 9.14** Rhodium-catalyzed enantioselective radical addition to olefins.

Rh(III) intermediate, which undergoes reductive elimination to generate the product **39**. Alternatively, it could directly abstract bromine from the Rh(II)BrCl species in an outer-sphere mechanism to give the product **39.**

## 9.4 Iridium-Catalyzed Asymmetric Radical Reactions

The iridium-catalyzed asymmetric radical reactions, in which the iridium center captures the generated radical, are also rare. In 2021, Melchiorre and co-workers [42] demonstrated that chiral ($\eta^3$-allyl)iridium(III) complex (**Ir-40**) with an established thermal reactivity can be repurposed to mediate mechanistically different enantioselective processes using visible light excitation (Scheme 9.15). This photochemical

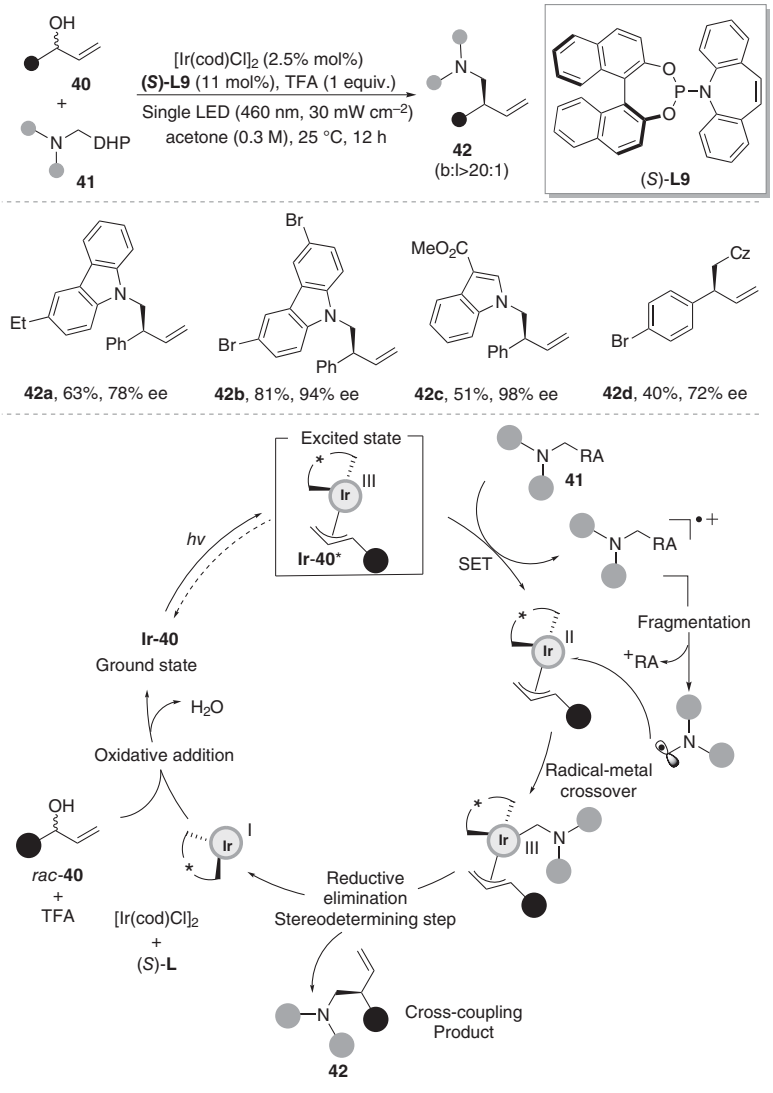


**Scheme 9.15** Catalytic asymmetric C—C cross-couplings enabled by photoexcitation.

strategy enables the enantioselective C($sp^3$)—C($sp^3$) cross-coupling of racemic allylic alcohols **40** with stable radical precursors **41**, which is difficult to achieve under thermal activation. With the optimal reaction conditions, various allylic alcohols and readily available radical precursors could undergo this reaction smoothly, giving the corresponding products **42** in excellent yields and enantioselectivity (up to 81% yield, 98% ee). A plausible catalytic cycle is depicted (Scheme 9.15, bottom): the oxidative addition of the chiral Ir(I) precatalyst to allylic alcohol **40** provides a ($\eta^3$-allyl)iridium(III) complex **Ir-40**. Then, **41** acts as a reductive quencher of **Ir-40***, undergoing a single-electron transfer pathway to provide the iridium(II) intermediate and the radical intermediate. Followed by radical–metal crossover, the iridium(II) intermediate intercepts the radical to get a more stable iridium(III) complex. Eventually, the C($sp^3$)—C($sp^3$) bond is forged via regio- and stereo-determining reductive elimination, and the active Ir(I) catalyst is regenerated.

## 9.5 Summary and Perspectives

Precious metal catalysis has shown synthetic potential in asymmetric radical reactions. Enantioselective Pd/photoredox dual catalysis showed its ability in radical AAA reactions. This strategy needs to be extended to other type of reactions. Limited success has been achieved in other precious metals. The synthetic potential of Rh, Ir, and other metal-mediated asymmetric radical reactions needs to be further explored.

## References


1 Chirik, P. and Morris, R. (2015). *Acc. Chem. Res.* 48: 2495–2495.
2 Wen, J., Wang, F., and Zhang, X. (2021). *Chem. Soc. Rev.* 50: 3211–3237.
3 Miyaura, N. and Suzuki, A. (1995). *Chem. Rev.* 95: 2457–2483.
4 Muci, A.R. and Buchwald, S.L. (2002). *Top. Curr. Chem.* 219: 131–209.
5 Negishi, E. and Anastasia, L. (2003). *Chem. Rev.* 103: 1979–2018.
6 Beccalli, E.M., Broggini, G., Martinelli, M., and Sottocornola, S. (2007). *Chem. Rev.* 107: 5318–5365.
7 Lyons, T.W. and Sanford, M.S. (2010). *Chem. Rev.* 110: 1147–1169.
8 He, J., Wasa, M., Chan, K.S.L. et al. (2016). *Chem. Rev.* 117: 8754–8786.
9 Ruiz-Castillo, P. and Buchwald, S.L. (2016). *Chem. Rev.* 116: 12564–12649.
10 Shao, Q., Wu, K., Zhuang, Z. et al. (2020). *Acc. Chem. Res.* 53: 833–851.
11 Tietze, L.F., Ila, H., and Bell, H.P. (2004). *Chem. Rev.* 104: 3453–3516.
12 Margalef, J., Biosca, M., de la Cruz Sánchez, P. et al. (2021). *Coord. Chem. Rev.* 446: 214120–214204.
13 Noreen, S., Zahoor, A.F., Ahmad, S. et al. (2019). *Curr. Org. Chem.* 23: 1168–1213.
14 Pàmies, O., Margalef, J., Cañellas, S. et al. (2021). *Chem. Rev.* 121: 4373–4505.
15 Kitagawa, O. (2021). *Acc. Chem. Res.* 54: 719–730.
16 Peng, J.-B., Liu, X.-L., Li, L., and Wu, X.-F. (2022). *Sci. China Chem.* 65: 441–461.

**17** Milhau, L. and Guiry, P.J. (2011). *Top. Organomet. Chem.* 38: 95–153.
**18** Lucas, E.L., Lam, N.Y.S., Zhuang, Z. et al. (2022). *Acc. Chem. Res.* 55: 537–550.
**19** Zhan, B.-B., Jin, L., and Shi, B.-F. (2022). *Trends. Chem.* 4: 220–235.
**20** Trost, B.M., Jiao, Z., and Hung, C. (2019). *Angew. Chem. Int. Ed.* 58: 15154–15158.
**21** Zhang, Z., Xu, B., Wu, L. et al. (2019). *Angew. Chem. Int. Ed.* 58: 14653–14659.
**22** Zhang, W., Wang, F., McCann, S.D. et al. (2016). *Science* 353: 1014–1018.
**23** Ge, L., Zhou, H., Chiou, M.-F. et al. (2020). *Nat. Catal.* 4: 28–35.
**24** Zhang, C., Li, Z.-L., Gu, Q.-S., and Liu, X.-Y. (2021). *Nat. Commun.* 12: 475–483.
**25** Zhou, Q., Chin, M., Fu, Y. et al. (2021). *Science* 374: 1612–1616.
**26** Zhang, H.-H., Chen, H., Zhu, C., and Yu, S. (2020). *Sci. China Chem.* 63: 637–647.
**27** Nagib, D.A. (2022). *Chem. Rev.* 122: 15989–15992.
**28** Lang, S.B., O'Nele, K.M., Douglas, J.T., and Tunge, J.A. (2015). *Chem. Eur. J.* 21: 18589–18593.
**29** Zhang, H.-H., Zhao, J.-J., and Yu, S. (2018). *J. Am. Chem. Soc.* 140: 16914–16919.
**30** Zhang, H.-H., Zhao, J.-J., and Yu, S. (2020). *ACS Catal.* 10: 4710–4716.
**31** Shen, X., Qian, L., and Yu, S. (2020). *Sci. China Chem.* 63: 687–691.
**32** Bai, X., Qian, L., Zhang, H.-H., and Yu, S. (2021). *Org. Lett.* 23: 8322–8326.
**33** Zhang, H.-H., Tang, M., Zhao, J.-J. et al. (2021). *J. Am. Chem. Soc.* 143: 12836–12846.
**34** Song, C., Zhang, H.-H., and Yu, S. (2022). *ACS Catal.* 12: 1428–1432.
**35** Tang, S., Zhang, H.-H., and Yu, S. (2023). *Chem. Commun.* 59: 1153–1156.
**36** Zheng, J., Nikbakht, A., and Breit, B. (2021). *ACS Catal.* 11: 3343–3350.
**37** Zheng, J., Tang, N., Xie, H., and Breit, B. (2022). *Angew. Chem. Int. Ed.* 61: e202200105.
**38** Cheung, K.P.S., Fang, J., Mukherjee, K. et al. (2022). *Science* 378: 1207–1213.
**39** Ding, W., Li, M., Fan, J., and Cheng, X. (2022). *Nat. Commun.* 13: 5642–5652.
**40** Huang, X. and Meggers, E. (2019). *Acc. Chem. Res.* 52: 833–847.
**41** Chen, B., Fang, C., Liu, P., and Ready, J.M. (2017). *Angew. Chem. Int. Ed.* 56: 8780–8784.
**42** Crisenza, G.E.M., Faraone, A., Gandolfo, E. et al. (2021). *Nat. Chem.* 13: 575–580.

# 10

# Chiral Lewis Acid-Catalyzed Asymmetric Radical Transformations

*Yu-Mei Lin, Haichao Huang, Jiabin Liao, Yuhang He, and Lei Gong*

*Key Laboratory of Chemical Biology of Fujian Province, College of Chemistry and Chemical Engineering, Xiamen University, Xiamen, China*

## 10.1 Introduction

Radical chemistry has long been recognized as a potent and indispensable tool in synthetic chemistry due to its unique ability to cleave and construct chemical bonds [1–3]. This makes it an essential route for a variety of organic reactions that offer several advantages, such as mild conditions, high functional group compatibility, and chemoselectivity [4–6]. As a result, a plethora of methods based on thermally, photochemically, and electrochemically triggered radical formations and transformations have been developed, enabling the synthesis of diverse organic molecules in both stoichiometric and catalytic manners [7–9]. Despite these advances, asymmetric catalysis via radical processes remains a significant challenge [10–14]. The high reactivity and low reaction barriers of radical species often result in background reactions, making it remarkably difficult to achieve high levels of diastereo- and enantioselectivity [15–20]. The development of effective strategies to control stereochemistry in radical-involved processes is an active area of research, with many promising approaches being explored.

Chiral Lewis acids (CLAs) are essential components of modern organic synthesis, providing strong activation toward substrate molecules and exceptional asymmetric induction in many ionic and concerted reactions [21]. In the 1990s, pioneering studies by Sibi, Porter, and others demonstrated the power of CLA catalysts in controlling the stereochemistry of free radical reactions [22, 23]. These catalysts can efficiently activate substrates by reducing the LUMO energies of unsaturated bonds through coordination, thereby inducing stereodiscrimination in subsequent reactions with nucleophilic alkyl radicals generated in situ (Scheme 10.1a) [24]. Over the next three decades, numerous enantioselective radical reactions have been developed using CLA catalysis, including enantioselective conjugate radical addition, hydrogen atom transfer (HAT), and radical cyclization. More recently, the combination of CLA catalysis with photoredox or electrolysis has emerged as a new research field. These progresses have inspired chemists to design new

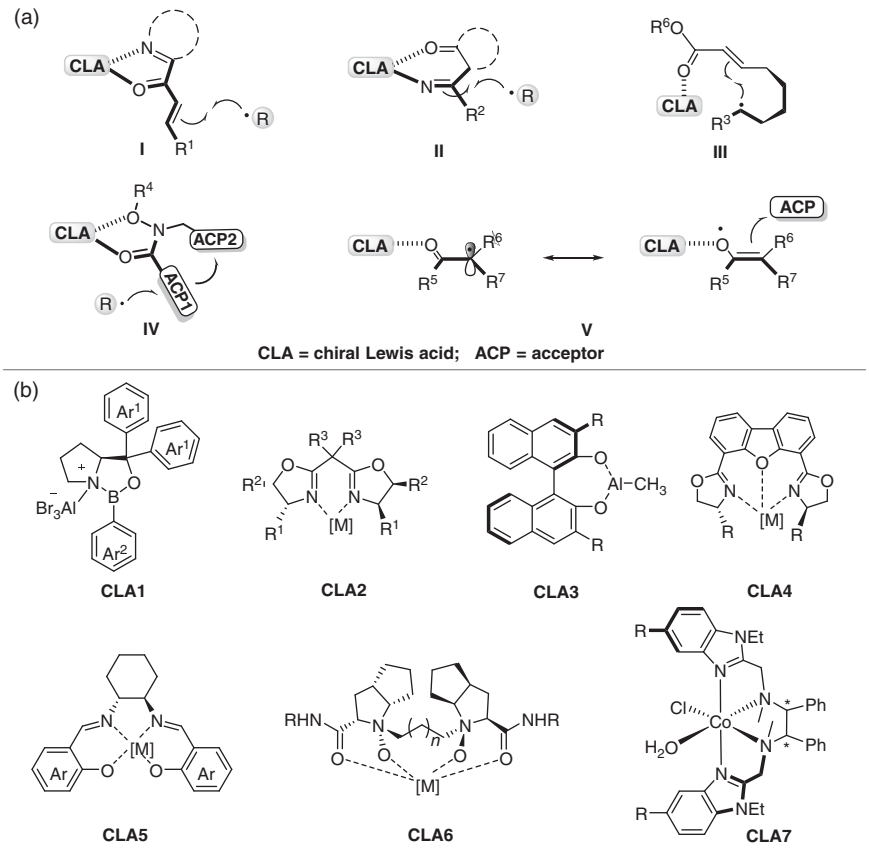


**Scheme 10.1** (a) Representative activation models by chiral Lewis acid catalysts in enantioselective radical transformations. (b) Representative chiral Lewis acid catalysts.

asymmetric synthetic methods based on radical chemistry, some of which have been documented in recent reviews [25–28].

This chapter provides a brief overview of enantioselective radical reactions catalyzed by classic CLAs, such as chiral boranes (e.g., **CLA1**) and complexes of magnesium, lanthanum metals, or other transition metals (e.g., Zn, Al, Ti, Cu, Ni, Co) bearing bidentate, tridentate, or multidentate chiral ligands (e.g., **CLA2–CLA7**) (Scheme 10.1b). Enantioselective transformations catalyzed by unique iridium or rhodium complexes with exclusive metal-centered chirality will be discussed separately in other chapters [29].

## 10.2 Asymmetric Radical Reactions Initiated by Classical Chemical Methods

### 10.2.1 Enantioselective Conjugate Radical Addition Reactions

Conjugate addition to α,β-unsaturated systems is a fundamental reaction in organic chemistry, enabling the direct installation of β-functionalities adjacent

to carbonyl moieties [30, 31]. In 1996, Sibi and Porter et al. demonstrated that chiral bisoxazoline complexes of magnesium or zinc, functioning as CLAs, could catalyze an enantioselective conjugate radical addition to α,β-unsaturated *N*-acyloxazolidinones (**1**) at −78 °C (Scheme 10.2a) [32]. In the presence of $Et_3B$/oxygen as the initiator, an alkyl iodide (**2**) was converted into the corresponding alkyl radical, which underwent stereocontrolled β-addition to the C=C double bond of substrate **1** activated by the CLA catalyst. At this low temperature, the non-Lewis acid-mediated process was suppressed, and chelation of the substrate (**1**) and chiral ligand (**L1a** or **L1b**) to the Lewis acid center (Mg or Zn) generated reactive complex intermediates that captured the nucleophilic radical intermediate. The β-alkylated products (**3**) were obtained in good yield (71–86%) with moderate enantioselectivity (67–70% ee), even when the CLA loading was reduced from a stoichiometric amount (entry 1) to 20 mol% (entries 2, 4, and 5). This work represents the first example of radical addition enabled by substoichiometric CLAs, opening new avenues for catalytic enantioselective radical transformations. Further development of chiral Lewis acid catalysts with improved reactivity and selectivity will undoubtedly lead to more efficient approaches to enantioselective radical reactions. This group later optimized the same reaction by employing a chiral bisoxazoline ligand with a spiro ring (**L2**) to adjust the bite angle (Scheme 10.2b) [33]. The chiral product (**3a**) was obtained with significantly increased enantioselectivity (97% ee) under similar conditions. When the reaction was conducted at room temperature, high enantioselectivity (93% ee) was retained, enabling more convenient setups for this challenging transformation.

(a)

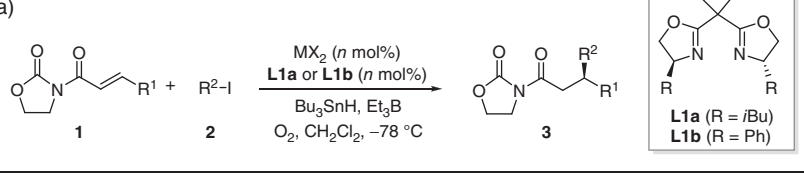


| entry | product | CLA ($MX_2$/chiral ligand) | amout of CLA (*n* mol%) | yield (%) | ee (%) |
|---|---|---|---|---|---|
| 1 | **3a** ($R^1$ = Ph, $R^2$ = *i*Pr) | $MgI_2$/**L1a** | 100 | 88 | 82 |
| 2 | **3a** ($R^1$ = Ph, $R^2$ = *i*Pr) | $MgI_2$/**L1a** | 20 | 86 | 67 |
| 3 | **3a** ($R^1$ = Ph, $R^2$ = *i*Pr) | $MgI_2$/**L1a** | 5 | 57 | 40 |
| 4 | **3b** ($R^1$ = $CH_3$, $R^2$ = *t*Bu) | $MgI_2$/**L1a** | 20 | 73 | 66 |
| 5 | **3b** ($R^1$ = $CH_3$, $R^2$ = *t*Bu) | $Zn(OTf)_2$/**L1b** | 20 | 71 | 70 |

(b)

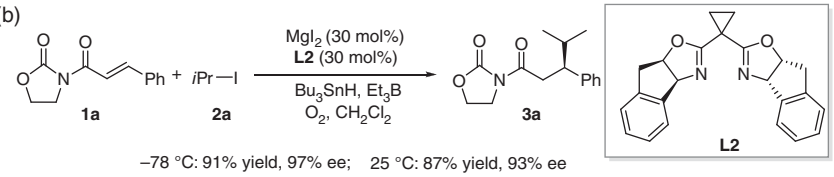


–78 °C: 91% yield, 97% ee; 25 °C: 87% yield, 93% ee

**Scheme 10.2** (a) Pioneering work on CLA-catalyzed enantioselective conjugate radical addition. (b) An optimized reaction using a spiro-derived chiral ligand.

The pioneering studies in this area have inspired chemists to explore more combinations of chiral ligands, metal salts, various auxiliaries, and substrate partners to develop enantioselective radical reactions [34–40]. For instance, Murakata, Hoshino et al. reported a zinc-catalyzed enantioselective conjugate addition to an *N*-cinnamoyloxazolidinone (**4**) with alkyl iodines (**2**) as radical precursors (Scheme 10.3) [34]. By using a chiral Lewis acid derived from $Zn(OTf)_2$ (25 mol%) and a chiral ligand (**L3**, 25 mol%), the reaction was executed with moderate to good enantioselectivity (72–84% ee). The addition of 5-diphenyloxazolidin-2-one (**5**) as an achiral additive proved to be the key to success, perhaps because it could coordinate with the zinc center to tune the steric environment of the CLA catalyst. These findings highlight the importance of rational design of substrates and careful selection of reaction conditions.

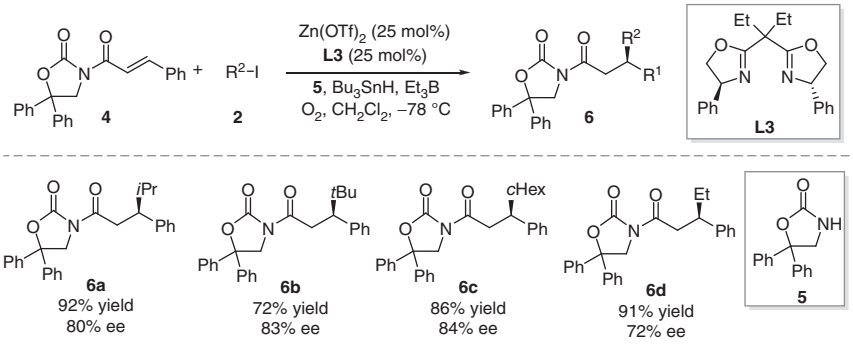


**Scheme 10.3** Zn/bisoxazoline-catalyzed enantioselective conjugate radical addition.

Furthermore, Sibi et al. found that a lanthanide complex bearing a proline-derived ligand (**L4**) could catalyze a similar reaction (Scheme 10.4a) [35]. Using an *N*-acyl oxazolidinone (**7**) and 4 Å molecular sieves as additives, the desired adduct (**3a**) was obtained with dramatically improved enantioselectivity (92% ee) compared to previous studies. In a follow-up study, they reported an enantioselective conjugate radical addition to α′-hydroxy α,β-unsaturated ketones (**8**) catalyzed by 30 mol% of $Mg(NTf_2)_2$/chiral bisoxazoline ligand (**L1b**) (Scheme 10.4b) [36]. This reaction demonstrated the effectiveness of employing a carbonyl and a hydroxyl group of the enone substrate as bidentate chelation sites instead of an achiral template, such as alkylidene malonates and oxazolidinones. The formation of chiral α-hydroxy ketone products (**9**) proceeded with good yields (63–86%) and enantioselectivities (66–86% ee).

Kim et al. revealed that α′-phosphoric enone substrates are also applicable in enantioselective radical addition (Scheme 10.4c) [37]. Among various combinations of metal salts and chiral ligands, $Zn(OTf)_2$ and a tetraphenyl-substituted $C_2$-symmetric bisoxazoline ligand (**L5**) were found to be the most effective for the reaction between the α′-phosphoric enone (**10**) and alkyl iodide (**2**), resulting in corresponding products (**11**) with up to 98% yields and 95% ee. Moreover, the addition of allyltributylstannane as a third reaction component led to the

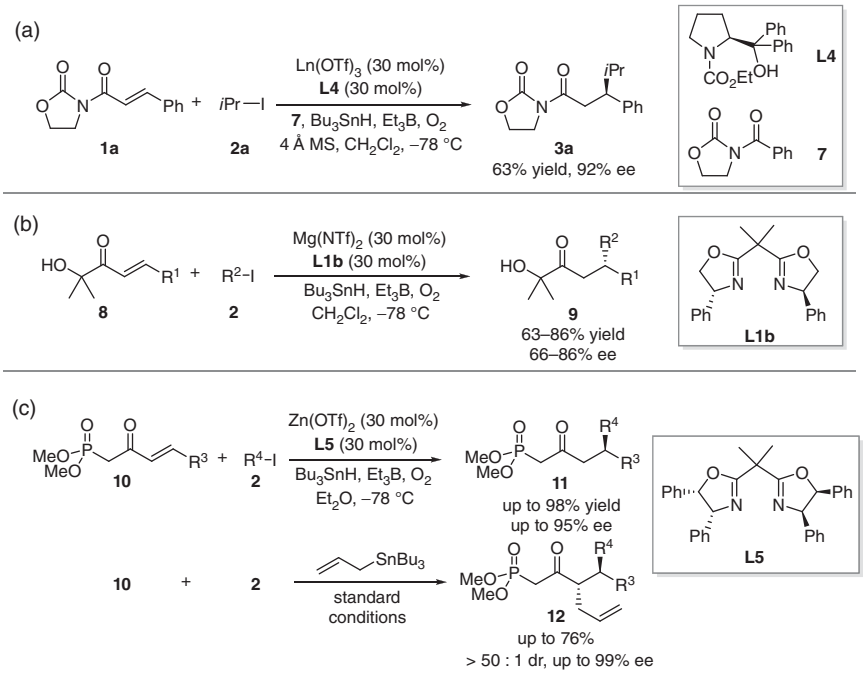


**Scheme 10.4** Other selected examples of CLA-catalyzed enantioselective conjugate radical addition reactions. (a) $Ln(OTf)_3$-catalyzed enantioselective conjugate radical addition. (b) $Mg(NTf)_2$-catalyzed enantioselective conjugate radical addition. (c) $Zn(OTf)_2$-catalyzed enantioselective conjugate radical addition.

formation of *anti*-isomers of further addition products (**12**) with >50 : 1 dr and up to 99% ee. These results demonstrate the compatibility of CLA-catalyzed conjugate radical additions with external radical acceptors, enabling the development of multi-component asymmetric synthesis.

### 10.2.2 Enantioselective Hydrogen Atom Transfer Reactions

Enantioselective hydrogen atom transfer (HAT) reactions, which involve the stereodetermining step in hydrogen atom transfer processes, remain challenging in organic synthesis [41]. This is because hydrogen is the smallest atom, making it difficult to discriminate stereoselectivity [42]. However, certain CLAs have been established to have potential in controlling stereoselectivity in HAT to α-carbonyl radicals, either derived from a single-electron reduction of α-halo carbonyl compounds or from a conjugate radical addition to α,β-unsaturated compounds (Scheme 10.5) [43].

An earlier report by Hoshino et al. demonstrated that the combination of $MgI_2$ and a $C_2$-symmetric diamine ligand (**L6**) could promote a stoichiometric enantioselective reduction of α-alkyl-α-iodo hydrocoumarins (**13**) using $Bu_3SnH$ as the hydrogen atom source (Scheme 10.6) [44]. Despite the moderate enantioselectivities

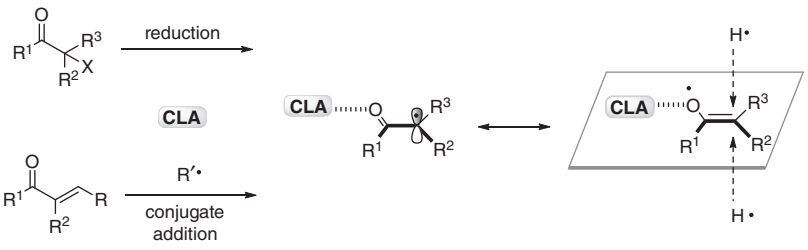


**Scheme 10.5** CLA-controlled HAT to α-carbonyl radicals.

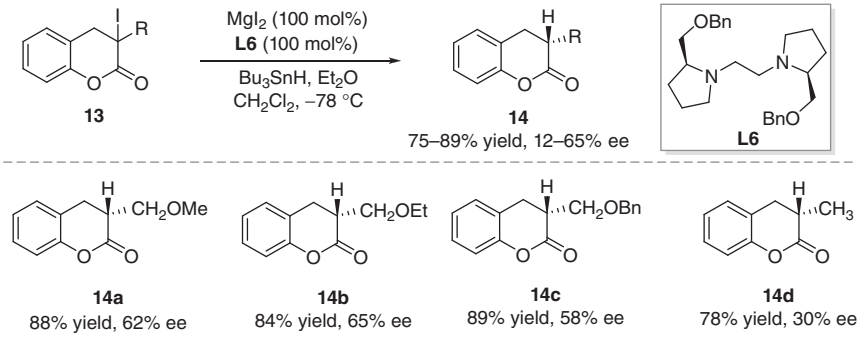


**Scheme 10.6** An enantioselective reduction of α-alkyl-α-iodo hydrocoumarins.

(12–65% ee) and the requirement for stoichiometric CLAs, this study exhibits the potential for enantiodiscrimination in HAT-triggered radical processes.

Sibi et al. also made significant contributions to enantioselective HAT reactions. They reported a CLA-promoted conjugate addition of nucleophilic radicals to α-methacrylates, followed by an enantioselective HAT process (Scheme 10.7) [45]. The effects of various achiral auxiliaries, such as pyrazole (**15a**), 3,5-dimethylpyrazole (**15b**), indazole (**15c**), 2-(α-methacryloyl)azetidinone (**15d**), 2-oxazolidinone (**15e**), pyrrolidinone (**15f**), *N*-phenylpyrazolone (**15g**), 1,8-naphthosultam (**15h**), and 1,8-naphtholactam (**15i**), were evaluated. With the use of a stoichiometric amount of $MgBr_2 \cdot Et_2O$ and a spiro-derived chiral bisoxazoline (**L2**), the reaction of α-methacrylates bearing a naphthosultam moiety (**15h**) delivered the best results in terms of yield (90%) and enantioselectivity (78% ee). After optimization of reaction conditions, a catalytic reaction was achieved by 30 mol% of chiral magnesium Lewis acid, which provided the enantioenriched products (**16i**–**16m**) with up to 90% ee. This study represents the first example of CLA-catalyzed enantioselective HAT reactions, highlighting the potential of CLAs in controlling stereoselectivity in otherwise challenging HAT reactions.

Toru et al. reported an enantioselective HAT reaction to sulfonyl α-carbon radicals facilitated by the Zn/bisoxazoline ligand (**L1b**)-based chiral Lewis acid (Scheme 10.8) [46]. When a stoichiometric quantity of the chiral Lewis acid was employed, vinylsulfones (**17**) were converted to the corresponding α-chiral sulfonyl products (**18**) with up to 99% yields and 93% ee. In one instance, a yield of 67%

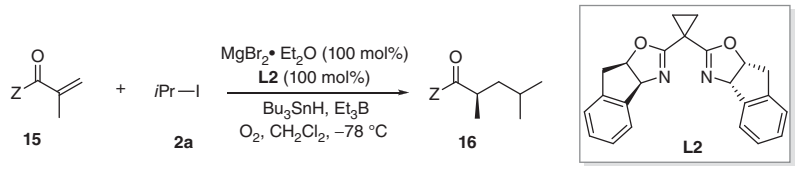


| entry | Z | product | yield (%) | ee (%) | entry | Z | product | yield (%) | ee (%) |
|---|---|---|---|---|---|---|---|---|---|
| 1 | | **16a** | 52 | 15 | 6 | | **16f** | 76 | 42 |
| 2 | | **16b** | 54 | 38 | 7 | 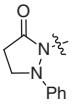 | **16g** | 67 | 28 |
| 3 | 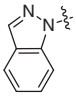 | **16c** | 66 | 15 | 8 | 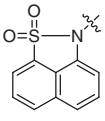 | **16h** | 90 | 78 |
| 4 | | **16d** | 54 | 15 | | | | | |
| 5 | | **16e** | 80 | 65 | 9 | 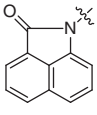 | **16i** | 55 | 22 |

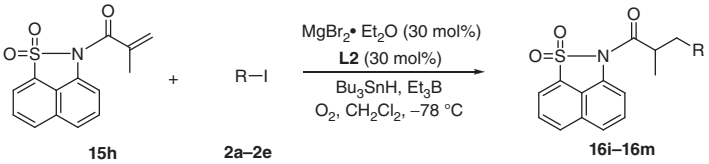


**Scheme 10.7** The enantioselective HAT reaction to α-methacrylates using a naphthosultam template.

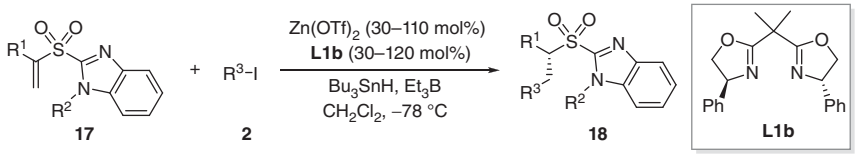


**$Zn(OTf)_2$ (110 mol%), L1b (120 mol%):**
up to 99% yield, up to 93% ee
**$Zn(OTf)_2$ (30 mol%), L1b (30 mol%):**
67% yield, 55% ee ($R^1$ = Ph, $R^2$ = Me, $R^3$ = Et)

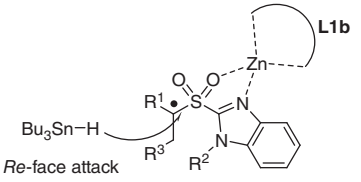


**Scheme 10.8** CLA-promoted enantioselective HAT to sulfonyl α-carbon radicals.

and enantioselectivity of 55% were still achieved even when the chiral Lewis acid was reduced to 30 mol%. The reaction proceeded through a conjugate addition of nucleophilic alkyl radicals, followed by an enantioselective HAT to α-sulfonyl radicals. A plausible transition state indicates that the tetrahedral zinc center of the Lewis acid coordinates with one oxygen atom of the sulfonyl group and one nitrogen atom of the benzimidazolyl moiety, while a hydrogen atom from $Bu_3SnH$ attacks the sulfonyl radical from the *Re*-face.

Sibi et al. discovered that phthalimide-derived α,β-unsaturated esters (**19**) served as effective radical acceptors in this type of transformation (Scheme 10.9) [47]. The reaction of **19** and alkyl halides (**20**) at −78 °C, in the presence of 100 mol% $MgI_2$ and a chiral ligand (**L2**), yields chiral adducts (**21**) in 71–95% yield and with 20–98% ee. Remarkably, up to 90% ee could still be achieved with a catalytic amount (30 mol%) of the CLA catalyst. The proposed transition state featured a flexible eight-membered chelation of the α,β-unsaturated ester substrate (**19**) with the chiral Lewis acid. The conformation of the ester substituent (*S-cis* or *S-trans*) was dependent on its size and was controlled by the chiral ligand. The face selectivity of the H atom transfer from $Bu_3SnH$ to the α-carbonyl radical was influenced by the size of the ester substituent and that of the radical fragments. This method presents new opportunities for the preparation of α-substituted β-amino acids ($\beta^2$-amino acids) of synthetic and biological interest.

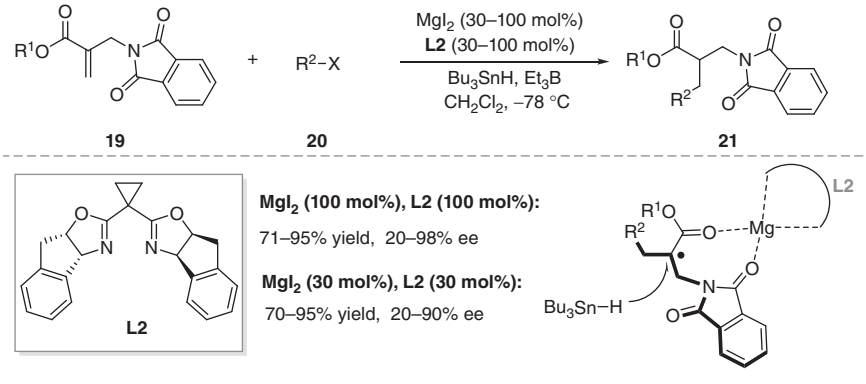


**Scheme 10.9** CLA-enabled enantioselective HAT to α-carbonyl radicals.

The conjugate addition of nucleophilic alkyl radicals to α,β-disubstituted unsaturated systems, followed by enantioselective HAT, has the potential to install two vicinal stereocenters. In 2005, Sibi et al. reported an enantioselective radical addition/trapping reaction of α,β-disubstituted unsaturated imides (**22**) with alkyl iodides (**2**) as the radical precursors (Scheme 10.10a) [48]. In the presence of a 30 mol% CLA catalyst derived from $MgI_2$ and a chiral ligand (**L2**), the anti-propionate aldol products (**23**) were obtained as major isomers with a 3 : 1—99 : 1 diastereomeric ratio and 56—94% ee. In a plausible transition state, an alkyl radical generated in situ attacks the β-carbon of the CLA-bonded substrate from the top face, opposite the aryl group of the chiral ligand (Scheme 10.10,

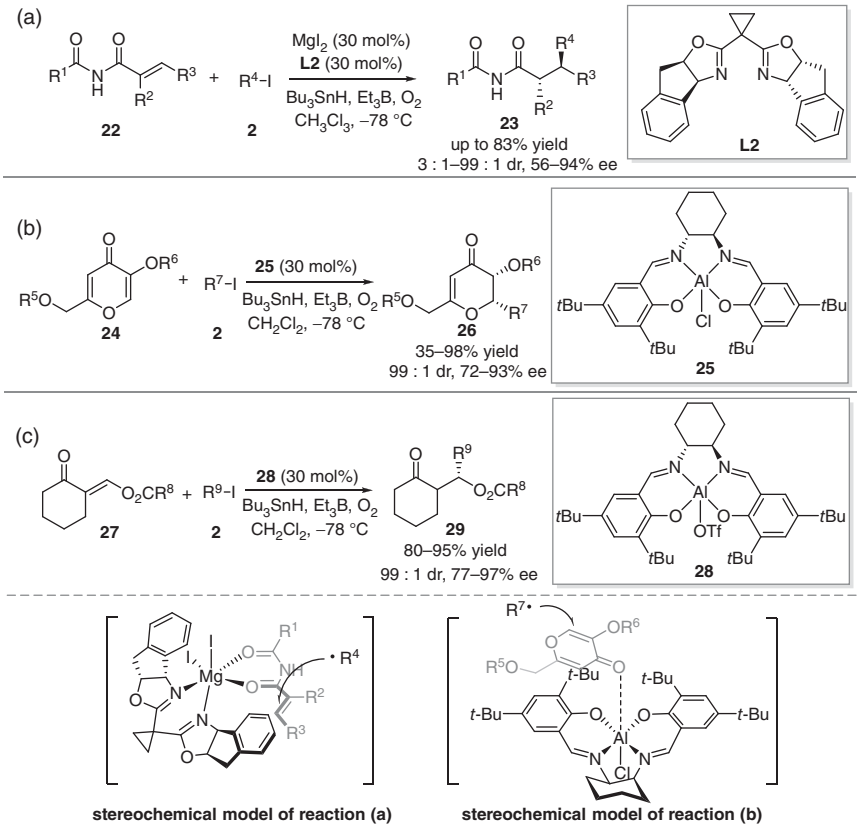


**Scheme 10.10** Selected examples of CLA-catalyzed enantioselective conjugate radical addition to α,β-disubstituted unsaturated compounds for: (a) α,β-disubstituted unsaturated imides derivatives; (b) pyromeconic acid derivatives; (c) benzoate derivatives.

bottom, left side). Subsequent HAT from $Bu_3SnH$ to the α-carbon of the substrate is believed to be controlled by the newly formed β-stereocenter.

Later, they developed similar diastereo- and enantioselective reactions of alkyl radicals with pyromeconic acid derivatives (**24**) (Scheme 10.10b) [49] or benzoate derivatives (**27**) (Scheme 10.10c) [50]. In the case of the reaction in Scheme 10.10b, the combination of magnesium or scandium and bisoxazoline ligands was ineffective in producing high asymmetric induction. A chiral salen aluminum complex (**25**) was the best catalyst, yielding the addition products (**26**) with a 99 : 1 dr and 72–93% ee. A stereochemical model was proposed to explain the formation of the major isomers with a *syn*-configuration (Scheme 10.10, bottom, right side). The pyromeconic acid substrate (**24**) bonds through the carbonyl group with the chiral salen aluminum catalyst (**25**), where the more bulky substituent ($OR^6$) is positioned away from the axial hydrogen atoms on the cyclohexane ring, leaving the *Si* face more open for the initial addition of the nucleophilic radical ($R^7\cdot$). A subsequent HAT to the α-carbon atom is affected by the newly formed β-stereocenter, where the $R^7$ group shields the *Si* face, resulting in an overall *anti*-addition of $R^7\cdot$ and an H atom.

### 10.2.3 Radical Cyclization

Radical-mediated cyclization can form multiple chemical bonds and install several stereogenic centers in a single step, making it a valuable tool for the synthesis of carbocyclic and heterocyclic molecules [5, 8, 51–53]. However, enantioselective radical cyclization remains a significant challenge, due to the lack of effective chiral reagents or catalysts capable of controlling stereochemistry during the ring-forming process [54–56]. Earlier studies by Nishida, Toru, Yang, and others have shown that the addition of stoichiometric CLAs to radical reaction systems can be a promising method for achieving asymmetric radical cyclization [57–62]. For instance, Nishida et al. reported in 1996 an enantioselective intramolecular radical cyclization enabled by a stoichiometric amount of an aluminum-based chiral Lewis acid (Scheme 10.11a) [57]. Upon the reaction of α,β-unsaturated esters bearing a terminal iodoalkenyl moiety (**30**) with a structurally defined aluminum complex (**31**, 4.0 equiv.) at 0 °C, 5- or 6-membered cyclic products (**32**) were obtained with 36–48% ee. A plausible transition state was proposed in which the α,β-unsaturated ester (**30**) coordinated with the Lewis acid in an *s-trans* conformation, resulting

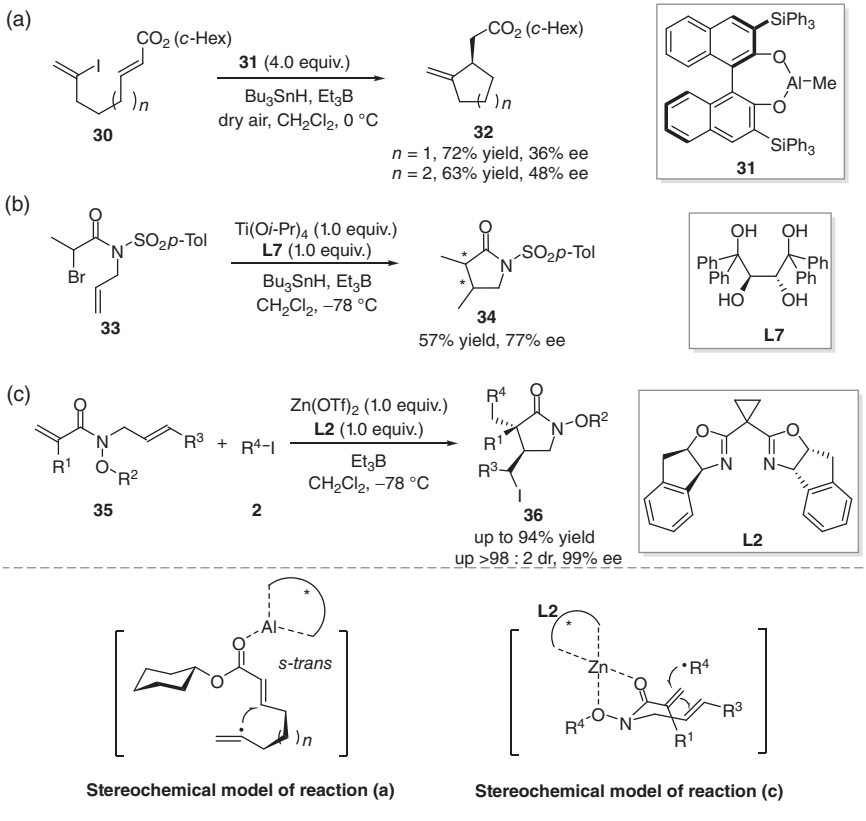


**Scheme 10.11** Selected examples of enantioselective radical cyclization reactions using stoichiometric amounts of CLA. (a) Al-based CLA catalysis. (b) Ti-based CLA catalysis. (c) Zn-based CLA catalysis.

in the products (**32**) possessing an *R*-enantiomer excess. Subsequently, Ishii et al. developed an asymmetric cyclization of α-bromo-*N*-allylamides, facilitated by a chiral titanium Lewis acid (Scheme 10.11b) [58]. In the presence of 1.0 equivalent of the chiral Lewis acid derived from $Ti(OiPr)_4$ and a chiral diol ligand (**L7**), the reaction of an α-bromo-*N*-allylamide (**33**) furnished the cyclized product (**34**) in 57 % yield and with 77% ee. Additionally, Miyabe and Takemoto et al. reported a zinc-catalyzed radical cyclization reaction of hydroxamate esters (**35**) via a radical addition-cyclization-trapping sequence (Scheme 10.11c) [59]. Coordination of the chiral Lewis acid with the substrate (**35**) occurred via a bidentate manner, enabling the formation of a stable five-membered chelation to enhance stereoselectivity.

In 2001, Yang et al. developed the first example of using catalytic amounts of CLAs for radical cyclization transformations. In an atom-transfer radical cyclization reaction of unsaturated β-keto esters (**37**), they found that high enantioselectivity could be achieved by using a chiral magnesium complex of a chiral bisoxazoline ligand (**L8**), even at a loading of 30 mol% (Scheme 10.12) [63]. For instance, the 5-membered ring (**38a**) was obtained in 68% yield and with 92% ee, which was comparable to those of a stoichiometric reaction (67% yield, 94% ee). The proposed model explained how the chiral Lewis acid controls stereochemistry. The β-keto ester group of the substrate (**37**) coordinates with the magnesium center, creating a planar geometry. The steric hindrance between the substrate and *tert*-butyl groups of the chiral ligand (**L8**), along with the interactions among substituents on the C=C bond ($R^1$, $R^2$) and the methyl-substituted β-dicarbonyl group, dictates that the radical cyclization proceeds from the *Re*-face with the orientation. Despite low diastereoselectivity (1 : 1–1 : 1.4), this study demonstrates the potential of CLAs as catalysts for asymmetric radical cyclization reactions.

The same group subsequently developed similar strategies and applied them to other substances and reactions. In 2006, they reported the preparation of

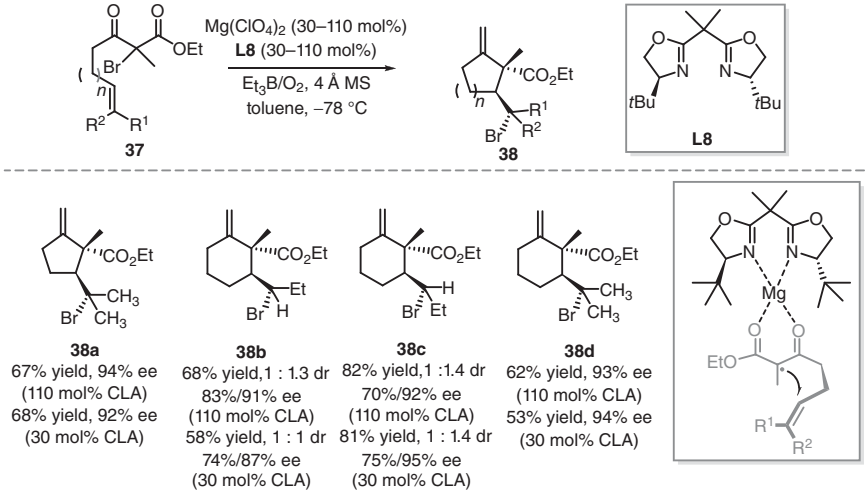


**Scheme 10.12** The development of a CLA-catalyzed enantioselective radical cyclization reaction.

monocyclic and bicyclic ring skeletons through a magnesium-catalyzed enantioselective PhSe-group-transfer/radical cyclization tandem reaction (Scheme 10.13) [64]. The best catalyst was found to be a chiral Lewis acid derived from $Mg(ClO_4)_2$ and a chiral bisoxazoline ligand (**L8**), which dramatically facilitated the reaction and provided the cycloadducts (**40**) as exclusive diastereomers and with high ee values. Reactions using 100 and 30 mol% of the CLA catalyst had similar reaction rates, but the latter affords relatively lower enantioselectivities. In contrast to the bromine atom transfer process (Scheme 10.12), this reaction was diastereospecific, likely due to the higher steric hindrance and relatively lower transfer rate of the SePh group.

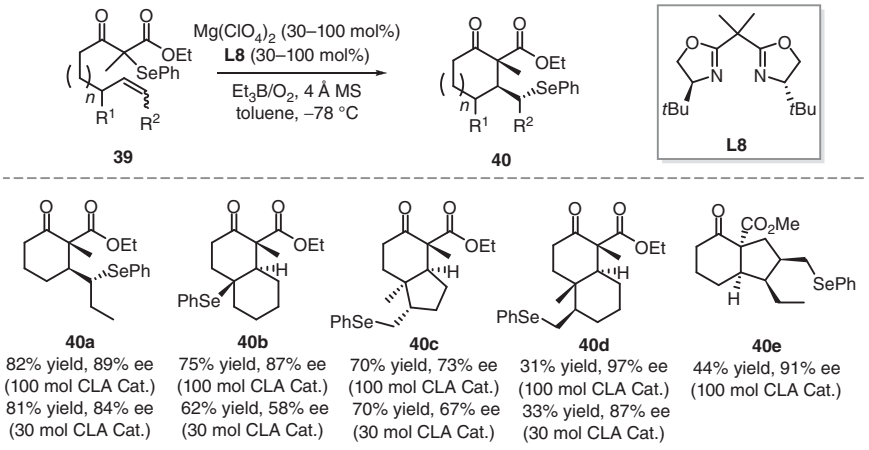


**Scheme 10.13** Another CLA-catalyzed enantioselective radical cyclization reaction.

Streuff et al. reported a titanium-catalyzed intramolecular enantioselective reductive coupling between a ketone moiety and a nitrile fragment in 1,5-ketonitriles (**41**) in 2012 (Scheme 10.14) [65]. The commercially available ansa-titanocene ((*R*,*R*)-**42**) was identified as the best pre-catalyst (10 mol%), along with zinc as the reductant. After workup with *tetra*-$^n$butylammonium fluoride (TBAF), the cyclic α-hydroxyketone products (**43**) were obtained in good yields (42–99%) and high enantioselectivity (42–99% ee). Various aromatic (e.g., **43a**), heterocyclic (e.g., **43b**), aliphatic (e.g., **43c**), allylic substitution patterns (e.g., **43d**), and annulated rings (e.g., **43e**) were well tolerated. In a plausible reaction mechanism, ansa-titanocene ((*R*,*R*)-**42**) is reduced by zinc to generate a low-valent titanium catalyst ([$Ti^{III}$]*), which coordinates with the carbonyl group of the substrate (**41a**). An intramolecular single-electron transfer (SET) from the metal to the C=O bond leads to a radical complex (**Ia**). Subsequently, **Ia** undergoes an intramolecular radical addition through a stereocontrolled 5-*exo* cyclization to generate an *N*-centered radical complex (**Ib**). **Ib** is reduced by the $Ti^{III}$ species and protonated by $HCl{\cdot}NEt_3$, affording titanium(IV) alcoholate (**Ic**). Finally, a single-electron reduction of **Ic** by zinc and treatment with TMSCl reproduce the low-valent titanium catalyst ([$Ti^{III}$]*), meanwhile releasing a TMS-derived product **(Id)**. The latter is converted into the chiral product (**43a**) after workup. In summary, the chiral titanium catalyst

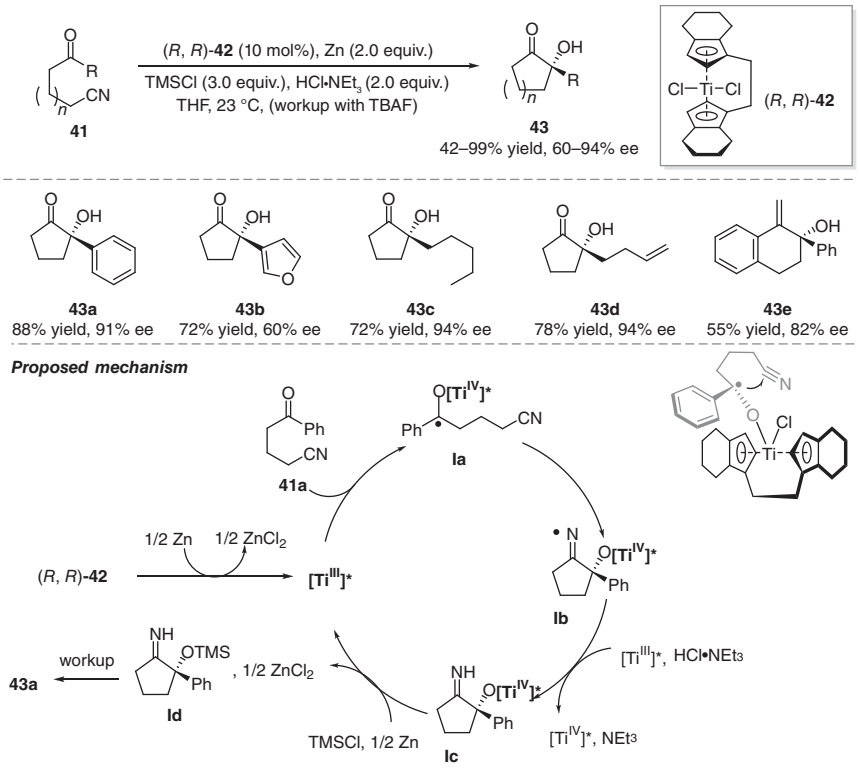


**Scheme 10.14** Titanium-catalyzed enantioselective reductive cyclization of ketonitriles.

not only participates in SET steps but also serves as a chiral Lewis acid to modulate stabilized radical intermediates, thus controlling stereochemistry during the radical cyclization process.

Chiral titanium complexes have been utilized in other radical-mediated asymmetric synthesis, such as asymmetric epoxide openings, which were developed by the groups of Gansaeuer, Lin, and others [66–73]. In these methods, chiral titanium catalysts exhibit high chemoselectivity for electron transfer to epoxides, while demonstrating remarkably low Lewis acidity [74, 75]. Since these titanium complexes act as electron transfer catalysts rather than classic CLA catalysts, the relevant studies are not further discussed in this chapter.

### 10.2.4 Other Reactions

The asymmetric addition of nucleophiles or radicals to C=N double bonds is one of the most straightforward strategies for synthesizing chiral amines. In this regard, Friestad et al. developed a variety of useful reactions based on the implementation of chiral *N*-acylhydrazones as versatile imino acceptors for asymmetric radical additions [76–78]. In 2003, they developed the first example of catalytic enantioselective reductive radical additions to non-chiral *N*-acylhydrazones

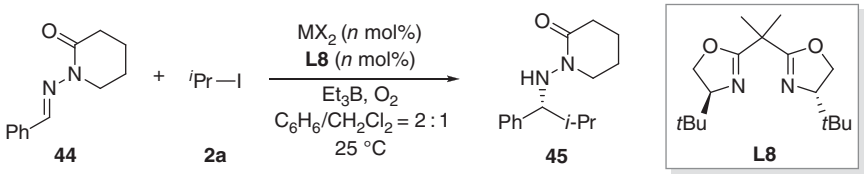


| $MX_2$ | *n* | yield (%) | ee (%) |
|---|---|---|---|
| $Mg(ClO_4)_2$ | 100 | 21 | 30 |
| $Cu(OTf)_2 \cdot 2\,H_2O$ | 100 | 66 | 95 |
| $Cu(OTf)_2 \cdot 2\,H_2O$ | 50 | 71 | 81 |
| $Cu(OTf)_2 \cdot 2\,H_2O$ | 20 | 83 | 58 |
| $Cu(OTf)_2 \cdot 2\,H_2O$ | 10 | 74 | 46 |

**Scheme 10.15** Copper-catalyzed enantioselective radical addition to *N*-acylhydrazones.

using a bisoxazoline copper complex as the CLA catalyst (Scheme 10.15) [79]. A stoichiometric reaction of an *N*-acylhydrazone (**44**) and isopropyl iodide (**2a**) was first optimized, and the chiral bisoxazoline (**L8**)/$Cu(OTf)_2 \cdot 2H_2O$ combination was found to be the best option, providing a 66% yield and 95% ee. Reducing the loadings of the chiral Lewis acid gave similar yields but decreased enantioselectivities. In the presence of 10 mol% of the chiral copper catalyst, the corresponding amine product (**45**) was produced with 46% ee and a yield of 74%, indicating a turnover number (TON) of 7.4.

Hypervalent iodine compounds can serve as radical precursors in various radical-involved transformations. In 2018, Feng et al. reported a nickel-catalyzed enantioselective α-alkylation of β-ketoamides (**46**) with phenyliodonium ylide (**47**) (Scheme 10.16) [80]. Using 10 mol% of the chiral tetradentate *N,N′*-dioxide ligand (**L9**)/$Ni(OTf)_2$, a range of enantioenriched 1,4-dicarbonyl compounds were obtained in good yields (up to 91%) with high enantioselectivity (up to 97% ee). The proposed mechanism involves the decomposition of phenyliodonium ylide (**47**), followed by intersystem crossing (ISC) to form a triplet-state carbene intermediate ($^3$**:**$C(CO_2Me)_2$, **IIa**). A subsequent HAT from complex **IIa** to the chiral nickel-coordinated β-ketoamide (**IIb**) generates a carbene radical species (**IIc**) and a radical complex (**IId**), which undergo stereoselective radical-radical coupling to form a nickel-bonded complex (**IIe**). The final dissociation from the metal leads to the chiral product (**48**). The use of a well-tailored *N,N′*-dioxide ligand to create a specific steric environment for stereodiscrimination in the radical-radical coupling step is critical for achieving high enantioselectivity. Notably, the catalytic system is insensitive to air and moisture, and gram-scale reactions could be easily achieved, making it highly beneficial for further synthetic applications.

In 2021, the same research group discovered that an iron catalyst supported by an *N,N′*-dioxide ligand (**L10**) could effectively catalyze the enantioselective radical carboazidation and diazidation of α,β-unsaturated carbonyl compounds (**49**) (Scheme 10.17) [81]. By employing hypervalent iodines or peroxides as the alkyl radical precursors, and $TMSN_3$ as the azide source, various α-azido carbonyl

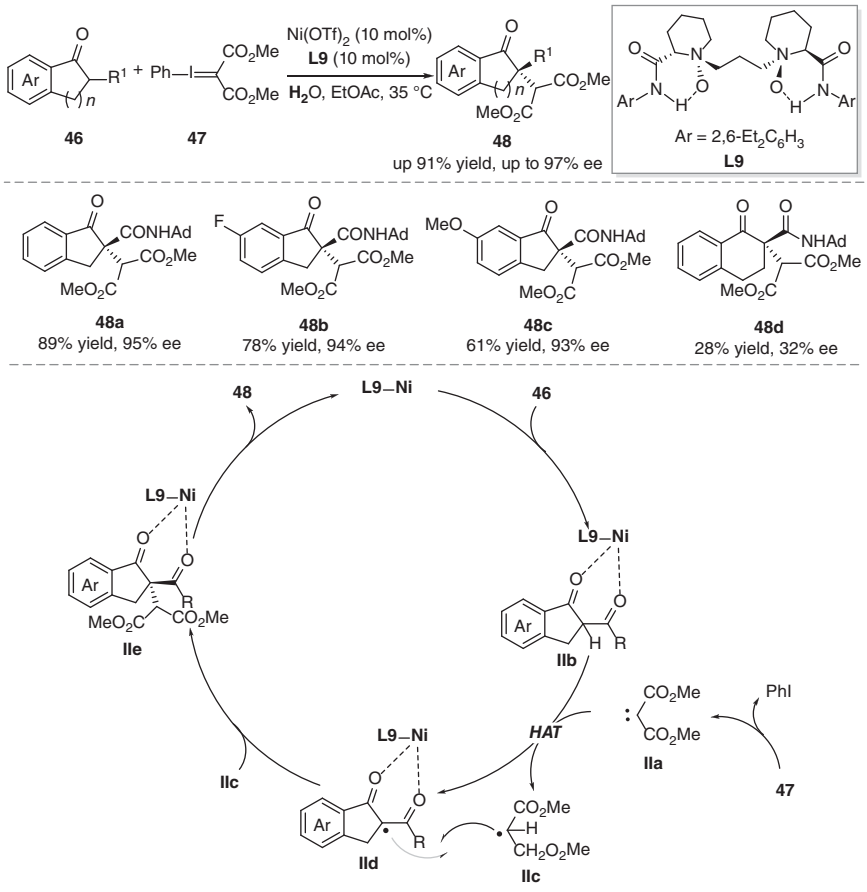


**Scheme 10.16** Nickel-catalyzed enantioselective α-alkylation of β-ketoamides with phenyliodonium ylide.

derivatives were obtained in good yields (up to 84%) and with high enantioselectivity (up to 96% ee). These products are synthetically valuable and can be readily converted into optically active α-amino ketones, vicinal amino alcohols, and vicinal diamines. DFT calculations suggest that the reaction might involve azido transfer from an internal nitrogen of the Fe—$N_3$ species (**IIId**) to a bonded α-carbonyl radical via an intramolecular five-membered transition state.

Katayev et al. developed an enantioselective trifluoromethylation of oxindoles (**53**) using a hypervalent iodine reagent (**54**) in combination with magnesium-based CLA catalysis (Scheme 10.18) [82]. PyBOX-type chiral ligands (**L11** or **L12**) were found to be the best ligands, enabling high conversions (81–99%) and excellent enantioselectivity (90–99% ee). Mechanistic studies based on experimental and computational methods suggest a reaction sequence involving a SET and a stereocontrolled $S_N2$-type transfer of trifluoromethyl radicals. This method is highly compatible with various oxindole substrates and provides appealing access to synthetically and biologically interesting chiral trifluoromethylated oxindoles.

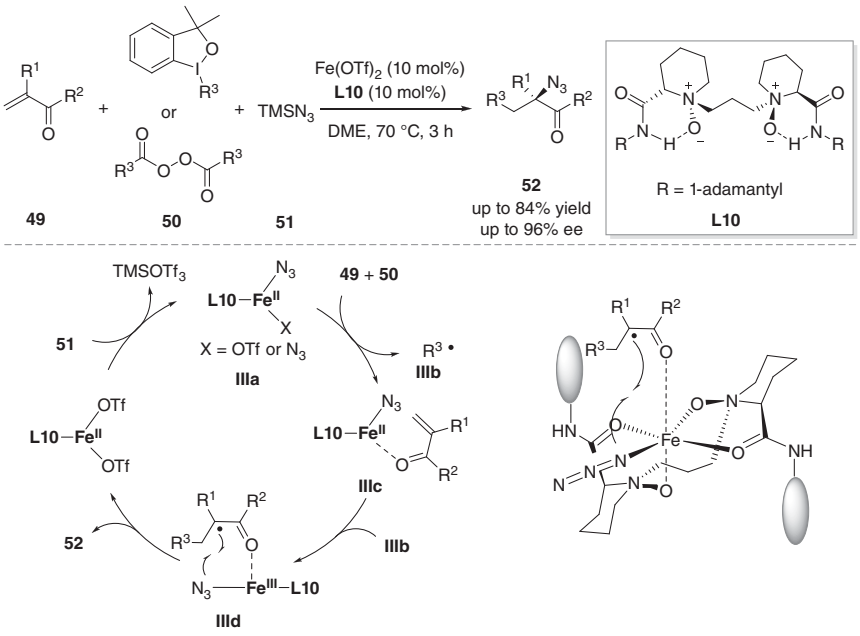


**Scheme 10.17** Iron-catalyzed enantioselective radical carboazidation and diazidation of α,β-unsaturated carbonyl compounds.

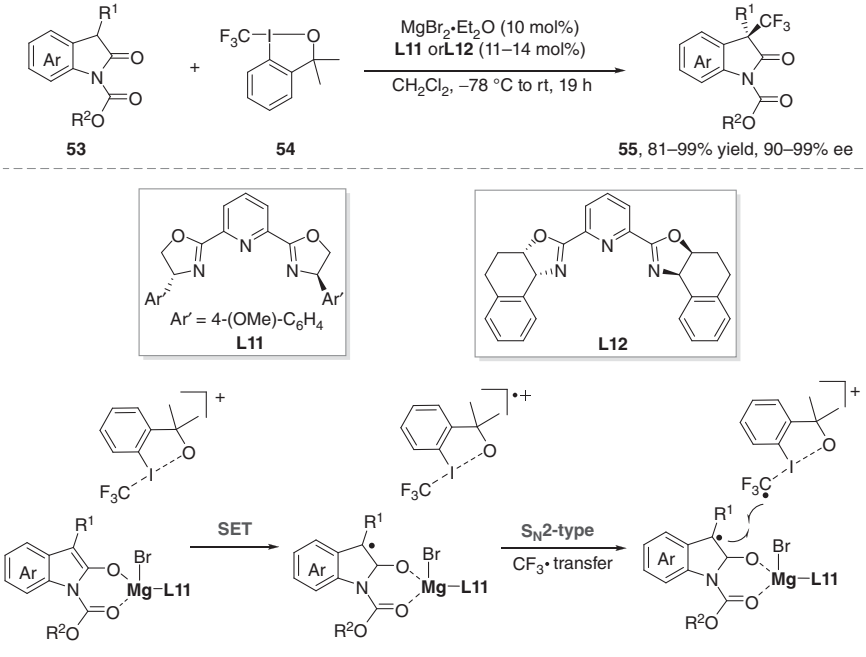


**Scheme 10.18** Enantioselective trifluoromethylation of oxindoles using a hypervalent iodine reagent in combination with magnesium-based Lewis acid catalysis.

Catalytic asymmetric dehydrogenative cross-coupling for the stereoselective construction of carbon–carbon bonds is a challenging process in synthetic chemistry. In 2019, Liu reported an enantioselective oxidative coupling of saturated ethers (**56**) with carboxylic amide derivatives (**57**) [83]. $Ni(OTf)_2$ and a chiral diphosphine ligand (**L13** or **L14**) were identified as the most effective combination of CLA catalysts (Scheme 10.19) [83]. In the presence of *tert*-butyl hydroperoxide (TBHP), the desired products (**58**) were obtained with moderate diastereoselectivity and excellent enantioselectivity (86–99% ee). This one-pot protocol exhibits high functionality compatibility and is applicable to various saturated ethers, such as prevalent tetrahydrofurans (e.g., products **58a**, **58b**), medium and large-sized cyclic moieties (e.g., **58c**), and acyclic ethers (e.g., **58d**). The reaction mechanism is inferred to involve oxidative acetal formation (**56 → IVa → IVb**), probably going through a peroxide-triggered HAT and nickel-mediated CLA catalysis (**L13-Ni → IVd → IVe → L13-Ni**). The authors believe that this process will provide

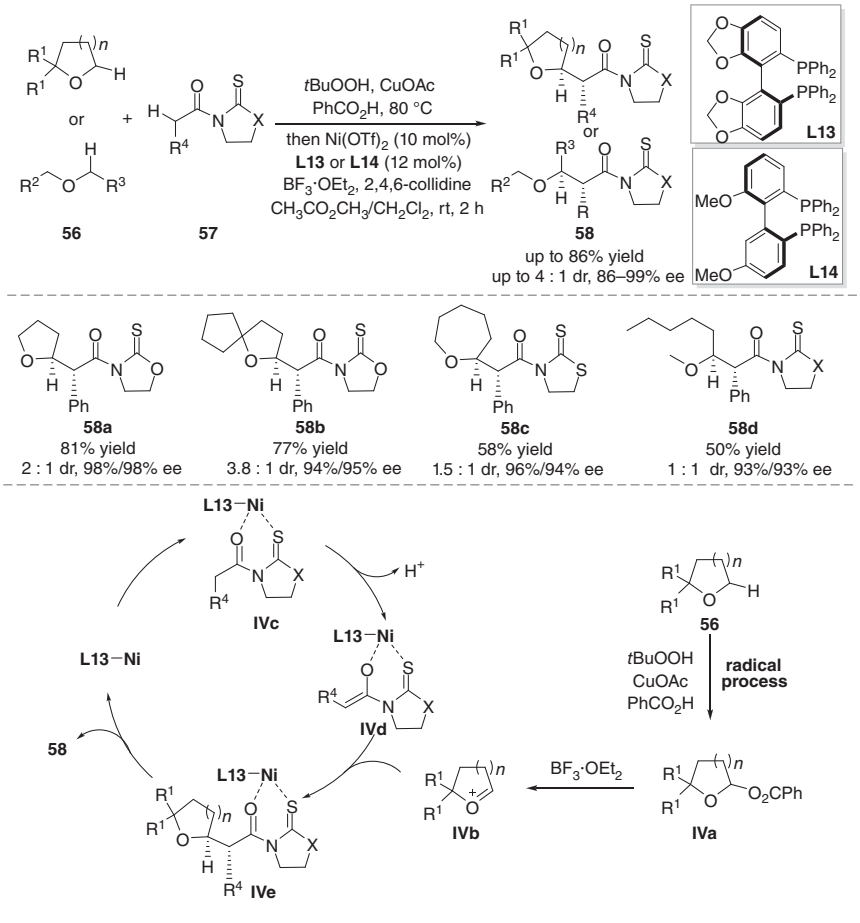


**Scheme 10.19** Enantioselective oxidative coupling of saturated ethers with carboxylic acid derivatives.

new opportunities for the development of asymmetric synthesis starting from abundant C($sp^3$)—H resources.

## 10.3 Merging CLA Catalysis with Photocatalysis

Photocatalysis has emerged as a powerful tool in organic synthesis, enabling the convenient construction of carbon–carbon and carbon–heteroatom bonds under mild conditions [84–88]. Asymmetric photocatalysis, which combines asymmetric catalysis with photocatalysis, is an attractive strategy for synthesizing chiral compounds via mechanistic scenarios different from those of traditional thermal reactions [89–93]. Various asymmetric photocatalytic reactions have been developed using chiral organocatalysts, organometallic catalysts, and transition metal catalysts to achieve stereodiscrimination [94–108]. Among them, CLAs show great promise in achieving such transformations by activating excited states of some specific substrates (**S1**) and controlling the stereochemistry of subsequent transformations with other reactants (**S2**) (Scheme 10.20a). Alternatively, CLA-substrate (**S3**) intermediates generated in situ absorb photons and react with other components (**S4**), in which the chiral environment of the CLA catalyst affects the stereochemistry (Scheme 10.20b). Furthermore, the addition of external photosensitizers (**PS**) can promote light-triggered single-electron transfer (SET), hydrogen atom transfer (HAT), and/or energy transfer (EnT) processes to generate high-energy intermediates such as radicals or radical ions, which then incorporate with CLA-substrate (**S6**) intermediates at ground states (Scheme 10.20c). These pathways provide flexibility for the design of diverse asymmetric photochemical synthesis [27].

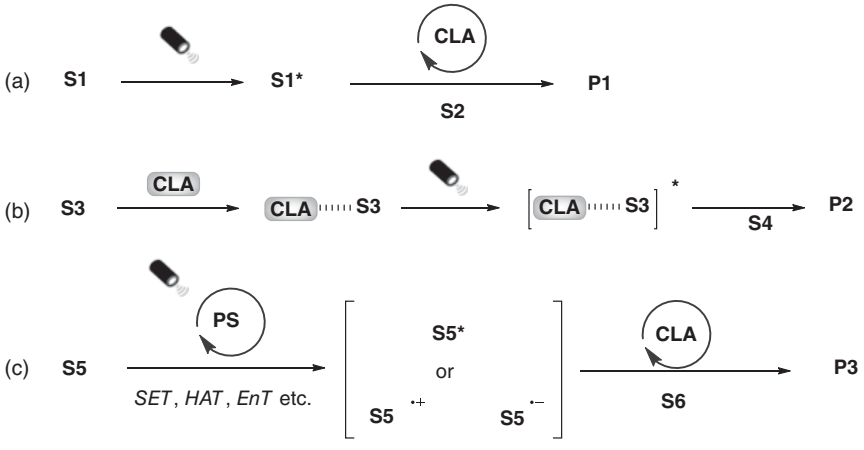


**Scheme 10.20** Several representative pathways of CLA-mediated asymmetric photochemical reactions. (a) CLA-mediated photoactivated substrates reacting with other substrates. (b) Photoactivated CLA-mediated substrates reacting with other substrates. (c) CLA-mediated high-energy intermediates created by the interaction with **PS** reacting with other substrates.

### 10.3.1 CLA-Catalyzed Asymmetric Photochemical Reactions in the Absence of External Photosensitizers

Photoinduced [2 + 2] cycloadditions are effective for the construction of cyclobutane scaffolds, which can be employed either as key building blocks for the synthesis of cyclobutane-containing molecules or upon ring opening for the generation of strategic bonds [25, 26]. Achieving high diastereo- and enantioselectivity in such reactions is challenging, perhaps due to the involvement of highly reactive intermediates such as triplet diradical species.

The pioneering work by Lewis and Barancyk demonstrated that Lewis acids, such as $BF_3 \cdot Et_2O$, can accelerate a [2 + 2] photochemical cycloaddition of coumarin with alkenes via binding with the UV light-activated coumarin [109]. Such binding modes of Lewis acid lead to an increase in the singlet-state lifetime and the electrophilicity of the reactant. In 2012, Bach et al. developed a catalytic enantioselective fashion using a substoichiometric amount of an oxazaborolidine (**60**) as the chiral Lewis acid (Scheme 10.21a) [110]. Irradiating a 4-(pent-4-enyl)coumarin derivative (**59**) with Philips black light blue lamps ($\lambda = 366$ nm) for 3.5−9 h in the presence of 50 mol% of **60** yielded chiral products bearing a tetracyclic 3,3a,4,4a-tetrahydro-1*H*-cyclopenta [2,3]cyclobuta [1,2-c]chromen-5(2*H*)-one skeleton (**61**) in up to 96% yield with up to 90% ee. The amount of the borane catalyst could be reduced to 20 mol%, still providing a good enantioselectivity (78% ee). Although this protocol relies on UV light-activated substrates, it provides the first example of asymmetric photochemical reactions enabled by a single CLA catalyst.

In 2014, Bach et al. reported a CLA-catalyzed intramolecular [2 + 2] photocycloaddition of 5,6-dihydro-4-pyridones (**62**), a versatile class of enone substrates (Scheme 10.21b) [111]. Under similar conditions, a range of 5,6-dihydro-4-pyridone substrates (**62**) were successfully converted into tricyclic or bicyclic products (**63**) as single diastereomers in 48−87% yield with 80−90% ee. One of the products was applied as a key intermediate in the total synthesis of (+)-lupinine and the formal synthesis of (+)-thermopsine, demonstrating the synthetic utility of this reaction. A postulated coordination of the substrate (**62**) to the chiral Lewis acid (**60**) indicated an intramolecular approach of the olefin moiety to the double bond in a *Si*-face attack relative to the enone fragment. Moreover, UV-Vis experiments revealed significant absorption shifts (>50 nm) of 5,6-dihydro-4-pyridone substrates upon Lewis acid coordination. The good enantioselectivity might be attributed to the high absorption coefficient of CLA-substrate complexes at 366 nm, which prevented racemic background reactions of the non-binding enone substrates.

This strategy was later extended to intramolecular photocycloadditions of other substrates. For example, irradiation of 3-alkenyloxy-2-cycloalkenones (**64**) at a wavelength of 300 nm using a trifluoro-substituted oxazaborolidine (**65**) as the CLA catalyst led to the formation of chiral tricyclic products (**66**) in 69−93% yield with 75−94% ee (Scheme 10.22a) [112]. The products could be easily converted into anellated seven- or eight-membered-ring systems without racemization via ring-expansion reactions under acidic conditions. Building upon these observations, Bach et al. recently developed an asymmetric cycloaddition/rearrangement cascade

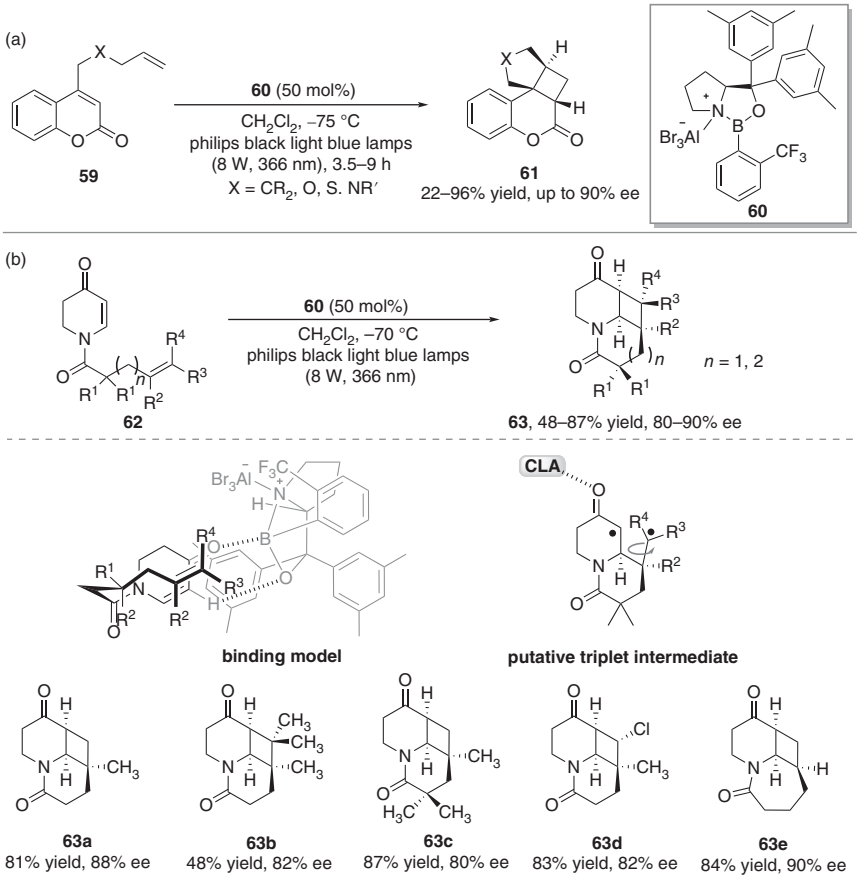


**Scheme 10.21** Enantioselective intramolecular [2 + 2] photoaddition reactions catalyzed by chiral borane Lewis acids. (a) Intramolecular [2+2] photoaddition reactions of 4-(pent-4-enyl)coumarin derivates. (b) Intramolecular [2+2] photoaddition reactions of 5,6-dihydro-4-pyridone substrates.

triggered by visible light (Scheme 10.22b) [113]. This one-pot reaction involves a photochemical dearomatization of 1-naphthaldehyde derivatives (**67**), followed by a thermal acid-catalyzed rearrangement to produce structurally unique polycyclic compounds (**69**).

A visible light-driven enantioselective intermolecular [2 + 2] photocycloaddition was achieved using a CLA-activation strategy similar to that involved in previous studies (Scheme 10.22c) [114]. UV-Vis spectroscopy revealed that phenanthrene-9-carboxaldehyde had maximum absorption at 316 nm, and underwent an extensive bathochromic shift ($\lambda_{max}$ = 387 nm) upon coordination with a Lewis acid such as $EtAlCl_2$. Under irradiation with a blue LED lamp ($\lambda_{max}$ = 457 nm) and in the presence of the chiral oxazaborolidine (**68**, 20 mol%), phenanthrene-9-carboxaldehyde derivatives (**70**) underwent intermolecular cycloaddition with olefins (**71**), delivering corresponding adducts (**72**) with up to

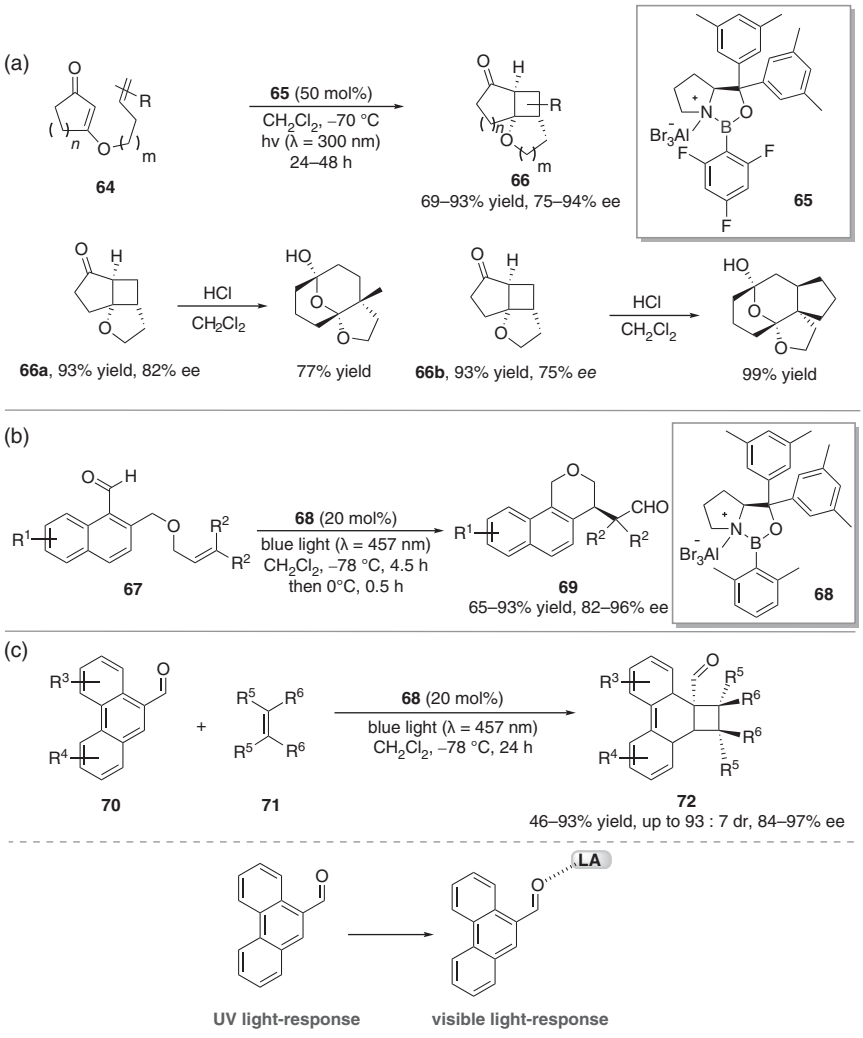


**Scheme 10.22** Chiral borane Lewis acid catalytic asymmetric [2 + 2] photoaddition reactions. (a) Intramolecular [2+2] photoaddition reactions of 3-alkenyloxy-2-cycloalkenones. (b) Intramolecular [2+2] photoaddition rearrangement cascade reactions of 1-naphthaldehyde derivatives. (c) Intermolecular [2+2] photoaddition reactions of phenanthrene-9-carboxaldehyde derivatives.

93 : 7 dr and 84–97% ee. This study indicates that the aldehyde binding motif is useful for achieving high enantiodiscrimination in photocatalytic transformations.

Electron donor-acceptor (EDA) complexes generated by the association of an electron acceptor with an electron donor have received significant attention in organic synthesis [115]. Such intermediates can initiate radical processes and enable various photochemical reactions in the absence of additional photosensitizers [116, 117]. In 2021, Ryu et al. reported an enantioselective radical addition reaction of α,β-unsaturated carbonyl compounds (**73** or **74**) with α-silyl amines (**75**) as the

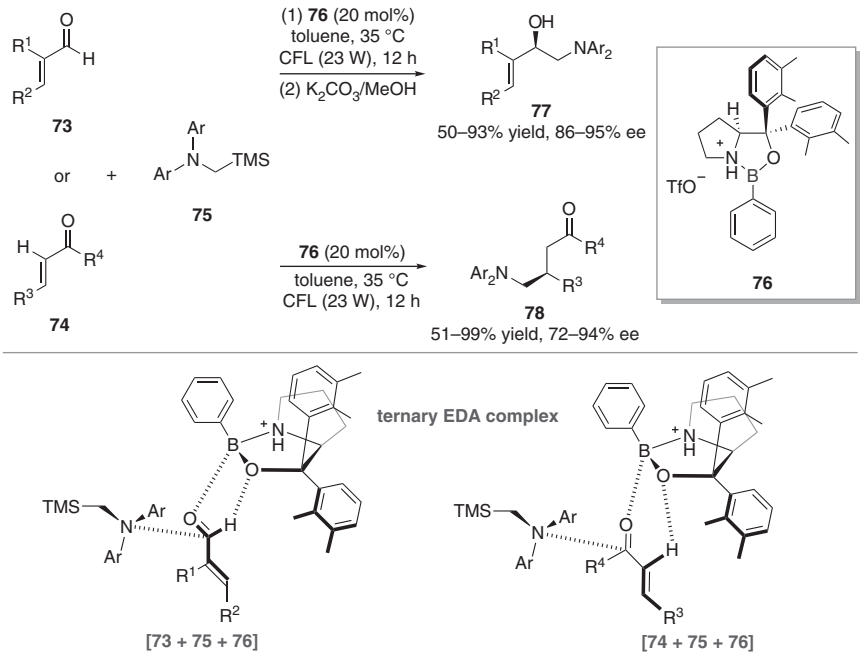


**Scheme 10.23** Enantioselective radical addition enabled by ternary electron donor-acceptor complexes.

radical precursors (Scheme 10.23) [118]. The reactions proceeded smoothly without external photosensitizers, yielding 1,2-addition (**77**) or 1,4-addition products (**78**) in good yields with high enantioselectivities. Mechanistic experiments suggested the formation of ternary EDA complexes consisting of an α,β-unsaturated carbonyl substrate (**73** or **74**), an α-silyl amine (**75**), and a chiral oxazaborolidinium ion catalyst (**76**). This strategy provides effective access to simplified approaches for asymmetric photochemical synthesis.

Our group has long been interested in the development of visible light asymmetric photochemical synthesis based on 3d transition metal catalysis [119, 120]. In 2018, we developed an enantioselective conjugated radical addition to α,β-unsaturated carbonyl compounds (**79**) with α-silylamines (**80**) as the radical precursors (Scheme 10.24) [121]. The combination of $Ni(ClO_4)_2 \cdot 6H_2O$ and a chiral dibenzofuran-4,6-bisoxazoline (DBFOX) ligand (**L15**) facilitated the preparation of γ-amino carboxylic acid products ($R^2$ = alkyl, aryl) or γ-lactams ($R^2$ = H) (**81**). The reaction did not require external photosensitizers, where CLA-substrate complexes (intermediate **Va**) might act as the light-responsive components. This simplified catalytic system provided satisfactory yields (up to 86%) and high enantiomeric excess (87−99% ee) under mild conditions, thus offering methods for synthesizing potential molecules of biological interest.

We later applied this chiral DBFOX nickel catalyst to regiodivergent asymmetric cycloadditions of α,β-unsaturated carbonyl compounds (**82**) with dienes (**83**) or electronically rich olefins (**84**) (Scheme 10.25) [122]. An asymmetric [2 + 2]

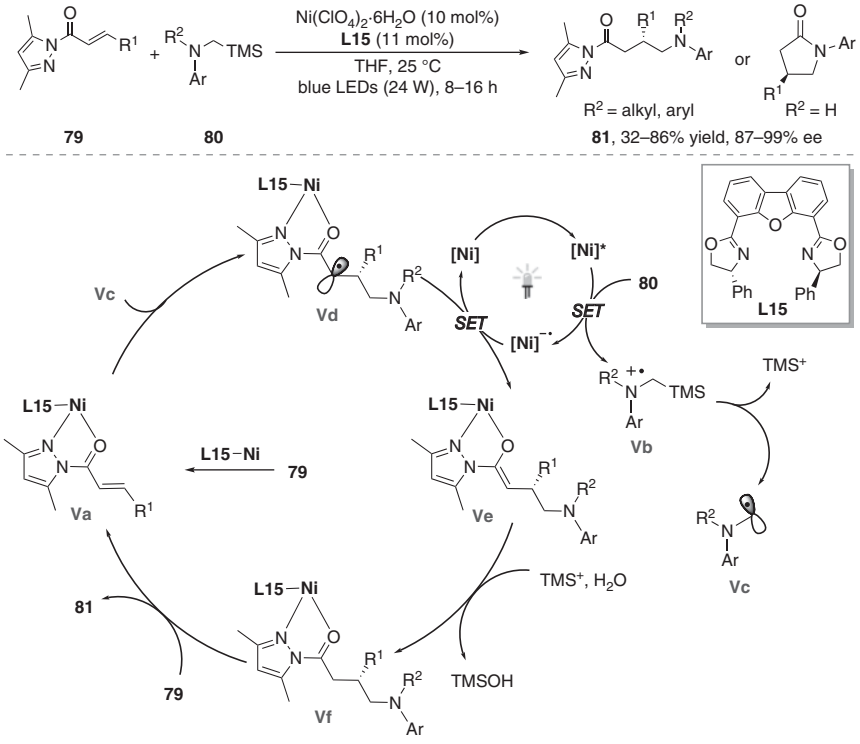


**Scheme 10.24** Catalytic enantioselective radical addition to α,β-unsaturated carbonyl compounds by a chiral nickel catalyst.

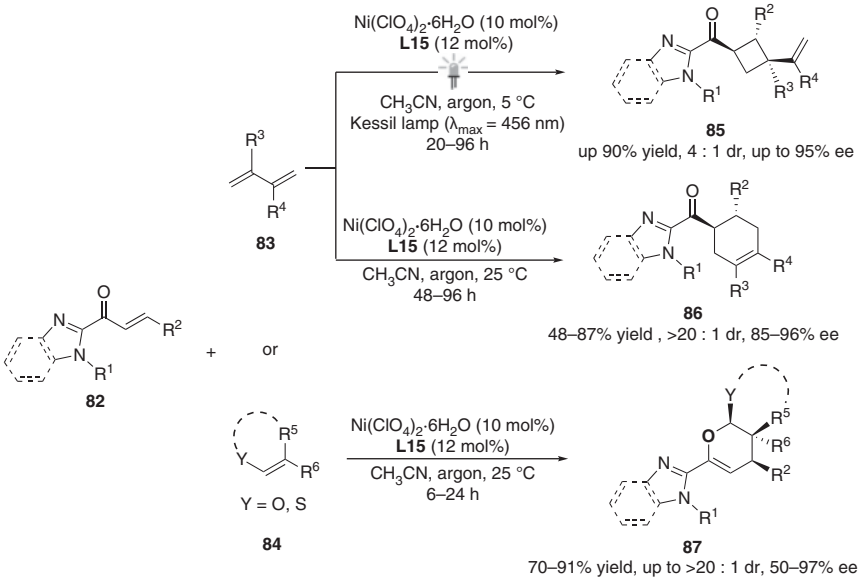


**Scheme 10.25** Regiodivergent asymmetric cycloadditions of α,β-unsaturated carbonyl compounds with olefins.

photocycloaddition was achieved without external photosensitizers, yielding chiral cyclobutanes with a 4 : 1 dr and up to 95% ee. By switching the reaction conditions from light irradiation to darkness, or by adjusting the electronic features of the reaction partners, diastereo- and enantioselective Diels–Alder or *oxa*-Diels–Alder reactions were realized. These results enable the divergent synthesis of optically active carbocycles and heterocycles starting from the same set of substrates and CLA catalysts.

Chiral copper catalysts have shown significant potential in radical-mediated asymmetric synthesis, as the metal can adopt different oxidation states (0, +1, +2, and +3), allowing for one-electron or two-electron transfer processes [123–136]. In 2018, we reported a copper-catalyzed photochemical enantioselective alkylation of imines with alkyl trifluoroborates as radical precursors (Scheme 10.26) [137]. The use of a copper/chiral bisoxazoline ligand (**L16** or **L17**) facilitated the photochemical alkylation of *N*-sulfonylimines (**88**) or isatin-derived ketimines (**89**) in the

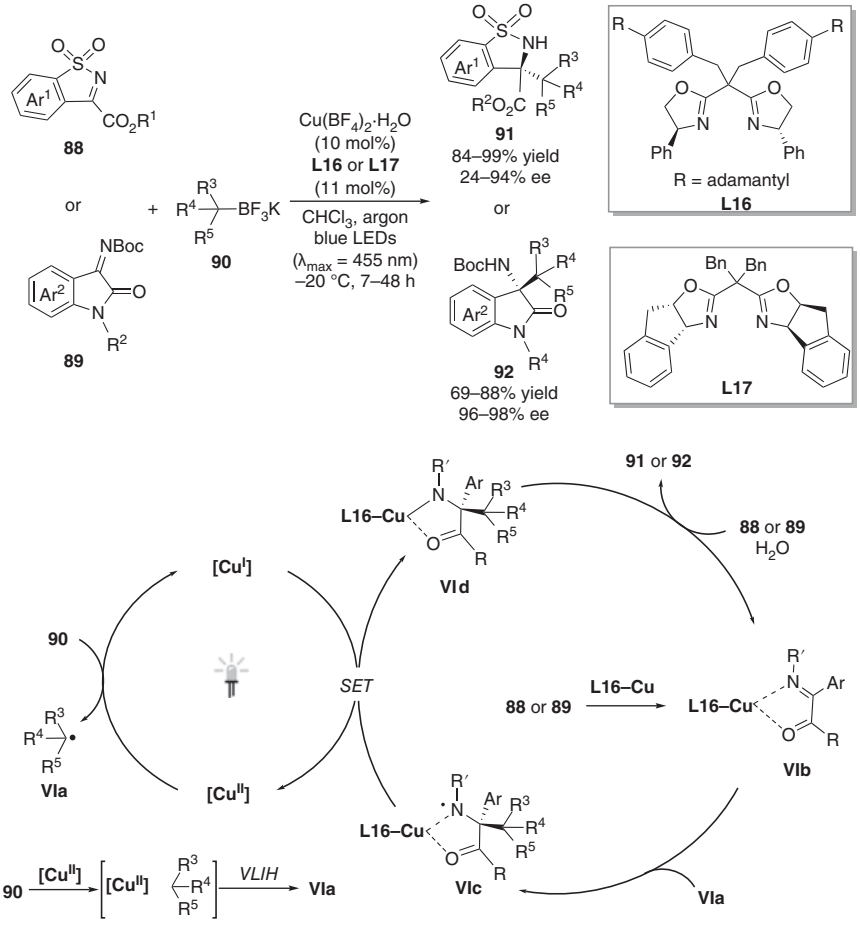


**Scheme 10.26** Copper-catalyzed photochemical alkylation of imines.

absence of photosensitizers, affording chiral *N*-sulfonylamines (**91**) or ketamines (**92**) bearing a tetrasubstituted carbon stereocenter in 69–99% yield with 24–98% ee. Mechanistic studies, such as radical quenching experiments, UV-Vis spectroscopic analysis, and control experiments, revealed that the reaction involved an enantioselective radical addition to copper-bonded substrates. First, the copper catalyst undergoes transmetallation with the trifluoroborate (**90**) to generate an alkyl-copper(II) intermediate, followed by visible-light-induced homolysis (VLIH) to produce an alkyl radical (**VIa**) and copper(I) species. The alkyl radical (**VIa**) then reacts with the copper-coordinated imine substrate (**VIb**) via enantioselective radical addition, yielding a radical complex (**VIc**). A subsequent SET and ligand exchange process lead to the formation of the chiral amine product (**91**) and the regeneration of the key intermediate complex (**VIb**). For the first time, copper catalysts with chiral bisoxazoline ligands were found to initiate the photochemical generation of alkyl radicals and simultaneously control stereochemistry as CLA.

Chiral copper-induced photochemical reactions have been further developed by us and others. For instance, we reported a photochemical enantioselective α-aminoalkylation of *N*-acylhydrazones catalyzed by a copper complex of a bisoxazoline ligand bearing 2,4,6-trimethylbenzyl substituents (**L18**) (Scheme 10.27a) [138]. This catalyst was found to be involved in single-electron oxidation steps, photoredox processes, and provided Lewis acid activation and stereodiscrimination. In addition, we developed a copper-catalyzed photochemical asymmetric cross-dehydrogenative coupling of 2-acyl imidazoles (**95**) and xanthene derivatives (**96**) using molecular oxygen as the oxidant (Scheme 10.27b) [139]. This reaction forged C—C bonds and vicinal stereocenters under mild conditions, providing moderate diastereoselectivity (up to 2.3 : 1 dr) but high enantioselectivity (up to 97% ee).

Chiral *N,N′*-dioxide/metal complexes have demonstrated excellent chiral induction in many asymmetric transformations by the groups of Feng and others.

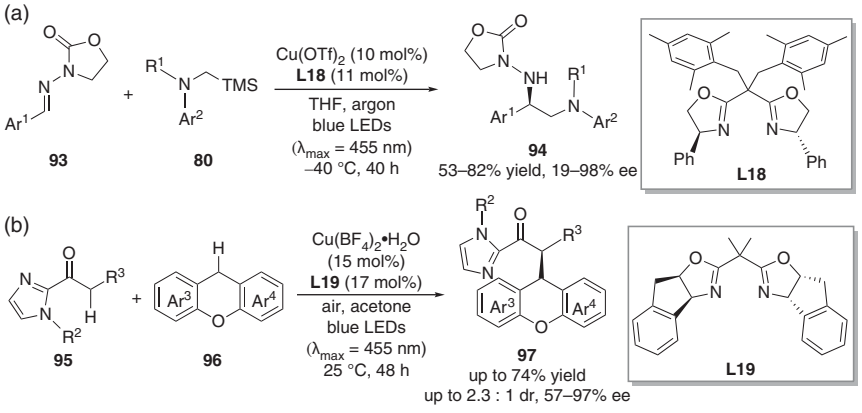


**Scheme 10.27** Copper-catalyzed photochemical radical addition to imines and aerobic asymmetric cross-dehydrogenative coupling of C($sp^3$)—H bonds. (a) Enantioselective α-aminoalkylation of *N*-acylhydrazones. (b) Asymmetric cross-dehydrogenative coupling reaction.

Recently, they found that the chiral *N,N′*-dioxide (**L20**)/Ni(OTf)$_2$ complex could catalyze an asymmetric photoenolization/Mannich (PEM) cascade of *ortho*-alkyl aromatic ketones (**98**) with benzosulfonimides (**88**), producing a variety of α-amino acid esters with high diastereo- and enantioselectivity (up to 96 : 4 dr and 95% ee) (Scheme 10.28) [140]. Experimental results indicate that the combination of a chiral *N,N′*-dioxide nickel catalyst and the LiNTf$_2$ additive effectively suppresses the background reaction and epimerization of products. The reaction proceeds via direct nucleophilic addition rather than a hetero-Diels–Alder/ring-opening sequence. Mechanistically, the 2-benzylbenzophenone substrate is excited upon UV light irradiation ($\lambda = 365$ nm), transferring to its triplet state with biradical characters (**VIIa**). An intramolecular 1,5-HAT of **VIIa** forms the other diradical species (**VIIb**) followed by bond rotation and ISC, giving rise to an *E*-photoenol intermediate (**VIIc**). Meanwhile, the *N,N′*-dioxide/Ni$^{II}$ catalyst undergoes ligand exchange with the imine substrate (**88a**) to generate a chiral ligand-transition metal-substrate intermediate, in which the *Si* face of the imine is shielded by the amide unit of the ligand. Thus, the favored *Re–Re* nucleophilic addition occurs, furnishing the Mannich product (**99a**) with a (*S,R*)-configuration. The $\pi$–$\pi$ interactions between the aryl group at the benzyl position of the photoenol and the aryl group of the *N*-sulfonyl cyclic ketimine might exist, facilitating further stereocontrolled transformations.

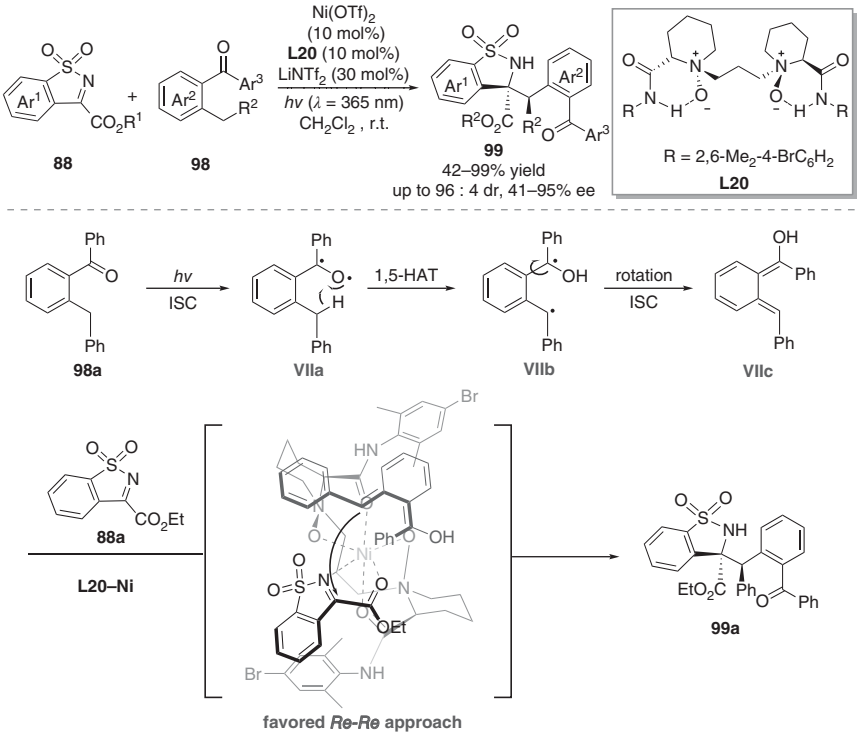


**Scheme 10.28** Nickel-catalyzed asymmetric photoenolization/Mannich reaction of (2-alkylphenyl) ketones.

The combination of an adamantanyl-substituted chiral *N,N′*-dioxide ligand (**L21**) with $Ga(OTf)_3$ was found to be effective in a light-triggered stereoselective α-C($sp^3$)—H functionalization of sulfides (**101**) with isatins (**100**) (Scheme 10.29) [141]. The reaction proceeded under irradiation of a blue LED lamp without external photosensitizers, and it provided facile access to optically active sulfur-containing 2-oxindoles (**102**) with excellent regio- (20 : 1 rr) and enantioselectivity (77–97% ee). The isatin substrates (**100**) not only serve as photoredox reagents but also as coupling partners. Regarding the reaction mechanism, a SET between the triplet excited state of **100** and the sulfide substrate (**101**) promotes the formation of a *C*-centered radical, which undergoes subsequent enantioselective radical-radical coupling. The late-stage modification of sulfur-containing amino acids and methionine-related peptides was also achieved, demonstrating the synthetic utility of this protocol.

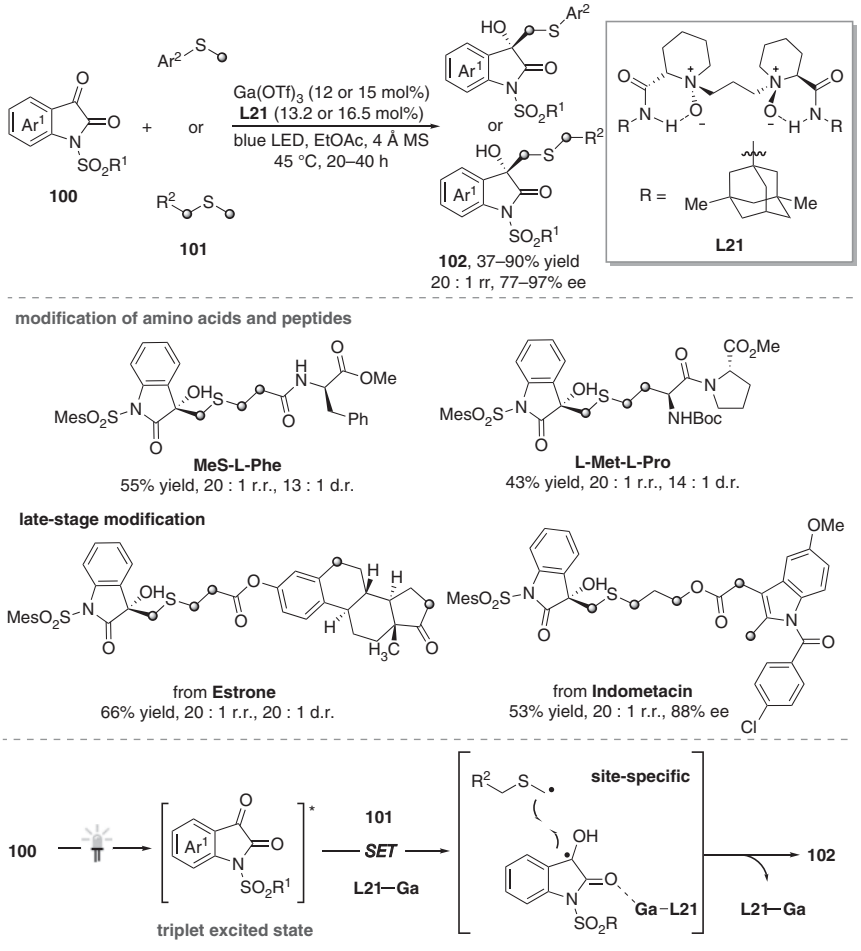


**Scheme 10.29** Photoinduced stereoselective α-C($sp^3$)—H functionalization of sulfides catalyzed by a gallium-based chiral Lewis acid.

In 2022, Feng et al. developed an enantioselective radical addition to ketones (**103**) with α-silylamines (**104**) as radical precursors and chiral *N,N′*-dioxide ligand (**L22**)/$Sc(OTf)_3$ as the CLA catalyst (Scheme 10.30) [142]. The reaction delivered *aza*-heterocycle-based tertiary alcohols (**105**) in 30–98% yields with 42–97% ee. Kinetic studies indicated a first-order kinetic dependence on the chiral Lewis acid and the two substrates (**103, 104**). DFT calculations revealed that the rate-determining step might be a SET to form active radical species (**VIIIc, VIIId**). Based on these outcomes, a reaction pathway involving a chiral Sc(III)-ketone intermediate (**VIIIa**) generated in situ as the temporary photoredox catalyst is proposed. This intermediate can not only initiate the formation of a *C*-centered radical via a SET with the radical precursor (**104**) but also govern enantioselectivity during the radical addition process (**VIIIc + VIIIa → VIIIe**).

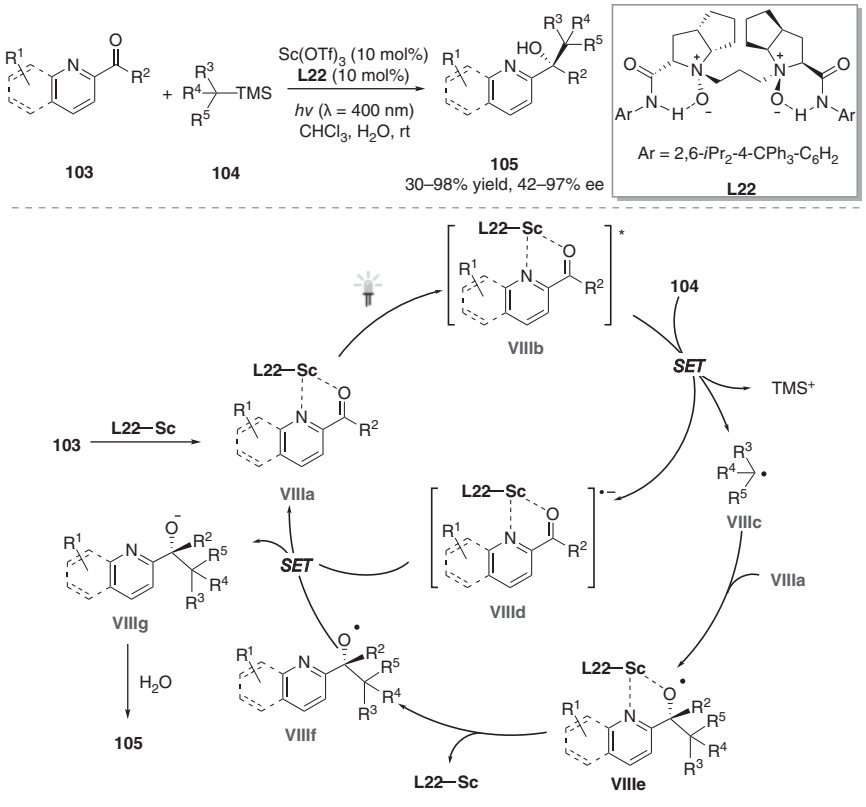


**Scheme 10.30** Enantioselective radical addition to ketones through Lewis acid-enabled photoredox catalysis.

## 10.3.2 CLA-Catalyzed Asymmetric Photochemical Reactions in the Presence of External Photosensitizers

Photosensitizers, such as polypyridyl complexes of iridium and ruthenium, as well as organic dyes, have been extensively employed for the development of flexible

synthetic approaches under visible light conditions [84]. The merger of CLAs with photosensitizers is a useful tool for the design of photocatalytic asymmetric synthesis [25].

In 2014, Yoon et al. demonstrated that the use of a lanthanum-based chiral Lewis acid (**L23**/$Eu(OTf)_3$) and a Ru-based photosensitizer (**PC1**) as co-catalysts effectively promoted a diastereo- and enantioselective photocycloaddition between two different α,β-unsaturated ketones (**106**, **107**) (Scheme 10.31a) [143]. The [2 + 2] adducts (**108**) were formed in 34–72% yields with a 2.5 : 1−9 : 1 dr and 86–93% ee in the presence of $Eu(OTf)_3$ (10 mol%), **L23** (20 mol%), **PC1** (2 mol%), and $iPr_2NEt$ (2.0 equiv.). Mechanistically, the reaction begins with the visible light excitation of the photosensitizer (**PC1**). A subsequent SET between **PC1*** and $iPr_2NEt$ gives rise to a reduced photosensitizer (**PC1**$^{\cdot-}$) and an *N*-centered radical cation. The metal-bonded substrate (**IXb**) undergoes a second SET with **PC1**$^{\cdot-}$, producing an enolate radical complex (**IXc**) and regenerating the photosensitizer (**PC1**). A stereocontrolled radical addition of **IXc** to the substrate (**107**), followed by a third SET with the *N*-centered radical cation and ligand dissociation, affords the chiral product (**108**) and the CLA catalyst. Soon after, they extended the strategy to an

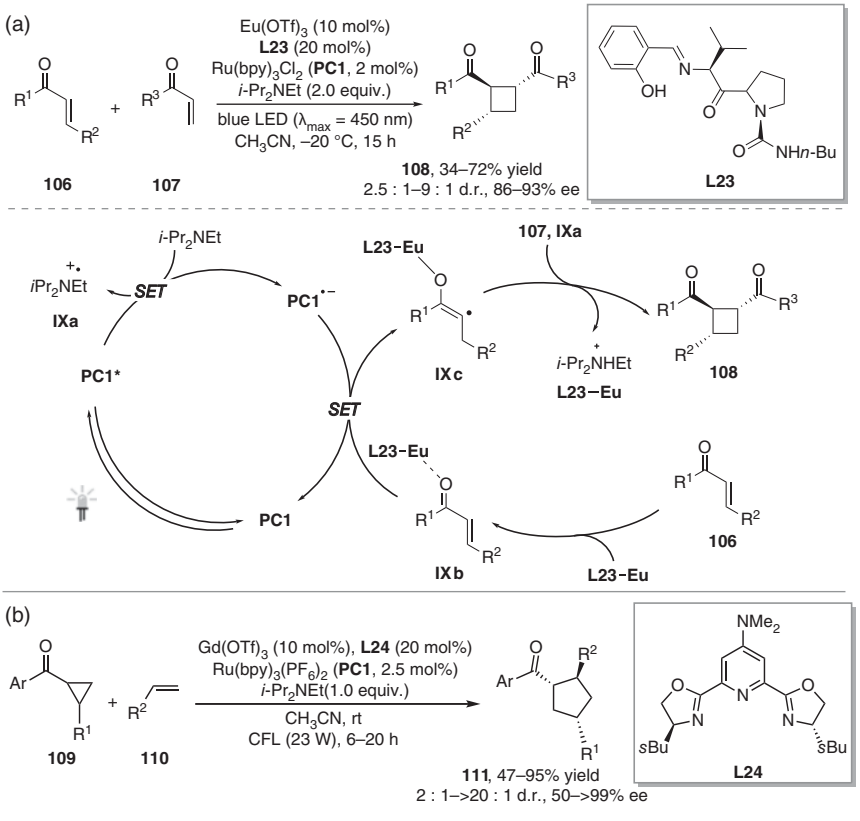


**Scheme 10.31** Asymmetric photocycloaddition enabled by synergistic photoredox and lanthanide metal-based CLA catalysis.

intermolecular formal [3 + 2] photocycloaddition of aryl cyclopropyl ketones (**109**) and olefins (**110**) (Scheme 10.31b) [144]. A chiral Gd(III)/tridentate ligand (**L24**) and the same ruthenium photosensitizer (**PC1**) were identified as the best combination of catalysts, which afforded multi-substituted chiral cyclopentanes with high diastereo- and enantioselectivity (up to >20 : 1 dr and 99% ee). These studies demonstrate that the combination of versatile CLAs with photoredox-induced intermediates of unique reactivity has significant potential in developing stereoselective transformations.

Such synergistic systems, consisting of a photoredox and lanthanide metal-based CLA catalyst, were effective in more photoredox-triggered asymmetric conjugate radical additions. For instance, an enantioselective radical addition of α-silyl amines (**80**) to α,β-unsaturated carbonyl compounds bearing an oxopyrazolidinyl fragment (**112**) was achieved by (**L25**)/$Sc(OTf)_3$ and $Ru(bpy)_3Cl_2$ (**PC1**), giving γ-aminocarbonyl products (**113**) with 85–96% ee (Scheme 10.32a) [145]. In terms of the mechanism, the reaction sequence involves a light-induced SET to generate an α-amino radical (**Xb**) and a key enantioselective radical β-addition to a CLA-activated radical acceptor (**Xc**). Furthermore, an enantioselective addition of α-alkoxy radicals derived from α-silyl ethers was developed, allowing the preparation of valuable γ-oxycarbonyl motifs (**115**) in 22–96% yield with 81–98% ee (Scheme 10.32b) [146].

The dual catalysis strategy is also applicable in asymmetric photocycloadditions via triplet-energy transfer. For example, a diastereo- and enantioselective [2 + 2] cycloaddition of 2′-hydroxychalcones (**116**) and alkenes (**110**) was realized by a chiral Sc(III) complex and ruthenium-based photocatalysis (Scheme 10.33a) [147]. This reaction gave good to excellent stereodiscrimination (up to >10 : 1 dr, >99% ee) when using a tridentate Pybox ligand (**L25**) as the chiral ligand. The mechanism involves the conversion of the ruthenium photosensitizer (**PC1)** into its singlet state ($^1Ru(bpy)_3{}^{2+}$) upon light irradiation, followed by an ISC to form a triplet state ($^3Ru(bpy)_3{}^{2+}$). Energy transfer then occurs between $^3Ru(bpy)_3{}^{2+}$ and the chiral Sc(III)-bonded substrate (**X1a**), affording a diradical complex (**X1b**) and regenerating **PC1**. The reaction of **X1b** with the styrene derivative (**117**) yields the 1,4-diradical intermediate (**X1c**), which undergoes an intramolecular radical combination. The final ligand exchange between the resultant metal-coordinated product and the 2′-hydroxychalcones substrate (**116**) leads to the formation of the chiral product (**117**) and the regeneration of complex **X1a**. The key to the success of this reaction is the dramatic lowering of the singlet-triplet gap of 2′-hydroxychalcone ($E_T$ = 54 kcal mol$^{-1}$) upon Lewis acid coordination, rendering triplet-energy transfer from the photosensitizer ($E_T$ = 45 kcal mol$^{-1}$) to the CLA-bound substrate ($E_T$ = 32 kcal mol$^{-1}$) thermodynamically favorable. Chiral oxazaborolidine-based Lewis acids (**119**) were found to be useful co-catalysts with an iridium photosensitizer (**PC3**), enabling a triplet-sensitized [2 + 2] photocycloaddition of simple cinnamate esters (**118**) with highly diastereo- and enantioselectivity (Scheme 10.33b) [148].

Asymmetric reductive cross-coupling of two *C*-centered electrophiles is an attractive strategy in organic synthesis due to its ability to forge C—C bonds with

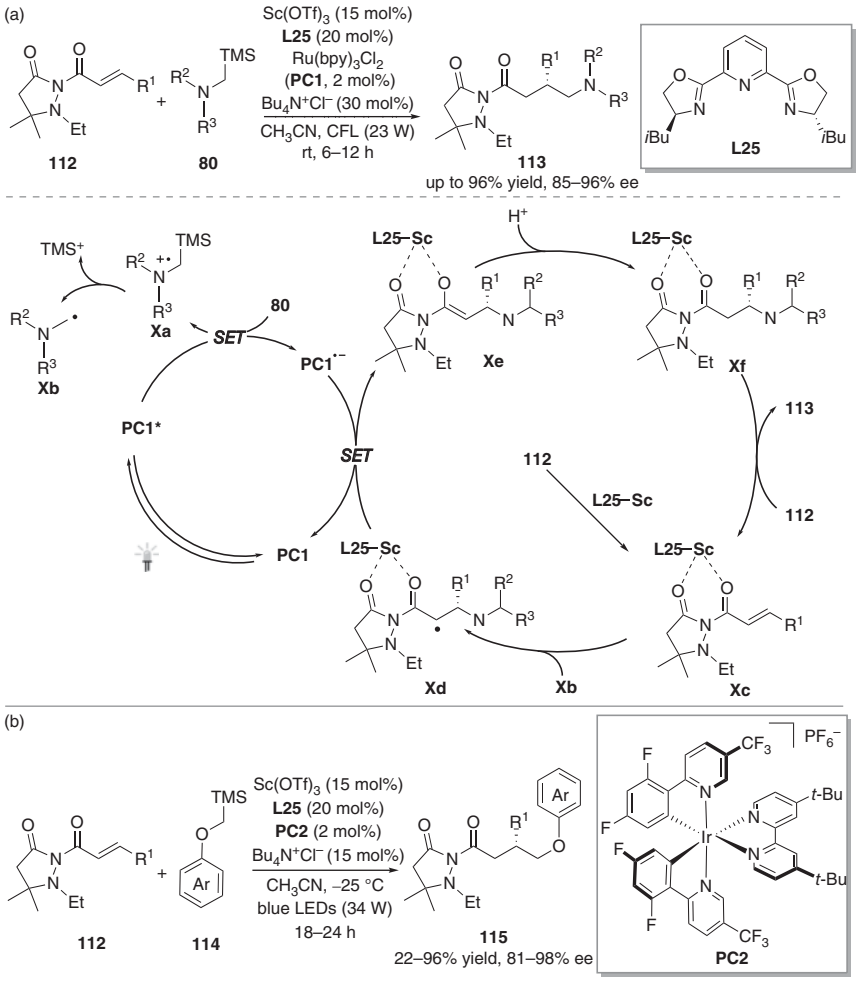


**Scheme 10.32** Enantioselective conjugate radical addition enabled by synergistic photoredox and lanthanide metal-based CLA catalysis. (a) Enantioselective α-aminoalkyl radical addition reactions catalyzed synergistically by Ru-based and Sc-based catalysts. (b) Enantioselective α-alkoxy radical addition reactions catalyzed synergistically by Ir-based and Sc-based catalysts.

two stereocenters. In 2019, Huang et al. reported the asymmetric synthesis of chiral vicinal amino alcohols (**123**) via a photocatalytic reductive cross-coupling of nitrones (**121**) with aryl aldehydes (**122)** (Scheme 10.34) [149]. Dual catalysis by a ruthenium polypyridine complex (**PC1**) and the chiral lanthanum catalyst provided high diastereo- (up to 12 : 1 dr) and enantioselectivity (up to 99% ee) during the process of forming adjacent carbon-centered stereocenters. The proposed reaction pathway starts with the visible light excitation of **PC1**. This is followed by a SET with an amine additive to form the reduced photocatalyst (**PC1**$^{\bullet-}$) and a nitrogen radical cation. On the other hand, the two substrates (**121** and **122**) coordinate with the

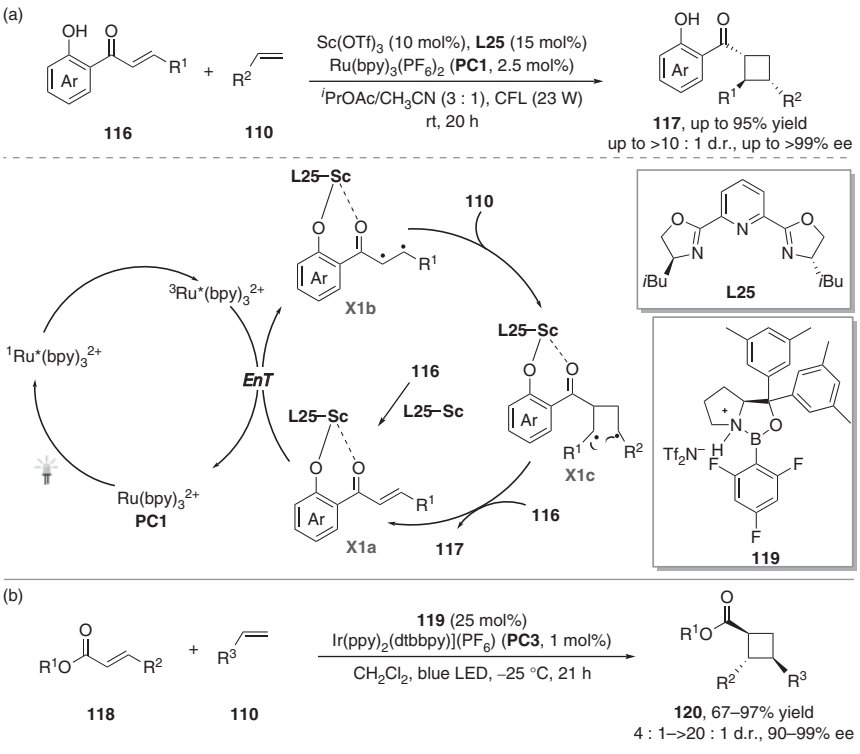


**Scheme 10.33** Asymmetric [2 + 2] photocycloaddition through CLA-catalyzed triplet-energy transfer (a) enabled by a chiral Sc(III) complex along with a Ru-based photocatalyst, or (b) enabled by an oxazaborolidinium ion catalyst along with an Ir-based photocatalyst.

scandium CLA catalyst to form a ternary complex (**X2a**), which undergoes a SET with **PC1**$^{\cdot-}$ to close the photoredox cycle and simultaneously generates a radical complex (**X2b**). An *N*-radical intermediate complex (**X2c**) is subsequently produced with a *syn*-configuration through an analogous 6-*endo*-trig radical annulation. Further hydrogen abstraction from the nitrogen radical cation results in a neutral complex (**X2d**). The final protonation and ligand exchange lead to the formation of the chiral product (**123**) and the regeneration of the CLA-substrate complex (**X2a**) for the next cycle.

Chiral copper complexes have been recognized as efficient co-catalysts with photosensitizers, facilitating visible light-driven asymmetric catalysis. Li et al. demonstrated that a copper complex featuring a chiral Pybox ligand (**L28**) could function as a CLA catalyst, working in concert with an iridium photoredox catalyst (**PC4**) to enable an enantioselective oxidative C($sp^3$)—H arylation (Scheme 10.35a) [150]. The reaction of *N*-aryltetrahydroisoquinolines (**124**) with arylboronic acids (**125**) proceeded under mild conditions, producing α-arylated *N*-aryltetrahydroisoquinoline products (**126**) with up to 80% ee. In the proposed reaction mechanism, a SET between the excited photocatalyst (**PC4***) and the

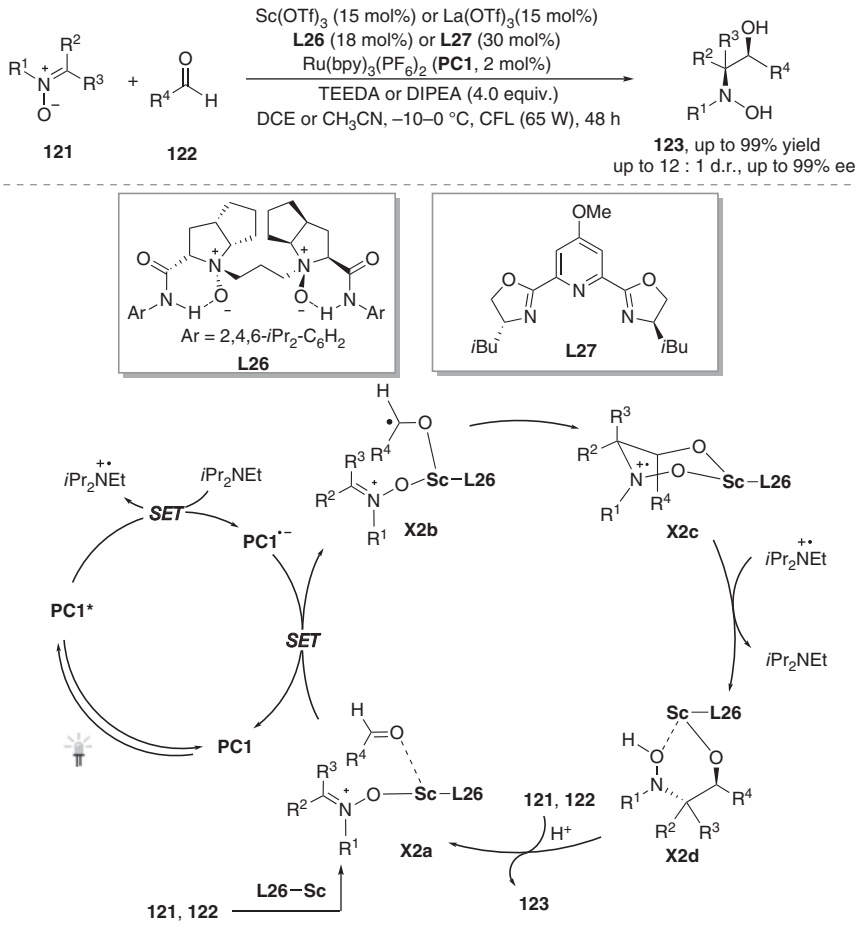


**Scheme 10.34** Photocatalytic enantioselective synthesis of chiral amino alcohols.

*N*-aryltetrahydroisoquinoline substrate (**124**) gives the reduced photocatalyst (**PC4**$^{\bullet-}$) and a radical cation (**X3a**). Intermediate **X3a** undergoes hydride abstraction to furnish an iminium cation, which is then coordinated with the copper center via a $\eta^2$-coordination mode. The resultant intermediate (**X3b**) is attacked by the arylboronic acid (**125**), releasing the chiral product (**126**). The copper catalyst acts as a chiral Lewis acid to activate the key electrophilic intermediate (**X3b**) and facilitates enantiodiscrimination in the nucleophilic addition step.

Shibasaki et al. developed an enantioselective aminomethylation of α,β-unsaturated amides (**127**) with α-silylamine (**80**) through the synergistic combination of copper-based CLA catalysis and photoredox catalysis (Scheme 10.35b) [151]. The incorporation of a 7-aza-6-MeO-indoline auxiliary into the substrates (**127**) was essential for achieving high enantioselectivity, which allowed the production of β-chiral amines (**128**) in good yields (66–97%) and with high enantioselectivity (74–99% ee). Mechanistically, the iridium photocatalyst (**PC4**) enables the mild

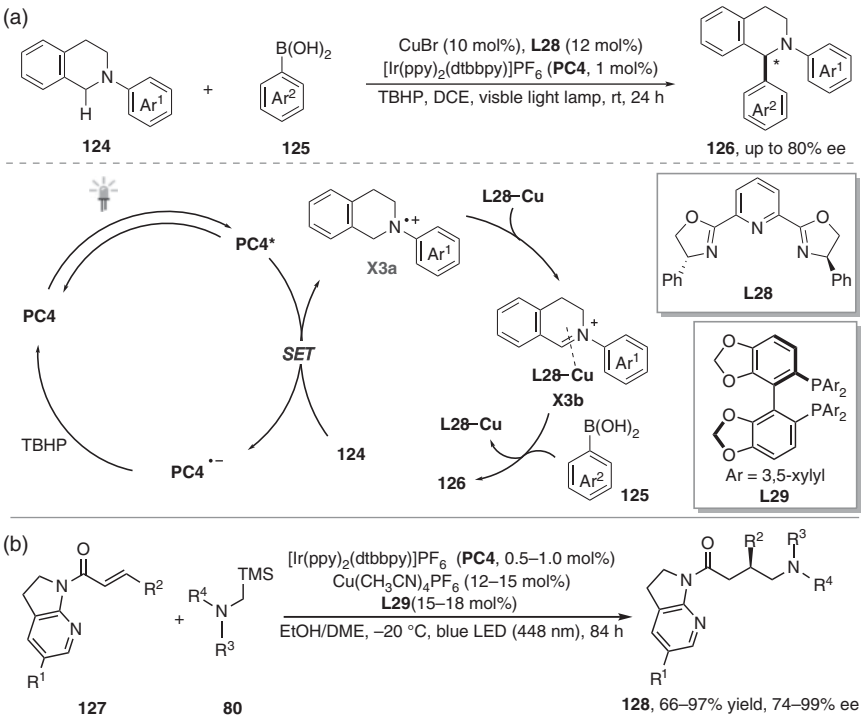


**Scheme 10.35** Development of synergistic photoredox and copper-based CLA catalysis for: (a) asymmetric C($sp^3$)—H arylation of tetrahydroisoquinoline, and (b) enantioselective conjugate radical addition to α,β-unsaturated amides.

release of α-aminomethyl radicals via photoinduced single-electron oxidation of α-silylamines (**80**), and the copper catalyst controls the stereochemistry in the radical addition step.

The selective functionalization of aliphatic C—H bonds is valuable in organic synthesis [152]. In this field, the site- and stereoselective modification of non-activated C($sp^3$)—H bonds, such as those in alkanes and cycloalkanes, remains remarkably challenging [153, 154]. Our group developed a strategy relying on synergistic organophotocatalysis and copper-based CLA catalysis for a photochemical stereoselective C($sp^3$)—H alkylation (Scheme 10.36) [155]. Using the 5,7,12,14-pentacenetetrone (**PC5**) and chiral copper co-catalyst, *N*-sulfonylimines (**88**) as the reaction partners, a regio- and stereoconrolled functionalization of various C—H bonds in unactivated alkanes (**129**) was achieved. A wide variety of enantioenriched *N*-sulfonylamine products (**91**) were formed with high site- and stereoselectivity (up to >50 : 1 rr and 99.5% ee). Interestingly, the replacement of the chiral copper catalyst with zinc, nickel, and cobalt yielded an inverted enantioselectivity under identical reaction conditions and with the same chiral ligand. The reaction proceeds through a light-induced HAT to activate a C($sp^3$)—H bond, single-electron reduction of the metal-bonded *N*-sulfonylamine, and enantioselective radical-radical cross-coupling governed by the CLA catalyst. This

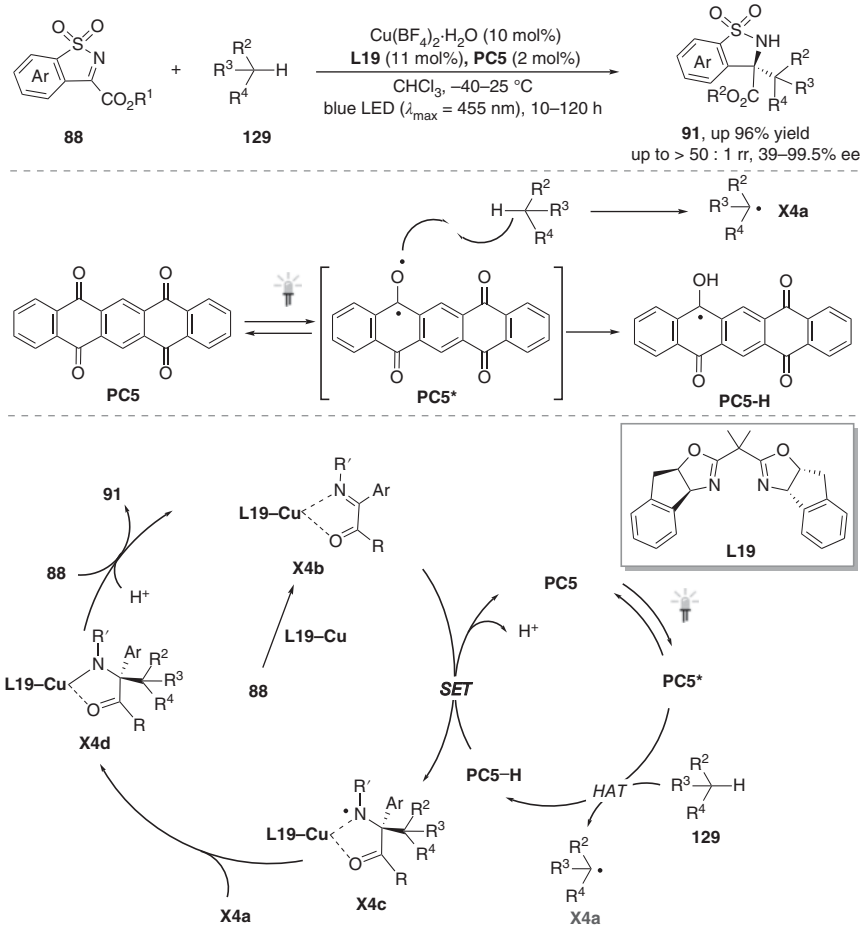


**Scheme 10.36** Photochemical selective C($sp^3$)—H functionalization enabled by synergistic HAT photocatalysis and copper-based CLA catalysis.

study introduces new pathways for synthesizing chiral molecules that are both synthetically and biologically valuable, utilizing readily available and abundant hydrocarbon feedstocks.

In 2021, we conducted a study on photochemical three-component asymmetric synthesis, which involved direct C($sp^3$)—H functionalization through synergistic organophotocatalysis and CLA catalysis (Scheme 10.37a) [156]. The use of 5,7,12,14-pentacenetetrone (**PC5**) and a nickel complex of a chiral bisoxazoline ligand (**L30**) with higher steric hindrance as co-catalysts was found to be effective for the C($sp^3$)—H functionalization. This led to the corresponding products with high regio- and enantioselectivity (up to >50 : 1 rr and 95% ee). Experiment studies revealed a radical relay sequence of light-induced HAT catalysis, nickel-based asymmetric catalysis and sulfur dioxide insertion. The third reaction component

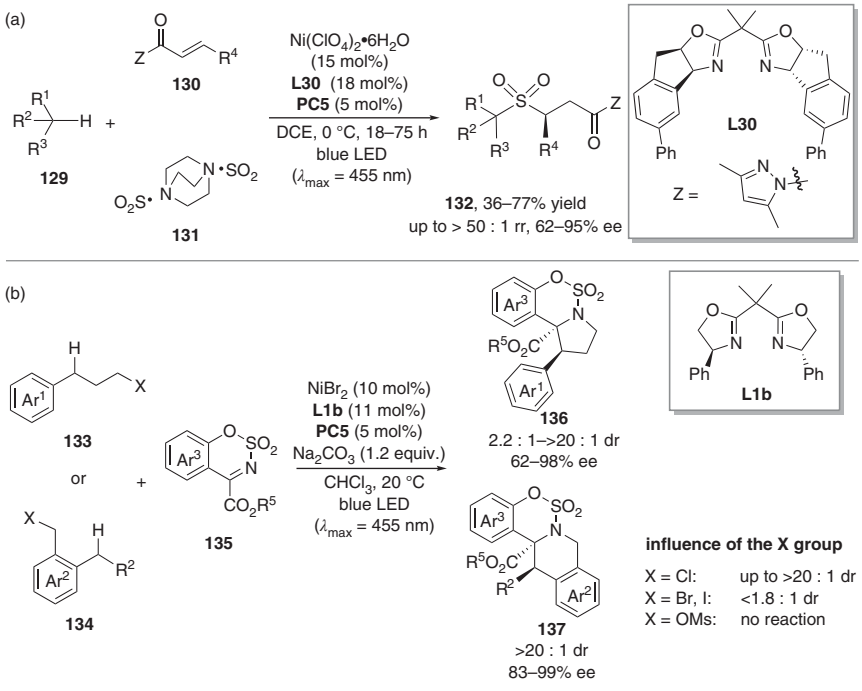


**Scheme 10.37** Synergistic HAT photocatalysis and nickel-based CLA catalysis for: (a) photochemical three-component asymmetric sulfonylation via direct C($sp^3$)—H functionalization, and (b) photochemical diastereo- and enantioselective benzylic C—H functionalization.

(**131**) as a $SO_2$ surrogate is critical for stabilizing high-energy alkyl radicals, thus ensuring excellent chemo- and stereoselectivity.

Later, we developed a visible light-induced diastereo- and enantioselective cascade benzylic C—H functionalization/cyclization via a similar cooperative organophotocatalysis and nickel-based CLA catalysis (Scheme 10.37b) [157]. The reaction of (3-chloropropyl)benzenes (**133**) or 1-(chloromethyl)-2-methylbenzene derivatives (**134**) with *N*-sulfonylimines (**135**) produced chiral benzosultams (**136**) or fused tetrahydroisoquinolines (**137**) with up to >20 : 1 dr and 99% ee. Importantly, the introduction of remote chlorine substituents to the benzylic C—H substrates is crucial in achieving both reactivity and stereoselectivity, allowing the rapid construction of chiral polycyclic compounds with vicinal stereocenters.

Recently, Feng et al. expanded photocatalytic stereoselective C—H activation by utilizing lanthanide metal-catalyzed asymmetric radical addition to different acceptors. For example, dual catalysis consisting of a chiral *N,N′*-dioxide (**L31**)/$Gd(OTf)_3$) and anthraquinone (**PC6**) as a HAT photocatalyst was developed. This system exhibited high catalytic efficiency and enantioselectivity in an acyl radical-mediated hydroacylation of α,β-unsaturated carbonyl compounds (**139**) with aldehydes (**138**) (Scheme 10.38a) [158]. Upon irradiation with a wavelength of 390 nm, **PC6** is converted into its excited state of diradical characters, which undergoes HAT with

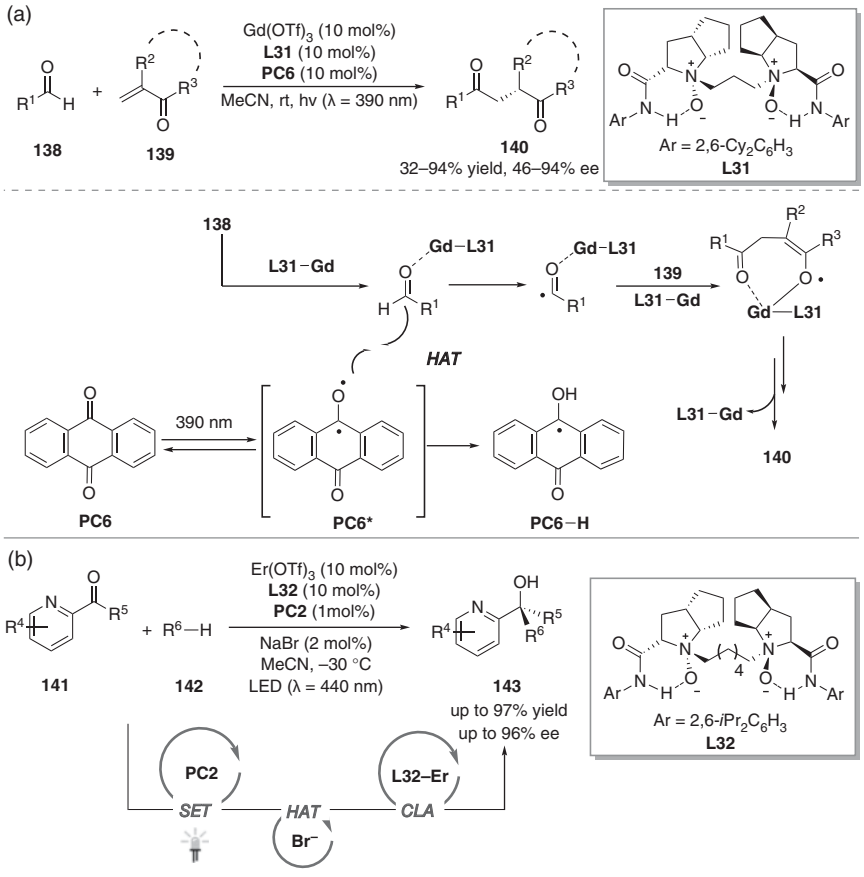


**Scheme 10.38** Synergistic HAT photocatalysis and CLA catalysis for: (a) enantioselective radical-mediated hydroacylation of α,β-unsaturated carbonyl compounds, and (b) enantioselective addition of hydrocarbons to pyridine-based ketones.

the metal-coordinated aldehyde to generate an acyl radical complex. This radical species then adds to the CLA-activated α,β-unsaturated carbonyl compound for further transformations. This protocol provides facile access to a wide array of enantioenriched 1,4-diketones under mild conditions. Furthermore, a ternary system comprising Er(III)-based chiral Lewis acid catalysis, photoredox catalysis, and bromide-radical-mediated HAT was developed and proved to be effective for a photochemical asymmetric radical addition of hydrocarbons (**142**) to pyridinyl ketones (**141**) (Scheme 10.38b) [159].

Xiao et al. designed a class of unique octahedral cobalt complexes (e.g., **146**) with both metal-centered (Δ) and ligand chirality (*R*,*R*), which were later used as co-catalysts with an organic photosensitizer (**PC7**) (Scheme 10.39) [105]. A visible light-driven asymmetric Giese reaction between alkyl/acyl radical precursors (**145**) and α,β-unsaturated carbonyl compounds (**144**) was achieved, delivering chiral ketones or 1,4-dicarbonyls (**147**) with up to >99% yields and 78–94% ee.

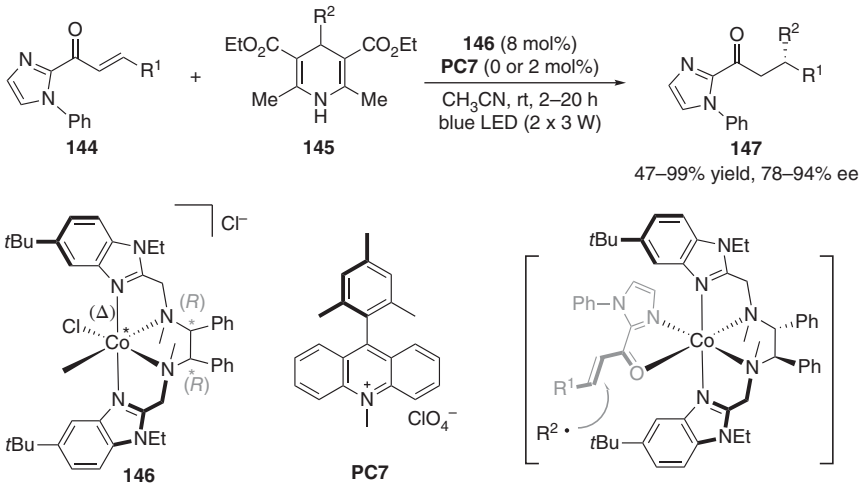


**Scheme 10.39** Photocatalytic asymmetric Giese reaction enabled by organocatalysis and cobalt-based CLA catalysis.

## 10.4 Merging CLA Catalysis with Electrochemical Reactions

Electrochemical organic synthesis has been extensively investigated, presenting new opportunities for the development of practical and environmentally appealing synthetic methodologies [160–171]. Several strategies, including the use of chiral auxiliaries and chiral electrodes, have been established to control stereoselectivity [172–175]. However, achieving electrolysis-triggered asymmetric catalysis has been a rare accomplishment.

In 2019, Guo et al. developed a novel enantioselective alkylation reaction of 2-acyl imidazoles (**148**) and phenols (**149**) using a combination of electrosynthesis with nickel-based CLA catalysis (Scheme 10.40) [176]. Conducted under mild conditions, this protocol enabled the synthesis of various alkylation products (**150**) in good yields (35–85%) with excellent enantioselectivities (76–97% ee). One of the products (**148a**) could be converted into a compound with antibacterial activity (WO 2003/018017) by multiple steps, while retaining its ee. Mechanistic investigations revealed a plausible sequence through an enantioselective radical-radical cross-coupling pathway. The reaction initiates with the bidentate chelation of 2-acyl imidazole (**148**) with the nickel catalyst (**L33-Ni**) to form a ketone intermediate (**X5a**), followed by deprotonation to generate an enolate complex (**X5b**). A subsequent electrolysis-induced SET oxidation of **X5b** leads to an α-carbonyl radical (**X5c**), which undergoes a radical-radical coupling with a benzylic radical intermediate (**X5d**) derived from the anodic oxidation of the phenol substrate (**149**). Ultimately, ligand exchange of the resulting nickel-bonded product (**X5e**) and **148** produces the chiral product and intermediat**e X5a** for the next cycle. The study highlights the compatibility of CLA catalysis with electrochemically formed radical intermediates and suggests the potential of such strategies in the development of new asymmetric synthesis.

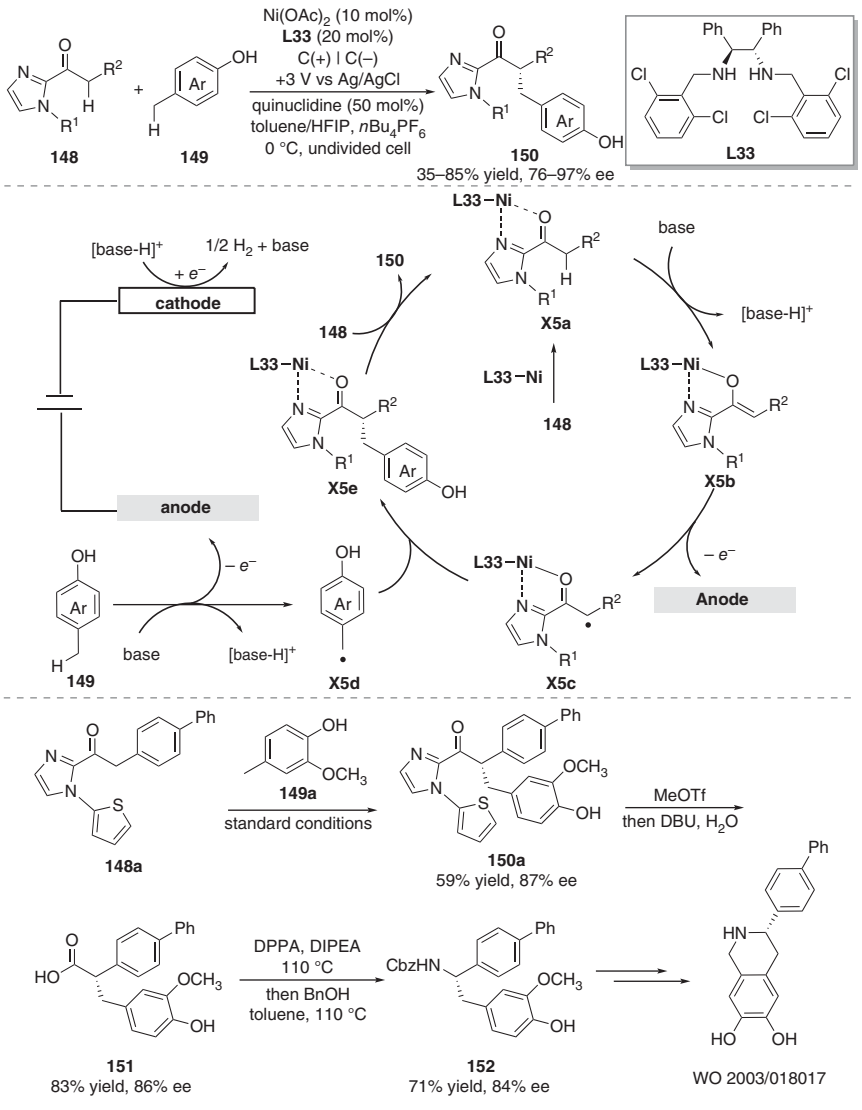


**Scheme 10.40** Enantioselective C–H alkylation of 2-acyl imidazoles enabled by electrolysis in combination with nickel-based CLA catalysis.

In 2021, the application of CLA-catalyzed electrolysis systems was reported by Guo in an enantioselective C—H arylation of 2-acyl imidazoles (**148**) (Scheme 10.41a) [177]. In contrast to the above-mentioned method, the catechol reaction partner (**153**) can be anodically oxidized to a *para*-phenoxyl radical species. This active intermediate is then converted to the corresponding chiral products through stereocontrolled radical-radical coupling. The utilization of an in situ generated nickel complex bearing a modified chiral diamine ligand (**L34**) as the CLA catalyst ensures a high level of enantiodiscrimination (86–94% ee). Finally, an enantioselective formal synthesis of (+)-Amurensinine was achieved, demonstrating the synthetic utility of this method. In 2022, they reported a nickel-catalyzed electrochemical

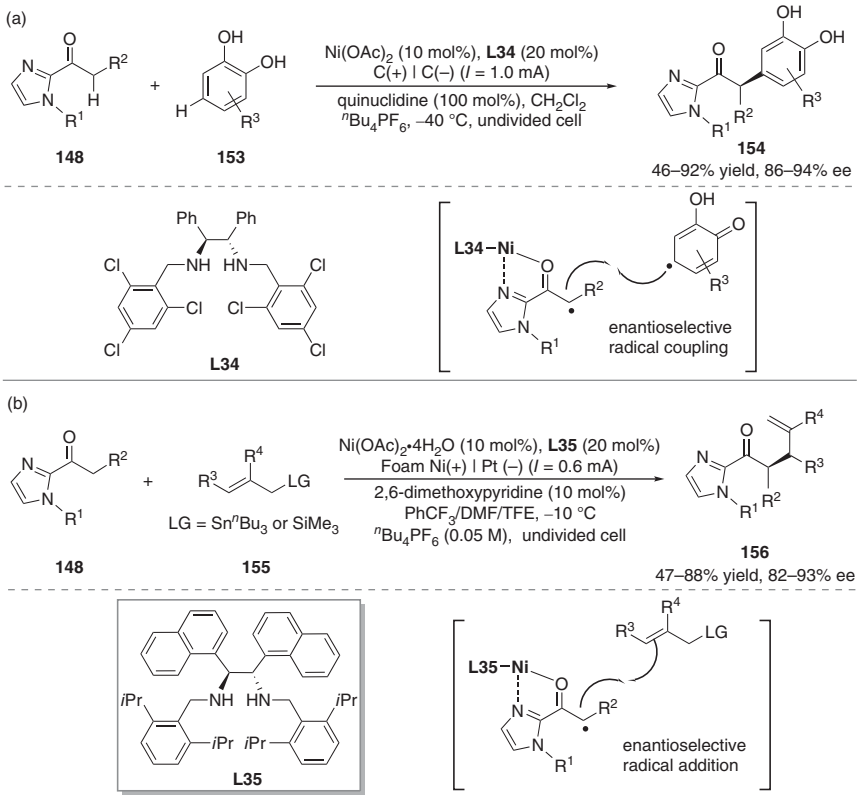


**Scheme 10.41** (a) Enantioselective electrochemical C–H arylation and (b) C—H allylation reactions enabled by nickel-based CLA catalysis.

radical asymmetric allylation of 2-acyl imidazoles (**148**) with allyltributylstannanes or allylsilanes (**155**) in an undivided cell equipped with a nickel (Ni) foam anode and platinum (Pt) cathode under constant-current conditions (Scheme 10.41b) [178]. The reaction involves a different exergonic addition of the anodically generated electrophilic nickel-coordinated radical cation with the double bond of the electron-rich allyltributylstannanes or allylstannane (**155)** and a β-scission process.

Although research in this field is still limited, these advances showcase the significant potential of strategies utilizing the anodic single-electron oxidation of well-organized CLA-bound enolates and introduce new avenues for radical-mediated asymmetric synthesis.

## 10.5 Conclusion

Radical-mediated asymmetric catalysis by CLAs is an emerging field and a powerful tool for constructing optically active molecules. This is due to its ability to forge diverse chemical bonds in a stereocontrolled fashion and its introduction of new

mechanistic scenarios. Classic CLAs, including chiral boranes and chiral complexes of magnesium and transition metals (Ln, Zn, Al, Ti, Cu, Ni, Co, etc.), exhibit multiple functions in these reactions. Different CLA catalysts with well-tailored chiral architectures and readily tunable reactivity can provide strong Lewis acid activation to various substrates, adjust the energy levels of excited states, stabilize radical species, and enable effective diastereo- and enantiodiscrimination. Significant success has been achieved in CLA-catalyzed radical reactions triggered by traditional thermal processes, merged with photocatalysis or electrolysis. These developments have led to the discovery of valuable synthetic methods that are reagent-efficient and easy to operate. It is believed that these studies will stimulate further applications in asymmetric synthesis, sustainable chemistry, and other research fields.

## References


1 Gisese, B. (1986). *Radicals in Organic Synthesis. Formation of Carbon-Carbon Bonds*. Oxford: Pergamon.
2 Renaud, P. and Sibi, M.P. (2001). *Radicals in Organic Synthesis*. Weinheim: Wiley.
3 Parsons, A.F. (2000). *An Introduction to Free Radical Chemistry*. Oxford: Blackwell Science.
4 Pattenden, G. (1988). *Chem. Soc. Rev.* 17: 361–382.
5 Jasperse, C.P., Curran, D.P., and Fevig, T.L. (1991). *Chem. Rev.* 91: 1237–1286.
6 Beckwith, A.L.J. (1993). *Chem. Soc. Rev.* 143–151.
7 Molander, G.A. and Harris, C.R. (1996). *Chem. Rev.* 96: 307–338.
8 Snider, B.B. (1996). *Chem. Rev.* 96: 339–363.
9 Zard, S.Z. (1997). *Angew. Chem. Int. Ed.* 36: 673–685.
10 Urabe, H., Yamashita, K., Suzuki, K. et al. (1995). *J. Organomet. Chem.* 60: 3576–3577.
11 Renaud, P. and Gerster, M. (1998). *Angew. Chem. Int. Ed.* 37: 2562–2579.
12 Liu, J., Lu, L., Wood, D. et al. (2020). *Science* 6: 1317–1340.
13 Wu, X., Chang, Y., and Lin, S. (2022). *Chem* 8: 1805–1821.
14 Zhang, C., Li, Z.-L., Gu, Q.-S., and Liu, X.-Y. (2021). *Nat. Commun.* 12: 475–483.
15 Xia, Q., Dong, J., Song, H., and Wang, Q. (2019). *Chem. Eur. J.* 25: 2949–2961.
16 Gu, Q.-S., Li, Z.-L., and Liu, X.-Y. (2020). *Acc. Chem. Res.* 53: 170–181.
17 Huo, H. and Meggers, E. (2016). *Chimia* 70: 186–191.
18 Mondal, S., Dumur, F., Gigmes, D. et al. (2022). *Chem. Rev.* 122: 5842–5976.
19 Gansäuer, A., Lauterbach, T., and Narayan, S. (2003). *Angew. Chem. Int. Ed.* 42: 5556–5573.
20 Schwinger, D.P. and Bach, T. (2020). *Acc. Chem. Res.* 53: 1933–1943.
21 Mlynarski, J. (2017). *Chiral Lewis Acids in Organic Synthesis*, 1e. KGaA: Wiley-VCH Verlag GmbH & Co.
22 Sibi, M.P. and Porter, N.A. (1999). *Acc. Chem. Res.* 32: 163–171.
23 Sibi, M.P., Manyem, S., and Zimmerman, J. (2003). *Chem. Rev.* 103: 3263–3296.
24 Zimmerman, J. and Sibi, M.P. (2006). *Top. Curr. Chem.* 263: 107–162.

**25** Yoon, T.P. (2016). *Acc. Chem. Res.* 49: 2307–2315.
**26** Amador, A.G. and Yoon, T.P. (2016). *Angew. Chem. Int. Ed.* 55: 2304–2306.
**27** Xiong, T. and Zhang, Q. (2021). *Chem. Soc. Rev.* 50: 8857–8873.
**28** Genzink, M.J., Kidd, J.B., Swords, W.B., and Yoon, T.P. (2022). *Chem. Rev.* 122: 1654–1716.
**29** Huang, X. and Meggers, E. (2019). *Acc. Chem. Res.* 52: 833–847.
**30** Perlmutter, P. (1992). *Conjugate Addition Reactions in Organic Synthesis*. Oxford: Pergamon.
**31** Sibi, M.P., Jasperse, C.P., and Ji, J. (1995). *J. Am. Chem. Soc.* 117: 10779–10780.
**32** Sibi, M.P., Ji, J., Wu, J.H. et al. (1996). *J. Am. Chem. Soc.* 118: 9200–9201.
**33** Sibi, M.P. and Ji, J. (1997). *J. Organomet. Chem.* 62: 3800–3801.
**34** Murakata, M., Tsutsui, H., and Hoshino, O. (2001). *Org. Lett.* 3: 299–302.
**35** Sibi, M.P. and Manyem, S. (2002). *Org. Lett.* 4: 2929–2932.
**36** Lee, S., Lim, C.J., Kim, S. et al. (2006). *Org. Lett.* 8: 4311–4313.
**37** Lee, S. and Kim, S. (2008). *Org. Lett.* 10: 4255–4258.
**38** Sibi, M.P. and He, L. (2004). *Org. Lett.* 6: 1749–1752.
**39** Sibi, M.P. and Prabagaran, N. (2004). *Synlett* 13: 2421–2424.
**40** Sibi, M.P. and Yang, Y.-H. (2008). *Synthesis* 1: 83–88.
**41** Vedejs, E., Kruger, A.W., Lee, N. et al. (2000). *J. Am. Chem. Soc.* 122: 460–465.
**42** Nakamura, S., Kaneeda, M., Ishihara, K., and Yamamoto, H. (2000). *J. Am. Chem. Soc.* 122: 8120–8130.
**43** Sibi, M.P., Asano, Y., and Sausker, J.B. (2001). *Angew. Chem. Int. Ed.* 40: 1293–1296.
**44** Murakata, M., Tsutsui, H., Takeuchi, N., and Hoshino, O. (1999). *Tetrahedron* 55: 10295–10304.
**45** Sibi, M.P. and Sausker, J.B. (2002). *J. Am. Chem. Soc.* 124: 984–991.
**46** Sugimoto, H., Nakamura, S., Watanabe, Y., and Toru, T. (2003). *Tetrahedron Asymmetry* 14: 3043–3055.
**47** Sibi, M.P. and Patil, K. (2004). *Angew. Chem. Int. Ed.* 43: 1235–1238.
**48** Sibi, M.P., Petrovic, G., and Zimmerman, J. (2005). *J. Am. Chem. Soc.* 127: 2390–2391.
**49** Sibi, M.P. and Zimmerman, J. (2006). *J. Am. Chem. Soc.* 128: 13346–13347.
**50** Sibi, M.P. and Nad, S. (2007). *Angew. Chem. Int. Ed.* 46: 9231–9234.
**51** Parsons, P.J., Penkett, C.S., and Shell, A.J. (1996). *Chem. Rev.* 96: 195–206.
**52** Malacria, M. (1996). *Chem. Rev.* 96: 289–306.
**53** McCarroll, A.J. and Walton, J.C. (2001). *Angew. Chem. Int. Ed.* 40: 2224–2248.
**54** Miyabe, H. and Takemoto, Y. (2007). *Chem. Eur. J.* 13: 7280–7286.
**55** Miyabe, H., Kawashima, A., Yoshioka, E., and Kohtani, S. (2017). *Chem. Eur. J.* 23: 6225–6236.
**56** Miyabe, H. (2017). *Eur. J. Org. Chem.* 2017: 3302–3310.
**57** Nishida, M., Hayashi, H., Nishida, A., and Kawahara, N. (1996). *Chem. Commun.* 579–580.
**58** Hiroi, K. and Ishii, M. (2000). *Tetrahedron Lett.* 41: 7071–7074.
**59** Miyabe, H., Asada, R., Toyoda, A., and Takemoto, Y. (2006). *Angew. Chem. Int. Ed.* 45: 5863–5866.

**60** Yang, D., Yang, M., and Zhu, N.-Y. (2003). *Org. Lett.* 5: 3749–3752.
**61** Yang, D., Yan, Y.-L., Law, K.-L., and Zhu, N.-Y. (2003). *Tetrahedron* 59: 10465–10475.
**62** Yang, D., Gu, S., Yan, Y.-L. et al. (2001). *J. Am. Chem. Soc.* 123: 8612–8613.
**63** Yang, D., Gu, S., Yan, Y.-L. et al. (2002). *Angew. Chem. Int. Ed.* 41: 3014–3017.
**64** Yang, D., Zheng, B.-F., Gao, Q. et al. (2006). *Angew. Chem. Int. Ed.* 45: 255–258.
**65** Streuff, J., Feurer, M., Bichovski, P. et al. (2012). *Angew. Chem. Int. Ed.* 51: 8661–8664.
**66** Gansäuer, A., Lauterbach, T., Bluhm, H., and Noltemeyer, M. (1999). *Angew. Chem. Int. Ed.* 38: 2909–2910.
**67** Gansäuer, A., Bluhm, H., and Lauterbach, T. (2001). *Adv. Synth. Catal.* 343: 785–787.
**68** Gansäuer, A., Shi, L., and Otte, M. (2010). *J. Am. Chem. Soc.* 132: 11858–11859.
**69** Mühlhaus, F., Weißbarth, H., Dahmen, T. et al. (2019). *Angew. Chem. Int. Ed.* 58: 14208–14212.
**70** Xu, Z., Shen, J., Li, L. et al. (2022). *Angew. Chem. Int. Ed.* 61: e202214111.
**71** Hao, W., Harenberg, J.H., Wu, X. et al. (2018). *J. Am. Chem. Soc.* 140: 3514–3517.
**72** Ye, K.-Y., McCallum, T., and Lin, S. (2019). *J. Am. Chem. Soc.* 141: 9548–9554.
**73** Robinson, S.G., Wu, X., Jiang, B. et al. (2020). *J. Am. Chem. Soc.* 142: 18471–18482.
**74** Streuff, J. and Gansäuer, A. (2015). *Angew. Chem. Int. Ed.* 54: 14232–14242.
**75** Weißbarth, H., Mühlhaus, F., and Gansäuer, A. (2020). *Synthesis* 52: 2940–2947.
**76** Friestad, G.K. (2005). *Eur. J. Org. Chem.* 2005: 3157–3172.
**77** Ding, H. and Friestad, G.K. (2005). *Synthesis* 2005: 2815–2829.
**78** Friestad, G.K. and Mathies, A.K. (2007). *Tetrahedron* 63: 2541–2569.
**79** Friestad, G.K., Shen, Y., and Ruggles, E.L. (2003). *Angew. Chem. Int. Ed.* 42: 5061–5063.
**80** Guo, J., Liu, X., He, C. et al. (2018). *Chem. Commun.* 54: 12254–12257.
**81** Liu, W., Pu, M., He, J. et al. (2021). *J. Am. Chem. Soc.* 143: 11856–11863.
**82** Calvo, R., Comas-Vives, A., Togni, A., and Katayev, D. (2019). *Angew. Chem. Int. Ed.* 58: 1447–1452.
**83** Wang, G., Xin, X., Wang, Z. et al. (2019). *Nat. Commun.* 10: 559–567.
**84** Prier, C.K., Rankic, D.A., and MacMillan, D.W.C. (2013). *Chem. Rev.* 113: 5322–5363.
**85** Narayanam, J.M.R. and Stephenson, C.R.J. (2011). *Chem. Soc. Rev.* 40: 102–113.
**86** Xuan, J. and Xiao, W.-J. (2012). *Angew. Chem. Int. Ed.* 51: 6828–6838.
**87** Chen, J.-R., Hu, X.-Q., Lu, L.-Q., and Xiao, W.-J. (2016). *Chem. Soc. Rev.* 45: 2044–2056.
**88** Zhu, J., Yang, W.-C., Wang, X.-D., and Wu, L. (2018). *Adv. Synth. Catal.* 360: 386–400.
**89** Lipp, A., Badir, S.O., and Molander, G.A. (2021). *Angew. Chem. Int. Ed.* 60: 1714–1726.
**90** Meggers, E. (2015). *Chem. Commun.* 51: 3290–3301.
**91** Wang, C. and Lu, Z. (2015). *Org. Chem. Front.* 2: 179–190.

**92** Meggers, E. (2017). *Angew. Chem. Int. Ed.* 56: 5668–5675.
**93** Jiang, C., Chen, W., Zheng, W.-H., and Lu, H. (2019). *Org. Biomol. Chem.* 17: 8673–8689.
**94** Nicewicz, D.A. and MacMillan, D.W.C. (2008). *Science* 322: 77–80.
**95** Arceo, E., Jurberg, I.D., Álvarez-Fernández, A., and Melchiorre, P. (2013). *Nat. Chem.* 5: 750–756.
**96** Tellis, J.C., Primer, D.N., and Molander, G.A. (2014). *Science* 345: 433–436.
**97** Huo, H., Shen, X., Wang, C. et al. (2014). *Nature* 515: 100–103.
**98** Alonso, R. and Bach, T. (2014). *Angew. Chem. Int. Ed.* 53: 4368–4371.
**99** Gutierrez, O., Tellis, J.C., Primer, D.N. et al. (2015). *J. Am. Chem. Soc.* 137: 4896–4899.
**100** Silvi, M., Verrier, C., Rey, Y.P. et al. (2017). *Nat. Chem.* 9: 868–873.
**101** Ma, J., Rosales, A.R., Huang, X. et al. (2017). *J. Am. Chem. Soc.* 139: 17245–17248.
**102** Ding, W., Lu, L.-Q., Zhou, Q.-Q. et al. (2017). *J. Am. Chem. Soc.* 139: 63–66.
**103** Li, J., Kong, M., Qiao, B. et al. (2018). *Nat. Commun.* 9: 2445–2453.
**104** Zhang, H.-H., Zhao, J.-J., and Yu, S. (2018). *J. Am. Chem. Soc.* 140: 16914–16919.
**105** Zhang, K., Lu, L.-Q., Jia, Y. et al. (2019). *Angew. Chem. Int. Ed.* 58: 13375–13379.
**106** Shin, N.Y., Ryss, J.M., Zhang, X. et al. (2019). *Science* 366: 364–369.
**107** Fu, M.-C., Shang, R., Zhao, B. et al. (2019). *Science* 363: 1429–1434.
**108** Hörmann, F.M., Kerzig, C., Chung, T.S. et al. (2020). *Angew. Chem. Int. Ed.* 59: 9659–9668.
**109** Lewis, F.D., Howard, D.K., and Oxman, J.D. (1983). *J. Am. Chem. Soc.* 105: 3344–3345.
**110** Brimioulle, R., Guo, H., and Bach, T. (2012). *Chem. Eur. J.* 18: 7552–7560.
**111** Brimioulle, R. and Bach, T. (2013). *Science* 342: 840–843.
**112** Brimioulle, R. and Bach, T. (2014). *Angew. Chem. Int. Ed.* 53: 12921–12924.
**113** Stegbauer, S., Jandl, C., and Bach, T. (2022). *Chem. Sci.* 13: 11856–11862.
**114** Stegbauer, S., Jandl, C., and Bach, T. (2018). *Angew. Chem. Int. Ed.* 57: 14593–14596.
**115** Foster, R. (1980). *J. Phys. Chem.* 84: 2135–2141.
**116** Miyasaka, H. (2013). *Acc. Chem. Res.* 46: 248–257.
**117** Crisenza, G.E.M., Mazzarella, D., and Melchiorre, P. (2020). *J. Am. Chem. Soc.* 142: 5461–5476.
**118** Kim, J.Y., Lee, Y.S., and Ryu, D.H. (2021). *ACS Catal.* 11: 14811–14818.
**119** Gong, L. (2022). *Nat. Synth.* 1: 915–916.
**120** Song, L.L., Cai, L., Gong, L., and Van der Eycken, E.V. (2023). *Chem. Soc. Rev.* 52: 2358–2376.
**121** Shen, X., Li, Y., Wen, Z. et al. (2018). *Chem. Sci.* 9: 4562–4568.
**122** Cao, S., Ye, Z., Chen, Y. et al. (2021). *CCS Chem.* 4: 3122–3133.
**123** Wang, F., Yang, C., Liu, J. et al. (2022). *Nat. Chem.* 14: 949–957.
**124** Dong, X.-Y., Li, Z.-L., Gu, Q.-S., and Liu, X.-Y. (2022). *J. Am. Chem. Soc.* 144: 17319–17329.

**125** Li, Z.-L., Fang, G.-C., Gu, Q.-S., and Liu, X.-Y. (2020). *Chem. Soc. Rev.* 49: 32–48.
**126** Choi, J. and Fu, G.C. (2017). *Science* 356: eaaf7230.
**127** Zhang, Z.-H., Dong, X.-Y., Du, X.-Y. et al. (2019). *Nat. Commun.* 10: 5689–5698.
**128** Zhang, W., Wang, F., McCann, S.D. et al. (2016). *Science* 353: 1014–1018.
**129** Li, J., Zhang, Z., Wu, L. et al. (2019). *Nature* 574: 516–521.
**130** Zhang, W., Chen, P., and Liu, G. (2017). *J. Am. Chem. Soc.* 139: 7709–7712.
**131** Zhang, W., Wu, L., Chen, P., and Liu, G. (2019). *Angew. Chem. Int. Ed.* 58: 6425–6429.
**132** Fu, L., Zhang, Z., Chen, P. et al. (2020). *J. Am. Chem. Soc.* 142: 12493–12500.
**133** Jiang, C., Chen, P., and Liu, G. (2020). *CCS Chem.* 2: 1884–1893.
**134** Wang, F., Chen, P., and Liu, G. (2018). *Acc. Chem. Res.* 51: 2036–2046.
**135** Yu, Z.-L., Cheng, Y.-F., Liu, J.-R. et al. (2023). *J. Am. Chem. Soc.* 145: 6535–6545.
**136** Chen, J.-J., Fang, J.-H., Du, X.-Y. et al. (2023). *Nature* 618: 294–300.
**137** Li, Y., Zhou, K., Wen, Z. et al. (2018). *J. Am. Chem. Soc.* 140: 15850–15858.
**138** Han, B., Li, Y., Yu, Y., and Gong, L. (2019). *Nat. Commun.* 10: 3804–3812.
**139** Zhou, K., Yu, Y., Lin, Y.-M. et al. (2020). *Green Chem.* 22: 4597–4603.
**140** Yang, L., Li, W.-Y., Hou, L. et al. (2022). *Chem. Sci.* 13: 8576–8582.
**141** Tan, Z., Zhu, S., Liu, Y., and Feng, X. (2022). *Angew. Chem. Int. Ed.* 61: e202203374.
**142** Hou, L., Zhou, Y., Yu, H. et al. (2022). *J. Am. Chem. Soc.* 144: 22140–22149.
**143** Du, J., Skubi, K.L., Schultz, D.M., and Yoon, T.P. (2014). *Science* 344: 392–396.
**144** Amador, A.G., Sherbrook, E.M., and Yoon, T.P. (2016). *J. Am. Chem. Soc.* 138: 4722–4725.
**145** Ruiz Espelt, L., McPherson, I.S., Wiensch, E.M., and Yoon, T.P. (2015). *J. Am. Chem. Soc.* 137: 2452–2455.
**146** Dong, X., Li, Q.Y., and Yoon, T.P. (2021). *Org. Lett.* 23: 5703–5708.
**147** Miller, Z.D., Lee, B.J., and Yoon, T.P. (2017). *Angew. Chem. Int. Ed.* 56: 11891–11895.
**148** Daub, M.E., Jung, H., Lee, B.J. et al. (2019). *J. Am. Chem. Soc.* 141: 9543–9547.
**149** Ye, C.-X., Melcamu, Y.Y., Li, H.-H. et al. (2018). *Nat. Commun.* 9: 410–418.
**150** Querard, P., Perepichka, I., Zysman-Colman, E., and Li, C.-J. (2016). *Beilstein J. Org. Chem.* 12: 2636–2643.
**151** Pagire, S.K., Kumagai, N., and Shibasaki, M. (2020). *Chem. Sci.* 11: 5168–5174.
**152** Cuthbertson, J.D. and MacMillan, D.W.C. (2015). *Nature* 519: 74–77.
**153** Cook, A.K., Schimler, S.D., Matzger, A.J., and Sanford, M.S. (2016). *Science* 351: 1421–1424.
**154** Hu, A., Guo, J.J., Pan, H., and Zuo, Z. (2018). *Science* 361: 668–672.
**155** Li, Y., Lei, M., and Gong, L. (2019). *Nat. Catal.* 2: 1016–1026.
**156** Cao, S., Hong, W., Ye, Z., and Gong, L. (2021). *Nat. Commun.* 12: 2377–2388.
**157** Zhang, S., Dong, S., Cheng, X. et al. (2022). *Org. Chem. Front.* 9: 6853–6860.
**158** Luo, Y., Wei, Q., Yang, L. et al. (2022). *ACS Catal.* 12: 12984–12992.
**159** Yu, H., Zhan, T., Zhou, Y. et al. (2022). *ACS Catal.* 12: 5136–5144.

**160** Yoshida, J.-I., Kataoka, K., Horcajada, R., and Nagaki, A. (2008). *Chem. Rev.* 108: 2265–2299.
**161** Francke, R. and Little, D. (2014). *Chem. Soc. Rev.* 43: 2492–2521.
**162** Yan, M., Kawamata, Y., and Baran, P.S. (2017). *Chem. Rev.* 117: 13230–13319.
**163** Jiang, Y., Xu, K., and Zeng, C. (2018). *Chem. Rev.* 118: 4485–4540.
**164** Waldvogel, S.R., Lips, S., Selt, M. et al. (2018). *Chem. Rev.* 118: 6706–6765.
**165** Wiebe, A., Gieshoff, T., Mçhle, S. et al. (2018). *Angew. Chem. Int. Ed.* 57: 5594–5619.
**166** Tang, S., Liu, Y., and Lei, A. (2018). *Chem* 4: 27–45.
**167** Hayashi, R., Shimizu, A., and Yoshida, J.-I. (2016). *J. Am. Chem. Soc.* 138: 8400–8403.
**168** Horn, E.J., Rosen, B.R., Chen, Y. et al. (2016). *Nature* 533: 77–81.
**169** Hruszkewycz, D.P., Miles, K.C., Thiel, O.R., and Stahl, S.S. (2017). *Chem. Sci.* 8: 1282–1287.
**170** Kawamata, Y., Yan, M., Liu, Z. et al. (2017). *J. Am. Chem. Soc.* 139: 7448–7451.
**171** Imada, Y., Rçckl, J., Wiebe, A. et al. (2018). *Angew. Chem. Int. Ed.* 57: 12136–12140.
**172** Cai, C.-Y., Lai, X.-L., Wang, Y. et al. (2022). *Nat. Catal.* 5: 943–951.
**173** Yang, Z., Shi, W., Alhumade, H. et al. (2023). *Nat. Synth.* 2: 217–230.
**174** Libendi, S.S., Demizu, Y., Matsumura, Y., and Onomura, O. (2008). *Tetrahedron* 64: 3935–3942.
**175** Watkins, B.F., Behling, J.R., Kariv, E., and Miller, L.L. (1975). *J. Am. Chem. Soc.* 97: 3549–3550.
**176** Zhang, Q., Chang, X., Peng, L., and Guo, C. (2019). *Angew. Chem. Int. Ed.* 58: 6999–7003.
**177** Zhang, Q., Liang, K., and Guo, C. (2021). *CCS Chem.* 3: 338–347.
**178** Zhang, Q., Liang, K., and Guo, C. (2022). *Angew. Chem. Int. Ed.* 61: e202210632.

# 11

# Chiral-at-Metal Complex-Catalyzed Asymmetric Radical Reactions

*Jiajia Ma*

*Frontiers Science Center for Transformative Molecules, School of Chemistry and Chemical Engineering, Shanghai Jiao Tong University, Dongchuan Road 800, Shanghai 200240, P. R. China*

## 11.1 Introduction

Platinum-group metal complexes encompass remarkable photophysical properties and photochemical activities and are widely investigated across many disciplines such as pharmaceutical, material, and synthetic chemistry. In particular, polypyridyl coordinated ruthenium complex $Ru(bpy)_3^{+2}$ (bpy = 2,2′-bipyridine) and cyclometalated iridium complex $[Ir(ppy)_2(dtbbpy)]^{+1}$ (ppy = phenyl pyridine; dtbbpy = 4,4′-di-*tert*-butyl-2,2′-bipyridine) as well as their derivatives are privileged photocatalysts that have been extensively used in photoinduced radical chemistry [1]. Numerous transformations that are otherwise challenging under conventional thermal conditions have been accomplished by these photocatalysts-enabled radical chemistry.

Thanks to Alfred Werner's pioneering work on chiral metal complexes, metal-centered chirality has been established for octahedral platinum-group metal complexes for more than a century (Figure 11.1) [2]. Soai demonstrated that the chiral-at-metal complexes can be used as chiral initiators in asymmetric autocatalysis [3]. Fontecave introduced the concept of using (reactive) chiral-at-metal complexes for asymmetric transition metal catalysis, although the stereocontrol was inferior [4]. Gladysz demonstrated for the first time that inert chiral-at-metal Werner-type complexes can be used for asymmetric catalysis through the ligand sphere (metal-templated organocatalysis) [5]. The Meggers group pioneered the use of chiral-at-metal complexes as highly efficient chiral catalysts over the last decade [6]. A range of privileged chiral-at-metal catalysts with metal chirality have been invented and showcased unprecedented catalytic activities towards various synthetic transformations [7].

Intriguingly, the bis-cyclometalated chiral-at-Ir/Rh complexes are the enantioenriched analogs of the widely used photocatalysts and are found to enable photoinduced asymmetric radical reactions. As outlined in Figure 11.2a, chiral-at-metal complexes used in asymmetric photoinduced radical reactions are divided

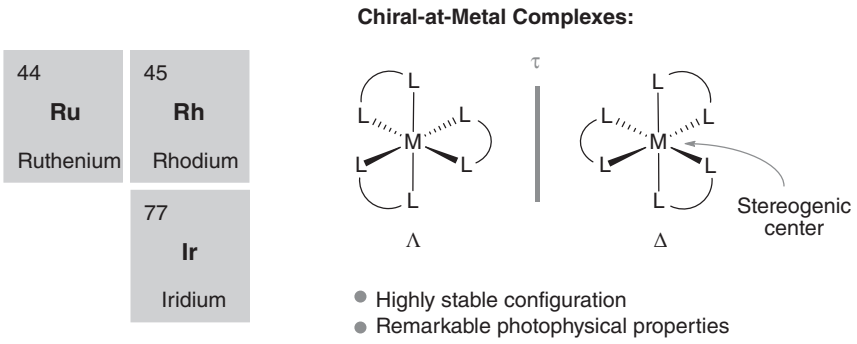


**Figure 11.1** Chiral-at-metal platinum-group metal complexes.

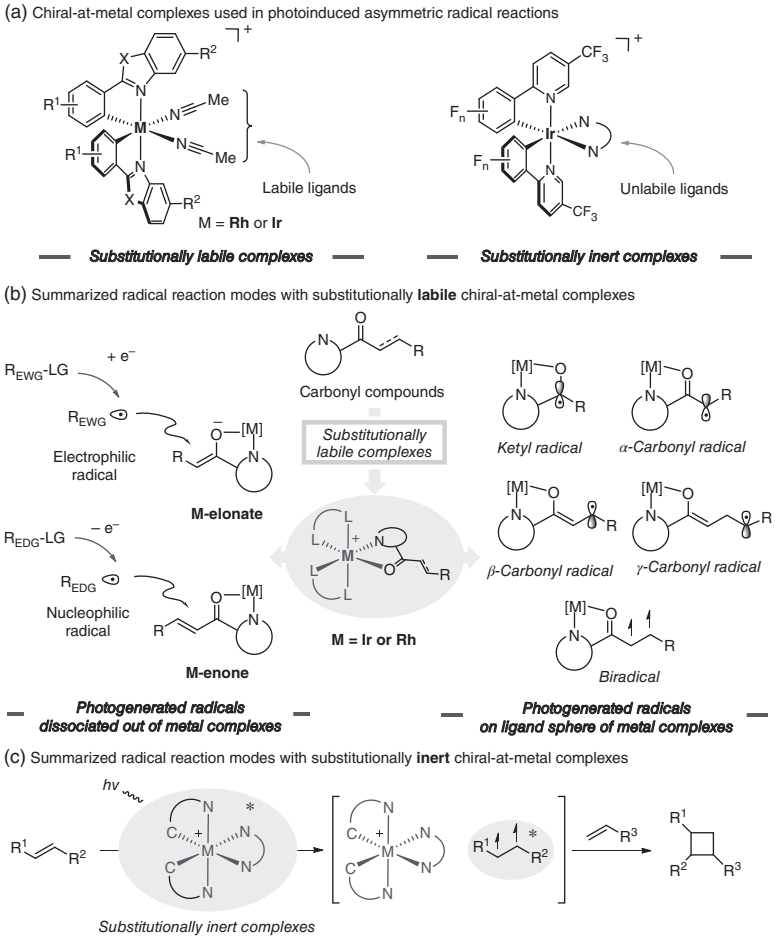


**Figure 11.2** Chiral-at-metal complexes enabled asymmetric radical reactions. (a) Chiral-at-metal complexes discussed in this chapter; (b) Asymmetric radical reaction modes with substitutionally labile chiral-at-metal complexes; (c) Asymmetric radical reaction modes with substitutionally inert chiral-at-metal complexes.

into substitutionally labile [7a, 7b] and inert [8] ones. The substitutionally labile ones contain two bidentate cyclometalating 5-*tert*-butyl-2-phenylbenzoxazole or 5-*tert*-butyl-2-phenylbenzothiazole ligands, in addition to two labile acetonitriles. In contrast, the substitutionally inert ones encompass two bidentate cyclometalating phenyl pyridine ligands, in addition to a third bidentate ligand, thus a 2-(1*H*-pyrazol-3-yl)pyridine or 2,2′-bipyridine derivative. These complexes are Λ-configured (left-handed propeller) or Δ-configured (right-handed propeller) and are monocationic being associated with hexafluorophosphate or tetrakis[3,5-bis (trifluoromethyl)phenyl]borate counterions. The synthesis of these complexes relies on the sequence of chiral-auxiliary mediated resolution and stereospecific ligand exchange described by the Meggers group [9].

In this chapter, the asymmetric radical reactions are divided into sections according to the types of employed chiral-at-metal complexes, substitutionally labile or inert variants.

(1) The substitutionally labile chiral-at-iridium and rhodium complexes typically play the role of Lewis acid that interacts with the substrate by coordination and meanwhile are often precursors for assembling the photocatalyst *in-situ* (Figure 11.2b). In particular, the chiral-at-Rh Lewis acid can cooperate with an additional photocatalyst or redox mediator, thus triggering an extended scope for asymmetric radical reactions. Furthermore, due to the much faster ligand exchange kinetics for Rh compared to Ir, chiral-at-Rh Lewis acid catalysis is very suitable for capturing radicals with shorter lifetimes. The photogenerated bonding radicals either dissociate out of the chiral-at-metal complexes or directly delocalize on the ligand sphere. The following asymmetric induction over bond formations is directed by the metal chirality. The asymmetric radical reactions relying on chiral-at-iridium or rhodium complexes are presented individually in the next two sections.
(2) The substitutionally inert chiral-at-metal complex is used as the chiral photosensitizer to facilitate the production of biradical intermediates from activated alkenes which can then engage in stereocontrolled [2+2] cycloadditions with a second alkene (Figure 11.2c). The asymmetric induction is directed by the metal chirality and optionally in cooperation with an additional chiral Brønsted acid. Substitutionally inert chiral-at-metal complex catalyzed radical reactions are discussed in the last section.

## 11.2 Asymmetric Radical Reactions Enabled by Chiral-at-Iridium Lewis Acid

Asymmetric photocatalysis is a significant tool for enabling stereocontrolled synthetic radical chemistry. In most reported examples, asymmetric photocatalysis is driven by two individual catalysts: a photocatalyst for triggering radical chemistry and a chiral catalyst for providing stereocontrol [10]. In compassion, developing a single catalytic system combining the dual roles of photocatalysis and asymmetric

catalysis is sustainable and valuable, rendering reaction optimization simple. In this context, the Meggers group demonstrated that the substitutionally labile chiral-at-Ir complex can serve as the dual role of Lewis acid and a precursor for *in-situ* assembled photocatalyst, thus enabling a variety of asymmetric radical reactions [7a]. The photogenerated bonding radicals can either dissociate out the chiral-at-metal complexes or directly delocalize on their ligand sphere, and they will be discussed individually in the section.

### 11.2.1 Radicals Dissociated out of Chiral-at-Iridium Complexes

In 2014, Meggers and coworkers disclosed the proof-of-concept that a single chiral-at-Ir complex was capable of facilitating photoinduced asymmetric radical reaction by intertwining the dual function of chiral Lewis acid catalysis and photocatalysis [11]. The reported stereocontrolled radical reaction of 2-acylimidazoles **1** with activated alkyl bromides **2** provides the α-alkylation products **4** in excellent to quantitative yields and with high enantioselectivities of up to 99% ee (Figure 11.3). In this unique catalytic system, the chiral-at-Ir complex serves a dual function of chiral Lewis acid and a precursor for *in-situ* assembled photoredox catalyst. As proposed by the authors, the catalytic cycle is initiated by bidentate coordination of the 2-acyl imidazole **1** to the chiral-at-Ir complex Λ-**IrS**. The afforded intermediate **I** is converted to an electron-rich iridium enolate **II** by base-promoted deprotonation. Notably, the Ir-enolate **II** can be directly excited by visible-light and then is oxidatively quenched by activated alkyl bromides **2** to generate the corresponding alkyl radicals. The subsequent enantioselective addition of this electrophilic alkyl radical to the Ir-enolate (**II**) provides the intermediate **III**, which is then oxidized to an iridium-bound product **IV**. The following ligand exchange of product **4** with substrate **1** leads to a new catalytic cycle. In subsequent work, the same group extended this remarkable dual-functional single catalytic system to enantioselective α-trichloromethylations of 2-acylimidazoles and 2-acylpyridines [12].

This asymmetric radical α-alkylation can proceed sequentially with asymmetric transfer hydrogenation by using the sole chiral-at-Ir complex Λ-**IrS** [13]. As outlined in Figure 11.4, the α-alkylation product **7** obtained under photoredox conditions is then subjected to asymmetric transfer hydrogenation, thus affording an enantioenriched alcohol **8** with excellent diastereoselectivities. This sequential asymmetric radical reaction and transfer hydrogenation were performed in two separate steps but in one pot, in which the sole chiral-at-Ir complex Λ-**IrS** was employed.

Next, Meggers and coworkers further developed a photocatalyzed enantioselective perfluoroalkylation of 2-acylimidazoles (Figure 11.5) [14]. The asymmetric radical reaction proceeds through the enantioselective addition of an electrophilic perfluoroalkyl radical to Ir-enolate intermediate under visible light photocatalysis. It's worth noting that the original chiral-at-Ir complex Λ-**IrS** can enable this transformation but with inferior yields. Structural optimization of the Λ-**IrS** by introducing two additional *t*-Bu groups to the cyclometalated phenyl rings delivers a new chiral-at-Ir complex Λ-**IrS(*t*Bu)** which can promote the enantioselective perfluoroalkylation with significantly improved yields. The introduced *t*-Bu groups render the increased HOMO energy of the chiral-at-Ir complex, thus making it a better single electron

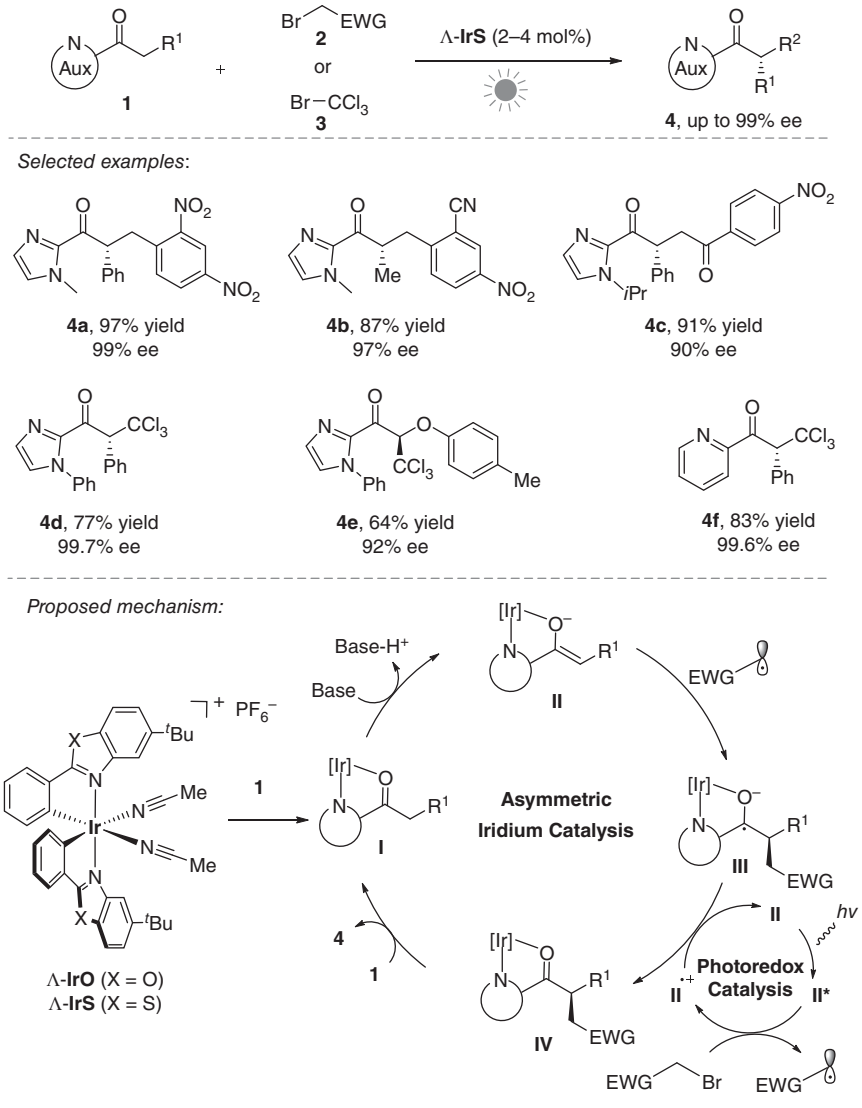


**Figure 11.3** Electrophilic alkyl or trichloromethyl radicals interfacing with Ir-enolate: asymmetric radical α-alkylation of 2-acyl imidazoles and pyridines.

donor at both ground and excited states which is beneficial for single electron reduction of feedstock perfluoroalkyl iodides **9** and **10**. As a result, the yields of the enantioselective perfluoroalkylation of 2-acylimidazoles **11** are improved.

The radicals generated from chiral-at-Ir photoredox catalysis can interface with the Ir-enolate to give enantioenriched α-alkylation products. Likewise, the photogenerated radical could further undergo single electron oxidation with terminal oxidants to produce a reactive cation, which then interfaces with Ir-enolate. In 2015, Meggers and coworkers reported a photoinduced enantioselective oxidative α-alkylation of 2-acyl-1-phenylimidazoles **1** with *N*,*N*-diaryl-*N*-(tri-methylsilyl)

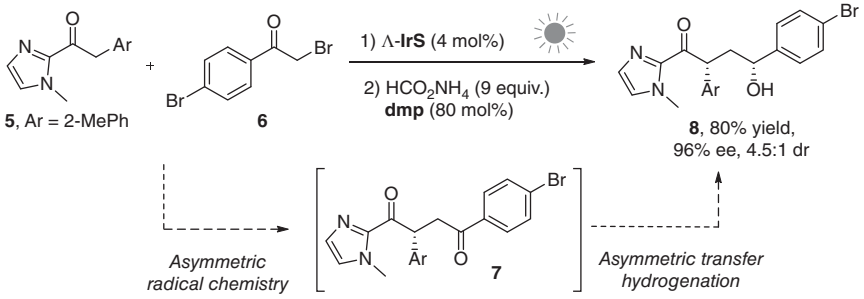


**Figure 11.4** Sequential asymmetric radical α-alkylation and transfer hydrogenation.

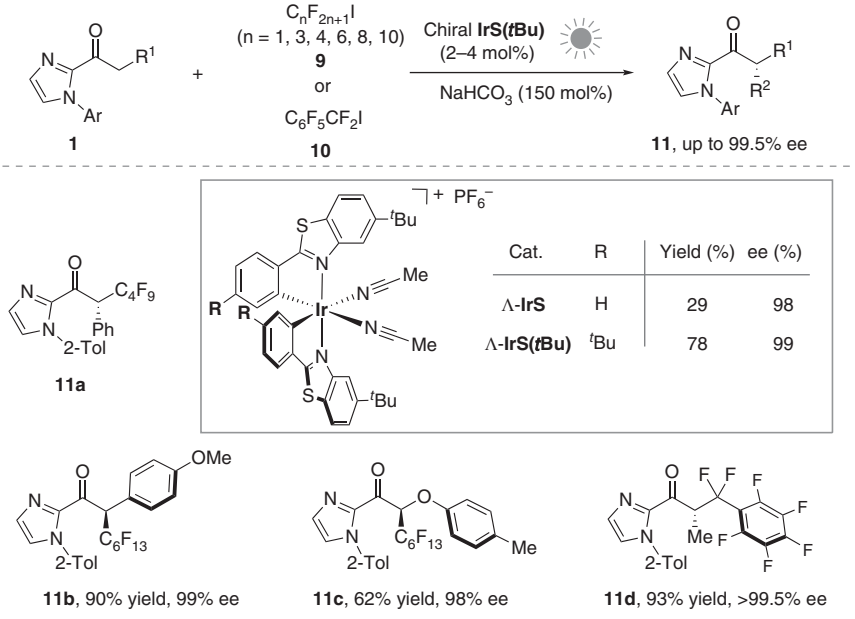


**Figure 11.5** Electrophilic perfluoroalkyl radicals interfacing with Ir-enolate: asymmetric radical perfluoroalkylation of 2-acyl imidazoles.

methylamines **12** under air (Figure 11.6) [15]. The reaction provides aminoalkylation products **13** in good yields (up to 93% yield) with up to 98% ee. The catalytic cycle is initiated upon the coordination of the 2-acylimidazole substrate **1** with chiral-at-Ir complex to provide intermediate **I**. The subsequent deprotonation at the α-position of the carbonyl affords the nucleophilic Ir-enolate intermediate **II**. The α-silylamine **12** undergoes single electron oxidation by photoexcited Ir-complex $\mathbf{I}^*$ to afford α-aminoalkyl radical after the release of trimethylsilyl cation. This α-aminoalkyl radical is then oxidized by molecule oxygen to generate an electrophilic iminium ion. The subsequent enantioselective trap of this iminium ion by iridium enolate intermediate **II** provides the corresponding products **13** after release from the iridium complex.

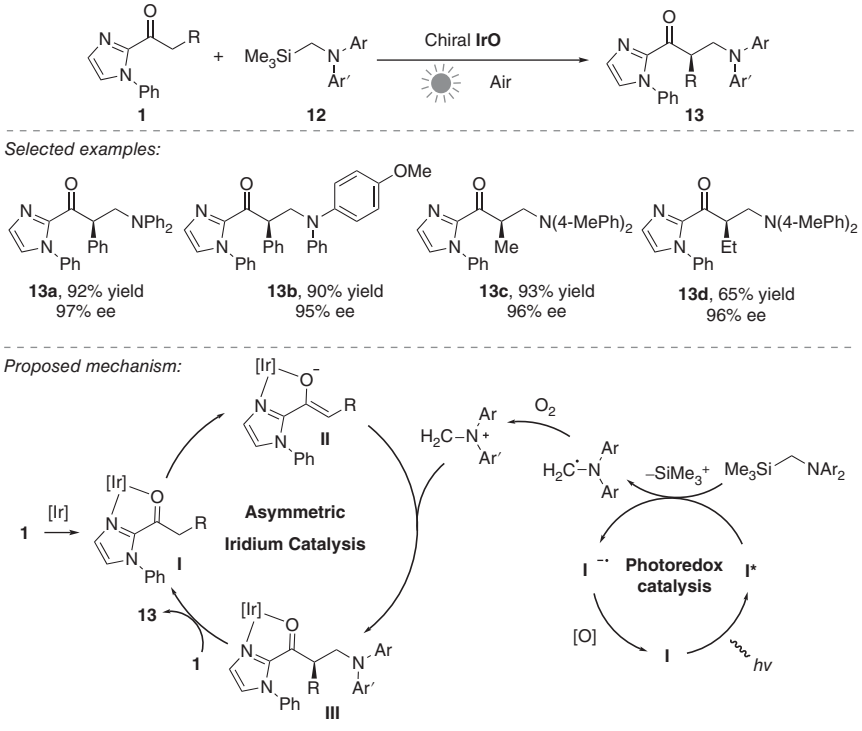


**Figure 11.6** Iminium ions interfacing with Ir-enolate: asymmetric α-aminoalkylation by chiral-at-Ir photoredox catalysis.

### 11.2.2 Radicals Delocalized on the Ligand Sphere of Chiral-at-Iridium Complexes

In this section, the ligand sphere radicals of chiral-at-Ir complexes that undergo stereocontrolled radical transformations are documented. In 2016, Meggers and coworkers reported an asymmetric cross-coupling reaction between the trifluoromethyl ketones **14** and tertiary amines **15** through visible-light activated chiral-at-Ir catalysis (Figure 11.7) [16]. Enantioenriched 1,2-amino alcohols **16** were obtained with excellent enantioselectivities. An iridium-ketyl intermediate has been suggested as the key for success in this transformation. As proposed by the authors, the chiral-at-Ir complex is initially coordinated by the trifluoromethyl ketone **14** to produce the intermediate **I**. Subsequently, this Ir-bound trifluoromethyl ketone intermediate **I** is excited by visible light and then reductively quenched by a tertiary amine **15** to give the Ir-ketyl radical **III**. Meanwhile, the tertiary amine **15** is converted to the amino radical cation which undergoes proton transfer with intermediate **III** to deliver **IV** and α-aminoalkyl radical. The following radical-radical cross-coupling gives the intermediate **V**. Finally, the ligand exchange with a new substrate **14** leads to a new catalytic cycle and the terminal product **16**.

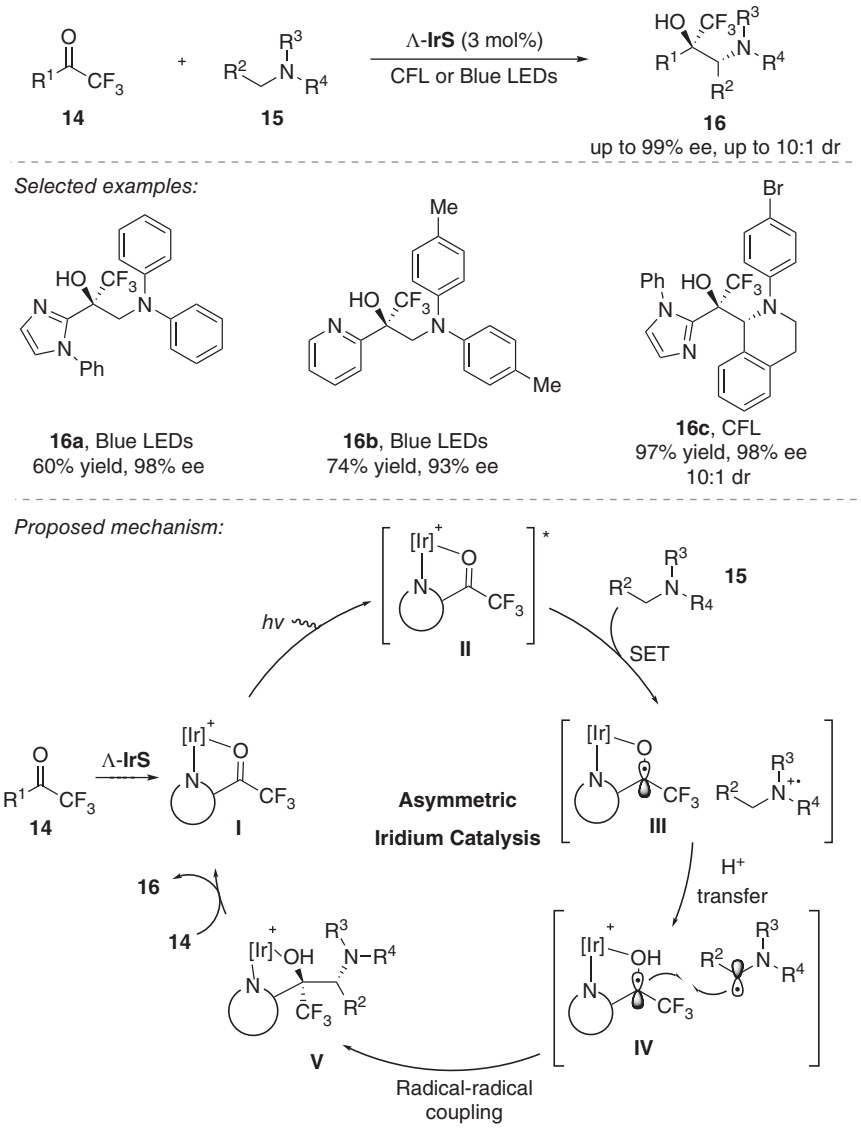


**Figure 11.7** Ligand sphere Ir-ketyl radical interfacing with α-aminoalkyl radical.

## 11.3 Asymmetric Radical Reactions Enabled by Chiral-at-Rhodium Lewis Acid

Compared with the chiral-at-iridium complexes, their rhodium congeners typically showcase higher catalytic reactivities, thus leading to an extended reaction scope. In addition, the rhodium-based chiral-at-metal Lewis acid can cooperate with an additional racemic or achiral photocatalyst/mediator to promote more transformations.

Similar with the case of iridium complexes, the photogenerated binding radicals can also either dissociate out the chiral-at-Rh complexes or directly delocalize on their ligand sphere.

## 11.3.1 Radicals Dissociated out of Chiral-at-Rhodium Complexes

### 11.3.1.1 Electrophilic Radicals Interfacing with Rhodium-Enolate

Electrophilic carbon or nitrogen centered radicals are readily accessible under photoredox conditions and can undergo highly stereocontrolled bond formations with rhodium-enolate intermediate by chiral-at-Rh Lewis acid catalysis. In 2016, Meggers and coworkers demonstrated an enantioselective α-amination reaction of 2-acyl imidazoles **1** in which the Rh-enolate intermediate was recognized as both the nitrogen radical acceptor and a "smart initiator" of a radical-chain process for enabling nitrogen radical production (Figure 11.8) [17]. Lately, the same group reported that aryl azides and α-diazo carboxylic esters **19** were used as precursors for providing the electrophilic carbon or nitrogen radicals which then engaged in stereocontrolled C—C/N bonds formations under cooperative photoredox and chiral-at-Rh Lewis acid catalysis (Figure 11.9) [18]. The external photocatalyst $[Ru(bpy)_3](PF_6)_2$ is responsible for the redox process. Interestingly, among all these transformations, the chiral-at-Rh catalyst (**RhO**) has been observed to be superior over its iridium congener (**IrO/S**) and the **RhS** with benzothiazolyl ligands is better than its analog **RhO** with benzoxazoles.

Mechanistic experiments shed light on the different catalytic activities of **IrO**, **RhO**, and **RhS**. As outlined in Figure 11.10, kinetic investigations reveal that the

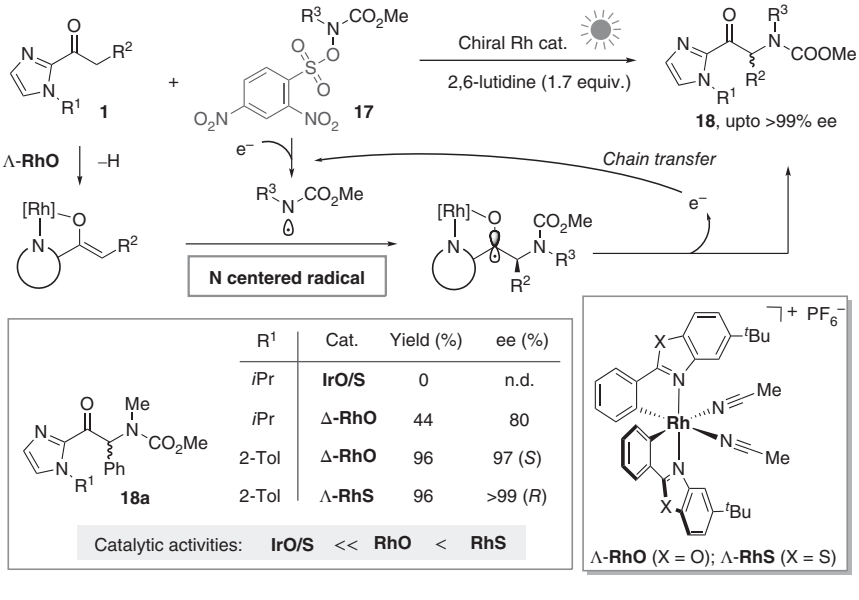


| $R^1$ | Cat. | Yield (%) | ee (%) |
|---|---|---|---|
| *i*Pr | **IrO/S** | 0 | n.d. |
| *i*Pr | Δ-**RhO** | 44 | 80 |
| 2-Tol | Δ-**RhO** | 96 | 97 (*S*) |
| 2-Tol | Λ-**RhS** | 96 | >99 (*R*) |

**Figure 11.8** Electrophilic nitrogen-centered radical interfacing with Rh-enolate: asymmetric α-amination of 2-acylimidazoles.

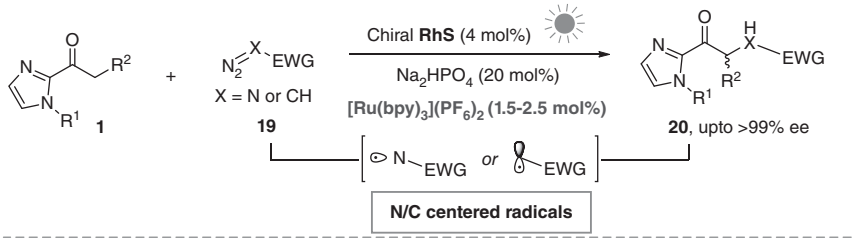


| Cat. | Base | Yield (%) | ee (%) |
|---|---|---|---|
| IrS | DIPEA | 0 | n.d. |
| Δ-RhO | DIPEA | 24 | 86 |
| Δ-RhS | DIPEA | 70 | 97.7 |
| Δ-RhS | $Na_2HPO_4$ | 82 | 98.4 |

Catalytic activities:
IrS << RhO < RhS

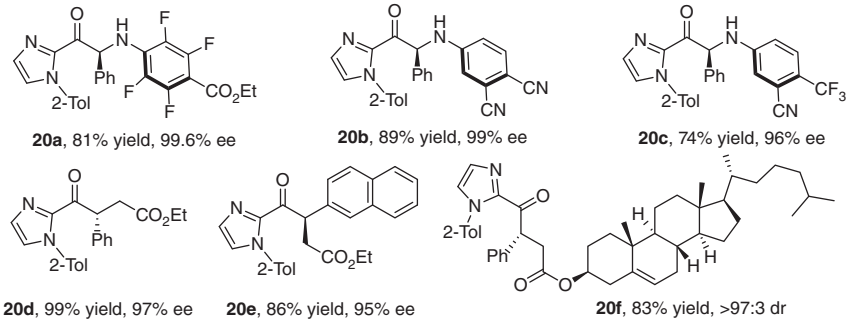


**Figure 11.9** Electrophilic nitrogen and carbon-centered radical interfacing with Rh-enolate: asymmetric α-amination and alkylation of 2-acylimidazoles.

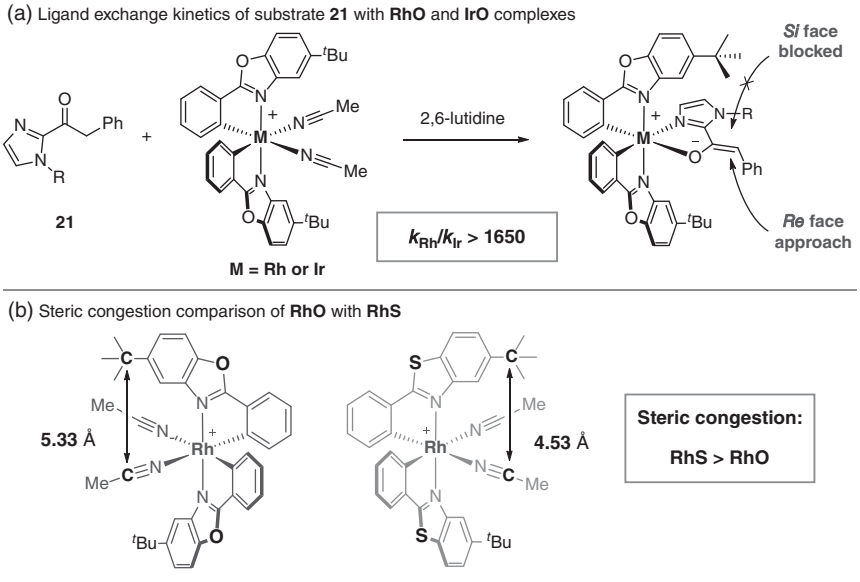


**Figure 11.10** Explanation for the catalytic activity difference of IrO, RhO, and RhS.

initial rate of acetonitrile ligand exchange by the substrate **21** within the **RhO** complex is over 1650 times higher than within the **IrO** complex [17a]. Meanwhile, the electrophilic radicals are known to be short-lived and prone to be reduced under redox conditions [19]. Therefore, the superiority of **RhO** over **IrO** in asymmetric radical reactions can be attributed to the significantly faster turnover frequency of the catalytic cycle with **RhO**. This higher turnover frequency allows **RhO** to effectively keep pace with the short-lived electrophilic free radicals. The crystallography analysis suggests that the quaternary carbon of the *tert*-butyl group within **RhS** is in closer proximity to the carbon of acetonitrile by 0.8 Å than that of **RhO** [17b]. This observation can be traced back to the increased C—S bond length compared to the C—O bond length, which positions the two *tert*-butyl groups closer to the substrate coordination site. In addition, the co-crystal structure analysis of rhodium bound enolate intermediate reveals that the *Si* face of the prochiral C($sp^2$) is sterically shielded by the *tert*-butyl groups of the $C_2$ symmetric **RhO**, while the *Re* face can be readily approached [20]. Collectively, the improved ligand exchange kinetics of rhodium over iridium and the increased steric congestion of **RhS** over **RhO** enable the high asymmetric induction of **RhS**.

In 2019, Xu and coworkers realized an enantioselective α-difluoroalkylation of 2-acyl imidazoles **1** with bromodifluoroacetamide **22** by merging visible-light photocatalysis and chiral-at-Rh Lewis acid catalysis (Figure 11.11) [21]. As shown in the outlined mechanism, the stereocontrolled addition of the fluorinated carbon-centered radical generated from the photocatalysis to the rhodium enolate intermediate **II** gives the ketyl radical **III**. The subsequent oxidation of this ketyl radical by the photoexcited catalyst produces a Rh-coordinated product **IV**, which is followed by a ligand exchange to release the difluoroalkylated product **23**. In consistent with the previous observation, the chiral-at-Ir complex failed to enable this transformation.

Structural diversification of chiral-at-Rh complexes was further developed to meet the request for enabling diverse asymmetric radical reactions. Relying on the seminal Rh-based Lewis acids [9b, 17b, 20], the Meggers group designed a new chiral-at-rhodium catalyst with two cyclometalated 6-*tert*-butyl-2-phenyl-2*H*-indazole ligands, which served the dual function of a precursor for *in-situ* assembled photocatalyst and the chiral Lewis acid catalyst (Figure 11.12) [22]. This newly developed chiral **RhInd** could promote the enantioselective α-cyanoalkylation of 2-acylimidazoles **1** and showcased superior catalytic activity over the previous **RhS** and **IrS**. The higher ligand exchange kinetics of **RhInd** over **IrS** and the slower unstereocontrolled $S_N2$ background reaction with **RhInd** to **RhS** can account for the good catalytic performance.

Photoredox-generated radicals after undergoing further single electron oxidation can lead to electrophilic species such as imines or iminium ions which can then interface with rhodium-enolate intermediate. In 2015, Meggers and Gong reported a photoinduced asymmetric aerobic dehydrogenative cross-coupling of 2-acyl imidazoles **1** with glycine esters **26** or *N*-methyl anilines **27** [23]. Autoxidation of glycine esters **26** or the rhodium complex enabled photo-oxidation of *N*-methyl anilines **27** under air atmosphere furnished the corresponding imines or iminium ions. The

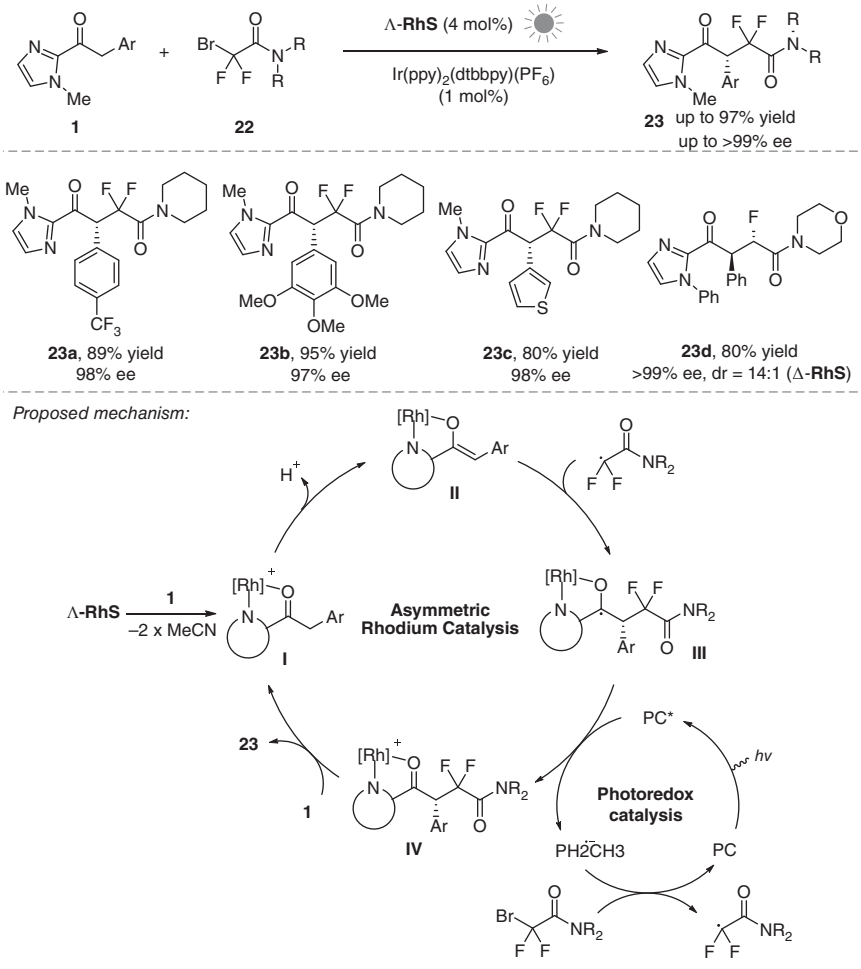


**Figure 11.11** Electrophilic difluoroalkyl radical interfacing with Rh-enolate: α-difluoroalkylation of 2-acyl imidazoles.

following C-C bond formation with 2-acyl imidazoles **1** under chiral-at-Rh Lewis acid catalysis produced the enantioenriched γ-amino carbonyl compounds **28** or **29** with excellent stereoselectivities, respectively (Figure 11.13).

#### 11.3.1.2 Nucleophilic Radicals Interfacing with Rhodium-Enone

The conjugate addition of a carbon-centered radical to an α,β-unsaturated alkene is defined as the Giese reaction [24]. The remarkably low energy barrier of C—C bond formation in this reaction makes the stereocontrol a formidable challenge in asymmetric catalysis. The seminal work by Sibi and coworkers demonstrates that chiral Lewis acid is a promising tool for high stereocontrol in Giese reaction [25]. Yoon and coworkers reported a pioneering study that dual chiral Lewis acid and photoredox catalysis could enable asymmetric Giese reaction with excellent enantioselectivities [26]. Meanwhile, the structurally unique chiral-at-Rh Lewis

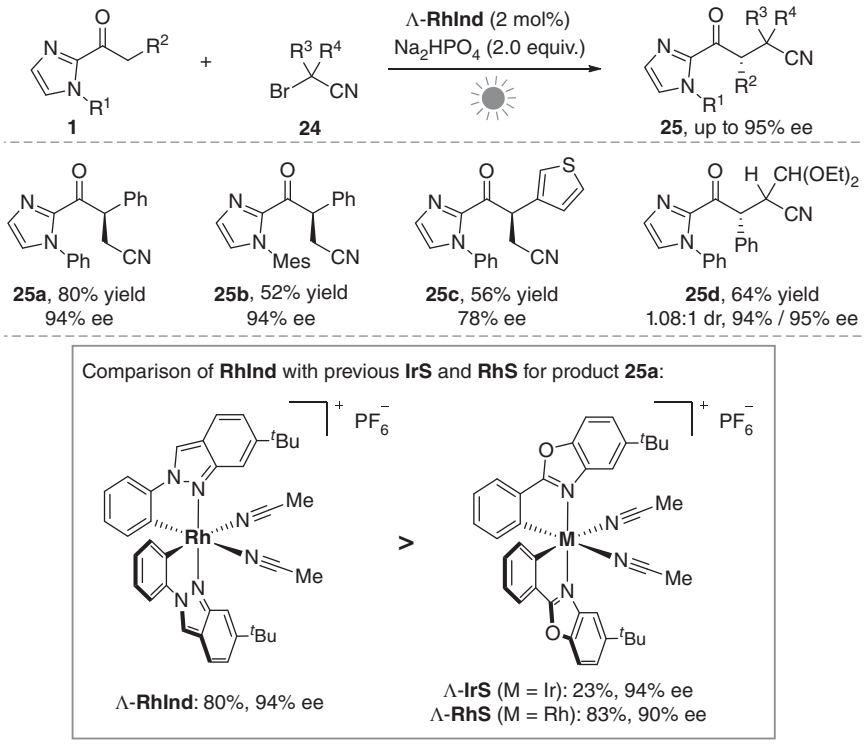


**Figure 11.12** Electrophilic cyanoalkyl radical interfacing with Rh-enolate intermediate: α-cyanoalkylation of 2-acylimidazoles with an advanced chiral-at-Rh complex.

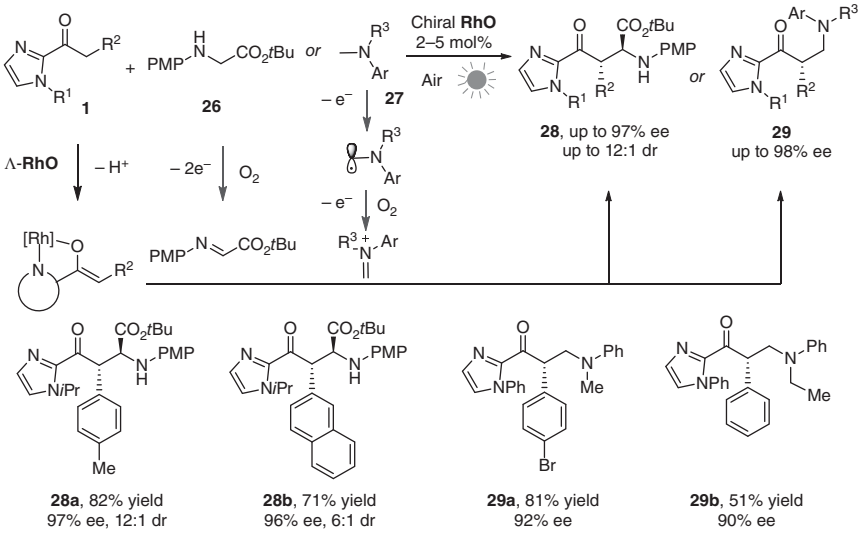


**Figure 11.13** Imine or iminium ion interfacing with Rh-enolate: asymmetric α-aminoalkylation.

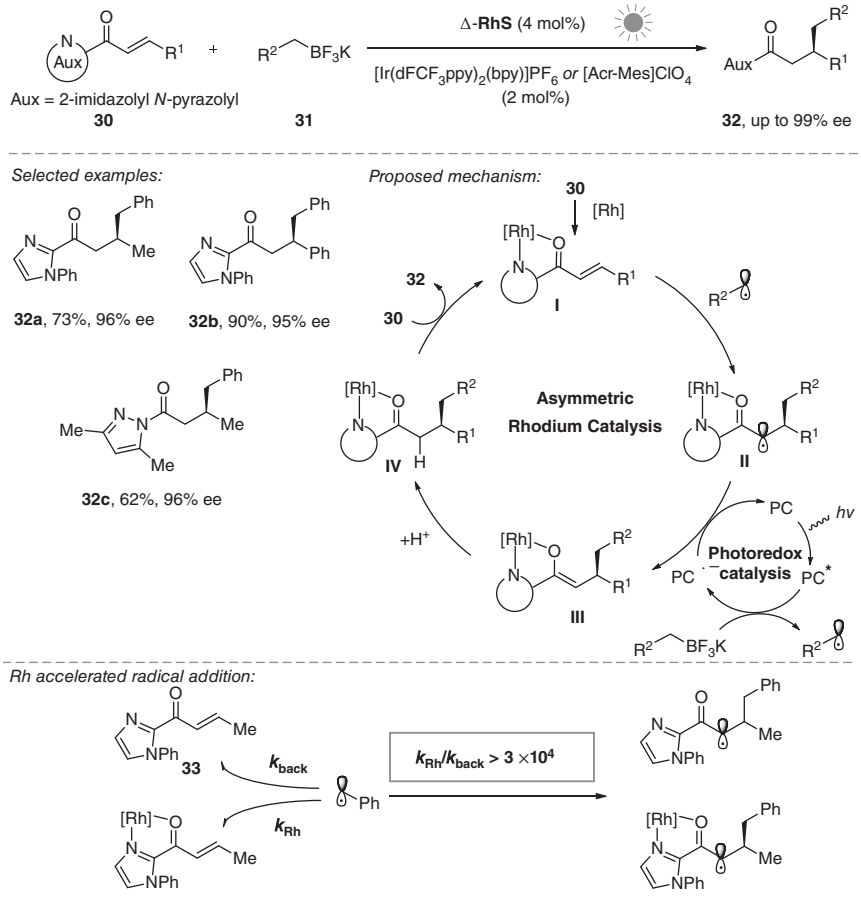


**Figure 11.14** Nucleophilic radical interfacing with Rh-enone: asymmetric β-alkylation of unsaturated alkenes.

acid developed by Meggers and coworkers was proven a privileged chiral catalyst for triggering asymmetric Giese reaction (Figures 11.14 and 11.15) [7b]. In 2016, Meggers and coworkers demonstrated that the alkyl radicals which were generated by the single-electron oxidation of organotrifluoroborates **31**, could undergo enantioselective addition to electron-deficient alkenes **30** under cooperative chiral-at-Rh Lewis acid and photoredox catalysis [27]. Excellent enantioselectivities (up to 99%) were obtained with the chiral catalyst loading of merely 4 mol%. Mechanistic investigations suggested that the chiral-at-Rh Lewis acid could accelerate the radical conjugate addition rate by 4–5 orders of magnitudes over the non-catalyzed background reaction, which was further supported by the Wiest group's computational study [28].

Next, various radical precursors were found to be applicable in this catalytic asymmetric Giese reaction (Figure 11.16). For example, the single-electron reduction of *N*-alkoxyphthalimides **34** by *fac*-Ir(ppy)$_3$ provides the oxygen-centered

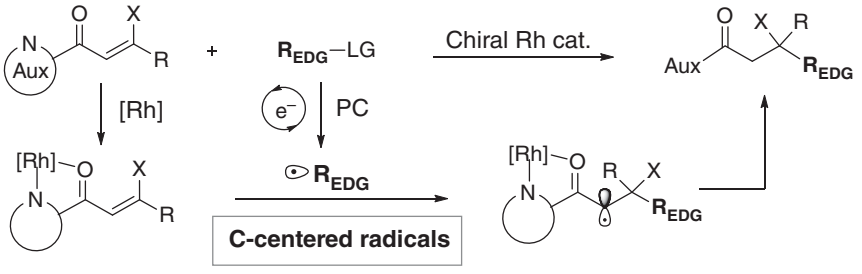


**Figure 11.15** A general blueprint of nucleophilic radical interfacing with Rh-enone: asymmetric Giese reaction.

radical species which then undergo an intramolecular 1,5-hydrogen atom transfer (HAT) to give alkyl radicals [29]. The chiral-at-Rh Lewis acid catalysis then enables an enantioselective conjugate addition of these alkyl radicals to enones **30**. Alternatively, glycine-derived *N*-acyloxy phthalimides **36** undergo the photoinduced decarboxylation with Hantzsch ester (HE) as photoredox mediator, leading to α-aminoalkyl radicals which are also applicable in the chiral-at-Rh Lewis acid-catalyzed Giese reaction [30]. Notably, a fluorinated quaternary stereocenter is accessible for the first time in the catalytic asymmetric Giese reaction. Except for the phthalimides, Hantzsch esters are also suitable redox handles for the production of alkyl radicals and have been applied in this transformation [31].

The direct cleavage of a C—H bond is unarguably a sustainable method for accessing alkyl radicals and this strategy is also compatible with the chiral-at-Rh Lewis acid-catalyzed Giese reaction. Kang and coworkers reported that the direct single-electron oxidation of tertiary amines **39** could afford the α-aminoalkyl radicals which were then involved in the asymmetric Giese reaction [32]. Wu, Meggers, and coworkers demonstrated that photoexcited neutral Eosin Y could enable hydrogen atom transfer (HAT) of C—H bonds within diverse feedstocks such as aldehyde, acetal, tetrahydrofuran, aniline, phosphine oxide, and hydrosulfone, thus generating various radicals [33]. These intermediates could interface with enones **30** under the chiral-at-Rh Lewis acid catalysis, thus giving the corresponding enantioenriched β-carbonyl compounds **41**. Apart from the two-component asymmetric Giese reaction, Meggers and coworkers introduced a three-component version in which perfluoroalkyl sulfinates **42**, vinyl ethers **43**, and α,β-unsaturated *N*-acyl pyrazoles **30** were coupled to provide enantioenriched fluoroalkyl-containing compounds **44** with up to 98% ee [34].

### 11.3.2 Radicals Delocalized on the Ligand Sphere of Chiral-at-Rhodium Complexes

After binding with the chiral-at-rhodium complexes (operationally by deprotonation), acceptor-substituted ketones can undergo single electron reduction to give rhodium-bound ketyl or formal β-carbonyl radicals. Alternatively, with proper substituents such as cyclopropyl, the rhodium-bound ketyl radicals could be transformed into α or γ-carbonyl radicals. Meanwhile, α,β-unsaturated carbonyl

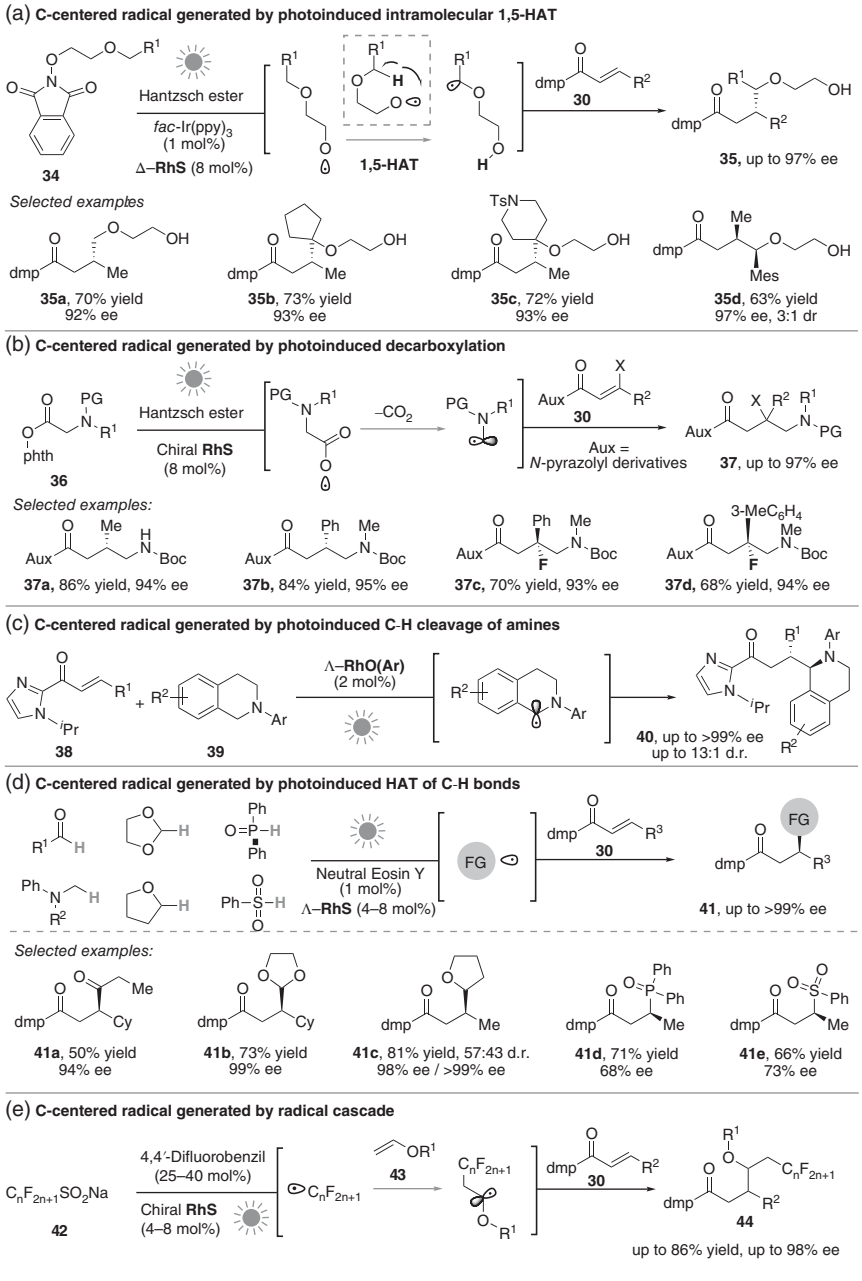


**Figure 11.16** Chiral-at-Rh complex catalyzed asymmetric radical conjugate additions with various radical precursors. Aux. = auxiliary; dmp = 3,3-dimethyl pyrazole.

compounds, binding with rhodium complexes, can be promoted to the excited state to give a biradical intermediate under direct photoirradiation. Overall, these radicals delocalize on the ligand sphere of the chiral-at-rhodium complexes and can interface with diverse trapping reagents such as alkenes, alkynes, or a second dissociated free radical, to produce enantioenriched products. The ligand sphere radicals generated by single electron transfer (SET) or direct photoexcitation are discussed individually in this section.

#### 11.3.2.1 Ligand Sphere Radical by Single Electron Transfer of Rhodium Complexes

(1) Rh-bound ketyl radical

In 2016, Meggers and coworkers reported an asymmetric cross-coupling reaction between 2-acyl imidazoles **1** and α-silylmethylamines **45** under dual photoredox and chiral-at-Rh Lewis acid catalysis conditions, thus providing enantioenriched 1,2-amino alcohols **46** in excellent yields and enantioselectivities after desilylation (**Figure** 11.17**a**) [35]. In the proposed mechanism, the photoexcited $[Ru(II)]^*$ was reductively quenched by α-silylmethylamines **45** to give a highly reducing [Ru(I)], which promoted the efficient single electron reduction of rhodium-bound imidazolyl ketone. As a result, rhodium-bound ketyl radical was furnished and then underwent a stereocontrolled radical-radical cross-coupling with the α-amino alkyl radical. This transformation is related to the author's previous work using trifluoromethyl ketone under chiral-at-Ir photocatalysis [16], but encompasses an extended scope of aryl and alkyl ketones. This is ascribed to the higher catalytic activities of chiral-at-Rh complex in cooperation with an external photoredox catalyst.

In a subsequent report, Meggers, Chen, and coworkers demonstrated a photochemical α-deracemization of ketones in which a similar rhodium-bound ketyl radical was recognized as a key intermediate [36]. As outlined in **Figure** 11.17**b**, the chiral-at-Rh Lewis acid is initially coordinated by the pyridylketone **47** to produce the complex **I** which is the mixture of two diastereomers. Subsequently, it could be excited by visible light to deliver the excited intermediate $\mathbf{I}^*$ and the following reductive quenching by the tertiary amine **45** furnishes a Rh-bound ketyl radical **II**. Meanwhile, the tertiary amine **45** was converted to the amino radical cation which underwent hydrogen atom transfer with intermediate **II** to give a Rh-enolate intermediate **III** and a protonated amine. The following stereocontrolled proton transfer regenerates the rhodium-bound ketone as a single diastereomer. Dissociation of the enantioenriched ketone upon the coordination of a new substrate leads to the next catalytic cycle. The key to producing these ketyl radicals in these reports is the remarkable decrease of the LUMO of ketones after complexation with Rh-based Lewis acids, which renders the Rh-bound ketones more amendable for single electron reduction at both ground and excited states.

Notably, as shown by the mechanistic experiments in **Figure** 11.17**b,** the enantioenriched (*R*)-**47b** undergoes a remarkable racemization under the standard deracemization conditions rather than removing the visible light. Likewise, the

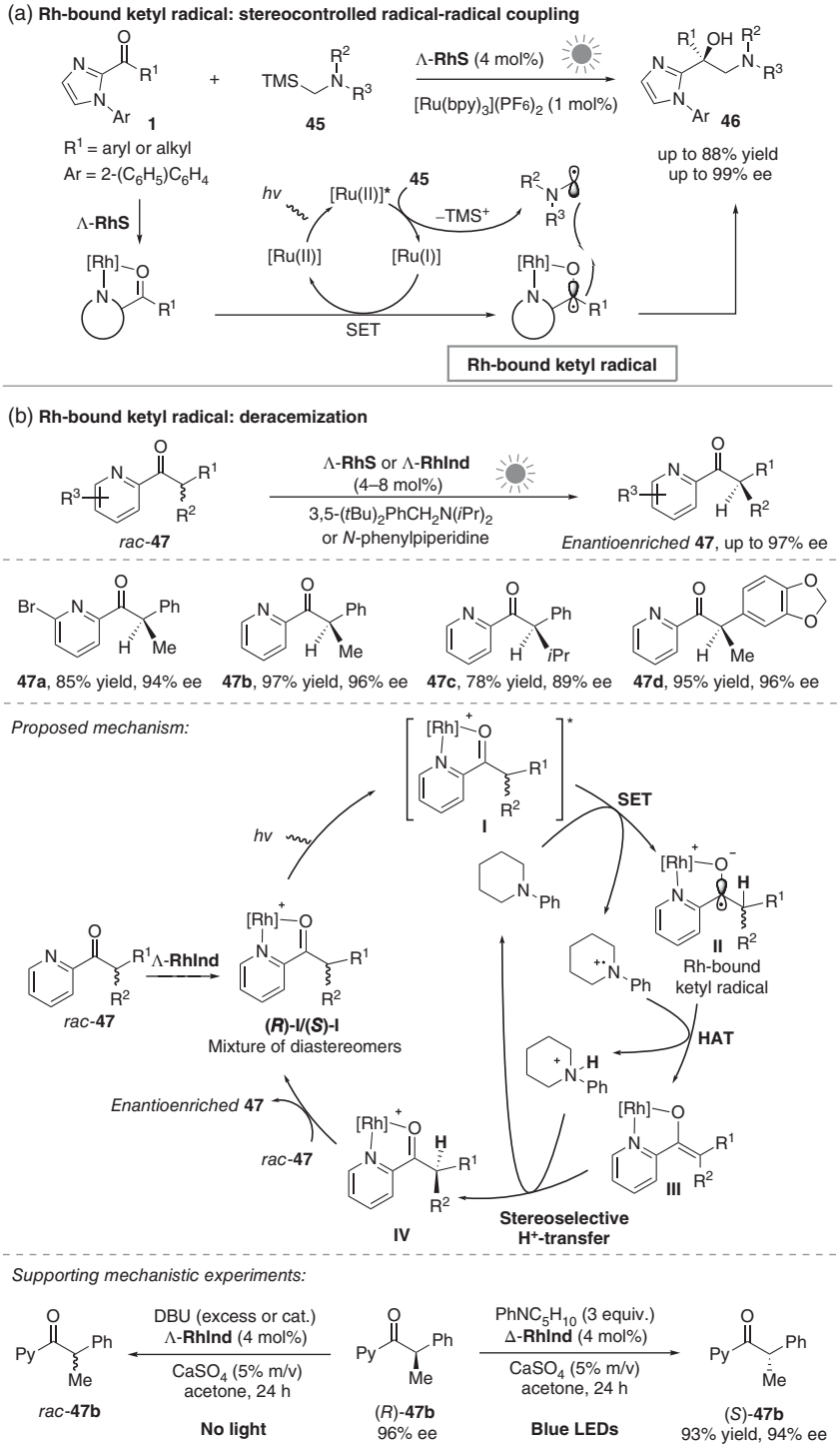


**Figure 11.17** Ligand sphere Rh-bound ketyl radical.

enantioenriched (*R*)-**47b** underwent a stereochemistry inversion thus producing (*S*)-**47b** under the standard photo deracemization conditions by using the mirror-imaged catalyst Δ-**RhInd**. These results suggested that a base-catalyzed deracemization is not feasible in the absence of light and the rhodium-bound ketyl radical is the intermediate involved.

(2) Rh-bound α-carbonyl radical

The ketyl radical can trigger the fragmentation of α-C—X bond, thereby generating a Rh-bound α-carbonyl radical, which can then be utilized in asymmetric radical transformations (For ketyl radical fragmented to γ-carbonyl radical, shown below). In 2019, Meggers and coworkers demonstrated an enantioconvergent cross-coupling of α-chloro 2-imidazolyl ketones **48** with *N*-aryl glycines **49** under photoinduced single chiral-at-Rh catalysis (**Figure** 11.18) [37]. As proposed by the authors,

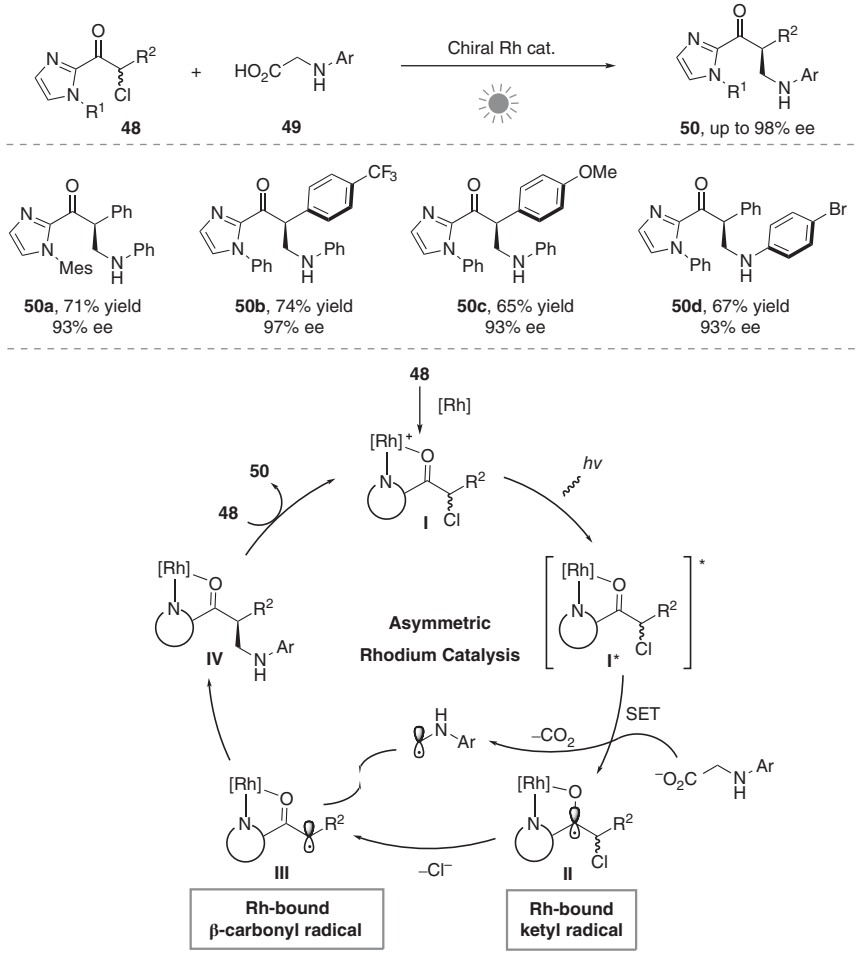


**Figure 11.18** Ligand sphere Rh-bound α-carbonyl radical from ketyl radical triggered fragmentation.

the Rh-substrate complex **I** can be directly photoexcited and then be reductively quenched by the *N*-aryl glycinate, thus providing a Rh-ketyl radical intermediate **II**. This species then undergoes fast dechlorination to give the Rh-bound α-carbonyl radical (**III**). Meanwhile, an α-aminoalkyl radical is generated from the *N*-aryl glycinate oxidation under the release of $CO_2$. The subsequent enantioselective radical-radical cross-coupling proceeds under the asymmetric induction of Rh chirality to give the C—C formation intermediate **IV**. Ligand exchange between a new substrate **48** and the product **50** leads to a new catalytic cycle.

The rhodium-bound α-carbonyl radical can also be produced by single electron oxidation of the corresponding enolate intermediate. In 2018, Meggers and coworkers demonstrated an asymmetric oxidative cross-coupling of 2-acyl imidazoles **51** with silyl enol ethers **52** under electrochemical conditions [38]. As outlined in **Figure** 11.19, a rhodium-enolate intermediate (**II**) is generated by the coordination of substrate **51** to the Rh Lewis acid, followed by deprotonation. This intermediate is then oxidized in anode to furnish the key Rh-bound α-carbonyl radical, which is subsequently trapped by a silyl enol ether in a stereocontrolled fashion. The newly afforded radical intermediate **IV** undergoes a second anodic oxidation, followed by desilylation and substrate-product exchange to close the catalytic cycle.

In a following report, the same group demonstrated that the redox mediator ferrocene (FC) was employed to enable the single electron oxidation of Rh-enolate intermediate under electrochemical conditions, thus giving the key rhodium-bound α-carbonyl radical (**Figure** 11.20) [39]. The subsequent radical trapping with the alkenyl trifluoroborate **54**, single electron oxidation, and $BF_3$ elimination sequence affords the product **55** with excellent enantioselectivities. A remarkable α-carbonyl radical trapping experiment with TEMPO delivers the TEMPO-adduct **57** with 98% yield and 73% ee, which provided strong evidence for the existence of rhodium-bound α-carbonyl radical. Upon hydrogenation and imidazolyl cleavage of the alkylation product **55e**, an enantiopure carboxylic acid **59** was obtained with 99.5% ee. Compound **59** was the key intermediate for synthesizing the cathepsin K inhibitor **60**, which was previously accessed by multiple recrystallization and acidification from the corresponding racemic mixture with a chiral amine auxiliary [40].

(3) Rhodium-bound β-carbonyl radical

The single electron reduction of the rhodium-enone can furnish the corresponding rhodium-bound β-carbonyl radical which then undergoes enantioselective C—C or C—N bond formation. In 2017, Meggers and coworkers reported an asymmetric coupling reaction of α,β-unsaturated *N*-acyl pyrazoles **61** and allyl sulfones **62** with rhodium-bound β-carbonyl radical as the key intermediate (**Figure** 11.21**a**) [41]. As proposed by the authors, LUMO-lowering activation of **61** by the Rh Lewis acid coordination facilitates an efficient single electron reduction by the photoexcited Hantzsch ester, thus leading to the formation of a rhodium-bound β-carbonyl radical. The subsequent enantioselective trap by the allyl sulfone **62** gives the allylation

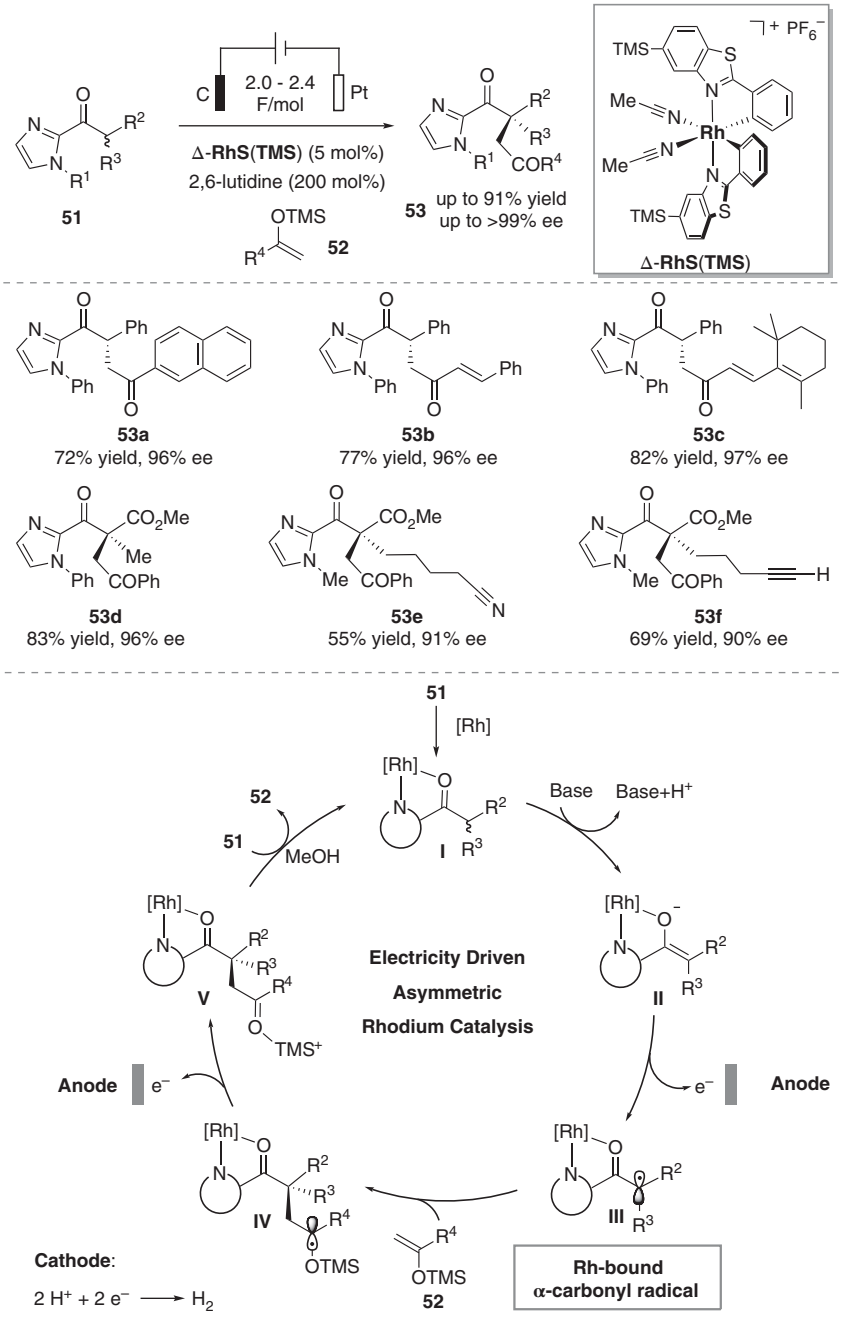


**Figure 11.19** Ligand sphere Rh-bound α-carbonyl radical via single electron oxidation of enolate under electrochemical conditions: asymmetric α-alkylation of 2-acylimidazoles.

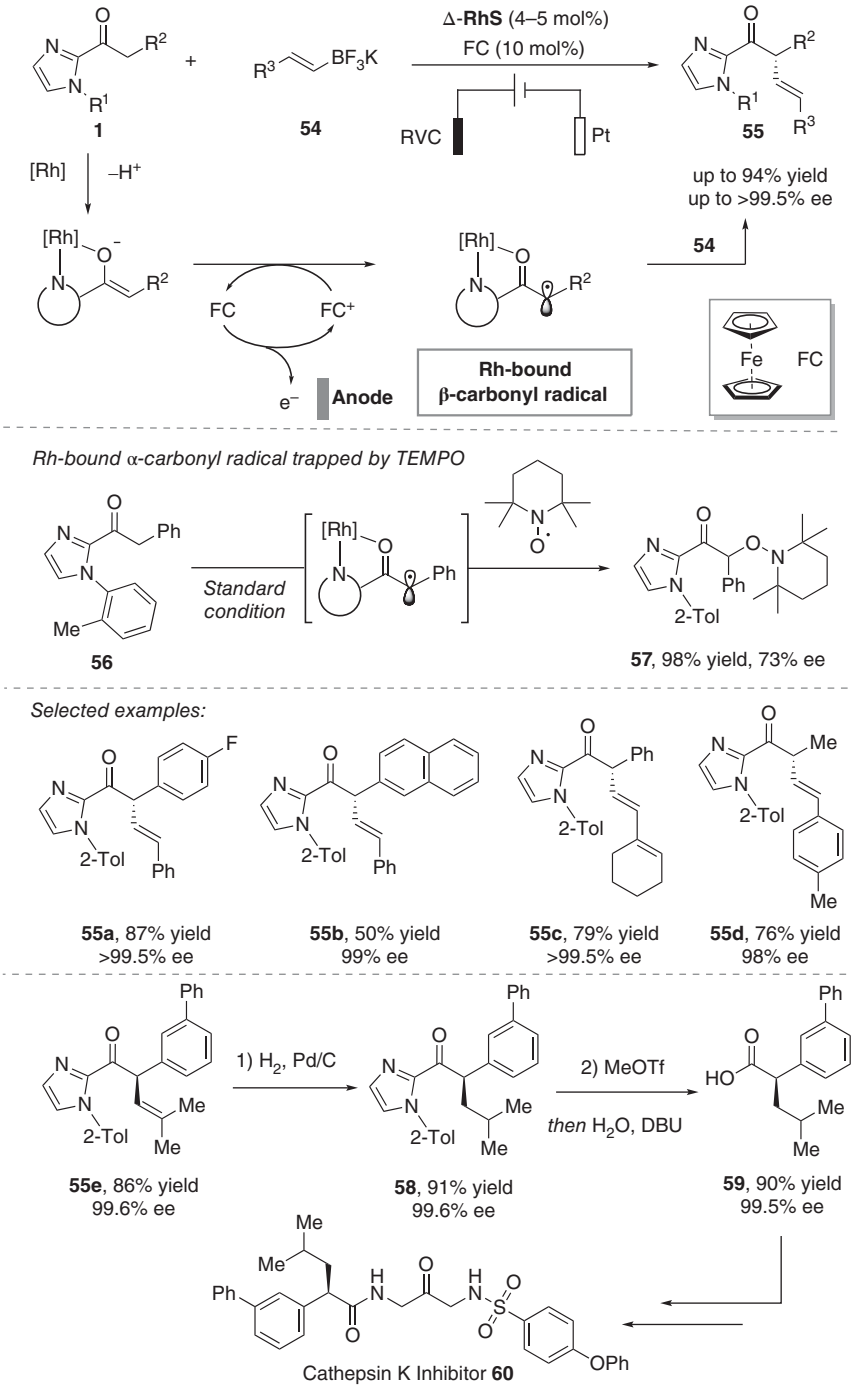


**Figure 11.20** Ligand sphere Rh-bound α-carbonyl radical via single electron oxidation of enolate under electrochemical conditions: asymmetric α-alkenylation of 2-acylimidazoles.

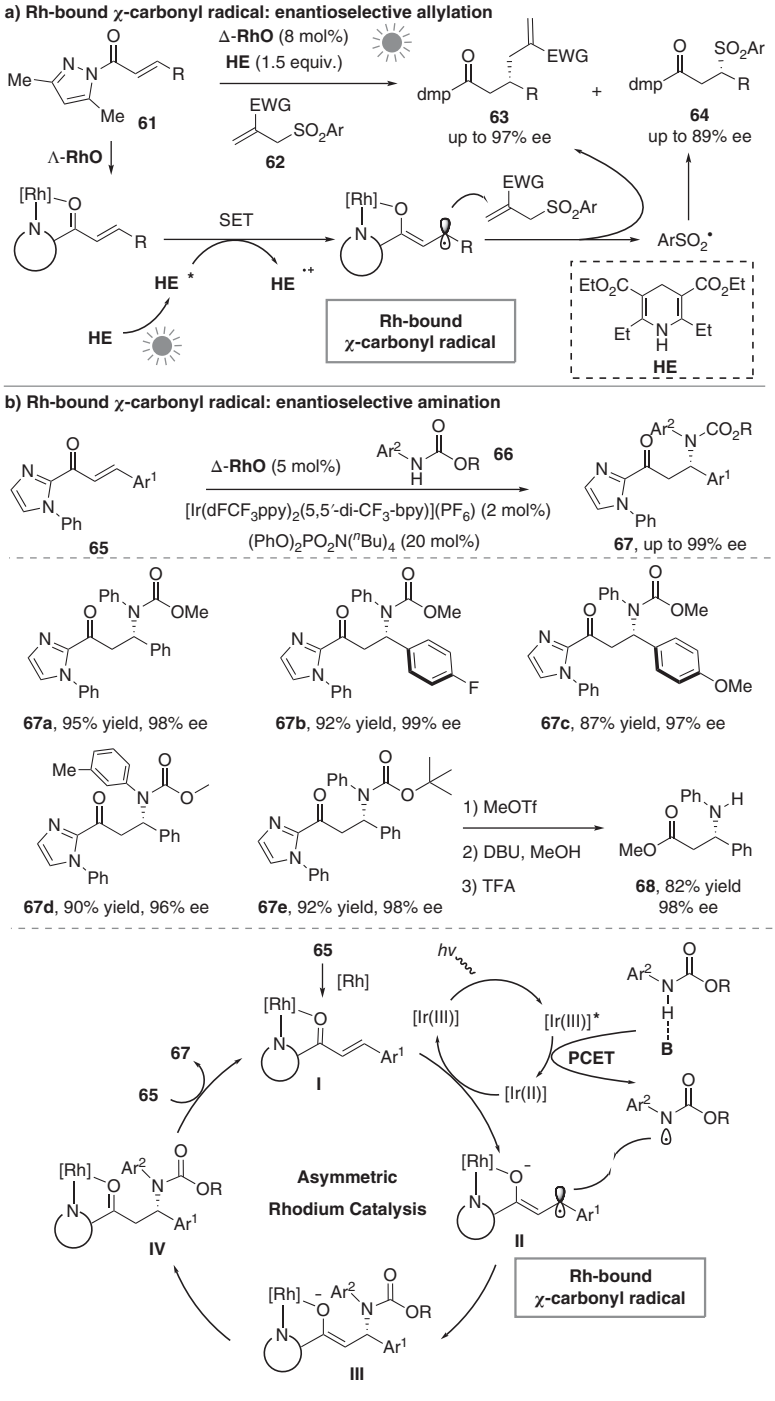


**Figure 11.21** Ligand sphere Rh-bound β-carbonyl radical via single electron reduction of enone.

product **63** under the release of a sulfonyl radical, which then adds to a second rhodium-enone to produce the enantioenriched sulfone **64**.

In addition, the rhodium-bound β-carbonyl radicals can interface with nitrogen-centered radicals to generate enantioenriched β-amino acid derivatives with excellent yields and enantioselectivities (**Figure** 11.21**b**) [42]. As proposed by the authors, the reaction relies on the cooperative Lewis acid and photoredox catalysis. Accordingly, the photoexcited iridium catalyst [Ir(III)]* is reductively quenched by the base-associated **66** through a proton-coupled electron transfer (PCET) pathway. As a result, a carbamoyl radical and a highly reducing [Ir(II)] species are afforded. This [Ir(II)] species then interfaces with the Lewis acid catalytic cycle by enabling the single electron reduction of the Rh-enone **I** to give the key rhodium-bound β-carbonyl radical **II**. The ultimate stereocontrolled radical-radical cross-coupling with the carbamoyl radical, followed by protonation and ligand exchange in rhodium complexes, leads to the enantioenriched β-amino acid derivative **67**.

Even though the single electron reduction of enone under Rh Lewis acid catalysis and redox conditions is a powerful avenue to the β-carbonyl radical, the more sustainable and ideal path is the direct conversion of the β-carbonyl C($sp^3$)—H to the corresponding radical. In 2017, Meggers and coworkers accomplished this goal by demonstrating an asymmetric β-C—H functionalization reaction between 2-acyl imidazoles/pyridines **68** with 1,2-dicarbonyls **69** (**Figure** 11.22). Excellent enantioselectivities (up to >99% ee) and diastereoselectivities (up to >20:1 dr) were obtained [43]. The auxiliary imidazolyl can be readily removed under mild conditions to give an enantioenriched lactone **71** with retained enantioselectivity and diastereoselectivity. Mechanistically, the single rhodium complex is proposed to intertwine the dual function of photoredox and asymmetric catalysis. As outlined in **Figure** 11.22, substrate **68** binds with rhodium Lewis acid to deliver a Rh-enolate intermediate **II** which is a highly reducing species after photoexcitation. The single electron transfer from photoexcited intermediate **II** to **69** furnished intermediate **III** and a ketyl radical. The following β-deprotonation provides the formal β-carbonyl radical **IV** which then undergoes a stereocontrolled radical-radical recombination. The subsequent protonation and substrate-product exchange sequence leads to a new catalytic cycle.

This sustainable fashion for producing a β-carbonyl radical from the corresponding C($sp^3$)—H bond was further extended to the synthesis of enantioenriched pyrroline derivatives. In 2021, Alemán and coworkers found that the chiral-at-Rh Lewis acid could cooperate with an additional photoredox catalyst to enable the asymmetric cascade cyclization of 2-acyl imidazoles/pyridines **68** with imines **72** (**Figure** 11.23). The pyrroline derivatives **73** were obtained with excellent enantioselectivities [44]. Mechanistic investigations suggest that the formation of the key β-carbonyl radical **III** might be achieved by DABCO radical cation-enabled hydrogen atom transfer (HAT) from the corresponding C($sp^3$)—H bond. Meanwhile, the α-amino radical is formed by single electron reduction of the imines under the cooperative photoredox catalysis. The following stereocontrolled cross-coupling of

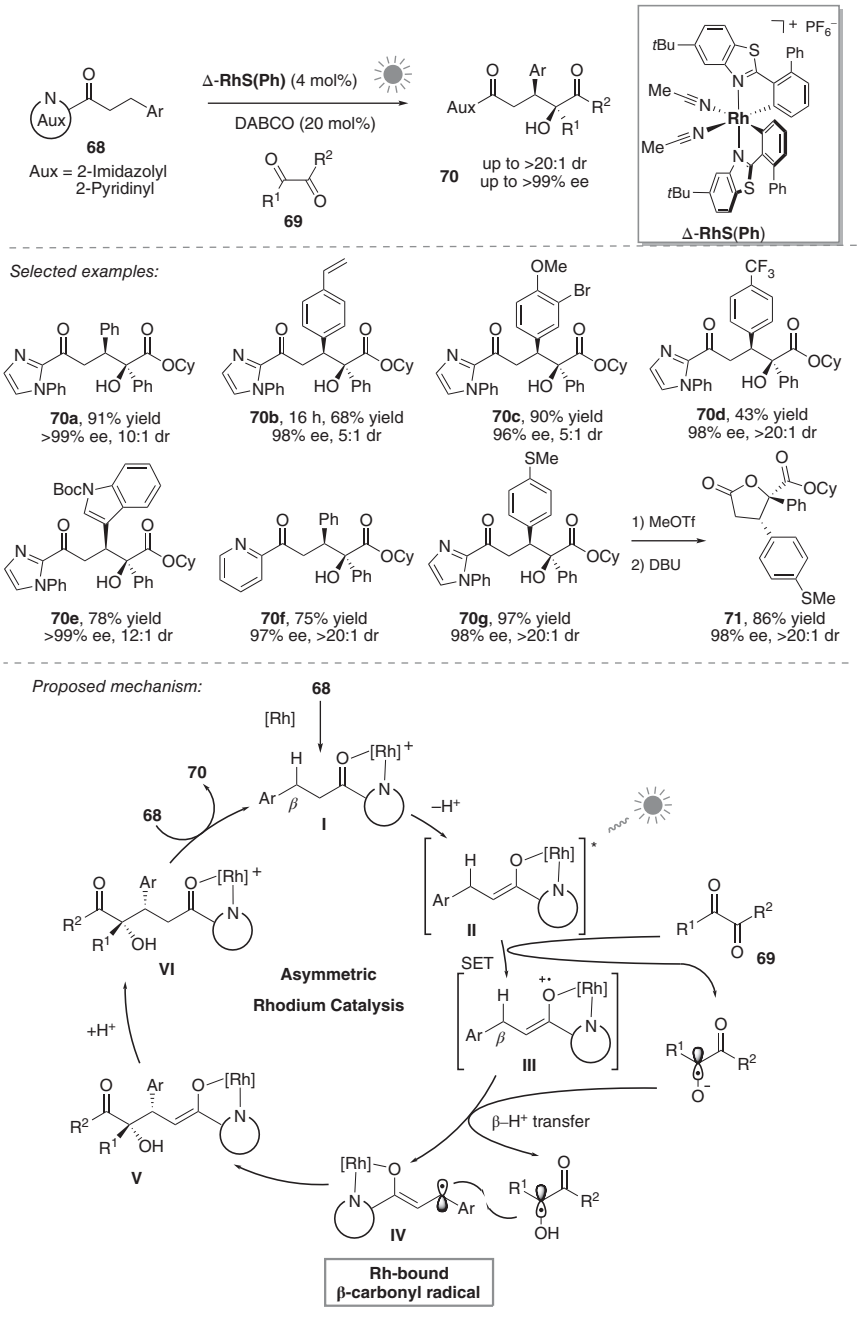


**Figure 11.22** Ligand sphere Rh-bound β-carbonyl radical from C(sp3)-H: stereocontrolled coupling with carbonyls.

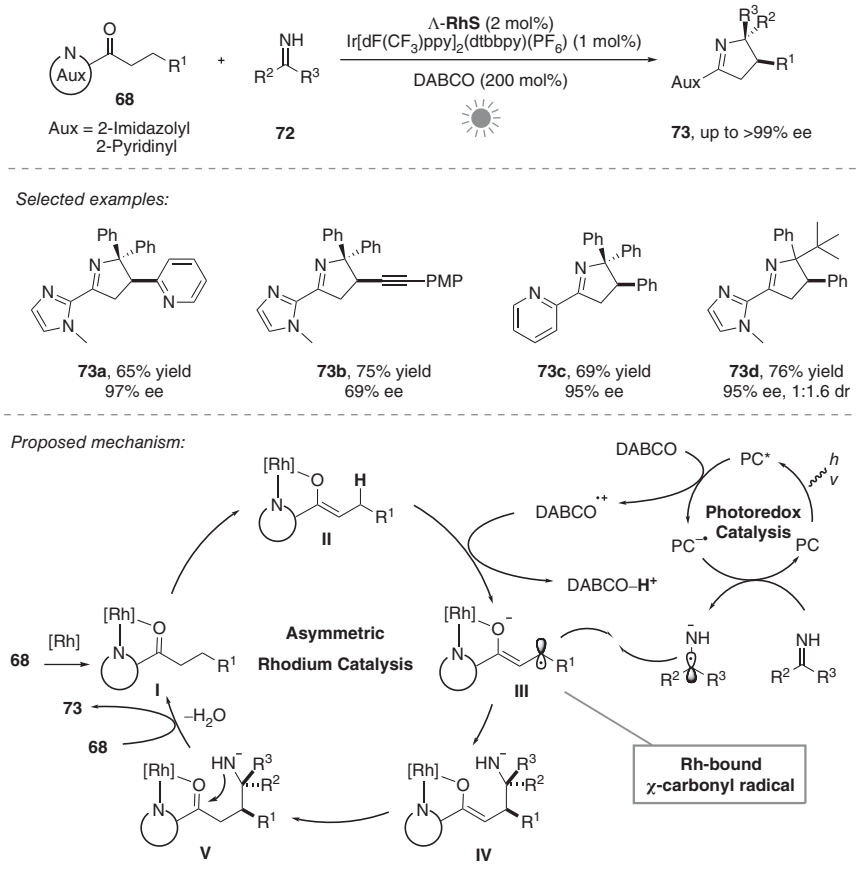


**Figure 11.23** Ligand sphere Rh-bound β-carbonyl radical from C(sp3)-H: stereocontrolled coupling with imines.

β-carbonyl radical **III** with α-aminoalkyl radical furnishes the intermediate **IV**. The sequence of protonation, intramolecular cyclization and dehydration provides the terminal product **73** after release from the rhodium center.

(4) Rh-bound γ-carbonyl radical

Compared to the ahead rhodium-bound ketyl and formal α or β-carbonyl radicals, achieving a controllable Rh-bound γ-carbonyl radical is more challenging but offers significant potential for further unprecedented transformations. In 2018, Meggers and coworkers reported that the Rh-bound γ-carbonyl radical can be obtained through the rearrangement of corresponding cyclopropyl adjacent Rh-bound ketyl radical (**Figure** 11.24) [45]. The furnished Rh-bound γ-carbonyl radical can interface with alkenes or alkynes through asymmetric [3+2] cycloadditions, thus leading to enantioenriched cyclopentane (**77**) and cyclopentene (**78**) derivatives, respectively.

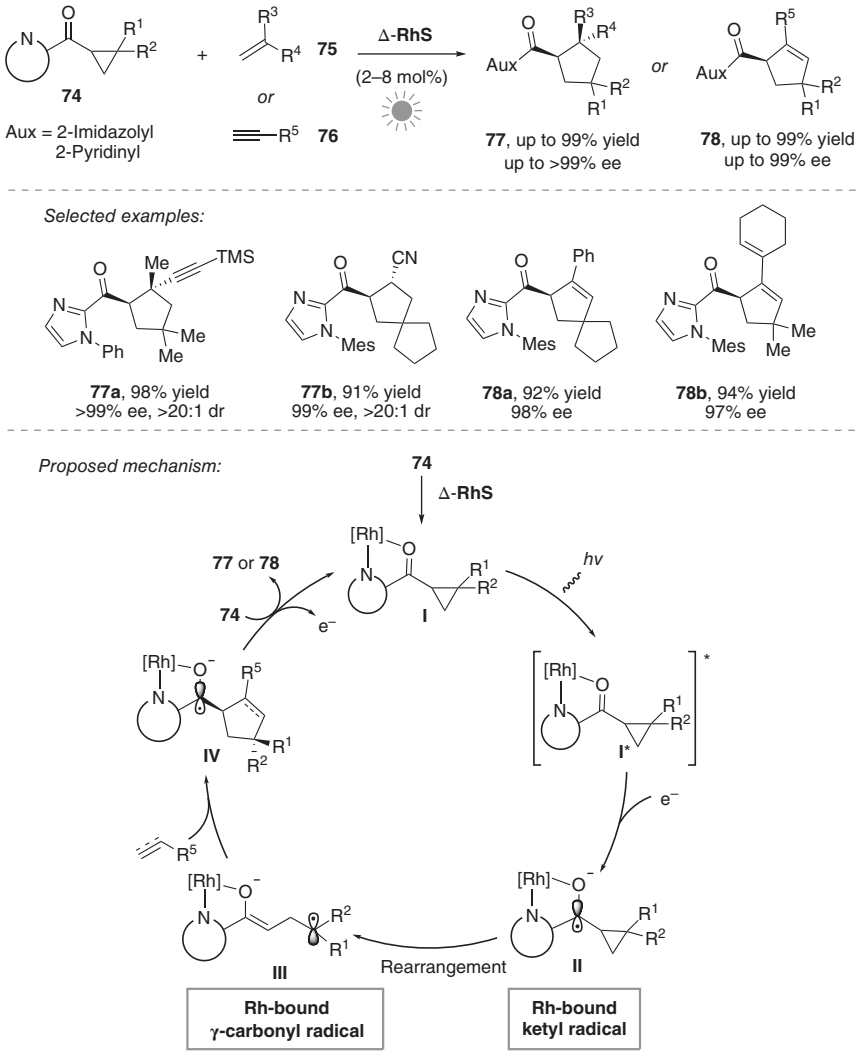


**Figure 11.24** Ligand sphere Rh-bound γ-carbonyl radical from C(sp3)-H from ketyl radical triggered fragmentation: stereocontrolled [3+2] cycloadditions.

### 11.3.2.2 Ligand Sphere Biradical by Direct Photoexcitation of Rhodium Complexes

Enones can be irradiated to the excited state on the ligand sphere of photoactivated chiral-at-Rh complexes. These excited enones are recognized as delocalized biradical on the conjugated alkenes which can subsequently engage in diverse stereocontrolled cycloadditions. For example, by utilizing this biradical strategy, Meggers and coworkers demonstrated highly stereocontrolled [2+2] and [3+2] cycloadditions of enones **79** with alkenes **75** and vinyl azides **80**, thus providing enantioenriched cyclobutanes **81** and 1-pyrrolidines **82**, respectively (**Figure** 11.25) [46]. Up to three

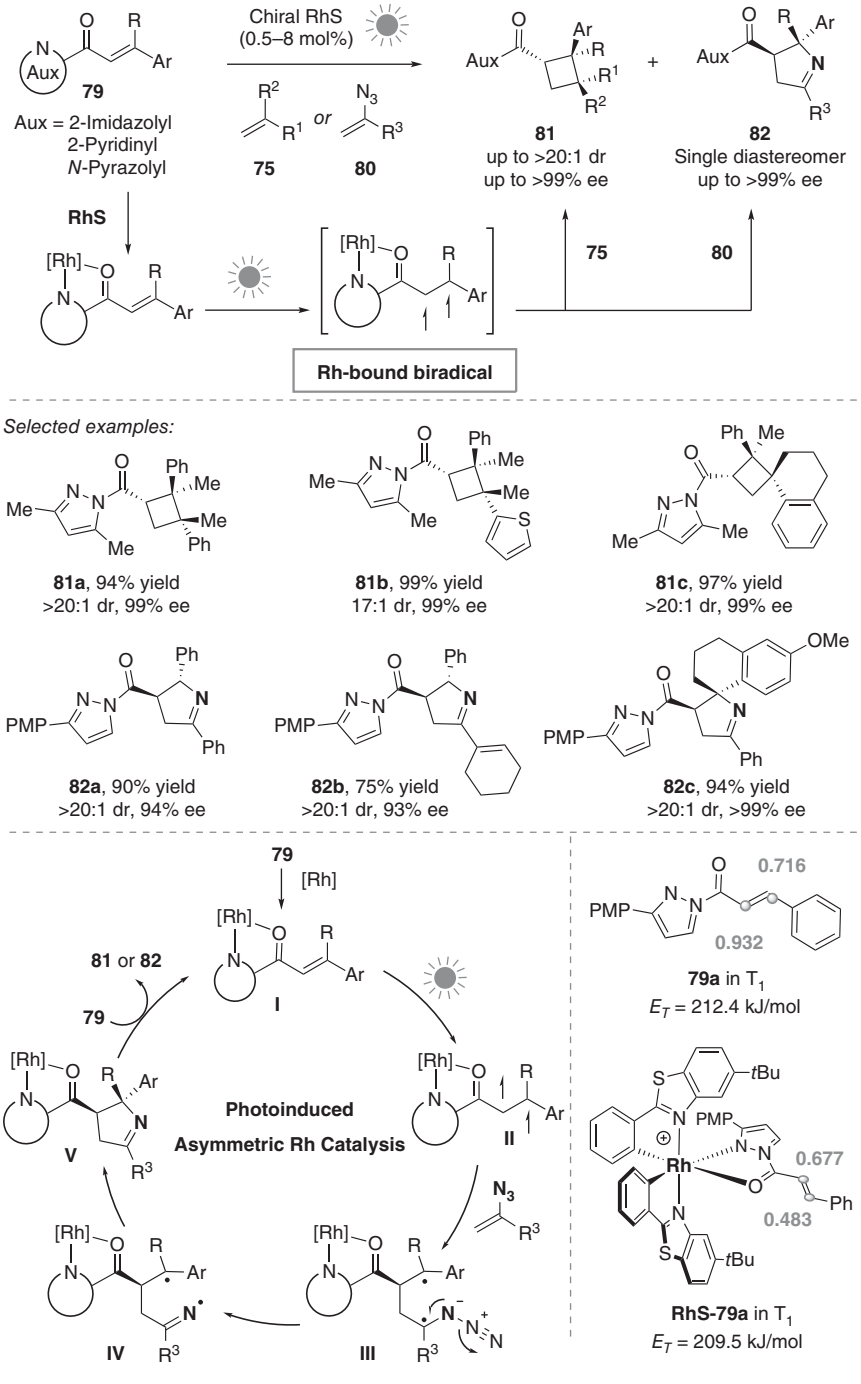


**Figure 11.25** Ligand sphere Rh-bound biradical: stereocontrolled [2+2] and [3+2] cycloadditions.

consecutive stereocenters and optionally all-carbon quaternary ones are readily accessible. The proposed catalytic cycle concerning the representative [3+2] photocycloaddition is presented to illustrate the reaction pathway. Initially, substrate **79** coordinates to the chiral-at-Rh Lewis acid through N,O-bidentate chelation, and the subsequent photoactivation irradiates the intermediate to the lowest singlet state. After intersystem crossing, the triplet excited state **II** is furnished and then interfaces with a vinyl azide **80** to give the 1,4-diradical intermediate **III**. This species then transforms into a 1,5-diradical intermediate **IV** with the release of $N_2$. The stereocontrolled carbon- and nitrogen-based radical-radical recombination gives the intermediate **V**. The subsequent ligand exchange of **82**→**79** in the rhodium complex leads to a new catalytic cycle. Computational study reveals that the spin density of both the excited substrate and rhodium complex **II** delocalize on the alkene sphere of the conjugated enone, thus suggesting a formal biradical intermediate. In a later report, the stereocontrolled [2+2] cycloaddition also proceeded smoothly under the photocatalysis of a non-$C_2$-symmetric chiral-at-Rh complex with two different cyclometalating ligands [47].

In 2021, Bach and coworkers reported a chiral-at-rhodium complex-enabled [2+2] photocycloaddition of 2-benzimidazolyl styryl sulfones **83** with 2,3-dimethyl-2-butene, providing sulfonyl-substituted cyclobutanes **84** (**Figure** 11.26) [48]. Although it provides moderate enantioselectivities, the asymmetric induction of the chiral-at-Rh catalyst is superior to that of other common chiral Lewis acids in this reaction.

In addition to the bimolecular [2+2] photocycloaddition, Bach and coworkers subsequently established an intramolecular version with the chiral-at-Rh catalyst (**Figure** 11.27) [49]. Substrate **84** underwent a smooth crossed [2+2] cycloaddition, thus giving enantioenriched bridged skeletons **85** which were otherwise difficult to obtain.

Meggers, Baik and coworkers further extended this photocycloaddition protocol from alkenes to aromatics (**Figure** 11.28) [50]. Various substituted benzofurans and benzothiophene underwent the stereocontrolled dearomative [2+2] photocycloaddition with styrenes to provide enantioenriched tricyclic products **88** with high yields and selectivities. Up to four consecutive stereocenters are accessible

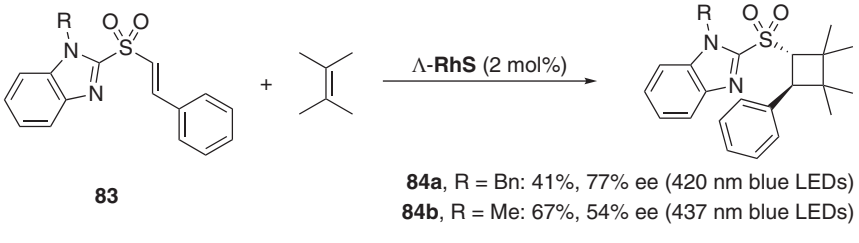


**Figure 11.26** Stereocontrolled [2+2] cycloadditions of 2-benzimidazolyl styryl sulfones with 2,3-dimethyl-2-butene.

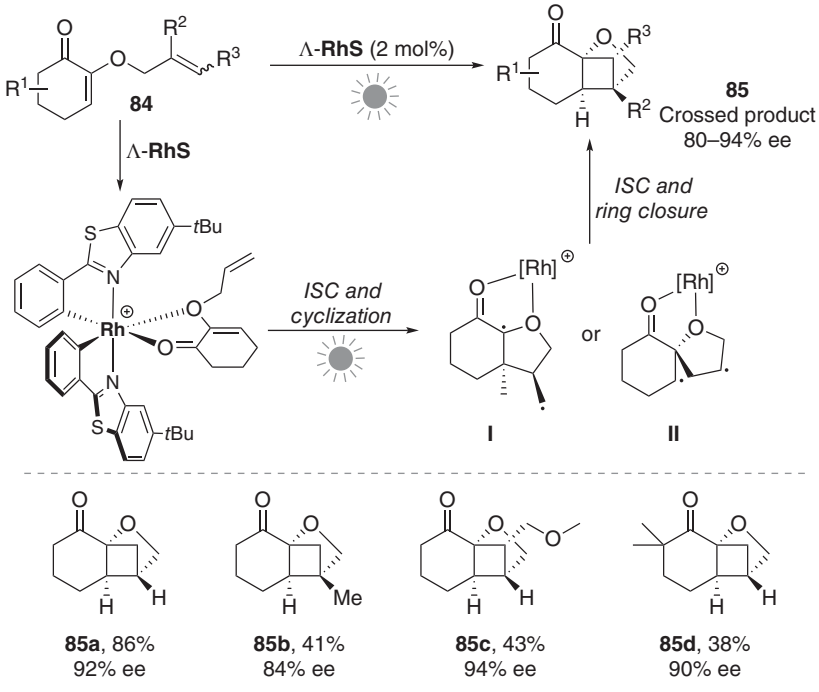


**Figure 11.27** Ligand sphere Rh-bound biradical: stereocontrolled intramolecular crossed [2+2] cycloadditions.

in which complete regio- and diastereoselectivities as well as excellent enantioselectivities are obtained. An unforeseen head-to-tail regioselectivity was observed, that can be traced back to the remarkable energy gap between two key 1,4-biradical intermediates.

Apart from the C—C bond formation, the enone biradical intermediate can abstract the hydrogen atom from aldehydes, thus triggering the subsequent asymmetric transformations. In 2019, Meggers, Houk and coworkers reported that 3-(2-formylphenyl)-1-pyrazol-1-yl-propenones **89** underwent a highly stereocontrolled rearrangement to furnish benzo-[*d*]cyclopropa[*b*]pyranones **90** under photoinduced chiral-at-Rh catalysis (**Figure** 11.29) [51]. Various enantioenriched products with 6-6-3 ring system were obtained as single diastereomers and up to >99% ee. As proposed by the authors, the intramolecular hydrogen atom transfer (HAT) within the photoexcited Rh-bound biradical leads to a ketene intermediate after intersystem crossing. The following hetero-Diels-Alder cycloaddition gives the terminal products along with the regeneration of the Rh-substrate complex.

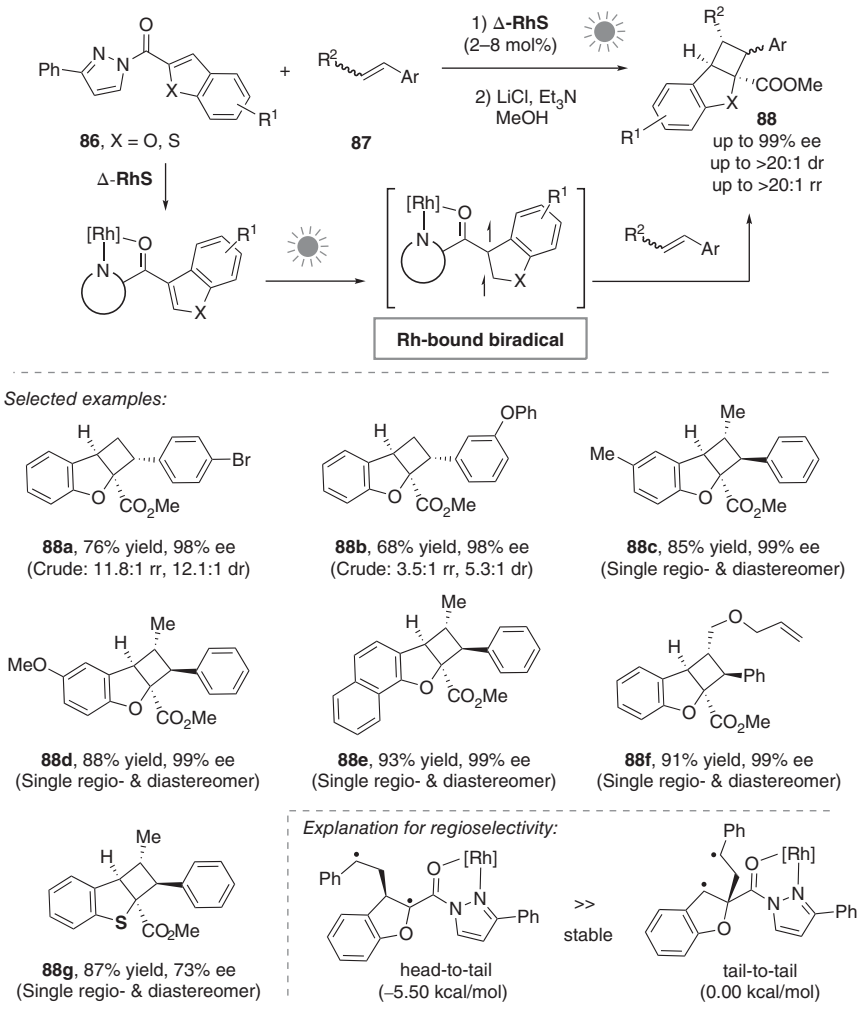


**Figure 11.28** Ligand sphere Rh-bound biradical: stereocontrolled dearomative [2+2] cycloadditions.

## 11.4 Asymmetric Radical Reactions Enabled by Substitutionally Inert Chiral-at-Iridium Complexes

Pioneering work by Meggers and coworkers has showed the significant value of chiral-at-metal complexes in photoinduced asymmetric radical reactions [7a, 7b]. These chiral-at-metal complexes are substitutionally labile and typically serve as Lewis acids to activate the corresponding substrate by coordination which lays the

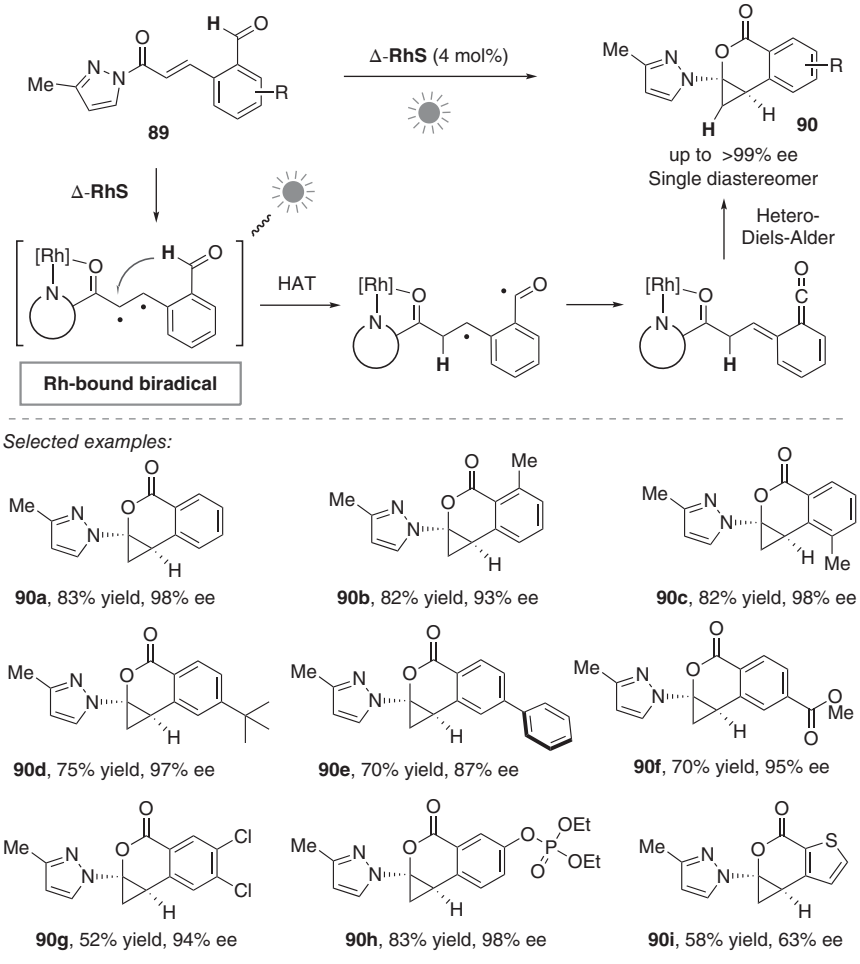


**Figure 11.29** Ligand sphere Rh-bound biradical triggered hydrogen atom transfer (HAT): stereocontrolled hetero-Diels-Alder cycloadditions.

foundation for high asymmetric induction. In contrast, although the seminal work by Meggers and Gong reveals that substitutionally inert chiral-at-metal complexes can be introduced as metal-templated "organocatalysts" to enable asymmetric reactions in the ground state [6a, 52], their application in asymmetric photocatalysis remains elusive. It was not until 2017 that Yoon and Baik demonstrated an elegant work showing that a substitutionally inert chiral-at-Ir complex was capable of catalyzing photochemical asymmetric intramolecular [2+2] cycloadditions (**Figures** 11.30 and 11.31**a**) [8a]. Mechanistic investigations revealed that the sole chiral-at-Ir complex Λ-**Ir-HB1** played a dual role of asymmetric hydrogen bonding and photosensitization catalysis. Accordingly, the NH moiety of pyrazolyl ligand interfaces with the amide group of the quinolone substrate by hydrogen bonding interaction. The cyclometalated ligand interacts with the quinolone by π–π stacking. These non-covalent interactions are responsible for the orbital overlap required for

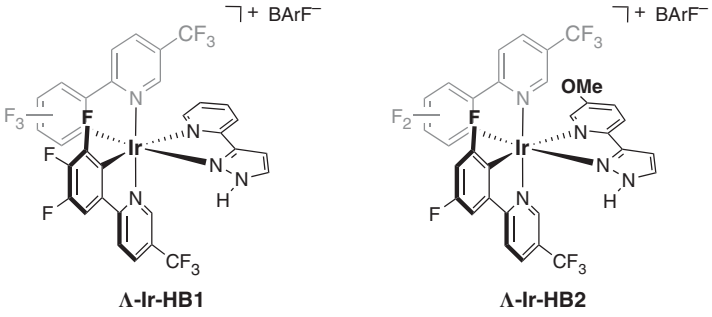


**Figure 11.30** Substitutionally inert chiral-at-iridium complexes used as chiral photosensitizers.

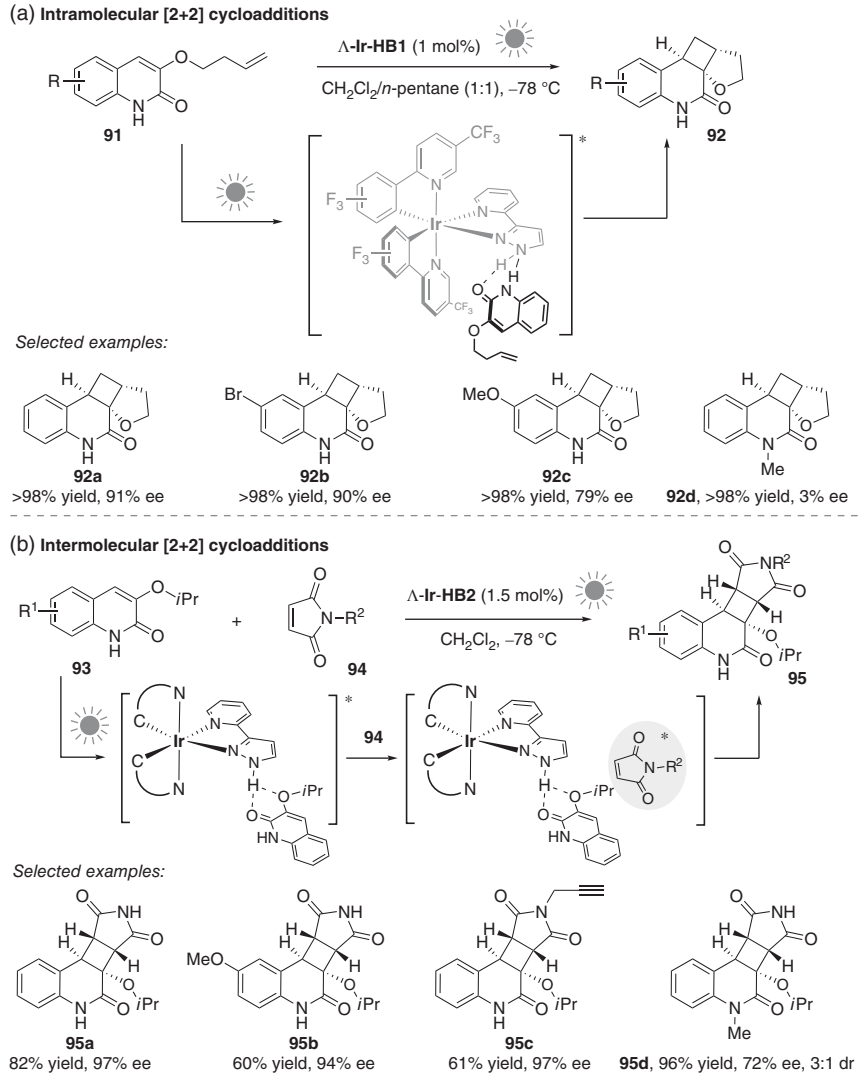


**Figure 11.31** Asymmetric [2+2] cycloadditions enabled by substitutionally inert chiral-at-iridium complexes.

triplet energy transfer between the chiral-at-Ir complex Λ-**Ir-HB1** and the substrates for the efficient asymmetric induction of the following [2+2] cycloaddition.

In a subsequent work, Yoon, Baik, and Meyer further extended this protocol to a bi-molecular [2+2] cycloadditions of quinolones **93** and maleimides **94** in excellent enantioselectivities (**Figure** 11.31**b**) [8b]. Different from the ahead photosensitization from chiral-at-Ir complex to the hydrogen bonding bound quinolone pathway, the excited state iridium complex Λ-**Ir-HB2** preferentially sensitizes the maleimide **94**. The following [2+2] cycloaddition still proceeds under the metal chirality-mediated chiral environment. Mechanistic experiments support an alternative hydrogen bonding fashion of the pyrazolyl with the two oxygen atoms of quinolone **93**, which is different from the author's precedent report [8a]. Computational investigations reveal that this bonding mode is the lowest-energy version and doesn't favor the orbital overlap required for triplet energy transfer to quinolone **93**. As a result, the triplet energy transfer to maleimide **94** is feasible.

In 2022, Yoon and Toste further disclosed that a hydrogen-bond free, substitutionally inert chiral-at-Ir complex **Δ-Ir-PS** could cooperate with a chiral Brønsted acid to achieve the photoinduced stereocontrolled [2+2] cycloadditions of vinylpyridines **96** with styrenes **97** (**Figure** 11.32) [8c]. Excellent enantio- (up to 96%) and diastereoselectivities (up to >20 : 1) were obtained. Notably, this protocol

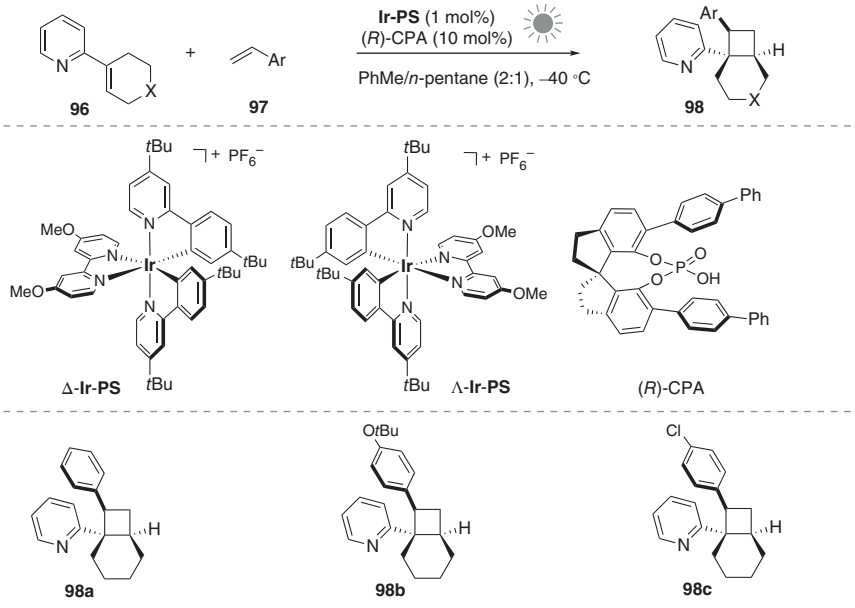


| Ir-PS | Yield (%) | dr | ee (%) |
|---|---|---|---|
| *rac* | 83 | >20:1 | 94 |
| Δ | 90 | >20:1 | 95 |
| Λ | 34 | 18:1 | 45 |

| Ir-PS | Yield (%) | dr | ee (%) |
|---|---|---|---|
| *rac* | 88 | -- | 93 |
| Δ | 95 | >20:1 | 95 |
| Λ | 12 | 16:1 | 42 |

| Ir-PS | Yield (%) | dr | ee (%) |
|---|---|---|---|
| *rac* | 80 | -- | 89 |
| Δ | 94 | 12:1 | 96 |
| Λ | 21 | 4:1 | 34 |

**Figure 11.32** Cooperative effect of substitutionally inert chiral-at-iridium complexes with a chiral Brønsted acid.

doesn't rely on the carbonyl-based alkenes which are mandatory in the previous work [53]. Mechanistically, the Ir complex plays the role of photosensitizer to enable the triplet energy transfer to chiral Brønsted acid-bound vinylpyridine. A biradical intermediate is then afforded and undergoes a subsequent stereocontrolled [2+2] cycloaddition mediated by the chirality of both chiral Ir complex and Brønsted acid. Interestingly, the Δ-enantiomer of iridium complexes typically leads to higher yields and selectivities over the Λ-enantiomer and the racemic mixture thus indicating a notable cooperative asymmetric induction effect. This remarkable matched/mismatched effect suggests the great relevance of metal chirality in asymmetric photoinduced radical reactions.

## 11.5 Summary

Although the photoinduced chiral-at-metal complex-catalyzed asymmetric radical reactions are a recent advance, it has emerged as an intriguing realm amongst synthetic chemistry. Biscyclometalated chiral-at-iridium and rhodium complexes are found as privileged scaffolds, thus enabling numerous stereocontrolled radical transformations such as alkylation, alkenylation, amination, conjugate addition, deracemization, rearrangement, and cycloaddition, etc. The substitutionally labile chiral-at-metal complexes typically play a dual role of Lewis acid and precursors for assembling photocatalysts *in situ*. In addition, the chiral-at-rhodium complexes can cooperate with an external photocatalyst or photoactive redox mediator to provide many asymmetric radical transformations. Particularly, the direct photoexcitation of rhodium-bound alkenes leads to ligand sphere biradicals that are readily involved in stereocontrolled bond formations. Likewise, the substitutionally inert chiral-at-iridium complexes are utilized as photosensitizers and optionally as hydrogen bonding catalysts to facilitate stereocontrolled radical [2+2] cycloadditions.

## Acknowledgments

Jiajia Ma thanks Prof. Eric Meggers for his kind revisions and great support. Yun-Peng Chu, Hui Liang, De-Hai Liu, and Xue-Lin Yue are acknowledged for assistance for the preparation of this chapter. National Key R&D Program of China (2023YFA1508900), the National Nature Science Foundation of China (22201174), the Natural Science Foundation of Shanghai (23ZR1432000), the Shanghai Rising-Star Program (24QA2704100), and the Shanghai Jiao Tong University 2030 Initiative are gratefully acknowledged.

## References

**1** (a) Prier, C.K., Rankic, D.A., and MacMillan, D.W.C. (2013). *Chem. Rev.* 113: 5322–5363. (b) Narayanam, J.M.R. and Stephenson, C.R.J. (2011). *Chem. Soc.*

*Rev.* 40: 102–113. (c) Yoon, T.P., Ischay, M.A., and Du, J. (2010). *Nat. Chem.* 2: 527–532.

**2** (a) Bowman-James, K. (2005). *Acc. Chem. Res.* 38: 671–678. (b) von Zelewsky, A. (2014). *Chimia* 68: 297–298.

**3** (a) Soai, K., Shibata, T., Morioka, H., and Choji, K. (1995). *Nature* 378: 767–768. (b) Tsuneomi, K., Toshiki, O., Mirai, S. et al. (2007). *Chem. Lett.* 36: 30–31. (c) Islas, J.R., Lavabre, D., Grevy, J.-M. et al. (2005). *Proc. Natl. Acad. Sci.* 102: 13743–13748.

**4** (a) Chavarot, M., Ménage, S., Hamelin, O. et al. (2003). *Inorg. Chem.* 42: 4810–4816. (b) Hamelin, O., Rimboud, M., Pécaut, J., and Fontecave, M. (2007). *Inorg. Chem.* 46: 5354–5360.

**5** Ganzmann, C. and Gladysz, J.A. (2008). *Chem. Eur. J.* 14: 5397–5400.

**6** (a) Chen, L.-A., Xu, W., Huang, B. et al. (2013). *J. Am. Chem. Soc.* 135: 10598–10601. (b) Gong, L., Chen, L.A., and Meggers, E. (2014). *Angew. Chem. Int. Ed.* 53: 10868–10874.

**7** (a) Zhang, L. and Meggers, E. (2017). *Acc. Chem. Res.* 50: 320–330. (b) Huang, X. and Meggers, E. (2019). *Acc. Chem. Res.* 52: 833–847. (c) Genzink, M.J., Kidd, J.B., Swords, W.B., and Yoon, T.P. (2022). *Chem. Rev.* 122: 1654–1716.

**8** (a) Skubi, K.L., Kidd, J.B., Jung, H. et al. (2017). *J. Am. Chem. Soc.* 139: 17186–17192. (b) Zheng, J., Swords, W.B., Jung, H. et al. (2019). *J. Am. Chem. Soc.* 141: 13625–13634. (c) Chapman, S.J., Swords, W.B., Le, C.M. et al. (2022). *J. Am. Chem. Soc.* 144: 4206–4213.

**9** (a) Gong, L., Mulcahy, S.P., Harms, K., and Meggers, E. (2009). *J. Am. Chem. Soc.* 131: 9602–9603. (b) Ma, J., Zhang, X., Huang, X. et al. (2018). *Nat. Protoc.* 13: 605–632. (c) Chu, Y.-P., Yue, X.-L., Liu, D.-H., Wang, C., and Ma, J. (2025). *Nat. Commun.* 16: 1177. (d) Liang, H., Morais, G.N., Chen, G. et al. (2025). *J. Am. Chem. Soc.* 147: 6825–6834.

**10** (a) Hopkinson, M.N., Sahoo, B., Li, J.L., and Glorius, F. (2014). *Chem. Eur. J.* 20: 3874–3886. (b) Skubi, K.L., Blum, T.R., and Yoon, T.P. (2016). *Chem. Rev.* 116: 10035–10074. (c) Meggers, E. (2015). *Chem. Commun.* 51: 3290–3301.

**11** Huo, H., Shen, X., Wang, C. et al. (2014). *Nature* 515: 100–103.

**12** Huo, H., Wang, C., Harms, K., and Meggers, E. (2015). *J. Am. Chem. Soc.* 137: 9551–9554.

**13** Zhang, X., Qin, J., Huang, X., and Meggers, E. (2018). *Eur. J. Org. Chem.* 2018: 571–577.

**14** Huo, H., Huang, X., Shen, X. et al. (2016). *Synlett* 27: 749–753.

**15** Wang, C., Zheng, Y., Huo, H. et al. (2015). *Chem. Eur. J.* 21: 7355–7359.

**16** Wang, C., Qin, J., Shen, X. et al. (2016). *Angew. Chem. Int. Ed.* 55: 685–688.

**17** (a) Shen, X., Harms, K., Marsch, M., and Meggers, E. (2016). *Chem. Eur. J.* 22: 9102–9105. (b) Ma, J., Shen, X., Harms, K., and Meggers, E. (2016). *Dalton Trans.* 45: 8320–8323.

**18** Huang, X., Webster, R.D., Harms, K., and Meggers, E. (2016). *J. Am. Chem. Soc.* 138: 12636–12642.

**19** Zard, S.Z. (2008). *Chem. Soc. Rev.* 37: 1603–1618.

**20** Wang, C., Chen, L.-A., Huo, H. et al. (2015). *Chem. Sci.* 6: 1094–1100.

**21** Liang, H., Xu, G.-Q., Feng, Z.-T. et al. (2019). *J. Org. Chem.* 84: 60–72.

**22** Steinlandt, P.S., Zuo, W., Harms, K., and Meggers, E. (2019). *Chem. Eur. J.* 25: 15333–15340.

**23** Tan, Y., Yuan, W., Gong, L., and Meggers, E. (2015). *Angew. Chem. Int. Ed.* 54: 13045–13048.

**24** Giese, B. (1983). *Angew. Chem. Int. Ed.* 22: 753–764.

**25** (a) Sibi, M.P., Ji, J., Wu, J.H. et al. (1996). *J. Am. Chem. Soc.* 118: 9200–9201. (b) Sibi, M.P. and Ji, J. (1997). *J. Org. Chem.* 62: 3800–3801.

**26** Ruiz Espelt, L., McPherson, I.S., Wiensch, E.M., and Yoon, T.P. (2015). *J. Am. Chem. Soc.* 137: 2452–2455.

**27** Huo, H., Harms, K., and Meggers, E. (2016). *J. Am. Chem. Soc.* 138: 6936–6939.

**28** Tutkowski, B., Meggers, E., and Wiest, O. (2017). *J. Am. Chem. Soc.* 139: 8062–8065.

**29** Wang, C., Harms, K., and Meggers, E. (2016). *Angew. Chem. Int. Ed.* 55: 13495–13498.

**30** Ma, J., Lin, J., Zhao, L. et al. (2018). *Angew. Chem. Int. Ed.* 57: 11193–11197.

**31** de Assis, F.F., Huang, X., Akiyama, M. et al. (2018). *J. Org. Chem.* 83: 10922–10932.

**32** Lin, S.-X., Sun, G.-J., and Kang, Q. (2017). *Chem. Commun.* 53: 7665–7668.

**33** Kuang, Y., Wang, K., Shi, X. et al. (2019). *Angew. Chem. Int. Ed.* 58: 16859–16863.

**34** Ma, J., Xie, X., and Meggers, E. (2018). *Chem. Eur. J.* 24: 259–265.

**35** Ma, J., Harms, K., and Meggers, E. (2016). *Chem. Commun.* 52: 10183–10186.

**36** Zhang, C., Gao, A.Z., Nie, X. et al. (2021). *J. Am. Chem. Soc.* 143: 13393–13400.

**37** Zhou, Z., Nie, X., Harms, K. et al. (2019). *Sci. China Chem.* 62: 1512–1518.

**38** Huang, X., Zhang, Q., Lin, J. et al. (2019). *Nat. Catal.* 2: 34–40.

**39** Xiong, P., Hemming, M., Ivlev, S.I., and Meggers, E. (2022). *J. Am. Chem. Soc.* 144: 6964–6971.

**40** DesJarlais, R.L., Yamashita, D.S., Oh, H.-J. et al. (1998). *J. Am. Chem. Soc.* 120: 9114–9115.

**41** Huang, X., Luo, S., Burghaus, O. et al. (2017). *Chem. Sci.* 8: 7126–7131.

**42** Zhou, Z., Li, Y., Han, B. et al. (2017). *Chem. Sci.* 8: 5757–5763.

**43** Ma, J., Rosales, A.R., Huang, X. et al. (2017). *J. Am. Chem. Soc.* 139: 17245–17248.

**44** Rodríguez, R.I., Mollari, L., and Alemán, J. (2021). *Angew. Chem. Int. Ed.* 60: 4555–4560.

**45** Huang, X., Lin, J., Shen, T. et al. (2018). *Angew. Chem. Int. Ed.* 57: 5454–5458.

**46** (a) Huang, X., Quinn, T.R., Harms, K. et al. (2017). *J. Am. Chem. Soc.* 139: 9120–9123. (b) Huang, X., Li, X., Xie, X. et al. (2017). *Nat. Commun.* 8: 2245–2252.

**47** Grell, Y., Hong, Y., Huang, X. et al. (2019). *Organometallics* 38: 3948–3954.

**48** Jeremias, N., Mohr, L.-M., and Bach, T. (2021). *Org. Lett.* 23: 5674–5678.

**49** Rigotti, T., Schwinger, D.P., Graßl, R. et al. (2022). *Chem. Sci.* 13: 2378–2384.

**50** Hu, N., Jung, H., Zheng, Y. et al. (2018). *Angew. Chem. Int. Ed.* 57: 6242–6246.

**51** Zhang, C., Chen, S., Ye, C.-X. et al. (2019). *Angew. Chem. Int. Ed.* 58: 14462–14466.

**52** (a) Ma, J., Ding, X., Hu, Y. et al. (2014). *Nat. Commun.* 5: 4531–4536.
(b) Xu, W., Arieno, M., Löw, H. et al. (2016). *J. Am. Chem. Soc.* 138: 8774–8780.
(c) Cruchter, T., Medvedev, M.G., Shen, X. et al. (2017). *ACS Catal.* 5151–5162.
(d) Cao, Z.-Y., Brittain, W.D., Fossey, J.S., and Zhou, F. (2015). *Catal. Sci. Technol.* 5: 3441–3451.

**53** Poplata, S., Tröster, A., Zou, Y.-Q., and Bach, T. (2016). *Chem. Rev.* 116: 9748–9815.

# 12

# Chiral Photochemical Reactions in Supramolecular Assemblies

*Yanling Shen, Yulin Mao, Tong Shan, Wanhua Wu, and Cheng Yang*

*Key Laboratory of Green Chemistry & Technology, College of Chemistry, Laboratory of Precision Cancer Therapeutics, Precision Medicine Research, State Key Laboratory of Biotherapy, West China Hospital, Sichuan University, 29 Wangjiang Road, Chengdu 610064, China*

## 12.1 Introduction

An abundance of research has been performed on asymmetric synthesis, a fundamental topic in the chemical sciences, with considerable success. Nevertheless, the synthesis of polycyclic or highly strained chiral molecules is still difficult when utilizing regular thermal or enzyme reactions. Excited-state photochemical reactions offer a promising solution for the synthesis of these molecules, providing an efficient and environmentally friendly approach that aligns with the principles of green chemistry [1]. On account of the challenges, such as a short lifetime of the excited state and high substrate sensitivity, the achievement of a high stereo-selection in an excited state photochemical reaction is still a major challenge. Supramolecular photochemical reaction, which involves pre-arrangements of the substrates within a limited chiral space prior to the radiation, may overcome these problems. In this strategy, non-covalent interactions, such as hydrogen bonding, hydrophobic interactions, and van der Waals forces, work together to confine the substrates in the microenvironment of the chiral source, fixing their conformation/arrangement through ground-state and/or excited-state supramolecular interactions. This approach was extensively studied by utilizing a variety of pre-organized host molecules, such as cyclodextrins [2], cucurbit[n]urils [3], and biomacromolecules [4], as well as chiral templates that engage in strong supramolecular interactions. By employing supramolecular photoinduced chirality methods, chiral photochemical reactions with almost quantitative enantiomeric excess (*ee*) values have been achieved [5].

In order to prevent the formation of racemic products in the solution of the substrate due to an uncomplexed substrate, an excess chiral source is generally used by increasing the complexation ratio of the substrate [6]. The practical application of supramolecular photochirogenesis is thus restricted due to the challenges associated with obtaining chiral hosts/templates, along with the considerations of atom economy and green chemistry. Hence, catalytic supramolecular photochirogenesis through sub-stoichiometric chiral sources is a more

sensible option [7]. Theoretically, it is possible to implement this process, as the photo-reaction can be accelerated when the substrate is confined in a host cavity due to pre-arrangement, confining, and/or concentration effects; furthermore, the moderate affinity and non-covalent nature of the host-guest interactions make it possible to reuse the chiral cavity by releasing the photo-products and taking up new substrates. Eliminating or diminishing non-chiral photoreactions outside the chiral environment is essential for catalytic supramolecular photochemistry.

This chapter will summarize recent reports on the pre-organization of photosubstrates through supramolecular complexation for excited-state chiral photoreactions before photo-irradiation. It should be noted that although the focus of this chapter is radical reactions, we do not limit the reactions to radical photochemistry but rather emphasize excited-state chiral photochemistry. We will highlight enantioselective excited-state photo-reactions in the past ten years with supramolecular chiral sources as the classification criteria.

## 12.2 Chiral Photoreactions with Cyclodextrins

Cyclodextrins (CDs), cyclic oligosaccharides linked by 1,4-glycosidic bonds, are the most extensively studied chiral host molecules. Due to their high solubility in water, inherent chirality, and biocompatibility, CDs are widely used in various applications such as pharmaceuticals, asymmetric catalysis, and organic functional materials. The first reported CD-mediated asymmetric photoreaction is the enantiodifferentiating photoisomerization of (*Z*)-cyclooctene (**1Z)** and (*Z*,*Z*)-1,3-cyclooctadiene (**2ZZ)** (Scheme 12.1). Previous studies showed that direct excitation of **1Z** with β-CD resulted in an approximate racemic mixture of planar-chiral (*E*)-cyclooctene (**1E)** and the CD-based sensitizers do not show significant temperature-dependent behavior since the low-entropy environment of CD cavity, in contrast to the conventional chiral sensitizers. Inoue and coworkers introduced aromatic ester-modified CDs **3** (Figure 12.1) as supramolecular sensitizers to improve the enantioselectivity of **1E**. By choosing the solvent condition and the substituent on the sensitizer, they were able to enhance the *ee* value of **1E** to as much as 24% [8]. Subsequently,

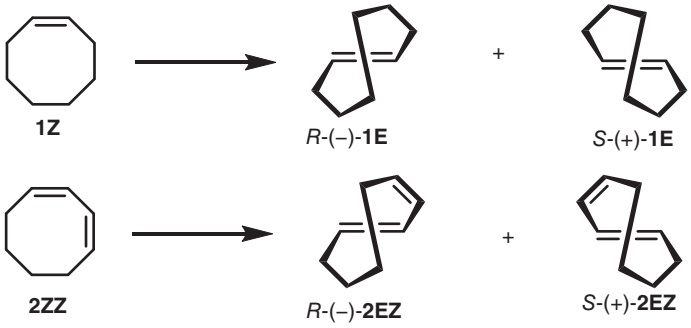


**Scheme 12.1** Photosensitized isomerization of cyclooctenes.

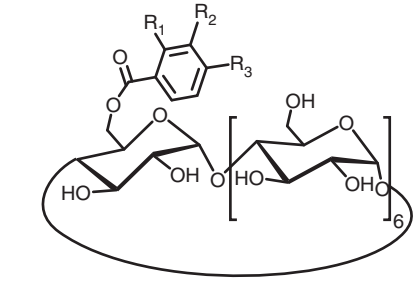


| | $R_1$ | $R_2$ | $R_3$ |
|---|---|---|---|
| **3** | H | H | H |
| **4a** | $OCH_3$ | H | H |
| **4b** | H | $OCH_3$ | H |
| **4c** | H | H | $OCH_3$ |
| **5a** | $CO_2CH$ | H | H |
| **5b** | H | $CO_2CH$ | H |
| **5c** | H | H | $CO_2CH$ |

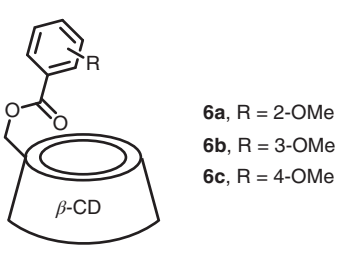


**6a**, R = 2-OMe
**6b**, R = 3-OMe
**6c**, R = 4-OMe

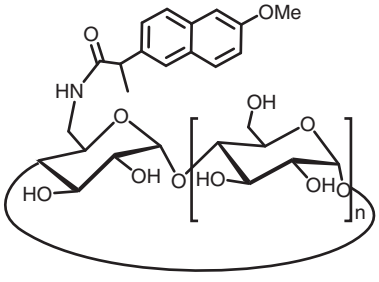


**7a**, n=5
**7b**, n=6
**7c**, n=7

**Figure 12.1** Benzoate-modified CDs as supramolecular sensitizers.

they explored the use of chiral sensitizers **4a-c** and **5a-c** (Figure 12.1). While the *ortho*- and *para*-substituted counterparts **4a** and **4c** showed poor performance in asymmetric catalysis of **1E**, the *meta*-methoxy benzoylated CD **4b** showed a significant improvement in enantioselectivity, reaching to 46% *ee* [9]. Inoue, Yang, and coworkers used 6-O-(*o*-, *m*-, or *p*-methoxy-benzoyl)-β-CD (**6a-c**) (**Figure** 12.1) as supramolecular sensitizers in aqueous solutions, achieving 67% *ee* of **1E**. This represents the highest enantioselectivity reported to date for the supramolecular photoisomerization of **1Z** mediated by sensitizer-modified β-CDs [10]. However, achieving stereochemical control of the photoisomerization of **2ZZ** has proven to be more challenging. The highest reported *ee* value was only 17%, even at low temperatures of −110 °C. Moreover, due to the poor size matching of α- or β-CD-based sensitizers, negligible *ee* values were obtained. With naproxen-bearing β-CD **7a-c** in 20% aqueous methanol solution (**Scheme** 12.2), the (*Z*,*E*)-1,3-cyclooctadiene (**2EZ)** was obtained in an enhanced optical yield of 4.6% *ee* [11]. Yang and coworkers also synthesized a [4]rotaxane **8** (**Scheme** 12.2), where the biphenyl photosensitizer axle was sealed in the cavities of γ-CD using cucurbit[6]uril-catalyzed click reaction of azide and alkyne [12]. It is expected that breaking the symmetry of the large chiral cavity of γ-CD by the implanted sensitizer axle can significantly enhance the enantioselectivity of the photoreaction that occurs within this highly defined chiral cavity. Indeed, with 0.2 equiv. of the rotaxanes as the sensitizer and catalysts, photoisomerization of **2ZZ** gave the highest recorded ee as high as 15.3% at 0.5 °C.

CD nanosponges (CDNS) (**9–11**), which are based on CD crosslinked with pyromellitic dianhydride, have been employed in the study of enantiodifferentiating photoisomerizations of **1Z** and **2ZZ** (Figure 12.2). Notably, by gradually

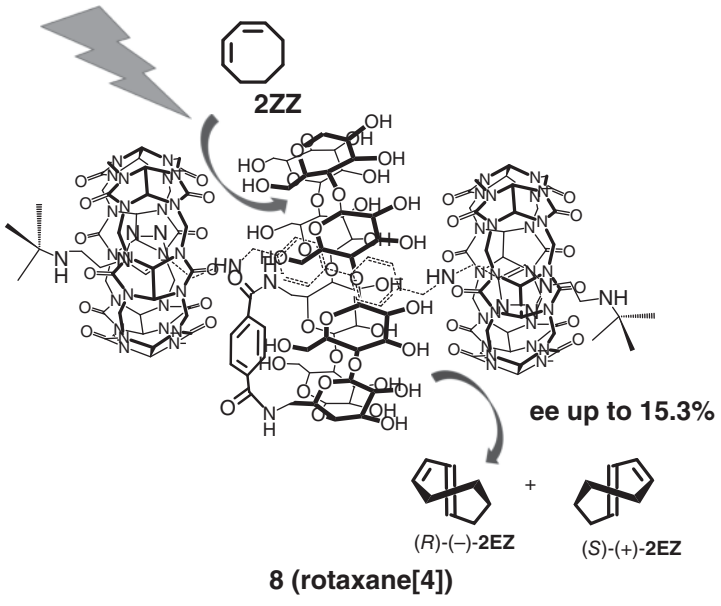


**Scheme 12.2** Supramolecular photoisomerization of 2ZZ sensitized by chiral [4]rotaxane 8.

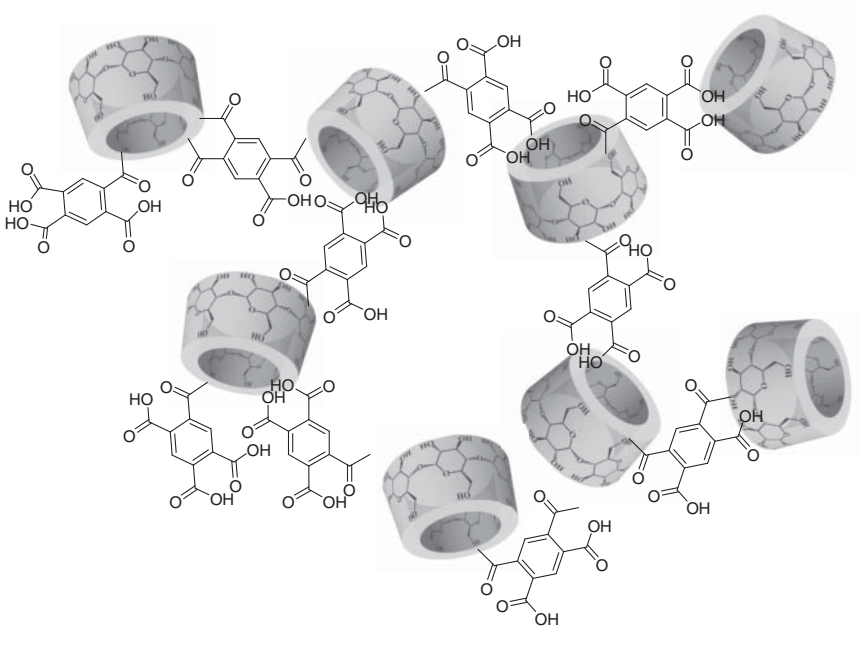

**9-11**

**9:** β-CD:PDA = 1:2
**10:** β-CD:PDA = 1:4
**11:** γ-CD:PDA = 1:4

**Figure 12.2** Cyclodextrin nanosponges prepared by cross-linking CDs with pyromellitic dianhydride.

increasing the concentrations of CDNS from 0.2–2000 mg/ml, the phase condition of the mixture undergoes a transformation from solution to suspension, flowing gel, and finally rigid gel. Intriguingly, it has been observed that the enantioselectivity of **1Z** and **2ZZ** is strongly correlated with the phase conditions of CDNS. For example, in solution or suspensions, the photoisomerization of **2ZZ** in γ-CDNS produces nearly racemic products, whereas, at the interface between flowing and rigid gels, the *ee* value jumps to 13.3% [13]. This effect is due to the alteration in the recognition and reaction site for the photoreaction from the cavities of CDs in solution to the void space within the gel phase.

Furthermore, by crosslinking cyclic nigerosylnigerose (CNN) or linear maltodextrin (LM) with pyromellitic dianhydride, CNN-based nanosponges **12a**, **12b** [14] and LM-based nanosponges **13a**, **13b** [15] (**Figure** 12.3) were synthesized. Different from the previous CDNS, CNN-NS/LM-NS lacks a confining cavity that can fully accommodate a guest substrate, resulting in a very low *ee* value in the enantiodifferentiating photoisomerization of **1Z** mediated by the solution or suspension phase of CNN-NSs. However, at the phase border of flowing gel and rigid gel, the *ee* values suddenly leaped to 22–24%, which is the highest enantioselectivity obtained in nanosponges [14]. Similar results were observed in the LM-NS media [15], indicating that the chiral polymer void formed by CNN-NS aggregation plays a decisive role in the selectivity of the photoreaction.

For a larger ring electrocyclization reaction of (1*R*,5*R*)-2-azabicyclo[3.2.0]heptan-3-one **14** (**Scheme** 12.3), Aitken and coworkers discovered that the interactions between **14** and native β-CD were weak, with a binding constant of only 35.4 $M^{-1}$ in water. As a result, no enantiodifferentiation in solution was observed for the photoproduct. However, when an equimolar mixture of **14** and β-CD was used, a opalescent suspension was formed, and further photoreaction exhibited high enantiodifferentiation of up to 45% *ee* of **15** [16]. This study expanded the application of CD derivatives as supramolecular sensitizers in photogenic reactions.

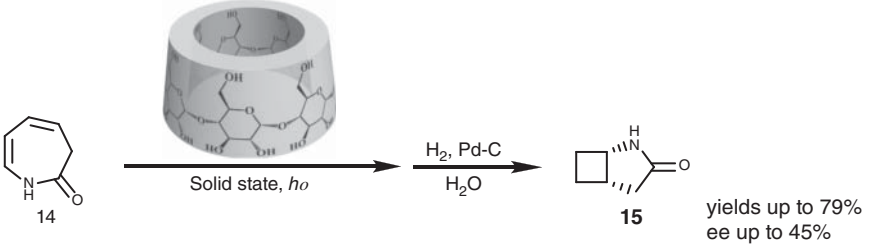


**Scheme 12.3** Sequential photochemical electrocyclization–reduction of azepinone 14 in the presence of native β-CD.

The first [4 + 4] photocyclodimerization at the chiral level is the photocyclodimerization of anthracenecarboxylic acid (AC) mediated by native γ-CD (**Scheme** 12.4). Since the cavity of γ-CD is big enough to form 1 : 2 host-guest complex with **16a** in an aqueous solution, the proximity of two molecules of **16a** in space significantly accelerates the photocyclodimerization of **16a** [17]. Recently, Inoue, Sugiyama, and

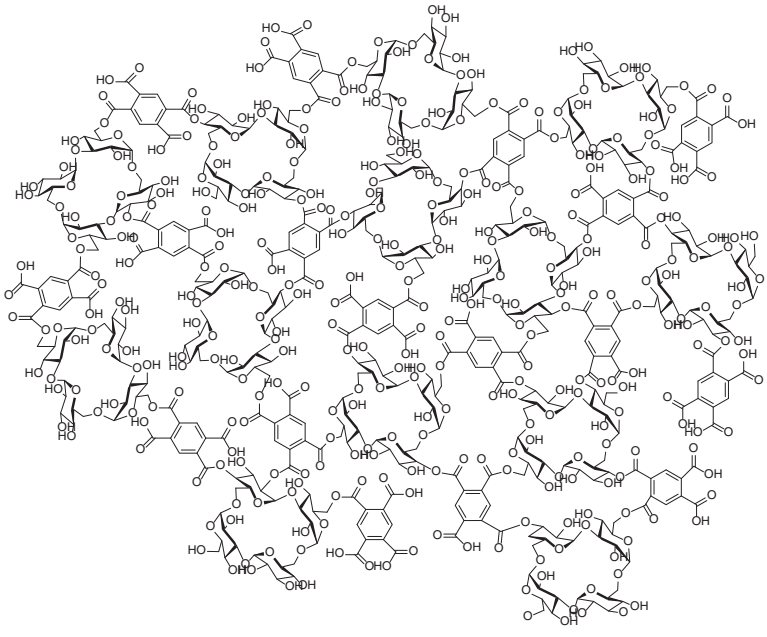

**12a:** CNN:PDA = 1:2
**12b:** CNN:PDA = 1:4

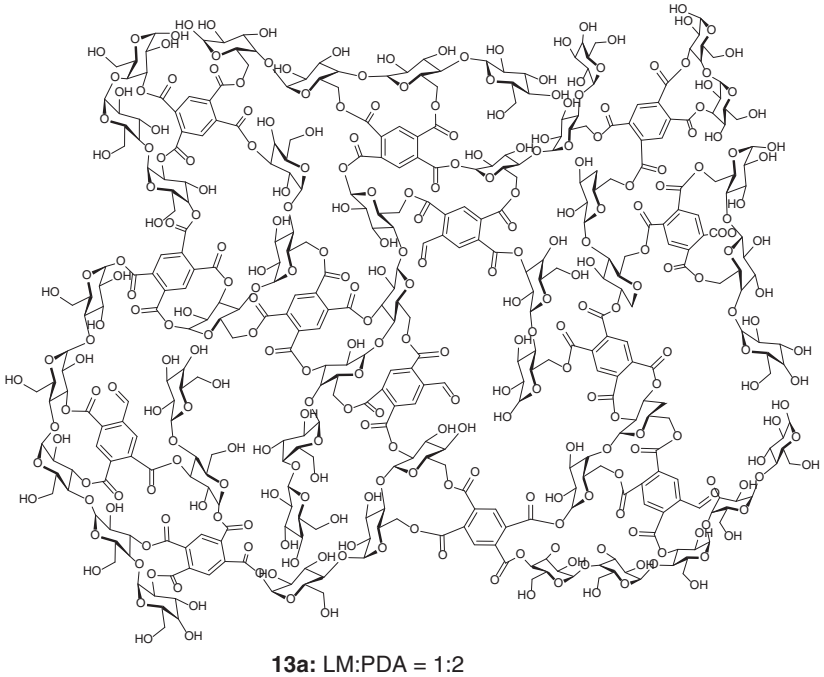

**13a:** LM:PDA = 1:2
**13b:** LM:PDA = 1:4

**Figure 12.3** Nanosponges 11a, 11b and 12a, 12b prepared by crosslinking CNN, and LM with PDA.

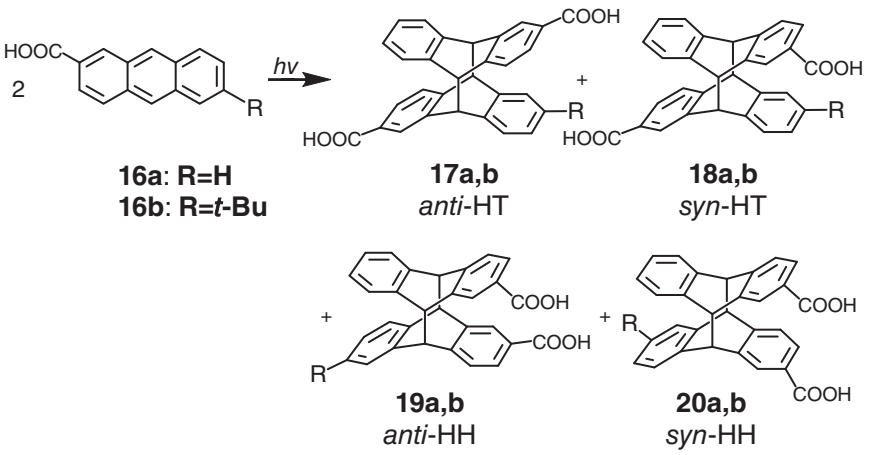


**Scheme 12.4** Photocyclodimerization of anthracenecarboxylic derivatives.

coworkers found that with focused laser beam irradiation, the higher-order 2 : 4 complex can form, consisting of two 1 : 2 complexes stabilized by inter-complex hydrogen bonds between the carboxylic acid residues of **16a** [18]. Experimental results show that native γ-CD prefers to give the HT (head to tail) dimers **17a** and **18a**, with the chiral dimer **18a** obtained in 41% *ee* [6a].

The study with modified γ-CDs reveals a critical correlation between the hosts' structure and the reaction stereoselectivity. Modification of the CD parts with positively charged groups can change the spatial arrangement of **16a** in the CD cavity, in particular, **16a** existing in the form of carboxylate under basic conditions. For example, γ-CDs bearing pyridiums (**21a–21d**) [19] or two amino groups **(22a–22d**) [20] successfully improved the stereoselectivity of HH (head to head) dimers (**Figure** 12.4). To further restrict the spatial position of **16a** in the cavity of γ-CD, capped γ-CDs **23** (**Figure** 12.4) have been investigated, which showed an improved and inverted enantioselectivity of **18a** in −58% *ee* [21]. A dual supramolecular strategy was attempted to manipulate the selectivity of the reaction. In this approach, **16a** was covalently linked to the primary rim of α-CD, resulting in *mono*- and *di*-substituted α-CDs **24** and **25** (Figure 12.4) [22]. The photocyclodimerization of **24** gives HT dimers **17a** and **18a** as the main products, with **18a** being formed with >90% *ee*. Furthermore, researchers have also investigated the impact of reaction conditions on the selectivity of the photocyclodimerization of ACs. For example, **26a** and **26b** exhibit spectral dependence with pH, and a reversal of the chiral selectivity of **19a** was observed (*ee* value change from −5% to 28%) when pH was changed from 11 to 6 [23]. The pH effect was further explored by Kanagaraj *et al*., who used two bis-quinoline-modified γ-CD as chiral hosts. Upon changing the solution pH in the presence of **27**, the chiral selectivity of HH dimer **19a** was reversed, with the *ee* value changing from 25.2% to −64.6%, and with **28**, the *ee* value changing from 41.2% to −76.2% (Figure 12.5) [24] (**Figure** 12.5).

The properties of the photosubstrate are also a critical factor in the stereoselectivity. 2,6-anthracenedicarboxylate (**ADC**) with an additional carboxylate group

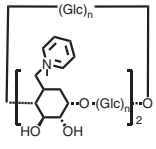

**21a**: n = 0, $6^A,6^B$-dipyridyl-$6^A,6^B$-dideoxy-gCD
**21b**: n = 1, $6^A,6^C$-dipyridyl-$6^A,6^C$-dideoxy-gCD
**21c**: n = 2, $6^A,6^D$-dipyridyl-$6^A,6^D$-dideoxy-gCD
**21d**: n = 3, $6^A,6^E$-dipyridyl-$6^A,6^E$-dideoxy-gCD

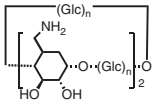

**22a**: n = 0, $6^A,6^B$-diamino-$6^A,6^B$-dideoxy-γCD
**22b**: n = 1, $6^A,6^C$-diamino-$6^A,6^C$-dideoxy-γCD
**22c**: n = 2, $6^A,6^D$-diamino-$6^A,6^D$-dideoxy-γCD
**22d**: n = 3, $6^A,6^E$-diamino-$6^A,6^E$-dideoxy-γCD

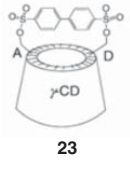

**23**

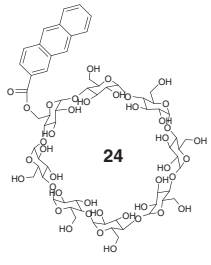

**24**

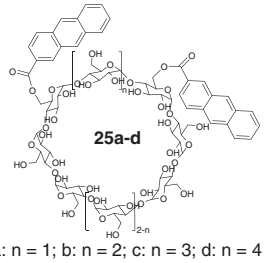

**25a-d**

a: n = 1; b: n = 2; c: n = 3; d: n = 4

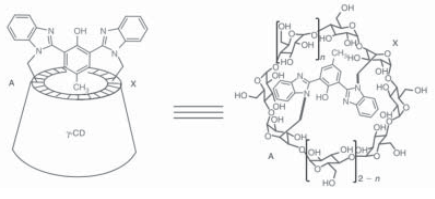

**26a**: n = 0, x = D
**26b**: n = 1, x = E

**Figure 12.4** Photocyclodimerization of 16a with modified γ-CDs.

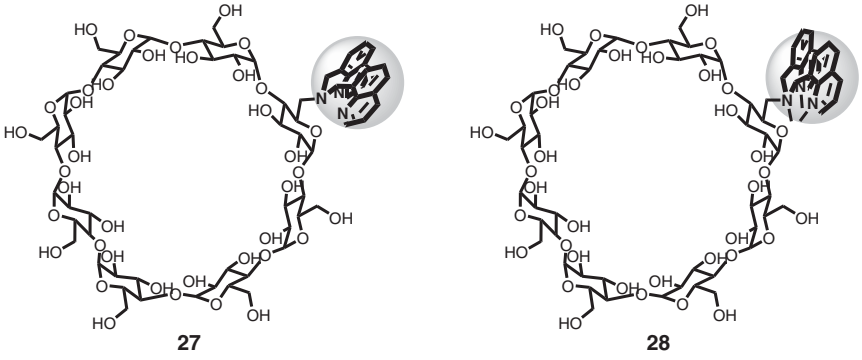


**Figure 12.5** Chemical structure of supramolecular hosts 27 and 28.

at the 6-position is expected to have stronger electrostatic attraction interactions than monoanionic **16a** with positively charged γ-CDs but suffer stronger repulsion between ADC (**Scheme** 12.5). With **31** as the chiral host at optimized external conditions, dimer **29** (or *ent*-**29**) was afforded with up to 58% yield and −72% *ee*. Meanwhile, using chiral host **32**, **29** (or *ent*-**29**) is achieved with 94% yield and −69% *ee* [25].

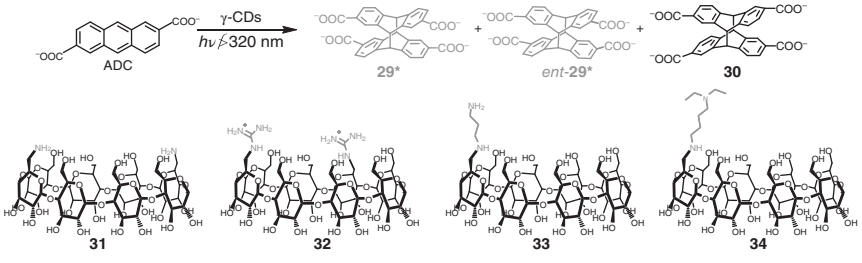


**Scheme 12.5** Enantiodifferentiating [4 + 4] photocyclodimerization of 2,6-anthracenedicarboxylic acid (ADC), and chemical structure of chiral host 31–34.

Native β-CD form a relatively stable 1 : 1 host-guest complexes with **16a**, which further leads to 2 : 2 complexes formed with π-π interaction and inter-CD hydrogen bonding interactions, which can accelerate the photocyclodimerization reaction [26]. Photoreaction of **16a** with native β-CD led to the preferential production of chiral slipped cyclodimers **35** and **36** over classical cyclodimers. The stereoselectivity is manipulable by various factors, enabling the selective production of slipped cyclodimers. The dual β-CD capsule acts as a chiral organophotocatalyst, mimicking a catalytic antibody in triggering and accelerating the nonclassical photochirogenic route. Furthermore, a series of functionalized β-CD derivates (**Scheme** 12.6) have been applied to the photoreaction of **16a**. In the photocyclodimerization mediated by amino-modified β-CD derivatives **37a-f** (**Scheme** 12.6), nonclassical slipped cyclodimers **35** and **36** are further preferred. By exploring conditions such as host/guest ratio, wavelength, pressure, salt effect, and host modification, **35** and

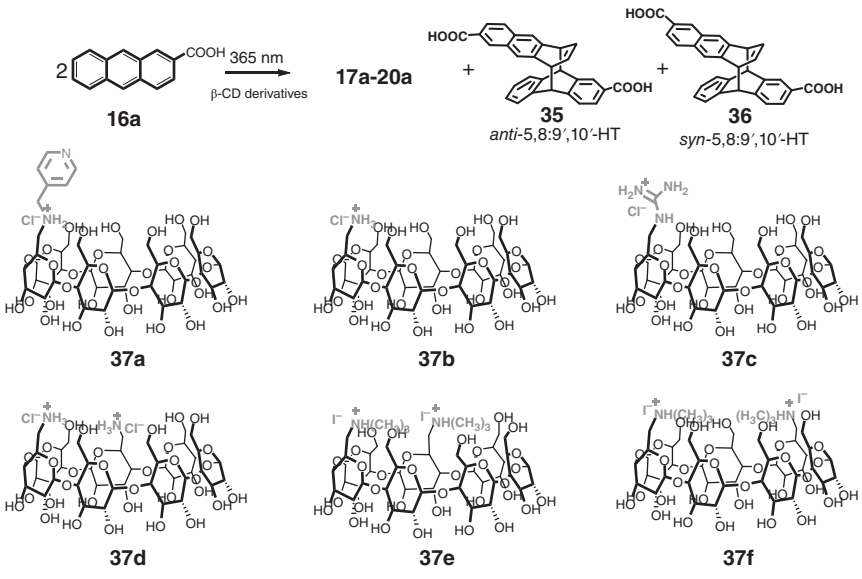


**Scheme 12.6** Enantiodifferentiating [4 + 4] photocyclodimerization of 16a to give non-classical 5,8:9′,10′-cyclodimers 35 and 36 and classical 9,10:9′,10′-cyclodimers 17a-20a, and modified β-CD derivatives 37a-f.

**36** could be increased with higher enantioselectivity. With **37d** and **37e** as host molecules, the conversion of slipped dimer can be significantly improved to 100% in pH 9.0 phosphate buffer solution with 6 M CsCl at −20 °C and the *ee* value of dimer **35** and **36** reaching 71% and −45% [26].

The primary-face-modified β-CD **38** affords dimer **35** with a 61% relative yield and 65% *ee*, while dimer **36** is achieved with 33% relative yield and −49% *ee* in pH 9.0 phosphate buffer solution at 40 °C. The enantiodifferentiating photocyclodimerization reactions of **16a** were also mediated by the secondary-face-modified β-CDs (**38**, **39**) (**Figure** 12.6). Additionally, the secondary-face-modified β-CD **40** afforded dimer **36** with a higher *ee* of 70% in the presence of 6 M CsCl at −20 °C in pH 9.0 phosphate buffer solution, which is the highest reported selectivity for the non-classic dimer **36** [27].

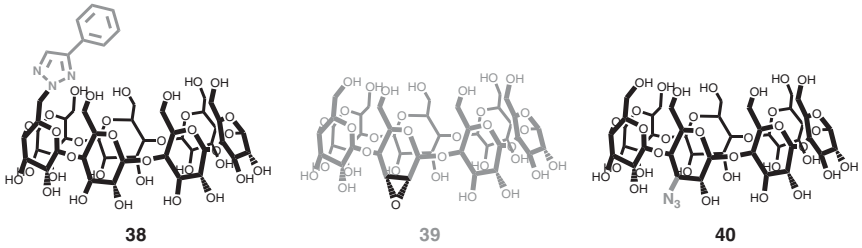


**Figure 12.6** Primary-face and secondary-face-modified modified β-CD derivatives 38–40.

In supramolecular photochirogenesis, achieving catalytic selectivity is challenging, and it often requires the use of excess amounts of host molecules to bind as many substrate molecules as possible and inhibit the photoreactions of uncomplexed photosubstrate, which will lead to racemic products. Inoue and coworkers addressed this issue by synthesizing a γ-CD-based Cu complex catalyst for the photocyclodimerization of **16a**. The Cu complex chelated in the γ-CD could pre-organize two **16a** molecules in the HH orientation within the cavity and facilitate the photoreaction, while the unchelated $Cu^{2+}$ in the solvent quenches the excited-state of free **16a**. As a result, HH-dimers **19a** and **20a** were obtained in up to 80% combined yield, and **19a** was afforded with 70% *ee* using only a catalytic amount (0.1 equiv.) of the γ-CD-Cu complex [28]. Selective photoactivation of **16a** bound in the cavity of host molecules is another interesting strategy to avoid photoreactions in the bulky solution. Yang and coworkers designed and synthesized chiral host **41** by grafting Pt(II) Schiff base complex to γ-CD derivatives (Scheme 12.7). The Pt(II) Schiff base complex serves as a triplet sensitizer to initiate the triplet-triplet annihilation (TTA) upconversion of **16a**. Under visible light irradiation where **16a** molecules have no absorption, the Pt complex undergoes intersystem crossing to give a triplet excited state efficiently, which transfers energy to **16a** bound in the cavity of hosts. Triplet **16a** is not photoreactive, and only singlet **16a** could result in cyclodimers. The two triplet **16a** molecules, thereby generated, give one singlet **16a** through TTA upconversion, leading to photocyclodimerization in the cavity. This energy transfer ensures that the reaction only occurs within the cavity, avoiding racemic photoreactions in solution. With only 0.5 mol% equiv. of host **41**, *syn*-HT dimer **18a** was obtained with 61% yield and 31.4% *ee* [29]. Furthermore, a temperature effect was observed in this system, where the *ee* value of **18a** increased from 2.1% to 31.6% when the temperature was changed from 0 °C to 30 °C using 5% equiv. of host **41** [30]. Additionally, the enantiodifferentiating photocyclodimerization can be triggered under near-infrared light irradiation at 980 nm by introducing γ-CD-grafted lanthanide-doped upconverted nanoparticles (UCNP) [31].

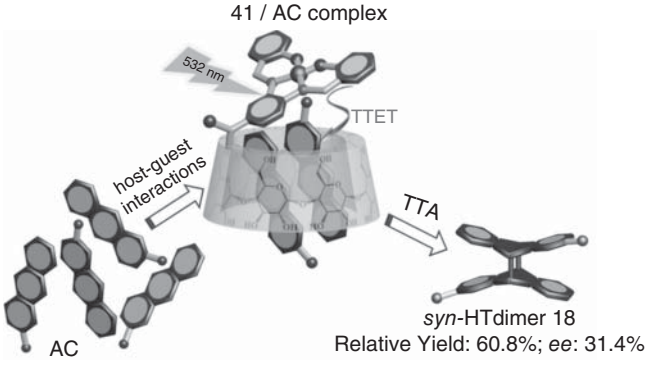


**Scheme 12.7** Schematic representation of visible-light-driven catalytic dimerization of AC mediated by sensitizer/host 41.

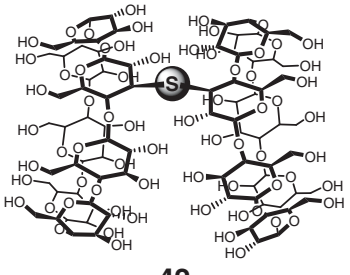

42

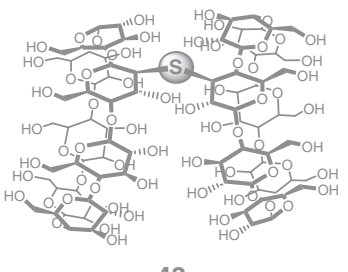

43

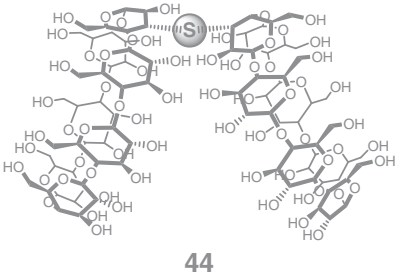

44

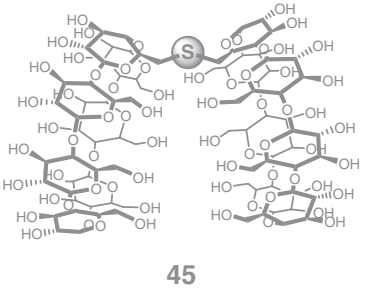

45

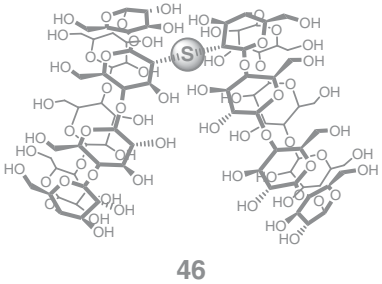

46

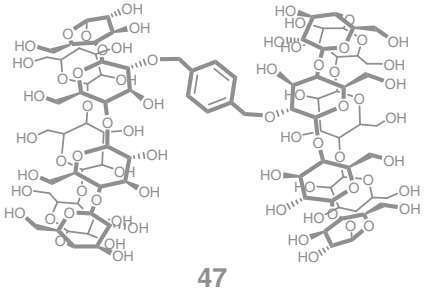

47

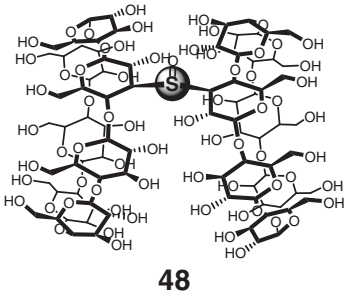

48

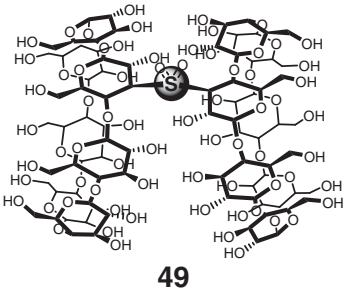

49

**Figure 12.7** Chemical structure of sulfur-, arene-bridged, sulfoxide- or sulfone- β-CD dimers 42–49.

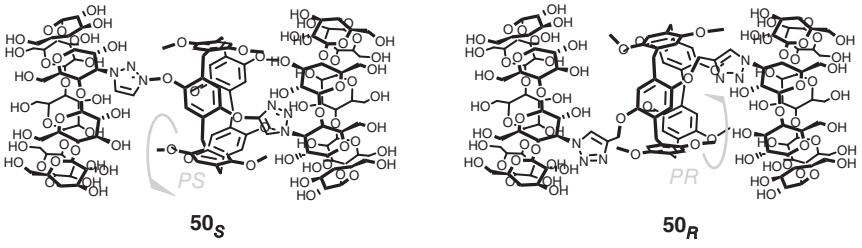


$50_S$ $50_R$

**Figure 12.8** Chemical structure of trimer chiral host 50R and 50S.

In the above chiral photoreactions, enantioselective photoreactions primarily occurred in the host-guest complexes where the substrate was spatially restricted within the cavity of CD. However, it remained difficult to obtain single enantiomeric products with high yields in supramolecular photochirogenesis as most supramolecular complexation are not highly chiral discriminating. To further improve the stereoselectivity of the photocyclodimerization of **16a** with β-CD, several CD dimers (**42**–**47**) in which two β-CDs were linked by a sulfur atom or an arene spacer to create a more compact and less flexible capsule (Figure 12.7). The CD capsules formed 1 : 1 and 1 : 2 host-guest complexes with **16a** in aqueous solutions, with only the 1 : 2 complex being photoactive. Among these capsules, **42** exhibited excellent selectivity in phosphate buffer solution (pH = 5.1) at 0.5 °C, with the *syn*-HT cyclodimer **18a** formed in 100% *ee* and 97–98% relative yield [32]. Moreover, several sulfoxide- and sulfone-bridged β-CD dimers are also synthesized(**48**, **49**) [33]. These β-CD dimers only have small structural change compared with **42**. However, the *ee* value of **18a** was −96.7% with the sulfur-bridged CD **48**, while with CD **49**, the *ee* value decreased to −20.3%, indicating that even slight structural changes can significantly alter the stereochemical outcome of supramolecular photochirogenic systems.

Recently, a series of chiral tri-cavity hosts with sandwich-like structures were synthesized by combining two β-CDs with a pillar[5]arene, in which the pillar[5]arene unit could adapt a *PR* or *PS* configuration. The diastereomeric pairs thus formed were successfully separated (Figure 12.8). When these chiral hosts were introduced in the photocyclodimerization of **16a**, they exhibited a preference for the formation of nonclassical cyclodimers **35** and **36**. Notably, when using $\mathbf{50}_{\boldsymbol{R}}$ as the chiral host, the *ee* value of **35** was enhanced to 87%, which is the highest reported ee value for nonclassical cyclodimers. In contrast, using $\mathbf{50}_{\boldsymbol{S}}$ as the chiral host resulted in the formation of **34** with an opposite *ee* value [34]. This work gives an interesting concept to constructing novel chiral hosts by combining natural and artificial hosts, which should be effective, especially considering that achieving inverted enantioselectivity in supramolecular photogenesis with native chiral hosts is a challenging task.

## 12.3 Supramolecular Photochirogenesis with Chiral Zeolites

Zeolites are porous aluminosilicates with three-dimensional supercages of varying sizes, which can act as hosts in various photoreactions. The negative charge surface of zeolites is composed of $Si^{4+}$, $Al^{3+}$, and oxygen, and is balanced by exchangeable cations. The mesoporous structures and strong cation-organic interaction of zeolites facilitate the adsorption of molecules, and their UV–Vis light-transmitting properties allow for photoexcitation of adsorbed molecules to the excited state [35] Zeolites' supercage is not chiral by itself but can be modified by immobilizing chiral inductors on the inside walls. The modified zeolites are prepared by adsorbing chiral neutral organic molecules or replacing the zeolite's countercations with chiral organic ammonium ions [36].

Photoreactions that take place within zeolite supercages often result in stereochemical outcomes that are different from those obtained in isotropic solutions. Ramamurthy *et al*. investigated the photocyclization of tropolone (S)-2-methylbutyl ether **51b** in hexane, both with and without zeolite (**Scheme** 12.8). In hexane, the reaction yielded the non-diastereoselective formation of **52b** and *ent*-**52b** (*de* = 0%). However, when conducted within NaY zeolite as a hexane slurry at −20 °C, the diastereoselectivity improved, and **52b** was obtained in 68% *de*, which was further enhanced to 92% *de* by using (−)-norephedrine-modified NaY zeolite. This demonstrates that the zeolite's supercage and cation play a crucial role in achieving high diastereoselectivity, as conducting the same reaction on the silica gel surface resulted in negligible *de* for **52b** [37]. Further mechanical studies showed that the performance of a chiral auxiliary improves when it is restricted by cation binding and confinement, and empty cages (without a chiral inductor) do not yield the product with 100% *de* [38].

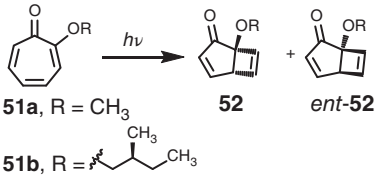


**Scheme 12.8** Enantiodifferentiating photocyclization of tropolone

The photorearrangement of 2,4-cyclohexadienones **53** within zeolite NaY results in the formation of **54** in 73% *de* (**Scheme** 12.9). Similar reactions conducted with other ion-exchanged Y zeolites, such as LiY (40%), KY (1%), RbY (−25%), and CsY (−20%), also yield the corresponding products with varying diastereoselectivities [39]. The stereochemistry of the dominant photoproduct is highly sensitive to the size of the supercage and can be tuned by the cation species present in the zeolite. Hence, exchanging the cation of the zeolite can switch the diastereoselectivity of the product.

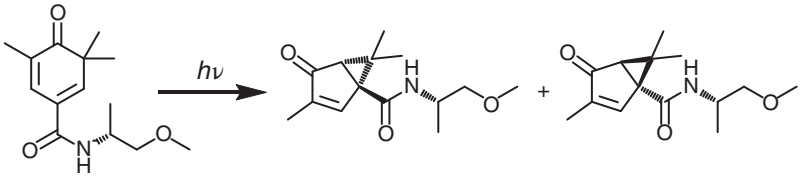


**Scheme 12.9** Oxa-di-π-methane rearrangement of cyclohexadienone derivatives.

The *cis*-to-*trans* photoisomerization of 1,2-diphenylcyclopropane **55** (**Scheme** 12.10) has been established in the supercage of MY zeolites (M = alkali metal). When 4′-methoxyacetophenone is used as the sensitizer, **55a** affords cis/trans ratios of 95 : 5 and 92 : 8 with LiY and NaY zeolites, respectively. No *ee* value is determined for **56** in NaY zeolite, but the *ee* value of **56b** is enhanced to 20% by using ephedrine as a chiral inductor, and **56c** increases to 17% by using cyclohexyl ethylamine [40]. The chiral inductors can be further covalently attached to afford intramolecular chiral auxiliaries, such as 2,3-diphenylcyclopropane **57** (**Scheme** 12.11). The *meta*-substituted ketone **57b** undergoes photoisomerization in NaY zeolite to give **57b** in 71% *de*, while irradiation of **57c** and **57d** at room temperature results in the formation of **57a** with near quantitative *ee*, respectively [41].

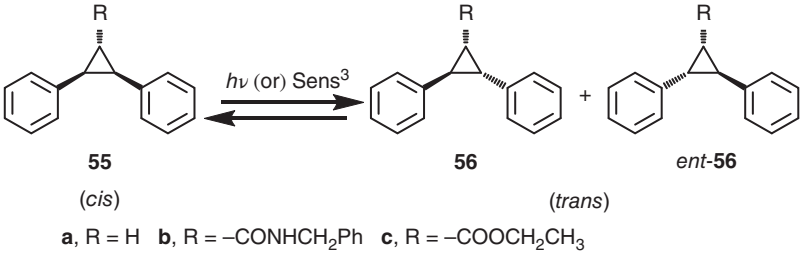


**Scheme 12.10** Photoisomerization of benzoylcyclopropane derivatives.

Turro *et al*. investigated the photolysis of aryl ketones **59** (**Scheme** 12.12). In solution, the photolysis process resulted in the formation of radical combination products **60** and **61** in yields of 23% and 70%, respectively. However, in NaY zeolite, the formation of combination products was strongly suppressed, and instead, the *para*-coupled product **62** was obtained with yields of up to 70%. Interestingly, when photolyzed in NaY zeolites in the presence of a chiral guest, such as (*D*)-diethyl-tartrate, the recombination product *S*-**59** was obtained with enantiomeric enrichment of 9.2% *ee* [42].

Singlet oxygen ($^1O_2$) is the smallest possible cyclophile, and as a substrate of [4 + 2] cycloaddition, it can control the stereoselectivity through an appropriate chiral inductor [43]. For example, the photooxygenation of the enecarbamate **63** with methylene blue (MB) as a sensitizer affords nonracemic methyldesoxybenzoin

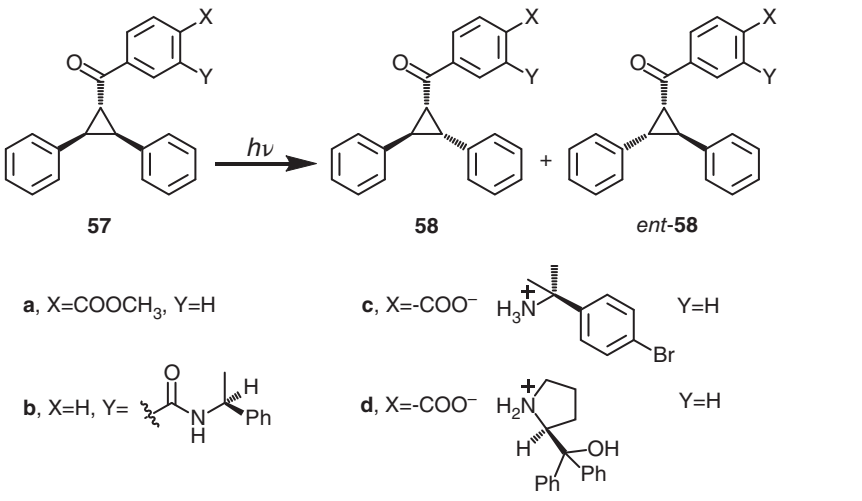


**Scheme 12.11** Photoisomerization of chirally modified benzoylcyclopropanes

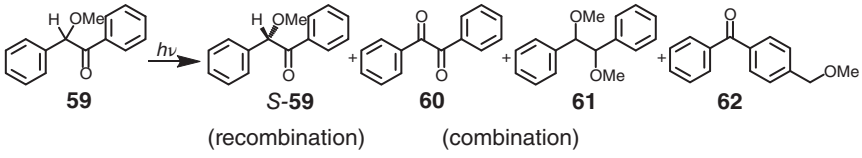


**Scheme 12.12** Photoreaction of benzoin methyl ether.

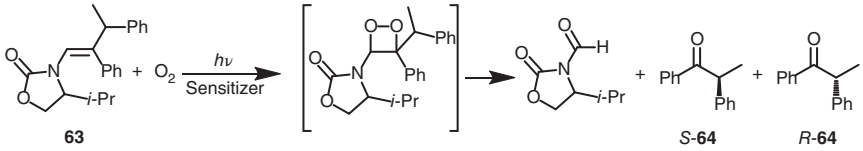


**Scheme 12.13** Singlet oxygenation of diastereomeric enecarbamates and subsequent decomposition to two carbonyl compounds.

**64** (**Scheme** 12.13), when the reaction was carried out in $CDCl_3$ slurry. The *Z*-isomers (*Z*)-(4*R*, 3'*R*/*S*)- and (*Z*)-(4*S*, 3'*R*/*S*)-**63** give (*R*)- and (*S*)-**64** in 27% and 11% *ee*, respectively, and the *E*-isomers (*E*)-(4*R*, 3'*R*/*S*)- and (*E*)-(4*S*, 3'*R*/*S*)-**63** give (*R*)- and (*S*)-**64** in 55% and 40% *ee*, respectively [43b]. Interestingly, when the *Z*-isomers **63** are irradiated in NaY zeolite exchanged with MB, the corresponding products (*S*)- and (*R*)-**64** are obtained with inverted stereoselectivity, yielding 80% and 71% *ee*, respectively, while the *E*-isomers **63** yield (*R*)- and (*S*)-**64** with 62% and 63% *ee*, respectively [43c]. Further studies have revealed that the anchoring of the enecarbamate substrate by the metal ion in the zeolite supercage, as well as the more rigid structure of *Z*-isomers, enhance the π-facial-selective attack by $^1O_2$ on the alkene, leading to improved stereoselectivity in the photooxygenation process [43c, d].

## 12.4 Chiral Photoreactions with Chiral Templates

Chiral templates are also significant supramolecular sources. Unlike host molecules mentioned above, which possess a cavity for accommodating guest substrates, chiral templates rely on direct interactions with target substrates through strong and directional non-covalent interactions, such as hydrogen bonding and electrostatic interactions. The relatively simpler structures of chiral templates allow for versatile design and synthesis, making them an effective and convenient chiral platform for achieving chirality transfer in photochirogenesis.

Generally, substrates can reach the triplet state through direct excitation following intersystem crossing or energy transfer from a triplet chiral template sensitizer. One of the most exemplary chiral template sensitizers is Kemp's triacid derivatives **65–70** (**Figure** 12.9), which have amide groups that function as both hydrogen bonding donors and acceptors, allowing them to bind with another lactam molecule. The bulky aromatic fence in **65–70** plays the role of sensitizer, which shields one enantioface of the photosubstrate to prevent self-association into a homodimer and allow for the attack of certain reagents from another side. Chiral templates **65** and **66** have mediated the photoreaction of the prochiral 2-quinolone allyl ether **71** to afford enantioselective intramolecular [2 + 2] photocycloaddition products **72** (**Scheme** 12.14). It was demonstrated that **65** and **66** form stable dual hydrogen

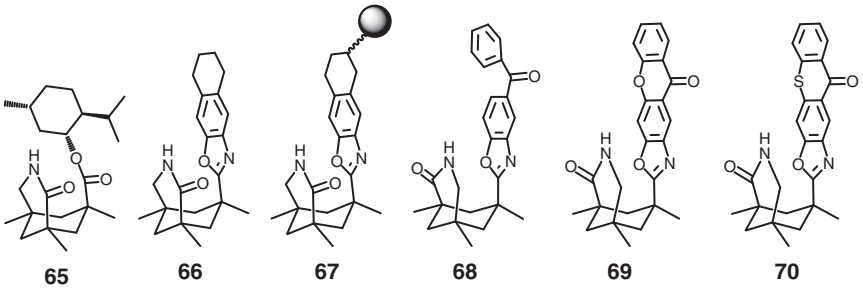


**Figure 12.9** Chiral γ-lactam templates of Kemp's triacid derivatives.

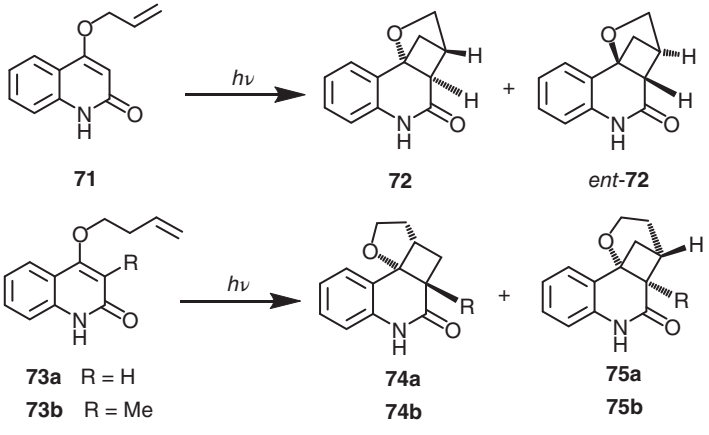


**Scheme 12.14** Intramolecular [2 + 2] photocyclization of quinolone.

bonds with **71**, and the bulky moiety makes the allyl group attack only from the opposite side, leading to high enantioselectivity. Increasing the amount of template, lowering reaction temperature, and decreasing solvent polarity can further promote enantioselectivity. For example, irradiating ($\lambda$ = 254 nm) **71** with *ent*-**66** at −60 °C resulted in *ent*-**72** with 93% *ee* [44]. Moreover, the methoxypolyethylene glycol (average molecular mass of 2000 Da, MPEG 2000) bound template **67** (**Figure** 12.9) could further enhance the selectivity, and under optimized conditions, the recovery yield of **67** and the conversions of **71** can reach up to 97% and 96%, respectively, after five catalytic cycles [45].

The xanthone **69** has relatively high triplet energy and comparably long-wavelength absorption and is more active than benzophenone **68**, **73a**, and **69** (**Scheme** 12.14) when irradiated ($\lambda$ = 366 nm) at −25 °C to obtain **74a** and **75b** with 78% yield and 94% *ee* [46]. The thioxanthone **70** can sensitize the intermolecular [2 + 2] photocycloaddition reactions under visible light irradiation and photosensitization of **76** and **70** with 10 equiv. of methyl acrylate irradiate ($\lambda$ = 419 nm) at −25 °C resulted in the regio- and simple diastereoselectivity product **77** in 74% *ee* [47]. (**Scheme** 12.15) As the wavelength of irradiation increases, solar irradiation can be utilized for this process. The alkyl group at the 3-position significantly decreases the triplet energy of 2-quinolone **73b**, and the intramolecular [2 + 2] photocycloaddition of **73b** is mediated by template **70** to afford a single regioisomer product **74b** with 88% *ee* [48].

2-Hydroxy-1,4-naphthoquinone **78** can form dual hydrogen bonds with template **66** (**Scheme** 12.16). However, when **78** reacted with alkene under photosensitization with **66** at −60 °C, the [3 + 2] photocycloaddition product **79** was given with a low

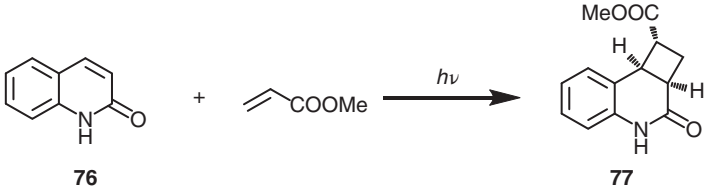


**76** **77**

**Scheme 12.15** Intramolecular [2 + 2] photocyclization of alkene to quinolone.

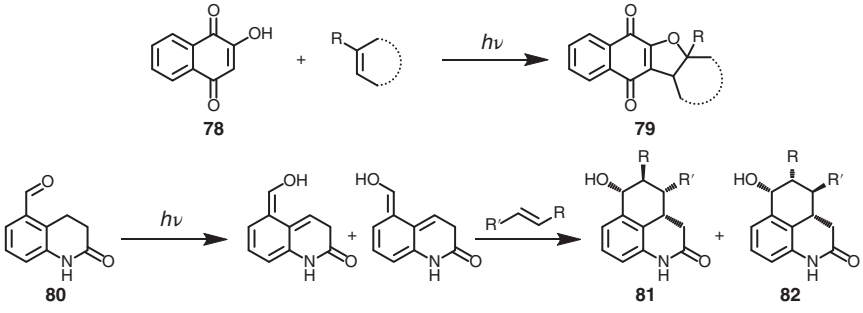


**Scheme 12.16** Intermolecular photocycloaddition of alkene to naphthoquinone and quinolone.

enantioselectivity of only 11%. This was attributed to the fact that **78** has two n-$\pi^*$ electronic transitions and exhibits a prolonged wavelength absorption in the range of 400–500 nm, which allows it to be directly excited by light rather than undergoing energy transfer through a chiral template sensitizer [49]. The in-situ two-step [4 + 2] Diels-Alder reaction between aldehyde **80** and dienophiles has been carried out in the presence of template **66**. (**Scheme** 12.16) Upon irradiation at $\lambda > 300$ nm, the aromatic aldehyde **80** undergoes hydrogen abstraction to form (*Z*)- and (*E*)-dienols. Subsequently, the longer-lived intermediate (*E*)-dienol undergoes cycloaddition with dienophiles in-situ. The reaction is conducted at −60 °C, forming the *exo*-adduct **81** as the major product with up to 94% *ee* [50].

Chiral templates **68** and **69** could also undergo photoinduced electron transfer (PET) to conduct chiral cyclization of spirocyclic pyrrolizidine. Photoirradiation initiates a PET process from the pyrrolidine nitrogen to the benzophenone moiety, followed by a proton transfer, resulting in the generation of the α-aminoalkyl radical. This radical then attacks intramolecularly at the C-4 position of the quinolone from the open face, leading to the formation of the chiral cyclization product. When compound **83** is irradiated with 0.3 equiv. of template **68,** the spiro product **84** was obtained with 64% yield and up to 70% *ee* [7a] (**Scheme** 12.17).

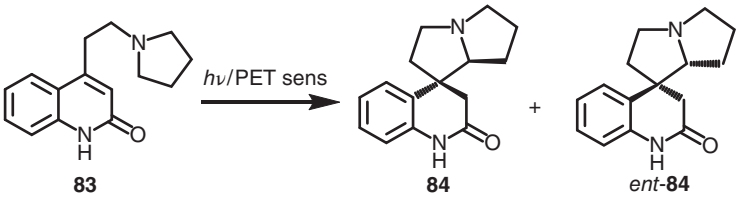


**Scheme 12.17** Photocyclization sensitized by chiral templates.

Chiral benzamide derivative 4-aminoprolinol TKS159 **85a** (**Figure** 12.10) has been employed as chiral templates in the supramolecular enantiodifferentiating photocyclodimerization of anthracene derivatives. **85a** bound **16a** through a nine-membered dual hydrogen-bonding motif incorporating the carboxylic acid and 2-hydroxymethylpyrrolidine moieties. The benzoyl moiety of **85a** could cover one of the enantiofaces of **16a** to block the attack of other molecules, while the opposite face is accessible to the free or another complexed **16a**. Photoirradiation of **16b** (**Scheme** 12.4) at $\lambda > 320$ nm with template **85a** is performed at −50 °C to obtain *syn*-HT dimer **18a** in 20% yields and −36% *ee* and *anti*-HH dimer **19a** with 31% yield and −40% *ee*, respectively. Due to the lower partial overlap of the template **85b** with the **16a** plane, photoirradiation with **85b** afforded the chiral cyclodimers with <3% *ee* [51]. Circular dichroism spectral studies discover the formation of a novel 2 : 1 HH-oriented hydrogen bonding/π -stacked complex between **16b** and **85a**, which causes significant circular dichroism spectral changes due to the exciton coupling interaction of two **16a** chromophores and a significant acceleration of the HH photocyclodimerization [52].

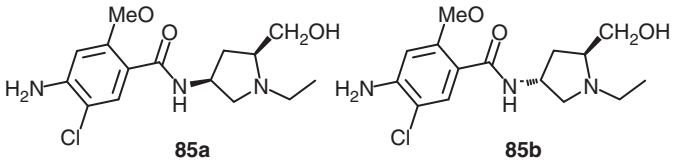


**Figure 12.10** Chiral hydrogen-bonding templates: epimeric 2-methoxybenzamide derivatives of 4-aminoprolinol.

## 12.5 Supramolecular Photochirogenesis with Biomolecular Hosts

Certain biomolecules, such as proteins, antibodies, and DNA, have high affinities and selectivities for organic molecules, making them ideal candidates as chiral supramolecular hosts for achieving photochirogenesis. When chiral organic guests are selectively bound by these bio-supramolecular hosts, photochemical reactions occur in the guest molecules after absorbing photons and reaching excited states. Typically, bio-supramolecular hosts absorb light in the UV–Vis region, with proteins absorbing UV light at 320 nm due to the presence of tryptophan and tyrosine moieties. Therefore, it is essential to identify the optimal irradiation wavelength to ensure the efficient transformation of guests while avoiding damage to the host structure.

Serum albumins are widely used as bio-supramolecular hosts in supramolecular photochirogenesis due to their accessibility and cost-effectiveness. Zandomennghi *et al.* investigated the photodecarboxylation kinetic of racemic 1,1′-binaphthol **86** in an aqueous solution with bovine serum albumin (BSA) (**Scheme** 12.18). BSA selectively binds to (*S*)-**86**, resulting in a bathochromic shift of the UV–Vis spectrum of **86**. Photoirradiation at the bathochromic shifted band resulted in enantiomeric isomerization, giving **86** with 77% conversion and 99.5% *ee* [53]. This reaction was reexamined with BSA and human serum albumin (HAS) using phosphate buffer at pH 7 instead of water. The results show that both BSA and HAS have a higher affinity for (*S*)-**86**, with affinity ratios ($K_S/K_R$) of 8.9 and 160, respectively. Additionally, the kinetic resolution of *rac*-**1** is less efficient, leading to (*R*)-**86** with 98% *ee* only at 99% decomposition with BSA and with 46% *ee* at 65% decomposition with HAS [54].

Serum albumins are also employed as chiral hosts in photocyclodimerization of **16a** (see **Scheme** 12.4). A series of research has been conducted on the interaction

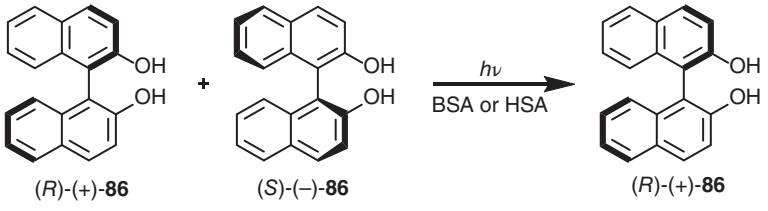


**Scheme 12.18** Photochemical kinetic resolution of racemic 1,1′-binaphthol.

between **16a** and various types of serum albumins, giving a variety of complexation information [55]. BSA has four independent binding sites, which were proved by UV–Vis, fluorescence, and CD spectral tests. Therefore, BSA can accommodate one, three, two, and three **16a**, respectively, by order of their binding constants. In the first unimolecular binding site, two different fluorescence lifetimes, 4.8 ns and 2.1 ns, respectively, were observed due to two different binding modes. The fluorescence lifetime of **16a** bound to the second site is 13.2 ns, much longer than the lifetimes of **16a** bound to sites 3 and 4, whose lifetimes are indistinguishable from the free **16a** in bulk water, which has a lifetime of 15.8 ns. This suggests that sites 3 and 4 are highly hydrophilic and possibly exposed to bulk water. This is supported by the effective quenching of **16a** fluorescence after adding nitromethane to the solution. In the photocyclodimerization of **16a** mediated by BSA, HH dimers dominate over HT dimers in solution because HH dimers are hindered sterically and electrostatically. The *anti*-HH dimer **19a** is obtained with 40% yield and 58% *ee* at **16a**/BSA = 3.8 condition. Furthermore, after adding 18 mM nitromethane, the *ee* of *syn*-HT dimers **16a** was enhanced to 38% [55a].

Although HSA and BSA differ by only 26 amino acid residues (out of approximately 600), their functional differences are significant when it comes to complex **16a** and photocyclodimerization. HSA possesses five independent binding sites, with sites 1–4 capable of binding one, one, three, and five molecules of **16a**, respectively. Weak binding occurs only at site 5 [4a, 56]. The two unimolecular binding sites (sites 1 and 2) correspond to Sudlow's drug sites II and I, respectively, and their affinities to **16a** are the highest, up to $10^{7-8}\ M^{-1}$. However, these sites are unproductive for photocyclodimerization entirely. On the contrary, **16a** bound to sites 3 and 4 are photoreactive and gave cyclodimers **17a**-**20a** (see **Scheme** 12.4) as final products. The ratios of these cyclodimers are similar to those obtained for free AC in bulk solution but differ significantly from those obtained with BSA [55c]. *syn*-HT dimer **18a** and *anti*-HH dimer **19a** can be produced with 82% and 90% *ee,* respectively, mediating HSA [55b]. These results demonstrate a significantly higher enantioselectivity than those mediated by BSA. Furthermore, the excited states of **16a,** which are bound to site 3, exhibit a long rotational correlation time of 36 ns, indicating limited mobility of **16a** in site 3 and explaining elevated *ee* with HSA [4b].

While serum albumins are strongly binding hosts and usually produce photoproducts with significant enantioselectivities, they often demand a great amount of albumin to prevent the possible photoreaction of free substrates in bulk solution, which is not desirable from the point of view of chirality source economy. An approach for catalytic photochirogenesis with HSA involving the recycling of HSA in a batch process has been reported. This method maintains a low **16a**/HSA ratio at *ca*. 3 to keep **16a** only in the highly enantiodifferentiating site 3 through incremental additions of extra **16a** to compensate consumption after photoirradiation [57]. As a result, after three incremental additions, a turnover number of 3.4 is achieved without significantly reducing the original high *ee* values.

Yokoyama *et al*. have published a study that describes the enantiodifferentiating 6π-photocyclization of photochromic diarylethenes (*M*)- and (*P*)-**87** to (*S*,*S*)- and (*R*,*R*)-**88** with the mediation of HSA (**Scheme** 12.19) [58]. The diarylethenes display

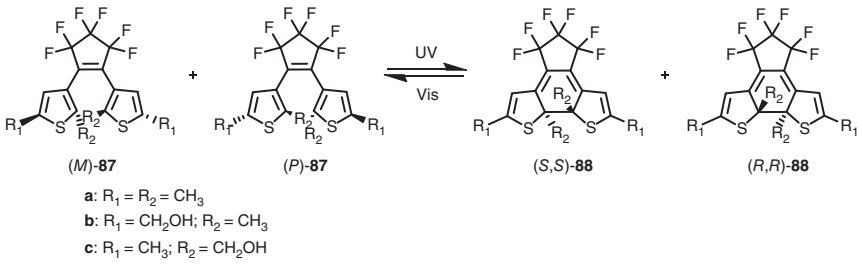


**Scheme 12.19** Enantiodifferentiating photocyclization of diarylethenes.

induced circular dichroism spectra as they are bound to HSA weakly in Sudlow's drug site I with $K = 8200\ M^{-1}$ for **87b**. When **87a**-**c** was irradiated at 313 nm in the presence of 0.2–10 equivalents of HSA, it yielded the ring-closed **88a**-**c** with *ee* values ranging from 8 to 42%, 18–63%, and 3–27%, respectively, at room temperature. Additionally, the highest *ee* of 71% was achieved when **87b** was irradiated at −4 °C with 10 equivalents of HSA.

More recently, Yokoyama *et al.* investigated the enantioselective photochromic ring closure of diarylethenes mediated by HAS (**Scheme** 12.20) [59]. Bis(thiophen-2-yl)hexafluorocyclopentenes **89a** and **89b** bearing a close resemblance to the previously reported isomer **87** were used in the study. Highly enantioselective photochromic ring closure was observed in **89a** and **89b** upon exposure to HSA, and they exhibited absorption of longer-wavelength UV light compared to the corresponding isomer of the thiophen-3-yl family (such as 313 nm for **87**). Therefore, the photochromism of **89a** and **89b** could be achieved using less harmful UV light (366 nm) compared to that required for **87**. $^{19}F$ nuclear magnetic resonance analysis revealed that in the presence of 1 equiv. of HSA at 323 K, **89a** exhibited six distinct signals, in contrast to the two signals observed in the absence of HSA. This indicates that all six fluorine atoms of the **89a** molecule are situated in different environments, suggesting the presence of a highly asymmetric environment within HSA. Furthermore, the addition of chiral HSA resulted in the highest *ee* value of 98% for **90a** in an acetonitrile/phosphate-buffered saline (PBS) solution with a 1 : 99 ratio after reaching the photostationary state. This *ee* value remained unchanged even when the incubation temperature was lowered from ambient temperature to −4 °C. On the other hand, **90b** exhibited a maximum *ee* value of 81.4% after irradiation with 366 nm light in an acetonitrile/PBS solution with a 13 : 87 ratio.

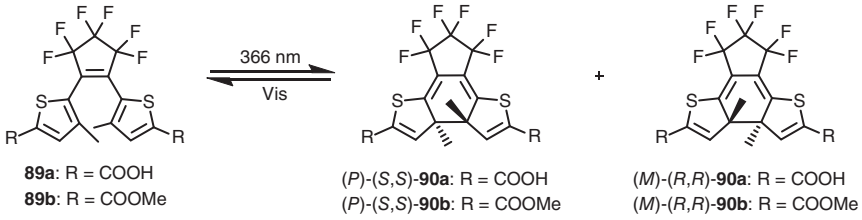


**Scheme 12.20** Enantiodifferentiating photocyclization of diarylethenes.

The *ee* value of **90b** slightly increased to 82.8% when the incubation temperature was lowered to −4 °C.

It has been demonstrated that (*Z*)-cyclooctene can undergo enantiodifferentiating photoisomerization from the *Z*-configuration to the *E*-configuration using chiral sensitizers (see **Scheme** 12.1), such as nucleosides and nucleotides [60]. Pyrimidine and purine nucleosides are used as chiral sensitizers and yield **1E** with 5.2% *ee* in the photostationary state. However, the utilization of calf thymus DNA could increase the *ee* value to −15.2%. The most likely explanation for this phenomenon is that **1Z** binds to the hydrophobic minor groove of double-stranded DNA before photosensitization. This is supported by the observation that the *ee* of **1E** significantly decreases, approaching zero, upon irradiation at higher temperatures or in 50% aqueous methanol. These results suggest that supramolecular interactions play a critical role in the enantiodifferentiating process.

Despite the advantages mentioned above and the widespread utilization of serum albumins, there are limitations, such as long wavelength absorption caused by the tryptophan moiety and complicated complexation due to multi-binding sites in experiments. As an alternative, prefoldin (PFD), a chaperone protein derived from archaeal *pyrococcus horikoshii* OT3, has gained attention. PFD is a tryptophan-free, jellyfish-like heterohexamer with a semi-cage structure and hydrophobic amino acid moieties on the inside surfaces. These unique features make it an attractive candidate for supramolecular photochirogenesis, as non-productive unimolecular binding and electron-transfer quenching by tryptophan will be inhibited. Therefore, PFD has been employed as a chiral protein host to facilitate the photocyclodimerization of **16a** (see **Scheme** 12.4) [61]. CD spectrum showed that multiple **16a** binds to PFD at relatively distant positions without exciton-coupling interactions. Even in the presence of an eightfold excess of PFD, the photocyclodimerization of **16a** is not slowed down, which indicates a weak binding constant, but rather biasedly produced the HH dimers, resulting in chiral dimers **18a** and **19a** with 10% and 16% *ee*, respectively.

Recently, chiral variants of amyloid fibrils have been used in supramolecular photocyclodimerization of **16a** [62]. Those fibrils are prepared by agitating acidified solutions of bovine insulin. The (+)- and (−)-insulin fibrils prepared by the chiral bifurcation induce a quasi-mirror-imaged circular dichroism spectrum upon complexation with **16a**. Upon photoirradiation, these fibrils also afford *anti*-HH dimer **19a** of the opposite absolute configuration with −10% and +17% *ee*, respectively. While the *ee* values obtained are not very high, it is noteworthy that both enantiomers can be obtained by modifying the chiral type of **16a**-binding amyloid matrix, which is not practically feasible with normal biological hosts.

## 12.6 Supramolecular Photochirogenesis with Circularly Polarized Light in Supramolecular Systems

Circularly polarized light (CPL) is a chiral electromagnetic field that can convey chiral bias information to materials. CPL could be generated by passing non-polarized

light through a polarizer and a quarter-wave plate, resulting in left-handed (*l*-) or right-handed (*r*-) CPL, depending on the direction of rotation of the electric vector ***E*** when the light approaches the observer. The wave emitted from CPL is considered a true chiral entity [63] capable of inducing photochirogenesis in asymmetric photochemistry, which has been proposed as a possible explanation for the homochirality of life [64]. While CPL has found applications in various fields [65], its use in introducing chiral biases into molecules is relatively limited compared to chiral catalysts and even fewer in supramolecular photochirogenesis.

There are three mechanisms of CPL-induced asymmetric photochemical reactions (A–C), which are often used to induce photochirogenesis at the molecular level [66]. However, the resulting chiral biases in these mechanisms can also be amplified by enantioselective association, leading to a predominant helical sense at the supramolecular scale. Furthermore, chiral biases can also arise from the self-assembly or polymerization of achiral molecules or a combination of chiral and achiral molecules under CPL irradiation in the field of supramolecular chemistry (D):

A. Asymmetric photodegradation;
B. Photoderacemization;
C. CPL-induced asymmetric synthesis;
D. CPL-induced asymmetric assembly or polymerization.

Recently, Zou *et al.* studied the enantioselective photopolymerization of thiol-ene [67]. Racemic allyl-(1-((3-[dimethylamino]propyl)amino)-4-mercapto-1-oxobutan-2-yl)carbamates (DPAMOC) were used as substrates in polymerization. In a previous study published by the authors, chiral bias was observed due to a difference in absorption coefficients for chiral light between the enantiomers under CPL irradiation. As a result, one enantiomer with a certain chirality exhibited preferential activation of the thiyl radical intermediate during the photopolymerization process [65c]. Furthermore, a significant improvement in *ee* (ca. 20%) was achieved by adding HAD (hydrogen atom donors), which effectively suppressed undesirable carbon-centered side reactions. Furthermore, HAD also quenched the racemic thiyl radical, allowing the substrate enantiomers to be re-triggered by CPL and produce the preferential enantiomer again, akin to a refined procedure. The resulting poly(thioether) displayed high luminescence in aggregated states, known as clusterization-triggered emission (CTE), and exhibited strong circularly polarized luminescence (Scheme 12.21).

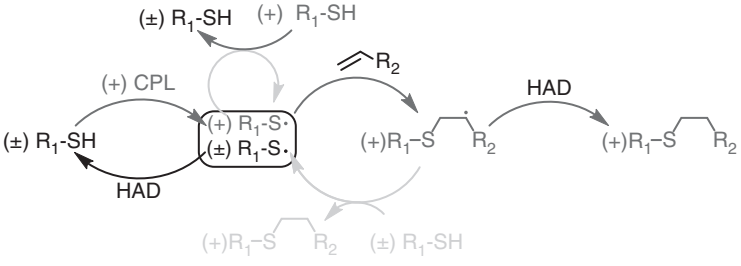


**Scheme 12.21** Kinetics diagrams of CPL-triggered enantioselective thiol–ene click reaction with additional HAD.

Seo *et al.* reported a process involving the self-assembly of triarylamine, known as the "sergeants and soldiers" process, to control the formation of *M*-type (left-handed) and *P*-type (right-handed) helices from achiral triarylamine (DA-TAA) through enantioselective polymerization via *l*- and *r*-CPL [68]. In this study, CPL acts as "photonic sergeant"and competes with sergeant molecules in the chirality induction process. Copolymerization of DA-TAA with sergeant molecule S-TAA (<10 mol% loading) mainly produced *M*-type helix with *P*-superhelix formed by the opposite coiling of the *M*-helix under UV irradiation. In contrast, both *l*- and *r*-CPL irradiation produced an opposite CD sign in the presence of 5 mol% S-TAA. *P*-helix and *P*-superhelix were identified as being generated by *r*- and *l*-CPL, respectively, based on CD spectrum features. Irradiating DA-TAA with CPL produced *P*-helix, indicating that CPL overrode the chiral information from S-TAA. However, increasing S-TAA loading to 10 mol% results in more *M*-helix forming *P*-superhelix under UV irradiation, overriding the chiral information from *r*-CPL and producing a similar CD sign with lower intensity (Figure 12.11).

Nakano *et al.* recently reported a CPL irradiation-induced enantioselective self-assembly of preferred axial chiral regional molecules of **93–95** [69]. The CPL-induced photoreaction of these molecules is conducted in the solid state using thin film samples to limit the rotational freedom of the single bonds. The mirror image CD spectra of **93–95** are obtained upon irradiation with *l*-CPL and *r*-CPL. Further analysis using DTF calculations suggests that the changes in spectra can be attributed to variations in the average dihedral angle around the single bonds (Figure 12.12).

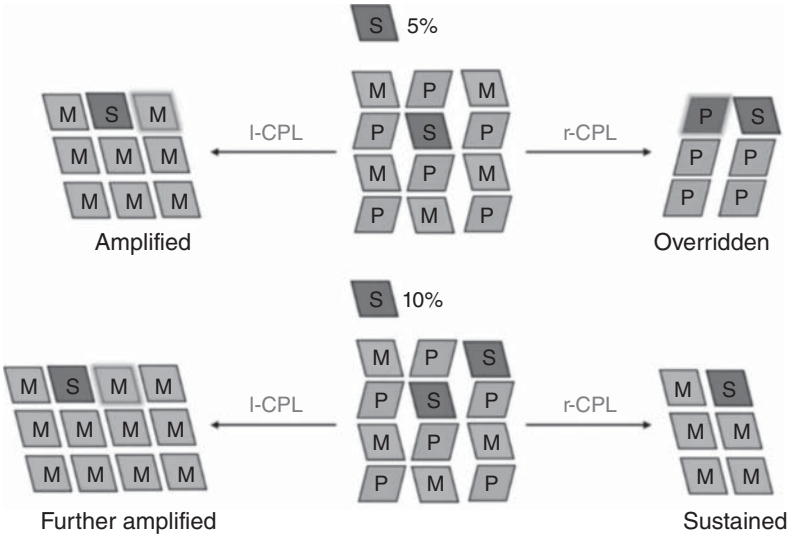


**Figure 12.11** Transmission of chiral information from molecular chirality and CPL as an external input. Possible scenarios of chirality induction when molecular and photonic sergeants coexist.

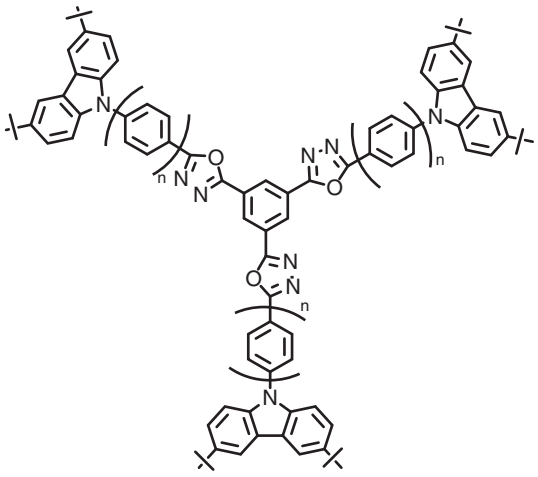

**93** n = 1; **94** n = 2; **95** n = 3

**Figure 12.12** Structures of star-shaped oligomers (93–95).

## 12.7 Supramolecular Photochirogenesis in Other Supramolecular Systems

The aqueous organopalladium octahedral cage **96** (**Scheme** 12.22) is another representative supramolecular host in photochemistry, which assembles from *cis* end-capped Pd(II) ions and triazine-cored tridentate ligands [70]. The cage **96** induced a [2 + 2] photoaddition of a maleimide derivative **100** (**Scheme** 12.22) with fluoranthene **97a** and **97b** in an aqueous solution by co-including the photosubstrates at room temperature to give product **101a** and **101b** with 40% and 50% *ee*, respectively [70d]. The similar [2 + 2] photo- or [2 + 4] Diels–Alder additions of **100** with aceanthrylene **98** and phenanthrene **99** in the cavity of **96** give the corresponding products **102** and **103** in 60% and 50% yields, respectively [70e].

Photochemical asymmetric syntheses are also performed in organized assemblies, such as gels and liquid crystals (LCs). The gel sample that mixed gelator **109** (**Figure** 12.13) with methylcyclohexane/*n*-hexane (1 : 1 v/v) was photoirradiated at 5 °C to obtain *syn*-HT dimer **18a** with 41% *ee* and *anti*-HH dimer **19a** with −56% *ee* in the **109**-glycidyl methyl ether gel sample [71].

The equimolar amounts of amino alcohol **110**–**112** (**Figure** 12.13) and carboxylic acids were mixed to form two-component crystals, which could be considered "flexible crystals" or "ordered solvents". The LC of **110** and **16a** (see **Scheme** 12.4) was irradiated at $\lambda > 380$ nm at 45 °C (smectic state) to afford *anti*-HH dimer **19a** in 81% *ee* [72]. The amino alcohols **110**–**112** exhibit different stereochemistries but similar sizes and shapes, leading to distinct results in the photocyclodimerization of **16a**. When **16a** and **111** are in the crystalline phase at 40 °C and irradiated at $\lambda > 380$ nm, *anti*-HH dimer **19a** was given with −15% *ee*. However, **110** was unidentified mesophase at 45 °C and afforded **19a** with up to 86% *ee*, while **112** was the smectic state at 40 °C and gave **19a** with 32% *ee*. The overall yields increase with longer irradiation time, but the enantioselectivity decreases.

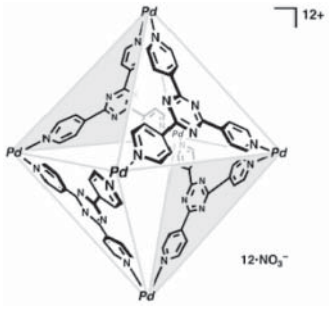


96

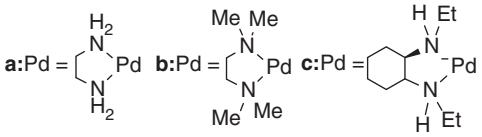


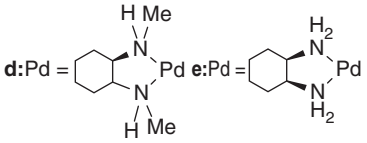


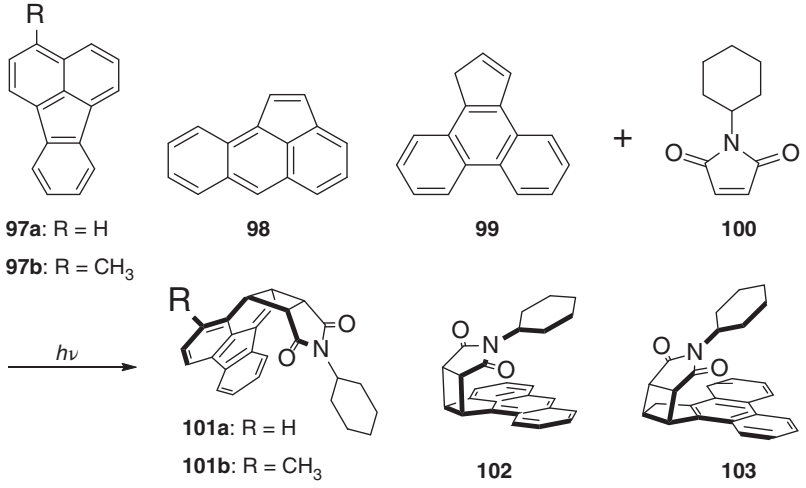


**Scheme 12.22** Photocycloaddition in the cavity of M6L4 cage incorporating chiral ligands.

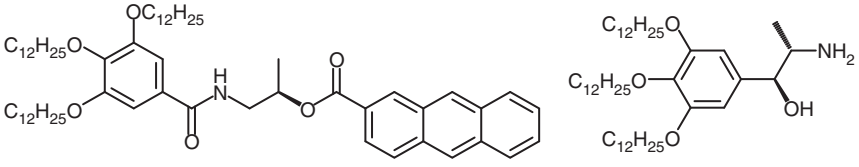


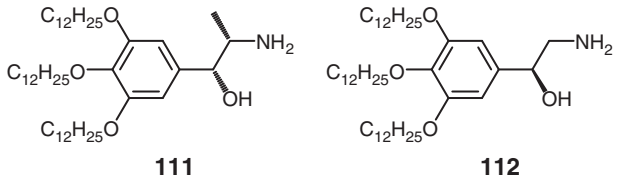


**Figure 12.13** The structure of liquid crystal and amphiphilic amino alcohol.

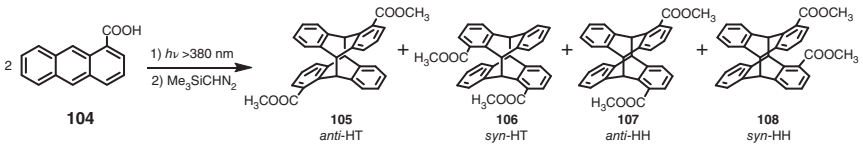


**Scheme 12.23** Enantiodifferentiating photocyclodimerization of 1-anthracenecarboxylic acid.

However, the in situ photocyclodimerization of 1-anthracenecarboxylic acid **104** with **110** at 25 °C afforded **107** with the highest *ee* value (−13%), probably due to less chirally ordered alignment of **106** in the LC phase [73] (**Scheme** 12.23). Isothermal annealing processes can also affect enantioselectivity, as cooling the LC of **16a** and **110** from 115 °C to 45 °C and then irradiated at 45 °C for 1 h afforded *anti*-HH dimer **19a** with 86% *ee*, while keeping it at 45 °C for 20 h before being photoirradiated for 1 h gave **19a** with −94% *ee* [74]. More recently, the cross-photocyclodimerization between two photo reactants was achieved by applying the LCs strategy. The overall chemo ratio of the cross-cyclodimer **17b**–**20b** was 58%, with corresponding regiochemistry ratios of 1%, 1%, 83%, and 15%, respectively, and the cross *anti*-HH dimer **19b** was obtained with up to 90% *ee* [75].

The hexagonal liquid crystal (HLC) **113** (**Figure** 12.14) is formed by mixing *n*-pentanol, sodium dodecyl sulfate (SDS), and $H_2O$ in a weight ratio of 1 : 6 : 9, with (1*R*,2*S*)-(−)-norephedrine **115** serving as the chiral inductor. The photochemical reaction of **51a** at −10 °C in HLC **113** afforded **52a** and *ent*-**52a** up to 40% ee, while using (1*S*,2*R*)-(+) **115** as the chiral inductor afforded the opposite result (−40% *ee*) (**Scheme** 12.24). When menthol and decanol were used as chiral inductors, low *ee* was obtained (5%), and undoped LC resulted in a racemic product [76]. *p*-Xylene, (*S*)-3-hexadecyl-1-(1-hydroxy-propan-2-yl)imidazolium bromide and $H_2O$ were

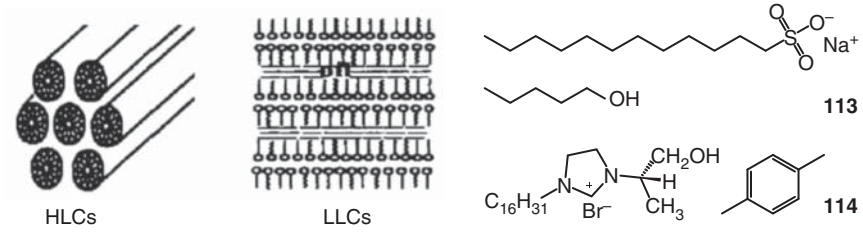


**Figure 12.14** The hexagonal liquid crystal (HLC) and lamellar liquid crystals (LC).

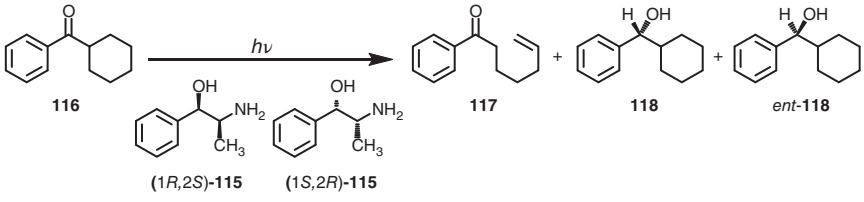


**Scheme 12.24** Photochemical reduction and cleavage of cyclohexyl phenyl ketone.

mixed in a ratio of 0.25 : 0.50 : 0.25 and gave HLC **114**. Upon irradiation of **116** in **114** with hydrogen donor triethylamine, the inter- and intra-molecular hydrogen abstraction products **117** and **118** were obtained in 0 : 100 ratio with 13% *ee* [77].

## References


**1** (a) Ramamurthy, V. and Sivaguru, J. (2016). *Chem. Rev.* 116: 9914–9993. (b) Ramamurthy, V. and Inoue, Y. (2011). *Supramolecular Photochemistry, Supramolecular Photochemistry: Controlling Photochemical Processes*. John Wiley & Sons. (c) Brimioulle, R., Lenhart, D., Maturi, M.M., and Bach, T. (2015). *Angew. Chem. Int. Ed.* 54: 3872–3890.

**2** Yang, C. and Inoue, Y. (2014). *Chem. Soc. Rev.* 43: 4123–4143.

**3** (a) Pattabiraman, M., Sivaguru, J., and Ramamurthy, V. (2017). *Isr. J. Chem.* 58: 264–275. (b) Liu, J., Lan, Y., Yu, Z. et al. (2017). *Acc. Chem. Res.* 50: 208–217.

**4** (a) Nishijima, M., Pace, T.C.S., Nakamura, A. et al. (2007). *J. Org. Chem.* 72: 2707–2715. (b) Fuentealba, D., Kato, H., Nishijima, M. et al. (2013). *J. Am. Chem. Soc.* 135: 203–209.

**5** Urushima, A., Taura, D., Tanaka, M. et al. (2020). *Angew. Chem. Int. Ed.* 59: 7478–7486.

**6** (a) Nakamura, A. and Inoue, Y. (2003). *J. Am. Chem. Soc.* 125: 966–972. (b) Wang, Q., Yang, C., Ke, C. et al. (2011). *Chem. Commun.* 47: 6849–6851.

**7** (a) Bauer, A., Westkamper, F., Grimme, S., and Bach, T. (2005). *Nature* 436: 1139–1140. (b) Brimioulle, R. and Bach, T. (2013). *Science* 342: 840–843.

**8** Inoue, Y., Wada, T., Sugahara, N. et al. (2000). *J. Org. Chem.* 65: 8041–8050.

**9** Lu, R., Yang, C., Cao, Y. et al. (2008). *J. Org. Chem.* 73: 7695–7701.

**10** Jin, P., Rong, Y., Liang, W. et al. (2021). *J. Org. Chem.* 87: 1679–1688.

**11** Yang, C., Mori, T., Wada, T., and Inoue, Y. (2007). *New J. Chem.* 31: 697–702.

**12** Yan, Z., Huang, Q., Liang, W. et al. (2017). *Org. Lett.* 19: 898–901.

**13** Liang, W., Yang, C., Zhou, D. et al. (2013). *Chem. Commun.* 49: 3510–3512.

**14** Wei, X., Liang, W., Wu, W. et al. (2015). *Org. Biomol. Chem.* 13: 2905–2912.

**15** Liang, W., Zhao, M., Wei, X. et al. (2017). *RSC Adv.* 7: 17184–17192.

**16** Mansour, A.T., Buendia, J., Xie, J. et al. (2017). *J. Org. Chem.* 82: 9832–9836.

**17** Tamaki, T. and Kokubu, T. (1984). *J. Incl. Phenom. Macrocycl. Chem.* 2: 815–822.

**18** Shih, T.-W., Chen, Y.-R., Wei, X. et al. (2023). *Cell Rep. Phys. Sci.* 4: 101216–101255.

**19** Ikeda, H., Nihei, T., and Ueno, A. (2005). *J. Org. Chem.* 70: 1237–1242.

**20** Yang, C., Fukuhara, G., Nakamura, A. et al. (2005). *J. Photoch. Photobio. A* 173: 375–383.

**21** Yang, C., Mori, T., and Inoue, Y. (2008). *J. Org. Chem.* 73: 5786–5794.

**22** (a) Yang, C., Mori, T., Origane, Y. et al. (2008). *J. Am. Chem. Soc.* 130: 8574–8575. (b) Yang, C., Ke, C., Liang, W. et al. (2011). *J. Am. Chem. Soc.* 133: 13786–13789.

**23** Yang, C., Ke, C., Kahee, F. et al. (2008). *Aust. J. Chem.* 61: 565–568.

**24** Kanagaraj, K., Liang, W., Rao, M. et al. (2020). *Org. Lett.* 22: 5273–5278.

**25** Wang, Q., Liang, W., Wei, X. et al. (2020). *Org. Lett.* 22: 9757–9761.
**26** Wei, X., Wu, W., Matsushita, R. et al. (2018). *J. Am. Chem. Soc.* 140: 3959–3974.
**27** Wei, X., Yu, X., Zhang, Y. et al. (2019). *J. Photoch. Photobio. A* 371: 374–381.
**28** Ke, C., Yang, C., Mori, T. et al. (2009). *Angew. Chem. Int. Ed.* 48: 6675–6677.
**29** Rao, M., Kanagaraj, K., Fan, C. et al. (2018). *Org. Lett.* 20: 1680–1683.
**30** Rao, M., Wu, W., and Yang, C. (2019). *Molecules* 24: 1502–1506.
**31** Rao, M., Fan, C., Ji, J. et al. (2022). *ACS Appl. Mater. Inter.* 14: 21453–21460.
**32** Ji, J., Wu, W., Liang, W. et al. (2019). *J. Am. Chem. Soc.* 141: 9225–9238.
**33** Wang, X., Ji, J., Rao, M. et al. (2021). *Chem. Asian J.* 16: 3091–3096.
**34** Ji, J., Wu, W., Wei, X. et al. (2020). *Chem. Commun.* 56: 6197–6200.
**35** (a) Sivaguru, J., Natarajan, A., Kaanumalle, L.S. et al. (2003). *Acc. Chem. Res.* 36: 509–521. (b) Ramamurthy, V. (2019). *Molecules* 24: 3570–3588.
**36** (a) Sen, S.E., Smith, S.M., and Sullivan, K.A. (1999). *Tetrahedron* 55: 12657–12698. (b) Hutchings, G.J. (1999). *Chem. Commun.* 301–306. (c) van de Velde, F., Arends, I., and Sheldon, R.A. (2000). *Top. Catal.* 13: 259–265. (d) Suslov, E.V., Korchagina, D.V., Komarova, N.I. et al. (2006). *Mendeleev Commun.* 16: 202–204.
**37** Joy, A., Uppili, S., Netherton, M.R. et al. (2000). *J. Am. Chem. Soc.* 122: 728–729.
**38** Joy, A., Kaanumalle, L.S., and Ramamurthy, V. (2005). *Org. Biomol. Chem.* 3: 3045–3053.
**39** Uppili, S. and Ramamurthy, V. (2002). *Org. Lett.* 4: 87–90.
**40** Kaanumalle, L.S., Sivaguru, J., Sunoj, R.B. et al. (2002). *J. Org. Chem.* 67: 8711–8720.
**41** Chong, K.C.W., Sivaguru, J., Shichi, T. et al. (2002). *J. Am. Chem. Soc.* 124: 2858–2859.
**42** Kaprinidis, N.A., Landis, M.S., and Turro, N.J. (1997). *Tetrahedron Lett.* 38: 2609–2612.
**43** (a) Poon, T., Turro, N.J., Chapman, J. et al. (2003). *Org. Lett.* 5: 2025–2028. (b) Poon, T., Sivaguru, J., Franz, R. et al. (2004). *J. Am. Chem. Soc.* 126: 10498–10499. (c) Sivaguru, J., Poon, T., Franz, R. et al. (2004). *J. Am. Chem. Soc.* 126: 10816–10817. (d) Sivaguru, J., Saito, H., Solomon, M.R. et al. (2006). *Photochem. Photobiol.* 82: 123–131.
**44** Bach, T., Bergmann, H., Grosch, B., and Harms, K. (2002). *J. Am. Chem. Soc.* 124: 7982–7990.
**45** Breitenlechner, S. and Bach, T. (2008). *Angew. Chem. Int. Ed.* 47: 7957–7959.
**46** Muller, C., Bauer, A., and Bach, T. (2009). *Angew. Chem. Int. Ed.* 48: 6640–6642.
**47** Troster, A., Alonso, R., Bauer, A., and Bach, T. (2016). *J. Am. Chem. Soc.* 138: 7808–7811.
**48** Li, X., Jandl, C., and Bach, T. (2020). *Org. Lett.* 22: 3618–3622.
**49** Muller, C., Bauer, A., and Bach, T. (2011). *Photochem. Photobiol. Sci.* 10: 1463–1468.
**50** Grosch, B., Orlebar, C.N., Herdtweck, E. et al. (2004). *Chem. Eur. J.* 10: 2179–2189.
**51** Mizoguchi, J., Kawanami, Y., Wada, T. et al. (2006). *Org. Lett.* 8: 6051–6054.

**52** Kawanami, Y., Katsumata, S.Y., Mizoguchi, J.I. et al. (2012). *Org. Lett.* 14: 4962–4965.

**53** (a) Festa, C., Levi-Minzi, N., and Zandomeneghi, M. (1996). *Gazz. Chim.* 126: 599–603. (b) Levi-Minzi, N. and Zandomeneghi, M. (1992). *J. Am. Chem. Soc.* 114: 9300–9304. (c) Ouchi, A., Zandomeneghi, G., and Zandomeneghi, M. (2002). *Chirality* 14: 1–11.

**54** Nishijima, M., Chang, J.-W., Yang, C. et al. (2013). *Res. Chem. Intermed.* 39: 371–383.

**55** (a) Asaoka, S., Wada, T., and Inoue, Y. (2003). *J. Am. Chem. Soc.* 125: 3008–3027. (b) Nishijima, M., Wada, T., Mori, T. et al. (2007). *J. Am. Chem. Soc.* 129: 3478–3479. (c) Pace, T.C.S., Nishijima, M., Wada, T. et al. (2009). *J. Phys. Chem. B* 113: 10445–10453.

**56** Nishijima, M., Pace, T.C.S., Bohne, C. et al. (2016). *J. Photoch. Photobio. A* 331: 89–94.

**57** Nishijima, M., Kato, H., Yang, C. et al. (2013). *ChemCatChem* 5: 3237–3240.

**58** Mai, F., Kawamura, I., Ubukata, T., and Yokoyama, Y. (2013). *Chem. Eur. J.* 19: 9401–9401.

**59** Saeki, Y., Kayanuma, M., Nitta, A. et al. (2021). *J. Org. Chem.* 86: 12549–12558.

**60** Wada, T., Sugahara, N., Kawano, M., and Inoue, Y. (2000). *Chem. Lett.* 29: 1174–1175.

**61** Bando, K., Zako, T., Sakono, M. et al. (2010). *Photoch. Photobio. Sci.* 9: 655–660.

**62** Nishijima, M., Tanaka, H., Yang, C. et al. (2013). *Chem. Commun.* 49: 8916–8918.

**63** (a) Barron, L.D. (1987). *Biosystems* 20: 7–14. (b) Chela-Flores, J. and Ponnamperuma, C. (1992). *Chemical Evolution: Origin Of Life*. A. Deepak Publishing.

**64** (a) Balavoine, G., Moradpour, A., and Kagan, H.B. (1974). *J. Am. Chem. Soc.* 96: 5152–5158. (b) Cronin, J.R. and Pizzarello, S. (1997). *Science* 275: 951–955. (c) Hao, C., Xu, L., Sun, M. et al. (2019). *Chem. Eur. J.* 25: 12235–12240.

**65** (a) Rong, R., Liu, Y., Nie, X. et al. (2023). *Adv. Sci.* 10: 2206191. (b) Saito, K. and Tatsuma, T. (2018). *Nano Lett.* 18: 3209–3212. (c) Yang, G., Xu, Y.Y., Zhang, Z.D. et al. (2017). *Chem. Commun.* 53: 1735–1738.

**66** (a) Rau, H. (1983). *Chem. Rev.* 83: 535–547. (b) Inoue, Y. (1992). *Chem. Rev.* 92: 741–770.

**67** He, C.-L., Feng, Z., Li, Y. et al. (2021). *Polym. Chem.* 12: 2433–2438.

**68** Kang, J.S., Kang, S., Suh, J.M. et al. (2022). *J. Am. Chem. Soc.* 144: 2657–2666.

**69** Zhang, Z., Harada, T., Pietropaolo, A. et al. (2021). *Chem. Commun.* 57: 1794–1797.

**70** (a) Yoshizawa, M., Tamura, M., and Fujita, M. (2006). *Science* 312: 251–254. (b) Furusawa, T., Kawano, M., and Fujita, M. (2007). *Angew. Chem. Int. Ed.* 46: 5717–5719. (c) Yoshizawa, M., Takeyama, Y., Okano, T., and Fujita, M. (2003). *J. Am. Chem. Soc.* 125: 3243–3247. (d) Nishioka, Y., Yamaguchi, T., Kawano, M., and Fujita, M. (2008). *J. Am. Chem. Soc.* 130: 8160–8161. (e) Horiuchi, S., Nishioka, Y., Murase, T., and Fujita, M. (2010). *Chem. Commun.* 46: 3460–3462.

**71** Dawn, A., Shiraki, T., Haraguchi, S. et al. (2010). *Chem. Eur. J.* 16: 3676–3689.

**72** Ishida, Y., Kai, Y., Kato, S.Y. et al. (2008). *Angew. Chem. Int. Ed.* 47: 8241–8245.

**73** Ishida, Y., Achalkumar, A.S., Kato, S. et al. (2010). *J. Am. Chem. Soc.* 132: 17435–17446.
**74** Ishida, Y., Matsuoka, Y., Kai, Y. et al. (2013). *J. Am. Chem. Soc.* 135: 6407–6410.
**75** Kanai, H., Yamada, K., Salikolimi, K. et al. (2022). *Chem. Eur. J.* 28: e202201940.
**76** Lv, F.F., Chen, B., Wu, L.Z. et al. (2008). *Org. Lett.* 10: 3473–3476.
**77** Yang, X., Li, X., Chen, B. et al. (2013). *Chin. J. Chem.* 31: 603–606.

# 13

# Organocatalysis via Covalent Bonds for Asymmetric Radical Transformations

*Danqing Zheng*

*State Key Laboratory of Materials-Oriented Chemical Engineering, College of Chemical Engineering, Nanjing Tech University, Nanjing, China*

## 13.1 Introduction

It is a fundamental task to develop methods for the preparation of chiral molecules as single enantiomers in organic synthesis [1, 2]. Asymmetric organocatalysis, which uses organic molecules as chiral catalysts, has been extensively developed and offers a powerful tool for asymmetric synthesis [3–5]. This field has recently been recognized by the 2021 Chemistry Nobel Prize for the outstanding achievements of Benjamin List and David MacMillan. It is noteworthy that early studies of asymmetric organocatalysis mainly focused on two-electron-pair transformations [6–8]. The area of radical chemistry has recently flourished [9]. Impressive achievements have been witnessed using these reactive single-electron species to solve synthetic challenges. Along these lines, organocatalyzed enantioselective radical reactions have been developed, in particular thanks to the progression of photocatalytic reactions [10, 11]. In this chapter, we will summarize the recent advances in organocatalyzed asymmetric radical transformations, with an emphasis on covalent bonding activation modes.

Asymmetric organocatalysis via covalent modes has pioneered the early studies of asymmetric radical reactions. In covalent bonding activation modes, organocatalysts react with the substrates covalently to produce chiral transient reactive intermediates, which are further transferred to radicals or react with radicals [12, 13]. Impressive enantioselective control could be obtained in these processes. According to the types of organocatalysts, the covalent activation modes of organocatalyzed asymmetric radical transformations mainly include: (i) chiral amine-catalyzed transformations of carbonyl compounds via enamine catalysis or iminium catalysis; (ii) nitrogen-heterocyclic carbene (NHC) catalysis; (iii) Si/Sn/S-centered radical-induced asymmetric radical reactions such as thiol catalysis (Figure 13.1) [14, 15]. In this chapter, advances in organocatalyzed asymmetric radical transformations will be discussed according to the modes of organocatalysts, with an

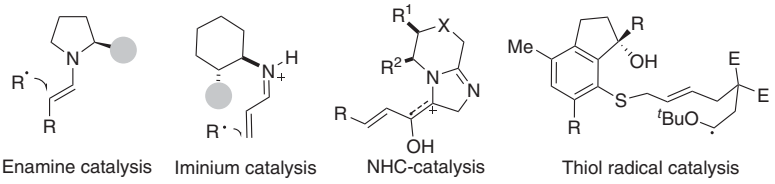


**Figure 13.1** Different modes of organocatalyzed radical reactions via covalent interaction.

emphasis on landmark discoveries in this field. As the third covalent activation mode of Si/Sn/S-centered radical-induced asymmetric radical reactions will be discussed in other parts, this chapter will not discuss it.

## 13.2 Aminocatalysis for Asymmetric Radical Transformations

Chiral amines such as pyrrolidines, imidazolidinones, and cinchona alkaloids have been extensively used in the enantioselective functionalization of carbonyl compounds via traditional ionic, two-electron-pair approaches [4]. However, there have still remained specific challenges that could not be solved with these established methods. Along these lines, aminocatalysis was combined with radical transformations to expand its synthetic potential in synthesizing enantiopure chiral compounds. The condensation of a chiral amine catalyst with a carbonyl compound or an α,β-unsaturated carbonyl compound produces enamine or iminium intermediates, leading to two different activation modes [14, 15]. In the former case, the stereocontrol is delivered via the covalent bond between the chiral amine and π-bond of the enamine (Figure 13.2a). For asymmetric enamine activation, there are two major pathways. First, the singly occupied molecular orbital (SOMO) activation through an α-iminyl radical cation intermediate generated from the single-electron oxidation of the electron-rich enamine that engages in classical radical reactions such as addition, cyclization, coupling (path a), and photoredox organocatalysis via the direct radical addition of an electrophilic radical to the nucleophilic enamine (path b). Second, in radical iminium activation, the electrophilic iminium ion generated from amine condensation with α,β-unsaturated aldehyde reacts with a nucleophilic radical via radical addition (path c) or undergoes a single-electron reduction to give a chiral β-enaminyl radical intermediate which couples with another radical (path d, Figure 13.2b).

### 13.2.1 Enamine Catalysis for Asymmetric Radical Transformations

#### 13.2.1.1 Enamine Catalysis via α-Iminyl Radical Cation Intermediates

The concept of SOMO catalysis developed by MacMillan demonstrated that radical intermediates could be stereoselectively trapped by chiral enamines, thus increasing the potential for chiral bond formation. The single-electron oxidant of enamine creates a transient radical species. This α-iminyl radical cation intermediate

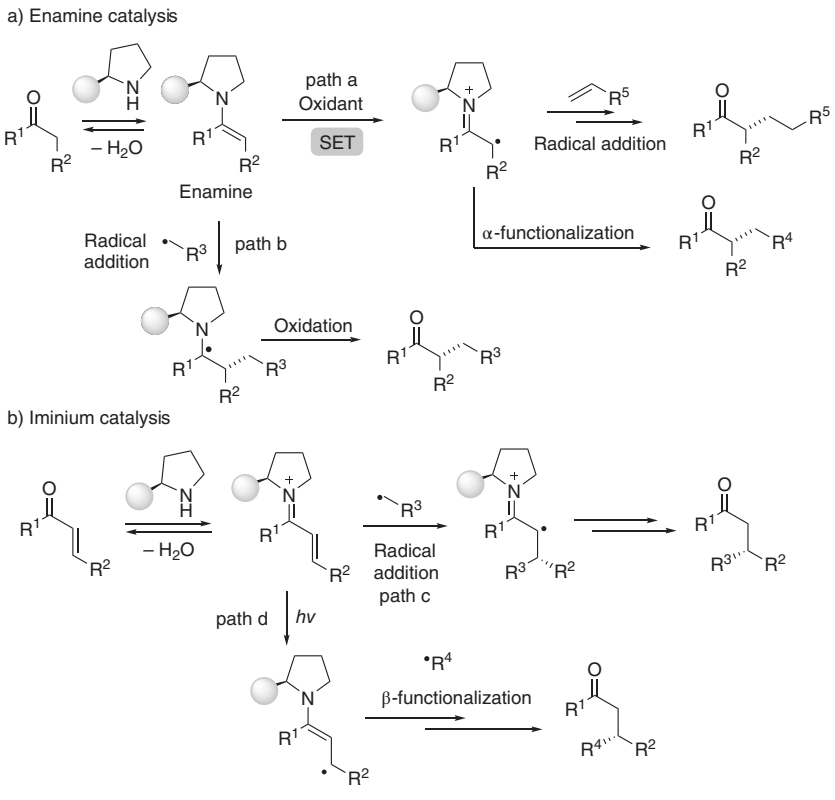


**Figure 13.2** Principles of chiral amine-catalyzed radical transformations.

could undergo a series of radical transformations such as radical addition, radical cyclization, as well as radical coupling. This section will be discussed according to the types of the radical trapping process.

***Radical Addition*** As mentioned above, the MacMillan group pioneered the concept of SOMO activation. In 2007, the breakthrough was achieved via the reaction of α-allylation of aldehydes **1** using ceric ammonium nitrate (CAN) as the oxidant in stoichiometric amounts and allylsilanes **2** as the radical acceptors (Scheme 13.1) [16]. This activation mode expanded the reaction class of enamine catalysis by using radical addition instead of electrophilic addition. Good yields and excellent enantioselectivities could be obtained using the chiral imidazolidinone catalyst **4** under a low temperature of –20 °C, generating compounds **3a**–**3h** with 87–94% ee. The authors proposed the formation of enamine **5** through the condensation of the aldehyde **1** and chiral amine catalyst **4**, followed by a selective single-electron oxidation to afford a radical cation intermediate **6** (Scheme 13.2). This radical cation could add to the allylsilane **2** to produce another radical cation intermediate **7**. Next, another equivalent of CAN oxidized the radical cation intermediate to give a β-silyl cation, which underwent β-elimination and hydrolysis to afford the product **3** along with the regeneration of catalyst **4**.

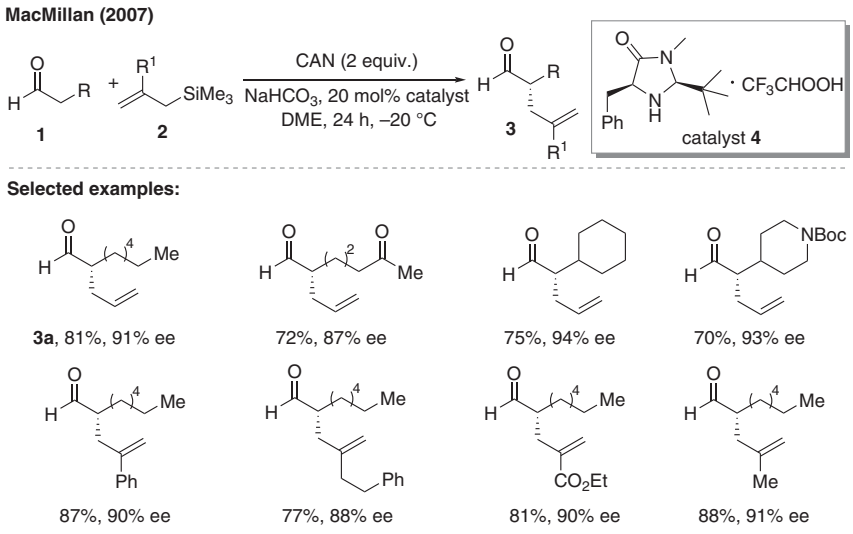


**Scheme 13.1** α-Allylation of aldehydes with allylsilanes.

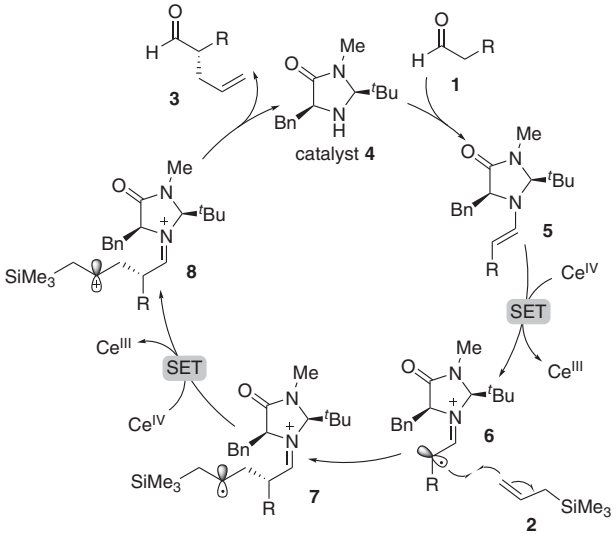


**Scheme 13.2** Mechanism of the α-allylation of aldehydes.

Shortly after that, the MacMillan group applied the SOMO catalysis to achieve the enantioselective α-enolation [17] and α-vinylation [18] of aldehydes using the same chiral imidazolidinone catalyst **4** (Scheme 13.3). Enolsilanes **9** and vinyltrifluoroborate **11** were demonstrated to be good radical acceptors, giving rise to a wide range of chiral α-substituted-γ-ketoaldehydes **10** and α-vinyl aldehydes **12** with good yields and high ee. For the α-vinylation reaction of aldehydes, the elimination step of boron via a β-radical intermediate gave excellent *trans*-selectivity.

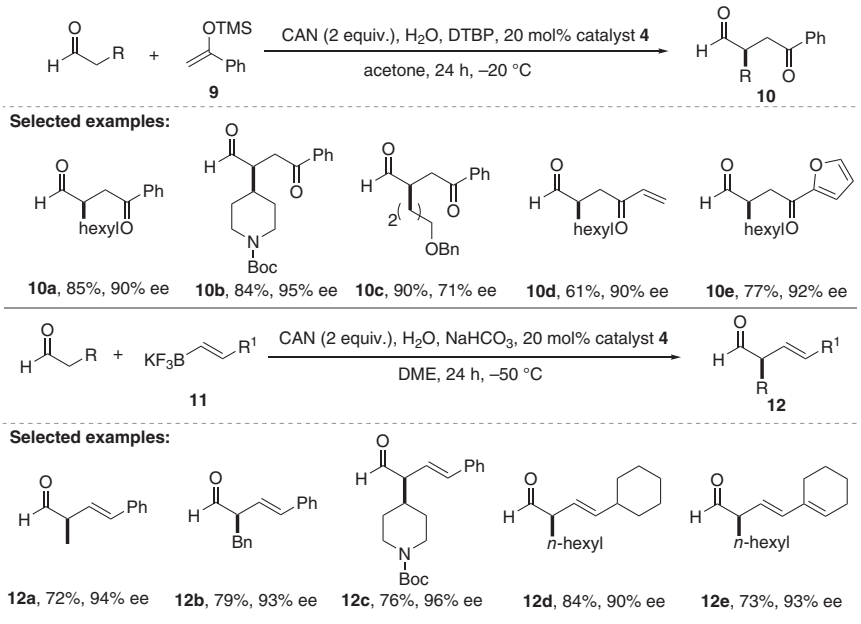


**Scheme 13.3** α-Enolation and α-vinylation of aldehydes.

In the SOMO catalysis mode, when the elimination step could not easily occur, the cation intermediates could then be trapped by nucleophiles such as the nitrate group. In 2008, the MacMillan group reported the reaction of aldehydes with styrenes **13** in the presence of CAN and chiral imidazolidinone catalyst **15** (Scheme 13.4) [19]. After the intermolecular radical addition and single-electron

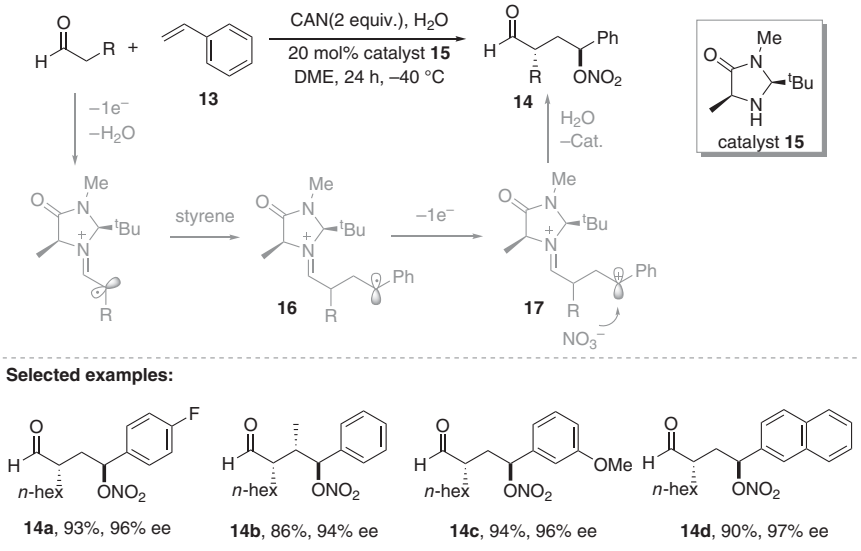


**Scheme 13.4** Carbooxidation of styrenes.

oxidation steps, the cation intermediate **17** could react with the anionic $NO_3^-$ from CAN. A series of electron-rich or electron-deficient styrenes could participate in the reaction smoothly, leading to the γ-nitrate-α-alkyl aldehyde products **14a**–**14d** in 86–94% yields with 94–97% ee. These nitrate ester products were easily converted to various enantioenriched heterocyclic rings such as tetrahydrofurans, pyrrolidines, and γ-lactones.

This SOMO activation mode was further extended to α-nitroalkylation [20] and α-chlorination [21] of aldehydes through oxidative organocatalysis. The catalytic process provided a highly efficient tool for α-functionalization of aldehydes, extensively extending the potential of aminocatalysis for asymmetric transformations.

Compared to the aldehyde partner, ketones have different electronic and steric interactions with the amine catalyst, leading to new challenges for the α-functionalization of ketones using the same oxidative activation mode. Despite the advances of transition-metal-catalyzed asymmetric allylation reactions, these reactions relied on either the enantioselective allylation of metal enolates or asymmetric decarboxylative conversion of allyl keto carbonates. The direct α-allylation of simple ketones remained the most straightforward process for asymmetric catalysis. In 2010, the MacMillan group developed new modified chiral imidazolidinone catalysts for the asymmetric allylation of cyclic ketones via SOMO catalysis (Scheme 13.5) [22]. In this system, the chiral amine catalysts and cyclic ketone substrates were stable in the presence of oxidants. The asymmetric induction was achieved via the selective engagement of the radical acceptor allylsilanes with the *Si* face of the α-iminyl radical intermediate **21**. Additionally, the enantioselective

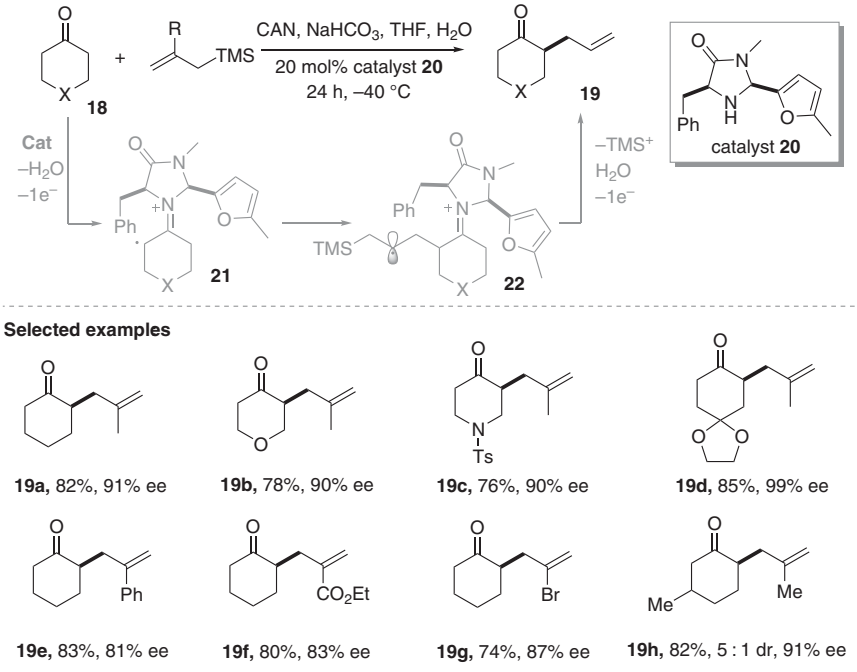


**Scheme 13.5** Enantioselective α-allylation of ketones.

α-enolation and α-carbooxidation of carbocyclic ketones were also developed using this catalytic process.

Considering the importance of bicyclo[1.1.1]pentanes (BCPs) in drug design and the difficulty of the synthesis of BCPs featuring adjacent stereocenters, the Anderson group recently reported the synthesis of α-chiral BCPs through the direct addition of aldehydes to [1.1.1]propellane **23** (Scheme 13.6) [23]. This work was inspired by the previously reported work by the MacMillan group [24]. The combination of photocatalysis and organocatalysis enabled the generation of the chiral α-iminyl radical cation **26**, which would add to [1.1.1]propellane and open the ring. The generated radical **27** would abstract a hydrogen atom from the thiol via hydrogen atom transfer (HAT) and give the desired product **24**. The reaction featured mild conditions and broad scope, providing a range of α-chiral BCPs with good yields and high enantioselectivities. A theoretical model for stereocontrol in this reaction revealed that noncovalent interactions between the substrate side chain and the prolinol substituents were crucial for achieving high enantioselectivity.

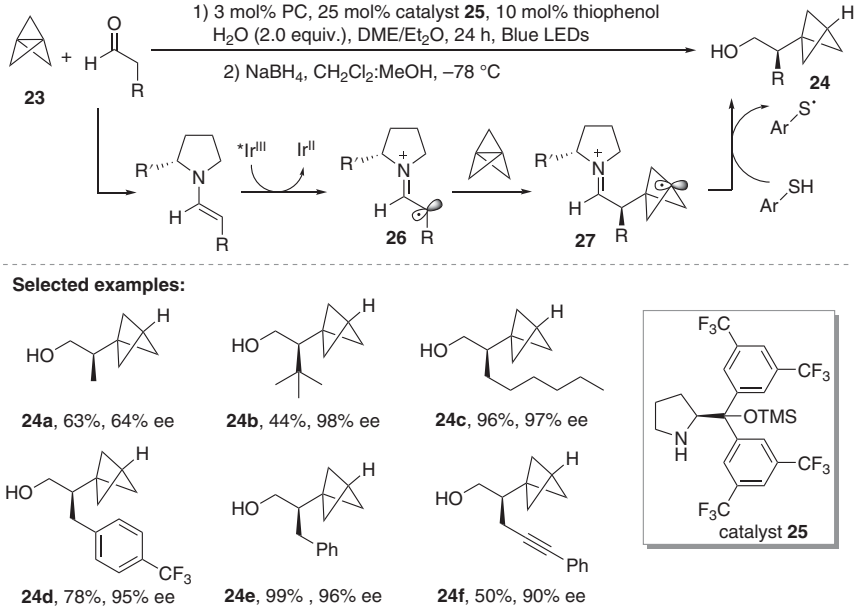


**Scheme 13.6** Asymmetric synthesis of α-chiral BCPs.

Very recently, the Luo group reported an asymmetric dehydrogenative coupling of β-ketocarbonyls and olefins enabled by a ternary catalytic system (Scheme 13.7) [25]. The reaction involved a photoredox catalyst, a chiral primary amine, and a cobaloxime cocatalyst. As mentioned above, if the elimination step is difficult, the radical could be trapped with other processes. In this work, the Co(II)-metalloradical was utilized to capture the radical intermediate generated from the radical addition of the α-iminyl radical cation **32** to the olefin **28**. Then, photomediated dehydrogenation of **33** and hydrolysis would lead to the desired

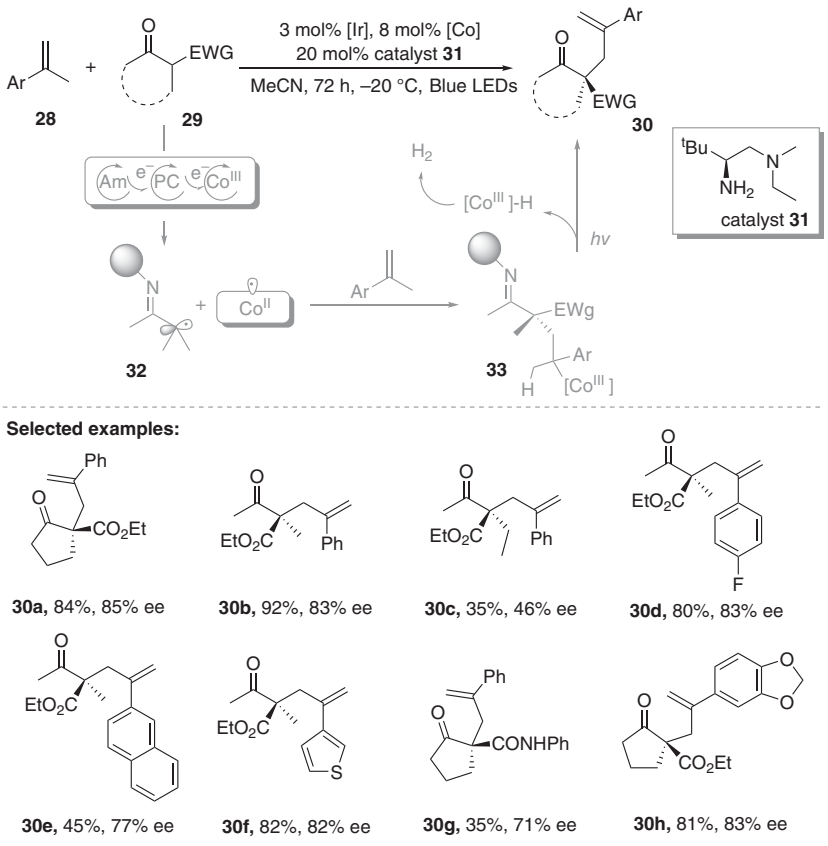


**Scheme 13.7** Asymmetric coupling of β-ketocarbonyls and olefins.

product **30** and regenerate the amine and Co(III) catalysts. Substrates such as cyclohexanecarboxylate esters and acyclic acetoacetate esters were both suitable for this transformation, leading to the allylation product **30a**–**30h** in 35–92% yields with 46–85% ee. It is worthy to mention that they also reported an enantioselective α-alkynylation of β-ketocarbonyls via photoredox catalysis [26].

***Radical Cyclization*** When the radical trapping process proceeds in an intramolecular manner, enantioenriched carbocycles and heterocycles could be obtained. In 2009, Nicolaou and coworkers reported an enantioselective intramolecular α-arylation of aldehydes **34** in the presence of the amine catalyst **36** with CAN as the oxidant (Scheme 13.8) [27]. In the same year, the MacMillan group also revealed a similar transformation using $[Fe(phen)_3](PF_6)_3$ as the oxidant [28]. The Nicolaou group proposed a Friedel-Crafts type reaction mechanism (Scheme 13.9). Firstly, the chiral amine catalyst combined with the aldehyde **34** to produce the enamine **36**, which was oxidized by CAN via single-electron transfer to give the reactive radical cation **37**. The radical cation **37** rapidly cyclized intramolecularly to the intermediate **38** in typical Friedel-Crafts reactions. This intermediate lost a proton and was

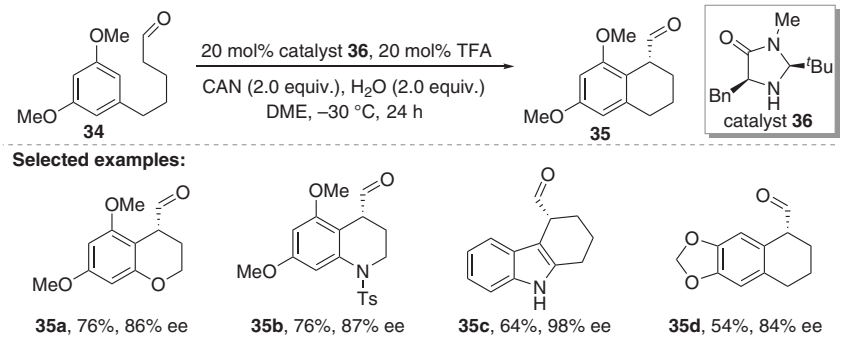


**Scheme 13.8** Asymmetric α-arylation of aldehydes.

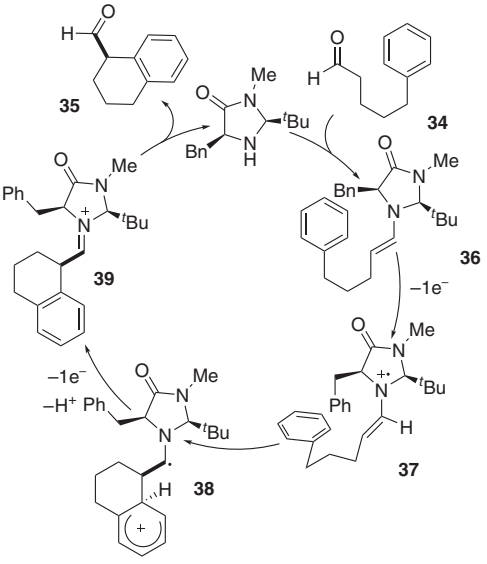


**Scheme 13.9** Mechanism of the asymmetric α-arylation of carbonyl compounds.

oxidized again by CAN. Further hydrolysis would afford the cyclized product **35** and regenerate the chiral amine catalyst. In contrast, the MacMillan group proposed a radical cyclization mechanism, which was supported by quantum mechanical calculations [29]. The *ortho*-regioselectivity for the 1,3-disubstituted aromatic system was also in agreement with the radical cyclization mechanism.

The radical polar crossover strategy was also applied to the asymmetric SOMO catalysis by the MacMillan group. In 2010, they developed an enantioselective radical-mediated (4 + 2) formal reaction of aldehydes **40** and conjugated alkenes **41** via amine catalysis (Scheme 13.10) [30]. The olefin trapped the α-iminyl radical cation **43** and resulted in a radical intermediate **44**. The radical **44** was oxidized to a cation **45**, which readily underwent the intramolecular nucleophilic addition.

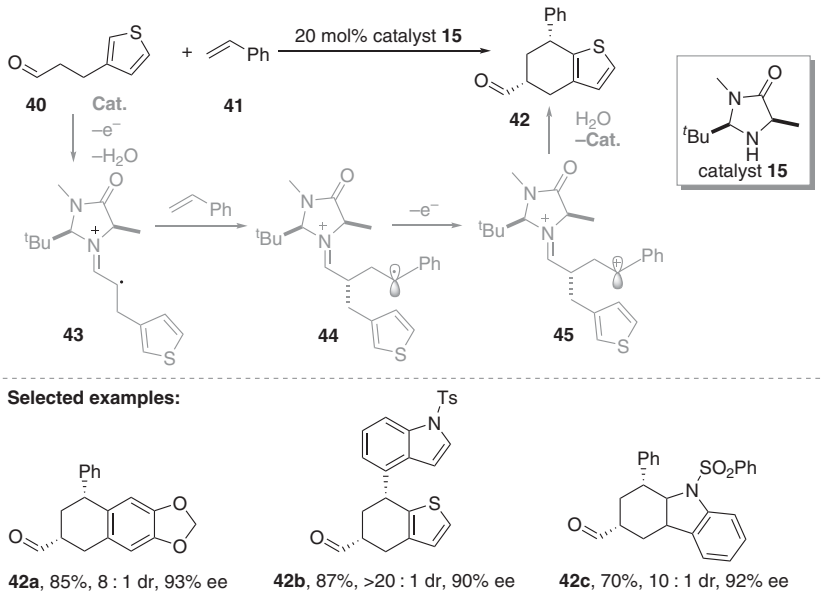


**Scheme 13.10** (4 + 2) Coupling reaction of aldehydes and conjugated olefins.

Various electron-rich benzenes and heteroarenes can be used as nucleophilic terminators to provide cyclohexyl products with excellent stereoselectivities.

In 2011, MacMillan and coworkers developed a direct cyclization reaction based on the enantioselective intramolecular α-allylation of aldehydes (Scheme 13.11) [31]. The reaction took place with chiral amine **36** as the catalyst and CAN as the oxidant. This method successfully converted a range of

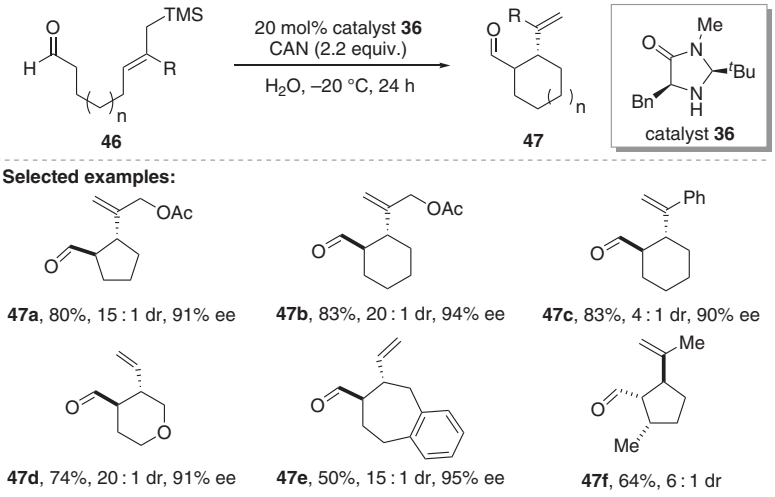


**Scheme 13.11** Intramolecular α-allylation of aldehydes.

allylsilane-tethered aldehydes into five-, six-, and seven-membered carbon rings and heterocycles with high efficiency and excellent enantioselectivities.

Using the radical polar crossover strategy, MacMillan and coworkers achieved the construction of enantioenriched pyrrolidines from β-amino aldehydes and alkenes (Scheme 13.12) [32]. A series of styrenes and dienes **49** were smoothly coupled in this cycloaddition cascade, giving rise to structurally complex pyrrolidines **50** with high efficiency and enantioselectivities. The mechanism is shown in Scheme 13.13. The condensation of chiral amine **51** with β-amino aldehyde **48** would generate

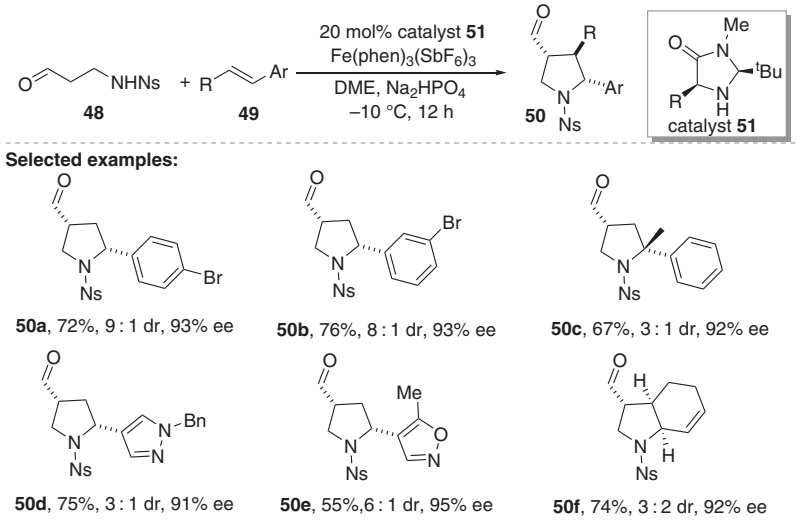


**Scheme 13.12** Enantioselective (3 + 2) cyclization of aldehydes and olefins.

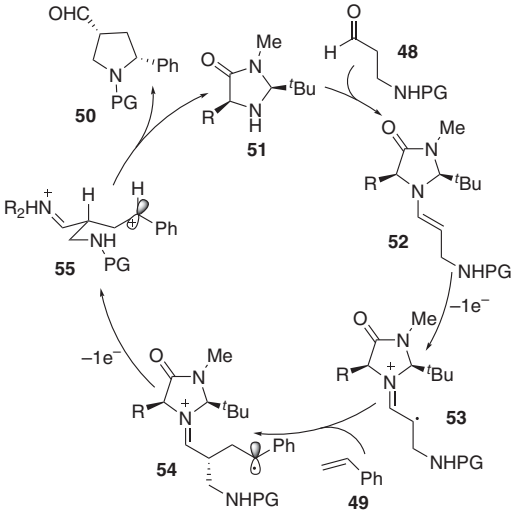


**Scheme 13.13** Mechanism of the (3 + 2) cyclization of aldehydes and olefins.

the enamine intermediate **52**, which could be oxidized to the α-iminyl radical cation **53**. The following intermolecular radical addition and further single-electron oxidation would afford the carbocation **55**, which was trapped by the intramolecular amide nucleophile. Further hydrolysis gave the pyrrolidine product and the chiral amine catalyst for the next catalytic cycle. The authors presumed that excellent enantiocontrol was obtained via the basis of 3π-electron geometry control in the radical cation intermediates.

In 2013, the MacMillan group developed an enantioselective α-allylation of non-activated aldehydes with intramolecular double bonds for the synthesis of chiral substituted carbocycles and heterocycles **57** (Scheme 13.14) [33]. No additional leaving group such as silane group was required in this process. In analogy to the carbonyl-ene type cyclization, this method provided an important approach for the construction of complex cyclic scaffolds bearing valuable aldehyde and olefin functional groups.

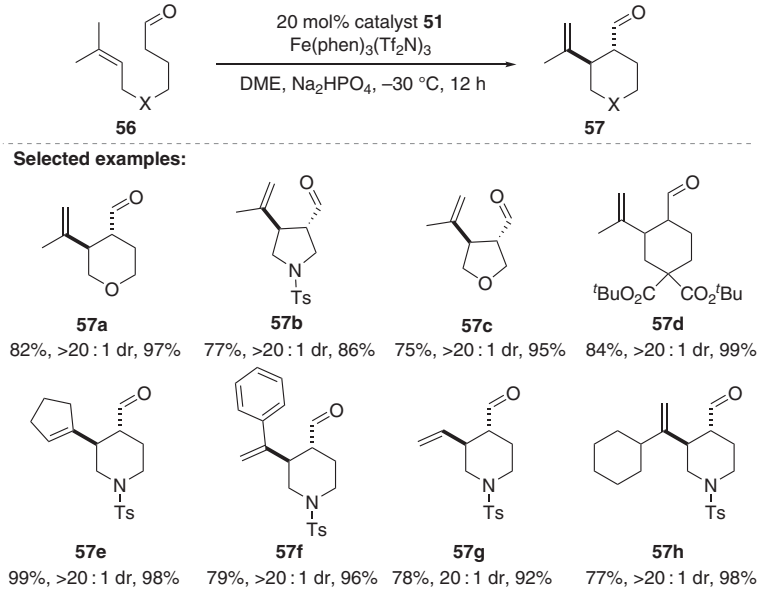


**Scheme 13.14** Enantioselective intramolecular α-allylation of aldehydes.

Combining photoredox, enamine, and thiol HAT catalysis, MacMillan and coworkers disclosed an intramolecular enantioselective α-alkylation of aldehydes in 2017 (Scheme 13.15) [24]. This visible-light-mediated transformation involved three discrete catalytic cycles that were matched to work synergistically. The α-iminyl radical cation generated via the oxidation of the enamine by the iridium photocatalyst at an excited state added to the olefin intramolecularly or intermolecularly to produce another radical intermediate, which could abstract a hydrogen atom from the thiophenol catalyst through the hydrogen atom transfer (HAT) process. This process was overall redox-neutral, and thus no additional oxidant was required. The reaction took place smoothly under visible light conditions with high atom and step-economy, increasing the possibility of their industrial applications.

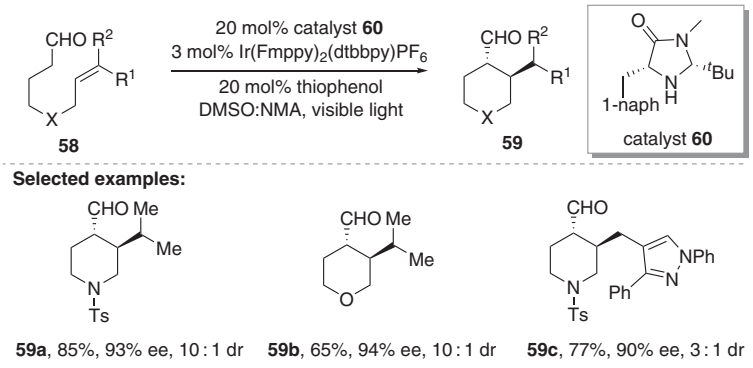


**Scheme 13.15** Enantioselective α-alkylation of aldehydes.

***Other Transformations Involving α-Iminyl Radical Cation Intermediates*** Instead of radical addition or cyclization, the α-iminyl radical could also undergo other transformations. In 2007, Sibi and coworkers reported an enantioselective α-oxyamination of aldehydes using TEMPO as the radical trapping reagent (Scheme 13.16) [34]. This transformation was supposed to be SOMO catalysis, in which a highly reactive radical species was formed followed by SET oxidation. Enantioselective α-oxyamination of aldehydes was established by combining chiral amine catalyst **63** with $FeCl_3/NaNO_2/O_2$ oxidative system. It was surprising that the aliphatic isovaleraldehyde was transferred to the desired product **62d** in high efficiency but with no enantioselectivity. The author proposed that the enamine **64** generated from the aldehyde chiral amine catalyst **63** was oxidized to produce the α-iminyl radical **65**. Subsequently, a radical coupling occurred between TEMPO and radical

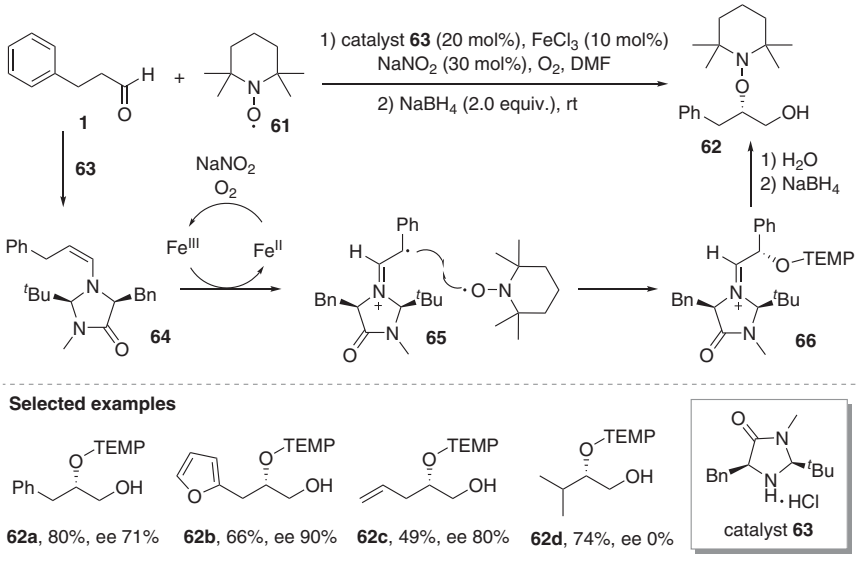


**Scheme 13.16** Enantioselective α-oxyamination of aldehydes.

**65** to forge an enantioselective C—O bond formation, and the final product **62** was obtained after hydrolysis.

However, the MacMillan group failed to introduce the Sibi oxidation conditions ($FeCl_3$, $NaNO_2/O_2$) into their transformations, which inspired them to study the mechanism of the Sibi oxidation system [35]. The authors selected *cis*-cyclopropane-substituted aldehyde **67** as a probe, which was converted into the *cis*-product **68** with a lower degree of isomerization under the Sibi oxidation conditions (Scheme 13.17). This experiment showed that the closed-shell addition to enamine **69** was favored for radical capture by TEMPO. Notably, the product could undergo *cis*/*trans* isomerization with changes in different TEMPO concentrations, which indicated that a radical mechanism was also involved.

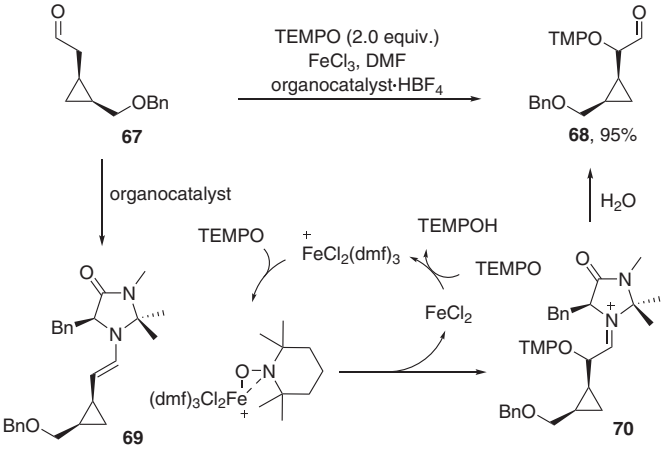


**Scheme 13.17** Mechanistic studies of the α-oxyamination of aldehydes.

In 2011, the chiral amine catalyst was combined with a heterogeneous $TiO_2$ photocatalyst to accomplish an α-oxyamination reaction of aldehydes, avoiding the utilization of a stoichiometric amount of strong oxidant, reported by the Jang group [36]. Later, the same group established an asymmetric difunctionalization of α,β-unsaturated aldehydes [37]. The asymmetric Michael addition/oxyamination was enabled via chiral enamine and photoredox dual catalysis. The Ru(II)@$TiO_2$/chiral amine combined catalytic process exhibited excellent catalytic activity with a low catalyst loading.

In 2013, the Melchiorre group demonstrated that the electron-rich chiral enamine intermediate could participate in the photoexcitation of an electron donor–acceptor (EDA) complex with electron-deficient 2,4-dinitrobenzyl bromide **71** [38]. The transient formation of the photon-absorbing EDA complex underwent a SET event to produce the corresponding α-iminyl radical and benzyl radical. The subsequent radical coupling and hydrolysis gave the alkylated product **72**. The authors used *cis*-cyclopropyl-substituted aldehyde as a radical probe and proposed that the radical-chain pathway was negligible. However, in their later works, the

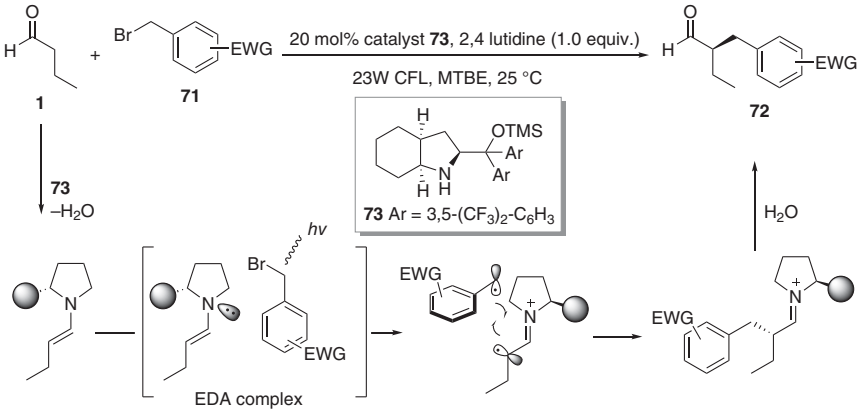


**Scheme 13.18** α-Alkylation of aldehydes via EDA complex.

measurements of quantum yield and determination of redox potentials suggested that the radical-chain process was more likely to be dominant (Scheme 13.18).

More recently, Jørgensen and coworkers have shown that the chiral enamine intermediates could undergo double oxidation with additional oxidants to obtain the α-iminyl cation intermediates (Scheme 13.19) [39]. These intermediates could

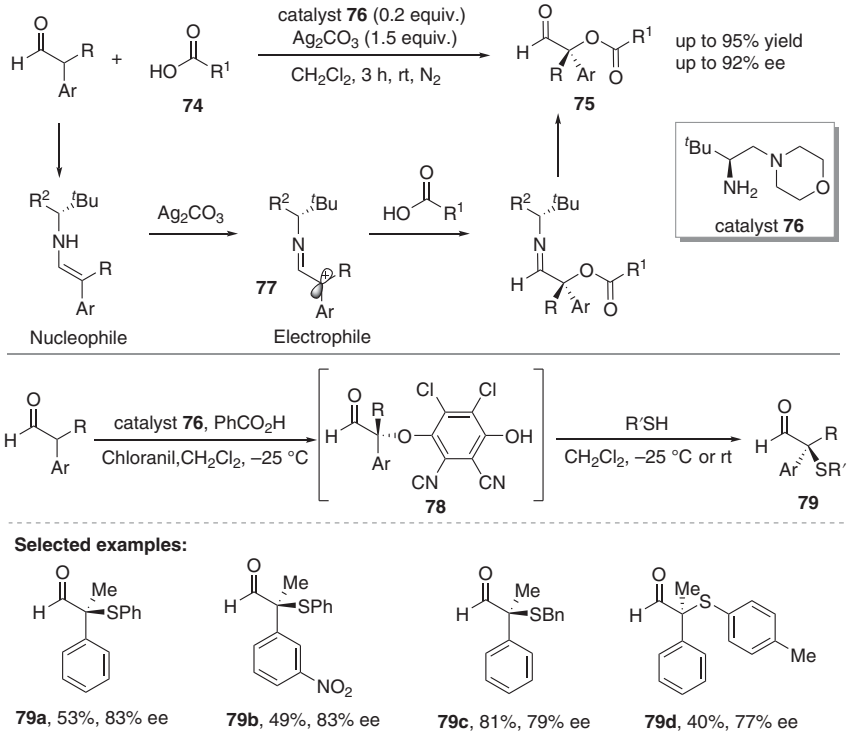


**Scheme 13.19** The umpolung strategy for α-functionalization of aldehydes.

react with nucleophiles such as carboxylic acids **74** to furnish the organocatalytic cycle. This strategy broke the limitation of coupling with electrophiles in the SOMO activation mode. They also applied this umpolung strategy to generate the O-bound quinol-intermediate **78,** which could undergo nucleophilic substitution with various nucleophiles, such as water, methanol, phenol, and chloride [40]. The organocatalytic enantioselective α-thiolation of aldehydes could afford various quaternary thioethers with high enantioselectivities. In 2019, the same group reported an enantioselective coupling of indoles with aldehydes using the same strategy [41].

#### 13.2.1.2 Enamine Catalysis via Radical Addition to Enamine Intermediates

The combination of photoredox catalysis and aminocatalysis has been extensively explored in the field of organic chemistry. The pioneering work was achieved by the MacMillan group in 2008 [42]. They reported an enantioselective intermolecular α-alkylation of aldehydes with the photoredox catalyst $Ru(bpy)_3Cl_2$ and a chiral imidazolidinone catalyst **82** (Scheme 13.20), which laid the foundation of the photoredox and organo-dual catalysis for asymmetric radical transformations. A range of electron-deficient α-bromo carbonyl substrates **80** were smoothly coupled, affording the desired alkylated products **81** in good yields with excellent enantioselectivities. Since chiral amine catalysts are generally low-cost and the use of electrophilic radical precursors can overcome the high energy barriers of conventional photocatalysts, an increasing number of asymmetric organocatalysis strategies for photocatalytic transformations have been developed.

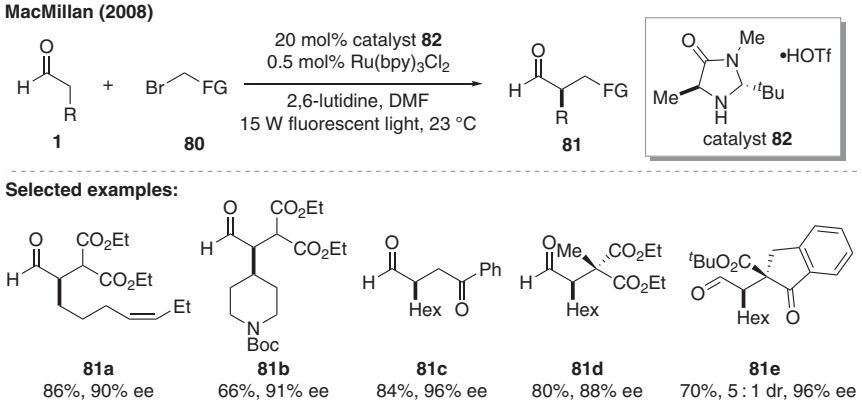


**Scheme 13.20** Enantioselective intermolecular α-alkylation of aldehydes.

The authors proposed that the single-electron reduction of the α-bromo carbonyl substrate by $Ru(bpy)_3^+$ would generate the electron-deficient alkyl radical **84.** At the same time, electron-rich chiral enamine **83** was formed through the condensation of aldehyde **1** with chiral amine catalyst **82**. Then, the electron-deficient radical **84** added to the enamine intermediate **83** to obtain an electron-rich α-amino radical **85**, which could be oxidized by the photocatalyst $[Ru(bpy)_3^{2+}]^*$ at an excited state

to give the imine ion **86**. Further hydrolysis produced the alkylation product **81** and catalyst **82** for the next catalytic cycle. Mechanistic investigations also revealed that a radical-chain reaction was involved, suggesting the electron-rich α-amino radical **85** could reduce the α-bromo carbonyl **80** to propagate the reaction chain. The enantiocontrol mainly came from the radical addition of **84** to the *Si* face of the enamine intermediate **83**, while the *Re* face was shielded by the methyl group on the amine catalyst (Scheme 13.21).

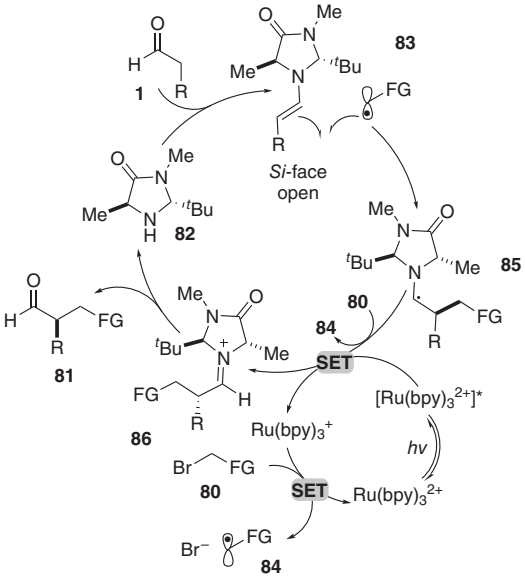


**Scheme 13.21** Mechanism of the enantioselective α-alkylation of aldehydes.

Based on the photoredox and enamine dual catalytic system, the MacMillan group developed the enantioselective α-trifluoromethylation, α-benzylation, and α-cyanoalkylation of aldehydes using different radical precursors including trifluoromethyl iodide **87**, benzylic bromide **90**, and bromo acetonitrile **93** (Scheme 13.22) [43–45]. The trifluoromethyl, benzyl, and cyanoalkyl radicals generated via single-electron reduction by the photoredox system were electron-deficient radicals, which could efficiently undergo radical addition to the electron-rich enamine intermediates to furnish this asymmetric organocatalysis. These reactions rely on the use of transition-metal-based photoredox catalysts.

To overcome the requirement for expensive noble-metal photocatalysts, chemists have turned to inexpensive organic dyes and recyclable heterogeneous semiconductor photocatalysts in asymmetric photoredox organocatalysis (Scheme 13.23). In 2011, Zeitler and coworkers utilized an easily available organic dye eosin Y to replace the metal photocatalyst, successfully achieving the asymmetric intermolecular α-alkylation of aldehydes by combining with aminocatalysis [46]. This purely organic asymmetric photoredox organocatalysis worked as efficiently as that with the metal photocatalysts, proving that eosin derivatives exhibited similar redox

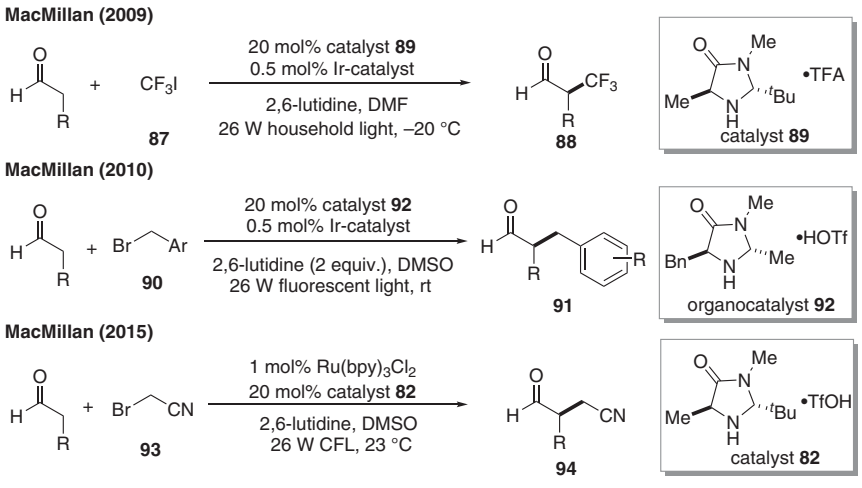


**Scheme 13.22** Enantioselective α-functionalization of aldehydes.

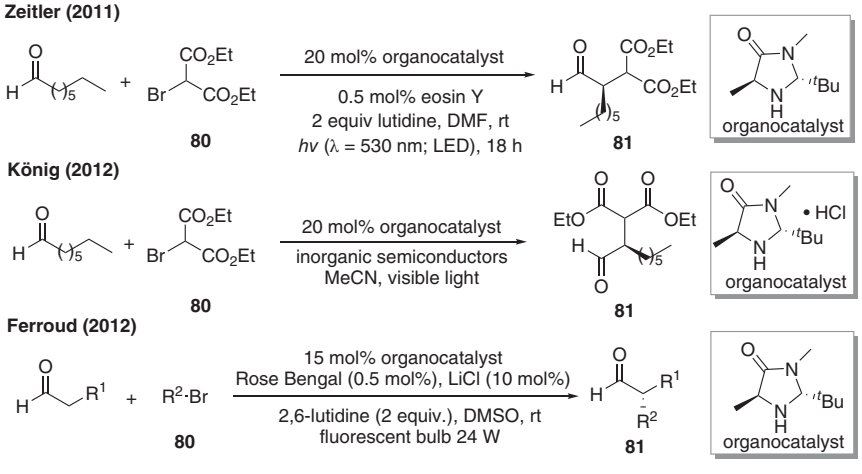


**Scheme 13.23** Enantioselective α-alkylation of aldehydes with different photocatalysts.

properties. The König group showed that the CdS heterogeneous semiconductor was a suitable photocatalyst for this transformation [47]. This inorganic photocatalyst can also promote the oxidative Mannich-type reaction with ketones under blue light irradiation with proline as an organic catalyst. The simple removal from the reaction mixture ensures convenient recovery of the photocatalyst, thereby enhancing the practicality of photocatalysis. In 2012, Ferround and coworkers developed a Rose Bengal photocatalyst, leveraging mild room temperature conditions and shorter irradiation time [48]. The reaction can be completed in only 2 hours without the need for any heating or cooling systems.

Taking advantages of photoredox organocatalysis, various electrophilic radical precursors have been developed for these transformations. In 2013, MacMillan

and coworkers reported an enantioselective α-amination of aldehydes through the addition of *N*-centered radicals generated by photocatalysis to the chiral enamine intermediate formed via organocatalysis (Scheme 13.24, above) [49]. The amine radical precursor **95** incorporated a photolabile group, thereby obviating the need for additional photocatalysts in this process. The α-amino aldehyde products **96** are useful synthons, which could be successfully converted into β-amino alcohols and α-amino acids. It was found that the C-2 position of the amino group on the imidazolidinone skeleton of the chiral organic catalyst was susceptible to H-atom extraction by *N*-radicals, resulting in decreased reaction efficiency. The design of an imidazolidinone catalyst **97** that contained a fully substituted carbon stereocenter at the C-2 position of the amino group suppressed this influence. Alcohols are unreactive alkylating agents as C-radical precursors. In 2018, MacMillan and coworkers utilized a radical-mediated "spin-center shift" (SCS) strategy to access benzylic radicals from electron-deficient heterobenzylic alcohols **98** [50]. The benzylic radicals smoothly participated in reactions with the catalytically generated enamines. This elegant design enabled the α-benzylation of aldehydes from alcohols by SCS.

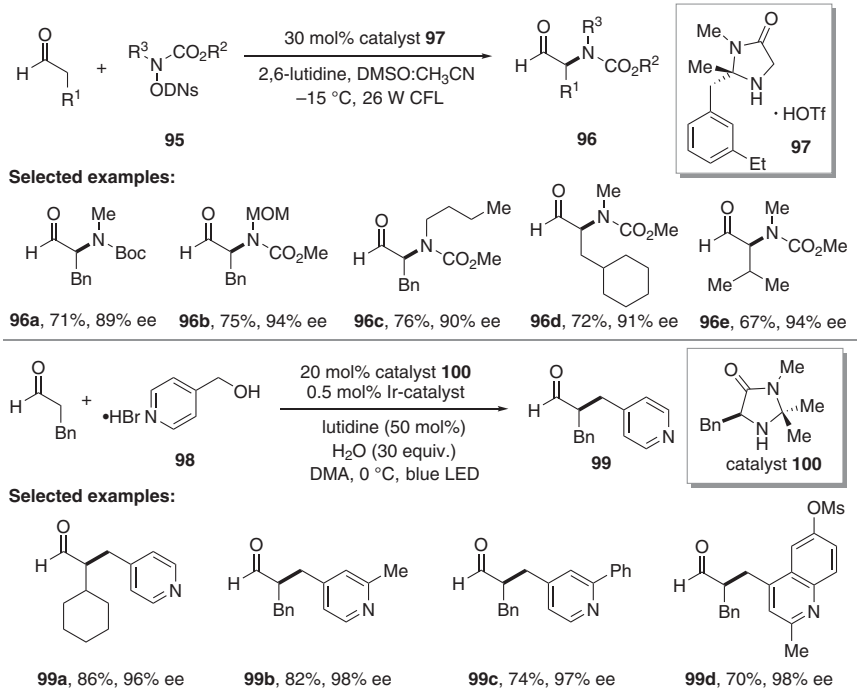


**Scheme 13.24** Enantioselective α-amination and α-benzylation of aldehydes.

Melchiorre reported a photoredox organocatalyzed enantioselective α-alkylation of aldehydes using a diarylprolinol ether organocatalyst **102** without the addition of an external photocatalyst (Scheme 13.25) [51]. The transiently generated enamine intermediate **103** was able to directly reach an excited state **103*** upon light

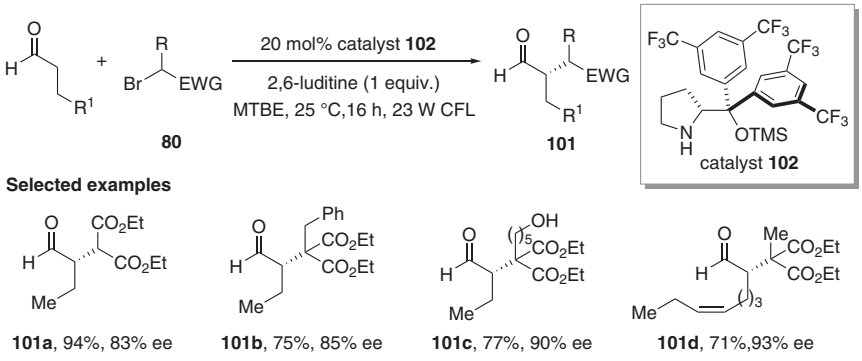


**Scheme 13.25** Photocatalyst-free enantioselective α-alkylation of aldehydes.

absorption and react with bromomalonate **80** to form a reactive radical species **104** (Scheme 13.26). This electrophilic radical could add to the enamine **103** to generate another radical **105**, which would undergo single-electron oxidation and hydrolysis to give the desired product **101** and regenerate the organocatalyst **102**. Meanwhile, bromomalonate **80** was reduced to radical **104** to propagate the radical chain. The success of this transformation relied on the photosensitive property of the enamine and the high reduction potential of the photoexcited enamine. The same group showed that (phenylsulfonyl)alkyl iodides could also participate in this photoorganocatalytic enantioselective α-alkylation reaction of aldehydes [52].

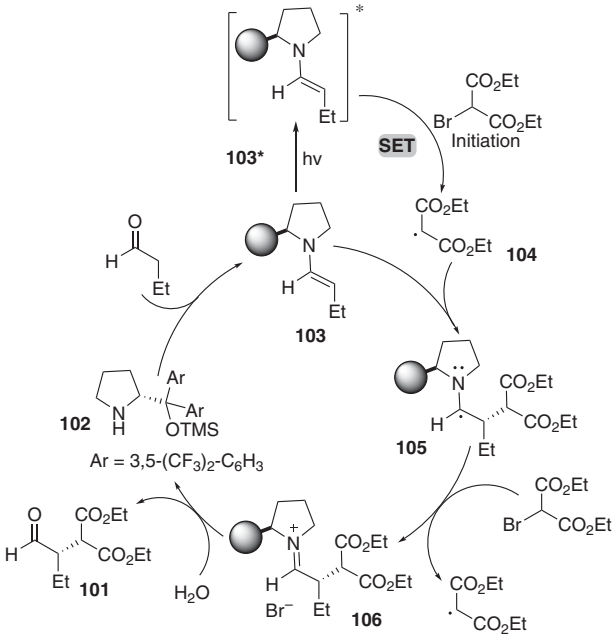


**Scheme 13.26** Mechanism of the photocatalyst-free α-alkylation of aldehydes.

In 2018, Aleman and coworkers fixed the photosensitive thioxanthone motif to the imidazolidinone organocatalyst and prepared a new type of photoaminocatalyst **108** (Scheme 13.27) [53]. This photoaminocatalyst could be easily synthesized in only two steps, and the introduction of the thioxanthone motif would modify the steric properties of the aminocatalyst. The α-alkylation of aldehydes with this photoaminocatalyst afforded the desired product **107** in moderate to good yields with high enantiomeric excess.

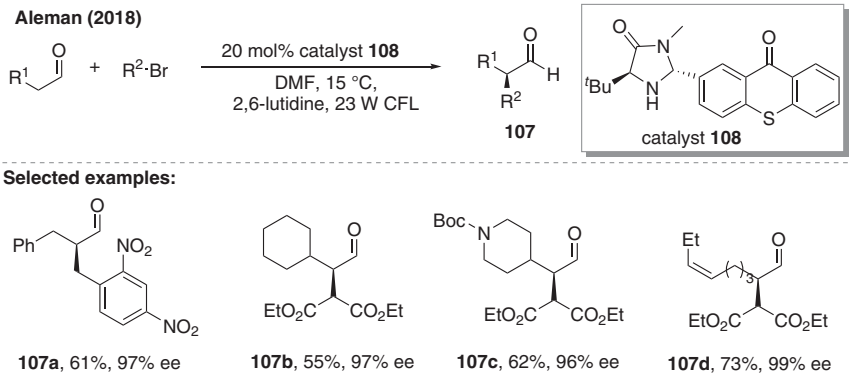


**Scheme 13.27** The application of the bifunctional photoaminocatalyst.

Despite these achievements with aldehyde substrates, the functionalization of ketone substrates via chiral amine and photoredox dual catalysis remained challenging. Luo and coworkers realized the enantioselective α-alkylation of β-ketocarbonyls **110** using a chiral primary amine catalyst **112** (Scheme 13.28). In their pioneering work, the ruthenium-based photoredox catalyst served as the photocatalyst to furnish the photoredox catalytic cycle [54].

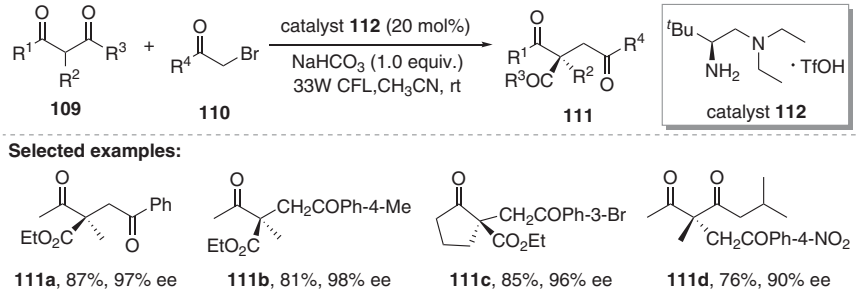


**Scheme 13.28** Enantioselective α-alkylation of β-ketocarbonyls.

Later, they found that this photoalkylation reaction could take place solely with the amine catalyst without an external photosensitizer [55]. These transformations were used to construct quaternary carbon stereocenters that were difficult to form. The reaction process was similar to the corresponding transformation with

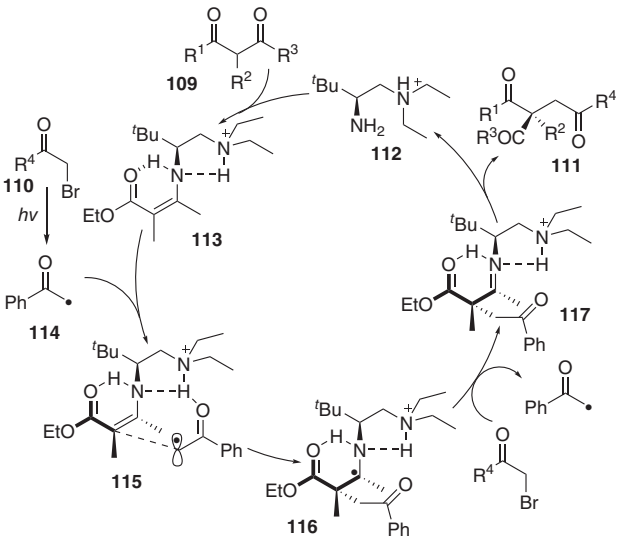


**Scheme 13.29** Mechanism of the enantioselective α-alkylation of β-ketocarbonyls.

aldehydes (Scheme 13.29). The primary amine catalyst **112** condensed with the encumbered ketone **109**, enabling the formation of the key enamine intermediate **113**. The radical **114** generated from **110** was trapped by the enamine to give an amino radical **116**, which could undergo single-electron transfer with bromo ketone **110** and complete the amino catalytic cycle after hydrolysis. A range of β-oxo esters **109** and bromo ketone substrates **110** were compatible with this reaction, affording the alkylated products **111** in moderate to good yields with excellent enantioselectivities.

### 13.2.2 Iminium Catalysis for Asymmetric Radical Transformations

In iminium activation mode, the electrophilic iminium ion is generated via the condensation of the chiral amine catalyst with an α,β-unsaturated carbonyl substrate. As mentioned in the introduction, two major pathways are included in iminium catalysis [14, 15]. Some iminium ion intermediates can be excited to an excited state upon light excitation. Subsequently, they can participate in single-electron transfer with another substrate, forming a chiral β-enaminyl radical intermediate which can couple with another in situ generated radical. This process can achieve photoinduced reactions that were previously inaccessible without the need for additional photocatalysts. On the other hand, this iminium ion could trap a nucleophilic radical generated by an additional photocatalytic system. This approach usually requires photocatalysts or photosensitive substrates as radical precursors. The iminium catalysis enables the enantioselective β-functionalization of α,β-unsaturated carbonyls to give enantio-enriched β-functionalized carbonyl compounds. It is worth mentioning that the Melchiorre group has made outstanding contributions to this field. In this section, the iminium activation mode will be discussed based on these two types of radical trapping processes.

### 13.2.2.1 Radical Coupling

In 2017, the Melchiorre group reported an enantioselective β-alkylation of enals catalyzed by an amine catalyst under visible light irradiation (Scheme 13.30) [56]. The iminium ions were shown to be able to reach the excited state via absorption of light and act as strong oxidants to initiate radical reactions. The amine catalyst **123a** was crucial for the success of this stereoselective β-alkylation transformation, as it not only determined the photoelectronic property of the iminium ion intermediate but also induced the stereocontrol.

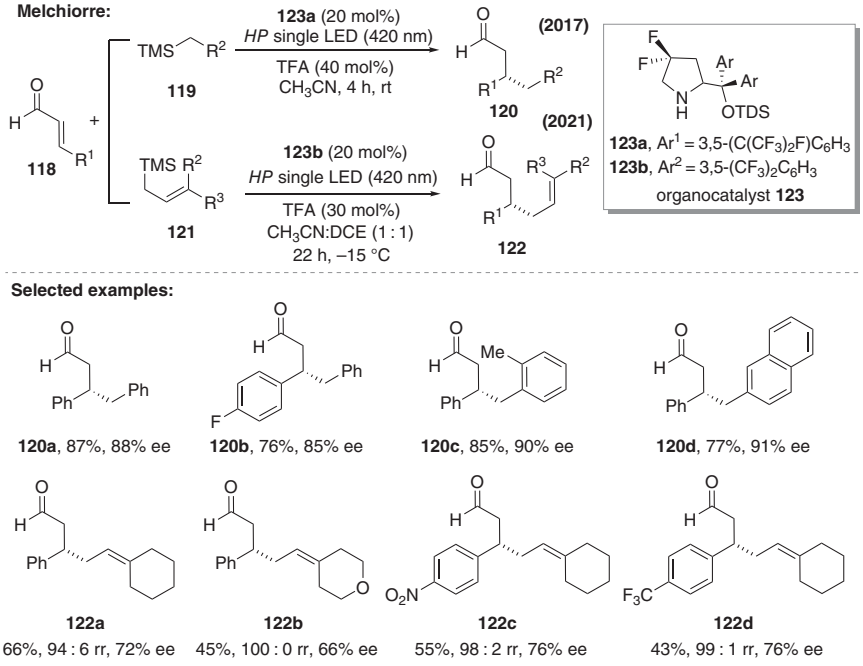


**Scheme 13.30** Enantioselective β-alkylation of enals with alkyl silanes.

Mechanistically, the chiral amine catalyst **123a** condensed with the α,β-unsaturated aldehyde **118** to generate the iminium ion intermediate **124**, which absorbed visible light to reach the excited state (Scheme 13.31). The iminium ion **124*** at an excited state showed strong oxidizing properties. The single-electron transfer between **124*** and the alkyl silanes **119** would generate the radical **125** and alkyl radical **126**. The subsequent radical-radical coupling and hydrolysis afforded the final β-alkylation **120**. In 2021, the same group revealed that allyl silanes **121** could be oxidized to allyl radicals by the photoexcited iminium ions, which could accomplish the enantioselective β-allylation of enals [57]. This radical conjugate allylation pathway proceeded smoothly with high regio- and chemoselectivities.

The Melchiorre group next combined the photoexcited iminium ions with the direct sequential multisite proton-coupled electron transfer (MS-PCET) process to generate benzyl radicals, realizing the enantioselective C–H functionalization of toluene derivatives **129** (Scheme 13.32a) [58]. The enantioselective β-alkylation

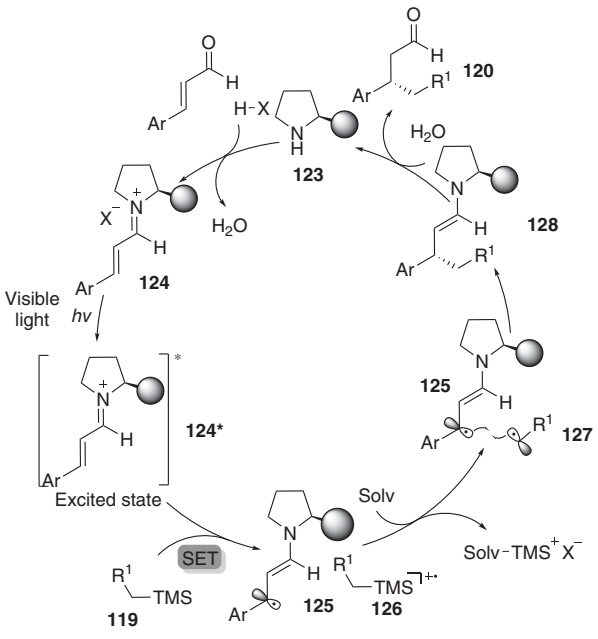


**Scheme 13.31** Mechanism of the β-alkylation of enals with alkyl silanes.

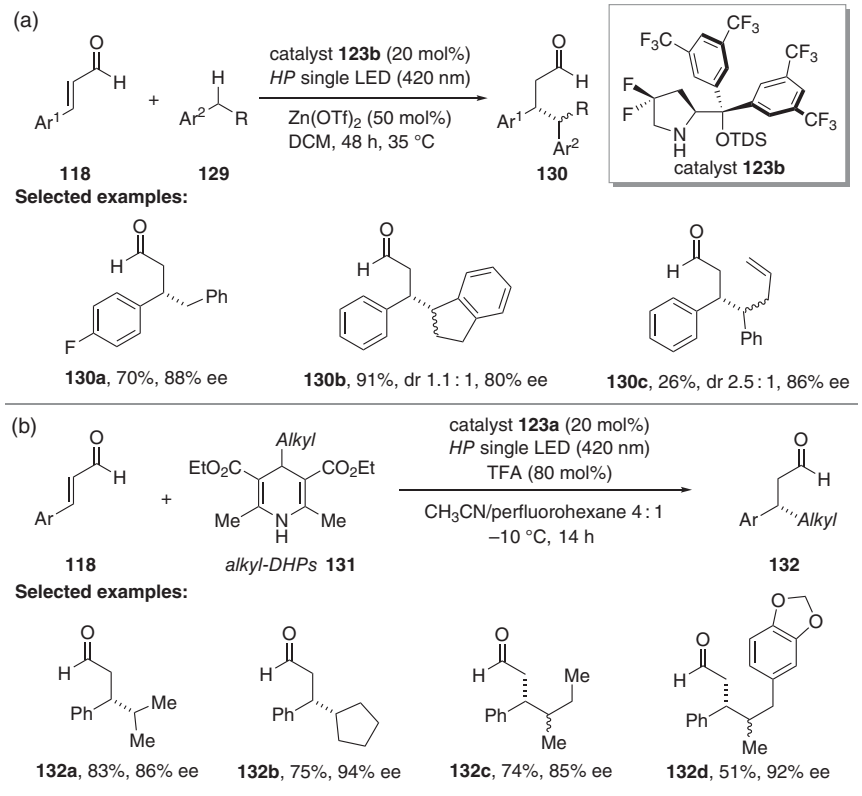


**Scheme 13.32** Enantioselective β-alkylation of enals.

of enals with simple substrates enhanced the functionality and practicality of this iminium catalytic strategy. Subsequently, this process was extended to the enantioselective β-alkylation reaction of α,β-unsaturated aldehydes with 4-alkyl-1,4-dihydropyridines (alkyl-DHPs) (Scheme 13.32b) [59]. The photoexcited iminium ions could oxidize the alkyl-DHPs to deliver the corresponding alkyl radicals.

In the same year, Melchiorre and coworkers used excited iminium ion **124*** to oxidize cyclopropanol **133**, followed by rapid ring opening to form a β-ketoalkyl radical **136** (Scheme 13.33a) [60]. The radical coupling of **136** with chiral radical **137** and subsequent cyclization afforded the highly substituted cyclopentanols **134** with excellent enantioselectivities (up to 99% ee). Later, the asymmetric photocatalytic radical cascade reactions of unactivated alkenes **139** and allenes **140** were developed to furnish **145** with high stereoselectivity, as illustrated in Scheme 13.33b [61, 62]. To further obtain multi-substituted bicyclic lactones, they designed substrates to introduce an intramolecular Aldol-type cyclization to this process, which finally triggered the acyl migration to give the final products **146.**

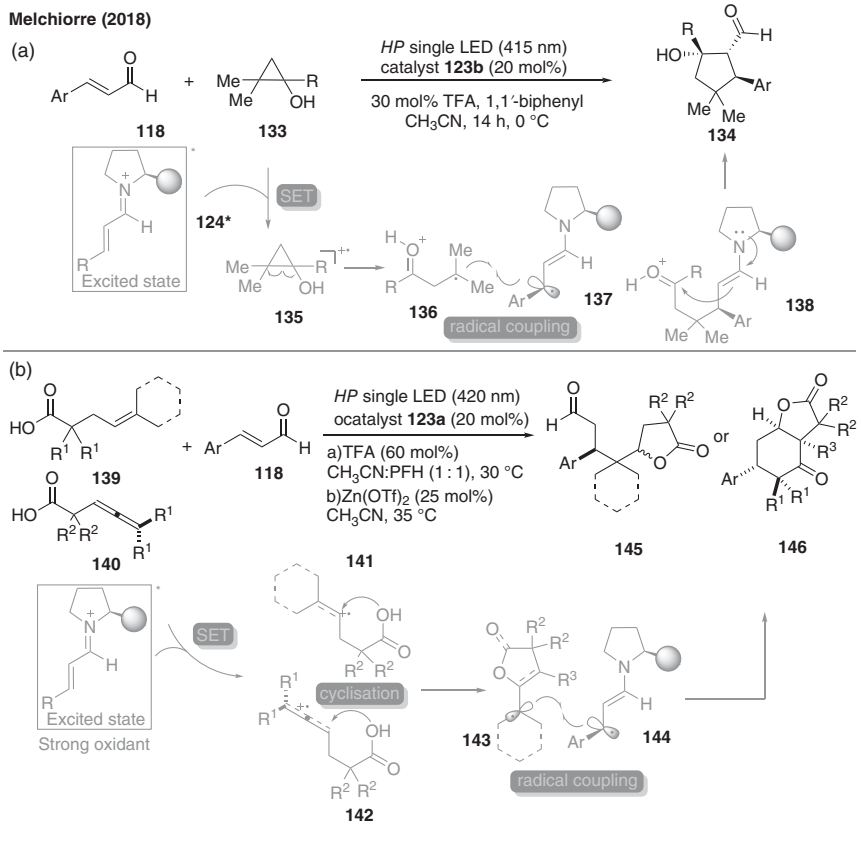


**Scheme 13.33** Enantioselective radical cascades with enals.

Inspired by previous works, the Alemán group used *gem*-difluorinated sulfinates as the source of difluoroalkyl radicals in the photocatalytic enantiocontrolled

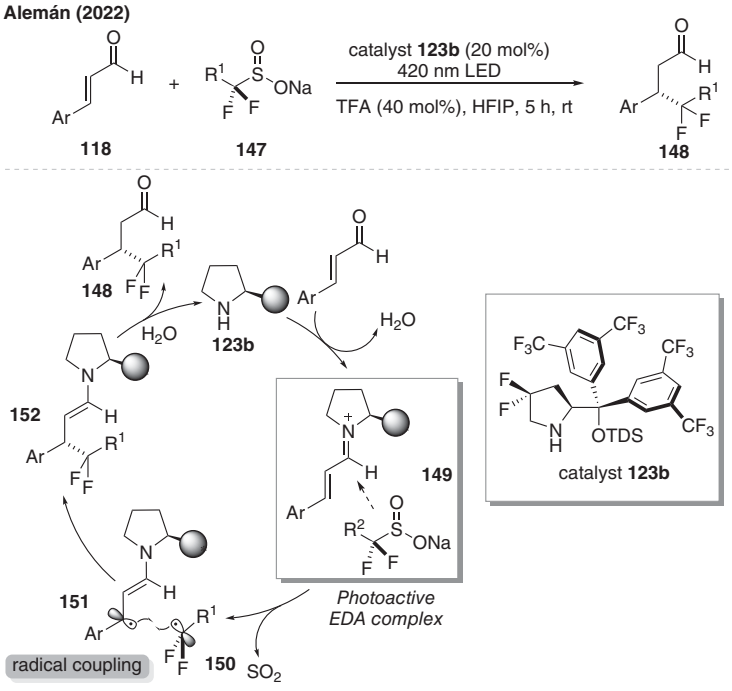


**Scheme 13.34** Enantioselective β-difluoroalkylation of enals.

β-functionalization of enals (Scheme 13.34) [63]. Unlike previous works that utilized the strong oxidizing properties of the photoexcited iminium ions, this work was enabled by the formation of an electron donor–acceptor (EDA) complex between the sulfinate and iminium ion. Single-electron transfer and the following release of sulfur dioxide generated the radicals **150** and **151**, which were smoothly coupled. The enantioselective introduction of the *gem*-difluoro moiety was important for drug design and was applied to the preparation of attractive bioactive molecules.

#### 13.2.2.2 Radical Addition

In the last section, these reactions utilize the excited iminium ions to oxidize the other substrates or rely on the formation of electron donor–acceptor (EDA) complexes to generate two radicals that could be coupled. These transformations are enabled by the unique photoelectronic property of the iminium ions, which usually require specialized amine catalysts. With the assistance of an additional photocatalytic system, the generated radicals could also undergo radical addition to the iminium ions to furnish the enantioselective β-functionalization of α,β-unsaturated carbonyls.

In 2016, the Melchiorre group designed a chiral amine catalyst with a carbazole motif and constructed quaternary carbon stereocenters with β,β-disubstituted cyclic enones via the combination of photoredox and organic catalysis (Scheme 13.35) [64]. Photochemically generated benzodioxole-derived radicals and α-amino radicals from substrates **154** or **157** were successfully applied. The condensation of the chiral

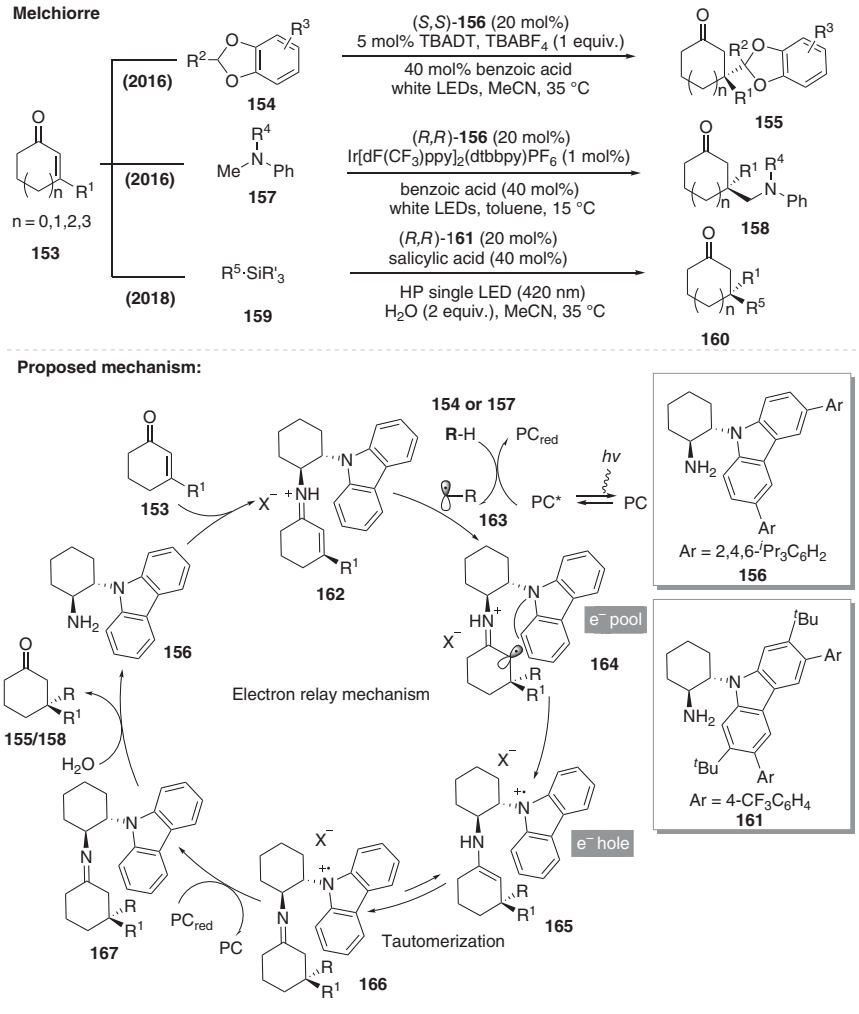


**Scheme 13.35** Enantioselective radical conjugate addition to enones.

amine catalyst with the unsaturated ketone substrate generated the imine ion intermediate **162**. The radical addition of the carbon radical **163** to **162** gave the unstable radical cation **164**, which underwent tautomerism to produce the enamine intermediate **165**. The subsequent electron transfer and hydrolysis led to the products and completed the catalytic cycle. In 2018, the same group expanded this strategy by using an intramolecular EDA complex [65]. The intramolecular iminium-ion-based EDA complex could oxidize the electron-rich alkyl trimethylsilane to generate alkyl radicals. This novel design can avoid the use of photocatalysts.

Using the same strategy, the Melchiorre group next developed an enantioselective acylation of enals to access valuable chiral 1,4-dicarbonyl compounds (Scheme 13.36a) [66]. In this transformation, 4-acyl-1,4-dihydropyridine **168** reached the excited state under visible-light irradiation and generated the acyl

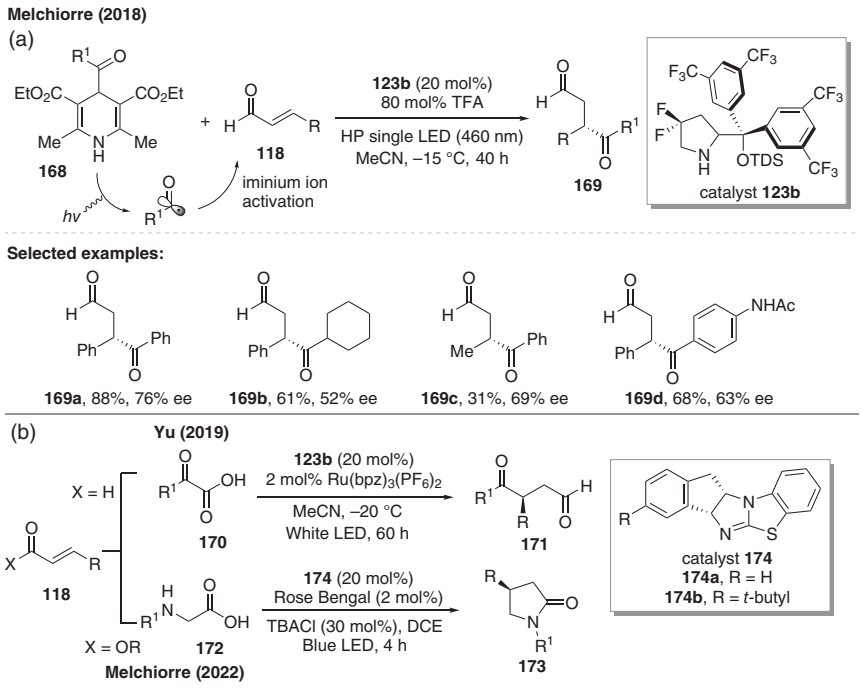


**Scheme 13.36** Asymmetric radical addition to α,β-unsaturated anhydrides and esters.

radicals. The subsequent stereoselective radical capture by the iminium ions ensured the generation of enantioenriched 1,4-dicarbonyl compounds **169**. In 2019, the Yu group utilized easily available α-ketocarboxylic acids as acyl radical precursors via single-electron oxidation and decarboxylation, furnishing the enantioselective β-acylation of enals (Scheme 13.36b) [67]. In 2022, the Melchiorre group reported the decarboxylation of amino acids to provide chiral pyrrolidinones with a chiral isothiourea catalyst **174** (Scheme 13.36b) [68]. The β-acylation product would undergo an intramolecular condensation to afford the pyrrolidinone product.

To address the issue of substrate scope in β-alkylation reactions of enals, the Melchiorre group next developed the iminium ion-based catalytic method for the enantioselective conjugate addition of primary radicals to aliphatic and aromatic alkenals (Scheme 13.37) [69]. This method required an additional photocatalyst but did not require an aromatic substituent in the β-position of enones, greatly expanding the substrate applicability. Mechanistically, the TMS reagent was oxidized to radical **179** by the excited photocatalyst. The alkyl radical **179** added to the iminium ion **177**, which was generated via the condensation of alkenal **118** with organocatalyst **123b**, generating the intermediate **180**. The subsequent single-electron reduction and hydrolysis afforded the final product **176** and completed the catalytic cycle.

In 2022, the Melchiorre group reported an asymmetric γ-functionalization of enals via a dual organocatalytic platform (Scheme 13.38) [70]. The dithiocarbonyl anion

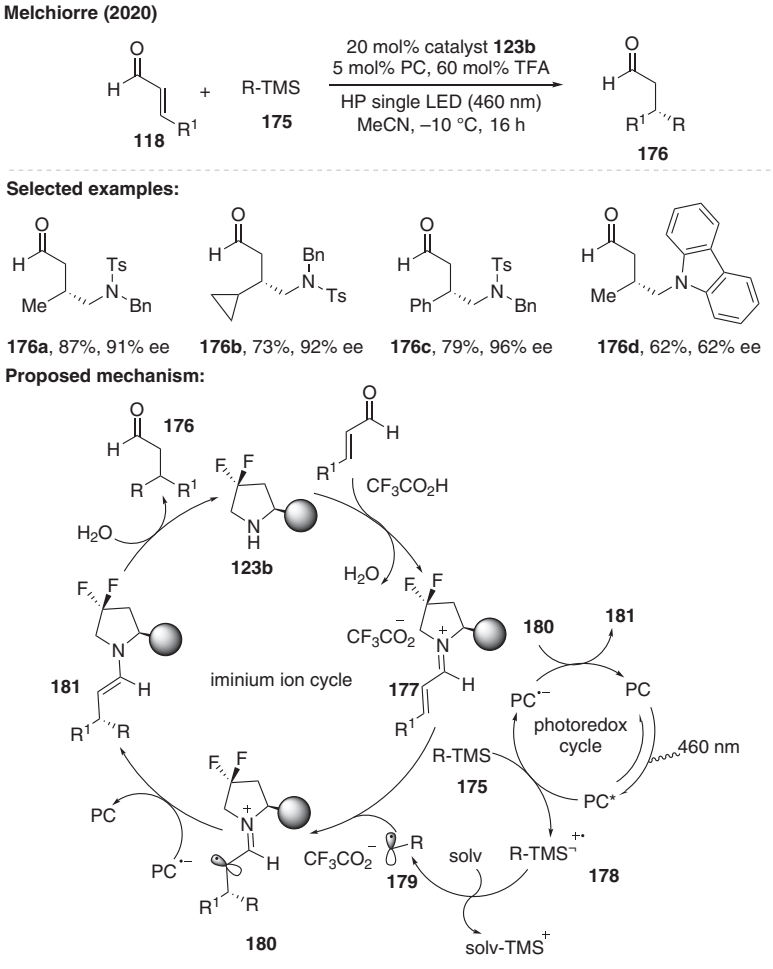


**Scheme 13.37** The β-alkylation of enals via the dual photoredox/organo catalysis.

(DTC) organocatalyst **186** was employed to initiate the radical reaction. Commercially available alkyl halides reacted with the DTC catalyst **186** via $S_N2$ to form an intermediate **187**. The S—C bond underwent homolytic cleavage to generate alkyl radical **188** and thiyl radical **189** under visible light irradiation. The addition of alkyl radical **188** to dienylamine **190** generated the allyl radical **191** or **192** intermediates, which could be oxidized by the thiyl radical **189**. The subsequent hydrolysis afforded the product **184** and regenerated chiral amine catalyst **185**.

In the same year, the Melchiorre group reported an asymmetric synthesis of 1,7-dicarbonyl compounds by combining photoredox catalysis with chiral amine catalysis (Scheme 13.39) [71]. Cyclobutanols **193** were used as the precursors of γ-ketone radicals. These unstable primary radicals could be stereoselectively trapped by the iminium ion intermediates. This strategy provided an attractive approach for the efficient synthesis of chiral 1,7-dicarbonyl compounds.

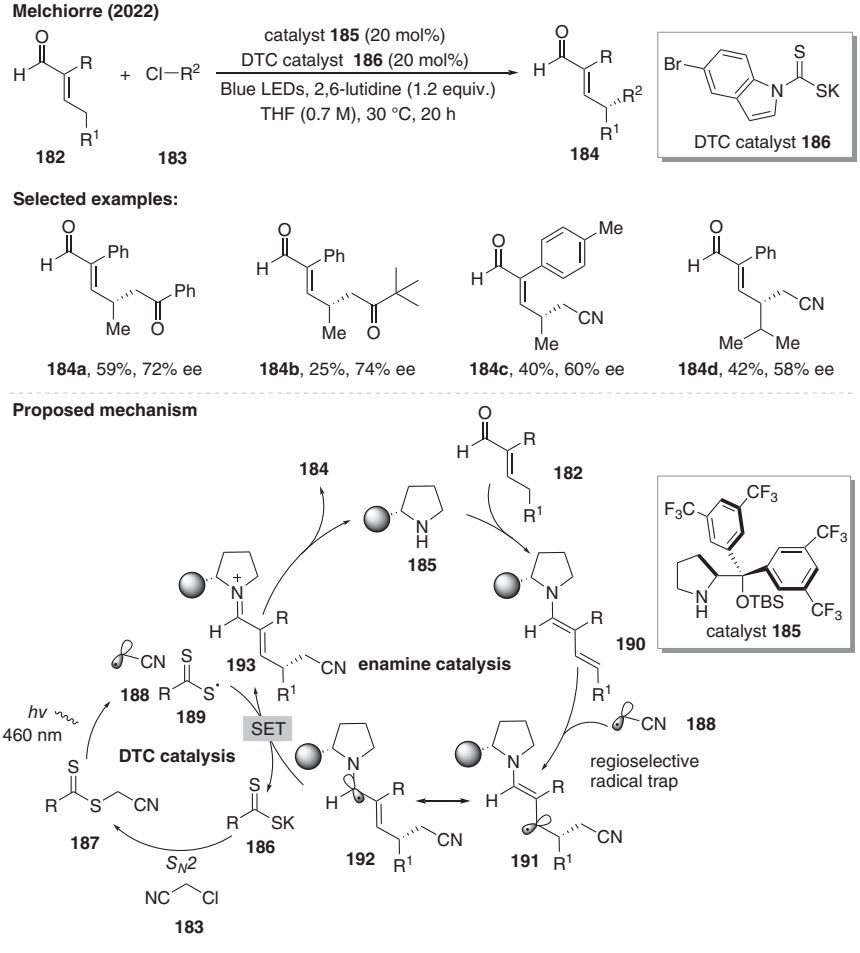


**Scheme 13.38** Enantioselective radical γ-functionalization of α-branched enals.

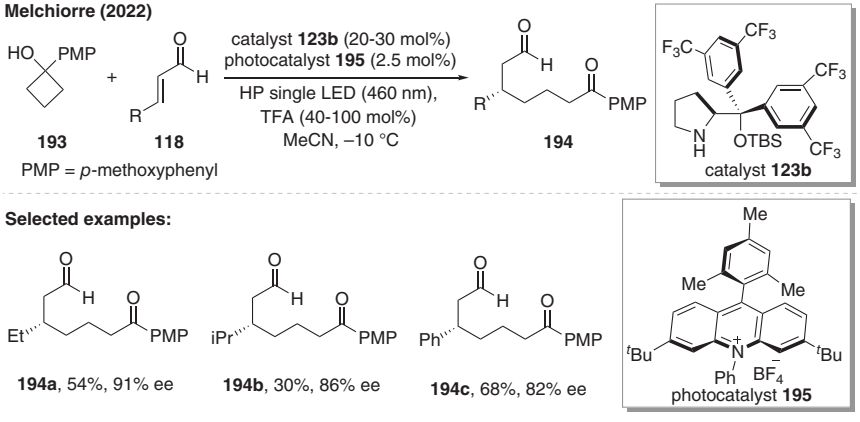


**Scheme 13.39** Enantioselective synthesis of 1,7-dicarbonyl compounds.

## 13.3 Nitrogen-Heterocyclic Carbene Catalysis for Asymmetric Radical Transformations

In the past decades, the vast potential of enantioselective reactions related to NHC as a chiral organocatalyst has unfolded before our eyes [72]. However, little attention has been paid to asymmetric radical reactions involving NHC catalysis. The reaction combining NHC catalysis with photoredox catalysis was first reported by the Rovis group in 2012, which achieved an asymmetric α-acylation of tertiary amines [73]. This strategy utilized a photocatalyst to oxidize tertiary amines under oxygen conditions to form an iminium ion. The iminium ion intermediates next participate in the NHC-catalyzed reaction with aldehydes to afford the α-acylation products. The Smith group also developed a method for the oxidation of amines to imines, which subsequently reacted with activated aryl esters to produce chiral tetrahydro-isoquinolines with good yields and enantioselectivities via the combination of chiral NHC and photoredox catalysis [74]. Since radicals did not directly participate in the stereocontrol steps, these reactions will not be discussed in detail in this chapter.

The pioneering works of NHC-catalyzed enantioselective radical reactions were reported by the Rovis group [75] and Chi group [76] independently (Scheme 13.40). They developed an enantioselective β-hydroxylation of enals via oxygen atom transfer from electron-deficient nitro compounds (4-nitropyridine *N*-oxide or

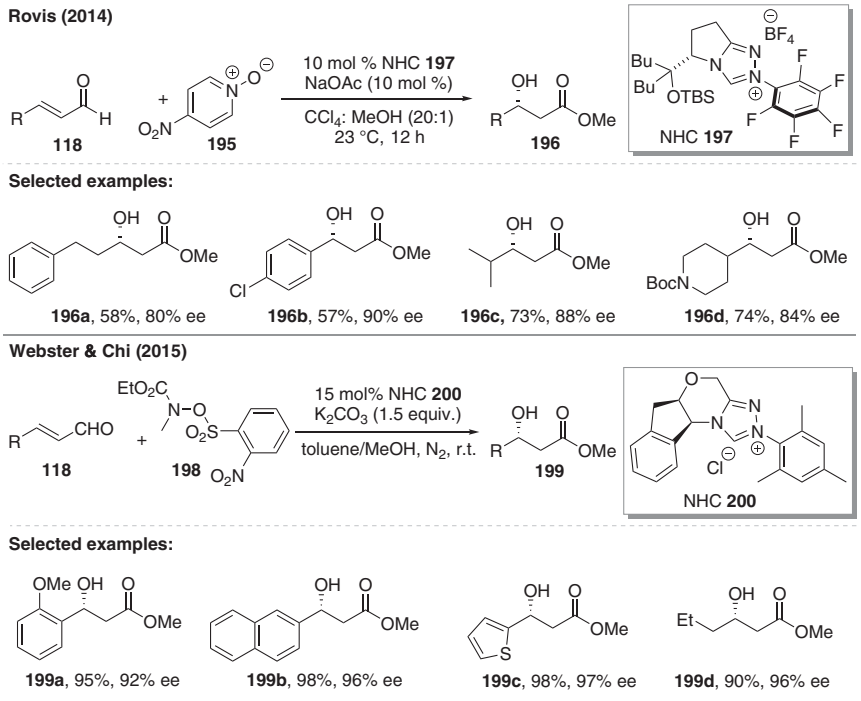


**Scheme 13.40** Enantioselective β-hydroxylation of enals.

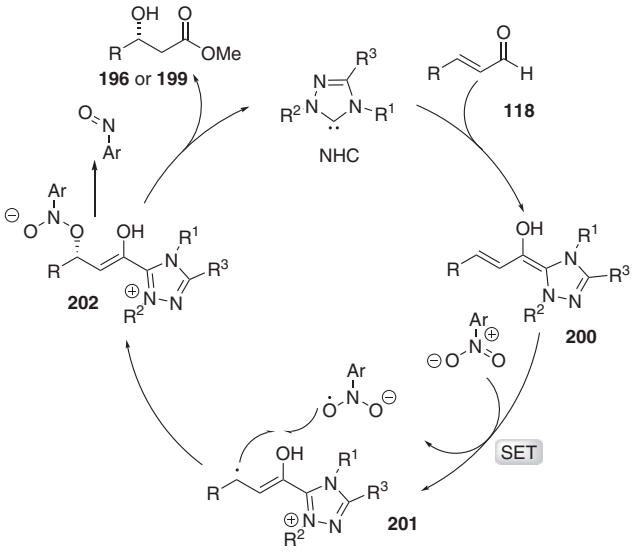


**Scheme 13.41** Mechanism of the enantioselective β-hydroxylation of enals.

nitrobenzenesulfonic carbamate). The enal substrate reacted with the NHC catalyst to form a Breslow intermediate **200**, which could undergo single-electron transfer with the nitro compound to produce the radical cation **201** (Scheme 13.41). The radical cation **201** next coupled with the oxygen-centered radical to form an enol intermediate **202**, which excluded a molecule of nitroso benzene and regenerate the NHC catalyst (in the presence of methanol), leading to the desired β-hydroxylated products **196** or **199** (Scheme 13.41). Better functional group tolerance, higher yields, and ee values were obtained in Chi's work.

Later, the Rovis group extended this strategy to the enantioselective dimerization of α,β-unsaturated aldehydes to generate 3,4-disubstituted cyclopentanones (Scheme 13.42) [77]. This transformation gave *trans*-diarylcyclopentanones **203**

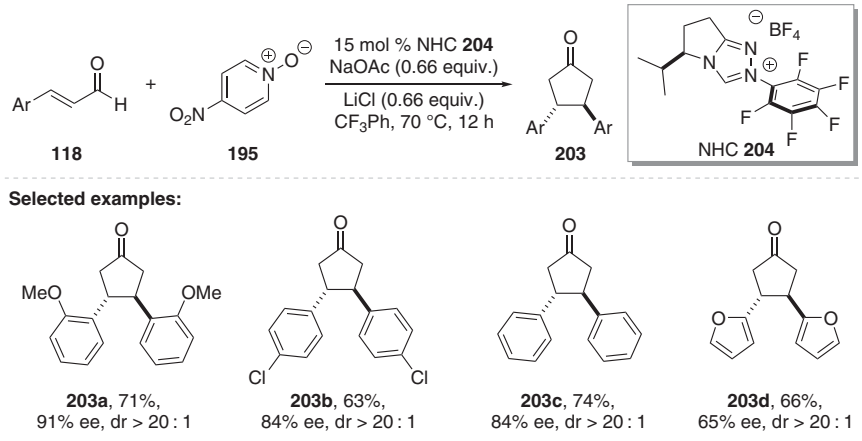


**Scheme 13.42** NHC-catalyzed enantioselective annulation of enals.

with good yields, dr, and ee using only 0.66 equivalent of oxidant. The reaction was enabled by a radical/polar crossover strategy with an initiation process with 4-nitropyridine *N*-oxide via SET. Similar to the previous method, the Breslow radical cation intermediate **206** was formed and underwent a conjugate addition to another Breslow intermediate **205**, leading to the coupled intermediate **207** (Scheme 13.43). A second SET occurred between intermediate **207** and the oxygen-centered radical to afford an acyl azolium **208**. The following intramolecular displacement released one equivalent of NHC to form cyclopentanone **209**, which underwent hydrolysis to produce the β-keto acid **210** and regenerated the second equivalent NHC. Further decarboxylation of **210** afforded the desired product **203**. In addition, the use of mixed α,β-unsaturated aldehydes can also form unsymmetric 3,4-disubstituted cyclopentanones with good yields and ee.

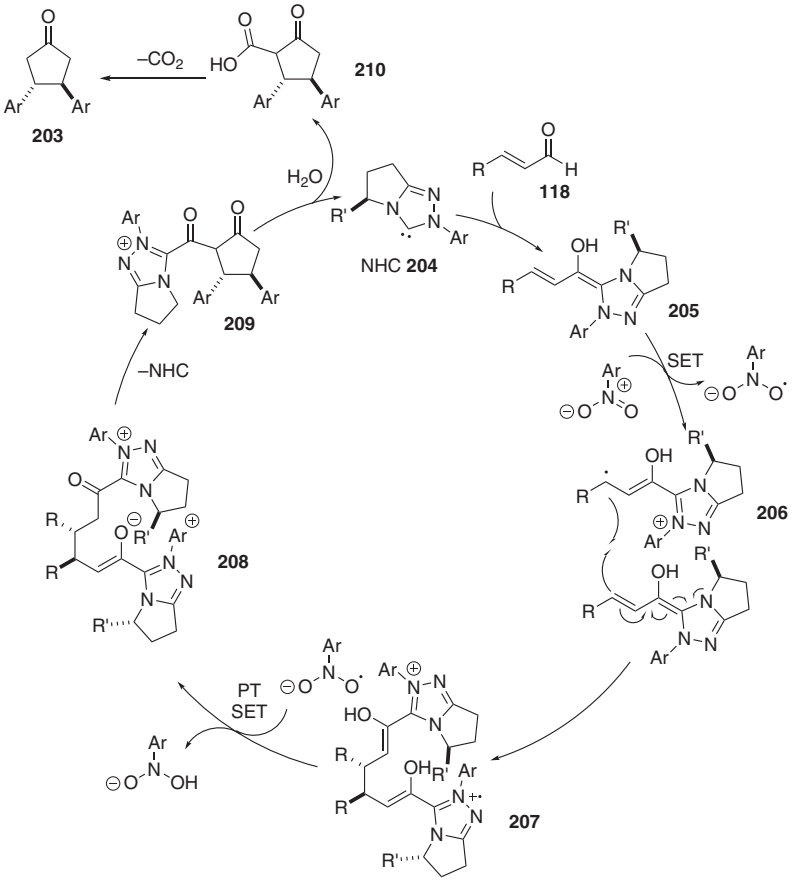


**Scheme 13.43** Mechanism of the enantioselective annulation of enals.

In 2018, the Chi group developed an enantioselective NHC-catalyzed oxidative coupling reaction of enals and di(hetero)arylmethanes to afford benzimidazole fused lactams **212** (Scheme 13.44) [78]. The benzyl radical generated from the oxidation

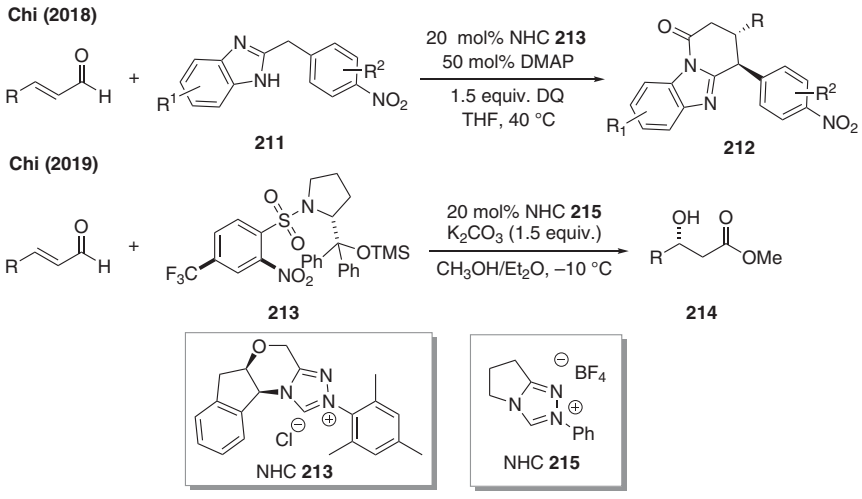


**Scheme 13.44** NHC-catalyzed enantioselective functionalization of enals.

of diarylmethane acted as the key intermediate to furnish the enantioselective functionalization of inactivated carbon–hydrogen bonds. Subsequently, the same group developed an enantioselective β-hydroxylation of enals using nitro compounds with chiral auxiliary groups (Scheme 13.44) [79]. The achiral NHC catalyst **215** was capable of catalyzing this reaction. These nitro compounds can be easily prepared from commercially available nitrobenzenesulfonyl chloride with chiral amines.

Another application involving HAT to generate benzyl radicals, combined with NHC catalysis, was developed by the Ye group (Scheme 13.45) [80, 81]. They reported the NHC-catalyzed radical [3 + 2] cyclization reaction of dioxindoles **216** and enals provided spirooxindole-γ-lactones **217** with good enantioselectivities using nitrobenzene as an oxidant. The NHC-catalyzed enantioselective β-alkylation was combined with a lactonization process to produce the spirooxindole-γ-lactones. Both aliphatic and aromatic enals reacted well with oxindoles bonded to electron-withdrawing and

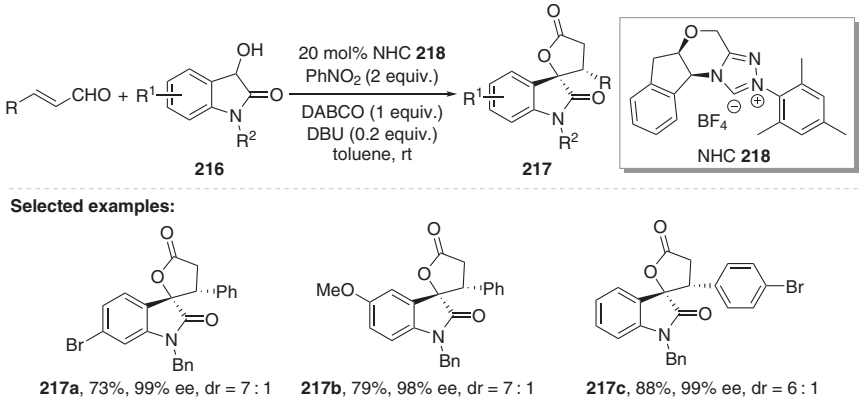


**Scheme 13.45** NHC-catalyzed oxidative [3 + 2] annulation of dioxindole and enals.

electron-donating groups, showing excellent functional group tolerance. Later, they extended this NHC-catalyzed radical reaction to β,β-disubstituted enal substrates to synthesize the spirocyclic oxindole-γ-lactones bearing two contiguous tetrasubstituted stereocenters.

Since nitrobenzene ($E$red = −0.9 V) is not oxidative enough to undergo a SET process with Breslow intermediate, Bertrand and Martin carefully investigated the reaction mechanism and proposed that the deprotonated Breslow intermediate was the true reductant to reduce the nitrobenzene [82].

Very recently, the Hong group [83] revealed an asymmetric β-pyridylation reaction of α,β-unsaturated aldehydes by using an NHC-catalyzed radical process.

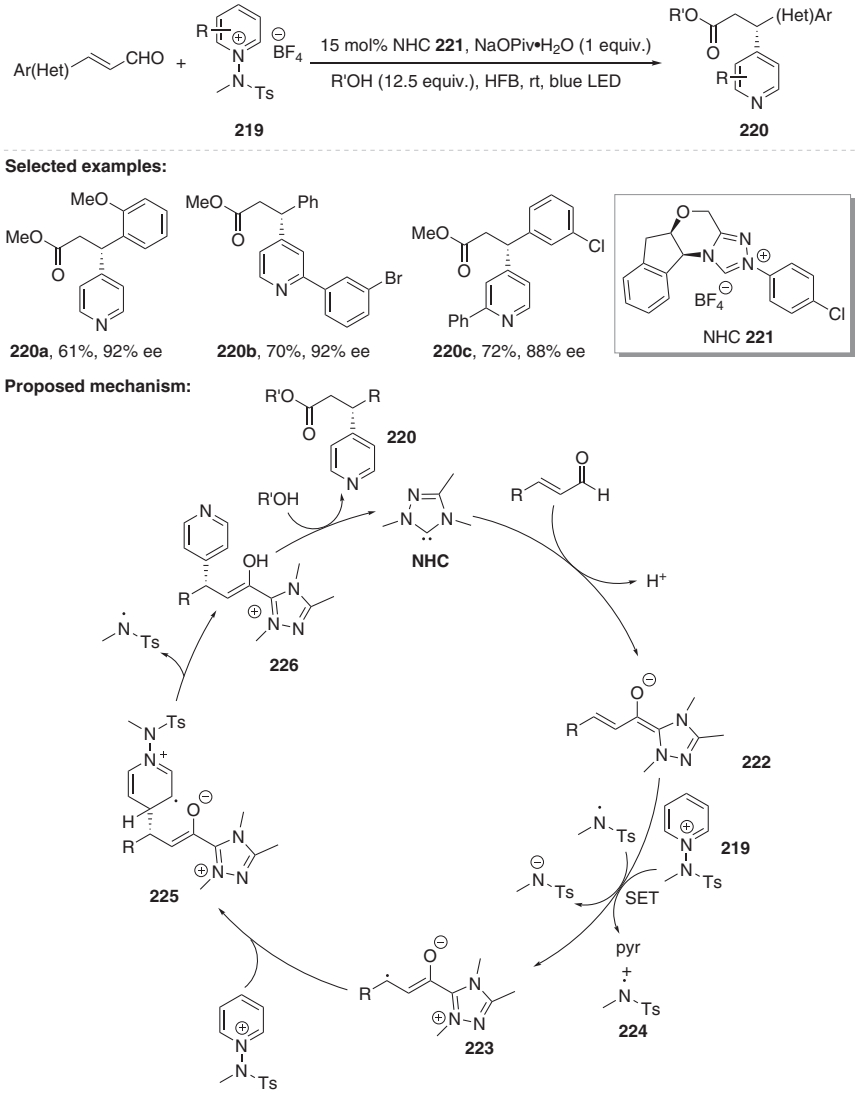


**Scheme 13.46** Enantioselective functionalization of pyridine derivatives.

The NHC catalyst **225** was used to obtain good controllability of enantiomeric and C4-selective functionalization of pyridine. Mechanistically, the single-electron transfer occurred between Breslow intermediate **222** and *N*-aminopyridine salt **219** to produce the Breslow radical cation **223**, which added to the C4 position of an additional *N*-aminopyridine salt **219**. The subsequent deprotonation and homolytic cleavage of the N—N bond gave the intermediate **226**, which reacted with alcohol via nucleophilic substitution to yield the final product **220** (Scheme 13.46). Considering the ubiquity of carbonyls and pyridines in active molecules, this approach is promising to be applied in synthesizing chemical and biological molecules.

## 13.4 Conclusion

This chapter has reviewed the versatility of organocatalysis in asymmetric radical transformations and highlighted the exciting achievements of organocatalyzed enantioselective radical reactions. These reactions provide a platform to access chiral molecules that are difficult to synthesize via conventional two-electron transformations. We discussed the transformations according to the types of organocatalysts with an emphasis on covalent bonding activation modes. Amine catalysis involving enamine catalysis and iminium catalysis, as well as NHC catalysis, were introduced in detail. Despite these elegant works, many challenges remain to be addressed in organocatalyzed asymmetric radical transformations. For example, the asymmetric functionalization of unreactive C—H bonds via the combination of photoredox catalysis and organocatalysis using PCET and HAT processes is expected. The emerging excited-state organocatalytic reactivity can be further revealed by exploring new bifunctional organocatalysts that work as asymmetric catalysts and internal photocatalysts. The development of continuous-flow photochemistry and easy-recyclable heterogeneous photocatalysts may assist the scale-up and practicality of photoredox organocatalyzed asymmetric reactions. Finally, organocatalyzed radical-mediated cascade reactions are highly attractive for the one-step divergent synthesis of chiral molecules with complexity.

## References


1 Yoon, T.P. and Jacobsen, E.N. (2003). *Science* 299: 1691–1693.
2 Blaser, H.U. and Federsel, H.J. (2011). *Asymmetric Catalysis on Industrial Scale: Challenges, Approaches and Solutions*. John Wiley & Sons.
3 Mukherjee, S., Yang, J.W., Hoffmann, S., and List, B. (2007). *Chem. Rev.* 107: 5471–5569.
4 Melchiorre, P., Marigo, M., Carlone, A., and Bartoli, G. (2008). *Angew. Chem. Int. Ed.* 47: 6138–6171.
5 Dalko, P.I. (2013). *Comprehensive Enantioselective Organocatalysis: Catalysts, Reactions, and Applications*. Weinheim: Wiley-VCH.
6 MacMillan, D.W.C. (2008). *Nature* 455: 304–308.

7 Grondal, C., Jeanty, M., and Enders, D. (2010). *Nat. Chem.* 2: 167–178.
8 Jones, S.B., Simmons, B., Mastracchio, A., and MacMillan, D.W.C. (2011). *Nature* 475: 183–188.
9 Yan, M., Lo, J.C., Edwards, J.T., and Baran, P.S. (2016). *J. Am. Chem. Soc.* 138: 12692–12714.
10 Schultz, D.M. and Yoon, T.P. (2014). *Science* 343: 1239176.
11 Romero, N.A. and Nicewicz, D.A. (2016). *Chem. Rev.* 116: 10075–10166.
12 Silvi, M. and Melchiorre, P. (2018). *Nature* 554: 41–49.
13 Proctor, R.S.J., Colgan, A.C., and Phipps, R.J. (2020). *Nat. Chem.* 12: 990–1004.
14 Mondal, S., Dumur, F., Gigmes, D. et al. (2022). *Chem. Rev.* 122: 5842–5976.
15 Nagib, D.A. (2022). *Chem. Rev.* 122: 15989–15992.
16 Beeson, T.D., Mastracchio, A., Hong, J. et al. (2007). *Science* 316: 582–585.
17 Jang, H., Hong, J., and MacMillan, D.W.C. (2007). *J. Am. Chem. Soc.* 129: 7004–7005.
18 Kim, H. and MacMillan, D.W.C. (2008). *J. Am. Chem. Soc.* 130: 398–399.
19 Graham, T.H., Jones, C.M., Jui, N.T., and MacMillan, D.W.C. (2008). *J. Am. Chem. Soc.* 130: 16494–16495.
20 Wilson, J.E., Casarez, A.D., and MacMillan, D.W.C. (2009). *J. Am. Chem. Soc.* 131: 11332–11334.
21 Amatore, M., Beeson, T.D., Brown, S.P., and MacMillan, D.W.C. (2009). *Angew. Chem. Int. Ed.* 48: 5121–5124.
22 Mastracchio, A., Warkentin, A.A., Walji, A.M., and MacMillan, D.W.C. (2010). *Proc. Natl. Acad. Sci. USA* 107: 20648–20651.
23 Wong, M.L.J., Sterling, A.J., Mousseau, J.J. et al. (2021). *Nat. Commun.* 12: 1644.
24 Capacci, A.G., Malinowski, J.T., McAlpine, N.J. et al. (2017). *Nat. Chem.* 9: 1073–1077.
25 Jia, Z., Zhang, L., and Luo, S. (2022). *J. Am. Chem. Soc.* 144: 10705–10710.
26 Wang, D., Zhang, L., and Luo, S. (2017). *Org. Lett.* 19: 4924–4927.
27 Nicolaou, K.C., Reingruber, R., Sarlah, D., and Bräse, S. (2009). *J. Am. Chem. Soc.* 131: 2086–2087.
28 Conrad, J.C., Kong, J., Laforteza, B.N., and MacMillan, D.W.C. (2009). *J. Am. Chem. Soc.* 131: 11640–11641.
29 Um, J.M., Gutierrez, O., Schoenebeck, F. et al. (2010). *J. Am. Chem. Soc.* 132: 6001–6005.
30 Jui, N.T., Lee, E.C.Y., and MacMillan, D.W.C. (2010). *J. Am. Chem. Soc.* 132: 10015–10017.
31 Pham, P.V., Ashtona, K., and MacMillan, D.W.C. (2011). *Chem. Sci.* 2: 1470–1473.
32 Jui, N.T., Garber, J.A.O., Finelli, F.G., and MacMillan, D.W.C. (2012). *J. Am. Chem. Soc.* 134: 11400–11403.
33 Comito, R.J., Finelli, F.G., and MacMillan, D.W.C. (2013). *J. Am. Chem. Soc.* 135: 9358–9361.
34 Sibi, M.P. and Hasegawa, M. (2007). *J. Am. Chem. Soc.* 129: 4124–4125.
35 Van Humbeck, J.F., Simonovich, S.P., Knowles, R.R., and MacMillan, D.W.C. (2010). *J. Am. Chem. Soc.* 132: 10012–10014.
36 Ho, X., Kang, M., Kim, S. et al. (2011). *Catal. Sci. Technol.* 1: 923–926.

**37** Ho, H.X., Jang, J., Lee, H. et al. (2012). *Org. Lett.* 14: 3272–3275.

**38** Arceo, E., Jurberg, I.D., Álvarez-Fernández, A., and Melchiorre, P. (2013). *Nat. Chem.* 5: 750–756.

**39** Leth, L.A., Næsborg, L., Reyes-Rodríguez, G.J. et al. (2018). *J. Am. Chem. Soc.* 140: 12687–12690.

**40** Blom, J., Reyes-Rodríguez, G.J., Tobiesen, H.N. et al. (2019). *Angew. Chem. Int. Ed.* 58: 17856–17862.

**41** Rezayee, N.M., Tobiesen, H.N., Lauridsen, V.H. et al. (2019). *Chem. Sci.* 10: 3586–3591.

**42** Nicewicz, D.A. and MacMillan, D.W.C. (2008). *Science* 322: 77–80.

**43** Nagib, D.A., Scott, M.E., and MacMillan, D.W.C. (2009). *J. Am. Chem. Soc.* 131: 10875–10877.

**44** Shih, H., Vander Wal, M.N., Grange, R.L., and MacMillan, D.W.C. (2010). *J. Am. Chem. Soc.* 132: 13600–13603.

**45** Welin, E.R., Warkentin, A.A., Conrad, J.C., and MacMillan, D.W.C. (2015). *Angew. Chem. Int. Ed.* 54: 9668–9672.

**46** Neumann, M., Füldner, S., König, B., and Zeitler, K. (2011). *Angew. Chem. Int. Ed.* 50: 951–954.

**47** Cherevatskaya, M., Neumann, M., Füldner, S. et al. (2012). *Angew. Chem. Int. Ed.* 51: 4062–4066.

**48** Fidaly, K., Ceballos, C., Falguières, A. et al. (2012). *Green Chem.* 14: 1293–1297.

**49** Cecere, G., König, C.M., Alleva, J.L., and MacMillan, D.W.C. (2013). *J. Am. Chem. Soc.* 135: 11521–11524.

**50** Nacsa, E.D. and MacMillan, D.W.C. (2018). *J. Am. Chem. Soc.* 140: 3322–3330.

**51** Silvi, M., Arceo, E., Jurberg, I.D. et al. (2015). *J. Am. Chem. Soc.* 137: 6120–6123.

**52** Filippini, G., Silvi, M., and Melchiorre, P. (2017). *Angew. Chem. Int. Ed.* 56: 4447–4451.

**53** Rigotti, T., Casado- Sánchez, A., Cabrera, S. et al. (2018). *ACS Catal.* 8: 5928–5940.

**54** Zhu, Y., Zhang, L., and Luo, S. (2014). *J. Am. Chem. Soc.* 136: 14642–14645.

**55** Zhang, W., Zhu, Y., Zhang, L., and Luo, S. (2018). *Chin. J. Chem.* 36: 716–722.

**56** Silvi, M., Verrier, C., Rey, Y.P. et al. (2017). *Nat. Chem.* 9: 868–873.

**57** Berger, M., Carboni, D., and Melchiorre, P. (2021). *Angew. Chem. Int. Ed.* 60: 26373–26377.

**58** Mazzarella, D., Crisenza, G.E.M., and Melchiorre, P. (2018). *J. Am. Chem. Soc.* 140: 8439–8443.

**59** Verrier, C., Alandini, N., Pezzetta, C. et al. (2018). *ACS Catal.* 8: 1062–1066.

**60** Woźniak, Ł., Magagnano, G., and Melchiorre, P. (2018). *Angew. Chem. Int. Ed.* 130: 1080–1084.

**61** Bonilla, P., Rey, Y.P., Holden, C.M., and Melchiorre, P. (2018). *Angew. Chem. Int. Ed.* 130: 13001–13005.

**62** Perego, L.A., Bonilla, P., and Melchiorre, P. (2020). *Adv. Synth. Catal.* 362: 302–307.

**63** Rodríguez, R.I., Sicignano, M., and Alemán, J. (2022). *Angew. Chem. Int. Ed.* 134: e202112632.

**64** Murphy, J.J., Bastida, D., Paria, S. et al. (2016). *Nature* 532: 218–222.

**65** Cao, Z.Y., Ghosh, T., and Melchiorre, P. (2018). *Nat. Commun.* 9: 3274.

**66** Goti, G., Bieszczad, B., Vega-Peñaloza, A., and Melchiorre, P. (2019). *Angew. Chem. Int. Ed.* 58: 1213–1217.

**67** Zhang, M., Ruzi, R., Xi, J. et al. (2019). *Org. Lett.* 21: 913–916.

**68** Hartley, W.C., Schiel, F., Ermini, E., and Melchiorre, P. (2022). *Angew. Chem. Int. Ed.* 61: e202204735.

**69** Saux, E.L., Ma, D., Bonilla, P. et al. (2021). *Angew. Chem. Int. Ed.* 60: 5357–5362.

**70** Balletti, M., Marcantonio, E., and Melchiorre, P. (2022). *Chem. Commun.* 58: 6072–6075.

**71** Wong, T.H., Ma, D., Sanza, R.D., and Melchiorre, P. (2022). *Org. Lett.* 24: 1695–1699.

**72** Biju, A.T. (2018). *N-Heterocyclic Carbenes in Organocatalysis*. Weinheim: Wiley-VCH.

**73** DiRocco, D.A. and Rovis, T. (2012). *J. Am. Chem. Soc.* 134: 8094–8097.

**74** Arokianathar, J.N., Frost, A.B., Slawin, A.M.Z. et al. (2018). *ACS Catal.* 8: 1153–1160.

**75** White, N.A. and Rovis, T. (2014). *J. Am. Chem. Soc.* 136: 14674–14677.

**76** Zhang, Y., Du, Y., Huang, Z. et al. (2015). *J. Am. Chem. Soc.* 137: 2416–2419.

**77** White, N.A. and Rovis, T. (2015). *J. Am. Chem. Soc.* 137: 10112–10115.

**78** Chen, Q., Zhu, T., Majhi, P.K. et al. (2018). *Chem. Sci.* 9: 8711–8715.

**79** Wang, H., Wang, Y., Chen, X. et al. (2019). *Org. Lett.* 21: 7440–7444.

**80** Chen, X., Chen, K., Sun, D., and Ye, S. (2017). *Chem. Sci.* 8: 1936–1941.

**81** Song, Z., Chen, K., Chen, X., and Ye, S. (2018). *J. Org. Chem.* 83: 2966–2970.

**82** Regnier, V., Romero, E.A., Molton, F. et al. (2019). *J. Am. Chem. Soc.* 141: 1109–1117.

**83** Choi, H., Mathi, G.R., Hong, S., and Hong, S. (2022). *Nat. Commun.* 13: 1776.

# 14

# Organocatalysis via Hydrogen Bonding for Asymmetric Radical Transformations

*Xu Ban, Xiangbin Bai, and Zhiyong Jiang*

*School of Chemistry and Chemical Engineering, Henan Normal University, Xinxiang, P. R. China*

## 14.1 Introduction

The use of small organic molecules to catalyze organic transformations, especially in an enantioselective manner, has been sporadically reported in the literature since the 1970s. However, it was not until 2000 that the terminology "organocatalysis" was popularized, and the field grew exponentially [1]. Over the years, several classes of organocatalysts have been developed to enable asymmetric reactions through either covalent catalysis (iminium, enamine, Lewis base, SOMO catalysis, etc.) or noncovalent catalysis (ion-pairing, hydrogen bonding, Brønsted acid/base catalysis, etc.) [2]. Among them, hydrogen bonding (H-bonding) has been established as one of the most important interactions to control the stereoselectivity of various chemical transformations [3]. However, applying H-bonding catalysts into asymmetric radical transformations is a recent development that poses a significant challenge due to the weak interactions involved and the high reactivity of the radical species [4]. Although the conventional asymmetric radical transformations based on the ground state have been continually reported, they have been limited to a narrow scope. However, a significant turning point occurred in the early twenty-first century with the resurgence of photocatalysis. This resurgence coincided with notable advancements in utilizing radical-based reactions to construct C—C and C–heteroatom bonds in organic synthesis [5]. The main advantages of photocatalysis include its ability to operate under mild conditions, the absence of stoichiometric oxidant/reductant, and a high tolerance for functional groups. These characteristics make photocatalysis an ideal platform for investigating the impact of hydrogen bonding in asymmetric radical reactions. Furthermore, the integration of photocatalysis with transition metal catalysis [6], Lewis acid catalysis [7], and supramolecular chemistry [8] has significantly advanced the field. The discovery of chiral bifunctional photocatalysts featuring H-bonding domains [9], and cooperative chiral H-bonding catalysts coupled with achiral photocatalysts [10], marked the true inception of research dedicated to asymmetric photoinduced radical-based reactions. Since this moment, intense research into H-bonding mediated asymmetric radical transformations

in organic synthesis has commenced. More importantly, a burst of new ideas has emerged, leading to a plethora of catalytic modes related to H-bonding. These advancements enable the utilization of photoinduced electron transfer, energy transfer (EnT), and hydrogen atom transfer (HAT) mechanisms to facilitate asymmetric radical reactions under mild and sustainable experimental conditions [11].

This section aims to provide a comprehensive overview of the progress made over the past two decades, focusing on the role of hydrogen-bonding interactions in the construction of stereocenters via radical intermediates. The term "radical-based transformation" has been used somewhat ambiguously in the literature of contemporary synthetic catalysis. However, when discussing "organocatalysis via H-bonding," this topic predominantly focuses on photoinduced excitation modes, with relatively few examples conducted under ground-state conditions. To provide a logically organized framework, we have categorized this topic into eight common radical transformations based on the distinct bond-forming patterns where the construction of stereocenters occurs. These categories are radical cycloaddition, radical cyclization, radical addition, radical coupling, Minisci reactions, asymmetric protonation, radical/polar crossover reactions, and deracemizations. In each section, emphasis will be placed on the role of H-bonding catalysis and the underlying mechanisms. Additionally, examples will be selected to highlight their potential in the asymmetric synthesis of small molecules.

## 14.2 Asymmetric Cycloaddition via H-Bonding Organocatalysis

Asymmetric cycloadditions are one of the most employed radical-based reactions. They have attracted significant attention due to their remarkable ability to synthesize highly functionalized compounds with multiple stereocenters in one step. Over the years, numerous synthetic strategies have been developed to effectively control the stereochemistry of these reactions [12]. Among the various approaches, the use of organocatalysis through H-bonding has emerged as a particularly promising avenue. This method involves employing organic catalysts that can interact with the reactants through H-bonding interactions. The result is exceptional catalytic activity and enantioselectivity, enabling the synthesis of chiral compounds with high precision. Different types of H-bonding organocatalysts have been extensively explored in the context of asymmetric cycloadditions, including chiral diols, lactams, urea/thiourea, phosphonic acids, and others. By incorporating these catalysts into the reaction system, it becomes possible to exert control over the regio- and stereochemical outcomes, facilitating the formation of complex molecules with desired stereocenters.

Chiral diols, such as BINOLs, VANOLs, and tartaric acid derivatives, are commonly used as chiral templates in asymmetric synthesis [13]. This is mainly because the OH group has the ability to coordinate with substrates through a single H-bond, creating a stereo-differentiating environment that ensures subsequent bond formations in an asymmetric manner. The use of chiral diols in asymmetric radical

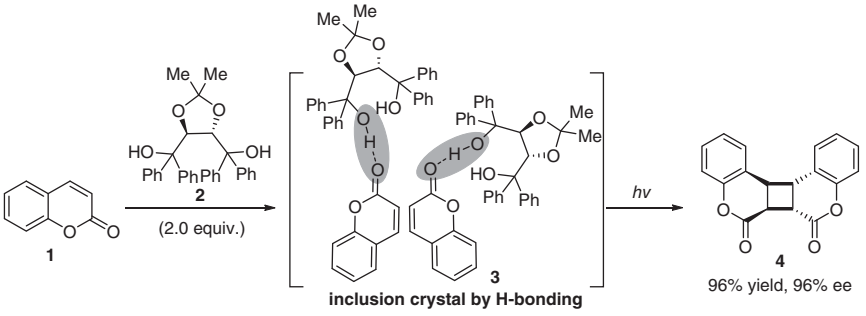


**Scheme 14.1** Chiral diol as H-bonding template for solid-state [2 + 2] cycloaddition.

cycloaddition was initially studied as a complexing agent with an excess amount in solid-phase conditions. In 1992, Toda reported that irradiation of inclusion crystals of chalcones **1** and 2.0 equiv. diol **2** resulted in an asymmetric [2 + 2] cycloaddition with a high enantiomeric excess of up to 96% ee (Scheme 14.1) [14]. The authors proposed that chiral inclusion crystal **3**, acting as photoactive exciplexes, was formed via H-bonding interactions between the OH of **2** and C=O of **1**, leading to high enantioselectivities. It should be noted that this work provides solid evidence that the relatively weak H-bond can participate in the radical reaction process. However, it is important to point out that this irradiation was conducted using high-energy ultraviolet light, and a high amount (2.0 equiv.) of chiral H-bond complexing agent **2** was required.

In 2005, Tanaka developed this strategy for a homogeneous solution system using 2.0 equiv. chiral diol **2** as an optically active host (Scheme 14.2) [15]. Although this process was carried out in cyclohexane, an H-bonding mediated dynamic kinetic resolution was involved. One enantiomer of the formed adduct (−)-**6** interacted with the chiral diols, leading to the precipitation of inclusion crystal **2**, which was favored. These inclusion crystals acted as protective shields, preventing the reverse reaction back to the racemic monomer substrate. On the other hand, the other

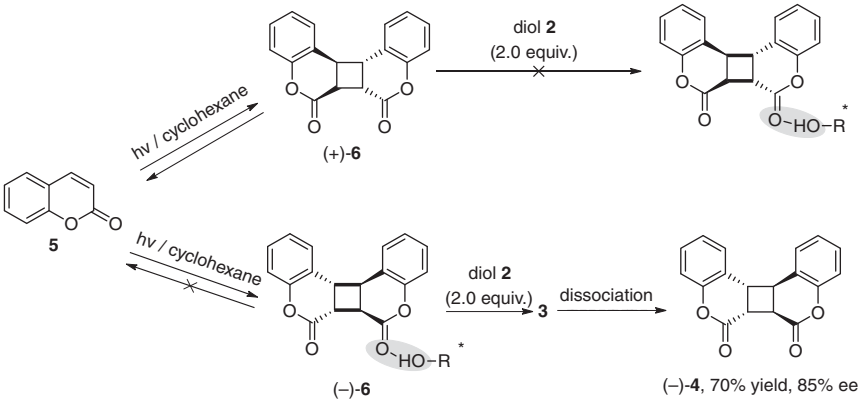


**Scheme 14.2** Chiral diol as H-bonding template for asymmetric [2 + 2] cycloaddition.

enantiomer (+)-**6** (which was disfavored) decomposed back to the monomer upon direct irradiation in the solution. As a result, the final dimer product was obtained with 70% yield and 85% ee. It is worth noting that the success of this method heavily relied on the formation of inclusion crystals between the substrate and diols through H-bonding, which significantly limited its further applications regarding the substrate scope in organic synthesis.

In addition to chiral diols, secondary chiral lactam has been extensively studied as an ideal H-bonding catalyst with NH as the donor and C=O as the acceptor in asymmetric radical transformations. Starting from 1999, Bach and coworkers have reported a series of chiral lactams that serve as H-bonding skeletons for conducting asymmetric radical reactions (**7**–**10** in Scheme 14.3) [16]. These chiral lactams are typically synthesized based on Kemp's triacid and related imides, which feature a U-shaped two-point H-bonding site. The lactams form complexes with various substrates containing amide groups, leading to stable and effective enantioface discrimination through twofold H-bonding interactions. This arrangement effectively shields one face of the substrate with oxazole-tethered substitutions, allowing for highly selective reactions on the open face of the substrate.

The initial applications of chiral lactam **7** involved the utilization of 4-alkenyloxyquinolone **11** as substrates [17]. These substrates have been known

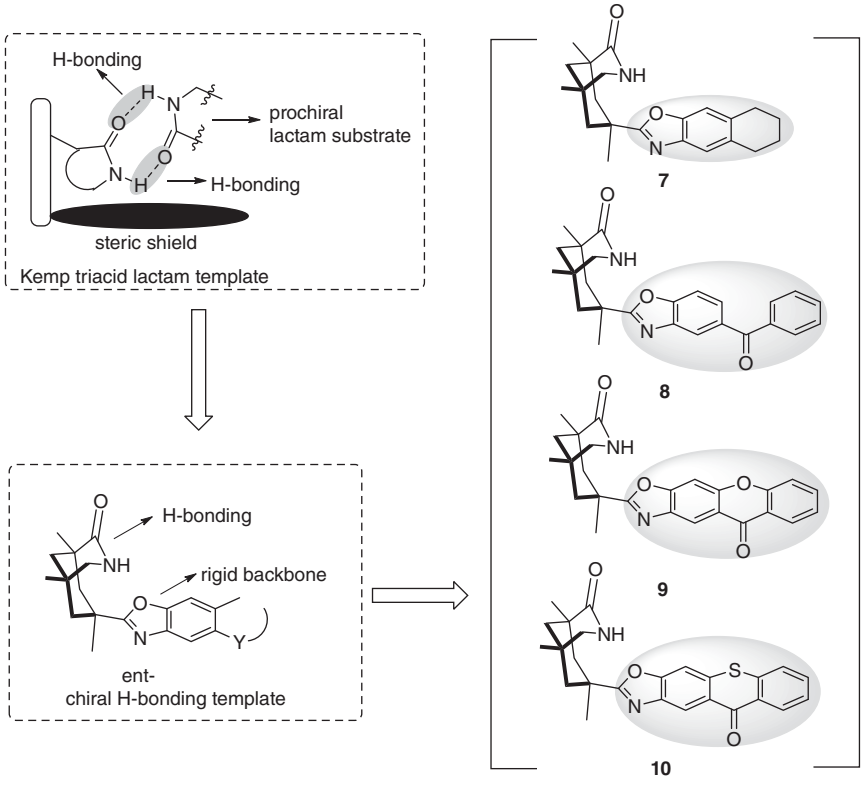


**Scheme 14.3** Design concept for chiral lactams as H-bonding catalysts by Bach.

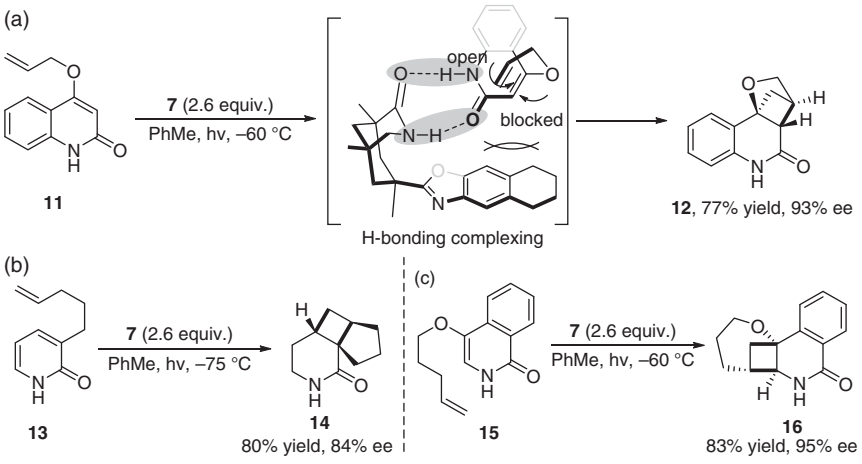


**Scheme 14.4** Chiral lactams in asymmetric intramolecular [2 + 2] cycloaddition: (a) 4-spiops xmltex28alkenyloxyquinolone; (b) 5,6-dihydropyridone; (c) isoquinolone.

to undergo an intramolecular [2 + 2] cycloaddition under irradiation conditions, resulting in polycyclic products **12**. Interestingly, it was discovered that the introduction of 2.6 equivalents of chiral lactam **7** induced a high degree of enantioselectivity, achieving 93% ee (Scheme 14.4a). It is worth noting that the use of an H-bonding complexing agent **7** in this process does not participate in the stoichiometry of individual reactions. Instead, it only transfers chirality to the reaction products. The recovery of the complexing agent can be easily achieved in quantitative yields through chromatography. Mechanistic studies have revealed that the presence of a tetrahydronaphthalene unit in the chiral lactam **7** prevents internal attack of the olefin from the bottom face. Instead, the olefin approaches the photoexcited quinolone from the top face. The regioselectivity of the reaction is determined by the ease of ring closure to form a five-membered ring, ultimately resulting in cycloaddition products **12**. Building upon a similar mechanistic approach, it has been found that these conditions can also be applied to the asymmetric [2 + 2] cycloaddition of 5,6-dihydropyridone **13** and isoquinolone **15**, yielding **14** and **16** with high yields and ee (Scheme 14.4b, c) [18]. Despite the instability of chiral lactam catalyst **7**, like many organic molecules under short wavelengths ($\lambda = 254$ nm), it has been observed to withstand irradiation conditions sufficiently well to maintain a high level of enantioselectivity.

In 2000, the same lactam catalyst **7** was utilized to carry out asymmetric intermolecular [2 + 2] cycloadditions between 2-quinolone **17** and common alkene **18** [19]. The approach encompassed the initial formation of an H-bonded complex between the 2-quinolone and the lactam **7** through dual hydrogen bonds. This complexation process facilitated the differentiation of the enantiotropic faces, thus enabling the subsequent [2 + 2] cycloaddition with the approaching alkenes (Scheme 14.5a). A significant achievement resulting from this synthetic strategy was the successful total synthesis of the Melodinus alkaloid (+)-meloscine (Scheme 14.5b). By utilizing 2.5 equivalents of the chiral template, the key synthon **22** was obtained as a single isomer with excellent yield and 79% ee. After

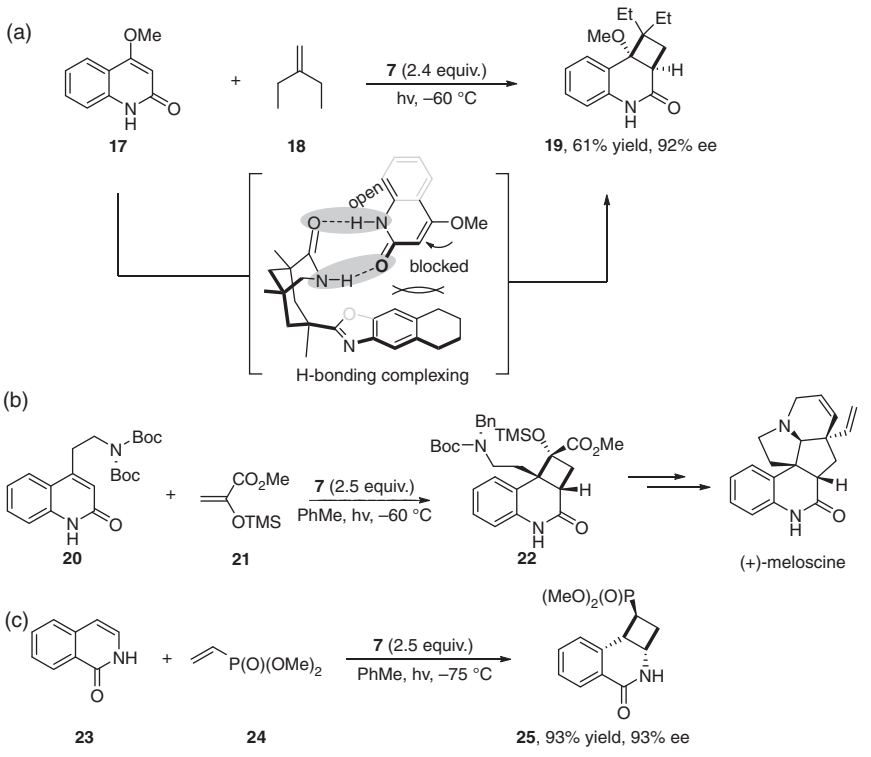


**Scheme 14.5** Chiral lactam in intermolecular [2 + 2] cycloaddition: (a) cycloaddition of 2-quinolone with alkene; (b) Total synthesis of (+)-meloscine; (c) cycloaddition of isoquinolone with alkenes.

a straightforward crystallization step for downstream modifications, the desired enantiomer (+)-meloscine was ultimately obtained [20]. Similarly, isoquinolone **23** also undergoes efficient [2 + 2] photocycloaddition with a range of electron-deficient alkenes. This reaction generates functionalized cyclobutane **25** in 93% yield with 93% ee [21].

Later, the Bach group expanded their strategy to encompass other cycloaddition reactions [22]. A notable example is the [4 + 4] cycloaddition of 2-pyridone **26**, which demonstrates the suitability of this heterocyclic compound class for H-bonding with the chiral lactam **7**. Remarkably, even with a relatively low loading (1.2 equivalents), the desired adduct **28** could be obtained with high enantioselectivity (Scheme 14.6a). Furthermore, the chiral lactam exhibited excellent performance in facilitating asymmetric intermolecular [4 + 2] cycloadditions (Scheme 14.6b) [23]. The Bach group reported an enantioselective Diels–Alder-type reaction of functionalized benzaldehyde **29** and activated olefin. This reaction employed an *ortho*-quinodimethane generated through intramolecular H-abstraction from a photochemically excited *ortho*-alkyl-substituted benzaldehyde. The chiral lactam catalyst **7** played a crucial role in differentiating the enantiotopic face of the photochemically generated *o*-quinodimethane for the subsequent [4 + 2] cycloaddition with alkenes. In 2012, Bach further applied this strategy to a chiral

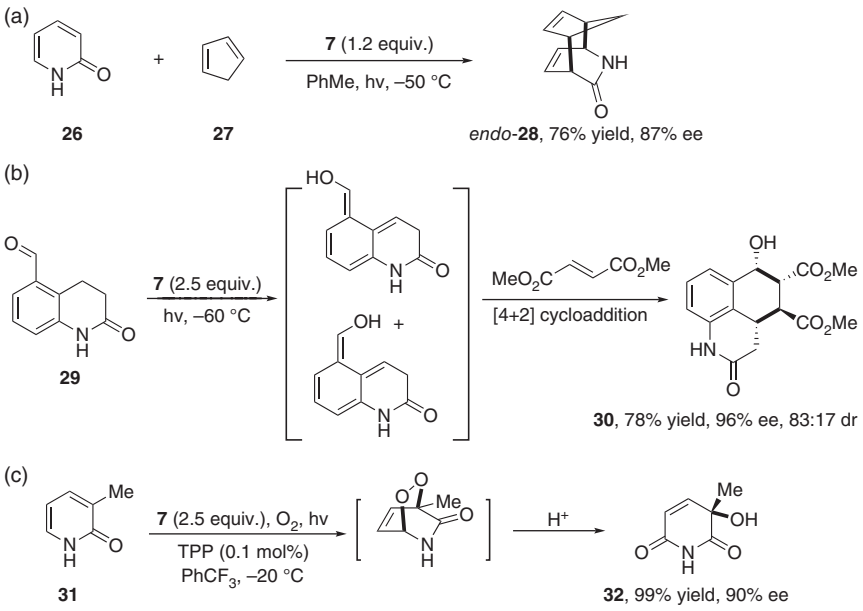


**Scheme 14.6** Chiral lactam in other asymmetric cycloadditions: (a) 2-pyridone; (b) benzaldehyde; (c) cycloaddition of 2-pyridone with singlet oxygen.

template-mediated enantioselective [4 + 2] photocycloaddition of 2-pyridone **31** with singlet oxygen (Scheme 14.6c) [24]. This transformation was carried out in the presence of TPP as a photoredox catalyst, ultimately affording a series of chiral tertiary alcohols **32**.

Impressive breakthroughs have been made in radical reactions using chiral lactam **7** as H-bonding templates. However, the requirement for excessive amounts of chiral lactam and the use of high-pressure mercury lamps have limited its further applications in synthetic chemistry. Therefore, there is an urgent need to develop catalytic conditions that can solve the limitations and operate under mild irradiation conditions.

Regarding the mechanism, it is widely believed that most photocycloaddition reactions proceed through triplet processes. The triplet state can theoretically be populated through intersystem crossing (ISC) from the directly accessible excited *S1* state using a high-pressure mercury lamp in Pyrex glass ($\lambda > 280$ nm) [25]. The relevance of the triplet state to catalytic enantioselective photochemical reactions arises from the fact that it can be accessed not only directly via *S1*, but also indirectly through a process known as triplet energy transfer or sensitization. A typical triplet sensitizer (Sens) that can catalyze a photochemical reaction exhibits a long-wavelength absorption beyond that of the substrate and a high ISC rate to efficiently populate its *T1* state. Previous attempts to employ chiral triplet sensitizers for asymmetric radical reactions have failed to achieve satisfactory enantioselectivity. This is likely due to the poor enantioface differentiation caused by the chiral catalysts, rather than a failure to meet the energy-transfer criterion. As a result, linking Bach's chiral lactam with a rigid oxazole unit has proven to be a superior solution, providing a stable

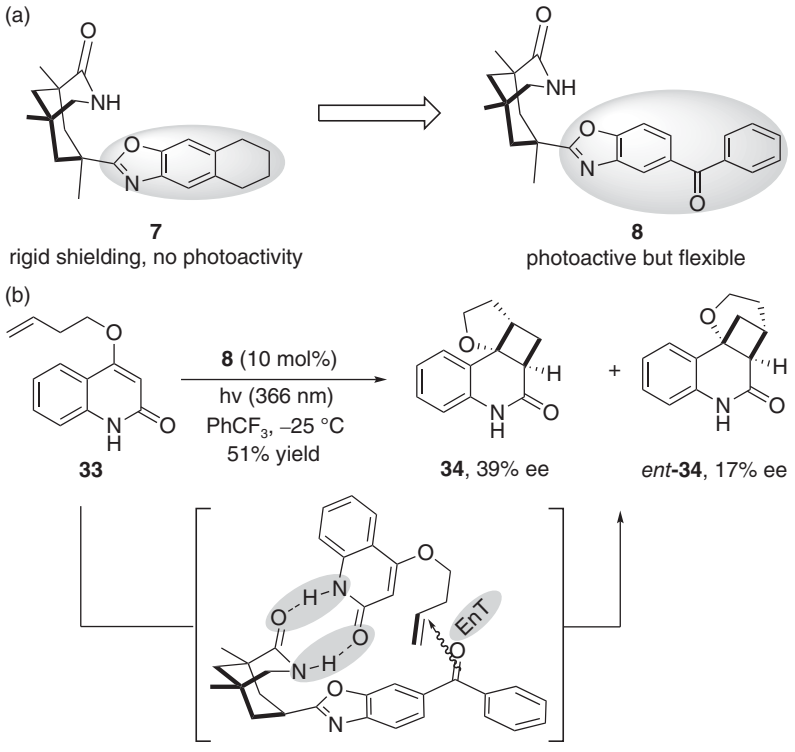


**Scheme 14.7** Benzophenone-incorporated chiral lactams in intramolecular [2 + 2] cycloaddition: (a) design of aromatic ketone containing photosensitizer 8; (b) applications of photosensitizer 8.

steric shield. In this context, the Bach group has developed their second generation of H-bonding organocatalyst by incorporating an aromatic ketone group as a photosensitizer, resulting in lactam **8** (Scheme 14.7a) [26]. The triplet energy of this compound was measured as 291 kJ mol$^{-1}$ (pentane/isopentane). Subsequent investigations focused on the intramolecular [2 + 2] cycloaddition reaction of quinolone **33** in the presence of 10 mol% of the lactam **8**. While a rate acceleration of the reaction was observed, the enantioselectivities remained low. The best result was achieved in trifluorotoluene at –25 °C, with only 39% ee for the major product and 17% ee for the minor product (Scheme 14.7b). The relatively low triplet energy and the comparatively short-wavelength absorption of the chiral benzophenone **8** are responsible for the disappointing enantioselective results. Another factor to consider is the flexibility of the benzophenone moiety, which provides less steric shielding compared to the oxazolotetrahydronaphthalene unit in the chiral template. Nevertheless, this work represents a significant milestone in the pursuit of catalytic asymmetric radical reactions through H-bond interactions.

Bach developed a novel photocatalyst by substituting the benzophenone group with a more rigid and photoactive xanthone unit (Scheme 14.8a). The xanthone unit exhibited a higher triplet energy (approximately 310 kJ mol$^{-1}$) compared to benzophenone (approximately 287 kJ mol$^{-1}$) [27]. This higher energy level,

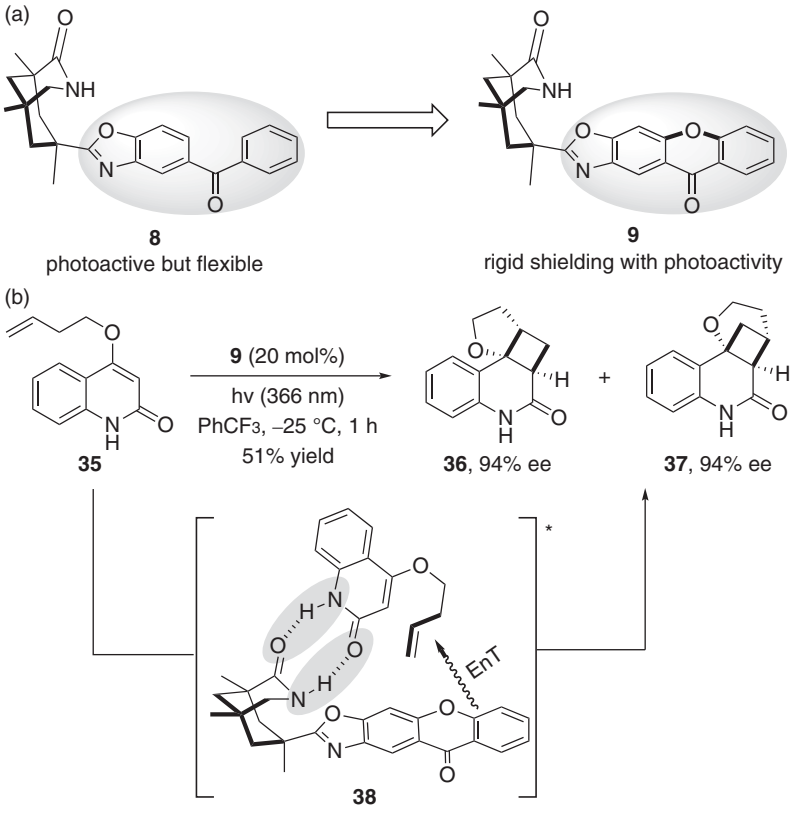


**Scheme 14.8** Xanthone-incorporated chiral lactams in intramolecular [2 + 2] cycloaddition: (a) Design of photosensitizer 9; (b) applications of photosensitizer 9.

combined with the inflexible and planar nature of the xanthone moiety, was expected to provide superior steric shielding capabilities. In subsequent studies, the xanthone unit of **9** displayed a relatively high absorption coefficient for wavelengths above 350 nm. Additionally, the chirality turnover was remarkably high, with up to 90% ee achieved after one hour of irradiation at –25 °C in $PhCF_3$. The proposed mechanism suggests that irradiation of the H-bonding chiral complex **38**, formed between the xanthone **9** and substrate **35**, facilitates rapid energy transfer from the xanthone chromophore to **35**, exciting the substrate to its triplet excited state (Scheme 14.8b). This is followed by an intramolecular [2 + 2] cycloaddition process. Furthermore, the xanthone moiety in **9** acts as a steric shield, ensuring that cycloaddition occurs only from the open face of the substrate. It is important to note that reducing the catalyst loading from 20 to 10 mol% resulted in a significant decrease in ee values due to the decomposition of the photocatalyst under irradiation. To overcome this issue, the author suggested stopping the reaction before complete conversion to minimize catalyst degradation [28].

In comparison to xanthone, thioxanthone demonstrates a bathochromic shift in its UV/Vis spectra, exhibiting an absorption maximum centered at 390 nm with significant absorption in the visible region. The parent thioxanthone possesses a triplet

energy of 264 kJ mol$^{-1}$, while xanthone has a triplet energy of 310 kJ mol$^{-1}$. This difference in triplet energy allows thioxanthone to efficiently excite most organic substrates under visible light irradiation, thus suppressing the decomposition pathway typically caused by high-energy UV light. Building upon these considerations, a recent report by Bach introduced a novel bifunctional photocatalyst incorporating thioxanthone as the chromophore in H-bonding lactams (Scheme 14.9a) [29]. This catalyst exhibited remarkable absorption in the visible light region and enabled efficient asymmetric catalysis of the intramolecular [2 + 2] cycloaddition reaction of **39**, presumably through triplet energy transfer via the H-bonding complex **41** (Scheme 14.9b). Notably, the chiral thioxanthone photocatalyst **10** surpassed benzophenone **8** and xanthone **9** by being the first chiral photocatalyst capable of utilizing visible light for highly enantioselective photochemical reactions while accommodating a wide range of substrates [30].

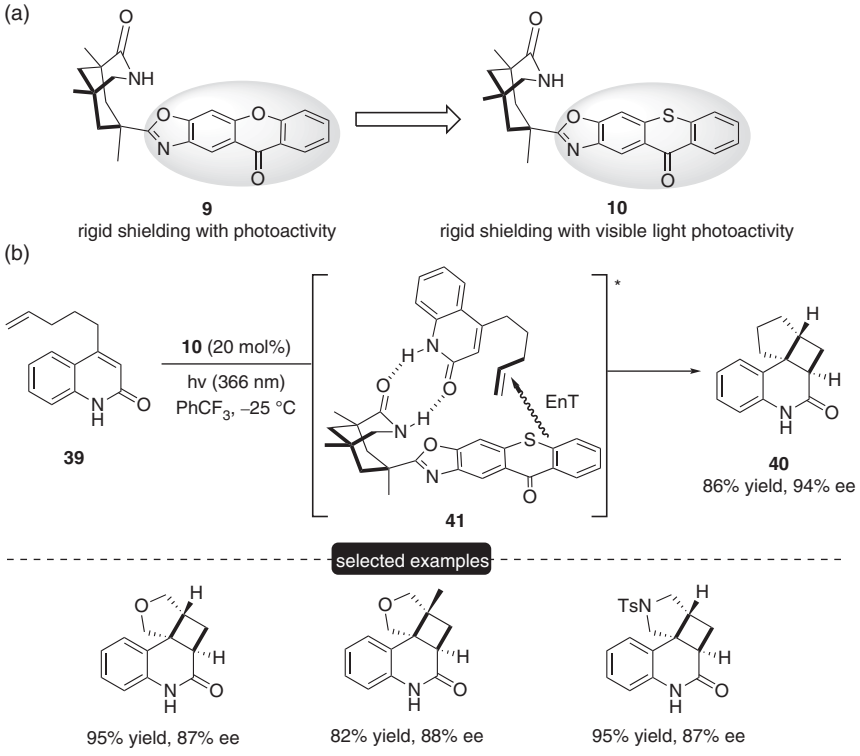


**Scheme 14.9** Thioxanthone-incorporated chiral lactam in asymmetric intramolecular [2 + 2] cycloaddition: (a) design of photosensitizer 10; (b) applications of photosensitizer 10.

Like lactams, ureas/thioureas, a class of readily available and widely used organocatalysts, have long been attractive due to their dual H-donor capabilities from the NH and CO groups. In 1990, Etter's group reported the formation of crystals between diaryl ureas and carbonyl compounds as H-bonding acceptors [31]. This discovery laid the foundation for the utilization of urea as a novel achiral H-bonding catalyst in various applications. One significant application

was demonstrated later by Curren, who used the achiral thiourea catalyst to enhance the reaction rate and increase diastereoselectivity in the allylation of cyclic-sulfinyl radicals under sunlamp irradiation [32]. The interaction between the sulfide and thiourea through hydrogen bonding played a crucial role in this transformation. This pioneering work inspired the remarkable development of urea/thiourea catalysts, particularly after Jacobsen's discovery of their asymmetric activation of electrophiles in 1998 [33]. Notably, Sivaguru and coworkers made impressive advancements in this field by reporting a chiral atropisomeric urea catalyst **42** for an asymmetric intramolecular [2 + 2] photocycloaddition of coumarin **43** (Scheme 14.10) [34]. These reactions yielded the corresponding cycloadduct **44** with high yields and excellent enantioselectivities (up to 96% ee). Mechanistic investigations revealed that the binaphthyl-based urea catalyst possessed lower excited-state energies than the pure starting coumarin substrates. Through a 3-fold hydrogen-bond interacting mode, an exciplex **45** was formed, facilitating efficient energy transfer within a chiral environment. However, despite the widespread use of urea and thiourea in ionic reactions, their application in asymmetric radical transformations remains relatively underdeveloped.

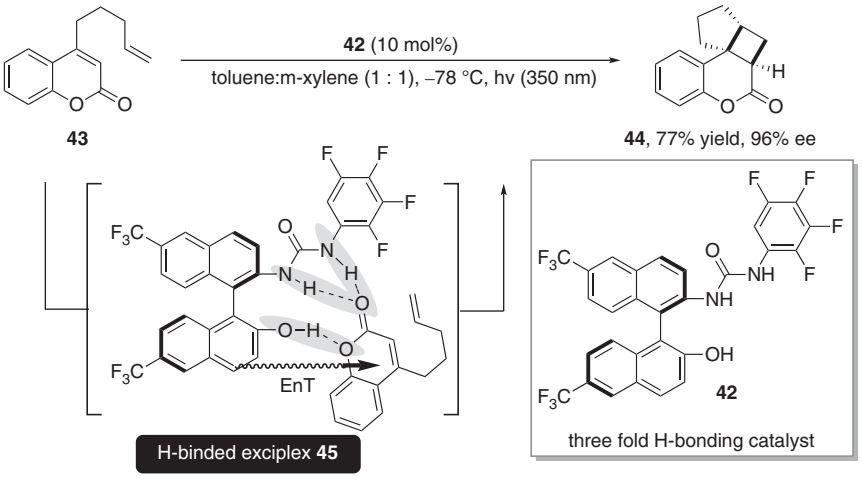


**Scheme 14.10** Chiral urea in asymmetric intramolecular [2 + 2] cycloaddition.

Brønsted acids, specifically chiral phosphonic acids (CPAs), have recently garnered significant attention due to their explosive applications in asymmetric chemical transformations [35]. The Jiang group has developed a transition metal-free platform that combines cooperative photocatalysis and CPAs as H-bonding catalysis (Scheme 14.11a). This platform utilizes a highly efficient organophotosensitizer, which is based on dicyanopyrazine-derived push–pull chromophores (Scheme 14.11b) [36]. Among these chromophores, DPZ stands out as the most promising photocatalyst. It incorporates a 5-methoxy-thiophen-2-yl moiety as an electron-donating group, resulting in favorable photoelectrical properties and high catalytic efficiency. The Jiang group has successfully utilized DPZ in a series of important asymmetric transformations. These transformations involve the

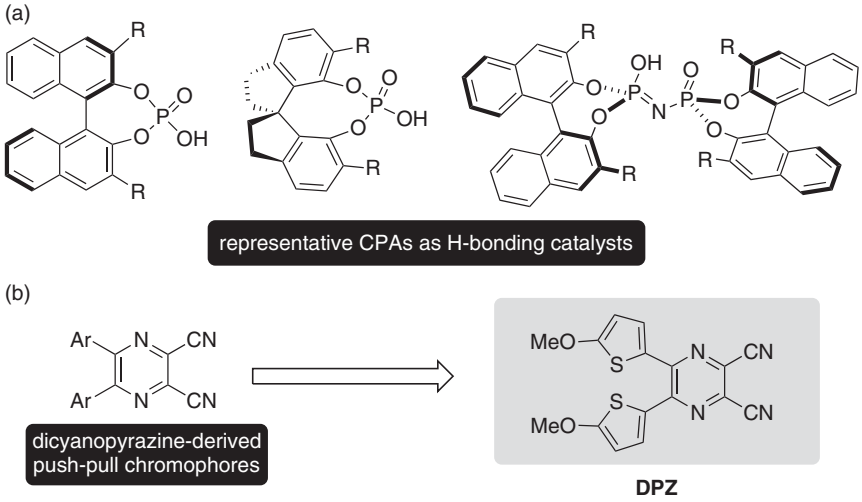


**Scheme 14.11** Jiang's cooperative photocatalytic system: (a) representative CPAs as H-bonding catalysts; (b) design of DPZ as photosensitizer.

formation of stereocenters through either ionic-type or radical-type bond-forming pathways, further expanding the scope and potential of this innovative catalytic system [37].

In 2020, the Jiang group published groundbreaking work on an asymmetric [3 + 2] cycloaddition of cyclopropylamines with 2-vinylazaarenes (Scheme 14.12a) [38]. This method allows for the rapid formation of all-carbon quaternary stereocenters. Jiang utilized a C2-symmetric imidodiphosphoric acid **46** as the chiral catalyst, which interacts with heteroarenes through H-bonding interactions. By employing a cooperative photoredox DPZ/CPA system, the Jiang group successfully synthesized valuable chiral azaarene-substituted cyclopentanes **49** with high yields, enantioselectivities, and diastereoselectivities. Detailed mechanistic studies provided evidence supporting a mechanism involving the initial single-electron-transfer (SET) oxidation of cyclopropylamines to open the ring, followed by two sequential radical additions to yield enantioenriched cyclopentanes. The authors emphasized the importance of a rigid and confined ternary complex **50**, consisting of cyclopropylamines as the H-bonding donor and the heteroatom in azaarenes as the H-bonding acceptor, in conjunction with the catalyst CPA. This arrangement ensures the differentiation of enantiofacial outcomes in the radical cycloadditions. Building upon this success, the Jiang group further expanded the scope by incorporating electron-rich alkenes with protecting groups containing an H-bonding acceptor domain (Scheme 14.12b). Through this approach, they successfully prepared cyclopentylamines **53** with high yields, ee, and dr in a fully atom-economical manner [39]. Overall, this study represents a significant advancement in asymmetric catalysis and offers valuable insights into the design of efficient methodologies for the construction of complex molecular architectures.

In addition to cooperative asymmetric photocatalysis, the utilization of catalysts with dual functions in asymmetric photoreactions is a relatively uncommon practice. However, there are still notable examples worth mentioning. The Yoon research

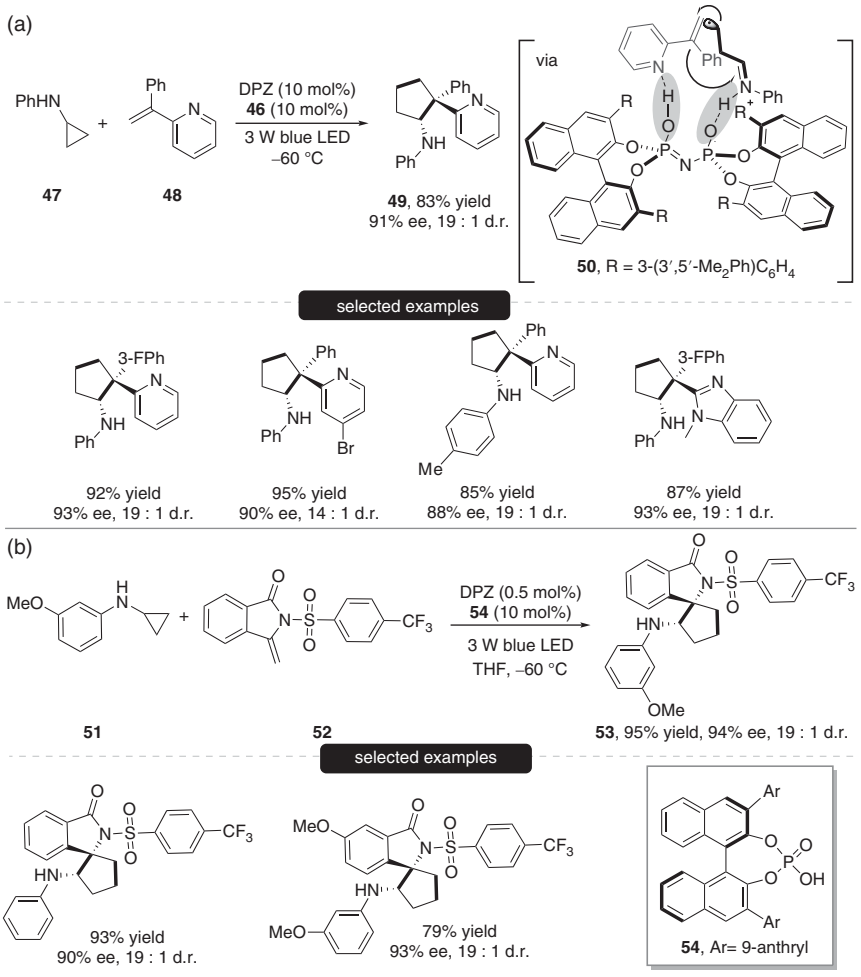


**Scheme 14.12** CPA/DPZ cooperative catalysis in asymmetric intermolecular [3 + 2] cycloaddition: (a) [3 + 2] cycloaddition of cyclopropylamines with 2-vinylazaarenes; (b) synthesis of cyclopentylamines through [3 + 2] cycloaddition.

group reported a noteworthy case involving the use of CPA as the only catalyst, which effectively controlled an intermolecular asymmetric [2 + 2] cycloaddition between $\alpha,\beta$-unsaturated ketones **56** and alkenes (Scheme 14.13) [40]. Initially, they attempted to combine a metal-based photoredox catalyst with CPA **55** to facilitate this challenging intermolecular coupling. However, they ultimately discovered that the presence of CPA **55** alone was sufficient to drive the reaction smoothly, resulting in a range of enantioenriched substituted cyclobutanes **57**. Yoon proposed that an excited complex **58** formed between **55** and the substrates **56** through hydrogen-bonding interactions in their ground state, accounting for the observed high reactivity and selectivity.

Another notable approach involving the use of CPAs as bifunctional catalysts in asymmetric photoreactions was reported by Bach (Scheme 14.14) [41]. In this strategy, a triplet organic chromophore, thioxanthone, was incorporated into the CPA

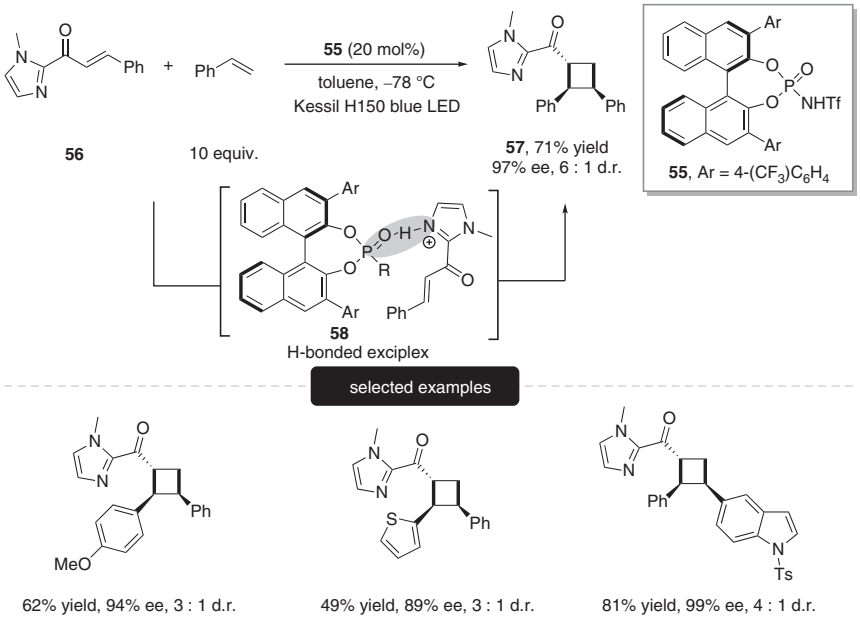


**Scheme 14.13** CPA as bifunctional catalyst in asymmetric intermolecular [2 + 2] cycloaddition.

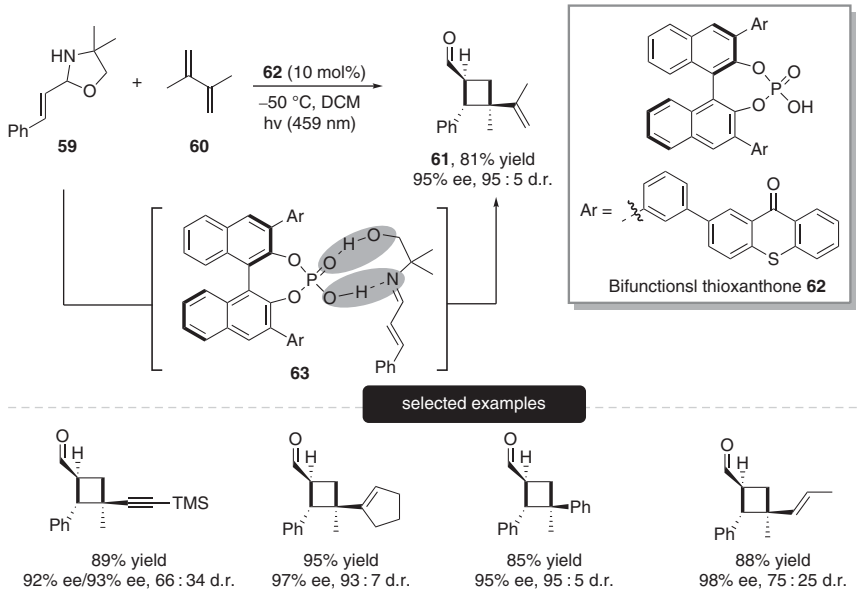


**Scheme 14.14** Thioxanthone-incorporated-CPA as bifunctional catalyst in asymmetric intermolecular [2 + 2] cycloaddition.

structure, forming a novel bifunctional photoredox catalyst **62**. This catalyst exhibited easy excitation upon exposure to visible light. Subsequently, an enantioselective [2 + 2] photocycloaddition between N,O-acetals **59** and olefins **60** via iminium ions was investigated. Remarkably, this transformation resulted in a diverse range of cyclobutane-carbaldehydes **61** with high yields and ee. NMR studies provided evidence for the formation of an iminium ion **63**, which was bound to the acid counterion through H-bonding interactions in an ion pair arrangement. The catalytic activity of the acid component was attributed to the presence of thioxanthone moieties, which facilitated efficient triplet energy transfer and enabled effective differentiation of the enantiofaces.

## 14.3 Asymmetric Cyclization via H-Bonding Organocatalysis

Asymmetric radical cyclization, a powerful approach for constructing chiral ring structures, relies on the key step of radical addition with unsaturated substrates [42]. In a pioneering study by Bach, inspired by the behavior of chiral H-bonding lactams in asymmetric radical cycloaddition, the application of chiral lactam **7** in asymmetric cyclization reactions was explored. This involved a reductive radical cyclization of piperidin-2-one **64** using $Bu_3SnH$ and $Et_3B$ as radical initiators in toluene at –78 °C (Scheme 14.15a) [43]. The cyclic product **65** was obtained in 81% yield with 84% ee. Mechanistic studies revealed that in nonpolar solvents, the chiral lactam bound to the lactam moiety of **65** enables the differentiation of enantiotopic faces. The key stereocontrolling step in this reaction was the hydrogen transfer from $Bu_3SnH$ to the intermediate radical **66**. It is important to note that although this process does not involve photocatalysis, a super-stoichiometric amount of the chiral lactam **7** was still required. Subsequently, the use of chiral complexing agent **7** for stereocontrol in the 6-endo (**67**) and 5-exo (**69**) cyclization of quinolone derivatives was investigated

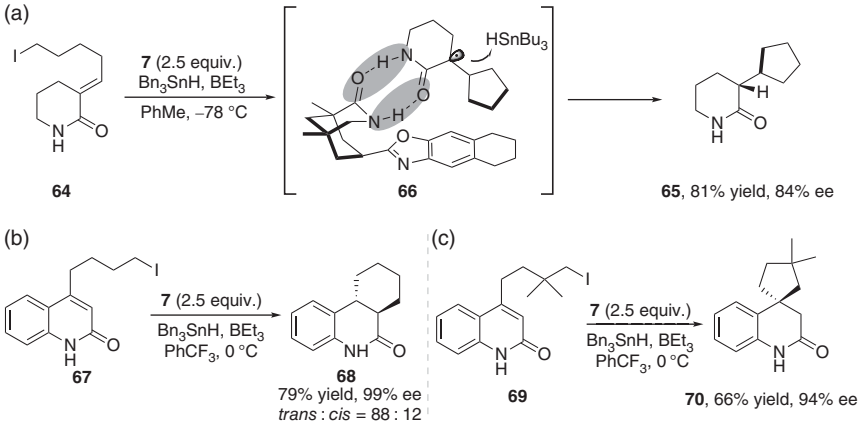


**Scheme 14.15** Chiral lactam in asymmetric radical cyclization: (a) intramolecular cyclization of piperidin-2-one; (b) 6-endo and 5-exo cyclization of quinolone.

(Scheme 14.15b). In the presence of a chiral lactam **7** as the complexing agent, the radical cyclization of iodide was carried out using $Bu_3SnH$ and $Et_3B$ in $PhCF_3$ at 0 °C [44]. The 6-*endo* cyclized product **68** was obtained with 99% ee. When a substituted iodide was employed as the substrate, the 5-*exo* radical cyclization proceeded, yielding the 5-*exo* cyclized product **70** with 94% ee [45]. Generally, high levels of enantioselectivity were observed when a stoichiometric excess of the chiral complexing agent was used.

The second generation of H-bonding catalyst **8** modified by Bach has demonstrated dual functionality as both stereocontrolling and photoinduced electron transfer catalysts, utilizing benzophenone as the chromophore. In the context of photoinduced enantioselective cyclization of quinolone **71** (Scheme 14.16), these catalysts have been able to achieve the desired spirocyclic product **72** with 70% ee using a catalytic amount of **8** at a temperature of –40 °C [26]. It should be noted that the unsatisfactory ee values were attributed to the flexibility of the benzophenone unit, which is similar to that observed in asymmetric cycloaddition reactions.

In 2017, Bach proposed the integration of a thioxanthone triplet sensitizer into a chiral thiourea framework **73** [46]. This envisioned bifunctional photocatalyst was anticipated to possess two-point H-bond sites, while simultaneously utilizing the

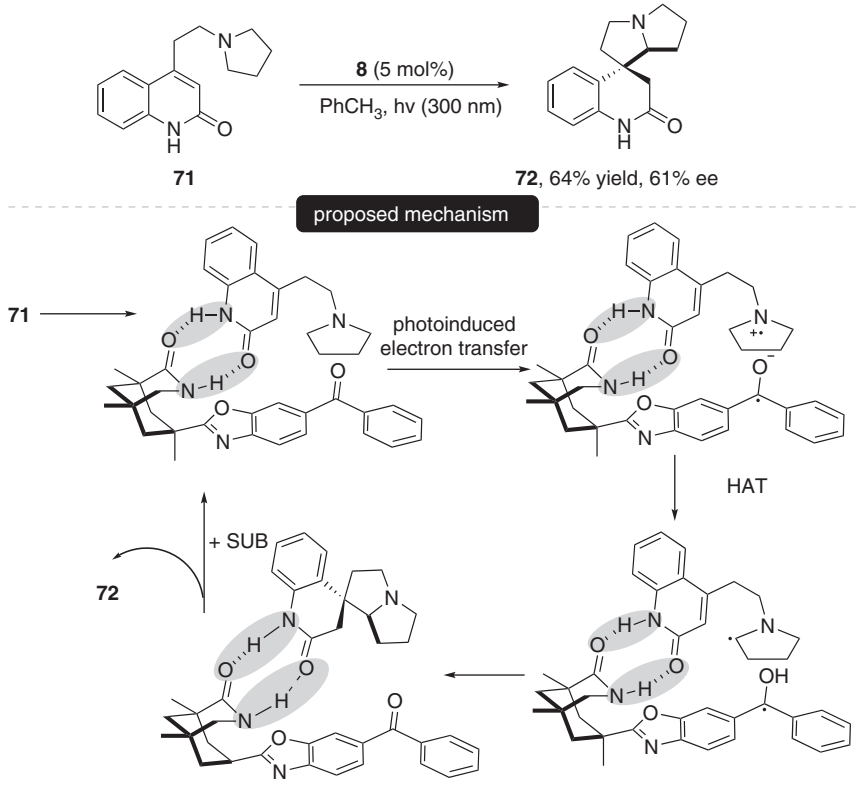


**Scheme 14.16** Chiral lactams as bifunctional catalyst in asymmetric cyclization.

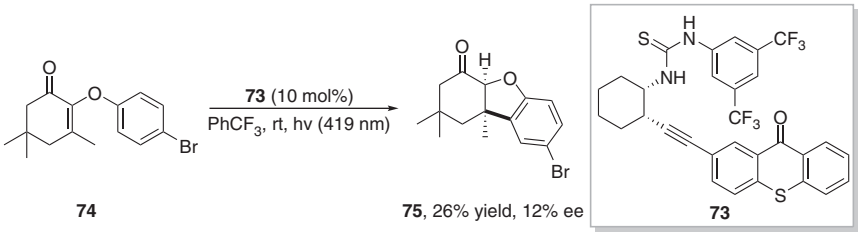


**Scheme 14.17** Chiral lactams as bifunctional catalyst in asymmetric cyclization.

thioxanthone as a sensitizer to facilitate the photoexcitation of bound substrates (Scheme 14.17). However, when an intramolecular cyclization reaction of **74** was performed, both the yields and ee values were low. This can likely be attributed to the absence of a rigid and confined chiral environment within the thiourea catalyst **73**, which hindered the effectiveness of the catalytic process.

The Knowles group reported a noteworthy advancement in asymmetric intramolecular aza-pinacol cyclization [47]. Their pioneering work involved the use of a cooperative catalyst system comprising a chiral phosphoric acid **76** derived from BINOL and $Ir(ppy)_2(dtbpy)PF_6$ as a photosensitizer, along with Hantzsch dihydropyridine (**HEH**) serving as a terminal reductant (Scheme 14.18). CPA **76** played a crucial role in reducing the ketone moiety through a proton-coupled electron transfer (PCET) process, which is believed to occur via H-bonding interactions via **80** and **81**. Furthermore, mechanistic studies have demonstrated the robust basicity of the resulting ketyl intermediate **80**, enabling the CPA **76** to closely interact with the substrate **77**. This interaction facilitated impeccable enantiocontrol for the subsequent radical addition **80** to an imine. This remarkable achievement marked the first successful demonstration of cooperative photoredox and H-bonding catalysis, resulting in cyclized adducts with exceptional enantioselectivity. The findings provided an exciting starting point for harnessing the power of chiral H-bonding catalysis in radical cyclization processes.

In a recent development, Knowles successfully employed a synergistic system comprising a chiral phosphonate salt and thiol for an intramolecular enantioselective hydroamination of alkenes with sulfonamides (Scheme 14.19) [48]. This groundbreaking transformation was proposed to proceed through *N*-centered radicals, facilitated by the H-bonding-assisted proton-coupled electron transfer (PCET) activation of sulfonamide N—H bonds. The high enantioselectivity observed can be attributed to the H-bonding interactions between the neutral sulfonamidyl radical and a chiral phosphoric acid **82**. These interactions play a crucial role in providing asymmetric induction during the subsequent C—N bond formation step. To enhance the solubility of the phosphonate salt **82**, two long lipophilic chains were incorporated into the BINOL skeleton, ensuring optimal functioning of the catalytic system. This significant advancement showcases the potential of utilizing synergistic effects, such as H-bonding interactions, in achieving enantioselectivity and expanding the scope of intramolecular hydroamination reactions.

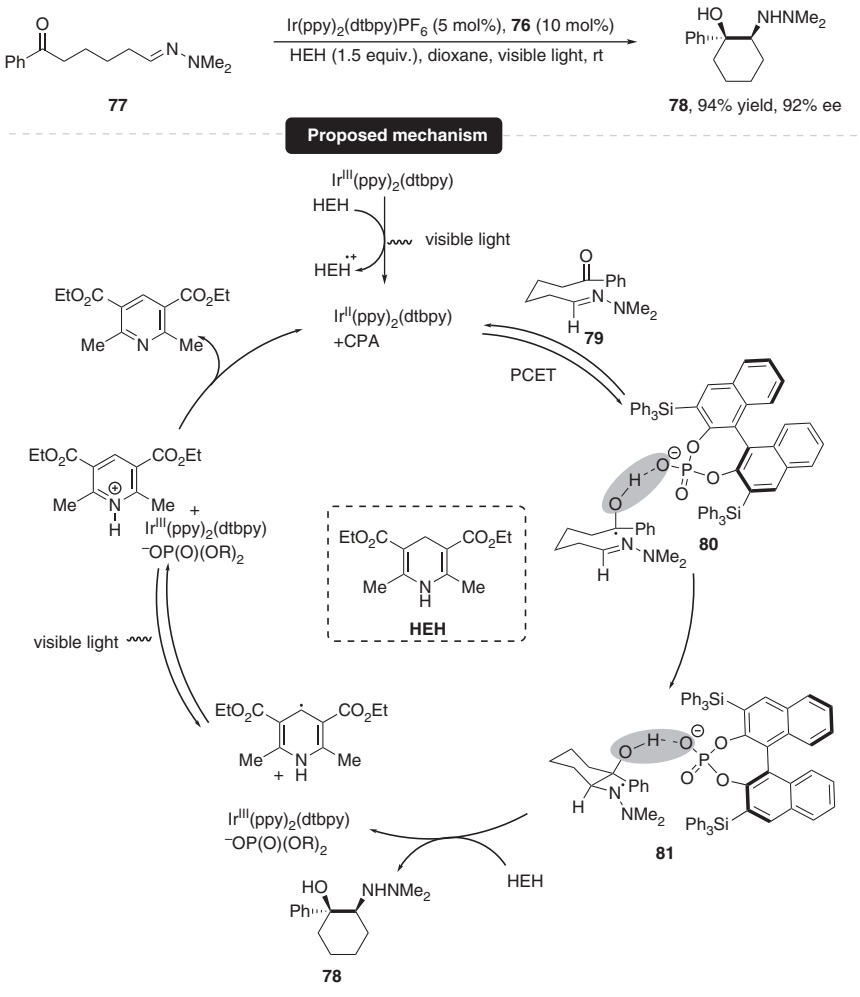


**Scheme 14.18** CPA in asymmetric cyclization via PCET.

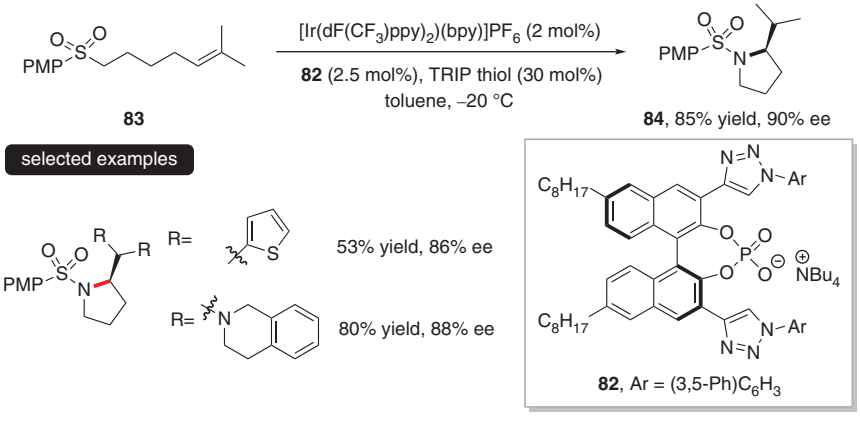


**Scheme 14.19** CPA in asymmetric cyclization by Knowles.

In a parallel effort, the Jiang group drew inspiration from the widespread applications of cooperative photocatalysis involving DPZ/CPA in organic radical synthesis (Scheme 14.20) [49]. They successfully disclosed a novel enantioselective Beckwith-Enholm cyclization of ketyls to generate azaarene-based olefins. This work, distinct from Knowles' study, revealed that the azaarenes, rather than the carbonyl group, functioned as the acceptor for H-bonding interactions. Mechanistic investigations further provided insights into the reaction pathway, highlighting the crucial role of H-bonding interactions with the azaarenes **86**. By leveraging this innovative approach, they synthesized a diverse array of enantioenriched azaarene-functionalized carbocyclic and heterocyclic alcohols **87**. These compounds exhibited excellent yields, enantiomeric excesses, and diastereomeric ratios, showcasing the successful incorporation of adjacent 1,2- or nonadjacent 1,3-stereocenters within distinct cyclic frameworks. This study not only advances their understanding of cooperative photocatalysis but also underscores its potential in enabling the synthesis of complex and highly functionalized molecules with significant synthetic value.

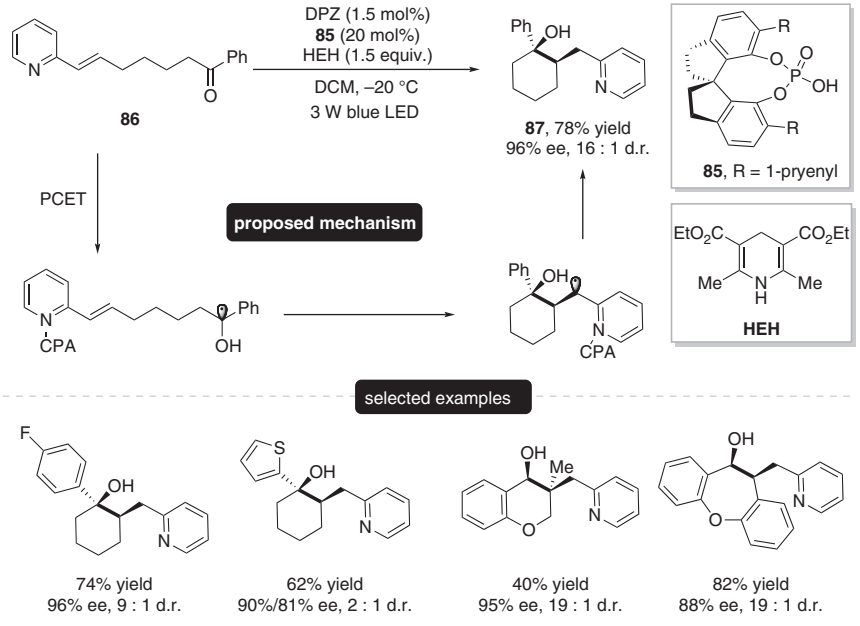


**Scheme 14.20** CPA in asymmetric intramolecular cyclization.

## 14.4 Asymmetric Radical Addition via H-Bonding Organocatalysis

Radical addition, such as radical cycloaddition and cyclization, also occurs with unsaturated substrates. However, in the context of an organized framework, radical addition typically refers to a process that yields linear products with stereocenters formed during the radical addition step [50].

In modern asymmetric synthesis, the use of enamine catalysts has become widespread. A significant development in asymmetric radical transformations is the combination of enamine catalysts with photocatalysts. In 2014, the Luo group reported an enantioselective $\alpha$-photoalkylation of $\beta$-ketocarbonyl compound **89** using a cooperative photocatalysis system (Scheme 14.21) [51]. In this system, a chiral primary amine **88** was employed as a cocatalyst along with Ru(II) as a photoredox catalyst. When a wide range of $\beta$-ketocarbonyl compounds were reacted with $\alpha$-bromocarbonyl compounds under visible light irradiation, a series of all-carbon quaternary stereocenters with excellent enantioselectivities were formed. The proposed mechanism involves the formation of an $\alpha$-acyl radical, which is generated through photoredox catalysis, and an enamine **92** from primary amine catalysis. Subsequent radical addition occurs within the tertiary chiral complex **93** through H-bond interactions. The presence of this rigid chiral complex ensures high enantioselectivity.

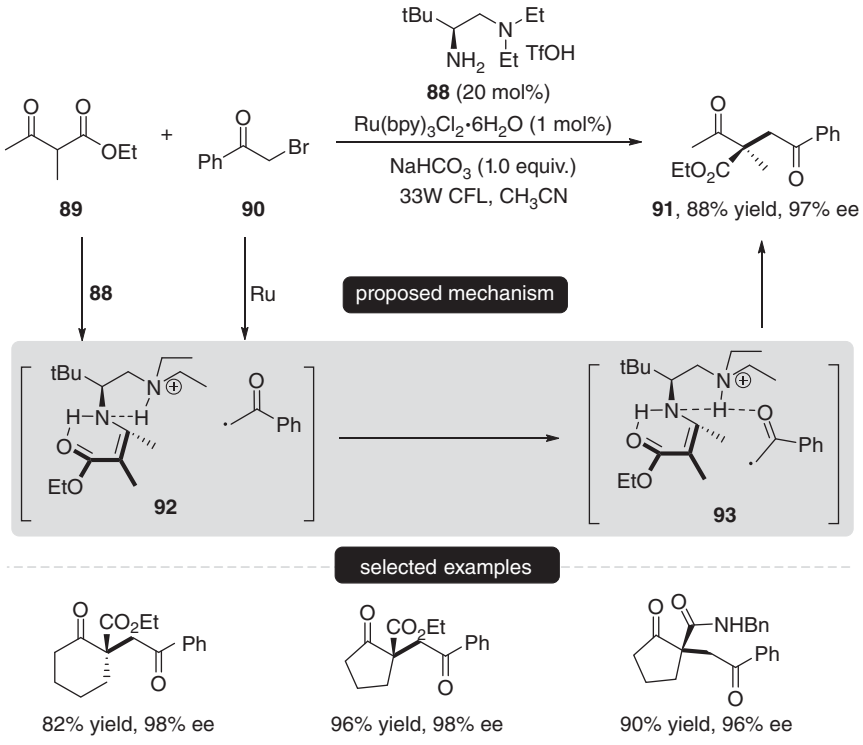


**Scheme 14.21** Primary amine as H-bonding catalyst in radical addition.

The same research group reported an interesting advancement in the field of asymmetric decarboxylative $\alpha$-alkynylation of $\beta$-ketocarbonyls (Scheme 14.22). This process utilizes a synergistic combination of photoredox catalysis and primary amine catalysis **88** [52]. In this reaction, the key step involves the addition of an $\alpha$-imino radical intermediate, which is generated through SET oxidation of a

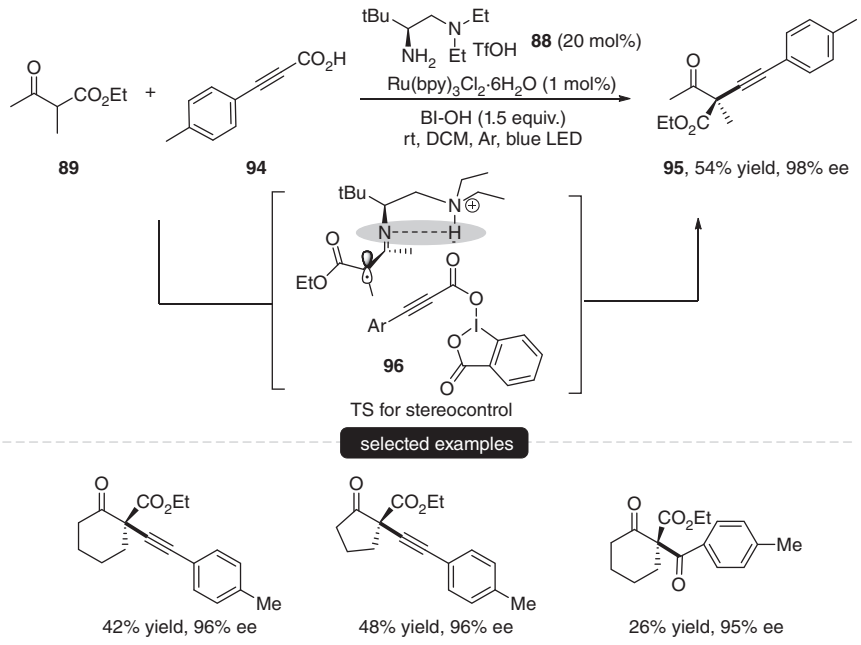


**Scheme 14.22** Primary amine as H-bonding catalyst in decarboxylative $\alpha$-alkynylation of $\beta$-ketocarbonyls.

secondary enamine, to propiolic acid **94**. The presence of hydroxybenziodoxole (BI-OH) is crucial for the oxidative quenching of the excited state of the photocatalyst Ru(II). Similar to the previous example, it is proposed that H-bonding assistance plays a significant role in achieving high stereocontrol during the formation of quaternary carbon centers. Overall, this research provides valuable insights into the development of efficient methodologies for the construction of complex and enantioenriched molecules, offering new possibilities for synthetic organic chemistry.

In addition to the conventional utilization of Ir(III) and Ru(II) complexes in asymmetric photoreactions, the Jiang group has recently reported a form of cooperative photocatalysis (Scheme 14.23) [53]. This pioneering approach involves the amalgamation of tungstate salts as HAT catalyst and chiral phosphoric acid **97** as H-bonding catalyst to facilitate an asymmetric sequential conjugate addition/enantioselective protonation process. The methodology provides a diverse collection of highly valuable enantioenriched $\alpha$-tertiary azaarene **99** with exceptionally high yields and commendable enantioselectivities.

H-bonding interactions play a crucial role in chemical reactions, requiring substrates to possess specific functional groups capable of acting as H-bonding acceptors or donors. These functional groups include carbonyls, alcohols, amines, amides, and imines found in azaarenes such as pyridines, quinolines, isoquinolines, and imidazoles. These imine-bearing azaarenes are widely present in various natural products, pharmaceuticals, and materials, making them significant

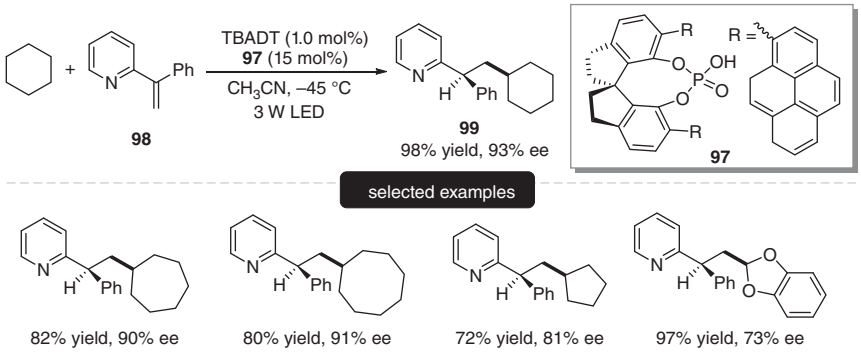


**Scheme 14.23** TBADT/CPA for asymmetric conjugate addition/protonation.

structural motifs [54]. Due to their electron-deficient nature, chemists have increasingly employed these azaarenes as analogues of carbonyls to induce asymmetric transformations of prochiral azaarene-based substrates [55]. However, the limited ability of azaarenes to activate functional groups has inspired the community to explore highly reactive radical pathways by combining photoredox and H-bonding catalysis.

Building upon the success of achiral phosphoric acid-catalyzed conjugate addition reactions involving $\alpha$-amino radicals derived from the single-electron oxidation of *N*,*N*-dimethyl anilines to alkenyl-pyridines, the Melchiorre group attempted an enantioselective variant in 2016 (Scheme 14.24) [56]. In this case, azaarene-activated alkene **101** served as representative substrates, with BINOL-derived **100** utilized as the chiral H-bonding catalyst. However, the desired product **102** was obtained with only 35% ee. Interestingly, both the *E*-7 and *Z*-7 diastereomers displayed the same enantioselectivity, indicating a Curtin-Hammett-type kinetic situation. Although the enantioselectivity was not satisfactory, the use of only 10 mol% of **100** resulted in a product with 35% ee, demonstrating the potential of asymmetric H-bonding catalysis in radical reactions involving azaarenes through the H-bond interaction between the basic nitrogen of the azaarene and a chiral Brønsted acid.

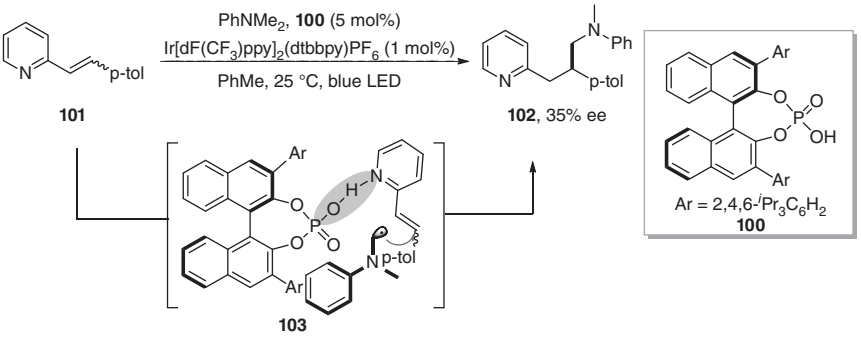


**Scheme 14.24** Chiral lactams as bifunctional catalyst in asymmetric radical addition.

Overall, the asymmetric formation of stereocenters at the $\beta$-position of azaarenes under the catalysis of CPA remains a challenging task. This difficulty can be attributed to the distance between the $\alpha$-amino radical and the nitrogen-coordinated chiral catalyst, which compromises the effectiveness of enantiofacial induction. Despite these challenges, the Jiang group has explored the potential of H-bonding catalysis in constructing distant γ-stereocenters through the conjugate addition of prochiral radicals to vinylazaarenes (Scheme 14.25a) [57]. Specifically, they investigated the addition of aldehydes, ketones, aldimines, and ketimines to vinylpyridines using a reductive coupling strategy. The utilization of DPZ with SPINOL-derived **104** as cooperative catalysts afforded the desired adduct **106** with up to 90% yield and >99% ee. Notably, the substrate scope was extensive, encompassing various pro-nucleophiles and pyridine electrophiles. Chiral secondary and tertiary alcohols/amines were successfully incorporated at the γ-position of both 2-pyridines and 4-pyridines. The high enantioselectivity observed with complex

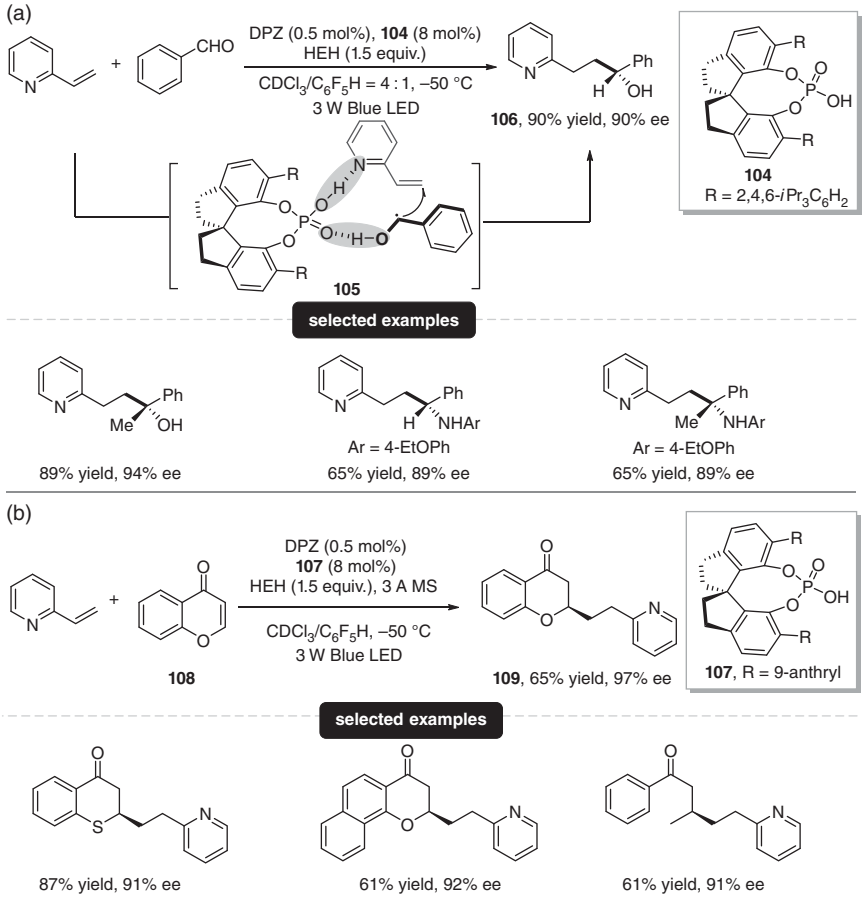


**Scheme 14.25** CPA as H-bonding catalyst in the construction of γ-stereocenters to azaarenes: (a) constructing of distant γ-stereocenters; (b) constructing of enantioenriched pyridine derivatives featuring diverse γ-tertiary carbon stereocenters.

oestrone-derived ketones and 4-vinylpyridine as substrates further demonstrated the robust capabilities of **104** as chiral H-bonding catalysts in asymmetric photoredox-catalyzed reactions of prochiral azaarenes. Interestingly, this strategy can also be applied to electron-deficient alkenes, extending beyond carbonyl and its derivatives. In 2022, the Jiang group reported the use of visible-light-driven cooperative photoredox and chiral Brønsted acid-catalyzed reactions, employing Hantzsch ester as the terminal reductant (Scheme 14.25b) [58]. Through this approach, various cyclic and acyclic enones **108** with 2-vinylpyridines were successfully converted to a wide range of enantioenriched pyridine derivatives **109** featuring diverse γ-tertiary carbon stereocenters, with yields as high as 93% and excellent enantioselectivities. These findings highlight the promising potential of H-bonding catalysis and cooperative catalyst systems in achieving selective formation of stereocenters in azaarenes, thereby enabling the synthesis of valuable chiral molecules with significant structural complexity.

Through the utilization of a chiral phosphoric acid **110** as an H-bonding catalyst and DPZ as the photoredox sensitizer, a highly efficient hydroaminoalkylation reaction has been recently achieved (Scheme 14.26) [59]. This reaction involves the addition of *N*-arylglycines to alkenyl azaarenes, resulting in enantioenriched molecules that possess stereocenters at the *β*-position of the azaarenes. Control experiments and density functional theory (DFT) calculations were conducted to gain insight into the origin of the observed stereoselectivity. It was found that H-bonding interactions played a crucial role in assisting the chiral catalyst **110** in achieving sufficient enantiocontrol. What sets this work apart from previous studies, such as the one conducted by Melchiorre, is the involvement of the H-bonding

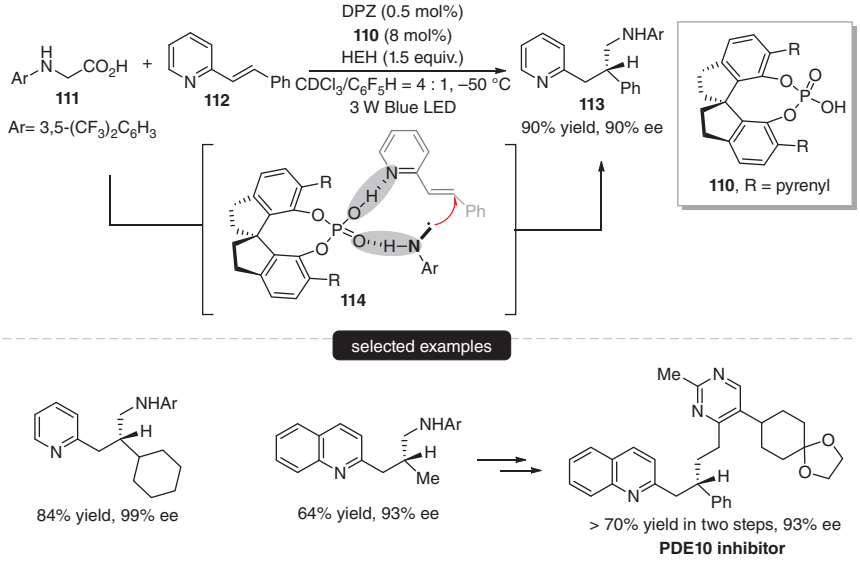


**Scheme 14.26** CPA as H-bonding catalyst in the construction of *β*-stereocenters to azaarenes.

donor NH in the radical precursor **111**. This NH group facilitates the formation of a ternary complex **114**, ensuring that the radical addition takes place within a chiral environment. As a result, the asymmetric radical addition at the $\beta$-position of the azaarenes is realized. Overall, this development represents a significant advancement in the synthesis of enantioenriched molecules with stereocenters at the $\beta$-position of azaarenes. The use of chiral phosphoric acid **110** as an H-bonding catalyst, combined with DPZ as the photoredox sensitizer, offers new possibilities for the creation of complex organic compounds.

## 14.5 Asymmetric Minisci Reaction via H-Bonding Organocatalysis

The asymmetric Minisci reaction, developed by Francesco Minisci, involves the addition of nucleophilic radicals to electron-deficient heterocycles. This reaction has found wide application in medicinal chemistry due to the prevalence of basic heterocycles in drug-like molecules [60]. However, for a long time, chemists have faced challenges in achieving selectivity in this reaction. One prominent challenge is regioselectivity, specifically the tendency to form regioisomers when multiple electronically similar positions are available on a heteroarene, such as the 2- and 4-positions. Another challenge is the control of absolute stereochemistry when using a prochiral radical nucleophile. To address these challenges, H-bonding catalysts have been explored, such as CPAs. These catalysts can activate the heteroarene by making it more electron-deficient and engage in attractive noncovalent interactions, such as H-bonding, with suitably functionalized nucleophilic radicals [61]. This arrangement positions the radical near the C2 position of the activated heteroarene, allowing for control of regioselectivity in the addition. If the catalyst is chiral and enantiopure, it may also enable control of enantioselectivity in the formation of a new stereocenter when using a prochiral radical precursor.

In 2018, the Phipps group demonstrated how a combination of CPAs and an Ir(III) complex could achieve enantioselectivity in the Minisci-type alkylation of heteroarenes (Scheme 14.27) [62]. Their proposal was based on the idea that a racemic Minisci reaction with a Brønsted acid catalyst lowers the LUMO of the heteroarene **116**, allowing nucleophilic radicals **120** to attack the π-system. By using BINOL-derived chiral phosphonic acid **115**, they were able to create a network of attractive noncovalent H-bonding interactions among different reactive intermediates, thereby achieving enantiocontrol. The H-bonding interactions with the incoming radical **120** and the heteroatom ring **116** in a ternary complex **121** were crucial for both high reactivity and selectivity.

Shortly after Phipps' groundbreaking report, Jiang and colleagues published a similar protocol independently to show its effectiveness on isoquinolines (Scheme 14.28) [63]. This development was significant because isoquinolines exhibited poor enantioselectivities under Phipps' original conditions. In this study, Jiang utilized the organic photocatalyst DPZ as the photosensitizer and employed an H-bonding catalyst **122** derived from SPINOL to achieve the highest ee. By

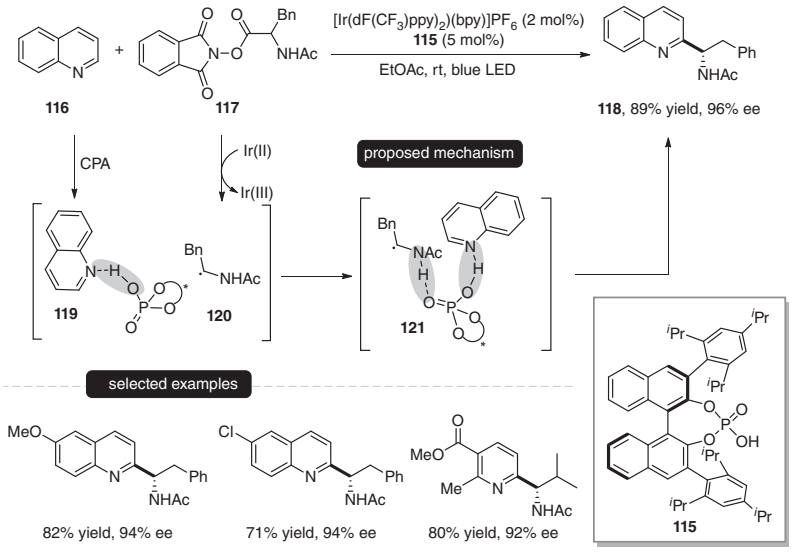


**Scheme 14.27** CPA in asymmetric Minisci reaction by Phipps.

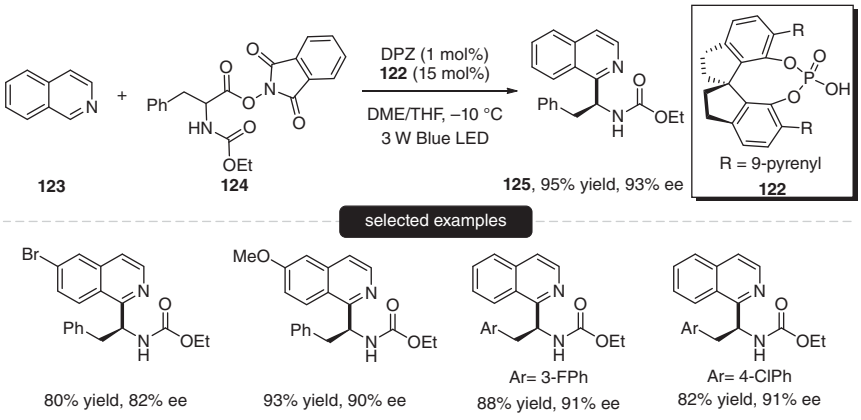


**Scheme 14.28** CPA as H-bonding catalyst in asymmetric Minisci reaction by Jiang.

employing amino acid-derived RAEs **124** derived from phenylalanine, the scope of the reaction was notably broad, allowing for extensive substitution on the phenylalanine arene.

In the aforementioned protocols, redox-active esters (RAEs) were utilized as the radical precursor through photoredox reactions. Subsequently, Phipps proposed an alternative approach to generate $\alpha$-amino radical intermediates from the $\alpha$-position of *N*-acetylamine via HAT [64]. This method avoids the elaborate steps in preparing the RAEs. In 2022, they found that by employing diacetyl as a HAT catalyst and **126** as a chiral H-bonding catalyst, asymmetric Minisci reactions of heteroazarenes with *N*-acetylamine **127** could be achieved with similar levels of enantioselectivity compared to using RAEs (Scheme 14.29a). Notably, the use of

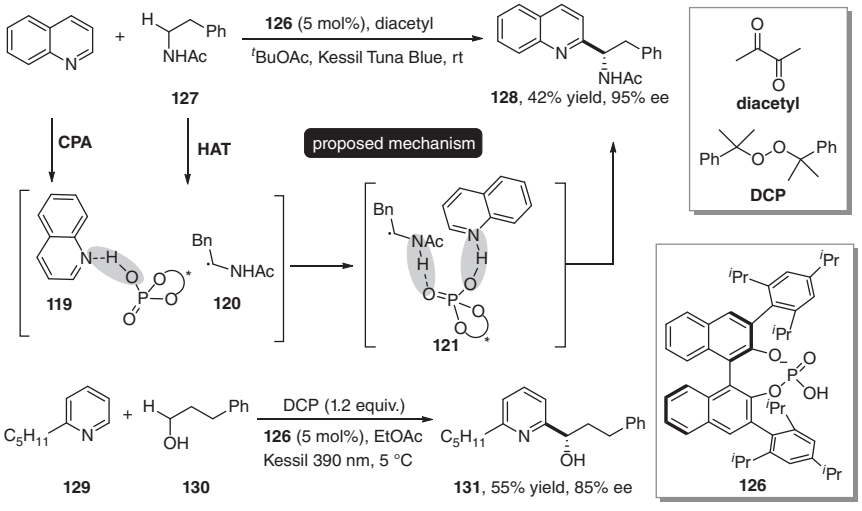


**Scheme 14.29** CPA as H-bonding catalyst in asymmetric Minisci reaction by Phipps.

a photocatalyst is not required as diacetyl can be directly photoexcited. Parallel to the aforementioned work, Phipps focused on utilizing $\alpha$-hydroxy radicals in the enantioselective Minisci reaction to generate enantioenriched secondary alcohols (Scheme 14.29b) [65]. While $\alpha$-oxy radicals have been extensively employed in Minisci reactions through HAT from ethers, there are fewer reports on HAT from alcohols to produce $\alpha$-hydroxy radicals. Several well-precedented side reactions exist for $\alpha$-hydroxy radicals, including further oxidation to form an aldehyde. This aldehyde can then undergo HAT to generate an acyl radical, which can participate in Minisci additions to yield a different product. Additionally, upon successful addition to the heteroarene and subsequent deprotonation, the resulting neutral radical can undergo spin-center-shift elimination of water. To overcome the issue of low yields, the authors conducted an extensive optimization process to evaluate various oxidants, HAT reagents, and photocatalysts. Ultimately, it was discovered that irradiation using a 390 nm Kessil lamp was sufficient to promote the heterolytic cleavage of dicumylperoxide (DCP), enabling it to function as both a HAT reagent and an oxidant without the need for an additional photocatalyst. By carefully controlling the reaction temperature at 5 °C and making a slight modification to the CPA catalyst by using DIP, favorable levels of yield and enantioselectivity could be achieved.

In 2019, Zheng and Studer introduced a remarkable discovery [66]. They presented an innovative asymmetric three-component Minisci reaction, which involves the formation of an *N*-acyl, $\alpha$-amino radical by combining an $\alpha$-bromo ester with an enamide (Scheme 14.30). This transformation is achieved through the photocatalytic reduction of the $\alpha$-bromo ester, resulting in an electrophilic radical that exhibits a matching polarity with the electron-rich enamide **133**. The resulting adduct comprises an *N*-acyl, $\alpha$-amino radical, which has proven to be highly effective in driving the asymmetric Minisci reaction. This elegant advance serves as a compelling

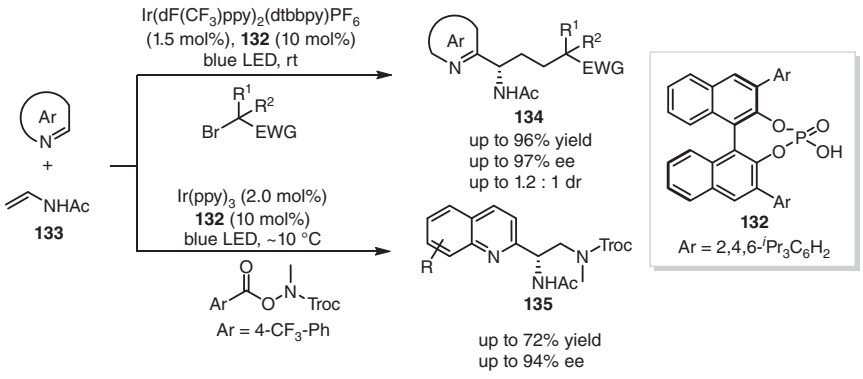


**Scheme 14.30** CPA as H-bonding catalyst in asymmetric three-component Minisci reactions.

demonstration of augmenting the complexity of the reaction mechanism while preserving the pivotal role of asymmetric catalysis.

In a recent breakthrough, the Jiang group unveiled their findings on asymmetric three-component Minisci reactions involving 2-bromo-1-arylethan-1-ones **137**, styrenes, and quinoxalin-2(1H)-ones **138** (Scheme 14.31) [67]. This approach employs a dual-catalyst system comprising DPZ as a photosensitizer and CPA **136** as an H-bonding catalyst. Under basic conditions, a diverse array of quinoxalin-2(1H)-one derivatives **141** bearing $\alpha$-tertiary stereocenters were successfully synthesized. Notably, by fine-tuning the basic conditions from $Na_3PO_4$

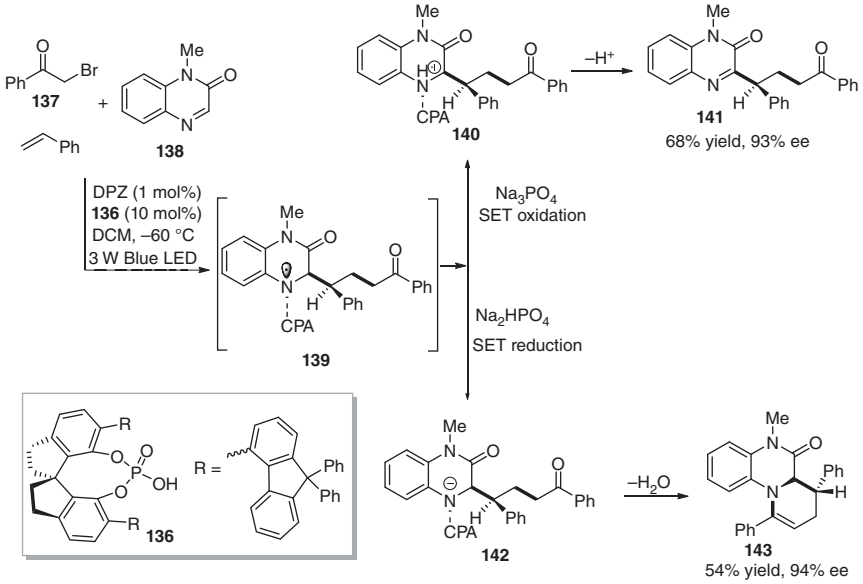


**Scheme 14.31** CPA as H-bonding catalyst in chemodivergent asymmetric Minisci reaction by Jiang.

to slightly acidic $Na_3HPO_4$, the reaction yielded dihydroquinoxalin-2-one-based bicyclic variants **143** featuring two adjacent tertiary stereocenters. This accomplishment represents a significant advancement in achieving chemodivergent photocatalytic asymmetric synthesis, a highly sought-after objective in both radical chemistry and the pharmaceutical industry. Mechanistic investigations have revealed that the different pKa environments play a crucial role in inducing the quinoxalin-2(1H)-ones **137** to form radicals **139** after the second radical addition. These radicals can undergo either single-electron oxidation via **140**, leading to Minisci-type reactions, or single-electron reduction via **142**. In the latter case, the bromide anion (Br−) released from ketones was identified as the essential reductant, enabling the successful synthesis of the bicyclic products **143** without an external reductant. These insightful mechanistic studies shed light on the underlying principles governing this remarkable transformation.

## 14.6 Asymmetric Radical Cross-Coupling via H-Bonding Organocatalysis

Radical cross-coupling reactions are known for their ability to form new chemical bonds through the seamless joining of two different odd-electron partners. This characteristic makes radical cross-coupling a highly efficient approach for the creation of molecules with a wide range of functional groups and complexities. However, this advantage poses challenges when aiming to achieve enantioselective variants. The highly reactive nature of radical intermediates hinders precise stereocontrol and often results in significant racemic background reactions. Additionally, chemoselectivity becomes a significant challenge due to the easily-occurring homocoupling reactions between radicals [68]. Therefore, it is crucial to develop effective platforms that can enable diverse asymmetric radical cross-coupling reactions in both fundamental research and practical applications.

In 2015, Ooi et al. demonstrated the use of photoredox neutral catalysis combined with the unique properties of *P*-spiro chiral arylaminophosphonium barfate as an ion-pairing catalyst [69]. This approach enabled highly enantioselective coupling of *N*-arylaminomethanes and *N*-sulfonyl aldimines. Building on this pioneering work, the Jiang group developed an asymmetric radical coupling of *N*-aryl glycines and activated ketones (Scheme 14.32) [70]. They achieved this by harnessing the cooperative catalytic effects of photoredox DPZ and CPA as H-bonding catalysts. Notably, this strategy allowed for the construction of more challenging heteroquaternary stereocenters, resulting in products **148** with high yields and ee. Overall, these advancements in the utilization of noncovalent catalysis in radical cross-coupling reactions have opened up new possibilities for the synthesis of complex molecules with improved stereocontrol and selectivity. Such developments hold great promise for both fundamental research and practical applications in asymmetric synthesis.

Alkyl halides are abundant and readily accessible compounds that play a crucial role in organic synthesis. The nucleophilic substitution of alkyl halides is a fundamental chemical transformation to introduce molecular fragments

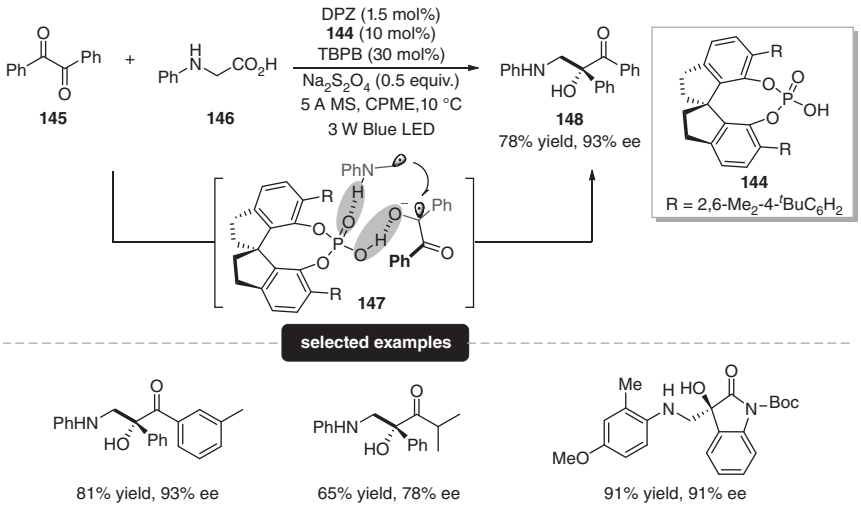


**Scheme 14.32** CAP as H-bonding catalyst in asymmetric radical coupling by Jiang.

onto $sp^3$-hybridized carbon atoms, with the halide acting as a directing group. While various methods, such as classic $S_N1$ and $S_N2$ reactions, have been well established and widely utilized for the synthesis of complex molecules, achieving enantioconvergent substitutions that create a carbon stereocenter in simple alkyl halides remains a significant challenge. Recognizing the oxidative potential of alkyl halides and the availability of a wide range of easily obtainable and stable reducible organic molecules strategy offers a direct synthetic approach. The Jiang group has explored the feasibility of transforming *N*-aryl amino acid **146** and $\alpha$-halo carbonyl compound **150** using cooperative photoredox and chiral bifunctional H-bonding catalysis (Scheme 14.33). By employing this net redox-neutral pathway, two distinct radical species **152** and **153** can be generated. The chiral catalyst **149**, through H-bonding interactions, enhances the nucleophilicity of $\alpha$-amino radical 152 and the electrophilicity of $\alpha$-radicals of the carbonyl compound **153**. This creates a stereocontrolling environment conducive to C—C bond formation in radical cross-coupling reactions [71]. Specifically, the use of DPZ and CPA **149** as catalysts enables smooth reactions between various $\alpha$-bromo ketones and diverse *N*-aryl amino acids, resulting in valuable enantiomerically pure $\beta$2- and $\beta$2,2-amino ketones **151** in satisfactory yields with excellent ee. Additionally, this methodology enables the construction of fluorinated heteroquaternary and fully carbon quaternary stereogenic centers, which are typically challenging to prepare. It is noteworthy that after single-electron reductive debromination, the generated radicals exhibit an enhanced ease of undergoing single-electron reduction-protonation in the absence of CPA **149**, underscoring the crucial role of H-bonding catalysis in achieving chemoselectivity.

Following the aforementioned success, the Jiang group conducted subsequent investigations on the synergistic catalytic platform in the radical coupling of 3-chlorooxindole **156** with *N*-aryl glycine **157** due to the significant biological

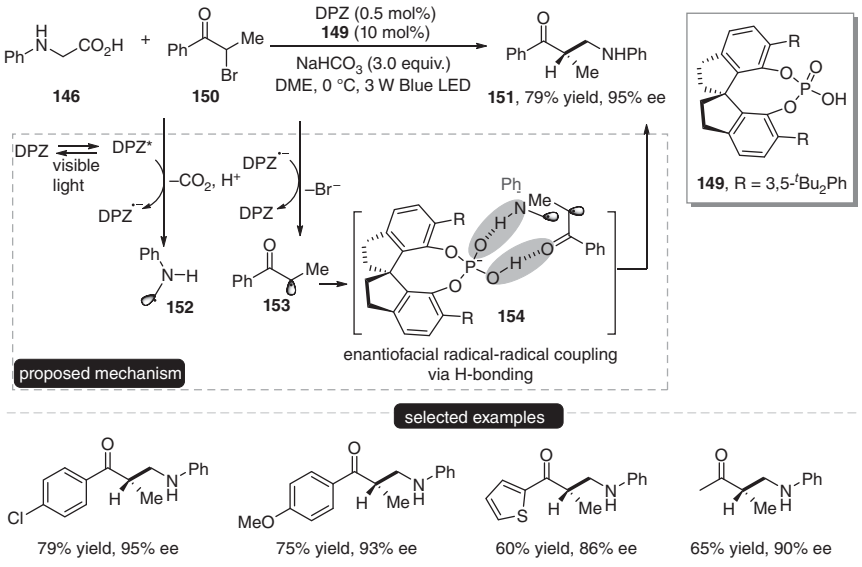


**Scheme 14.33** CPA as H-bonding catalyst in the asymmetric radical coupling of alkyl halides by Jiang.

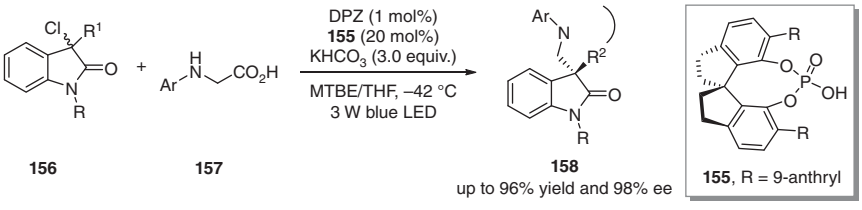


**Scheme 14.34** CAP as H-bonding catalyst in the asymmetric radical coupling of 3-chlorooxindole by Jiang.

significance of the resulting adducts (Scheme 14.34) [72]. The presence of DPZ and CPA **155** facilitated the efficient production of **158** with up to 96% yield and 98% ee. The substrate scope exhibited satisfactory compatibility, encompassing 3-aryl, 3-alkyl, and 3-allyl 3-chlorooxindoles. This innovative method enables the synthesis of spiro-five and -six-membered ring-based products, including horsfiline and analgesic therapeutic derivatives.

2,2-Disubstituted indolin-3-ones are present in various pseudoindoxyl alkaloids. In 2014, both the Brasholz [73] and Xiao [74] groups independently reported an efficient synthetic approach to access these valuable compounds (Scheme 14.35a). This method involved a visible light-driven photoredox-catalyzed aerobic oxidation and semi-pinacol rearrangement of 2-aryl-3-alkyl-substituted indoles **160**. Mechanistically, the radical species **163** derived from the single-electron oxidation of **160**, along with oxygen gas through single-electron reduction (superoxide anion radical), underwent coupling to generate intermediates **164**. Subsequently, a semipinacol transformation led to racemic 2,2-disubstituted indolin-3-one **161**.

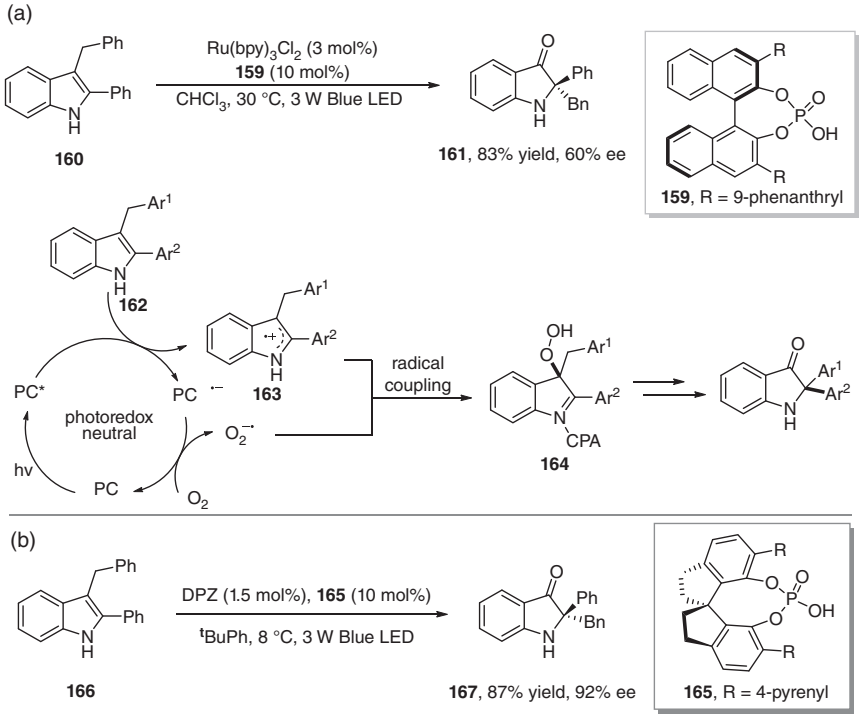


**Scheme 14.35** CPA as H-bonding catalyst in asymmetric radical coupling via aerobic oxidation: (a) aerobic oxidation and semi-pinacol rearrangement of 2-aryl-3-alkyl-substituted indoles; (b) Jiang's enantioselective version.

It is worth noting that achieving enantioselective radical coupling would result in enantioenriched intermediates **164**. The feasibility of this hypothesis was demonstrated by the Xiao group utilizing a dual catalysis comprising a Ru-based photosensitizer and CPA **159** under a pure oxygen atmosphere, albeit with only moderate ee. In 2018, the Jiang group accomplished the first highly enantioselective example using a more convenient ambient atmosphere (Scheme 14.35b) [75]. Their organocatalytic system employed DPZ and CPA **165**. The investigation also revealed that the presence of chiral 3-hydroxy intermediates could influence the enantioselectivity of the radical coupling, thereby making enantiocontrol more challenging.

In 2018, Knowles and colleagues employed TEMPO as the radical counterpart and TIPS-EBX as the sacrificial oxidant and proton acceptor in order to achieve an enantioselective synthesis of pyrroloindolines **170** from *N*-Cbz-protected tryptamines **169** through a sequential single-electron oxidation/radical coupling/addition process (Scheme 14.36) [76]. The Brønsted base BINOL-derived CPA **168** interacts with the generated radical cations from **169**, resulting in the crucial radical species **171** for the construction of stereocenters via C—O bond formation. The obtained products are highly valuable as they have demonstrated reactivity toward various nucleophiles, leading to the synthesis of important derivatives, particularly the synthesis of (−)-calycanthidine.

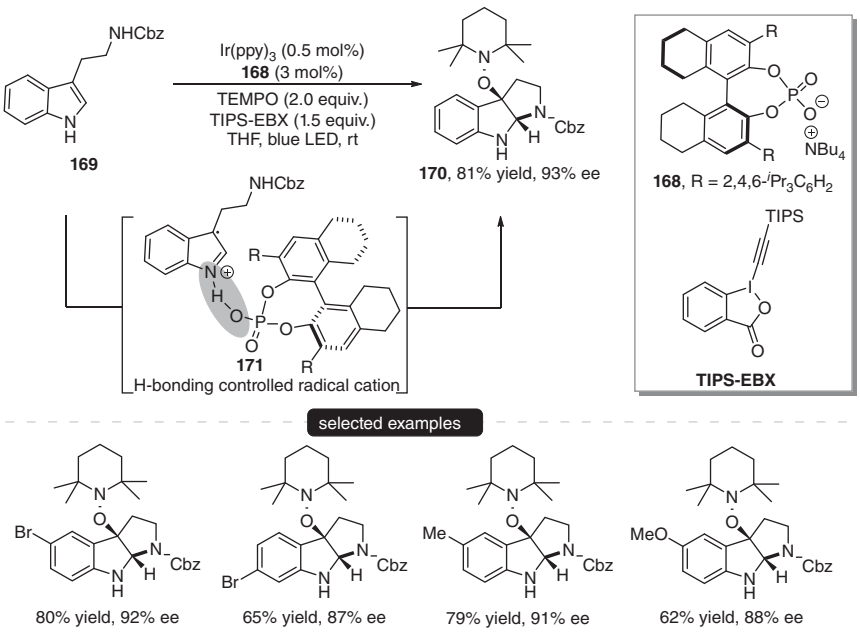


**Scheme 14.36** CPA as H-bonding catalyst in asymmetric radical coupling by Knowles.

Recently, the Jiang group has unveiled a method for the asymmetric azaarylation of enones **173** utilizing readily available cyanoazaarenes **174** as starting materials through a radical coupling pathway (Scheme 14.37) [77]. This groundbreaking approach enables the synthesis of valuable enantioenriched azaarene derivatives **175** with high yields and ee. The transformation of cyanoazaarene **174** with both acyclic and cyclic enones is facilitated by the cooperative catalysis of a photosensitizer and a chiral CPA **172**, in conjunction with an amine HEH as the sacrificial reductant. This strategy yields a broad spectrum of hydroazaarylation products **175**, featuring tertiary or quaternary carbon stereocenters. Notably, the choice of chiral catalysts plays a pivotal role in achieving satisfactory enantioselective outcomes, necessitating careful regulation depending on the specific enone substrate. Significantly, this pioneering work demonstrates the effectiveness of chiral H-bonding catalysts in providing adequate enantiocontrol for highly reactive radical coupling processes. This breakthrough is expected to inspire rapid advancements in other reductive azaarylation reactions and radical coupling-based reactions in asymmetric synthesis.

In a remarkable study, Akiyama discovered that the complex formed between an imine **180** and a chiral CPA **179** exhibited intrinsic photoactivity, avoiding the need for an external photosensitizer. This unique feature allowed the complex to be photoexcited, facilitating the subsequent radical coupling process (Scheme 14.38) [78]. Chiral CPA **179** played a crucial role in this process by providing dual H-bonding sites, which formed a ternary intermediate complex **183**. It is this complex that was responsible for the remarkable enantioselectivity observed

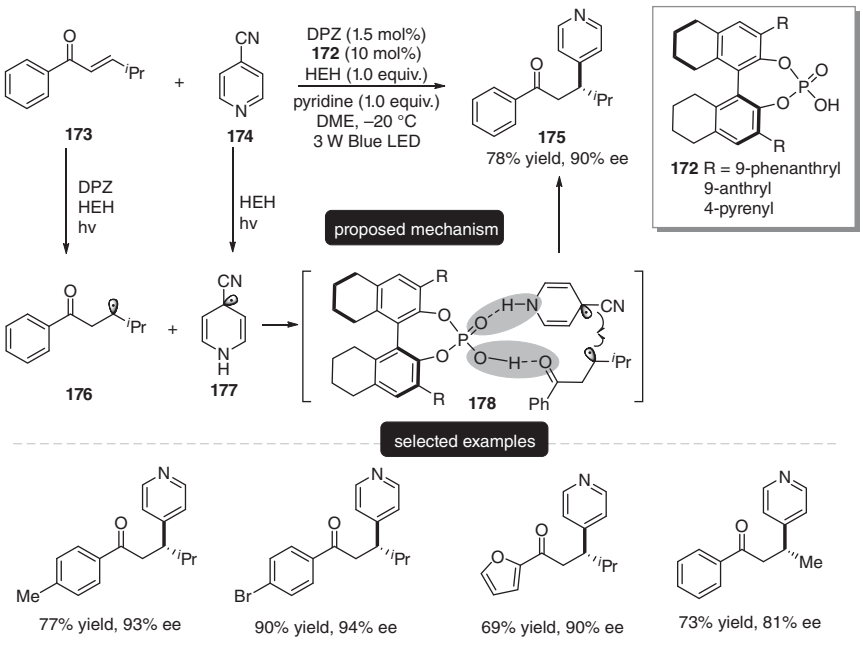


**Scheme 14.37** CPA as H-bonding in the asymmetric radical coupling of cyanoazaarenes by Jiang.

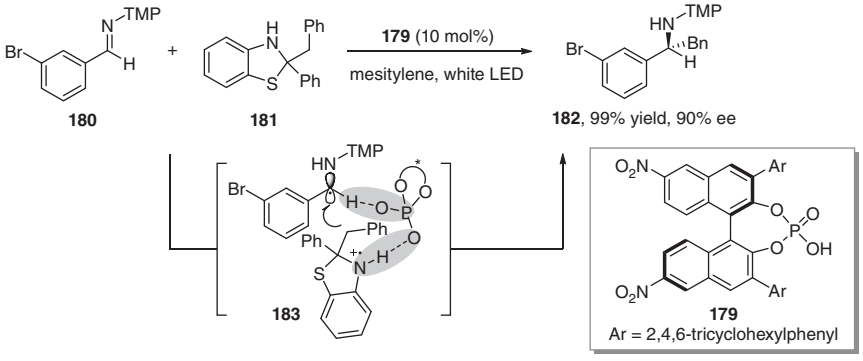


**Scheme 14.38** CPA as H-bonding catalyst in asymmetric radical coupling by Akiyama.

in the reaction. This intriguing finding suggests new avenues for utilizing chiral Brønsted acid-containing compounds in radical coupling reactions and highlights the potential of intrinsic photoactivity in catalytic processes. The discovery also underscores the significance of dual H-bonding interactions in achieving high enantioselectivity in asymmetric synthesis.

## 14.7 Asymmetric Protonation via H-Bonding Organocatalysis

The incorporation of stereocenters through enantioselective protonation has been widely exploited in asymmetric synthesis to access enantioenriched compounds featuring diverse tertiary carbon stereogenic centers [79]. The quest for novel strategies to expand the utility of this classic transformation presents an appealing opportunity for advancement. In this regard, the amalgamation of radical-based photoredox catalysis and catalytic asymmetric protonation emerges as a significant and promising research area. Such a merger holds the potential to provide a new pathway for accessing essential chiral compounds and enabling the utilization of readily available but poorly reactive feedstocks as direct substrates. However, the achievement of excellent enantioselectivity in enantioselective protonation poses a formidable challenge due to the high mobility of exceedingly small protons. Additionally, the rapid radical process leading to the prochiral tertiary carbon anion intermediate introduces a racemic background reaction, further compounding the difficulty in attaining high levels of enantioselectivity. Notwithstanding these challenges, the Jiang research group has directed their efforts toward the development of photoredox-catalyzed asymmetric protonation. This choice stems from a significant advantage offered by this approach – the ability to generate anion intermediates under controllable and nearly neutral conditions via a radical process. Such controlled generation of anion intermediates would facilitate the construction of acid/base-labile tertiary stereocenters, advancing the field of asymmetric synthesis [80].

As a starting point, Pete presented a significant advancement in the field of photodeconjugation in 1990 (Scheme 14.39) [81]. He demonstrated that $\alpha$-methyl

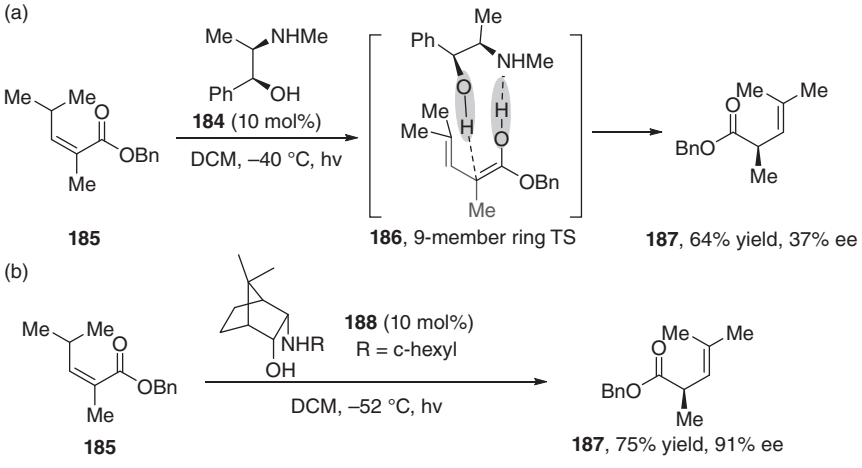


**Scheme 14.39** $\beta$-amino alcohol as H-bonding catalyst in asymmetric deconjugation: (a) pioneer work in photodeconjugation; (b) enantioselective photodeconjugation.

conjugated esters **185** could undergo this process with moderate ee when catalyzed by chiral $\beta$-amino alcohol **184**. The authors proposed an intriguing model involving a nine-membered ring transition state **186** formed via hydrogen-bonding interactions. This model provided a rational explanation for the enantioselective protonation process. The $\beta$-amino alcohol **184** acted as a dual hydrogen-bonding donor, effectively interacting with the enolate intermediate from **185** and facilitating the subsequent enantioselective protonation. To enhance the efficiency of the asymmetric processes, Pete and his team explored cyclic and rigid amino alcohols **188** as inducers for the photodeconjugation reaction (Scheme 14.39b). Remarkably, cyclic $\beta$-amino alcohol **188** led to an impressive ee of up to 91%. This result indicated a modified steric influence on the enantio-inducing step of the photodienol process. Overall, these findings represent a significant contribution to the understanding and optimization of asymmetric photochemical reactions.

Recently, Gilmour presented an intriguing study on the photoinduced deconjugative isomerization of activated alkene **188** (Scheme 14.40) [82, 83]. This transformation was achieved solely with the assistance of quinine **189** in catalytic amounts. As depicted in Scheme 14.40, mechanistic investigations uncovered the crucial role of H-bonding interactions between the enol and the quinuclidine nitrogen. It was found that the energy difference between distinct enantiomers played a pivotal role in determining the rate and enantioselectivity of the protonation step. Additionally, this interaction effectively suppressed the undesired uncatalyzed background reaction through precise temperature regulation. These findings shed light on the intricate mechanistic aspects underlying this photochemical process and provided valuable insights for the development of catalytic strategies in deconjugative isomerizations.

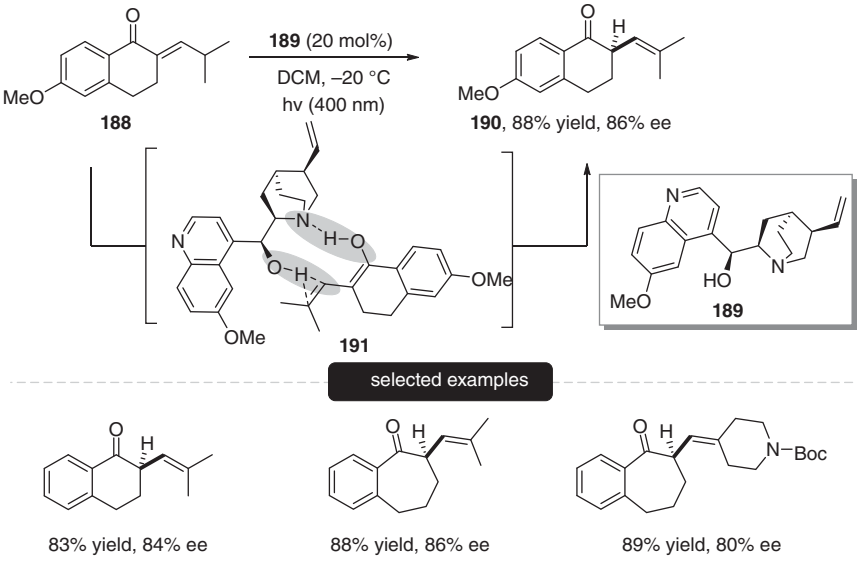


**Scheme 14.40** Quinine as H-bonding catalyst in asymmetric deconjugative isomerization.

Willner et al. reported the reduction of benzil to benzoin using $[Ru(bpy)_3]Cl_2$ as a photoredox catalyst and $Et_3N$ as a sacrificial reductant [84]. Protonation was proposed as the final step in the formation of the secondary alcohol. This work, along with Knowles' study on ketyl intermediates featuring strong basicity [47], served as inspiration for the Jiang group.

In 2017, the Jiang group developed a highly enantioselective reduction of 1,2-diketones by employing a dual catalytic system consisting of DPZ and a chiral guanidinium salt **192** as an H-bonding catalyst (Scheme 14.41) [85]. Symmetric 1,2-diketone **193** was used as an example. The reductive quenching of photoactivated DPZ by *N*-2-naphthyl tetrahydroisoquinoline (THIQ) generated the DPZ−· species, which could then reduce 1,2-diketone to form ketyl intermediates. These intermediates were subsequently captured by the chiral guanidinium salt, leading to the neutral radical species. The second single-electron reduction by THIQ resulted in the generation of an anion. Within the stereocontrolled environment provided by the H-bonding catalyst, enantioselective protonation was achieved with high levels of enantioselectivity (up to 98% ee). Interestingly, this transformation could occur even in the absence of DPZ, operating through an 'electron donor–acceptor' (EDA) mechanism. However, the enantioselectivities of most products were lower than those obtained with the photoredox catalytic system. To further evaluate the method, the Jiang group investigated the reduction of 1-phenyl-1,2-propanedione as a representative unsymmetrical diketone. It was determined that a chiral catalyst derived from *tert*-L-leucine-derived urea-tertiary amine provided the best results, yielding chiral alcohol in 67% yield with 80% ee, along with excellent

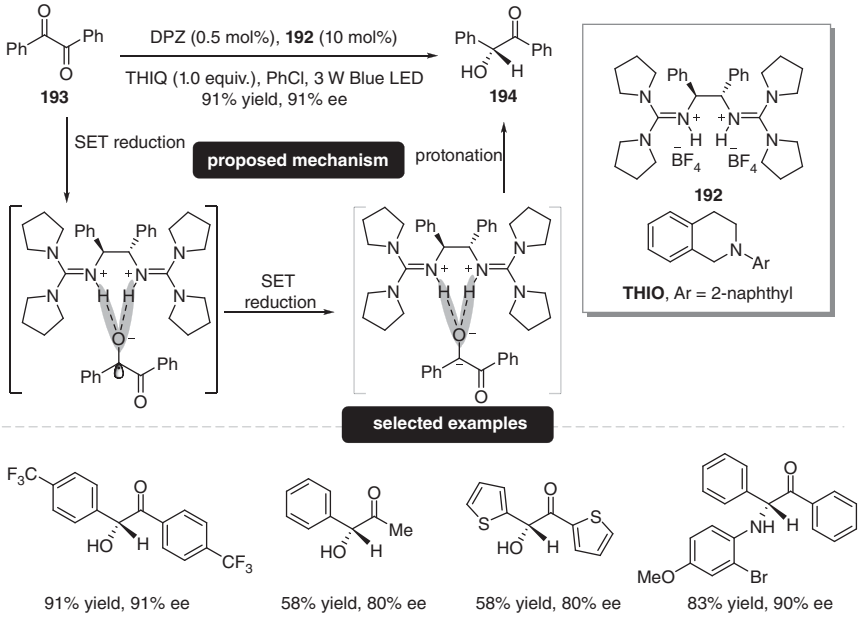


**Scheme 14.41** Reductive asymmetric protonation by Jiang.

regioselectivity and chemoselectivity. Additionally, by employing Takemoto's 1,2-cyclo-hexanediamine-based urea-tertiary amine and DPZ as the catalytic system, $\alpha$-keto ketimines could be efficiently reduced to $\alpha$-amino ketones with high yields (up to 95%) and enantioselectivities (up to 90% ee). The successful utilization of three different H-bonding catalysts in achieving excellent enantioselectivities suggests that similar dual-catalyst systems can yield favorable results through careful catalyst selection. Furthermore, this study highlights the effectiveness of chiral H-bonding catalysis in radical transformations.

The success of their previous work prompted the Jiang group to explore the potential of using this dual catalysis platform for the synthesis of secondary $\alpha$-halo ketones (Scheme 14.42) [86]. This type of bond is important in the pharmaceutical and synthetic fields, but achieving high enantioselectivity is challenging due to the inherent instability of stereocenters. To address this issue, the Jiang group prepared a range of $\alpha$,$\alpha$-dihaloketone **195** as starting materials. They utilized a combination of 0.5 mol% DPZ and 5.0 mol% L-tert-leucine-derived squaramide-tertiary amine **193** as catalysts, with a secondary amine **194** serving as the terminal reductant. This reaction setup enabled the formation of **196** containing secondary C—F, C—Cl, and C—Br bonds up to 96% yield and >99% ee. The control experiment revealed the presence of a competitive racemic background reaction within the system. The photoredox catalytic cycle was initiated through SET between photoactivated DPZ and secondary amine **194**. Subsequently, DPZ−·, facilitated by its matching redox potentials, selectively reduced the C—Cl or C—Br bond of substrate **195**. The stability of the radical intermediates was ensured by two crucial hydrogen-bonding interactions between the squaramide's two N—H units and the oxygen of the carbonyl group (**197**). Following another SET process to generate anions, enantioselective

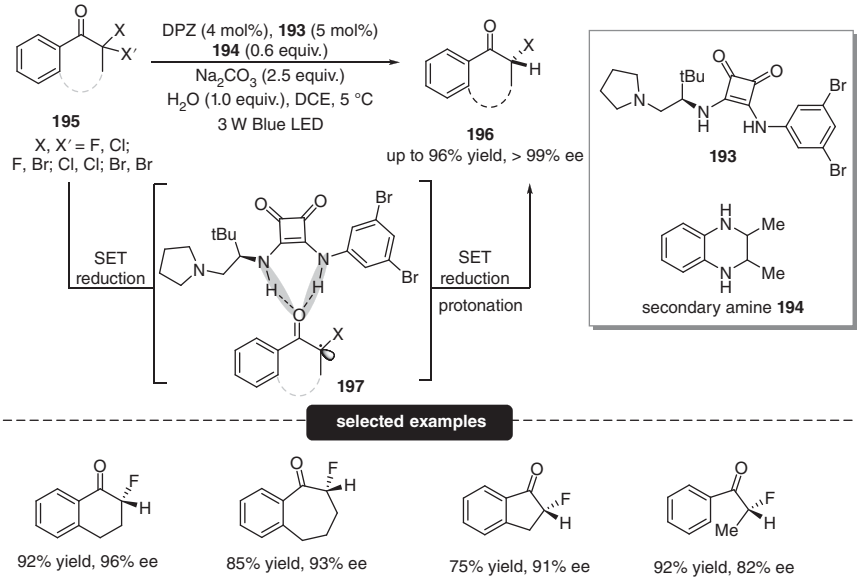


**Scheme 14.42** Asymmetric protonation via dehalogenation by Jiang.

protonation was achieved to afford the desired product **196** with satisfactory results. However, the Jiang group also discovered the susceptibility of C—Cl/Br bond-based stereocenters to degradation during flash column chromatography, resulting in a deterioration of the products' ee values. To overcome this challenge, they established a sequential strategy involving a one-pot reduction of ketones using diisobutylaluminium hydride (DIBAL-H). This approach allowed them to prepare a series of chloro/bromo-hydrins.

Later, the Jiang group studied the enantioselective reduction of azaarene-based ketones using visible light-driven photoredox asymmetric catalysis [87]. This study represents a significant advancement, as there is a lack of general and efficient catalytic methods for accessing imine-bearing azaarene-substituted secondary alcohols (Scheme 14.43a). In their investigation, the Jiang group employed a dual catalytic system consisting of CPA **198** as an H-bonding catalyst and DPZ as a photosensitizer. *N*-phenyl piperidine **199** served as the terminal reductant. Through this tandem process involving two SET reductions and an enantioselective protonation, various azaarene-bearing ketones **200** could be efficiently transformed into chiral azaarene-based secondary alcohols **201**. High yields (up to >99%) and moderate to excellent enantioselectivity (up to 97% ee) were achieved for the synthesis of chiral azaarene-based secondary alcohols with diverse aryl and alkyl substituents.

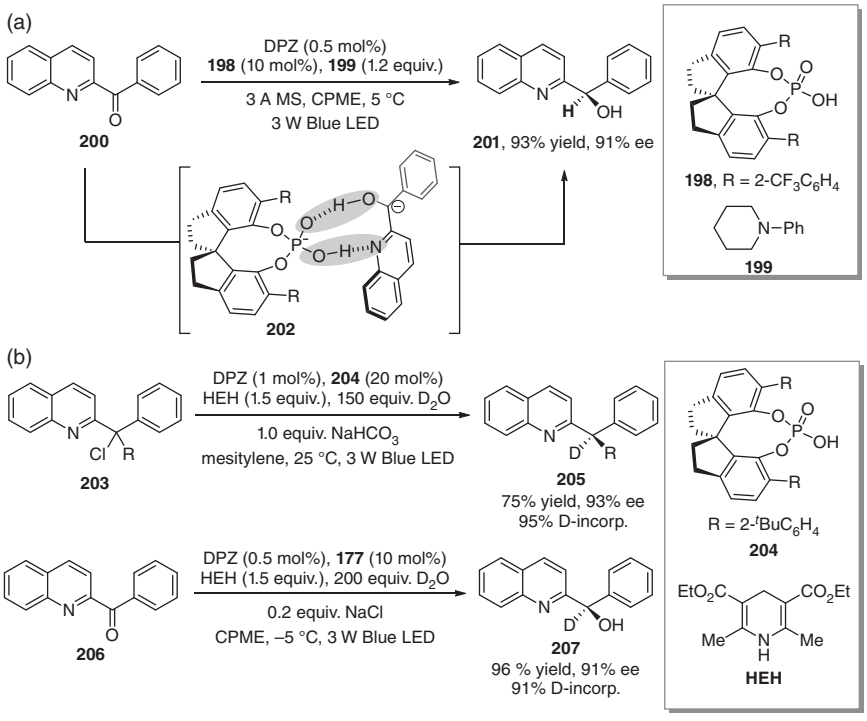


**Scheme 14.43** CPA as H-bonding catalyst in asymmetric protonation via SET: (a) enantioselective reduction of azaarene-based ketones; (b) an enantioselective reductive dehalogenative deuteration.

Building upon these achievements, the Jiang group also developed an enantioselective reductive deuteration of azaarene-substituted ketones **206** and an enantioselective reductive dehalogenative deuteration of racemic $\alpha$-chloro-azaarenes **203** (Scheme 14.43b) [88]. Inexpensive $D_2O$ was used as the deuterium source. By employing cooperative photoredox and H-bonding catalysis, utilizing DPZ with CPA **204**, the Jiang group successfully obtained a variety of chiral $\alpha$-deuterated azaarenes **205** and **207** in satisfactory yields. These products exhibited good to excellent enantioselectivities (up to 99% ee) and substantial deuterium incorporation. Overall, the work represents a logical and useful extension of previous research on photoreduction reactions. Their findings provide valuable insights into the synthesis of biologically important compounds and offer a general catalytic method for accessing imine-bearing azaarene-substituted secondary alcohols.

In 2018, the Jiang group reported an advancement in the construction of chiral azaarene-based derivatives through enantioselective protonation (Scheme 14.44) [89]. Their approach involved a radical conjugate addition-enantioselective protonation of *N*-aryl glycine **210**, affording $\alpha$-branched 2-vinylazaarenes **211**. To achieve this, they employed a dual catalytic system comprising DPZ and CPA **208**, which allowed for the transformation of *N*-aryl glycine into various valuable chiral 3-(2-pyridine/quinoline)-3-substituted amines with up to 97% yield and >99% ee. Mechanistic studies revealed that the process involved the generation of $\alpha$-amino radicals from amino acids through a sequential process of single-electron oxidation, deprotonation, proton transfer, and decarboxylation. These $\alpha$-amino radicals selectively attacked Brønsted acid-activated olefins, leading to radical species **212** and **213**. The subsequent single-electron reduction resulted in anionic species, which underwent enantioselective protonation to yield the desired products. The importance of maintaining a low reaction temperature

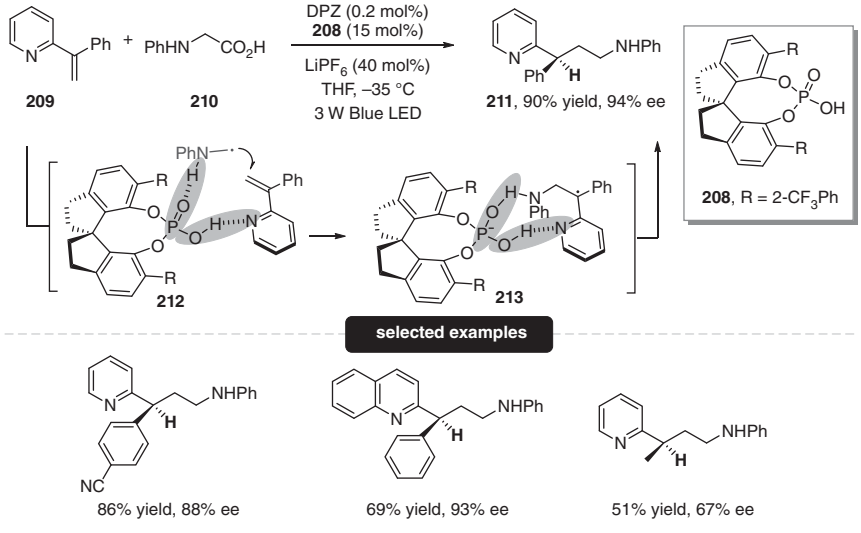


**Scheme 14.44** CPA as H-bonding catalyst in asymmetric protonation via radical addition.

was highlighted as it played a crucial role in achieving excellent enantioselectivity. By minimizing the occurrence of racemic background reactions, the desired enantiomerically pure therapeutic compound pheniramine (Avil) could be conveniently synthesized from the obtained product.

A recent advancement has been made in the enantioselective protonation through dual photoredox catalysis [90]. This breakthrough pertains to the reductive cross-coupling of two distinct olefins **215** and **216**, as depicted in Scheme 14.45. By employing a cooperative system involving photoredox catalysts and chiral H-bonding catalyst **214**, along with a terminal reductant HEH, a wide range of $\alpha$-branched vinylketones **215** can be efficiently transformed into enantioenriched azaarene derivatives **217**. These derivatives contain tertiary stereocenters at their remote δ-position and exhibit high yields and enantioselectivities. Moreover, this reaction system also proves effective for $\alpha$-branched vinylazaarenes, thereby enabling the formation of elusive 1,4-distereocenters. Collectively, these results highlight the exceptional enantio-control capabilities of the synergistic CPA/DPZ photoredox catalysis in the asymmetric protonation process.

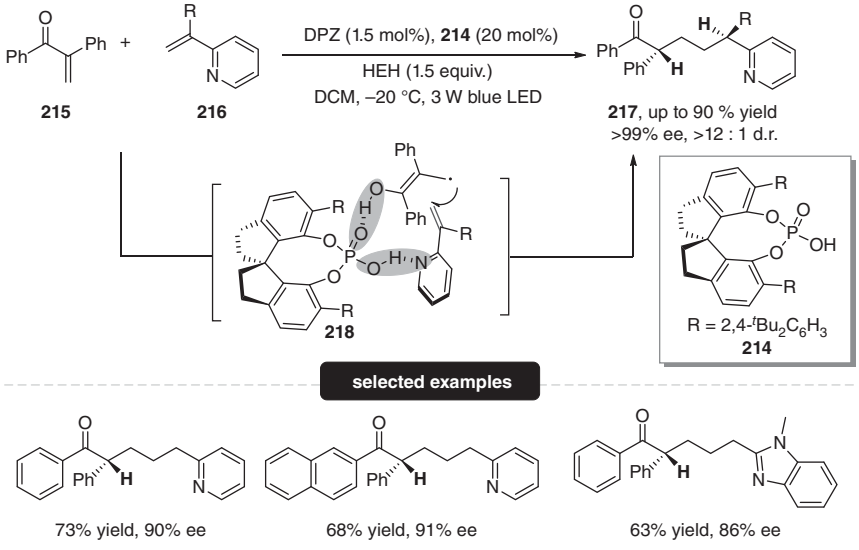


**Scheme 14.45** CPA as H-bonding catalyst in asymmetric protonation via radical coupling.

Very recently, the Jiang group introduced an innovative method for asymmetric olefin isomerization through a photoredox catalytic HAT and enantioselective protonation strategy (Scheme 14.46) [91]. In this study, chiral phosphonic acid was employed as a bifunctional catalyst, serving as both enantiocontrol elements through H-bonding and activators of the azaarenes. To achieve this, the Jiang group established a dual-catalyst system involving a visible light photosensitizer DPZ and chiral phosphoric acid **219**. *N*-hydroxyimide (**NHI-6**) was used to facilitate the HAT process. By utilizing this approach, a diverse range of allylic azaarene derivatives **221**, featuring $\alpha$-tertiary carbon stereocenters and $\beta$-C=C bonds, were synthesized

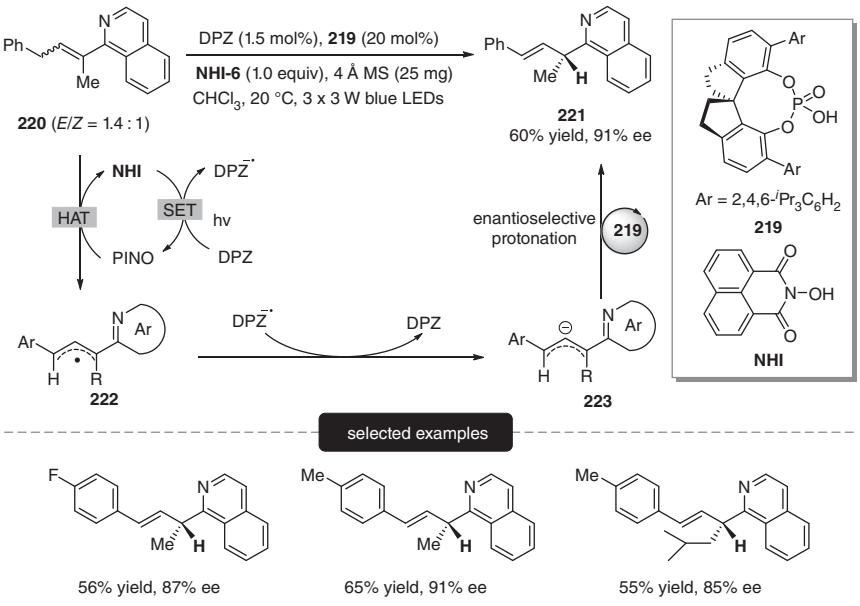


**Scheme 14.46** CPA as H-bonding catalyst in asymmetric isomerization of alkenes.

with excellent yields, enantioselectivities, and $E/Z$ ratios. Notably, this transformation demonstrated good compatibility with deuterium labeling, using affordable $D_2O$ as a deuterium source, further highlighting its broad applicability and potential utility. The proposed mechanism involves the reductive quenching of *DPZ by the HAT agent **NHI-6**, leading to the generation of PINO. The PINO molecule abstracts a γ-H atom from the substrate **220**, resulting in the formation of neutral radical intermediates **222**. These intermediates are subsequently reduced by DPZ−· to generate anions **223**, which can then undergo highly $\alpha$-regioselective and enantioselective protonation with the assistance of the chiral catalyst through H-bonding interactions with the azaarenes. Overall, this study demonstrates a novel and efficient strategy for asymmetric olefin isomerization, offering valuable insights into the design and development of catalyst systems for complex molecule synthesis.

## 14.8 Asymmetric Radical/Polar Crossover Reaction via H-Bonding Organocatalysis

Photoredox catalysis, in conjunction with extrinsic asymmetric catalysis, has emerged as a powerful strategy for the synthesis of optically pure compounds. This approach involves the generation of key ionic intermediates through a double SET process, which is often difficult to achieve or unstable using other methods. This innovative technique has been termed the radical/polar crossover reaction and has found wide application in the formation of C—C or C–heteroatom bonds [92].

One notable example of this catalytic system involves *N*-aryl α-amino acids, which can undergo single-electron oxidation to generate α-amino radicals (Scheme 14.47) [93]. These radicals can then be further oxidized, leading to imines. However, the purification of these imines is challenging due to their instability on acidic silica gel. Additionally, alkyl-substituted imines are prone to tautomerization, resulting in the formation of enamines. To overcome these challenges, the Jiang group developed a dual catalysis enantioselective manifold for the aerobic decarboxylative Povarov reaction of *N*-aryl alanines (Scheme 14.47a) [94]. The desired products **226** were obtained in high yields, with high enantioselectivity and diastereomeric ratios, using a combination of 1.0 mol% DPZ, 10 mol% CPA **224**, and 1.0 equiv. of tetra-*n*-octylammonium bromide (TOAB) as an additive under ambient conditions. This achievement represented a significant advancement in the synthesis of chiral 4-amino-2-methyl-substituted THQs. Furthermore, the Jiang group extended their research to include the enantioselective aerobic decarboxylative Povarov reaction of *N*-aryl α-amino acids with methylenephthalimidines (Scheme 14.47b) [95]. This reaction, facilitated by a dual catalysis system involving DPZ and CPA **227**, produced a range of important optically pure isoindolin-1-ones **230**. These isoindolin-1-ones featured a 3,3-spiro-tetrahydroquinoline-based stereocenter and were obtained in high yields, enantioselectivities, and diastereomeric ratios. Importantly, this study represented the first construction of the 3,3-spiro-six-membered ring of isoindolin-1-ones through asymmetric catalysis. The unsatisfactory results observed during the CPA **227** catalyzed three-component Povarov reaction underscored the significance of the developed protocol. This work highlights the synthetic importance of the proposed methodology and its potential for further advancements in the field of asymmetric catalysis.

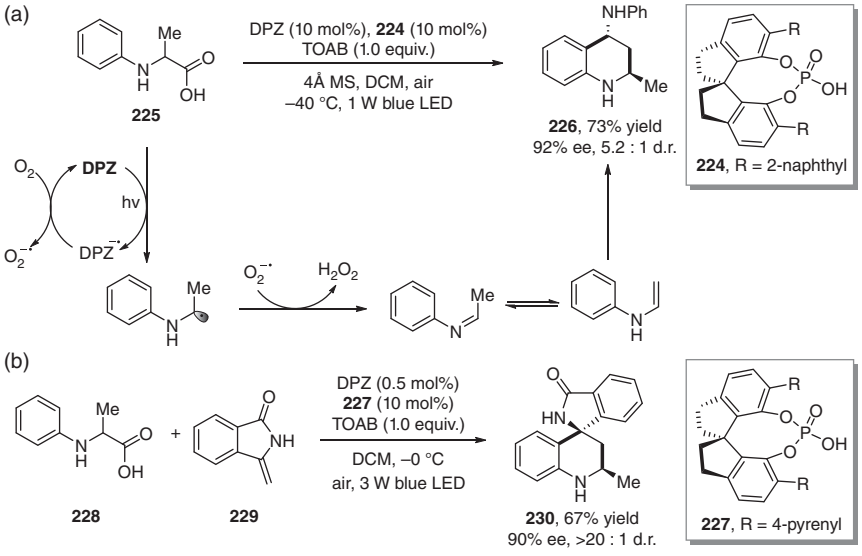


**Scheme 14.47** CPA as H-bonding catalyst in radical/polar crossover reactions by Jiang: (a) aerobic decarboxylative Povarov reaction; (b) enantioselective aerobic decarboxylative Povarov reaction of N-aryl α-amino acids with methylenephthalimidines.

Wang and his colleagues have also made advancements in creating oxygen-free conditions by oxidizing $\alpha$-amino acid-derived RAEs **233**, which serve as precursors for imines (Scheme 14.48) [96]. This process involves an asymmetric Friedel-Crafts reaction in the presence of CPA **231**, acting as an H-bonding catalyst. The reaction utilizes indoles **232** as the reaction partners, resulting in enantioenriched 1-indolyl-1-alkylamine derivatives **235** with yields of up to 95% and enantiomeric excess of up to 97%. A ternary transition state **234** is proposed, where the catalyst functions as a Lewis acid-Brønsted base bifunctional catalyst, interacting with both the N atom of the imine and the H atom of the indole. In another study, Knowles reported an enantioselective synthesis of pyrroloindolines through a sequential process involving single-electron oxidation, radical coupling, and addition reactions (Scheme 14.48b) [76]. The formation of the stereocenter at the 3-position of the indole ring (**239**) occurs via a radical coupling prior to the formation of the stereocenter at the 2-position through the aza-Mannich reaction.

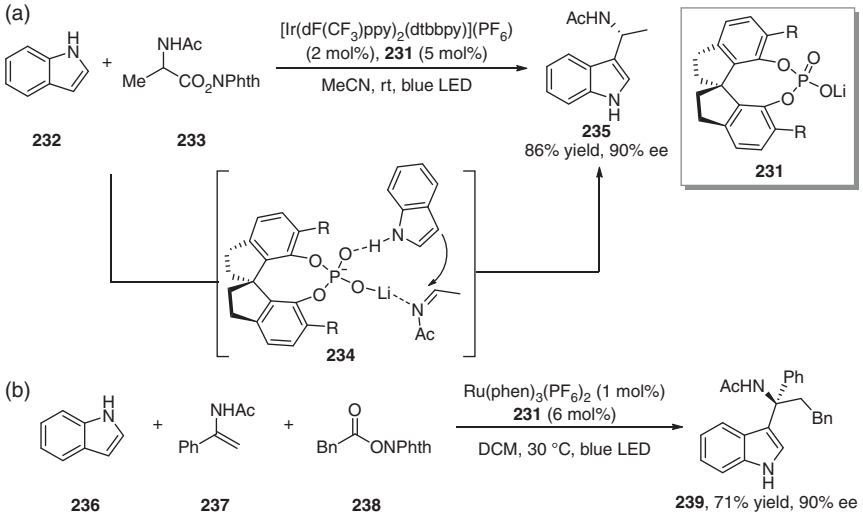


**Scheme 14.48** CPA as H-bonding catalyst in asymmetric Friedel-Crafts and aza-Mannich reactions: (a) photocatalytic asymmetric Friedel-Crafts reaction; (b) enantioselective synthesis of pyrroloindolines.

In 2017, Tung and his colleagues introduced a groundbreaking cooperative catalysis platform for the cross-dehydrogenative coupling of tertiary amine **237** with ketone under visible light conditions (Scheme 14.49) [97]. This innovative process was made possible by the utilization of a simple chiral primary amine catalyst **236**. The reaction proceeds through an enamine intermediate formed between catalyst **236** and the ketone, which is subsequently trapped by in-situ generated iminium cation species derived from tetrahydroisoquinoline derivatives under the influence of coupled Ru/Co catalysis. Importantly, the primary amine catalyst **236** plays a dual role in this process, acting both as an enamine catalyst and as an H-bonding donor, thereby ensuring high levels of enantioselectivity and diastereoselectivity in the reaction.

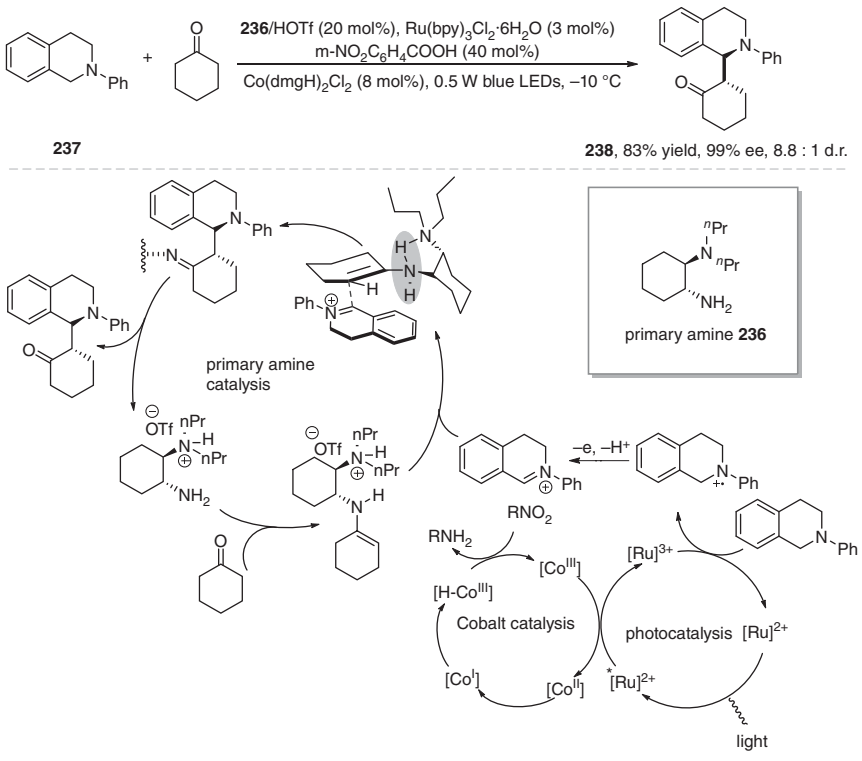


**Scheme 14.49** Primary amine as H-bonding in asymmetric cross-dehydrogenative coupling of amines to ketone.

In 2019, the Vila group unveiled an innovative cooperative organocatalyst strategy for the enantioselective oxidative alkylation of dihydroquinoxalinone **239** with a ketone through an asymmetric Mannich reaction [98]. This strategy involved the integration of the photoredox catalyst Eosin Y with (S)-proline (Scheme 14.50). Under visible light irradiation and in the presence of Eosin Y and oxygen, dihydroquinoxalin-2-one **239** undergoes initial oxidation to form iminium salt **241**, which serves as an intermediate for the subsequent asymmetric Mannich reaction. The enantioselectivity of the reaction is further modulated through H-bonding interactions between the carboxylic acid moiety of *S*-proline and the cyclic imine. Remarkably, the conversion of dihydroquinoxalinone was complete, resulting in chiral Mannich products **240** with excellent yields and ee.

Recently, the Guan group described a photocatalyzed oxidative dearomatization/asymmetric Mannich reaction of 2-substituted indole **242** and ketones or aldehydes (Scheme 14.51) [99]. In this work, they employed a cooperative photocatalysis system utilizing $Ru(bpy)_3Cl_2{\cdot}6H_2O$ as the photosensitizer, combined with L-proline as an enamine catalyst. The reaction proceeded as follows: First, the indole substrate **242** was photooxidized to an iminium salt. Subsequently, the iminium salt reacted with the superoxide anion $O_2^{\cdot-}$, which was generated through a SET process involving Ru(I) and $O_2$ within the photoredox catalysis cycle. This step

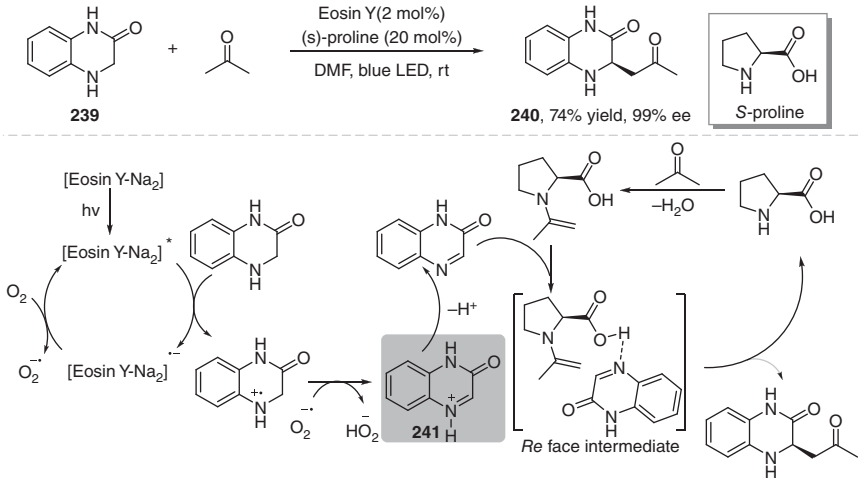


**Scheme 14.50** *S*-proline as H-bonding catalyst in asymmetric Mannich reaction.

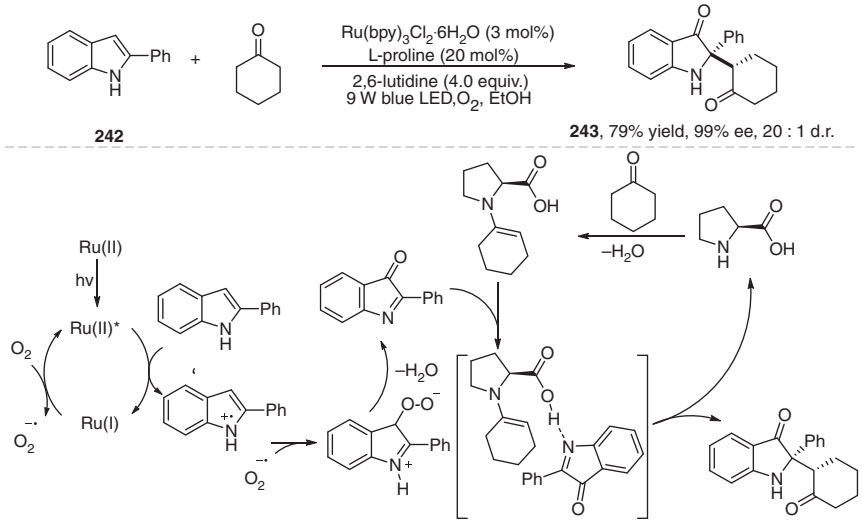


**Scheme 14.51** L-proline as H-bonding catalyst in oxidative dearomatization/asymmetric Mannich reaction.

ultimately resulted in an indolone intermediate. Finally, the indolone intermediate was trapped by the enamine of ketones in the presence of L-proline via an asymmetric Mannich reaction. Notably, L-proline played a dual role as a catalyst in the reaction system. Firstly, acting as a Brønsted acid, the proton from the carboxylic acid moiety of L-proline interacted with the intermediate through an H-bonding. Additionally, L-proline served as an enamine catalyst, effectively activating the ketone component of the reaction. This study provides valuable insights into the development of new synthetic methodologies for the synthesis of complex organic molecules, showcasing the potential of cooperative photocatalysis and asymmetric catalysis in achieving challenging transformations.

## 14.9 Deracemization via H-Bonding Organocatalysis

Deracemization, the process of converting a racemate into its single enantiomer without separating the intermediates, has recently gained renewed interest in asymmetric synthesis due to its inherent atomic economy and high efficiency [100]. However, achieving this ideal process requires selective energy input and careful reaction design to overcome thermodynamic and kinetic challenges. While asymmetric catalysis, including enzymes, transition metals, and organocatalysts, has been employed for deracemizations, traditional chemical energy-driven deracemizations have always relied on stoichiometric amounts of redox reagents, compromising the overall reaction economy [101]. The combination of radical intermediates with organic photochemical processes circumvents these limitations and offers a new approach to effective deracemization [102]. By selectively exciting molecules with photons, high-energy intermediates can be generated that easily overcome thermodynamic barriers. This process also breaks the microscopic reversibility of the existing chemical cycle due to the unique light responsiveness of the photosensitizer compared to other species in the reaction system [103].

In the 1970s, attempts were made to achieve photopromoted deracemization using radical intermediates in cases involving trans-1,2-diphenyl-cyclopropane, penta-2,3-diene, and methyl tolyl sulfoxide [104]. These attempts involved the use of ultraviolet irradiation and a stoichiometric amount of chiral sensitizers. However, the enantiomeric enrichment achieved in these studies was poor, with less than 3% ee. Significant progress in deracemization was not achieved until 2018 when Bach reported a breakthrough in the form of an effective deracemization of allenes (Scheme 14.52) [29]. This breakthrough was catalyzed by a designed bifunctional chiral photosensitizer **244** that utilized H-bonding interactions. The catalysis effectively promoted the deracemization of allene lactam **245**, resulting in excellent yield and enantioselectivity. Mechanistic studies revealed that the catalyst could

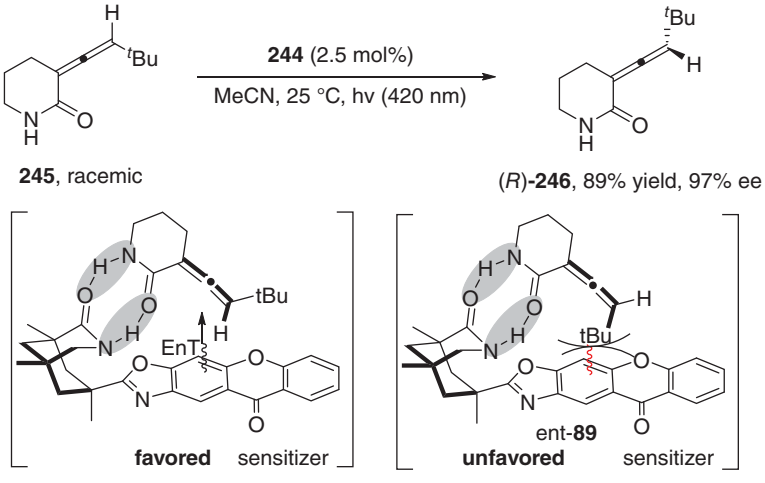


**Scheme 14.52** Chiral lactam as H-bonding catalyst in deracemization.

differentiate between the two enantiomers. The (*R*)-isomer of allene demonstrated a higher association constant with the catalyst, leading to a closer distance for triplet energy transfer and the generation of an achiral biradical intermediate related to the (*S*)-enantiomer of X. This enhanced the stereoinversion of the (*R*)-isomer compared to the weak-binding (*S*)-isomer. In this reaction design, the challenging tasks of enantioselectivity control and racemization are accomplished within a single catalytic cycle using only one catalyst.

The aforementioned strategy has also demonstrated successful application in the deracemization of molecules with central chirality, such as aryl-substituted cyclopropane spirocyclopropyl oxindoles and sulfoxides. In these examples, moderate to good ee was achieved by employing the photocatalysts **247** (Scheme 14.53) [105]. The reaction was proposed to involve light-induced σ-bond homolysis, leading to diradical intermediates that bridge the enantiomers.

In a recent publication, Bach and colleagues reported their advancements in the photochemical deracemization of primary allene amides, supported by

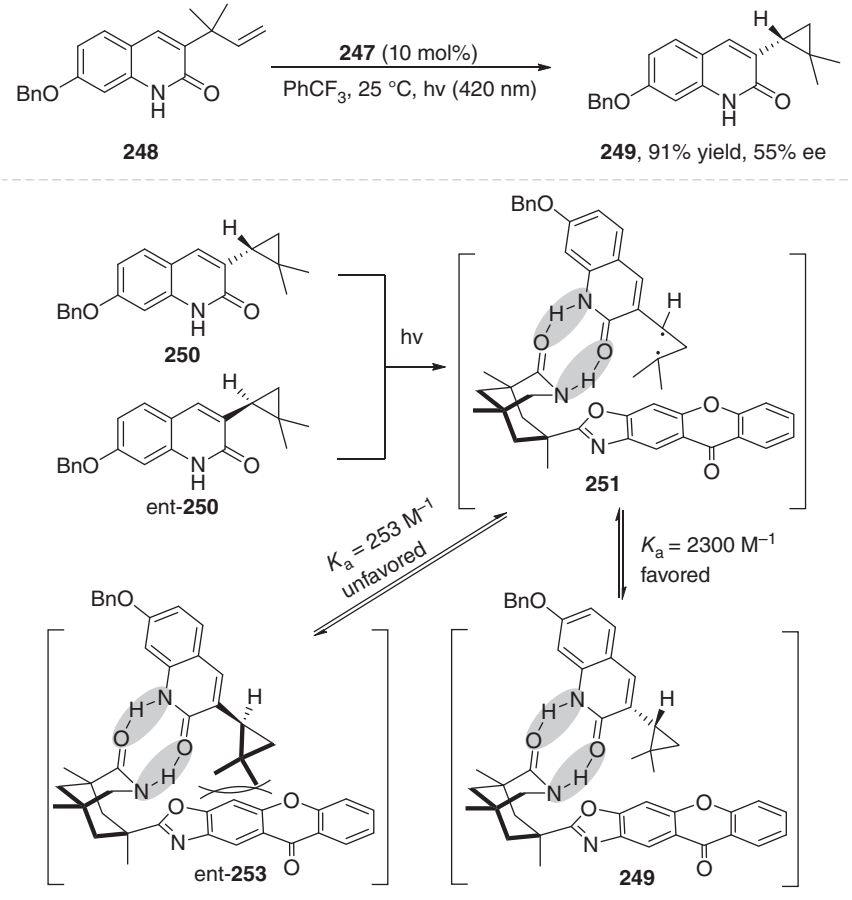


**Scheme 14.53** Enantioselective three-component Minisci-type addition.

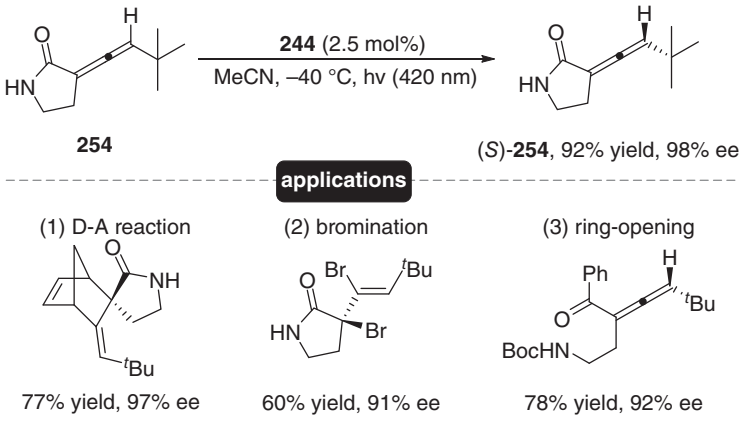


**Scheme 14.54** Enantioselective three-component Minisci-type addition.

experimental and theoretical investigations (Scheme 14.54) [106]. The mechanistic studies confirmed that the selective transfer of triplet energy, resulting from chiral recognition, played a critical role in determining the stereochemistry. Furthermore, this approach was extended to substrates with axial chirality, including tetrasubstituted alkenes. Through precise energy transfer, the desired alkene enantiomers were obtained in high yield and exceptional enantioselectivity. A proposed triplet intermediate, specifically a 1,2-radical, was identified as the key species responsible for the interconversion of enantiomers. By selectively recognizing one enantiomer of the allene through hydrogen-bonding interactions and employing a triplet-sensitized racemization process, Bach and the research team further demonstrated the photochemical deracemization of 3-(1'-alkenylidene)-pyrrolidin-2-one. This process involved the use of a photoredox catalyst and subsequent modifications, allowing for the transfer of chirality to various promising structures [107].

In 2019, Knowles and Miller presented a ternary catalytic system for the efficient deracemization of cyclic ureas, achieving high yields and ee (Scheme 14.55) [108]. The process commenced through photoinduced electron transfer (PET) between the racemic urea substrate **256** and an excited Ir-based photosensitizer. Subsequently, the resulting cation radical engaged in a series of selective reactions, including proton transfer (PT) with a chiral phosphate anion denoted as **255**, followed by stereoselective HAT facilitated by a cysteine-embedded peptide catalyst. This sequence of steps collectively governed the observed stereoselectivity, as confirmed by DFT calculations. Further analysis of each chiral catalyst demonstrated the synergistic manipulation of enantioselectivity by the chiral phosphate anion and the peptide component.

In 2021, Bach presented a benzophenone-containing chiral amide catalyst **257**, designed for the deracemization of hydantoin derivatives (Scheme 14.56) [109]. The catalyst demonstrated remarkable efficiency in producing a single enantiomer **259** with high yields and enantioselectivity. Mechanistic investigations indicated that the photocatalytic process proceeded through a HAT mechanism, as illustrated in Scheme 14.56. Detailed analysis using transient absorption spectroscopy

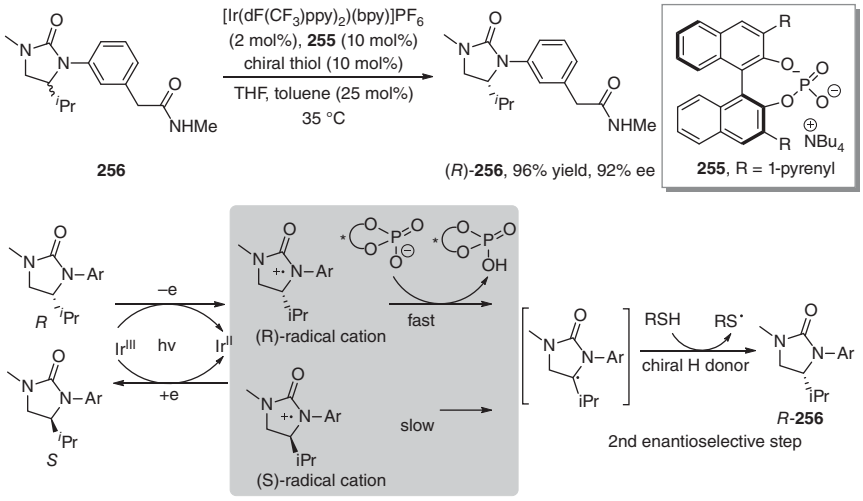


**Scheme 14.55** Enantioselective three-component Minisci-type addition.

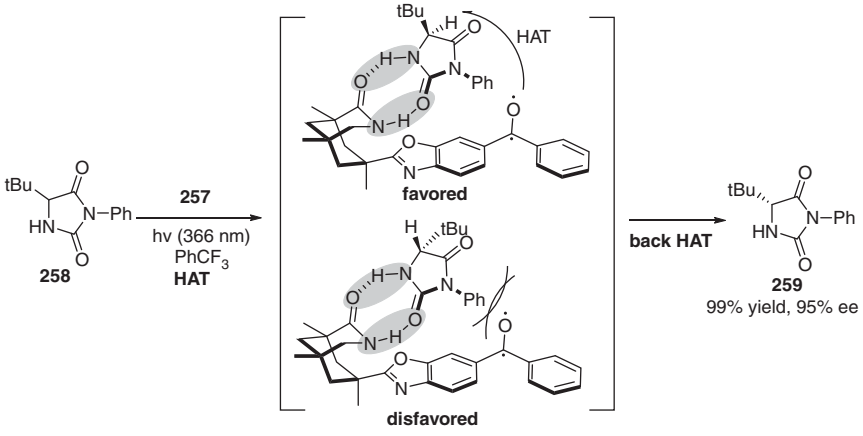


**Scheme 14.56** Enantioselective three-component Minisci-type addition.

identified a crucial ketyl radical intermediate, which exhibited HAT exclusively for one enantiomer. Furthermore, the subsequent back HAT step generated an enol intermediate, and subsequent tautomerization resulted in both enantiomers without discrimination [110]. Notably, the continuous depletion of one enantiomer during the catalytic cycle contributed to the enrichment of the desired enantiomer.

In a recent development, Jiang realized the deracemization of $\alpha$-amino esters **261** by combining the organo-photocatalyst DPZ with a chiral phosphoric acid catalyst **262**, as depicted in Scheme 14.57 [111]. This approach allowed for the effective transformation of various amino esters bearing diverse $\alpha$-alkyl, $\alpha$-aryl, and cyclic frameworks. Remarkably, the enantioselectivity of the process was maintained even in the presence of a substantial amount of $D_2O$, enabling the deuteration of the products. Notably, the integration of an electron-rich *N*-protecting group

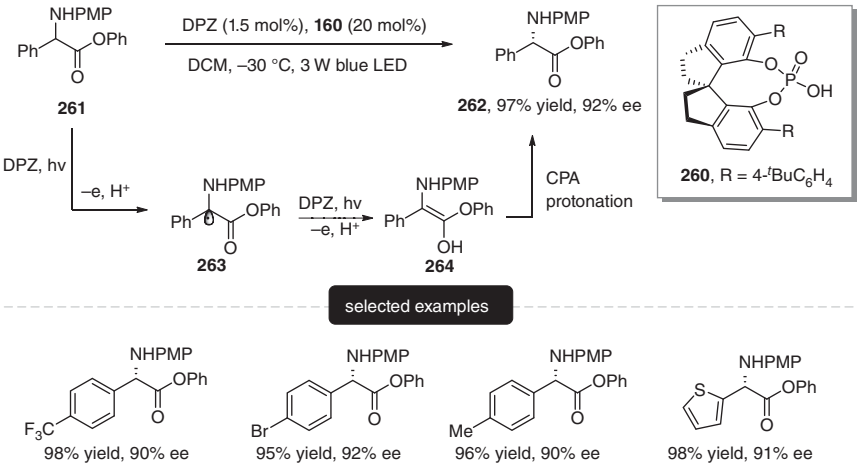


**Scheme 14.57** Enantioselective three-component Minisci-type addition.

proved to be crucial for promoting the PET of the amino esters. Through a cascade of electron–proton–back electron transfer events, a pivotal enol intermediate was generated, introducing a novel photochemical process that differs from the conventional enol formation through proton transfer. The enantioselective tautomerization of the enol, facilitated by the chiral phosphoric acid catalyst, resulted in the reconstruction of the chiral center, thus achieving the desired deracemization of the $\alpha$-amino esters.

## 14.10 Summary and Perspective

Chiral H-bonding catalysis has revolutionized the field of asymmetric radical reactions, particularly in the last two decades. The integration of photoredox catalysis with H-bonding interactions has emerged as a powerful and versatile catalytic platform, enabling a wide range of radical transformations with unprecedented stereoselectivity. However, there are still several challenges for the further development of HBD-mediated asymmetric catalysis. First, compared to its role in thermal asymmetric radical transformations, the repertoire of catalytic reactions and catalysts in H-bonding mediated photoredox catalysis is currently limited. There is a need for expanding the types of catalytic radical reactions and diversifying the catalog of catalysts. In particular, the development of novel substrate-differentiating-based synergistic catalysis holds great promise and is highly desirable. Second, since H-bonding catalysts originate from the biosystem, there is a need for more complex catalytic systems. Efforts are already underway to develop catalysis platforms consisting of three distinct catalytic molecules, mirroring the complexity of enzymes and proteins. These advancements will pave the way for a more systematic approach to catalysis using HBD-mediated processes. Last, the emerging concept of multiphoton-induced photoredox catalysis has

garnered significant attention in recent years. This subdiscipline focuses on the co-development of organic radical chemistry and physical inorganic chemistry to overcome the thermodynamic limitations imposed by the energy of a single photon. By harnessing the combined energy of multiple photons, this approach allows for a broader range of applicable redox potentials and mitigates the risk of photodamage and undesired side reactions. Introducing HBD into the multiphoton excitation system holds tremendous potential for advancing synthetic strategies in this field.

Overall, the integration of chiral H-bonding catalysis with photoredox catalysis has opened up new avenues in asymmetric radical organic synthesis. Addressing the challenges of expanding catalytic reactions and catalyst diversity, developing more complex catalytic systems, and exploring multiphoton-induced photoredox catalysis will undoubtedly enhance the synthetic art and further propel this field forward.

## References


**1** a) List, B. (2007). *Chem. Rev.* 107: 5413–5415. b) MacMillan, D.W.C. (2008). *Nature* 455: 304–308.

**2** Xiang, S.H. and Tan, B. (2020). *Nat. Commun.* 11: 3786.

**3** Doyle, A.G. and Jacobsen, E.N. (2007). *Chem. Rev.* 107: 5713–5743.

**4** a) Bauer, T., Hakim, Y.Z., and Morawska, P. (2023). *Molecules* 28: 6252–6369. b) Yu, X. and Wang, W. (2008). *Chem. Asian J.* 3: 516–532. c) Knowles, R.R. and Jacobsen, E.N. (2010). *Proc. Natl. Acad. Sci. USA* 107: 20678–20685.

**5** a) Prier, C.K., Rankic, D.A., and MacMillan, D.W.C. (2013). *Chem. Rev.* 113: 5322–5363. b) Reckenthaler, M. and Griesbeck, A.G. (2013). *Adv. Synth. Catal.* 355: 2727–2744. c) Narayanam, J.M.R. and Stephenson, C.R.J. (2011). *Chem. Soc. Rev.* 40: 102–113.

**6** Twilton, J., Le, C., Zhang, P. et al. (2017). *Nat. Rev. Chem.* 1: 52–70.

**7** Fukuzumi, S., Jung, J., Lee, Y.-M., and Nam Asian, W. (2017). *J. Organomet. Chem.* 6: 397–409.

**8** a) Ramamurthy, V. and Sivaguru, J. (2016). *Chem. Rev.* 116: 9914–9993. b) Tuten, B.T., Wiedbrauk, S., and Barner-Kowollik, C. (2020). *Prog. Polym. Sci.* 100: 101183–101195.

**9** Nicewicz, D.A. and MacMillan, D.W.C. (2008). *Science* 322: 77–80.

**10** Bach, T., Bergmann, H., and Harms, K. (1999). *J. Am. Chem. Soc.* 121: 10650–10651.

**11** a) Skubi, K.L., Blum, T.R., and Yoon, T.P. (2016). *Chem. Rev.* 116: 10035–10074. b) Genzink, M.J., Kidd, J.B., Swords, W.B., and Yoon, T.P. (2022). *Chem. Rev.* 122: 1654–1716.

**12** a) Woldegiorgis, G., Suleman, M., and Lin, X. (2022). *Eur. J. Org. Chem.* 34: e20220062. b) Li, X., Zheng, H., Xia, Y. et al. (2017). *Acc. Chem. Res.* 50: 2621–2631.

**13** a) Chen, Y., Yekta, S., and Yudin, A.K. (2003). *Chem. Rev.* 103: 3155–3212. b) Nguyen, T.N., Chen, P.A., Setthakarn, K., and May, J.A. (2018). *Molecules* 23: 2317–2353.

**14** Tanaka, K. and Toda, F.J. (1992). *J. Chem. Soc. Chem. Commun.* 943.

**15** Tanaka, K. and Fujiwara, T. (2005). *Org. Lett.* 7: 1501–1503.

**16** a) Poplata, S., Troster, A., Zou, Y.Q., and Bach, T. (2016). *Chem. Rev.* 116: 9748–9815. b) Proctor, R.S.J., Colgan, A.C., and Phipps, R.J. (2020). *Nat. Chem.* 12: 990–1004.

**17** Bach, T., Bergmann, H., and Harms, K. (2000). *Angew. Chem. Int. Ed.* 39: 2302–2304.

**18** a) Albrecht, D., Vogt, F., and Bach, T. (2010). *Chem. Eur. J.* 16: 4284–4296. b) Austin, K.A.B., Herdtweck, E., and Bach, T. (2011). *Angew. Chem. Int. Ed.* 50: 8416–8419.

**19** a) Bach, T. and Bergmann, H. (2000). *J. Am. Chem. Soc.* 122: 11525–11526. b) Coote, S.C., Pothig, A., and Bach, T. (2015). *Chem. Eur. J.* 21: 6906–6912.

**20** a) Selig, P. and Bach, T. (2008). *Angew. Chem. Int. Ed.* 47: 5082–5084. b) Selig, P., Herdtweck, E., and Bach, T. (2009). *Chem. Eur. J.* 15: 3509–3525.

**21** Coote, S.C. and Bach, T. (2013). *J. Am. Chem. Soc.* 135: 14948–14951.

**22** Bach, T., Bergmann, H., and Harms, K. (2001). *Org. Lett.* 3: 601–603.

**23** a) Grosch, B., Orlebar, C.N., Herdtweck, E. et al. (2003). *Angew. Chem. Int. Ed.* 42: 3693–3696. b) Grosch, B., Orlebar, C.N., Herdtweck, E. et al. (2004). *Chem. Eur. J.* 10: 2179–2189.

**24** Wiegand, C., Herdtweck, E., and Bach, T. (2012). *Chem. Commun.* 48: 10195–10197.

**25** Burg, F. and Bach, T. (2019). *J. Organomet. Chem.* 84: 8815–8836.

**26** Bauer, A., Westkamper, F., Grimme, S., and Bach, T. (2005). *Nature* 436: 1139–1140.

**27** Herkstroeter, W., Lamola, A.A., and Hammond, G.S. (1964). *J. Am. Chem. Soc.* 86: 4537–4540.

**28** a) Muller, C., Bauer, A., Maturi, M. et al. (2011). *J. Am. Chem. Soc.* 133: 16689–16697. b) Maturi, M.M., Wenninger, M., Alonso, R. et al. (2013). *Chem. Eur. J.* 19: 7461–7472.

**29** Holzl-Hobmeier, A., Bauer, A., Silva, A.V. et al. (2018). *Nature* 564: 240–243.

**30** Alonso, R. and Bach, T. (2014). *Angew. Chem. Int. Ed.* 53: 4368–4371.

**31** Etter, M.C., Lipkowska, Z.U., Ebrahimi, M.Z., and Panunto, T.W. (1990). *J. Am. Chem. Soc.* 112: 8415–8426.

**32** Curran, D.P. and Kuo, L.H. (1994). *J. Organomet. Chem.* 59: 3259–3261.

**33** Sigman, M.S. and Jacobsen, E.N. (1998). *J. Am. Chem. Soc.* 120: 4901–4902.

**34** Vallavoju, N., Selvakumar, S., Jockusch, S. et al. (2014). *Angew. Chem. Int. Ed.* 53: 5604–5608.

**35** Li, S., Xiang, S.H., and Tan, B. (2019). *Chin. J. Chem.* 38: 213–214.

**36** Zhao, Y., Zhang, C., Chin, K.F. et al. (2014). *RSC Adv.* 4: 30062–30067.

**37** a) Lv, X., Xu, H., Yin, Y. et al. (2020). *Chin. J. Chem.* 38: 1480–1488. b) Yin, Y., Zhao, X., and Jiang, Z. (2020). *ChemCatChem* 12: 4471–4489.

**38** Yin, Y., Li, Y., Goncalves, T.P. et al. (2020). *J. Am. Chem. Soc.* 142: 19451–19456.

**39** Dai, Y., Liang, S., Zeng, G. et al. (2022). *Chem. Sci.* 13: 3787–3795.

**40** Sherbrook, E.M., Genzink, M.J., Park, B. et al. (2021). *Nat. Commun.* 12: 5735.

**41** Pecho, F., Sempere, Y., Gramuller, J. et al. (2021). *J. Am. Chem. Soc.* 143: 9350–9354.

**42** Miyabe, H., Kawashima, A., Yoshioka, E., and Kohtani, S. (2017). *Chem. Eur. J.* 23: 6225–6236.

**43** Aechtner, T., Dressel, M., and Bach, T. (2004). *Angew. Chem. Int. Ed.* 43: 5849–5851.

**44** Rressel, M. and Bach, T. (2006). *Org. Lett.* 8: 3145–3147.

**45** Kapitán, P. and Bach, T. (2008). *Synthesis* 10: 1559–1564.

**46** Edtmueller, V., Poethig, A., and Bach, T. (2017). *Tetrahedron* 73: 5038–5047.

**47** Rono, L.J., Yayla, H.G., Wang, D.Y. et al. (2013). *J. Am. Chem. Soc.* 135: 17735–17738.

**48** Roos, C.B., Demaerel, J.D., Graff, D.E., and Knowles, R.R. (2020). *J. Am. Chem. Soc.* 142: 5974–5979.

**49** Guo, Z., Chen, X., Fang, H. et al. (2021). *Sci. China Chem.* 64: 1522–1529.

**50** a) Renaud, P. and Sibi, M.P. (2001). *Radicals in Organic Synthesis*. Weinheim, Germany: Wiley-VCH. b) Togo, H. (2004). *In Advanced Free Radical Reactions for Organic Synthesis*. Elsevier Science: Amsterdam.

**51** Zhu, Y., Zhang, L., and Luo, S. (2014). *J. Am. Chem. Soc.* 136: 14642–14645.

**52** Wang, D., Zhang, L., and Luo, S. (2017). *Org. Lett.* 19: 4924–4927.

**53** Tan, Y., Yin, Y., Cao, S. et al. (2022). *Chin. J. Catal.* 43: 558–563.

**54** Pozharskii, A.F., Soldatenkov, A.T., and Katritzky, A.R. (2011). *Heterocycles in Life and Society: An Introduction to Heterocyclic Chemistry, Biochemistry and Applications*. Weinheim, Germany: Wiley-VCH.

**55** a) Yu, S., Sang, H.L., and Ge, S. (2017). *Angew. Chem. Int. Ed.* 56: 15896–15900. b) Xu, C., Muir, C.W., Leach, A.G. et al. (2018). *Angew. Chem. Int. Ed.* 57: 11374–11377.

**56** Hepburn, H.B. and Melchiorre, P. (2016). *Chem. Commun.* 52: 3520–3523.

**57** Cao, K., Tan, S.M., Lee, R. et al. (2019). *J. Am. Chem. Soc.* 141: 5437–5443.

**58** Cao, K., Li, C., Tian, D. et al. (2022). *Org. Lett.* 24: 4788–4792.

**59** Chai, X., Hu, X., Zhao, X. et al. (2022). *Angew. Chem. Int. Ed.* 61: e202115110.

**60** Proctor, R.S.J. and Phipps, R.J. (2019). *Science* 58: 13666.

**61** Bacos, P.D., Lahdenpera, A.S.K., and Phipps, R.J. (2023). *Acc. Chem. Res.* 56: 2037–2049.

**62** Proctor, S.J., Davis, H.J., and Phipps, R.J. (2018). *Science* 360: 419–422.

**63** Liu, X., Liu, Y., Chai, G. et al. (2018). *Org. Lett.* 20: 6298–6301.

**64** Proctor, R.S.J., Chuentragool, P., Colgan, A.C., and Phipps, R.J.J. (2021). *J. Am. Chem. Soc.* 143: 4928–4934.

**65** Colgan, A.C., Proctor, R.S.J., Gibson, D.C. et al. (2022). *Angew. Chem. Int. Ed.* 61: e202200266.

**66** Zheng, D. and Studer, A. (2019). *Angew. Chem. Int. Ed.* 58: 15803–15807.

**67** Ma, C., Shen, J., Qu, C. et al. (2023). *J. Am. Chem. Soc.* 145: 20141–20148.

**68** a) Yi, H., Zhuang, G., Wang, H. et al. (2017). *Chem. Rev.* 117: 9016–9085. b) Xie, J., Jin, H., and Hashmi, A.S.K. (2017). *Chem. Soc. Rev.* 46: 5193–5203.

**69** Uraguchi, D., Kinoshita, N., Kizu, T., and Ooi, T. (2015). *J. Am. Chem. Soc.* 137: 13768–13771.

**70** Liu, Y., Liu, X., Li, J. et al. (2018). *Chem. Sci.* 9: 8094–8098.
**71** Li, J., Kong, M., Qiao, B. et al. (2018). *Nat. Commun.* 9: 2445.
**72** Zeng, G., Li, Y., Qiao, B. et al. (2019). *Chem. Commun.* 55: 11362–11365.
**73** Lerch, S., Unkel, L.-N., and Brasholz, M. (2014). *Angew. Chem. Int. Ed.* 53: 6558–6562.
**74** Ding, W., Zhou, Q.-Q., Xuan, J. et al. (2014). *Tetrahedron Lett.* 55: 4648–4652.
**75** Bu, L., Li, J., Yin, Y. et al. (2018). *Chem. Asian J.* 13: 2382–2387.
**76** Gentry, E.C., Rono, L.J., Hale, M.E. et al. (2018). *J. Am. Chem. Soc.* 140: 3394–3402.
**77** Li, Y., Han, C., Wang, Y. et al. (2022). *J. Am. Chem. Soc.* 144: 7805–7814.
**78** Uchikura, T., Kamiyama, N., Mouri, T., and Akiyama, T. (2022). *ACS Catal.* 12: 5209–5216.
**79** Mohr, J.T., Hong, A.Y., and Stoltz, B.M. (2009). *Nat. Chem.* 1: 359–369.
**80** Yin, Y., Zhao, X., Qiao, B., and Jiang, Z. (2020). *Org. Chem. Front.* 7: 1283–1296.
**81** Piva, O. and Pete, J.P. (1990). *Tetrahedron Lett.* 31: 5157–5160.
**82** Morack, T., Onneken, C., Nakakohara, H. et al. (2021). *ACS Catal.* 11: 11929–11937.
**83** Henin, F., Muzart, J., Pete, J.P. et al. (1991). *Angew. Chem. In. Ed.* 30: 416–418.
**84** Willner, I., Tsfania, T., and Eichen, Y. (1990). *J. Organomet. Chem.* 55: 2656–2662.
**85** Lin, L., Bai, X., Ye, X. et al. (2017). *Angew. Chem. Int. Ed.* 56: 13842–13846.
**86** Hou, M., Lin, L., Chai, X. et al. (2019). *Chem. Sci.* 10: 6629–6634.
**87** Qiao, B., Li, C., Zhao, X. et al. (2019). *Chem. Commun.* 55: 7534–7537.
**88** Shao, T., Li, Y., Ma, N. et al. (2019). *iScience* 16: 410–419.
**89** Yin, Y., Dai, Y., Jia, H. et al. (2018). *J. Am. Chem. Soc.* 140: 6083–6087.
**90** Kong, M., Tan, Y., Zhao, X. et al. (2021). *J. Am. Chem. Soc.* 143: 4024–4031.
**91** Liu, Y., Zhang, L., Zhang, Y. et al. (2023). *J. Am. Chem. Soc.* 145: 18307–18315.
**92** a) Bergonzini, G., Schindler, C.S., Wallentin, C.-J. et al. (2014). *Chem. Sci.* 5: 112–116. b) Wei, G., Zhang, C., Bureš, F. et al. (2016). *ACS Catal.* 6: 3708–3712.
**93** Kizu, T., Uraguchi, D., and Ooi, T. (2016). *J. Organomet. Chem.* 81: 6953–6958.
**94** Shao, T., Yin, Y., Lee, R. et al. (2018). *Adv. Synth. Catal.* 360: 1754–1760.
**95** Li, J., Gu, Z., Zhao, X. et al. (2019). *Chem. Commun.* 55: 12916–12919.
**96** Shen, M.-L., Shen, Y., and Wang, P.-S. (2019). *Org. Lett.* 21: 2993–2997.
**97** Yang, Q., Zhang, L., Ye, C. et al. (2017). *Angew. Chem. In. Et.* 56: 3694–3698.
**98** Rostoll-Berenguer, J., Blay, G., Munoz, M.C. et al. (2019). *Org. Lett.* 21: 6011–6015.
**99** Dong, C.L., Ding, X., Huang, L.Q. et al. (2020). *Org. Lett.* 22: 1076–1080.
**100** a) Gruber, C.C., Lavandera, I., Faber, K., and Kroutil, W. (2006). *Adv. Synth. Catal.* 348: 1789–1805. b) Faber, K. (2001). *Chem. Eur. J.* 7: 5004–5010.
**101** a) Lackner, A.D., Samant, A.V., and Toste, F.D. (2013). *J. Am. Chem. Soc.* 135: 14090–14093. b) Ji, Y., Shi, L., Chen, M.W. et al. (2015). *J. Am. Chem. Soc.* 137: 10496–10499. c) Wan, M., Sun, S., Li, Y., and Liu, L. (2017). *Angew. Chem. Int. Ed.* 56: 5116–5120.
**102** Huang, M., Pan, T., Jiang, X., and Luo, S. (2023). *J. Am. Chem. Soc.* 145: 10917–10929.

**103** a) Marzo, L., Pagire, S.K., Reiser, O., and König, B.V. (2018). *Angew. Chem. Int. Ed.* 57: 10034–10072. b) Wang, H., Tian, Y.M., and König, B. (2022). *Nat. Rev. Chem.* 6: 745–755.

**104** a) Ouannes, C., Beugelmans, R., and Roussi, G. (1973). *J. Am. Chem. Soc.* 95: 8472–8474. b) Drucker, C.S., Toscano, V.G., and Weiss, R.G. (1973). *J. Am. Chem. Soc.* 95: 6482–6484. c) Balavoine, G., Jugé, S., and Kagan, H.B. (1973). *Tetrahedron Lett.* 14: 4159–4162.

**105** a) Tröster, A., Bauer, A., Jandl, C., and Bach, T. (2019). *Angew. Chem. Int. Ed.* 58: 3538–3541. b) Li, X., Kutta, R.J., Jandl, C. et al. (2020). *Angew. Chem. Int. Ed.* 59: 21640–21647. c) Wimberger, L., Kratz, T., and Bach, T. (2019). *Synthesis* 51: 4417–4424.

**106** Plaza, M., Jandl, C., and Bach, T. (2020). *Angew. Chem. Int. Ed.* 59: 12785–12788.

**107** Plaza, M., Großkopf, J., Breitenlechner, S. et al. (2021). *J. Am. Chem. Soc.* 143: 11209–11217.

**108** Shin, N.Y., Ryss, J.M., Zhang, X. et al. (2019). *Science* 366: 364–369.

**109** Großkopf, J., Plaza, M., Seitz, A. et al. (2021). *J. Am. Chem. Soc.* 143: 21241–21245.

**110** Kutta, R.J., Großkopf, J., van Staalduinen, N. et al. (2023). *J. Am. Chem. Soc.* 145: 2354–2363.

**111** Gu, Z., Zhang, L., Li, H. et al. (2022). *Angew. Chem. Int. Ed.* 61: e202211241.

# 15

# Covalent Interaction (S-/Sn-/B-Centered Radical)-Induced Asymmetric Radical Reactions

*Yee Lin Phang, Feng-Lian Zhang, and Yi-Feng Wang*

*Department of Chemistry, University of Science and Technology of China, Hefei, China*

## 15.1 Introduction

In modern synthetic chemistry, the exploration of asymmetric radical reactions has emerged as a cornerstone for the construction of intricate and architecturally diverse enantioenriched compounds. Among the myriad of asymmetric radical transformations enabled by organocatalysts, atom-centered radicals stand as a beacon of innovation, offering alternative pathways for asymmetric reactions. In the radical reactions induced by atom-centered radicals, as depicted in Scheme 15.1, the radical was initially added to the substrate through covalent bonding. Subsequently, the resulting radical intermediate underwent a series of radical transformations to deliver another radical species. Finally, an elimination reaction took place to release the final product while regenerating the atom-centered radical catalyst.

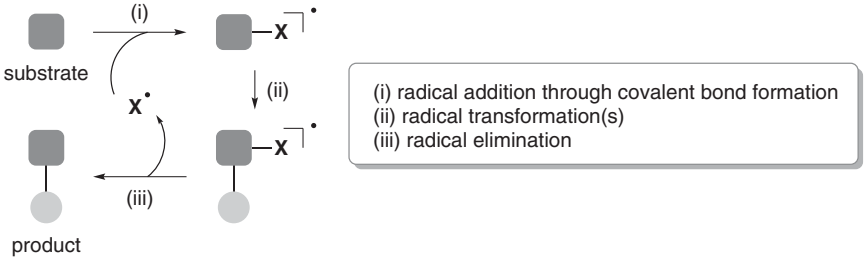


**Scheme 15.1** Atom-centered radical-induced radical reactions through covalent bonding.

In this catalytic cycle, there are two main ways in which asymmetric control could be achieved: *radical-controlled* or *substrate-controlled*. In the *radical-controlled* asymmetric reaction, a radical species bearing the chiral moiety is added to a racemic substrate through covalent bond formation. The chiral properties of this radical species guided the enantioselective control of the subsequent radical transformation steps through noncovalent interactions such as hydrogen bonding

or steric properties. For the *substrate-controlled* asymmetric reaction, an achiral radical species added to the chiral substrate, where the substrate played the role of determining the enantioselectivity of the subsequent reactions.

Hitherto, several efforts have been devoted to developing atom-centered radical-induced asymmetric radical reactions following the corresponding concept [1]. New methods and strategies were developed to control the enantioselectivity of radical reactions by the syntheses and applications of several chiral heteroatom-centered radicals, including the thiyl, stannyl, and boryl radicals [2, 3]. In addition, the enantioselective synthesis of natural products has also been achieved by asymmetric radical reactions, through which the enantioselective control was governed by the chiral substrate [4].

In this chapter, remarkable progress in the heteroatom-centered radical-induced asymmetric radical transformations was presented. The examples of those works were systematically discussed based on the types of radical species following the chronological order. A brief historical overview of the development of atom-centered radical-induced radical reactions was introduced in the following subsection.

## 15.2 Thiyl Radicals

The seminal work on atom-centered radical-induced reactions was disclosed by the Oshima group in 1988 [5]. In their pioneering study, a phenylthiyl or triphenylstannyl radical participated in an intramolecular [3 + 2] cycloaddition reaction to deliver five-membered carbocycles. As shown in Scheme 15.2, 1,3-butadienylcyclopropanes substituted with two electron-withdrawing groups were employed as the substrates and treated with azobisisobutyronitrile (AIBN), benzenethiol (PhSH) or triphenyltin hydride ($Ph_3SnH$) in benzene solution at 60 °C, constructing racemic products with vinylcyclopentene scaffold. Control experiments revealed that the presence of dienic moiety and two electron-withdrawing substituents was mandatory for the reaction.

The mechanism for this reaction was illustrated in Scheme 15.3. Initially, the thermal decomposition of radical initiator AIBN provided an isobutyronitrile radical

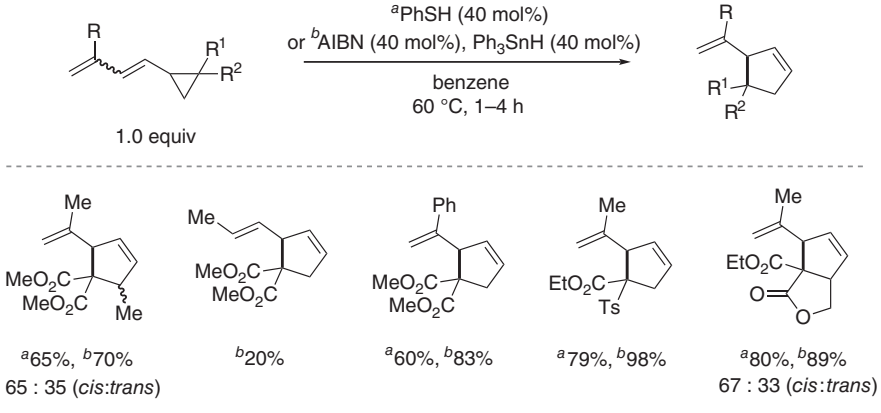


**Scheme 15.2** Intramolecular [3 + 2] cycloaddition of 1,3-butadienylcyclopropanes.

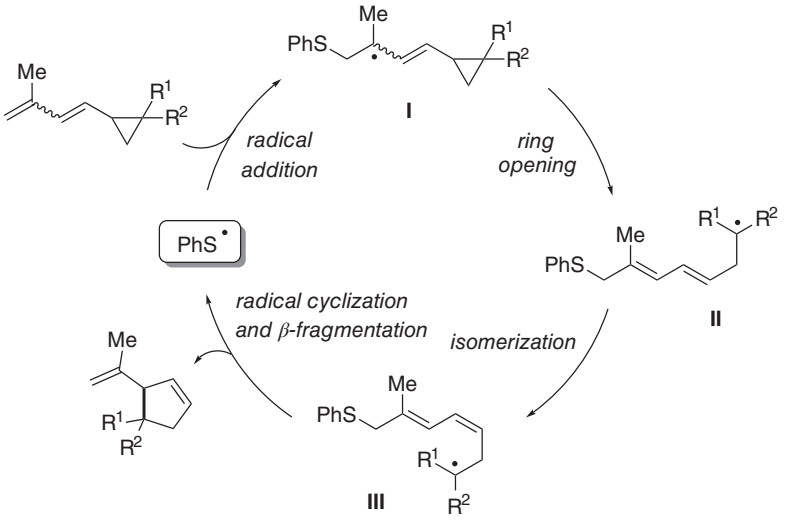


**Scheme 15.3** Proposed mechanism for the intramolecular [3 + 2] cycloaddition of 1,3-butadienylcyclopropanes.

that reacted with benzenethiol (or triphenyltin hydride) to deliver a phenylthiyl radical (or triphenylstannyl radical) as the active catalytic species. The addition of this phenylthiyl radical to the terminus of diene gave a new radical intermediate **I** that was prompted to a ring-opening process to generate electron-withdrawing groups-stabilized alkyl radical **II**. After double bond isomerization, the subsequent radical cyclization and $\beta$-fragmentation yielded the cyclopentene product exclusively without any seven-membered-ring product.

Oshima's study of the intramolecular radical [3 + 2] cycloaddition soon paved the way for the intermolecular version of the same reaction. In the same year, the groups of Oshima [6] and Feldman [7] independently developed a phenylthiyl radical-mediated intermolecular cycloaddition of vinylcyclopropanes and alkenes (Scheme 15.4). The reaction by Oshima involved the synthesis of cyclopentane derivatives from various substituted cyclopropanes and alkenes, mediated by a catalytic amount of benzenethiol at 60 °C. On the other hand, the Feldman group disclosed the radical cycloaddition between the vinylcyclopropanes and electron-poor alkenes. Notably, the reaction was still feasible with single-electron-withdrawing group-substituted vinylcyclopropanes. Complete regioselective control with moderate C1 : C3 *cis* stereoselectivity was achieved. The addition of 0.8 equivalents of trimethylaluminum, a Lewis acid, under low-temperature conditions could improve the stereoselectivity of this reaction.

The reaction mechanism of the intermolecular radical [3 + 2] cycloaddition is similar to that of the intramolecular version (Scheme 15.5). The sulfur atom-centered radical, generated from radical initiator, was added to the C—C double bond of vinylcyclopropane to afford a radical intermediate **I**, which underwent a ring-opening process to release the ring strain of a three-membered ring. The subsequent addition of this resulting radical **II** to an alkene delivered another alkyl radical **III** that was

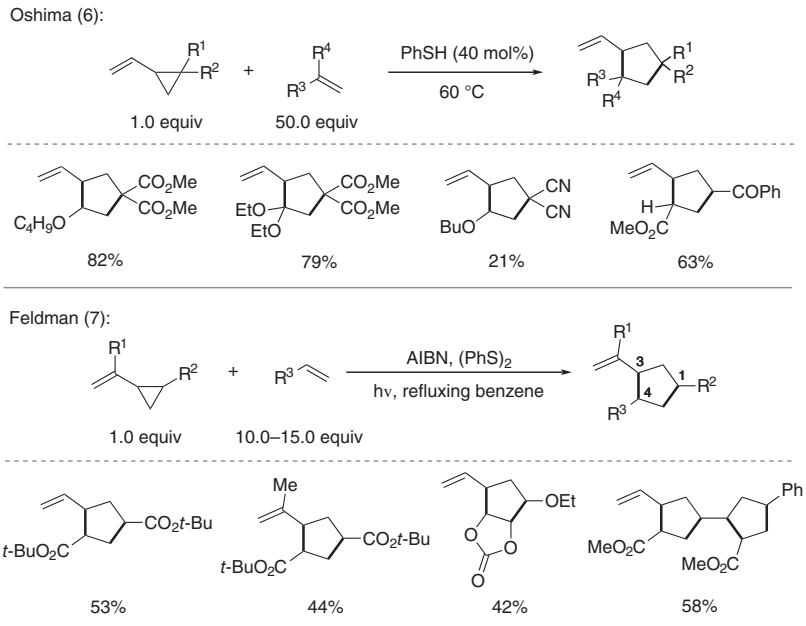


**Scheme 15.4** Intermolecular [3 + 2] cycloaddition of vinylcyclopropanes and alkenes.

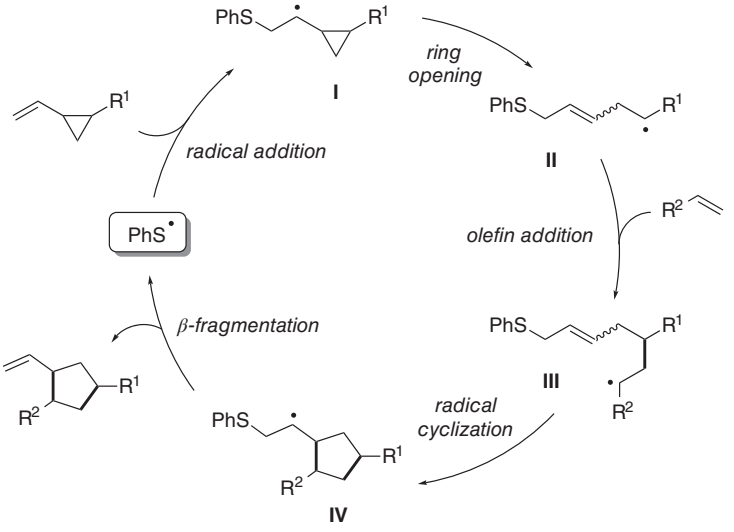


**Scheme 15.5** Proposed mechanism for the intermolecular [3 + 2] cycloaddition of vinylcyclopropanes and alkenes.

then intramolecularly cyclized with the pendent alkene. Further $\beta$-fragmentation of radical **IV** released the final product while regenerating the active thiyl radical species.

Since the initial disclosure of the intermolecular [3 + 2] cycloaddition of vinylcyclopropanes and functionalized alkenes, the Feldman group continued to expand

their interest by investigating various substrate scopes of this reaction [8–13]. During this time, they proposed the synthesis of chiral binaphthyldisulfide as an enantiopure radical precursor to enable the asymmetric variant of the developed [3 + 2] cycloaddition reaction [1]. As indicated by the molecular modeling studies, the covalently bound thiyl radical could form a chiral cleft as defined by its steric properties. This imparts a conformational bias on the enantiofacial selectivity of the bond-forming process.

Structurally, the designed chiral disulfide pre-catalyst is characterized by two linked naphthalene rings. One of these rings is substituted with two phenyl rings that are positioned *para* to each other. Starting with naphthylpropyne and diphenylisobenzofuran, the substituted binaphthyl core was constructed through the Diels-Alder reaction and oxygen extrusion (Scheme 15.6). Conversion of iodide to thiol in the presence of *tert*-butyl lithium, sulfur, and lithium aluminum hydride afforded a racemic thiol intermediate. The sequential transformation of this thiol to its Mosher ester derivative enabled chiral resolution to deliver two thiol enantiomers after ester hydrolysis. Finally, the dimerization of thiol with *tert*-butyl hydroperoxide led to the binaphthyldisulfide pre-catalyst. Unfortunately, the asymmetric [3 + 2] cycloaddition reaction mediated by this chiral thiol catalyst was not reported.

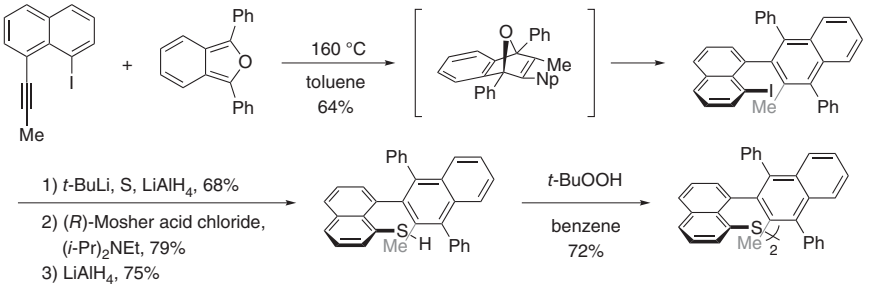


**Scheme 15.6** Synthesis of chiral binaphthyldisulfide via resolution.

The important contribution to asymmetric radical reactions was then reported by Roberts through his introduction of the concept of polarity reversal catalysis [14–17]. In his efforts to achieve enantioselective hydrosilylation and enantioselective carboxyalkylation of prochiral alkenes, homochiral thiol was employed as a polarity reversal catalyst for enantioselective hydrogen atom abstraction (Scheme 15.7) [18]. As illustrated, the reaction proceeded through hydrogen atom abstraction of the silane by thiyl radical. The resulting silyl radical added to the alkene substrate to form a $\beta$-silylalkyl radical. Since this alkyl radical is prochiral, the subsequent hydrogen atom transfer from a chiral thiol catalyst was envisioned to produce an enantioselective product.

Having this concept in mind, the Roberts team reported an enantioselective radical-chain hydrosilylation of prochiral alkenes using chiral thiol catalysts [19]. Treatment of methylene tetrahydropyranone with di-*tert*-butyl hyponitrite (TBHN)

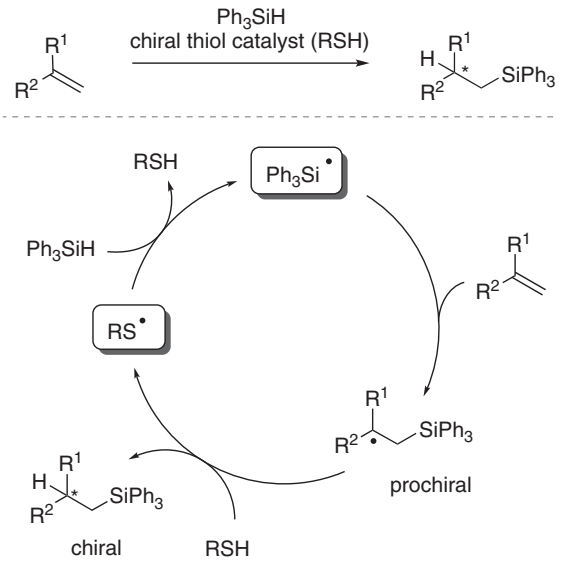


**Scheme 15.7** Proposed mechanism for asymmetric hydrosilylation.

as initiator, triphenylsilane and chiral thiol as catalyst, resulted in sequential hydrogen atom abstraction process to furnish the corresponding hydrosilylation product (Scheme 15.8). Four chiral thiol pre-catalysts were screened, including the commercially available thiocholesterol (catalyst **A**), 2,3,4,6-tetra-*O*-acetyl-l-thio-$\beta$-D-glucopyranose (**B**), neomenthyl mercaptan (**C**) and thiol **D** derived from (1*R*)-(+)-camphor. Unfortunately, low enantiomeric excess (ee) was generally obtained from these reactions, except with the carbohydrate-thiol pre-catalyst **B**, which exhibited moderate enantioselective control (40% ee in 1,4-dioxane and 50% ee in hexane).

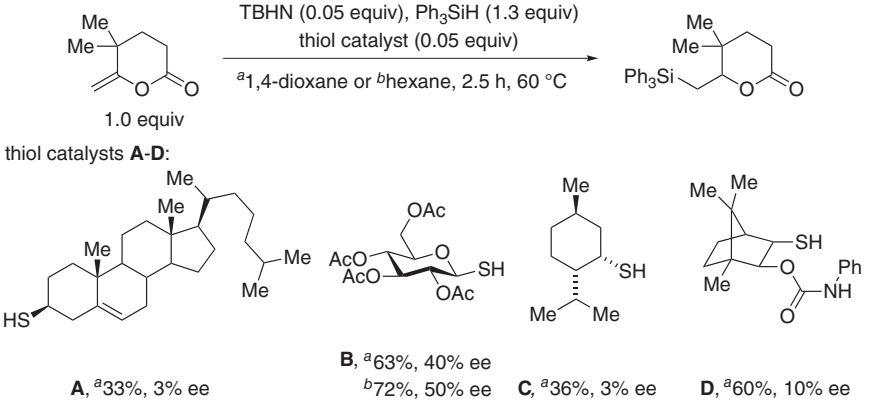


**Scheme 15.8** Screening of chiral thiol pre-catalysts on asymmetric hydrosilylation of methylene tetrahydropyranone.

Given the moderate yield and enantioselectivity of the hydrosilylation reaction catalyzed by thiyl catalyst **B**, the Roberts group further screened several chiral carbohydrates bearing a thiol group at the anomeric position (Scheme 15.9) [20]. Replacing the $\beta$-glucopyranose thiol (catalyst **B**) with $\beta$-mannopyranose thiol (catalyst **E**) resulted in an enhancement of both yield and ee of the reaction. Specifically, the yield increased from 72% to 84%, and the ee was improved from 50% to 76%. Moreover, the substrate with an increased steric bulk provided by the geminal diphenyl substituents was evidenced to raise the yield to 90% with 95% ee. In contrast to the reaction where *tert*-dodecanethiol served as the pre-catalyst, the carbohydrate-derived thiol resulted in a higher chemical yield. This was attributed to the relatively high-electrophilic nature of the corresponding thiyl radicals as well as the stronger S—H bond strength owing to the presence of electronegative oxygen atoms in the thiol compound.

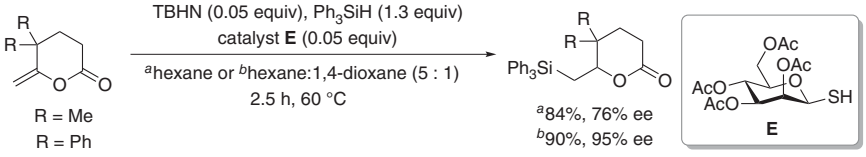


**Scheme 15.9** Asymmetric hydrosilylation of methylene tetrahydropyranone catalyzed by carbohydrate-derived thiol.

Since the emergence of the polarity reversal catalysis concept for the enantioselective hydrosilylation using homochiral thiols in the 1990s, a glaring gap was observed in atom-centered radical-induced asymmetric radical reactions until 2014. In that year, the Maruoka group accomplished a diastereo- and enantioselective [3 + 2] cyclization of electron-deficient vinylcyclopropanes and alkenes, delivering highly substituted cyclopentane products. Similar to Feldman's idea of chiral binaphthyldisulfide pre-catalyst [1], pre-catalysts with binaphthyl-based scaffold (catalyst **F**) were designed by the group of Maruoka (Scheme 15.10) [21].

In the initial study outlined in Scheme 15.10, the treatment of dibenzyl vinylcyclopropanedicarboxylate and *tert*-butyl vinyl ether with chiral thiyl catalyst generated from photolytic homolysis of binaphthyldisulfide $\mathbf{F_I}$, furnished the desired product mostly in its *trans* configuration. This reaction exhibited a high yield of 89% and a diastereomeric ratio (dr) of 80 : 20. A slight preference over a single enantiomer was observed, as reflected by the 13% ee of the isolated product. It was proposed that the diastereoselectivity of this reaction was not affected by thiyl radical-mediated hydrogen atom abstraction after the radical cyclization step as the reaction with diphenyl disulfide pre-catalyst gave products with similar dr (83 : 17 dr) despite lower yield (59%). Increasing the steric bulk around the silicon atom by replacing the trimethyl silyl (TMS) group (catalyst $\mathbf{F_I}$) with the triisopropyl silyl (TIPS) group (catalyst $\mathbf{F_{II}}$) seemed to enhance the enantioselective control (25% ee). Nevertheless, attempts to synthesize bulkier disulfides failed.

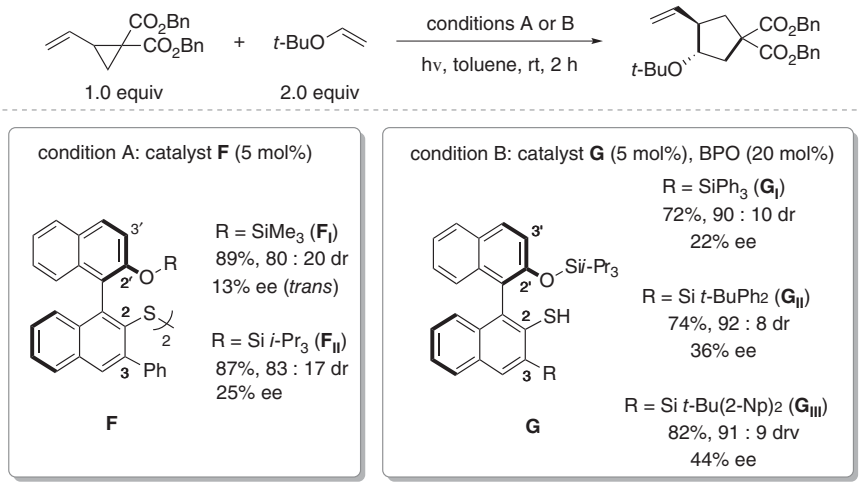


**Scheme 15.10** Screening of chiral disulfide and thiol catalyst for asymmetric [3 + 2] cycloaddition.

The solution to this challenge was the alternative method to generate thiyl radical through photoirradiation of chiral thiol (catalyst **G**) in the presence of benzoyl peroxide (BPO), likely to be an oxidant (condition B, Scheme 15.10). Fixing the TIPS ether group on one of the naphthyl rings (C-2′), the phenyl moiety on the other naphthyl ring (C-3) was substituted by several sterically encumbered silyl groups. For instance, thiols $\mathbf{G_{II}}$ and $\mathbf{G_{III}}$ with a diaryl(*tert*-butyl)silyl group substituted at C-3 increased the enantioselective control of the reaction to 36% and 44% ee, respectively. Remarkably, the diastereoselectivity was also improved with catalysts $\mathbf{G_{I\text{-}III}}$.

Subsequent trials to enhance the enantioselectivity through this binaphthyl-based thiol catalyst proved futile, prompting the design of a chiral catalyst with a new molecular scaffold. Based on the stereochemical model to rationalize the observed stereoselectivity of the reaction, the bulky silyl group at the C-3 position of catalyst **G** effectively blocked the first and second quadrants around the sulfur atom (Scheme 15.11). The third quadrant, on the other hand, was poorly occupied by the TIPS ether group, possibly accounting for the moderate enantioselectivity of the cycloaddition reaction. With this conjecture, the authors designed an indanol-based chiral thiol catalyst that effectively blocked the third quadrant by an aryl group at C-1. While all three quadrants were blocked with different bulky groups, the alkyl radical was confined to a chiral pocket that allowed the reaction to take place stereochemically.

Subsequently, the indanol-based chiral thiol catalysts with diverse substituents on the C-1 aryl and diaryl-(*tert*-butyl)silyl groups were screened for their control over diastereoselectivity and enantioselectivity. Catalyst $\mathbf{H_{optimized}}$ bearing a 10-butyl-9-anthryl group at the 3,5-positions of the C-1 aryl group, and two 4-(trifluoromethyl)phenyl groups-substituted silyl moiety was found to be the ideal catalyst (Scheme 15.12). The reaction optimization studies revealed that the cycloaddition between dibenzyl vinylcyclopropanedicarboxylate and *tert*-butyl

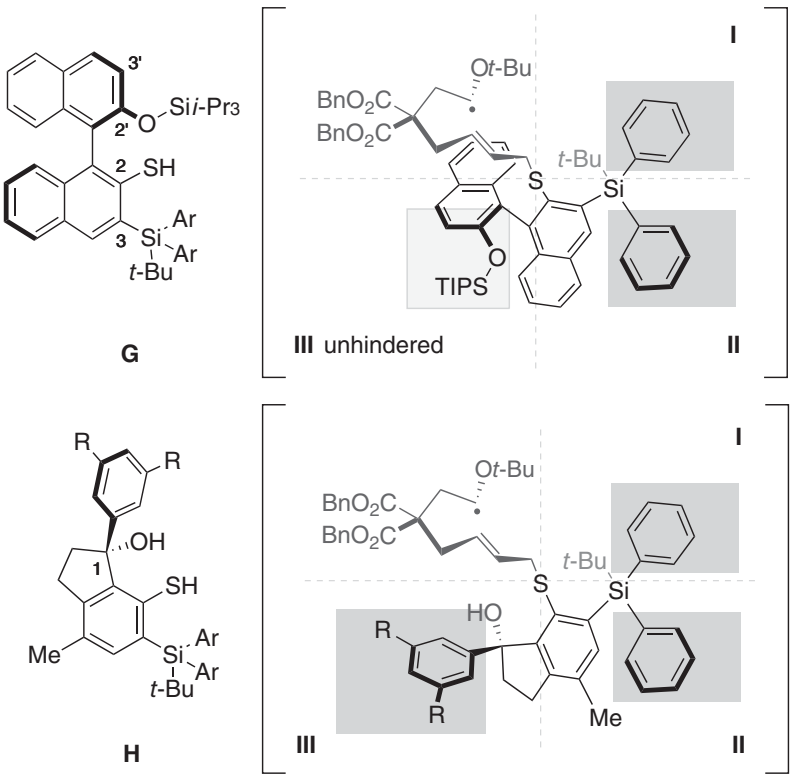


**Scheme 15.11** Stereochemical model of the transition states leading to cyclization by catalysts **G** and **H**.

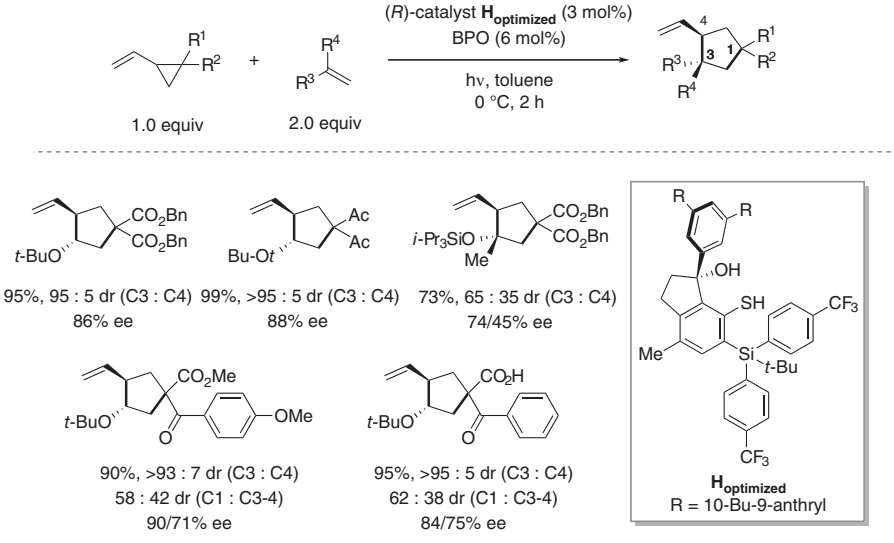


**Scheme 15.12** Asymmetric [3 + 2] cycloaddition catalyzed by indanol-based chiral thiol.

vinyl ether, catalyzed by catalyst $\mathbf{H_{optimized}}$ in the presence of BPO under UV lamp at 0 °C for 2 hours yielded the cyclopentane product in 95% yield with excellent diastereoselectivity (95 : 5 dr) and high enantioselectivity (86% ee). Vinylcyclopropanes substituted with diesters or diketones delivered products with comparable stereoselectivity. The reaction of vinylcyclopropanes substituted with the keto ester unit also demonstrated excellent control over the C-3 and C-4 stereocenters despite the poorly controlled C-1 stereocenters.

Recently, the group of Miller developed a cysteine-based disulfide-catalyzed enantioselective [3 + 2] cycloaddition of substituted vinylcyclopropanes and alkenes [22]. As opposed to the steric blocking strategy to achieve enantioselective control reported by Maruoka, this work focused on the use of noncovalent interactions, for instance, the hydrogen bonding provided by multiple amide structures in the peptide linkage. Screening of the various peptide-based catalysts, such as catalysts **I** and **J**, revealed no effective control over enantioselectivity despite moderate diastereoselective control (Scheme 15.13). It was postulated that the chiral information on the catalyst lay distantly from the radical intermediate, and an extended substituent at the C-4 position of proline may enhance the stereochemical communication. Indeed, the use of catalyst **K** proved to deliver the cyclopentane products with increased enantioselectivity of both diastereomers.

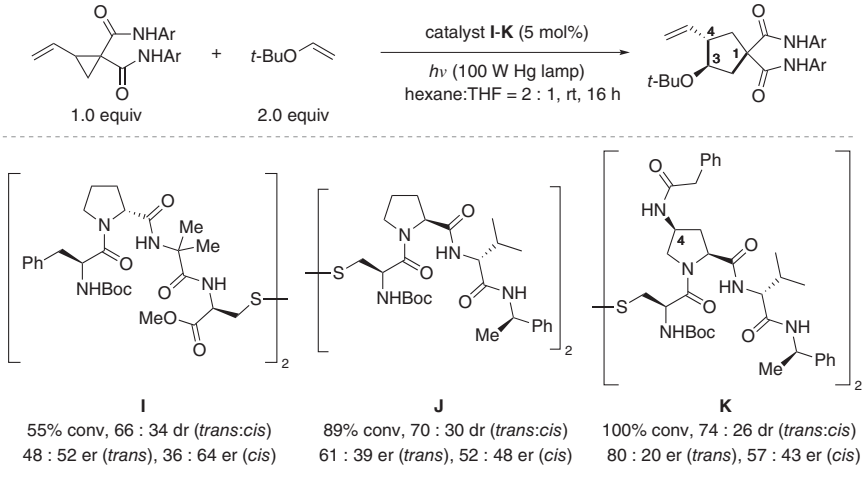


**Scheme 15.13** Screening of chiral disulfide-bridged peptides for asymmetric [3 + 2] cycloaddition.

Further screening of various substituents at the C-4 position of cysteine-based dimers demonstrated that the presence of amide holds greater potential for achieving high levels of enantioselectivity, among which catalyst **L** bearing a diphenylmethylacetamide moiety was the optimized catalyst (Scheme 15.14). The reaction of diverse diamide-substituted vinylcyclopropanes with *tert*-buyl vinyl ether proceeded smoothly to give the desired cyclopentane products, with a higher yield and enantioselectivity on *trans* diastereomers compared to the *cis* diastereomers. The use

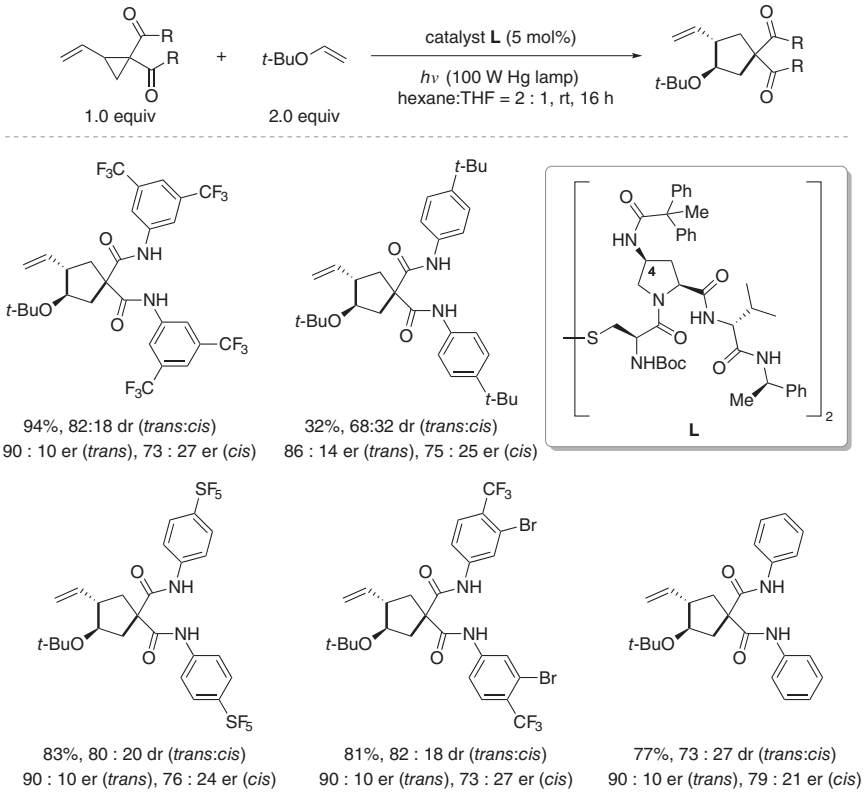


**Scheme 15.14** Asymmetric [3 + 2] cycloaddition catalyzed by chiral disulfide-bridged peptide: substrate scope of vinylcyclopropanes.

of diester-substituted vinylcyclopropanes as substrates delivered a nearly racemic product, which was reasoned to be related to the hydrogen-bonding interactions with the peptide catalyst. Electron-rich alkenes bearing an $\alpha$-heteroatom were proved to be a polarity-matched partner to react with the electron-deficient $\alpha$-dicarbonyl radical intermediate (Scheme 15.15).

An in-depth kinetic analysis of this cysteine-derived thiyl radical-catalyzed cycloaddition reaction was carried out by the same group [23]. As illustrated in Scheme 15.16, the ring opening of vinylcyclopropanes after thiyl radical addition was likely a rate- and enantio-determining step to furnish the intermediate **I** with either (*R*)- or (*S*)-configuration (the latter was not depicted for clarity). The varied binding modes of vinylcyclopropanes to the catalyst and the differing reactivity of intermediate **I** accounted for the stereochemical outcomes of the products. In addition, this pair of enantiomeric intermediates also determined the stereochemistry at the vinyl group of alkenes, as influenced by the steric properties of the C-4 proline substituent. Subsequently, the cyclization of radical species **II** was diastereodetermining on the configuration *tert*-butoxy group. Then, the final $\beta$-fragmentation redelivered the thiyl radical catalyst.

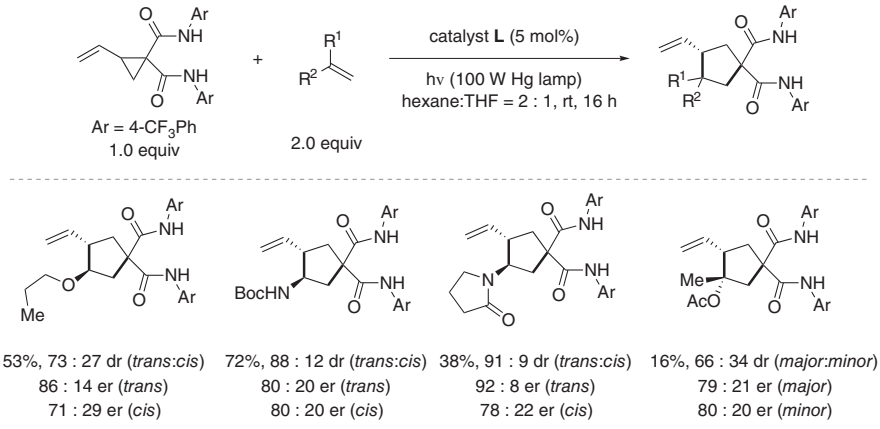


**Scheme 15.15** Asymmetric [3 + 2] cycloaddition catalyzed by chiral disulfide-bridged peptide: substrate scope of alkenes.

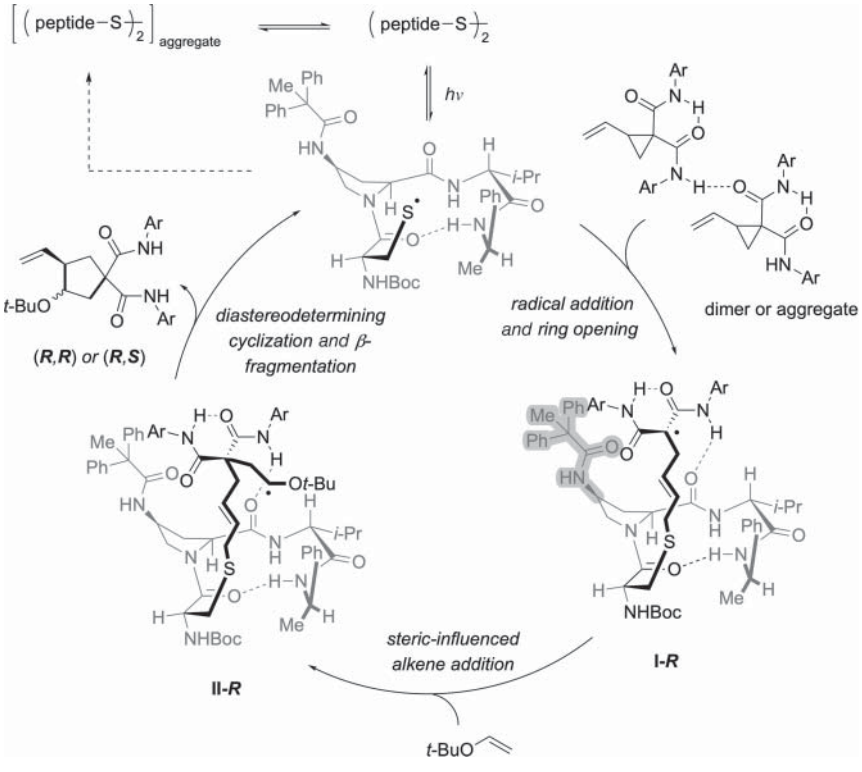


**Scheme 15.16** Proposed mechanism for the stereochemical control of intermolecular [3 + 2] cycloaddition catalyzed by disulfide-bridged peptide.

As a promising strategy to synthesize highly functionalized cyclopentane frameworks, the Gong and Yang research team envisioned that the [3 + 2] cycloaddition of vinylcyclopropanes and alkenes might be a key step in forging an intermediate that allowed access to the asymmetric total synthesis of (−)-pavidolide B (Scheme 15.17) [4]. Initially, they attempted the reaction under palladium catalysis by screening various phosphine ligands. Unfortunately, no reaction or decomposition of the substrates was observed in most cases. Thus, the attention was shifted to radical-mediated cyclization reaction. Generation of the thiyl radical species through thermal conditions or irradiation by either ultraviolet or visible light afforded the desired cyclopentane product. The optimized reaction condition was found to be the visible light irradiation of phenythiol in the presence of an iridium photocatalyst. Remarkably, the poor diastereoselectivity on the C-12 of substrate (1.5 : 1 dr) would not affect the following cyclization step.

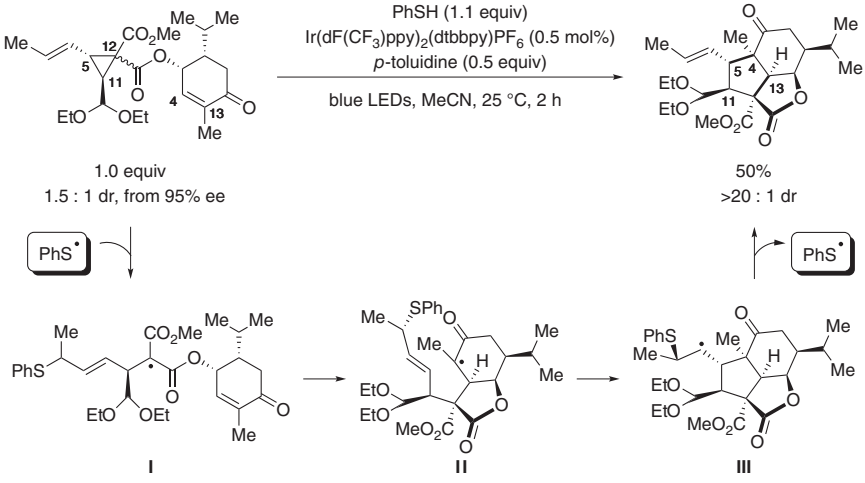


**Scheme 15.17** Synthesis of a key intermediate of (−)-pavidolide B via thiyl radical catalysis.

This substrate-controlled asymmetric thiyl radical reaction was initiated through the addition of phenylthiyl radical on the vinyl moiety to deliver the diester-stabilized tertiary alkyl radical **I** (Scheme 15.17). Notably, the reaction with only monoester-substituted vinylcyclopropane led to the decomposition of the radical intermediate. Then, *5-exo* conjugate addition took place, resulting in intermediate **II** with fixed stereocenters at C-12 and C-13. Another cyclization of **II** afforded species **III** with a *trans* relationship between C-5 and C-11. At this point, two rings with four consecutive stereocenters were forged. The final $\beta$-elimination released the phenylthiyl radical.

## 15.3 Stannyl Radicals

In 2013, the Maruoka group disclosed an enantioselective radical cyclization of aldehydes catalyzed by chiral organotin hydride, with silyl hydride acting as a stoichiometric reducing agent and AIBN as the radical initiator (Scheme 15.18) [24]. Under the treatment of (*S*)-catalyst **M**, the aldehyde substrates were converted to the corresponding chromanol derivatives in good yield and diastereoselectivity, albeit with moderate enantioselectivity. This reaction was also applicable to the synthesis of other heteroatom-containing six-membered rings, including chiral thiochroman and tetrahydroquinoline compounds.

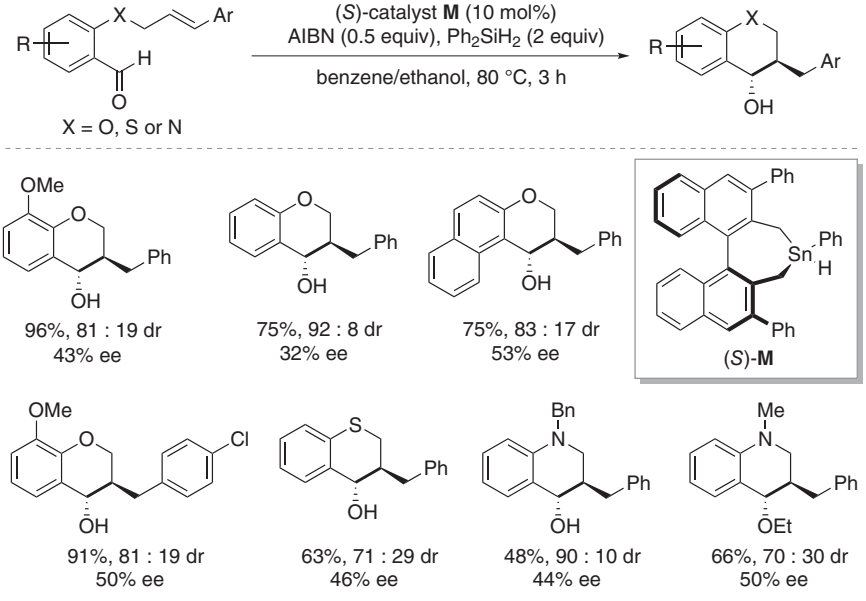


**Scheme 15.18** Asymmetric radical cyclization of aldehydes catalyzed by chiral organotin hydride.

The mechanism of this reaction was proposed in Scheme 15.19. The stannyl radical, generated from radical initiation of chiral organotin hydride by AIBN, selectively added to the carbonyl oxygen of aldehyde to deliver an *O*-stannyl ketyl radical **I**, which then underwent an intramolecular radical cyclization stereoselectively. The resulting radical species **II** abstracted a hydrogen atom from the chiral tin catalyst, forming the organotin alkoxide **III** and a regenerated stannyl radical. The subsequent reaction with ethanol converted intermediate **III** to the final product while releasing tin ethoxide. Reduction of this stannane reagent by stoichiometric diphenylsilane regenerated organotin hydride catalyst.

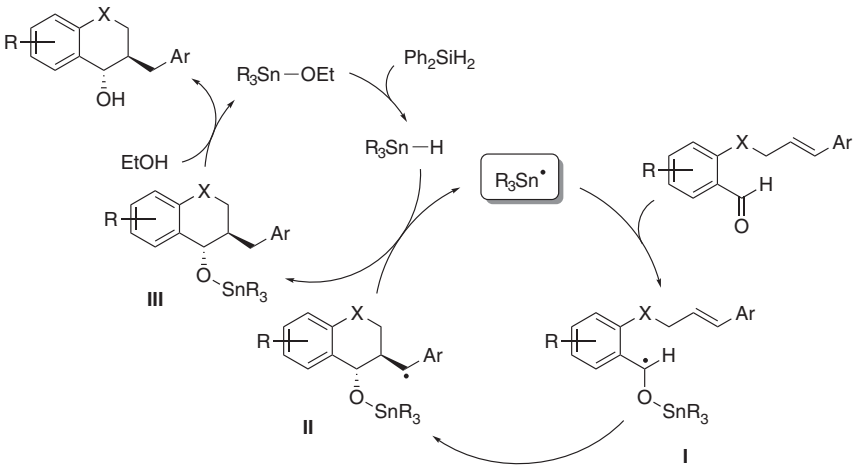


**Scheme 15.19** Proposed mechanism for asymmetric cyclization of aldehydes.

## 15.4 Boryl Radicals

In the ongoing effort to practice the concept of polarity reversal catalysis through enantioselective hydrogen atom abstraction, the Roberts group discovered that an optically active amine-boryl radical could abstract an electron-deficient $\alpha$-hydrogen from the ester substrate [25]. As the enantiomeric pairs of the chiral ester exhibited different reactivity toward the boryl-radical species, the kinetic resolution of the substrate could be realized [26]. In the work reported by Roberts in 1993, it was observed that exposure of amine borane to photolysis of di-*tert*-butyl peroxide (DTBP) led to chiral amine boryl radical through hydrogen atom abstraction. Then, the abstraction of the $\alpha$-C-H hydrogen of the racemic ester was facilitated by the amine-boryl radical (Scheme 15.20). After 75% of the substrate was consumed, the remaining substrate

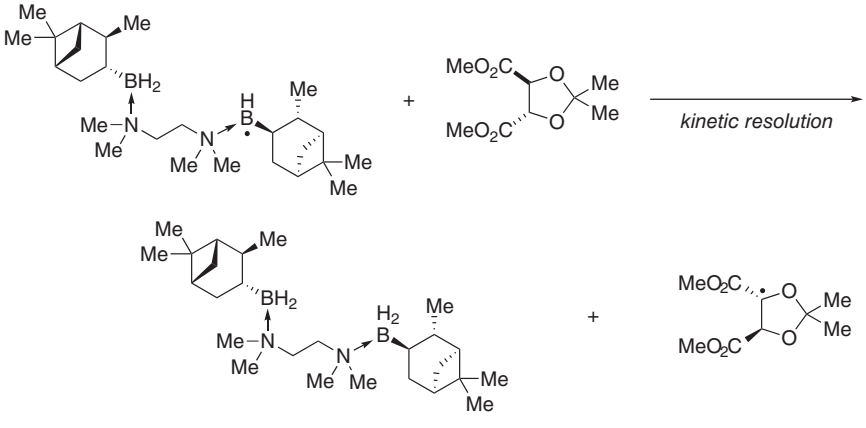


**Scheme 15.20** Kinetic resolution of esters catalyzed by chiral amine-boryl radical.

was found to have a 97% ee in favor of the (*R*,*R*)-enantiomer, allowing the resolution of racemic ester to take place.

In 2019, the Wang group disclosed an *N*-heterocyclic carbene (NHC)-boryl radical-catalyzed cycloisomerization of *N*-(2-ethynylaryl)arylamides to build a quinolinone framework through carbon–carbon triple bond reorganization [27]. Taking advantage of the large library of readily accessible chiral NHCs, the authors envisioned that a conceptually distinct catalytic reaction could be developed to facilitate asymmetric radical reactions. This is in contrast to the chiral sulfur-based pre-catalyst which required tedious preparation steps. In recent study, the team reported a chiral NHC-boryl radical-catalyzed asymmetric cycloisomerization reaction of *N*- or *O*-benzyl homopropargyl amines utilizing 1,1′-azobis(cyclohexanecarbonitrile) (ACCN) as radical initiator, forging pyrrolidines or tetrahydrofurans in high to excellent control of geometric isomerism and enantioselectivity (Scheme 15.21) [28].

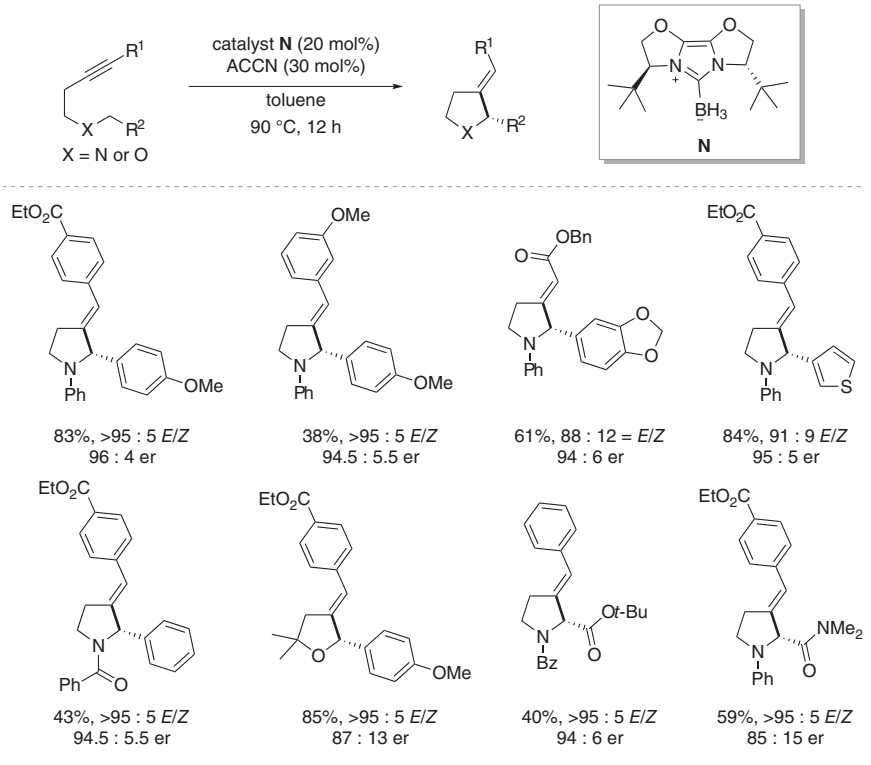


**Scheme 15.21** Asymmetric cycloisomerization of *N*- or *O*-benzyl homopropargyl amines by NHC-boryl radical.

The reaction was initiated by the addition of the boryl radical to the alkyne moiety to afford the alkenyl radical intermediate **I** (Scheme 15.22). The selective addition of boryl radical to either terminus of alkyne moiety was affected by the radical-stabilizing effect of alkynyl substituents [27, 29, 30]. Notably, this

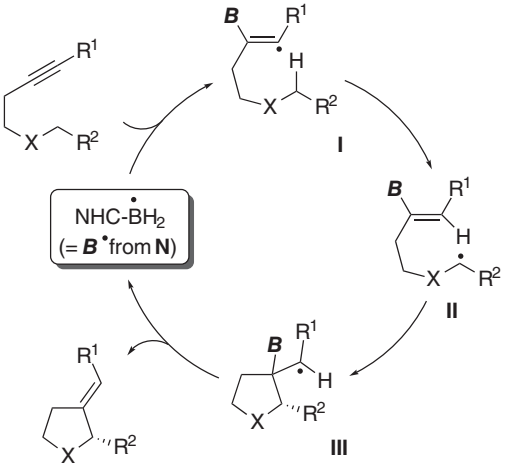


**Scheme 15.22** Proposed mechanism for radical cycloisomerization reaction involving 1,6-hydrogen atom transfer.

nucleophilic radical addition reaction proceeded with higher yield when the $R^1$ substituent was an electron-deficient aryl ring. Subsequent 1,6-hydrogen atom transfer was promoted by stabilization of the $R^2$ group, generating an intermediate **II** in a preferred *trans* relationship due to steric control. Cyclization of **II** to **III** then proceeded under asymmetric induction of bulky *tert*-butyl of oxazole ring, which then led to five-membered rings with excellent ee over the *R*-isomer. Last, the radical elimination step occurred with high stereoselectivity as both $R^1$ and $R^2$ groups of **III** preferred to stay apart from each other to avoid steric congestion; hence, the *E*-isomer was obtained as the major product while regenerating the catalyst.

In addition, the Wang group demonstrated a radical cycloisomerization reaction of *N*-benzyl-indol-7-yl propiolates to afford pyrrolo[3,2,1-*ij*]quinolines (Scheme 15.23) [28]. In this reaction, an aminoindanol-derived NHC-borane was used as a pre-catalyst while the radical initiator was changed to 2,2′-azobisisoheptonitrile (ABVN). Similarly, the reaction proceeded with high to excellent ee. The presence of the methoxycarbonyl group was necessary to enable an efficient boryl radical addition step, as switching to other functionality led to no desired product at all.

The proposed mechanism was illustrated in Scheme 15.24. After radical initiation by ABVN, the boryl radical added to the alkyne moiety of substrate to deliver an alkenyl radical **I**. The formation of the more stabilized benzyl radical **II** then drove the 1,5-hydrogen atom transfer reaction forward. Similarly, the *trans* isomer of **II** was preferentially generated. The ensuing 6-*endo-trig* cyclization of **II** delivered an intermediate **III** with excellent enantioselective control governed by noncovalent interaction. The subsequent elimination of the radical species completed the catalytic cycle by releasing the final product. By introducing chirality on the boryl radical species, the stereoselective control in a radical reaction was governed by the radical itself but not the substrates. This allows broad substrate scope tolerance while

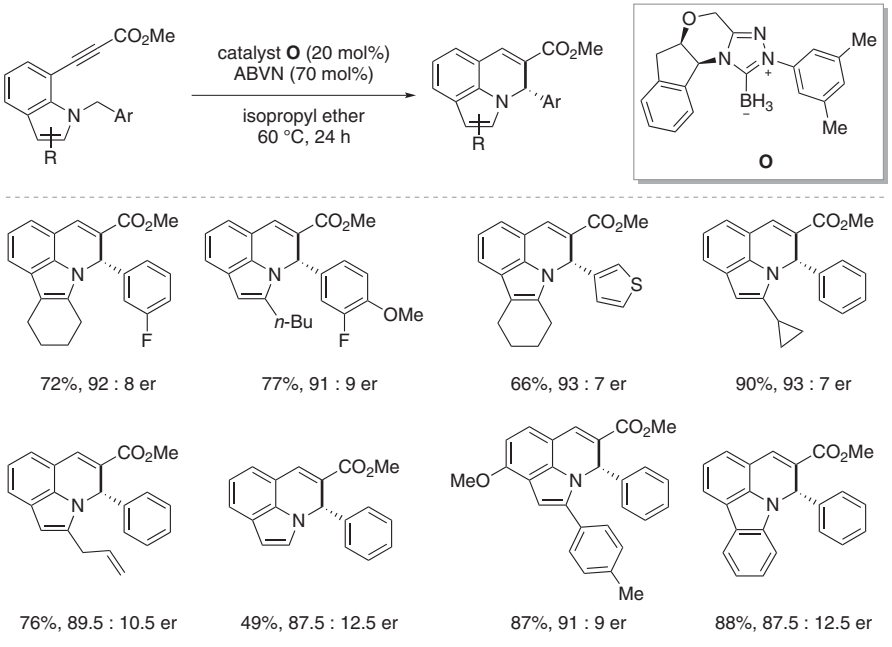


**Scheme 15.23** Asymmetric cycloisomerization of *N*-benzyl-indol-7-yl propiolate by NHC-boryl radical.

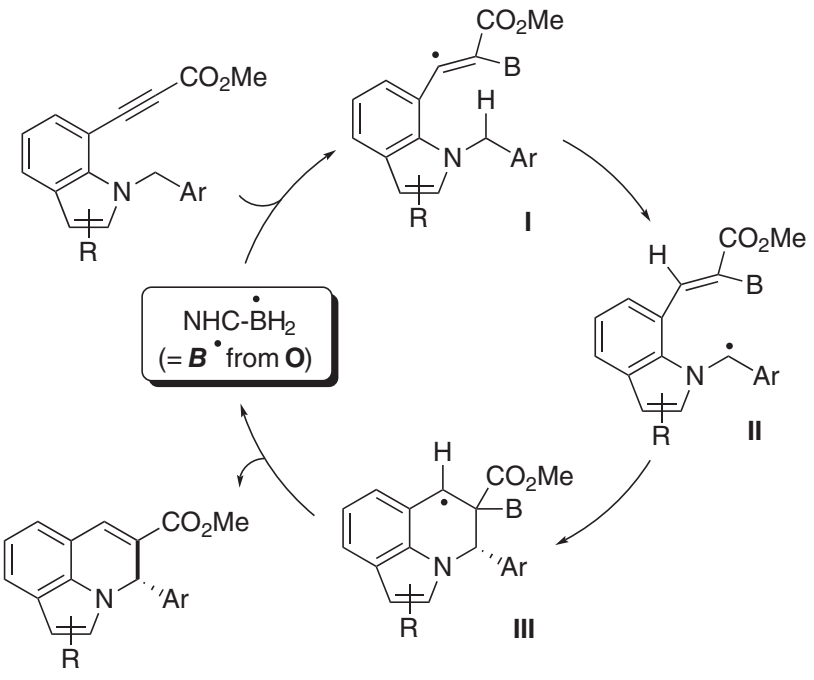


**Scheme 15.24** Proposed mechanism for radical cycloisomerization reaction involving 1,5-hydrogen atom transfer.

offering high enantioselectivity. The authors speculated that the chiral NHC-boryl radicals may offer great opportunities in enantioselective radical catalysis.

In the attempt to accomplish an intermolecular enantioselective boryl radical-catalyzed reaction, the Wang group demonstrated that this asymmetric NHC-boryl radical catalysis could also apply to a three-component cyclization reaction [28]. This [2 + 2 + 2] cyclization reaction was previously accomplished by stannyl radical catalysis, delivering products as regioisomeric and diastereomeric mixtures [31]. Exposure of adamantan-1-yl propiolate to 10 equivalents of 4-fluorostyrene, boryl radical pre-catalyst **N** and TBHN resulted in chiral six-membered rings (Scheme 15.25). Albeit in lower yield, the product featured a high diastereoselective and enantioselective ratio.

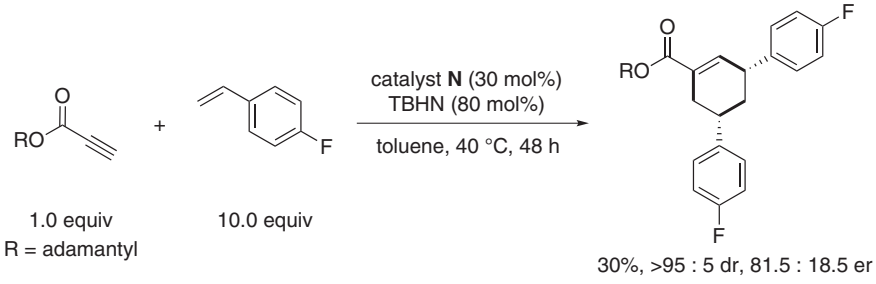


**Scheme 15.25** Asymmetric [2 + 2 + 2] cyclization of propiolate and styrene catalyzed by chiral NHC-boryl radical.

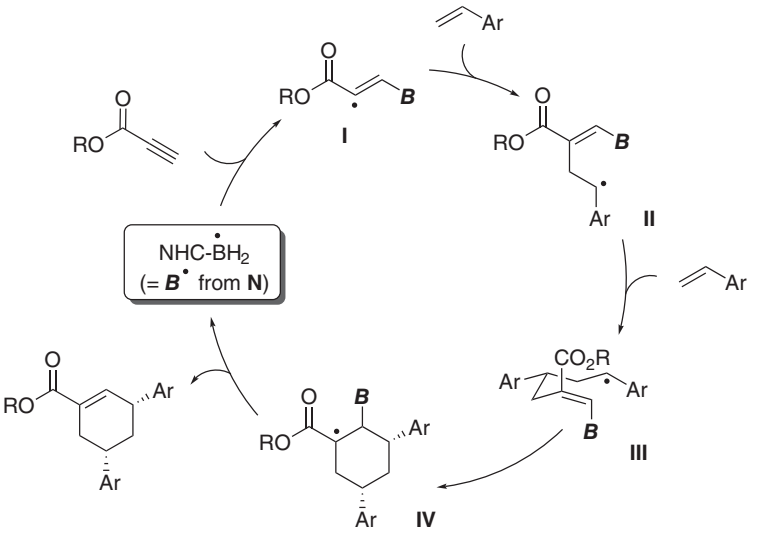


**Scheme 15.26** Proposed mechanism for the intermolecular [2 + 2 + 2] cyclization.

The [2 + 2 + 2] cyclization was proposed to proceed through a catalytic cycle shown in Scheme 15.26. The radical addition of imidazolyl-NHC boryl radical to the alkynyl terminus of propiolate delivered an alkenyl radical species **I**. The following addition to one molecule of alkene provided a new alkyl radical **II** that was then added to the second molecule of alkene to deliver the aryl-stabilized radical species **III**. The intramolecular radical cyclization provided the cyclohexane ring **IV**, which then released the final product via the $\beta$-elimination process.

## 15.5 Conclusions

In this chapter, the exploration of atom-centered radicals in asymmetric radical reactions has been discussed. The unique reactivity and enantioselectivity of these radicals compared to other approaches offered a versatile platform for the development of novel and efficient synthetic methodologies. As evidenced by the successful applications across multiple chemical transformations, including the [3 + 2] cycloadditions, hydrosilylations, aldehyde cyclizations, and cycloisomerizations, heteroatom-centered radicals hold great promise and underexplored potential to unlock new avenues for the synthesis of enantioenriched compounds. Despite impressive efforts presented, relentless efforts to expand the types of reactions and scope of substrates are in high demand.

## References

**1** Feldman, K.S., Ruckle, R.E., Ensel, S.M., and Weinreb, P.H. (1992). *Tetrahedron Lett.* 33: 7101–7102.

2 Xiao, W. and Wu, J. (2023). *ChemCatChem* 15: e202300541.
3 Phang, Y.L., Zhang, F.-L., and Wang, Y.-F. (2024). *ARKIVOC* 2: 202312052.
4 Zhang, P., Li, Y., Yan, Z. et al. (2019). *J. Org. Chem.* 84: 15958–15971.
5 Miura, K., Fugami, K., Oshima, K., and Utimoto, K. (1988). *Tetrahedron Lett.* 29: 1543–1546.
6 Miura, K., Fugami, K., Oshima, K., and Utimoto, K. (1988). *Tetrahedron Lett.* 29: 5135–5138.
7 Feldman, K.S., Romanelli, A.L., Ruckle, R.E., and Miller, R.F. (1988). *J. Am. Chem. Soc.* 110: 3300–3302.
8 Feldman, K.S. and Fisher, T.E. (1989). *Tetrahedron* 45: 2969–2977.
9 Feldman, K.S. and Simpson, R.E. (1989). *J. Am. Chem. Soc.* 111: 4878–4886.
10 Feldman, K.S., Ruckle, R.E., and Romanelli, A.L. (1989). *Tetrahedron Lett.* 30: 5845–5848.
11 Feldman, K.S., Romanelli, A.L., Ruckle, R.E., and Jean, G. (1992). *J. Org. Chem.* 57: 100–110.
12 Feldman, K.S., Berven, H.M., and Weinreb, P.H. (1993). *J. Am. Chem. Soc.* 115: 11364–11369.
13 Feldman, K.S. (1995). *Synlett* 1995: 217–225.
14 Paul, V. and Roberts, B.P. (1987). *J. Chem. Soc., Chem. Commun.* 1322–1324.
15 Paul, V. and Roberts, B.P. (1988). *J. Chem. Soc., Perkin Trans. 2* 1183–1193.
16 Paul, V., Roberts, B.P., and Willis, C.R. (1989). *J. Chem. Soc., Perkin Trans. 2* 1953–1961.
17 Kaushal, P., Mok, P.L.H., and Roberts, B.P. (1990). *J. Chem. Soc., Perkin Trans. 2* 1663–1670.
18 Roberts, B.P. (1999). *Chem. Soc. Rev.* 28: 25–35.
19 Haque, M.B. and Roberts, B.P. (1996). *Tetrahedron Lett.* 37: 9123–9126.
20 Haque, M.B., Roberts, B.P., and Tocher, D.A. (1998). *J. Chem. Soc., Perkin Trans. 1* 2881–2890.
21 Hashimoto, T., Kawamata, Y., and Maruoka, K. (2014). *Nat. Chem.* 6: 702–705.
22 Ryss, J.M., Turek, A.K., and Miller, S.J. (2018). *Org. Lett.* 20: 1621–1625.
23 Turek, A.K., Sak, M.H., and Miller, S.J. (2021). *J. Am. Chem. Soc.* 143: 16173–16183.
24 Shirakawa, S., Usui, A., Kan, S.B.J., and Maruoka, K. (2013). *Asian J. Org. Chem.* 2: 916–919.
25 Mok, P.L.H. and Roberts, B.P. (1992). *Tetrahedron Lett.* 33: 7249–7252.
26 Mok, P.L.H., Roberts, B.P., and McKetty, P.T. (1993). *J. Chem. Soc., Perkin Trans. 2* 665–674.
27 Xu, A.-Q., Zhang, F.-L., Ye, T. et al. (2019). *CCS Chem.* 1: 504–512.
28 Wang, C.-L., Wang, J., Jin, J.-K. et al. (2023). *Science* 382: 1056–1065.
29 Walton, J.C., Brahmi, M.M., Fensterbank, L. et al. (2010). *J. Am. Chem. Soc.* 132: 2350–2358.
30 Qi, J., Zhang, F.-L., Huang, Y.-S. et al. (2018). *Org. Lett.* 20: 2360–2364.
31 Lee, E., Hur, C.U., Rhee, Y.H. et al. (1993). *J. Chem. Soc., Chem. Commun.* 1466–1468.

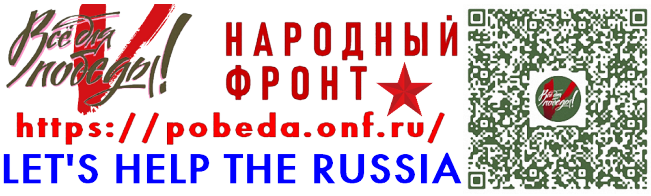


# Index

***a***

absorption spectroscopy 491
α-acetoxy redox-active ester 105
acyclic amides 110, 111
acyclic and cyclic racemic tertiary alkyl electrophiles 93
acylation of α-$CF_3$ alkyl bromides 130
acylation of benzyl chlorides 129
β-acylation product 430
*N*-acylhydrazones 299, 300, 311
*O*-acyl hydroxamides 237
2-acylimidazoles 10, 336–338, 341–343, 345, 353, 354
acyl-Ni(III)-alkyl species 104
α-$CF_3$-benzyl bromides 94
aldehydes
  α-enolation and α-vinylation of 407
aliphatic aldehyde-derived *N*-sulfonylhydrazones 38
aliphatic ketones 176
aliphatic secondary amides 109
*E*-and *Z*-alkenes 108
alkenylation of alkyl chlorides 131
alkenyl-cyclization of 2-bromo-1,6-dienes with alkenyl halides 150
4-alkenyloxyquinolone 446
alkoxyallenes 280
N-alkoxypyridinium salt 167, 235
α-alkylated amides 89
α-alkylation 301
  of aldehydes 417, 420, 422
β-alkylation, of enals with alkyl silanes 425, 426
alkylation of α-boryl alkyl chlorides with alkyl iodides 142
alkylation of aryl iodides
  with aziridines 137
  with epoxides 136
1,2-alkylborated products 120
1,1-alkyl-borylation products 120
alkylboronate esters 81
alkylcopper(III) intermediate 241
4-alkyl-1,4-dihydropyridines (DHPs) 103, 251, 275–277, 427
alkyldinitriles 235
alkyl iodide 90
α-alkyl-α-iodo hydrocoumarins 292
alkyl-nickel complex 89
alkyl-nickel(I) intermediate 116
alkylsilyl peroxide 248
alkyl-substituted Hantzsch esters 265
1-alkyl-substituted (hetero)arenes 160
alkyltrifluoroborates 117, 250, 251
alkylzinc reagent 78–92, 104, 105
alkynyl aluminum reagents 93
alkynyl bromide 262
alkynylboronic esters 170
1-alkynyl tetrahydroisoquinolines 232
allenylsilanes 85
α-allylation
  of aldehydes with allylsilanes 406
  of ketones 408
allyl azidoformate, asymmetric radical bicyclization of 46
*N*-allyl-diphenylamine 263
allylic sulfonamides 92

π-allyl palladium species 280
α-boryl radicals 12
amine-boryl radical 513
α-amino acids 81, 102–104, 245, 261, 274, 280, 281, 312, 421, 485, 486
β-amino alcohol 294, 356, 477
amino alcohol 313, 391, 393, 396, 397, 430, 468, 472, 482
α-amino alkyl halides 81
α-amino arylation product 103
α-amino carbon radical 246, 250, 255, 257
α-amino C($sp^3$)–H arylation via dual nickel/photoredox-catalysis 110, 113
aminocatalysis 404–432
α-amino C($sp^3$)–H functionalization 112
2-amino-2′-hydroxy-1,1′-binaphthyls (NOBINs) 6
α-aminoketones 110
2-aminonaphthalene 6, 7
α-amino NHP esters 104
(*S*)-3-amino-3-phenylpropanoic acid 13
aminopyridine ligands 211
α-amino radical 103, 112, 255, 316, 356, 418, 419, 428, 464, 465, 468, 469, 472, 482, 485
anilines 183, 241, 275, 276
anthracenecarboxylic 375, 377, 398
1-anthracenecarboxylic acid 398
2,6-anthracenedicarboxylate (ADC) 377
anthraquinone-type photocatalyst 163
anti-HIV drug Maraviroc 13
arylation of α-borylalkyl iodides with aryl iodides 135
arylation of α-$CF_3$ alkyl bromides 130, 134, 139
arylation of α-chlorosulfones with aryl halides 135
arylation of α-phosphoryl alkyl bromides with aryl iodides 141
arylation of alkyl halides with aryl iodides 140
arylation of epoxides with aryl iodides 139
aryl-alkylation of alkenes with alkyl halides 147
α-aryl alkylnitriles 133
α-aryl amides 95, 108
aryl-amination of alkenes with O-acyl hydroxylamines 148
α-aryl and α-alkenyl esters 95
aryl bromides 99–102, 105, 114, 117, 139, 142, 144, 151, 153, 248–253, 260–262, 281
aryl carbamoyl chloride-tethered alkenes 116
*N*-aryl glycine 351, 471, 472, 482
aryl iodides 133–141, 143, 146, 258, 259, 261
α-aryl ketones 78, 108
aryl-sulfonylation of enamide 118
arylboron reagent 95, 97, 116
arylboronic acids 96, 97, 168, 233, 318, 319
aryldiazomethanes 35–37
2-arylpyrrolidine 109
*N*-aryl-tetrahydroisoquinolines 232, 233
asymmetric α-arylation
  of aldehydes 411
  of α-halo-α-fluoro ketones 79
  of carbonyl compounds 411
asymmetric β-arylation of cyclopropanols 106
asymmetric alkynylation
  with alkynyl indium and aluminum reagents 93
  of C($sp^3$)–H bonds 169–173
asymmetric amination of C($sp^3$)–H bonds 175–179
asymmetric arylation of C($sp^3$)–H bonds 167–169
asymmetric benzylic C–H acylation of alkylarenes 108
asymmetric C–C coupling of alkyl halides 11–13
asymmetric C–N bond formation 13–18
asymmetric coupling
  with aliphatic C($sp^3$)–H bonds 107–115

of 3-bromo-phthalides with arylboronic acids 96
of β-ketocarbonyls and olefins 410
with redox auxiliaries 101–107
of secondary α-*N*-heterocyclic trifluoroborates 100
asymmetric couplings of C($sp^2$)-halides with C($sp^3$) pseudo-electrophiles
couplings with aziridines 137
couplings with epoxides 136–137
asymmetric couplings of C($sp^3$) halides with C($sp^2$) halides
couplings with acyl chlorides 129–131
couplings with alkenyl halides 131–132
couplings with aryl halides 133–135
asymmetric C($sp^3$)–C($sp^2$) XECs enabled by metallaphotoredox or electrocatalysis 137–143
asymmetric cyanation of benzylic C–H bonds 160, 161, 167
asymmetric cyanation of benzylic radical 161
asymmetric cyanation of C($sp^3$)–H bonds 160–167
asymmetric cyclization, via H-bonding organocatalysis 457–461
asymmetric cycloaddition, via H-bonding organocatalysis 444–457
asymmetric decarboxylation arylation of α-amino acids 102
asymmetric fluoroalkylation of C($sp^3$)–H bonds 173–174
asymmetric Hiyama α-arylation of α-bromo esters 96
asymmetric hydroamination of alkenes with *N*-heterocycles 59
asymmetric hydrosilylation 504, 505
asymmetric Kumada cross-coupling 64–66
asymmetric Minisci reaction 467–471
asymmetric Negishi α-alkylation 105
asymmetric Negishi cross-coupling of racemic secondary allylic chlorides 83–84
asymmetric Negishi reaction of cyclopropyliczinc reagents and alkyl electrophiles 91
asymmetric nickel-catalyzed regio-and stereoselective cross-electrophile coupling of 3,4-epoxyalcohols 137
asymmetric organocatalysis, with covalent modes 403
asymmetric oxidative coupling of C–H bonds
for binaphthyl synthesis 4–7
of other C–H bonds 7–11
asymmetric α-oxygen C($sp^3$)–H functionalization 112
asymmetric protonation 444, 477–484
via dehalogenation 480
asymmetric radical cross-coupling 63–70, 77–121, 127–154, 159–179, 471–476
asymmetric radical reactions
CLA catalysis with photocatalysis 304
external photosensitizers 305–314
photochemical reactions 314–324
CLA electrochemical reactions 324–326
enantioselective conjugate radical addition reactions 288–291
enantioselective hydrogen atom transfer (HAT) reactions 291–295
iron-catalyzed enantioselective radical carboazidation 302
radical-mediated cyclization 296–299
asymmetric radical/polar crossover reaction 484–488
asymmetric redox-neutral alkene functionalization 115–120
asymmetric reductive alkylarylation of bromoaryl-tethered alkenes with alkyl bromides 147
asymmetric reductive carboalkylation of acyl chloride-tethered styrenes 145
asymmetric Suzuki α-arylation of α-chloro amides 96

asymmetric Suzuki arylation of racemic α-haloamides 95
asymmetric Suzuki-Miyaura coupling of α-bromobenzyl trifluoromethyl ethers 96
asymmetric tertiary C($sp^3$)–H bond functionalization 176
asymmetric three-component carboarylation of alkenes 118
azepinone 375
aziridination
  of alkenes with $TcesN_3$ azides 42
  with fluoroaryl azides 45
  intramolecular, of allylic sulfamoyl azides 43
  of styrene derivatives with phosphoryl azides 42
  of styrene derivatives with $TrocN_3$ 46
azobisisobutyronitrile (AIBN) 500
1,1′-azobis(cyclohexanecarbonitrile) (ACCN) 514
2,2′-azobisisoheptonitrile (ABVN) 515
azoles 189, 190, 201, 245

## b

Beckwith-Enholm cyclization 461
benzenethiol (PhSH) 500, 501
benzoate 81, 295, 373
benzoin methyl ether 386
benzophenone 388, 389, 450, 452, 458, 491
benzoylcyclopropane 385, 386
O-benzoyl-hydroxylamines 148
benzoyl peroxide (BPO) 506
benzyl alcohols 179, 506
benzylation of alkenyl bromides with N-hydroxyphthalimide esters 132
*N*-benzyl heterocycles 103
benzylic bromide 83, 87, 88, 93, 419
benzylic C–H bonds 38, 48, 160–162, 167, 168, 170, 171, 173, 178, 208, 239, 257
benzylic chlorides 101, 129, 131, 132, 139, 142, 147, 260
benzylic radical 14, 234, 237, 240, 261, 283, 324, 421
benzylic trifluoroborates 249
*N*-benzyl-indol-7-yl propiolate 515, 516
benzyl trifluoroborates 99, 250
bicyclo[1.1.1]pentanes (BCPs) 409
bidentate chiral diamine 243
bidentate isoquinoline-oxazoline ligand 87
bidentate phosphine 243
bifunctional catalysis by a single chiral copper catalyst 241–248
bifunctional electrophile 95
bifunctional photoaminocatalyst 423
biimidazoline (BiIM) 139
bimetallic-mediated hydroacyloxylation of alkenes 57
binaphthyldisulfide 503, 505
biomolecular hosts 390–393
bipyrrolidine-derived iron aminopyridine complexes 5
bisarenesulfonimide 170
2,2′-bis(arylamino)-1,1′-biaryls 7
bisoxazoline diphenylamine (BOPA) 244, 245
bisoxazoline diphenylalanine (BOPA) catalyst 200
bisoxazoline ligand 25, 64–67, 182, 200, 249, 263, 289, 290, 292, 295, 297, 298, 310, 311, 321
Boc-protected oxime esters 246
boryl radicals 500, 513–518
$Box^{OH}$ ligand 164
bromo acetonitrile 419
α-bromoamides 78, 114, 200
bromoaryl-tethered acrylamides 144
α-bromobenzyl fluoroalkanes 97
α-bromo esters 64–66, 95, 96, 469
(1-bromoethyl)benzene 88
α-bromo ketones 94
α-bromophosphates 259
α-bromophosphonates 262
α-bromosulfonamides 92
1,3-butadienylcyclopropanes 500, 501
*tert*-butoxyl radical 177, 178

*tert*-butyl α-bromopropionate 12
*tert*-butyl hydroperoxide (TBHP) 6, 233, 303, 503
*tert*-butylperoxybenzoate (TBPB) 17
γ-butyrolactone 114
*tert*-butyl vinyl ether 505

## C

C($sp^3$)–C(sp) cross-coupling 185–188, 198–202
C–C bond formation 60, 71, 78, 120, 181, 198, 267, 274, 344, 362, 472
C=C double bond 501
1,5-C–H amination
  of alkoxysulfonyl azides 51
  of sulfamoyl azides 50
  of sulfonyl azides 47, 48
1,6-C–H amination, of sulfamoyl azides 48, 49
  enantioconvergent radical amination process 49
(–)-calycanthidine 474
Candida antarctica lipase B (CALB) 243
carbon-based organometallic reagents 182
carbooxidation 407, 409
carboxylic acid-derived redox-active *N*-hydroxyphthalimide (NHP) esters 131
cascade reactions 1, 39–40, 307, 427, 438
catalytic asymmetric C–C cross-couplings enabled by photoexcitation 284
celestolide, chiral manganese-salen catalyzed enantioselective C–H azidation of 213
ceric ammonium nitrate (CAN) 405
α-$CF_3$-substituted alkyl bromides 259
$CF_3O$-substituted stereogenic centers 96
chiral α-alkynyl phosphonates 262
chiral α-aryl *N*-heterocycles 109
chiral α-arylated carbonyls 252
α-chiral BCPs 409
chiral α-quaternary β-lactams 197
chiral ($\eta^3$-allyl)iridium(III) complex 284
chiral 1,1-diaryl-2,2,2-trifluoroethanes 94
chiral 1,6-dinitriles 235
chiral 2-imidazolidinones 17
chiral 3-aryl-phthalides 97
chiral 4-heptyl biOx ligand 133, 137
chiral 4-heptyl-substituted biOx 151
chiral 8-quinoline imidazoline ligand (Quinim) 149
chiral aliphatic amines 80, 193
chiral alkyl-Ni(II) complex 89
chiral alkynes 85, 169, 185, 244
chiral allylic esters 247
chiral amino alcohols 319
chiral anionic ligands-tuned enantioconvergent radical cross-coupling
  chiral anionic N,N,N-ligands with long spreading side arm 198–200
  chiral anionic tridentate N,N,N-ligands 193–195
  chiral anionic tridentate N,N,P-ligands 184–192
  hemilabile chiral anionic N,N,N-ligands 195–198
  other ligands 200–202
chiral anionic N,N,N-ligands with long spreading side arm 198–200
chiral anionic tridentate N,N,N-ligands 193–195
chiral anionic tridentate N,N,P-ligands 184–192
chiral-at-iridium complexes
  asymmetric radical reactions 363–367
  radicals delocalized 339–340
  radicals dissociated out of 336–339
chiral-at-iridium Lewis acid 335–340
chiral-at-rhodium complexes
  radicals delocalized on 347–363
  radicals dissociated out of 341–347
chiral-at-rhodium Lewis acid 340–363
chiral benzyl azides 16
chiral benzyl nitriles 234, 237
chiral bioactive molecules
  (*R*)-δ-decalactone 141

chiral bioxazoline (biOx) ligand 109, 133, 137, 138, 144, 146, 147, 151, 152
chiral bis-amino-bis-pyridine manganese complexes 211
chiral bis(imidazoline) catalyst 252
chiral bis(oxazoline) (Box) ligand 175, 234
chiral bisoxazoline ligand 1, 65, 67, 105, 175, 200, 234, 245, 249, 289, 290, 292, 297, 298, 300, 310, 311, 321
chiral bisphosphine ligand 64, 202, 245
chiral Box-copper complex 170
chiral *t*-Bu-pyox ligand 150
chiral $CF_3$-substituted alcohols and ethers 95
chiral $CF_3$-substituted thioethers 93
chiral cyano-Box ligand 250
chiral cyclopropanes 71, 91
chiral dialkyl carbinols 104
chiral diols 444
  as H-bonding template for asymmetric [2+2] cycloaddition 445
  as H-bonding template for solid-state [2+2] cycloaddition 445
chiral diphosphine oxide–iron(II) complexes (*S*)-xylyl-$^{i}$PrO-BIPHEP-oxide 5
chiral disulfide 503, 506, 508–510
chiral guanidine hybrid ligand 202
chiral Haixi-BOX ligand 15–16
chiral heterobiaryl products 266
chiral homoallylic alcohol 107, 263, 265, 279
chiral imidazolidinone catalyst 405–408, 418
chiral inductors 384, 385, 398
chiral lactams
  in asymmetric intramolecular [2+2] cycloaddition 447, 452
  in asymmetric radical cyclization 457
  as bifunctional catalyst in asymmetric cyclization 458, 459
  as bifunctional catalyst in asymmetric radical addition 464
  as H-bonding catalysts 446
  in intermolecular [2+2] cycloaddition 448
  in intramolecular [2+2] cycloaddition 450, 451
  in other asymmetric cycloadditions 449
chiral Lewis acids (CLA) 287, 324–326
  activation models by 288
  catalyzed enantioselective conjugate radical addition 289
  C($sp^3$)–H functionalization 321
  catalysis with photocatalysis 304
  conjugate radical addition 317
  electrochemical reactions 324–326
  enantioselective radical cyclization reaction 297
  gallium-based 313
  HAT to α-carbonyl radicals 292
  HAT photocatalysis and nickel-based 322
  photocatalysis
    external photosensitizers 305–314
    photochemical reactions 314–324
  [2 + 2] photocycloaddition 318
  synergistic photoredox and lanthanide metal-based 315
chiral ligands, in metallaphotoredox catalysis 231
chiral manganese catalysts 207, 213, 214
chiral Mn(III)–porphyrin complex catalyzed enantioselective benzylic C–H hydroxylation 208
chiral *N*-donor hybrid ligand 201
chiral nickel/bis(imidazoline) 260
chiral nickel/PHOX complex 257
α-chiral organosulfur compounds 191
chiral organosilanes 81
chiral organotin hydride 512
chiral oxazolines 18, 171, 175, 240
chiral Phosferrox ligand 144
chiral phosphonic acid (CPA) 5, 7, 453, 456, 460, 467, 483
chiral polydentate ligand 266
chiral propargyl compounds 93

chiral PyBOX ligand 9, 151, 233, 318
chiral pyridineoxazoline ligand 250
chiral secondary amides 242
chiral sensitizers 372, 373, 393, 489
chiral silanes 83
chiral templates 290, 371, 387–390, 444, 447, 448, 450
chiral thiol catalysts 503, 506
chiral vinyl germanes 85
chiral zirconium–metallosalen 214
α-chloroarenes 133
α-chloroboronates 141, 259, 262
α-chloroboronates with alkyl iodides 141
α-chloroesters 133, 138, 143, 258, 259
3-chlorooxindole 472, 473
α-chlorosulfones 132, 134, 135
cinacalcet 191
cinchona alkaloid-derived bidentate sulfonamide N,N-anionic ligand 193
circularly polarized light (CPL) 393–396
classic Kharasch-Sosnovsky reaction 175
clusterization-triggered emission (CTE) 394
*C*-nucleophiles 57, 60–61
Co(II) complexes of $C_2$-symmetric chiral bis-binaphthyl porphyrins 30
Co(II)-based MRC system, for asymmetric intramolecular C–H alkylation 36
Co(II)-complexes of $D_2$-symmetric chiral amidoporphyrins 28, 29
Co-catalyzed asymmetric hydrofunctionalization of alkenes 54
  catalytic cycle 54
  with C-based nucleophiles 60
  [Co(Salen)] complexes 55, 56
  with nitrogen nucleophiles 58
  with oxygen-based nucleophiles
    electricity-driven method 58
    using hypervalent iodine(III) reagent 57
Co-catalyzed asymmetric intramolecular hydroalkoxylation of tertiary allylic alcohols 55
Co-catalyzed asymmetric Kumada cross-coupling
  with cyclopropane-based bisoxazoline ligands 65
  of racemic α-bromo esters and aryl Grignard reagents 65
Co-catalyzed asymmetric Negishi cross-coupling
  of fluorinated secondary benzyl bromide and lithium aryl boronates/$ZnBr_2$ 67
  of racemic α-bromo esters with arylzinc reagents 66
Co-catalyzed asymmetric radical cross-coupling reactions 63–70
Co-catalyzed asymmetric radical reactions 23–71
Co-catalyzed asymmetric remote borylation of alkyl halides 70
Co-catalyzed enantioconvergent radical Negishi cross-coupling
  with α-bromoketones 68
  with chiral multidentate *N,N,P*-ligand 67
Co-catalyzed enantioselective $C(sp^3)$–$C(sp^3)$ coupling 68
Co-catalyzed facial-selective hydroalkylation of cyclopropenes 68
Co-catalyzed highly enantioselective hydroamination of alkenes
  with NFSI 59
  with secondary amines 60
Co-catalyzed hydroamination of alkenes 62
Co-catalyzed radical cross-coupling reactions
  asymmetric Kumada 64–66
  asymmetric Negishi 66–68
CoH-catalyzed symmetric hydrofunctionalization 60
[Co(HuPhyrin)] 31

[Co(II)(Por)]-catalyzed asymmetric radical aziridination 40–47
[Co(II)(Por)]-catalyzed asymmetric radical C–H alkylation 36–39
[Co(II)(Por)]-catalyzed asymmetric radical C–H amination 47–54
[Co(II)(Por)]-catalyzed asymmetric radical cyclopropanation 26
[Co(**P3**)]-catalyzed asymmetric cyclopropanation
of alkene with acceptor/acceptor-substituted diazo compounds 31
[Co(P3)]-catalyzed intramolecular cyclopropanation 32
of 2-vinylaryl diazomalonates 32
[Co(P8)]-catalyzed asymmetric cyclopropanation
of alkene with methyl phenyl diazomalonate 33
[Co(P9)]-catalyzed asymmetric intramolecular cyclopropanation 34
[Co(P12)]-catalyzed intramolecular asymmetric cyclopropanation with in situ generated aryldiazomethanes 36
[Co(**P17**)]-catalyzed asymmetric cyclopropenation
of alkynes with acceptor/acceptor-substituted diazo compounds 39
[Co(Por)]-catalyzed asymmetric cyclopropanation
of alkene with diazoacetates 30
of alkene with diazosulfones 33
of alkene with in situ-generated donor/H substituted diazo compounds 35
[Co(Por)]-catalyzed asymmetric olefin cyclopropanation 28
[Co(Por)]-catalyzed cyclopropanation reactions
of styrene with EDA 28, 29
[Co(Por)]-catalyzed intramolecular radical C–H alkylation 38
[Co(Por)]-MRC
aziridination of alkenes 41, 42
aziridination of allylic sulfamoyl azides 44
C–H amination with organic azides 47
intramolecular radical C–H alkylation 37, 38
commercially available amino acid derivatives 104
cooperative photoredox 173, 239, 248, 341, 356, 454, 459, 466, 472, 482
copper(I) imidate complex 240
copper(II) acetylide 245
copper-catalyzed asymmetric arylation of benzylic C–H bonds 168
copper-catalyzed asymmetric cyanation of allylic C–H bonds 163
copper-catalyzed asymmetric trifluoromethylation of C–H bonds 174
copper-catalyzed benzylic C–H arylation 168
copper-catalyzed C($sp^3$)–H polyfluoroarylation using polyfluoroarenes 168
copper-catalyzed enantioconvergent radical cross-coupling, design of 183
copper-catalyzed enantioselective C–H cyanation 166
copper-catalyzed enantioselective intermolecular C–H amination 177
copper-catalyzed enantioselective radical addition 300
copper-catalyzed oxidative asymmetric radical cross-coupling of C($sp^3$)–H bonds
asymmetric alkynylation of 169–173
asymmetric amination of 175–179
asymmetric arylation of 167–169
asymmetric cyanation of 160–167
asymmetric fluoroalkylation of 173–174

copper-catalyzed photochemical alkylation 310
copper-catalyzed radical relay pathway 159
copper-catalyzed radical relay strategy for benzylic C–H bonds 160
copper/chiral cinchona alkaloid-based N,N,P-ligand catalyst 171
copper/chiral N,N,P-ligand catalyst 189
[Co(**S3**)] catalyst 57
[Co(Salen)] complexes 55, 56
(3+2) coupling, of aldehydes and olefins 413
(4+2) coupling reaction 412
covalent bonding 403, 438, 499
CPA/DPZ cooperative catalysis 455
cross-coupling of organohalides
  with aryl and primary alkylzinc reagents 78–87
  with organosilicon and organoboron reagents 95–101
  with organozirconium, organoindium, organotitanium and Grignard reagents 92–95
  with secondary alkylzinc reagents 87–92
crosslinking cyclic nigerosylnigerose (CNN) 375
Cu/anionic ligand-catalyzed diverse asymmetric radical reactions of alkynes 188
Cu/anionic N,N-ligand-catalyzed radical asymmetric oxytrifluoromethylation of alkenyl oximes 184
Cu/CPA-catalyzed radical asymmetric difunctionalization of alkenes 184
Cu/N,N,P-ligand complex 185
**L**$Cu^{II}$NuX complex 186
cyanoalkyl radicals 235, 247, 345, 419
cyanoazaarenes 475, 476
cyclic alkyl halides 89
cyclic amides 110, 111
cyclic carbamates 110
cyclic meso-anhydrides 99, 250
cyclic tertiary amides 111
cycloalkylzinc reagents 87, 88
cyclobutane-carbaldehydes 457
cyclobutanols 431
cyclodextrins (CDs) 371–383
cyclohexadienone 384, 385
cyclohexyl phenyl ketone 398
cyclooctenes 235, 372
cyclopentane products 505, 508, 511
cyclopentylamines 454
cyclopropane-fused tricyclic chromanones 32
cyclopropanes 26, 28, 30–35, 39, 40, 65, 69, 71, 91, 105, 490, 501
cyclopropanols 105, 106, 173, 427
cyclopropyl α-iodo alkylsilane 83
cyclopropyl-linked bis(oxazoline) 141
cyclopropylamines 454
cysteine-based dimers 508

## *d*

dapoxetine 190, 191
density functional theory (DFT) 26, 28, 100, 141, 161, 216, 241, 466
deracemization 349, 351, 367, 444, 489–493
desymmetric carbamoylalkylation of carbamoyl chloride-tethered 1,6-dienes with alkyl iodides 150
desymmetrization of cyclic meso-anhydrides with benzyl trifluoroborates 99
deuterium-containing coupling products 88
deuterium-labeled cyclopentyl zinc reagent 88
deuterium-labeled tetrahydrofuran 114
dexibuprofen 11
di-*tert*-butyl hyponitrite (TBHN) 503
di-*tert*-butyl peroxide (DTBP) 5, 60, 177, 513
dialkyl acetate 105
1,1-diaryl alkane 107, 139, 253
dialkylamines 81, 104

1,1-diarylethane product 99
diarylethenes 391, 392
1,1-diaryl fluoroalkanes 97
diarylprolinol ether organocatalyst 421
diastereo-and enantioselective alkyl-borylation of heterocyclic alkenes 118, 119
dibenzofuran-4,6-bisoxazoline (DBFOX) 308
dibenzyl vinylcyclopropanedicarboxylate 505, 506
1,7-dicarbonyl compounds 431, 432
dicumylperoxide (DCP) 469
Diels-Alder reaction 389, 503
*oxa*-Diels-Alder reactions 310
1,3-dienes 235, 246, 247, 265, 281
*gem*-difluoroalkenes 144
1,4-dihydropyridine (DHP) substrates 266
3,4-dihydroquinolinones 148, 212
(di-μ-hydroxo)iron$^{III}$(salan) catalyst 5
2,6-dimethyl benzoic acid (DMBA) 129
diisobutylaluminium hydride (DIBAL-H) 481
diisopropylethylamine or Hantzsch ester 278
diphenylisobenzofuran 503
diphenylmethylacetamide moiety 508
direct photoexcitation 349, 359–363, 367
2,2-disubstituted indolin-3-ones 473
2,4-disubstituted heterocycles 118
3,3-disubstituted oxindoles 116
α,β-disubstituted unsaturated systems 294
disulfide-bridged peptide 508–510
DPAMOC 394
dual catalytic decarboxylative allylations of α-amino acids 274
dual electrocatalysis 61
dual Ni/photoredox catalyzed cross-electrophile coupling 138
dual nickel/photoredox-catalyzed modular approach 103
dual photoinduced copper catalyzed asymmetric radical trifluoromethylation of benzylic C–H bonds 239
dual photoredox/chromium or cobalt-catalyzed asymmetric radical reactions 262
dual photoredox/chromium-catalyzed asymmetric radical 1,4-functionalization of 1,3-enynes 265
dual photoredox/chromium-catalyzed asymmetric radical allylation of aldehydes 264
dual photoredox/copper catalyzed asymmetric dehydrogenative cross-couplings of *N*-aryl tetrahydroisoquinolines 233
dual photoredox/copper catalyzed enantioselective asymmetric deoxygenative cyanation 236
dual photoredox/copper catalyzed enantioselective benzylic and allylic cyanation 234
dual photoredox/copper catalyzed enantioselective radical C-H amination reactions 240
dual photoredox/nickel asymmetric XEC reaction 141
dual photoredox/nickel catalyzed direct asymmetric C($sp^3$)–H radical arylation 253
dual photoredox/nickel catalyzed enantioselective benzylic C($sp^3$)–H arylation and alkenylation of alkylbenzenes 254
dual photoredox/nickel catalyzed enantioselective decarboxylative arylation 250
dual photoredox/nickel catalyzed enantioselective three-component radical carboarylation of alkenes 252
dual photoredox/nickel-catalyzed asymmetric reductive alkenylation 260

dual photoredox/nickel-catalyzed asymmetric reductive C($sp^3$/sp)-C($sp^3$) cross-couplings 262
dual photoredox/nickel-catalyzed cross-coupling of organotrifluoroborates with aryl bromides 101
dual photoredox/nickel-catalyzed enantioselective cross-electrophile coupling reactions 261
dual photoredox/organo catalysis 431
dual photoredox/palladium enantioselective alkylation 277
dual photoredox/palladium-catalyzed decarboxylative hydroamino-alkylation of allenes 280
dual photoredox/palladium-catalyzed enantioselective reductive cross-coupling 279

## *e*

electrocatalytic oxidative hydroetherification of alkenes 58
electrochemical organic synthesis 324
electrochemically driven alkenylation of benzylic chlorides 142
electrolysis-enabled alkenylation or arylation of aryl aziridines 143
electrolysis-enabled arylation of α-chloroesters 143
electron donor-acceptor (EDA) 307, 308, 416, 417, 428, 479
electron-rich BiIM ligand 139, 143
electrophoto-copper-catalyzed asymmetric cyanation of benzylic C–H bonds 162
enamine catalysis
  via **α**-iminyl radical cation intermediates 404–418
  via radical addition to enamine intermediates 418–424
enantioconvergent cross-coupling of α-zincated *N*-Boc-pyrrolidines with alkyl iodides 90
enantioconvergent cross-coupling of α-zincated amides with alkyl iodides 90
enantioconvergent Miyaura borylation of benzylic chlorides 101
enantioconvergent Negishi coupling of α-zincated *N*-Boc-pyrrolidine with alkyl halides 89
enantioconvergent radical *N*-alkylation of aliphatic amines 194
enantioconvergent radical amination process 49
enantioconvergent radical C($sp^3$)–C cross-coupling of racemic alkyl halides 181
enantioconvergent radical C($sp^3$)–C(sp) cross-coupling of racemic alkyl halides and terminal alkynes 187
enantioconvergent radical C($sp^3$)–N cross-coupling with sulfoximines 190
enantioconvergent radical C($sp^3$)–C($sp^2$) cross-coupling with azoles 190
enantioconvergent radical C($sp^3$)–C(sp) cross-coupling 185
enantioconvergent radical C($sp^3$)–N cross-coupling of aromatic amine 196
enantioconvergent radical C($sp^3$)–O cross-coupling of O-nucleophiles 201
enantioconvergent radical Suzuki-Miyaura C($sp^3$)–C($sp^2$) cross-coupling 189
enantiodivergent 1,5-C-H amination, of sulfamoyl azides 50
enantioenriched α-aryl alkylboronates 139
enantioenriched α-arylnitriles and allylic nitriles 79
enantioenriched α-lithiated benzoates 81
enantioenriched α-substituted ketones 103

enantioenriched α-trifluoromethyl-and perfluoroalkyl-containing benzylic and allylic ethers 95
enantioenriched β-alkyl-α-arylated carbonyls 117
enantioenriched β-aryl homoallylic amines 143
enantioenriched β-arylated sulfones 134
enantioenriched 1,1-diarylalkanes 83, 139
enantioenriched 2,2-diaryl alcohols 138, 261
enantioenriched 2-aryl phenethylamines 137
enantioenriched *β*-chiral sulfones 261
enantioenriched *δ*-amino nitrile 167
enantioenriched *trans* and *cis* α-alkenyl phosphonates 117
enantioenriched alkylboronate esters 81
enantioenriched benzylic boronic esters 101
enantioenriched dialkyl-substituted isoindoline skeletons 145
enantioenriched dialkylamines 104
enantioenriched organosilanes 82
enantioenriched oxindole synthesis with alkyl iodides 146
enantioenriched pyrrolines 257
enantioenriched trans-β-arylcycloalkanols 136
enantiomerically enriched 1,1-diarylalkanes 168
enantiomerically enriched *N*-benzyl heterocycles 103
enantioselective α-allylation of anilines by photoredox/palladium cocatalysis 276
enantioselective α-alkylation
  of β-ketocarbonyls 423, 424
  of aldehydes 415, 419
enantioselective α-alkylation of nitroalkanes 115
enantioselective α-amination 421
enantioselective α-amino C($sp^3$)–H acylation of acyclic amides 111
enantioselective α-amino C($sp^3$)–H arylation of amides 110
enantioselective α-benzylation 421
enantioselective α-functionalization, of aldehydes 420
enantioselective α-oxy C($sp^3$)–H functionalization 113, 114
enantioselective α-oxyamination, of aldehydes 415
enantioselective β-hydroxylation, of enals 433, 434
enantioselective β-alkylation, of enals 426
enantioselective β-difluoroalkylation, of enals 428
enantioselective acyl-carbamoylation of alkenes 116, 117
enantioselective alkenyl-and aryl-sulfonylation of alkenes 119
enantioselective alkenyl-sulfonylation of styrenes 118
enantioselective alkyl-alkenylation of vinyl phosphonates 118
enantioselective alkyl-borylation of terminal alkenes 120
enantioselective allylic alkylation enabled by photoredox/palladium cocatalysis 275
enantioselective annulation, of enals 435
enantioselective arylation of benzylic C-H bonds 168
enantioselective benzylic C($sp^3$)–H acylation and carbamoylation 109
enantioselective benzylic C($sp^3$)–H arylation 108
enantioselective benzylic C($sp^3$)–H cyanation 233
enantioselective benzylic C–H alkenylation of alkylbenzenes 253
enantioselective C($sp^3$)–H functionalization of oxacycles 112

enantioselective $C(sp^3)$–$C(sp^3)$ cross-coupling of racemic α-silylated alkyl iodides 83
enantioselective carboxyalkylation 503
enantioselective C–H lactonization, of carboxylic acids 221
enantioselective copper-catalyzed cyanation of propargylic C–H bonds via radical relay 164
enantioselective (3 + 2) coupling 413
enantioselective coupling of propargylic (pseudo)-halides with organozinc reagents 85
enantioselective coupling of secondary benzylic bromides with cycloalkylzinc reagents 88
enantioselective cross-coupling of α-bromoketones with arylzinc reagents 78
enantioselective cross-coupling of α-bromonitriles with organozinc reagents 80
enantioselective cross-coupling of α-halosilanes with organozinc reagents 82
enantioselective cross-coupling of allylic chlorides with alkylzinc reagents 84
enantioselective cross-coupling of benzylic halides with alkylzinc reagents 83
enantioselective cross-coupling of $CF_3$-substituted alkyl halides with organozinc reagents 79
enantioselective desymmetrization
  of carbonyl group-substituted indane derivatives 217
  of meso-pyrrolidine and tetrahydrofuran derivatives 216
enantioselective functionalization, of enals 436
enantioselective hydrocyanation of conjugated alkenes 61
enantioselective hydrogen atom transfer (HAT) reactions 291
enantioselective hydrosilylation 503, 505
enantioselective intramolecular lactonization, of methylene C–H bonds of adamantaneacetic acids 220
enantioselective oxidative desymmetrization
  of ketone-based spirocyclic hydrocarbons 219
  of monosubstituted cycloalkanes 218
  of spirocyclic oxindoles and dihydroquinolinones 219
enantioselective photoredox/palladium cocatalytic allylic alkylation reaction 274
enantioselective radical cascades 427
enantioselective radical decarbonylative azidation 17
enantioselective reductive arylation of α-chloro esters 138
enantioselective reductive arylation of α-chlorosulfones 134
enantioselective reductive cross-couplings 257
enantioselective tertiary C-H bond hydroxylation, of *cis*-3,5-dimethyl substituted cyclohexane derivatives 217
enantioselective three-component carboarylation of alkenes 251
6-*endo-trig* cyclization 515
energy transfer (EnT) 107, 108, 175, 229, 240, 255, 260, 267, 304, 316, 366, 367, 381, 387, 389, 444, 449, 451–453, 457, 490, 491
engineered cytochrome P450s 3
1,3-enynes 186, 235, 248, 265
eosin Y 260, 347, 419, 487
ephedrine 385
E-rich and E-poor heteroarenes 163
exogenous carboxylic acids 246

## *f*

$Fe(acac)_3$/chiral biphosphine ligand 11
$Fe^{I}$(BenzP*)Cl complex 12

Fe(III)-ligated naphthoxy radical 10
$Fe(NTf_2)_2$/chiral BOX ligand 13
(fluoro)alkyl halides 12
*N*-fluoroamides 171
4-fluorobenzaldehyde 263
four-membered oxanickelacycle intermediate 107
Friedel-Crafts type 410
α-functionalization, of aldehydes 417
γ-functionalization, of α-branched enals 432
1,2-functionalized chiral allyl cyanides 235

## g

Giese reaction 323, 324, 344, 346, 347
Glaser homocoupling 171, 185
Grignard reagents 11, 12, 63–66, 78, 92–95

## h

α-haloesters 11
α-halogenated borates with organolithium/organomagnesium reagents 81
H-bonding catalysts 446
  in asymmetric deconjugation 477
  in asymmetric deconjugative isomerization 478
  in asymmetric Friedel-Crafts 486
  in asymmetric Mannich reaction 488
  in asymmetric protonation via radical addition 482
  in asymmetric protonation via radical coupling 483
  in asymmetric protonation via SET 481
  in asymmetric radical coupling 473–475
  in aza-Mannich reactions 486
  in decarboxylative α-alkynylation of β-ketocarbonyls 463
  in deracemization 489–493
  in oxidative dearomatization/asymmetric Mannich reaction 488
  in radical addition 462
  in radical/polar crossover reactions 484–488
H-bonding organocatalysis
  asymmetric cyclization via 457–461
  asymmetric cycloaddition via 444–457
  asymmetric Minisci reaction via 467–471
  asymmetric protonation via 477–484
  asymmetric radical addition via 461–467
  asymmetric radical cross-coupling via 471–476
  asymmetric radical/polar crossover reaction via 484–488
  deracemization via 489–493
hemilabile chiral anionic N,N,N-ligands 195–198
hept-4-yl-substituted PyBox ligand 85
heteroaryl iodides 133
α-*N*-heterobenzylic trifluoroborates with aryl bromides 100
α-heterocyclic carboxylic acids 103, 251
hexagonal liquid crystal (HLC) 398
Hofmann-Löffler-Freytag reaction 166, 170
homoallylic alcohols 106, 107, 263, 265, 279
homochiral thiols 503, 505
human serum albumin (HSA) 390, 392
hydrogen atom abstraction (HAA) 26, 107, 165, 173, 187, 208, 209, 214, 503–505, 513
hydrogen atom transfer (HAT) 287, 304, 347, 362, 414
  α-methacrylates 293
  sulfonyl α-carbon radicals 293
  to α-carbonyl radicals 294
hydrogen-bonding interactions 31, 212, 216, 224, 364, 379, 444, 455, 478, 480, 491, 509
hydrosilylation reaction 505

hydroxybenziodoxole (BI-OH) 463
*N*-hydroxyimide 483
2-hydroxy-1,4-naphthoquinone 388
*δ*-hydroxyl nitrile 167
*N*-hydroxyphthalimide ether 104, 167, 234, 235
α′-hydroxy α,β-unsaturated ketones 290

## *i*

imidazolidinone catalyst 405–408, 418, 421
iminium catalysis
  radical addition 428–432
  radical coupling 425–428
**α**-iminyl radical cation intermediates 404–418
IndaBOX ligand 131
indane, enantioselective hydroxylation 210
indanol-based chiral thiol 506, 507
indoline compounds 213
in situ diazo generation 34
in situ generated Cu(I)-chiral complex 233
intermolecular α-alkylation, of aldehydes 418
intermolecular benzylic C–H amination with fluoroaryl azides 52
intermolecular convergent C–H amination, with fluoroaryl azides 53
intermolecular olefin cyclopropanation, catalytic cycle of 27
intramolecular α-allylation, of aldehydes 414
intramolecular α-allylation, of aldehydes 412
intramolecular alkyl-acylation of alkenes with alkyl iodides 148
intramolecular aryl-alkenylation of alkenes with alkenyl triflates 146
intramolecular aryl-allylation of alkenes with allyl carbonates 147
intramolecular arylation and alkenylation of acrylamides 145
intramolecular C–H amination, of aliphatic azide compounds 53
intramolecular 1,5-HAT 245
intramolecular radical C–H alkylation 37, 38
iridium-catalyzed asymmetric radical reactions 284–285
iron(III) azide species 13, 14
iron-catalyzed asymmetric aminoazidation and diazidation of styrenes 15
iron-catalyzed asymmetric azidation of alkenes 16
iron-catalyzed asymmetric azidation of benzylic peresters 15
iron-catalyzed asymmetric Kumada reaction 11
iron-catalyzed asymmetric radical ring contraction and C–H amination 18
iron-catalyzed asymmetric Suzuki–Miyaura coupling 13
iron-catalyzed C–H/C–H cross-coupling of 2-naphthols 4–6
iron-catalyzed coupling of 2-naphthols and nitroalkanes 8
iron-catalyzed enantioselective three-component coupling reaction 12
iron-catalyzed radical asymmetric carboazidation 14
iron-catalyzed radical asymmetric reactions
  asymmetric C–C coupling of alkyl halides 11–13
  asymmetric C–N bond formation 13–18
  asymmetric oxidative coupling of C–H bonds
    coupling for binaphthyl synthesis 4–7
    coupling of other C—H bonds 7–11
iron-catalyzed Suzuki–Miyaura coupling reaction 12
iron-porphyrins 2, 18

isobutyronitrile radical 500
Ito's enantioconvergent C($sp^3$)–B cross-coupling 202

## k

Kemp's triacid 387, 446
β-ketoamides 300, 301
β-ketoester derivatives 8
kinetic resolution (KR)
  Mn-catalyzed oxidative
    cyclic benzylic azides 223
    saturated cyclic ethers 222
  principle of 221
Kumada reaction 11, 94

## l

L*ArFe$^{II}$Cl species 12
L*Fe(II) species 16
L*Fe(III)-azide species 16
L-proline 487, 488
lactams 110, 148, 214, 216, 387, 435, 444, 446–452, 457–459, 464, 489
lamellar liquid crystals (LLC) 398
lauroyl peroxide 6, 248
ligand-controlled cobalt-hydride-catalyzed regio-, enantio-, and diastereoselective oxyheterocyclic alkene hydroalkylation 69
ligand relay 62, 63
linear maltodextrin (LM) 375
lithium aryl boronates 67, 96, 97
lithium arylborates 12
lithium organoboronate 97

## m

manganese-catalyzed asymmetric radical reactions
  asymmetric transformations 208–214
  enantioselective desymmetrization 214–221
  kinetic resolution 221–225
manganese-catalyzed enantioselective C–H azidation 213
manganese-catalyzed enantioselective C–H bond hydroxylation 208
manganese catalyzed enantioselective desymmetrization
  to alcohols 214–218
  to ketones 218–219
  to lactones 220–221
manganese-catalyzed enantioselective hydroxylation
  of arylalkanes 211
  of 3,4-dihydroquinolones 212
  of tertiary propargylic C($sp^3$)–H bonds 224
Mannich reaction of (2-alkylphenyl) ketones 312
β-mannopyranose thiol 505
Markovnikov rule 23
metal-hydride-mediated hydrogen atom transfer (MHAT) 54–56
metalloporphyrins 2, 28
metalloradical activation (MRA) of azide compounds 26, 40
metalloradical catalysis (MRC)
  with diazo and azide compounds 27
  intermolecular olefin cyclopropanation, catalytic cycle of 27
metalloradical catalysis 25–54
metalloradical Cu(II) 182
α-methacrylates 293
4-methoxy-NHPI (N-hydroxyphthalimide) 176
methylene-linked bis(oxazoline) 141
methylene tetrahydropyranone 503–505
Minisci-type addition 490–493
Mn(III)–porphyrin complex catalyzed C–H hydroxylation with $H_2O_2$ 210
Mn(III)–salen complexes catalyzed enantioselective C–H oxidation 209
modern organic synthesis 1, 207, 287
modified γ-CDs 377
3Å molecular sieves (3Å MS) 129
Morita–Baylis–Hillman (MBH) adducts 277
multisite proton-coupled electron transfer (MS-PCET) 425

multivariate linear regression (MVLR) analysis 133, 139

***n***

nanosponges 373–376
2-naphtholated iron$^{III}$(salan) species 5
2-naphtholated iron$^{IV}$(salan) species 5
2-naphthols 4–10
naphthylpropyne 503
1-naphthyl-substituted Quinim 149
*N*-containing chiral drugs 191
Negishi arylations of propargylic bromides 86, 87
Negishi coupling 78, 80, 83, 89
*N*-fluoroalkylsulfonamide (NFAS) 164
*N*-fluorobenzenesulfonimide (NFSI) 59
NHC-boryl radical 516, 517
*N*-hydroxy 2,3-naphthalimide (NNaphth)-derived esters 243
*N*-hydroxyphthalimide (NHP) esters 233, 235
N-hydroxyphthalimide (NHP)-type esters of carboxylic acids 186
Ni-catalyzed asymmetrc cross-electrophile coupling (XEC)
  asymmetric C($sp^3$)–C($sp^2$) XECs enabled by metallaphotoredox or electrocatalysis 137–143
  asymmetric couplings of C($sp^2$)-halides with C($sp^3$) pseudo electrophiles
    couplings with aziridines 137
    couplings with epoxides 136–137
  asymmetric couplings of C($sp^3$) halides with C($sp^2$) halides
    couplings with acyl chlorides 129–131
    couplings with alkenyl halides 131–132
    couplings with aryl halides 133–135
  asymmetric reductive difunctionalization of alkenes with electrophiles
    tethered activated alkenes 144–146
    tethered nonactivated alkenes 146–151
  three-component asymmetric coupling with alkenes 151–153
Ni-catalyzed asymmetric reductive alkenylation 132, 260
Ni-catalyzed asymmetric reductive dicarbofunctionalization of enamines with aryl halides and alkyl halides 151
Ni/(Ph)-Box 79
Ni/photoredox catalyzed enantioselective XEC of benzylic chlorides with aryl bromides 139
Ni/photoredox dual catalysis 100
Ni/pyridine-oxazoline-based catalyst 91
$NiBr_2 \cdot$ diglyme 93
nickel/bisphosphine-catalyzed stereoconvergent cross-coupling of epoxides 106
nickel-catalyzed asymmetric Negishi cross-coupling of racemic propargylic carbonates 85
nickel-catalyzed asymmetric reductive alkylarylation of bromoaryl-tethered enamides 145
nickel-catalyzed asymmetric reductive divinylation of 2-bromo-1,6-dienes with vinyl bromides 150
nickel-catalyzed asymmetric XEC reaction of acyl chloride-tethered alkenes with alkyl iodides 147
nickel-catalyzed cross-coupling of secondary α-haloketones 92
nickel-catalyzed diastereo-and enantioselective alkyl-borylation of heterocyclic alkenes 118
nickel-catalyzed electrophile-nucleophile and related asymmetric radical cross-couplings
  asymmetric cross-coupling with aliphatic C($sp^3$)–H bonds 107
  asymmetric cross-coupling with redox auxiliaries 101
  asymmetric redox-neutral alkene functionalization 115

nickel-catalyzed electrophile-nucleophile and related asymmetric radical cross-couplings (*contd.*)
of organohalides with aryl and primary alkylzinc reagents 78–87
of organohalides with organosilicon and organoboron reagents 95–101
of organohalides with organozirconium, organoindium, organotitanium and Grignard reagents 92–95
of organohalides with secondary alkylzinc reagents 87–92
nickel-catalyzed enantioselective arylation and alkenylation of racemic α-halonitriles 79
nickel-catalyzed Hiyama arylation 95
nickel-catalyzed regioselective cross-coupling of α-silylated propargylic bromides 85
nickel-catalyzed stereoconvergent Hiyama cross-coupling 95
nickel-catalyzed stereoconvergent Negishi arylation of racemic alkyl electrophiles 80
nickel-catalyzed Suzuki-Miyaura cross-coupling of racemic 3-bromo-phthalides 97
nickel/PyBox-catalyzed enantioselective cross-coupling of racemic α-bromoketones 78
nickel/PyBox-catalyzed stereoconvergent cross-coupling of alkyl chlorides 101
nickel/Pyrox-catalyzed asymmetric Suzuki-Miyaura coupling of α-bromobenzyl trifluoro-/difluoro-/mono-fluoromethanes 97
niraparib 166
nitroalkanes 7, 8, 114, 115
nitrobenzene 436, 437
nitro compounds 433, 434, 436
nitrogen-heterocyclic carbene (NHC) 403, 433–438, 514
β-nitroamides 114
$^{15}N$ labeling ammonium chloride 179
NNHP-type esters 243, 244
*N*-nucleophiles 58–60
nonactivated alkanes 10
5-nonyl-substituted biOx 151
(–)-norephedrine 384, 398
Nozaki-Hiyama-Kishi (NHK) reaction 263

***O***

oligomers 396
*O*-nucleophiles 55–58, 246
optically active β-cyano ketones 235
optically active diarylalkanes 276
optically active propargyl cyanides 237
organoaluminum reagents 93
organoboron compounds 81, 97
organoboron reagent 95–102, 116, 189, 195, 248
organocatalysts 304, 364, 403, 404, 416, 421–423, 430, 431, 433, 438, 443, 444, 450, 452, 487, 489, 499
organocatalyzed radical reactions 404
organoindium compounds 93
organophotoredox acridinium catalyst 263
organotitanium reagents 93, 94
organozinc reagent 78–83, 85, 87, 88, 92, 93, 105
Oxa-di-π-methane rearrangement 385
oxime ester 151, 235, 246–248, 257
oxime imidates 175
oxindoles 116, 144, 145, 219, 257, 301, 302, 313, 436, 490
α-oxyamination, of aldehydes 416
α-oxy C($sp^3$)–H arylation via dual nickel/photoredox-catalysis 113
oxygen extrusion 503
α-oxy TCNHP esters 104

## p

palladium catalysis 273, 276, 277, 279, 281, 511
palladium/photoredox-catalyzed regio-and enantioselective decarboxylative allylic benzylation 279
(-)-pavidolide B 511
Pd-catalyzed asymmetric radical reactions 273–282
Pd-catalyzed cross-coupling reactions 181
pendant olefin 80, 116
phenylnickel(I) complex 86
phenylnickel(II) complex 86, 87
*N*-phenyl piperidine 481
phenylthiyl 500, 501, 511
phenythiol 511
phosphino-oxazoline (PHOX) ligand 133
phosphoric acids 9, 18, 176, 179, 182, 459, 463, 464, 466, 467, 483, 492, 493
[2+2] photoaddition reactions 306, 307
photocatalyst Ir(III)* oxidizes cyclopropanols 105
photocatalyst-free α-alkylation 422
photocatalytic iminyl radical 235
photocatalytic system 424, 428, 454
photocycloaddition reactions 388, 449
photocyclodimerization 375, 377–381, 383, 389–391, 393, 396, 398
photoelectrocatalysis 237, 239
photoenolization/Mannich (PEM) 312
photoexcited Ir(III) catalyst 232
photoinduced copper-catalyzed asymmetric C($sp^3$)–H alkynylation of unactivated cyclic 2-iodo-benzamides 245
photoinduced copper-catalyzed asymmetric C($sp^3$)–H radical alkynylation 244
photoinduced copper-catalyzed asymmetric radical alkylation of azoles 245
photoinduced copper-catalyzed enantioselective C($sp^3$)–H alkylation 246
photoinduced copper-catalyzed enantioselective radical C–O coupling 247
photoinduced copper-catalyzed enantioselective radical cross-coupling 242
photoinduced copper-catalyzed enantioselective radical cyanofluoroalkylation of alkenes 243
photoinduced Cu-catalyzed radical cross-coupling 183
photoinduced electron transfer (PET) 389, 444, 458, 491
photoinduced enantioselective C($sp^3$)–N cross-coupling strategy 241
photoirradiation 349, 389–391, 393, 506
photonic sergeant 395
photoredox catalysis 137, 166, 167, 173, 174, 230, 232, 233, 249, 251, 262, 263, 281, 314, 319, 323, 337, 339, 344, 346, 356, 410, 418, 431, 433, 438, 462, 477, 483, 484, 487, 493, 494
photoredox/copper-catalyzed asymmetric radical reactions
  bifunctional catalysis 241–248
  dual catalysis 232–241
photoredox/nickel dual catalyzed enantioselective radical acylation of alkenes 258
photoredox/nickel dual catalyzed enantioselective radical C($sp^3$)–H acylation 256
photoredox/nickel dual-catalysis platform 102
photoredox/nickel-catalyzed asymmetric radical reactions
  enantioselective reductive cross-couplings 257–262
  redox-neutral enantioselective radical transformations 248–257

photoredox/nickel-catalyzed enantioselective desymmetrization of cyclic meso-anhydrides 250
photoredox/nickel-catalyzed enantioselective radical acylation reaction 251
photoredox/palladium cocatalyzed-AAA reaction 276
photoredox/palladium-cocatalyzed enantioselective alkylation of secondary benzyl carbonates 277
photoredox/Pd-cocatalyzed reductive homocoupling of allylic electrophiles 278
photoredox sensitizer 466, 467
photosensitizers (PS) 173, 186, 240, 251, 304–324, 335, 365, 367, 373, 423, 450, 459, 467, 470, 474, 475, 481, 483, 487, 489, 491
(+)-physostigmine 144
(+)-physovenine 144
2-piperidinones 148
plausible reaction mechanism 298
potassium alkoxymethyl trifluoroborate 99
potassium benzyltrifluoroborates 248
potassium organotrifluoroborates 99
potassium trifluoroborates 250
potent GPR40 agonist AMG 837 170
precious transition metal-catalyzed asymmetric radical reactions
  iridium-catalyzed asymmetric radical reactions 284–285
  Pd-catalyzed asymmetric radical reactions 273–282
  rhodium-catalyzed asymmetric radical reactions 283–284
prefoldin (PFD) 393
prochiral α-amino carbon radical 255, 257
prochiral alkenes 503
*S*-proline 487, 488
propargyl esters 237
propargylic bromide 85–87, 91
proton-coupled electron transfer (PCET) 105, 356, 425, 459, 460
purine nucleosides 393
(*i*-Pr)-PyBox 78
(*S*)-($^{i}$Pr)-PyBox 93
pyridine derivatives 437, 466
pyrimidine 133, 393

## *q*

quinine 478
2-quinolone 387, 388, 447
quinolone 364, 366, 387–389, 447, 450, 457, 458
8-Quniox ligand 148

## *r*

racemic alkyl-DHPs 103
racemic α-γ-silylated allylic halides 85
racemic α-amino alkyl chlorides 81
racemic α-bromoamide 78
racemic α-halogenborates 81
racemic α-haloglycine derivatives 81
racemic α-halosilanes 82
racemic α-zincated *N*-Boc pyrrolidine 88
racemic β-zincated amides 91
racemic benzyl bromides 93
racemic 1,1′-binaphthol 390
racemic cyclopropylzinc reagents 91
racemic germylated allylic bromides 85
racemic heterobiaryls 266
racemic hydrazones 176
racemic ketones 176
racemic propargylic bromides 91
racemic pyrrolidine-derived nucleophiles 89
racemic Reformatsky reagents 89
racemic secondary propargylic bromides 91
racemic styrene oxides 261
racemic tertiary alkyl halides 93, 198, 241
racemic trifluoroborate 99
radical addition (RA) 17, 25, 26, 114, 117, 118, 135, 153, 170, 194, 249, 252, 257, 267, 283, 287–291, 294,

295, 297–300, 307–309, 311, 314–317, 320, 322, 323, 326, 346, 404, 405, 407, 410, 414, 415, 418–424, 428–432, 444, 454, 457, 459, 461–467, 471, 482, 509, 515, 518
radical-based transformation 444
radical chemistry 25, 53, 287, 288, 333, 335, 403, 471, 494
radical conjugate addition 346, 348, 429, 482
radical coupling 243, 251, 265, 266, 274, 300, 313, 324, 325, 405, 415, 416, 425–428, 444, 471–476, 483, 486
radical cyclization 28, 80, 287, 296–299, 405, 410–415, 444, 457–459, 501, 505, 512, 518
radical cycloisomerization reaction 515, 517
radical cyclopropenation 39–40
radical-mediated asymmetric catalysis 225, 299, 310, 326
radical-mediated cyclization 296, 511
radical rebound mechanism, for manganese-catalyzed C–H hydroxylation 208
(+)-Radulanin J 36
redox-active esters 105, 468
redox auxiliary 101–107
redox $Cu^{I}$/chiral phosphoric acid (CPA) catalytic system 176
redox-neutral enantioselective radical transformations 248–257
reductive asymmetric protonation 479
regio-and enantioselective α-amino C($sp^3$)–H acylation of cyclic amides 111
regioselectivity in asymmetric cyanation of propargylic C–H bonds 165
Rh-bound α-carbonyl radical 351, 354
Rh-bound γ-carbonyl radical 358, 359
Rh-bound ketyl radical 349, 350
rhodium-bound β-carbonyl radical 352, 358
rhodium-catalyzed asymmetric radical reactions 283
rhodium complexes
  direct photoexcitation of 359–363
  single electron transfer of 349–359
rhodium-enolate 341–344
rhodium-enone 344–347
rivastigmine 191
ryl iodides 133–141, 143, 146, 258, 259, 261

## S

saturated azacycles 110
Schwartz reagent 92
secondary α-chloronitriles 133
secondary alkyl bromides 88, 97, 245, 279
secondary alkyl halide 67, 79, 94, 116, 185, 190, 198
secondary benzylic bromides 83, 88, 93
self-designed chiral bis-imidazoline (BiIM) ligand 107
seminal photoredox/nickel-catalyzed decarboxylative arylation of amino acids 250
sergeants and soldiers process 395
(*S*)-sertraline tetralone 83
serum albumins 390–393
silane-controlled enantioselective intramolecular hydroalkoxylation of alkenes 57
α-silyl benzyl halides 188
silyl hydride 512
single-electron oxidation 99, 311, 320, 326, 337, 338, 343, 346, 352–354, 404, 405, 407, 414, 422, 430, 464, 471, 473, 474, 482, 485, 486
single-electron transfer (SET) 10, 13, 25, 101, 103, 104, 107, 112, 114, 116, 129, 181, 229, 232, 273, 281, 285, 298, 304, 349–359, 410, 424, 425, 428, 434, 438, 454, 462
singlet oxygen 385, 386, 449
singly occupied molecular orbital (SOMO) 404

site-and enantioselective α-acylation of saturated *N*-heterocycles 257
sodium benzene sulfinates 261
sodium dodecyl sulfate (SDS) 398
($sp^2$)–C/X cross-coupling for achiral products 181
spin-center shift (SCS) 421, 469
spiroepoxyoxindoles 106
Stannyl radicals 512–513, 517
stereo-and enantioselective benzylic C($sp^3$)–H alkenylation 109
stereoconvergent coupling of α-halogenborates with organozinc reagents 82
stereoconvergent Negishi reactions of racemic benzylic bromides 87
γ-stereogenic vinyl halides 85
sterically hindered phenanthrene methyl box ligand 130
stoichiometric chiral auxiliaries 81
stoichiometric diphenylsilane 512
α-substituted ketones 251
3,5-substituted N,N,P-ligands 192
substrate-controlled asymmetric reaction 500
supramolecular photochemical reaction 371
supramolecular photochirogenesis 371, 381, 383–386, 390–399
supramolecular systems 393–399
Suzuki-Miyaura cross-coupling of tertiary α-bromide-β-lactams 198
$C_1$-symmetric 1,1′-bi-2,2′-naphthols (BINOLs) 4

## *t*

TBADT/CPA 464
TCNHPI ester 105
TEMPO 28, 86, 106, 278, 352, 415, 416, 474
terminal alkynes 39, 62, 170, 171, 185–187, 198–201, 232, 243
tertiary α-fluorinated ketones 79
tethered activated alkenes 144–146
tethered nonactivated alkenes 146–151
tetrabutylammonium chloride (TBAC) 135
tetrabutylammonium decatungstate (TBADT) 257
tetrahydrofuran-3-one 114
tetrahydroisoquinolines 232, 233, 320, 322, 479, 486
tetrahydronaphthalene unit 447, 450
1,2,3,5-tetrakis(carbazole-9-yl)-4,6-dicyanobenzene (4CzIPN) 138
tetrakis(dimethylamino)ethylene (TDAE) 132
tetrakis[3,5-bis(trifluoromethyl)phenyl] borate anion ($BAr_F$) 177
*tetra*-$^n$butylammonium fluoride (TBAF) 298
tetra-*n*-octylammonium bromide (TOAB) 485
*p*-thiocresol 145
thiol catalyst 503, 506
thiophosphoric imide 263
thioxanthone 388, 423, 451, 452, 455–459
thiyl radicals 394, 431, 500–511
three-component asymmetric coupling with alkenes 151–153
Togni-II reagent 173, 240
*p*-toluenesulfonohydrazide 176
transition metal-catalyzed enantioconvergent radical cross-coupling of alkyl halides 182
transition metal-mediated oxidative C–H/C–H coupling reactions 4
trialkynyl lithium reagents 93
trifluoromethyl iodide 419
trifluoromethyl ketone 339, 349
triisopropyl silyl (TIPS) 505
trimethylaluminum 501
trimethylsilyl cyanide (TMSCN) 233
triphenylstannyl 500, 501
triphenyltin hydride ($Ph_3SnH$) 500, 501
triplet energy transfer 139, 316, 318, 366, 367, 449, 452, 457, 490
triplet-excited ketone 252

triplet-triplet annihilation (TTA) 381
tropolone 384
two-component asymmetric couplings with tethered alkenes
  tethered activated alkenes 144–146
  tethered nonactivated alkenes 146–151

***u***

unnatural α-amino acids 245
α,β-unsaturated anhydrides 430
α,β-unsaturated alkene 344
α,β-unsaturated compounds 291
α,β-unsaturated systems 288
β,γ-unsaturated ketones 92

***v***

vinyl boronates 12
vinyl bromides 131, 144, 150, 253, 260
vinylcyclopentene 500
vinylcyclopropanes 501, 502, 505, 506, 508, 509, 511
visible light 229
visible-light-driven photocatalytic cycles 231
visible light irradiation 107, 108, 244–246, 266, 381, 388, 425, 429, 431, 452, 462, 487, 511
visible-light-induced homolysis (VLIH) 311

***x***

xanthone 388, 450–452

***z***

zeolites 384–386
Zhang's Enantioconvergent Radical $C(sp^3)$–C(sp) Cross-Coupling 188
α-zincated *N*-Boc pyrrolidine 88–90
Zoloft 83